ASYMMETRIC PERICYCLIC TRANSFORMATIONS
FROM REACTIVE PALLADIUM INTERMEDIATES

Thesis by

Alexander Quinn Cusumano

In Partial Fulfillment of the Requirements for

the Degree of

Doctor of Philosophy

CALIFORNIA INSTITUTE OF TECHNOLOGY

Pasadena, California

2024

(Defended June 5, 2023)

Alexander Quinn Cusumano
ORCID: 0000-0002-2914-2008

To my loving parents

ACKNOWLEDGEMENTS

There are numerous people I wish to thank for their support, encouragement, mentorship, and friendship during my time in graduate school. The culmination of all of these interactions and memories has made this time a truly unique experience – one far more exhilarating and rewarding than I could have ever imagined.

First, I have to thank Professor Brian Stoltz for his guidance, support, and unwavering enthusiasm over the past five years. Brian is an amazing scientist. He is always thinking outside the box, taking on hard challenges, and getting everyone else excited about chemistry. I also want to acknowledge how Brian is a role model of a PI. During my time in the Stoltz group, I have been continually impressed with his people skills – his patience, optimism, ability to foster scientific growth in his mentees, and his genuine investment in our personal development as young adults. Brian offers us an immense amount of freedom in our research directions and the types of challenges we wish to pursue. This level of autonomy allows us to explore our unique interests and define our own scientific identities, all while still benefiting from his support and guidance. I am extremely grateful to have had the opportunity to pursue doctoral studies in the Stoltz group.

I would also like to thank Professor William (Bill) Goddard for being a second mentor to me on the fronts of theoretical and computational chemistry. Bill has unique insights, perspectives, and is always excited to talk about research. I have especially enjoyed taking and TA-ing the Ch120–CH121 series. The concepts we talked about and the intuitive picture of quantum mechanics painted from these courses has changed the way I think about chemistry at the deepest level. I would also like express my appreciation for the members of my thesis committee. In addition to being a supportive thesis chair, Professor Gregory Fu

was always there to offer professional advice and chemistry wisdom. From our chats about postdoc plans and grantsmanship to kinetic queries, Greg has been a phenomenal resource. I would also like to thank Professors Ryan Hadt, Theo Agapie, and Sarah Reisman for their support over the years.

We are lucky at Caltech to have amazing staff that make everyone's research possible. To that end, I am grateful for the plethora of help and guidance I have received over the years from Dr. Scott Virgil. I need to thank Dr. David VanderVelde, Dr. Mike Takase, and Dr. Mona Shahgholi for their expertise and assistance in NMR spectroscopy, X-ray crystallography, and mass spectrometry. Beth Marshall, Joe Drew, Alison Ross, and Tomomi Kano are all thanked for keeping everything in Schlinger running.

I am lucky to have had a number of outstanding project partners during my time in the Stoltz group. The guidance of Dr. Eric Alexy and Dr. Tyler Fulton were critical when I first arrived. From teaching me laboratory techniques to offering big-picture career advice, their direction was treasured. I am thankful to Dr. Trevor Lohrey for all of the help with organometallic-related synthesis and questions, as well as insights on life as a postdoc. I have learned a ton from our conversations and had a great time working with Ni and Pd together. Working with Adrian Samkian and Zack Sercel on the synthesis of OSDAs has been a pleasure. I have also had the opportunity to work with Dr. Steven Sardini and Dr. Veronica Hubble on a variety of projects over the last years, all of which have been an awesome time (besides our "asymmetric" protonation). I am thankful for our "[4+2] team" – Kali Flesch, Ruby Chen, and Christian Strong – for being an amazingly supportive group in our efforts to hijack Pd enolates. Lastly, I am grateful for the opportunity to mentor Tianyi Zhang, an

amazingly talented undergraduate, over the past two years. Tianyi continually impressed me with his intellect, fun personality, and ability to rapidly acquire and apply new skills.

The Stoltz group is full of interesting characters that make coming to work each day that much more enjoyable. I got lucky to have an awesome cohort, with Alexia Kim, Zack Sercel, and Tyler Casselman (TC). Officer Kim has been the perfect hood-mate and partner on our bad boy police force over these 5 years. If you are reading this, I am sorry for the embarrassing photos in my defense. Thank you for putting up with me and blessing our bay with good tunes – sorry for the dances. Zack has been not only a source of encouragement, but also a great sounding board for wacky ideas, a fun project partner, and just a pleasure to talk to about life. Hopefully we get to cross paths again someday. TC was the addition to our cohort that we needed. From random fist-bumps when I looked stressed at my desk to hilarious one-liners, Tyler has been a great moral booster. I am also thankful for the following class, Melinda Chan and Ally Stanko. I need to thank Melinda for support and friendship over the years. I remember when we first met, you almost called the police because you didn't have my number saved and I convinced you over text that you were being roped in to a cocaine smuggling ring in the Cats. Anyways, thank you for the Ting Ting workouts, letting me babysit Poo, and the life advice. Our group then rapidly expanded two classes of seven graduate students. Jay Barbor, Kali Flesch, Kevin Gonzales, Elliot Hicks, Farbod Moghadam, Samir Rezgui, and Adrian Samkian were all amazing additions to the group. The following year we were blessed with Ruby Chen, Ben Gross, Kim Sharp, Christian Strong, Camila Suarez, Marva Tariq, and Hao Yu. It was fun watching all of this new talent flood into the group as the size of our family grew dramatically. I am excited to see what our

most recent class, Adrian de Almenara, Sydney Bottcher, Chloe Cerione, and Jonathan Farhi, will accomplish over the next few years.

I am grateful for the talented group of postdocs I have overlapped with over the years. Dr. Stephen Sardini has been an awesome friend and project partner. Stephen is a talented chemist and has started and developed several exciting projects in his time in the Stoltz group. Thank you for helping me out whenever I got stuck and always pushing me to be a hard little worker. Dr. Veronica Hubble has been another key figure during my time in the Stoltz group. I remember chatting on the phone about Brian and research in the Stoltz group when you were considering pursuing a postdoc here. Fortunately, you decided to come to Caltech, and the rest is history. Dr. Melissa Ramirez has been an awesome addition to the group. Our conversations on academia, science, and life never failed to offer me a new perspective on things – this I value a ton. In addition to the former group members mentioned earlier, I have to give a special thanks to Dr. Chris Reimann for being a "fatherly" figure to me and Alexia when we were baby G1s. Thank you for always supporting us regardless of whatever wild situation in which we found ourselves. Long live "Bible Club."

My years prior to Caltech were formative. I am indebted to Professor Markus Etzkorn at UNC Charlotte for welcoming me into his research group during my high school years. Those early experiences introduced me to the exciting field that is organic chemistry, about which I have remained passionate ever since. Following this, I had the great fortune of working with Professor Joshua Pierce during my undergraduate years at NC State. His guidance and support (and patience) were crucial to my development as a young scientist and ultimately led to me pursuing graduate school. I would also especially like to thank Dr.

Yasamin Moazami and the entirety of the Pierce group for being amazing mentors during these years.

Lastly, I would like to extend my gratitude to my loving family, without whom none of this would be possible. My parents, and sister Nicki, have been an amazing support system every step of the way. To this day, without fail, I receive embarrassingly decorated "care packages" all the way from North Carolina for even the smallest of holidays. Thank you for always encouraging me to pursue my passions, and for the endless love. Of course, I have to thank my amazing girlfriend, Meagan Castañeda, for being by my side through this crazy journey. Meeting you was the best thing to happen to me during my time here. I am so lucky to have you and I am excited for the next steps in our life together. At last, mga anak natin Pingu, Koala, at Kokak – salamat sa support.

ABSTRACT

Research in the Stoltz group is centered around the development of novel tactics and strategies for the synthesis of complex organic molecules. The Pd-catalyzed decarboxylative asymmetric allylic alkylation of enolate nucleophiles is a cornerstone of our groups' efforts to develop methodologies that directly facilitate the synthesis of stereochemically complex molecular building blocks. This thesis first focuses on our efforts to deepen our mechanistic understanding of these transformations. We then employ our insights as a base from which we expand the scope of the decarboxylative asymmetric allylic alkylation reaction, as well as develop entirely novel reaction paradigms.

PUBLISHED CONTENT AND CONTRIBUTIONS

1. Duquette, D. C.; Cusumano, A. Q.; Lefoulon, L.; Moore, J. T.; Stoltz, B. M. Probing Trends in Enantioinduction via Substrate Design: Palladium-Catalyzed Decarboxylative Allylic Alkylation of α-Enaminones. *Org. Lett.* **2020**, *22*, 4966–4969. DOI: 10.1021/acs.orglett.0c01441.

    A.Q.C. participated in manuscript preparation.

2. Cusumano, A. Q.; Stoltz, B. M.; Goddard, W. A. III. Reaction Mechanism, Origins of Enantioselectivity, and Reactivity Trends in Asymmetric Allylic Alkylation: A Comprehensive Quantum Mechanics Investigation of a $C(sp^3)$–$C(sp^3)$ Cross-Coupling. *J. Am. Chem. Soc.* **2020**, *142*, 13917–13933. DOI: 10.1021/jacs.0c06243.

    A.Q.C. carried out computational studies, experimental work, data analysis, and manuscript preparation.

3. Cusumano, A. Q.; Goddard, W. A. I.; Stoltz, B. M. The Transition Metal Catalyzed [π2s + π2s + σ2s + σ2s] Pericyclic Reaction: Woodward–Hoffmann Rules, Aromaticity, and Electron Flow. *J. Am. Chem. Soc.* **2020**, *142*, 19033–19039. DOI: 10.1021/jacs.0c09575.

    A.Q.C. carried out computational studies, data analysis, and manuscript preparation.

4. Zhang, T.; Cusumano, A. Q.; Hafeman, N. J.; Loskot, S. A.; Reimann, C. E.; Virgil, S. C.; Goddard, W. A. I.; Stoltz, B. M. Investigations of an Unexpected [2+2] Photocycloaddition in the Synthesis of (−)-Scabrolide A from Quantum Mechanics Calculations. *J. Org. Chem.* **2022**, *87*, 14115–14124. DOI: 10.1021/acs.joc.2c01693.

    A.Q.C. carried out computational studies, data analysis, and manuscript preparation.

5. Flesch, K. N.; Cusumano, A. Q.; Chen, P.-J.; Strong, C. S.; Sardini, S. R.; Du, Y. E.; Bartberger, M. D.; Goddard, W. A. I.; Stoltz, B. M. Divergent Catalysis: Catalytic Asymmetric [4+2] Cycloaddition of Palladium Enolates. *J. Am. Chem. Soc.* **2023**. *In press*. DOI: 10.1021/jacs.3c02104.

A.Q.C. carried out experimental work, computational studies, data analysis, and manuscript preparation.

TABLE OF CONTENTS

CHAPTER 1   **1**

Mechanism of the Pd-catalyzed Asymmetric Allylic Alkylation: A Comprehensive Quantum Mechanics Investigation

APPENDIX 1   **80**

Spectra Relevant to Chapter 1

CHAPTER 2   **83**

Analysis of the Pd [π2s + π2s + σ2s + σ2s] Pericyclic Reaction

CHAPTER 3   **136**

Catalytic Asymmetric [4+2] Cycloaddition of Pd Enolates

APPENDIX 3   644

Spectra Relevant to Chapter 5

APPENDIX 4   753

Notebook Cross-Reference for New Compounds

ABOUT THE AUTHOR   757

LIST OF FIGURES

CHAPTER 1
Mechanism of the Pd-catalyzed Asymmetric Allylic Alkylation: A Comprehensive Quantum Mechanics Investigation of a C(sp³)–C(sp³) Cross-Coupling

APPENDIX 1
Spectra Relevant to Chapter 1

CHAPTER 2

Analysis of the Pd [π2s + π2s + σ2s + σ2s] Pericyclic Reaction

CHAPTER 3
Catalytic Asymmetric [4+2] Cycloaddition of Pd Enolates

APPENDIX 2

Spectra Relevant to Chapter 3

CHAPTER 4

Quantum Mechanics Investigations of the [2+2] Photocycloaddition in the Synthesis of (–)-Scabrolide A

CHAPTER 5

Development of a Branched-selective Asymmetric Allylic Alkylation of Hard Pd-Enolate Nucleophiles

APPENDIX 3

Spectra Relevant to Chapter 5

LIST OF SCHEMES

CHAPTER 1

Mechanism of the Pd-catalyzed Asymmetric Allylic Alkylation: A Comprehensive Quantum Mechanics Investigation of a $C(sp^3)$–$C(sp^3)$ Cross-Coupling

CHAPTER 3

Catalytic Asymmetric [4+2] Cycloaddition of Pd Enolates

CHAPTER 4

Quantum Mechanics Investigations of the [2+2] Photocycloaddition in the Synthesis of (−)-Scabrolide A

LIST OF TABLES

CHAPTER 3

Catalytic Asymmetric [4+2] Cycloaddition of Pd Enolates

CHAPTER 4

Quantum Mechanics Investigations of the [2+2] Photocycloaddition in the Synthesis of (−)-Scabrolide A

LIST OF ABBREVIATIONS

$[\alpha]_D$	specific rotation at wavelength of sodium D line
ºC	degrees Celsius
Å	Angstrom
Aq	aqueous
Ar	aryl
atm	atmosphere
Bn	benzyl
Boc	*tert*-butyloxycarbonyl
bp	boiling point
br	broad
Bz	benzoyl
c	concentration for specific rotation measurements
calc'd	calculated
cm^{-1}	wavenumer(s)
d	doublet
D	deuterium
dba	dibenzylideneacetone
DMF	*N,N*-dimethylformamide
dr	diastereomeric ratio
ee	enantiomeric excess
equiv	equivalent(s)

ESI	electrospray ionization
Et	ethyl
EtOAc	ethyl acetate
G	grams
GC	gas chromatography
h	hours
HPLC	high-performance liquid chromatography
HRMS	high-resolution mass spectrometry
Hz	hertz
IPA	isopropanol
IR	infrared (spectroscopy)
J	coupling constant (NMR), exchange coupling constant (diradicals)
K	Kelvin (absolute temperature)
kcal	kilocalorie
KHMDS	potassium hexamethyldisilazide
L	liter; ligand
LDA	lithium diisopropylamide
m/z	mass to charge ratio
Me	methyl
mg	milligram(s)
MHz	megahertz
min	minutes
mol	mole(s)

n-Bu	*n*-butyl
NMR	nuclear magnetic resonance
Pd/C	palladium on carbon
Ph	phenyl
PHOX	phosphinooxazoline (ligand)
ppm	parts per million
R	generic for any atom or functional groups
SCF	self-consistent field
SFC	supercritical fluid chromatography

CHAPTER 1

Mechanism of the Pd-catalyzed Asymmetric Allylic Alkylation: A

Comprehensive Quantum Mechanics Investigation

1.1   INTRODUCTION

The construction of chiral all-carbon quaternary centers remains a forefront challenge in synthetic chemistry[1] Over the years, our group has pursued the development of the decarboxylative asymmetric allylic alkylation reaction as a practical entry into these highly sought-after structural motifs (Figure 1.1A).[2] This approach has proved fruitful in asymmetric synthesis,[3] particularly in the early-stage preparation of chiral building blocks. However, our efforts to further extend the scope of these transformations have highlighted limitations of the current catalytic systems.[4] We recognize that a comprehensive mechanistic understanding is crucial in our ability to address these shortcomings and to realize general improvements. Owing to the interplay of several plausible inner- and outer-sphere processes (Figure 1.1B), the unification of a comprehensive, stereochemically complete mechanistic hypothesis has remained elusive for the Pd(PHOX) system. Determination of inner- or outer-sphere nucleophilic attack through observation of retention (outer-sphere) or inversion (inner-sphere) of stereochemistry when employing chiral cyclic allyl electrophiles is not applicable as such substitution patterns are not

tolerated by the system at hand. Surprisingly, allylic alkylation with the Pd(PHOX) system

demonstrates remarkable tolerance to exogenous water, with reaction yields and

enantioselectivity largely unaffected.[5] These results suggest that the presence of an

unbound enolate with a conjugate acid pK_a significantly higher than that of water is

unlikely. Given the tolerance to water, an inner-sphere mechanism for C–C bond formation

is generally invoked for the Pd(PHOX) system.

Figure 1.1. *(A) Original report of the decarboxylative asymmetric allylic alkylation of*

β-ketoesters by Stoltz.[2a] (B) Inner- and outer-sphere allylic alkylation. (C) Isolation of

the catalyst resting state.[5] (D) This research.

A. Allylic alkylation of β-ketoesters to forge chiral all-carbon quaternary centers.[2a]
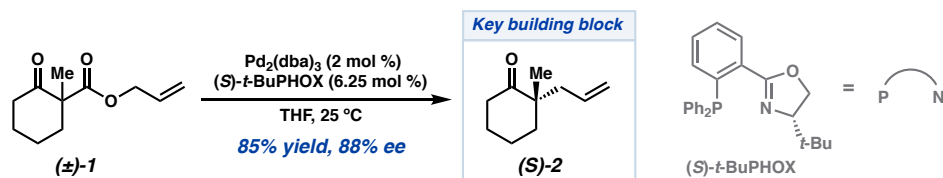
B. Outer- versus inner-sphere allylic alkylation.
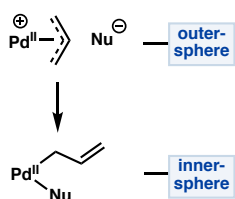
C. Mechanistic Developments.[5]

D. This research.

- DLPNO-CCSD(T) & DFT Invesitgation
- Origins of Enantioselectivity
- Mechanism of Decarboxylation
- Inner- versus outer-sphere
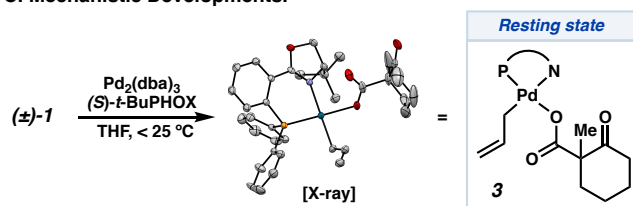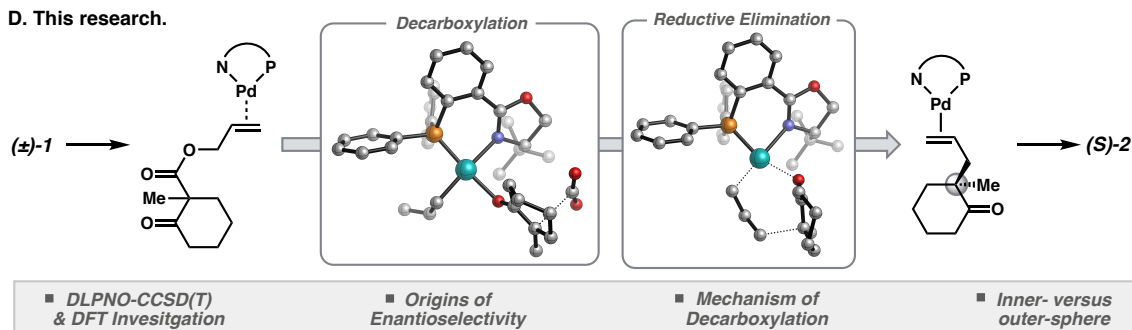
In contrast, mechanistic studies by Trost and coworkers with the bis-phosphine (*R,R*)-ANDEN-phenyl ligand on related substrates suggest alkylation occurs via an outer-sphere mechanism.[6] As anticipated with an ionic outer-sphere mechanism, highly charge stabilized "soft" enolates perform well in these systems.[7] Unlike the outer-sphere conditions of Trost, the Pd(PHOX) catalytic manifold provides low levels of enantioselectivity with stabilized enolate nucleophiles,[4,8] yet the Pd(PHOX) system excels with basic "hard" enolates, as well as substrates that contain heteroatoms.[9]

Key to the inner-sphere C–C bond formation hypothesis is the intermediacy of a square planar C- or O-bound Pd^{II} enolate complex. In our efforts to directly observe such a species, our group isolated a unique η^1-allyl Pd^{II} carboxylate complex (**3**) from the reaction of Pd$_2$(dba)$_3$, *(S)-t*-BuPHOX, and β-ketoester **1** (Figure 1.1C). The carboxylate complex was determined to be the catalyst resting state, with decarboxylation as the rate-limiting process (k = 1.58 x 10^{-3} s^{-1} at 24 °C, corresponding to a free energy barrier of 21.2 kcal/mol).[5]

In addition to experimental studies, our groups have turned to quantum mechanics (QM) calculations as a powerful tool to interrogate the mechanism of the stereoablative transformation of (±)-**1** to *(S)*-**2**.[10] These investigations focused on post-decarboxylation intermediates, and ultimately led to the discovery of a low energy pathway for inner-sphere C–C bond formation via a seven-centered cyclic reductive elimination transition state (Figure 1.1D). Analogous fully carbocyclic mechanisms have been proposed by Morken and Echavarren.[11] While these initial studies offer an invaluable knowledge base, the

mechanism of decarboxylation and the precise origins of enantioinduction remained unclear. To address these questions, we returned to computational and experimental studies. During our group's ongoing efforts to explore the mechanism, Sargent and coworkers reported an all-DFT-based investigation of the Pd(PHOX)-catalyzed transformation of **1** to **2**. [12] Unfortunately, the computationally-derived barrier to decarboxylation was significantly less than that of experiment, with the rate-limiting step as an isomerization to a pre-decarboxylation intermediate. Nevertheless, other aspects of their study regarding decarboxylation and C–C bond formation corroborate our computational and experimental findings herein. Taken together, these studies bring an unprecedented level of clarity to the mechanism of the decarboxylative asymmetric allylic alkylation reaction.

Herein, we outline a detailed QM investigation into each step of the reaction mechanism: oxidative addition, decarboxylation, and C–C bond formation, revealing a mechanistic picture that unites all current experimental observations, including enantioinduction, reaction rate, identity of the catalyst resting state, enolate cross-over, water tolerance, and solvent effects on the interplay between inner- and outer-sphere pathways in the PHOX system (Figure 1.1D). To provide useful insight into factors underlying enantiomeric selectivity, very high quantum mechanical accuracy is required. Given this, we use this study as an opportunity to compare the efficacy of various modern computational methods (density functional theory and localized coupled-cluster theory) in the context of asymmetric Pd^0/Pd^{II} catalysis. Further experiments are carried out to explore the mechanistic hypotheses derived from the ab initio calculations. Lastly, we address the

shortcomings of the present state-of-the-art catalyst systems and offer theory-based insight into future development.

1.2 COMPUTATIONAL METHODS

Density functional theory (DFT) geometry optimizations, energy, vibrational frequency, and coupled-cluster calculations were performed using Orca version 4.1.2.[13] Geometry optimizations were carried out with the BP86 generalized gradient approximation (GGA) functional[14] with Becke-Johnson damped D3 dispersion corrections (herein referred to as D3).[15] A mixed basis set was implemented, in which Pd is described by the small core LANL2TZ(f) basis set with the Hay–Wadt effective core potential (ECP),[16] while the 6-31G(d) basis set was used on all other atoms. Key structures were optimized at various levels of theory and compared to crystallographic data to ensure that consistent results are obtained across multiple methodologies (see 1.5 Supporting Information for details).

Triple-ζ quality single point calculations were carried out on all stationary points with a variety of density functionals, including BP86-D3,[14] B3LYP-D3,[17] PBE0-D3,[18] M06,[19] and DSD-BLYP-D3[20] with the def2-TZVP basis set[21] on all atoms (including the small core ECP28MWB pseudopotential[22] on Pd). Corrections for solvation (THF or otherwise as specified) were carried out for single point calculations with the implicit Conductor-like Polarizable Continuum Model (CPCM).[23] Unless otherwise noted, all energies reported are G_{298} values from single point calculations at the M06/def2-TZVP/CPCM(THF) level of theory on BP86-D3/LANL2TZ(f)–6-31G(d) optimized

geometries with thermodynamic corrections applied from frequency calculations obtained at the optimization level of theory. The Quasi-RRHO method is applied to correct for the breakdown of the harmonic oscillator approximation for low frequency vibrations.[24] All stationary points are characterized by the appropriate number of imaginary vibrational modes (zero for optimized geometries and one for transition states). Intrinsic reaction coordinate (IRC) analyses were carried out to ensure all transition states connect the appropriate starting materials and products. Molecular illustrations were made from CLYview.[25]

Additional single point calculations were performed on all optimized structures with the domain based local pair natural orbital coupled-cluster (DLPNO-CCSD(T), "NormalPNO" settings unless otherwise noted) method as described by Neese and coworkers and as implemented in Orca (further details included in Supporting Information).[26] The cc-pVTZ basis set is used on all atoms in the DLPNO-CCSD(T) calculations, with the SK-MCDHF-RSC effective core potential[27] on Pd. Throughout the text, free energies calculated from electronic energies at the DLPNO-CCSD(T)/cc-pVTZ/CPCM(THF) level of theory are provided in brackets next to the DFT (M06/CPCM(THF)) values for comparison.

1.3 RESULTS

Our investigation began with the experimental observation of the [(PHOX)Pd(η^1-allyl)(RCO$_2$)] complex (**3**) as the resting state of the catalyst (Figure 1.2). The structure of this unusual η^1–allyl complex was previously confirmed by X-ray crystallography while

the solution phase behavior was studied by NMR spectroscopy.[5] Importantly, **3** is competent in the reaction, and affords the ketone product **2** from β-ketoester **1** in similar yield and enantioselectivity to that obtained from the catalytic transformation. Kinetic studies revealed first order rate dependence of this process in **3**,[5] with an overall rate constant measured to be 1.58 x 10^{-3} s^{-1} (at 24 °C in THF-d_8). Given that loss of CO_2 is the rate limiting step, the experimental $\Delta G^{\ddagger}$ of decarboxylation is calculated to be 21.2 kcal/mol.

1.3.1   OXIDATIVE ADDITION

To better understand the role of the catalyst resting state (**3**) in the overall mechanistic picture, we first sought to examine the mechanism of oxidative addition of allyl β-ketoester **1** to the Pd^0(PHOX) precatalyst. Oxidative addition of allyl acetate to Pd^0 complexes is generally represented as directly generating the $[L_nPd(\eta^3\text{-allyl})](OAc)$ ion pair in situ in a reversible fashion.[28] This prompted us to question whether oxidative addition proceeds through a unique mechanism in which **3** is yielded directly, or if an analogous $[(PHOX)Pd(\eta^3\text{-allyl})]^+(RCO_2^-)$ ion pair (**4**) is first formed followed by rapid equilibration to **3** (Figure 1.2A).

While the stereoablative transformation employs racemic substrate (**1**), the chiral center is not directly involved but rather appended to the site of oxidative addition through freely rotatable bonds. Hence, we expect comparable energies of the diastereomeric transition states arising from both enantiomers of **1**. Our initial explorations considered the (*S*) enantiomer of **1**, but the relevant oxidative addition pathways were also evaluated for

(**R**)-**1**. A similar consideration is employed with regard to the orientation of the allyl

fragment in the η^3–bound form. Here, the prefix *endo* describes the η^3–(allyl) conformer

in which the apical carbon (*i.e.,* C2) of the allyl group is *cis* to the *t*-Bu group of the PHOX

ligand, and *exo* corresponds to the *trans* isomer. Experimentally the *endo* and *exo* isomers

were found to be nearly identical in energy. Both *endo* and *exo* geometries will be

considered. Unless otherwise stated, free energy comparisons are from the lowest energy

conformer.

Figure 1.2. *(A) Four general classes of Pd⁰ allyl carboxylate oxidative addition*

*mechanisms (B) Stereoretentive three-centered (**TS1**), seven-centered (**TS2**), and syn*

*S$_N$2′-like (**TS3**) transition states.[a]*
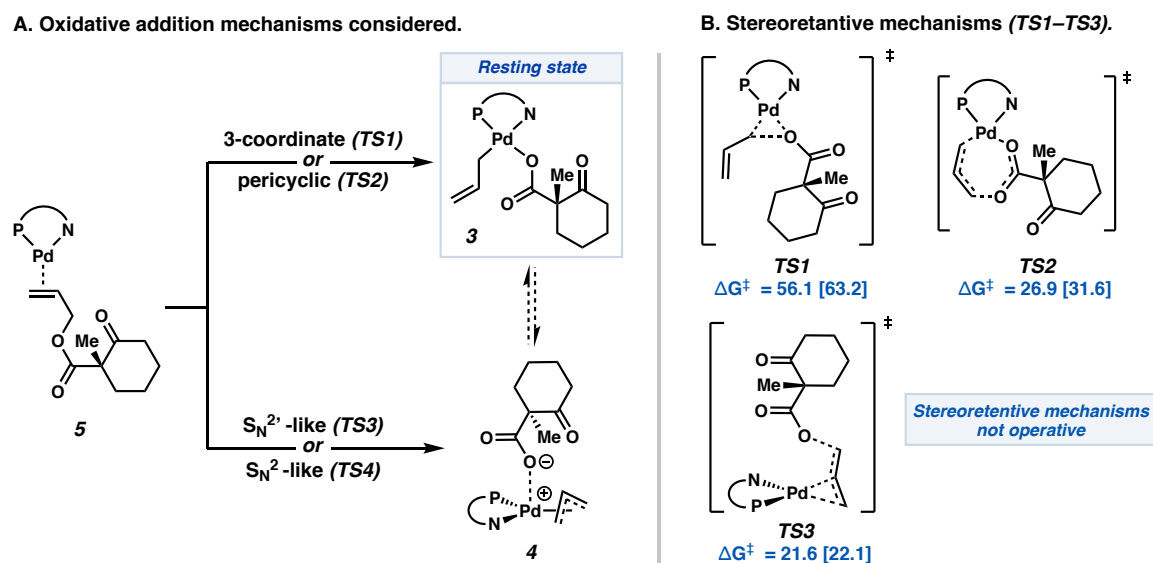
A. Oxidative addition mechanisms considered.

B. Stereoretantive mechanisms (TS1–TS3).

Resting state

3-coordinate (TS1)
— or —
pericyclic (TS2)

3

5

S$_N$2′-like (TS3)
— or —
S$_N$2-like (TS4)

4

TS1
$\Delta G^\ddagger = 56.1\ [63.2]$

TS2
$\Delta G^\ddagger = 26.9\ [31.6]$

Stereoretentive mechanisms not operative

TS3
$\Delta G^\ddagger = 21.6\ [22.1]$

[a] Relative Gibbs free energies in kcal/mol (M06). Free energies derived from DLPNO-CCSD(T)

calculations in brackets.

Starting from olefin-bound Pd^0(PHOX) complex **5**, a variety of transition states that achieve C–O bond cleavage were considered (Figure 1.2A). Three- (**TS1**)[29,30] and seven-membered (**TS2**) cyclic transition states,[31] as well as a *syn* conjugate displacement-type mechanism (**TS3**) afford barrier heights greater than that of the rate-limiting step ($\Delta G^\ddagger$ = 21.2 kcal/mol) (Figure 1.2B).[5]

Figure 1.3. *Isomeric transition states for the anti displacement-type oxidative addition mechanisms.*[a]
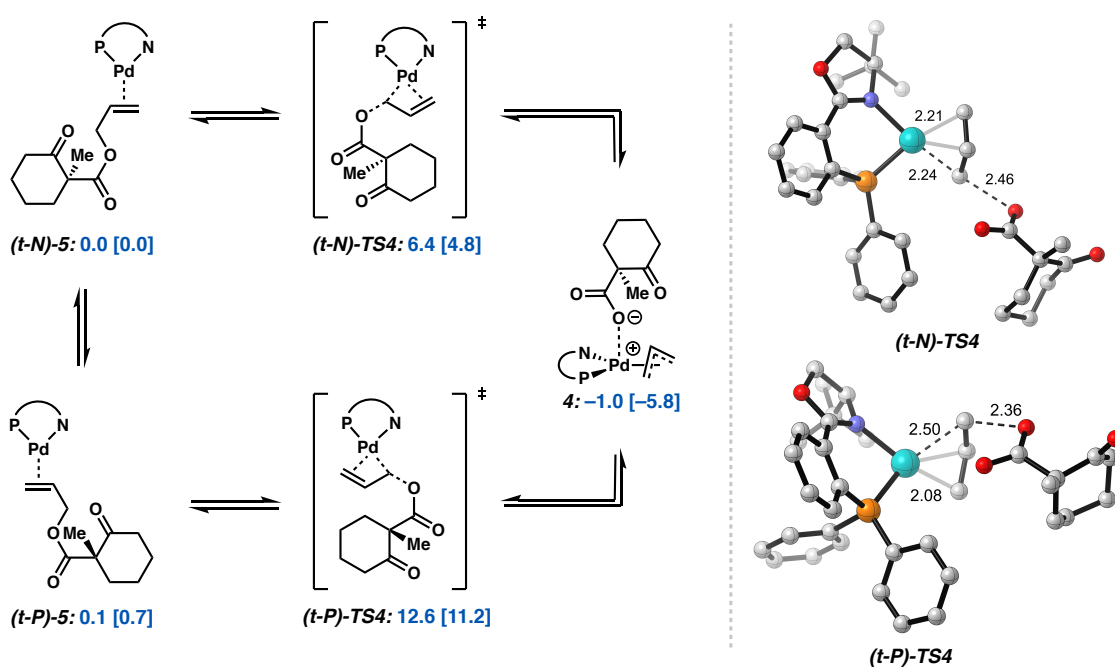
[a] Relative Gibbs free energies in kcal/mol (M06). Free energies derived from DLPNO-CCSD(T) calculations in brackets. *Endo* η^3–allyl **4** is 0.3 [0.4] kcal/mol higher in energy than its *exo* isomer depicted above.

Analogous to **TS3**, an *anti* displacement-type mechanism (**TS4**) via electrophilic addition to Pd^0 presents a substantially lower barrier than that of the other pathways

considered (Figure 1.3). Unlike **TS3**, in which C–O bond breaking occurs through the filling of σ^*(C–O) by the olefin-based π(C–C) orbital, **TS4** achieves the same overall result with direct overlap between σ^*(C–O) and the Pd d(x^2–y^2)-based HOMO.

Isomeric transition states are possible, in which the displacement event occurs *trans* to either the nitrogen or phosphorus of the PHOX ligand. The abbreviations *t*-N and *t*-P refer to C–O bond breaking occurring *trans* to N and *trans* to P, respectively. Here, we assume free equilibration between the isomers of **5**. Therefore, we consider the apparent barrier height to be that of the lowest energy transition state from the lowest energy isomer (***t*-N)-5**.

From the corresponding olefin-bound Pd precursors (**5**), we found a barrier height of 12.6 [11.2] kcal/mol for (***t*-P)-TS4**. Interestingly, considerably lower energy pathways were obtained for displacements *trans* to nitrogen, with a barrier of 6.4 [4.8] kcal/mol for (***t*-N)-TS4**. A similar energetic preference for displacement *trans* to nitrogen is observed across several DFT methods. Oxidative addition via these mechanisms leads directly to ion pair **4**. Additionally, as anticipated by experiment, the energy of *endo* and *exo* isomers of **4** were found to be nearly identical, with the *exo*-isomer favored by 0.3 [0.4] kcal/mol. Henceforth, reference to **TS4** will specifically refer to the lowest energy isomer, (***t*-N)-TS4**.

In summary, of the oxidative addition pathways considered, olefin binding, followed by *anti* displacement (**TS4**) affords the lowest barrier height by a considerable margin. The displacement is stereospecific to inversion of chirality with respect to that of the leaving group, whereas the pathways involving a three-centered transition state (**TS1**),

a seven-membered pericyclic transition state (**TS2**), or a *syn* conjugate displacement (**TS3**) would be anticipated to retain the configuration of the carboxylate leaving group (when substitution is present on the allyl terminus). We emphasize that consideration of each mechanistic pathway is crucial in order to reliably interpret net inversion/retention of stereochemistry as a general mechanistic probe in the Tsuji–Trost reaction.[32]

Furthermore, the two lowest energy pathways (direct/*anti* and conjugate/*syn* displacement) directly afford ion pair **4** rather than **3** as the product of oxidative addition. These results suggest that the observed η^1–allyl catalyst resting state (**3**) is *not* the direct product of oxidative addition but is generated through a subsequent equilibration from ion pair **4**. Curious as to the magnitude of the difference in energy between η^1–allyl **3** and ion pair **4**, we compared the calculated free energies of the two isomeric complexes. In accord with experiment, $[(PHOX)Pd(\eta^1–allyl)(RCO_2)]$ (**3**) is computed to be favored over the $[(PHOX)Pd(\eta^3–allyl)]^+(RCO_2^-)$ ion pair (**4**) by 5.4 kcal/mol (Figure 1.4). Single point calculations with several other density functionals give rise to similar results ($\Delta G = 4.6$ to 9.3 kcal/mol), showing that this outcome is not an artifact of the DFT functional. In agreement with the DFT values, a difference in free energy of 5.2 kcal/mol favoring **3** over **4** is obtained at the DLPNO-CCSD(T) level of theory and is taken to be our reference value.

Interestingly, this trend appears not to be due to an extraneous effect of the β-ketocarboxylate leaving group, but rather a general feature of the Pd(PHOX) system with allyl acetates. Control experiments have been previously reported by our group in which the allyl β-ketoester was replaced with allyl acetate to similar effect.[5] The corresponding

[(PHOX)Pd(η^1–allyl)(OAc)] complex (**6**) was isolated and characterized by X-ray crystallography and solution-phase NMR spectroscopy. Accordingly, the difference in free energies between **6** and ion pair **7** was calculated to be 6.6 [6.0] kcal/mol, favoring the η^1–allyl form (Figure 1.4).

Figure 1.4. *Relative free energies of constitutional isomers of η^1– and η^3–allyl Pd complexes from masked enolate synthons, and acetate for comparison.*[a]
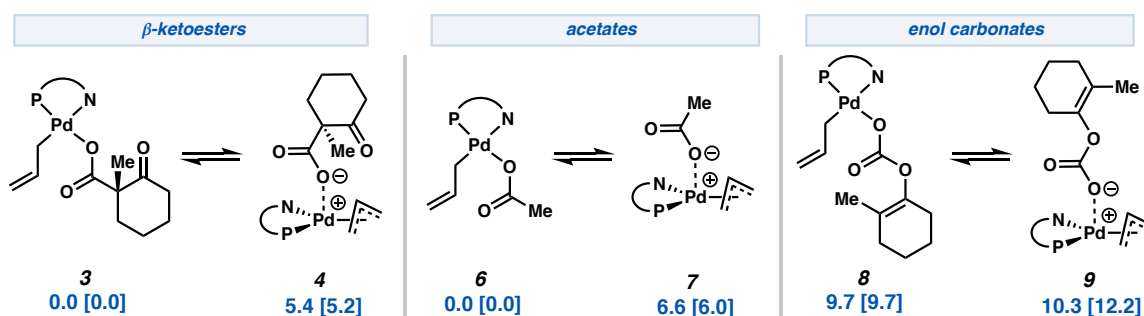
[a] Relative Gibbs free energies in kcal/mol (M06). Free energies derived from DLPNO-CCSD(T) calculations in brackets.

We then sought to explore these trends for the allyl enol carbonate substrate class,[2b] for which a crystal structure of the catalyst resting state has yet to be obtained. As with the β-ketocarboxylates, the corresponding η^1–allyl carbonate complex (**8**) was predicted to be favored over the η^3–allyl carbonate ion pair (**9**) (Figure 1.4). Calculations with the M06 density functional predict a 0.6 kcal/mol preference for the η^1-allyl form, while DLPNO-CCSD(T) theory refines the energy difference to 2.5 kcal/mol, still favoring the η^1–allyl form. Accordingly, ^{31}P NMR studies suggest the catalyst resting state may be an analogous η^1–allyl complex.[5] Taking experimental and theoretical results into account, we anticipate

that the η^1–allyl form similarly dominates the solution phase character of the catalyst resting state.

Complexes **3**, **4**, **8**, and **9**, are constitutional isomers. Since the subsequent reaction yields identical Pd enolate intermediates, we note that the enol carbonate substrate is predicted to undergo a more exergonic reaction than the β-ketocarboxylate isomer by *ca.* 10 kcal/mol. While investigation into the mechanism of decarboxylation of the enol carbonates **8/9** lies outside the scope of this investigation, we postulate the following: If the resting state of the catalyst in the enol carbonate system is described by **8/9** (analogous to the carboxylates), and if the absolute energy of the barrier to decarboxylation is similar to that of **3**, then a significantly higher reaction rate is anticipated. We therefore wish to highlight the design of the enolate synthon as one avenue by which future improvements to the reaction rate may be achieved.

1.3.2 DECARBOXYLATION

We then sought to explore the mechanism through which decarboxylation occurs. Loss of CO_2 was experimentally determined to be the rate-limiting step of catalyst turnover.[4] Deriving inspiration from the canonical decarboxylation of β-ketocarboxylic acids, we explored analogous cases for a Pd^{II} β-ketocarboxylate (Figure 1.5). Two isomeric square pyramidal transition states may be envisioned: one in which the carboxylate group is apically bound to Pd (**TS5**), and another with an equatorially bound carboxylate (**TS6**). Alternatively, decarboxylation could occur through a Zwitterionic square planar complex wherein the ketone of the β-ketocarboxylate is coordinated to η^1–allyl Pd (**TS14**) or the

analogous η^1–allyl case (**TS15**). As noted previously, the minimum energy pathway through oxidative addition directly affords ion pair **4**, rather than the catalyst resting state **3**. To explore the interconnectivity between these intermediates, as well as our postulated decarboxylative pathways, we constructed the free energy network depicted in Scheme 1.1. Beginning from the product of oxidative addition, ion pair **4**, the catalyst resting state (**3**) can be reached via square pyramidal intermediate **11** (a higher energy conformer of **3**) with an overall effective barrier of 4.3 [5.0] kcal/mol and ΔG of –5.4 [–5.2] kcal/mol (Scheme 1.1).

Figure 1.5. *(A) Experimentally-derived parameters for decarboxylation. (B) Decarboxylation pathways considered.*

A. Experimental rate and corresponding barrier for rate-limiting decarboxylation.
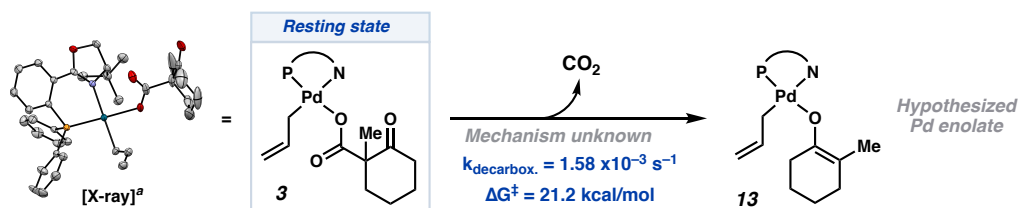
B. Possible decarboxylation mechanisms.
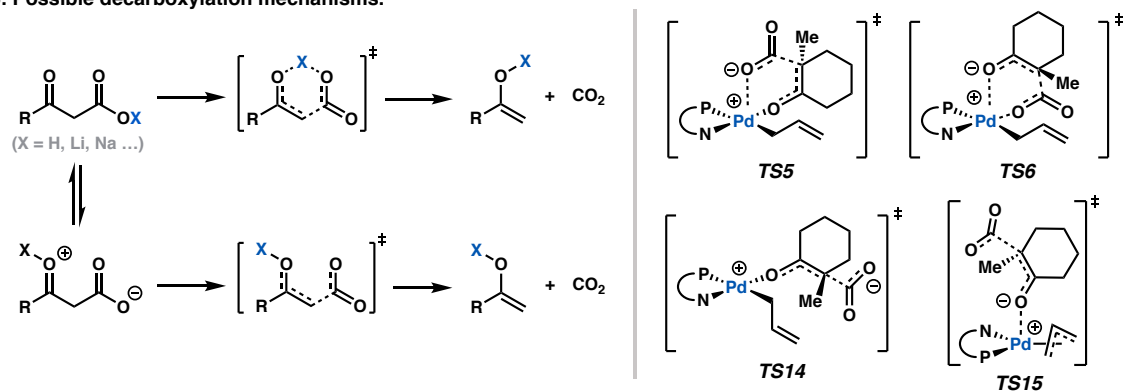
Scheme 1.1. *Free energy network from resting state **3** to decarboxylation pathways.[a]*
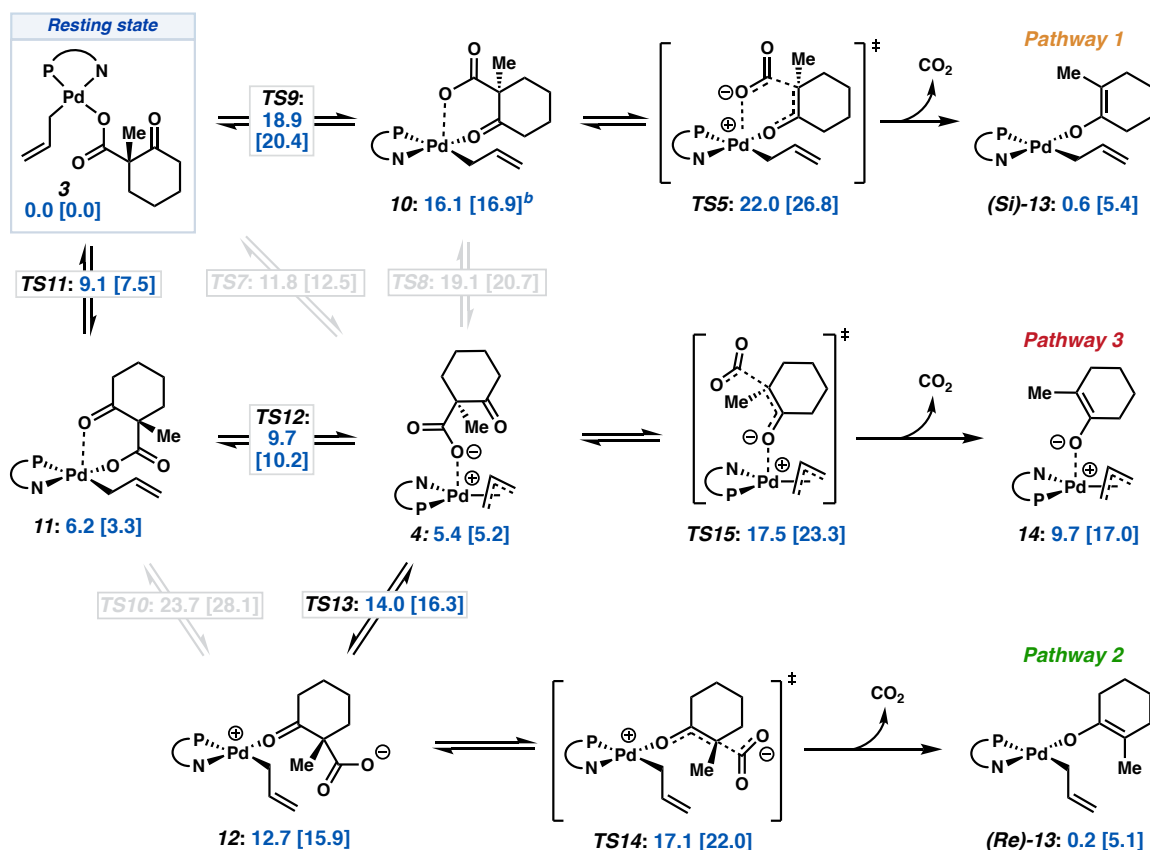
[a] Free energies in kcal/mol (M06) with energies derived from DLPNO-CCSD(T) calculations in brackets. Minimum energy pathways through decarboxylation colored with higher energy alternatives in grey. Lowest energy conformers depicted.

We then turned our attention to decarboxylation. Transition states **TS5** and **TS6** require the square pyramidal precursors **10** and **11**, respectively (Scheme 1.1). Sufficiently low energy pathways connecting the resting state (**3**) to **10** and **11** are found. Decarboxylation is observed only through transition states in which the carboxylate group is poised axially on the six-membered ring, whether it be in a boat (**(boat)-TS5**) or chair (**(chair)-TS5**). This may result from the C–CO$_2^-$ σ orbital experiencing enhanced overlap

with the π^* of the ketone when occupying an axial position. While the chair conformers

dominate the equilibrium geometries of **10**, both M06 and DLPNO-CCSD(T) methods

predict decarboxylation through **(boat)-TS5** to be lower in energy than **(chair)-TS5** by 1.8

and 2.8 kcal/mol, respectively. An apparent $\Delta G^{\ddagger}$ value of 22.0 [26.8] kcal/mol is calculated

from resting state **3** to **TS5**. We will henceforth refer to this sequence as *decarboxylative*

pathway 1.

While the barrier to decarboxylation via **TS5** is quite low with respect to **10** (5.9

[9.9] kcal/mol), decarboxylation directly from **11** (via **TS6**) is not observed. This result is

not unexpected, since weak axial binding is generally observed in square planar d^8

complexes (in the absence of π back bonding) by virtue of the filled, axially-oriented metal-

based $d(z^2)$ orbital, here of slight Pd–O σ^* character. Considering the role of the Pd^{II} center

as a Lewis acid in promoting the decarboxylation, the weak axial binding of the ketone

carbonyl in **11** to the metal center results in a complex that is poorly predisposed to

decarboxylation. Furthermore, the LUMO of the square planar/square pyramidal d^8

complexes are largely of metal-based $d(x^2-y^2)$ character. As such, compared to **11**, the

equatorially-bound carbonyl of **10** exhibits greater overlap with the Pd-based LUMO,

allowing for more effective charge transfer to the electropositive metal center. This,

combined with the greater positive partial charge of the Pd center in **10** due to the weakly

bound axial carboxylate counterion, results in facile decarboxylation.

Analogous to the highly charge-separated cyclic form of **10**, we were intrigued to

find an acyclic variant, **12**, as a stable intermediate on the potential energy surface.

Calculations reveal **12** equilibrates with resting state **3** via **TS11–11–TS12–4–TS13** (Scheme 1.1). The highest barrier is that of **TS13** at 14.0 [16.3] kcal/mol, with **12** at 12.7 [15.9] kcal/mol higher in energy than **3**. As with **10**, decarboxylation from **12** may then occur with the carboxylate oriented axially in either a chair or boat conformer, with the chair being lowest in energy (**TS14**). From **12**, a barrier height of 4.4 [6.1] kcal/mol through **TS14** is found. With respect to resting state **3**, the overall barrier to decarboxylation through this pathway is 17.1 [22.0] kcal/mol. As with **TS5**, decarboxylation through this route directly affords the η^1–allyl O–bound Pd enolate (***Re*)-13** (a rotamer of (***Si*)-13**). We will henceforth denote this sequence as *decarboxylative pathway 2.*

We next envisioned the possibility for decarboxylation to occur directly from the $[\eta^3$–(allyl)Pd(PHOX)$]^+$(RCO$_2^-$) ion pair, **4**. We will term this sequence *decarboxylative pathway 3*. In pathway 3, the overall barrier height through decarboxylation was found to be 17.5 [23.2] kcal/mol via the lowest energy conformer of **TS15**. Dissimilar to pathways 1 and 2, pathway 3 does not lead directly to (***Re/Si*)-13** but rather the η^3–allyl isomer **14**. The relevance of this detail becomes apparent below in the free energy networks through which C–C bond forming occurs (Scheme 1.3).

Loss of CO_2 is the overall rate determining step for pathways 1, 2, and 3. Of the three, we found pathway 2 to have the lowest barrier at 17.1 [22.0] kcal/mol; however, pathway 3 is comparable in energy, with a barrier height of 17.5 [23.2] kcal/mol, and the difference between these pathways is likely within the accuracy of DFT. Single point calculations with B3LYP-D3, PBE0-D3 and DSD-BLYP-D3 favor **TS14** by 5.0, 2.0, and

0.4 kcal/mol, respectively. Moreover, DLPNO-CCSD(T) calculations favor **TS14** by 1.2 kcal/mol. Thus, we suggest an energetic preference for pathway 2. However, both pathways 2 and 3 remain mechanistically relevant under the reaction conditions.

As previously mentioned, NMR experiments determined the rate constant of decarboxylation of isolated **3** to be 1.58 $\times 10^{-3}$ s^{-1} at 24 ºC, corresponding to $\Delta G^{\ddagger}$ of 21.2 kcal/mol, which is consistent with the observed reaction time of a few hours. This experimental data affords an opportunity to compare the computational methods utilized in this study. Interestingly, all density functionals employed predict lower barriers than that of experiment. The most accurate values are obtained with the global hybrid PBE0-D3 and the spin-component-scaled double-hybrid DSD-BLYP-D3, with calculated barriers of 20.2 kcal/mol and 18.6 kcal/mol, respectively. The popular B3LYP-D3 density functional affords the least accurate $\Delta G^{\ddagger}$ of 16.5 kcal/mol. With a barrier of 17.1 kcal/mol, M06 also overestimates the rate of decarboxylation. High-quality coupled-cluster calculations with DLPNO-CCSD(T) provide an accurate barrier height of 22.0 kcal/mol, within 1.0 kcal/mol of experiment. Employing "TightPNO" cutoff criteria refines this value to 21.9 kcal/mol.

Since the dipole moment of **TS15** (19.7 D) is large compared to that of **TS5** (12.2 D) and **TS14** (13.6 D) (with M06/CPCM(THF)) we investigated the effect of solvation on the relative free energy barriers of the three pathways. Experimentally, high yields and enantioselectivities are observed across a variety of non-polar aprotic solvents, while yields and enantioselectivities diminish in polar, aprotic solvents.[4]

Figure 1.6. *Structures of rate-limiting transition states for decarboxylation pathways*

1–3 and apparent barriers as a qualitative function of solvation.[a]

		toluene ($\varepsilon = 2.4$)	Et$_2$O ($\varepsilon = 4.3$)	THF ($\varepsilon = 7.3$)	DMF ($\varepsilon = 38.2$)
TS14	*Pathway 2*	15.4	16.5	17.1	17.9
TS15	*Pathway 3*	19.6	18.3	17.5	16.6
TS5	*Pathway 1*	21.9	22.0	22.0	22.0
TS16		–	–	20.3[b]	–
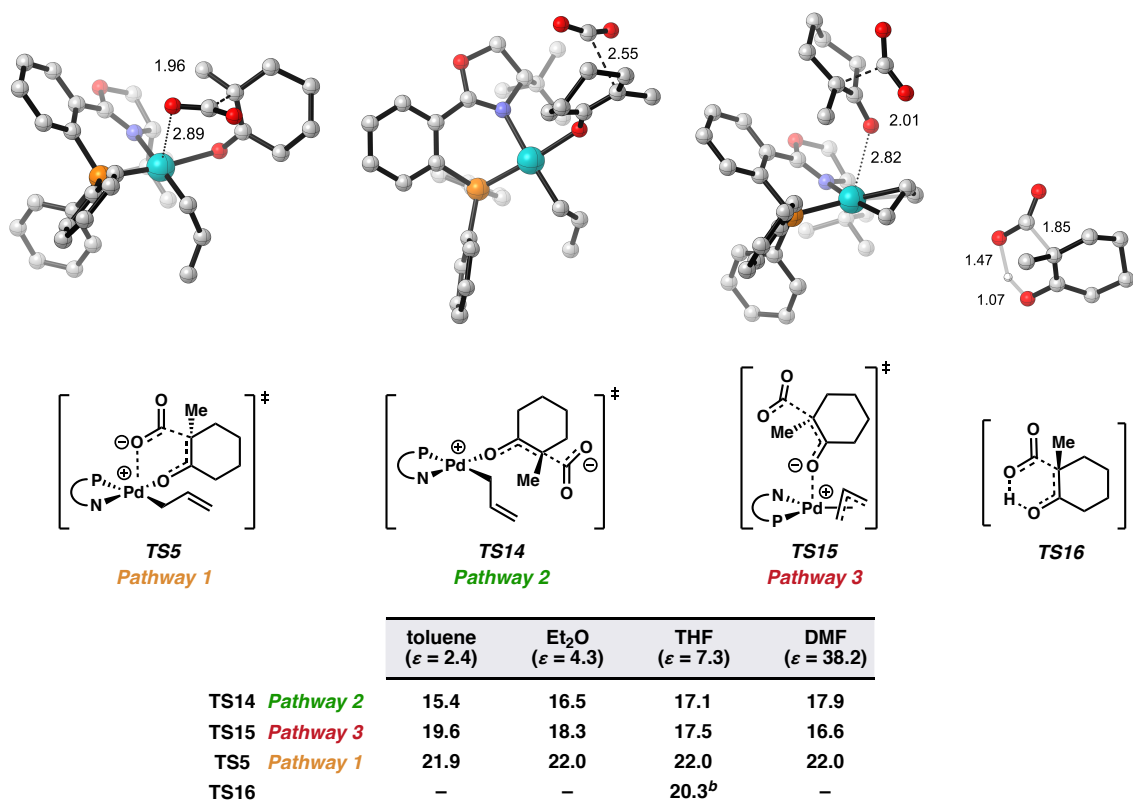
[a] Apparent barriers to decarboxylation ($\Delta G^{\ddagger}$ from **3**). Free energies reported in kcal/mol, calculated

with M06/def2-TZVP/CPCM(*solvent*) on gas phase geometries. [b] With respect to the corresponding

β-ketoacid (**16-H**).

Our initial efforts to assess solvent dependence focused on solvent effects from

single point calculations using the implicit Conductor-like Polarizable Continuum Model

(CPCM) for geometries optimized in the gas phase. As stated above, we found net barrier

heights of 17.1, 17.5, and 22.0 kcal/mol in THF ($\varepsilon = 7.3$) for decarboxylation pathways 2,

3, and 1, respectively. Control computation experiments were carried out in which

optimizations of select intermediates were additionally carried out in THF (see 1.5 Supporting Information), yielding similar results but with an even greater preference for pathway 2.

In addition to THF ($\varepsilon = 7.3$), we compared the barrier heights of the three decarboxylative pathways in the less polar solvents toluene ($\varepsilon = 2.4$) and diethyl ether ($\varepsilon = 4.3$), along with the more polar DMF ($\varepsilon = 38.3$). A clear trend arises in which a continuum with a reduced charge permittivity ($\varepsilon < 8$) favors pathway 2 (**TS14**), while pathway 3 (**TS15**) is preferred in solvents with higher dielectric constants ($\varepsilon > 8$) (Figure 1.6).

Specifically, **TS14** is 4.2 kcal/mol lower in energy than **TS15** in toluene, compared to a $\Delta\Delta G^{\ddagger}$ of 1.8 and 0.4 kcal/mol (favoring **TS14**) in Et$_2$O and THF, respectively. In DMF, pathway 3 is predicted to be most favorable, with **TS15** 1.3 kcal/mol lower in energy than **TS14**. Furthermore, we found these trends to be a result of the simultaneous lowering of the barrier of **TS14** and raising that of **TS15** with decreasing solvent polarity. For example, $\Delta G^{\ddagger}$ of decarboxylation through **TS14** with M06/def2-TZVP/CPCM(toluene) was found to be 15.4 kcal/mol, compared to 17.1 kcal/mol in THF. Meanwhile, the barrier height to **TS15** is 19.6 kcal/mol in toluene, compared to 17.5 kcal/mol in THF. In conclusion, less polar solvents afford greater selectivity for pathway 2 while lowering the overall barrier height to decarboxylation through this pathway.

Since the polarizable continuum implicit solvation model considers electrostatics as the sole component of solute-solvent interaction, it may be inadequate to *quantitatively* capture all effects in the experimental solvent variations – particularly when comparing

solutes with very different cavities. We expect the general trends to remain qualitatively consistent with these findings, and thus, valuable for considerations in future reaction development. Recently, a new CPCM model was developed and implemented in ORCA (versions 5 and above) that employs a polarization charge density made of spherical Gaussians, rather than point charges, spread over the surface of the solute cavity resulting in a smoother potential. For future investigations, we recommend the use of this improved Gaussian charge scheme (GCS) for geometry optimization and single-point energy evaluation.

As racemic allyl β-ketoester **1** is employed in the stereoablative transformation, we carried out an analogous investigation from the other diastereomer of **3**, derived for the **(R)-1**. A qualitatively similar situation is encountered (see 1.5 Supporting Information).

Previous mechanistic studies found both the reaction yield and product enantioenrichment to be tolerant of super-stoichiometric equivalencies of water.[5] This result formed the basis of evidence for an inner-sphere mechanism. Additionally, crossover experiments with deuterium labeling of both the allyl fragment and enolate were performed. Since nearly equal quantities of the crossed products were observed, the involvement of an outer-sphere mechanism in which a solvated free enolate is indifferent to attacking either the labeled or unlabeled η^3–allyl complexes may be considered but is inconsistent with the water-stability of the system. These results may also be accommodated within the inner-sphere mechanistic hypothesis as well when considering the carboxylate/carbonate intermediates are sufficiently stable to undergo exchange prior to decarboxylation.

Scheme 1.2. *Relative energy of select η^1– and η^3–allyl intermediates.[a]*
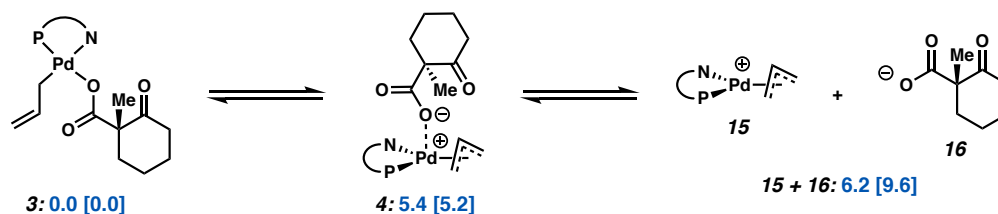
3: 0.0 [0.0]   **4: 5.4 [5.2]**   **15**   **16**   **15 + 16: 6.2 [9.6]**

[a] Relative Gibbs free energies in kcal/mol (M06). Free energies derived from DLPNO-CCSD(T) calculations in brackets.

For the β-ketocarboxylate intermediate, this mechanism appears to take place. Comparing the difference in free energy between ion pair **4** and solvent separated ions **15** and **16**, it is reasonable that free exchange between the carboxylate anion and Pd cation may occur at a rate superseding that of decarboxylation (Scheme 1.2). Both inner and outer-sphere mechanisms may thus accommodate the results of the crossover experiments. Therefore, under these conditions, the observation of enolate/allyl electrophile crossover is irrelevant to differentiation between the two mechanistic pathways.

With regard to water tolerance, we compared the barrier heights to decarboxylation for the conjugate acid of β-ketocarboxylate **16** (**16-H**) via the canonical six-membered cyclic transition state to those of the Pd-catalyzed pathways mentioned above. With $\Delta G^{\ddagger} =$ 20.3 [26.1] kcal/mol for **TS16**, the lowest apparent barriers to decarboxylation remain those involving the Pd catalyst (pathways 2 and 3). Furthermore, the lower pKa of **16-H** compared to water (*ca.* 10 units) affords a low effective concentration **16-H**, and thus, a substantially slower reaction than would be indicated from the relative $\Delta G^{\ddagger}$ from **16-H** is expected. This offers an explanation as to why, in the Pd(PHOX)-catalyzed systems, the

decarboxylated but non-alkylated starting material is not observed. Hence, the experimentally observed water tolerance is well explained for this system.

1.3.3   C–C BOND FORMATION VIA REDUCTIVE ELIMINATION

Given post-decarboxylation Pd enolate intermediates **14**, **(*Re*)-13**, and **(*Si*)-13**, we then sought to explore possible mechanisms for $C(sp^3)$–$C(sp^3)$ bond formation. We further exploit this opportunity to revise and expand upon previous investigations in this area.[10]

Figure 1.7. *Inner-sphere C–C bond forming transition states considered.*

TS17   TS18 (not observed)   TS19   TS20
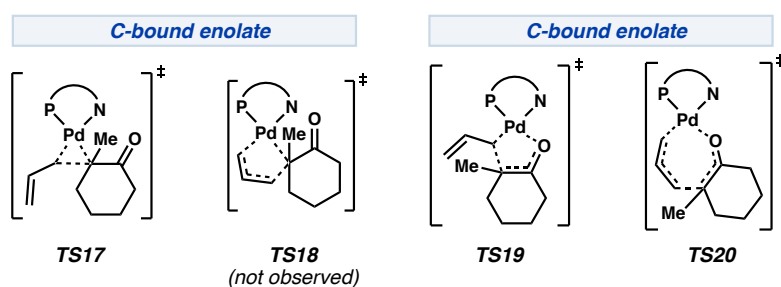
First, inner-sphere mechanisms are considered. We envisioned four unique classes of transition states through which reductive elimination may occur: (1) a three-membered ring transition state from a C–bound Pd enolate (**TS17**), (2) a five-membered cyclic transition state from a C–bound Pd enolate in which the carbon atom of the Pd enolate migrates to the distal carbon of the η^1-allyl fragment (**TS18**), (3) a five-membered ring transition state from an O–bound Pd enolate in which the carbon atom of the enolate bonds with the proximal carbon of the η^1-allyl fragment (**TS19**), and (4) a seven-membered cyclic transition state (**TS20**)[33] (Figure 1.7). Previous investigation suggests the isomerization between oxygen and carbon-bound Pd enolates to be facile.[10] Thus, we initially focused on evaluating the barrier to the $C(sp^3)$–$C(sp^3)$ bond forming event.

Consistent with previous observations,[10] three-centered transition state **TS17** was calculated to be intractably high in energy, with an apparent barrier of 33.7 [46.4] kcal/mol. To determine whether a lower energy transition state could be found by expanding the ring size, we considered the vinylogous case of the 5-centered transition state (**TS18**). However, the planarity of the allyl fragment in the transition state mandates a still highly strained five-membered ring. Despite our best efforts, a transition state fitting this connectivity was never found on the PES, and any transformation similar would likely be intractably high in energy. Next, we turn our attention to an alternative five-membered cyclic transition state, **TS19**. Beginning from O–bound Pd enolate **13**, the barrier to **TS19** is found to be 32.6 [46.3] kcal/mol, and thus, likely not responsible for C–C bond formation.

Lastly, we considered the fully expanded seven-membered cyclic transition state, **TS20**. Here, the seven-membered ring may adopt either a boat or chair conformer for both *Re* and *Si* faces of the enolate. Additionally, the six-membered ring of the cyclohexanone enolate fragment may adopt two unique half chair conformers, giving rise to eight total transition states to be considered (Figure 1.8). Here, bond formation from the *Re* and *Si* faces afford the *S* and *R* enantiomer of product, respectively. The prefixes *chair*/*boat* refer to the conformation of the seven-membered ring, and *axial*/*equatorial* denote the half chair geometry of the cyclic enolate (Figure 1.8A).

Figure 1.8. *(A) Reductive elimination from axial versus equatorial Pd enolate half-chairs. (B) Lowest energy chair and boat conformers for each diastereomeric seven-centered C–C bond forming transition state.[a]*

A. Axial versus equatorial attack from Pd enolate half-chairs.

Axial attack (favored)   *Equatorial attack (disfavored)*

B. Four lowest energy (axial attack) transition states.
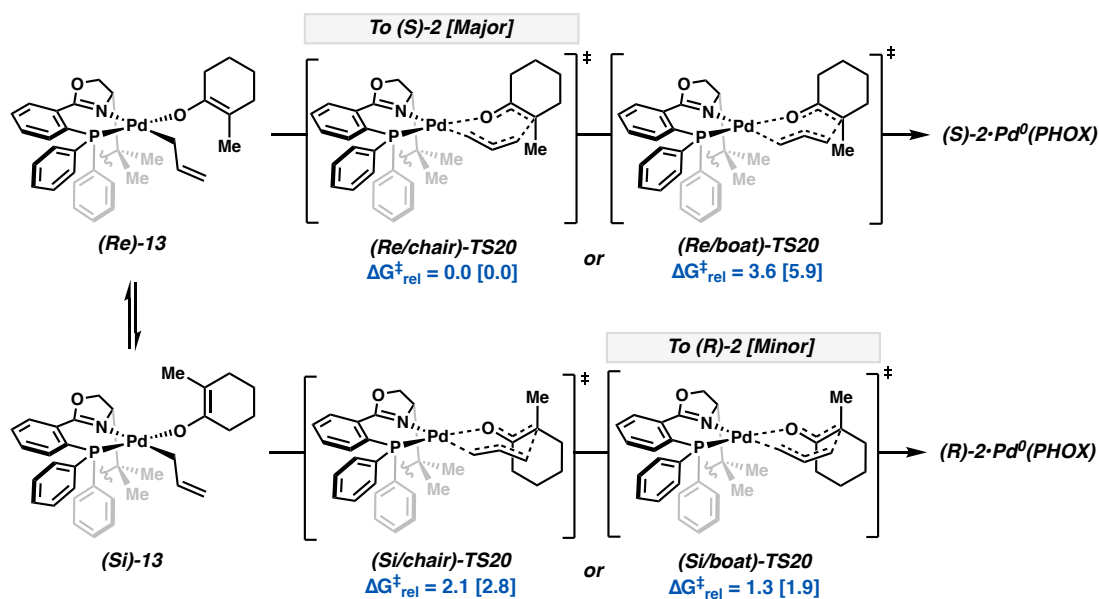
[a] Relative free energies given in kcal/mol from final electronic energies at the M06/def2-TZVP/CPCM(THF) level of theory with DLPNO-CCSD(T) values in brackets. For **(Si/boat)-TS20**, the DLPNO-CCSD(T) value was refined with TightPNO settings.

Transition states that feature *equatorial* attack of the allyl fragment by the enolate half chair are all higher in energy than their *axial* counterparts by 0.4 to 1.5 kcal/mol. Henceforth, in our discussion the *axial/equatorial* suffix will be omitted with all references

being to the favorable *axial* transition states. In comparison with the previously mentioned inner-sphere transition states, all eight of the seven-membered cyclic transition states (**TS20**) offer substantially lower barriers to C–C bond formation, with $\Delta G^\ddagger$ ranging from 10.8 [18.5] to 15.1 [24.6] kcal/mol.

Figure 1.9. *Structures of the two lowest energy diastereomeric transition states of* **TS20**.[a]
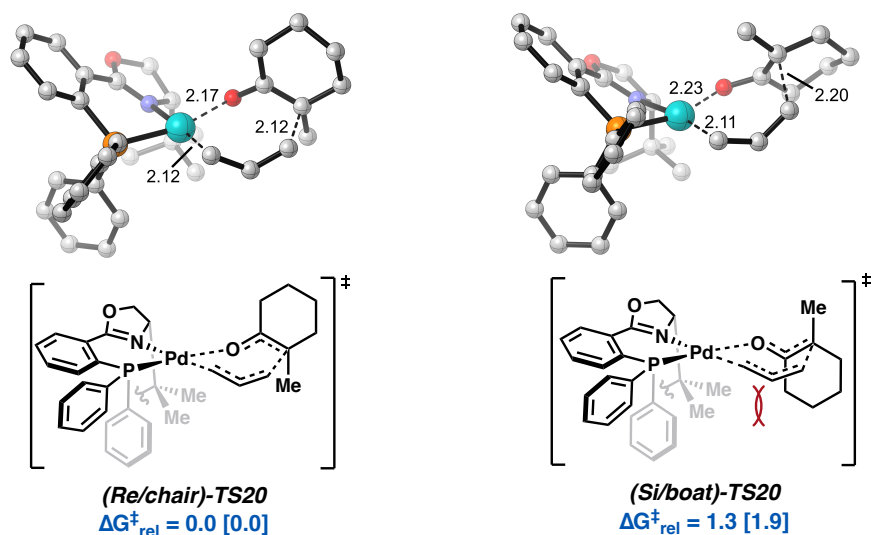
(Re/chair)-TS20
$\Delta G^\ddagger_{rel}$ = 0.0 [0.0]

(Si/boat)-TS20
$\Delta G^\ddagger_{rel}$ = 1.3 [1.9]

[a] Relative free energies given in kcal/mol from final electronic energies at the M06/def2-TZVP/CPCM(THF) level of theory with DLPNO-CCSD(T) values in brackets.

Experimentally, the *(S)-* enantiomer of the *t*-BuPHOX ligand yields *(S)*-2-allyl-2-methylcyclohexan-1-one (**(S)-2**) as the major product with 88% ee. At a reaction temperature of 25 ºC, this corresponds to an effective energetic difference of 1.6 kcal/mol between the enantiodetermining transition states. From O-bound Pd enolate (**Si/Re**)-**13**, we found the lowest energy difference between *Re/Si* diastereomeric transition states to be (**Re/chair**)-**TS20** and (**Si/boat**)-**TS20**, with barrier heights of 10.8 and 12.1 kcal/mol,

respectively ($\Delta\Delta G^{\ddagger} = 1.3$ [1.9] kcal/mol) (Figure 1.8B). This initial result is in good agreement with the experimentally observed enantioselectivities.

Because reliably obtaining relative energies within a sub-kcal/mol error from QM is challenging, we performed a variety of control calculational experiments. Single point calculations on the BP86-D3/LANL2TZ(f)-6-31G(d) optimized geometries were carried out with a suite of 15 density functionals, encompassing several classes of functionals. Electronic energies obtained at the DLPNO-CCSD(T) level of theory (with both NormalPNO and TightPNO settings) were employed for benchmarking. The four lower energy *axial* conformations of **TS20** (Figure 1.8B) were also optimized with a subset of density functionals (with and without empirical dispersion corrections (D3)), followed by single point calculations as previously described (see 1.5 Supporting Information). All results from the control experiments correctly predict **(*Re*/chair)-TS20** to be the overall lowest energy transition sate, with **(*Si*/boat)-TS20** as the lowest energy pathway for the formation of the minor product **(R)-2**. Thus, we propose C–C bond formation via **TS20** to be the enantiodetermining step in the decarboxylative asymmetric allylic alkylation reaction with the Pd(PHOX) catalyst (Figure 1.9).

An investigation of a related system by our groups highlighted internal rearrangements of a Pd enolate as a potential mechanism by which product enantioselectivity is determined.[10b] Although outside the scope of that investigation, the authors noted that a subsequent equilibration between *(Si/Re)* enolates may be facile. Thus, a definite conclusion as to the origin of the enantioinduction was not drawn. Accordingly, we found a facile interconversion between **(*Si*)-13** and **(*Re*)-13**, with a rotational barrier

several kcal/mol lower in energy than that of C–C bond formation (**TS24**) (vide infra, Scheme 1.3). Therefore, the rate of kinetic quenching of intermediates *(Si)*-**13** and *(Re)*-**13** will not be sufficient to preserve any stereochemical induction of previous mechanistic steps. A similar conclusion was posited by McPherson and coworkers.[12]

Upon further examination, it becomes clear that in the case of the favored **(Re)-TS20** geometries, adverse interaction between the α-methyl substituent of the enolate fragment and the *t*-Bu group of the PHOX ligand is minimal compared to the analogous clash between the *t*-Bu group and the carbocyclic backbone of the enolate found in **(Si)-TS20**. The four atoms ligating Pd, along with the two carbon termini of the newly forming σ (C–C) bond, are nearly coplanar (Figure 1.9). In the *Si* transition states, the resulting steric clash between the ligand and substrate leads to a distorted chair/boat transition state as well as deviation from square planarity at the Pd center. We performed a control calculation in which the *t*-Bu group of the PHOX ligand was replaced with a hydrogen atom, followed by subsequent transition state optimization. The optimized *(Si)-des-t*-Bu transition state regained planarity resembling the favored **(Re)-TS20** geometry. These results suggest that the steric interaction from the carbocyclic scaffold and the *t*-Bu group of the PHOX ligand, along with the accompanying distortion from square planarity, is the primary origin of enantioinduction.

Although previous work suggests an inner-sphere mechanism to be prevalent, we do not discount the possibility that a competing outer-sphere mechanism is also present. In fact, with the Pd(PHOX) system, stabilized "soft" enolates generally remain competent in

the reaction, albeit with substantially reduced enantioselectivities.[4] In the canonical Tsuji–

Trost allylic alkylation, differentiation between inner- and outer-sphere pathways is highly

reliant on the nature of the nucleophile,[34] with hard nucleophiles proceeding through inner-

sphere attack and soft nucleophiles via outer-sphere mechanisms. As such, we hypothesize

that the poor enantioselectivities observed with stabilized enolates are likely the result of a

less selective outer-sphere mechanism dominating the C–C bond formation step. In an

effort to continue the development of this methodology to include previously inaccessible

substrate classes, we sought to explore the intricacies of the interplay between outer-sphere

and inner-sphere mechanisms.

From O–bound enolates *(Si)*-**13** and *(Re)*-**13**, an associative displacement of the

enolate by the olefin of the allyl fragment (*(Si/Re)*-**TS21**) directly affords **14** (as two

inconsequential rotamers) (Scheme 1.3). Its noteworthy that **14** is also the product of

decarboxylation through **TS15** (decarboxylative pathway 3) (Scheme 1.1). As expected, in

14, bonding between the axial enolate oxygen and Pd is dominated by electrostatic

attraction. Intermediate **14** presents a Pd–O bond length of 2.72 Å and Löwden bond order

of 0.23, compared to the 2.08 Å Pd–O bond length and bond order of 0.60 as observed in

(Re)-**13**. As such, disassociated ions **15** and **17** are comparable in free energy to **14**. This

was found to be the lowest energy entry into the outer-sphere mechanistic space (Scheme

1.3).

Scheme 1.3. *Various C–C bond forming pathways.[a]*
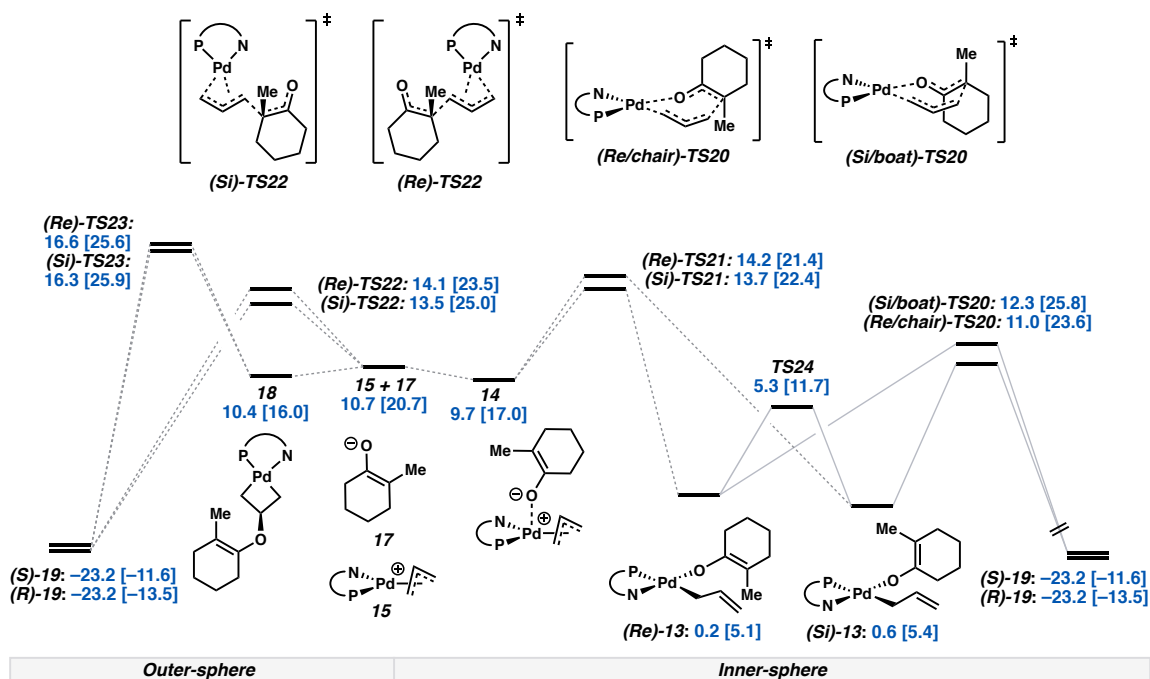
[a] Free energies relative to **3** (in kcal/mol) obtained with M06/def2-TZVP/CPCM(THF), with energies

derived from electronic energies at the DLPNO-CCSD(T)/cc-pVTZ/CPCM(THF) level of theory in

brackets. Lowest energy conformers depicted. $\Delta\Delta G^{\ddagger}$ refined to 1.9 kcal/mol with TightPNO settings.

In considering C–C bond formation through an outer-sphere attack of enolate **17** on

the $[\eta^3–(\text{allyl})\text{Pd}(\text{PHOX})]^+$ complex (**15**), we note that attack may occur either *trans* to N

or P, from the *Si* or *Re* face of the enolate, in both enolate half chairs, and to either *exo-* or

endo-allyl **15**. Based on our previous findings, we considered only the enolate half chair

which gives rise to the favored axial attack. Here, we found six of the eight hypothesized

transition states for this outer-sphere process (**TS22**).

Unlike the inner-sphere transition states **TS20**, which give rise to $\Delta\Delta G^{\ddagger}$ of 1.3 [1.9]

kcal/mol between the lowest energy diastereomeric transition states, the outer-sphere

transition states afford reduced selectivity. From transition states **(*Si*)-TS22** and **(*Re*)-TS22**, a $\Delta\Delta G^{\ddagger}$ of 0.6 [1.4] kcal/mol was calculated. We note that the presence of numerous nearly degenerate rotameric transition states complicated obtaining accurate $\Delta\Delta G^{\ddagger}$ for this pathway.

In addition to reactivity at the π-allyl carbon termini, nucleophilic attack at the central carbon of the allyl fragment to afford palladacyclobutane species is known.[35] Previous experimental and computational studies find the mode of reactivity to be highly dependent on the σ-donating/π-accepting nature of the ancillary ligand and the basicity of the nucleophile. Palladacyclobutane complexes have been proposed as mechanistic intermediates in palladium-mediated cyclopropanation reactions,[36] as well as isolated and characterized by X-ray crystallography.[37]

Of relevance to this work, we considered that **15** and **17** may combine in such a way that the oxygen atom of **17** forms a covalent bond with the β carbon of the allyl fragment to afford metallacyclobutane **18**. The C–C π orbitals of the enolate fragment are in potentially good overlap with the Pd–C σ* of the allyl terminus. Thus, we envisioned intermediate **18** may be a competent precursor to the desired C–C bond formation via **(*Si/*Re)-TS23**. IRC analysis reveals **(*Si/*Re)-TS23** directly connects metallacyclobutane **18** and the complexed ketone product **(*R/S*)-19** on the potential energy surface without the intermittency of ion pair **15+17**. Therefore, **TS23** represents a C–C bond forming pathway unique to that of **TS22**. Complex **18** is well poised for reductive elimination to form **19**.

The apparent barrier to this process (relative to enolate **(*Si*)-13**) is 16.4 [20.5] and 16.1 [20.8] kcal/mol for **(*Si*)-TS23** and **(*Re*)-TS23**, respectively.

From analysis of the free energy network encompassing Pd enolates **(*Si*)-13**, **(*Re*)-13**, and **14**, with the accompanying C–C bond forming pathways, the following conclusions are drawn:

1. Given facile rotation about the Pd–O and C–O σ bonds in Pd enolates **(*Si*)-13** and **(*Re*)-13**, preservation of stereochemical information through differentiation in energy between prior diastereomeric transition states should largely be erased. We found the rotational barrier from **(*Si*)-13** to **(*Re*)-13** to be 5.1 [6.6] kcal/mol (via **TS24**), whereas the minimum energy barrier to C–C bond formation is 10.8 [18.5] kcal/mol. Therefore, the rate of kinetic quenching of intermediates **(*Si*)-13** and **(*Re*)-13** will not be sufficient to preserve any stereochemical induction from previous mechanistic steps. However, this feature of the PES may be substrate specific and more extrapolated scaffolds may experience rotational barriers similar to or greater than that of C–C bond formation.

2. The mechanism through which decarboxylation of the β-ketoester occurs plays an important role in determining the predisposition for C–C bond formation to occur through either an inner or outer-sphere process. As previously mentioned, decarboxylation via **TS5**, **TS14**, and **TS15**, yield Pd enolates **(*Si*)-13**, **(*Re*)-13**, and **14**, respectively. From **(*Re*/*Si*)-13**, direct C–C bond formation through the inner-sphere transition states **(*Re*/chair)-TS20** or **(*Si*/boat)-TS20** represent the lowest energy pathway to the product. From **(*Re*/*Si*)-13**, the apparent barrier height to C–C bond formation via an outer-sphere

mechanism corresponds to the isomerization of **(*Re*/*Si*)-13** to the axially-bound enolate **14** via **(*Re*/*Si*)-TS21**, as **(*Re*/*Si*)-TS21** are found to be higher in energy than the outer-sphere C–C bond forming transition states (**TS22**). Therefore, decarboxylation through **TS5** or **TS14** (pathway 1 or 2) to directly afford **(Re/*Si*)-13** carries a predisposition for inner-sphere C–C bond formation.

Alternatively, decarboxylation via **TS15** (pathways 3) directly leads to apical enolate **14**. When this is the case, C–C bond formation through both inner and outer-sphere processes becomes highly competitive. From **14**, the highest barrier to the outer-sphere mechanism is that of the outer-sphere C–C bond forming event (**TS22**). While the barrier heights for the inner-sphere C–C bond forming transition states are lower in energy than those of the outer-sphere mechanism, the Pd enolate must first undergo an isomerization from apically-bound **14** to square planar complexes **(*Re*/*Si*)-13**. In fact, the barrier heights of these isomerizations (via **(*Re*/*Si*)-TS21**) are comparable to that of the outer-sphere C–C bond formation. Therefore, less preference for the inner over outer-sphere mechanism is expected for the case in which decarboxylation proceeds through **TS15** (pathway 3). Qualitatively similar results are obtained across a variety of density functional methods.

3. We previously discussed the effects of solvation on differentiating between decarboxylative pathways. We find that nonpolar solvents such as toluene impose a large preference for decarboxylation through the less polar **TS14**, while polar solvents result in preference for the more charge-separated **TS15**. Given the similarities in the free energies of the inner- and outer-sphere mechanisms, along with the experimentally observed solvent dependencies described in the literature, an analogous investigation into the solvent effects

Chapter 1 – Mechanism of the Pd-catalyzed Asymmetric Allylic Alkylation: A Comprehensive Quantum Mechanics Investigation

34

on differentiation of the inner- and outer-sphere mechanistic pathways was carried out. For the reasons described above, this investigation is *qualitative* in nature, highlighting the expected reactivity trends.

First, we note the relative free energies between the low energy Pd enolates (***Re/Si***)-**13** and the transition states for their isomerization to **14** are independent of the continuum dielectric constant (Table 1.1). However, the barrier for C–C bond formation via inner-sphere **TS20** demonstrates a dependence on solvent polarity in which less polar solvents afford reduced barrier heights. As anticipated, the generation of solvent separated ions **15** and enolate **17** from **14** becomes increasingly unfavorable with decreasing dielectric constant of the solvent. As the relative free energy of **15** and **17** increases dramatically in nonpolar solvents, the outer-sphere C–C bond formation from the separate ions via **TS22** is anticipated to become less prevalent. In contrast, solvation in a continuum with a high dielectric constant favors the separate ions **15** and **17** over Pd enolate **14**. The barriers to outer-sphere C–C bond formation also decrease, now favoring an outer-sphere mechanism from **14**.

Taken together with the results for solvent effects on decarboxylation, we conclude that in polar solvent, decarboxylation via **TS15** is favored, affording intermediate **14**. From **14**, the minimum energy pathway to C–C bond formation is via a less enantioselective outer-sphere mechanism (**TS22**). Conversely, nonpolar solvents favor loss of CO_2 through **TS14**, yielding enolate (***Si***)-**13**. Reductive elimination via the 7-membered pericyclic transition state **TS20** then ensues. Given the sensitivity of relative barrier heights to changes in solvation, we highlight the need to consider both the mechanism of

decarboxylation and that of the C–C bond forming pathways in determining the inner-sphere or outer-sphere mechanism to be more favorable.

Table 1.1. *Qualitative comparison of relative free energy barrier heights along reductive elimination pathways.[a]*

Intermediate	PhMe	Et$_2$O	THF	DMF
(*Re*)-13	0.6	0.5	0.5	0.4
(*Si*)-13	0.0	0.0	0.0	0.0
14	8.8	9.3	9.5	9.8
15 + 17	33.2	17.5	9.2	-0.5
(*Re*)-TS21	13.5	13.5	13.5	13.6
(*Si*)-TS21	14.1	14.1	14.1	14.1
(*Re*/chair)-TS20	9.5	10.3	10.8	11.5
(*Si*/boat)-TS20	10.9	11.7	12.1	12.7
(endo/*Re*/*t*-P)-TS22	14.9[b]	13.9[b]	13.3	12.6
(exo/*Si*/*t*-N)-TS22	16.0[b]	14.7[b]	13.9	12.9
(endo/*Re*/*t*-P)-TS23	19.8	17.8	16.6	15.1
(endo/*Si*/*t*-P)-TS23	19.1	17.2	16.1	14.8

[a] Relative free energies given in kcal/mol at the M06/def2-TZVP/CPCM(*solvent*) level of theory on geometries obtained in the gas phase. [b] Barrier less than free energy of separated ions **15** and **17.**

1.3.4 COMPLETE CATALYTIC CYCLE

Considering the findings for each step of the decarboxylative allylic alkylation reaction, we now construct a mechanistic picture that unites theoretical and experimental findings (Figure 1.10). First, the π-basic Pd^0(PHOX) precatalyst coordinates to the olefin

of the allyl β-ketoester starting material (**1**), followed by oxidative addition to form the

[Pd(PHOX)(η^3–allyl)]$^+$(RCO$_2^-$) ion pair (**4**). Oxidative addition occurs *trans* to the

nitrogen of the PHOX ligand via direct displacement of the carboxylate leaving group

(**TS4**). Validation of this displacement-type mechanism supports the basis from which

previous claims have been made using inversion/retention of stereochemistry as a probe

for determination of inner versus outer-sphere mechanisms (when substitution on the allyl

terminus is present).[6,32] The mechanism of Bäckvall was found to be unlikely for these

substrates.[31] Furthermore, both enantiomers of the starting material have similar barriers to

oxidative addition. This is in accordance with experimental evidence that a kinetic

resolution of the allyl β-ketoester starting material is generally not observed to great

extent.[38]

Figure 1.10. *Complete catalytic cycle for the inner-sphere allylic alkylation reaction.*
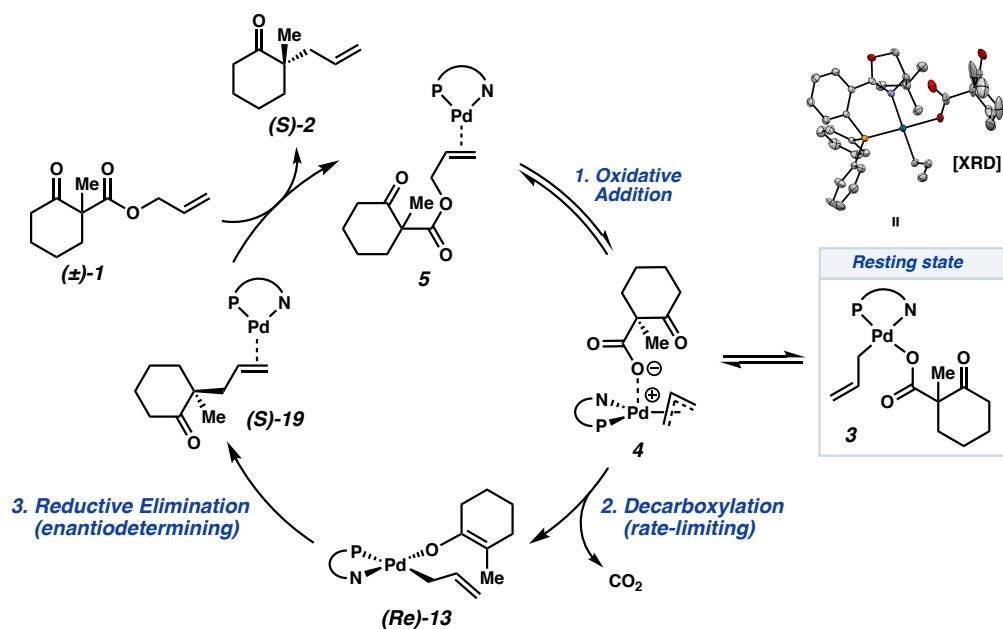
Ion pair **4** readily equilibrates to the more thermodynamically stable [Pd(PHOX)(η^1–allyl)(RCO$_2$)] complex (**3**). Experiment and computation agree in identifying **3** as the resting state of the catalyst. We further extend the analogous comparison to that of the enol carbonate substrate class (**8/9**). Given the equilibration between **3** and **4**, along with the similar relative energies of the separated ions, we conclude that observation of crossover products in deuterium labeling experiments does not necessarily indicate an outer-sphere C–C bond forming mechanism, but rather is still accommodated within the inner-sphere mechanistic hypothesis.[2] That is, charge-separated ion pairs may undergo facile anion exchange to afford the observed cross-products. Additionally, the pK_b of the carboxylate/carbonate anions is such that quenching with water to render an inactive or decomposed species is not anticipated, in accordance with the observed water tolerance experiments.[5]

Subsequent loss of CO$_2$ occurs through one (or more) of three unique decarboxylative transition states, each leading to a different Pd enolate intermediate. Our investigation determines that ion pair **4** (the initial product of oxidative addition) is a common intermediate along the two lowest energy pathways through decarboxylation. Therefore, the catalyst resting state (**3**) is best described as an off-cycle intermediate (Figure 1.11). In agreement with experiment, decarboxylation is determined here to be rate-limiting. Furthermore, the calculated rate of decarboxylation (4.65 x10^{-4} s^{-1}, $\Delta G^{\ddagger}$ = 21.9 kcal/mol) is in excellent agreement with that of experiment (1.58 x10^{-3} s^{-1}; $\Delta G^{\ddagger}$ = 21.2 kcal/mol).[5]

Figure 1.11. *Free energy profile of minimum energy pathway through full catalytic cycle (green) as well as pathway for equilibration to off-cycle resting state* **3** *(orange).*[a]
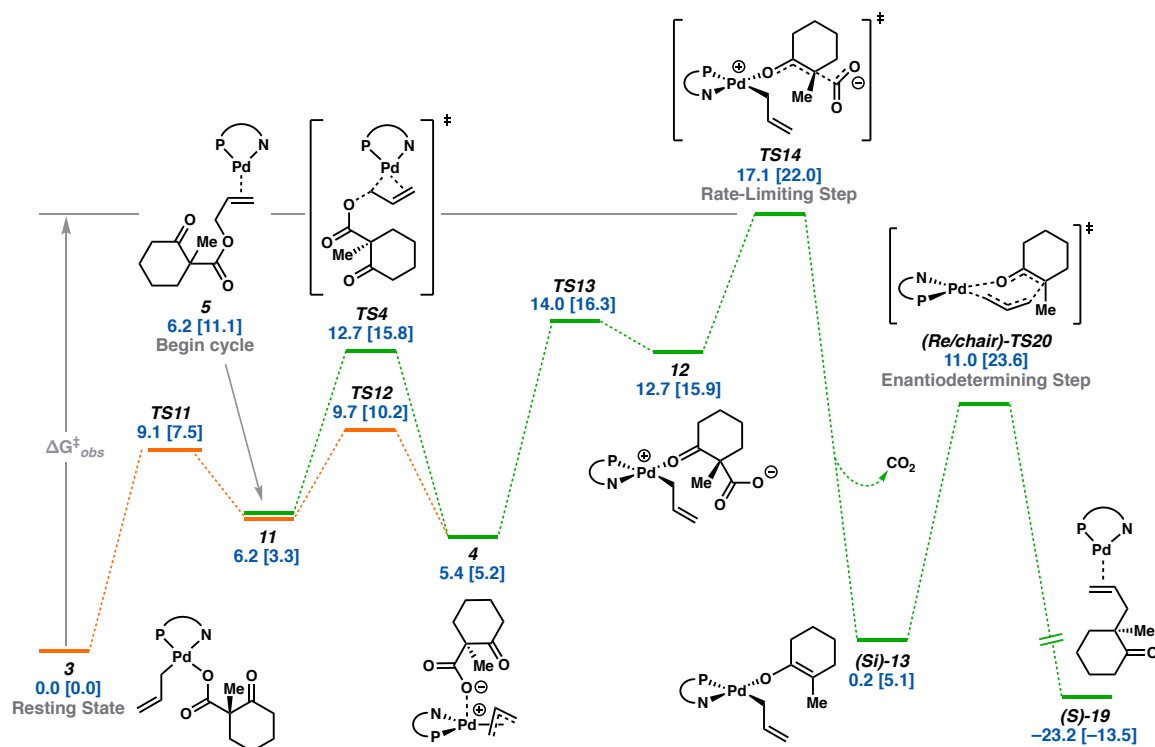
[a] Note that decarboxylation is considered irreversible as CO_2 is lost to reaction headspace/atmosphere.

From the four-coordinate Pd enolates **(Re/Si)-13**, the most facile pathway to C–C bond formation is inner-sphere reductive elimination via a seven-membered pericyclic transition state (**TS20**). We establish that this C–C bond forming event is the enantiodetermining step (Figure 1.8). Calculated enantioselectivities agree with experiment and are assessed across a variety of computational methods.

We investigated the interplay of inner and outer-sphere mechanisms. In particular, we assess effects of solvation on the differentiation of these two processes. The highly enantioselective inner-sphere process is favored in nonpolar solvents, whereas the less selective outer-sphere mechanisms become increasingly relevant in polar solvents. The origin of this solvent dependence is two-fold. In addition to stabilization of charged intermediates encountered in the outer-sphere processes, we find that increasingly polar solvents favor decarboxylation via the formally charge-separated transition state **TS15**, leading directly to the square pyramidal enolate complex **14**. Above, we discuss the implications of this in the context of a more facile entry into the outer-sphere mechanistic space.

1.3.5   EXPERIMENT AND DISCUSSION

We then sought to experimentally evaluate the mechanistic predictions obtained in our computational investigation. In the case of α-methyl allyl enol carbonate **8**, prior research reveals that the reaction rate is increased with the use of the more electron poor *(S)*-(CF$_3$)$_3$-*t*-BuPHOX ligand.[39] While a similar trend for the analogous β-ketoester (**1**) may be anticipated, reaction time course studies reveal that the same rate enhancement is not observed (Figure 1.12). In fact, when the catalyst resting state (**3**), and both low energy transition states responsible for decarboxylation (**TS14** and **TS15**) are re-optimized with the *(S)*-(CF$_3$)$_3$-*t*-BuPHOX ligand, the barrier to decarboxylation is calculated to be 22.2 kcal/mol (DLPNO-CCSD(T), TightPNO) — within error of the 21.9 kcal/mol (DLPNO-CCSD(T), TightPNO) barrier height of the original system. This experiment further

highlights the fidelity of the computational methods employed in this study in describing

the reactivity trends in the catalytic system.

Figure 1.12. *Conversion of **1** to **(S)-2** under standard reaction conditions.*[a]
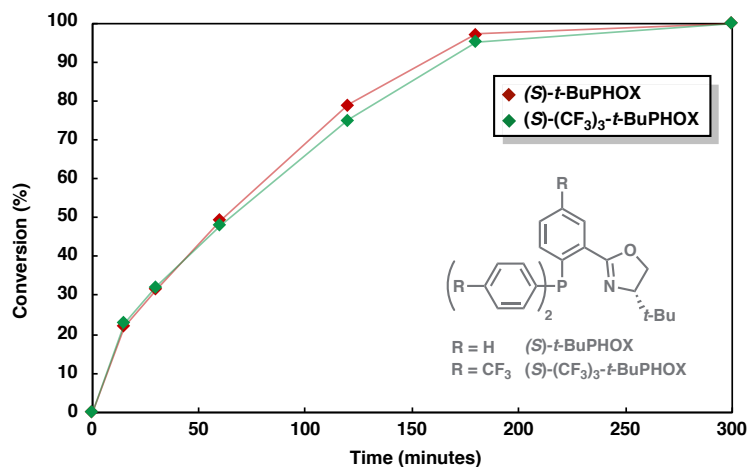
[a] Conversion as determined by GC-FID with respect to tetradecane internal standard.

We prepared α-phenyl allyl β-ketoester substrate **20** to probe the interplay of inner

and outer-sphere processes (Figure 1.13). Compared to α-methylated β-ketoester **1**, the

enolate derived from **20** experiences significant electronic stabilization through

conjugation. As anticipated from the discussion provided above, as well as prior

experimental trends, substrate **20** affords the desired product **(S)-22** in 99% yield, however,

in a modest 23% ee. It is worth noting that the reduction in enantioselectivity is likely not

exclusively a consequence of steric interactions. A variety of sterically encumbered

substrates, which do not provide significant electronic stabilization, such as the analogous

α-*t*-Bu, α-Bn, α-prenyl, etc., compounds afford the corresponding allylic alkylation

products in 82–91% ee.[2,]**Error! Bookmark not defined.** Furthermore, we compute a

$\Delta\Delta G^{\ddagger}$ of 1.3 kcal/mol between the enantiodetermining inner-sphere transition states derived from substrate **20** (corresponding to 80% ee at 25 ºC). These results suggest that an enantioselective inner-sphere pathway persists, however, under the standard reaction conditions, the less selective outer-sphere mechanisms dominate.

Figure 1.13. *Effect of decarboxylation mechanism on downstream enantioselectivity.*[a]
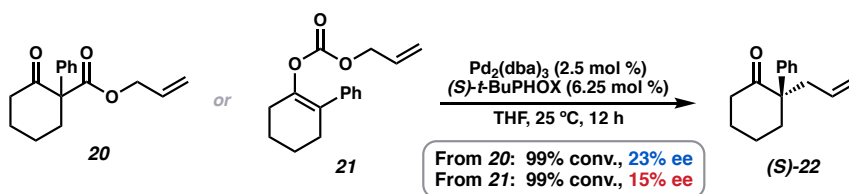
[a] Enantiomeric excess determined by chiral SFC analysis.

In addition to α-phenyl β-ketoester **20**, the corresponding α-phenyl allyl enol carbonate (**21**) was also evaluated in the transformation (Figure 1.13). Interestingly, under identical conditions to those employed with β-ketoester **20**, enol carbonate **21** affords *(S)-***22** in a reduced 15% ee, compared to 23% ee as obtained starting from **20**.[8] After decarboxylation, both **20** and **21** share access to the same network of enolate intermediates (Scheme 1.3). However, by virtue of the differing mechanisms of decarboxylation, the point at which the intermediates derived from each substrate enter the post-decarboxylation mechanistic space is anticipated to vary. As prefaced by our computational investigation, this may lead to altered levels of product enantioenrichment due to the resulting predisposition for C–C bond formation to occur via inner- or outer-sphere mechanisms to varying extent (vida supra). Naturally, differences in enantioselectivities based on enolate

synthon (*i.e.,* β-ketoester versus enol carbonate) are expected to be increasingly pronounced in the case of stabilized enolates (**20/21**), for which an outer-sphere mechanism is readily accessible. These results highlight the importance in considering the effect of the mechanism of decarboxylation and subsequent behavior of enolate intermediates in the overall enantioselectivity of the transformation.

With compound **20** in hand, we then sought to probe the effects of solvation and ligand electronics on observed enantioselectivity (Figure 1.14). As previously mentioned, the enantioselective inner-sphere pathway to C–C bond formation to *(S)*-**22** is expected to be largely outcompeted by less selective outer-sphere mechanisms. Our computational investigations suggest that, for allyl β-ketoesters, inner-sphere mechanisms are favored by: (1) disfavoring the charge-separated intermediates required for an outer-sphere approach, and (2) favoring decarboxylative mechanisms that lead directly to η^1–allyl square planar palladium enolates (*i.e.*, via decarboxylation pathways 1 and 2). Calculations further predicted that this may be accomplished by utilizing nonpolar solvents, as well as through the installation of electron withdrawing groups on the PHOX ligand framework.

Indeed, we observe an increase from 23 to 28% ee simply by implementing toluene ($\varepsilon = 2.4$) in place of THF ($\varepsilon = 7.3$) as the reaction solvent (entries 1–2, Figure 1.14). Utilizing the more electron poor *(S)*-$(CF_3)_3$-*t*-BuPHOX ligand in toluene (entry 3) and a 2:1 methylcyclohexane/toluene solvent mixture ($\varepsilon = 2.1$), enantioselectivity was further enhanced to 32% and 36% ee, respectively (entries 3–4). Given the initial improvements from perturbations of ligand electronics and solvation alone, we suggest in silico high-

throughput screening of ligands with different steric environments as a practical next step

in future developmental efforts.

Figure 1.14. *Effect of solvation and ligand electronics on enantioselectivity.*

Entry	Ligand	Solvent [ε]	ee (%)[a]	Yield 22 (%)[b]	ΔG$_{eq}$[c]
1	(S)-t-BuPHOX	THF [7.4]	23	99	1.8
2	(S)-t-BuPHOX	PhMe [2.4]	28	96	24.0
3	(S)-(CF$_3$)$_3$-t-BuPHOX	PhMe [2.4]	32	90	31.0
4	(S)-(CF$_3$)$_3$-t-BuPHOX	2:1 MeCy/PhMe [2.1]	36	69[d]	35.2

R = H   (S)-t-BuPHOX
R = CF$_3$ (S)-(CF$_3$)$_3$-t-BuPHOX
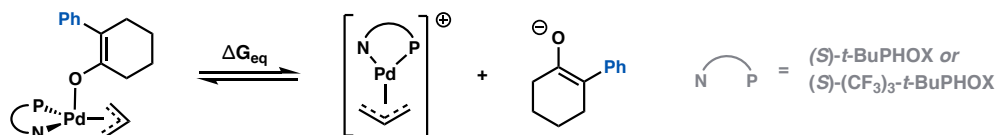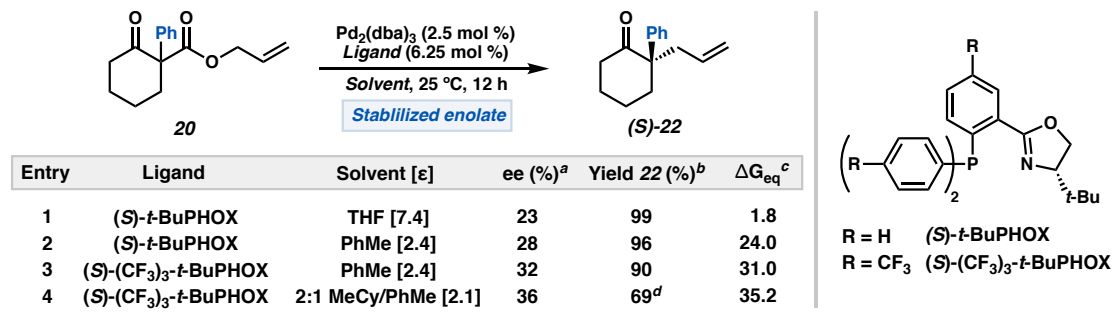
[a] Determined by chiral SFC analysis. [b] Determined by ^{1}H NMR with respect to 1,3,5-trimethoxybenzene as an internal standard. [c] Change in free energy (in kcal/mol, 1 M standard state) from square pyramidal enolate to separated ions. [d] 34% of **20** remaining after 12 hours.

1.4   CONCLUSIONS

We report a detailed quantum mechanics investigation into the three mechanistic

steps (oxidative addition, decarboxylation, and reductive elimination) of the

decarboxylative asymmetric allylic alkylation with the Pd(PHOX) catalyst system.

Experiments were carried out to explore the mechanistic hypotheses derived from the ab

initio calculations.

Beginning with allyl β-ketoester **1**, oxidative addition of Pd^0(PHOX) proceeds

through pre-coordination of the olefin of the allyl fragment of **1** (to give **5**), followed by an

S$_N$2-like electrophilic addition to Pd to yield the [(PHOX)Pd(η^3-allyl)]$^+$(RCO$_2^-$) ion pair

(**4**). Ion pair **4** then rapidly equilibrates to the catalyst resting state, [(PHOX)Pd(η^1-allyl)(RCO$_2$)] (**3**). Complex **3** is best described as an off-cycle intermediate. Given the equilibration between **3** and **4**, along with the similar relative energies of the separated ions, we corroborate that the results from our previously reported cross-over experiments are not necessarily indicative of an outer-sphere mechanism, but still are accommodated within the inner-sphere mechanistic hypothesis.

From the catalyst resting state (**3**), we find three dominant pathways (1, 2, and 3) through which decarboxylation may occur. Each pathway leads to a unique palladium enolate with the ability for subsequent interconversion between the three. However, ensuing analysis of the C–C bond forming potential energy surface reveals that the enolates derived from pathways 1 and 2 are more predisposed to undergo an inner-sphere C–C bond formation via the seven-membered pericyclic transition state, **TS20**. On the other hand, decarboxylation via pathway 3 directly affords square pyramidal enolate **14** which may undergo a more facile dissociation and enter the outer-sphere mechanistic space.

We predict relative barrier heights among the decarboxylative and $C(sp^3)$–$C(sp^3)$ bond forming pathways to be highly solvent dependent. Decreasing solvent polarity favors inner-sphere processes by destabilizing the ionic intermediates of the outer-sphere mechanism, as well as promoting decarboxylation via Pathway 2. Decarboxylation is determined to be rate-limiting in accordance with experiment. Furthermore, the calculated decarboxylation rate constant in THF obtained with DLPNO-CCSD(T) (4.65×10^{-4} s^{-1}; $\Delta G^\ddagger$ = 21.9 kcal/mol) is in excellent agreement with that of experiment (1.58×10^{-3} s^{-1}; $\Delta G^\ddagger$ =

21.2 kcal/mol).[4] In comparison, the DFT methods applied in this study all predict a rate constant 10^3–10^7 times larger in magnitude ($\Delta G^{\ddagger}$ = 12.5–18.9 kcal/mol) than experimentally observed.

We considered several inner-sphere reductive elimination transition states. In accordance with previous research in our group, the seven-membered, doubly-vinylogous transition state (**TS20**)[39] provides the lowest energy pathway to C–C bond formation in nonpolar solvents. We establish that the $C(sp^3)$–$C(sp^3)$ bond forming event is the enantiodetermining step. Calculated $\Delta\Delta G^{\ddagger}$ are in excellent agreement with experimentally observed enantioselectivities and are assessed across a variety of computational methods.[40] A model is proposed for the origin of the enantioinduction.

We also investigated outer-sphere processes, which we found to be competitive in barrier height with the inner-sphere reactions, albeit slightly less favorable. Unlike the inner-sphere transition states, however, severely degraded enantiocontrol is anticipated for outer sphere mechanisms.

Additionally, enolate synthon design is highlighted as an area for future development. Herein, we compare the relative thermodynamics of catalyst resting states derived from different enolate precursors. From this, we suggest that in conjunction with catalyst design, the development of more activated masked enolates may achieve a desirable increase in reaction rate. With a complete mechanistic picture in hand, in silico development may now accompany ensuing experimental efforts.

In order to evaluate the fidelity of the mechanistic hypotheses, a stabilized enolate equivalent (**20**) was employed as a probe for inner and outer-sphere competition.

Experimental results support the computation-based predictions in solvent trends as well as effects of ligand substitution. Furthermore, comparison between **20** and **21** demonstrates the intricacies in the equilibration of the palladium enolate intermediates as described herein. While α-methyl ketone **1** is employed throughout the majority of this study as a "standard" substrate, many of the experimentally observed trends mentioned throughout the text remain consistent amongst more highly decorated heterocyclic scaffolds alike. Thus, the conclusions presented herein are expected to serve as robust first-order approximations to a broad variety of substrate classes.

Density functional theory and localized coupled-cluster theory are employed in this study. We find the DLPNO-CCSD(T) method of Neese *et. al.* highly effective in obtaining accurate barrier heights and thermodynamic relations.[26] Thus, we recommend DLPNO-CCSD(T) for routine use in future quantum mechanics-based investigations in asymmetric catalysis.

These avenues of thought, coupled with the detailed mechanistic hypothesis presented herein, provide a powerful tool in addressing the current limitations and aiding in the future development of the decarboxylative asymmetric allylic alkylation reaction.

1.5   SUPPORTING INFORMATION

1.5.1   GENERAL COMPUTATIONAL DETAILS

Density functional theory calculations

All quantum mechanical calculations were performed with ORCA version 4.1 and 4.2.[13] Unless otherwise noted, geometry optimizations were carried out with the BP86

generalized gradient approximation (GGA) functional[14] [Becke '88 exchange functional paired with the Perdew '86 correlation functional] with Becke–Johnson damped D3 dispersion corrections (henceforth referred to as D3).[15] A mixed basis set was implemented, in which palladium is described by the small core LANL2TZ(f) basis set with the Hay Wadt effective core potential[16] (ECP) [28 core electrons on Pd], and the 6-31G(d) basis set was used on all other atoms. Thermal corrections (at 298 K) were calculated from the unscaled vibrational frequencies at this level of theory. The Quasi-RRHO method was applied to correct for the breakdown of the harmonic oscillator approximation for low frequency vibrations.[24] All stationary points are characterized by the appropriate number of imaginary vibrational modes (zero for optimized geometries and one for transition states). Intrinsic reaction coordinate (IRC) analyses were carried out to ensure all transition states connect the appropriate starting materials and products.

Triple-ζ quality single point calculations were carried out on all stationary points with the BP86-D3, B3LYP-D3,[17] PBE0-D3,[18] M06,[19] and DSD-BLYP-D3[20] functionals with the def2-TZVP basis set[21] on all atoms (with the small core ECP28MWB pseudopotential[22] on Pd). The Conductor-like Polarizable Continuum Model (CPCM)[23] was employed in these single point calculations to include effects of solvation. Thermal corrections obtained at the previous level of theory are then applied to these electronic energies to obtain the reported free energies (G_{298}). Calculated free energy changes are for a 1 M standard state at 25 ºC, apart from decarboxylation where CO_2 is given a standard state of 1 atm.

These methods encompass a range of functional classes, including GGA (BP86-D3), hybrid GGA (B3LYP-D3), non-empirical hybrid GGA (PBE0-D3), hybrid meta-GGA (M06), and spin-component-scaled double hybrid (DSD-BLYP-D3), where effects from dispersion are accounted for either in parameterization or empirically with *ad-hoc* corrections. As the M06 density functional is parameterized to offer a suitable balance between transition metals and main group elements, we report these energies in the text of the manuscript. However, we encourage comparison of these results to those obtained with the other methods. The values obtained from all quantum mechanical calculations are included in the supporting excel file available online (https://pubs.acs.org/doi/10.1021/jacs.0c06243?ref=pdf).

The resolution of identity (RI) and chain-of-spheres[40] (keyword = RIJCOSX) approximations were utilized for coulomb and exchange integrals, respectively, where applicable. Automatic generation of the auxiliary basis sets was employed (keyword = AutoAux).[41] The finest integration grid settings (Grid7, GridX9, NoFinalGrid) were utilized in all calculations.

DLPNO-CCSD(T) Calculations

Additional single point calculations were performed on all optimized structured with the domain based local pair natural orbital coupled-cluster (DLPNO-CCSD(T)) method as described by Neese *et. al.* and as implemented in ORCA.[26] Here, we find the cc-pVTZ basis set (with the corresponding cc-pVTZ/C and def2/J auxiliary basis sets), along with the small core SK-MCDHF-RSC effective core potential[27] on Pd (*i.e.,* the cc-pVTZ-PP main basis set with cc-pVTZ-PP/C and def2/J auxiliary basis sets) with the

"NormalPNO" cutoffs to offer an appropriate balance between cost and accuracy for routine use. As before, the CPCM(THF) was employed to account for effects of solvation. Thermal corrections obtained at the BP86-D3/LANL2TZ(f)–6-31G(d) are applied to the DLPNO-CCSD(T)/cc-pVTZ/CPCM(THF) electronic energies to afford the corresponding free energies. The "TightPNO" settings are employed to further refine correlation energy for comparison of select structures.

Notes:

- Similar results are obtained with the def2-TZVP basis set in control experiments, although we elected to employ Dunning's cc-pVnZ family of basis sets for ease of basis set extrapolation with further calculations should the need arise.

- "NormalPNO": $T_{CutPairs} = 10^{-3}$, $T_{CutDO} = 1 \times 10^{-2}$, $T_{CutPNO} = 3.33 \times 10^{-7}$, $T_{CutMKN} = 10^{-3}$

- "TightPNO": $T_{CutPairs} = 10^{-5}$, $T_{CutDO} = 5 \times 10^{-3}$, $T_{CutPNO} = 1.00 \times 10^{-7}$, $T_{CutMKN} = 10^{-3}$

- "TightPNO" settings may be employed, however, the computational cost increases dramatically. Thus, we have found an efficient approach is to perform routine single point calculations with "NormalPNO" cutoffs, then refine these values for key intermediates with the "TightPNO" settings.

- When CPCM implicit solvation is employed (ORCA 4), the Hartree–Fock reference is optimized self-consistently with respect to the solvent reaction field, but the subsequent optimization of the cluster amplitudes is not. [An alternative is to apply ΔG(solv) from DFT calculations to a gas phase DLPNO-CCSD(T) energy.]

1.5.2   INITIAL BENCHMARKING

We explore density functional and basis set dependence on the geometry optimization of the Pd^{II} resting state complex **3**. These calculated geometries are then compared to that of the recently reported crystallographic structure (CCDC 695531) (Table 1.2).[5] While slight discrepancies between crystallographic and solution phase structure may persist, we utilize this data as a reference point to which we may calibrate our methodology, as well as explore general trends in basis set and functional dependencies.

Table 1.2. *Comparison of geometric parameters obtained from geometry optimization with various functionals and basis sets.[a]*
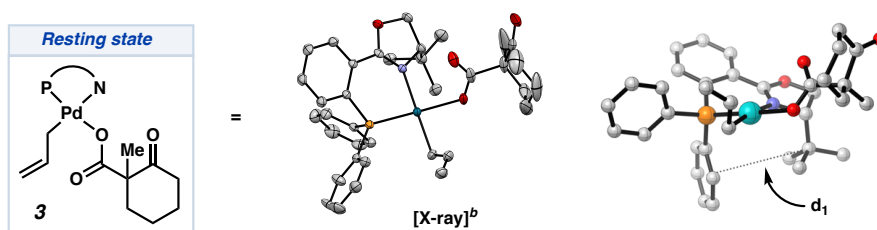
Basis Set	Functional	Pd–P	Pd–N	Pd–O	Pd–C	d_1	MUE[a]	MSE
Crystal XRD		2.189	2.133	2.136	2.055	4.687	-	-
LANL2DZ[Pd]/6-31G(d)	BP86-D3	2.217	2.201	2.159	2.082	4.610	3.65	3.65
LANL2TZ [Pd]/6-31G(d)	BP86-D3	2.213	2.192	2.151	2.082	4.618	3.12	3.12
LANL2TZ(f) [Pd]/6-31G(d)	**BP86-D3**	**2.206**	**2.148**	**2.107**	**2.067**	**4.598**	**1.83**	**0.38**
def2-TZVP [all atoms]	BP86-D3	2.182	2.136	2.111	2.070	4.632	1.25	-0.35
LANL2TZ(f) [Pd]/6-31G(d)	PBE-D3	2.214	2.162	2.117	2.069	4.701	2.17	1.22
LANL2TZ(f) [Pd]/6-31G(d)	TPSS-D3	2.217	2.154	2.101	2.071	4.673	2.50	0.75
LANL2TZ(f) [Pd]/6-31G(d)	BLYP-D3	2.233	2.208	2.152	2.095	4.645	4.38	4.38
LANL2TZ(f) [Pd]/6-31G(d)	B3LYP-D3	2.228	2.209	2.134	2.066	4.683	3.20	3.10
LANL2TZ(f) [Pd]/6-31G(d)	B3PW-D3	2.204	2.145	2.088	2.045	4.586	2.13	-0.78
LANL2TZ(f) [Pd]/6-31G(d)	PBE0-D3	2.211	2.150	2.086	2.040	4.673	2.60	-0.65
LANL2TZ(f) [Pd]/6-31G(d)	TPSSh-D3	2.215	2.153	2.091	2.059	4.653	2.37	0.12
LANL2TZ(f) [Pd]/6-31G(d)	wB97X-D3	2.226	2.179	2.097	2.033	4.612	2.75	-0.80

LANL2DZ [Pd]/6-31G(d)	B3LYP	2.278	2.234	2.133	2.079	5.102	5.43	5.28

[a] Geometric parameters (Pd–X bond lengths, and d_1) given in angstrom (Å). MUE and MSE (excluding d_1) given in pm. Optimization carried out beginning from the known X-ray crystal structure. [b] CCDC 695531 (ref. 5).

From these controls, the following trends are observed:

(1) Greatly reduced errors in Pd–X bond lengths with minimal increase in computational cost are obtained by employing the larger triple-ζ quality basis set with polarization functions, LANL2TZ(f), on Pd in place of the double-ζ (LANL2DZ) basis set.

(2) The use of Becke-Johnson D3 damped dispersion corrections (-D3) in the optimization greatly aids in capturing perturbations of the ligand geometry arising from noncovalent interactions (see d_1).

(3) Density functionals constructed with the Lee–Yang–Parr correlation functional (BLYP, B3LYP) present elongated Pd–X bonds and are among the functionals with the highest MUEs. This trend has been previously described in the literature[19] and has been attributed to the LYP functional underestimating correlation at the uniform electron gas (UEG) limit.[42]

Thus, for geometry optimization we employ the BP86 density functional with Becke–Johnson damped dispersion corrections (BP86-D3), with a mixed basis set comprised of the LANL2TZ(f) basis set on Pd with 6-31G(d) on all other atoms. *We do not recommend the use of the B3LYP/LANL2DZ–6-31G(d) level of theory as is employed in select literature investigations. We believe more suitable geometries may be obtained with D3BJ dispersion*

Chapter 1 – Mechanism of the Pd-catalyzed Asymmetric Allylic Alkylation: A Comprehensive Quantum Mechanics Investigation

52

corrections and triple-ζ basis sets with polarization functions on the metal center. Apart from B3LYP and BLYP, all other functionals evaluated perform comparably well.

1.5.3 DECARBOXYLATION AND CONTROL EXPERIMENTS

In order to obtain accurate barrier heights for the rate determining decarboxylative step, geometry/transition state optimizations were also carried out with CPCM(THF) for comparison to the structures optimized in the gas phase (Table 1.3).

Table 1.3. *Decarboxylation barrier heights with geometries optimized in gas phase and with CPCM(THF).*[a]

Method (for single point calculations)	(boat/ax)-TS5 (gas)	(chair/ax)-TS14 (gas)	(exo/chair/ax)-TS15 (gas)	(boat/ax)-TS5 (THF)	(chair/ax)-TS14 (THF)	(exo/chair/ax)-TS15 (THF)
BP86-D3	16.5	**12.5**	16.4	15.1	**11.5**	21.7
B3LYP-D3	18.4[b]	**16.5**	21.5	19.2	**15.4**	27.7
PBE0-D3	21.0[b]	**18.9**[c]	21.0	23.9	**19.0**	27.8
M06	22.0	**17.1**	17.5	21.8	**15.2**	19.8
DSD-BLYP-D3	20.6[d]	**18.6**	19.0	22.5	**17.1**	24.1
DLPNO-CCSD(T)[e]	26.8	**22.0**	23.2[c]	26.8	**19.8**	28.2

[a] Comparison of barrier heights obtained across a variety of methods with geometries optimized in gas phase and with CPCM(THF). Barrier heights given in kcal/mol from *"Method"*/def2-TZVP–CPCM(THF)//BP86-D3/LANL2TZ(f)–6-31G(d) (with or without CPCM(THF)). [b] **(chair/ax)-TS5**. [c] **(boat/ax)-TS14**. [d] **(exo/boat/ax)-TS15**. [e] Single point with the cc-pVTZ basis set (with SK-MCDHF-RSC pseudopotential on Pd; *i.e.,* cc-pVTZ-PP), "NormalPNO" settings.

For completeness, intermediates derived from the *R* enantiomer of starting material **1** were also investigated (Table 1.4). An analogous result was obtained. *Note: Transition*

state geometries obtained with CPCM(THF) solvation were prone to an additional small imaginary vibrational mode (<5 cm^{-1}) corresponding to a rocking of the ligand backbone. With the point charge CPCM scheme these were unable to be eliminated, however they bear no consequences on the final results.

Table 1.4. *Decarboxylation barrier heights of complexes derived from the (R) enantiomer of* **1**.[a]

Method	*(chair/ax)-TS14_diast2*	*(exo/chair/ax)-TS15_diast2*
BP86-D3	12.3	18.5
B3LYP-D3	16.7	24.8
PBE0-D3	21.0	25.5
M06	17.4	21.5
DSD-BLYP-D3	18.8	23.1
DLPNO-CCSD(T)[b]	21.6	27.7

[a] Barrier heights reported in kcal/mol from single point calculations with the listed functional/method, the def2-TZVP basis set on all atoms and CPCM(THF) on geometries obtained with BP86-D3/LANL2TZ(f)–6-31G(d). [b] Single point with the cc-pVTZ basis set (with SK-MCDHF-RSC pseudopotential on Pd; *i.e.,* cc-pVTZ-PP) and "NormalPNO" settings.

1.5.4 PREDICTION OF ENANTIOSELECTIVITY

Given the challenge of calculating energies to within the sub-kcal/mol level of accuracy required for accurate prediction of reaction enantioselectivity, we chose to employ a variety of control experiments to assess the fidelity of our results. With geometries obtained at the BP86-D3/LANL2TZ(f)–6-31G(d) level, we began by evaluating single point energies with a variety of density functional methods (Table 1.5). These methods include generalized gradient approximation (GGA), meta-GGA, hybrid

meta-GGA, range-separated hybrid GGA, and double hybrid functionals. Similar trends in

relative free energies are obtained across each of the methods tested.

Table 1.5. *Comparison of relative free energies obtained across a variety of density*

functional methods.[a]

	BP86-D3	BLYP-D3	revPBE-D3	M06-L	B3LYP-D3	B3LYP-D3[b]
(*Re*/chair/ax)-TS20	0.0	0.0	0.0	0.0	0.0	0.0
(*Re*/boat/ax)-TS20	5.4	6.0	5.3	4.2	6.1	5.7
(*Re*/chair/eq)-TS20	1.6	2.2	1.7	1.4	2.0	1.9
(*Re*/boat/eq)-TS20	5.5	5.3	5.0	4.3	5.6	5.2
(*Si*/chair/ax)-TS20	2.0	2.4	1.9	1.8	2.8	2.6
(*Si*/boat/ax)-TS20	1.0	0.8	0.9	0.3	1.1	1.0
(*Si*/chair/eq)-TS20	4.2	5.0	4.1	3.7	5.0	4.9
(*Si*/boat/eq)-TS20	3.2	3.4	2.9	2.6	3.6	3.4

	PBE0-D3	TPSSh-D3	M06	M06-2X	ωB97X-D3	mPW2PLYP-D
(*Re*/chair/ax)-TS20	0.0	0.0	0.0	0.0	0.0	0.0
(*Re*/boat/ax)-TS20	5.2	5.9	3.6	4.3	6.1	5.1
(*Re*/chair/eq)-TS20	1.2	1.7	0.4	1.2	1.6	1.4
(*Re*/boat/eq)-TS20	5.6	5.8	4.0	4.4	5.8	5.8
(*Si*/chair/ax)-TS20	2.5	2.2	2.1	2.8	2.8	2.2
(*Si*/boat/ax)-TS20	1.5	1.0	1.3	1.0	0.9	1.9
(*Si*/chair/eq)-TS20	4.1	4.2	3.2	4.0	4.3	4.0
(*Si*/boat/eq)-TS20	3.5	3.3	2.8	2.8	3.0	4.1

	PWPB95-D3	DSD-BLYP-D3	DSD-PBEP86-D3
(*Re*/chair/ax)-TS20	0.0	0.0	0.0
(*Re*/boat/ax)-TS20	5.5	5.1	5.0
(*Re*/chair/eq)-TS20	1.3	1.1	1.0
(*Re*/boat/eq)-TS20	5.5	5.6	5.6

(*Si*/chair/ax)-TS20	2.4	2.2	2.1
(*Si*/boat/ax)-TS20	1.4	2.1	2.1
(*Si*/chair/eq)-TS20	3.9	3.8	3.6
(*Si*/boat/eq)-TS20	3.3	3.7	3.7

[a] Relative free energies reported in kcal/mol from single point calculations with the listed functional, the def2-TZVP basis set on all atoms and CPCM(THF) on geometries obtained with BP86-D3/LANL2TZ(f)–6-31G(d). [b] A mixed basis set consisting of LANL2TZ(f) on palladium and 6-311+G(d) on all other atoms utilized.

Given the potentially significant role of noncovalent interactions in differentiating the energy between diastereomeric transition states, we sought to further refine our calculated $\Delta\Delta G^{\ddagger}$ by employing single point calculations with domain based local pair natural orbital coupled-cluster theory (DLPNO-CCSD(T)) (Table 1.6). For these calculations, we employ the cc-pVTZ basis set on all atoms, with the SK-MCDHF-RSC relativistic effective core potential on palladium. Calculations are additionally carried out with the "TightPNO" criteria for the two lowest energy diastereomeric transition states found from calculations with the "NormalPNO" settings.

Under standard conditions at 25 ºC, an enantiomeric excess of 88% is experimentally observed, corresponding to an apparent $\Delta\Delta G^{\ddagger}$ of 1.6 kcal/mol. Comparing the relative energies of only the two lowest energy diastereomeric transition states with "NormalPNO" and "TightPNO" cutoffs affords a calculated $\Delta\Delta G^{\ddagger}$ of 2.3 and 1.9 kcal/mol, respectively, corresponding to 96% ee and 92% ee. From a Boltzmann-weighted average over unique transition states (with "NormalPNO"), 94% ee is calculated. These results are

in good agreement with experimentally obtained values, and thus highlight the efficacy of

the DLPNO-CCSD(T) in the context of asymmetric catalysis.

Table 1.6. *Comparison of relative free energies obtained at the DLPNO-CCSD(T)*

level of theory.[a]

	DLNO-CCSD(T)[b] NormalPNO	DLNO-CCSD(T) NormalPNO	DLNO-CCSD(T) TightPNO
(*Re*/chair/ax)-TS20	0.0	0.0	0.0
(*Re*/boat/ax)-TS20	6.6	5.9	–
(*Re*/chair/eq)-TS20	1.4	1.0	–
(*Re*/boat/eq)-TS20	6.6	6.1	–
(*Si*/chair/ax)-TS20	3.0	2.8	–
(*Si*/boat/ax)-TS20	2.2	2.3	1.9
(*Si*/chair/eq)-TS20	4.5	4.0	–
(*Si*/boat/eq)-TS20	4.4	4.2	–

[a] Relative free energies reported in kcal/mol with DLPNO-CCSD(T)/cc-pVTZ–CPCM(THF)//BP86-
D3/LANL2TZ(f)–6-31G(d). [b]Using the def2-TZVP basis set on all atoms.

Further controls were carried out in which transition state optimizations were

carried out without D3 dispersion correction (Table 1.7), and with the B3LYP-D3 hybrid

functional (Table 1.8). Both of these trials offer similar overall results to those obtained

with BP86-D3 geometries.

Table 1.7. *Optimization without D3 corrections (BP86).[a]*

	M06[b]	DLNO-CCSD(T)[c]
(*Re*/chair/ax)-TS20	0.0	0.0
(*Re*/boat/ax)-TS20	4.4	5.9
(*Re*/chair/eq)-TS20	1.6	2.2
(*Re*/boat/eq)-TS20	5.3	6.7

(*Si*/chair/ax)-TS20	2.6	1.8
(*Si*/boat/ax)-TS20	1.7	2.7
(*Si*/chair/eq)-TS20	4.2	4.3
(*Si*/boat/eq)-TS20	3.5	5.0

[a] Relative free energies reported in kcal/mol with geometries obtained with BP86/LANL2DZ–6-31G(d). [b] Single point calculation with M06/def2-TZVP–CPCM(THF). [c] Single point calculation with DLPNO-CCSD(T)/cc-pVTZ–CPCM(THF) with "NormalPNO" settings.

Table 1.8. *Optimization with B3LYP-D3.[a]*

	M06[b]	DLNO-CCSD(T)[c]
(*Re*/chair/ax)-TS20	0.0	0.0
(*Re*/boat/ax)-TS20	2.8	3.7
(*Si*/chair/ax)-TS20	1.7	1.9
(*Si*/boat/ax)-TS20	1.5	2.3

[a] Relative free energies reported in kcal/mol with geometries obtained with B3LYP-D3/LANL2DZ–6-31G(d). The four lowest energy "axial" transition states were considered here. [b] Single point calculation with M06/def2-TZVP–CPCM(THF). [c] Single point calculation with DLPNO-CCSD(T)/cc-pVTZ–CPCM(THF) with "NormalPNO" settings.

1.5.5   ADDITIONAL NOTES

Facile interconversion between *(Re)*-13 and *(Si)*-13

A previous computational investigation into the reaction mechanism of a truncated system (beginning from enolate intermediates) highlights internal rearrangements of palladium enolates prior to C–C bond formation as a possible origin of enantioinduction.[21] This hypothesis is dependent on kinetic quenching (rather than equilibration) of enolates *(Re)*-13 and *(Si)*-13 by their corresponding C–C bond forming events. However, the authors of that study recognize that a transition state leading to the facile equilibration of

(Re/Si)-**13** may exist, but do not explore further, leaving the origins of enantioinduction

unresolved. In this investigation, a low energy transition state connecting *(Re)*-**13** and *(Si)*-

13 on the PES is found (**TS24**, $\Delta G^{\ddagger} \sim 5$ kcal/mol). **TS24** is significantly lower in energy

than the next lowest transition states, which are those of C–C bond formation (**TS20**). Thus,

enolates *(Re)*-**13** and *(Si)*-**13** are expected to be in thermal equilibrium. Hence, internal

rearrangements of palladium enolates, followed by kinetic quenching via C–C bond

formation, is not responsible for enantioinduction.

Additional potentially lower energy transition states for the interconversion of *(Re)*-

13 and *(Si)*-**13** likely persist, however are challenging to optimize given the flat nature of

the PES and conformational flexibility of the enolate fragment. It is worth noting that

highly decorated, sterically encumbered substrates may experience a barrier to enolate

equilibration similar or greater in magnitude to that of C–C bond formation. Should this be

the case, the mechanism of decarboxylation and/or choice of masked enolate synthon

would play a large role in the resultant product enantioselectivity. The pathways,

intermediates, and consideration described in this research provide a framework from

which this would be evaluated.

Trans Influence in Oxidative Addition

Our investigations into the mechanism of oxidative addition reveal the lowest

energy process for C–O bond cleavage to be that of an *anti* displacement-type of

mechanism (Figure 1.3). The lowest energy conformer of four unique transition states are

considered, in which displacement of the carboxylate leaving group occurs *trans* to either

the nitrogen (*t*-N) or phosphorus (*t*-P) of the PHOX ligand, with either *exo* or *endo* approach of the allylic fragment.

Table 1.9. *Relative free energies (in kcal/mol) of isomeric oxidative addition transition states at various levels of theory.*[a]

	BP86-D3	B3LYP-D3	PBE0-D3	M06	DLPNO-CCSD(T)[b]
(exo/*t*-N)-TS4	0.0	0.0	0.0	0.0	0.0
(endo/*t*-N)-TS4	1.4	2.0	1.9	2.3	2.7
(exo/*t*-P)-TS4	5.9	7.6	7.3	7.5	9.3
(endo/*t*-P)-TS4	3.8	4.8	5.5	6.2	6.5

[a] Relative free energies reported in kcal/mol with geometries obtained with BP86-D3/LANL2TZ(f)–6-31G(d). Single point calculation with def2-TZVP basis set on all atoms (def2-ECP on Pd) and CPCM(THF). [b] Single point calculation with DLPNO-CCSD(T)/cc-pVTZ/CPCM(THF) with "NormalPNO" settings.

An energetic preference of 3.8–6.5 kcal/mol is found for the *t*-N transition states across the various levels of theory investigated (Table 1.9). While this may be in part due to steric interactions between the carboxylate leaving group and the phenyl rings of the triaryl phosphine ligand, we also consider electronic effects. In accordance with the anticipated trans influence, elongated Pd–X bond lengths trans to phosphorus are observed (Figure 1.3). As a hypothesis for the origins of the preference for *t*-N transition states, we consider the research of De Proft and co-workers,[43] who provide a ligand-field-based rational for the trans influence in related square planar Pt(II) complexes. In brief, the authors suggest the repulsion between a strong trans ligand (T) and the ligand trans to T (L) arises from further hybridization (in unsymmetrical d^8 complexes) between the occupied 2a' and

virtual 3a' MOs (Figure 1.15) resulting in a net decrees in Pt–L σ-bonding character, and

thus, a longer bond length.

Figure 1.15. *Select frontier MOs of a model Pt^{II} complex highlighting potential*

hybridization of 2a' and 3a'.
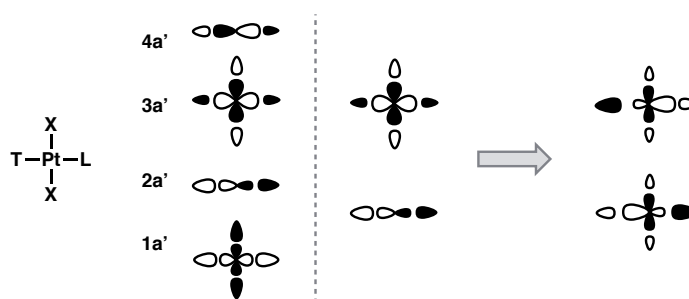
In the case of the (PHOX)Pd complexes, we consider this effect may play a role in the

calculated preference for displacement *trans* to nitrogen. The reduced Pd–C(OCOR) bond

length in the *t*-N transitions states should be conducive to enhanced overlap with the σ*(C–

O), thus, facilitating displacement of the carboxylate leaving group.

Additional Computations for "Experiment and Discussion" Section of Manuscript

Experimentally, it was determined that for β-ketoester substrate **1**, employing the more

electron poor (*S*)-(CF$_3$)$_3$-*t*-BuPHOX ligand in place of the standard (*S*)-*t*-BuPHOX ligand,

with otherwise identical reaction conditions, did not result in a significant change in

reaction rate. Computationally, an identical result was obtained. Henceforth, the suffix

"**_CF₃**" denotes structures that are re-optimized using the (*R*)-(CF$_3$)$_3$-*t*-BuPHOX ligand.

The apparent barrier heights of the two lowest energy decarboxylation pathways (Pathways

2 and 3, see text) were then compared with both ligands at the DLPNO-CCSD(T) level of

theory. Similar results are obtained with "NormalPNO" and "TightPNO" cutoffs (Table

1.10).

Table 1.10. *Comparison of barrier heights to decarboxylation with the standard (S)-*

t-BuPHOX and electron poor (S)-(CF$_3$)$_3$-t-BuPHOX ligands.[a]

	TS14	**TS15**	**TS14_CF$_3$**	**TS15_CF$_3$**
NormalPNO	22.0	23.5	22.4	21.6
TightPNO	21.9	24.3	22.2	22.4

[a] Free energies reported in kcal/mol with geometries obtained with BP86-D3/LANL2TZ(f)–6-31G(d).

Single point calculation with DLPNO-CCSD(T)/cc-pVTZ–CPCM(THF).

In order to experimentally probe the interplay of inner- and outer-sphere

mechanistic pathways, we prepared α-phenyl β-ketoester **20** as well as the corresponding

enol carbonate **21**. Highlighting the role of decarboxylative pathway on subsequent C–C

bond formation, compounds **20** and **21** both yield α-phenyl product **22**, however with

differing degrees of enantioenrichment. In analogous fashion to intermediates derived from

substrate **1** (R = Me), the corresponding set of seven-membered pericyclic inner-sphere C–

C bond forming transition states (**TS20_Ph**) are considered. These initial results suggest

that inner-sphere C–C bond formation for these α-phenyl enolates may give rise to a similar

degree of product enantioenrichment as the α-methyl case (Table 1.11).

Table 1.11. *Inner-sphere reductive elimination transition states with α-phenyl*

substrate.

Transition State	G(rel)
(*Re*/chair/axial)-TS20_Ph_i	0.0

(*Re*/chair/axial)-TS20_Ph_ii	1.3
(*Re*/boat/axial)-TS20_Ph_i	4.9
(*Re*/boat/axial)-TS20_Ph_ii	3.6
(*Si*/chair/axial)-TS20_Ph_i	4.1
(*Si*/chair/axial)-TS20_Ph_ii	4.1
(*Si*/boat/axial)-TS20_Ph_i	1.3
(*Si*/boat/axial)-TS20_Ph_ii	1.3

[a] Relative free energies reported in kcal/mol from the M06/def2-TZVP–CPCM(THF)//BP86-D3/LANL2TZ(f)–6-31G(d) level of theory. Note that Re and Si exchange compared to **TS20** with α-Me groups due to the priority of the Ph substituent.

1.5.6   EXPERIMENTAL PROCEDURES AND SPECTROSCOPIC DATA
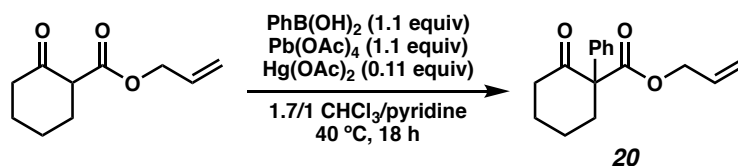
Allyl 2-oxo-1-phenylcyclohexane-1-carboxylate (20)

Compound **20** was prepared in following literature precedent.[44] To a flame dried flask equipped with a stir bar under a nitrogen atmosphere were added phenylboronic acid (1.46 g, 12.1 mmol, 1.10 equiv), lead(IV) acetate (5.34 g, 12.1 mmol, 1.10 equiv), and mercury(II) acetate (0.38 g, 1.21 mmol). The solids were dissolved in anhydrous chloroform (20 mL) and the solution was heated to 40 ºC. After one hour at 40 ºC, a solution of allyl 2-oxocyclohexane-1-carboxylate[2] (2.00 g, 11.0 mmol, 1.00 equiv) in pyridine (11.0 mL, 1.0 M) was added to the reaction, and stirring at 40 ºC was continued for 18 hours. Upon complete consumption of β-ketoester starting material, as determined by TLC (10%

EtOAc/hexanes), the reaction mixture was let cool, then filtered through a plug of Celite®

washing with chloroform. The combined organic phase was washed with aqueous H_2SO_4

(3 M, 20 mL). The resulting aqueous layer was extracted twice with chloroform (20 mL).

The combined organic layer was once again washed with water (20 mL), dried over

anhydrous Na_2SO_4, filtered, and volatiles were removed in vacuo. The crude oil was

purified by flash column chromatography (10% EtOAc/hexanes) to afford β-ketoester **20**

(2.00 g, 70% yield) as a colorless oil, which solidifies to an amorphous solid upon

refrigeration.

^{1}H NMR (400 MHz, CDCl$_3$): δ 7.41 – 7.35 (m, 2H), 7.34 – 7.29 (m, 1H), 7.27 – 7.23 (m,

2H), 5.86 (ddt, J = 17.2, 10.5, 5.6 Hz, 1H), 5.25 – 5.17 (m, 2H), 4.65 (dq, J = 5.6, 1.5 Hz,

2H), 2.81 – 2.73 (m, 1H), 2.60 – 2.53 (m, 2H), 2.48 – 2.40 (m, 1H), 2.03 – 1.93 (m, 1H),

1.90 – 1.73 (m, 3H).

^{13}C NMR (100 MHz, CDCl$_3$): δ 206.8, 171.1, 136.6, 131.6, 128.6, 128.0, 127.8, 118.6,

66.7, 66.1, 40.8, 35.2, 27.8, 22.1

IR (Neat Film, NaCl): 2989, 1714, 1434, 1214 cm^{-1}.

HRMS (MM: FD+): *m/z* calc'd for $C_{16}H_{18}O_3$ [M]$^+$: 258.1256, found 258.1265.
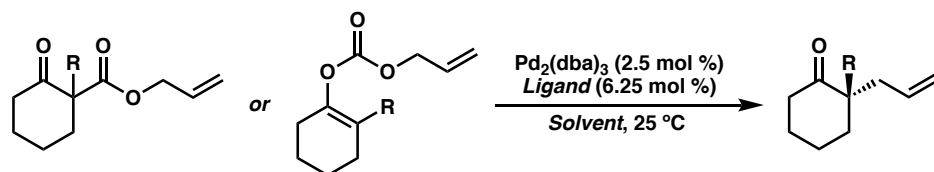
General procedure for asymmetric allylic alkylation screening

The procedure for the Pd-catalyzed dicarboxylic allylic alkylation is followed as described

in our previous reports.[2,Error! Bookmark not defined.] In a nitrogen filled glovebox, an oven dried

vial is charged with a stir bar, tris(dibenzylideneacetone)dipalladium(0) (2.28 mg, 2.50

µmol), and *ligand* (6.25 µmol). *Solvent* (1.0 mL) is added, and the catalyst stock solution

is pre-stirred for 30 minutes at 25 ºC. To a separate vial equipped with a stir bar is added a

solution of *substrate* (0.05 mmol) in *solvent* (1.0 mL, 0.05 M). To the solution of substrate

is added 0.50 mL of the pre-stirred catalyst stock solution [1.25 µmol Pd$_2$(dba)$_3$, 3.13 µmol

ligand]. The reaction vessel is then sealed with electrical tape and removed from the

glovebox. Stirring is continued at 25 ºC for 12 hours (unless otherwise noted). Volatiles

are then removed in vacuo and the product is purified by silica gel flash column

chromatography or preparatory-scale TLC.

(S)-2
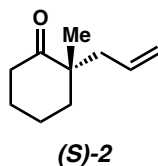
(S)-2-allyl-2-methylcyclohexan-1-one ((S)-2)

Known compound – Spectral data matches that of prior literature reports.[2,**Error! Bookmark not**

defined.]

 ¹H NMR (500 MHz, CDCl$_3$): δ 5.69 (ddt, *J* = 16.2, 10.9, 7.4 Hz, 1H), 5.07 – 5.01 (m,

2H), 2.42 – 2.33 (m, 3H), 2.23 (dd, *J* = 13.8, 7.2 Hz, 1H), 1.91 – 1.67 (m, 5H), 1.64 – 1.55

(m, 1H), 1.07 (s, 3H).

Note: Compound is moderately volatile, and care should be exercised when removing

solvent in vacuo.

(S)-22
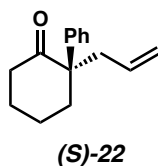
(S)-2-allyl-2-phenylcyclohexan-1-one ((S)-22)

Known compound – Spectral data matches that of prior literature reports.[45]

^{1}H NMR (500 MHz, CDCl$_3$): δ 7.35 (t, J = 7.7 Hz, 2H), 7.26 – 7.22 (m, 1H), 7.15 (d, J = 7.5 Hz, 2H), 5.44 (dddd, J = 17.0, 10.2, 7.9, 6.7 Hz, 1H), 4.92 (d, J = 10.2 Hz, 1H), 4.88 (d, J = 17.0 Hz, 1H), 2.67 (dq, J = 14.4, 3.0 Hz, 1H), 2.51 (dd, J = 14.0, 6.7 Hz, 2H), 2.44 (dd, J = 14.0, 8.0 Hz, 2H), 2.38 – 2.26 (m, 2H), 1.99 – 1.91 (m, 1H), 1.83 – 1.63 (m, 4H).

SFC conditions: 5% IPA, 2.5 mL/min, Chiralpak OJ-H column, λ = 210 nm, t$_R$ (min): minor = 3.31, major = 3.07.

Racemic 22:
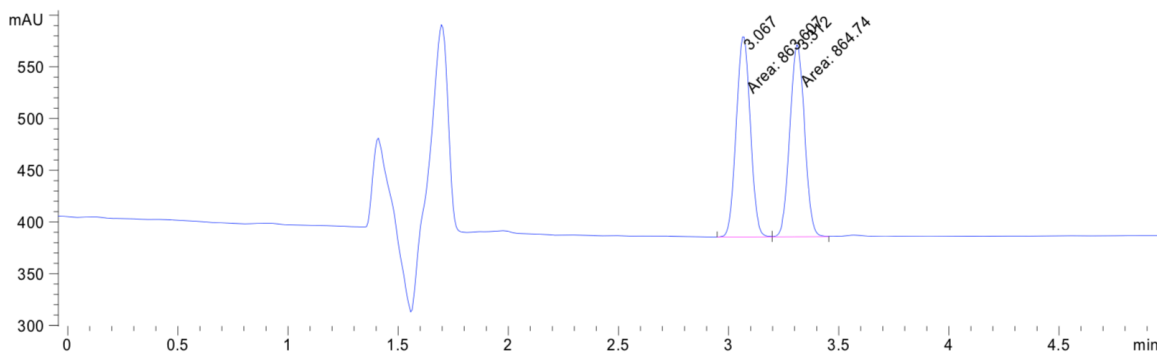
From enol carbonate 21:
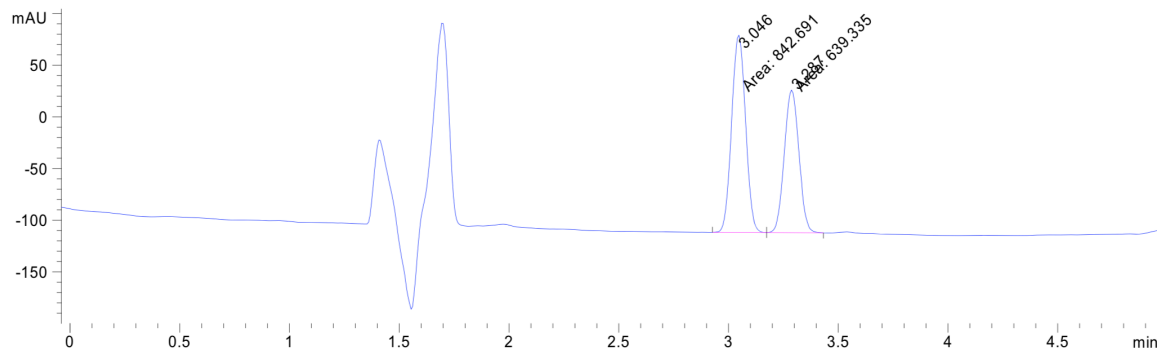
Peak	RetTime [min]	Type	Width [min]	Area [mAU*s]	Height [mAU]	Area %
1	3.046	MF	0.0731	842.69116	192.14436	56.8607
2	3.287	FM	0.0768	639.33521	138.66087	43.1393

From β-ketoester **20**:

Peak	RetTime [min]	Type	Width [min]	Area [mAU*s]	Height [mAU]	Area %
1	3.169	MM	0.0760	269.91296	59.16746	61.6800
2	3.420	MF	0.0784	167.68944	35.64637	38.3200
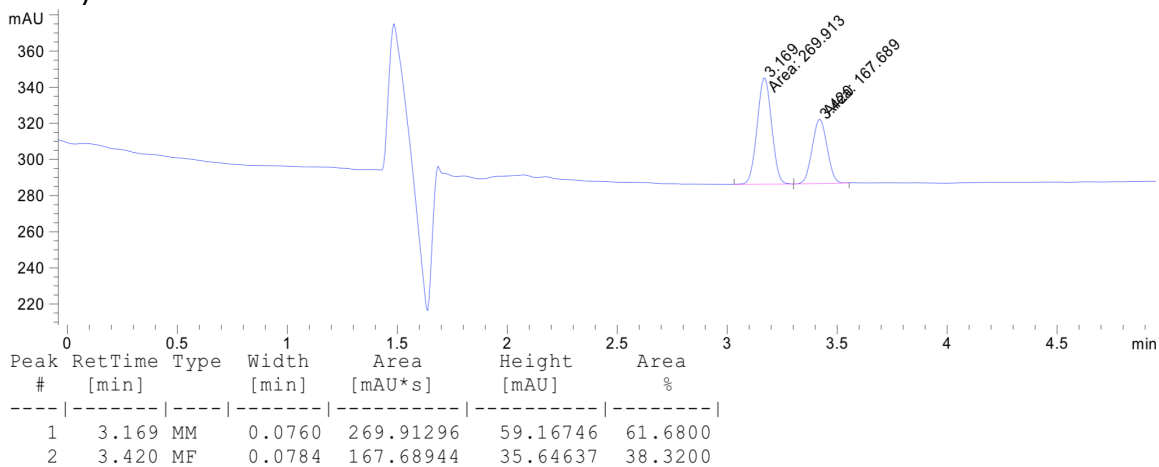
From β-ketoester **20** *with optimal conditions (entry 4 in Figure 1.14):*

Peak	RetTime [min]	Type	Width [min]	Area [mAU*s]	Height [mAU]	Area %
1	2.861	MF	0.0622	505.43756	135.37050	68.0706
2	3.027	FM	0.0634	237.08202	62.32189	31.9294
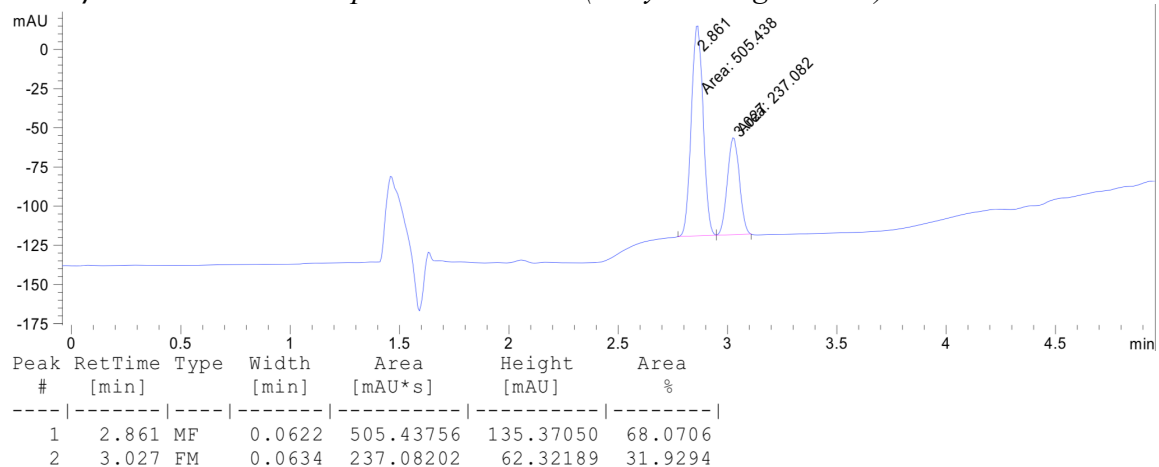
1.6   REFERENCES AND NOTES

(1)   (a) Trost, B. M.; Jiang, C. Catalytic Enantioselective Construction of All-Carbon Quaternary Stereocenters. *Synthesis* **2006**, *3*, 369–396. (b) Corey, E. J.; Guzman-Perez, A. The Catalytic Enantioselective Construction of Molecules with Quaternary Carbon Stereocenters. *Angew. Chem. Int. Ed.* **1998**, *37*, 388–401.

(2)   (a) Mohr, J. T.; Behenna, D. C.; Harned, A. M.; Stoltz, B. M. Deracemization of Quaternary Stereocenters by Pd-Catalyzed Enantioconvergent Decarboxylative Allylation of Racemic β-Ketoesters. *Angew. Chem. Int. Ed.* **2005**, *44*, 6924–6927. (b) Behenna, D. C.; Stoltz, B. M. The Enantioselective Tsuji Allylation. *J. Am. Chem. Soc.* **2004**, *126*, 15044–15045. (c) Ngamnithiporn, A.; Iwayama, T.; Bartberger, M. D.; Stoltz, B. M. Enantioselective Synthesis of Highly Oxygenated Acyclic Quaternary Center-Containing Building Blocks via Palladium-Catalyzed Decarboxylative Allylic Alkylation of Cyclic Siloxyketones. *Chem. Sci.* **2020**, *11*, 11068–11071. (d) Alexy, E. J.; Fulton, T. J.; Zhang, H.; Stoltz, B. M. Palladium-Catalyzed Enantioselective Decarboxylative Allylic Alkylation of Fully Substituted N-Acyl Indole-Derived Enol Carbonates. *Chem. Sci.* **2019**, *10*, 5996–6000. (e) Lu, Y.; Goldstein, E. L.; Stoltz, B. M. Palladium-Catalyzed Enantioselective $C(sp^3)$–$C(sp^3)$ Cross-Coupling for the Synthesis of (Poly)Fluorinated Chiral Building Blocks. *Org. Lett.* **2018**, *20*, 5657–5660. (f) Alexy, E. J.; Zhang, H.; Stoltz, B. M. Catalytic Enantioselective Synthesis of

Acyclic Quaternary Centers: Palladium-Catalyzed Decarboxylative Allylic Alkylation of Fully Substituted Acyclic Enol Carbonates. *J. Am. Chem. Soc.* **2018**, *140*, 10109–10112. (g) Alexy, E. J.; Virgil, S. C.; Bartberger, M. D.; Stoltz, B. M. Enantioselective Pd-Catalyzed Decarboxylative Allylic Alkylation of Thiopyranones. Access to Acyclic, Stereogenic α-Quaternary Ketones. *Org. Lett.* **2017**, *19*, 5007–5009.

(3)   (a) Liu, Y.; Han, S.-J.; Liu, W.-B.; Stoltz, B. M. Catalytic Enantioselective Construction of Quaternary Stereocenters: Assembly of Key Building Blocks for the Synthesis of Biologically Active Molecules. *Acc. Chem. Res.* **2015**, *48*, 740–751. (b) Pritchett, B. P.; Stoltz, B. M. Enantioselective Palladium-Catalyzed Allylic Alkylation Reactions in the Synthesis of Aspidosperma and Structurally Related Monoterpene Indole Alkaloids. *Nat. Prod. Rep.* **2018**, *35*, 559–574.

(4)   Behenna, D. C.; Mohr, J. T.; Sherden, N. H.; Marinescu, S. C.; Harned, A. M.; Tani, K.; Seto, M.; Ma, S.; Novák, Z.; Krout, M. R.; McFadden, R. M.; Roizen, J. L.; Enquist, J. A.; White, D. E.; Levine, S. R.; Petrova, K. V.; Iwashita, A.; Virgil, S. C.; Stoltz, B. M. Enantioselective Decarboxylative Alkylation Reactions: Catalyst Development, Substrate Scope, and Mechanistic Studies. *Chem. Eur. J.* **2011**, *17*, 14199–14223.

(5)   Sherden, N. H.; Behenna, D. C.; Virgil, S. C.; Stoltz, B. M. Unusual Allylpalladium Carboxylate Complexes: Identification of the Resting State of Catalytic

Enantioselective Decarboxylative Allylic Alkylation Reactions of Ketones. *Angew. Chem. Int. Ed.* **2009**, *48*, 6840–6843. Note that product enantioenrichment follows a linear correlation with PHOX ligand enantioenrichment. An error was found in a unit conversion (minutes to seconds) in the supporting information data. The correct rate in inverse seconds is $k = 1.58 \times 10^{-3}$ s^{-1}. While this error was initially propagated it is minor and does not affect any subsequent conclusions.

(6)   Trost, B. M.; Xu, J.; Schmidt, T. Palladium-Catalyzed Decarboxylative Asymmetric Allylic Alkylation of Enol Carbonates. *J. Am. Chem. Soc.* **2009**, *131*, 18343–18357.

(7)   For review of classes of nucleophiles as well as mechanistic implications: (a) Trost, B. M.; Crawley, M. L. Asymmetric Transition-Metal-Catalyzed Allylic Alkylations: Applications in Total Synthesis. *Chem. Rev.* **2003**, *103*, 2921–2944. Highlighting the challenge of employing "hard" ketone enolate nucleophiles: (b) Trost, B. M.; Schroeder, G. M. Palladium-Catalyzed Asymmetric Alkylation of Ketone Enolates. *J. Am. Chem. Soc.* **1999**, *121*, 6759–6760. For examples of stabilized ketone enolates with Trost system: (c) Trost, B. M.; Schroeder, G. M.; Kristensen, J. Palladium-Catalyzed Asymmetric Allylic Alkylation of α-Aryl Ketones. *Angew. Chem. Int. Ed.* **2002**, *41*, 3492–3495. (d) Trost, B. M.; Radinov, R.; Grenzer, E. M. Asymmetric Alkylation of β-Ketoesters. *J. Am. Chem. Soc.* **1997**, *119*, 7879–7880.

(8)   McDougal, N. T.; Virgil, S. C.; Stoltz, B. M. High-Throughput Screening of the

        Asymmetric Decarboxylative Alkylation Reaction of Enolate-Stabilized Enol

        Carbonates. *Synlett* **2010**, 11, 1712–1716.

(9)   (a) Sun, A. W.; Hess, S. N.; Stoltz, B. M. Enantioselective Synthesis of Gem-

        Disubstituted N-Boc Diazaheterocycles via Decarboxylative Asymmetric Allylic

        Alkylation. *Chem. Sci.* **2019**, *10*, 788–792. (b) Sun, A. W.; Bulterys, P. L.;

        Bartberger, M. D.; Jorth, P. A.; O'Boyle, B. M.; Virgil, S. C.; Miller, J. F.; Stoltz,

        B. M. Incorporation of a Chiral Gem-Disubstituted Nitrogen Heterocycle Yields an

        Oxazolidinone Antibiotic with Reduced Mitochondrial Toxicity. *Bioorg. Med.*

        Chem. Lett. **2019**, *29*, 2686–2689. (c) Numajiri, Y.; Jiménez-Osés, G.; Wang, B.;

        Houk, K. N.; Stoltz, B. M. Enantioselective Synthesis of Dialkylated N-

        Heterocycles by Palladium-Catalyzed Allylic Alkylation. *Org. Lett.* **2015**, *17*,

        1082–1085. (d) Behenna, D. C.; Liu, Y.; Yurino, T.; Kim, J.; White, D. E.; Virgil,

        S. C.; Stoltz, B. M. Enantioselective Construction of Quaternary N-Heterocycles

        by Palladium-Catalysed Decarboxylative Allylic Alkylation of Lactams. *Nat. Chem*

        2012, *4*, 130–133. (e) Bennett, N. B.; Duquette, D. C.; Kim, J.; Liu, W.-B.; Marziale,

        A. N.; Behenna, D. C.; Virgil, S. C.; Stoltz, B. M. Expanding Insight into

        Asymmetric Palladium-Catalyzed Allylic Alkylation of N-Heterocyclic Molecules

        and Cyclic Ketones. *Chem.: Eur. J.* **2013**, *19*, 4414–4418. (f) Korch, K. M.;

        Eidamshaus, C.; Behenna, D. C.; Nam, S.; Horne, D.; Stoltz, B. M. Enantioselective

Synthesis of α-Secondary and α-Tertiary Piperazin-2-Ones and Piperazines by Catalytic Asymmetric Allylic Alkylation. *Angew. Chem. Int. Ed.* **2015**, *54*, 179–183. (g) Sercel, Z. P.; Sun, A. W.; Stoltz, B. M. Synthesis of Enantioenriched Gem-Disubstituted 4-Imidazolidinones by Palladium-Catalyzed Decarboxylative Asymmetric Allylic Alkylation. *Org. Lett.* **2021**, *23*, 6348–6351. (h) Duquette, D. C.; Cusumano, A. Q.; Lefoulon, L.; Moore, J. T.; Stoltz, B. M. Probing Trends in Enantioinduction via Substrate Design: Palladium-Catalyzed Decarboxylative Allylic Alkylation of α-Enaminones. *Org. Lett.* **2020**, *22*, 4966–4969. (i) Sercel, Z. P.; Sun, A. W.; Stoltz, B. M. Palladium-Catalyzed Decarboxylative Asymmetric Allylic Alkylation of 1,4-Diazepan-5-Ones. *Org. Lett.* **2019**, *21*, 9158–9161.

(10)   (a) Keith, J. A.; Behenna, D. C.; Mohr, J. T.; Ma, S.; Marinescu, S. C.; Oxgaard, J.; Stoltz, B. M.; Goddard, W. A. The Inner-Sphere Process in the Enantioselective Tsuji Allylation Reaction with *(S)-t*-Bu-Phosphinooxazoline Ligands. *J. Am. Chem. Soc.* **2007**, *129*, 11876–11877. (b) Keith, J. A.; Behenna, D. C.; Sherden, N.; Mohr, J. T.; Ma, S.; Marinescu, S. C.; Nielsen, R. J.; Oxgaard, J.; Stoltz, B. M.; Goddard, W. A. The Reaction Mechanism of the Enantioselective Tsuji Allylation: Inner-Sphere and Outer-Sphere Pathways, Internal Rearrangements, and Asymmetric C–C Bond Formation. *J. Am. Chem. Soc.* **2012**, *134*, 19050–19060.

(11)   (a) Pérez-Rodríguez, M.; Braga, A. A. C.; de Lera, A. R.; Maseras, F.; Álvarez, R.; Espinet, P. A DFT Study of the Effect of the Ligands in the Reductive Elimination

from Palladium Bis(Allyl) Complexes. *Organometallics* **2010**, *29*, 4983–4991. (b) Méndez, M.; Cuerva, J. M.; Gómez-Bengoa, E.; Cárdenas, D. J.; Echavarren, A. M. Intramolecular Coupling of Allyl Carboxylates with Allyl Stannanes and Allyl Silanes: A New Type of Reductive Elimination Reaction? *Chem. Eur. J.* **2002**, *8*, 3620–3628. (c) Zhang, P.; Brozek, L. A.; Morken, J. P. Pd-Catalyzed Enantioselective Allyl−Allyl Cross-Coupling. *J. Am. Chem. Soc.* **2010**, *132*, 10686–10688.

(12)   McPherson, K. E.; Croatt, M. P.; Morehead, A. T. Jr.; Sargent, A. L. DFT Mechanistic Investigation of an Enantioselective Tsuji–Trost Allylation Reaction. *Organometallics* **2018**, *37*, 3791–3802.

(13)   (a) Neese, F. Software Update: The ORCA Program System, Version 4.0. *Wiley Interdisciplinary Reviews: Computational Molecular Science* **2018**, *8*, e1327. (b) Neese, F. The ORCA Program System. *Wiley Interdisciplinary Reviews: Computational Molecular Science* **2012**, *2*, 73–78.

(14)   (a) Perdew, J. P. Density-Functional Approximation for the Correlation Energy of the Inhomogeneous Electron Gas. *Phys. Rev. B* **1986**, *33*, 8822–8824. (b) Becke, A. D. Density-Functional Exchange-Energy Approximation with Correct Asymptotic Behavior. *Phys. Rev. A* **1988**, *38*, 3098–3100.

(15)   (a) Grimme, S.; Antony, J.; Ehrlich, S.; Krieg, H. A A consistent and accurate *ab initio* parametrization of density functional dispersion correction (DFT-D) for the

94 elements H-Pu. *J. Chem. Phys.* **2010**, *132*, 154104. (b) Grimme, S.; Ehrlich, S.; Goerigk, L. Effect of the Damping Function in Dispersion Corrected Density Functional Theory. *J. Comput. Chem.* **2011**, *32*, 1456–1465. (c) Becke, A. D.; Johnson, E. R. A density-functional model of the dispersion interaction. *J. Chem. Phys.* **2005**, *122*, 154101. (d) Johnson, E. R.; Becke, A. D. A post-Hartree–Fock model of intermolecular interactions. *J. Chem. Phys.* **2005**, *123*, 024101. (e) Johnson, E. R.; Becke, A. D. A post-Hartree-Fock model of intermolecular interactions: Inclusion of higher-order corrections. *J. Chem. Phys.* **2006**, *124*, 174104.

(16)   Hay, P. J.; Wadt, W. R. Ab Initio Effective Core Potentials for Molecular Calculations. Potentials for the Transition Metal Atoms Sc to Hg. *J. Chem. Phys.* **1985**, *82*, 270–283.

(17)   Stephens, P. J.; Devlin, F. J.; Chabalowski, C. F.; Frisch, M. J. Ab Initio Calculation of Vibrational Absorption and Circular Dichroism Spectra Using Density Functional Force Fields. *J. Phys. Chem.* **1994**, *98*, 11623–11627.

(18)   Adamo, C.; Barone, V. Toward Reliable Density Functional Methods without Adjustable Parameters: The PBE0 Model. *J. Chem. Phys.* **1999**, *110*, 6158–6170.

(19)   Zhao, Y.; Truhlar, D. G. The M06 Suite of Density Functionals for Main Group Thermochemistry, Thermochemical Kinetics, Noncovalent Interactions, Excited States, and Transition Elements: Two New Functionals and Systematic Testing of

Four M06-Class Functionals and 12 Other Functionals. *Theor Chem Account* **2008**, *120*, 215–241.

(20)   Kozuch, S.; Gruzman, D.; Martin, J. M. L. DSD-BLYP: A General Purpose Double Hybrid Density Functional Including Spin Component Scaling and Dispersion Correction. *J. Phys. Chem. C* **2010**, *114*, 20801–20808.

(21)   Weigend, F.; Ahlrichs, R. Balanced Basis Sets of Split Valence, Triple Zeta Valence and Quadruple Zeta Valence Quality for H to Rn: Design and Assessment of Accuracy. *Phys. Chem. Chem. Phys.* **2005**, *7*, 3297–3305.

(22)   Andrae, D.; Häußermann, U.; Dolg, M.; Stoll, H.; Preuß, H. Energy-Adjusted ab Initio Pseudopotentials for the Second and Third Row Transition Elements. *Theoret. Chim. Acta* **1990**, *77*, 123–141.

(23)   Barone, V.; Cossi, M. Quantum Calculation of Molecular Energies and Energy Gradients in Solution by a Conductor Solvent Model. *J. Phys. Chem. A* **1998**, *102*, 1995–2001.

(24)   Grimme, S. Supramolecular Binding Thermodynamics by Dispersion-Corrected Density Functional Theory. *Chem. Eur. J.* **2012**, *18*, 9955–9964.

(25)   Legault, C. Y. CYLView, 1.0b; Université de Sherbrooke, Canada, 2009; http://www.cylview.org. Note that solvent exposed surface plots were generated with Chimera: Petterson, E. F.; Goddard T. D.; Huang, C. C.; Couch, G. S.; Greenblatt, D. M.; Meng, E. C.; Ferrin, T. E. UCSF Chimera – a visualization

system for exploratory research and analysis. *J. Comput. Chem.* **2004**, *25*, 1605–
1612.

(26) (a) Riplinger, C.; Neese, F. An Efficient and near Linear Scaling Pair Natural
Orbital Based Local Coupled Cluster Method. *J. Chem. Phys.* **2013**, *138*, 034106.
(b) Riplinger, C.; Sandhoefer, B.; Hansen, A.; Neese, F. Natural Triple Excitations
in Local Coupled Cluster Calculations with Pair Natural Orbitals. *J. Chem. Phys.*
2013, *139*, 134101. (c) Riplinger, C.; Pinski, P.; Becker, U.; Valeev, E. F.; Neese,
F. Sparse Maps—A Systematic Infrastructure for Reduced-Scaling Electronic
Structure Methods. II. Linear Scaling Domain Based Pair Natural Orbital Coupled
Cluster Theory. *J. Chem. Phys.* **2016**, *144*, 024109.

(27) Peterson, K. A.; Figgen, D.; Dolg, M.; Stoll, H. Energy-Consistent Relativistic
Pseudopotentials and Correlation Consistent Basis Sets for the 4d Elements Y–Pd.
J. Chem. Phys. **2007**, *126*, 124101.

(28) (a) Yamamoto, T.; Saito, O.; Yamamoto, A. Oxidative Addition of Allyl Acetate
to Palladium(0) Complexes. *J. Am. Chem. Soc.* **1981**, *103*, 5600–5602. (b)
Yamamoto, T.; Akimoto, M.; Saito, O.; Yamamoto, A. Interaction of Palladium(0)
Complexes with Allylic Acetates, Allyl Ethers, Allyl Phenyl Chalcogenides,
Allylic Alcohols, and Allylamines. Oxidative Addition, Condensation,
Disproportionation, and π-Complex Formation. *Organometallics* **1986**, *5*, 1559–
1567. (c) Amatore, C.; Jutand, A.; Meyer, G.; Mottier, L. Evidence of the

Reversible Formation of Cationic π-Allylpalladium(II) Complexes in the Oxidative

Addition of Allylic Acetates to Palladium(0) Complexes. *Chem.: Eur. J.* **1999**, *5*,

466–473.

(29)   Ariafard, A.; Lin, Z. Understanding the Relative Easiness of Oxidative Addition of

Aryl and Alkyl Halides to Palladium(0). *Organometallics* **2006**, *25*, 4030–4033

(30)   Low, J. J.; Goddard, W. A. Theoretical Studies of Oxidative Addition and

Reductive Elimination. 3. Carbon-Hydrogen and Carbon-Carbon Reductive

Coupling from Palladium and Platinum Bis(Phosphine) Complexes. *J. Am. Chem.*

Soc. **1986**, *108*, 6115–6128.

(31)   Grennberg, H.; Langer, V.; Bäckvall, J.-E. Structure and Reactivity of Cis- and

Trans-Bis-[{5-Carbomethoxy-(1,2,3-η)-Cyclohexenyl}palladium]. Evidence for a

(σ-Allyl)Palladium Intermediate in the Cis-Migration of Acetate from Palladium to

Coordinated π-Allyl. *J. Chem. Soc., Chem. Commun.* **1991**, 17, 1190–1192

(32)   Trost, B. M.; Verhoeven, T. R. Allylic Substitutions with Retention of

Stereochemistry. *J. Org. Chem.* **1976**, *41*, 3215–3216.

(33)   (a) Pérez-Rodríguez, M.; Braga, A. A. C.; de Lera, A. R.; Maseras, F.; Álvarez, R.;

Espinet, P. A DFT Study of the Effect of the Ligands in the Reductive Elimination

from Palladium Bis(Allyl) Complexes. *Organometallics* **2010**, *29*, 4983–4991. (b)

Méndez, M.; Cuerva, J. M.; Gómez-Bengoa, E.; Cárdenas, D. J.; Echavarren, A. M.

Intramolecular Coupling of Allyl Carboxylates with Allyl Stannanes and Allyl

Silanes: A New Type of Reductive Elimination Reaction? *Chem. Eur. J.* **2002**, *8*, 3620–3628. (c) Zhang, P.; Brozek, L. A.; Morken, J. P. Pd-Catalyzed Enantioselective Allyl−Allyl Cross-Coupling. *J. Am. Chem. Soc.* **2010**, *132*, 10686–10688.

(34)   (a) Trost, B. M.; Thaisrivongs, D. A. Strategy for Employing Unstabilized Nucleophiles in Palladium-Catalyzed Asymmetric Allylic Alkylations *J. Am. Chem. Soc.* **2008**, *130*, 14092–14093. (b) Zhang, K.; Peng, Q.; Hou, X.-L.; Wu, Y.-D. Highly Enantioselective Palladium-Catalyzed Alkylation of Acyclic Amides *Angew. Chem. Int. Ed.* **2008**, *47*, 1741–1744. (c) Trost, B. M.; Xu, J.; Schmidt, T. Palladium-Catalyzed Decarboxylative Asymmetric Allylic Alkylation of Enol Carbonates *J. Am. Chem. Soc.* **2009**, *131*, 18343–18357.

(35)   (a) Aranyos, A.; Szabó, K. J.; Castaño, A. M.; Bäckvall, J.-E. Central versus Terminal Attack in Nucleophilic Addition to (π-Allyl)Palladium Complexes. Ligand Effects and Mechanism. *Organometallics* **1997**, *16*, 1058–1064. (b) Szabó, K. J. Effects of the Ancillary Ligands on Palladium−Carbon Bonding in (η^3−Allyl)Palladium Complexes. Implications for Nucleophilic Attack at the Allylic Carbons. *Organometallics* **1996**, 15, 1128–1133. (c) Castaño, A. M.; Aranyos, A.; Szabó, K. J.; Bäckvall, J.-E. Nucleophilic Attack on (π-Allyl)Palladium Complexes: Direction of the Attack to the Central or Terminal Carbon Atom by Ligand Control. *Angew. Chem. Int. Ed.* **1995**, *34*, 2551–2553.

(36)   Hegedus, L. S.; Darlington, W. H.; Russell, C. E. Cyclopropanation of Ester Enolates by π-Allylpalladium Chloride Complexes. *J. Org. Chem.* **1980**, *45*, 5193–5196.

(37)   Hoffmann, H. M. R.; Otte, A. R.; Wilde, A.; Menzer, S.; Williams, D. J. Isolation and X-Ray Crystal Structure of a Palladacyclobutane: Insight into the Mechanism of Cyclopropanation. *Angew. Chem. Int. Ed.* **1995**, *34*, 100–102.

(38)   Note that in reference 2h a slight kinetic resolution was observed.

(39)   Tani, K.; Behenna, D. C.; McFadden, R. M.; Stoltz, B. M. A Facile and Modular Synthesis of Phosphinooxazoline Ligands. *Org. Lett.* **2007**, *9*, 2529–2531.

(40)   Neese, F.; Wennmohs, F.; Hansen, A.; Becker, U. Efficient, Approximate and Parallel Hartree-Fock and Hybrid DFT Calculations. A 'Chain-of-Spheres' Algorithm for the Hartree-Fock Exchange. *Chemical Physics* **2009**, *356*, 98–109.

(41)   Stoychev, G. L.; Auer, A. A.; Neese, F. Automatic Generation of Auxiliary Basis Sets. *J. Chem. Theory Comput.* **2017**, *13*, 554–562.

(42)   (a) Chéron, N.; Jacquemin, D.; Fleurat-Lessard, P. A Qualitative Failure of B3LYP for Textbook Organic Reactions. *Phys. Chem. Chem. Phys.* **2012**, *14*, 7170–7175. (b) Burke, K.; Perdew, J. P.; Ernzerhof, M. Why the Generalized Gradient Approximation Works and How to Go beyond It. *International Journal of Quantum Chemistry* **1997**, *61*, 287–293.

(43)   Pinter, B.; Speybroek, V. V.; Waroquier, M.; Geerlings, P.; De Proft, F. *trans* effect and *trans* influence: importance of metal mediated ligand-ligand repulsion. *Phys. Chem. Chem. Phys.* **2013**, *15*, 17354–17365.

(44)   Akula, R.; Doran, R.; Guiry, P. J. Highly Enantioselective Formation of α-Allyl-α-Arylcyclopentanones via Pd-Catalysed Decarboxylative Asymmetric Allylic Alkylation. *Chem. Eur. J.* **2016**, *22*, 9938–9942.

(45)   Trost, B. M.; Schroeder, G. M.; Kristensen, J. Palladium-Catalyzed Asymmetric Allylic Alkylation of α-Aryl Ketones. *Angew. Chem. Int. Ed.* **2002**, *41*, 3492–3495.

APPENDIX 1

Spectra Relevant to Chapter 1: Mechanism of the Pd-catalyzed

Asymmetric Allylic Alkylation: A Comprehensive Quantum Mechanics

Investigation
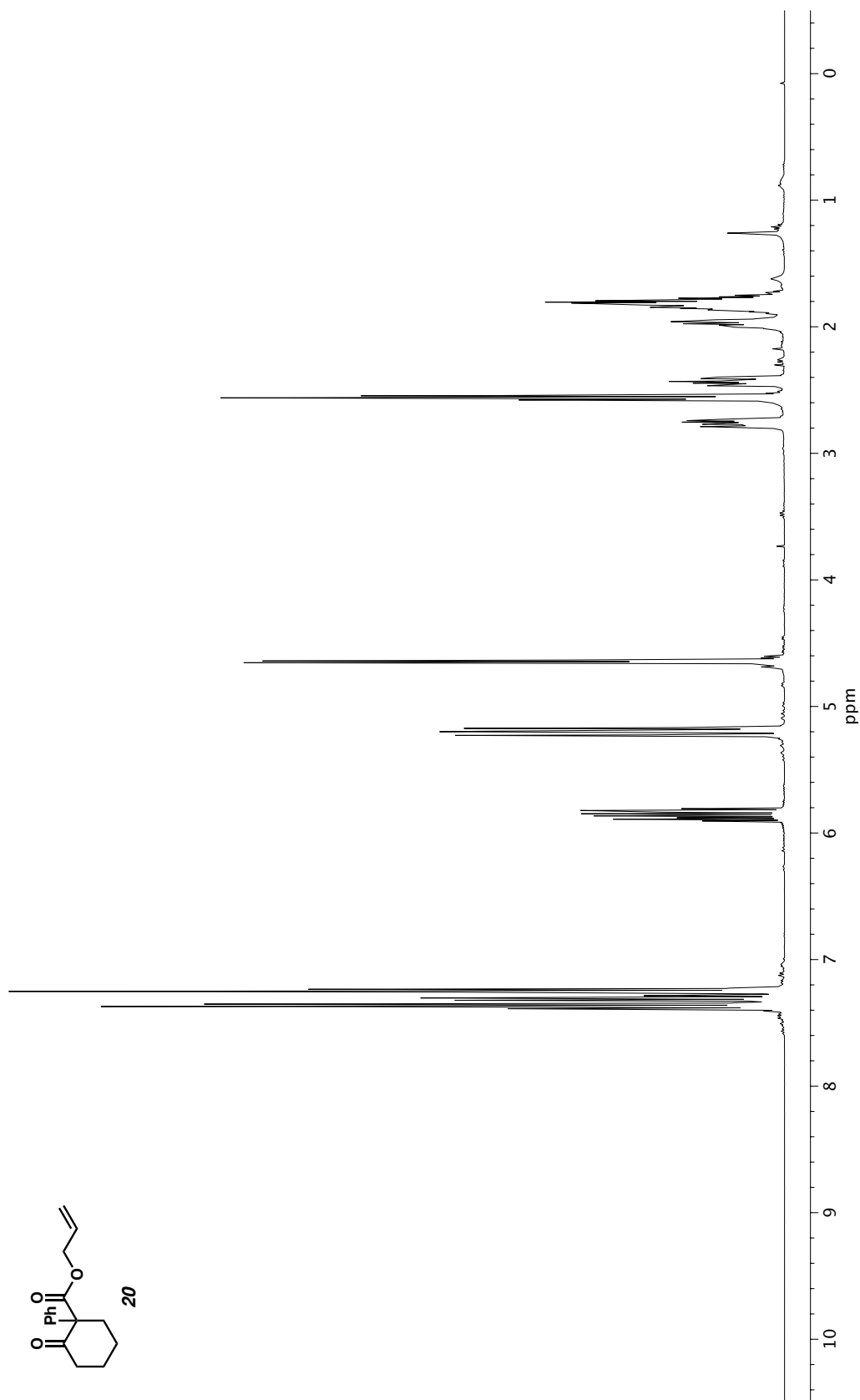
Figure A1.1. ^1H NMR (400 MHz, CDCl$_3$) of compound **20**.
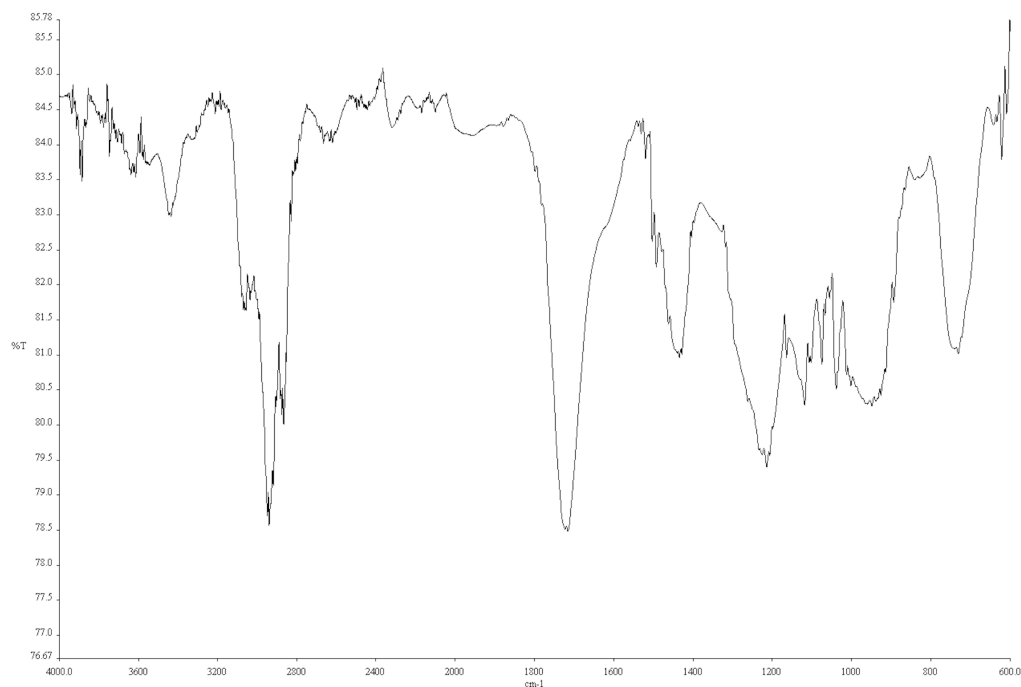
Figure A1.2. Infrared spectrum (Thin Film, NaCl) of compound **20**.
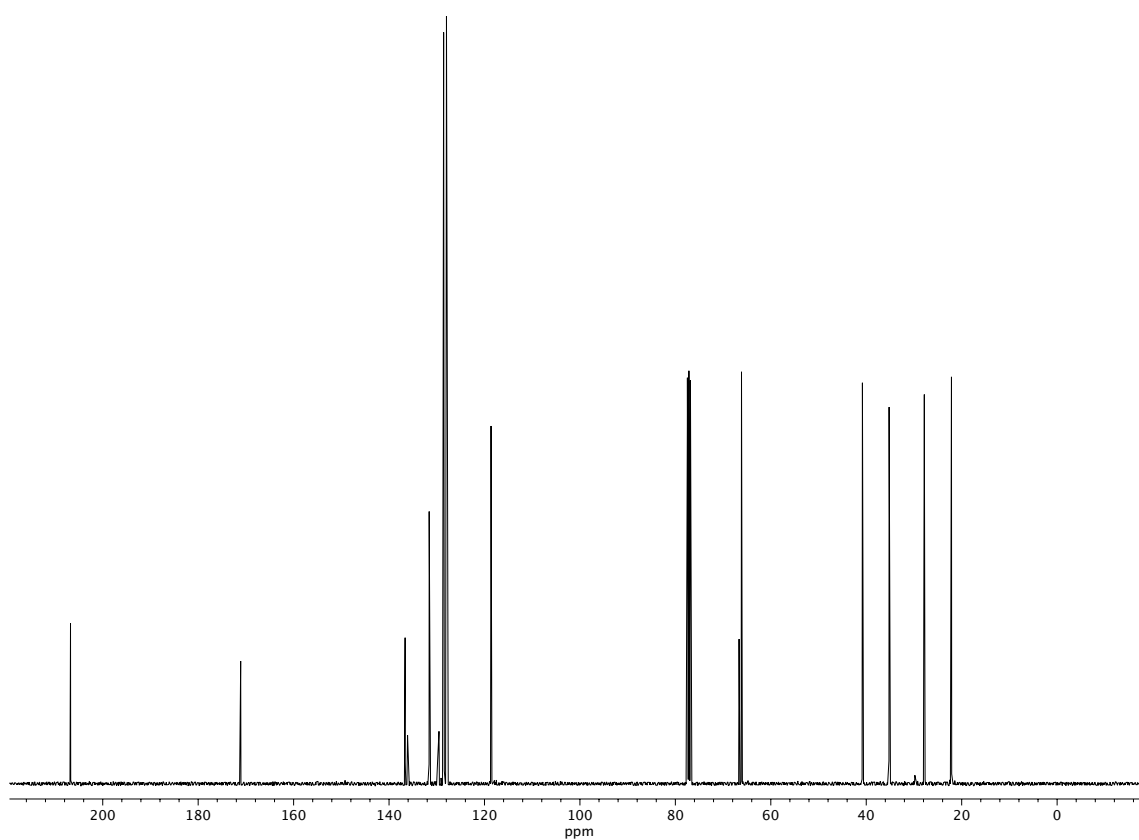
Figure A1.3. ^{13}C NMR (100 MHz, CDCl$_3$) of compound **20**.

CHAPTER 2

Analysis of the Pd [π2s + π2s + σ2s + σ2s] Pericyclic Reaction†

2.1 INTRODUCTION

Selectivity in pericyclic reactions is a tangible manifestation of the quantum mechanical wave-like behavior of electrons. Bringing an acyclic system to a cyclic transition state introduces constructive/destructive interferences amongst the spatial wavefunctions of the component electrons, which are governed by orbital orthogonality requirements as prescribed by the Pauli principle. With proper constructive overlaps, the bond order of the transition state will match that of the reactant(s) and product(s) – *i.e.,* net covalent bonding is *maintained* through the transition state. Alternatively, destructive interferences are incurred that do not allow for continual bonding – *i.e.,* a covalent bonding interaction is *lost*, and the electronic configuration is that of a diradical. Several conceptual frameworks are commonly employed to analyze the nature of bonding in pericyclic transition states, though these are simply different projections of the same underlying physics. These tools include orbital and state correlation diagrams, frontier molecular orbital (FMO) theory, [1] the orbital phase continuity principle [2] in valence bonding wavefunctions, and the concept of transition state (anti)aromaticity. [3]

Pericyclic reactivity is also commonplace in organometallic systems. [4] In fact, the elementary step responsible for enantioinduction in the inner-sphere asymmetric Tsuji

allylic alkylation is C–C bond formation through a synchronous, seven-membered pericyclic transition state (**TS20**) (Figure 2.1A).[5] Since the original computational reports by our groups [6] and others, [7] the relationship between this class of seven-membered transition states to those of the canonical pericyclic reactions as described by Woodward and Hoffmann is underexplored. [8] Exemplifying the peculiar nature of the reaction, an analogous transformation in a system comprised of main group elements remains elusive.[9] Given the key role of this seven-membered pericyclic process in asymmetric catalysis, we sought to delineate the underlying reactivity paradigm that enables this unique transformation (Figure 2.1B).

Figure 2.1. *Seven-centered cyclic transition states in Pd catalysis.*

2.2   RESULTS AND DISCUSSION
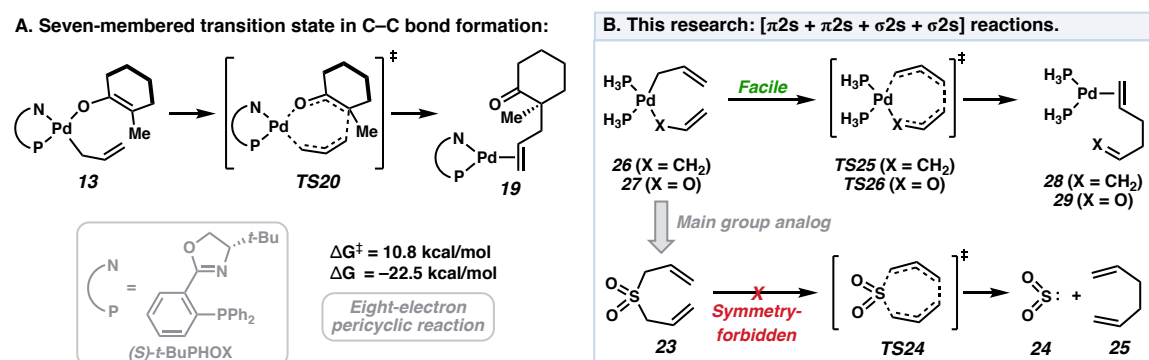
To obtain a general understanding of this bond forming event, we first examined an analogous system comprised of main group elements, namely the reaction of diallyl sulfone (**23**) to sulfur dioxide (**24**) and 1,5-hexadiene (**25**) (Figure 2.1B). If the geometry of the seven-membered cheletropic transition state (**TS24**) is constrained to match that of **TS20**, then a suprafacial relationship amongst the eight correlating orbitals with linear departure of the chelefuge is mandated. Thus, the transformation of **23** to **24** + **25** is designated [π2s

+ π2s + σ2s + σ2s] and the reverse as [ω2s + π2s + π2s + σ2s]. With four suprafacial two-electron terms, the ground-state pericyclic reaction of **23** to **24** + **25** is anticipated to be symmetry-forbidden by the generalized Woodward–Hoffmann rules.[8] An identical conclusion is reached for chelefuges such as CO and N_2 in the ground state.[10] Given the low thermal barriers with which the Pd-catalyzed transformations proceed ($\Delta G^{\ddagger} = 10$–20 kcal/mol),[5] we became curious as to whether the transformation is similarly forbidden for a L_nPd^0-like chelefuge.

To uncover the electronic origins that enable the transition metal-mediated pericyclic processes, we turned to ab initio Quantum Mechanics (QM) calculations. Calculations were carried out with the ORCA ab initio package (see 2.4. Supporting Information for full details).[11] Complete active space self-consistent field (CASSCF) theory is utilized to capture the multiconfigurational nature of the potential energy surface (PES), where the (8,8) active space is defined to be the eight valence electrons in eight correlating orbitals as described by orbital correlation diagrams. Dynamical correlation is accounted for via N-electron valence state perturbation theory[12] (NEVPT2) single point calculations on the CASSCF wavefunctions. All geometry optimizations and frequency calculations were carried out with the triple-ζ quality def2-TZVP basis set[13] on all atoms (with the small core ECP28MWB pseudopotential[14] on Pd, *i.e.,* 18 explicit electrons including the 4s and 4p core electrons). For transition metal complexes with insignificant multiconfigurational character, geometries were obtained with density functional theory (DFT) (PBE0-D3(BJ)/def2-TZVP)[15] followed by CASSCF/NEVPT2 single point calculations with the def2-TZVPP basis set. Solvation was accounted for in single point

Figure 2.2. *(A) Orbital correlation diagram for the [π2s + π2s + σ2s + σ2s] quasi-cheletropic reaction of diallyl sulfone.[a] (B) Symmetry-forbidden C–C bond formation from diallyl sulfone **23**.[b]*

A. Orbital correlation diagram for the [π2s + π2s + σ2s + σ2s] reaction of diallyl sulfone:
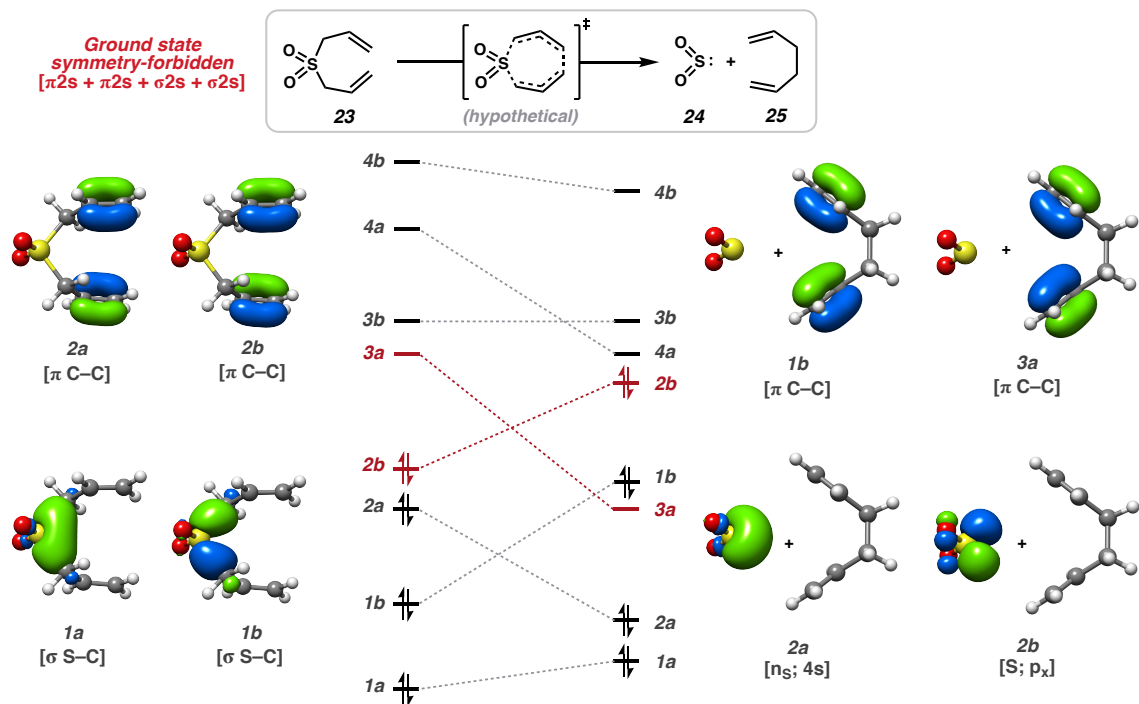
B. Ground state reaction of *23* to *24* + *25*:
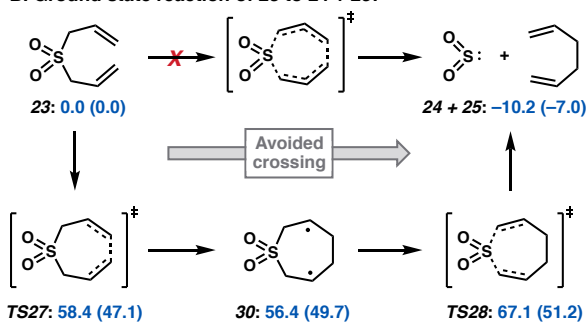
C. Electronic structure of diradical *30*:
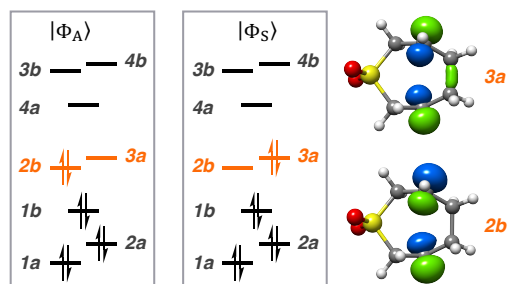
[a] Select natural orbitals from the CAS(8,8) active space shown. [b] CASSCF-based free energy estimates in kcal/mol with the NEVPT2 corrected values in parentheses.

calculation with the SMD model for THF.[16] All energies reported are solvated free energies at 298.15 K.

Beginning with main group analog diallyl sulfone (**23**), generation of symmetry-adapted linear combinations of correlating valence orbitals under approximate C_2 symmetry affords symmetric (*a*) and antisymmetric (*b*) sets of σ/σ^*(C–S) and π/π^*(C–C) orbitals (Figure 2.2A). Correlating these orbitals to those of the product implies an avoided crossing along the ground sate potential energy surface (PES) as the diabatic state describing **23**, $|\Phi_A\rangle$, corresponds to a doubly excited state of the products. Likewise, a single transition state connecting **23** to **24** + **25** was not found on the CASSCF potential energy surface. Rather, a stepwise process involving singlet diradical intermediate **30** was found (Figure 2.2B).[17] At this point, the ground state configuration interaction (CI) vector possesses nearly equal contributions of configurations $|\Phi_S\rangle$ and $|\Phi_A\rangle$, leading to a diradical index d = 98.0% (Figure 2.2C).[18] Calculations with multireference iterative Difference Dedicated CI (IDDCI) theory provide d = 95.4% and a singlet/triplet exchange coupling constant (J) of 83 cm^{-1}.[19]

In summary, the required crossing of the starting material (**23**) and product (**24** + **25**) diabatic ground states renders the concerted [π2s + π2s + σ2s + σ2s] reaction symmetry-forbidden. The ground state PES of **23** → **24** + **25** is characterized by a stepwise mechanism involving weakly coupled diradical **30**, with an overall $\Delta G^{\ddagger}$ of >50 kcal/mol — contrasting the low thermal barriers of Pd-catalyzed transformations ($\Delta G^{\ddagger}$ = 10–20 kcal/mol).[5] Given this, we became curious as to whether the Pd-catalyzed transformation is similarly symmetry-forbidden, proceeding through a low energy diradical intermediate/state, or whether a unique set of symmetry elements describe the transformation that conserves orbital symmetry through the reaction.

In order to probe this hypothesis, we first considered the case of a simplified bis-(η^1–allyl)Pd^{II} complex **26** (Figure 2.3A). Contrary to **23**, we find a single low energy transition state (**TS25**), with $\Delta G^{\ddagger}$ =13.4 kcal/mol, on the spin-restricted DFT (PBE0-D3(BJ)/def2-TZVP) PES connecting **26** to **28** (Figure 2.3B). We obtain a similar result for (η^1-allyl)Pd^{II} enolate **27**. We find that the ground-state single-determinant wavefunction along the PES is stable with respect to symmetry breaking, suggesting a single closed-shell singlet (CSS) configuration is dominant. The existence of a saddle point smoothly connecting **26** to **28** on a PES derived from the CSS state of a single-determinant wavefunction points to the absence of an avoided crossing. Moreover, this suggests that simple DFT geometries should be reliable for these Pd complexes and will be used in the following.

For comparison to the symmetry-forbidden transformation of **23** to **24** + **25**, we construct the corresponding orbital correlation diagram for the conversion of **26** to **28** (Figure 2.3A). The four occupied correlating orbitals of starting complex **6** are identical in symmetry to those of diallyl sulfone **13** (two *a* and two *b* symmetry elements). However, unlike the products of the thermally-forbidden reaction (**24** + **25**), complex **28** maintains the symmetry of ground-state minimum **26**. This is further evident in the composition of the ground-state CASSCF wavefunction at **TS25**, with weights of 0.86 and 0.02 for the dominant CSS configuration and second largest contributor, respectively. Note the absence of configurations corresponding Zwitterionic states or mixing of ground and doubly excited states describing a diradical configuration. Control experiments do not find evidence of redox noninnocence of the PHOX ligand scaffold. Thus, our calculations suggest the Pd

[π2s + π2s + σ2s + σ2s] reaction is symmetry-allowed. While introducing heteroatoms into the system formally lowers the symmetry, this has no effect on the underlying physics. Hence, the transformation of Pd^{II} enolate complex **27** to **29** is also symmetry-allowed in the ground-state (Figure 2.3B).

The symmetry of the lone pair-like orbital of the chelefuge differentiates between the thermally-allowed and forbidden scenarios. In ground state SO_2, the lone pair occupies a symmetric sp^2 valence orbital (*2a* in Figure 2.2A), whereas in **8/9**, this corresponds to the antisymmetric Pd-based $d(x^2–y^2)$ orbital (*2b* in Figure 2.3A). Thus, the eight-electron seven-membered pericyclic transition is thermally-allowed in the case of Pd complexes **27**, **29**, and **13** by virtue of the parity of the $d(x^2–y^2)$ orbital involved in σ bonding with the organic scaffold (Figure 2.3C).[20] Other metal-based d orbitals can be included in this analysis but bear no consequence as these orbitals remain doubly occupied throughout the transformation.

From the perspective of frontier molecular orbital (FMO) theory, the transformation is readily interpreted as the (in)ability of the chelefuge HOMO/donor to constructively interact with the antisymmetric LUMO/acceptor of the 1,5-hexadiene in the appropriate geometry (Figure 2.4A). If constructive overlap is achieved, then *net bonding is preserved through the transition state* and the reaction is symmetry-allowed.[20a–b] This is the case for the Pd-catalyzed transformation as the Pd-based $d(x^2–y^2)$ HOMO of hypothetical L_2Pd^0 chelefuge σ bonds with the diene in a suprafacial/antaranodal fashion, *i.e.*, with phase inversion, constructively mixing with the diene LUMO (Figure 2.4A).[21] This is not the case for the symmetric nucleophile lone pair orbitals of SO_2 and CO.[10]

Figure 2.3. *(A) Orbital correlation diagram for the pericyclic reaction of **26** to **28**. Select natural orbitals of CAS(8,8) wavefunction shown. (B) Free energy changes and barriers (in kcal/mol). (C) Orbital topologies.*

A. Orbital correlation diagram for the [π2s + π2s + σ2s + σ2s] reaction of bis-(η¹–allyl)Pd^{II} complex *26*:

B. The [π2s + π2s + σ2s + σ2s] reaction of *6/7* to *8/9*:

26   TS25   28
ΔG‡ = 13.4 (12.3); ΔG = −27.8 (−29.9)

27   TS26   29
ΔG‡ = 13.8 (13.7); ΔG = −31.5 (−38.8)
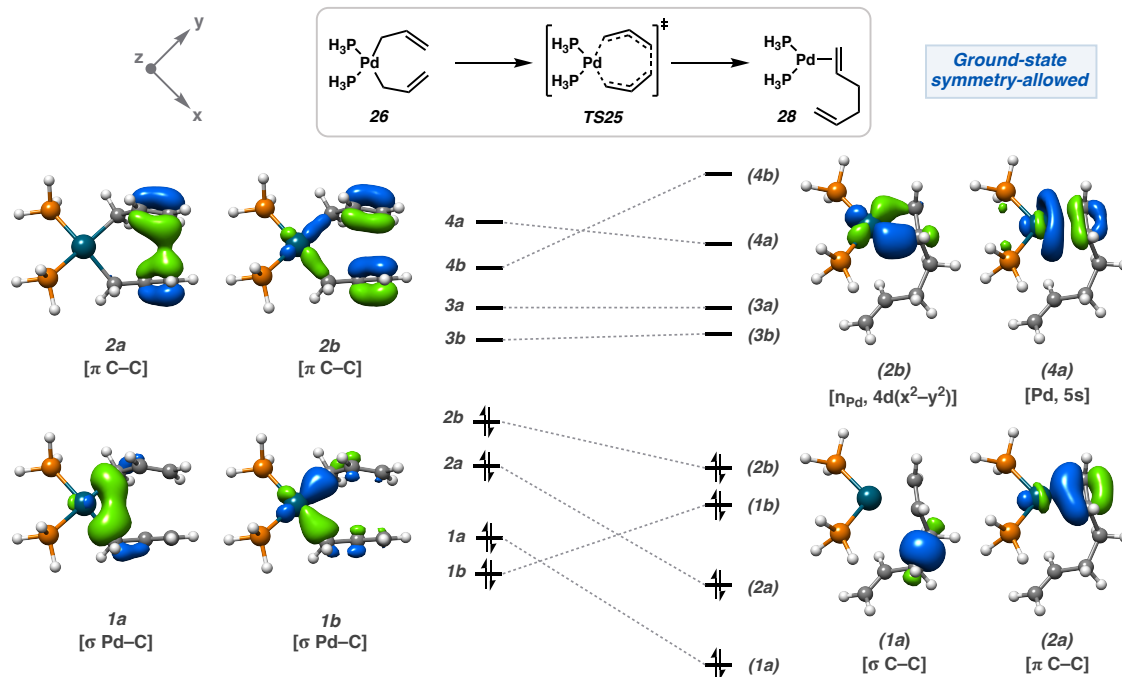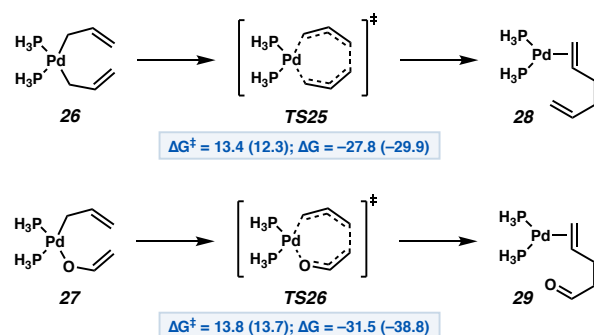
C. Relevant orbital topologies:
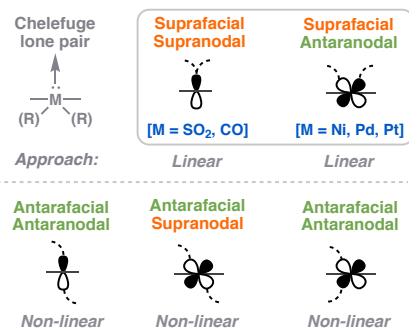
[a] Free energies calculated using NEVPT2 electronic energies with thermal corrections and geometries from DFT (PBE0-D3(BJ)). Full DFT energies in parenthesis.

Figure 2.4. *(A) FMO perspective of the [π2s + π2s + σ2s + σ2s] reaction. (B) Relevant MOs from the CAS(8,8) active space that contribute to the aromaticity of* **TS25**. *(C) NICS analysis of* **TS25** *(green and red spheres denote negative and positive NICS values).*[a]

A. Reactivity paradigm from FMOs:

Allowed   Forbidden

donor   acceptor   donor   acceptor

B. Elements of Craig–Möbius aromaticity in TS25:

HOMO

HOMO –2

C. NICS analysis of TS25:

−19.4
+1.0
3.1 Å
+0.5   4.7 Å
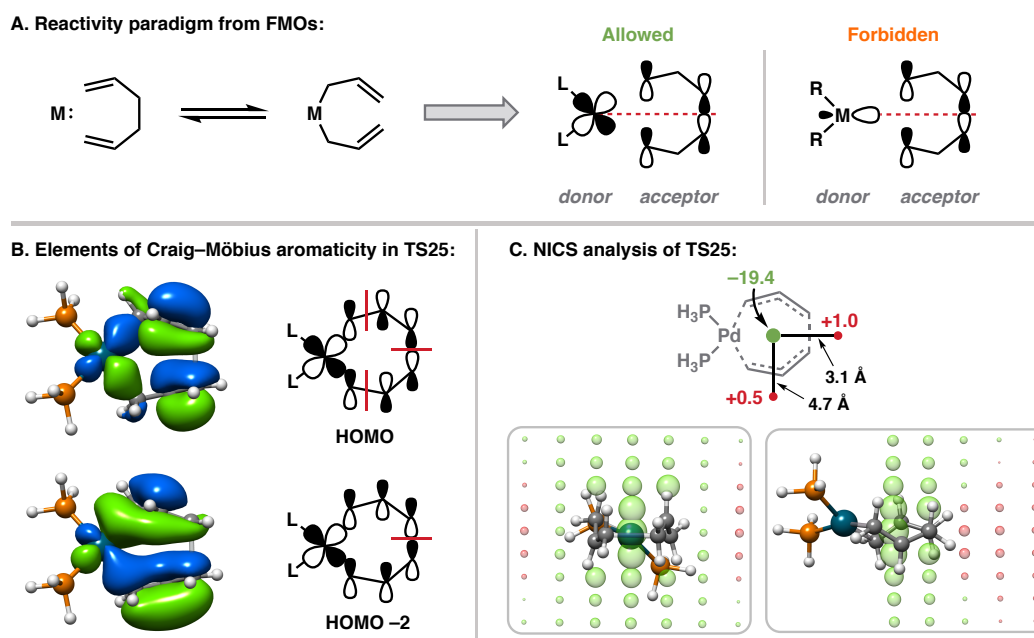
[a] NICS values in ppm with sphere radius depicting magnitude of the shift ($r = \left(\left|\delta_{ppm}\right|\right)^{1/3}$).

It is well understood that concerted, symmetry-allowed pericyclic reactions proceed through aromatic transition states.[3] Thus, if the Pd [π2s + π2s + σ2s + σ2s] reaction of **26** to **28** is indeed symmetry-allowed, then **TS25** should be aromatic in nature. From analysis of the active space MOs at **TS25** we find elements of Craig–Möbius-like aromaticity within the σ bonding framework.[22] Of particular interest, the HOMO and HOMO–2 conform to a Möbius topology with the Pd $d(x^2-y^2)$ generating a phase inversion and an odd number of nodes (1 and 3) along the ring (Figure 2.4B).[23] To probe this suspected aromaticity, we

employ the Nucleus-Independent Chemical Shift (NICS) method of Schleyer and coworkers.[24] A NICS(0) of –19.4 ppm is calculated at the geometric center of the seven-membered ring of **TS25**, indicating aromaticity.[25] Likewise, a positive NICS is found at various points along the external periphery. For enhanced visualization, the NICS at points along 2D grids are displayed in Figure 2.4C.

A principal objective of our investigation is to relate electronic structure to intuitive concepts in chemical bonding. As such, we sought to explore whether the Pd-catalyzed [π2s + π2s + σ2s + σ2s] transformation could be properly described by valence bonding concepts such as the ubiquitous "arrow-pushing" formalism of Robinson and Ingold.[26] Given the single-configurational nature of the ground state density, the concept of bond reorganization is addressed through analysis of Intrinsic Bonding Orbitals (IBOs) as described by Knizia and co-workers.[27] Previously, IBO analysis was implemented to highlight "electron flow" through transition states, discern between classes of mechanisms, and evaluate synchronicity of bond making/breaking in these events.[27] Generation of IBOs proceeds through a Pipek–Mezey-style localization of Kohn–Sham orbitals where orbital charge contribution to an atomic center is measured by Intrinsic Atomic Orbital (IAO) charge.[27a–b] At no point in the localization are empirical concepts of valence bonding introduced, yet IBOs correspond well to two-center two-electron bonds (or lone pairs) as depicted in Lewis structures. IBOs of forming/breaking bonds at transition structures generally resemble three-center two-electron bonds describing the transformation of one localized bond to another. Hence, the progression of IBOs along a reaction coordinate offers a connection to the "arrow-pushing" formalism of Robinson and Ingold. So long as

the localized orbitals are adequately portrayed by a Lewis structure and the system is well described by a single reference wavefunction then there is utility in such analysis.

IBO analysis was carried out with the full (PHOX)Pd enolate system (Figure 2.5). Four IBOs (ϕ_i) undergo significant displacement along the intrinsic reaction coordinate (IRC) through **13**→**TS20**→**19**.[28] The first of these, ϕ_1, corresponds to the localized π(C–C) bond of the enolate fragment, which smoothly progresses to encapsulate the density of the newly formed σ(C–C) bond of the product. Likewise, ϕ_2, ϕ_3, and ϕ_4 track the transformations of π(C–C) → π(C–C)', σ(Pd–C) → n(Pd; d(x^2–y^2)),[29] and σ(Pd–O) → π(C–O), respectively. Considering these transformations together reveals an intrinsic directionality to the evolution of the local orbitals in the Pd-catalyzed [π2s + π2s + σ2s + σ2s] reaction. Inspection of the relative magnitudes of net orbital displacement along the IRC further suggests synchronicity in the bond making/breaking events of the [π2s + π2s + σ2s + σ2s] process (Figure 2.5). In accord with the initial reports of Knizia and co-workers, we also find the localized IBOs obtained from the ground state densities closely resemble valence orbitals as portrayed in simple Lewis structures. Thus, tracking the net flow of electron density is carried out in the same valence bonding framework. The result is a mechanism described by the synchronous movement of valence bonding electron pairs, or more precisely, a first principles-derived "arrow-pushing" mechanism that accounts for the net change in bonding along the reaction coordinate in a chemically intuitive orbital basis (Figure 2.5).[27b–c]

Figure 2.5. *IBO analysis the Pd [π2s + π2s + σ2s + σ2s] reaction.*
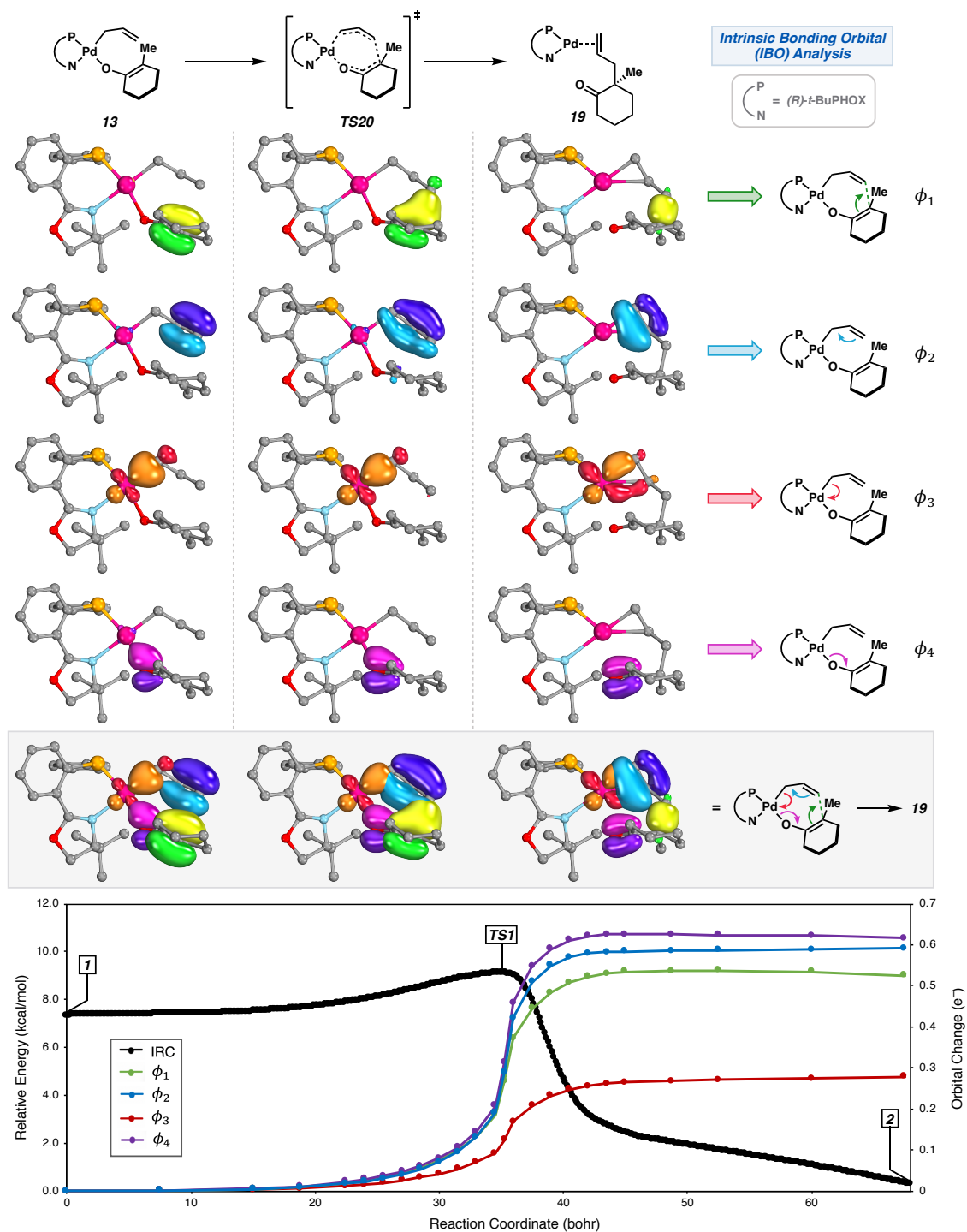
[a] Note that the *R* enantiomer of the *t*-BuPHOX ligand employed. Select atoms omitted for clarity.

2.3   CONCLUSIONS

In conclusion, we find the Pd-catalyzed [π2s + π2s + σ2s + σ2s] reaction to be symmetry-allowed in the ground-state owing to phase inverting role of the Pd $d(x^2–y^2)$ orbital in the σ bonding framework of the transition state. Insights from this investigation are contextualized within the Woodward–Hoffmann rules, orbital correlation diagrams, and FMO theory. As with prototypical thermally-allowed pericyclic reactions, we find the Pd-catalyzed [π2s + π2s + σ2s + σ2s] reaction proceeds through an aromatic transition state. Lastly, we describe a first principles-derived "arrow-pushing" mechanism from analysis the transformation of IBOs along the reaction coordinate. These efforts highlight the connection between ab initio electronic structure calculations and empirical bonding concepts, thus, facilitating a natural conceptualization of chemical bonding in these unique systems.

2.4   SUPPORTING INFORMATION

2.4.1   GENERAL COMPUTATIONAL DETAILS

All quantum mechanical calculations were performed with ORCA version 4.1 and 4.2.[11] Geometries of open-shell species (**TS27**, **30**, and **TS28**) and their precursors (**23**, **24** and **25**) were optimized with complete active space self-consistent field (CASSCF) theory. The active space was defined as the correlating valence electrons and orbitals as obtained by the corresponding orbital correlation diagrams (see below). The triple-ζ quality def2-TZVP basis set[13] was used on all atoms. Further details on choice of active spaces are provided below. Results obtained via broken-symmetry density functional theory (BS-DFT) are provided below for comparison. For transition metal complexes with insignificant

multiconfigurational character (**26**, **27**, **TS25**, **TS26**, **28**, and **29**), geometries were obtained from dispersion-corrected DFT. The PBE0 global hybrid density functional[15] paired with Becke–Johnson damped D3 dispersion corrections (henceforth referred to as PBE0-D3(BJ)) and the def2-TZVP basis set on all atoms was employed. The small-core ECP28MWB pseudopotential[14] was used on Pd (18 explicit electrons including the 4s and 4p core shells are defined).

To account for dynamical correlation, N-electron valence state perturbation theory[12] (NEVPT2) single point calculations were carried out on all stationary points (CASSCF and DFT geometries) from the corresponding CAS references. The strongly contracted variant of NEVPT2 was employed. Solvation was accounted for in these single point calculations with the SMD model for THF.[16] In addition to single point calculations with NEVPT2/def2-TZVPP/SMD(THF), for the compounds that were optimized with PBE0-D3(BJ)/def2-TZVP, additional single point calculations were carried out with PBE0-D3(BJ)/def2-TZVP/SMD(THF) for comparison.

Thermal corrections were obtained from the unscaled vibrational frequencies computed at the level of theory employed for geometry optimization. The Quasi-RRHO method [30] was applied to correct for the breakdown of the harmonic oscillator approximation in low frequency vibrations. For CASSCF and DFT calculations these frequencies were computed numerically and analytically, respectively. All stationary points were characterized by the appropriate number of imaginary vibrational modes (zero for optimized geometries and one for transition states). Intrinsic reaction coordinate (IRC) analyses were carried out to ensure all transition states connect saddle points to the

appropriate minima. Conformer searching was carried out manually and energies reported are from lowest energy conformers. All energies reported in the manuscript are free energies calculated at 298.15 K and at a 1 atm standard state. Applying thermal corrections obtained at the optimization level of theory to the single point electronic energies (and solvation free energies), final Gibbs free energies are accordingly:

$$G_{solv} = E(el)^{SP} + ZPE + E(vib) + E(rot) + E(trans) + k_b T - TS + \Delta G(solv)^{SP}$$

The resolution of identity (RI) and chain-of-spheres[31] (keyword = RIJCOSX) approximations were utilized for coulomb and exchange integrals, respectively. Automatic generation of auxiliary basis sets was employed (keyword = AutoAux).[32] [Note that in geometry optimization, frequency, and IRC calculations with CASSCF, the RI and COS approximations were not used as they are not implemented with analytical (nuclear) gradients in ORCA version 4.2.0]. The finest integration grid settings (Grid7, GridX9, NoFinalGrid) were utilized in all calculations.

2.4.2   NEVPT2/CASSCF ACTIVE SPACE RESULTS

Unless otherwise specified, energies provided below are solvated CASSCF and NEVPT2 free energies (in Hartree) with the def2-TZVP basis set and SMD implicit solvation model for THF. Energies further refined with the def2-TZVPP basis set are provided in the text and supporting excel document (nearly identical results were obtained). Weights (C_i^2) of the three configurations with the largest contributions to the ground state CI coefficient vector are provided. The notation [2200] corresponds to a configuration with double occupancy of the first and second MOs of the active space and zero occupancy of the third and fourth active space MOs. Unless otherwise noted, active space MOs are

depicted as the natural orbitals of the CAS wavefunction and are rendered with a contour value of 0.07. Active spaces were chosen to include the correlating valence orbitals as determined by the corresponding Woodward–Hoffmann orbital correlation diagrams.[8] The active space may be localized to confirm the correct active space compositions. Unless otherwise specified, state-averaging was not employed, and results are that of the lowest energy singlet state. Occupancy numbers are provided in parentheses next to MO numbers. Orbital energy eigenvalues (from NEVPT2) are listed when the ordering of the active space MOs by occupancy number is different than the ordering by energies.

Figure 2.6. *MCSCF active space orbitals and energies of complex **13**.[a]*
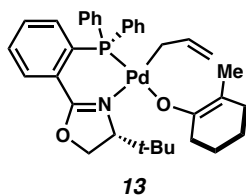
CASSCF(8,8)	-2022.394386
NEVPT2(8,8)	-2030.146571
Weight	Configuration
0.87749	[22220000]
0.02871	[21211010]
0.02357	[22020200]
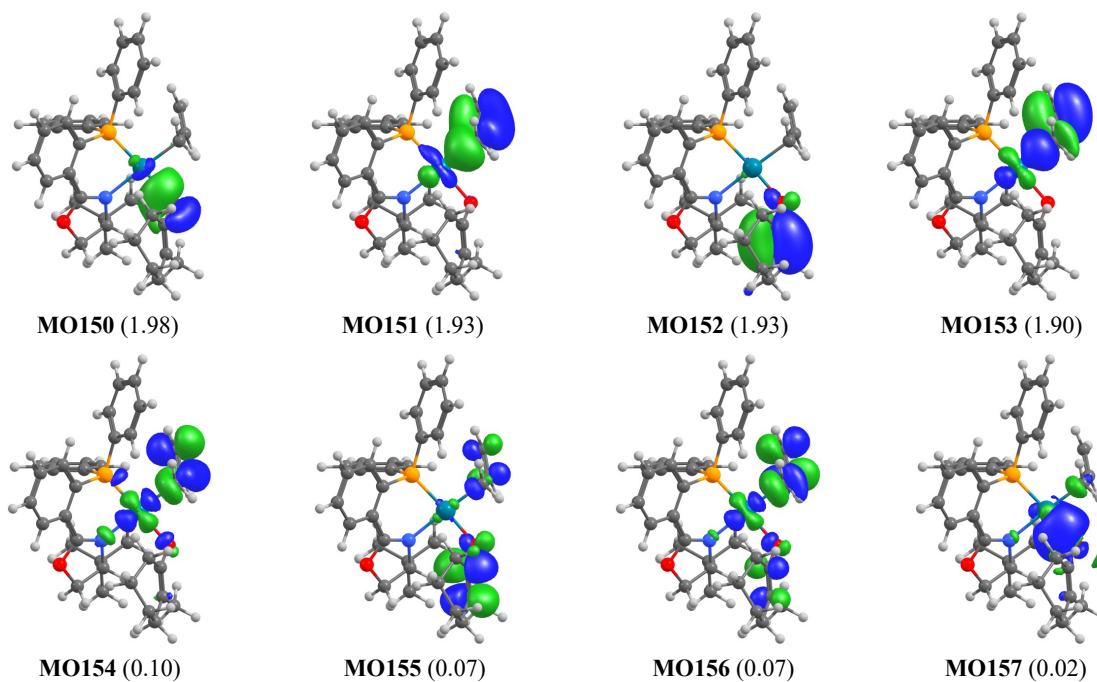
MO150 (1.98)   **MO151** (1.93)   **MO152** (1.93)   **MO153** (1.90)

MO154 (0.10)   **MO155** (0.07)   **MO156** (0.07)   **MO157** (0.02)

[a] Geometry taken from reference 5 (BP86-D3/LANL2TZ(f)[Pd],6-31G(d)). Energies above are CASSCF and NEVPT2 solvated electronic energies in Hartree. Orbital energy eigenvalues (by ascending MO) in eV: –0.5516, –0.4294, –0.2868, –0.3067, 0.1907, 0.3014, 0.3116, 0.9729. Isosurface level adjusted to 0.03 for ease of visualization.

Figure 2.7. *MCSCF active space orbitals and energies of* **TS20**.[a]
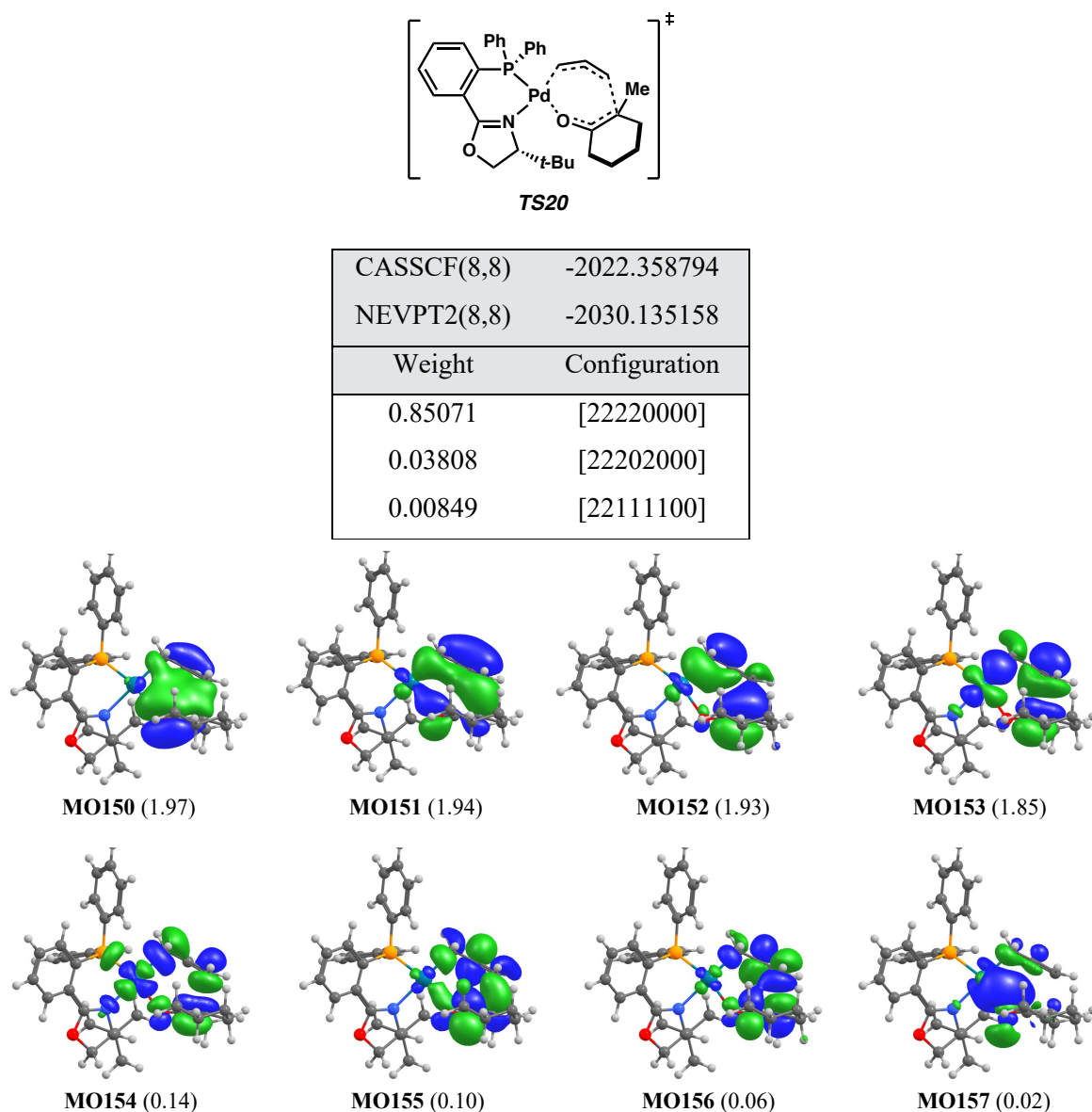
TS20

CASSCF(8,8)	-2022.358794
NEVPT2(8,8)	-2030.135158
Weight	Configuration
0.85071	[22220000]
0.03808	[22202000]
0.00849	[22111100]

MO150 (1.97)   **MO151** (1.94)   **MO152** (1.93)   **MO153** (1.85)

MO154 (0.14)   **MO155** (0.10)   **MO156** (0.06)   **MO157** (0.02)

[a] Geometry taken from reference 5 (BP86-D3/LANL2TZ(f)[Pd],6-31G(d)). Energies above are CASSCF and NEVPT2 solvated electronic energies in Hartree. Orbital energy eigenvalues (by ascending MO) in eV: –0.5101, –0.4084, –0.3196, –0.2322, 0.1617, 0.2167, 0.3781, 0.7215. Isosurface level adjusted to 0.04 for ease of visualization.

Figure 2.8. *MCSCF active space orbitals and energies of complex* **19**.[a]
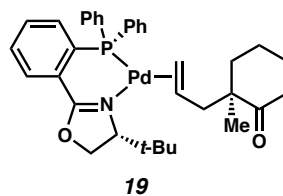
CASSCF(8,8)	-2022.420396
NEVPT2(8,8)	-2030.191318
Weight	Configuration
0.90785	[22220000]
0.02896	[22020200]
0.02830	[22202000]
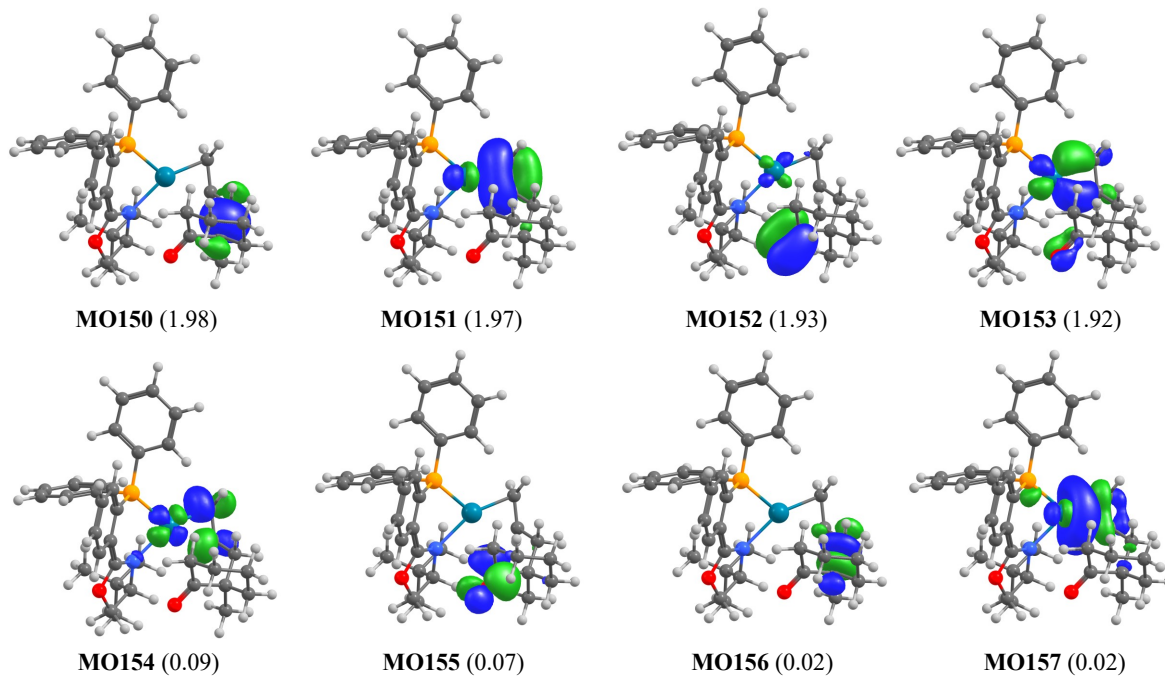
MO150 (1.98)   MO151 (1.97)   MO152 (1.93)   MO153 (1.92)

MO154 (0.09)   MO155 (0.07)   MO156 (0.02)   MO157 (0.02)

[a] Geometry taken from reference 5 (BP86-D3/LANL2TZ(f)[Pd],6-31G(d)). Energies above are CASSCF and NEVPT2 solvated electronic energies in Hartree. Orbital energy eigenvalues (by ascending MO) in eV: –0.6097, –0.4323, –0.4795, –0.3032, 0.2540, 0.2951, 0.7745, 0.5139. Isosurface level adjusted to 0.04 for ease of visualization.

Figure 2.9. *MCSCF active space orbitals and energies of diallyl sulfone **23**.*
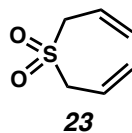
CASSCF(8,8)	-780.349971
NEVPT2(8,8)	-782.106985
Weight	Configuration
0.90106	[22220000]
0.03843	[22111100]
0.01005	[22202000]

MO35 (1.98)   **MO36** (1.98)   **MO37** (1.98)   **MO38** (1.08)

MO39 (0.92)   **MO40** (0.02)   **MO41** (0.02)   **MO42** (0.02)
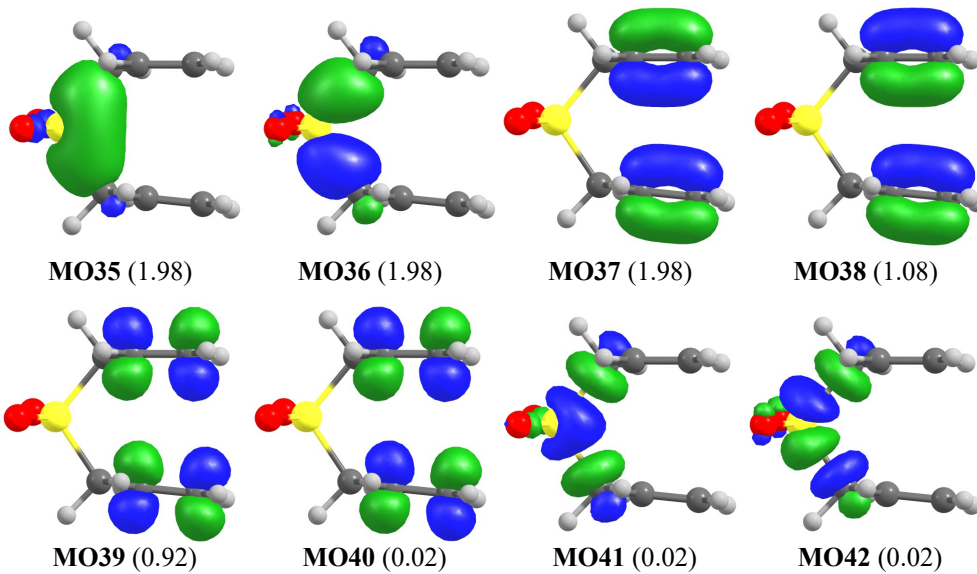
Figure 2.10. *MCSCF active space orbitals and energies of **TS27**.*

TS27
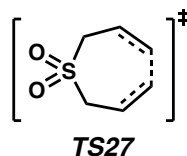
CASSCF(8,8)	-780.258382
NEVPT2(8,8)	-782.031183
Weight	Configuration
0.68584	[22220000]
0.26002	[22202000]
0.01996	[22111100]

MO35 (1.98)   **MO36** (1.98)   **MO37** (1.95)   **MO38** (1.44)

MO39 (0.56)   **MO40** (0.05)   **MO41** (0.02)   **MO42** (0.02)
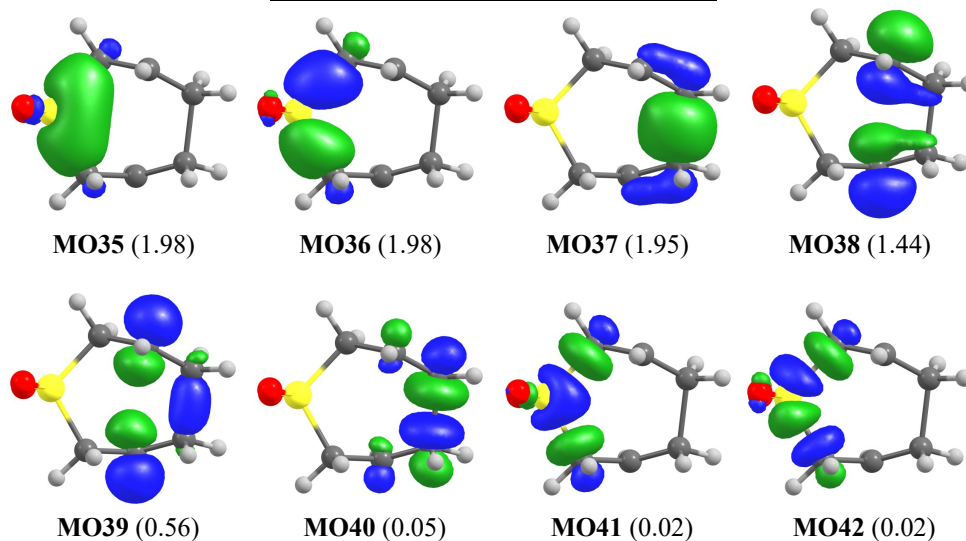
Figure 2.11. *MCSCF active space orbitals and energies of diradical* **30**.
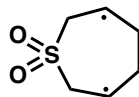
30

CASSCF(8,8)	-780.261600
NEVPT2(8,8)	-782.026896
Weight	Configuration
0.52173	[22220000]
0.44492	[22202000]
0.00405	[12120101]
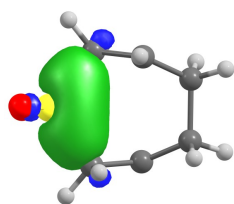
MO35 (1.98)   **MO36** (1.98)   **MO37** (1.98)   **MO38** (1.08)
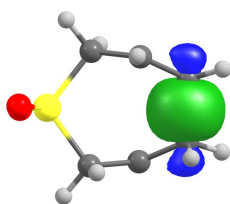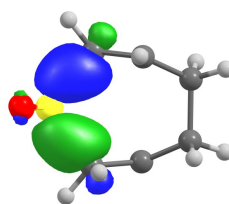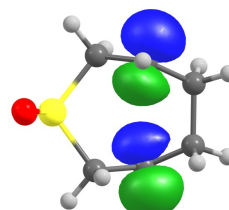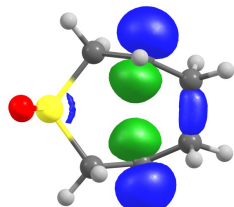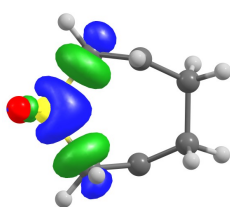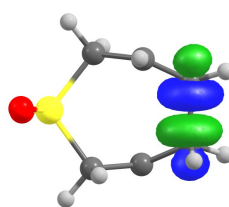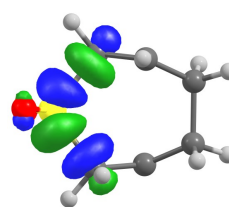
MO39 (0.92)   **MO40** (0.02)   **MO41** (0.02)   **MO42** (0.02)

Figure 2.12. *MCSCF active space orbitals and energies of **TS28**.*

TS28
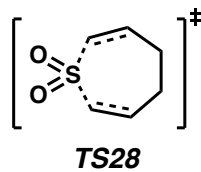
CASSCF(8,8)	-780.244658
NEVPT2(8,8)	-782.024561

Weight	Configuration
0.61644	[22220000]
0.29502	[22202000]
0.04355	[22111100]

MO35 (1.98)   **MO36** (1.98)   **MO37** (1.92)   **MO38** (1.33)

MO39 (0.67)   **MO40** (0.08)   **MO41** (0.03)   **MO42** (0.02)
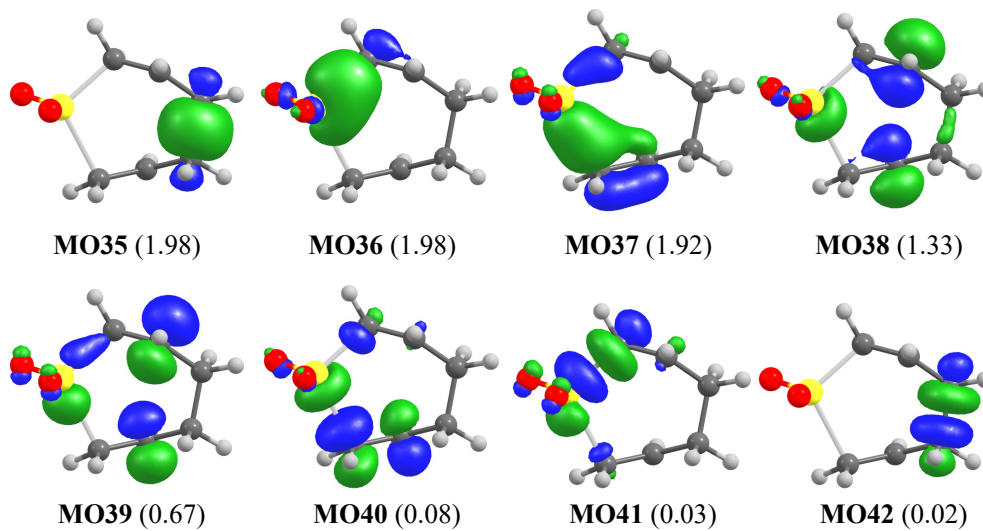
Figure 2.13. *MCSCF active space orbitals and energies of SO$_2$ (**24**).*

24
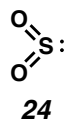
CASSCF(2,2)	-547.345604
NEVPT2(2,2)	-548.090971
Weight	Configuration
0.98002	[20]
0.01998	[02]
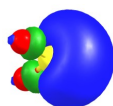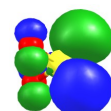
MO15 (1.96)   **MO16** (0.04)

Figure 2.14. *MCSCF active space orbitals and energies of (s-cis)-1,5-hexadiene (**25_cis**).*[a]
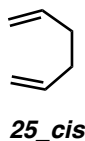
25_cis

CASSCF(6,6)	-233.022382
NEVPT2(6,6)	-234.026032
Weight	Configuration
0.91161	[222000]
0.03853	[211110]
0.01066	[220200]

MO20 (1.98)   **MO21** (1.92)   **MO22** (1.92)

MO23 (0.08)   **MO24** (0.08)   **MO25** (0.02)
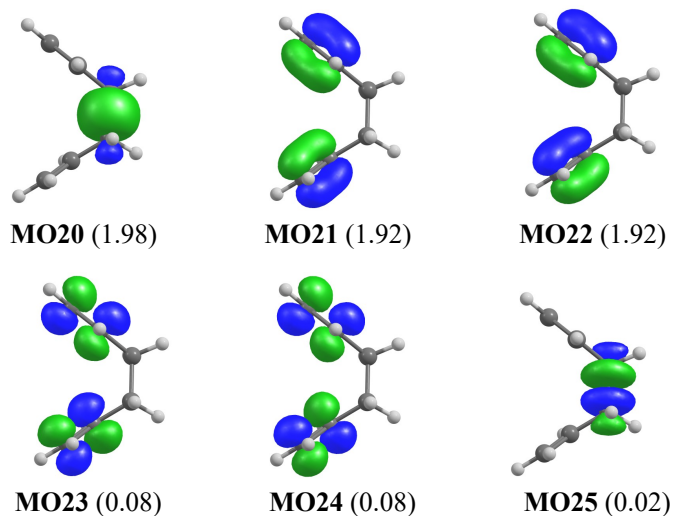
[a] Active space orbitals for compound **25_cis**. (Not visible at isosurface printed above: MO23 and MO24 experience slight mixing with MO25 and MO20, respectively, such that the resulting orbital energy eigenvalue for MO23 is lower than that of the symmetric MO24 (0.2332 eV and 0.2374 eV).

Figure 2.15. *MCSCF active space orbitals and energies of (s-trans)-1,5-hexadiene* (**25_trans**).
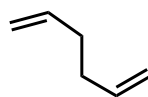
25_trans

CASSCF(6,6)	-233.004232
NEVPT2(6,6)	-234.022461
Weight	Configuration
0.92057	[222000]
0.03724	[211110]
0.00985	[202200]
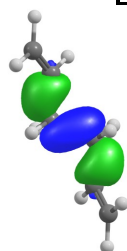
MO20 (1.99)   **MO21** (1.92)   **MO22** (1.92)
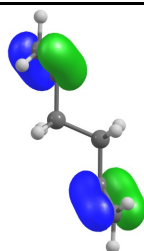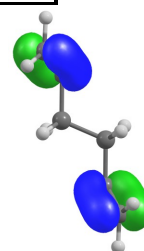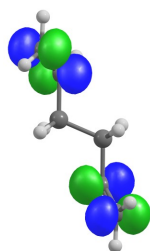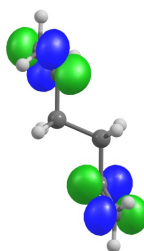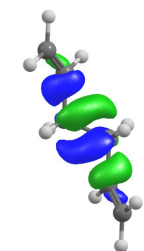
MO23 (0.08)   **MO24** (0.08)   **MO25** (0.00)*

Figure 2.16. *MCSCF active space orbitals and energies of complex* **26**.[a]

26
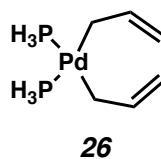
CASSCF(8,8)	-1044.976965
NEVPT2(8,8)	-1047.103294
Weight	Configuration
0.88527	[22220000]
0.01649	[22111100]
0.01002	[21211010]

MO46 (1.97)   **MO47** (1.95)   **MO48** (1.92)   **MO49** (1.92)

MO50 (0.09)   **MO51** (0.07)   **MO52** (0.06)   **MO53** (0.02)
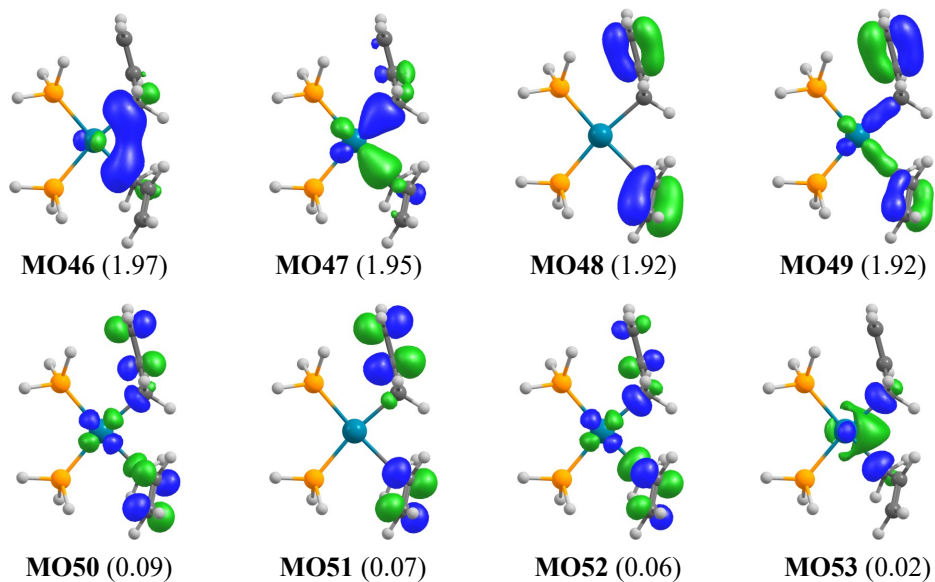
[a] Active space orbitals for compound **26**. Orbital energy eigenvalues (by ascending MO) in eV: –0.4110, –0.4486, –0.3197, –0.3230, 0.1931, 0.2702, 0.3169, 0.6241. In this (low energy) conformation, the antisymmetric Pd–L σ* and the antisymmetric C–C π* symmetry adapted linear combinations mix to give rise to MO50 and MO52.

Figure 2.17. *MCSCF active space orbitals and energies of complex* ***27***.[a]
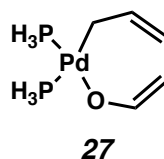
CASSCF(8,8)	-1080.874182
NEVPT2(8,8)	-1083.041153
Weight	Configuration
0.88716	[22220000]
0.03125	[22111100]
0.02575	[20220020]
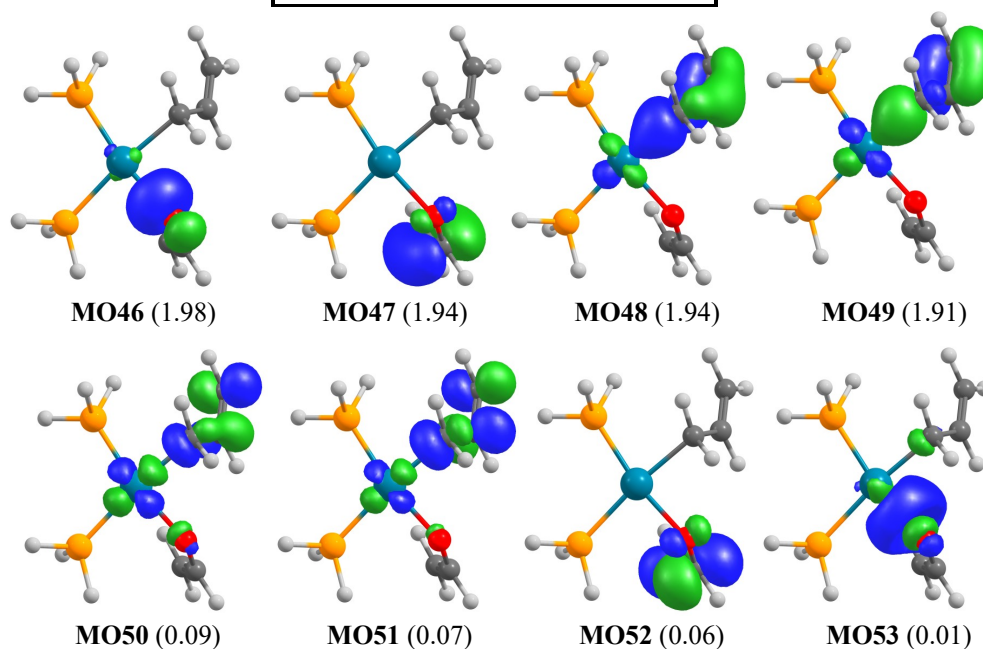
[a] Active space orbitals for compound **27**. Orbital energy eigenvalues (by ascending MO) in eV: –0.5622, –0.3144, –0.4403, –0.3213, 0.1826, 0.2975, 0.2983, 0.9742. In this conformation, the η^1-allyl ligand C–C π orbitals are nearly coplanar and further mix with the Pd-based $d(x^2–y^2)$ (MO48–MO51). If the active space is localized (Foster–Boys) the C–C π/π* and Pd–C σ/σ* may be separated for ease of interpretation.

Figure 2.18. *MCSCF active space orbitals and energies of* **TS25***.*[a]
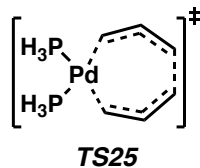
TS25

CASSCF(8,8)	-1044.936576
NEVPT2(8,8)	-1047.082378
Weight	Configuration
0.85693	[22220000]
0.01682	[22202000]
0.01094	[22111100]

MO46 (1.96)   **MO47** (1.93)   **MO48** (1.92)   **MO49** (1.88)

MO50 (0.13)   **MO51** (0.10)   **MO52** (0.10)   **MO53** (0.02)
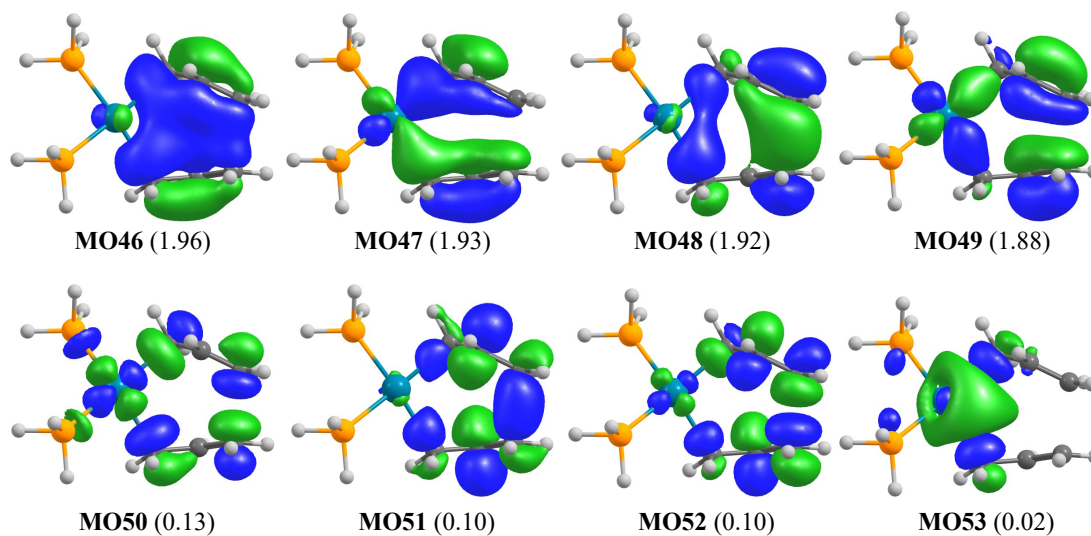
[a] Active space orbitals for compound **TS25**. Isosurface value adjusted to 0.04 for ease of visualization. Orbital energy eigenvalues (by ascending MO) in eV: –0.4443, –0.4016, –0.3064, –0.2400, 0.1574, 0.2046, 0.3684, 0.5126.

Figure 2.19. *MCSCF active space orbitals and energies of **TS26**.*[a]

TS26

CASSCF(8,8)	-1080.838314
NEVPT2(8,8)	-1083.018807
Weight	Configuration
0.86058	[22220000]
0.03715	[22202000]
0.00724	[22020200]

MO46 (1.97)   **MO47** (1.94)   **MO48** (1.93)   **MO49** (1.86)

MO50 (0.13)   **MO51** (0.08)   **MO52** (0.06)   **MO53** (0.02)
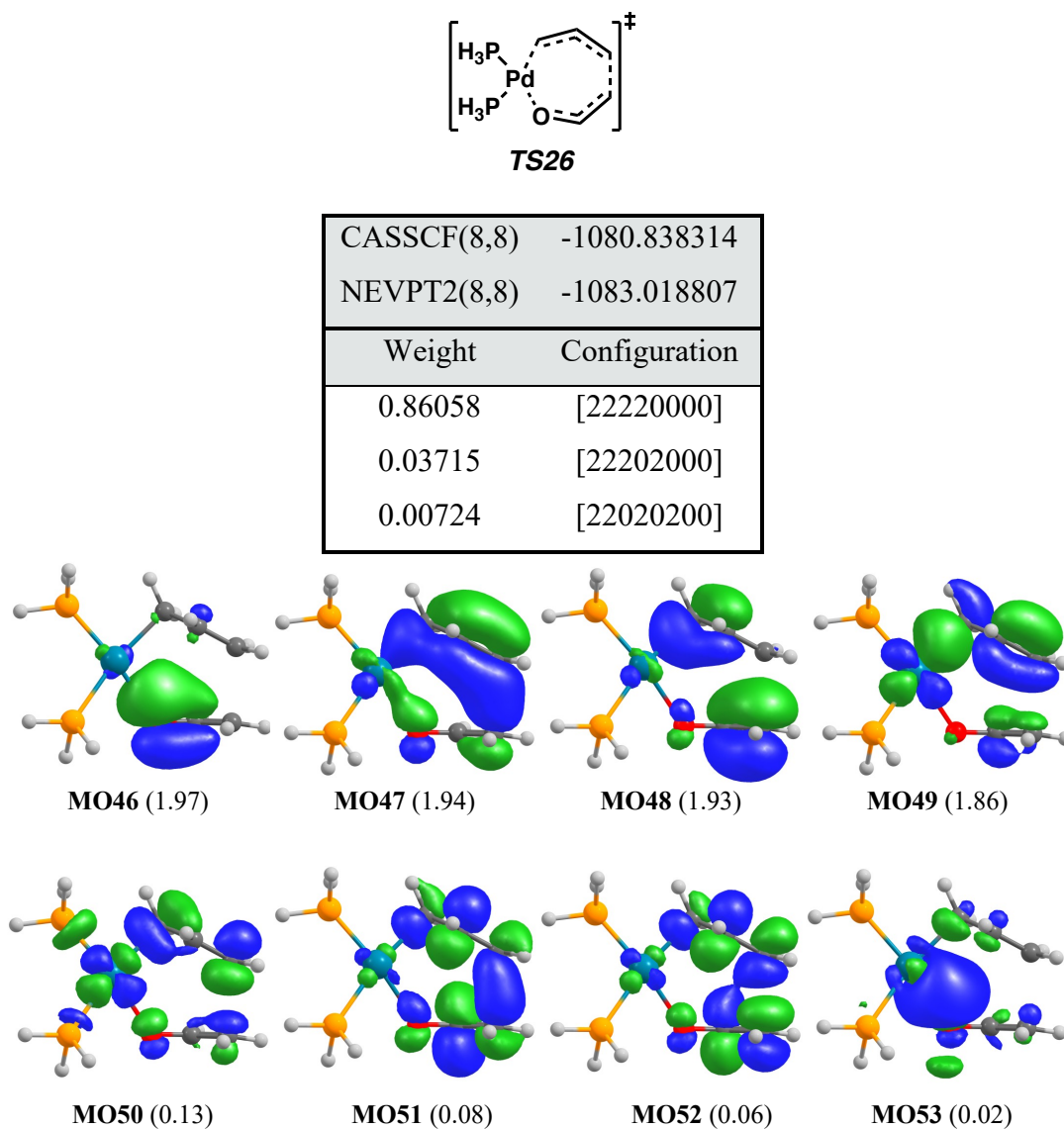
[a] Active space orbitals for compound **TS26**. Isosurface value adjusted to 0.04 for ease of visualization. Orbital energy eigenvalues (by ascending MO) in eV: –0.5448, –0.4209, –0.3126, –0.2783, 0.1404, 0.2406, 0.3519, 0.7700.

Figure 2.20. *MCSCF active space orbitals and energies of **28**.[a]*

28
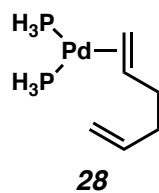
CASSCF(8,8)	-1045.009114
NEVPT2(8,8)	-1047.148494
Weight	Configuration
0.88527	[22220000]
0.01649	[22111100]
0.01002	[21211010]

MO46 (1.98) **MO47** (1.97) **MO48** (1.95) **MO49** (1.92)

MO50 (0.08) **MO51** (0.06) **MO52** (0.02) **MO53** (0.01)
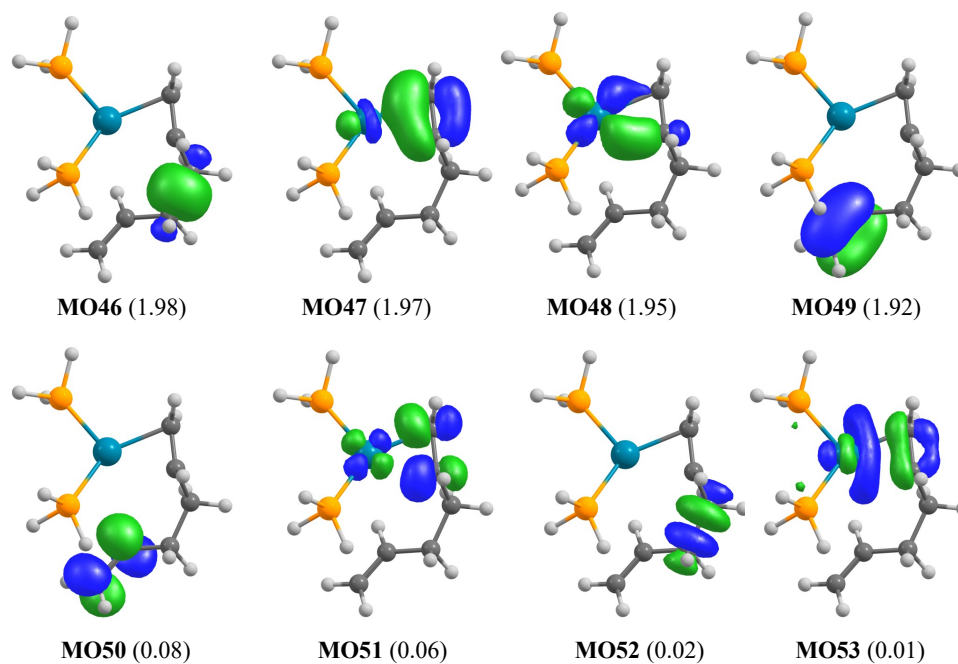
[a] Active space orbitals for compound **28**. Isosurface value adjusted to 0.04 for ease of visualization.

Orbital energy eigenvalues (by ascending MO) in eV: –0.6193, –0.4392, –0.3288, –0.3509, 0.2247, 0.2579, 0.8061, 0.4683.

Figure 2.21. *MCSCF active space orbitals and energies of **29**.[a]*
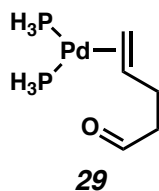
CASSCF(8,8)	-1080.909107
NEVPT2(8,8)	-1083.101216
Weight	Configuration
0.92253	[22220000]
0.02687	[22202000]
0.01400	[22020200]

MO46 (1.98)   **MO47** (1.97)   **MO48** (1.95)   **MO49** (1.92)

MO50 (0.08)   **MO51** (0.06)   **MO52** (0.02)   **MO53** (0.01)
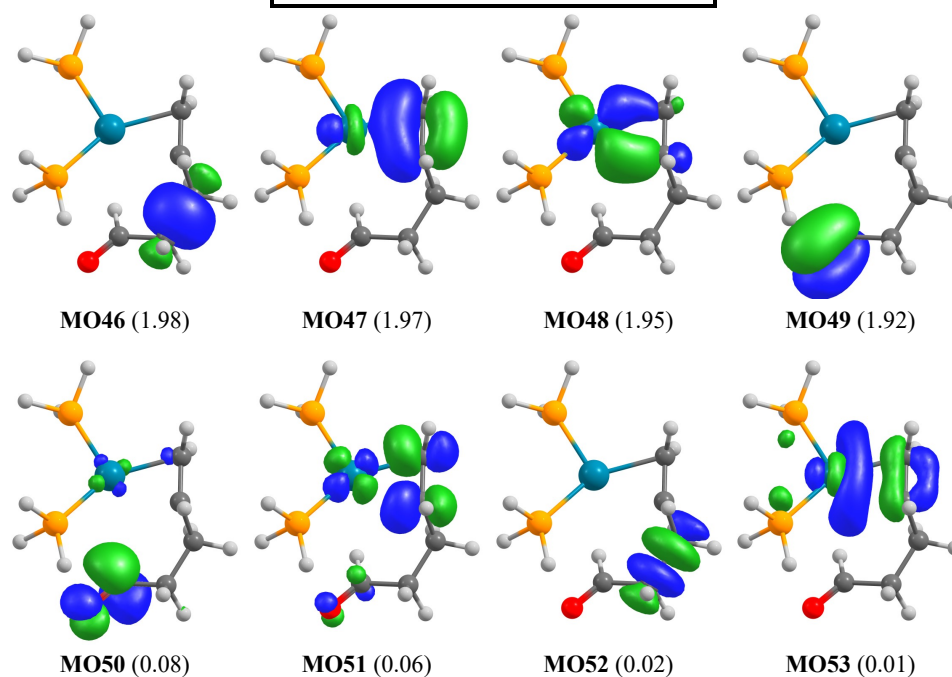
[a] Active space orbitals for compound **29**. Isosurface value adjusted to 0.06 for ease of visualization.

Orbital energy eigenvalues (by ascending MO) in eV: –0.6342, –0.4444, –0.3324, –0.5055, 0.2854,

0.2572, 0.8066, 0.4687.

2.4.3   ADDITIONAL NOTES ON NEVPT2/CASSCF CALCULATIONS

The frozen core approximation was not used in the NEVPT2 calculations (keyword: "! NoFrozenCore"). Solvated free energies include the cavitation, dispersion, structure (CDS) terms as calculated in the SMD model.[16] *Practical note to users:* For efficiently converging active spaces with weakly correlated valence-bond-like orbitals (such as the C–C σ/σ^*) in the starting complexes and products, we recommend use of the PMO virtual orbital optimization feature in ORCA. A standard procedure involved converging the MCSCF with an active space excluding the weakly correlating pair, localization of the internal space, locating the valence bond orbital of interest, then optimization of a corresponding virtual orbital (using the PMO methodology (RefMO)). Generally, expanding the active space to include the natural orbital-like pair affords smoothly convergence of the MCSCF.

2.4.4   DISCUSSION ON OTHER MAIN GROUP CHELEFUGES

In our investigation of the [π2s + π2s + σ2s + σ2s] reaction, we employ diallyl sulfone (**23**) as a main group analog to bis(η^1-allyl)Pd(PH$_3$)$_2$ complex **26**. In addition to SO$_2$, CO and N$_2$ are also viable main group chelefuges. Thus, the [π2s + π2s + σ2s + σ2s] reactions of hepta-1,6-dien-4-one or diallyl isodiazene may be considered. For these scenarios, there are *nine* correlating valence orbitals – occupied by 10 valence electrons (see Chapter 3 of reference 8). Both reactions are similarly symmetry forbidden. As a representative example, the orbital correlation diagram for the reaction of hepta-1,6-dien-4-one to CO and 1,5-hexadiene is provided below (Figure 2.22). In the general [π2s + π2s + σ2s + σ2a] reaction, we only consider linear departure/approach of the chelefuge due to

the geometric/steric constraints of the seven-membered transition state. An exception to this may be methylene carbene, which could possibly undergo the thermally allowed [π2s + π2s + σ2s + σ2a]/[ω2a + π2s + π2s + σ2s] reaction, *i.e.*, with non-linear departure/approach of the carbene.

Figure 2.22. *Orbital correlation diagram for the ground state symmetry-forbidden [π2s + π2s + σ2s + σ2s] extrusion of CO from hepta-1,6-dien-4-one.*
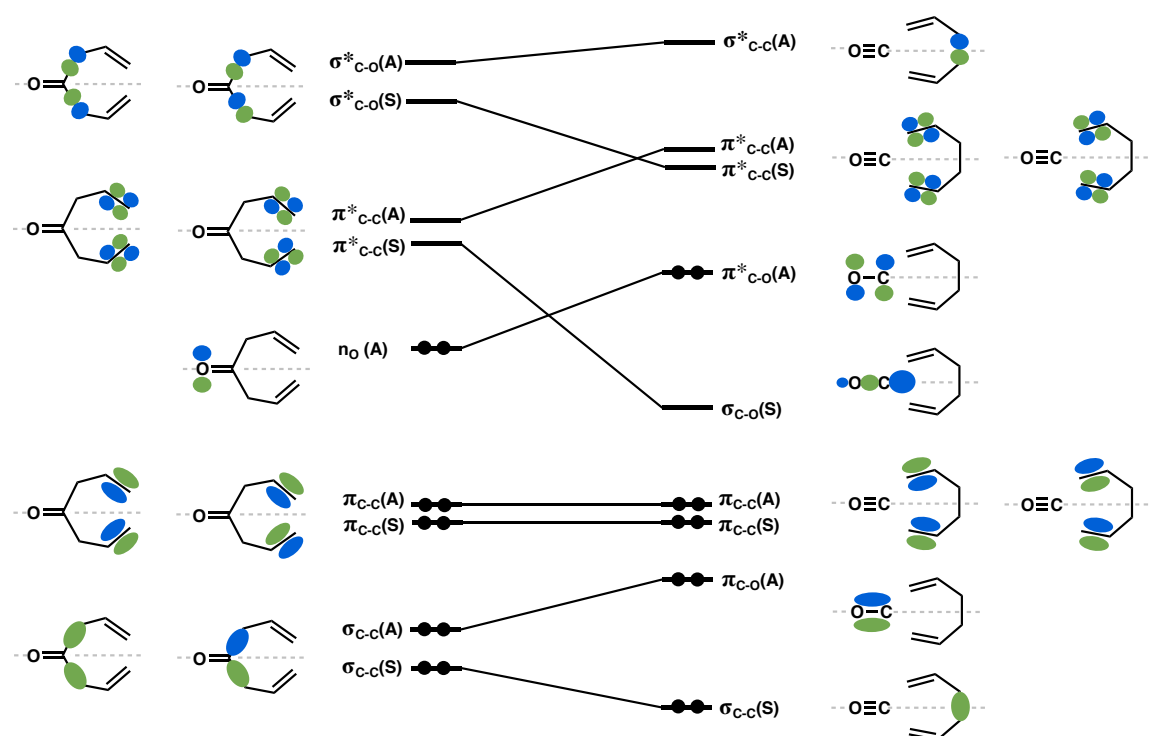
From the FMO perspective, it is important to note that the π systems of CO and N$_2$ are of the correct symmetry to constructively interact with the diene LUMO (in its reactive conformer), but these π orbitals ultimately correlate to lone pairs on O (in CO) and N (in N$_2$) and thus cannot serve as the "donor" in the donor-acceptor relationship.

2.4.5   EXCHANGE COUPLING IN DIRADICAL INTERMEDIATE 30

The RI and COS integral approximations were not used in calculations evaluating exchange coupling. All computations were carried out in the gas phase. State averaging over the relevant singlet and triplet diradical states was employed in CASSCF calculations. Results obtained with the minimal (2,2) active space, *i.e.,* including only the local spin centers, are provided for comparison. Hypothetical diradical species **30** is a metastable intermediate on the singlet CAS(8,8) and BS-DFT ($M_S = 0$) potential energy surfaces. In the case of BS-DFT, the diradical was found as an intermediate regardless of choice of functional ((U)PBE0-D3(BJ), (U)PBE-D3(BJ), (U)M06-2X).[33]

Exchange coupling interaction may be described through the phenomenological Heisenberg–Dirac–van Vleck Hamiltonian[34]:

$$\hat{H}_{\mathrm{HDvV}} = -2J\hat{S}_A\hat{S}_B$$

where $\hat{S}_A$ and $\hat{S}_B$ are "local" spin operators on spin sites A and B. J is defined as the exchange coupling constant. Thus, for the coupling of two spin-1/2 magnetic sites, J is expressed as:

$$J = -\frac{1}{2}(E_T - E_S)$$

where E_T and E_S are the energies of the triplet- and singlet-coupled diradical states, respectively. When $J > 0$, *i.e.*, $E_T < E_S$, the interaction is termed ferromagnetic. Likewise, $J < 0$ implies an antiferromagnetic coupling of the two spins. As a consequence of a single determinant formulation, the broken-symmetry DFT solution of an open-shelled singlet state is a mixture of the $M_S = 0$ singlet and triplet states.[35] Thus, calculation of exchange

coupling was performed after removal of spin contamination. The spin projection to the "true" singlet energy was carried out via the Yamaguchi equation[36]:

$$E_T - E_S = \frac{2}{\langle S^2 \rangle_T - \langle S^2 \rangle_{BS}} (E_T - E_{BS})$$

As such, the J values we report via BS-DFT are calculated as:

$$J = -\frac{E_T - E_{BS}}{\langle S^2 \rangle_T - \langle S^2 \rangle_{BS}}$$

Single point calculations with SA-CAS(8,8) on the CAS(8,8) PES initially suggest an antiferromagnetic coupling between the two spin-1/2 centers ($J = -12.1$ cm^{-1}) of **30**. However, inclusion of dynamical correlation via SC-NEVPT2, with the SA-CAS(8,8) reference, reveals a weak ferromagnetic coupling ($J = 3.2$ cm^{-1}) (Table 2.1, entry 5). BS-DFT single point calculations carried out on the CAS(8,8) geometry also suggest a singlet-coupled diradical, with $J = -38.9$ cm^{-1}. Conversely, DFT single point calculations at both the high spin and broken-symmetry (BS-)DFT-optimized geometries suggest ferromagnetism (Table 2.1, entries 9 and 10). Unsurprisingly, these data suggest the treatment of dynamical electron correlation is crucial in obtaining qualitatively meaningful results.

Table 2.1. *Calculation of spin exchange coupling constant (J) between spin centers in 1,4-diradical **30**.*[a]
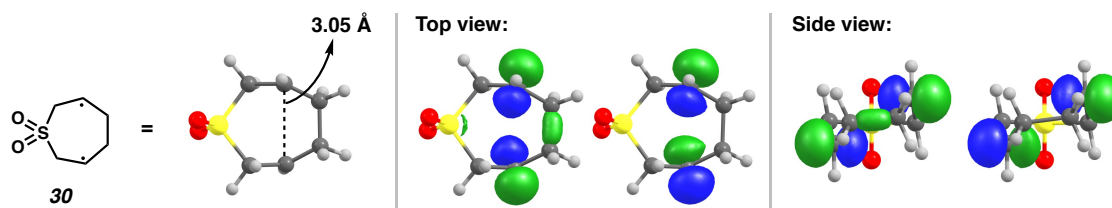
Entry No.	Method	$J\,(\mathrm{cm}^{-1})$
1	SA-CAS(2,2)	59.1
2	SA-CAS(8,8)	−12.1
3	SC-NEVPT2/SA-CAS(2,2)	−14.1
4	FIC-NEVPT2/SA-CAS(2,2)	−14.0
5	SC-NEVPT2/SA-CAS(8,8)	3.2
6	FIC-NEVPT2/SA-CAS(8,8)	7.0
7	**IDDCI**[b]	**82.9**
8	(U)PBE0-D3(BJ)[c]	−38.9
9	(U)PBE0-D3(BJ)[d]	30.0
10	(U)PBE0-D3(BJ)[e]	37.0

[a] Unless otherwise noted, performed on the singlet CAS(8,8)/def2-TZVP geometry **30**. All calculations above employ the def2-TZVP basis set on all atoms, no integral approximations, and are carried out in the gas phase. Pictured above are the two natural orbitals in the CAS(8,8) active space describing bonding and antibonding pairing in diradical **30**. [b] IDDCI (see below) starting from the SA-CAS(2,2) wavefunction. [c] BS-DFT single point calculation on CAS(8,8)/def2-TZVP geometry. [d] Single point calculation on broken-symmetry ($M_s = 0$) (U)PBE0-D3(BJ)/def2-TZVP optimized geometry. [e] Single point calculation on high spin ($S = 1$) (U)PBE0-D3(BJ)/def2-TZVP optimized geometry.

For a more rigorous treatment of static and dynamic correlation, multireference calculations were carried out with the Iterative Difference Dedicated Configuration

Interaction (IDDCI) method. [37] The standard DDCI approach resembles that of an uncontracted MRCI (singles and doubles), where completely inactive double excitations are omitted. The reference states were defined to be the singlet and triplet diradical states. The state-averaged CAS(2,2) wavefunction was taken to be the initial orbitals. The results obtained with DDCI are highly depended on the choice of reference orbitals. To help alleviate this starting orbital dependence and generally obtain more accurate results, we employed the Iterative DDCI method (IDDCI) of Malrieu and coworkers.[11b] In IDDCI, an iterative MO improvement strategy is utilized in which a DDCI calculation is first converged, followed by construction of the state-averaged single-particle density matrix and diagonalization to give a set of new set of state-averaged natural orbital-like MOs. These MOs then serve as the starting orbital basis for a subsequent DDCI calculation. The process is repeated until self-consistency (*i.e.*, the energies of the states stabilize).

As implemented in the ORCA program, convergence of the calculated exchange coupling constant and state energies is achieved with the parameters $T_{sel} = 1 \times 10^{-11}$ (default 1×10^{-6}) and $T_{pre} = 1 \times 10^{-4}$ (default 1×10^{-4}). A sample input for the IDDCI calculation is provided below:

```
! def2-TZVP NoPop Grid7 NoFinalGrid
! MORead VeryTightSCF NoIter AllowRHF

%base "SampleName"
%moinp "SampleStart.gbw"
%method
FrozenCore fc_ewin
end

%mrci
        EWin -10,1000
        CIType MRDDCI3
```

```
            Solver DIIS
            UseIVOs true
            Tsel 1e-11
            Tpre 1e-5
            AllSingles true
            DavidsonOpt none
            NatOrbIters 5
            NewBlock 1 *
               NRoots 1
               refs cas(2,2) end
               end
            NewBlock 3 *
               NRoots 1
               refs cas(2,2) end
               end
      end

      * xyzfile 0 1 Sample.xyz
```

Due to the rapid increase in computational cost with increase in the size of the active space, we elected to employ the (2,2) active space consisting of the two local magnetic orbitals. Calculations with the (8,8) active space were explored; however, it was found that convergence of the exchange coupling constant and state energies was not fully achieved with values of T_{sel} that yield a reasonable computational cost. Thus, we suggest the results obtained from the tightly converged (2,2) active space to be more robust. *Note that the results are qualitatively similar regardless – both (2,2) and (8,8) active spaces afford J > 0.* After five iterations, the IDDCI(2,2) method converges to an exchange coupling constant of 82.9 cm^{-1} (Figure 2.23). These results are in accord with that of NEVPT2(8,8) and BS-DFT, suggesting a triplet ground state of diradical **30**.

In summary, the concerted ground state [π2s + π2s + σ2s + σ2s] reaction of diallyl sulfone **23** to SO$_2$ (**24**) and 1,5-hexadiene (**25**) is symmetry forbidden. Owing to the triplet

ground state of diradical **30**, the individual steps of the stepwise mechanism are formally spin forbidden — granted the singlet and triplet states are nearly degenerate (ΔE_{T-S} of *ca.* 0.5 kcal/mol) in the weakly coupled diradical.

Figure 2.23. *Exchange coupling via IDDCI.*[a]
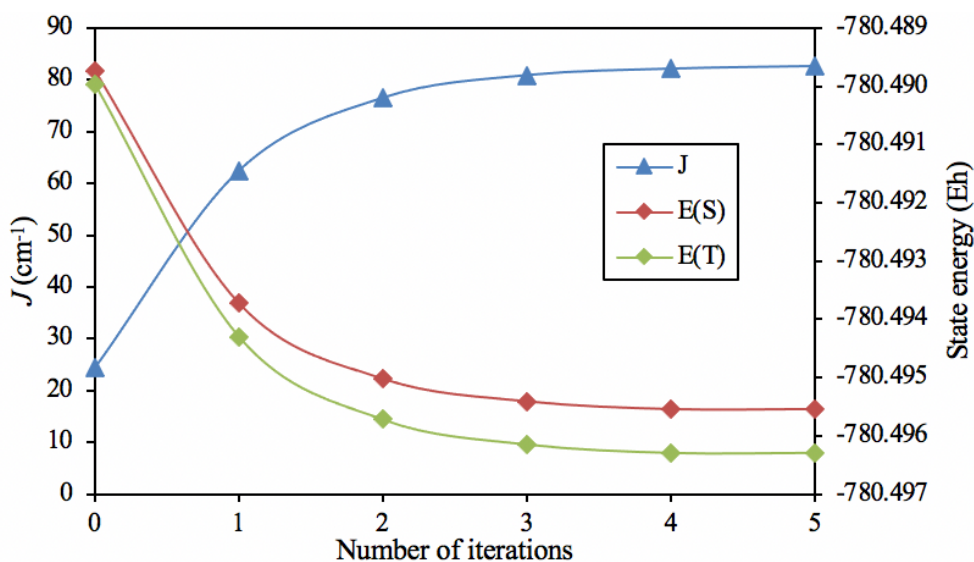
[a] Convergence of exchange coupling and state energies via iterative MO optimization in DDCI (IDDCI).

2.4.6   REDOX INNOCENCE OF THE PHOX LIGAND

The general Pd-catalyzed [π2s + π2s + σ2s + σ2s] pericyclic reaction is symmetry allowed without mandatory implication of ligand-based excited states/configurations. However, in the case of Pd(PHOX) complexes, we sought to evaluate whether the π system of the PHOX ligand is capable of facilitating the reductive elimination through ligand-based redox activity. First, we note that the ground state densities obtained with PBE0-D3(BJ)/def2-TZVP are stable with respect to spin symmetry breaking. Thus, at the DFT level, the ground state along the reaction path **13 → TS20 → 19** is well represented as a

closed-shell singlet (CSS). Time-dependent density functional theory (TD-DFT) calculations were then carried out on stationary points **13**, **TS20**, and **19** at the PBE0-D3(BJ)/def2-TZVP/SMD(THF) level of theory. The TD-DFT calculations suggest no low energy excited states along the ground state PES. The lowest of these vertical transitions is that of the ^{3}(M/L→L) at **TS20**, which is calculated to be nearly 1.0 eV (Table 2.2). All other excitations (M→M, L→M/L, etc.) are found to be > 2 eV. The PHOX π*-based LUMO (Figure 2.24) serves as a common acceptor in each of the lowest energy transitions in Table 2. These results suggest that redox contribution of the PHOX ligand along the ground state PES is likely trivial.

Table 2.2. *TD-DFT vertical excitations at stationary points **13**, **TS20**, and **19**.^{a}*

	13		TS20		19	
	Excitation	Energy (eV)	Excitation	Energy (eV)	Excitation	Energy (eV)
Singlet	L → L	1.463	M/L → L	1.401	MLCT	2.264
Triplet	L → L	1.014	M/L → L	0.986	MLCT	1.941

[a] Lowest energy TD-DFT vertical excitations with PBE0-D3(BJ)/def2-TZVP/SMD(THF) and adapted triplets from the RKS reference. L = ligand, M = metal, M/L = mixed metal/ligand.

Figure 2.24. *Orbitals involved in the vertical transitions to the lowest energy singlet and triplet excited states at **TS20**.*

^{1}(M/L to L) = 1.40 eV
^{3}(M/L to L) = 0.99 eV

Pd/allyl/enolate-based HOMO   **PHOX π*-based LUMO**
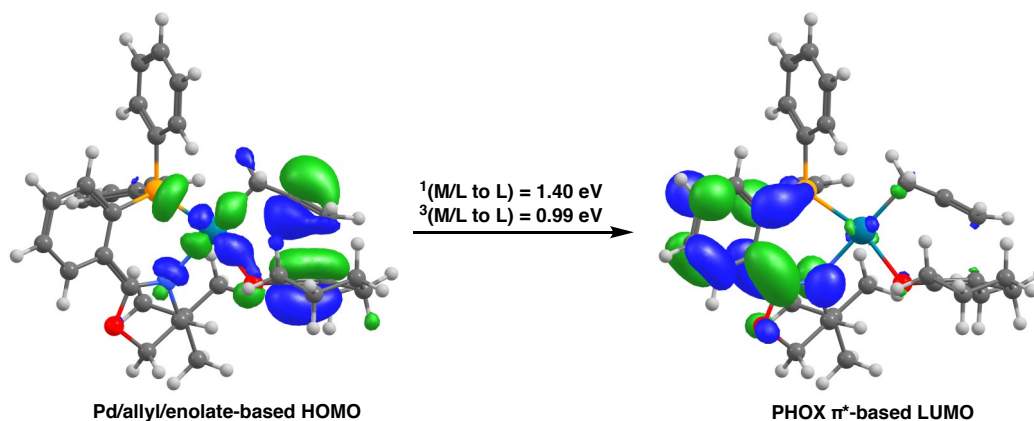
2.4.7   NUCLEUS INDEPENDENT CHEMICAL SHIFT CALCULATIONS

Calculations of Nucleus Independent Chemical Shift (NICS) were carried out in order to probe the aromatic character of **TS25**. In this investigation, the formalism of Schleyer and coworkers is followed.[24] Reported NICS values are the negative of the calculated isotropic chemical shift/shielding at the geometric center of the ring in question. These calculations were carried out with the NMR module in ORCA. Calculations of NICS were conducted in the gas phase at the PBE0-D3(BJ)/def2-TZVP level of theory. Gauge independent atomic orbitals (GIAO) were used and the relevant one-electron and two-electron integrals were evaluated analytically and with the RIJK approximation, respectively. A ghost atom ("H:", no nuclear charge nor electrons) was used to define a point in space at which shielding was to be determined. A highly contracted basis (and auxiliary basis) function was then assigned to the ghost atom. This procedure was used to ensure the proper grid points were assigned to the point in space without significantly perturbing the ground state density. Note that the results are independent of the chosen

exponent as long as the exponent is large. For example, the following would be added to the geometry block of an input file to define a point with cartesian coordinates (0.00, 1.00, 2.00):

H: 0.00 1.00 2.00 newgto S 1 1 1000000 1 end newauxJKgto S 1 1 2000000 1 end

At the PBE0-D3(BJ)/def2-TZVP level of theory, NICS values of –8.9 and 28.8 ppm were obtained for benzene and cyclobutadiene, respectively. These controls are in good agreement with literature values of –9.7 and 27.6 ppm (HF/6-31+G(d)).[24] As described in the text, an NICS value of –19.4 ppm is found at the geometric center of the seven-membered ring of **TS25** (Figure 2.4C). A NICS value of –19.4 ppm reveals a significant diatropic ring current. Thus, **TS25** is characterized as aromatic.[25]

2.4.8   INTRINSIC BONDING ORBITAL ANALYSIS

Analysis of the net flow of electron density through the Pd-catalyzed [π2s + π2s + σ2s + σ2s] pericyclic reaction was carried out by Intrinsic Bonding Orbital (IBO) analysis.[27] IBO analysis was carried out along the IRC describing **19** → **TS20** → **19**. SCF densities were obtained at the M06/def2-TZVP/CPCM(THF) level of theory and on BP86-D3(BJ)/LANL2TZ(f)[Pd]–6-31G(d) geometries, consistent with reference 5. Localization of the SCF density, frame alignment, and calculation of IBO displacement were carried out with the IBOView program. For further details of this procedure and additional discussion of the relevant theory, see the seminal reports of Knizia and coworkers.[27] Note that results are largely independent of choice in density functional, and qualitatively identical results may be obtained with densities from an ab initio wavefunction method.

2.5   REFERENCES AND NOTES

(1)   Fukui, K. A Simple Quantum-Theoretical Interpretation of the Chemical Reactivity of Organic Compounds, in Molecular orbitals in chemistry, physics, and biology. A Tribute to R. S. Mulliken, (Eds,: Löwdin, P. O.; Pullman, B.), Academic Press, New York, **1964**, 513–537.

(2)   Goddard, W. A. I. Orbital Phase Continuity Principle and Selection Rules for Concerted Reactions. *J. Am. Chem. Soc.* **1970**, *92*, 7520–7521.

(3)   For further discussion of aromaticity in pericyclic transition states, see: (a) Schleyer, P. von R.; Wu, J. I.; Cossío, F. P.; Fernández, I. Aromaticity in Transition Structures. *Chem. Soc. Rev.* **2014**, *43*, 4909–4921. (b) Dewar, M. J. S. Aromaticity and Pericyclic Reactions. *Angew. Chem. Int. Ed.* **1971**, *10*, 761–776. and references therein.

(4)   Such as three-centered reductive elimination and [2+2] cycloadditions in olefin metathesis.

(5)   (a) Cusumano, A. Q.; Stoltz, B. M.; Goddard III, W. A. Reaction Mechanism, Origins of Enantioselectivity, and Reactivity Trends in Asymmetric Allylic Alkylation: A Comprehensive Quantum Mechanics Investigation of a $C(sp^3)$–$C(sp^3)$ Cross-Coupling. *J. Am. Chem. Soc.* **2020**, *In-Press*. (b) McPherson, K. E.; Croatt, M. P.; Morehead, A. T.; Sargent, A. L. DFT Mechanistic Investigation of an Enantioselective Tsuji–Trost Allylation Reaction. *Organometallics* **2018**, *37*, 3791–3802.

(6) (a) Keith, J. A.; Behenna, D. C.; Mohr, J. T.; Ma, S.; Marinescu, S. C.; Oxgaard, J.; Stoltz, B. M.; Goddard III, W. A. The Inner-Sphere Process in the Enantioselective Tsuji Allylation Reaction with (S)-*t*-Bu-Phosphinooxazoline Ligands. *J. Am. Chem. Soc.* **2007**, *129*, 11876–11877. (b) Keith, J. A.; Behenna, D. C.; Sherden, N.; Mohr, J. T.; Ma, S.; Marinescu, S. C.; Nielsen, R. J.; Oxgaard, J.; Stoltz, B. M.; Goddard III, W. A. The Reaction Mechanism of the Enantioselective Tsuji Allylation: Inner-Sphere and Outer-Sphere Pathways, Internal Rearrangements, and Asymmetric C–C Bond Formation. *J. Am. Chem. Soc.* **2012**, *134*, 19050–19060.

(7) (a) Pérez-Rodríguez, M.; Braga, A. A. C.; de Lera, A. R.; Maseras, F.; Álvarez, R.; Espinet, P. A DFT Study of the Effect of the Ligands in the Reductive Elimination from Palladium Bis(Allyl) Complexes. *Organometallics* **2010**, *29*, 4983–4991. (b) Méndez, M.; Cuerva, J. M.; Gómez-Bengoa, E.; Cárdenas, D. J.; Echavarren, A. M. Intramolecular Coupling of Allyl Carboxylates with Allyl Stannanes and Allyl Silanes: A New Type of Reductive Elimination Reaction? *Chem. Eur. J.* **2002**, *8*, 3620–3628. (c) Zhang, P.; Brozek, L. A.; Morken, J. P. Pd-Catalyzed Enantioselective Allyl−Allyl Cross-Coupling. *J. Am. Chem. Soc.* **2010**, *132*, 10686–10688.

(8) Woodward, R. B.; Hoffmann R.; *The Conservation of Orbital Symmetry*; Verlag Chemie GmbH (BRD) and Academic Press Inc. (USA), 1971.

(9) Despite our best efforts, we are unable to find literature examples of an identical main group analog fitting $\Delta\pi = 0$ and $\Delta\sigma = 1$ in this seven-membered geometry.

(10) See Supporting Information for a discussion on N_2 as a chelefuge. For examples of

reactivity of diazenes in cheletropic reactions, see Lemal, D. M.; McGregor, S. D. Dienes from 3-Pyrrolines. A Stereospecific Deamination. *J. Am. Chem. Soc.* **1966**, *88*, 1335–1336.

(11)   (a) Neese, F. Software Update: The ORCA Program System, Version 4.0. *Wiley Interdisciplinary Reviews: Computational Molecular Science* **2018**, *8*, e1327. (b) Neese, F. The ORCA Program System. *Wiley Interdisciplinary Reviews: Computational Molecular Science* **2012**, *2*, 73–78.

(12)   Angeli, C.; Cimiraglia, R.; Malrieu, J.-P. N-Electron Valence State Perturbation Theory: A Fast Implementation of the Strongly Contracted Variant. *Chemical Physics Letters* **2001**, *350*, 297–305. (b) Angeli, C.; Cimiraglia, R.; Malrieu, J.-P. N-Electron Valence State Perturbation Theory: A Spinless Formulation and an Efficient Implementation of the Strongly Contracted and of the Partially Contracted Variants. *J. Chem. Phys.* **2002**, *117*, 9138–9153.

(13)   Weigend, F.; Ahlrichs, R. Balanced Basis Sets of Split Valence, Triple Zeta Valence and Quadruple Zeta Valence Quality for H to Rn: Design and Assessment of Accuracy. *Phys. Chem. Chem. Phys.* **2005**, *7*, 3297–3305.

(14)   Andrae, D.; Häußermann, U.; Dolg, M.; Stoll, H.; Preuß, H. Energy-Adjusted ab Initio Pseudopotentials for the Second and Third Row Transition Elements. *Theoret. Chim. Acta* **1990**, *77*, 123–141.

(15)   PBE0-D3: PBE0 hybrid density functional coupled with Becke–Johnson damped D3 dispersion correction. PBE0: (a) Adamo, C.; Barone, V. Toward Reliable Density Functional Methods without Adjustable Parameters: The PBE0 Model. *J.*

Chem. Phys. **1999**, *110*, 6158–6170. D3(BJ): (b) Grimme, S.; Antony, J.; Ehrlich, S.; Krieg, H. A A consistent and accurate *ab initio* parametrization of density functional dispersion correction (DFT-D) for the 94 elements H-Pu. *J. Chem. Phys.* **2010**, *132*, 154104. (c) Grimme, S.; Ehrlich, S.; Goerigk, L. Effect of the Damping Function in Dispersion Corrected Density Functional Theory. *J. Comput. Chem.* **2011**, *32*, 1456–1465.

(16)   Marenich, A. V.; Cramer, C. J.; Truhlar, D. G. Universal Solvation Model Based on Solute Electron Density and on a Continuum Model of the Solvent Defined by the Bulk Dielectric Constant and Atomic Surface Tensions. *J. Phys. Chem. B* **2009**, *113*, 6378–6396.

(17)   Similar results were obtained with broken-symmetry DFT (see supporting information for details). We are unable to find a concerted closed-shell singlet [π2a + π2s + σ2s + σ2s] transition state. Additionally, singlet diradical **10** is in the boat conformation collapses to the corresponding cyclobutene.

(18)   Diradical index defined as described by Neese and coworkers, with $d = 98.0\%$ indicating of 98% diradical character. Here, c_0 and c_d are the factional contributions of the relevant bonding and antibonding configurations to the ground-state CI wavefunction.

$$d = 200 \sqrt{\frac{c_0^2 c_d^2}{c_0^2 + c_d^2}}$$

Herebian, D.; Wieghardt, K. E.; Neese, F. Analysis and Interpretation of Metal-Radical Coupling in a Series of Square Planar Nickel Complexes: Correlated Ab

Initio and Density Functional Investigation of [Ni(LISQ)₂] (LISQ=3,5-Di-Tert-Butyl-o-Diiminobenzosemiquinonate(1-)). *J. Am. Chem. Soc.* **2003**, *125*, 10997–11005.

Note that through-bond coupling of *2b* with σ*(C–C) and *3a* with σ(C–C) gives rise to *2b* being lower in energy than the symmetric *3a*. For further discussion see: Stuyver, T.; Chen, B.; Zeng, T.; Geerlings, P.; De Proft, F.; Hoffmann, R. Do Diradicals Behave Like Radicals? *Chem. Rev.* **2019**, *119*, 11291–11351.

(19)   Calculated from singlet and triplet diradical references starting from state-averaged CASSCF orbitals. Further details and comparison with other methods are included in SI section. For the DDCI method, see: (a) Miralles, J.; Daudey, J.-P.; Caballol, R. Variational Calculation of Small Energy Differences. The Singlet-Triplet Gap in [Cu2Cl6]2−. *Chem. Phys. Lett.* **1992**, *198*, 555–562. (b) García, V. M.; Castell, O.; Caballol, R.; Malrieu, J. P. An Iterative Difference-Dedicated Configuration Interaction. Proposal and Test Studies. *Chem. Phys. Lett.* **1995**, *238*, 222–229. (c) García, V. M.; Reguero, M.; Caballol, R. Application of the Iterative Difference-Dedicated Configuration Interaction Method to the Determination of Excitation Energies in Some Benchmark Systems: Be, CH+, BH and CH₂. *Theor. Chem. Acc.* **1997**, *98*, 50–56. As implemented in ORCA, we employ the uncontracted DDCI3 variant.

(20)   A similar effect was observed by Steigerwald and Goddard in studying the thermally *allowed* [2s + 2s] sigma bond metathesis of D₂ by transition metal hydrides. (a) Steigerwald, M. L.; Goddard III, W. A. The 2s + 2s Reactions at

Transition Metals. 1. The Reactions of Deuterium with Dichlorohydrotitanium(1+) Ion (Cl_2TiH+), Titanium Hydrogen Dichloride (Cl_2TiH), and Scandium Hydrogen Dichloride (Cl_2ScH). *J. Am. Chem. Soc.* **1984**, *106*, 308–311. (b) Steigerwald, M. L.; Goddard III, W. A. 2s + 2s Reactions at Transition Metals. Part 3. Dichlorotitanacyclopropane. The Structure and Reactivity of a Metallacyclopropane. *J. Am. Chem. Soc.* **1985**, *107*, 5027–5035. For further discussion on transition-metal enabled [2s + 2s], see (c) Mango, F. D.; Schachtschneider, J. H. Orbital Symmetry Restraints to Transition Metal Catalyzed [2+2] Cycloaddition Reactions. *J. Am. Chem. Soc.* **1971**, *93*, 1123–1130. For additional representative examples of transition-metal intervention in pericyclic reactions, see (d) Tantillo, D. J.; Hoffmann, R. Demoniac Intervention in the Thermal Electrocyclic Ring Opening of Cyclobutenes: $Fe(CO)_3$ Complexation of Pericyclic Transition Structures. *Helvetica Chimica Acta* **2001**, *84*, 1396–1404. (e) Siebert, M. R.; Tantillo, D. J. Transition-State Complexation in Palladium-Promoted [3,3] Sigmatropic Shifts. *J. Am. Chem. Soc.* **2007**, *129*, 8686–8687. (f) Tantillo, D. J.; Hoffmann, R. Complicated Goings-On in the Metal-Manipulated Ring-Opening of Cyclobutene. *J. Am. Chem. Soc.* **2001**, *123*, 9855–9859. (g) Tantillo, D. J.; Carpenter, B. K.; Hoffmann, R. Disrotatory and Conrotatory Transition Structures for the $Fe(CO)_3$-Templated Rearrangement of Methylenecyclopropane to Trimethylenemethane. *Organometallics* **2001**, *20*, 4562–4564.

(21)   LUMO as derived qualitatively for FMO analysis from two interacting three electron allyl fragments.

(22)   (a) Craig, D. P. A novel type of aromaticity. *Nature* **1958**, *181*, 1052–1053. (b) Zhu, C.; Luo, M.; Zhu, Q.; Zhu, J.; Schleyer, P. v R.; Wu, J. I.-C.; Lu, X.; Xia, H. Planar Möbius Aromatic Pentalenes Incorporating 16 and 18 Valence Electron Osmiums. *Nature Communications* **2014**, *5*, 3265. (c) An, K.; Shen, T.; Zhu, J. Craig-Type Möbius Aromaticity and Antiaromaticity in Dimetalla[10]Annulenes: A Metal-Induced Yin-and-Yang Pair. *Organometallics* **2017**, *36*, 3199–3204. For a review on Möbius topologies, see (d) Rzepa, H. S. Möbius Aromaticity and Delocalization. *Chem. Rev.* **2005**, *105*, 3697–3715.

(23)   Hua, Y.; Zhang, H.; Xia, H.; Houk, K. N. Three Classes of π-Aromaticity **2020**, *submitted*. Received as a personal communication.

(24)   (a) Schleyer, P. von R.; Maerker, C.; Dransfeld, A.; Jiao, H.; van Eikema Hommes, N. J. R. Nucleus-Independent Chemical Shifts: A Simple and Efficient Aromaticity Probe. *J. Am. Chem. Soc.* **1996**, *118*, 6317–6318. (b) Chen, Z.; Wannere, C. S.; Corminboeuf, C.; Puchta, R.; Schleyer, P. von R. Nucleus-Independent Chemical Shifts (NICS) as an Aromaticity Criterion. *Chem. Rev.* **2005**, *105*, 3842–3888.

(25)   For use of NICS for determination of transition state aromaticity, see Jiao, H.; Schleyer, P. von R. Aromaticity of Pericyclic Reaction Transition Structures: Magnetic Evidence. *J. Phys. Org. Chem.* **1998**, *11*, 655–662.

(26)   (a) Ingold, C. K. Principles of an Electronic Theory of Organic Reactions. *Chem. Rev.* **1934**, *15*, 225–274. (b) Kermack, W. O.; Robinson, R. LI.—An Explanation

of the Property of Induced Polarity of Atoms and an Interpretation of the Theory of Partial Valencies on an Electronic Basis. *J. Chem. Soc., Trans.* **1922**, *121*, 427–440.

(27)   (a) Knizia, G. Intrinsic Atomic Orbitals: An Unbiased Bridge between Quantum Theory and Chemical Concepts. *J. Chem. Theory Comput.* **2013**, *9*, 4834–4843. (b) Knizia, G.; Klein, J. E. M. N. Electron Flow in Reaction Mechanisms—Revealed from First Principles. *Angew. Chem. Int. Ed.* **2015**, *54*, 5518–5522. (c) Klein, J. E. M. N.; Knizia, G. CPCET versus HAT: A Direct Theoretical Method for Distinguishing X–H Bond-Activation Mechanisms. *Angew. Chem. Int. Ed.* **2018**, *57*, 11913–11917.

(28)   Ishida, K.; Morokuma, K.; Komornicki, A. The Intrinsic Reaction Coordinate. An Ab Initio Calculation for HNC→HCN and $H^-+CH4→CH4+H^-$. *J. Chem. Phys.* **1977**, *66*, 2153–2156.

(29)   Final IBO at **2** is of $d(x^2–y^2)$ parentage with π-back-bonding to the olefin observed.

(30)   Grimme, S. Supramolecular Binding Thermodynamics by Dispersion-Corrected Density Functional Theory. *Chem. Eur. J.* **2012**, *18*, 9955–9964.

(31)   Neese, F.; Wennmohs, F.; Hansen, A.; Becker, U. Efficient, Approximate and Parallel Hartree-Fock and Hybrid DFT Calculations. A 'Chain-of-Spheres' Algorithm for the Hartree-Fock Exchange. *Chem. Phys.* **2009**, *356*, 98–109.

(32)   Stoychev, G. L.; Auer, A. A.; Neese, F. Automatic Generation of Auxiliary Basis Sets. *J. Chem. Theory Comput.* **2017**, *13*, 554–562.

(33)   For PBE see: (a) Perdew, J. P.; Burke, K.; Ernzerhof, M. Generalized Gradient Approximation Made Simple. *Phys. Rev. Lett.* **1996**, *77*, 3865–3868. For M06-2X

see (b) Zhao, Y.; Truhlar, D. G. The M06 Suite of Density Functionals for Main Group Thermochemistry, Thermochemical Kinetics, Noncovalent Interactions, Excited States, and Transition Elements: Two New Functionals and Systematic Testing of Four M06-Class Functionals and 12 Other Functionals. *Theor Chem Account* **2008**, *120*, 215–241.

(34)   Heisenberg, W. Zur Theorie des Ferromagnetismus. *Z. Physik* **1928**, *49*, 619–636.

(35)   Neese, F. Definition of Corresponding Orbitals and the Diradical Character in Broken Symmetry DFT Calculations on Spin Coupled Systems. *J. Phys. Chem. Solids* **2004**, *65*, 781–785.

(36)   (a) Yamaguchi, K.; Takahara, Y.; Fueno, T. Ab-Initio Molecular Orbital Studies of Structure and Reactivity of Transition Metal-OXO Compounds. In *Applied Quantum Chemistry*; Smith, V. H., Schaefer, H. F., Morokuma, K., Eds.; Springer Netherlands: Dordrecht, 1986; pp 155–184. (b) Soda, T.; Kitagawa, Y.; Onishi, T.; Takano, Y.; Shigeta, Y.; Nagao, H.; Yoshioka, Y.; Yamaguchi, K. Ab Initio Computations of Effective Exchange Integrals for H–H, H–He–H and Mn_2O_2 Complex: Comparison of Broken-Symmetry Approaches. *Chem. Phys. Lett.* **2000**, *319*, 223–230. (c) Ferré, N.; Guihéry, N.; Malrieu, J.-P. Spin Decontamination of Broken-Symmetry Density Functional Theory Calculations: Deeper Insight and New Formulations. *Phys. Chem. Chem. Phys.* **2015**, *17*, 14375–14382.

(37)   (a) Miralles, J.; Castell, O.; Caballol, R.; Malrieu, J.-P. Specific CI Calculation of Energy Differences: Transition Energies and Bond Energies. *Chem. Phys.* **1993**, *172*, 33–43. For discussion on the iterative method (IDDCI) see: (b) García, V. M.;

Castell, O.; Caballol, R.; Malrieu, J. P. An Iterative Difference-Dedicated Configuration Interaction. Proposal and Test Studies. *Chem. Phys. Lett.* **1995**, *238*, 222–229.

Catalytic Asymmetric [4+2] Cycloaddition of Pd Enolates†

3.1   INTRODUCTION

Enantioselective construction of all-carbon quaternary stereogenic centers represents a central and ongoing challenge in synthetic organic chemistry. [1] The asymmetric allylic alkylation of enolate nucleophiles serves as a powerful strategy for accessing such motifs.[2]

A unique aspect of the Pd-catalyzed allylic alkylation methods developed by our group is the inner-sphere reductive elimination from a chiral O-bound Pd enolate intermediate (**32**), yielding enantioenriched ketones (**33**) (Figure 3.1A). [3,4] This intermediate is generated catalytically from achiral or racemic enolate precursors, such as allyl enol carbonates[5] and β-ketoesters[6] (**31**). The Pd enolate is accessed in the absence of a base, under neutral conditions, and in a regiospecific fashion. Conversely, canonical conditions for enolate formation are plagued by regioselectivity challenges and typically require the use of a strong base or Lewis acid. Given the inherent advantages of Pd enolates, we sought to exploit their reactivity beyond simple allylic alkylations in more general asymmetric transformations.

Highlighting the utility of this concept, our lab has demonstrated the enantioselective protonation of Pd enolates as a valuable strategy to access ketones with

tertiary stereocenters (**34**).[7] Building upon this success, we subsequently developed

methods to construct quaternary centers via enantioselective conjugate additions[8] (**35**) and

intramolecular aldol reactions (**36**).[9] Taken together, these advances underscore the

feasibility of employing Pd enolates as stereogenic nucleophiles.

Figure 3.1. *(A) Examples of chiral Pd enolate reactivity. (B) Lithium base-promoted*

intramolecular formal [4+2] cycloaddition. (C) Proposed asymmetric intramolecular
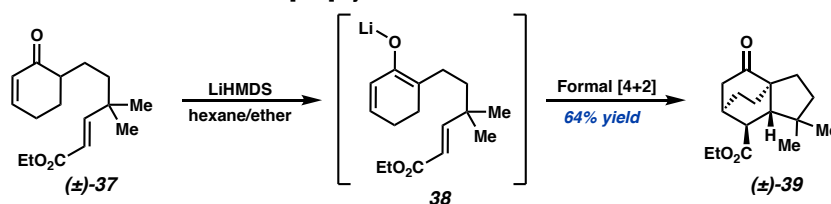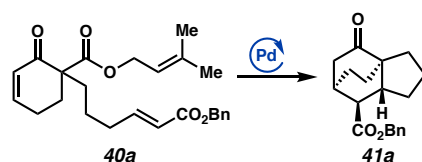
[4+2] reaction. (D) Divergent catalytic cycle.
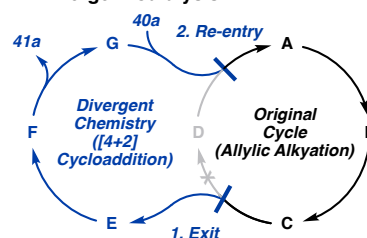
In a unique example of enolate reactivity, Fukumoto and coworkers reported a formal [4+2] reaction from in situ generated conjugated lithium enolate **38**, forging tricyclic adduct **39** in a racemic fashion (Figure 3.1B).[10] We envisioned that an analogous asymmetric transformation would be tractable from a chiral, conjugated Pd enolate – derived from the decarboxylation of unsaturated β-ketoester **40a** using an asymmetric ligand on Pd (Figure 3.1C).

To realize this transformation, we sought to develop a conceptual framework based on our mechanistic understanding to expand the general utility of the Pd enolate. As such, we employed a strategy of divergent catalysis (Figure 3.1D), where deviation occurs at the common Pd enolate (*i.e.*, **C**, Figure 3.1D, cf. Scheme 3.1, vide infra), allowing for desired alternative reactivity in the diverged cycle. Subsequent re-entry into the original catalytic cycle turns over the catalyst allowing regeneration of the Pd enolate.

Applying this strategy of divergent catalysis, we developed a catalytic decarboxylative asymmetric intramolecular [4+2] cycloaddition from conjugated Pd enolates. Mechanistic studies including quantum mechanics calculations, Eyring analysis, and KIE studies offer insights into the reaction mechanism. This transformation enables access to tricyclic scaffolds bearing at least four contiguous stereocenters, at least one of which is quaternary.

3.2   RESULTS AND DISCUSSION

3.2.1   REACTION DESIGN AND OPTIMIZATION

Employing unsaturated β-ketoester **42** as a precursor for conjugated Pd enolate **43**, we hypothesized that the precedented allylic alkylation forming **44** could be interrupted by

a [4+2] cycloaddition to generate **45** (Figure 3.2A). Alkylation of the transposed enolate

(**45**) would then turn over the catalyst and forge tricyclic product **46**.

Figure 3.2. *(A) General reactivity paradigm from Pd enolate **43**. (B) Computed*

substituent effects on the rate of C–C bond formation and successful application.[a]

A. Desired reactivity of chiral Pd enolate *43*.

B. Modulating barrier to reductive elimination.

Entry	R[1]	R[2]	ΔG‡	k_{rel} (60 °C)
1	H	H	12.9	1
2	Ph	H	16.5	4.0×10^{-3}
3	Me	Me	21.6	1.7×10^{-6}
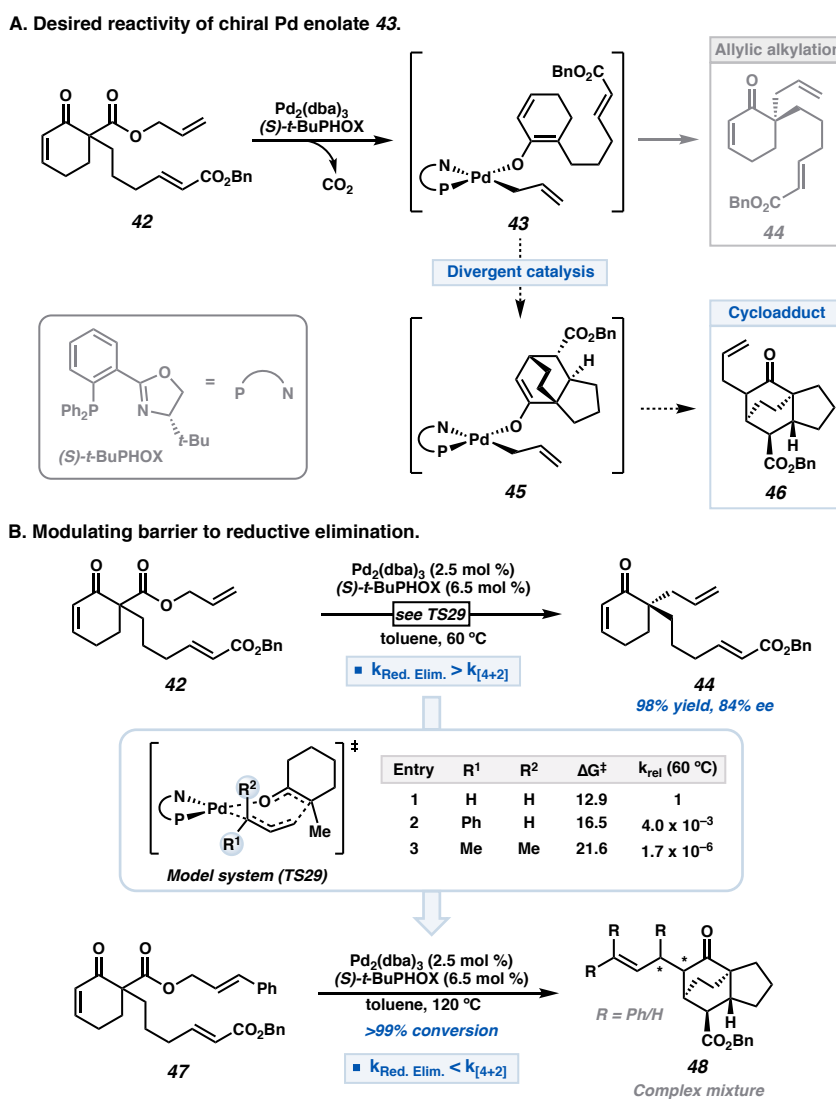
[a] See 3.4 Supporting Information for computational details and discussion of other isomeric

transition states. Yield determined by ^{1}H NMR with respect to 1,3,5-trimethoxybenzene as internal

standard. Enantiomeric excess determined by chiral SFC.

Unfortunately, the rate direct allylic alkylation of enolate **43** supersedes the desired divergent reactivity. Treatment of β-ketoester **42** under our standard conditions produces ketone **44** in 98% yield and 84% ee (Figure 3.2B). This prompted us to redesign our exit strategy (Figure 3.1D). Increasing the rate of the cycloaddition through modification of the diene or dienophile could circumvent formation of premature allylic alkylation product **44** but would limit the generality of this transformation. Therefore, we sought to impede alkylation through modification of the allyl moiety.

Computational investigation of a model system (**TS29**) suggested that introducing terminal substitution on the allyl group raises the barrier to reductive elimination, decreasing the rate of allylic alkylation (Figure 3.2B, see 3.4 Supporting Information for computational details).[11] For example, phenyl substitution (entry 2, Figure 3.2B) slows the rate of inner-sphere reductive elimination by roughly three orders of magnitude. Inspired by these computational results, we explored the efficacy of cinnamyl ester substrate **47** in the transformation. In line with our hypothesis, the desired tricyclic core was observed (**48**), albeit as a complex mixture of isomers – hampering the synthetic utility. To this end, we sought to develop an alternative strategy for catalyst turnover that could potentially simplify the product outcomes.

Building upon previous findings from our group, we sought to employ stoichiometric acidic additives for catalyst turnover. The exogenous acid serves the dual purpose of protonating the final enolate (analogous to **45**) and turning over the catalyst by trapping the cinnamyl group. Addition of 3,5-dimethylphenol[9] exclusively yielded undesired protonation product **49a** along with aryl ether **50** (Figure 3.3A). To our delight,

replacing the phenol additive with 4-methylaniline afforded the desired *endo* [4+2]

cycloadduct (**41a**) as a single diastereomer in 83% yield and 88% ee.

Figure 3.3. *(A) Sacrificial additives to enable catalyst turnover.*[a] *(B) Additive-free reaction with prenyl ester **40a**.*[b]

A. Alternative catalyst turnover strategy.

B. Additive-free catalyst turnover.
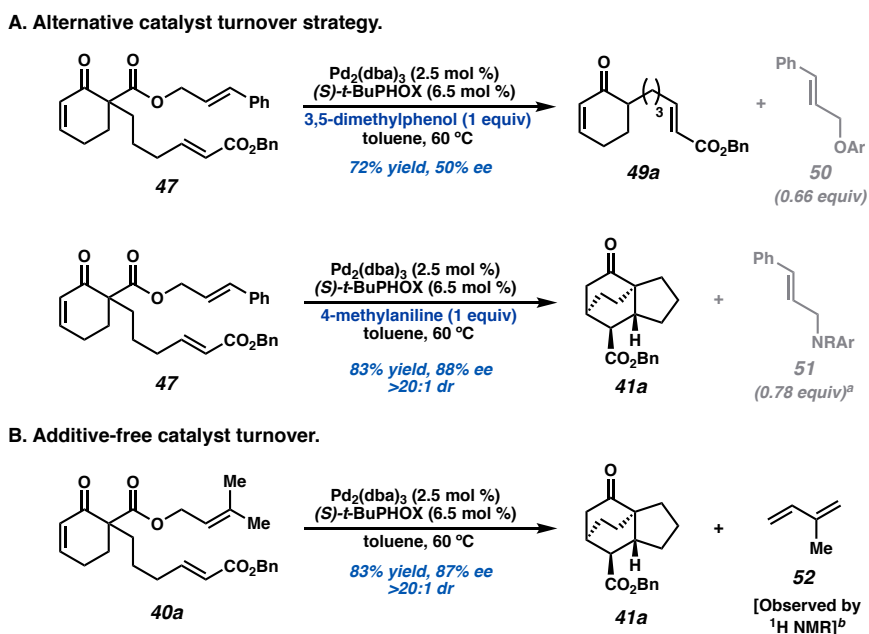
[a] Equivalents includes mixture of branched and linear constitutional isomers, as well as double-alkylation of aniline. [b] Isoprene (**52**) observed in 0.94:1 ratio with **41a** by ^{1}H NMR (J Young tube, toluene-d_8).

Seeking to improve the reaction yield, the competency of β-ketoester **40a**, derived

from the commodity chemical prenyl alcohol, was explored. According to our

computations, a substrate containing a di-substituted allyl fragment would be similarly

effective in hindering premature allylic alkylation by increasing the barrier to reductive

elimination (Figure 3.2B, entry 3). Perplexingly, while the desired tricyclic product was

generated in 73% isolated yield and 88% ee, no alkylated 4-methylaniline (analogous to

51) was observed as a byproduct.

Table 3.1. *Optimization of [4+2] reaction conditions.[a]*
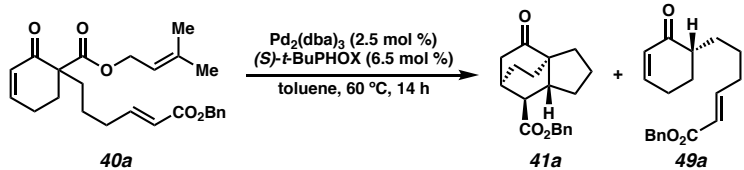
Entry	Deviation from standard conditions	Yield *41a* (%)[b]	ee *41a* (%)	Yield *49a* (%)[b]	ee *49a* (%)
1	none	96 (83)	87 (87)	–	–
2	THF	86	81	–	–
3	benzene	92	87	–	–
4	1,4-dioxane	12	–	63	49
5	40 °C	51	89	–	–
6	*(S)*-(CF$_3$)$_3$-*t*-BuPHOX	12	89	66	62
7	*(S)*-(OMe)$_3$-*t*-BuPHOX	40	88	26	65
8	4-methylaniline (1 equiv)	93 (73)	87 (88)	–	–
9	4-methylaniline (2 equiv)	78	87	–	–
10	3,5-dimethylphenol (1 equiv)	0	–	100	71
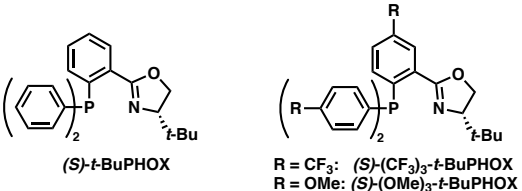
[a] Conditions: 0.02 mmol **40a**, 2.5 mol % Pd$_2$(dba)$_3$, 6.5 mol % ligand, in 1.0 mL of solvent (0.02 M). [b] Yields determined by ^{1}H NMR with respect to 1,3,5-trimethoxybenzene as internal standard. Isolated yields on 0.2 mmol scale in parentheses.

A control reaction excluding 4-methylaniline was carried out, and surprisingly, desired product **41a** was formed in 83% yield and 87% ee (Figure 3.3B). This suggests that an alternative catalyst turnover mechanism is operative. Further NMR experiments revealed the stoichiometric evolution of isoprene (**52**) accompanying formation of product **41a**. Intrigued by this unexpected finding and clean reaction profile, we pursued optimization of additive-free reaction conditions.

The reaction proceeds in THF and benzene albeit in slightly diminished yield and enantioselectivity (entries 2–3, Table 3.1). Employing 1,4-dioxane as the solvent, protonation product **49a** was obtained as the major product in 63% yield and 49% ee, while cycloadduct **41a** was observed in only 12% yield (entry 4, Table 3.1). Lowering the temperature to 40 ºC slightly improved the ee to 89% at the cost of decreased conversion (entry 5, Table 3.1). Modification of the electronic properties of the PHOX ligand deleteriously impacted the product distribution (entries 6–7, Table 3.1). Phenol and aniline additives do not improve the reaction (entries 8–10, Table 3.1). Ultimately, optimized reaction conditions were determined to be additive-free with *(S)-t*-BuPHOX in toluene at 60 ºC. The reaction affords **41a**, a bridged bicycle with a pendant fused ring, in 83% isolated yield and 87% ee. The transformation allows for the simultaneous construction of four contiguous stereocenters, including one all-carbon quaternary center. Gratifyingly, the reaction can be performed with reduced catalyst loading (0.625 mol %) on 1.0 mmol scale to afford **41a** in 59% yield and 89% ee. The ability to efficiently construct these complex building blocks on scale highlights the synthetic utility of this transformation.

3.2.2 PROPOSED MECHANISM

We sought to capitalize on these initial exciting results by constructing a mechanistic framework to inform rational design. Based on our lab's prior investigations of Pd-catalyzed decarboxylative asymmetric allylic alkylation reactions, we propose that oxidative addition of Pd^0 to β-ketoester **40a** proceeds through complex **53** to afford the η^1-allyl carboxylate resting state **54** (Scheme 3.1).[12] Rate-limiting decarboxylation ensues, affording O-bound Pd enolate **55**.[3,12] This chiral conjugated enolate then serves as the diene

in a [4+2] cycloaddition (**TS30**) with the pendant dienophile to form tricyclic enolate **56**.

Subsequent proton transfer would generate product **41a**. Concomitant isoprene generation,

followed by ligand exchange, allows for re-entry into the original catalytic cycle at **53**. We

posit that the formation of undesired ketone **49a** arises from an off-cycle pathway, where

catalyst turnover occurs prior to cycloaddition via premature proton transfer to **55**.

Scheme 3.1. *Proposed divergent catalytic cycle. Undesired reaction pathways in grey.*
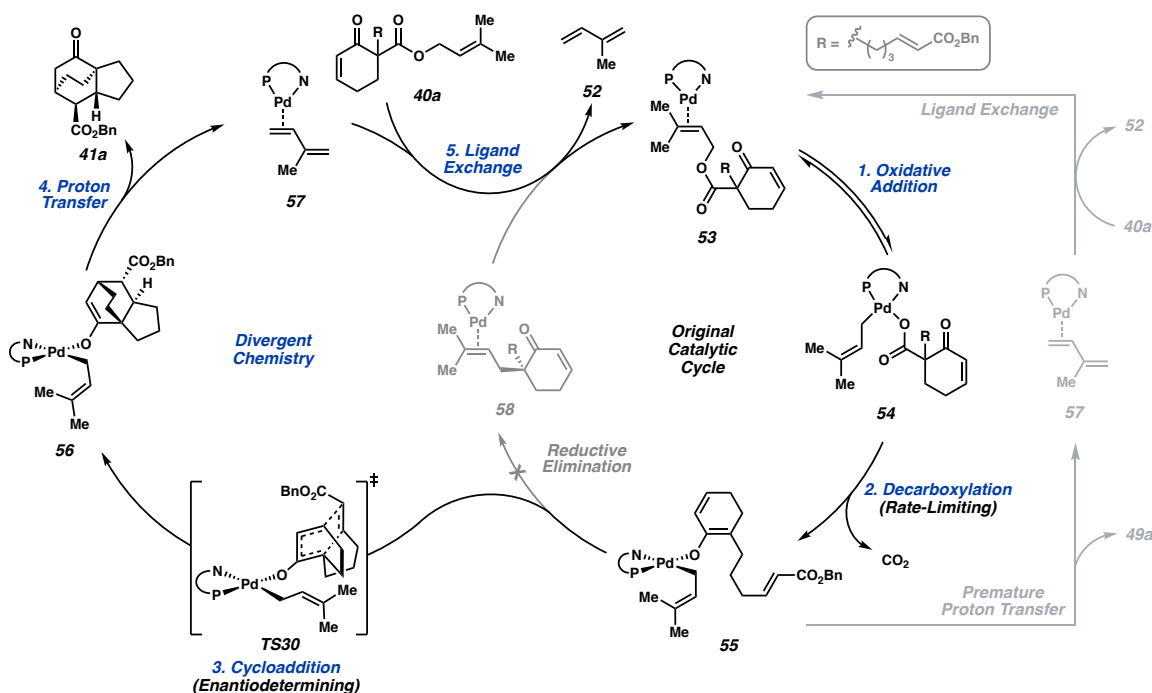
3.2.3 SUBSTRATE SCOPE

With a working mechanistic hypothesis in hand, we sought to draw further

mechanistic insights from substrate design, while simultaneously exploring limits of the

reaction. Considering the inverse relationship between diene ring size and Diels–Alder

Table 3.2. *Substrate scope of the [4+2] reaction.*[a]

Substrate	Product(s)
40h	**41h (endo)** (not observed) — **49h** 33% yield, 58% ee
40i	**41i (endo)** (not observed) — **49i** 80% yield, 7% ee
40j	**41j (endo)** 50% yield, 87% ee
40k	**41k (endo) 41k' (exo) 41k" (other)** 82% yield, 10.4:1.4:1 dr, 88% ee (endo)
40l	**41l (endo)** 90% yield, 89% ee
40m	**41m (endo) 41m' (exo)** 65% yield, 1.4:1 dr[b] 62% ee (endo), 62% ee (exo)
40n	**41n (endo)** 88% yield, 14.3:1 dr, 91% ee

Substrate	Product(s)
R = Bn **40a** / R = Et **40b**	**41a (endo)** 83% yield, 87% ee / **41b (endo)** 85% yield, 88% ee
40c	**41c (endo)** 65% yield, 65% ee
40d	**41d (endo)** 83% yield, 97% ee
40e	**41e (endo)** (not observed) — **49e** 81% yield, 47% ee
40f	**41f (endo)** 42% yield, 92% ee — **49f** 45% yield, 51% ee
40g	**41g (endo)** (not observed) — **49g** 74% yield, 56% ee

40o

41o (endo)   **41o' (exo)**
92% yield, 1.1:1 dr
84% ee (endo), 79% ee (exo)

40s

41s (endo)
69% yield, 83% ee

40p

41p (endo)
81% yield, 28.4:1 dr[b], 72% ee

40t

41t (endo)   **41t' (exo)**
89% yield, 2.6:1 dr[b]
85% ee (endo), 72% ee (exo)

40q

41q (endo)   **41q' (exo)**
92% yield, 1.6:1 dr
84% ee (endo), 29% ee (exo)

40u

41u (endo)
22% yield, >20:1 dr at *, 61% ee

40r

41r (endo)
47% yield, 89% ee

[a] Conditions: 0.2 mmol **40a**, 2.5 mol % Pd₂(dba)₃, 6.5 mol % ligand, in toluene (10 mL, 0.02 M), isolated yields, dr determined by ¹H NMR analysis of reaction crude. [b] dr determined by isolated yields of endo/exo products.

reaction rate [13],[2], we explored whether this trend impacts the generality of our transformation. However, with cyclopentyl diene derived from enone **40c**, a decrease in yield and ee, relative to six-membered parent substrate **40a**, was noted (Table 3.2). In comparison to smaller ring sizes, seven-membered cyclic dienes require increased distortion energy to reach the desired transition state.[13] Despite this, seven-membered ring substrate **40d** leads to a high yield and improved ee. Thus, this transformation represents a powerful method to synthesize various challenging bicyclic cores.

Figure 3.4. *Eyring analysis of* **41/49** *product ratio for propylene and butylene tethered substrates* **40a** *and* **40f**.[a]

T (°C)	41a : 49a	41f : 49f
60	–	1.5 : 1.0
80	8.7 : 1.0	1.0 : 1.0
100	5.9 : 1.0	1.0 : 2.2
120	3.4 : 1.0	1.0 : 2.8
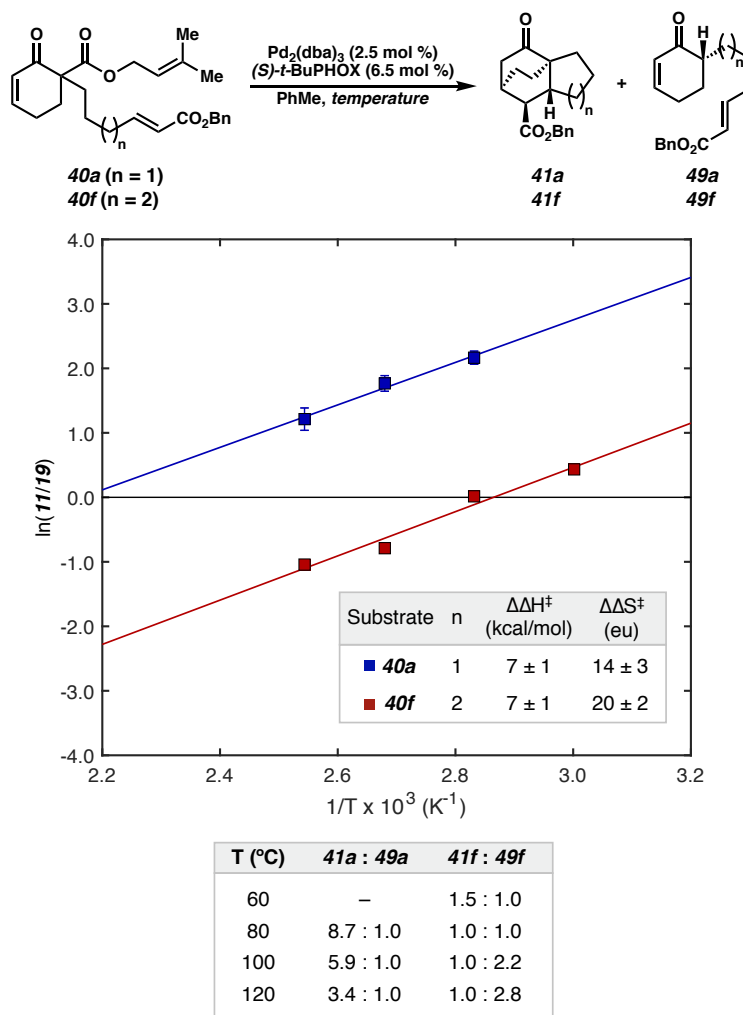
[a] All data points collected in triplicate, error bars and ranges reflect a 95% confidence interval.[14] Reactions carried out on 0.02 mmol scale with product ratios determined by crude ^{1}H NMR analysis.

The dienophile tether length was subsequently modulated to test its influence on product distribution. The ethylene tethered substrate **40e** yields solely the premature protonation product **49e**, likely due to insurmountable developing ring strain in the cycloaddition transition state. In contrast to the propylene tethered substrate **40a**, the

butylene tethered substrate **40f** leads to a near equal distribution of cycloadduct **41f** (42% yield) and prematurely protonation product **49f** (45% yield). Following this trend, the pentylene tethered substrate **40g** leads only to protonation product **49g**. Rationalizing this phenomenon, we propose that lengthening the tether increases conformational flexibility and imposes a greater entropic penalty to the highly organized [4+2] transition state. In contrast, increased tether length is inconsequential to the protonation process, which does not involve the dienophile.

Eyring analysis of product distributions from reactions of **40a** and **40f** further supports the hypothesis of an entropic preference for the formation of **49a/f** over **41a/f** (Figure 3.4). With **40a**, cycloaddition (**41a**) is enthalpically favored ($\Delta\Delta H^{\ddagger} = 7$ kcal/mol) but entropically disfavored ($\Delta\Delta S^{\ddagger} = 14$ eu) over protonation (**49a**). As anticipated, increasing the tether length to four methylene units (**40f**) further increases the relative entropic penalty for cycloaddition ($\Delta\Delta S^{\ddagger} = 20$ eu), while the differential enthalpy of activation remains similar ($\Delta\Delta H^{\ddagger} = 7$ kcal/mol). Hence, entropy differences associated with tether length lead to the formation of differential amounts of undesired ketones **49a** and **49f**.

We then surveyed the scope of functional groups that are tolerated in this reaction (Table 3.2). The cycloaddition does not proceed in the absence of a π-acceptor (**40h**), and carboxylic acid **40i** exclusively affords undesired ketone **49i**. To our delight, a variety of functional groups are compatible, including ethyl ester **10b**, phenyl ketone **10j**, phenyl ester **40k**, mesityl ester **40l**, N-hydroxyphthalimido (NHP) ester **40m**, enecarbamate **40n**, and *N*-acyl oxazolidinone **40o**. Additionally, further conjugated cinnamic ester dienophile **40p**

affords tetracycle **41p**. These results demonstrate the ability to tolerate varying dienophile electronics, incorporate additional functional handles, and access alternate ring systems.

The majority of the substrate scope is reflective of a stereospecific process, yielding only *endo* and *exo* diastereomers. We sought to exploit this property of the reaction to access other diastereomers of **41a** by employing *(Z)*-olefin dienophile **40q**. Gratifyingly, desired cycloadducts **41q** (*endo*) and **41q'** (*exo*) are furnished in a 1.6:1 ratio with a 92% combined yield, in 84% and 29% ee, respectively.

Further substitution patterns on the substrate were explored with the aim of increasing the stereochemical complexity of the products. Trisubstituted benzyl ester dienophile **40r** furnished cycloadduct **41r**, featuring two all-carbon quaternary centers, in 47% yield and 90% ee. β-Methyl (**40s**) and β-ethoxy (**40t**) α,β-unsaturated enones are also competent substrates, forging additional tetrasubstituted bridgehead stereocenters. Finally, we explored α-methyl substituted enone **40u**. The corresponding product **41u** was produced, bearing five contiguous stereocenters in >20:1 dr.

In summary, the transformation described herein represents a versatile method for the preparation of a variety of enantioenriched polycyclic scaffolds. Inspired by these results, we sought to explore the origins of enantioinduction and the mechanism by which catalyst turnover is achieved.

3.2.4   [4+2] CYCLOADDITION

In order to probe the origins of enantioinduction in the transformation, we first aimed to elucidate the enantiodetermining step in the catalytic cycle. We hypothesized that either the cycloaddition is irreversible and dictates the stereochemical outcome, or a

reversible [4+2] is coupled to a subsequent enantiodetermining step. First, we computationally evaluated the energetics of the [4+2] process. Cycloaddition directly from conjugated enolate **55** to transposed enolate **56** via **TS30** is achieved with a $\Delta G^{\ddagger}$ of 9.8 and ΔG of -22.3 kcal/mol (Figure 3.5A). The 32.1 kcal/mol barrier to the reverse process renders the cycloaddition step irreversible under the reaction conditions. Hence, our computations suggest that the cycloaddition step is enantiodetermining.

To assess this hypothesis experimentally, reaction product **41a** was converted to its corresponding prenyl enol carbonate **59**. Under the standard reaction conditions, Pd^0 undergoes oxidative addition to **59**, and decarboxylation affords target common intermediate **56** (Figure 3.5B).[5] When enantioenriched or racemic **59** is subjected to the reaction conditions, cycloadduct **41a** is obtained in high yield and identical enantiopurity to that of the respective enol carbonate precursor (**59**) (Figure 3.5B). No stereochemical resolution in product **41a** is observed from racemic enol carbonate **59**, indicating that a post-cycloaddition process is not responsible for enantioinduction. In addition to verifying the irreversibility of the cycloaddition step, these experiments also support the viability of enolate **56** as an intermediate in the catalytic cycle (Scheme 3.1).

Considering the [4+2] cycloaddition as the enantiodetermining process, the origin of enantioinduction in this step was investigated. As such, the lowest energy *endo* transition states giving rise to each enantiomer of **41a** were evaluated (Figure 3.5C). The minimum energy pathway to each enantiomer of product features a transition state in which the dienophile tether is *syn* to the *t*-Bu group of the PHOX ligand – in accord with prior observations in inner-sphere allylic alkylation transition states.[3,15] From this orientation,

***Figure* 3.5.** *(A) Computed barriers.[a] (B) Experimentally verifying irreversibility of the C–C bond formation. (C) Origins of enantioinduction in the [4+2] cycloaddition step.*

A. Thermodynamics of C–C bond formation.

$\Delta G^{\ddagger}_{forward} = 9.8$
$\Delta G^{\ddagger}_{reverse} = 32.1$

55
$G_{rel} = 0.0$

TS30
$G_{rel} = 9.8$

56
$G_{rel} = -22.3$
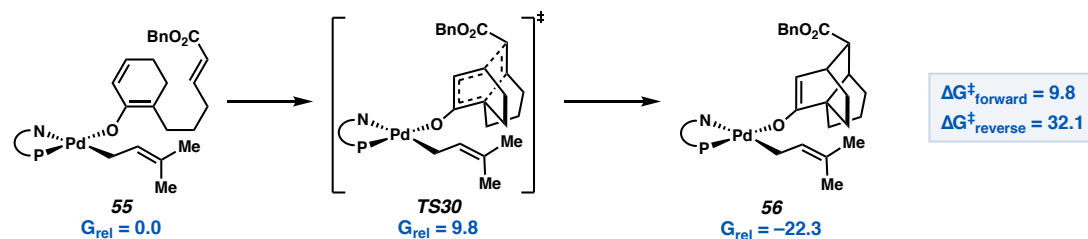
B. Enantioenrichment as readout of reversibility.

Pd$_2$(dba)$_3$ (2.5 mol %)
(S)-t-BuPHOX (6.5 mol %)
toluene, 60 °C

[4+2] step is irreversible and enantiodetermining

59

52

56

41a

ee *59* (%)	ee *41a* (%)	Yield *41a* (%)
87	87	92
0	0	92

C. Origins of enantioinduction (R = CO$_2$Bn).

Favored

External approach of dienophile (to 41a)

sterically accessible face

TS30
$\Delta G^{\ddagger}_{rel} = 0.0$

open back pocket

TS30

Disfavored

Internal approach of dienophile (to ent-41a)

steric clash

TS31
$\Delta G^{\ddagger}_{rel} = 1.6$

steric clash

TS31
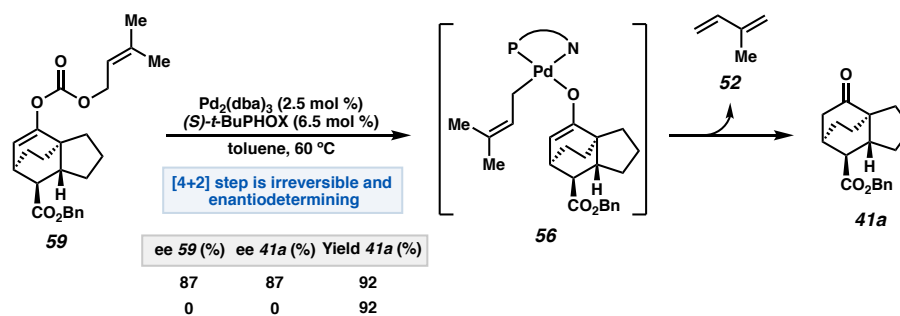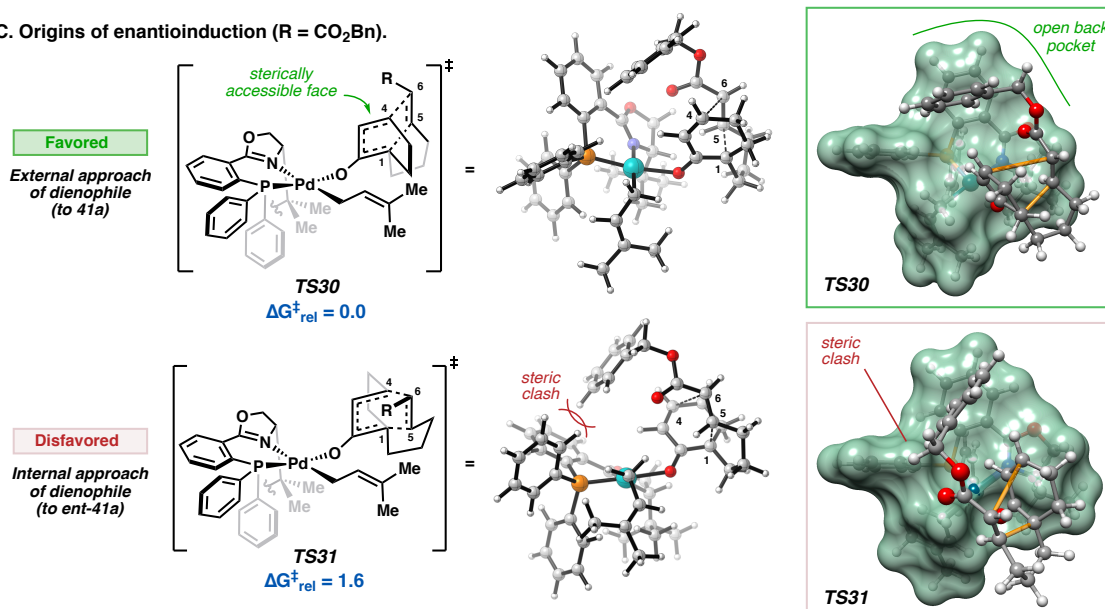
[a] Gibbs free energies in kcal/mol. See supporting information in section 3.4 for details.

the dienophile preferentially approaches the externally-exposed enantiotopic face of the diene to avoid steric clash between the benzyl ester and the phenyl groups of the PHOX ligand scaffold (Figure 3.5C). A 1.6 kcal/mol preference for external (**TS30**) over internal (**TS31**) approach is calculated, in accord with the experimentally observed 87% ee.[16] The major enantiomer of product (**41a**) predicted by computations matches that of the major enantiomer obtained experimentally, as confirmed by vibrational circular dichroism (VCD) spectroscopy (see 3.4 Supporting Information for details).

In summary, our investigations reveal C–C bond formation to be the enantiodetermining step, with enantioselectivity achieved by biasing *external* over *internal* dienophile approach (Figure 3.5).

3.2.5   CATALYST TURNOVER

Our [4+2] transformation is rendered catalytic by a unique reduction of Pd^{II} to Pd^0 that occurs concomitantly with formation of isoprene (**52**) and ketone **41a**. This observation motivated computational investigations to elucidate the catalyst turnover mechanism.

Of the numerous mechanisms explored, the minimum energy pathway involves isomerization of **56** to an N-detached π-allyl Pd species (**60**) and subsequent inner-sphere proton transfer (**TS4**) (Figure 3.6). Additionally, a pathway featuring outer-sphere proton transfer (**TS5**) was found to be highly competitive for catalyst turnover. These two processes present very similar free energy barriers of 22.3 and 22.4 kcal/mol, respectively, which are readily surmountable at 60 °C. A single favored pathway is not identified as the energy difference between the two mechanisms is within error of computations. In both pathways, subsequent ligand exchange of isoprene (**52**) for starting material **40a** completes

the catalytic cycle. Analysis of Intrinsic Bonding Orbitals (IBOs)[17] along the reaction coordinate suggest these processes are best conceptualized as the transfer of a proton, rather than a hydride, to the Pd enolate (see 3.4 Supporting Information for details).[18] Analogous mechanisms were found to be operative from pre-cycloaddition enolate **55**, giving rise to premature protonation product **49a**.

Figure 3.6. *Two lowest-energy pathways for catalyst turnover.*[a]
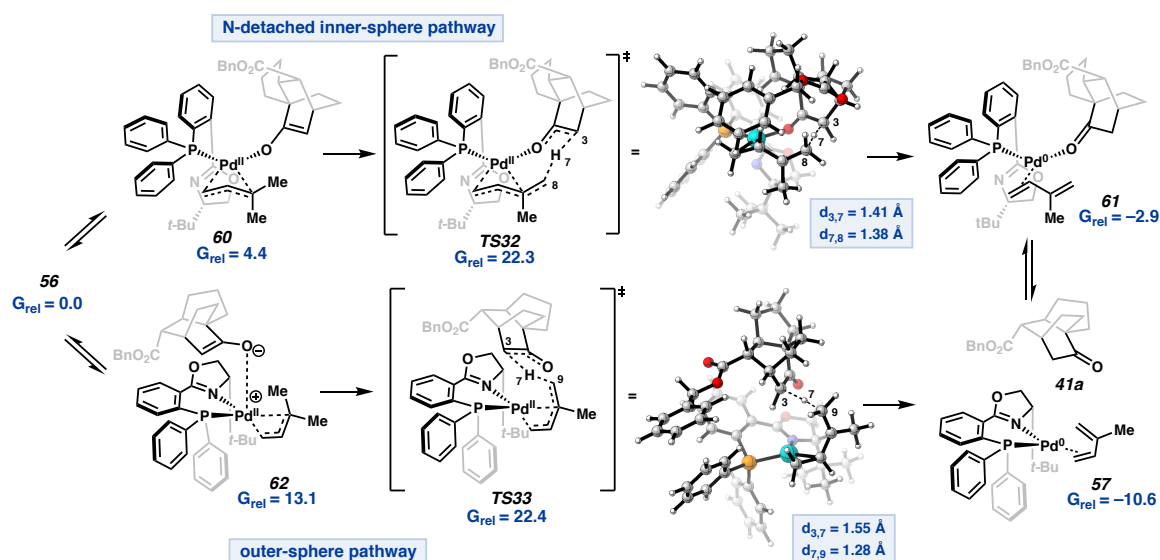
[a] Gibbs free energies in kcal/mol. See section 3.4 supporting information for details.

3.2.6   FURTHER MECHANISM-BASED DEVELOPMENTS

While this method allows access to a variety of complex scaffolds, premature protonation remains an outstanding challenge we sought to address. As such, we aimed to leverage our mechanistic insights surrounding this process to inhibit byproduct formation.

Figure 3.7. *(A) KIE study. (B) Prenyl ester modification.*

A. Leveraging kinetic isotope effect (KIE) to slow proton transfer.[a]

D-40f

Pd$_2$(dba)$_3$ (2.5 mol %)
*(S)-t-*BuPHOX (6.5 mol %)
toluene, 60 °C, 14 h

93% D[b]

D-41f
66% yield, 91% ee,
1.6:1 dr at *

64% D[b]

D-49f
24% yield, 55% ee

B. Modification of prenyl ester via cyclic and benzylic analogs.[c]

Pd$_2$(dba)$_3$ (2.5 mol %)
*(S)-t-*BuPHOX (6.5 mol %)
toluene, 60 °C, 14 h

41f

49f

Entry	R		Yield 41f (%)	ee 41f (%)	Yield 49f (%)	ee 49f (%)
1		(40f)	44	91	42	40
2[d]		(63)	25	92	44	46
3		(64)	8	–	89	48
4		(65)	63	92	21	44
5		(66)	48	92	46	38
6[e]		(67)	14	94	86	60

[a] Conditions: 0.20 mmol **D-40f**, 2.5 mol % Pd$_2$(dba)$_3$, 6.5 mol % ligand, in 10 mL of solvent (0.02 M). [b] Deuterium incorporation determined by HRMS. [c] Conditions: 0.02 mmol substrate, 2.5 mol % Pd$_2$(dba)$_3$, 6.5 mol % ligand, in 1.0 mL of solvent (0.02 M). Yield determined by ^{1}H NMR with respect to 1,3,5-trimethoxybenzene as internal standard. [d] 21% of allylic alkylation product was also observed. [e] The corresponding benzylic diene was also observed (see 3.4 Supporting Information for details).

To that end, we turned our attention to butylene tethered substrate **40f** given its similar yield of desired **41f** (44%) and byproduct **49f** (42%). We envisioned favoring the formation of **41f** by modification of the ancillary prenyl moiety. By introducing a kinetic isotope effect, we aimed to slow down the protonation processes. To our delight, employing hexa-deutero prenyl ester **D-40f** (Figure 3.7A) increases the yield of desired cycloadduct **D-41f** to 66%, with 91% ee.[19] Next, cyclic analogs of the prenyl ester **40f** were prepared (Figure 3.7B). At one extreme, seven-membered exocycle **66** affords a product distribution which closely mirrors that of parent substrate **40f** (entry 5). Excitingly, contracting the ring by one methylene (**65**) shifts the distribution favorably toward **41f** (entry 4, 3:1 ratio of **41f:49f**). However, five- and four-membered exocycles (**64** and **63**), as well as acyclic bis-benzylic allylic ester **67**, afford unfavorable product distributions.

In summary, we find appropriate modification of the prenyl moiety to be effective in suppressing deleterious side reactions. This is particularly important as the ring system generated in this reaction is a scaffold relevant to natural product synthesis.

3.2.7   PRODUCT DERIVATIZATIONS

To assess the utility of the asymmetric intramolecular [4+2] products, we started by altering the oxidation state of ketone **41a** (Figure 3.8A) through a 1,2-reduction, which provided alcohol **68** in quantitative yield and in 1.5:1 dr. Subsequently, we explored ring expansion strategies to incorporate heteroatoms and to furnish different ring systems (Figure 3.8A). From ketone **41a**, oxime condensation and subsequent Beckmann rearrangement afforded lactam **69** as a single isomer in 56% yield over two steps.

Analogously, Baeyer–Villiger oxidation furnished lactone **70** in 41% yield as a single isomer.

Furthermore, the tricyclic cycloaddition products closely resemble many members of the atisane family of diterpenoids (Figure 3.8B, **71-74**). Therefore, reactions to further functionalize these scaffolds were explored. First, hydrogenolysis followed by persulfate-mediated radical decarboxylation of **41f** afforded ketone **75** in 27% yield over two steps.[20] We were delighted to find that the exo-cyclic methylene motif presented in both crotogoudin (**71**) and campylopin (**74**) could be achieved through aldol condensations from both **75** and **41f** to yield crotogoudin-like enone **76** in 41% yield and analogous enone **77** in 26% yield.[21] Enone **77** can be further functionalized through dihydroxylation to furnish the primary and tertiary alcohol centers of the acochlearine (**72**) core in 13% yield and 10:1 dr (**78**).[22] A wider spectrum of natural product cores could also be accessed through oxidation at different sites of the tricyclic hydrocarbon backbone. For example, Riley oxidation of **41f** provided diketone **79** in 50% yield,[23] which can then be selectively mono-protected as acetal **80** in 41% yield.[24] Further manipulations to the exposed ketone of **80** could yield spiramilactam B (**73**)-like oxidation patterns. To that end, directed C–H oxidation following an oxime condensation of **41f** yielded oxime **81** in 30% yield. Deprotection of the oxime afforded the desired acetate on campylopin (**74**)-like tricycle **82** in 19% yield as a single diastereomer.[25] Overall, derivatization of the Diels–Alder product **41f** allowed access to four natural product-like motifs, demonstrating the potential of applying this transformation to asymmetric natural product syntheses.

Figure 3.8. *(A) Oxidation state alterations, ring system adjustments, and heteroatom incorporation on **41a**. (B) Reaction sequences to construct natural product-like cores.*

A. Reactivity of Diels–Alder product 41a.

NaBH$_4$, MeOH

1,2-Reduction

68
99% yield
*1.5:1 dr at ***

1. NaOAc, NH$_2$OH·HCl, MeOH
2. SOCl$_2$, THF

Beckmann Rearrangement

69
56% yield

m-CPBA, NaHCO$_3$, CH$_2$Cl$_2$

Baeyer–Villiger Oxidation

70
41% yield
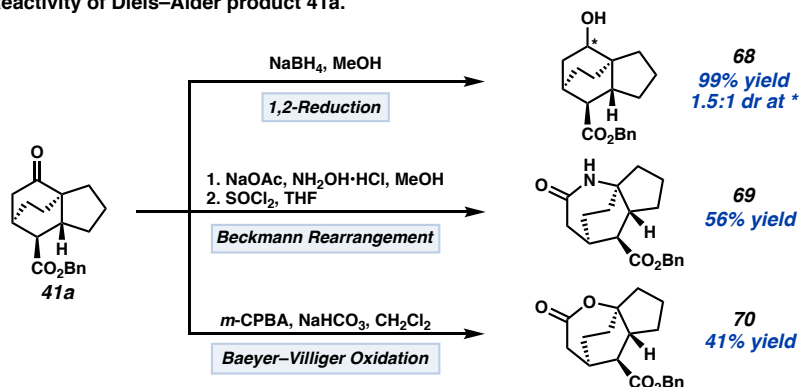
B. Construction of natural product-like cores from asymmetric Diels–Alder product 41f.

71
Crotogoudin

72
Acochlearine

73
Spiramilactam B

74
Campylopin

1. H$_2$, Pd/C, MeOH
2. 2,4,6-collidine, (NH$_4$)$_2$S$_2$O$_8$, DMSO

75
27% yield

i) HCO$_2$Et, KHMDS toluene
ii) HCHO$_{(aq)}$, THF

76
41% yield

i) HCO$_2$Et, KHMDS toluene
ii) HCHO$_{(aq)}$, THF

77
26% yield

K$_2$OsO$_4$·2H$_2$O NMO

acetone, H$_2$O

78
13% yield
10:1 dr

SeO$_2$

HOAc

79
50% yield

HC(OMe)$_3$
p-TsOH·H$_2$O

MeOH

80
41% yield

1. NH$_2$OH·HCl NaOAc, MeOH/H$_2$O
2. PhI(OAc)$_2$, Pd(OAc)$_2$ AcOH, Ac$_2$O

81
30% yield

K$_2$CO$_3$, NaHSO$_3$

MeOH/H$_2$O

82
19% yield
> 20:1 dr

3.3 CONCLUSIONS

We developed an asymmetric decarboxylative [4+2] cycloaddition employing a key catalytically-generated chiral Pd enolate intermediate – analogous to those implicated in inner-sphere allylic alkylation reactions. To enable this transformation, we first systematically modified the allyl moiety to disfavor undesired allylic alkylation. This allows the conjugated Pd enolate to engage in a [4+2] cycloaddition with a pendant dienophile. Computational and experimental analysis supports the role of C–C bond formation as the enantiodetermining step. Further computational investigation reveals that the catalyst turnover occurs through a proton transfer from the prenyl group directly to the transposed enolate, forming the desired product and releasing isoprene. Building upon these mechanistic insights, we were able to further favor the desired [4+2] cycloaddition over premature protonation for challenging substrates relevant to complex natural product synthesis. In summary, our approach of divergent catalysis serves as a powerful framework for rational design in asymmetric catalytic reactions. Studies applying this strategy more broadly in other synthetically relevant transformations are currently underway.

3.4 SUPPORTING INFORMATION

3.4.1 MATERIALS AND METHODS

Unless otherwise stated, reactions were performed in flame-dried glassware under an argon or nitrogen atmosphere using dry, deoxygenated solvents. Solvents were dried by passage through an activated alumina column under argon.[26] Reaction progress was monitored by thin-layer chromatography (TLC) or Agilent 1290 UHPLC-MS. TLC was performed using E. Merck silica gel 60 F254 precoated glass plates (0.25 mm) and

visualized by UV fluorescence quenching or KMnO$_4$ staining. Silicycle Silia*Flash*® P60 Academic Silica gel (particle size 40–63 nm) was used for flash chromatography. ^{1}H NMR spectra were recorded on a Bruker 400 MHz spectrometer and are reported relative to residual CHCl$_3$ (δ 7.26 ppm). ^{13}C NMR spectra were recorded on a Bruker 400 MHz spectrometer (100 MHz) and are reported relative to CHCl$_3$ (δ 77.16 ppm). ^{2}H NMR spectra were recorded on a Bruker 400 MHz (61 MHz) spectrometer and are reported relative to residual CDCl$_3$ (δ 7.26 ppm). Data for ^{1}H NMR are reported as follows: chemical shift (δ ppm) (multiplicity, coupling constant (Hz), integration). Multiplicities are reported as the peaks appear as follows: s = singlet, d = doublet, t = triplet, q = quartet, p = pentet, sept = septuplet, m = multiplet, br s = broad singlet, br d = broad doublet. Data for ^{13}C NMR are reported in terms of chemical shifts (δ ppm). Some reported spectra include minor solvent impurities of water (δ 1.56ppm), ethyl acetate (δ 4.12, 2.05, 1.26 ppm), methylene chloride (δ 5.30 ppm), acetone (δ 2.17 ppm), grease (δ 1.26, 0.86 ppm), and/or silicon grease (δ 0.07 ppm), which do not impact product assignments. ^{13}C NMR spectra of deuterated compounds are complicated by the low intensity of peaks of deuterium-substituted carbon atoms. IR spectra were obtained by use of a Perkin Elmer Spectrum BXII spectrometer or Nicolet 6700 FTIR spectrometer using thin films deposited on NaCl plates and reported in frequency of absorption (cm^{-1}). Optical rotations were measured with a Jasco P-2000 polarimeter operating on the sodium D-line (589 nm), using a 100 mm path-length cell. Analytical SFC was performed with a Mettler SFC supercritical CO$_2$ analytical chromatography system utilizing Chiralpak (AD-H or IC) or Chiralcel (OD-H, OJ-H, or OB-H) columns (4.6 mm x 25 cm) obtained from Daicel Chemical Industries, Ltd.

High resolution mass spectra (HRMS) were obtained from the Caltech Mass Spectral Facility using a JEOL JMS-600H High Resolution Mass Spectrometer in Field Desorption (FD+) mode. Absolute stereochemical assignments were made by vibrational circular dichroism analysis for select compounds with related compounds assigned by analogy.

Reagents were purchased from commercial sources and used as received unless otherwise stated. Ligands were prepared according to literature procedures.[27]

List of Abbreviations: ee – enantiomeric excess, SFC – supercritical fluid chromatography, TLC – thin-layer chromatography, IPA – isopropanol, VCD – vibrational circular dichroism.

3.4.2 EXPERIMENTAL PROCEDURES AND SPECTROSCOPIC DATA

Pd-Catalyzed Decarboxylative Cycloadditions

General Procedure A: Asymmetric Pd-Catalyzed Decarboxylative Cycloadditions.
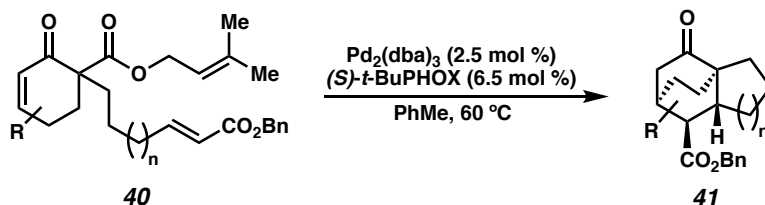
In a nitrogen filled glovebox, an oven-dried 20 mL vial was charged with a stir bar, Pd$_2$(dba)$_3$ (4.6 mg, 0.005 mmol, 2.5 mol %), *(S)-t*-BuPHOX (5.0 mg, 0.013 mmol, 6.5 mol %), and toluene (5 mL). The catalyst solution was stirred at 23 °C for 20 min. A solution of substrate **40** (0.2 mmol, 1 equiv) in toluene (5 mL) was added to the vial. The resultant solution was then heated to 60 °C for 14 h. The solution was then cooled to 23 °C and concentrated under reduced pressure. The crude reaction mixture was loaded directly

onto a flash column and the product (**41**) was isolated by silica gel flash column chromatography.

41a
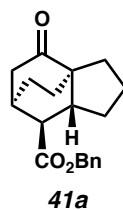
benzyl (3a*R*,6*R*,7*S*,7a*R*)-4-oxooctahydro-3a,6-ethanoindene-7-carboxylate (41a)

Prepared from **40a** following General Procedure A. Purification by flash column chromatography (0–35% EtOAc/hexanes) afforded the title compound as a colorless oil (49.7 mg, 0.167 mmol, 83% yield, 87% ee). Absolute and relative stereochemistry were assigned by VCD (vida infra). 2D NMR studies independently confirm the relative stereochemistry (vida infra).

^{1}H NMR (400 MHz, CDCl$_3$): δ 7.40 – 7.31 (m, 5H), 5.14 (d, *J* = 1.6 Hz, 2H), 2.54 (dt, *J* = 18.8, 2.3 Hz, 1H), 2.51 – 2.47 (m, 2H), 2.21 (dddd, *J* = 10.6, 8.7, 7.2, 1.7 Hz, 1H), 2.14 – 2.04 (m, 3H), 1.86 (ddd, *J* = 13.0, 11.1, 6.8 Hz, 1H), 1.81 – 1.72 (m, 2H), 1.70 – 1.52 (m, 3H), 1.44 (ddt, *J* = 12.9, 10.9, 1.8 Hz, 1H), 1.22 (ddd, *J* = 13.9, 9.2, 4.9 Hz, 1H).

^{13}C NMR (100 MHz, CDCl$_3$): δ 215.1, 174.7, 136.0, 128.8, 128.5, 128.2, 66.7, 54.2, 47.5, 43.3, 41.3, 32.9, 29.1, 27.4, 26.5, 25.1, 22.6.

IR (Neat Film, NaCl): 2947, 2873, 1726, 1455, 1267, 1160 cm^{-1}.

HRMS (MM: FD+): *m/z* calc'd for C$_{19}$H$_{22}$O$_3$ [M]$^+$: 298.1564, found 298.1576.

Optical Rotation: $[\alpha]_D^{21}$ –20.3 (c 1.00, CHCl$_3$).

SFC conditions: 15% IPA, 2.5 mL/min, Chiralpak AD-H column, λ = 210 nm, t$_R$ (min): minor = 4.21, major = 5.30

41b
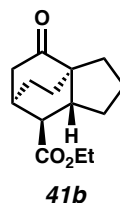
ethyl (3a*R*,6*R*,7*S*,7a*R*)-4-oxooctahydro-3a,6-ethanoindene-7-carboxylate (41b)

Prepared from **40b** following General Procedure A. Purification by flash column chromatography (5–30% EtOAc/hexanes) afforded the title compound as a colorless oil (39.9 mg, 0.169 mmol, 84% yield, 88% ee).

¹H NMR (400 MHz, CDCl₃): δ 4.15 (q, *J* = 7.1 Hz, 2H), 2.55 (dt, *J* = 18.8, 2.6 Hz, 1H), 2.49 – 2.44 (m, 1H), 2.42 (d, *J* = 8.6 Hz, 1H), 2.23 – 2.14 (m, 1H), 2.15 – 2.04 (m, 3H), 1.91 – 1.71 (m, 3H), 1.71 – 1.52 (m, 3H), 1.50 – 1.40 (m, 1H), 1.26 (t, *J* = 7.1 Hz, 3H), 1.21 (dt, *J* = 9.2, 4.9 Hz, 1H).

¹³C NMR (100 MHz, CDCl₃): δ 215.2, 174.9, 60.8, 54.2, 47.5, 43.3, 41.3, 32.9, 29.1, 27.4, 26.5, 25.1, 22.6, 14.4.

IR (Neat Film, NaCl): 2947, 2873, 1725, 1270, 1170 cm⁻¹.

HRMS (MM: FD+): *m/z* calc'd for C₁₄H₂₀O₃ [M]⁺: 236.1412, found 236.1415.

Optical Rotation: [α]_D²¹ –34.2 (c 1.00, CHCl₃).

Enantiomeric excess determined by converting ethyl ester to benzyl ester through saponification and Steglish esterification.

SFC conditions: 15% IPA, 2.5 mL/min, Chiralpak AD-H column, λ = 210 nm, t_R (min): minor = 4.21, major = 5.30

41c
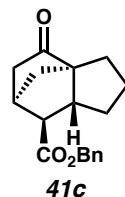
benzyl (3a*R*,6*R*,7*S*,7a*R*)-4-oxooctahydro-3a,6-methanoindene-7-carboxylate (41c)

Prepared from **40c** following General Procedure A. Purification by flash column chromatography (0–30% EtOAc/hexanes) afforded the title compound as a colorless oil (37.0 mg, 0.130 mmol, 65% yield, 65% ee).

^{1}H NMR (400 MHz, CDCl$_3$): δ 7.42 – 7.29 (m, 5H), 5.13 (dd, *J* = 12.3, 7.9 Hz, 2H), 2.96 (t, *J* = 4.2, 1H), 2.92 (ddd, *J* = 5.2, 3.7, 1.4, 1H), 2.42 – 2.35 (m, 1H), 2.22 – 2.17 (m, 1H), 2.16 – 2.05 (m, 3H), 1.95 (ddtd, *J* = 12.9, 8.4, 5.1, 2.2 Hz, 1H), 1.90 – 1.80 (m, 2H), 1.66 (dt, *J* = 10.6, 1.6 Hz, 1H), 1.52 – 1.37 (m, 2H).

^{13}C NMR (100 MHz, CDCl$_3$): δ 213.9, 173.3, 136.0, 128.8, 128.5, 128.3, 67.8, 66.6, 52.4, 48.5, 41.8, 40.6, 40.5, 32.2, 27.5, 22.1.

IR (Neat Film, NaCl): 2960, 2358, 1739, 1164, 730, 668 cm^{-1}.

HRMS (MM: FD+): *m/z* calc'd for C$_{18}$H$_{20}$O$_3$ [M]$^+$: 284.1414, found 284.1407.

Optical Rotation: $[\alpha]_D^{21}$ +20.0 (c 1.00, CHCl$_3$).

SFC conditions: 15% IPA, 2.5 mL/min, Chiralpak AD-H column, λ = 210 nm, t$_R$ (min): minor = 3.97, major = 4.33.

41d
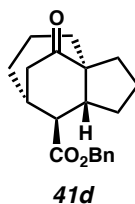
benzyl (3a*R*,7*R*,8*S*,8a*R*)-10-oxooctahydro-1*H*-3a,7-ethanoazulene-8-carboxylate (41d)

Prepared from **40d** following General Procedure A. Purification by flash column chromatography (0–35% EtOAc/hexanes) afforded the title compound as a colorless oil (51.8 mg, 0.166 mmol, 83% yield, 97% ee).

^{1}H NMR (400 MHz, CDCl$_3$): δ 7.40 – 7.31 (m, 5H), 5.16 (d, *J* = 12.4 Hz, 1H), 5.12 (d, *J* = 12.3 Hz, 1H), 2.70 – 2.63 (m, 2H), 2.64 – 2.56 (m, 1H), 2.25 (ddd, *J* = 18.5, 2.0, 1.0 Hz, 1H), 2.08 (td, *J* = 10.5, 7.8 Hz, 1H), 2.03 – 1.94 (m, 1H), 1.93 – 1.79 (m, 3H), 1.78 – 1.60 (m, 4H), 1.59 – 1.43 (m, 4H).

^{13}C NMR (100 MHz, CDCl$_3$): δ 215.7, 175.8, 136.0, 128.8, 128.5, 128.3, 66.7, 58.0, 50.2, 45.4, 41.0, 35.7, 33.6, 33.3, 32.0, 28.0, 21.8, 21.2.

IR (Neat Film, NaCl): 2934, 2873, 1727, 1713, 1455, 1161 cm^{-1}.

HRMS (MM: FD+): *m/z* calc'd for C$_{20}$H$_{24}$O$_3$ [M+H]$^+$: 312.1720, found 312.1734.

Optical Rotation: [α]$_D^{21}$ +21.4 (c 1.00, CHCl$_3$).

SFC conditions: 15% IPA, 2.5 mL/min, Chiralpak AD-H column, λ = 210 nm, t$_R$ (min): minor = 4.70, major = 6.23.

41f

benzyl (1*S*,2*R*,4a*R*,8a*R*)-4-oxooctahydro-2*H*-2,4a-ethanonaphthalene-1-carboxylate (41f).

Prepared from **40f** following General Procedure A. Purification by flash column chromatography (0–35% EtOAc/hexanes) afforded the title compound as a colorless oil (26.3 mg, 0.084 mmol, 42% yield, 92% ee).

¹H NMR (400 MHz, CDCl₃): δ 7.39 – 7.29 (m, 5H), 5.16 (d, *J* = 12.4 Hz, 1H), 5.10 (d, *J* = 12.2 Hz, 1H), 2.47 (dt, *J* = 17.0, 2.8 Hz, 2H), 2.28 – 2.19 (m, 2H), 2.14 (ddd, *J* = 19.7, 3.8, 1.8 Hz, 1H), 2.01 (dddd, *J* = 11.8, 6.8, 4.5, 1.7 Hz, 1H), 1.87 (ddtd, *J* = 12.8, 4.5, 3.4, 1.6 Hz, 1H), 1.83 – 1.71 (m, 1H), 1.71 – 1.56 (m, 4H), 1.51 – 1.11 (m, 5H).

¹³C NMR (100 MHz, CDCl₃): δ 216.3, 174.5, 136.0, 128.7, 128.4, 128.2, 66.7, 49.8, 45.1, 40.5, 37.1, 30.9, 30.0, 28.9, 26.2, 25.6, 21.7, 21.1.

IR (Neat Film, NaCl): 2928, 2856, 1721, 1170 cm⁻¹.

HRMS (MM: FD+): *m/z* calc'd for C₂₀H₂₄O₃ [M]⁺: 312.1720, found 312.1732.

Optical Rotation: [α]$_D^{21}$ −15.5 (c 1.00, CHCl₃).

SFC conditions: 15% IPA, 2.5 mL/min, Chiralpak AD-H column, λ = 210 nm, t$_R$ (min): minor = 4.70, major = 6.23.

41j
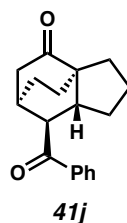
(3a*R*,6*R*,7*S*,7a*R*)-7-benzoylhexahydro-3a,6-ethanoinden-4(1*H*)-one (41j)

Prepared from **40j** following General Procedure A. Purification by flash column chromatography (0–30% EtOAc/hexanes) afforded the title compound as a colorless oil (27.1 mg, 0.101 mmol, 50% yield, 87% ee).

¹H NMR (400 MHz, CDCl₃): δ 7.97 – 7.94 (m, 2H), 7.61 – 7.56 (m, 1H), 7.51 – 7.46 (m, 2H), 3.42 (d, *J* = 8.5 Hz, 1H), 2.58 – 2.50 (m, 2H), 2.41 – 2.38 (m, 1H), 2.16 (ddd, *J* = 13.7, 11.1, 6.2 Hz, 1H), 2.08 – 1.87 (m, 4H), 1.82 – 1.74 (m, 1H), 1.70 – 1.50 (m, 4H), 1.25 (ddd, *J* = 14.0, 9.2, 5.1 Hz, 1H).

¹³C NMR (100 MHz, CDCl₃): δ 214.9, 201.0, 136.4, 133.4, 128.9, 128.5, 54.2, 49.4, 41.4, 40.8, 34.1, 28.9, 27.8, 26.5, 25.6, 22.7.

IR (Neat Film, NaCl): 2945, 2871, 1720, 1677, 1447, 1217 cm⁻¹.

HRMS (MM: FD+): *m/z* calc'd for C₁₈H₂₀O₂ [M]⁺: 268.1463, found 268.1463.

Optical Rotation: [α]_D²¹ –32.7 (c 1.00, CHCl₃).

SFC conditions: 30% IPA, 2.5 mL/min, Chiralpak AD-H column, λ = 210 nm, t_R (min): minor = 2.55, major = 3.40.

41k
(endo-trans)

41k'
(exo-cis)

41k"
(endo-cis)
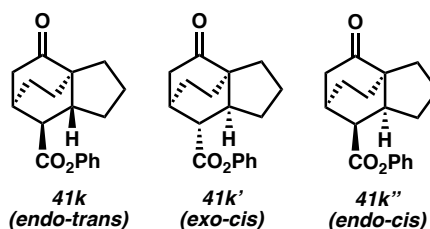
phenyl (3a*R*,6*R*,7*S*,7a*R*)-4-oxooctahydro-3a,6-ethanoindene-7-carboxylate (41k, 41k' and 41k'')

Prepared from **40k** following General Procedure A. Purification by flash column chromatography (0–35% EtOAc/hexanes) afforded the title compound as a colorless oil (47.2 mg, 0.166 mmol, 83% yield, 14.8:1.6:1.0 *endo-trans/endo-cis/exo-trans*, 88% ee (*endo-trans*)). Crude analysis by ¹H NMR affords a 10.4:1.4:1.0 ratio of *endo-trans/exo-trans/endo-cis*. The diastereomers were subsequently separated by preparative HPLC (15% IPA/hexanes, 25 mL/min, Chiralpak AD-H column) for independent characterization. Absolute and relative stereochemistry were assigned/confirmed by VCD where applicable (vida infra) in addition to 2D NMR.

41k (endo-trans):

¹H NMR (400 MHz, CDCl₃): δ 7.41 – 7.34 (m, 2H), 7.25 – 7.20 (m, 1H), 7.09 – 7.04 (m, 2H), 2.70 (d, *J* = 8.7 Hz, 1H), 2.67 – 2.60 (m, 2H), 2.31 (dddd, *J* = 10.6, 8.8, 7.3, 1.7 Hz, 1H), 2.23 – 2.09 (m, 3H), 1.97 – 1.76 (m, 3H), 1.67 (ddddd, *J* = 13.5, 11.1, 9.0, 6.2, 4.5 Hz, 3H), 1.50 (ddt, *J* = 12.5, 10.6, 1.7 Hz, 1H), 1.31 – 1.17 (m, 1H).

¹³C NMR (100 MHz, CDCl₃): δ 214.8, 173.4, 150.7, 129.6, 126.0, 121.5, 54.2, 47.5, 43.4, 41.2, 32.9, 29.1, 27.3, 26.5, 25.0, 22.5.

IR (Neat Film, NaCl): 2948, 2872, 1750, 1721, 1592, 1492, 1192, 1144 cm⁻¹.

HRMS (MM: FD+): *m/z* calc'd for $C_{18}H_{20}O_3$ [M]⁺: 284.1412, found 284.1411.

Optical Rotation: $[\alpha]_D^{21}$ –16.7 (c 0.20, CHCl₃). *(single major enantiomer of 11j)*

SFC conditions: 15% IPA, 2.5 mL/min, Chiralpak AD-H column, λ = 210 nm, t_R (min): minor = 4.09, major = 6.08.

41k' (exo-trans):

¹H NMR (400 MHz, CDCl₃): δ 7.39 – 7.34 (m, 2H), 7.25 – 7.19 (m, 1H), 7.06 – 7.01 (m, 2H), 3.30 (dt, *J* = 12.0, 2.3 Hz, 1H), 3.08 (dt, *J* = 19.5, 2.8 Hz, 1H), 2.58 (h, *J* = 2.8 Hz, 1H), 2.47 – 2.33 (m, 2H), 2.21 (dt, *J* = 19.6, 2.4 Hz, 1H), 2.08 – 2.01 (m, 2H), 1.93 – 1.71 (m, 5H), 1.70 – 1.59 (m, 1H), 1.04 (ddd, *J* = 12.8, 11.4, 6.7 Hz, 1H).

¹³C NMR (100 MHz, CDCl₃): δ 215.2, 171.8, 150.6, 129.6, 126.0, 121.7, 54.6, 45.8, 44.0, 40.1, 31.4, 28.4, 28.2, 27.0, 26.3, 21.8.

IR (CDCl₃ solution): 2951, 2870, 1751, 1717, 1194, 1163, 1146 cm⁻¹.

HRMS (MM: FD+): *m/z* calc'd for $C_{18}H_{20}O_3$ [M]⁺: 284.1412, found 284.1417.

41k'' (endo-cis):

¹H NMR (400 MHz, CDCl₃): δ 7.43 – 7.36 (m, 2H), 7.27 – 7.22 (m, 1H), 7.12 – 7.07 (m, 2H), 2.76 – 2.67 (m, 1H), 2.58 (dt, *J* = 8.3, 1.7 Hz, 1H), 2.48 – 2.33 (m, 4H), 2.12 – 2.01 (m, 2H), 1.91 – 1.63 (m, 5H), 1.10 (ddd, *J* = 13.0, 11.2, 6.5 Hz, 1H), 1.01 (ddd, *J* = 12.4, 9.5, 2.8 Hz, 1H).

¹³C NMR (100 MHz, CDCl₃): δ 215.1, 172.9, 150.9, 129.6, 126.1, 121.6, 53.8, 49.4, 46.0, 44.2, 32.7, 32.0, 28.6, 27.4, 22.6, 21.5.

IR (CDCl₃ solution): 2945, 2872, 1751, 1717, 1194, 1163, 1130 cm⁻¹.

HRMS (MM: FD+): *m/z* calc'd for C₁₈H₂₀O₃ [M]⁺: 284.1412, found 284.1407.

41l
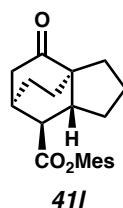
mesityl (3a*R*,6*R*,7*S*,7a*R*)-4-oxooctahydro-3a,6-ethanoindene-7-carboxylate (41l)

Prepared from **40l** following General Procedure A. Purification by flash column chromatography (0–35% EtOAc/hexanes) afforded the title compound as a colorless oil (58.6 mg, 0.180 mmol, 90% yield, 89% ee).

¹H NMR (400 MHz, CDCl₃):) δ 6.87 (s, 2H), 2.75 (d, *J* = 8.8 Hz, 1H), 2.72 – 2.65 (m, 2H), 2.36 (dddd, *J* = 10.6, 8.9, 7.3, 1.6 Hz, 1H), 2.26 (s, 3H), 2.24 – 2.09 (m, 3H), 2.08 (s, 6H), 1.98 – 1.78 (m, 3H), 1.75 – 1.61 (m, 3H), 1.55 – 1.48 (m, 1H), 1.31 – 1.24 (m, 1H).

¹³C NMR (100 MHz, CDCl₃): δ 214.8, 172.8, 145.9, 135.6, 129.5, 129.5, 54.2, 47.4, 43.5, 41.3, 33.2, 29.2, 27.5, 26.5, 25.1, 22.6, 20.9, 16.4.

IR (Neat Film, NaCl): 2946, 2873, 1747, 1723, 1485, 1458, 1189, 1137 cm⁻¹.

HRMS (MM: FD+): *m/z* calc'd for C₂₁H₂₆O₃ [M]⁺: 326.1877, found 326.1886.

Optical Rotation: $[\alpha]_D^{21}$ –25.8 (c 1.00, CHCl$_3$).

SFC conditions: 15% IPA, 2.5 mL/min, Chiralpak AD-H column, λ = 210 nm, t_R (min): minor = 4.06, major = 4.33.
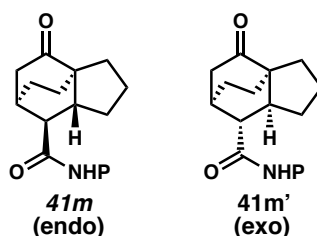
1,3-dioxoisoindolin-2-yl **(3a*R*,6*R*,7*S*,7a*R*)-4-oxooctahydro-3a,6-ethanoindene-7-carboxylate (41m and 41m')**

Prepared from **40m** following General Procedure A. Purification by flash column chromatography (0–35% EtOAc/hexanes) afforded the title compounds as colorless oils (**Endo**: 37.7 mg, 0.106 mmol, 53% yield, 62% ee; **Exo**: 8.6 mg, 0.024 mmol, 12% yield, 62% ee).

41m (endo):

^{1}H NMR (400 MHz, CDCl$_3$): δ 7.92 – 7.85 (m, 2H), 7.83 – 7.75 (m, 2H), 2.84 (dd, *J* = 8.7, 1.3 Hz, 1H), 2.71 (m, 1H), 2.64 (dt, *J* = 18.9, 2.5 Hz, 1H), 2.46 – 2.28 (m, 1H), 2.28 – 2.18 (m, 2H), 2.13 (m, 1H), 1.98 – 1.76 (m, 3H), 1.76 – 1.60 (m, 3H), 1.56 – 1.48 (m, 1H), 1.34 – 1.19 (m, 1H).

^{13}C NMR (100 MHz, CDCl$_3$): δ 214.0, 171.4, 162.1, 135.0, 129.0, 124.2, 54.1, 44.8, 43.3, 41.0, 33.2, 28.9, 27.2, 26.4, 24.9, 22.4.

IR (Neat Film, NaCl): 2948, 2873, 1782, 1742, 1718, 1466, 1362, 1185 cm^{-1}.

HRMS (MM: FD+): *m/z* calc'd for C$_{20}$H$_{19}$NO$_5$ [M]$^+$: 353.1263, found 353.1251.

Optical Rotation: $[\alpha]_D^{21}$ –0.2 (c 1.00, CHCl$_3$).

SFC conditions: 30% IPA, 2.5 mL/min, Chiralpak IC column, l = 210 nm, t$_R$ (min): minor = 4.03, major = 3.00

41m' (exo):

^{1}H NMR (400 MHz, CDCl$_3$): δ 7.90 (dd, *J* = 5.5, 3.1 Hz, 2H), 7.81 (dd, *J* = 5.5, 3.1 Hz, 2H), 2.77 (tt, *J* = 3.9, 2.2 Hz, 1H), 2.73 (d, *J* = 8.4 Hz, 1H), 2.47 – 2.28 (m, 4H), 2.19 – 2.02 (m, 2H), 1.92 – 1.71 (m, 4H), 1.71 – 1.61 (m, 1H), 1.11 (ddd, *J* = 13.1, 11.2, 6.6 Hz, 1H), 1.08 – 0.95 (m, 1H).

^{13}C NMR (100 MHz, CDCl$_3$): δ 214.2, 170.8, 162.1, 135.0, 129.1, 124.2, 53.7, 46.7, 46.0, 44.1, 32.9, 31.8, 28.4, 27.2, 22.5, 21.2.

IR (Neat Film, NaCl): 2947, 2868, 1809, 1784, 1743, 1717, 1466, 1362, 1185 cm^{-1}.

HRMS (MM: FD+): *m/z* calc'd for C$_{20}$H$_{19}$NO$_5$ [M]$^+$: 353.1263, found 353.1261.

Optical Rotation: $[\alpha]_D^{21}$ –13.6 (c 0.81, CHCl$_3$).

SFC conditions: 30% IPA, 2.5 mL/min, Chiralpak IC column, l = 210 nm, t$_R$ (min): minor = 4.98, major = 4.29.

41n
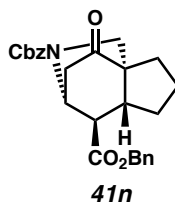
dibenzyl (3aR,4R,5R,7aS)-7-oxooctahydro-5,7a-(epiminomethano)indene-4,9-dicarboxylate (41n)

Prepared from **40n** following General Procedure A. Purification by flash column chromatography (0–40 % EtOAc/hexanes) afforded the title compound as a colorless oil (76.1 mg, 0.176 mmol, 88% yield, 14.3:1 endo/exo, 91% ee (endo)).

¹H NMR (400 MHz, CDCl₃): δ 7.35 (dd, J = 7.1, 4.9 Hz, 10H), 5.21 – 5.07 (m, 4H), 4.90 – 4.74 (m, 1H), 3.49 (dd, J = 12.1, 5.8 Hz, 1H), 3.40 – 3.27 (m, 1H), 2.88 (t, J = 8.9 Hz, 1H), 2.66 – 2.42 (m, 2H), 2.30 (p, J = 9.3 Hz, 1H), 2.23 – 2.10 (m, 2H), 1.91 – 1.56 (m, 3H), 1.33 – 1.14 (m, 1H).

¹³C NMR (100 MHz, CDCl₃): δ 210.1, 209.7, 172.2, 154.4, 136.3, 135.5, 128.9, 128.7, 128.7, 128.4, 128.4, 128.4, 128.3, 128.2, 128.1, 67.6, 67.2, 55.9, 55.8, 50.4, 50.0, 48.8, 48.6, 45.7, 45.6, 42.6, 42.6, 41.7, 41.6, 29.0, 28.9, 24.1, 22.9.

IR (Neat Film, NaCl): 3399, 2963, 2874, 2357, 1729, 1700, 1652, 1414, 1288, 1156, 1115, 748, 681 cm⁻¹.

HRMS (MM: FD+): *m/z* calc'd for C₂₆H₂₇NO₅ [M]⁺: 433.1889, found 433.1874.

Optical Rotation: $[\alpha]_D^{21}$ –39.8 (c 0.75, CHCl₃).

SFC conditions: 15% IPA, 2.5 mL/min, Chiralpak AD-H column, l = 210 nm, t_R (min): minor = 9.19, major = 11.59.

41o (endo)   **41o' (exo)**
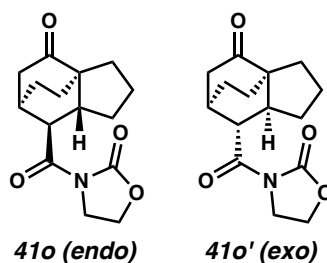
3-((3a*R*,6*R*,7*S*,7a*R*)-4-oxooctahydro-3a,6-ethanoindene-7-carbonyl)oxazolidin-2-one (41o and 41o')

Prepared from **40o** following General Procedure A. Purification by flash column chromatography (0–90 % EtOAc/hexanes) afforded the title compound as a colorless oil (51.2 mg, 0.185 mmol, 92% yield, 1.1:1 endo/exo (ratio from crude ^{1}H NMR analysis), 84% ee (endo), 79% ee (exo)).

41o (endo):

^{1}H NMR (400 MHz, CDCl$_3$): δ 4.43 (t, *J* = 8.1 Hz, 2H), 4.15 – 4.00 (m, 2H), 3.54 – 3.47 (m, 1H), 2.66 (ddd, *J* = 12.4, 8.3, 6.9 Hz, 1H), 2.52 – 2.25 (m, 4H), 1.92 – 1.68 (m, 5H), 1.67 – 1.53 (m, 2H), 1.08 (ddd, *J* = 12.9, 11.2, 6.4 Hz, 1H), 0.89 (tt, *J* = 12.3, 9.5 Hz, 1H).

^{13}C NMR (100 MHz, CDCl$_3$): δ 215.5, 173.8, 153.4, 62.1, 53.7, 48.3, 44.1, 44.0, 43.1, 33.8, 31.3, 28.7, 27.3, 22.8, 20.8.

IR (Neat Film, NaCl): 2942, 2867, 1775, 1714, 1693, 1387, 1267, 1222, 1040 cm^{-1}.

HRMS (MM: FD+): *m/z* calc'd for C$_{15}$H$_{19}$NO$_4$ [M]$^+$: 277.1314, found 277.1321.

Optical Rotation: [α]$_D^{21}$ –39.5 (c 1.00, CHCl$_3$).

SFC conditions: 20% IPA, 2.5 mL/min, Chiralpak AD-H column, λ = 210 nm, t$_R$ (min): minor = 4.15, major = 5.17.

41o' (exo):

^{1}H NMR (400 MHz, CDCl$_3$): δ 4.43 (t, *J* = 8.1 Hz, 2H), 4.13 – 3.97 (m, 2H), 3.71 (d, *J* = 8.8 Hz, 1H), 2.59 – 2.41 (m, 2H), 2.35 (dd, *J* = 3.5, 2.3 Hz, 1H), 2.19 – 1.84 (m, 5H), 1.81 – 1.41 (m, 6H), 1.27 – 1.18 (m, 1H).

^{13}C NMR (100 MHz, CDCl$_3$): δ 214.9, 174.6, 153.5, 62.13, 54.1, 45.6, 43.1, 41.2, 40.6, 34.5, 28.4, 27.3, 26.5, 25.3, 22.7.

IR (Neat Film, NaCl): 2949, 2872, 1775, 1718, 1692, 1387, 1221,1040, 759 cm^{-1}.

HRMS (MM: FD+): *m/z* calc'd for $C_{15}H_{19}NO_4$ [M]$^+$: 277.1314, found 277.1317.

Optical Rotation: $[\alpha]_D^{21}$ –5.8 (c 1.00, CHCl$_3$).

SFC conditions: 15% IPA, 2.5 mL/min, Chiralpak AD-H column, λ = 210 nm, t_R (min): minor = 6.80, major = 6.38.

41p (endo)   41p' (exo)
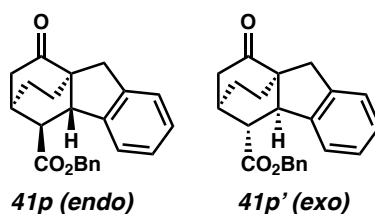
benzyl   (3R,4S,4aS,9aS)-1-oxo-1,2,3,4,4a,9-hexahydro-3,9a-ethanofluorene-4-carboxylate (41p and 41p')

Prepared from **40p** following General Procedure A. Purification by flash column chromatography (0–35% EtOAc/hexanes) afforded the title compounds as colorless oils (**Endo**: 56.8 mg, 0.156 mmol, 78% yield, 72% ee; **Exo**: 2.0 mg, 5.48 µmol, 3% yield).

41p (endo):

¹H NMR (400 MHz, CDCl₃): δ 7.28 – 7.20 (m, 5H), 7.14 – 7.05 (m, 4H), 5.13 (d, *J* = 2.4 Hz, 2H), 3.53 (dd, *J* = 9.4, 1.0 Hz, 1H), 3.16 (d, *J* = 15.7 Hz, 1H), 2.74 (dt, *J* = 9.3, 1.1 Hz, 1H), 2.61 (dt, *J* = 18.8, 2.4 Hz, 1H), 2.51 (ttd, *J* = 3.5, 2.2, 1.1 Hz, 1H), 2.31 (d, *J* = 15.8 Hz, 1H), 2.11 (ddd, *J* = 18.8, 3.5, 1.2 Hz, 1H), 1.70 – 1.56 (m, 2H), 1.54 – 1.45 (m, 1H), 1.42 – 1.34 (m, 1H).

¹³C NMR (100 MHz, CDCl₃): δ 214.0, 174.6, 142.3, 140.6, 135.8, 128.8, 128.6, 128.4, 127.3, 127.0, 125.5, 124.3, 67.1, 56.6, 47.8, 45.6, 42.1, 35.0, 33.2, 27.0, 24.8.

IR (Neat Film, NaCl): 2942, 2869, 1726, 1457, 1164 cm^{-1}.

HRMS (MM: FD+): *m/z* calc'd for $C_{23}H_{22}O_3$ [M+H]$^+$: 346.1564, found 346.1571.

Optical Rotation: $[\alpha]_D^{21}$ +1.4 (c 1.00, CHCl$_3$).

SFC conditions: 15% IPA, 2.5 mL/min, Chiralpak AD-H column, λ = 210 nm, t_R (min): minor = 6.74, major = 6.28.

41p' (exo):

^{1}H NMR (400 MHz, CDCl$_3$): δ 7.41 – 7.34 (m, 5H), 7.24 (d, *J* = 7.1 Hz, 1H), 7.14 – 7.07 (m, 3H), 5.30 (d, *J* = 12.3 Hz, 1H), 5.25 (d, *J* = 12.3 Hz, 1H), 3.85 (d, *J* = 9.4 Hz, 1H), 3.46 (d, *J* = 14.7 Hz, 1H), 2.75 (d, *J* = 9.3 Hz, 1H), 2.69 – 2.65 (m, 1H), 2.44 (d, *J* = 14.9 Hz, 1H), 2.37 (dd, *J* = 18.7, 2.1 Hz, 1H), 2.19 (ddd, *J* = 18.6, 3.4, 2.1 Hz, 1H), 2.15 – 2.07 (m, 2H), 1.90 – 1.84 (m, 1H), 1.81 – 1.76 (m, 1H).

^{13}C NMR (100 MHz, CDCl$_3$): δ 213.5, 174.0, 143.8, 142.7, 135.9, 128.8, 128.6, 128.4, 127.2, 126.6, 124.8, 122.5, 67.1, 56.4, 49.9, 48.3, 44.1, 35.3, 31.9, 27.5, 21.8.

IR (Neat Film, NaCl): 2918, 1727, 1161 cm^{-1}.

HRMS (MM: FD+): *m/z* calc'd for C$_{23}$H$_{22}$O$_3$ [M+H]$^+$: 346.1569, found 346.1568.

41q (endo) *41q' (exo)*
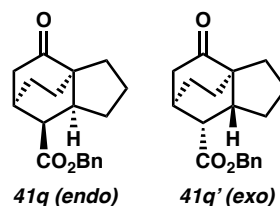
benzyl (3a*R*,6*R*,7*S*,7a*S*)-4-oxooctahydro-3a,6-ethanoindene-7-carboxylate (41q and 41q')

Prepared from **40q** following General Procedure A. Purification by flash column chromatography (0–35% EtOAc/hexanes) afforded the title compound as a colorless oil (54.9 mg, 0.183 mmol, 92% yield, 1.6:1 endo/exo, 84% ee (endo), 29% ee (exo)). The *endo* (**41q**) and *exo* (**41q'**) diastereomers were subsequently separated by preparative TLC (25%

EtOAc/hexanes) for independent characterization. Absolute and relative stereochemistry were assigned/confirmed by VCD (see below).

41q (endo):

^{1}H NMR (400 MHz, CDCl$_3$): δ 7.39 – 7.31 (m, 5H), 5.13 – 5.02 (m, 2H), 3.10 – 2.99 (m, 2H), 2.47 (h, J = 2.9 Hz, 1H), 2.36 – 2.21 (m, 2H), 2.15 (dt, J = 19.3, 2.3 Hz, 1H), 1.86 – 1.63 (m, 6H), 1.56 – 1.48 (m, 1H), 1.06 – 0.92 (m, 2H).

^{13}C NMR (100 MHz, CDCl$_3$): δ 215.5, 172.9, 135.9, 128.7, 128.7, 128.5, 66.3, 54.4, 45.9, 44.0, 40.2, 31.4, 28.3, 28.1, 27.0, 26.4, 21.8.

IR (Neat Film, NaCl): 2940, 2868, 1728, 1456, 1174, 1166, 1146 cm^{-1}.

HRMS (MM: FD+): *m/z* calc'd for C$_{19}$H$_{22}$O$_3$ [M]$^+$: 298.1564, found 298.1578.

Optical Rotation: [α]$_D^{21}$ –32.4 (c 1.00, CHCl$_3$).

SFC conditions: 15% IPA, 2.5 mL/min, Chiralpak AD-H column, λ = 210 nm, t$_R$ (min): minor = 5.44, major = 6.53.

41q' (exo):

^{1}H NMR (400 MHz, CDCl$_3$): δ 7.40 – 7.31 (m, 5H), 5.14 (d, J = 12.3 Hz, 1H), 5.09 (d, J = 12.2 Hz, 1H), 3.01 (ddd, J = 11.7, 3.3, 1.4 Hz, 1H), 2.46 (h, J = 3.3 Hz, 1H), 2.35 – 2.25 (m, 3H), 2.14 (tdd, J = 11.6, 7.9, 1.6 Hz, 1H), 2.07 – 1.94 (m, 2H), 1.88 – 1.69 (m, 3H), 1.63 – 1.57 (m, 1H), 1.47 – 1.34 (m, 2H), 1.16 (ddd, J = 13.9, 9.1, 5.0 Hz, 1H).

^{13}C NMR (100 MHz, CDCl$_3$): δ 215.5, 173.1, 136.0, 128.8, 128.5, 128.5, 66.3, 53.6, 45.4, 42.7, 41.2, 32.0, 26.4, 25.3, 24.4, 22.3, 21.8.

IR (Neat Film, NaCl): 2946, 2847, 1720, 1457, 1154 cm^{-1}.

HRMS (MM: FD+): *m/z* calc'd for C$_{19}$H$_{22}$O$_3$ [M]$^+$: 298.1564, found 298.1578.

Optical Rotation: $[\alpha]_D^{21}$ –5.1 (c 1.00, CHCl$_3$).

SFC conditions: 15% IPA, 2.5 mL/min, Chiralpak IC column, λ = 210 nm, t$_R$ (min): minor = 7.01, major = 7.42.
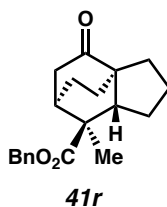
benzyl (3a*R*,6*R*,7*S*,7a*S*)-7-methyl-4-oxooctahydro-3a,6-ethanoindene-7-carboxylate (41r)

Prepared from **40r** following General Procedure A. Purification by flash column chromatography (0–30% EtOAc/hexanes) afforded the title compound as a colorless oil (29.4 mg, 0.094 mmol, 47% yield, 89% ee).

^{1}H NMR (400 MHz, CDCl$_3$): δ 7.39 – 7.29 (m, 5H), 5.16 (d, *J* = 12.4 Hz, 1H), 5.10 (d, *J* = 12.4 Hz, 1H), 2.49 – 2.38 (m, 2H), 2.32 (dt, *J* = 18.9, 2.8 Hz, 1H), 2.19 – 2.10 (m, 2H), 2.01 – 1.92 (m, 1H), 1.85 – 1.66 (m, 4H), 1.65 – 1.55 (m, 1H), 1.49 – 1.31 (m, 5H), 1.13 (ddd, *J* = 14.5, 9.1, 6.0 Hz, 1H).

^{13}C NMR (100 MHz, CDCl$_3$): δ 215.2, 177.8, 136.1, 128.7, 128.4, 128.0, 66.8, 54.37, 45.8, 44.7, 43.4, 37.3, 26.5, 24.4, 24.1, 22.7, 22.4, 20.8.

IR (Neat Film, NaCl): 2951, 2875, 1723, 1454, 1239, 1212, 1106 cm^{-1}.

HRMS (MM: FD+): *m/z* calc'd for C$_{20}$H$_{24}$O$_3$ [M]$^+$: 312.1725, found 312.1732.

Optical Rotation: $[\alpha]_D^{21}$ –15.3 (c 1.00, CHCl$_3$).

SFC conditions: 40% IPA, 2.5 mL/min, Chiralpak IC column, λ = 210 nm, t$_R$ (min): minor = 2.68, major = 3.51.

41s
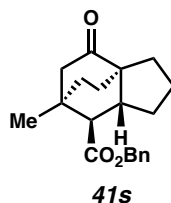
benzyl (3aR,6R,7R,7aR)-6-methyl-4-oxooctahydro-3a,6-ethanoindene-7-carboxylate (41s)

Prepared from **40s** following General Procedure A. Purification by flash column chromatography (0–25% EtOAc/hexanes) afforded the title compound as a colorless oil (43.6 mg, 0.140 mmol, 69% yield, 83% ee).

^{1}H NMR (400 MHz, CDCl$_3$): δ 7.42 – 7.29 (m, 5H), 5.13 (d, *J* = 1.1 Hz, 2H), 2.86 (dd, *J* = 18.5, 3.5 Hz, 1H), 2.37 (dd, *J* = 8.8, 1.4 Hz, 1H), 2.29 – 2.15 (m, 1H), 2.15 – 2.04 (m, 1H), 2.01 – 1.70 (m, 3H), 1.84 (dd, *J* = 18.7, 1.4 Hz, 1H), 1.68 – 1.36 (m, 4H), 1.30 – 1.15 (m, 2H), 0.94 (s, 3H).

^{13}C NMR (100 MHz, CDCl$_3$): δ 214.5, 174.9, 135.9, 128.8, 128.5, 128.5, 66.7, 54.2, 52.6, 47.0, 44.9, 38.0, 36.0, 28.7, 26.3, 26.0, 23.8, 22.8.

IR (Neat Film, NaCl): 2949, 2873, 1750, 1498, 1454, 1384, 1324, 1155, 1114, 977, 754, 698, 678, 556 cm^{-1}.

HRMS (MM: FD+): *m/z* calc'd for C$_{20}$H$_{24}$O$_3$ [M]$^+$: 312.1703, found 312.1720.

Optical Rotation: [α]$_D^{21}$ –68.2 (c 0.75, CHCl$_3$).

SFC conditions: 15% IPA, 2.5 mL/min, Chiralpak IC column, λ = 210 nm, t$_R$ (min): minor = 10.23, major = 12.31.

41t (endo)   **41t' (exo)**
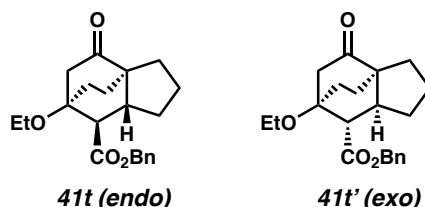
benzyl (3a*R*,6*S*,7*R*,7a*R*)-6-ethoxy-4-oxooctahydro-3a,6-ethanoindene-7-carboxylate (41t and 41t')

Prepared from **40t** following General Procedure A. Purification by flash column chromatography (0–50% EtOAc/hexanes) afforded the title compounds as colorless oils (**Endo**: 44.0 mg, 0.128 mmol, 64% yield, 85% ee; **Exo**: 17.0 mg, 0.050 mmol, 25% yield, 72% ee). Absolute and relative stereochemistry were assigned/confirmed by VCD (see below).

41t (endo):

^{1}H NMR (400 MHz, CDCl$_3$): δ 7.38 – 7.28 (m, 5H), 5.16 (d, *J* = 1.5 Hz, 2H), 3.55 – 3.32 (m, 2H), 3.17 (dd, *J* = 18.5, 3.1 Hz, 1H), 2.86 (dd, *J* = 8.5, 1.5 Hz, 1H), 2.38 – 2.25 (m, 2H), 2.16 – 2.02 (m, 1H), 2.02 – 1.86 (m, 3H), 1.87 – 1.39 (m, 5H), 1.20 (ddd, *J* = 14.1, 9.1, 5.1 Hz, 1H), 1.03 (t, *J* = 7.0 Hz, 3H).

^{13}C NMR (100 MHz, CDCl$_3$): δ 210.8, 173.7, 136.0, 128.7, 128.4, 128.3, 78.2, 66.8, 58.0, 54.2, 51.9, 45.1, 45.1, 30.7, 28.8, 25.8, 24.8, 22.9, 15.8.

IR (Neat Film, NaCl): 2944, 2875, 1726, 1458, 1390, 1320, 1282, 1153, 1110, 1039, 746, 700 cm^{-1}.

HRMS (MM: FD+): *m/z* calc'd for C$_{21}$H$_{26}$O$_4$ [M]$^+$: 342.1832, found 342.1826.

Optical Rotation: $[\alpha]_D^{21}$ –47.4 (c 0.75, CHCl$_3$).

SFC conditions: 15% IPA, 2.5 mL/min, Chiralpak AD-H column, λ = 210 nm, t_R (min): minor = 4.73, major = 5.13.

41t' (exo):

¹H NMR (400 MHz, CDCl₃): δ 7.42 – 7.28 (m, 5H), 5.19 (d, *J* = 1.1 Hz, 2H), 3.57 – 3.35 (m, 2H), 2.69 (dd, *J* = 7.8, 1.7 Hz, 1H), 2.60 – 2.47 (m, 1H), 2.47 – 2.44 (m, 2H), 2.39 (ddd, *J* = 12.5, 7.9, 6.9 Hz, 1H), 2.28 (ddd, *J* = 13.5, 9.4, 4.6 Hz, 1H), 1.92 – 1.78 (m, 3H), 1.77 – 1.66 (m, 1H), 1.67 – 1.58 (m, 1H), 1.11 (ddd, *J* = 11.3, 6.6, 3.7 Hz, 1H), 1.03 (t, *J* = 6.9 Hz, 3H), 0.89 (tt, *J* = 12.4, 9.6 Hz, 1H).

¹³C NMR (100 MHz, CDCl₃): δ 211.5, 173.4, 136.0, 128.7, 128.4, 128.3, 66.9, 58.1, 54.1, 52.8, 47.5, 46.8, 31,0, 27.7, 26.5, 25.9, 23.1, 15.7.

IR (Neat Film, NaCl): 2946, 1721, 1451, 1390, 1328, 1154, 1117, 767, 698 cm⁻¹.

HRMS (MM: FD+): *m/z* calc'd for $C_{21}H_{26}O_4$ [M]⁺: 342.1833, found 342.1826.

Optical Rotation: $[\alpha]_D^{21}$ +1.8 (c 0.75, CHCl₃).

SFC conditions: 15% IPA, 2.5 mL/min, Chiralpak IC column, λ = 210 nm, t_R (min): minor = 3.29, major = 4.04.

41u
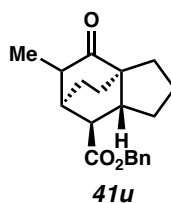
benzyl (3a*R*,6*R*,7*S*,7a*R*)-5-methyl-4-oxooctahydro-3a,6-ethanoindene-7-carboxylate (41u)

Prepared from **40u** following General Procedure A. Purification by flash column chromatography (0–25% EtOAc/hexanes) afforded the title compound as a colorless oil (13.6 mg, 0.044 mmol, 22% yield, 61% ee).

^{1}H NMR (400 MHz, CDCl$_3$): δ 7.39 – 7.32 (m, 5H), 5.14 (ddd, *J* = 17.8, 12.2 Hz, 2H), 2.61 (dd, *J* = 3.7, 2.1 Hz, 1H), 2.45 – 2.30 (m, 3H), 2.21 – 2.06 (m, 4H), 1.90 – 1.63 (m, 3H), 1.61 – 1.35 (m, 2H), 1.32 – 1.16 (m, 1H), 0.97 (d, *J* = 7.7 Hz, 3H).

^{13}C NMR (100 MHz, CDCl$_3$): δ 217.7, 174.8, 135.9, 128.7, 128.6, 128.5, 66.8, 54.2, 48.3, 46.9, 42.2, 38.1, 29.7, 28.9, 26.6, 24.1, 22.5, 15.8.

IR (Neat Film, NaCl): 2943, 2873, 1718, 1455, 1197, 1171 cm^{-1}.

HRMS (MM: FD+): *m/z* calc'd for C$_{20}$H$_{24}$O$_3$ [M]$^+$: 312.1725, found 312.1730.

Optical Rotation: [α]$_D^{21}$ +10.9 (c 0.75, CHCl$_3$).

SFC conditions: 15% IPA, 2.5 mL/min, Chiralpak AD-H column, λ = 210 nm, t$_R$ (min): minor = 5.84, major = 5.43.
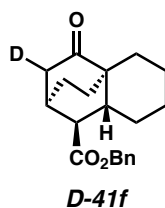
D-41f

benzyl (1*S*,2*R*,4a*R*,8a*R*)-4-oxooctahydro-2*H*-2,4a-ethanonaphthalene-1-carboxylate-3-*d* (*D*-41f)

Prepared from ***D*-40f** following General Procedure A. Purification by flash column chromatography (0–30% EtOAc/hexanes) afforded the title compound as a colorless oil (41.3 mg, 0.132 mmol, 66% yield, 91% ee).

¹H NMR (400 MHz, CDCl₃): δ 7.39 – 7.30 (m, 5H), 5.16 (d, *J* = 12.4 Hz, 1H), 5.11 (d, *J* = 12.2 Hz, 1H), 2.51 – 2.41 (m, 1.6H), 2.36 – 2.10 (m, 2.7H), 2.02 (dddd, *J* = 11.8, 9.1, 5.3, 2.9 Hz, 1H), 1.91 – 1.83 (m, 1H), 1.82 – 1.71 (m, 1H), 1.70 – 1.55 (m, 4H), 1.52 – 1.11 (m, 5H).

¹³C NMR (100 MHz, CDCl₃): δ 216.4, 174.5, 136.0, 128.8, 128.4, 128.2, 77.5, 77.2, 76.8, 66.7, 49.9, 45.1, 40.5, 37.1, 31.0, 30.9, 30.8, 30.0, 28.9, 26.2, 25.6, 21.8, 21.2.

*Partial deuteration complicates ¹³C NMR spectrum. Peaks are listed as they appear.

²H NMR (61 MHz, CHCl₃): δ 2.46, 2.14.

*Trace D-exchanged water observed in spectrum.

IR (Neat Film, NaCl): 2928, 2858, 1723, 1169 cm⁻¹.

HRMS (MM: FD+): *m/z* calc'd for C₂₀H₂₃DO₃ [M+H]⁺: 313.1783, found 313.1795.

Optical Rotation: [α]$_D^{21}$ –21.3 (c 1.00, CHCl₃).

SFC conditions: 15% IPA, 2.5 mL/min, Chiralpak AD-H column, λ = 210 nm, t$_R$ (min): minor = 5.07, major = 6.38.
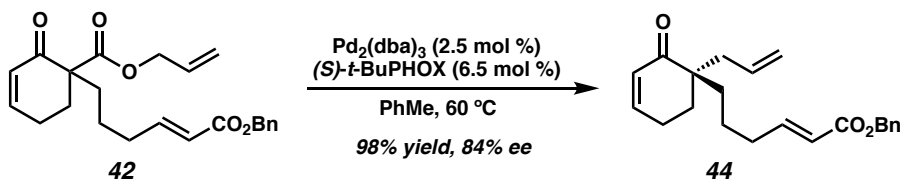
benzyl (*S*,*E*)-6-(1-allyl-2-oxocyclohex-3-en-1-yl)hex-2-enoate (44)

Prepared from **42** (0.02 mmol) following General Procedure A. Purification by preparatory thin layer chromatography (25% EtOAc/hexanes) afforded the title compound as a colorless oil (10.1 mg, 0.0196 mmol, 98% yield, 84 % ee).

¹H NMR (400 MHz, CDCl₃): δ 7.40 – 7.29 (m, 5H), 6.97 (dt, J = 15.6, 6.9 Hz, 1H), 6.85 (dt, J = 10.1, 3.9 Hz, 1H), 5.91 (dt, J = 10.0, 2.0 Hz, 1H), 5.85 (dt, J = 15.7, 1.6 Hz, 1H), 5.69 (ddt, J = 16.6, 10.5, 7.3 Hz, 1H), 5.17 (s, 2H), 5.09 – 5.00 (m, 2H), 2.41 – 2.29 (m, 3H), 2.26 – 2.13 (m, 3H), 1.87 (t, J = 6.1 Hz, 2H), 1.63 – 1.23 (m, 4H).

¹³C NMR (100 MHz, CDCl₃): δ 202.9, 166.6, 149.6, 148.7, 136.3, 134.0, 129.0, 128.7, 128.3, 128.3, 121.4, 118.3, 66.2, 47.6, 39.1, 33.9, 32.9, 30.8, 23.1, 22.4.

IR (Neat Film, NaCl): 2936, 2358, 1718, 1669, 1262, 992 cm⁻¹.

HRMS (MM: FD+): *m/z* calc'd for $C_{22}H_{26}O_3$ [M]⁺: 338.1881, found 338.1877.

Optical Rotation: [α]$_D^{21}$ –0.69 (c 0.62, CHCl₃).

SFC conditions: 15% IPA, 2.5 mL/min, Chiralpak IC column, λ = 210 nm, t$_R$ (min): minor = 14.49, major = 11.94.

83
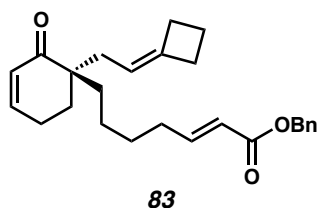
benzyl (*E*)-7-(1-(2-cyclobutylideneethyl)-2-oxocyclohex-3-en-1-yl)hept-2-enoateenoate (83)

Prepared from **63** following General Procedure A, with the modification of being on 0.1 mmol scale. Purification by preparatory thin layer chromatography (20% EtOAc/hexanes) afforded the title compound as a clear oil (2.4 mg, 0.006 mmol, 6% yield).

¹H NMR (400 MHz, CDCl₃): δ 7.41 – 7.29 (m, 5H), 6.99 (dt, J = 15.6, 6.9 Hz, 1H), 6.83 (dt, J = 10.0, 3.9 Hz, 1H), 5.92 – 5.81 (m, 2H), 5.17 (s, 2H), 5.01 – 4.92 (m, 1H), 2.67 –

2.54 (m, 3H), 2.40 – 2.30 (m, 2H), 2.27 – 1.99 (m, 4H), 1.96 – 1.82 (m, 3H), 1.63 – 1.49 (m, 3H), 1.49 – 1.36 (m, 3H), 1.32 – 1.13 (m, 2H).

13C NMR (100 MHz, CDCl₃): δ 203.6, 166.6, 150.1, 148.5, 143.1, 136.3, 129.1, 128.7, 128.3, 128.3, 121.1, 115.4, 66.2, 48.3, 34.1, 33.1, 32.3, 31.2, 30.8, 29.6, 28.8, 23.6, 23.2, 17.1.

IR (Neat Film, NaCl): 2929, 1720, 1670, 1185 cm⁻¹.

HRMS (MM: FD+): *m/z* calc'd for C₂₆H₃₂O₃ [M]⁺: 392.2351, found 392.2341.

84
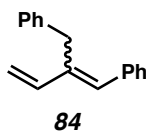
(2-vinylprop-1-ene-1,3-diyl)dibenzene (84)

Prepared from **67** following General Procedure A, with the modification of being on 0.1 mmol scale. Purification by flash column chromatography (0–35% EtOAc/hexanes) afforded the title compound as a colorless oil (6.5 mg, 0.03 mmol, 29% yield).

1H NMR (400 MHz, CDCl₃): δ 7.39 – 7.18 (m, 11.5H), 6.91 – 6.80 (m, 1.15H), 6.56 (ddd, *J* = 17.4, 10.8, 0.9 Hz, 0.15H), 6.45 (s, 1H), 5.42 – 5.33 (m, 1H), 5.19 – 5.13 (m, 1.15H), 5.11 – 5.06 (m, 0.15H), 3.90 (s, 0.3H), 3.73 (s, 2H).

*Isolated as an apparent 1:0.15 mixture of alkene isomers.

13C NMR (100 MHz, CDCl₃): δ 140.5, 140.2, 139.9, 137.7, 137.5, 137.3, 134.2, 133.8, 131.8, 129.6, 128.9, 128.8, 128.7, 128.5, 128.2, 128.2, 127.3, 127.0, 126.2, 126.1, 116.4, 114.8, 40.3, 33.2.

*Isolated as an apparent 1:0.15 mixture of alkene isomers.

IR (Neat Film, NaCl): 3060, 3023, 2919, 1601, 1493, 1455, 1165, 1074 cm⁻¹.

HRMS (MM: FD+): *m/z* calc'd for $C_{17}H_{16}$ [M]$^+$: 220.1252, found 220.1257.

Preparation of Unsaturated β-Ketoester Starting Materials

General Procedure B: Horner–Wadsworth–Emmons Olefination
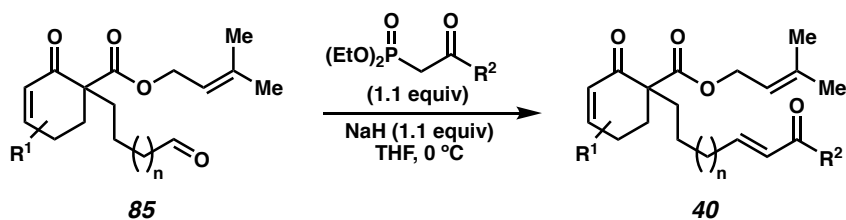
To a suspension of NaH (60% by weight in mineral oil, 1.1 equiv) in THF (0.5 M) at 0 ºC

was dropwise added a solution of the appropriate phosphonate ester (1.1 equiv) in THF

(1.0 M). Stirred at 0 ºC was continued for 30 minutes. To the reaction was then dropwise

added a solution of aldehyde **85** (1.0 equiv) in THF (0.5 M). Upon complete consumption

of starting material (as determined by TLC), the reaction mixture was diluted with a

saturated solution of NaHCO₃ and extracted with EtOAc (3x). The combined organic layers

were dried over Na₂SO₄, filtered, and concentrated under reduced pressure. The product

(**10**) was purified by silica gel flash column chromatography.
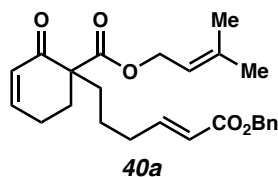
3-methylbut-2-en-1-yl (*E*)-1-(6-(benzyloxy)-6-oxohex-4-en-1-yl)-2-oxocyclohex-3-ene-1-carboxylate (40a)

Prepared from **85** and benzyl 2-(diethoxyphosphoryl)acetate [28] following General

Procedure B. Purification by flash column chromatography (20% EtOAc/hexanes)

afforded the title compound as a colorless oil (0.410 g, 1.00 mmol, 67 % yield).

^{1}H NMR (400 MHz, CDCl$_3$): δ 7.38 – 7.29 (m, 5H), 6.98 (dt, *J* = 15.7, 6.9 Hz, 1H), 6.90 – 6.84 (m, 1H), 6.02 (ddd, *J* = 10.1, 2.5, 1.5 Hz, 1H), 5.87 (dt, *J* = 15.6, 1.6 Hz, 1H), 5.31 – 5.24 (m, 1H), 5.17 (s, 2H), 4.58 (dt, *J* = 7.2, 1.0 Hz, 2H), 2.55 – 2.41 (m, 2H), 2.37 – 2.27 (m, 1H), 2.22 (qd, *J* = 7.3, 1.6 Hz, 2H), 1.97 – 1.86 (m, 2H), 1.77 – 1.69 (m, 4H), 1.67 (d, *J* = 1.4 Hz, 3H), 1.55 – 1.38 (m, 2H).

^{13}C NMR (100 MHz, CDCl$_3$): δ 196.3, 171.6, 166.5, 149.3, 149.3, 139.7, 136.3, 129.4, 128.7, 128.3, 128.3, 121.5, 118.3, 66.2, 62.3, 57.0, 33.5, 32.7, 30.5, 25.8, 23.9, 23.2, 18.2.

IR (Neat Film, NaCl): 3034, 2938, 1723, 1684, 1653, 1455, 1384, 1246, 1174, 1166 cm^{-1}.

HRMS (MM: FD+): *m/z* calc'd for C$_{25}$H$_{30}$O$_5$ [M]$^+$: 410.2088, found 410.2097.
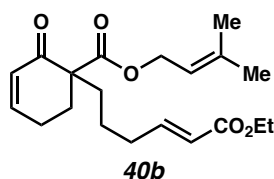
3-methylbut-2-en-1-yl (*E*)-1-(6-(benzyloxy)-6-oxohex-4-en-1-yl)-2-oxocyclohex-3-ene-1-carboxylate (40b)

Prepared from **85** and ethyl 2-(diethoxyphosphoryl)acetate following General Procedure B. Purification by flash column chromatography (20% EtOAc/hexanes) afforded the title compound as a colorless oil (0.291 g, 0.835 mmol, 47 % yield).

^{1}H NMR (400 MHz, CDCl$_3$): δ 6.97 – 6.85 (m, 2H), 6.02 (ddd, *J* = 10.0, 2.6, 1.5 Hz, 1H), 5.81 (dt, *J* = 15.6, 1.6 Hz, 1H), 5.31 – 5.24 (m, 1H), 4.64 – 4.54 (m, 2H), 4.18 (q, *J* = 7.1 Hz, 2H), 2.55 – 2.41 (m, 2H), 2.37 – 2.27 (m, 1H), 2.21 (qd, *J* = 7.3, 1.6 Hz, 2H), 1.98 –

1.87 (m, 2H), 1.78 – 1.69 (m, 4H), 1.68 (s, 3H), 1.55 – 1.37 (m, 2H), 1.28 (t, J = 7.1 Hz,

3H).

¹³C NMR (100 MHz, CDCl₃): δ 196.3, 171.6, 166.8, 149.3, 148.5, 139.7, 129.4, 121.8,

118.3, 62.3, 60.3, 57.0, 33.5, 32.6, 30.5, 25.8, 23.9, 23.3, 18.2, 14.4.

IR (Neat Film, NaCl): 2934, 1714, 1682, 1168 cm⁻¹.

HRMS (MM: FD+): *m/z* calc'd for $C_{20}H_{28}O_5$ [M]⁺: 348.1937, found 348.1943.

40d
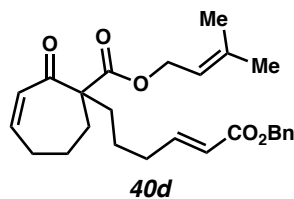
3-methylbut-2-en-1-yl   (*E*)-1-(6-(benzyloxy)-6-oxohex-4-en-1-yl)-2-oxocyclohept-3-ene-1-carboxylate (40d)

Prepared from cyclohept-2-en-1-one following General Procedures B–D. Note that

inseparable impurities plagued the β-ketoester and aldehyde intermediates. Fortunately,

these intermediates could be brought through the sequence in sub-optimal purity to still

afford the title compound **40d** as a colorless oil (265 mg, 0.62 mmol, 3.2% yield from

cyclohept-2-en-1-one) after a final purification by flash column chromatography (20%

EtOAc/hexanes).

¹H NMR (400 MHz, CDCl₃): δ 7.39 – 7.30 (m, 5H), 6.97 (dt, J = 15.6, 6.9 Hz, 1H), 6.36

(ddd, J = 12.3, 5.5, 3.9 Hz, 1H), 5.98 (ddd, J = 12.3, 2.4, 1.4 Hz, 1H), 5.86 (dt, J = 15.6,

1.6 Hz, 1H), 5.28 (ddp, J = 8.6, 5.7, 1.4 Hz, 1H), 5.17 (s, 2H), 4.57 (d, J = 7.2 Hz, 2H),

2.47 – 2.27 (m, 3H), 2.19 (qd, J = 7.2, 1.6 Hz, 2H), 1.99 – 1.79 (m, 3H), 1.77 – 1.69 (m,

4H), 1.69 – 1.61 (m, 4H), 1.43 – 1.32 (m, 2H).

¹³C NMR (100 MHz, CDCl₃): δ 201.1, 172.9, 166.5, 149.3, 143.2, 139.7, 136.3, 131.6, 128.7, 128.3, 128.3, 121.5, 118.2, 66.2, 63.9, 62.2, 36.5, 32.6, 32.3, 31.2, 25.8, 24.3, 23.0, 18.2.

IR (Neat Film, NaCl): 2927, 1720, 1686, 1453, 1162 cm⁻¹.

HRMS (MM: FD+): *m/z* calc'd for C₂₆H₃₂O₅ [M]⁺: 424.2244, found 424.2241.
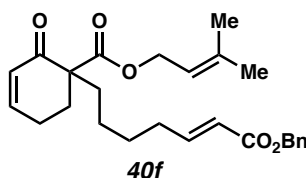
3-methylbut-2-en-1-yl **(*E*)-1-(7-(benzyloxy)-7-oxohept-5-en-1-yl)-2-oxocyclohex-3-ene-1-carboxylate (40f)**

Prepared from **86** and benzyl 2-(diethoxyphosphoryl)acetate[28] following General Procedure B. Purification by flash column chromatography (15–20% EtOAc/hexanes) afforded the title compound as a colorless oil (652 mg, 1.54 mmol, 69% yield).

¹H NMR (400 MHz, CDCl₃): δ 7.39 – 7.30 (m, 5H), 6.99 (ddd, *J* = 15.5, 7.3, 6.3 Hz, 1H), 6.90 – 6.84 (m, 1H), 6.01 (d, *J* = 10.1 Hz, 1H), 5.85 (d, *J* = 15.6 Hz, 1H), 5.30 – 5.25 (m, 1H), 5.17 (s, 2H), 4.58 (d, *J* = 6.6 Hz, 2H), 2.55 – 2.40 (m, 2H), 2.36 – 2.26 (m, 1H), 2.24 – 2.16 (m, 2H), 1.96 – 1.86 (m, 2H), 1.77 – 1.65 (m, 7H), 1.47 (p, *J* = 7.4 Hz, 2H), 1.38 – 1.24 (m, 2H).

¹³C NMR (100 MHz, CDCl₃): δ 196.2, 171.6, 166.5, 149.7, 149.2, 139.4, 136.2, 129.2, 128.6, 128.2, 128.2, 121.1, 118.2, 66.0, 62.1, 56.9, 33.5, 32.0, 30.2, 28.4, 25.7, 24.2, 23.7, 18.1.

IR (Neat Film, NaCl): 2932, 2861, 1722, 1684, 1653, 1456, 1263, 1181 cm⁻¹.

HRMS (MM: FD+): *m/z* calc'd for $C_{26}H_{32}O_5$ [M]$^+$: 424.2244, found 424.2247.
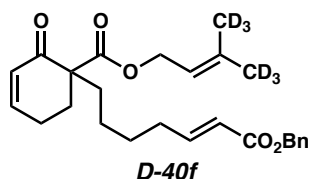
D-40f

3-(methyl-*d₃*)but-2-en-1-yl-4,4,4-*d₃*   **(*E*)-1-(7-(benzyloxy)-7-oxohept-5-en-1-yl)-2-oxocyclohex-3-ene-1-carboxylate (*D*-40f)**

Prepared from **D-86** and benzyl 2-(diethoxyphosphoryl)acetate[28] following General Procedure B. Purification by flash column chromatography (15–20% EtOAc/hexanes) afforded the title compound as a colorless oil (201 mg, 0.467 mmol, 48 % yield).

¹H NMR (400 MHz, CDCl₃): δ 7.39 – 7.30 (m, 5H), 6.99 (dt, *J* = 15.6, 6.9 Hz, 1H), 6.90 – 6.85 (m, 1H), 6.01 (ddd, *J* = 10.1, 2.6, 1.5 Hz, 1H), 5.85 (dt, *J* = 15.6, 1.5 Hz, 1H), 5.27 (t, *J* = 7.1 Hz, 1H), 5.17 (s, 2H), 4.58 (dd, *J* = 7.2, 1.7 Hz, 2H), 2.55 – 2.41 (m, 2H), 2.36 – 2.27 (m, 1H), 2.25 – 2.15 (m, 2H), 1.98 – 1.85 (m, 2H), 1.73 (ddd, *J* = 13.6, 11.2, 5.3 Hz, 1H), 1.51 – 1.42 (m, 2H), 1.37 – 1.25 (m, 2H).

¹³C NMR (100 MHz, CDCl₃): δ 196.4, 171.7, 166.6, 149.8, 149.3, 139.4, 136.3, 129.4, 128.7, 128.3, 128.3, 121.2, 118.4, 66.2, 62.3, 57.0, 33.6, 32.2, 30.3, 28.5, 24.3, 23.9.

²H NMR (61 MHz, CHCl₃): δ 1.69, 1.65.

IR (Neat Film, NaCl): 2930, 1720, 1683, 1264, 1167 cm^{-1}.

HRMS (MM: FD+): *m/z* calc'd for $C_{26}H_{26}D_6O_5$ [M]$^+$: 430.2621, found 430.2622.

40g
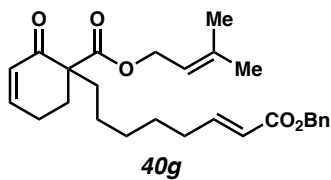
3-methylbut-2-en-1-yl (*E*)-1-(8-(benzyloxy)-8-oxooct-6-en-1-yl)-2-oxocyclohex-3-ene-1-carboxylate (40g)

Prepared from **87** and benzyl 2-(diethoxyphosphoryl)acetate[28] following General Procedure B. Purification by flash column chromatography (10–25% EtOAc/hexanes) afforded the title compound as a colorless oil (773 mg, 1.76 mmol, 65 % yield).

^{1}H NMR (400 MHz, CDCl$_3$): δ 7.40 – 7.29 (m, 5H), 6.99 (dt, *J* = 15.6, 6.9 Hz, 1H), 6.89 – 6.84 (m, 1H), 6.01 (ddd, *J* = 10.0, 2.5, 1.5 Hz, 1H), 5.85 (dt, *J* = 15.6, 1.6 Hz, 1H), 5.28 (ddp, *J* = 8.6, 5.7, 1.4 Hz, 1H), 5.17 (s, 2H), 4.63 – 4.53 (m, 2H), 2.55 – 2.40 (m, 2H), 2.36 – 2.26 (m, 1H), 2.19 (qd, *J* = 7.1, 1.6 Hz, 2H), 1.98 – 1.84 (m, 2H), 1.77 – 1.69 (m, 4H), 1.67 (s, 3H), 1.49 – 1.41 (m, 2H), 1.36 – 1.23 (m, 4H).

^{13}C NMR (100 MHz, CDCl$_3$): δ 196.5, 171.7, 166.6, 150.1, 149.3, 139.5, 136.3, 129.4, 128.7, 128.3, 128.3, 121.2, 118.4, 66.2, 62.2, 57.1, 33.7, 32.3, 30.3, 29.6, 27.8, 25.8, 24.4, 23.9, 18.2.

IR (Neat Film, NaCl): 2929, 2858, 1721, 1684, 1654, 1456, 1264, 1168 cm^{-1}.

HRMS (MM: FD+): *m/z* calc'd for C$_{27}$H$_{34}$O$_5$ [M]$^+$: 438.2401, found 438.2396.

40k
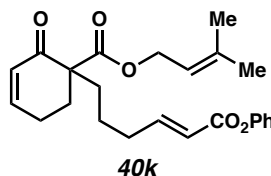
3-methylbut-2-en-1-yl (*E*)-2-oxo-1-(6-oxo-6-phenoxyhex-4-en-1-yl)cyclohex-3-ene-1-carboxylate (40k)

Prepared from **85** and benzyl 2-(diethoxyphosphoryl)acetate [29] following General Procedure B. Purification by flash column chromatography (20% EtOAc/hexanes) afforded the title compound as a colorless oil (409 mg, 1.03 mmol, 57 % yield).

¹H NMR (400 MHz, CDCl₃): δ 7.38 (t, J = 8.0 Hz, 2H), 7.22 (t, J = 7.4 Hz, 1H), 7.18 – 7.10 (m, 3H), 6.91 – 6.87 (m, 1H), 6.05 – 6.00 (m, 2H), 5.29 (tt, J = 7.1, 1.3 Hz, 1H), 4.61 (d, J = 7.1 Hz, 2H), 2.56 – 2.44 (m, 2H), 2.37 – 2.27 (m, 3H), 2.00 – 1.92 (m, 2H), 1.82 – 1.73 (m, 4H), 1.69 (s, 3H), 1.63 – 1.46 (m, 2H).

¹³C NMR (100 MHz, CDCl₃): δ 196.3, 171.6, 165.1, 150.9, 150.9, 149.3, 139.7, 129.5, 129.4, 125.8, 121.8, 121.1, 118.3, 62.4, 57.0, 33.6, 32.8, 30.5, 25.8, 23.9, 23.2, 18.2.

IR (Neat Film, NaCl): 2930, 1732, 1684, 1652, 1458, 1245, 1195 cm⁻¹.

HRMS (MM: FD+): m/z calc'd for $C_{24}H_{28}O_5$ [M]⁺: 396.1931, found 396.1945.

401
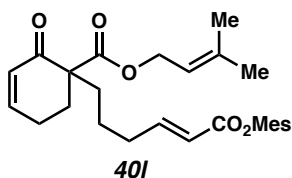
3-methylbut-2-en-1-yl (*E*)-1-(6-(mesityloxy)-6-oxohex-4-en-1-yl)-2-oxocyclohex-3-ene-1-carboxylate (40l)

Prepared from **85** and mesityl 2-(diethoxyphosphoryl)acetate [30] following General Procedure B. Purification by flash column chromatography (20% EtOAc/hexanes) afforded the title compound as a colorless oil (597 mg, 1.36 mmol, 76% yield).

¹H NMR (400 MHz, CDCl₃): δ 7.17 (dt, J = 15.7, 6.8 Hz, 1H), 6.92 – 6.84 (m, 3H), 6.09 – 6.01 (m, 2H), 5.32 – 5.26 (m, 1H), 4.61 (d, J = 5.6 Hz, 2H), 2.57 – 2.43 (m, 2H), 2.39 –

2.27 (m, 3H), 2.26 (s, 3H), 2.09 (s, 6H), 2.01 – 1.92 (m, 2H), 1.79 (ddd, J = 13.6, 11.9, 4.8 Hz, 1H), 1.73 (s, 3H), 1.69 (s, 3H), 1.64 – 1.46 (m, 2H).

^{13}C NMR (100 MHz, CDCl$_3$): δ 196.3, 171.6, 164.6, 150.7, 149.3, 146.0, 139.7, 135.3, 130.0, 129.4, 129.3, 120.7, 118.3, 62.4, 57.0, 33.6, 32.8, 30.5, 25.8, 23.9, 23.2, 20.9, 18.2, 16.4.

IR (Neat Film, NaCl: 2920, 1733, 1684, 1458, 1248, 1192, 1140 cm^{-1}.

HRMS (MM: FD+): *m/z* calc'd for C$_{27}$H$_{34}$O$_5$ [M]$^+$: 438.2401, found 438.2401.

40n
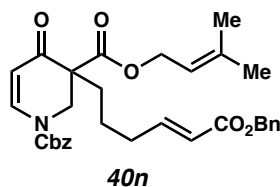
1-benzyl 3-(3-methylbut-2-en-1-yl) (*E*)-3-(6-(benzyloxy)-6-oxohex-4-en-1-yl)-4-oxo-3,4-dihydropyridine-1,3(2*H*)-dicarboxylate (40n)

Prepared from **88** and benzyl 2-(diethoxyphosphoryl)acetate[28] following General Procedure B. Purification by flash column chromatography (20-30% EtOAc/hexanes) afforded the title compound as a colorless oil (181.3 mg, 0.332 mmol, 55% yield).

^{1}H NMR (400 MHz, CDCl$_3$): δ 7.79 (s, 1H), 7.44 – 7.28 (m, 10H), 6.94 (dt, J = 15.5, 6.8 Hz, 1H), 5.85 (dt, J = 15.7, 1.6 Hz, 1H), 5.42 – 5.21 (m, 4H), 5.17 (s, 2H), 4.67 – 4.51 (m, 3H), 3.71 (d, J = 13.6 Hz, 1H), 2.20 (q, J = 7.3 Hz, 2H), 2.07 – 1.92 (m, 1H), 1.69 – 1.58 (m, 1H), 1.71 (s, 3H), 1.66 (s, 3H), 1.49 – 1.40 (m, 2H).

^{13}C NMR (100 MHz, CDCl$_3$): δ 190.5, 169.5, 166.4, 148.7, 142.7, 140.1, 136.2, 135.0, 129.0, 128.9, 128.7, 128.6, 128.4, 128.3, 121.7, 118.0, 106.5, 69.4, 66.2, 62.8, 55.3, 48.3, 32.4, 31.3, 25.8, 23.0, 18.2.

IR (Neat Film, NaCl): 2938, 2338, 1726, 1676, 1604, 1456, 1388, 1303, 1201, 975 cm^{-1}.

HRMS (MM: FD+): *m/z* calc'd for $C_{32}H_{35}NO_7$ [M]$^+$: 545.2414, found 545.2408.

40o
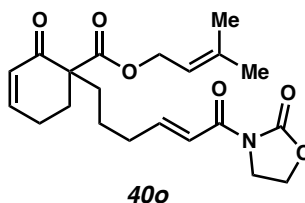
3-methylbut-2-en-1-yl (*E*)-2-oxo-1-(6-oxo-6-(2-oxooxazolidin-3-yl)hex-4-en-1-yl)cyclohex-3-ene-1-carboxylate (40o)

Prepared from **85** and diethyl (2-oxo-2-(2-oxooxazolidin-3-yl)ethyl)phosphonate [31] following General Procedure B. Purification by flash column chromatography (0-80% EtOAc/hexanes) afforded the title compound as a colorless oil (275.1 mg, 0.706 mmol, 71% yield).

^{1}H NMR (400 MHz, CDCl$_3$): δ 7.23 (d, *J* = 15.6 Hz, 1H), 7.12 (dt, *J* = 15.4, 6.7 Hz, 1H), 6.87 (ddd, *J* = 7.8, 6.0, 3.9 Hz, 1H), 6.01 (dt, *J* = 10.3, 2.0 Hz, 1H), 5.28 (tt, *J* = 7.2, 1.3 Hz, 1H), 4.62 – 4.54 (m, 2H), 4.41 (dd, *J* = 8.5, 7.6 Hz, 2H), 4.11 – 4.02 (m, 2H), 2.55 – 2.40 (m, 2H), 2.38 – 2.25 (m, 3H), 2.00 – 1.86 (m, 2H), 1.82 – 1.69 (m, 2H), 1.73 (s, 3H), 1.68 (s, 3H), 1.50 (dtd, *J* = 17.3, 12.4, 7.6 Hz, 2H).

^{13}C NMR (100 MHz, CDCl$_3$): δ 196.3, 171.6, 165.3, 153.6, 150.9, 149.4, 139.6, 129.3, 120.5, 118.3, 62.3, 62.2, 57.0, 42.8, 33.4, 33.1, 30.3, 25.8, 23.9, 23.3, 18.2.

IR (Neat Film, NaCl): 2927, 1774, 1724, 1684, 1636, 1385, 1359, 1222, 1042 cm^{-1}.

HRMS (MM: FD+): *m/z* calc'd for $C_{21}H_{27}NO_6$ [M]$^+$: 389.1838, found 389.1827.
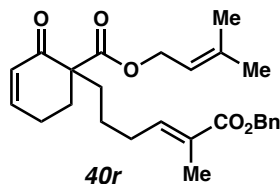
3-methylbut-2-en-1-yl (*E*)-1-(6-(benzyloxy)-5-methyl-6-oxohex-4-en-1-yl)-2-oxocyclohex-3-ene-1-carboxylate (40r)

Prepared from **85** and benzyl 2-(diethoxyphosphoryl)propanoate [32] following General Procedure B. Purification by flash column chromatography (0–30% EtOAc/hexanes) afforded the title compound as a colorless oil (220 mg, 0.518 mmol, 29% yield).

^{1}H NMR (400 MHz, CDCl$_3$): δ 7.39 – 7.29 (m, 5H), 6.87 (dddd, J = 10.1, 4.9, 3.0, 1.1 Hz, 1H), 6.78 (tq, J = 7.5, 1.5 Hz, 1H), 6.01 (ddd, J = 10.1, 2.5, 1.5 Hz, 1H), 5.31 – 5.24 (m, 1H), 5.18 (s, 2H), 4.58 (d, J = 6.9 Hz, 2H), 2.55 – 2.41 (m, 2H), 2.36 – 2.26 (m, 1H), 2.19 (qd, J = 7.5, 1.1 Hz, 2H), 1.98 – 1.87 (m, 2H), 1.85 (s, 3H), 1.79 – 1.69 (m, 4H), 1.67 (s, 3H), 1.53 – 1.37 (m, 2H).

^{13}C NMR (100 MHz, CDCl$_3$): δ 196.3, 171.6, 168.0, 149.3, 142.3, 139.6, 136.5, 129.3, 128.6, 128.2, 128.1, 128.1, 118.3, 66.3, 62.3, 57.0, 33.7, 30.4, 29.2, 25.8, 23.9, 23.9, 18.2, 12.6.

IR (Neat Film, NaCl): 2930, 1711, 1686, 1452, 1265, 1180 cm^{-1}.

HRMS (MM: FD+): *m/z* calc'd for C$_{26}$H$_{32}$O$_5$ [M]$^+$: 424.2250, found 424.2250.
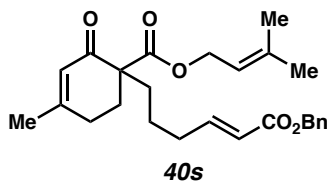
3-methylbut-2-en-1-yl (*E*)-1-(6-(benzyloxy)-6-oxohex-4-en-1-yl)-4-methyl-2-oxocyclohex-3-ene-1-carboxylate (40s)

Prepared from **89** and benzyl 2-(diethoxyphosphoryl)acetate[28] following General Procedure B. Purification by flash column chromatography (15–20–25% EtOAc/hexanes) afforded the title compound as a colorless oil (827.2 mg, 2.16 mmol, 64% yield).

^{1}H NMR (400 MHz, CDCl$_3$): δ 7.39 – 7.28 (m, 5H), 6.98 (dt, *J* = 15.6, 6.8 Hz, 1H), 5.87 (dq, *J* = 2.7, 1.3 Hz, 1H), 5.86 (dt, *J* = 15.6, 1.6 Hz, 1H), 5.27 (tp, *J* = 7.1, 1.4 Hz, 1H), 5.16 (s, 2H), 4.64 – 4.51 (m, 2H), 2.52 – 2.36 (m, 2H), 2.28 – 2.14 (m, 3H), 1.98 – 1.83 (m, 5H), 1.72 (s, 4H), 1.67 (s, 3H), 1.54 – 1.34 (m, 2H).

^{13}C NMR (100 MHz, CDCl$_3$): δ 195.9, 171.7, 166.5, 161.4, 149.3, 139.6, 136.3, 128.7, 128.3, 128.3, 126.1, 121.5, 118.4, 66.2, 62.3, 55.9, 33.5, 32.7, 30.2, 28.8, 25.8, 24.2, 23.3, 18.2.

IR (Neat Film, NaCl): 3032, 2938, 1723, 1674, 1438, 1379, 1264, 1212, 1168, 1013, 741, 698 cm^{-1}.

HRMS (MM: FD+): *m/z* calc'd for C$_{26}$H$_{32}$O$_5$ [M]$^+$: 424.2235, found 424.2244.

40t
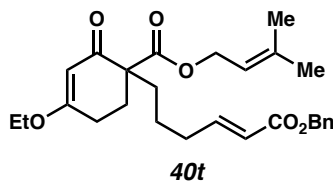
3-methylbut-2-en-1-yl (*E*)-1-(6-(benzyloxy)-6-oxohex-4-en-1-yl)-4-ethoxy-2-oxocyclohex-3-ene-1-carboxylate (40t)

Prepared from **90** and benzyl 2-(diethoxyphosphoryl)acetate[28] following General Procedure B. Purification by flash column chromatography (30% EtOAc/hexanes) afforded the title compound as a colorless oil (814.7 mg, 1.79 mmol, 88% yield).

^{1}H NMR (400 MHz, CDCl$_3$): δ 7.40 – 7.28 (m, 5H), 6.98 (dt, *J* = 15.6, 6.8 Hz, 1H), 5.86 (dt, *J* = 15.7, 1.6 Hz, 1H), 5.34 (d, *J* = 1.2 Hz, 1H), 5.28 (dddt, *J* = 7.0, 5.6, 2.8, 1.4 Hz, 1H), 5.16 (s, 2H), 4.66 – 4.52 (m, 2H), 3.89 (qd, *J* = 7.1, 1.6 Hz, 2H), 2.61 (dddd, *J* = 17.9, 10.1, 4.9, 1.2 Hz, 1H), 2.46 – 2.27 (m, 2H), 2.21 (qd, *J* = 7.3, 1.6 Hz, 2H), 2.02 – 1.83 (m, 2H), 1.82 – 1.72 (m, 1H), 1.71 (s, 3H), 1.67 (s, 3H), 1.45 (dddd, *J* = 13.3, 11.2, 6.4, 2.7 Hz, 2H), 1.35 (t, *J* = 7.0 Hz, 3H).

^{13}C NMR (100 MHz, CDCl$_3$): δ 195.8, 176.6, 171.8, 166.5, 149.4, 139.5, 136.3, 128.7, 128.3, 128.3, 121.4, 118.5, 102.3, 66.2, 64.5, 62.3, 56.0, 33.8, 32.7, 28.7, 26.6, 25.8, 23.3, 18.2, 14.3.

IR (Neat Film, NaCl): 2939, 1721, 1655, 1608, 1446, 1380, 1314, 1242, 1190, 1026, 736 cm^{-1}.

HRMS (MM: FD+): *m/z* calc'd for C$_{27}$H$_{34}$O$_6$ [M]$^+$: 454.2349, found 454.2350.
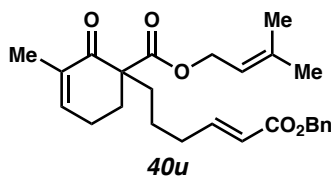
3-methylbut-2-en-1-yl   (*E*)-1-(6-(benzyloxy)-6-oxohex-4-en-1-yl)-3-methyl-2-oxocyclohex-3-ene-1-carboxylate (40u)

Prepared from **91** and benzyl 2-(diethoxyphosphoryl)acetate[28] following General Procedure B. Purification by flash column chromatography (10–25% EtOAc/hexanes) afforded the title compound as a colorless oil (1176.8 mg, 2.77 mmol, 71% yield).

^{1}H NMR (400 MHz, CDCl$_3$): δ 7.41 – 7.26 (m, 5H), 6.98 (dt, J = 15.6, 6.8 Hz, 1H), 6.59 (ddt, J = 4.7, 3.1, 1.3 Hz, 1H), 5.87 (dt, J = 15.6, 1.6 Hz, 1H), 5.27 (tdq, J = 7.1, 2.8, 1.5 Hz, 1H), 5.17 (s, 2H), 4.57 (d, J = 6.7 Hz, 2H), 2.50 – 2.36 (m, 2H), 2.33 – 2.16 (m, 3H), 1.98 – 1.83 (m, 2H), 1.78 (q, J = 1.7 Hz, 3H), 1.77 – 1.64 (m, 1H), 1.72 (s, 3H), 1.67 (s, 3H) 1.61 – 1.34 (m, 3H).

^{13}C NMR (100 MHz, CDCl$_3$): δ 197.0, 171.9, 166.5, 149.4, 143.8, 139.6, 136.3, 135.4, 128.7, 128.3, 128.3, 121.5, 118.3, 66.2, 62.2, 56.9, 33.6, 32.7, 30.9, 25.8, 23.6, 23.4, 18.2, 16.6.

IR (Neat Film, NaCl): 2921, 1721, 1677, 1450, 1377, 1248, 1168, 728 cm^{-1}.

HRMS (MM: FD+): *m/z* calc'd for C$_{26}$H$_{32}$O$_5$ [M]$^+$: 424.2244, found 424.2244.

42
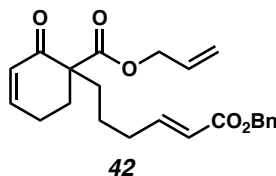
allyl (*E*)-1-(6-(benzyloxy)-6-oxohex-4-en-1-yl)-2-oxocyclohex-3-ene-1-carboxylate (42)

Prepared from **92** and benzyl 2-(diethoxyphosphoryl)acetate[28] following General Procedure B. Purification by flash column chromatography (20–25% EtOAc/hexanes) afforded the title compound as a colorless oil (599.1 mg, 1.41 mmol, 46% yield).

^{1}H NMR (400 MHz, CDCl$_3$): δ 7.41 – 7.26 (m, 5H), 6.98 (dt, J = 15.6, 6.9 Hz, 1H), 6.89 (dddd, J = 10.1, 4.8, 3.1, 1.0 Hz, 1H), 6.03 (ddd, J = 10.1, 2.5, 1.6 Hz, 1H), 5.93 – 5.77 (m,

2H), 5.27 (dq, J = 17.2, 1.5 Hz, 1H), 5.21 (dq, J = 10.4, 1.3 Hz, 1H), 5.17 (s, 2H), 4.60 (dq, J = 5.6, 1.6 Hz, 2H), 2.57 – 2.42 (m, 2H), 2.39 – 2.27 (m, 1H), 2.22 (qd, J = 7.3, 1.6 Hz, 2H), 2.02 – 1.87 (m, 2H), 1.77 (ddd, J = 13.7, 11.7, 5.2 Hz, 1H), 1.57 – 1.40 (m, 2H).

^{13}C NMR (100 MHz, CDCl$_3$): δ 196.0, 171.2, 166.5, 149.5, 149.1, 136.2, 131.7, 129.3, 128.7, 128.3, 128.3, 127.8, 127.1, 121.6, 118.7, 66.2, 65.9, 57.0, 33.4, 32.6, 30.3, 23.8, 23.2.

IR (Neat Film, NaCl): 2937, 2357, 1723, 1684, 1456, 1262, 1165, 992 cm^{-1}.

HRMS (MM: FD+): *m/z* calc'd for C$_{23}$H$_{27}$O$_5$ [M]$^+$: 383.1871, found 383.1853.
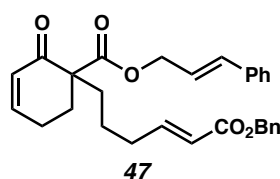
cinnamyl 1-((*E*)-6-(benzyloxy)-6-oxohex-4-en-1-yl)-2-oxocyclohex-3-ene-1-carboxylate (47)

Prepared from **93** and benzyl 2-(diethoxyphosphoryl)acetate[28] following General Procedure B. Purification by flash column chromatography (20% EtOAc/hexanes) afforded the title compound as a colorless oil (569 mg, 1.24 mmol, 67% yield).

^{1}H NMR (400 MHz, CDCl$_3$): δ 7.37 – 7.34 (m, 6H), 7.34 – 7.29 (m, 3H), 7.27 – 7.24 (m, 1H), 6.97 (dt, J = 15.6, 6.9 Hz, 1H), 6.89 (dddd, J = 10.1, 4.8, 3.1, 1.0 Hz, 1H), 6.62 (d, J = 15.9 Hz, 1H), 6.22 (dt, J = 15.9, 6.4 Hz, 1H), 6.04 (ddd, J = 10.1, 2.5, 1.6 Hz, 1H), 5.86 (dt, J = 15.7, 1.6 Hz, 1H), 5.16 (s, 2H), 4.76 (dt, J = 6.4, 1.4 Hz, 2H), 2.56 – 2.45 (m, 2H), 2.37 – 2.28 (m, 1H), 2.22 (ddd, J = 7.4, 7.4, 1.6 Hz, 2H), 1.95 (ddt, J = 16.8, 7.9, 5.7 Hz, 2H), 1.78 (ddd, J = 13.7, 11.7, 5.0 Hz, 1H), 1.56 – 1.42 (m, 2H).

^{13}C NMR (100 MHz, CDCl$_3$): δ 196.0, 171.4, 166.5, 149.5, 149.1, 136.2, 136.2, 134.7, 129.3, 128.7, 128.7, 128.3, 128.3, 126.8, 122.6, 121.6, 66.2, 65.9, 57.0, 33.4, 32.6, 30.3, 23.8, 23.2.

IR (Neat Film, NaCl): 3034, 2942, 1718, 1700, 1684, 1247, 1166 cm^{-1}

HRMS (MM: FD+): *m/z* calc'd for C$_{29}$H$_{30}$O$_5$ [M]$^+$: 458.2088, found 458.2082.
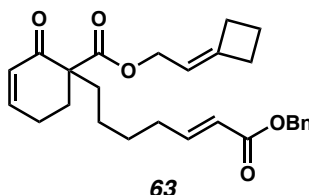
22-cyclobutylideneethyl   (*E*)-1-(7-(benzyloxy)-7-oxohept-5-en-1-yl)-2-oxocyclohex-3-ene-1-carboxylatecarboxylate (63)

Prepared from **94** and benzyl 2-(diethoxyphosphoryl)acetate[28] following General Procedure B. Purification by flash column chromatography (5–60% EtOAc/hexanes) afforded the title compound as a colorless oil (354 mg, 0.81 mmol, 39.8% yield).

^{1}H NMR (400 MHz, CDCl$_3$): δ 7.40 – 7.29 (m, 5H), 6.99 (dt, *J* = 14.9, 1.0 Hz, 1H), 6.91 – 6.84 (m, 1H), 6.02 (d, *J* = 1.2 Hz, 1H), 5.86 (d, *J* = 15.7 Hz, 1H), 5.24 – 5.13 (m, 3H), 4.51 – 4.41 (m, 2H), 2.75 – 2.62 (m, 4H), 2.56 – 2.39 (m, 2H), 2.36 – 2.27 (m, 1H), 2.25 – 2.16 (m, 2H), 2.02 – 1.84 (m, 4H), 1.73 (ddd, *J* = 13.6, 11.2, 5.3 Hz, 1H), 1.47 (p, *J* = 7.5 Hz, 2H), 1.40 – 1.23 (m, 2H).

^{13}C NMR (100 MHz, CDCl$_3$): δ 196.4, 171.6, 166.6, 149.8, 149.3, 148.8, 136.3, 129.4, 128.7, 128.3, 128.3, 121.2, 114.0, 66.2, 62.3, 57.1, 33.6, 32.2, 31.2, 30.3, 29.6, 28.5, 24.3, 23.9, 17.1.

IR (Neat Film, NaCl): 2945, 1722, 1687, 1446, 1169 cm^{-1}.

HRMS (MM: FD+): *m/z* calc'd for $C_{27}H_{32}O_5$ [M]$^+$: 436.2250, found 436.2222.

64
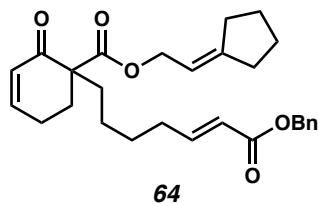
2-cyclopentylideneethyl (E)-1-(7-(benzyloxy)-7-oxohept-5-en-1-yl)-2-oxocyclohex-3-ene-1-carboxylate (64)

Prepared from **95** and benzyl 2-(diethoxyphosphoryl)acetate[28] following General Procedure B. Purification by flash column chromatography (10–60% EtOAc/hexanes) afforded the title compound as a colorless oil (1.40 g, 4.41 mmol, 38.9% yield).

^{1}H NMR (400 MHz, CDCl$_3$): δ 7.40 – 7.28 (m, 5H), 6.99 (dt, *J* = 15.6, 6.9 Hz, 1H), 6.91 – 6.83 (m, 1H), 6.01 (ddd, *J* = 10.1, 2.6, 1.5 Hz, 1H), 5.85 (dt, *J* = 15.6, 1.6 Hz, 1H), 5.37 (tp, *J* = 7.0, 2.2 Hz, 1H), 5.17 (s, 2H), 4.60 – 4.53 (m, 2H), 2.56 – 2.39 (m, 2H), 2.37 – 2.15 (m, 7H), 1.98 – 1.85 (m, 2H), 1.78 – 1.54 (m, 5H), 1.53 – 1.41 (m, 2H), 1.40 – 1.22 (m, 2H).

^{13}C NMR (100 MHz, CDCl$_3$): δ 196.4, 171.7, 166.6, 151.1, 149.8, 149.3, 136.3, 129.4, 128.7, 128.3, 128.3, 121.2, 113.8, 66.2, 63.7, 57.1, 33.9, 33.6, 32.2, 30.3, 29.0, 28.5, 26.4, 26.2, 24.3, 23.9.

IR (Neat Film, NaCl): 2946, 1719, 1686, 1457, 1165 cm^{-1}.

HRMS (MM: FD+): *m/z* calc'd for $C_{28}H_{34}O_5$ [M]$^+$: 450.2406, found 450.2394.

65
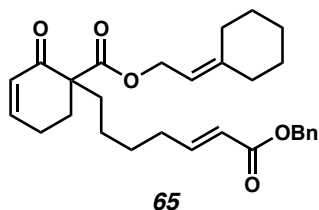
2-cyclohexylideneethyl (*E*)-1-(7-(benzyloxy)-7-oxohept-5-en-1-yl)-2-oxocyclohex-3-ene-1-carboxylate (65)

Prepared from **96** and benzyl 2-(diethoxyphosphoryl)acetate[28] following General Procedure B. Purification by flash column chromatography (10–60% EtOAc/hexanes) afforded the title compound as a colorless oil (81 mg, 0.17 mmol, 32.9% yield).

¹H NMR (400 MHz, CDCl₃): δ 7.41 – 7.27 (m, 5H), 6.99 (dt, *J* = 15.6, 6.9 Hz, 1H), 6.87 (dddd, *J* = 10.1, 5.2, 2.5, 1.1 Hz, 1H), 6.01 (ddd, *J* = 10.1, 2.6, 1.5 Hz, 1H), 5.85 (dt, *J* = 15.6, 1.6 Hz, 1H), 5.23 (tp, *J* = 7.3, 1.2 Hz, 1H), 5.17 (s, 2H), 4.59 (d, *J* = 7.2 Hz, 2H), 2.56 – 2.39 (m, 2H), 2.36 – 2.26 (m, 1H), 2.25 – 2.13 (m, 4H), 2.12 – 2.03 (m, 2H), 1.98 – 1.84 (m, 2H), 1.78 – 1.66 (m, 1H), 1.63 – 1.42 (m, 8H), 1.41 – 1.21 (m, 2H).

¹³C NMR (100 MHz, CDCl₃): δ 196.4, 171.6, 166.6, 149.8, 149.3, 147.7, 136.3, 129.4, 128.7, 128.3, 128.3, 121.2, 114.9, 66.2, 61.5, 57.0, 37.1, 33.6, 32.2, 30.4, 29.2, 28.5, 28.5, 27.9, 26.7, 24.3, 23.9.

IR (Neat Film, NaCl): 2929, 2853, 1723, 1681, 1456, 1385, 1266, 1184 cm⁻¹.

HRMS (MM: FD+): *m/z* calc'd for C₂₉H₃₆O₅ [M]⁺: 464.2563, found 464.2543.

66
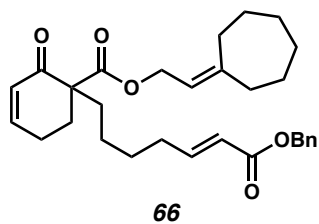
2-cycloheptylideneethyl (*E*)-1-(7-(benzyloxy)-7-oxohept-5-en-1-yl)-2-oxocyclohex-3-ene-1-carboxylate (66)

Prepared from **97** and benzyl 2-(diethoxyphosphoryl)acetate[28] following General Procedure B. Purification by flash column chromatography (5–70% EtOAc/hexanes) afforded the title compound as a colorless oil (135 mg, 0.28 mmol, 30% yield).

^{1}H NMR (400 MHz, CDCl$_3$): δ 7.43 – 7.29 (m, 5H), 6.99 (dt, J = 15.7, 6.9 Hz, 1H), 6.91 – 6.82 (m, 1H), 6.01 (ddd, J = 10.2, 2.6, 1.5 Hz, 1H), 5.85 (dt, J = 15.6, 1.6 Hz, 1H), 5.27 (tt, J = 7.1, 1.3 Hz, 1H), 5.17 (s, 2H), 4.59 (d, J = 7.1 Hz, 2H), 2.57 – 2.39 (m, 2H), 2.36 – 2.16 (m, 7H), 1.98 – 1.84 (m, 2H), 1.73 (ddd, J = 13.6, 11.3, 5.2 Hz, 1H), 1.61 – 1.43 (m, 10H), 1.31 (dddd, J = 13.2, 11.8, 8.6, 6.2 Hz, 2H).

^{13}C NMR (100 MHz, CDCl$_3$): δ 196.4, 171.7, 166.6, 149.8, 149.3, 149.0, 136.3, 129.4, 128.7, 128.3, 128.3, 121.2, 118.4, 66.2, 62.0, 57.0, 37.7, 33.6, 32.2, 30.4, 30.2, 29.8, 29.1, 28.9, 28.5, 27.3, 24.3, 23.9.

IR (Neat Film, NaCl): 2919, 2361, 1722, 1682, 1651, 1443, 1234, 1187 cm^{-1}.

HRMS (MM: FD+): *m/z* calc'd for C$_{30}$H$_{38}$O$_5$ [M]$^+$: 478.2719, found 478.2716.

67
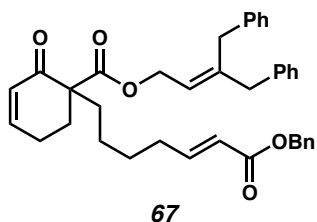
3-benzyl-4-phenylbut-2-en-1-yl   (*E*)-1-(7-(benzyloxy)-7-oxohept-5-en-1-yl)-2-oxocyclohex-3-ene-1-carboxylate (67)

Prepared from **98** and benzyl 2-(diethoxyphosphoryl)acetate[28] following General Procedure B. Purification by flash column chromatography (5–70% EtOAc/hexanes) afforded the title compound as a colorless oil (205 mg, 0.36 mmol, 39% yield).

¹H NMR (400 MHz, CDCl₃): δ 7.39 – 7.24 (m, 9H), 7.23 – 7.17 (m, 2H), 7.09 (dd, *J* = 11.6, 7.3 Hz, 4H), 6.98 (dt, *J* = 15.6, 6.9 Hz, 1H), 6.89 – 6.80 (m, 1H), 6.02 (d, *J* = 10.1 Hz, 1H), 5.85 (d, *J* = 16.1 Hz, 1H), 5.51 (t, *J* = 7.2 Hz, 1H), 5.17 (s, 2H), 4.83 – 4.69 (m, 2H), 3.36 (s, 2H), 3.23 (s, 2H), 2.55 – 2.40 (m, 2H), 2.37 – 2.24 (m, 1H), 2.18 (q, *J* = 7.2 Hz, 2H), 2.00 – 1.85 (m, 2H), 1.75 (ddd, *J* = 13.5, 11.1, 5.2 Hz, 1H), 1.46 (p, *J* = 7.4 Hz, 1H), 1.38 – 1.22 (m, 2H).

¹³C NMR (100 MHz, CDCl₃): δ 196.2, 171.6, 166.6, 149.8, 149.3, 144.8, 139.0, 138.8, 136.3, 129.4, 129.3, 128.8, 128.7, 128.7, 128.5, 128.3, 128.3, 126.5, 126.4, 121.7, 121.3, 66.2, 61.9, 57.1, 42.9, 35.8, 33.6, 32.1, 30.3, 28.5, 24.3, 23.9.

IR (Neat Film, NaCl): 3027, 2931, 1722, 1682, 1493, 1387, 1264, 1165 cm⁻¹.

HRMS (MM: FD+): *m/z* calc'd for C₃₈H₄₀O₅ [M]⁺: 576.2876, found 576.2857.
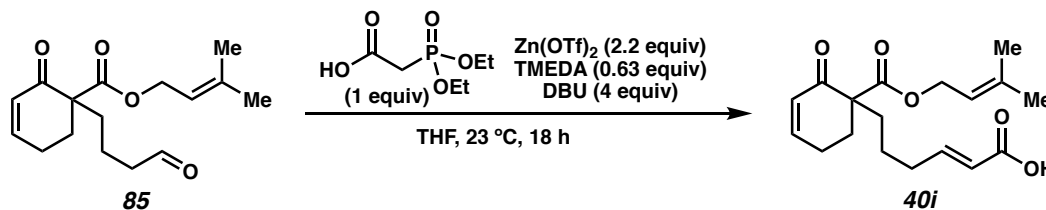
(*E*)-6-(1-(((3-methylbut-2-en-1-yl)oxy)carbonyl)-2-oxocyclohex-3-en-1-yl)hex-2-enoic acid (40i)[33]

To a suspension of Zn(OTf)₂ (6.6 mmol, 2.2 equiv) in THF (15 mL) was added (diethoxyphosphinyl)acetic acid (3 mmol, 1 equiv), followed by the addition of TMEDA (1.89 mmol, 0.63 equiv), DBU (12 mmol, 4 equiv), and then a solution of aldehyde **85** (3 mmol, 1 equiv) in THF (2 mL). The solution was stirred at 23 °C for 18 h, and the reaction was diluted with 1 M HCl and extracted with dichloromethane (4x). The combined organic layers were dried over Na₂SO₄, filtered, and concentrated under reduced pressure.

Purification by silica gel flash column chromatography (35% EtOAc/hexanes with 3% AcOH) afforded the title compound as a white solid (137.4 mg, 0.43 mmol, 43% yield).

^{1}H NMR (400 MHz, CDCl$_3$): δ 7.04 (dt, J = 15.7, 6.8 Hz, 1H), 6.93 – 6.84 (m, 1H), 6.03 (ddd, J = 10.2, 2.6, 1.5 Hz, 1H), 5.83 (dt, J = 15.6, 1.6 Hz, 1H), 5.28 (tp, J = 7.2, 1.4 Hz, 1H), 4.66 – 4.53 (m, 2H), 2.58 – 2.40 (m, 2H), 2.37 – 2.28 (m, 1H), 2.25 (qd, J = 7.3, 1.6 Hz, 2H), 1.98 – 1.87 (m, 2H), 1.80 – 1.68 (m, 1H), 1.73 (s, 3H), 1.68 (s, 3H), 1.61 – 1.37 (m, 3H).

^{13}C NMR (100 MHz, CDCl$_3$): δ 196.3, 171.6, 170.2, 151.4, 149.3, 139.7, 129.4, 120.8, 118.3, 62.4, 57.0, 33.5, 32.7, 30.5, 25.8, 23.9, 23.1, 18.2.

IR (Neat Film, NaCl): 2929, 1725, 1694, 1424, 1384, 1236, 1171 cm^{-1}.

HRMS (MM: FD+): *m/z* calc'd for C$_{18}$H$_{24}$O$_5$ [M]$^+$: 320.1624, found 320.1636.
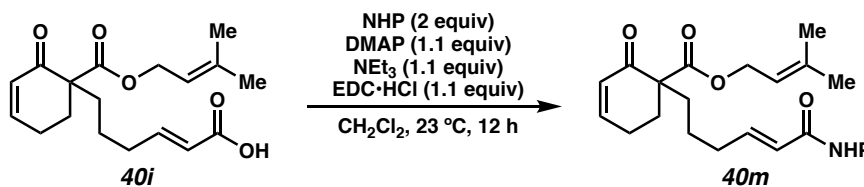
3-methylbut-2-en-1-yl (*E*)-1-(6-((1,3-dioxoisoindolin-2-yl)oxy)-6-oxohex-4-en-1-yl)-2-oxocyclohex-3-ene-1-carboxylate (40m)[34]

To a round bottom flask was added crude acid **40i** (assumed quantitative yield from previous reaction, 1 mmol, 1 equiv), DMAP (1.1 mmol, 1.1 equiv), NHP (2 mmol, 2 equiv), dichloromethane (9.5 mL), and triethylamine (1.1 mmol, 1.1 equiv). EDC•HCl (1.1 mmol, 1.1 equiv) was then added under N$_2$ atmosphere in a single portion, and the reaction was stirred vigorously at 23 °C for 12 h. The reaction mixture was diluted with dichloromethane and washed with 0.5 N HCl, saturated aqueous NaHCO$_3$, and brine. The combined organic

layers were dried over Na$_2$SO$_4$ and concentrated under reduced pressure. Purification by flash column chromatography (30–35% EtOAc/hexanes) afforded the title compound as a colorless oil (109.6 mg, 0.48 mmol, 24% yield over two steps).

^{1}H NMR (400 MHz, CDCl$_3$): δ 7.96 – 7.84 (m, 2H), 7.79 (dd, J = 5.5, 3.1 Hz, 2H), 7.30 (dd, J = 15.8, 6.7 Hz, 1H), 6.89 (dddd, J = 10.1, 4.9, 3.0, 1.1 Hz, 1H), 6.10 (dt, J = 15.8, 1.6 Hz, 1H), 6.04 (ddd, J = 10.1, 2.5, 1.5 Hz, 1H), 5.29 (tdt, J = 5.7, 2.8, 1.4 Hz, 1H), 4.67 – 4.55 (m, 2H), 2.58 – 2.40 (m, 2H), 2.35 (m, 3H), 2.03 – 1.89 (m, 2H), 1.87 – 1.74 (m, 1H), 1.74 (s, 3H), 1.69 (d, J = 1.3 Hz, 3H), 1.66 – 1.45 (m, 3H).

^{13}C NMR (100 MHz, CDCl$_3$): δ 196.2, 162.4, 162.2, 155.2, 149.3, 139.8, 134.8, 129.4, 129.1, 124.1, 118.3, 116.0, 62.4, 57.0, 33.5, 33.3, 30.6, 25.9, 23.9, 23.0, 18.3.

IR (Neat Film, NaCl): 1771, 1744, 1682, 1185 cm^{-1}.

HRMS (MM: FD+): *m/z* calc'd for C$_{26}$H$_{27}$NO$_7$ [M]$^+$: 465.1788, found 465.1779.

3-methylbut-2-en-1-yl (*Z*)-1-(6-(benzyloxy)-6-oxohex-4-en-1-yl)-2-oxocyclohex-3-ene-1-carboxylate (40q)

To a solution of benzyl 2-(bis(2-(*tert*-butyl)phenoxy)phosphoryl)acetate[35] (890 mg, 1.80 mmol, 1.00 equiv) in MeCN (18 mL, 0.1 M) was added K$_2$CO$_3$ (783 mg, 3.69 mmol, 2.05 equiv). The reaction was cooled to 0 ºC and a solution of **85** (500 mg, 1.80 mmol, 1.00 equiv) in MeCN (18 mL, 0.1 M) was dropwise added. The reaction was gradually warmed

to 25 ºC and stirring was continued until consumption of **85** as determined by TLC (around 16 h). The reaction mixture was filtered through a plug of Celite® to remove solids and volatiles were removed in vacuo. Purification by flash column chromatography (0–40% EtOAc/hexanes) afforded the title compound as a colorless oil (482 mg, 1.17 mmol, 65 % yield).

¹H NMR (400 MHz, CDCl₃): δ 7.39 – 7.29 (m, 5H), 6.90 – 6.84 (m, 1H), 6.24 (dt, *J* = 11.5, 7.4 Hz, 1H), 6.01 (ddd, *J* = 10.1, 2.5, 1.6 Hz, 1H), 5.83 (dt, *J* = 11.5, 1.7 Hz, 1H), 5.28 (ddp, *J* = 8.6, 5.7, 1.4 Hz, 1H), 5.15 (s, 2H), 4.59 (d, *J* = 7.2 Hz, 2H), 2.68 (qd, *J* = 7.4, 1.8 Hz, 2H), 2.53 – 2.41 (m, 2H), 2.35 – 2.26 (m, 1H), 1.98 – 1.87 (m, 2H), 1.79 – 1.71 (m, 4H), 1.67 (s, 3H), 1.52 – 1.37 (m, 2H).

¹³C NMR (100 MHz, CDCl₃): δ 196.4, 171.7, 166.2, 150.5, 149.3, 139.5, 136.3, 129.3, 128.7, 128.3, 128.3, 119.9, 118.4, 65.9, 62.3, 57.1, 33.4, 30.3, 29.4, 25.8, 24.2, 23.8, 18.2.

IR (Neat Film, NaCl): 2918, 1714, 1447, 1178, 1161 cm⁻¹.

HRMS (MM: FD+): *m/z* calc'd for C₂₅H₃₀O₅ [M]⁺: 410.2093, found 410.2108.

3-methylbut-2-en-1-yl (*E*)-2-oxo-1-(6-oxo-6-phenylhex-4-en-1-yl)cyclohex-3-ene-1-carboxylate (40j)

(2-oxo-2-phenylethyl)triphenylphosphonium bromide[36] (996 mg, 2.16 mmol, 1.2 equiv) was stirred in 26 mL of a 3:2 CH₂Cl₂/2 M aq. NaOH mixture for 30 minutes at 23 ºC. The layers were separated, and the aqueous layer was extracted twice with CH₂Cl₂. The

combined organic layers were washed with brine, dried over Na$_2$SO$_4$, filtered, and solvent was removed in vacuo. To a solution of this crude ylide in DCE (22 mL, 0.1 M) was added aldehyde **85** (500 mg, 1.80 mmol, 1 equiv). The reaction was stirred at 65 ºC for 36 hours. Upon complete consumption of **85**, as determined by TLC, volatiles were removed in vacuo. Purification by flash column chromatography (30% EtOAc/hexanes) afforded the title compound as a colorless oil (330 mg, 0.867 mmol, 48% yield).

^{1}H NMR (400 MHz, CDCl$_3$): δ 7.95 – 7.90 (m, 2H), 7.60 – 7.51 (m, 1H), 7.46 (tt, *J* = 6.8, 1.5 Hz, 2H), 7.02 (dt, *J* = 15.4, 6.7 Hz, 1H), 6.93 – 6.85 (m, 2H), 6.03 (ddd, *J* = 10.2, 2.6, 1.5 Hz, 1H), 5.30 – 5.25 (m, 1H), 4.59 (d, *J* = 7.1 Hz, 2H), 2.55 – 2.43 (m, 2H), 2.38 – 2.27 (m, 3H), 2.01 – 1.91 (m, 2H), 1.80 (ddd, *J* = 13.6, 12.0, 4.7 Hz, 1H), 1.72 (s, 3H), 1.67 (s, 3H), 1.63 – 1.47 (m, 2H).

^{13}C NMR (100 MHz, CDCl$_3$): δ 196.3, 191.0, 171.6, 149.3, 149.1, 139.7, 138.1, 132.8, 129.4, 128.7, 128.7, 126.4, 118.3, 62.4, 57.0, 33.6, 33.2, 30.5, 25.8, 23.9, 23.4, 18.2.

IR (Neat Film, NaCl): 2931, 1724, 1671, 1619, 1447, 1229, 1177 cm^{-1}.

HRMS (MM: FD+): *m/z* calc'd for C$_{24}$H$_{28}$O$_4$ [M]$^+$: 380.1988, found 380.1982.
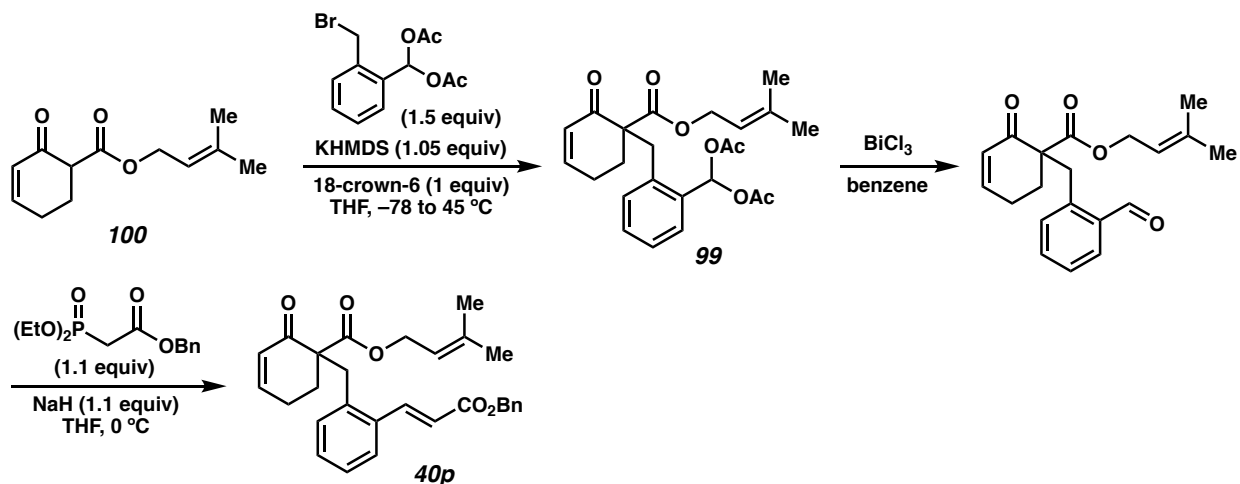
(2-((1-(((3-methylbut-2-en-1-yl)oxy)carbonyl)-2-oxocyclohex-3-en-1-yl)methyl)phenyl)methylene diacetate (99)

An oven dried round bottom flask was charged with KHMDS (837 mg, 4.20 mmol, 1.05 equiv), 18-crown-6 (1.06 g, 4.00 mmol, 1.0 equiv), and THF (21 mL). The mixture was cooled to –78 °C and a solution of enone **100** (830 mg, 4.00 mmol, 1.0 equiv) in THF (10 mL) was added. The reaction mixture was stirred for 15 minutes then (2-(bromomethyl)phenyl)methylene diacetate[37] (1.86 g, 6.00 mmol, 1.5 equiv) was added in a minimal amount of THF (*ca* 5 mL). The solution was slowly warmed to 45 °C and stirred for 14 h. Upon complete consumption of starting material (as determined by TLC), the solution was cooled to 23 °C, diluted with a saturated aqueous solution of NH$_4$Cl, and the reaction mixture was extracted thrice with EtOAc. The combined organic layers were dried over Na$_2$SO$_4$, filtered, and concentrated under reduced pressure. Purification by flash column chromatography (20–60% EtOAc/hexanes) afforded the title compound as a colorless oil (1.00 g, 2.33 mmol, 58% yield).

¹H NMR (400 MHz, CDCl₃): δ 7.87 (s, 1H), 7.58 – 7.52 (m, 1H), 7.30 – 7.24 (m, 2H), 7.21 – 7.16 (m, 1H), 6.88 – 6.82 (m, 1H), 6.07 (ddd, *J* = 10.1, 2.8, 1.3 Hz, 1H), 5.24 (ddq, *J* = 8.6, 5.7, 1.4 Hz, 1H), 4.56 (d, *J* = 7.2 Hz, 2H), 3.52 (d, *J* = 14.8 Hz, 1H), 3.45 (d, *J* = 14.8 Hz, 1H), 2.53 – 2.41 (m, 1H), 2.36 (dddd, *J* = 13.6, 4.9, 2.6, 1.3 Hz, 1H), 2.29 – 2.19 (m, 1H), 2.12 (s, 3H), 2.10 (s, 3H), 1.86 (ddd, *J* = 13.6, 10.4, 5.3 Hz, 1H), 1.73 (s, 3H), 1.67 (s, 3H).

¹³C NMR (100 MHz, CDCl₃): δ 195.4, 171.1, 168.8, 168.8, 149.6, 139.7, 135.5, 134.9, 131.5, 129.6, 129.5, 127.6, 127.2, 118.2, 88.4, 62.5, 58.2, 34.2, 30.2, 25.9, 24.1, 21.0, 21.0, 18.2.

IR (Neat Film, NaCl): 2935, 1759, 1731, 1682, 1447, 1371, 1236, 1206 cm⁻¹.

HRMS (MM: FD+): *m/z* calc'd for C₂₄H₂₈O₇ [M]⁺: 428.1835, found 428.1833.

3-methylbut-2-en-1-yl (*E*)-1-(6-(benzyloxy)-6-oxohex-4-en-1-yl)-2-oxocyclohept-3-ene-1-carboxylate (40p)

To a solution of diacetate **99** (500 mg, 1.17 mmol, 1 equiv) in benzene (11.7 mL, 0.1 M) was added bismuth chloride (38 mg, 0.12 mmol, 0.1 equiv). The reaction mixture was heated to 35 ºC for 3 hours. Upon cooling to 25 ºC, the reaction mixture was diluted with water and the layers were separated. The aqueous layer was extracted twice with chloroform. The combined organic layers were washed with brine, dried over Na₂SO₄, and volatiles were removed in vacuo. The crude aldehyde was used directly in the subsequent Horner–Wadsworth–Emmons olefination.

To a suspension of NaH (52 mg, 1.29 mmol, 60% by weight in mineral oil, 1.1 equiv) in THF (2.6 mL, 0.5 M) at 0 ºC was dropwise added a solution of benzyl 2-(diethoxyphosphoryl)acetate[28] (369 mg, 1.29 mmol, 1.1 equiv) in THF (1.3 mL, 1.0 M). Stirring at 0 ºC was continued for 30 minutes. To the reaction was then dropwise added a solution of the crude aldehyde in THF (2.4 mL, 0.5 M). Upon complete consumption of starting material (as determined by TLC), the reaction mixture was diluted with a saturated solution of $NaHCO_3$ and extracted with EtOAc (3x). The combined organic layers were dried over Na_2SO_4, filtered, and concentrated under reduced pressure. Purification by flash column chromatography (5–40% EtOAc/hexanes) afforded the title compound as a colorless oil (230 mg, 0.502 mmol, 43% yield).

¹H NMR (400 MHz, CDCl₃): δ 8.08 (d, J = 15.7 Hz, 1H), 7.57 (dd, J = 7.5, 1.9 Hz, 1H), 7.44 – 7.31 (m, 5H), 7.27 – 7.17 (m, 3H), 6.85 – 6.80 (m, 1H), 6.40 (d, J = 15.7 Hz, 1H), 6.06 (ddd, J = 10.1, 2.9, 1.2 Hz, 1H), 5.28 – 5.21 (m, 3H), 4.56 – 4.49 (m, 2H), 3.57 (d, J = 14.3 Hz, 1H), 3.31 (d, J = 14.4 Hz, 1H), 2.51 – 2.39 (m, 1H), 2.30 – 2.16 (m, 2H), 1.82 – 1.70 (m, 4H), 1.65 (s, 3H).

¹³C NMR (100 MHz, CDCl₃): δ 195.1, 170.4, 166.7, 149.7, 143.2, 139.7, 136.7, 136.2, 134.7, 132.1, 130.0, 129.3, 128.7, 128.4, 128.3, 127.5, 126.8, 119.4, 118.2, 66.5, 62.5, 58.4, 35.4, 30.2, 25.9, 24.1, 18.2.

IR (Neat Film, NaCl): 3028, 2927, 1720, 1686, 1629, 1168 cm⁻¹.

HRMS (MM: FD+): *m/z* calc'd for $C_{29}H_{30}O_5$ [M]⁺: 458.2088, found 458.2086.
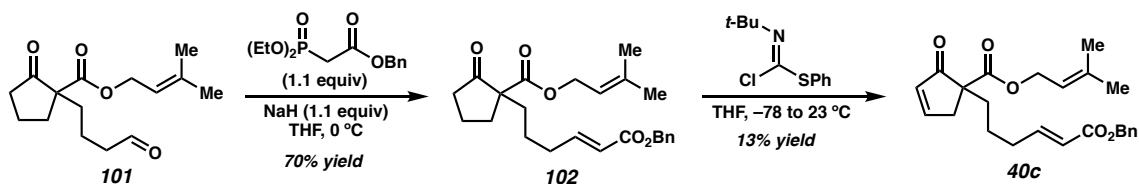
3-methylbut-2-en-1-yl (*E*)-1-(6-(benzyloxy)-6-oxohex-4-en-1-yl)-2-oxocyclopentane-1-carboxylate (102)

Prepared from **101** and benzyl 2-(diethoxyphosphoryl)acetate[28] following General Procedure B. Purification by flash column chromatography (15% EtOAc/hexanes) afforded the title compound as a colorless oil (1.40 g, 3.51 mmol, 70% yield).

^{1}H NMR (400 MHz, CDCl$_3$): δ 7.76 (dt, *J* = 5.6, 2.7 Hz, 1H), 7.42 – 7.26 (m, 5H), 6.95 (dt, *J* = 15.6, 6.9 Hz, 1H), 6.16 (dt, *J* = 5.8, 2.2 Hz, 1H), 5.85 (dt, *J* = 15.6, 1.6 Hz, 1H), 5.27 (tdq, *J* = 7.2, 2.9, 1.5 Hz, 1H), 5.16 (s, 2H), 4.59 (d, *J* = 7.1 Hz, 2H), 3.33 – 3.19 (m, 1H), 2.68 – 2.51 (m, 1H), 2.21 (qd, *J* = 7.3, 1.6 Hz, 2H), 1.99 (ddd, *J* = 13.7, 12.3, 4.5 Hz, 1H), 1.82 – 1.70 (m, 1H), 1.73 (s, 3H), 1.67 (s, 3H), 1.53 – 1.23 (m, 3H).

^{13}C NMR (100 MHz, CDCl$_3$): δ 205.7, 170.6, 166.4, 163.9, 148.9, 139.6, 136.2, 132.4, 128.7, 128.4, 128.3, 121.7, 118.3, 66.2, 62.7, 58.0, 39.5, 34.0, 32.4, 25.9, 23.2, 18.2.

IR (Neat Film, NaCl): 2932, 2356, 1715, 1263, 1164, 976, 754 cm^{-1}.

HRMS (MM: FD+): *m/z* calc'd for C$_{24}$H$_{28}$O$_5$ [M]$^+$: 396.1920, found 396.1931.

3-methylbut-2-en-1-yl (*E*)-1-(6-(benzyloxy)-6-oxohex-4-en-1-yl)-2-oxocyclopent-3-ene-1-carboxylate (40c)

A flame dried round bottom flask was charged with *i*-Pr$_2$NH (0.35 mL, 2.5 mmol, 1.25 equiv) and THF (8.0 mL, 0.25 M). The solution was cooled to –78 ºC and *n*-BuLi (0.96 mL, 2.4 mmol, 1.2 equiv) was added dropwise and the resultant solution was stirred for 30

min. Ketoester **102** (797 mg, 2.00 mmol, 1.0 equiv) in THF (8.0 mL, 0.25 M) was added

dropwise and the mixture was stirred for 1 h. *N-tert*-Butylbenzenesulfinimidoyl chloride[38]

(560.9 mg, 2.6 mmol, 1.3 equiv) in THF (4.0 mL, 0.5 M) was added dropwise and the

solution was slowly warmed to 23 ºC. Upon complete consumption of starting material (as

determined by TLC), the reaction mixture was diluted with saturated aqueous $NaHCO_3$

solution and extracted with Et_2O (25 mL x 3). The combined organic layers were dried

with Na_2SO_4, filtered, and concentrated under reduced pressure. The crude product was

purified by column chromatography (SiO_2, 0–40% EtOAc/Hexanes) to afford enone **40b**

as a colorless oil (100 mg, 0.25 mmol, 13% yield).

¹H NMR (400 MHz, CDCl₃): δ 7.76 (dt, $J = 5.6, 2.7$ Hz, 1H), 7.42 – 7.26 (m, 5H), 6.95

(dt, $J = 15.6, 6.9$ Hz, 1H), 6.16 (dt, $J = 5.8, 2.2$ Hz, 1H), 5.85 (dt, $J = 15.6, 1.6$ Hz, 1H),

5.27 (tdq, $J = 7.2, 2.9, 1.5$ Hz, 1H), 5.16 (s, 2H), 4.59 (d, $J = 7.1$ Hz, 2H), 3.33 – 3.19 (m,

1H), 2.68 – 2.51 (m, 1H), 2.21 (qd, $J = 7.3, 1.6$ Hz, 2H), 1.99 (ddd, $J = 13.7, 12.3, 4.5$ Hz,

1H), 1.82 – 1.70 (m, 1H), 1.73 (s, 3H), 1.67 (s, 3H), 1.53 – 1.23 (m, 3H).

¹³C NMR (100 MHz, CDCl₃): δ 205.7, 170.6, 166.4, 163.9, 148.9, 139.6, 136.2, 132.4,

128.7, 128.4, 128.3, 121.7, 118.3, 66.2, 62.7, 58.0, 39.5, 34.0, 32.4, 25.9, 23.2, 18.2.

IR (Neat Film, NaCl): 2932, 2356, 1715, 1263, 1164, 976, 754 cm⁻¹.

HRMS (MM: FD+): *m/z* calc'd for $C_{24}H_{28}O_5$ [M]⁺: 396.1920, found 396.1931.

3-methylbut-2-en-1-yl   (*E*)-1-(5-(benzyloxy)-5-oxopent-3-en-1-yl)-2-oxocyclohex-3-ene-1-carboxylate (40e)

To a solution of enone **100** (1.04 g, 5.00 mmol, 1.0 equiv) in DMF (10 mL, 0.5 M) at 25°C was added dropwise triethylamine (0.07 mL, 0.50 mmol, 0.1 equiv) followed by acrolein (0.50 mL, 7.50 mmol, 1.5 equiv). Upon consumption of starting material (as determined by TLC), the reaction mixture was diluted with water and extracted thrice with diethyl ether. The combined organic layers were washed with water followed by brine, dried over Na_2SO_4, and volatiles were removed in vacuo. The crude aldehyde was used directly in the subsequent Horner–Wadsworth–Emmons olefination. To a suspension of NaH (132 mg, 3.30 mmol, 60% by weight in mineral oil, 1.1 equiv) in THF (6 mL, 0.5 M) at 0 ºC was dropwise added a solution of benzyl 2-(diethoxyphosphoryl)acetate (945 mg, 3.30 mmol, 1.1 equiv) in THF (3.0 mL, 1.0 M). Stirred at 0 ºC was continued for 30 minutes. To the reaction was then dropwise added a solution of the crude aldehyde in THF (6.0 mL, 0.5 M). Upon complete consumption of starting material (as determined by TLC), the reaction mixture was diluted with a saturated solution of $NaHCO_3$ and extracted with EtOAc (3x). The combined organic layers were dried over Na_2SO_4, filtered, and concentrated under reduced pressure. Purification by flash column chromatography (10–20% EtOAc/hexanes) afforded the title compound as a colorless oil (490 mg, 1.24 mmol, 41% yield).

^{1}H NMR (400 MHz, CDCl₃): δ 7.41 – 7.29 (m, 5H), 6.99 (dt, *J* = 15.7, 6.8 Hz, 1H), 6.93 – 6.84 (m, 1H), 6.03 (ddd, *J* = 10.1, 2.5, 1.5 Hz, 1H), 5.88 (dt, *J* = 15.6, 1.6 Hz, 1H), 5.27 (ddt, *J* = 7.2, 5.8, 1.4 Hz, 1H), 5.17 (s, 2H), 4.59 (d, *J* = 7.1 Hz, 2H), 2.56 – 2.41 (m, 2H), 2.38 – 2.13 (m, 3H), 2.08 – 1.81 (m, 3H), 1.73 (s, 3H), 1.67 (s, 3H).

¹³C NMR (100 MHz, CDCl₃): δ 196.0, 171.4, 166.4, 149.3, 148.9, 139.9, 136.2, 129.4, 128.7, 128.3, 121.5, 118.2, 66.2, 62.4, 56.6, 32.2, 30.7, 27.6, 25.8, 23.8, 18.2.

IR (Neat Film, NaCl): 3032, 2934, 1737, 1681, 1445, 1384, 1265, 1175, 1137 cm⁻¹.

HRMS (MM: FD+): *m/z* calc'd for C₂₄H₂₈O₅ [M]⁺: 396.1937, found 396.1926.

Preparation of Aldehyde Precursors

General Procedure C: Alkylation of β-Ketoesters
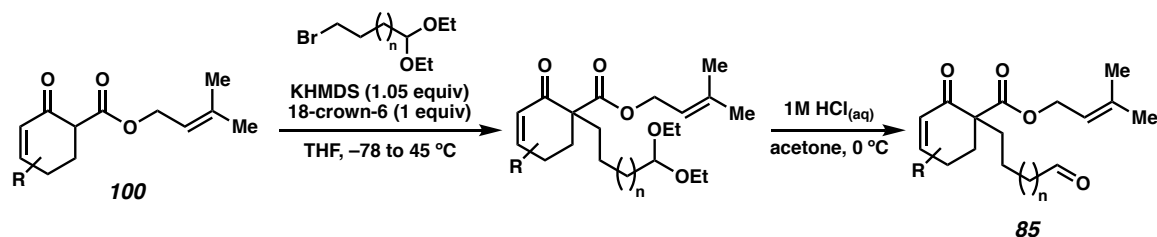
An oven dried round bottom flask was charged with KHMDS (1.05 equiv), 18-crown-6 (1.0 equiv), and THF (0.2 M with respect to KHMDS). The mixture was cooled to –78 ºC and a solution of acyclated enone **100** (1.0 equiv) in THF (0.4 M) was added. The reaction mixture was stirred for 15 minutes and then the appropriate alkyl bromide (1.5 equiv) was added neat dropwise. The solution was slowly warmed to 45 ºC and stirred for 14 h. Upon complete consumption of starting material (as determined by TLC), the solution was cooled to 23 ºC, diluted with a saturated aqueous solution of NH₄Cl and the reaction mixture was extracted thrice with EtOAc. The combined organic layers were dried over Na₂SO₄, filtered, and concentrated under reduced pressure to afford the crude diethyl acetal which was used directly in the next step. A round bottom flask was charged with the crude acetal and acetone (0.5 M), then cooled to 0 ºC. Aqueous 1 M HCl (1:1 volume with respect to acetone) was added and stirring was continued for 1 h. Upon complete consumption of starting material (as determined by TLC), the reaction mixture was extracted with EtOAc (3x). The

combined organic layers were washed with brine, dried over Na$_2$SO$_4$, filtered, and concentrated under reduced pressure. The crude product was purified by silica gel flash column chromatography to afford the respective aldehyde product (**85**).

85
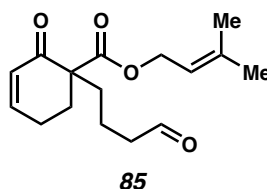
3-methylbut-2-en-1-yl 2-oxo-1-(4-oxobutyl)cyclohex-3-ene-1-carboxylate (85)

Prepared from **100** and 4-bromo-1,1-diethoxybutane[39] following General Procedure C. Purification by flash column chromatography (25% EtOAc/hexanes) afforded the title compound as a colorless oil (1.81 g, 6.50 mmol, 49% yield).

^{1}H NMR (400 MHz, CDCl$_3$): δ 9.75 (t, J = 1.5 Hz, 1H), 6.89 (dddd, J = 10.1, 4.4, 3.1, 1.1 Hz, 1H), 6.02 (ddd, J = 10.1, 2.5, 1.6 Hz, 1H), 5.31 – 5.25 (m, 1H), 4.59 (d, J = 6.8 Hz, 2H), 2.55 – 2.43 (m, 4H), 2.39 – 2.30 (m, 1H), 2.02 – 1.94 (m, 1H), 1.89 (ddd, J = 12.5, 11.7, 4.5 Hz, 1H), 1.78 (dd, J = 11.6, 4.9 Hz, 1H), 1.73 (s, 3H), 1.71 – 1.59 (m, 5H)

^{13}C NMR (100 MHz, CDCl$_3$): δ 202.2, 196.2, 171.5, 149.5, 139.7, 129.3, 118.3, 62.4, 57.0, 44.2, 33.2, 30.3, 25.8, 23.8, 18.2, 17.5.

IR (Neat Film, NaCl): 2942, 1732, 1716, 1456, 1180 cm^{-1}

HRMS (MM: FD+): *m/z* calc'd for C$_{16}$H$_{22}$O$_4$ [M]$^+$: 278.1518, found 278.1509.

86
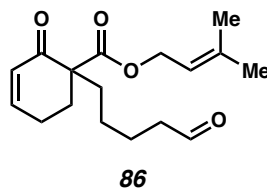
3-methylbut-2-en-1-yl 2-oxo-1-(5-oxopentyl)cyclohex-3-ene-1-carboxylate (86)

Prepared from **100** and 5-bromo-1,1-diethoxypentane[39] following General Procedure C. Purification by flash column chromatography (10–25% EtOAc/hexanes) afforded the title compound as a colorless oil (648 mg, 2.22 mmol, 38% yield).

¹H NMR (400 MHz, CDCl₃): δ 9.75 (s, 1H), 6.91 – 6.84 (m, 1H), 6.01 (ddd, J = 10.1, 2.6, 1.6 Hz, 1H), 5.27 (tdq, J = 7.1, 2.8, 1.4 Hz, 1H), 4.58 (d, J = 7.1 Hz, 2H), 2.54 – 2.40 (m, 4H), 2.36 – 2.27 (m, 1H), 1.98 – 1.86 (m, 2H), 1.78 – 1.60 (m, 10H), 1.40 – 1.26 (m, 2H).

¹³C NMR (100 MHz, CDCl₃): δ 202.6, 196.4, 171.7, 149.4, 139.6, 129.3, 118.3, 62.3, 57.0, 43.7, 33.6, 30.4, 25.8, 24.3, 23.8, 22.5, 18.2.

IR (Neat Film, NaCl): 2941, 1733, 1717, 1456, 1219 cm⁻¹

HRMS (MM: FD+): *m/z* calc'd for $C_{16}H_{22}O_4$ [M]⁺: 293.1747, found 293.1768.
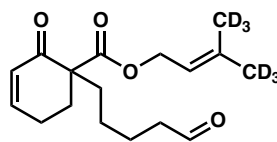
D-86

3-(methyl-*d₃*)but-2-en-1-yl-4,4,4-*d₃* **2-oxo-1-(5-oxopentyl)cyclohex-3-ene-1-carboxylate (*D*-86)**

Prepared from ***D*-100** and 5-bromo-1,1-diethoxypentane[39] following General Procedure C. Purification by flash column chromatography (10–25% EtOAc/hexanes) afforded the title compound as a colorless oil (290 mg, 0.971 mmol, 42% yield).

¹H NMR (400 MHz, CDCl₃): δ 9.75 (t, J = 1.7 Hz, 1H), 6.90 – 6.85 (m, 1H), 6.01 (ddd, J = 10.1, 2.6, 1.6 Hz, 1H), 5.27 (t, J = 7.2 Hz, 1H), 4.58 (dd, J = 7.2, 1.8 Hz, 2H), 2.55 – 2.41 (m, 4H), 2.36 – 2.26 (m, 1H), 1.97 – 1.86 (m, 2H), 1.74 (ddd, J = 13.6, 11.6, 5.1 Hz, 1H), 1.68 – 1.60 (m, 2H), 1.40 – 1.24 (m, 2H).

^{13}C NMR (100 MHz, CDCl$_3$): δ 202.6, 196.4, 171.7, 149.4, 139.4, 129.3, 118.4, 62.3, 57.0, 43.7, 33.6, 30.4, 24.3, 23.9, 22.5.

^{2}H NMR (61 MHz, CHCl$_3$): δ 1.69, 1.65.

IR (Neat Film, NaCl): 2941, 1726, 1682, 1238, 1186 cm^{-1}

HRMS (MM: FD+): *m/z* calc'd for C$_{17}$H$_{18}$D$_6$O$_4$ [M]$^+$: 298.2051, found 298.2052.

87
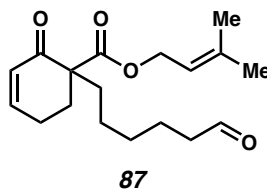
3-methylbut-2-en-1-yl 2-oxo-1-(6-oxohexyl)cyclohex-3-ene-1-carboxylate (87)

Prepared from **100** and 6-bromo-1,1-diethoxyhexane[39] following General Procedure C. Purification by flash column chromatography (10–25% EtOAc/hexanes) afforded the title compound as a colorless oil (838 mg, 2.73 mmol, 32% yield).

^{1}H NMR (400 MHz, CDCl$_3$): δ 9.75 (t, *J* = 1.8 Hz, 1H), 6.90 – 6.85 (m, 1H), 6.01 (ddd, *J* = 10.0, 2.5, 1.5 Hz, 1H), 5.30 – 5.25 (m, 1H), 4.62 – 4.55 (m, 2H), 2.54 – 2.39 (m, 4H), 2.36 – 2.27 (m, 1H), 1.98 – 1.84 (m, 2H), 1.73 (t, *J* = 1.2 Hz, 4H), 1.69 – 1.59 (m, 5H), 1.39 – 1.24 (m, 4H).

^{13}C NMR (100 MHz, CDCl$_3$): δ 202.8, 196.5, 171.7, 149.3, 139.5, 129.4, 118.4, 62.3, 57.1, 43.9, 33.6, 30.3, 29.6, 25.8, 24.4, 23.9, 21.9, 18.2.

IR (Neat Film, NaCl): 2934, 2864, 1733, 1717, 1684, 1456, 1220 cm^{-1}

HRMS (MM: FD+): *m/z* calc'd for C$_{18}$H$_{26}$O$_4$ [M]$^+$: 306.1831, found 306.1854.

93
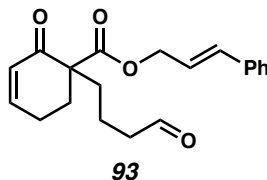
cinnamyl 2-oxo-1-(4-oxobutyl)cyclohex-3-ene-1-carboxylate (93)

Prepared from **103** and 4-bromo-1,1-diethoxybutane[39] following General Procedure C. Purification by flash column chromatography (10–25% EtOAc/hexanes) afforded the title compound as a colorless oil (0.607 g, 1.86 mmol, 49% yield).

^{1}H NMR (400 MHz, CDCl$_3$): δ 9.74 (t, J = 1.5 Hz, 1H), 7.38 – 7.35 (m, 2H), 7.35 – 7.30 (m, 2H), 7.28 – 7.24 (m, 1H), 6.91 (dddd, J = 10.1, 4.3, 3.1, 1.1 Hz, 1H), 6.63 (dt, J = 16.0, 1.4 Hz, 1H), 6.23 (dt, J = 15.8, 6.4 Hz, 1H), 6.05 (ddd, J = 10.1, 2.4, 1.7 Hz, 1H), 4.77 (dt, J = 6.5, 1.1 Hz, 2H), 2.57 – 2.45 (m, 4H), 2.42 – 2.32 (m, 1H), 2.05 – 1.98 (m, 1H), 1.93 (ddd, J = 13.2, 11.7, 5.1 Hz, 1H), 1.80 (ddd, J = 13.2, 11.1, 5.5 Hz, 1H), 1.73 – 1.63 (m, 2H).

^{13}C NMR (100 MHz, CDCl$_3$): δ 202.1, 196.0, 171.3, 149.7, 136.2, 134.7, 129.2, 128.8, 128.3, 126.8, 122.7, 66.0, 57.1, 44.1, 33.3, 30.1, 23.8, 17.5.

IR (Neat Film, NaCl): 2941, 1732, 1717, 1700, 1181, 734, 701 cm^{-1}

HRMS (MM: FD+): *m/z* calc'd for C$_{20}$H$_{22}$O$_4$ [M]$^+$: 326.1513, found 326.1510.

88
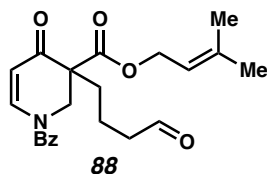
1-benzyl   3-(3-methylbut-2-en-1-yl)   4-oxo-3-(4-oxobutyl)-3,4-dihydropyridine-1,3(2*H*)-dicarboxylate (88)

Prepared from **104** and 4-bromo-1,1-diethoxybutane[39] following General Procedure C. Purification by flash column chromatography (15–30% EtOAc/hexanes) afforded the title compound as a colorless oil (603.9 mg, 1.46 mmol, 60% yield).

^{1}H NMR (400 MHz, CDCl$_3$): δ 9.73 (t, J = 1.4 Hz, 1H), 7.80 (s, 1H), 7.40 (d, J = 3.5 Hz, 5H), 5.27 (m, 4H), 4.61 (m, 3H), 3.78 (d, J = 13.6 Hz, 1H), 2.45 (tt, J = 6.8, 1.7 Hz, 2H), 2.03 – 1.90 (m, 1H), 1.72 (s, 3H), 1.67 (s, 3H), 1.70 – 1.60 (m, 1H).

^{13}C NMR (100 MHz, CDCl$_3$): δ 201.6, 190.5, 169.4, 142.7, 140.1, 135.0, 129.0, 128.9, 128.6, 118.0, 106.5, 69.4, 62.8, 55.4, 48.2, 43.9, 31.1, 25.8, 18.2, 17.2.

IR (Neat Film, NaCl): 2945, 2338, 1727, 1670, 1604, 1389, 1302, 1201, 932 cm^{-1}.

HRMS (MM: FD+): *m/z* calc'd for C$_{23}$H$_{27}$NO$_6$ [M]$^+$: 413.1838, found 413.1852.

89
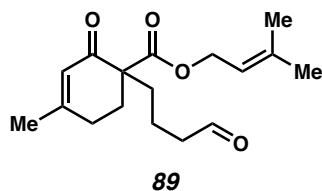
3-methylbut-2-en-1-yl   4-methyl-2-oxo-1-(4-oxobutyl)cyclohex-3-ene-1-carboxylate (89)

Prepared from **105** and 4-bromo-1,1-diethoxybutane[39] following General Procedure C. Purification by flash column chromatography (25–50% EtOAc/hexanes) afforded the title compound as a colorless oil (1141.4 mg, 3.90 mmol, 78% yield).

^{1}H NMR (400 MHz, CDCl$_3$): δ 9.74 (s, 1H), 5.87 (dt, J = 2.6, 1.2 Hz, 1H), 5.27 (tp, J = 7.1, 1.4 Hz, 1H), 4.58 (d, J = 7.2 Hz, 2H), 2.45 (ddd, J = 8.0, 4.8, 1.7 Hz, 4H), 2.29 – 2.18 (m, 1H), 1.92 (s, 3H), 2.00 – 1.84 (m, 2H), 1.72 (s, 3H), 1.67 (s, 3H), 1.79 – 1.54 (m, 3H).

¹³C NMR (100 MHz, CDCl₃): δ 202.2, 195.9, 171.7, 161.6, 139.6, 126.0, 118.3, 62.3, 56.0, 44.2, 33.2, 30.0, 28.7, 25.8, 24.2, 18.2, 17.5.

IR (Neat Film, NaCl): 3426, 2936, 2730, 1725, 1672, 1637, 1440, 1380, 1348, 1311, 1272, 1233, 1214, 1177, 1104, 1050, 1016, 986, 939, 870, 842, 820, 776 cm⁻¹.

HRMS (MM: FD+): *m/z* calc'd for $C_{17}H_{24}O_4$ [M]⁺: 292.1682, found 292.1669.

90
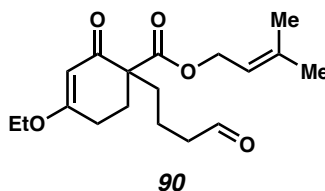
3-methylbut-2-en-1-yl   4-ethoxy-2-oxo-1-(4-oxobutyl)cyclohex-3-ene-1-carboxylate (90)

Prepared from **106** and 4-bromo-1,1-diethoxybutane[39] following General Procedure C. Purification by flash column chromatography (30–40% EtOAc/hexanes) afforded the title compound as a colorless oil (653.2 mg, 2.03 mmol, 21% yield).

¹H NMR (400 MHz, CDCl₃): δ 9.75 (t, *J* = 1.5 Hz, 1H), 5.34 (d, *J* = 1.1 Hz, 1H), 5.29 (tp, *J* = 7.2, 1.4 Hz, 1H), 4.66 – 4.53 (m, 2H), 3.86 (q, *J* = 7.18, 2H), 2.61 (dddd, *J* = 17.8, 10.3, 4.7, 1.3 Hz, 1H), 2.50 – 2.30 (m, 4H), 2.02 – 1.87 (m, 2H), 1.82 – 1.73 (m, 1H), 1.72 (s, 3H), 1.68 (s, 3H), 1.67 – 1.58 (m, 2H), 1.35 (t, *J* = 7.0 Hz, 3H).

¹³C NMR (100 MHz, CDCl₃): δ 201.9, 195.5, 176.5, 171.5, 139.1, 118.1, 101.9, 64.3, 62.0, 55.7, 43.9, 33.1, 28.2, 26.3, 25.5, 17.9, 17.2, 13.9.

IR (Neat Film, NaCl): 2939, 2728, 1723, 1659, 1608, 1447, 1380, 1315, 1242, 1179, 1108, 1027, 942, 816, 769 cm⁻¹.

HRMS (MM: FD+): *m/z* calc'd for $C_{18}H_{26}O_5$ [M]⁺: 322.1790, found 322.1775.

91
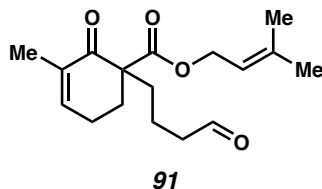
3-methylbut-2-en-1-yl 3-methyl-2-oxo-1-(4-oxobutyl)cyclohex-3-ene-1-carboxylate (91)

Prepared from **107** and 4-bromo-1,1-diethoxybutane[39] following General Procedure C. Purification by flash column chromatography (15–20% EtOAc/hexanes) afforded the title compound as a colorless oil (1.14 g, 3.90 mmol, 70% yield).

^{1}H NMR (400 MHz, CDCl$_3$): δ 9.75 (s, 1H), 6.64 – 6.57 (m, 1H), 5.27 (tt, *J* = 7.1, 1.4 Hz, 1H), 4.64 – 4.51 (m, 2H), 2.51 – 2.36 (m, 4H), 2.36 – 2.22 (m, 1H), 2.01 – 1.92 (m, 1H), 1.87 (m, 1H), 1.83-1.53 (m, 3H) 1.78 (s, 3H), 1.73 (s, 3H), 1.67 (d, *J* = 1.3 Hz, 3H).

^{13}C NMR (100 MHz, CDCl$_3$): δ 202.2, 196.9, 171.9, 143.9, 139.6, 135.3, 118.3, 62.2, 57.0, 44.2, 33.3, 30.7, 25.8, 23.5, 18.2, 17.7, 16.6.

IR (Neat Film, NaCl): 3500, 2925, 2333, 1725, 1681, 1449, 1361, 1182 cm^{-1}.

HRMS (MM: FD+): *m/z* calc'd for C$_{17}$H$_{24}$O$_4$ [M]$^+$: 292.1680, found 292.1669.

92
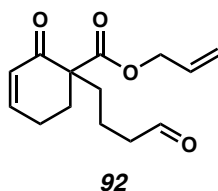
allyl 2-oxo-1-(4-oxobutyl)cyclohex-3-ene-1-carboxylate (92)

Prepared from allyl 2-oxocyclohex-3-ene-1-carboxylate [40] and 4-bromo-1,1-diethoxybutane[39] following General Procedure C. Purification by flash column

chromatography (15–30% EtOAc/hexanes) afforded the title compound as a colorless oil

(773.2 mg, 3.09 mmol, 21% yield).

¹H NMR (400 MHz, CDCl₃): δ 9.75 (t, *J* = 1.4 Hz, 1H), 6.91 (dddd, *J* = 10.1, 4.4, 3.1, 1.1

Hz, 1H), 6.03 (dt, *J* = 10.1, 2.0 Hz, 1H), 5.86 (ddt, *J* = 17.1, 10.2, 5.6 Hz, 1H), 5.28 (dq, *J*

= 17.2, 1.6 Hz, 1H), 5.22 (dq, *J* = 10.4, 1.3 Hz, 1H), 4.60 (dq, *J* = 5.4, 1.6 Hz, 2H), 2.58 –

2.43 (m, 4H), 2.43 – 2.30 (m, 1H), 2.07 – 1.95 (m, 1H), 1.91 (ddd, *J* = 13.2, 11.6, 5.2 Hz,

1H), 1.79 (ddd, *J* = 13.2, 10.9, 5.6 Hz, 1H), 1.75 – 1.56 (m, 2H).

¹³C NMR (100 MHz, CDCl₃): δ 202.1, 196.0, 171.2, 149.7, 131.7, 129.2, 118.7, 65.9,

57.1, 44.1, 33.1, 30.1, 23.7, 17.4.

IR (Neat Film, NaCl): 2947, 2732, 1726, 1680, 1238, 1184 cm⁻¹.

HRMS (MM: FD+): *m/z* calc'd for C₁₄H₁₉O₄ [M]⁺: 251.1281, found 251.1278.
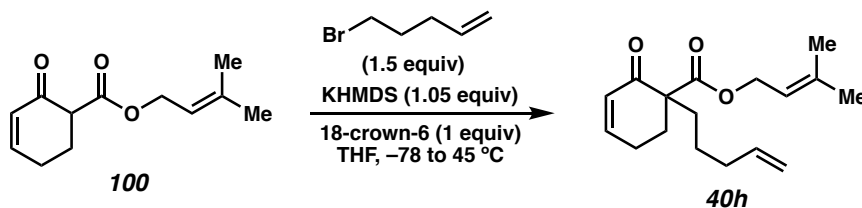
3-methylbut-2-en-1-yl 2-oxo-1-(pent-4-en-1-yl)cyclohex-3-ene-1-carboxylate (40h)

Prepared from **100** and 5-bromopent-1-ene following General Procedure C (without

hydrolysis step). Purification by flash column chromatography (0-20% EtOAc/hexanes)

afforded the title compound as a colorless oil (93.8 mg, 0.34 mmol, 23% yield).

¹H NMR (400 MHz, CDCl₃): δ 6.87 (dddd, *J* = 10.1, 4.8, 3.1, 1.1 Hz, 1H), 6.01 (ddd, *J* =

10.1, 2.5, 1.6 Hz, 1H), 5.78 (ddt, *J* = 16.9, 10.2, 6.6 Hz, 1H), 5.28 (tdq, *J* = 7.1, 2.9, 1.4 Hz,

1H), 5.00 (dq, *J* = 17.1, 1.6 Hz, 1H), 4.94 (ddt, *J* = 10.2, 2.2, 1.2 Hz, 1H), 4.59 (dd, *J* = 7.2,

3.7 Hz, 1H), 4.64 – 4.53 (m, 2H), 2.57 – 2.41 (m, 2H), 2.38 – 2.24 (m, 2H), 2.12 – 2.01 (m,

2H), 2.00 – 1.86 (m, 2H), 1.77 – 1.69 (m, 1H), 1.73 (s, 3H), 1.68 (s, 3H), 1.51 – 1.28 (m, 2H).

¹³C NMR (100 MHz, CDCl₃): δ 196.5, 171.7, 149.3, 139.5, 138.4, 129.4, 118.4, 114.9, 62.2, 57.1, 34.2, 33.4, 30.3, 25.8, 24.0, 23.9, 18.2.

IR (Neat Film, NaCl): 2928, 1726, 1683, 1440, 1383, 1186, 912 cm⁻¹.

HRMS (MM: FD+): *m/z* calc'd for $C_{17}H_{24}O_3$ [M]⁺: 276.1725, found 276.1718.

101
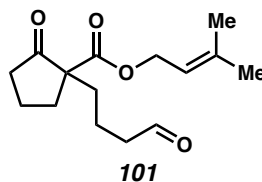
3-methylbut-2-en-1-yl 2-oxo-1-(4-oxobutyl)cyclopentane-1-carboxylate (101)

Prepared from 3-methylbut-2-en-1-yl 2-oxocyclopentane-1-carboxylate[41] and 4-bromo-1,1-diethoxybutane[39] following General Procedure C. Purification by flash column chromatography (20–25% EtOAc/hexanes) afforded the title compound as a colorless oil (1.86 g, 6.97 mmol, 87% yield).

¹H NMR (400 MHz, CDCl₃): δ 9.74 (t, *J* = 1.4 Hz, 1H), 5.29 (tp, *J* = 7.3, 1.4 Hz, 1H), 4.59 (d, *J* = 7.2 Hz, 2H), 2.58 – 2.47 (m, 1H), 2.44 (tt, *J* = 7.0, 1.5 Hz, 2H), 2.44 – 2.36 (m, 1H), 2.31 – 2.18 (m, 1H), 2.11 – 1.85 (m, 4H), 1.74 (s, 3H), 1.68 (s, 3H), 1.67 – 1.48 (m, 3H).

¹³C NMR (100 MHz, CDCl₃): δ 214.8, 201.9, 171.0, 139.7, 118.2, 62.5, 60.4, 44.0, 38.0, 33.2, 33.0, 25.9, 19.8, 18.2, 17.6.

IR (Neat Film, NaCl): 3456, 2954, 2724, 1745, 1721, 1446, 1406, 1384, 1154, 953 cm⁻¹.

HRMS (MM: FD+): *m/z* calc'd for $C_{15}H_{22}O_4$ [M]⁺: 266.1525, found 266.1513.

96
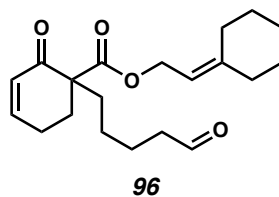
2-cyclohexylideneethyl 2-oxo-1-(5-oxopentyl)cyclohex-3-ene-1-carboxylate (96)

Prepared from **108** and 5-bromo-1,1-diethoxypentane[39] following General Procedure C. Purification by flash column chromatography (10–50% EtOAc/hexanes) afforded the title compound as a colorless oil (177 mg, 0.53 mmol, 25% yield).

^{1}H NMR (400 MHz, CDCl$_3$): δ 9.75 (t, *J* = 1.7 Hz, 1H), 6.93 – 6.83 (m, 1H), 6.02 (ddd, *J* = 10.1, 2.6, 1.6 Hz, 1H), 5.23 (tt, *J* = 7.2, 1.2 Hz, 1H), 4.60 (d, *J* = 7.2 Hz, 2H), 2.56 – 2.39 (m, 4H), 2.37 – 2.26 (m, 1H), 2.20 – 2.13 (m, 2H), 2.12 – 2.05 (m, 2H), 1.99 – 1.85 (m, 2H), 1.74 (ddd, *J* = 13.6, 11.7, 5.0 Hz, 1H), 1.64 (p, *J* = 7.5 Hz, 2H), 1.58 – 1.46 (m, 6H), 1.43 – 1.20 (m, 2H).

^{13}C NMR (100 MHz, CDCl$_3$): δ 202.6, 196.4, 171.6, 149.3, 147.7, 129.4, 114.8, 61.5, 57.0, 43.7, 37.1, 33.6, 30.4, 29.2, 28.5, 27.9, 26.7, 24.3, 23.9, 22.5.

IR (Neat Film, NaCl): 2929, 2858, 1731, 1446, 1170, 938 cm^{-1}.

HRMS (MM: FD+): *m/z* calc'd for C$_{20}$H$_{28}$O$_4$ [M]$^+$: 332.1988, found 332.1991.

95
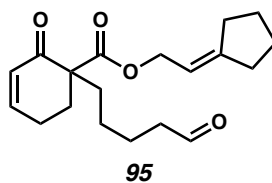
2-cyclopentylideneethyl 2-oxo-1-(5-oxopentyl)cyclohex-3-ene-1-carboxylate (95)

Prepared from **109** and 5-bromo-1,1-diethoxypentane[39] following General Procedure C. Purification by flash column chromatography (10–60% EtOAc/hexanes) afforded the title compound as a colorless oil (1.40 g, 4.40 mmol, 39% yield).

¹H NMR (400 MHz, CDCl₃): δ 9.75 (t, *J* = 1.7 Hz, 3H), 6.92 – 6.83 (m, 1H), 6.02 (ddd, *J* = 10.1, 2.6, 1.6 Hz, 1H), 5.41 – 5.32 (m, 1H), 4.64 – 4.50 (m, 2H), 2.56 – 2.39 (m, 4H), 2.37 – 2.20 (m, 5H), 1.99 – 1.83 (m, 2H), 1.80 – 1.57 (m, 7H), 1.45 – 1.22 (m, 2H).

¹³C NMR (100 MHz, CDCl₃): δ 202.6, 196.4, 171.7, 151.1, 149.4, 129.4, 113.8, 63.8, 57.0, 43.7, 33.9, 33.6, 30.4, 29.0, 26.4, 26.2, 24.3, 23.9, 22.5.

IR (Neat Film, NaCl): 2947, 2725, 1729, 1697, 1456, 1356, 1215 cm⁻¹.

HRMS (MM: FD+): *m/z* calc'd for $C_{19}H_{26}O_4$ [M]⁺: 318.1831, found 318.1809.

94
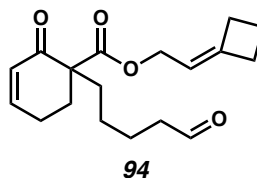
2-cyclobutylideneethyl 2-oxo-1-(5-oxopentyl)cyclohex-3-ene-1-carboxylate (94)

Prepared from **110** and 5-bromo-1,1-diethoxypentane[39] following General Procedure C. Purification by flash column chromatography (10–60% EtOAc/hexanes) afforded the title compound as a colorless oil (649 mg, 2.13 mmol, 29% yield).

¹H NMR (400 MHz, CDCl₃): δ 9.75 (t, *J* = 1.7 Hz, 1H), 6.94 – 6.83 (m, 1H), 6.02 (ddd, *J* = 10.1, 2.6, 1.5 Hz, 1H), 5.20 (tp, *J* = 7.1, 2.3 Hz, 1H), 4.46 (ddt, *J* = 7.4, 2.3, 1.1 Hz, 2H), 2.69 (dt, *J* = 16.0, 8.4 Hz, 4H), 2.56 – 2.40 (m, 4H), 2.37 – 2.26 (m, 1H), 2.03 – 1.84 (m, 4H), 1.75 (ddd, *J* = 13.6, 11.6, 5.1 Hz, 1H), 1.64 (p, *J* = 7.5 Hz, 2H), 1.42 – 1.26 (m, 2H).

^{13}C NMR (100 MHz, CDCl$_3$): δ 202.6, 196.4, 171.6, 149.4, 148.9, 129.4, 114.0, 62.3, 57.0, 43.7, 33.6, 31.2, 30.4, 29.6, 24.3, 23.9, 22.5, 17.1.

IR (Neat Film, NaCl): 2941, 1726, 1681, 1446, 1387, 1240, 1171, 1103 cm^{-1}.

HRMS (MM: FD+): *m/z* calc'd for C$_{18}$H$_{24}$O$_4$ [M]$^+$: 304.1675, found 304.1677.

98
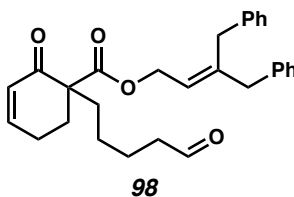
3-benzyl-4-phenylbut-2-en-1-yl   2-oxo-1-(5-oxopentyl)cyclohex-3-ene-1-carboxylate (98)

Prepared from **111** and 5-bromo-1,1-diethoxypentane[39] following General Procedure C. Purification by flash column chromatography (10–60% Et$_2$O/hexanes) afforded the title compound as a colorless oil (425 mg, 0.955 mmol, 18% yield).

^{1}H NMR (400 MHz, CDCl$_3$): δ 9.73 (t, *J* = 1.7 Hz, 1H), 7.32 – 7.27 (m, 4H), 7.21 (tt, *J* = 7.5, 2.3 Hz, 2H), 7.15 – 7.03 (m, 4H), 6.90 – 6.82 (m, 1H), 6.02 (ddd, *J* = 10.2, 2.5, 1.6 Hz, 1H), 5.51 (d, *J* = 7.4 Hz, 1H), 4.83 – 4.70 (m, 2H), 3.36 (s, 2H), 3.24 (s, 2H), 2.54 – 2.24 (m, 5H), 2.00 – 1.86 (m, 2H), 1.77 (ddd, *J* = 13.6, 11.6, 5.1 Hz, 1H), 1.63 (p, *J* = 7.5 Hz, 2H), 1.44 – 1.22 (m, 2H).

^{13}C NMR (100 MHz, CDCl$_3$): δ 202.5, 196.2, 171.6, 149.4, 144.8, 139.0, 138.8, 129.4, 129.3, 128.8, 128.7, 128.5, 126.5, 126.4, 121.7, 62.0, 57.0, 43.7, 42.9, 35.8, 33.6, 30.4, 24.3, 23.9, 22.5.

IR (Neat Film, NaCl): 2923, 1723, 1684, 1493, 1451, 1386, 1231 cm^{-1}.

HRMS (MM: FD+): *m/z* calc'd for C$_{29}$H$_{32}$O$_4$ [M]$^+$: 444.2301, found 444.2300.

97
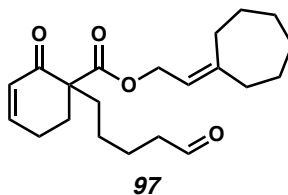
2-cycloheptylideneethyl 2-oxo-1-(5-oxopentyl)cyclohex-3-ene-1-carboxylate (97)

Prepared from **112** and 5-bromo-1,1-diethoxypentane[39] following General Procedure C.

Purification by flash column chromatography (10–70% Et$_2$O/hexanes) afforded the title

compound as a colorless oil (349 mg, 1.01 mmol, 15% yield).

^{1}H NMR (400 MHz, CDCl$_3$): δ 9.75 (t, *J* = 1.7 Hz, 1H), 6.91 – 6.84 (m, 1H), 6.02 (ddd, *J*

= 10.1, 2.6, 1.6 Hz, 1H), 5.28 (tt, *J* = 7.1, 1.3 Hz, 1H), 4.60 (d, *J* = 7.1 Hz, 2H), 2.56 – 2.40

(m, 4H), 2.38 – 2.20 (m, 5H), 1.98 – 1.87 (m, 2H), 1.76 (ddd, *J* = 13.7, 12.0, 4.8 Hz, 1H),

1.65 (p, *J* = 7.5 Hz, 2H), 1.57 (q, *J* = 5.4 Hz, 4H), 1.50 (dt, *J* = 5.2, 2.4 Hz, 4H), 1.42 –

1.27 (m, 2H).

^{13}C NMR (100 MHz, CDCl$_3$): δ 202.6, 196.4, 171.7, 149.4, 149.0, 129.4, 118.4, 62.1,

57.0, 43.7, 37.7, 33.6, 30.4, 30.2, 29.8, 29.1, 28.9, 27.3, 24.3, 23.9, 22.5.

IR (Neat Film, NaCl): 2923, 2854, 1737, 1681, 1443, 1385, 1235, 1172 cm^{-1}.

HRMS (MM: FD+): *m/z* calc'd for C$_{21}$H$_{30}$O$_4$ [M]$^+$: 346.2144, found 346.2139.

β-Ketoesters Synthesis

General Procedure D: Prenyl β-ketoesters Synthesis through Acylation
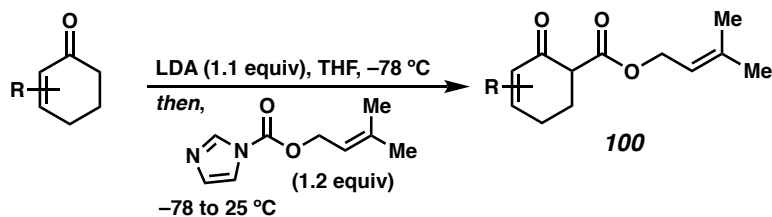
A flame dried round bottom flask was charged with iPr$_2$NH (1.1 equiv) and THF (1.75 M). The solution was cooled to 0 ºC and *n*-BuLi (2.5 M in hexanes, 1.05 equiv) was added dropwise. The resultant solution was stirred for 30 min at 0 ºC. The corresponding cyclohexenone (1.0 equiv) in THF (1.25 M) was added dropwise and stirring was continued at 0 ºC for 30 minutes. The solution was cooled to –78 ºC, and the appropriate N-acyl imidazole (1.2 equiv) in THF (3.25 M) was added dropwise. After 2 h, the reaction was gradually warmed to 23 ºC and diluted with 2 M aqueous HCl until reaching a pH < 7. The reaction mixture was extracted three times with EtOAc. The combined organic layers were washed with brine, dried over Na$_2$SO$_4$, filtered, and concentrated under reduced pressure. The crude product was purified by flash silica gel column chromatography to afford the corresponding acylated enone.

100
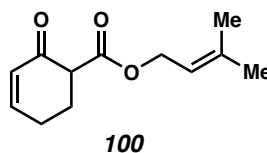
3-methylbut-2-en-1-yl 2-oxocyclohex-3-ene-1-carboxylate (100)

Prepared from 2-cyclohexen-1-one and 3-methylbut-2-en-1-yl 1H-imidazole-1-carboxylate [42] following General Procedure D. Purification by flash column chromatography (25% EtOAc/hexanes) afforded the title compound as a colorless oil (6.65 g, 31.9 mmol, 41% yield).

^{1}H NMR (400 MHz, CDCl$_3$): δ 7.02 – 6.97 (m, 1H), 6.07 (dt, *J* = 10.2, 2.0 Hz, 1H), 5.37 – 5.32 (m, 1H), 4.65 (d, *J* = 7.1 Hz, 2H), 3.42 – 3.39 (m, 1H), 2.55 – 2.45 (m, 1H), 2.44 – 2.34 (m, 2H), 2.26 – 2.18 (m, 1H), 1.75 (s, 3H), 1.71 (s, 3H).

^{13}C NMR (100 MHz, CDCl$_3$): δ 194.1, 170.2, 150.7, 139.6, 129.3, 118.4, 62.3, 53.6, 25.9, 25.8, 24.5, 18.2.

IR (Neat Film, NaCl): 3033, 2934, 1736, 1682, 1447, 1387, 1302, 1233, 1159, 1123 cm^{-1}

HRMS (MM: FD+): *m/z* calc'd for C$_{12}$H$_{16}$O$_3$ [M]$^+$: 208.1099, found 208.1090.
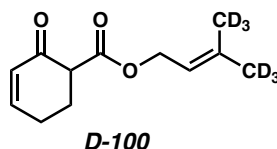
D-100

3-(methyl-*d$_3$*)but-2-en-1-yl-4,4,4-*d$_3$* 2-oxocyclohex-3-ene-1-carboxylate (D-100)

Prepared from 2-cyclohexen-1-one and 3-(methyl-*d$_3$*)but-2-en-1-yl-4,4,4-*d$_3$* 1*H*-imidazole-1-carboxylate [43] following General Procedure D. Purification by flash column chromatography (25% EtOAc/hexanes) afforded the title compound as a colorless oil (1.00 g, 4.67 mmol, 37% yield). *Note that 1.0 equiv of the N-acyl imidazole can be employed*.

^{1}H NMR (400 MHz, CDCl$_3$): δ 6.99 (dt, *J* = 10.0, 3.7 Hz, 1H), 6.06 (dt, *J* = 10.2, 2.1 Hz, 1H), 5.34 (t, *J* = 7.2 Hz, 1H), 4.65 (d, *J* = 7.2 Hz, 2H), 3.40 (dd, *J* = 9.7, 5.0 Hz, 1H), 2.54 – 2.44 (m, 1H), 2.44 – 2.32 (m, 2H), 2.22 (ddt, *J* = 13.7, 8.8, 3.0 Hz, 1H).

^{13}C NMR (100 MHz, CDCl$_3$): δ 194.1, 170.2, 150.7, 139.4, 129.3, 118.4, 62.3, 53.6, 25.8, 24.5.

^{2}H NMR (61 MHz, CHCl$_3$): δ 1.72, 1.67.

IR (Neat Film, NaCl): 2942, 1736, 1681, 1388, 1164 cm^{-1}

HRMS (MM: FD+): *m/z* calc'd for C$_{12}$H$_{10}$D$_6$O$_3$ [M]$^+$: 214.1476, found 214.1476.

103
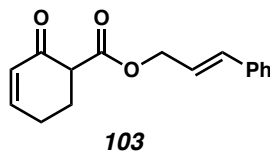
cinnamyl 2-oxocyclohex-3-ene-1-carboxylate (103)

Prepared from 2-cyclohexen-1-one and cinnamyl 1*H*-imidazole-1-carboxylate[42] following General Procedure D. Purification by flash column chromatography (15–25% EtOAc/hexanes) afforded the title compound as a colorless oil (0.98 g, 3.82 mmol, 39% yield).

^{1}H NMR (400 MHz, CDCl$_3$): δ 7.40 – 7.37 (m, 2H), 7.34 – 7.30 (m, 2H), 7.28 – 7.24 (m, 1H), 7.01 (dt, *J* = 10.3, 3.8 Hz, 1H), 6.67 (dt, *J* = 15.9, 1.3 Hz, 1H), 6.29 (dt, *J* = 15.9, 6.4 Hz, 1H), 6.09 (dt, *J* = 10.2, 2.0 Hz, 1H), 4.83 (d, *J* = 6.5 Hz, 2H), 3.47 (dd, *J* = 10.2, 4.9 Hz, 1H), 2.57 – 2.47 (m, 1H), 2.47 – 2.34 (m, 2H), 2.28 – 2.21 (m, 1H).

^{13}C NMR (100 MHz, CDCl$_3$): δ 193.9, 169.9, 150.8, 136.3, 134.6, 129.3, 128.7, 128.2, 126.8, 122.9, 65.9, 53.6, 25.8, 24.5.

IR (Neat Film, NaCl): 3024, 2940, 1734, 1676, 1304, 1223, 1157, 1123, 969 cm^{-1}

HRMS (MM: FD+): *m/z* calc'd for C$_{16}$H$_{16}$NaO$_3$ [M+Na]$^+$: 279.0997, found 279.0983.

107
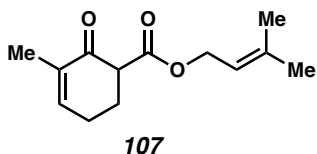
3-methylbut-2-en-1-yl 3-methyl-2-oxocyclohex-3-ene-1-carboxylate (107)

Prepared from 2-methylcyclohex-2-en-1-one[44] and 3-methylbut-2-en-1-yl 1H-imidazole-1-carboxylate[42] following General Procedure D. Purification by flash column

chromatography (10–20% EtOAc/hexanes) afforded the title compound as a colorless oil

(1.09 g, 4.90 mmol, 23% yield).

^{1}H NMR (400 MHz, CDCl$_3$): δ 6.78 – 6.69 (m, 1H), 5.35 (tdq, *J* = 7.2, 2.9, 1.5 Hz, 1H),

4.65 (d, *J* = 7.2 Hz, 2H), 3.42 – 3.36 (m, 1H), 2.48 – 2.11 (m, 5H), 1.79 (d, *J* = 1.6 Hz, 3H),

1.75 (s, 3H), 1.70 (s, 3H).

^{13}C NMR (100 MHz, CDCl$_3$): δ 194.7, 170.6, 145.5, 139.5, 135.4, 118.5, 62.2, 53.8, 26.3,

25.9, 24.6, 18.2, 16.2.

IR (Neat Film, NaCl): 2925, 1736, 1676, 1449, 1381, 1249, 1151 cm^{-1}.

HRMS (MM: FD+): *m/z* calc'd for C$_{13}$H$_{18}$O$_3$ [M]$^+$: 222.1255, found 222.1251.

105
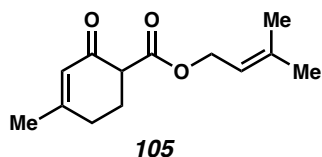
3-methylbut-2-en-1-yl 4-methyl-2-oxocyclohex-3-ene-1-carboxylate (105)

Prepared from 3-methylcyclohex-2-en-1-one and 3-methylbut-2-en-1-yl 1H-imidazole-1-

carboxylate[42] following General Procedure D. Purification by flash column

chromatography (10–20% EtOAc/hexanes) afforded the title compound as a colorless oil

(2.95 g, 13.3 mmol, 17% yield).

^{1}H NMR (400 MHz, CDCl$_3$): δ 5.91 (h, *J* = 1.4 Hz, 1H), 5.35 (tp, *J* = 7.1, 1.6 Hz, 1H),

4.65 (d, *J* = 7.2 Hz, 2H), 3.37 – 3.27 (m, 1H), 2.48 – 2.24 (m, 3H), 2.21 – 2.15 (m, 1H),

1.97 (s, 3H), 1.75 (d, *J* = 1.3 Hz, 3H), 1.70 (s, 3H).

^{13}C NMR (100 MHz, CDCl$_3$): δ 193.9, 170.5, 163.0, 139.5, 126.0, 118.5, 62.3, 52.6, 29.5,

25.9, 25.7, 24.5, 18.2.

IR (Neat Film, NaCl): 2938, 1732, 1668, 1632, 1434, 1378, 1357, 1302, 1246, 1216, 1170, 1152, 1018 cm^{-1}.

HRMS (MM: FD+): *m/z* calc'd for $C_{13}H_{18}O_3$ [M]$^+$: 222.1257, found 222.1251.

106
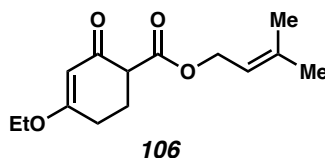
3-methylbut-2-en-1-yl 4-ethoxy-2-oxocyclohex-3-ene-1-carboxylate (106)

Prepared from 3-ethoxycyclohex-2-en-1-one and 3-methylbut-2-en-1-yl 1H-imidazole-1-carboxylate[42] following General Procedure D. Purification by flash column chromatography (25–30% EtOAc/hexanes) afforded the title compound as a colorless oil (2.84 g, 9.51 mmol, 19% yield).

^{1}H NMR (400 MHz, CDCl$_3$): δ 5.38 (s, 1H), 5.37 – 5.32 (m, 1H), 4.72 – 4.59 (m, 2H), 3.91 (qd, *J* = 7.0, 2.3 Hz, 2H), 3.36 – 3.27 (m, 1H), 2.56 (ddd, *J* = 16.6, 6.2, 4.5 Hz, 1H), 2.47 – 2.27 (m, 2H), 2.24 – 2.08 (m, 1H), 1.75 (s, 3H), 1.70 (s, 3H), 1.36 (t, *J* = 7.0 Hz, 3H).

^{13}C NMR (100 MHz, CDCl$_3$): δ 194.0, 177.7, 170.6, 139.4, 118.5, 102.3, 64.6, 62.3, 52.5, 27.5, 25.9, 24.3, 18.2, 14.2.

IR (Neat Film, NaCl): 2980, 2357, 1730, 1648, 1605, 1380, 1192, 1026, 668 cm^{-1}.

HRMS (MM: FD+): *m/z* calc'd for $C_{14}H_{20}O_4$ [M]$^+$: 252.1363, found 252.1356.
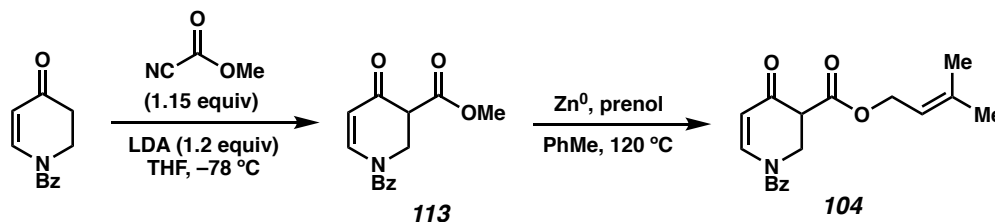
1-benzyl 3-methyl 4-oxo-3,4-dihydropyridine-1,3(2*H*)-dicarboxylate (113)

A flame dried round bottom flask was charged with *i*-Pr₂NH (2.52 mL, 18.0 mmol, 1.2 equiv) and THF (167 mL, 0.1 M). The solution was cooled to –78 ºC and *n*-BuLi (7.20 mL, 18.0 mmol, 1.2 equiv) was added dropwise. The resultant solution was slowly warmed to 0 ºC over 1 h and then cooled to – 78 ºC. The LDA solution was added dropwise to a solution of 1-benzoyl-2,3-dihydropyridin-4(1*H*)-one[45] (3.47 g, 15.0 mmol, 1.0 equiv) in THF (239 mL, 0.06 M) at –78 ºC. The resultant solution was stirred for 1 h. Then methyl cyanoformate (1.37 mL, 17.25 mmol, 1.15 equiv) was added dropwise. Upon complete consumption of starting material (as determined by TLC), the reaction was diluted with a saturated solution of NH₄Cl and the product was extracted with EtOAc (3 x 200 mL). The combined organic layers were dried over Na₂SO₄, filtered, and concentrated under reduced pressure. The crude product was purified by column chromatography (SiO₂, 20–30% EtOAc/Hexanes) to afford acylated enone **113** (1.17 g, 4.05 mmol, 27% yield).

¹H NMR (400 MHz, CDCl₃): δ 7.88 (s, 1H), 7.39 (d, *J* = 2.3 Hz, 5H), 5.40 (s, 1H), 5.28 (s, 1H), 4.39 (dd, *J* = 13.6, 8.9 Hz, 1H), 4.18 (dd, *J* = 13.6, 5.4 Hz, 1H), 3.76 (s, 3H), 3.51 (dd, *J* = 8.9, 5.4 Hz, 1H).

¹³C NMR (100 MHz, CDCl₃): δ 187.8, 168.2, 143.6, 134.8, 129.1, 128.9, 128.8, 128.7, 106.8, 69.6, 52.9, 50.6, 44.4.

IR (Neat Film, NaCl): 2952, 2332, 1734, 1670, 1601, 1388, 1293, 1213 cm⁻¹.

HRMS (MM: FD+): *m/z* calc'd for C₁₅H₁₅NO₅ [M]⁺: 289.0950, found 289.0948.

1-benzyl 3-(3-methylbut-2-en-1-yl) 4-oxo-3,4-dihydropyridine-1,3(2*H*)-dicarboxylate (104)

A flame dried round bottom flask equipped with a reflux condenser was charged with Zn^0 dust (51.5 mg, 0.787 mmol, 0.2 equiv), acylated enone **113** (1.14 g, 3.40 mmol, 1.0 equiv), and toluene (19.7 mL, 0.2 M). To the stirred solution, prenyl alcohol was added neat (2.00 mL, 19.68 mmol, 5.0 equiv). The resultant solution was heated to reflux for 3 days. The solution was cooled to 23 ºC, filtered through a celite plug and eluted with CH_2Cl_2, and concentrated under reduced pressure. The crude product was purified by column chromatography (SiO_2, 15–25% EtOAc/Hexanes) to afford acylated enone **104** (883 mg, 2.57 mmol, 65% yield).

¹H NMR (400 MHz, CDCl₃): δ 7.86 (s, 1H), 7.39 (m, 5H), 5.39 (s, 1H), 5.32 (tp, *J* = 7.3, 1.4 Hz, 1H), 5.27 (s, 2H), 4.65 (dd, *J* = 7.3, 2.9 Hz, 2H), 4.38 (dd, *J* = 13.6, 8.9 Hz, 1H), 4.17 (dd, *J* = 13.5, 5.4 Hz, 1H), 3.48 (dd, *J* = 9.1, 5.3 Hz, 1H), 1.74 (s, 3H), 1.69 (s, 3H).

¹³C NMR (100 MHz, CDCl₃): δ 187.9, 167.8, 143.5, 140.1, 134.9, 129.0, 128.9, 128.8, 128.7, 118.0, 106.9, 69.5, 62.8, 50.8, 44.5, 25.9, 18.2.

IR (Neat Film, NaCl): 2965, 1727, 1676, 1599, 1388, 1293, 1209, 940 cm⁻¹.

HRMS (MM: FD+): *m/z* calc'd for $C_{19}H_{21}HO_5$ [M]⁺: 343.1420, found 343.1420.

General Procedure E: Substituted β-Ketoesters Synthesis through Acylation[42]
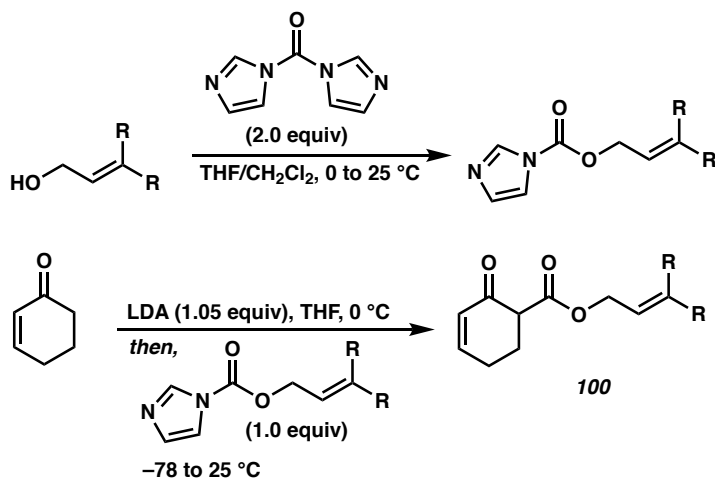
To a solution of di(1*H*-imidazol-1-yl)methanone (2.0 equiv) in THF (2.0 M) at 0 °C was added dropwise a solution of the corresponding alcohol (1.0 equiv) in CH₂Cl₂ (1.0 M). After 3 h, the reaction mixture was gradually warmed to 25 °C. Upon consumption of starting material (as determined by TLC), the reaction mixture was concentrated under reduced pressure then filtered through a silica plug and eluted with 50% EtOAc/Hexanes. The resulting solution was concentrated under reduced pressure.

A flame dried round bottom flask was charged with iPr₂NH (1.1 equiv) and THF (1.75 M). The solution was cooled to 0 ºC and *n*-BuLi (2.5 M in hexanes, 1.05 equiv) was added dropwise. The resultant solution was stirred for 30 min at 0 ºC. 2-cyclohexen-1-one (1.0 equiv) in THF (1.25 M) was added dropwise and stirring was continued at 0 ºC for 30 minutes. The solution was cooled to –78 ºC, and the corresponding crude 1*H*-imidazole-1-carboxylate (1.2 equiv) in THF (3.25 M) was added dropwise. After 2 h, the reaction was gradually warmed to 23 ºC and diluted with 2 M aqueous HCl until reaching a pH < 7. The reaction mixture was extracted three times with EtOAc. The combined organic layers were

washed with brine, dried over Na$_2$SO$_4$, filtered, and concentrated under reduced pressure. The crude product was purified by column chromatography to afford the corresponding acylated enone.

108
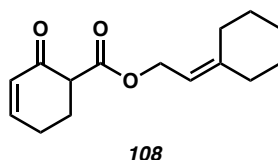
2-cyclohexylideneethyl 2-oxocyclohex-3-ene-1-carboxylate (108)

Prepared from 2-cyclohexen-1-one and 2-cyclohexylideneethan-1-ol[46] following General Procedure E, with the modification of 1.5 equiv of di(1*H*-imidazol-1-yl)methanone and 1.2 equiv of 2-cyclohexylideneethyl 1*H*-imidazole-1-carboxylate being used. Purification by flash column chromatography (5–30% EtOAc/hexanes) afforded the title compound as a colorless oil (535 mg, 2.15 mmol, 28% yield).

^{1}H NMR (400 MHz, CDCl$_3$): δ7.04 – 6.95 (m, 1H), 6.07 (dt, J = 10.1, 2.0 Hz, 1H), 5.29 (tt, J = 7.2, 1.2 Hz, 1H), 4.67 (d, J = 7.2 Hz, 2H), 3.45 – 3.36 (m, 1H), 2.56 – 2.30 (m, 3H), 2.27 – 2.15 (m, 3H), 2.14 – 2.08 (m, 2H), 1.60 – 1.48 (m, 6H).

^{13}C NMR (100 MHz, CDCl$_3$): δ 194.1, 170.2, 150.6, 147.5, 129.3, 115.0, 61.5, 53.6, 37.1, 29.2, 28.5, 27.9, 26.7, 25.8, 24.5.

IR (Neat Film, NaCl): 2930, 2852, 1735, 1683, 1447, 1388, 1298, 1169, 1122 cm^{-1}.

HRMS (MM: FD+): *m/z* calc'd for C$_{15}$H$_{20}$O$_3$ [M]$^+$: 248.1412, found 248.1418.

109
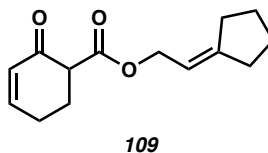
2-cyclopentylideneethyl 2-oxocyclohex-3-ene-1-carboxylate (109)

Prepared from 2-cyclohexen-1-one and 2-cyclopentylideneethan-1-ol[46] following General Procedure E. Purification by flash column chromatography (5–50% EtOAc/hexanes) afforded the title compound as a colorless oil (2.69 g, 11.46 mmol, 31.9% yield).

^{1}H NMR (400 MHz, CDCl$_3$): δ 6.99 (dt, J = 10.1, 3.8 Hz, 1H), 6.07 (dt, J = 10.2, 2.0 Hz, 1H), 5.50 – 5.40 (m, 1H), 4.64 (dt, J = 7.2, 1.1 Hz, 2H), 3.45 – 3.37 (m, 1H), 2.57 – 2.15 (m, 8H), 1.75 – 1.58 (m, 4H).

^{13}C NMR (100 MHz, CDCl$_3$): δ 194.1, 170.2, 151.2, 150.7, 129.3, 113.8, 63.8, 53.6, 34.0, 29.0, 26.4, 26.2, 25.8, 24.5.

IR (Neat Film, NaCl): 2946, 2869, 1782, 1681, 1455, 1387, 1304, 1224, 1156 cm^{-1}.

HRMS (MM: FD+): *m/z* calc'd for C$_{14}$H$_{18}$O$_3$ [M]$^+$: 234.1256, found 234.1255.

110
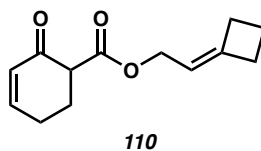
2-cyclobutylideneethyl 2-oxocyclohex-3-ene-1-carboxylate (110)

Prepared from 2-cyclohexen-1-one and 2-cyclobutylideneethan-1-ol[47] following General Procedure E. Purification by flash column chromatography (5–50% EtOAc/hexanes) afforded the title compound as a colorless oil (2.02 g, 9.19 mmol, 31.7% yield).

^{1}H NMR (400 MHz, CDCl$_3$): δ 7.00 (dt, J = 10.1, 3.7 Hz, 1H), 6.07 (dt, J = 10.2, 2.0 Hz, 1H), 5.27 (tp, J = 6.9, 2.2 Hz, 1H), 4.53 (d, J = 7.2 Hz, 2H), 3.45 – 3.36 (m, 1H), 2.80 – 2.65 (m, 4H), 2.56 – 2.31 (m, 3H), 2.28 – 2.15 (m, 1H), 1.98 (p, J = 8.0 Hz, 2H).

^{13}C NMR (100 MHz, CDCl$_3$): δ 194.1, 170.1, 150.7, 148.9, 129.3, 114.1, 62.3, 53.6, 31.2, 29.6, 25.8, 24.5, 17.1.

IR (Neat Film, NaCl): 2947, 1737, 1681, 1457, 1397, 1301, 1229, 1163, 1123 cm^{-1}.

HRMS (MM: FD+): *m/z* calc'd for $C_{13}H_{16}O_3$ [M]$^+$: 220.1099, found 220.1093.

111
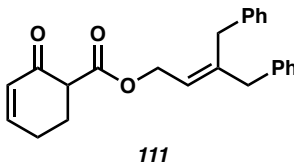
3-benzyl-4-phenylbut-2-en-1-yl 2-oxocyclohex-3-ene-1-carboxylate (111)

Prepared from 2-cyclohexen-1-one and 3-benzyl-4-phenylbut-2-en-1-ol [48] following General Procedure E. Purification by flash column chromatography (5–50% EtOAc/hexanes) afforded the title compound as a colorless oil (1.96 g, 5.43 mmol, 21.3% yield).

^{1}H NMR (400 MHz, CDCl$_3$): δ 7.33 – 7.25 (m, 4H), 7.24 – 7.18 (m, 2H), 7.17 – 7.07 (m, 4H), 7.03 – 6.97 (m, 1H), 6.08 (dt, *J* = 10.1, 2.0 Hz, 1H), 5.59 (tt, *J* = 7.1, 1.1 Hz, 1H), 4.86 – 4.80 (m, 2H), 3.48 – 3.35 (m, 3H), 3.26 (s, 2H), 2.55 – 2.32 (m, 3H), 2.30 – 2.15 (m, 1H).

^{13}C NMR (100 MHz, CDCl$_3$): δ 193.9, 170.1, 150.7, 144.4, 139.0, 138.9, 129.3, 129.3, 128.9, 128.7, 128.5, 126.5, 126.4, 121.9, 62.0, 53.6, 42.9, 35.9, 25.8, 24.5.

IR (Neat Film, NaCl): 3026, 2927, 1738, 1681, 1493, 1388, 1304, 1230, 1157, 1123 cm^{-1}.

HRMS (MM: FD+): *m/z* calc'd for $C_{24}H_{24}O_3$ [M]$^+$: 360.1725, found 360.17302.

112
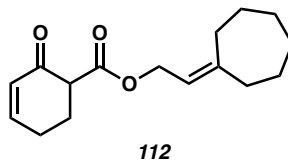
2-cycloheptylideneethyl 2-oxocyclohex-3-ene-1-carboxylate (112)

Prepared from 2-cyclohexen-1-one and 2-cycloheptylideneethan-1-ol[49] following General Procedure E. Purification by flash column chromatography (5–50% EtOAc/hexanes) afforded the title compound as a colorless oil (1.73 g, 5.43 mmol, 28.1% yield).

¹H NMR (400 MHz, CDCl₃): δ 6.99 (dt, J = 10.0, 3.8 Hz, 1H), 6.07 (dt, J = 10.1, 2.0 Hz, 1H), 5.34 (tt, J = 7.1, 1.3 Hz, 1H), 4.66 (d, J = 7.0 Hz, 2H), 3.45 – 3.37 (m, 1H), 2.57 – 2.15 (m, 8H), 1.63 – 1.44 (m, 8H).

¹³C NMR (100 MHz, CDCl₃): δ 194.1, 170.2, 150.6, 148.8, 129.3, 118.5, 62.1, 53.6, 37.8, 30.2, 29.9, 29.1, 28.8, 27.3, 25.8, 24.5.

IR (Neat Film, NaCl): 2923, 2853, 1736, 1681, 1442, 1388, 1300, 1231, 1155, 1122, 1076 cm⁻¹.

HRMS (MM: FD+): m/z calc'd for $C_{26}H_{22}O_3$ [M]⁺: 262.1569, found 262.1577. *Protonated*

Enone Byproducts
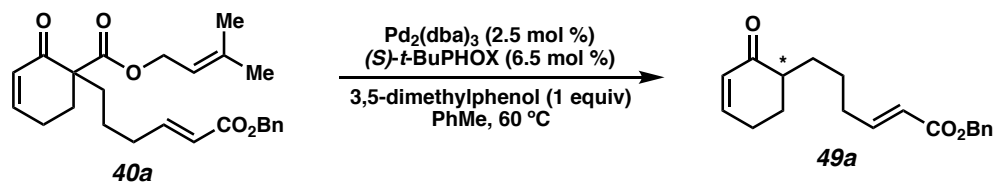
benzyl (R,E)-6-(2-oxocyclohex-3-en-1-yl)hex-2-enoate (49a)

In a nitrogen filled glovebox, an oven-dried 20 mL vial was charged with a stir bar, Pd₂(dba)₃ (0.46 mg, 0.50 μmol, 2.5 mol %), *(S)-t*-BuPHOX (0.50 mg, 1.3 μmol, 6.5 mol %), and toluene (0.5 mL). The catalyst solution was stirred at 23 ºC for 20 min. A solution of substrate **40a** (8.2 mg, 0.020 mmol, 1 equiv) and 3,5-dimethylphenol (2.4 mg, 0.020 mmol, 1 equiv) in toluene (0.5 mL) was added to the vial. The resultant solution was then heated to 60 ºC for 14 h. The solution was then cooled to 23 ºC and concentrated under reduced

pressure. NMR analysis of the crude reaction mixture affords an NMR yield of 100% (with respect to 1,3,5-trimethoxybenzene as an internal standard). The sample was purified by preparatory TLC (25% EtOAc/hexanes) to afford **49a** (71% ee).

^{1}H NMR (400 MHz, CDCl$_3$): δ 7.39 – 7.29 (m, 5H), 7.01 (dt, J = 15.7, 6.9 Hz, 1H), 6.92 (dddd, J = 10.1, 4.5, 3.5, 0.9 Hz, 1H), 5.98 (ddd, J = 10.1, 2.3, 1.7 Hz, 1H), 5.88 (dt, J = 15.6, 1.6 Hz, 1H), 5.17 (s, 2H), 2.46 – 2.34 (m, 2H), 2.32 – 2.20 (m, 3H), 2.09 (dqd, J = 13.3, 4.8, 1.0 Hz, 1H), 1.89 – 1.80 (m, 1H), 1.75 (dddd, J = 13.3, 11.0, 8.4, 5.8 Hz, 1H), 1.55 – 1.35 (m, 3H).

^{13}C NMR (100 MHz, CDCl$_3$): δ 201.6, 166.6, 149.7, 149.6, 136.3, 129.7, 128.7, 128.3, 128.3, 121.4, 66.2, 46.5, 32.5, 29.0, 28.0, 25.6, 25.3.

IR (Neat Film, NaCl): 2921, 1712, 1673, 1257 cm^{-1}.

HRMS (MM: FD+): *m/z* calc'd for C$_{19}$H$_{22}$O$_3$ [M]$^+$: 298.1569, found 298.1565.

Optical Rotation: [α]$_D^{21}$ +3.5 (c 0.20, CHCl$_3$).

SFC conditions: 40% IPA, 2.5 mL/min, Chiralpak IC column, λ = 210 nm, t$_R$ (min): minor = 3.81, major = 4.34.

49d
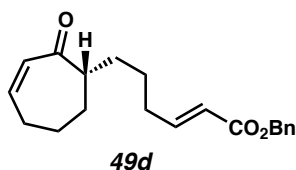
benzyl (*R,E*)-7-(2-oxocyclohex-3-en-1-yl)hept-2-enoate (49d)

Isolated as a byproduct from the reaction of **40d** to **41d** as a colorless oil (10.4 mg, 0.0332 mmol, 17% yield, 67% ee).

¹H NMR (400 MHz, CDCl₃): δ 7.32 – 7.22 (m, 5H), 6.93 (dt, *J* = 15.7, 6.9 Hz, 1H), 6.53 (ddd, *J* = 12.0, 6.7, 4.0 Hz, 1H), 5.94 (ddd, *J* = 11.9, 2.5, 0.9 Hz, 1H), 5.80 (dt, *J* = 15.6, 1.6 Hz, 1H), 5.10 (s, 3H), 2.59 – 2.49 (m, 1H), 2.42 – 2.25 (m, 2H), 2.14 (tdd, *J* = 7.7, 4.8, 1.4 Hz, 2H), 1.90 – 1.48 (m, 5H), 1.44 – 1.29 (m, 4H).

¹³C NMR (100 MHz, CDCl₃): δ 205.7, 166.5, 149.6, 146.0, 136.2, 132.8, 128.6, 128.2, 128.2, 121.2, 66.0, 51.7, 32.4, 31.1, 29.9, 29.5, 25.8, 25.4.

IR (Neat Film, NaCl): 2917, 1719, 1671, 1266, 1165 cm⁻¹.

HRMS (MM: FD+): *m/z* calc'd for C₂₀H₂₄O₃ [M]⁺: 312.1720, found 312.1734.

Optical Rotation: [α]_D²¹ –0.6 (c 1.00, CHCl₃).

SFC conditions: 15% IPA, 2.5 mL/min, Chiralpak AD-H column, λ = 210 nm, t_R (min): minor = 8.23, major = 7.63.

49e
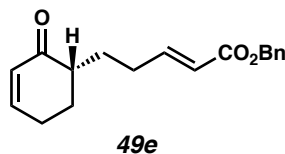
benzyl (*S,E*)-5-(2-oxocyclohex-3-en-1-yl)pent-2-enoate (49e)

Isolated as the major byproduct from the reaction of **40e** to **41e**. Purification by flash column chromatography (0–45% EtOAc/hexanes) afforded the title compound as a colorless oil (46.1 mg, 0.16 mmol, 81% yield, 47% ee).

¹H NMR (400 MHz, CDCl₃): δ 7.42 – 7.28 (m, 5H), 7.01 (dt, *J* = 15.6, 6.9 Hz, 1H), 6.92 (dddd, *J* = 10.0, 4.4, 3.6, 1.0 Hz, 1H), 5.98 (dt, *J* = 10.0, 2.0 Hz, 1H), 5.90 (dt, *J* = 15.7, 1.6 Hz, 1H), 5.17 (s, 2H), 2.44 – 2.24 (m, 5H), 2.15 – 1.96 (m, 2H), 1.82 – 1.69 (m, 1H), 1.62 – 1.44 (m, 1H).

¹³C NMR (100 MHz, CDCl₃): δ 201.3, 166.5, 149.6, 149.4, 136.2, 129.7, 128.7, 128.3, 128.3, 121.6, 66.2, 45.9, 29.7, 28.2, 27.8, 25.4.

IR (Neat Film, NaCl): 3032, 2932, 1719, 1675, 1455, 1386, 1265, 1171 cm⁻¹.

HRMS (MM: FD+): *m/z* calc'd for C₁₈H₂₀O₃ [M]⁺: 284.1412, found 284.1407.

Optical Rotation: [α]_D²¹ +11.8 (c 1.00, CHCl₃).

SFC conditions: 10% IPA, 2.5 mL/min, Chiralpak AS-H column, λ = 210 nm, t_R (min): minor = 5.69, major = 6.54.

49f
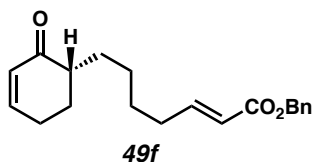
benzyl (*R,E*)-7-(2-oxocyclohex-3-en-1-yl)hept-2-enoate (49f)

Isolated as a byproduct from the reaction of **40f** to **41f** as a colorless oil (28.1 mg, 0.090 mmol, 45% yield, 51% ee). Absolute stereochemistry proposed based on VCD analysis (vide infra).

¹H NMR (400 MHz, CDCl₃): δ 7.42 – 7.29 (m, 5H), 7.00 (dt, *J* = 15.6, 6.9 Hz, 1H), 6.90 (dddd, *J* = 10.0, 4.5, 3.5, 0.9 Hz, 1H), 5.97 (dt, *J* = 10.1, 2.0 Hz, 1H), 5.86 (dt, *J* = 15.6, 1.6 Hz, 1H), 5.17 (s, 2H), 2.42 – 2.33 (m, 2H), 2.29 – 2.18 (m, 3H), 2.08 (dqd, *J* = 13.3, 4.8, 0.9 Hz, 1H), 1.88 – 1.80 (m, 1H), 1.78 – 1.69 (m, 1H), 1.52 – 1.29 (m, 5H).

¹³C NMR (100 MHz, CDCl₃): δ 201.8, 166.6, 150.0, 149.5, 136.3, 129.6, 128.6, 128.3, 128.3, 121.2, 66.1, 46.6, 32.2, 29.0, 28.2, 27.9, 26.6, 25.2.

IR (Neat Film, NaCl): 2927, 2859, 1716, 1675, 1652, 1262, 1172 cm⁻¹

HRMS (MM: FD+): *m/z* calc'd for C₂₀H₂₄O₃ [M]⁺: 312.1725, found 312.1737.

Optical Rotation: [α]_D²¹ +4.1 (c 1.00, CHCl₃).

SFC conditions: 15% IPA, 2.5 mL/min, Chiralpak AD-H column, λ = 210 nm, t_R (min):

minor = 7.77, major = 8.44.
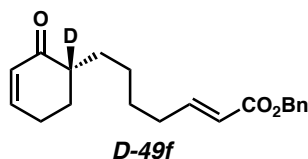
D-49f

benzyl (*R,E*)-7-(2-oxocyclohex-3-en-1-yl-1-*d*)hept-2-enoate (*D-49f*)

Isolated as a byproduct from the reaction of ***D-40f*** to ***D-41f*** as a colorless oil (14.9 mg,

0.0475 mmol, 24% yield, 55% ee).

¹H NMR (400 MHz, CDCl₃): δ 7.39 – 7.29 (m, 5H), 7.00 (dt, *J* = 15.6, 7.0 Hz, 1H), 6.91

(dddd, *J* = 10.1, 4.5, 3.5, 0.9 Hz, 1H), 5.97 (dddd, *J* = 10.0, 2.3, 1.6, 0.6 Hz, 1H), 5.86 (dt,

J = 15.6, 1.6 Hz, 1H), 5.17 (s, 2H), 2.44 – 2.33 (m, 2H), 2.28 – 2.18 (m, 2.5H), 2.09 (ddt,

J = 13.3, 5.8, 4.5 Hz, 1H), 1.87 – 1.70 (m, 2H), 1.53 – 1.27 (m, 5H).

¹³C NMR (100 MHz, CDCl₃): δ 201.9, 166.6, 150.0, 149.6, 129.7, 129.7, 128.7, 128.3,

128.3, 121.2, 66.2, 46.6, 32.3, 29.0, 28.9, 28.2, 27.9, 27.8, 26.7, 26.6, 25.3, 25.2.

²H NMR (61 MHz, CHCl₃): δ 2.25.

IR (Neat Film, NaCl): 2929, 2857, 1714, 1697, 1267, 1174 cm⁻¹.

HRMS (MM: FD+): *m/z* calc'd for $C_{20}H_{23}DO_3$ [M+H]⁺: 313.1783, found 313.1788.

Optical Rotation: [α]_D²¹ +5.8 (c 0.50, CHCl₃).

SFC conditions: 15% IPA, 2.5 mL/min, Chiralpak AD-H column, λ = 210 nm, t_R (min):

minor = 7.96, major = 8.67.

49g
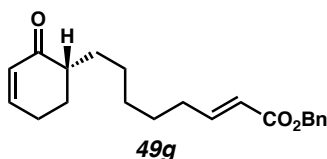
benzyl (*R*,*E*)-8-(2-oxocyclohex-3-en-1-yl)oct-2-enoate (49g)

Isolated as the major product from the reaction of **40g** to **41g** as a colorless oil (50.5 mg,

0.155 mmol, 77% yield, 56% ee).

¹H NMR (400 MHz, CDCl₃): δ 7.40 – 7.29 (m, 5H), 7.01 (dt, *J* = 15.6, 6.9 Hz, 1H), 6.91

(dddd, *J* = 10.0, 4.5, 3.5, 0.9 Hz, 1H), 5.97 (dt, *J* = 10.0, 2.0 Hz, 1H), 5.86 (dt, *J* = 15.6,

1.6 Hz, 1H), 5.17 (s, 2H), 2.45 – 2.33 (m, 2H), 2.30 – 2.16 (m, 3H), 2.09 (dqd, *J* = 14.5,

5.0, 0.9 Hz, 1H), 1.86 – 1.70 (m, 2H), 1.51 – 1.42 (m, 2H), 1.41 – 1.28 (m, 5H).

¹³C NMR (100 MHz, CDCl₃): δ 202.0, 166.7, 150.2, 149.5, 136.3, 129.7, 128.7, 128.3,

128.3, 121.1, 66.1, 46.6, 32.3, 29.3, 29.1, 28.0, 27.9, 26.8, 25.2.

IR (Neat Film, NaCl): 2927, 2859, 1718, 1677, 1555, 1450, 1257, 1165 cm⁻¹

HRMS (MM: FD+): *m/z* calc'd for C₂₁H₂₆O₃ [M]⁺: 326.1877, found 326.1891.

Optical Rotation: [α]$_D^{21}$ +7.0 (c 1.00, CHCl₃).

SFC conditions: 15% IPA, 2.5 mL/min, Chiralpak AD-H column, λ = 210 nm, t$_R$ (min):

minor = 9.70, major = 10.46.

49h
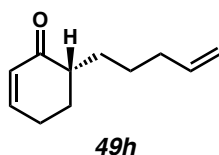
6-(pent-4-en-1-yl)cyclohex-2-en-1-one (49h)

Isolated as the major product from the reaction of **40h** to **41h** as a colorless oil. Purification

by flash column chromatography (0–15% EtOAc/hexanes) afforded the title compound as

a colorless oil (11.0 mg, 0.067 mmol, 33% yield, 58% ee).

¹H NMR (400 MHz, CDCl₃): δ 6.91 (dddd, *J* = 10.1, 4.4, 3.5, 0.9 Hz, 1H), 5.97 (dt, *J* = 10.0, 2.1 Hz, 1H), 5.81 (ddt, *J* = 16.9, 10.2, 6.6 Hz, 1H), 5.01 (dq, *J* = 17.2, 1.8 Hz, 1H), 4.94 (dd, *J* = 10.1, 1.3 Hz, 1H), 2.45 – 2.24 (m, 3H), 2.16 – 1.98 (m, 2=3H), 1.95 – 1.69 (m, 2H), 1.55 – 1.31 (m, 3H).

¹³C NMR (100 MHz, CDCl₃): δ 202.0, 149.5, 138.8, 129.7, 114.7, 46.6, 34.0, 28.8, 27.9, 26.4, 25.2.

IR (Neat Film, NaCl): 2925, 2859, 1677, 1639, 1456, 1387, 1215, 912 cm⁻¹.

HRMS (MM: FD+): *m/z* calc'd for C₁₁H₁₆O [M]⁺: 164.1201, found 164.1201.

Optical Rotation: [α]$_D^{21}$ –111.5 (c 1.00, CHCl₃).

SFC conditions: 3% IPA, 2.5 mL/min, Chiralpak AD-H column, λ = 210 nm, t$_R$ (min): minor = 4.41, major = 4.11.

49i
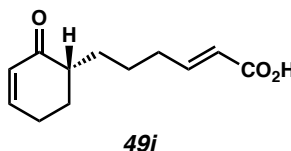
(*E*)-6-(2-oxocyclohex-3-en-1-yl)hex-2-enoic acid (49i)

Isolated as the major product from the reaction of **40i** to **41i** as a colorless oil. Purification by flash column chromatography (35% EtOAc/hexanes with 3% AcOH) afforded the title compound as a white solid (33.2 mg, 0.16 mmol, 80% yield, 9% ee).

¹H NMR (400 MHz, CDCl₃): δ 7.07 (dtd, *J* = 15.5, 7.0, 1.5 Hz, 1H), 6.97 – 6.87 (m, 1H), 5.98 (dq, *J* = 10.1, 1.9 Hz, 1H), 5.84 (dt, *J* = 15.6, 1.6 Hz, 1H), 2.49 – 2.35 (m, 2H), 2.34 – 2.19 (m, 3H), 2.16 – 2.04 (m, 1H), 1.92 – 1.81 (m, 1H), 1.81 – 1.70 (m, 1H), 1.63 – 1.48 (m, 2H), 1.48 – 1.35 (m, 1H).

13C NMR (100 MHz, CDCl3): δ 201.7, 171.5, 151.9, 149.7, 129.7, 120.9, 46.5, 32.5, 29.0, 28.0, 25.5.

IR (Neat Film, NaCl): 2928, 2857, 1731, 1454, 1155 cm^{-1}

HRMS (MM: FD+): *m/z* calc'd for $C_{12}H_{17}O_3$ [M]$^+$: 209.1178, found 209.1168.

Optical Rotation: $[\alpha]_D^{21}$ 2.2 (c 1.00, CHCl3).

SFC conditions: 30% IPA, 2.5 mL/min, Chiralpak IC column, l = 210 nm, t_R (min): minor = 3.30, major = 4.02

49m
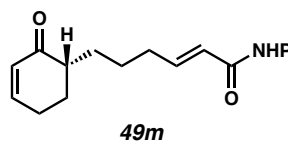
1,3-dioxoisoindolin-2-yl (*E*)-6-(2-oxocyclohex-3-en-1-yl)hex-2-enoate (49m)

Isolated as a byproduct product from the reaction of **40m** to **41m** as a colorless oil. Purification by flash column chromatography (0–35% EtOAc/hexanes) afforded the title compound as a white solid (7.7 mg, 0.022 mmol, 11% yield).

1H NMR (400 MHz, CDCl3): δ 7.89 (dd, *J* = 5.5, 3.1 Hz, 2H), 7.79 (dd, *J* = 5.5, 3.1 Hz, 2H), 7.32 (dt, *J* = 15.8, 6.9 Hz, 1H), 6.93 (dddd, *J* = 10.1, 4.5, 3.5, 1.0 Hz, 1H), 6.10 (dt, *J* = 15.8, 1.6 Hz, 1H), 5.99 (ddd, *J* = 10.0, 2.3, 1.7 Hz, 1H), 2.50 – 2.25 (m, 5H), 2.12 (m, 1H), 1.95 – 1.84 (m, 1H), 1.78 (m, 1H), 1.59 (m, 2H), 1.45 (m, 1H).

13C NMR (100 MHz, CDCl3): δ 201.5, 162.5, 162.2, 155.6, 149.7, 134.9, 129.7, 129.1, 124.1, 115.9, 46.5, 33.2, 29.1, 28.1, 25.4, 25.3.

IR (Neat Film, NaCl): 2931, 1770, 1745, 1673, 1466, 1360, 1186 cm^{-1}.

HRMS (MM: FD+): *m/z* calc'd for $C_{20}H_{19}NO_5$ [M]$^+$: 353.1263, found 353.1242.

49r
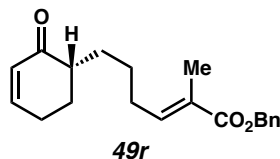
benzyl (*R*,*E*)-2-methyl-6-(2-oxocyclohex-3-en-1-yl)hex-2-enoate (49r)

Isolated as a byproduct from the reaction of **40r** to **41r** as a colorless oil (23.2 mg, 0.0743

mmol, 37% yield, 59% ee).

¹H NMR (400 MHz, CDCl₃): δ 7.40 – 7.29 (m, 5H), 6.91 (dddd, *J* = 10.1, 4.5, 3.5, 0.9 Hz,

1H), 6.81 (td, *J* = 7.5, 1.5 Hz, 1H), 5.97 (dt, *J* = 10.0, 1.9 Hz, 1H), 5.18 (s, 2H), 2.45 – 2.34

(m, 2H), 2.32 – 2.17 (m, 3H), 2.09 (dqd, *J* = 13.4, 4.9, 1.0 Hz, 1H), 1.90 – 1.81 (m, 4H),

1.80 – 1.71 (m, 1H), 1.55 – 1.36 (m, 3H).

¹³C NMR (100 MHz, CDCl₃): δ 201.7, 168.1, 149.6, 142.7, 136.6, 129.7, 128.6, 128.2,

128.1, 127.9, 66.3, 46.6, 29.2, 29.0, 28.0, 26.2, 25.2, 12.6.

IR (Neat Film, NaCl): 3033, 2932, 2861, 1710, 1677, 1256 cm⁻¹.

HRMS (MM: FD+): *m/z* calc'd for C₂₀H₂₄O₃ [M]⁺: 312.1725, found 312.1729.

Optical Rotation: [α]$_D^{21}$ +8.6 (c 1.00, CHCl₃).

SFC conditions: 15% IPA, 2.5 mL/min, Chiralpak AD-H column, λ = 210 nm, t$_R$ (min):

minor = 5.89, major = 6.22.

49t
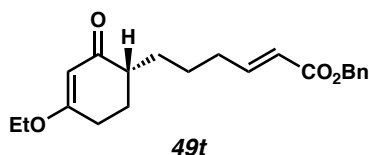
benzyl (*E*)-6-(4-ethoxy-2-oxocyclohex-3-en-1-yl)hex-2-enoate (49t)

Isolated as a byproduct from the reaction of **40t** to **41t** as a colorless oil (5.2 mg, 0.015

mmol, 8% yield, 45% ee).

¹H NMR (400 MHz, CDCl₃): δ 7.41 – 7.27 (m, 5H), 7.01 (dt, *J* = 15.6, 6.9 Hz, 1H), 5.87 (dt, *J* = 15.6, 1.6 Hz, 1H), 5.31 (s, 1H), 5.17 (s, 2H), 3.88 (qd, *J* = 7.1, 1.4 Hz, 2H), 2.41 (dd, *J* = 7.2, 5.3 Hz, 2H), 2.29 – 2.13 (m, 3H), 2.06 (dq, *J* = 13.2, 5.2 Hz, 1H), 1.86 (ddt, *J* = 13.3, 11.1, 5.2 Hz, 1H), 1.78 – 1.64 (m, 1H), 1.59 – 1.37 (m, 3H), 1.35 (t, *J* = 7.0 Hz, 3H).

¹³C NMR (100 MHz, CDCl₃): δ 201.4, 176.9, 166.6, 149.7, 136.3, 128.7, 128.3, 128.3, 121.3, 102.3, 66.1, 64.4, 45.1, 32.5, 29.3, 28.2, 26.4, 25.7, 14.3.

IR (Neat Film, NaCl): 2919, 1718, 1648, 1605, 1456, 1377, 1260, 1190, 732 cm⁻¹.

HRMS (MM: FD+): *m/z* calc'd for C₂₁H₂₆O₄ [M]⁺: 342.1828, found 342.1826.

Optical Rotation: [α]$_D^{21}$ –5.5 (c 0.34, CHCl₃).

SFC conditions: 15% IPA, 2.5 mL/min, Chiralpak AD-H column, λ = 210 nm, t$_R$ (min): minor = 10.17, major = 11.69.

49u
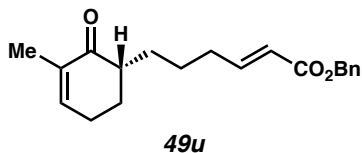
benzyl (*E*)-6-(3-methyl-2-oxocyclohex-3-en-1-yl)hex-2-enoate (49u)

Isolated as a byproduct from the reaction of **40u** to **41u** as a colorless oil (23.6 mg, 0.075 mmol, 37% yield, 46% ee).

¹H NMR (400 MHz, CDCl₃): δ 7.41 – 7.28 (m, 5H), 7.01 (dt, *J* = 15.5, 6.9 Hz, 1H), 6.71 – 6.63 (m, 1H), 5.88 (dt, *J* = 15.6, 1.6 Hz, 1H), 5.17 (s, 2H), 2.33 (ddq, *J* = 6.3, 4.8, 2.0 Hz, 2H), 2.29 – 2.19 (m, 3H), 2.10 – 2.01 (m, 1H), 1.88 – 1.77 (m, 1H), 1.76 (q, *J* = 1.7 Hz, 3H), 1.74 – 1.69 (m, 1H), 1.56 – 1.34 (m, 3H).

¹³C NMR (100 MHz, CDCl₃): δ 201.9, 166.6, 149.8, 144.5, 136.3, 135.3, 128.68, 128.3, 128.3, 121.3, 66.2, 46.6, 32.5, 29.2, 28.4, 25.7, 25.2, 16.3.

IR (Neat Film, NaCl): 2925, 1718, 1670, 1455, 1262, 1172, 1013 cm⁻¹.

HRMS (MM: FD+): *m/z* calc'd for C₂₀H₂₄O₃ [M]⁺: 312.1725, found 312.1721.

Optical Rotation: [α]_D²¹ –14.7 (c 0.35, CHCl₃).

SFC conditions: 10% IPA, 2.5 mL/min, Chiralpak OJ-H column, λ = 210 nm, t_R (min): minor = 7.18, major = 7.62.

Product Derivatizations
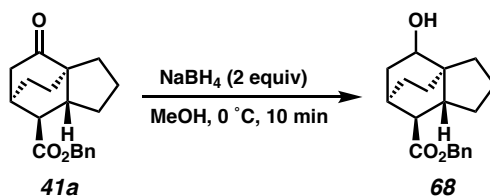
benzyl (3a*R*,6*R*,7*S*,7a*R*)-4-hydroxyoctahydro-3a,6-ethanoindene-7-carboxylate (68)

To a solution of ketone **41a** (0.125 mmol, 1 equiv) in methanol (4.4 mL) was added NaBH₄ (0.25 mmol, 2 equiv) at 0 ºC. The reaction was allowed to stir for 10 min at 0 ºC and then was diluted with water. The aqueous layer was extracted with dichloromethane (3x), and the combined organic layers were dried over Na₂SO₄. Concentration under reduced pressure afforded the title compound as a colorless oil (37.6 mg, 0.125 mmol, 99% yield).

¹H NMR (400 MHz, CDCl₃): δ 7.42 – 7.30 (m, 5H), 5.19 – 5.05 (m, 2H), 3.76 (dd, *J* = 8.9, 5.3 Hz, 0.4H, minor), 3.69 (dt, *J* = 8.9, 1.5 Hz, 0.6H, major), 2.35 – 2.24 (m, 1H), 2.15 – 1.95 (m, 2H), 1.95 – 1.83 (m, br, 1H), 1.83 – 1.56 (m, 6H), 1.53 – 1.23 (m, 5H), 1.15 – 1.01 (m, 1H).

¹³C NMR (100 MHz, CDCl₃): δ 175.8, 175.6, 136.3, 128.6, 128.2, 128.2, 128.0, 128.0, 75.6, 70.3, 66.3, 66.3, 49.21, 48.1, 44.5, 44.2, 43.2, 36.8, 35.0, 34.9, 34.0, 30.5, 30.3, 30.1, 29.6, 29.0, 26.7, 26.3, 22.8, 22.8, 20.3.

IR (Neat Film, NaCl): 3438, 3032, 2942, 2865, 1730, 1455, 1162 cm⁻¹

HRMS (MM: FD+): *m/z* calc'd for $C_{19}H_{24}O_3$ [M]⁺: 300.1725, found 300.1730.

Optical Rotation: $[\alpha]_D^{21}$ –31.1 (c 1.00, CHCl₃).
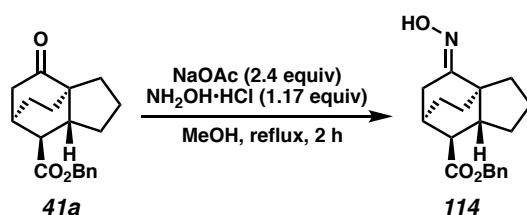
benzyl **(3a*R*,6*R*,7*S*,7a*R*,*E*)-4-(hydroxyimino)octahydro-3a,6-ethanoindene-7-carboxylate (114)**

To a stirred solution of ketone **41a** (0.125 mmol, 1 equiv) in methanol (1.25 mL) was added NaOAc (0.3 mmol, 2.4 equiv), NH₂OH•HCl (0.15 mmol. 1.17 equiv), and water (0.05 mL). The reaction was brought to reflux for 2 h and was subsequently cooled to 23 °C and concentrated under reduced pressure. The crude mixture was then diluted with water and extracted with EtOAc (3x), washed with a saturated aqueous solution of NaHCO₃ and brine, dried with Na₂SO₄, and concentrated under reduced pressure. The material was used in the next step without further purification assuming quantitative yield.

¹H NMR (400 MHz, CDCl₃): δ 7.42 – 7.28 (m, 5H), 5.20 – 5.06 (m, 2H), 2.52 – 2.46 (m, 2H), 2.43 – 2.39 (m, 1H), 2.39 – 2.36 (m, 1H), 2.15 (dtd, *J* = 10.2, 8.2, 1.8 Hz, 1H), 2.07 (ddt, *J* = 11.9, 8.3, 4.1 Hz, 1H), 1.98 (ddd, *J* = 13.0, 11.0, 8.0 Hz, 1H), 1.82 – 1.71 (m, 3H),

1.67 (ddd, *J* = 10.9, 3.6, 1.8 Hz, 1H), 1.48 (dddd, *J* = 12.5, 7.8, 6.5, 3.7 Hz, 2H), 1.36 (dddd,

J = 23.6, 11.1, 8.8, 2.6 Hz, 2H).

^{13}C NMR (100 MHz, CDCl$_3$): δ 174.8, 165.4, 136.2, 128.7, 128.4, 128.2, 66.5, 48.2, 45.7,

44.4, 30.6, 29.2, 28.9, 28.1, 27.2, 25.5, 22.6.

IR (Neat Film, NaCl): 2945, 1731, 1161 cm^{-1}.

HRMS (MM: FD+): *m/z* calc'd for C$_{19}$H$_{23}$NO$_3$ [M]$^+$: 313.1678, found 313.1676.

Optical Rotation: [α]$_D^{21}$ –22.0 (c 0.37, CHCl$_3$).
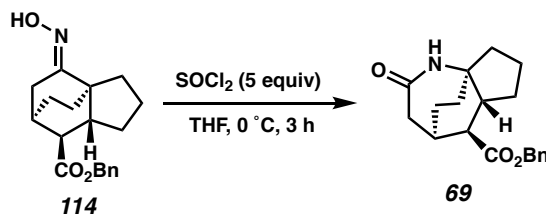
benzyl (4*R*,5*S*,5a*R*,8a*R*)-2-oxooctahydro-1*H*-4,8a-ethanocyclopenta[*b*]azepine-5-carboxylate (69)

To a solution of **114** (0.125 mmol, 1 equiv) in THF (1.25 mL) at 0 ºC was added a solution

of SOCl$_2$ (0.625 mmol, 5 equiv) in THF (0.23 mL). The reaction was stirred for 3 h at 0

ºC, followed by dilution with water. Aqueous solution NH$_4$OH was added to the reaction

mixture until neutral, and the aqueous layer was extracted with dichloromethane (3x). The

combined organic layers were washed with water and brine, dried over Na$_2$SO$_4$, and

concentrated under reduced pressure. Purification by flash column chromatography (35%

EtOAc/hexanes) afforded the title compound as a colorless oil (22 mg, 0.167 mmol, 56%

yield over two steps).

¹H NMR (400 MHz, CDCl₃): δ 7.41 – 7.27 (m, 5H), 6.67 (s, 1H, br), 5.15 (q, J = 12.3 Hz, 2H), 2.73 (dt, J = 18.1, 1.6 Hz, 1H), 2.62 (tdd, J = 9.9, 8.0, 1.4 Hz, 1H), 2.48 (dd, J = 18.4, 6.9 Hz, 1H), 2.40 – 2.32 (m, 2H), 2.29 – 2.16 (m, 1H), 1.95 (dtd, J = 12.7, 8.7, 2.2 Hz, 1H), 1.82 – 1.62 (m, 7H), 1.62 – 1.52 (m, 1H), 1.44 – 1.30 (m, 1H).

¹³C NMR (100 MHz, CDCl₃): δ 174.6, 174.2, 135.9, 128.8, 128.4, 128.3, 66.7, 59.9, 48.8, 48.5, 39.2, 33.3, 31.1, 29.8, 25.1, 23.3.

IR (Neat Film, NaCl): 3182, 3055, 2934, 1727, 1648, 1456, 1398, 1167 cm⁻¹.

HRMS (MM: FD+): m/z calc'd for C₁₉H₂₃NO₃ [M]⁺: 313.1678, found 313.1678.

Optical Rotation: $[\alpha]_D^{21}$ –5.5 (c 0.89, CHCl₃).
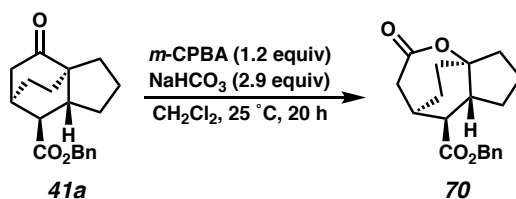
benzyl (4*R*,5*S*,5a*R*,8a*R*)-2-oxooctahydro-4,8a-ethanocyclopenta[*b*]oxepine-5-carboxylate (70)

To a solution ketone **41a** (37 mg, 0.13 mmol, 1 equiv) in CH₂Cl₂ (1.25 mL, 0.1 M) at 0°C was added NaHCO₃ (30.8 mg, 0.37 mmol, 2.9 equiv). Subsequently, *m*-CPBA (31 mg, 0.15 mmol, 1.2 equiv) was added and the reaction was allowed to warm to 25 °C. Upon complete consumption of starting material (as determined by TLC), the reaction mixture was diluted with a saturated solution of Na₂S₂O₃ and extracted with Et₂O (3x). The combined organic layers were washed with a saturated solution of NaHCO₃ followed by brine, dried over Na₂SO₄, and volatiles were removed in vacuo. Purification by preparatory

thin layer chromatography (30% EtOAc/hexanes) afforded the title compound as a clear oil (16 mg, 0.05 mmol, 41% yield).

^{1}H NMR (400 MHz, CDCl$_3$): δ 7.43 – 7.29 (m, 5H), 5.22 – 5.10 (m, 2H), 2.97 (ddd, J = 19.0, 2.5, 1.4 Hz, 1H), 2.83 – 2.61 (m, 2H), 2.41 – 2.32 (m, 2H), 2.28 – 2.09 (m, 3H), 2.05 – 1.93 (m, 1H), 1.81 – 1.56 (m, 5H), 1.40 – 1.26 (m, 1H).

^{13}C NMR (100 MHz, CDCl$_3$): δ 173.9, 172.9, 135.7, 128.8, 128.6, 128.3, 88.4, 66.9, 47.8, 46.5, 39.6, 39.1, 32.8, 30.4, 29.7, 24.9, 22.7.

IR (Neat Film, NaCl): 2943, 2873, 1722, 1255, 1189, 1167 cm^{-1}.

HRMS (MM: FD+): *m/z* calc'd for C$_{19}$H$_{22}$O$_4$ [M]$^+$: 314.1518, found 314.1521.

Optical Rotation: $[\alpha]_D^{21}$ –15.8 (c 1.00, CHCl$_3$).
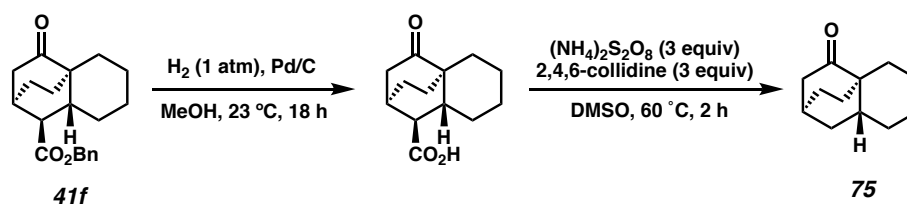
(2S,4aR,8aR)-octahydro-2H-2,4a-ethanonaphthalen-9-one (75)

A vial containing ketone **41f** (0.72 mmol, 1 equiv) and Pd/C (10 wt. % with 67% H$_2$O, 0.072 mmol, 0.1 equiv) was evacuated and backfilled with H$_2$. Methanol (1.06 mL) was subsequently added, and the reaction was stirred at 23 ºC overnight. The crude reaction mixture was filtered through a silica plug and concentrated under reduced pressure to afford the corresponding acid as a white solid, which was used without further purification.

To a solution of the crude acid (0.62 mmol, 1 equiv) in DMSO (1.24 mL) was added (NH$_4$)$_2$S$_2$O$_8$ (1.86 mmol, 3 equiv) and 2,4,6-collidine (1.86 mmol, 3 equiv). The mixture was purged with N$_2$ for 5 min and was subsequently sealed and heated to 60 ºC for 2 h with

stirring. The reaction mixture was diluted with dichloromethane, washed with brine (1x), and the aqueous layer was extracted with dichloromethane (3x). The combined organic layers were washed with brine (3x), dried over Na_2SO_4, and concentrated under reduced pressure. Purification by flash column chromatography (15% EtOAc/hexanes) afforded the title compound as a white solid (30.2 mg, 0.167 mmol, 27% yield).

¹H NMR (400 MHz, CDCl₃): δ 2.33 – 2.21 (m, 3H), 2.13 – 2.07 (m, 1H), 1.93 (dddd, *J* = 13.3, 10.6, 3.8, 2.8 Hz, 1H), 1.75 – 1.58 (m, 6H), 1.53 (dd, *J* = 13.6, 4.0 Hz, 1H), 1.47 – 1.38 (m, 2H), 1.38 – 1.28 (m, 1H), 1.27 – 1.17 (m, 1H), 1.17 – 1.05 (m, 2H).

¹³C NMR (100 MHz, CDCl₃): δ 218.6, 44.9, 43.9, 34.5, 34.1, 30.6, 29.0, 27.7, 25.9, 25.9, 21.8, 21.4.

IR (Neat Film, NaCl): 2925, 1716 cm⁻¹

HRMS (MM: FI+): *m/z* calc'd for $C_{12}H_{18}O$ [M]⁺: 178.1358, found 178.1359.

Optical Rotation: $[\alpha]_D^{21}$ –59.9 (c 0.89, CHCl₃).
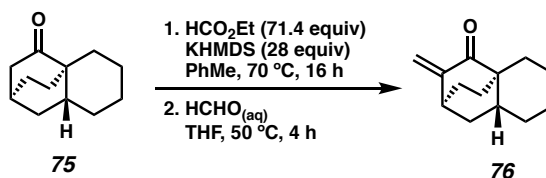
(2*S*,4a*R*,8a*R*)-10-methyleneoctahydro-2*H*-2,4a-ethanonaphthalen-9-one (76)

To a solution of ketone **75** (0.056 mmol, 1 equiv) and ethyl formate (4 mmol, 71.4 equiv) in toluene (3.2 mL) was added a solution of KHMDS (0.5 M in toluene, 1.6 mmol, 28 equiv) at 23 ºC. The reaction mixture was stirred at 70 ºC for 16 h. Upon cooling to 0 ºC, THF (6.4 mL) and formalin (37% in water, 3.2 mL) was added, and then the reaction was heated to 50 ºC for 4 h. The reaction mixture was diluted with a saturated aqueous solution

of NH$_4$Cl, extracted with EtOAc (3x), dried over Na$_2$SO$_4$, and concentrated under reduced pressure. Purification by preparatory thin layer chromatography (30% EtOAc/hexanes, 2x) afforded the title compound as a yellow oil (4.4 mg, 0.023 mmol, 41% yield).

^{1}H NMR (400 MHz, CDCl$_3$): δ 5.93 (d, *J* = 1.8 Hz, 1H), 5.15 (d, *J* = 1.8 Hz, 1H), 2.66 (p, *J* = 3.0 Hz, 1H), 2.39 – 2.19 (m, 1H), 1.98 (dddd, *J* = 13.2, 10.6, 3.9, 2.8 Hz, 1H), 1.81 – 1.61 (m, 6H), 1.51 – 1.42 (m, 2H), 1.41 – 1.31 (m, 2H), 1.23 – 1.15 (m, 2H), 1.11 (dt, *J* = 12.9, 3.6 Hz, 1H).

^{13}C NMR (100 MHz, CDCl$_3$): δ 205.3, 147.9, 116.3, 45.0, 36.1, 35.0, 34.7, 30.8, 29.0, 26.5, 26.0, 21.6, 21.3.

IR (Neat Film, NaCl): 2926, 2859, 1708, 1630, 1464, 1449 cm^{-1}

HRMS (MM: FD+): *m/z* calc'd for C$_{13}$H$_{18}$O [M]$^+$: 190.1358, found 190.1353.

Optical Rotation: [α]$_D^{21}$ –34.2 (c 0.29, CHCl$_3$).

41f → *77*
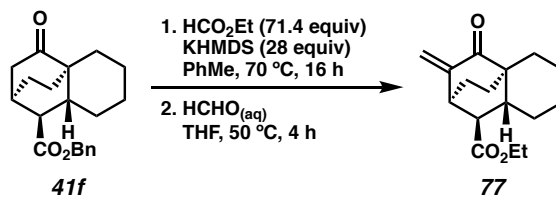
ethyl (1S,2S,4aR,8aR)-3-methylene-4-oxooctahydro-2H-2,4a-ethanonaphthalene-1-carboxylate (77)

To a solution of **41f** (0.192 mmol, 1 equiv) and ethyl formate (13.71 mmol, 71.4 equiv) in toluene (11.1 mL) was added a solution of KHMDS (0.5 M in toluene, 5.49 mmol, 28 equiv) at 23 ºC. The reaction mixture was stirred at 70 ºC for 16 h. Upon cooling to 0 ºC, THF (22.2 mL) and formalin (37% in water, 11.1 mL) was added, and then the reaction was heated to 50 ºC for 4 h. The reaction mixture was diluted with a saturated aqueous solution

of NH$_4$Cl, extracted with EtOAc (3x), dried over Na$_2$SO$_4$, and concentrated under reduced pressure. Purification by preparatory thin layer chromatography (30% EtOAc/hexanes, 2x) afforded the title compound as a yellow oil (13.1 mg, 0.05 mmol, 26% yield).

^{1}H NMR (400 MHz, CDCl$_3$): δ 5.99 (d, *J* = 1.7 Hz, 1H), 5.17 (d, *J* = 1.7 Hz, 1H), 4.21 – 4.01 (m, 2H), 3.04 (td, *J* = 3.1, 2.0 Hz, 1H), 2.27 (ddd, *J* = 14.2, 11.4, 5.4 Hz, 1H), 2.21 (dd, *J* = 6.8, 2.0 Hz, 1H), 2.01 (dddd, *J* = 11.6, 6.5, 4.4, 1.7 Hz, 1H), 1.92 – 1.75 (m, 3H), 1.73 – 1.65 (m, 2H), 1.56 – 1.50 (m, 1H), 1.47 – 1.31 (m, 2H), 1.29 – 1.16 (m, 6H).

^{13}C NMR (100 MHz, CDCl$_3$): δ 203.7, 173.8, 144.3, 119.0, 60.8, 51.1, 45.0, 39.1, 37.2, 30.3, 28.9, 26.2, 25.8, 21.3, 21.1, 14.4.

IR (Neat Film, NaCl): 2927, 2867, 1732, 1708, 1449, 1180 cm^{-1}.

HRMS (MM: FD+): *m/z* calc'd for C$_{16}$H$_{22}$O$_3$ [M]$^+$: 262.1569, found 262.1576.

Optical Rotation: [α]$_D^{21}$ –3.9 (c 0.38, CHCl$_3$).
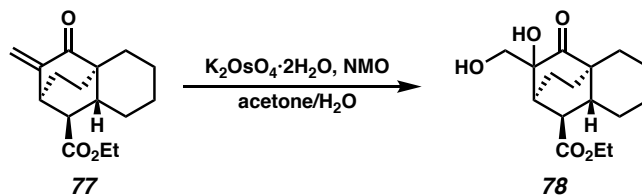
ethyl (1*R*,2*S*,4a*R*,8a*R*)-3-hydroxy-3-(hydroxymethyl)-4-oxooctahydro-2*H*-2,4a-ethanonaphthalene-1-carboxylate (78)

A flame dried vial was charged with enone **77** (14.7 mg, 0.056 mmol, 1 equiv) and acetone (2.3 mL, 0.024 M) and water (0.6 mL, 0.094 M). NMO (50 wt. % in H$_2$O) (23 μL, 0.112 mmol, 2 equiv) was added and the solution was cooled to 0 ºC. K$_2$OsO$_4$·2H$_2$O (2.1 mg, 0.006 mmol, 0.1 equiv) was added to the solution. The resultant solution was slowly warmed to 23 ºC. Upon complete consumption of starting material (as determined by TLC),

the reaction was quenched with a saturated solution of $Na_2S_2O_3$ and stirred for 30 min. The

mixture was then diluted with CH_2Cl_2 and the product was extracted with CH_2Cl_2 (2 x).

The combined organic layers were washed with brine, dried over Na_2SO_4, filtered, and

concentrated under reduced pressure. Purification by preparatory thin layer

chromatography (50% EtOAc/hexanes) afforded the title compound as a colorless oil (2.1

mg, 0.007 mmol,13% yield, 10:1 dr). In the ^1H NMR, peaks that correspond to the minor

diastereomer closely resemble the major diastereomer. dr was determine through

integration of ^1H NMR peaks 2.69 ppm (major) and 2.96 ppm (minor).

^1H NMR (400 MHz, CDCl₃): δ 4.15 (q, *J* = 7.1 Hz, 2H), 3.81 (dd, *J* = 11.8, 2.6 Hz, 1H),

3.54 (dd, *J* = 11.9, 2.7 Hz, 1H), 2.71 – 2.67 (m, 1H), 2.38 – 2.24 (m, 2H), 2.10 (d, *J* = 7.3

Hz, 1H), 1.94 – 1.64 (m, 7H), 1.47 – 1.18 (m, 9H).

^{13}C NMR (100 MHz, CDCl₃): δ 218.4, 174.8, 75.8, 65.8, 61.0, 48.9, 45.4, 37.3, 37.2, 30.3,

28.3, 25.6, 22.5, 21.0, 14.3.

IR (Neat Film, NaCl): 3468, 2930, 2355, 1716, 1197, 1033 cm⁻¹.

HRMS (MM: FD+): *m/z* calc'd for $C_{16}H_{24}O_5$ [M]⁺: 296.1624, found 296.1619.

Optical Rotation: $[\alpha]_D^{21}$ 2.1 (c 0.24, CHCl₃).
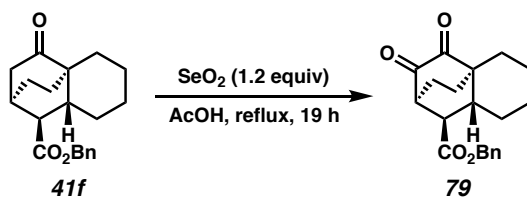
benzyl   (1*R*,2*S*,4a*R*,8a*R*)-3,4-dioxooctahydro-2*H*-2,4a-ethanonaphthalene-1-

carboxylate (79)

To a solution of **41f** (0.064 mmol, 1 equiv) in glacial acetic acid (0.1 mL) was added SeO_2 (0.077 mmol, 1.2 equiv). The reaction was brought to reflux for 19 h. After cooling to 23 ºC, the reaction mixture was filtered and concentrated under reduced pressure. The resulting crude mixture was dissolved in EtOAc and washed with water (5x), dried over Na_2SO_4, and concentrated under reduced pressure. Purification by preparatory thin layer chromatography (30% EtOAc/hexanes) afforded the title compound as a yellow oil (10.4 mg, 0.031 mmol, 48% yield).

¹H NMR (400 MHz, CDCl₃): δ 7.41 – 7.28 (m, 5H), 5.19 – 5.04 (m, 2H), 3.00 (m, 1H), 2.54 (dd, *J* = 6.4, 2.3 Hz, 1H), 2.40 (ddd, *J* = 14.6, 10.3, 6.9 Hz, 1H), 2.02 (m, 3H), 1.80 – 1.69 (m, 2H), 1.68 – 1.50 (m, 3H), 1.48 – 1.38 (m, 1H), 1.33 (dt, *J* = 13.4, 3.5 Hz, 1H), 1.29 – 1.15 (m, 2H).

¹³C NMR (100 MHz, CDCl₃): δ 198.7, 196.1, 173.2, 135.4, 128.8, 128.6, 128.4, 67.4, 49.9, 48.0, 46.3, 37.9, 30.2, 28.3, 25.5, 22.7, 20.5, 20.2.

IR (Neat Film, NaCl): 2932, 2857, 1731, 1454, 1155 cm⁻¹.

HRMS (MM: FD+): *m/z* calc'd for $C_{20}H_{22}O_4$ [M]⁺: 326.1518, found 326.1532.

Optical Rotation: $[\alpha]_D^{21}$ –49.2 (c 1.04, CHCl₃).
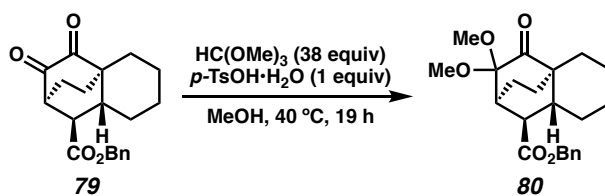
benzyl (1*R*,2*S*,4a*R*,8a*R*)-3,3-dimethoxy-4-oxooctahydro-2*H*-2,4a-ethanonaphthalene-1-carboxylate (80)

To a solution of diketone **79** (0.031 mmol, 1 equiv) in methanol (0.13 mL) was added

HC(OMe)$_3$ (1.2 mmol, 38 equiv) and *p*-TsOH•H$_2$O (0.031 mmol, 1 equiv). The reaction

was stirred for 19 h at 40 ºC, followed by dilution with a saturated aqueous solution of

NaHCO$_3$. The aqueous layer was extracted with EtOAc (4x), dried over Na$_2$SO$_4$, and

concentrated under reduced pressure. Purification by preparatory thin layer

chromatography (30% EtOAc/hexanes) afforded the title compound as a yellow oil (4.7

mg, 0.013 mmol, 41% yield).

¹H NMR (400 MHz, CDCl₃): δ 7.42 – 7.29 (m, 5H), 5.26 (d, *J* = 12.3 Hz, 1H), 5.02 (d, *J*

= 12.3 Hz, 1H), 3.20 (s, 3H), 3.06 (s, 3H), 2.93 (dt, *J* = 4.2, 2.2 Hz, 1H), 2.29 – 2.11 (m,

3H), 1.98 – 1.89 (m, 1H), 1.83 (dddd, *J* = 13.8, 11.4, 6.7, 2.4 Hz, 1H), 1.70 – 1.58 (m, 4H),

1.54 (d, *J* = 3.9 Hz, 1H), 1.31 (dd, *J* = 10.8, 2.4 Hz, 1H), 1.27 – 1.19 (m, 3H).

¹³C NMR (100 MHz, CDCl₃): δ 209.0, 173.5, 136.5, 128.6, 128.5, 128.2, 97.4, 66.4, 50.4,

48.8, 48.4, 45.5, 36.4, 34.9, 30.0, 29.1, 25.5, 23.1, 21.0, 21.0.

IR (Neat Film, NaCl): 2933, 2855, 1736, 1449, 1172 cm⁻¹

HRMS (MM: FD+): *m/z* calc'd for C₂₂H₂₈O₅ [M]⁺: 372.1937, found 372.1931.

Optical Rotation: [α]$_D^{21}$ –26.2 (c 0.42, CHCl₃).
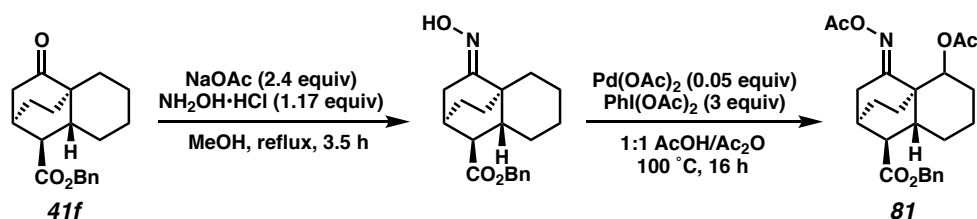
benzyl   (1*S*,2*R*,4a*S*,8a*R*,*E*)-5-acetoxy-4-(acetoxyimino)octahydro-2*H*-2,4a-

ethanonaphthalene-1-carboxylate (81)

To a stirred solution of ketone **41f** (0.096 mmol, 1 equiv) in methanol (0.93 mL) was added

NaOAc (0.23 mmol, 2.4 equiv), NH$_2$OH•HCl (0.111 mmol, 1.17 equiv), and water (0.033

mL). The reaction was brought to reflux for 3.5 h and was subsequently cooled to 23 ºC

and concentrated under reduced pressure. The crude mixture was then diluted with water

and extracted with EtOAc (3x), washed with a saturated aqueous solution of NaHCO$_3$ and

brine, dried with Na$_2$SO$_4$, and concentrated under reduced pressure. The crude oxime was

dissolved in a 1:1 mixture of AcOH/Ac$_2$O (0.78 mL). The reaction vessel was sealed and

stirred at 23 ºC for 2 h. Pd(OAc)$_2$ (0.0048 mmol, 0.05 equiv) and PhI(OAc)$_2$ (0.288 mmol,

3 equiv) were subsequently added, and the reaction was heated to 100 ºC for 16 h. The

reaction mixture was cooled to 23 ºC, filtered through a silica plug, and the filtrate was

diluted with EtOAc. The organic layer was washed with a saturated solution of NaHCO$_3$

until not acidic, washed with brine, dried over Na$_2$SO$_4$, and concentrated under reduced

pressure. Purification by preparatory thin layer chromatography (30% EtOAc/hexanes)

afforded the title compound (**81**) as a yellow oil (12.3 mg, 0.0288 mmol, 30% yield over

two steps).

^{1}H NMR (400 MHz, CDCl$_3$): δ 7.43 – 7.27 (m, 5H), 5.31 – 5.20 (m, 1H), 5.20 – 5.02 (m,

2H), 2.62 (dt, *J* = 20.2, 3.5 Hz, 1H), 2.40 – 2.29 (m, 2H), 2.27 – 2.17 (m, 1H), 2.14 (s, 3H),

2.02 (s, 3H), 1.89 (m, 1H), 1.83 – 1.69 (m, 4H), 1.62 (t, *J* = 2.8 Hz, 2H), 1.46 – 1.28 (m,

4H).

^{13}C NMR (100 MHz, CDCl$_3$): δ 173.9, 170.6, 170.4, 168.9, 135.9, 128.8, 128.5, 128.2,

71.7, 66.9, 49.6, 42.2, 39.1, 29.5, 28.9, 28.6, 26.9, 25.5, 23.0, 21.4, 20.2, 16.7.

IR (Neat Film, NaCl): 2930, 1764, 1731, 1456, 1371, 1248, 1210 cm^{-1}.

HRMS (MM: FD+): *m/z* calc'd for $C_{24}H_{29}NO_6$ [M]$^+$: 427.1995, found 427.2017.

Optical Rotation: $[\alpha]_D^{21}$ –27.6 (c 1.00, CHCl$_3$).
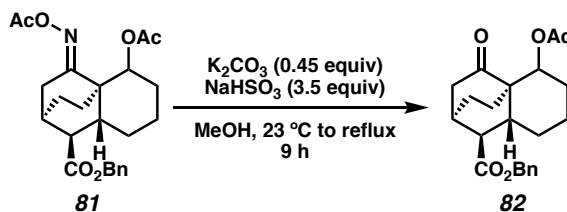
benzyl (1*S*,2*R*,4a*R*,8a*R*)-5-acetoxy-4-oxooctahydro-2*H*-2,4a-ethanonaphthalene-1-carboxylate (82)

To a solution of **81** (0.029 mmol, 1 equiv) in methanol (0.06 mL) in a loosely capped vial was added K$_2$CO$_3$ (0.013 mmol, 0.45 equiv) at 23 ºC in three portions over 6 h. NaHSO$_3$ (0.1 mmol, 3.5 equiv) and water (0.06 mL) were subsequently added, and the vial was sealed and heated to 80 ºC for 3 h. The reaction mixture was diluted with CHCl$_3$, rinsed with 1 M HCl, and the aqueous layer was extracted with CHCl$_3$ (3x). The combined organic layers were neutralized with a saturated solution of NaHCO$_3$, washed with brine, dried over Na$_2$SO$_4$, and concentrated under reduced pressure. Purification by preparatory thin layer chromatography (35% EtOAc/hexanes) afforded the title compound as a colorless oil (1.8 mg, 0.0056 mmol, 19% yield).

¹H NMR (400 MHz, CDCl₃): δ 7.41 – 7.30 (m, 5H), 5.19 – 5.06 (m, 3H), 2.48 (m, 1H), 2.41 (dt, *J* = 19.2, 2.8 Hz, 1H), 2.29 (dt, *J* = 6.9, 2.0 Hz, 1H), 2.16 – 2.04 (m, 3H), 1.98 (s, 3H), 1.94 – 1.89 (m, 1H), 1.87 – 1.79 (m, 3H), 1.78 – 1.73 (m, 1H), 1.71 (m, 2H), 1.46 – 1.29 (m, 3H).

¹³C NMR (100 MHz, CDCl₃): δ 212.2, 173.9, 170.2, 135.9, 128.8, 128.5, 128.3, 70.8, 66.9, 49.4, 48.5, 40.5, 37.9, 30.7, 29.0, 26.7, 25.8, 22.9, 21.3, 15.7.

IR (Neat Film, NaCl): 2928, 1781, 1375, 1246, 1173 cm^{-1}.

HRMS (MM: FD+): *m/z* calc'd for $C_{22}H_{26}O_5$ [M]$^+$: 370.1780, found 370.1774.

Optical Rotation: $[\alpha]_D^{21}$ –18.3 (c 0.18, CHCl$_3$).

Preparation of Additional Compounds
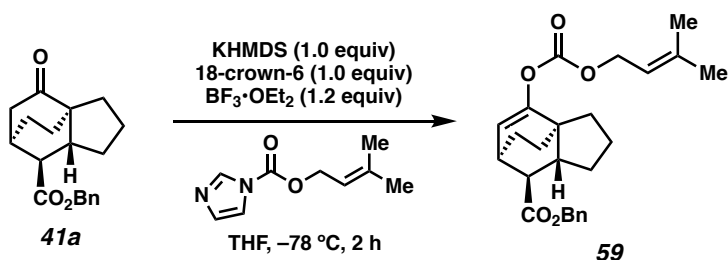
benzyl (3a*R*,6*R*,7*S*,7a*R*)-4-oxooctahydro-3a,6-ethanoindene-7-carboxylate (59)[42]

To a solution of KHMDS (40 mg, 0.20 mmol, 1.0 equiv) and 18-crown-6 (53 mg, 0.20 mmol, 1 equiv) in THF (2.0 mL) at –78 ºC was added a solution of **41a** (60 mg, 0.20 mmol, 1 equiv). Stirring was continued at –78 ºC for 30 minutes, then a pre-mixed solution of 3-methylbut-2-en-1-yl 1*H*-imidazole-1-carboxylate (43 mg, 0.24 mmol, 1.2 equiv) and boron trifluoride diethyl etherate (30 µL, 0.24 mmol, 1.2 equiv) in THF (1.2 mL) was added dropwise. After two additional hours of stirring at –78 ºC, EtOAc and saturated aqueous NH$_4$Cl were added. The layers were separated, and the aqueous layer was extracted twice with EtOAc. The combined organic layers were washed with brine, dried over Na$_2$SO$_4$, filtered, and solvent was removed in vacuo. The crude mixture was purified by silica gel flash column chromatography (0–40% EtOAc/hexanes) to afford enol carbonate **59** as a colorless oil (44 mg, 0.11 mmol, 55% yield).

^{1}H NMR (400 MHz, CDCl$_3$): δ 7.39 – 7.29 (m, 5H), 5.70 (d, *J* = 6.8 Hz, 1H), 5.42 – 5.36 (m, 1H), 5.09 (d, *J* = 3.6 Hz, 2H), 4.65 (d, *J* = 7.3 Hz, 2H), 3.08 – 2.96 (m, 1H), 2.25 (d, *J*

= 5.6 Hz, 1H), 2.07 – 1.97 (m, 2H), 1.91 – 1.79 (m, 3H), 1.77 (s, 3H), 1.73 (s, 3H), 1.63 –

1.54 (m, 2H), 1.52 – 1.38 (m, 3H), 1.35 – 1.28 (m, 1H).

^{13}C NMR (100 MHz, CDCl$_3$): δ 174.9, 155.6, 153.5, 140.6, 136.4, 128.7, 128.2, 128.0,

117.9, 112.8, 66.3, 65.3, 51.3, 48.1, 48.1, 35.5, 28.4, 28.4, 27.3, 25.9, 24.6, 22.8, 18.3.

IR (Neat Film, NaCl): 2953, 2870, 1754, 1735, 1241, 1226, 1150 cm^{-1}

HRMS (MM: FD+): *m/z* calc'd for C$_{25}$H$_{30}$O$_5$ [M]$^+$: 410.2093, found 410.2094.

SFC conditions: 20% IPA, 2.5 mL/min, Chiralpak IC column, λ = 210 nm, t$_R$ (min): minor

= 3.05, major = 3.40.

4.4.3 DETERMINATION OF ABSOLUTE AND RELATIVE

STEREOCHEMISTRY BY VCD SPECTROSCOPY

Experimental Protocol: A solution of the compound of interest (50 mg/mL) in CDCl$_3$ was

loaded into a front-loading SL-4 cell (International Crystal Laboratories) possessing BaF$_2$

windows and a 100 mm path length. Infrared (IR) and VCD spectra were acquired on a

BioTools ChiralIR-2X VCD spectrometer as a set of 24 one-hour blocks (24 blocks, 3120

scans per block) in dual PEM mode. A 15-minute acquisition of neat (+)-α-pinene control

yielded a VCD spectrum in agreement with literature spectra. IR and VCD spectra were

background corrected using a 30-minute block IR acquisition of the empty instrument

chamber under gentle N$_2$ purge, and were solvent corrected using a 16-hour (16 blocks,

3120 scans per block) IR/VCD acquisition of CDCl$_3$ in the same 100 μm BaF2 cell. The

reported spectra represent the result of block averaging.

Both enantiomers of compounds **41a**, **41q**, and **41q'** were prepared from the *(S)*

and *(R)* enantiomers of the *t*-BuPHOX ligand. Data were collected for both enantiomers of

compounds at identical concentration and the final reported VCD spectra are the half-difference of the spectra of the compounds derived from the *(S)* minus *(R)* enantiomer of ligand. Due to limited sample size, spectra of cycloadducts **41k'** and **41k''** were collected at concentrations of 11.7 and 9.3 mg/mL, respectively.

Computational Protocol: An arbitrarily chosen enantiomer of the compound of interest was subjected to an exhaustive initial molecular mechanics-based conformational search (OPLS_2005 force field, $CHCl_3$ solvent, 10.0 kcal/mol cutoff, "Enhanced" torsional sampling) as implemented in MacroModel program. [50] The resulting ensemble of conformers was subsequently optimized using the B3PW91 functional, cc-pVTZ(-f) basis, and implicit PBF solvation model for chloroform using the Jaguar program.[51] Harmonic frequencies computed at the B3PW91/cc-pVTZ(-f)/PBF(chloroform) level were scaled by 0.98. The resultant structurally unique conformers possessing all positive Hessian eigenvalues were Boltzmann weighted by relative free energy at 298.15 K. The predicted IR and VCD frequencies and intensities of the retained conformers were convolved using Lorentzian line shapes ($\gamma = 4$ cm^{-1}) and summed using the respective Boltzmann weights to yield the final predicted IR and VCD spectra. The predicted VCD of the opposite enantiomer was generated by inversion of sign.

VCD Analysis for diastereomers 41a, 41p, and 41p'

Figure 3.9. *Three diastereomers* ***41a****,* ***41q****, and* ***41q'*** *to be compared to spectra computed from all eight possible stereoisomers.*
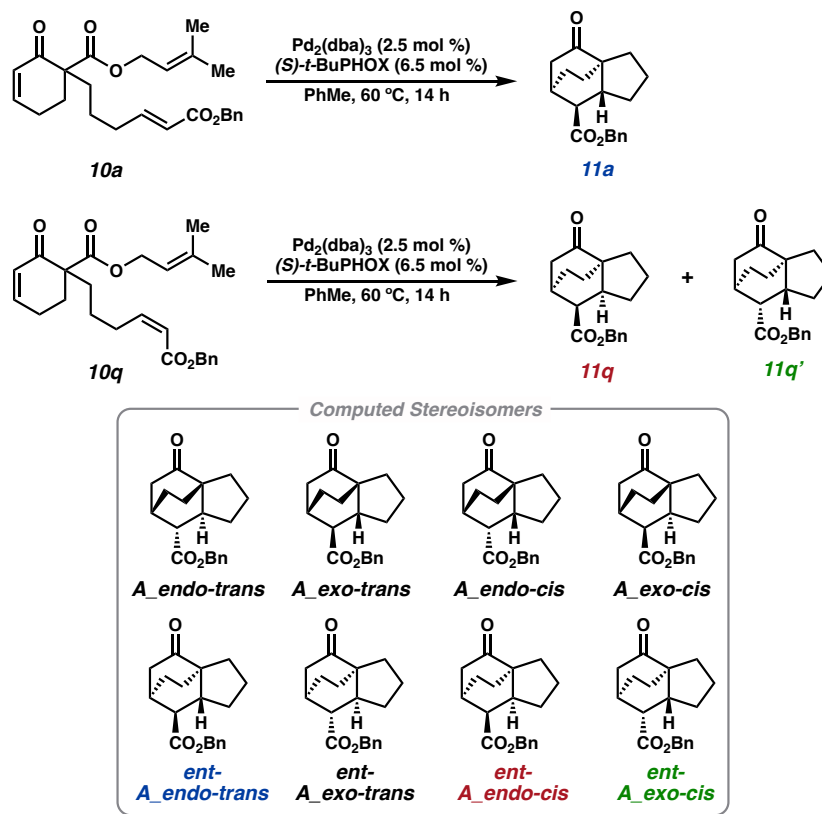
Figure 3.10. *Comparison of experimental VCD and IR spectra for product **41a** to computed spectra for **A_endo-trans**.[a]*
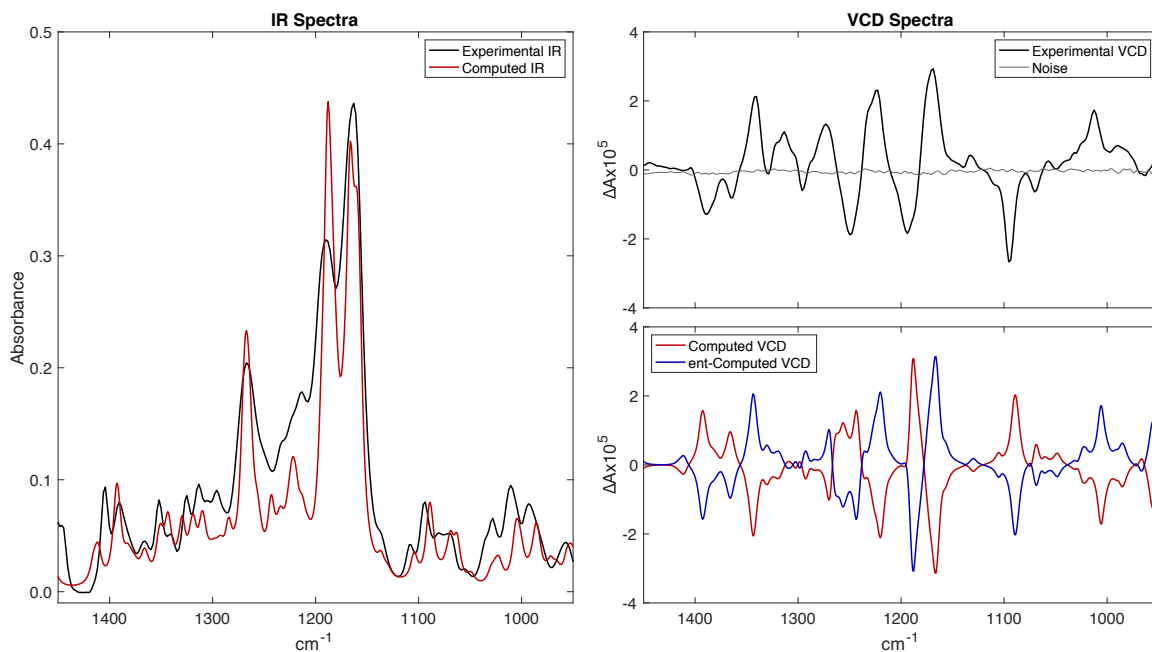
[a] Experimental IR spectrum in good agreement with computed spectrum. Experimental VCD spectrum for **41a** is in excellent agreement with computed spectrum for ***ent*-A_endo-trans**.

Figure 3.11. *Overlayed experimental and calculated VCD spectra for **41a** – assigned as **ent-A_endo-trans**.*
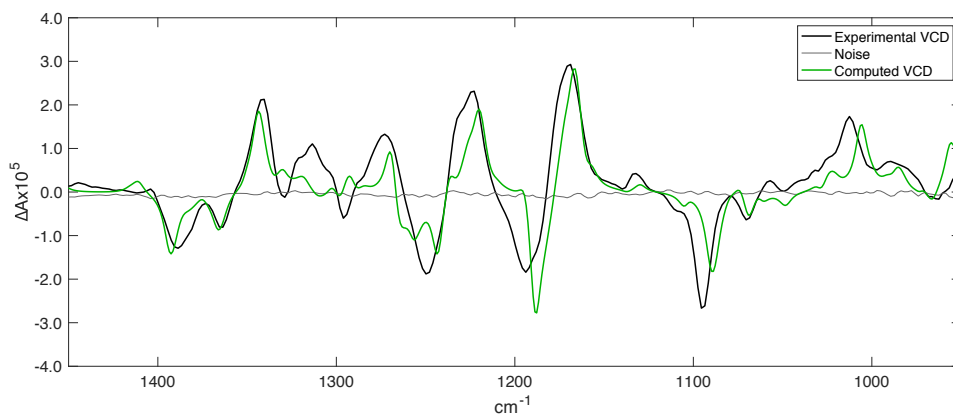
Figure 3.12. *Comparison of experimental VCD and IR spectra for product **41a** to computed spectra for **A_exo-trans**.[a]*
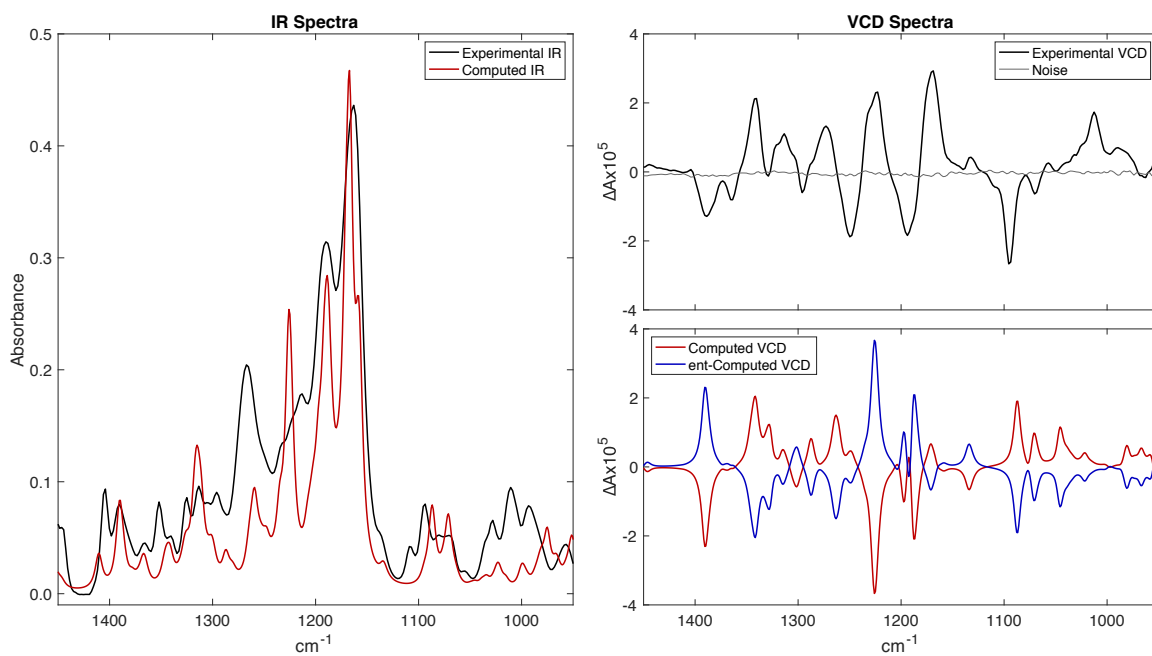
[a] A shift of –3 cm^{-1} along x-axis applied to computed spectra in fitting. Experimental data from **41a** do not match computed data of **A_exo-trans**.

Figure 3.13. *Comparison of experimental VCD and IR spectra for product **41a** to computed spectra for **A_endo-cis**.*[a]
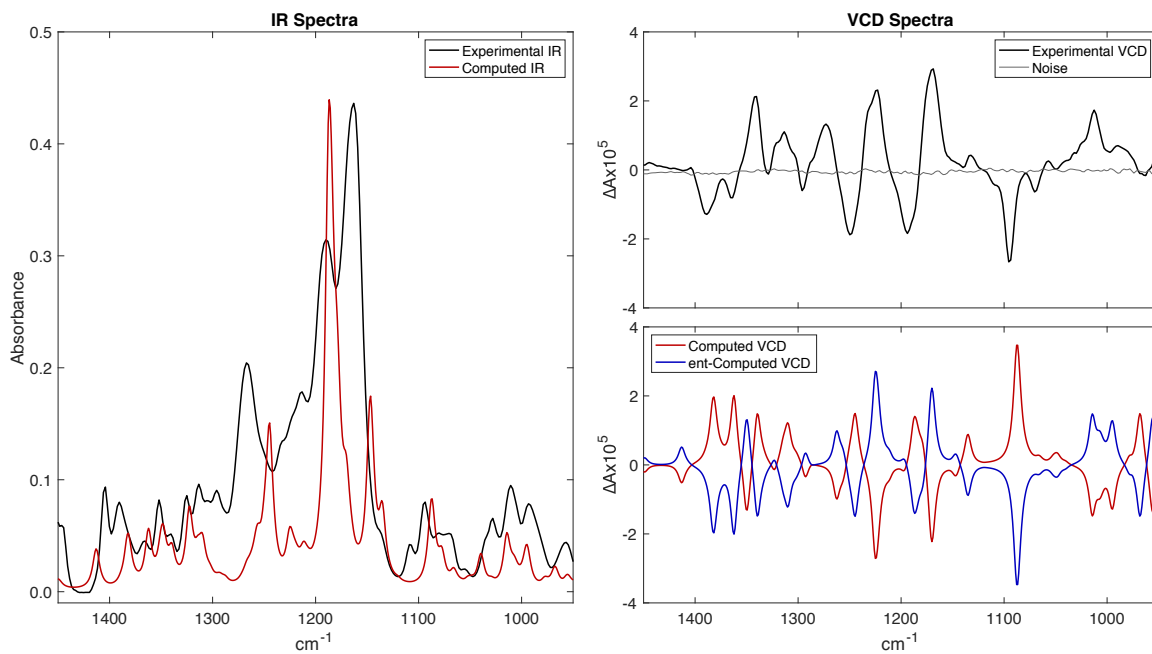
[a] Experimental data from **41a** do not match computed data of **A_endo-cis**.

***Figure* 3.14**. *Comparison of experimental VCD and IR spectra for product **41a** to computed spectra for **A_exo-cis**.*[a]
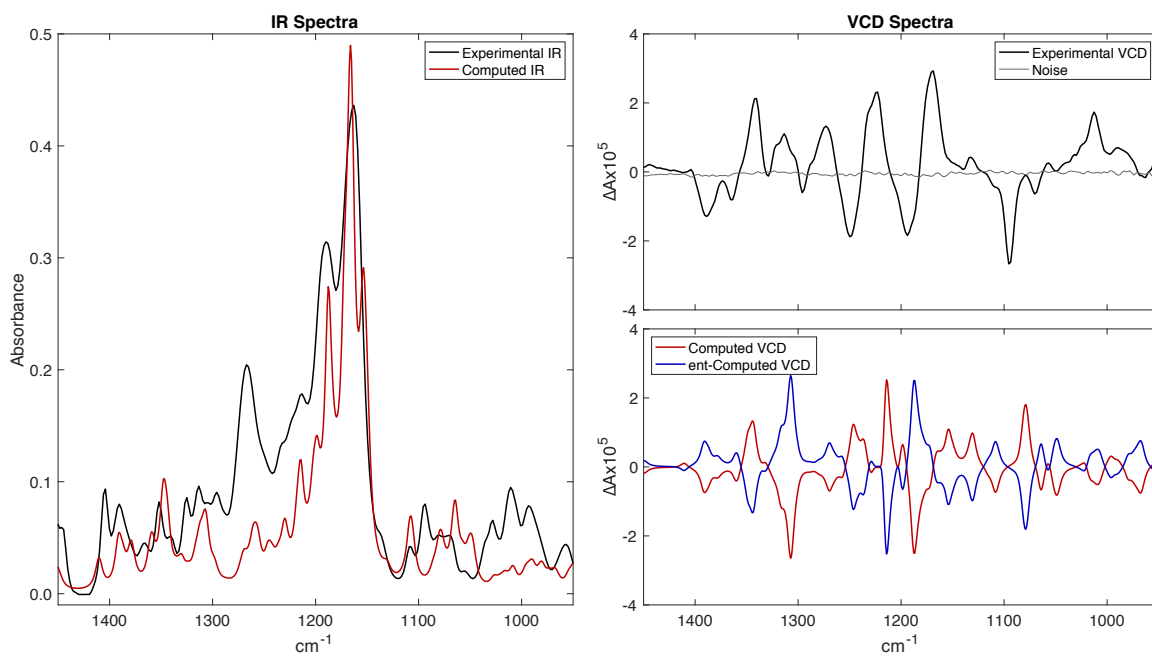
[a] A shift of –3 cm-1 along x-axis applied to computed spectra in fitting. Experimental data from **41a** do not match computed data of **A_exo-cis**.

Figure 3.15*. Comparison of experimental VCD and IR spectra for product **41q** to computed spectra for **A_endo-trans**.*[a]
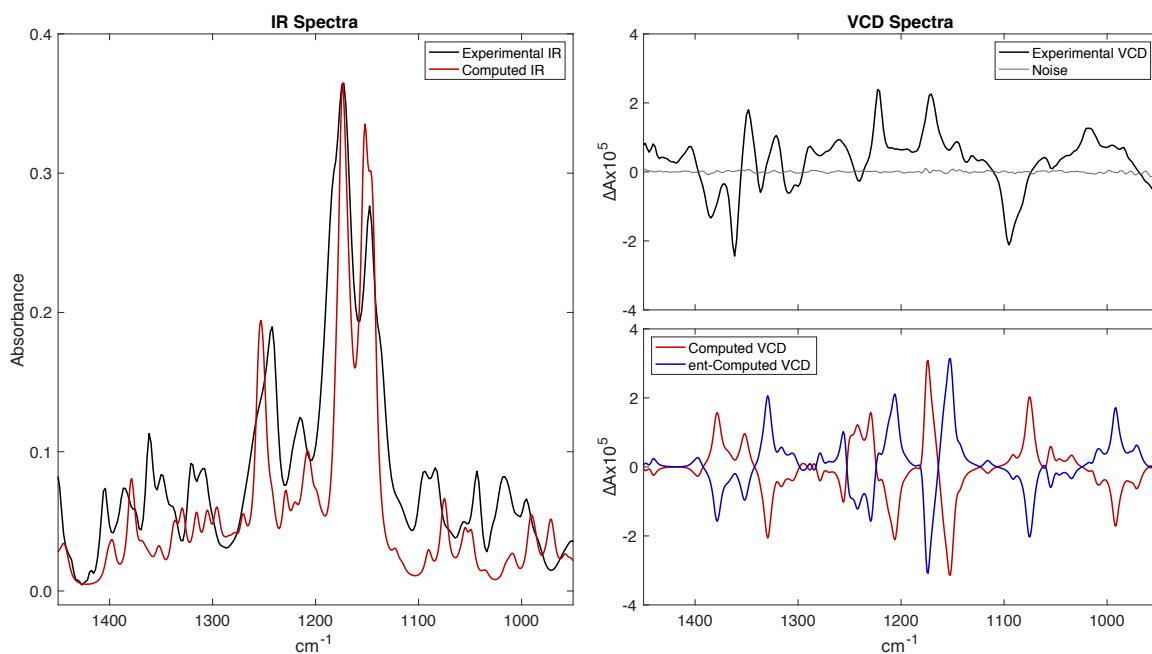
[a] A shift of +14 cm^{-1} along x-axis applied to computed spectra in fitting. The IR spectrum of **41q** contains similar features to the calculated spectrum for **A_endo-trans**; however, the VCD spectrum displays large discrepancies at 1174, 1152, 1330, 1076, and 992 cm^{-1}. **41q** is <u>not</u> assigned as **A_endo-trans**.

Figure 3.16. *Comparison of experimental VCD and IR spectra for product **41q** to computed spectra for **A_exo-trans**.*
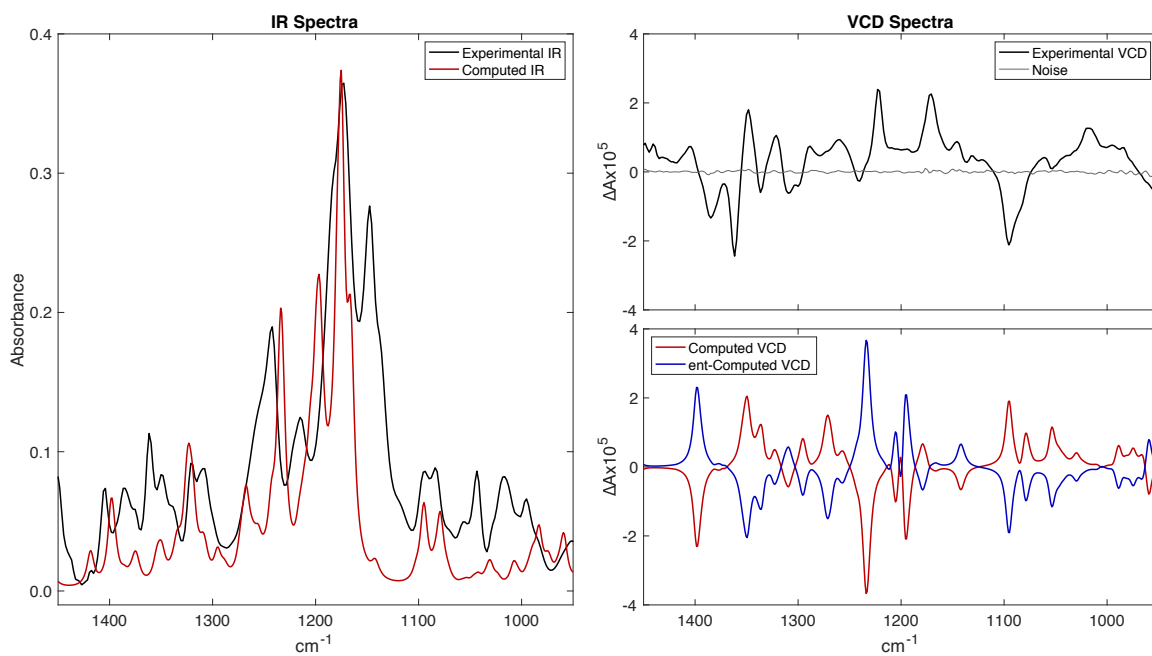
[a] Experimental data from **41q** do not match computed data of **A_exo-trans**.

Figure 3.17. *Comparison of experimental VCD and IR spectra for product **41q** to computed spectra for **A_endo-cis**.*
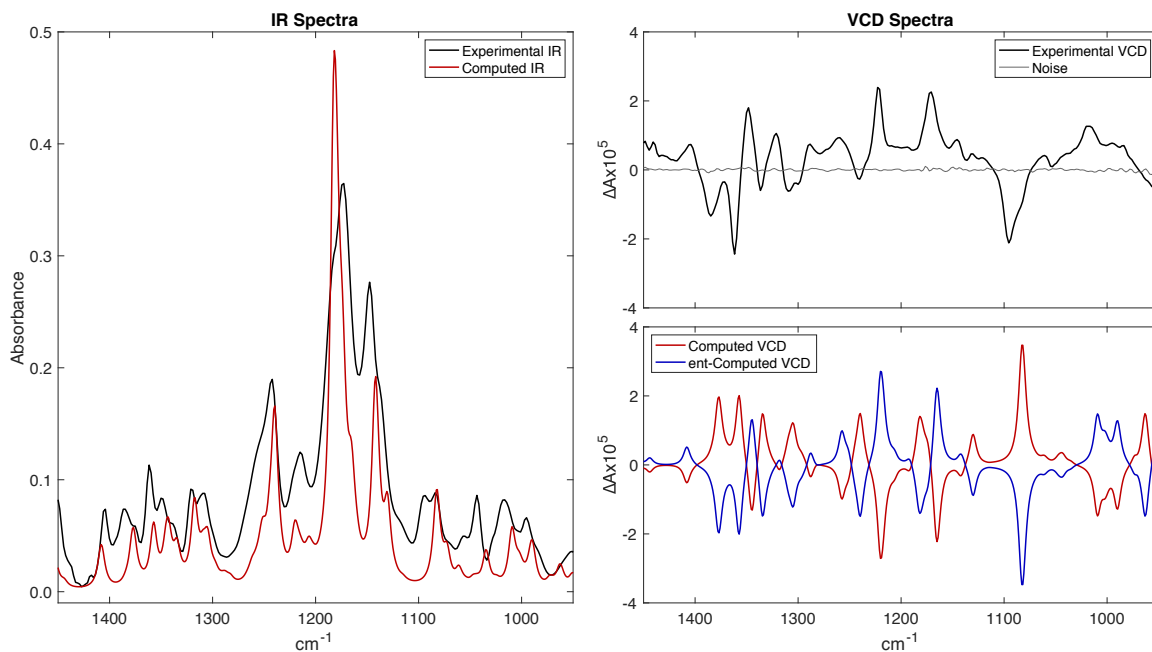
[a] A shift of +5 cm^{-1} along x-axis applied to computed spectra in fitting. The IR spectrum of **41q** is in good agreement with that of the computed IR spectrum of **A_endo-cis**. Experimental VCD spectrum for **41q** is in excellent agreement with computed spectrum for ***ent-*A_endo-cis**.

Figure 3.18. *Overlayed experimental and calculated VCD spectra for **41q** – assigned as **ent-A_endo-cis**.*
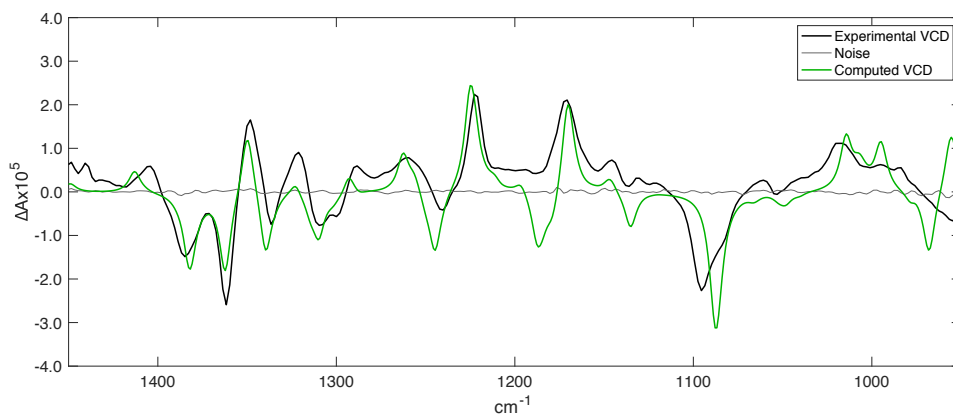
Figure 3.19. *Comparison of experimental VCD and IR spectra for product **41q** to computed spectra for **A_exo-cis**.[a]*
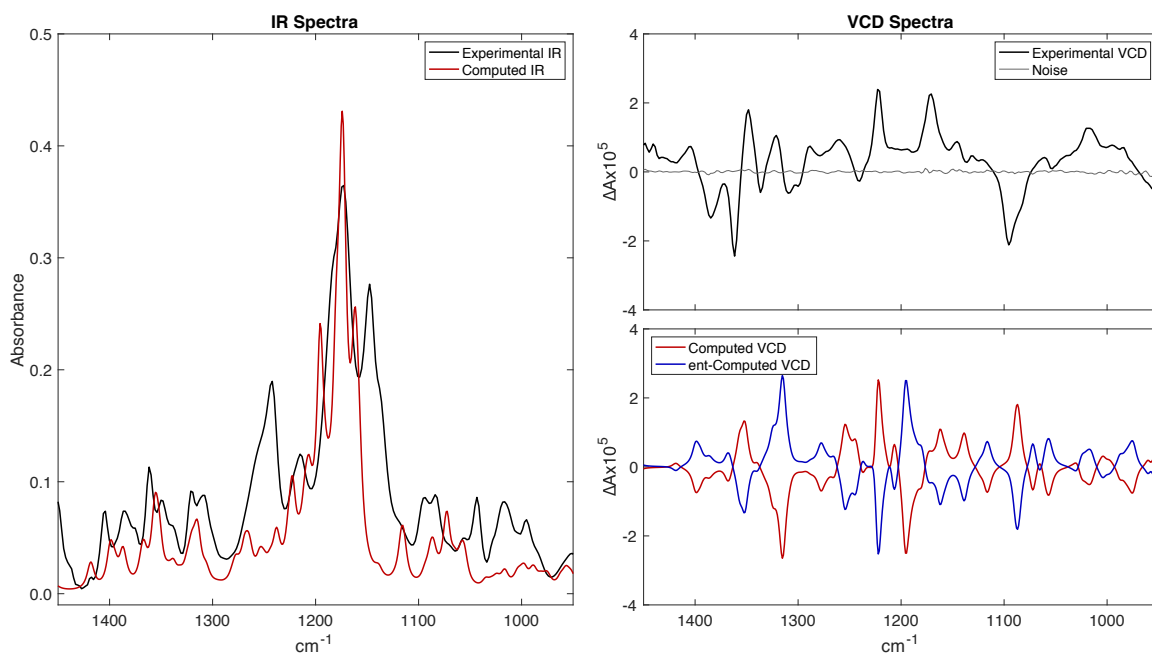
[a] Experimental data from **41q** do not match computed data of **A_exo-cis**.

Figure 3.20. *Comparison of experimental VCD and IR spectra for product **41q′** to computed spectra for **A_endo-trans**.*[a]
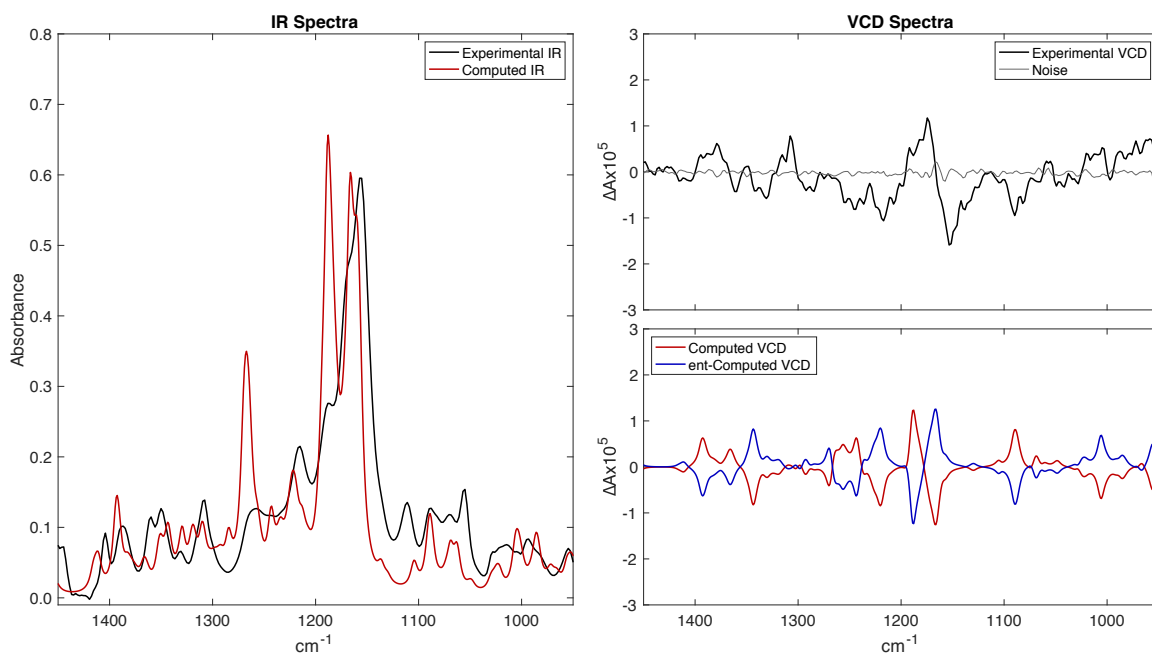
[a] The VCD spectrum was baseline-corrected with a shift of +7 cm^{-1} along y-axis. Experimental data from **41q′** do not match computed data of **A_endo-trans**.

Figure 3.21. *Comparison of experimental VCD and IR spectra for product **41q′** to computed spectra for **A_exo-trans**.*[a]
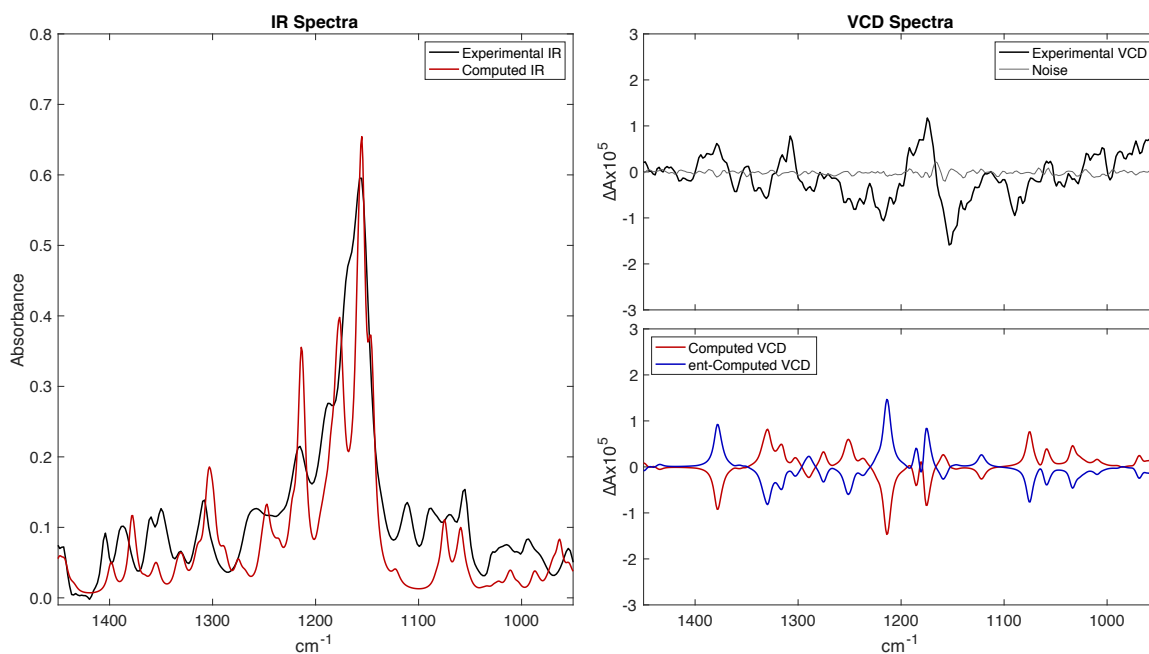
[a] The VCD spectrum of **41q′** was baseline-corrected with a shift of +7 cm⁻¹ along y-axis. A shift of -15 cm⁻¹ along x-axis applied to computed spectra in fitting. Experimental data from **41q′** do not match computed data of **A_exo-trans**.

Figure 3.22. *Comparison of experimental VCD and IR spectra for product **41q'** to computed spectra for **A_endo-cis**.[a]*
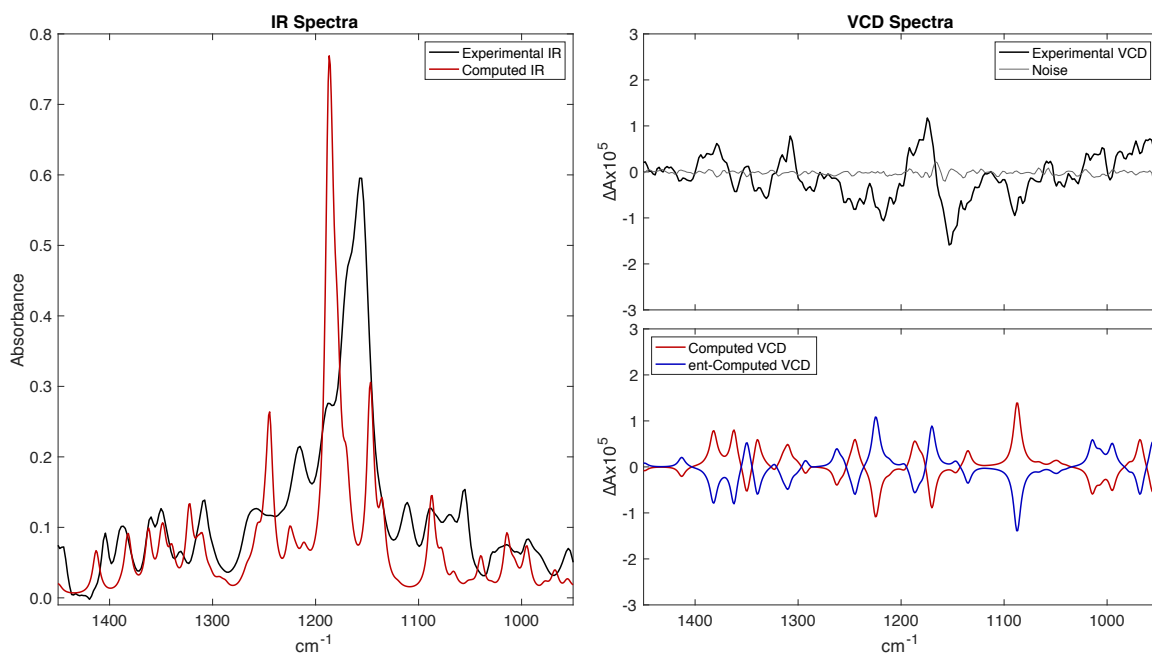
[a] The VCD spectrum of **41q'** was baseline-corrected with a shift of +7 cm^{-1} along y-axis. Experimental data from **41q'** do not match computed data of **A_endo-cis**.

Figure 3.23. *Comparison of experimental VCD and IR spectra for product* **41q′** *to computed spectra for* **A_exo-cis**.[a]
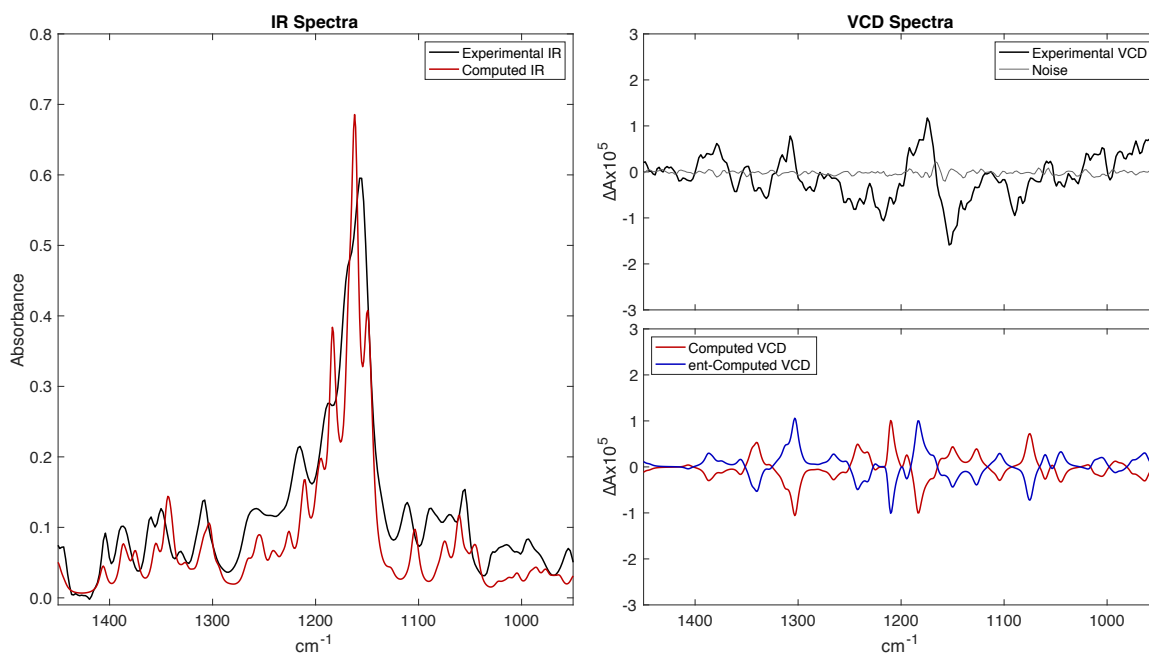
[a] The VCD spectrum of **41q′** was baseline-corrected with a shift of +7 cm^{-1} along y-axis. A shift of +7 cm^{-1} along x-axis applied to computed spectra in fitting. Experimental VCD spectrum for **41q′** is in good agreement with computed spectrum for **ent-A_exo-cis**.

Figure 3.24. *Overlayed experimental and calculated VCD spectra for* **41q′** *– assigned as* **ent-A_exo-cis**.
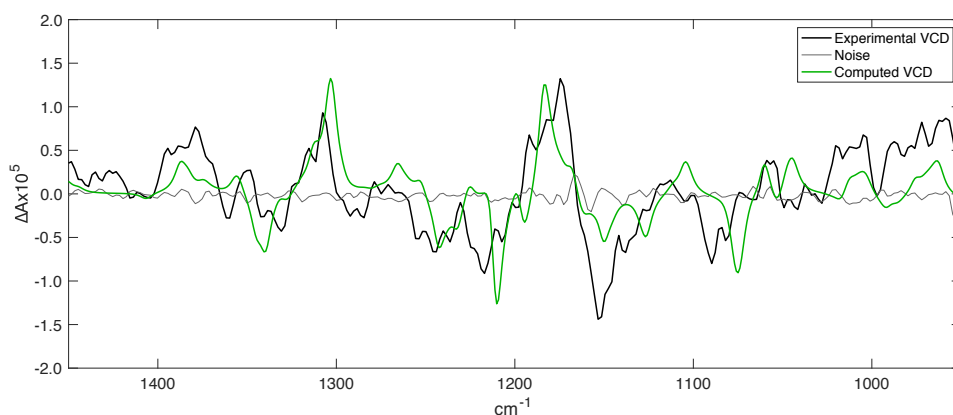
Figure 3.25. *Three diastereomers **41k, 41k', and 41k''** to be compared to spectra computed from all eight possible stereoisomers.*
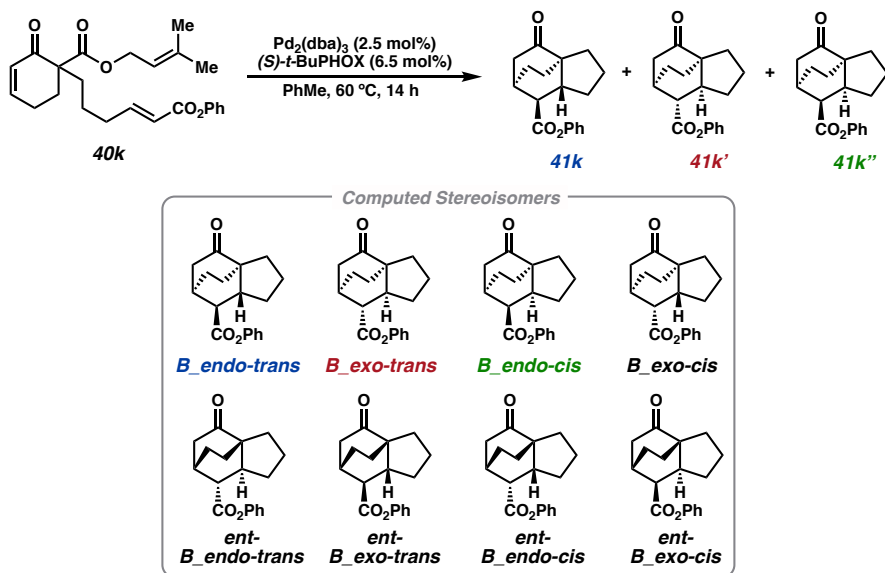
Figure 3.26. *Experimental VCD and IR spectra for product* **41k** *compared to computed spectra for* **B_endo-trans**.[a]
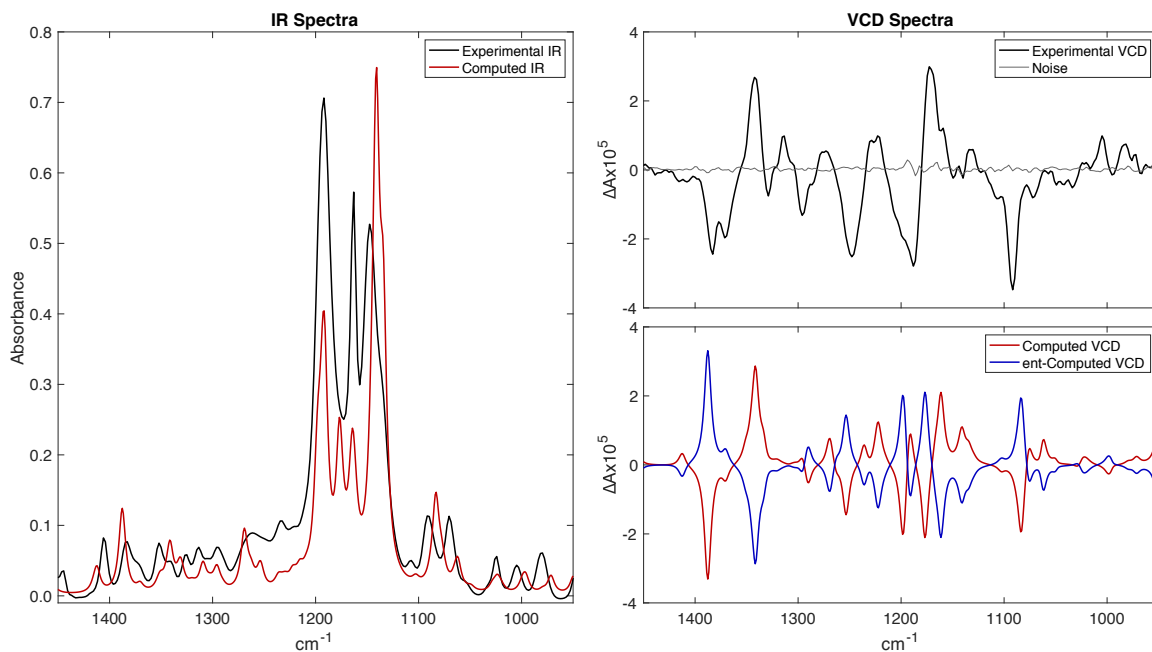
[a] Experimental IR spectrum in good agreement with computed spectrum. Experimental VCD spectrum for **41k** is in excellent agreement with computed spectrum for **B_endo-trans**.

Figure 3.27. *Overlayed experimental and calculated VCD spectra for* **41k** *– assigned as* **B_endo-trans**.
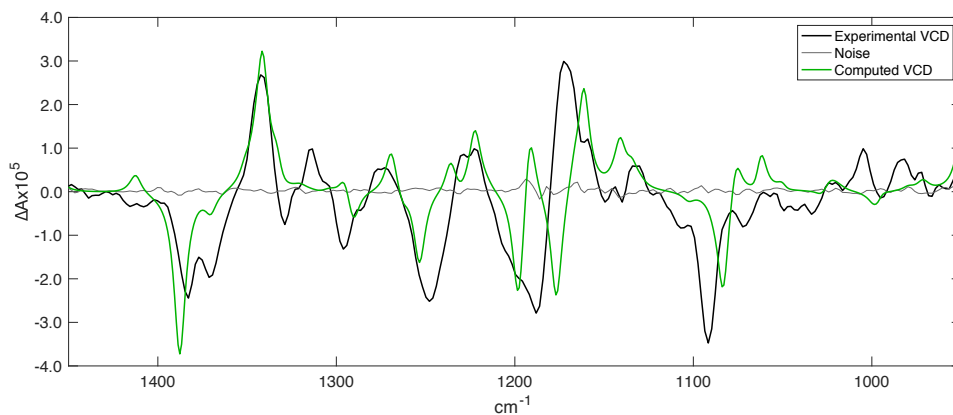
Figure 3.28. *Experimental VCD and IR spectra for product* ***41k*** *compared to computed spectra for* ***B_exo-trans***.[a]
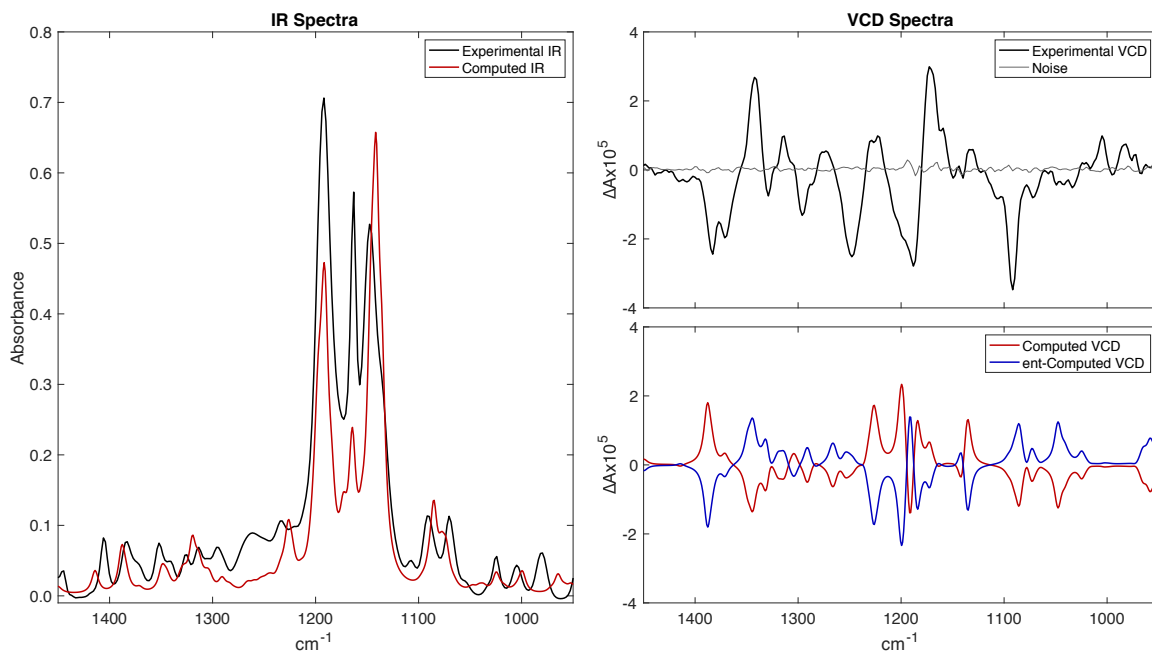
[a] Experimental IR spectrum in good agreement with computed spectrum. However, VCD spectrum contain key sign mismatches in regions around 1400 and 1100 cm^{-1}. Hence, **41k** is not assigned as **B_exo-trans**.

Figure 3.29. *Experimental VCD and IR spectra for product* ***41k*** *compared to computed spectra for* ***B_endo-cis***.[a]
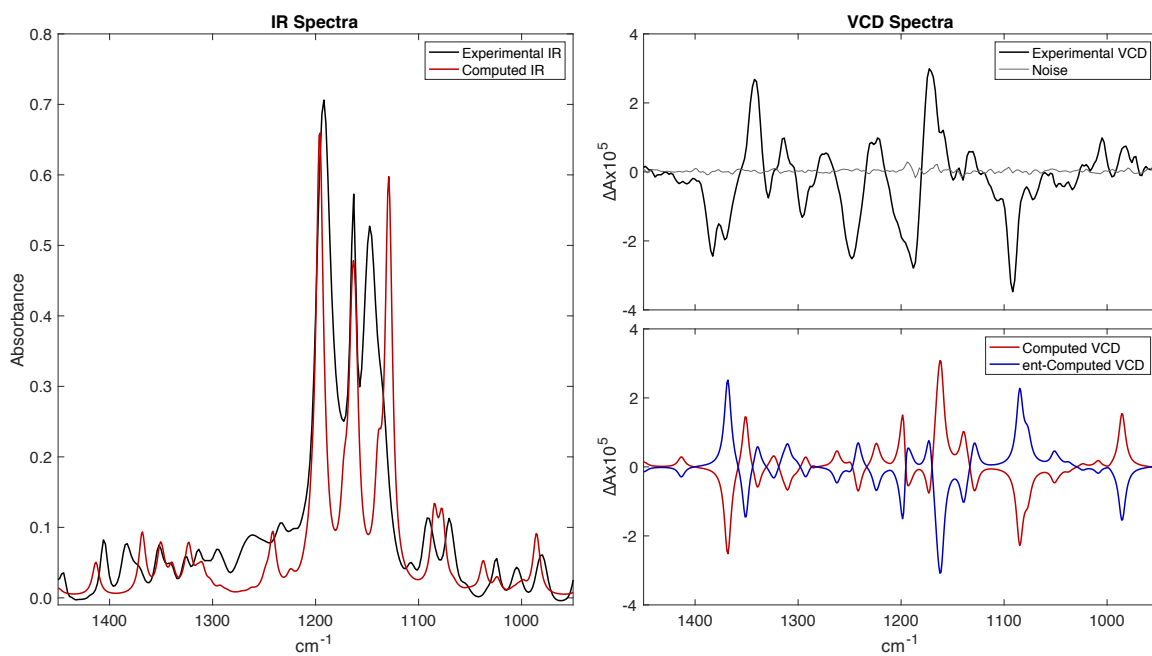
[a] Experimental data do not match computed data and **41k** is not assigned as **B_endo-cis**.

***Figure 3.30**. Experimental VCD and IR spectra for product **41k** compared to computed spectra for **B_exo-cis**.[a]*
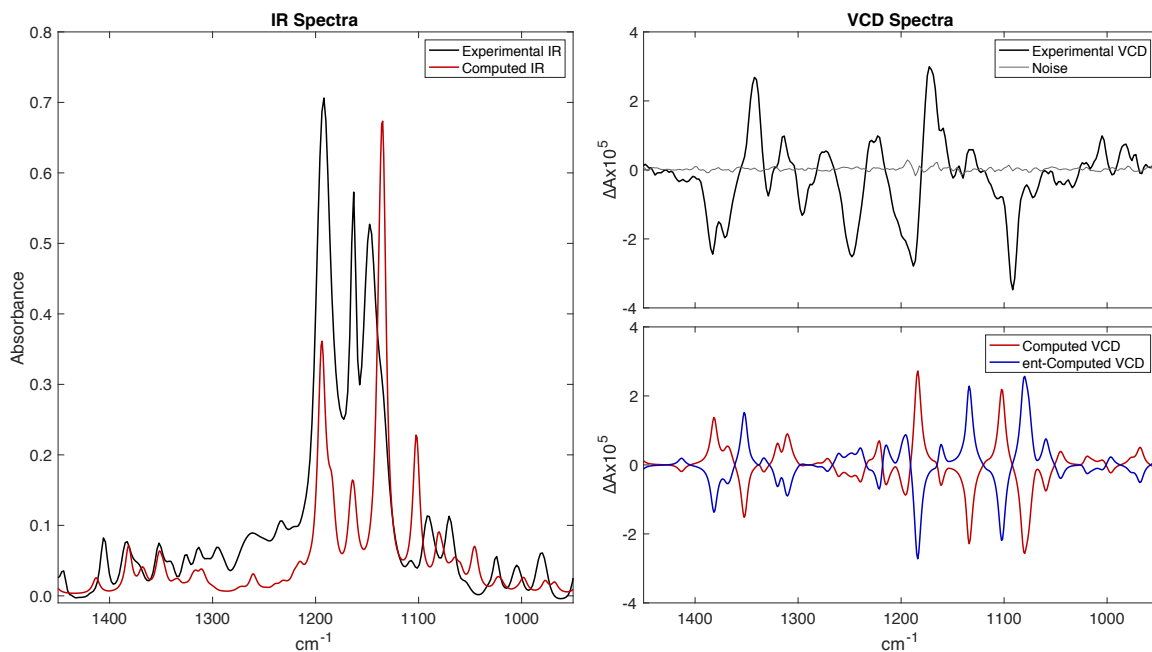
[a] Experimental data do not match computed data and **41k** is not assigned as **B_exo-cis**.

Due to limited sample size (< 3 mg), useful VCD spectra of **41k'** were unable to be obtained. Enantiomeric series was assigned by analogy to the **41a**, **41q** and **41q'** series. The 1000–1500 cm⁻¹ region of the IR spectra are still analyzed to support relative stereochemical assignments made by 2D NMR.

Figure 3.31. *Experimental IR spectrum for product **41k'** compared to computed spectra for **B_endo-trans** (top left), **B_exo-trans** (top right), **B_endo-cis** (bottom left), **B_exo-cis** (bottom right).[a]*
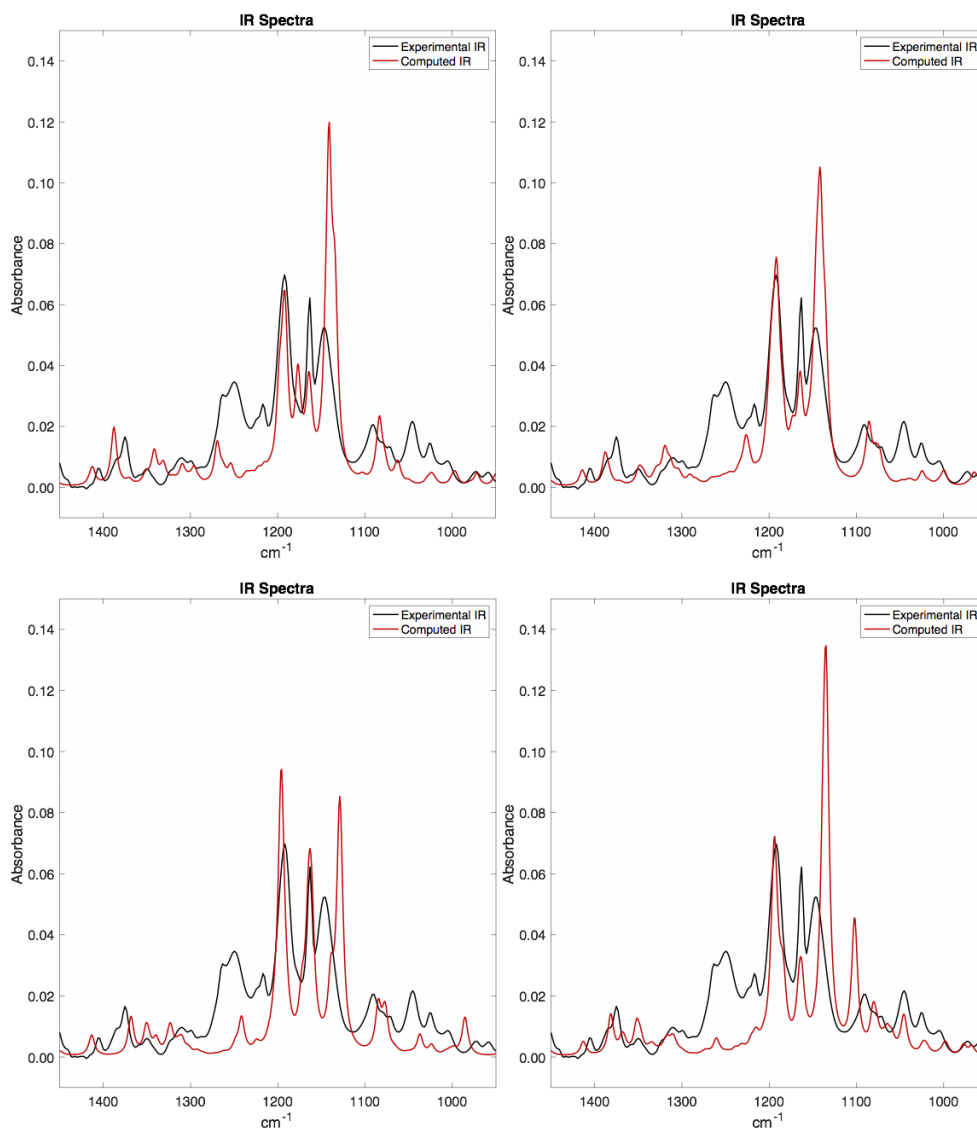
[a] The trans relationship is supported, in accord with 2D NMR data. In contrast to endo-cis and exo-cis, the computed IR spectra for both endo-trans and exo-trans are similar and do not offer key features for distinguishing the two. Given the trans stereochemistry, with **41k** known as **B_endo-trans**, **41k'** is assigned as **B_exo-trans** with absolute stereochemistry assigned based on analogy to **41q'**.

Figure 3.32. *Experimental VCD and IR spectra for product **41k″** compared to computed spectra for **B_endo-trans**.[a]*
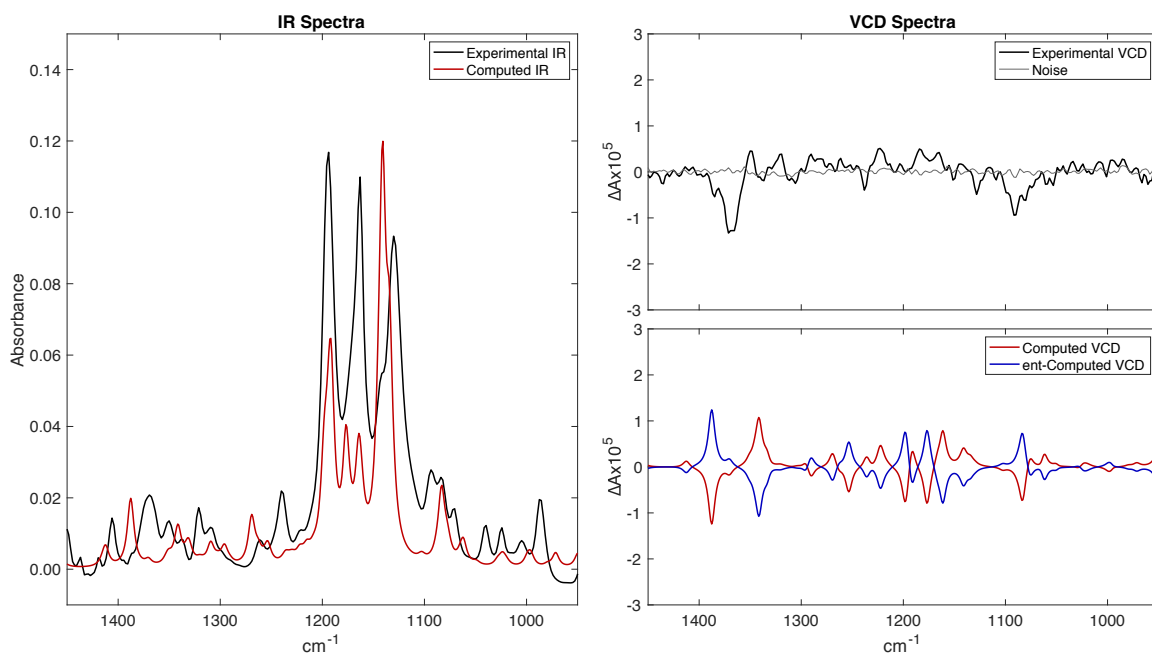
[a] Experimental data do not match computed data and **41k″** is not assigned as **B_endo-trans**.

Figure 3.33. *Experimental VCD and IR spectra for product **41k″** compared to computed spectra for **B_exo-trans**.[a]*
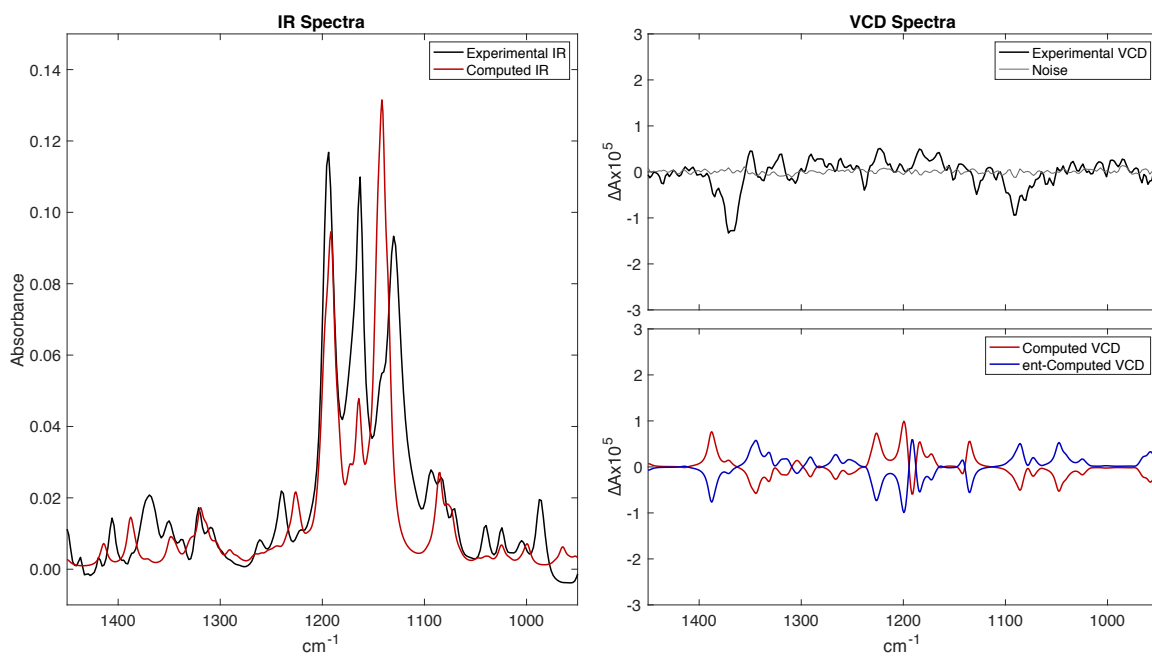
[a] Experimental data do not match computed data and **41k″** is not assigned as **B_exo-trans**.

Figure 3.34. *Experimental VCD and IR spectra for product* **41k″** *compared to computed spectra for* **B_endo-cis**.[a]
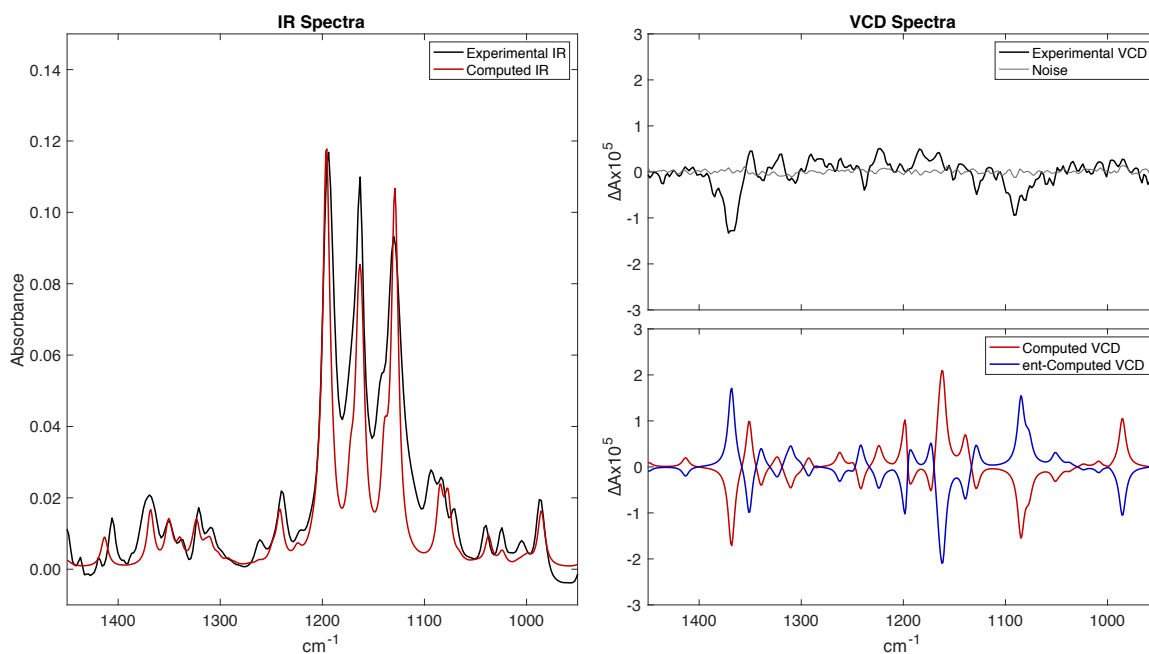
[a] Experimental IR spectrum is in agreement with the computed spectrum of **B_endo-cis**. Assignment of absolute stereochemistry is based the on the sign of the three most intense peaks in VCD spectrum, 1368, 1350, and 1085 cm^{-1}. These match **B_endo-cis**, the same enantiomeric series as **41k**.

Figure 3.35. *Overlayed experimental and calculated VCD spectra for* **41k″** *– assigned as* **B_endo-cis**.
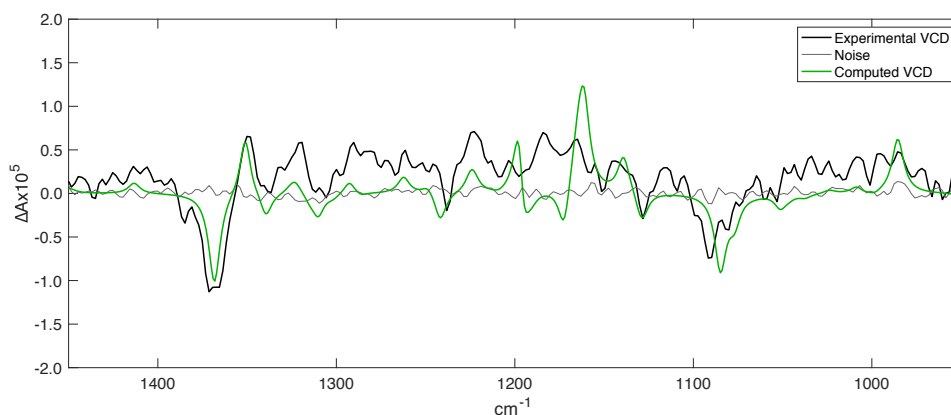
Figure 3.36. *Experimental VCD and IR spectra for product **41k″** compared to computed spectra for **B_exo-cis**.[a]*
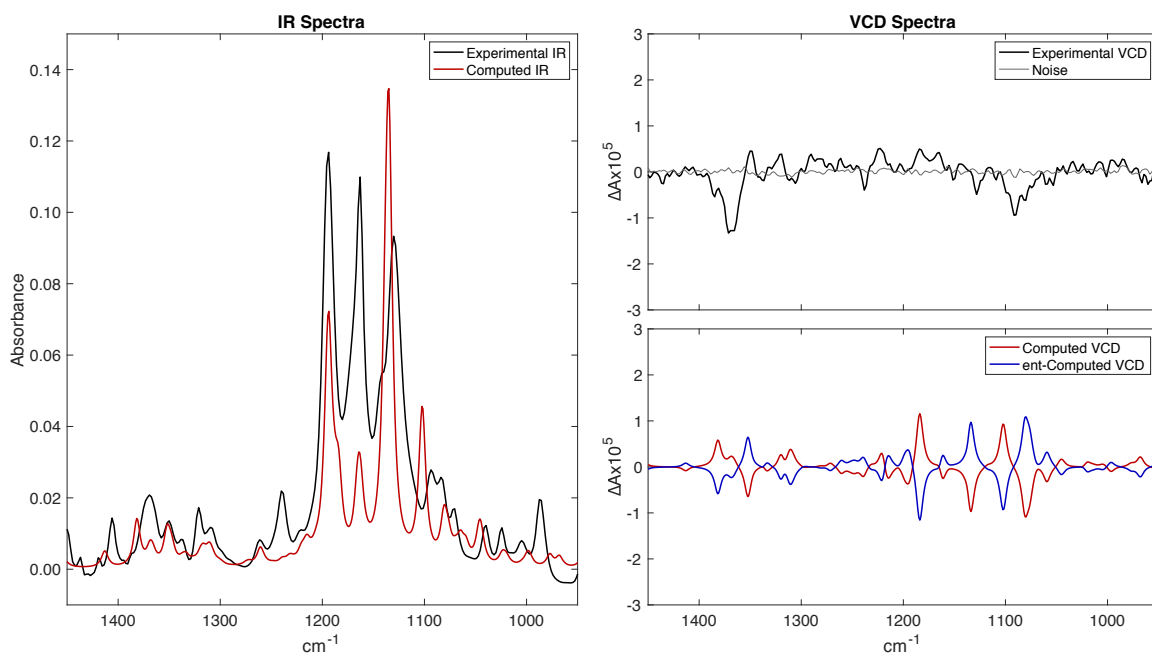
[a] Experimental data do not match computed data and **41k″** is not assigned as **B_exo-cis**.

3.4.4 2D NMR ANALYSIS OF SELECT COMPOUNDS

***Figure* 3.37.** *^{1}H-^{1}H COSY NMR spectrum of **41a** (400 MHz, CDCl$_3$).*
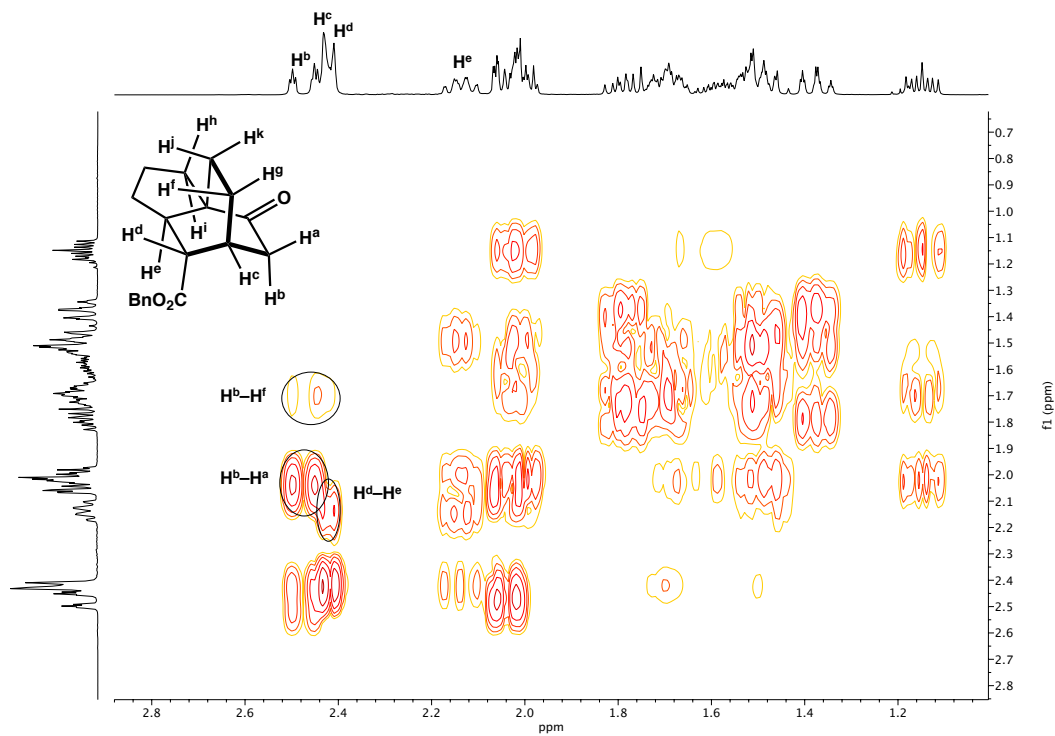
Figure 3.38. ^1H-^{13}C HSQC NMR spectrum of **41a** (400 MHz, CDCl$_3$).
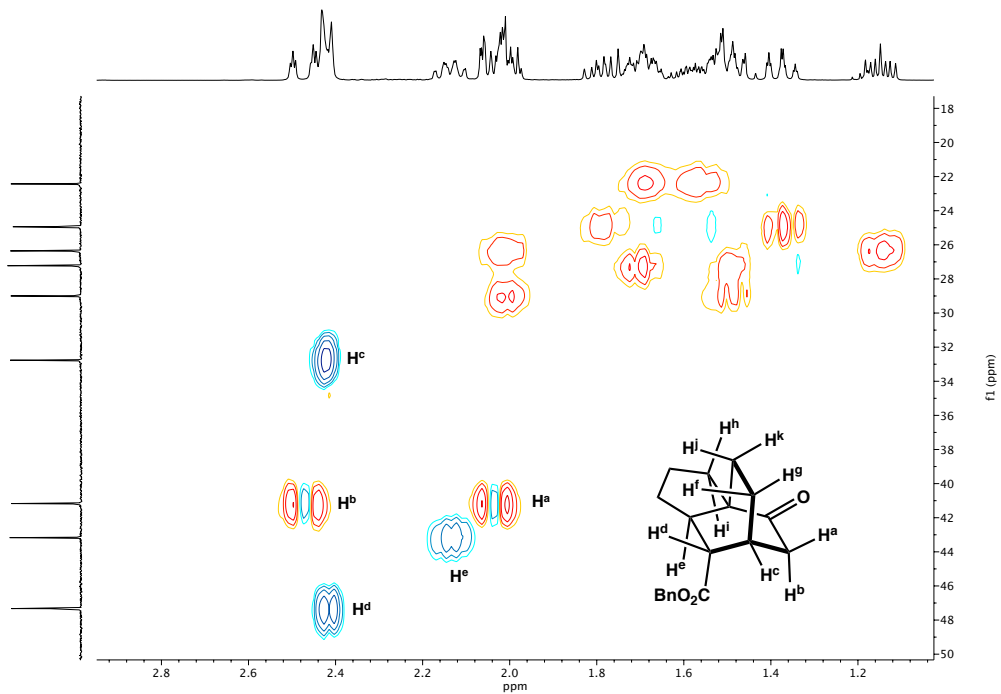
Figure 3.39. ^1H-^1H NOESY NMR spectrum of **41a** (400 MHz, CDCl$_3$).
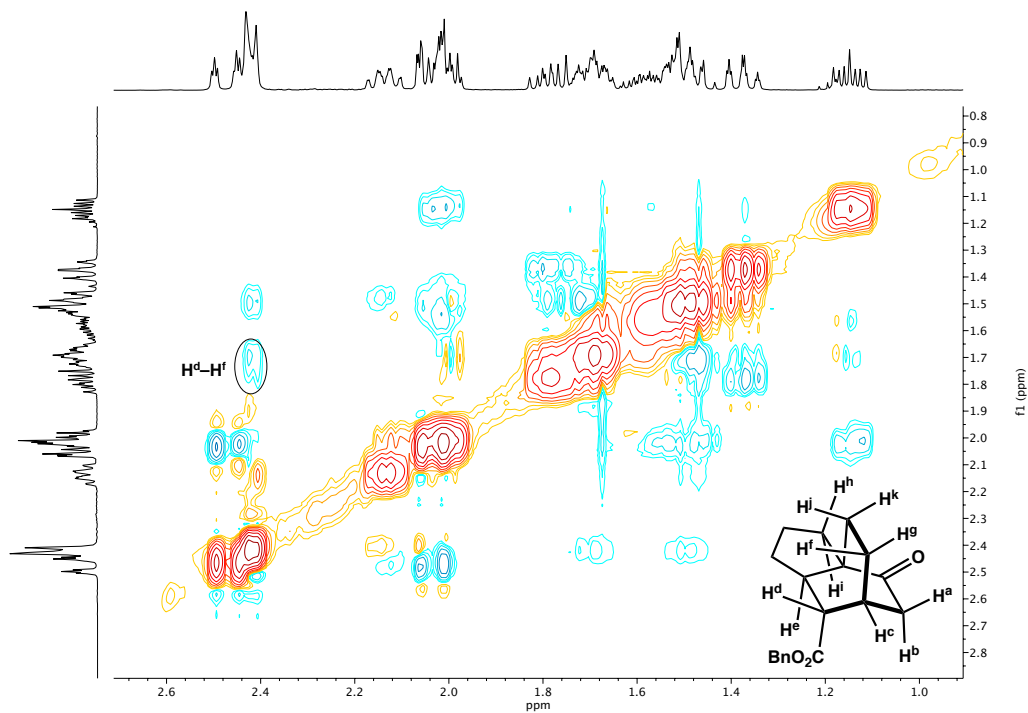
Figure 3.40. ^1H-^1H COSY NMR spectrum of **41p** (400 MHz, CDCl$_3$).
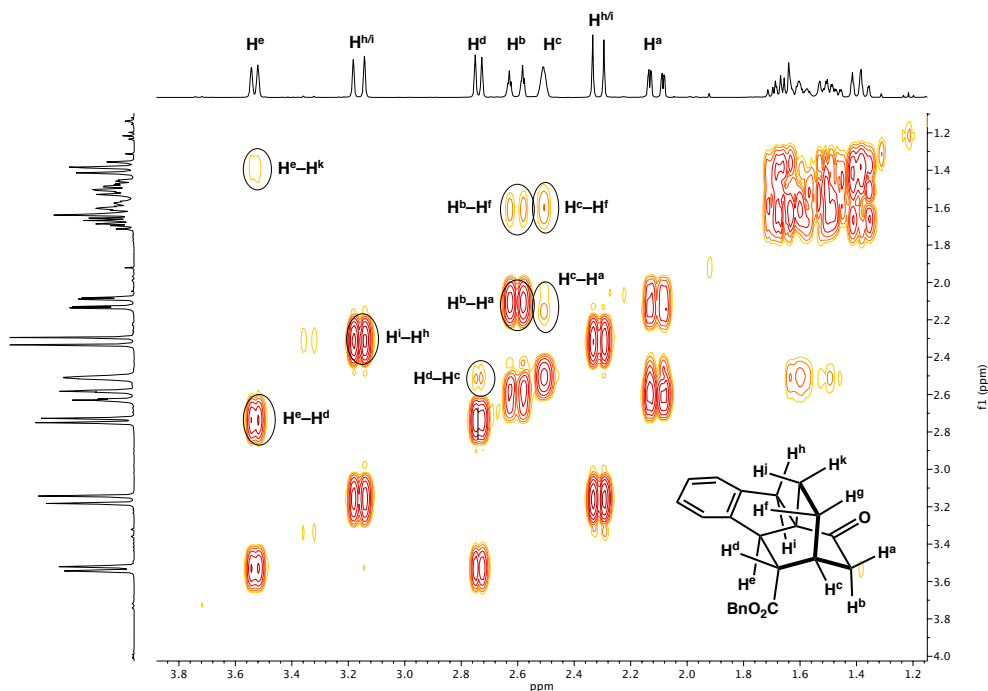
Figure 3.41. ^1H-^{13}C HSQC NMR spectrum of **41p** (400 MHz, CDCl$_3$).
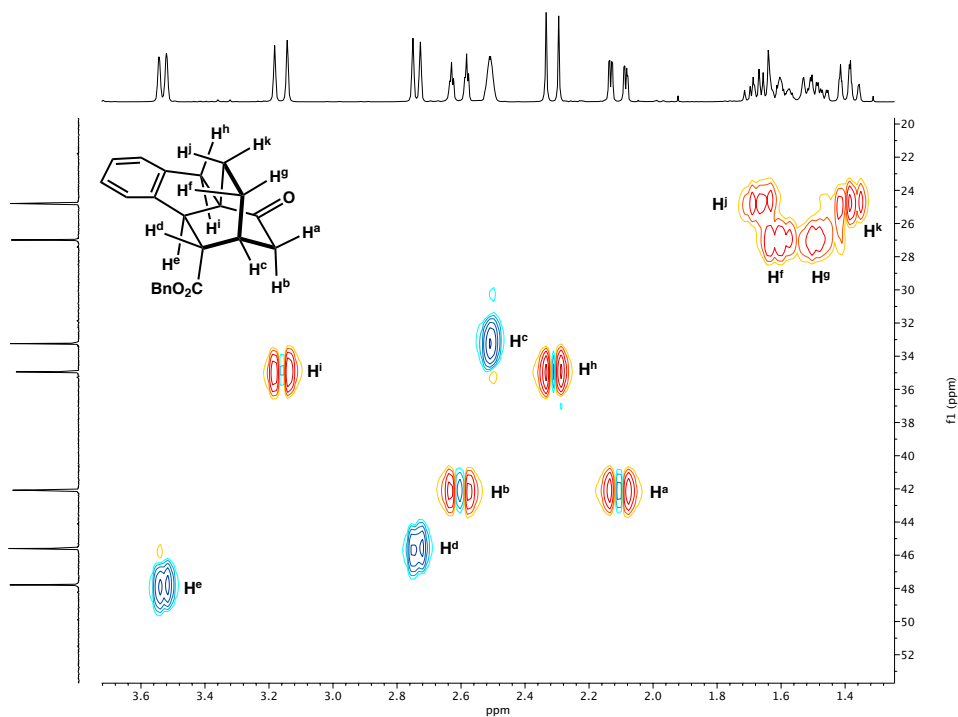
Figure 3.42. ^1H-^1H NOESY NMR spectrum of **41p** *(400 MHz, CDCl$_3$).*
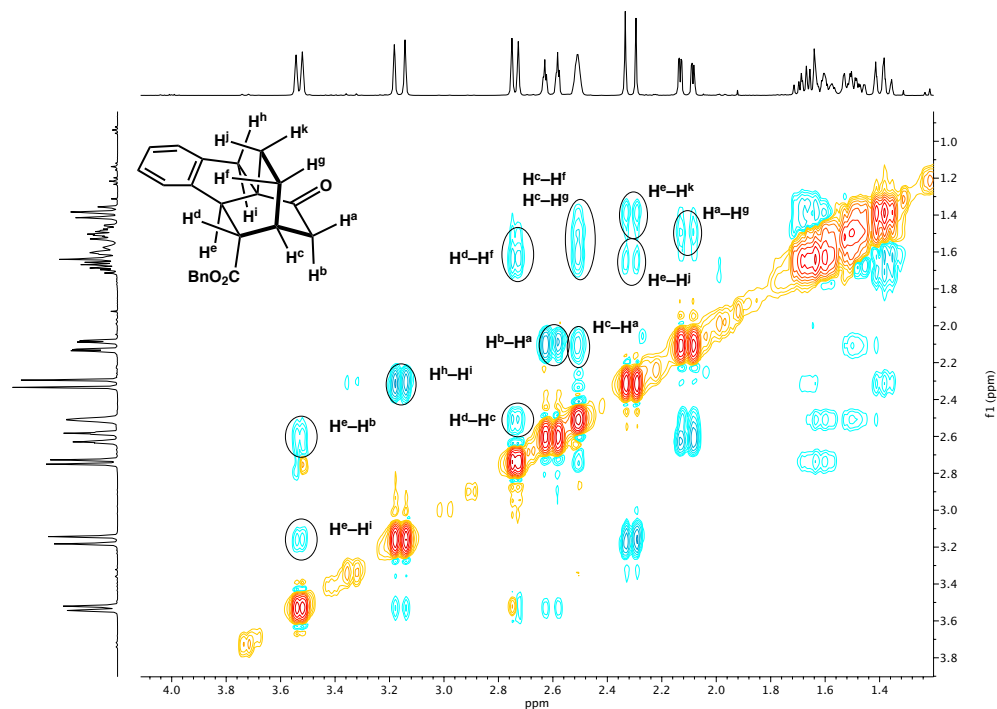
Figure 3.43. ^1H-^1H COSY NMR spectrum of **41q** *(400 MHz, CDCl$_3$).*
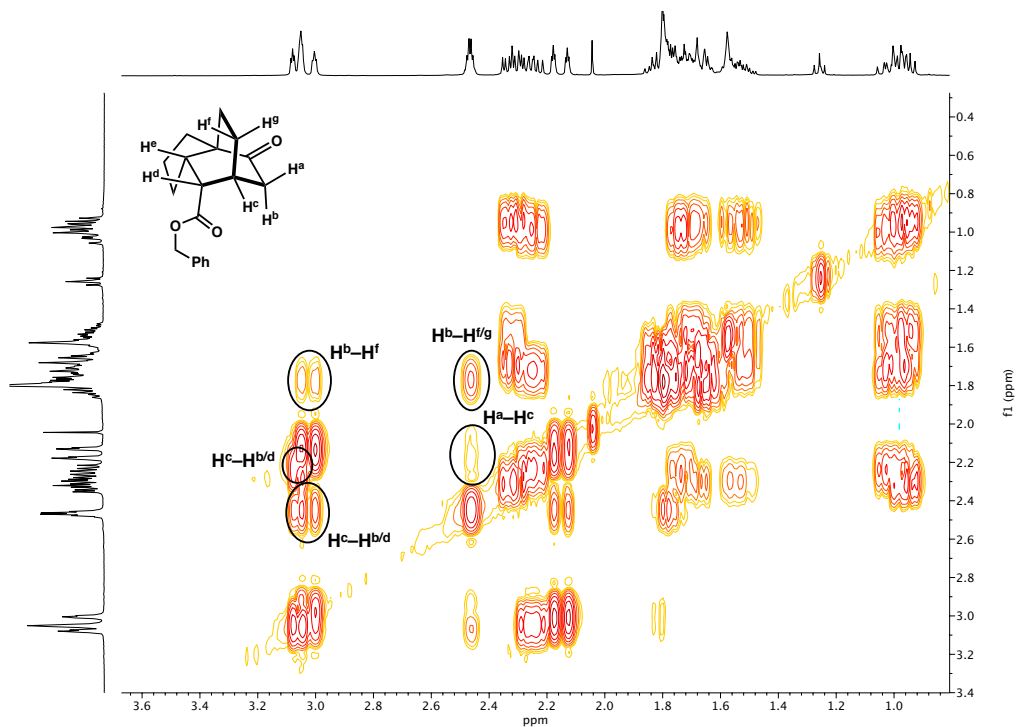
Figure 3.44. *¹H-¹³C HSQC NMR spectrum of* **41q** *(400 MHz, CDCl₃).*
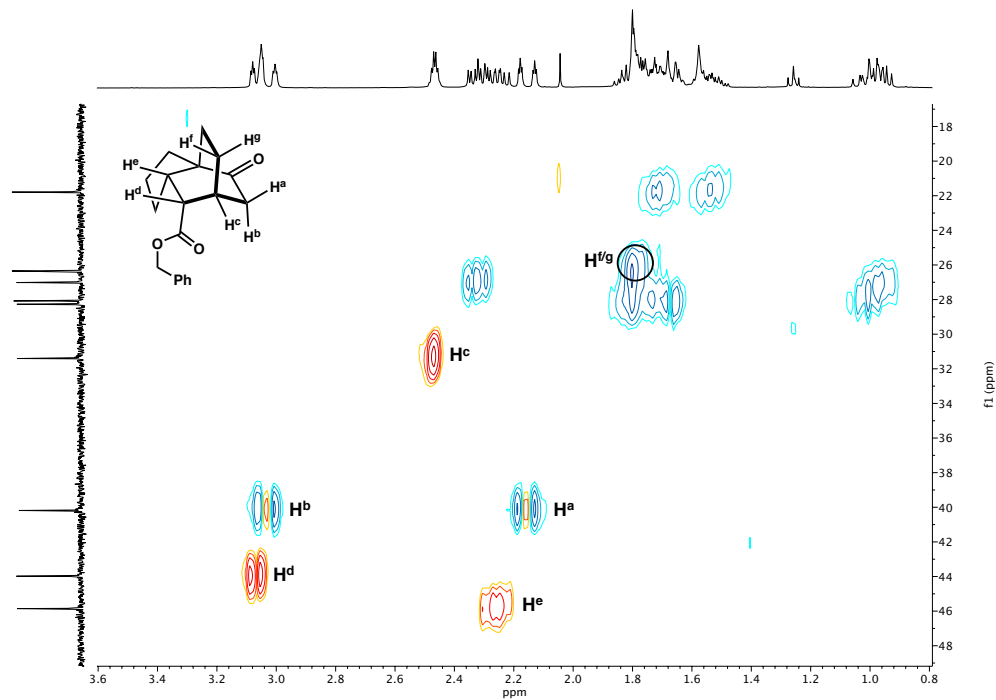
Figure 3.45. *¹H-¹H NOESY NMR spectrum of* **41q** *(400 MHz, CDCl₃).*
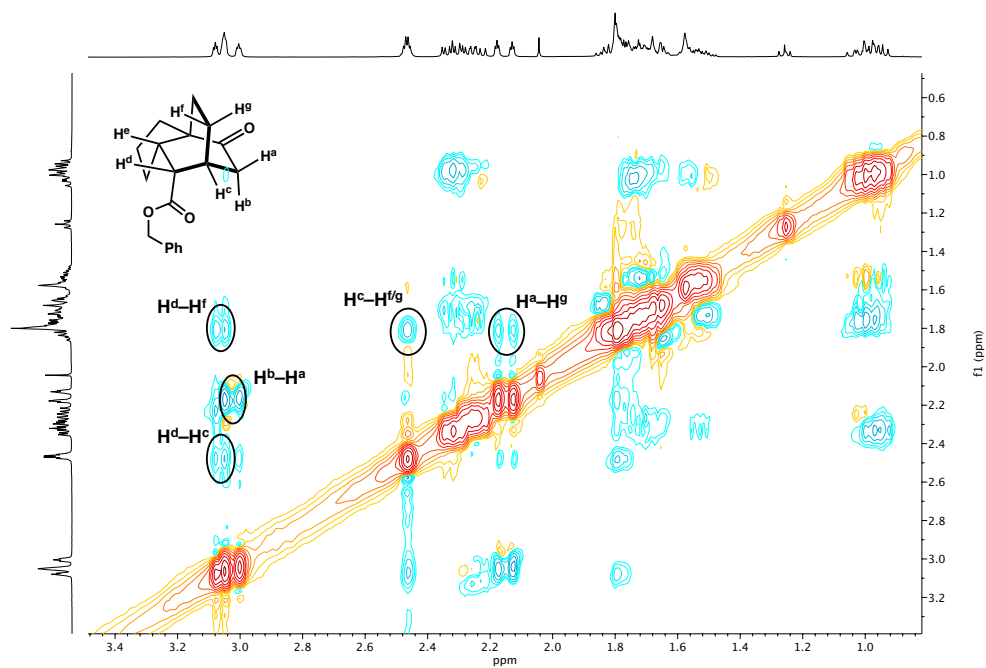
Figure 3.46. ^1H-^1H COSY NMR spectrum of **41q'** (400 MHz, CDCl$_3$).
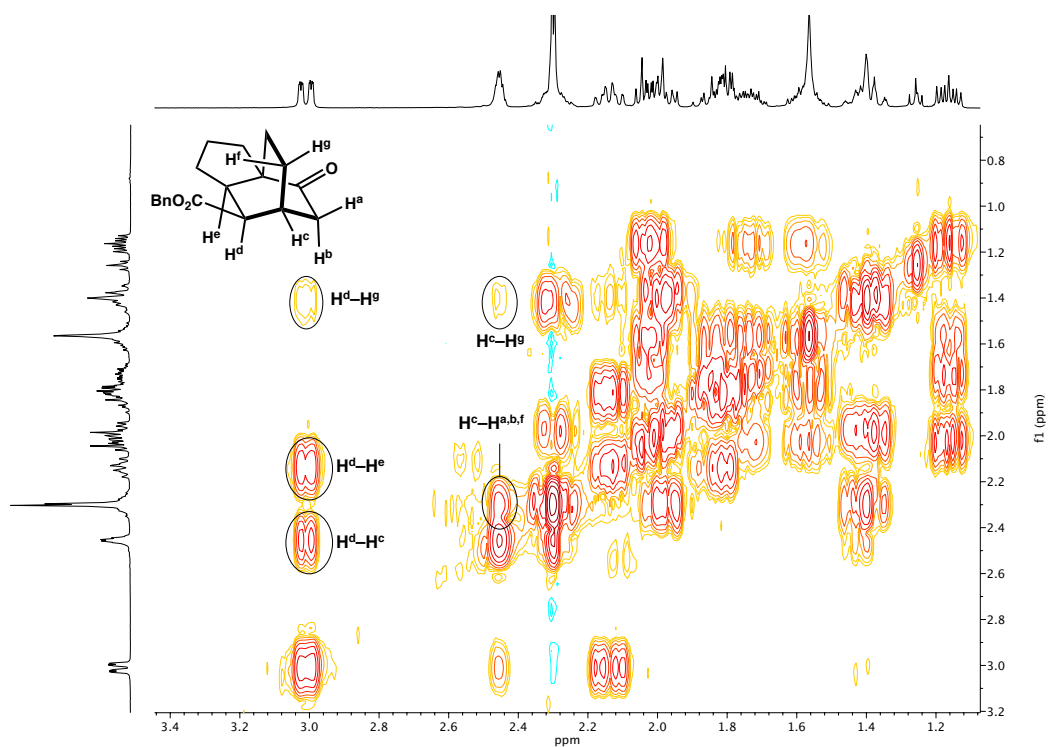
Figure 3.47. ^1H-^{13}C HSQC NMR spectrum of **41q'** (400 MHz, CDCl$_3$).
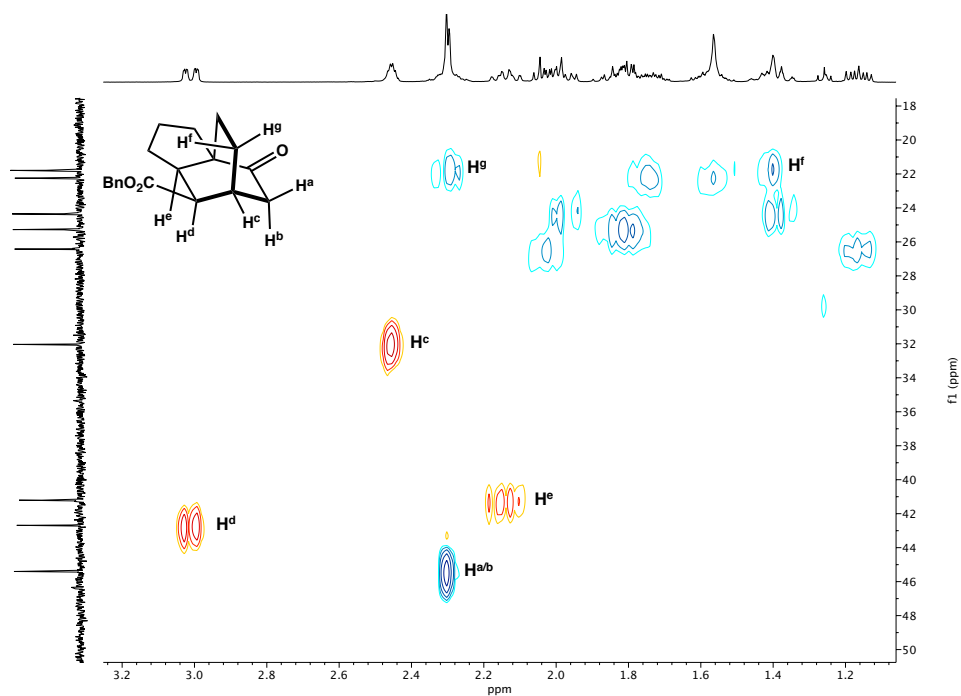
Figure 3.48. *^{1}H-^{1}H NOESY NMR spectrum of **41q'** (400 MHz, CDCl$_3$).*
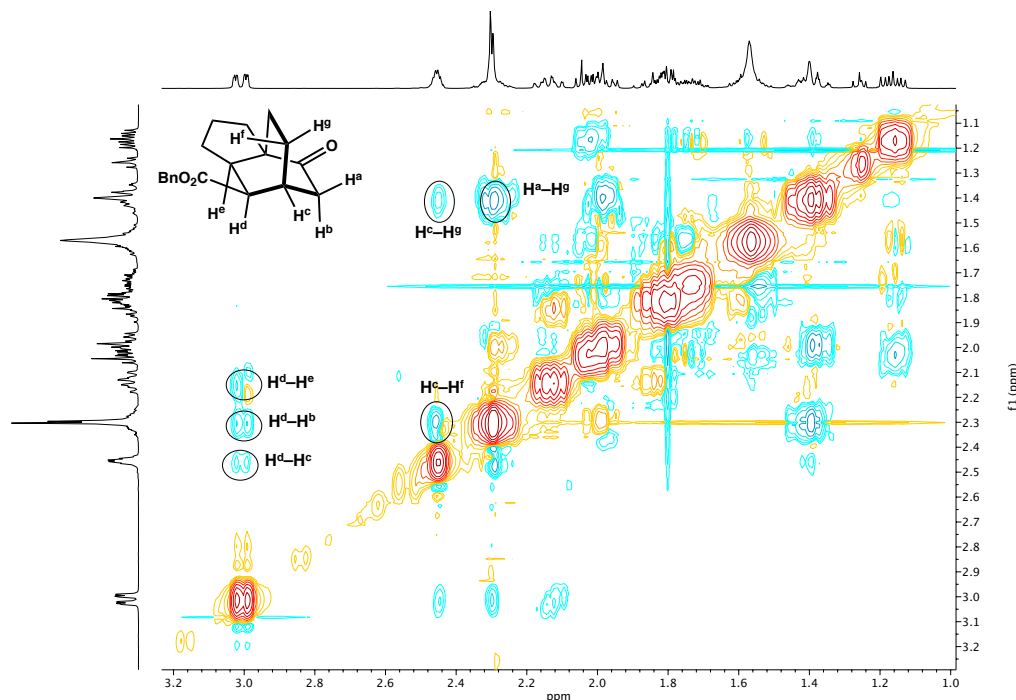
3.4.5   GENERAL COMPUTATIONAL DETAILS

General Notes

All quantum mechanics calculations were carried out with the ORCA program.[52] Geometry optimizations, harmonic frequency calculations, and single-point energy evaluations were carried out with density functional theory (DFT). The PBE0 functional[53] paired with Becke–Johnson damped D4 dispersion corrections[54], henceforth referred to as PBE0-D4, was used as it has proven a robust method for such systems in our prior studies.[55] For geometry optimization and harmonic frequency calculations, Pd is described by the def2-TZVP basis set[56] and the ECP28MWB small-core (18 explicit valence electrons) quasi-relativistic pseudopotential,[57] while C, H, N, and P are assigned the def2-SVP basis. Diffuse functions are added to oxygen (ma-def2-SVP). Herein, we refer to this composite

basis set as BS1. Geometry optimization and harmonic frequency calculations were carried out with the CPCM implicit solvation model for toluene (PhMe, $\varepsilon = 2.4$). For all calculations employing CPCM, surface charges are described by the improved Gaussian charge scheme of Neese and coworkers with a scaled Van der Waals cavity ($\alpha = 1.2$).[58] All Hessians were computed analytically. Stationary points are characterized by the correct number of imaginary vibrational modes (zero for minima and one for saddle points). Intrinsic reaction coordinate (IRC) analysis confirms the nature of transition states.[59] Cartesian coordinates of all optimized structures are included as ".xyz" files are available online in a compressed in a zip file format.

Electronic energies are further refined with single-point calculations employing the PBE0-D4 functional[60] and the def2-TZVPP basis set on all atoms (with the ECP28MWB pseudopotential for Pd) with additional diffuse functions on O (ma-def2-TZVPP). This mixed basis is henceforth referred to as BS2. Solvation was accounted for with CPCM as mentioned above (PhMe, $\varepsilon = 2.4$). Final Gibbs free energies were obtained by applying thermodynamic corrections obtained at the optimization level of theory to these refined electronic energies. Thermodynamic corrections from harmonic frequency calculations employ the quasi-ridged rotor harmonic oscillator approach to correct for the breakdown of the harmonic oscillator approximation at low vibrational frequencies.[61] Note that free energies are adjusted to a 1 M standard state. The translational (S_{trans}) and rotational entropy (S_{rot}) contributions to the Gibbs free energy calculated for a complex in condensed phase are *ca.* 40–60% of the values obtained assuming an ideal gas.[62] As suggested in the literature, S_{trans} and S_{rot} obtained by ideal gas treatment are scaled by a factor of 0.5 to

obtain the final condensed phase values.[63] Hence, the Gibbs free energy at 333.15 K is calculated as:

$$G_{solv}^* = E_{el,solv}^{BS2} + ZPE + E_{trans} + E_{rot} + E_{vib} + k_b T - T\left(S_{el} + S_{vib} + \frac{1}{2}S_{trans} + \frac{1}{2}S_{rot}\right)$$
$$+ \Delta G^{0\to*}$$

The resolution of identity (RI) and Chain-of-Spheres (COS) approximations are employed for efficient evaluation of Coulomb and exchange integrals, respectively.[64] The def2/J auxiliary basis[65] is employed for all atoms except oxygen, for which a suitable auxiliary was obtained via the automatic generation algorithm in the ORCA program (keyword: *AutoAux*). [66] Very fine grid settings are employed in all calculations (optimization/frequency calculations: DefGrid2, single point calculations: DefGrid3).

Conformer searching was carried out for each stationary point using the meta-dynamics-based CREST program (using GNF-FF) from the Grimme group. Duplicate conformers were removed, and low energy conformers were subsequently optimized and energies evaluated at the cheaper PBE0-D4/def2-TZVP (Pd), ma-def2-SVP (O), def2-SVP/CPCM(PhMe)//PBE-D4/def2-TZVP (Pd), ma-def2-SV(P) (O), def2-SV(P) level of theory. The final low energy conformers were further optimized at the level of theory mentioned prior. Note that for enantiodetermining transition states (such as TS2 and TS3) conformer searching also explicitly includes rotation about the Pd–O–C–C(enolate) dihedral, consideration of s-cis and s-trans ester conformations, as well as all permutations of the considered stereochemical elements.

Finally, conformational entropy [67] (entropy arising from multiple low energy thermally populated conformers) is accounted for by the *mixture of components* model of DeTar.[68] Conformational entropy (S_{conf}) is defined as:

$$S_{conf} = -R \sum \chi_i \ln (\chi_i)$$

where χ_i is the mole fraction (thermal population) of the ith conformer based on its relative free energy within the conformer ensemble. Given the computational demand for computing free energies for large ensembles of conformers, χ_i was derived from the free energies initially computed during the conformer screening process (PBE0-D4/def2-TZVP (Pd), ma-def2-SVP (O), def2-SVP/CPCM(PhMe)//PBE-D4/def2-TZVP (Pd), ma-def2-SV(P) (O), def2-SV(P))

$$G_{final} = G^*_{solv} - TS_{conf}$$

For the systems at hand, values of TS_{conf} (at 333.15 K) can be on the order of magnitude of a few kcal/mol.

Comparison of Barrier Heights to Inner-sphere Reductive Elimination

Employing cyclohexanone-derived Pd enolate as a model system (**13, 116, 117**), the barrier to inner-sphere reductive elimination was investigated while varying substitution on the allyl moiety (Figure 3.49). For further discussion on the seven-centered cyclic reductive elimination process, see Chapters 1–2.

Figure 3.49. *Relative free energies for various inner-sphere reductive elimination transition states from allyl (**13**), cinnamyl (**116**), and prenyl (**117**) complexes.*[a]
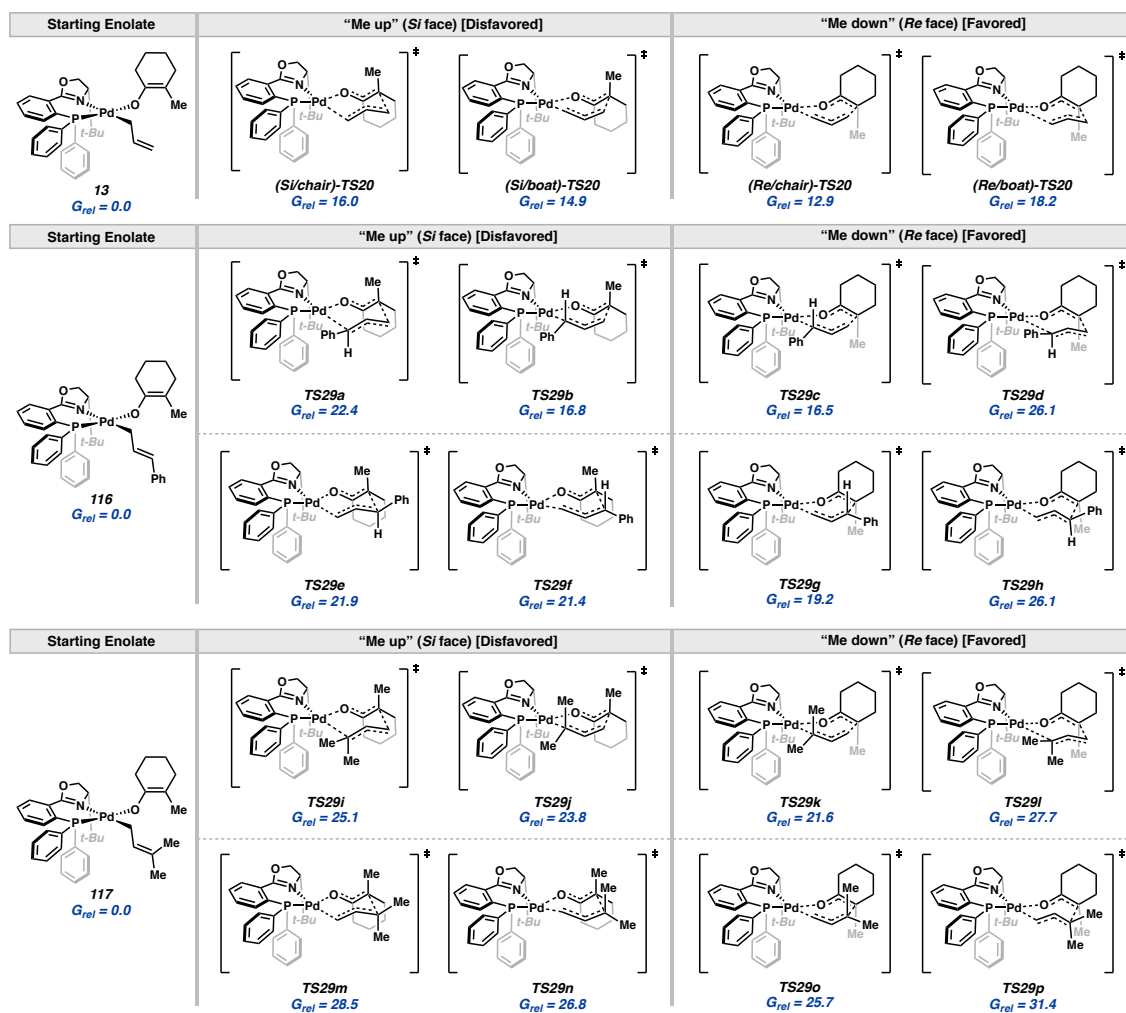
[a] Gibbs free energies in kcal/mol computed at the PBE0-D4/BS2/CPCM(PhMe)//PBE0-D4/BS1/CPCM(PhMe) level of theory at 333.15 K.

Mechanism of Catalyst Turnover

Of all the sampled transition states, we found the outer-sphere and N-detached inner-sphere

pathways to be highly competitive and lowest in energy. Additional transition states were

also explored, and the lowest energy pathway of each type of mechanism are shown in the following table.

Figure 3.50. *Relative free energies for various proton transfer transition states from post-cycloaddition enolate **56**.*[a]
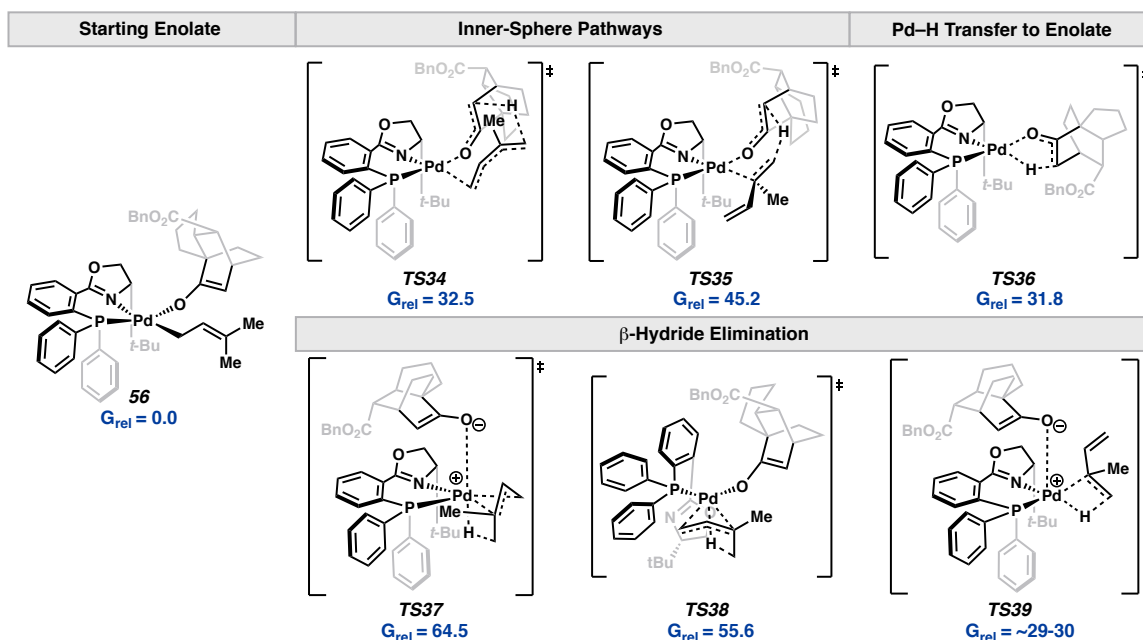
[a] Gibbs free energies in kcal/mol computed at the PBE0-D4/BS2/CPCM(PhMe)//PBE0-D4/BS1/CPCM(PhMe) level of theory at 333.15 K.

Mechanism of Premature Protonation

Analogous to the catalyst turnover mechanism, N-detached inner-sphere pathways were found to be lowest-energy for premature protonation. Of these transition states (**TS40a** and **TS40b**) that would yield enantiomeric protonation products, the lowest-energy **TS40a** provides the enantiomer consistent with the major reaction product. In addition, an outer-sphere pathway (**TS41**) was also found to be competitive.

Figure 3.51. *Relative free energies for various proton transfer transition states from pre-cycloaddition enolate **55**.*[a]
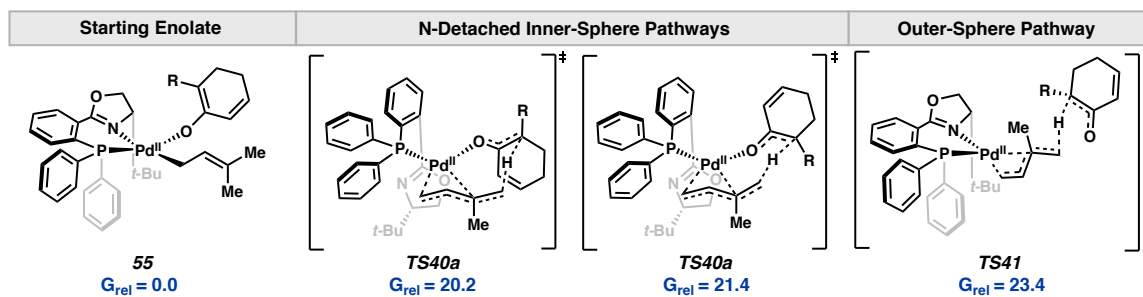
[a] Gibbs free energies in kcal/mol computed at the PBE0-D4/BS2/CPCM(PhMe)//PBE0-D4/BS1/CPCM(PhMe) level of theory at 333.15 K.

Intrinsic Bonding Orbital (IBO) Analysis of Inner-sphere Proton Transfer

IBO analysis along the reaction coordinate of the N-detached inner-sphere proton transfer

to post-cycloaddition enolate confirms the role of prenyl as a proton source.

Figure 3.52. *IBO analysis of N-detached inner-sphere mechanism and corresponding*

derived arrow-pushing mechanism.
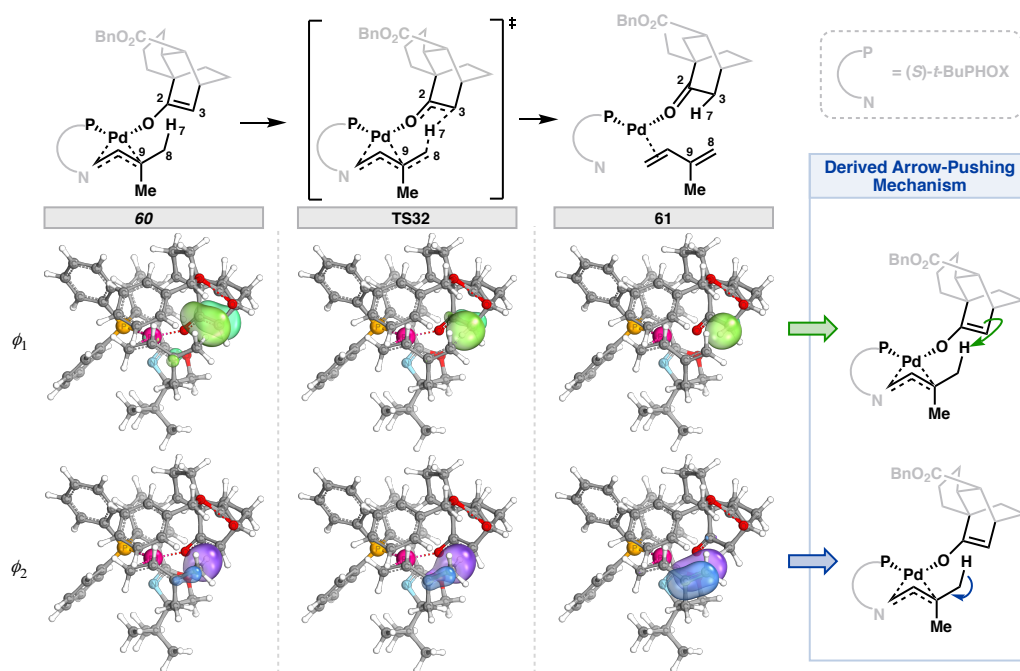
pKa Calculations and Thermodynamics of Outer-Sphere Proton Transfer

The pK_a values of the π-allyl Pd complex **118** and ketones were calculated, and the results

verify that the proton transfers to both pre- and post-cycloaddition enolates are

thermodynamically favorable.

Figure 3.53. *Computed pKa values of cationic π-allyl Pd complex **119** and ketones*

49a *and **41a**.*

Compound	Proton	pK_a in water	pK_a in DMSO
118	H_a	20.0	19.5
49a	H_b	30.1	30.3
41a	H_c	31.3	30.8
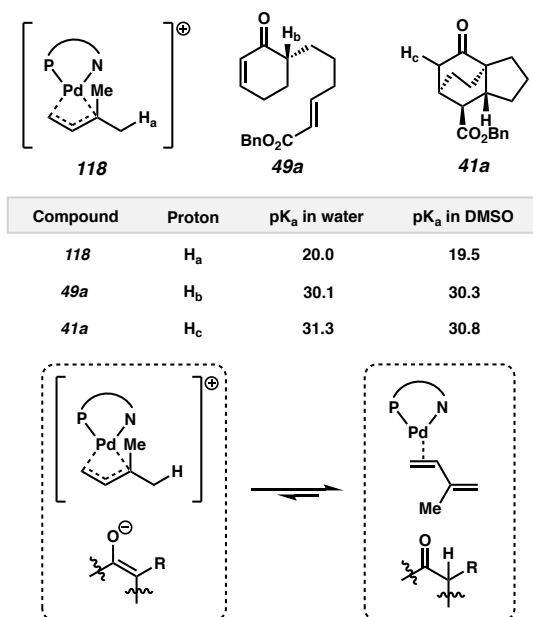
Enantiodetermining [4+2] cycloaddition

Figure 3.54. *(A) Comparison of internal versus external dienophile approach to both enantiotopic diene faces. (B) Select low energy conformers of **TS31** (allyl isomers not pictured). (C) Additional space-filling models for **TS30** and **TS31**.*

A. External versus internal dienophile approach in pathways to *41a* and *(ent)-41a*.

TS leading to *41a*		TS leading to *ent-41a* (minor)	
TS30	*TS42*	*TS31*	*TS43*
$\Delta G^{\ddagger}_{rel}$ = 0.0 kcal/mol	$\Delta G^{\ddagger}_{rel}$ = 6.4 kcal/mol	$\Delta G^{\ddagger}_{rel}$ = 1.6 kcal/mol	$\Delta G^{\ddagger}_{rel}$ = 3.5 kcal/mol
[Favored]		[Lowest energy to *ent-41a*]	

B. Select low energy conformers of TS31:

(G_{rel} = 1.6 kcal/mol) (G_{rel} = 2.3 kcal/mol) (G_{rel} = 2.3 kcal/mol)
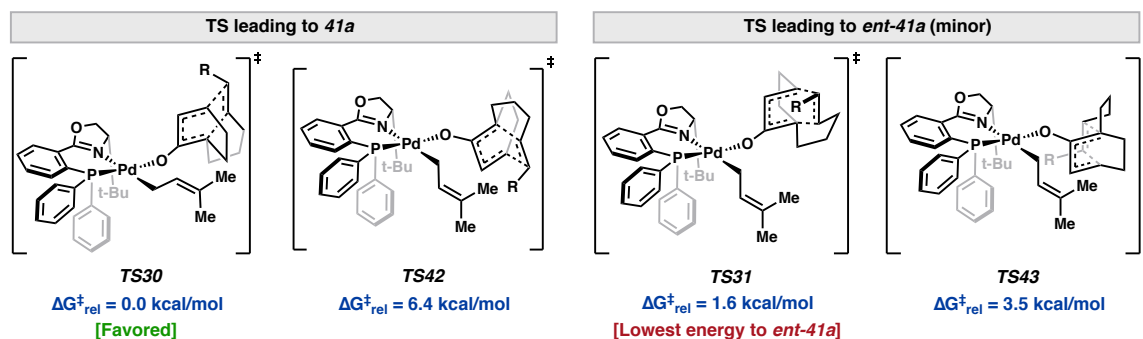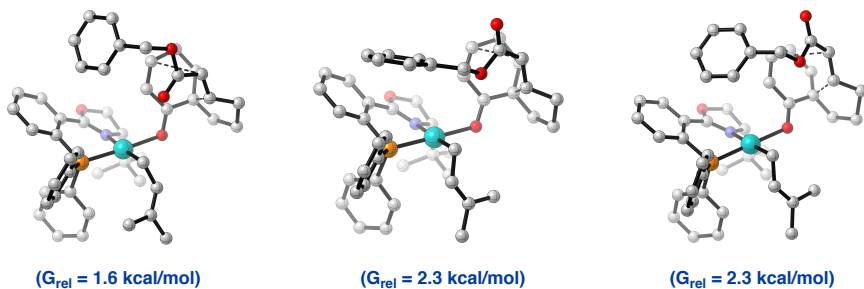
C. Additional space-filling models for TS30 versus TS31:

distorted and pushed back by PHOX ligand Ph group

TS31
[Disfavored]

TS30
[Favored]
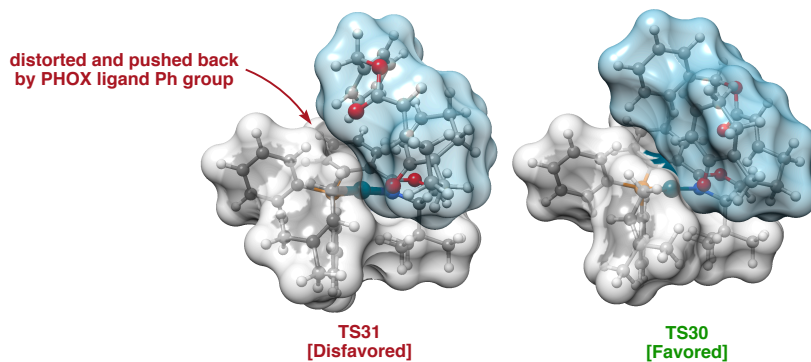
4.5   REFERENCES AND NOTES

(1)   (a) Christoffers, J.; Mann, A. Enantioselective Construction of Quaternary Stereocenters. *Angew. Chem. Int. Ed.* **2001**, *40*, 4591–4597. (b) Douglas, C. J.; Overman, L. E. Catalytic Asymmetric Synthesis of All-Carbon Quaternary Stereocenters. *Proc. Natl. Acad. Sci. U.S.A.* **2004**, *101*, 5363–5367.

(2)   (a) Liu, Y.; Han, S.-J.; Liu, W.-B.; Stoltz, B. M. Catalytic Enantioselective Construction of Quaternary Stereocenters: Assembly of Key Building Blocks for the Synthesis of Biologically Active Molecules. *Acc. Chem. Res.* **2015**, *48*, 740–751. (b) Trost, B. M.; Crawley, M. L. Asymmetric Transition-Metal-Catalyzed Allylic Alkylations: Applications in Total Synthesis. *Chem. Rev.* **2003**, *103*, 2921–2944.

(3)   Cusumano, A. Q.; Stoltz, B. M.; Goddard, W. A. Reaction Mechanism, Origins of Enantioselectivity, and Reactivity Trends in Asymmetric Allylic Alkylation: A Comprehensive Quantum Mechanics Investigation of a $C(sp^3)$–$C(sp^3)$ Cross-Coupling. *J. Am. Chem. Soc.* **2020**, *142*, 13917–13933.

(4)   (a) Keith, J. A.; Behenna, D. C.; Mohr, J. T.; Ma, S.; Marinescu, S. C.; Oxgaard, J.; Stoltz, B. M.; Goddard, W. A. The Inner-Sphere Process in the Enantioselective Tsuji Allylation Reaction with *(S)-t*-Bu-Phosphinooxazoline Ligands. *J. Am. Chem. Soc.* **2007**, *129*, 11876–11877. (b) Keith, J. A.; Behenna, D. C.; Sherden, N.; Mohr, J. T.; Ma, S.; Marinescu, S. C.; Nielsen, R. J.; Oxgaard, J.; Stoltz, B. M.; Goddard, W. A. The Reaction Mechanism of the Enantioselective Tsuji Allylation: Inner-Sphere and Outer-Sphere Pathways, Internal Rearrangements, and Asymmetric C–

C Bond Formation. *J. Am. Chem. Soc.* **2012**, *134*, 19050–19060. (C) McPherson, K. E.; Croatt, M. P.; Morehead, A. T.; Sargent, A. L. DFT Mechanistic Investigation of an Enantioselective Tsuji–Trost Allylation Reaction. *Organometallics* **2018**, *37*, 3791–3802.

(5)   Behenna, D. C.; Stoltz, B. M. The Enantioselective Tsuji Allylation. *J. Am. Chem. Soc.* **2004**, *126*, 15044–15045.

(6)   Mohr, J. T.; Behenna, D. C.; Harned, A. M.; Stoltz, B. M. Deracemization of Quaternary Stereocenters by Pd-Catalyzed Enantioconvergent Decarboxylative Allylation of Racemic β-Ketoesters. *Angew. Chem. Int. Ed.* **2005**, *44*, 6924–6927.

(7)   (a) Mohr, J. T.; Nishimata, T.; Behenna, D. C.; Stoltz, B. M. Catalytic Enantioselective Decarboxylative Protonation. *J. Am. Chem. Soc.* **2006**, *128*, 11348–11349. (b) Marinescu, S. C.; Nishimata, T.; Mohr, J. T.; Stoltz, B. M. Homogeneous Pd-Catalyzed Enantioselective Decarboxylative Protonation. *Org. Lett.* **2008**, *10*, 1039–1042.

(8)   Streuff, J.; White, D. E.; Virgil, S. C.; Stoltz, B. M. A Palladium-Catalysed Enolate Alkylation Cascade for the Formation of Adjacent Quaternary and Tertiary Stereocentres. *Nature Chem* **2010**, *2*, 192–196.

(9)   Inanaga, K.; Wollenburg, M.; Bachman, S.; Hafeman, N. J.; Stoltz, B. M. Catalytic Enantioselective Synthesis of Carbocyclic and Heterocyclic Spiranes via a Decarboxylative Aldol Cyclization. *Chem. Sci.* **2020**, *11*, 7390–7395.

(10)   (a) Ihara, M.; Ishida, Y.; Abe, M.; Toyota, M.; Fukumoto, K.; Kametani, T. Stereocontrolled Synthesis of the CDF Part of Aconitum Alkaloids via

Intramolecular Double Michael Reaction. *J. Chem. Soc., Perkin Trans. 1* **1988**, 5, 1155–1163. See also: (b) Ihara, M.; Makita, K.; Tokunaga, Y.; Fukumoto, K. Stereoselective Formation of Three Carbon-Carbon Bonds by Cascade Reaction with Enolate Anion: Synthesis of Tricyclo[6.2.2.0^{1,6}]Dodecane and Tricyclo[5.3.1.0^{3,8}]Undecane Derivatives. *J. Org. Chem.* **1994**, *59*, 6008–6013. (c) Ihara, M.; Toyota, M.; Fukumoto, K.; Kametani, T. Intramolecular Double Michael Reaction. Part II. Synthesis of Isoatisirene Type Compound. *Tetrahedron Lett.* **1984**, *25*, 3235–3238. (d) Ihara, M.; Suzuki, M.; Fukumoto, K.; Kabuto, C. Asymmetric Total Synthesis of Atisine via Intramolecular Double Michael Reaction. *J. Am. Chem. Soc.* **1990**, *112*, 1164–1171.

(11)   All quantum mechanics calculations were carried out with the ORCA program. Neese, F. Software Update: The ORCA Program System—Version 5.0. *WIREs Computational Molecular Science* **2022**, *12*, e1606.

(12)   Sherden, N. H.; Behenna, D. C.; Virgil, S. C.; Stoltz, B. M. Unusual Allylpalladium Carboxylate Complexes: Identification of the Resting State of Catalytic Enantioselective Decarboxylative Allylic Alkylation Reactions of Ketones. *Angew. Chem. Int. Ed.* **2009**, *48*, 6840–6843.

(13)   Paton, R. S.; Kim, S.; Ross, A. G.; Danishefsky, S. J.; Houk, K. N. Experimental Diels–Alder Reactivities of Cycloalkenones and Cyclic Dienes Explained through Transition-State Distortion Energies. *Angew. Chem. Int. Ed.* **2011**, *50*, 10366–10368.

(14)   Error bars are present for **40f** to **41f/49f** – they are smaller than the marker size in the figure.

(15)   Bennett, N. B.; Duquette, D. C.; Kim, J.; Liu, W.-B.; Marziale, A. N.; Behenna, D. C.; Virgil, S. C.; Stoltz, B. M. Expanding Insight into Asymmetric Palladium-Catalyzed Allylic Alkylation of N-Heterocyclic Molecules and Cyclic Ketones. *Chem. Eur. J.* **2013**, *19*, 4414–4418.

(16)   Unfortunately, attempts to further disfavor **TS31** by ortho-substitution of the PHOX ligand phenyl groups thwarted reactivity.

(17)   (a) Knizia, G. Intrinsic Atomic Orbitals: An Unbiased Bridge between Quantum Theory and Chemical Concepts. *J. Chem. Theory Comput.* **2013**, *9*, 4834–4843. (b) Knizia, G.; Klein, J. E. M. N. Electron Flow in Reaction Mechanisms—Revealed from First Principles. *Angew. Chem. Int. Ed.* **2015**, *54*, 5518–5522.

(18)   (a) Trost, B. M. When Is a Proton Not a Proton? *Chem. Eur. J.* **1998**, *4*, 2405–2412. See also: (b) Xu, L.; Hilton, M. J.; Zhang, X.; Norrby, P.-O.; Wu, Y.-D.; Sigman, M. S.; Wiest, O. Mechanism, Reactivity, and Selectivity in Palladium-Catalyzed Redox-Relay Heck Arylations of Alkenyl Alcohols. *J. Am. Chem. Soc.* **2014**, *136*, 1960–1967.

(19)   Note that on smaller scales (0.02 mmol) the ratio of ***D*-41f** to ***D*-49f** is 6.7:1 – in accord with a primary KIE. We hypothesize this may arise from the highly temperature-dependent nature of the product distribution paired with less homogenous reaction solution temperature on larger scales.

(20)   McLean, E. B.; Mooney, D. T.; Burns, D. J.; Lee, A.-L. Direct Hydrodecarboxylation of Aliphatic Carboxylic Acids: Metal- and Light-Free. *Org. Lett.* **2022**, *24* 686–691.

(21)   Nishiyama, Y.; Han-ya, Y.; Yokoshima, S.; Fukuyama, T. Total Synthesis of (–)-Lepenine. *J. Am. Chem. Soc.* **2014**, *136*, 6598–6601.

(22)   Kim, K. E.; Sakazaki, Y.; Stoltz, B. M. Synthesis of Non-Natural Cyanthiwigin–Gagunin Hybrids through Late-Stage Diversification of the Cyanthiwigin Natural Product Core. *Tetrahedron* **2020**, *76*, 130755.

(23)   Yang, T.-F.; Chang, C.-Y.; Lin, W.-F. Rearrangement of Acyclic-Alkyl [3.2.1]Bicyclic Alcohols to Free Methylene Dimethyl Alkyl [2.2.2]Bicyclic Octanes: Application to Preparation of Stereospecific Novel Sesquiterpene and Terpenoids. *Tetrahedron Letters* **2015**, *56*, 801–804.

(24)   Song, L.; Zhu, G.; Liu, Y.; Liu, B.; Qin, S. Total Synthesis of Atisane-Type Diterpenoids: Application of Diels–Alder Cycloadditions of Podocarpane-Type Unmasked *Ortho*- Benzoquinones. *J. Am. Chem. Soc.* **2015**, *137*, 13706–13714.

(25)   Neufeldt, S. R.; Sanford, M. S. O-Acetyl Oximes as Transformable Directing Groups for Pd-Catalyzed C–H Bond Functionalization. *Org. Lett.* **2010**, *12*, 532–535.

(26)   Pangborn, A. M.; Giardello, M. A.; Grubbs, R. H.; Rosen, R. K.; Timmers, F. J. Safe and Convenient Procedure for Solvent Purification. *Organometallics* **1996**, *15*, 1518–1520.

(27) McDougal, N. T.; Streuff, J.; Mukherjee, H.; Virgil, S. C.; Stoltz, B. M. Rapid synthesis of an electron-deficient *t*-BuPHOX ligand: cross-coupling of aryl bromides with secondary phosphine oxides. *Tetrahedron Lett.* **2010**, *51*, 5550–5554.

(28) Ando, K.; Narumiya, K.; Takada, H.; Teruya, T. Z-Selective Intramolecular Horner−Wadsworth−Emmons Reaction for the Synthesis of Macrocyclic Lactones. *Org. Lett.* **2010**, *12*, 1460–1463.

(29) Shelkov, R.; Nahmany, M.; Melman, A. Selective Esterifications of Alcohols and Phenols through Carbodiimide Couplings. *Org. Biomol. Chem.* **2004**, *2*, 397–401.

(30) Taguchi, T.; Sasaki, H.; Shibuya, A.; Morikawa, T. Regio- and Stereoselective Synthesis of Gem-Difluorocyclopropanes Using 4-Bromo-4,4-Difluorocrotonate. *Tetrahedron Lett.* **1994**, *35*, 913–916.

(31) Fornicola, R. S.; Subburaj, K.; Montgomery, J. A New Entry to the Isogeissoschizoid Skeleton. *Org. Lett.* **2002**, *4*, 615–617.

(32) Fillion, E.; Dumas, A. M. Synthesis of Fused 4,5-Disubstituted Indole Ring Systems by Intramolecular Friedel−Crafts Acylation of 4-Substituted Indoles. *J. Org. Chem.* **2008**, *73*, 2920–2923.

(33) Brandt, D.; Dittoo, A.; Bellosta, V.; Cossy, J. Synthetic Approach to Wortmannilactone C. *Org. Lett.* **2015**, *17*, 816–819.

(34) Fulton, T. J.; Cusumano, A. Q.; Alexy, E. J.; Du, Y. E.; Zhang, H.; Houk, K. N.; Stoltz, B. M. Global Diastereoconvergence in the Ireland–Claisen Rearrangement

of Isomeric Enolates: Synthesis of Tetrasubstituted α-Amino Acids. *J. Am. Chem. Soc.* **2020**, *142*, 21938–21947.

(35)   Touchard, F. P.; Capelle, N.; Mercier, M. Efficient and Scalable Protocol for the Z-Selective Synthesis of Unsaturated Esters by Horner–Wadsworth–Emmons Olefination. *Adv. Synth. Catal.* **2005**, *347*, 707–711.

(36)   Romano, C.; Fiorito, D.; Mazet, C. Remote Functionalization of α,β-Unsaturated Carbonyls by Multimetallic Sequential Catalysis. *J. Am. Chem. Soc.* **2019**, *141*, 16983–16990.

(37)   Sureshbabu, R.; Saravanan, V.; Dhayalan, V.; Mohanakrishnan, A. K. Lewis Acid Mediated One-Pot Synthesis of Aryl/Heteroaryl-Fused Carbazoles Involving a Cascade Friedel–Crafts Alkylation/Electrocyclization/Aromatization Reaction Sequence. *Eur. J. Org. Chem.* **2011**, 922–935.

(38)   Mukaiyama, T.; Matsuo, J.; Yanagisawa, M. A New and Efficient Method for Oxidation of Various Alcohols by Using N-Tert-Butyl Phenylsulfinimidoyl Chloride. *Chem. Lett.* **2000**, *29*, 1072–1073.

(39)   Inanaga, K.; Wollenburg, M.; Bachman, S.; Hafeman, N. J.; Stoltz, B. M. Catalytic Enantioselective Synthesis of Carbocyclic and Heterocyclic Spiranes via a Decarboxylative Aldol Cyclization. *Chem. Sci.* **2020**, *11*, 7390–7395.

(40)   Mohr, J. T.; Behenna, D. C.; Harned, A. M.; Stoltz, B. M. Deracemization of Quaternary Stereocenters by Pd-Catalyzed Enantioconvergent Decarboxylative Allylation of Racemic β-Ketoesters. *Angew. Chem. Int. Ed.* **2005**, *44*, 6924–6927.

(41)   Hierold, J.; Lupton, D. W. Synthesis of Spirocyclic γ-Lactones by Cascade Beckwith–Dowd Ring Expansion/Cyclization. *Org. Lett.* **2012**, *14*, 3412–3415.

(42)   Trost, B. M.; Xu, J. The O-Acylation of Ketone Enolates by Allyl 1H-Imidazole-1-Carboxylate Mediated with Boron Trifluoride Etherate: A Convenient Procedure for the Synthesis of Substituted Allyl Enol Carbonates. *J. Org. Chem.* **2007**, *72*, 9372–9375.

(43)   Prepared following ref. 42 with 3-(methyl-d_3)but-2-en-4,4,4-d_3-1-ol (Mosaferi, S.; Jelley, R. E.; Fedrizzi, B.; Barker, D. Scalable Synthesis of the Aroma Compounds D6-β-Ionone and D6-β-Cyclocitral for Use as Internal Standards in Stable Isotope Dilution Assays. *Tetrahedron Lett.* **2020**, *61*, 152642.

(44)   Shimizu, I.; Tsuji, J. Palladium-Catalyzed Decarboxylation-Dehydrogenation of Allyl β-Oxo Carboxylates and Allyl Enol Carbonates as a Novel Synthetic Method for α-Substituted α,β-Unsaturated Ketones. *J. Am. Chem. Soc.* **1982**, *104*, 5844–5846.

(45)   Knapp, S.; Yang, C.; Pabbaraja, S.; Rempel, B.; Reid, S.; Withers, S. G. Synthesis and Kinetic Analysis of the N-Acetylhexosaminidase Inhibitor XylNAc-Isofagomine. *J. Org. Chem.* **2005**, *70*, 7715–7720.

(46)   Srikrishna, A.; Kumar, P.P. Claisen Rearrangement Based Methodology for the Spiroannulation of a Cyclopentane Ring. Formal Total Synthesis of (±)-Acorone and Isoacorones. *Tetrahedron* **2000**, *56*, 8189–8195.

(47)   Szczesńiak, P.; Pieczykolan, M.; Steck, S. The Synthesis of α,α-Disubstituted α-Amino Acids via Ichikawa Rearrangement. *J. Org. Chem.* **2016**, *81*, 1057–1074.

(48)   Hou, H.; Xu, Y.; Yang, H.; Chen, X.; Yan, C.; Shi, Y.; Zhu, S. Visible-Light Mediated Hydrosilylative and Hydrophosphorylative Cyclizations of Enynes and Dienes. *Org. Lett.* **2020**, *22*, 1748-1753.

(49)   Yang, J.; Lu, K.; Li, C.; Zhao, Z.; Zhang, X.; Zhang, F.; Tu, Y. Chiral 1,2,3-Triazolium Salt Catalyzed Asymmetric Mono- and Dialkylation of 2,5-Diketopiperazines with the Construction of Tetrasubstituted Carbon Centers. *Angew. Chem. Int. Ed.* **2022**, *61*, e202114129.

(50)   **Schrödinger Release 2021-4:** MacroModel, Schrödinger, LLC, New York, NY, 2021.

(51)   Bochevarov, A.D.; Harder, E.; Hughes, T.F.; Greenwood, J.R.; Braden, D.A.; Philipp, D.M.; Rinaldo, D.; Halls, M.D.; Zhang, J.; Friesner, R.A., Jaguar: A high-performance quantum chemistry software program with strengths in life and materials sciences, *Int. J. Quantum Chem.*, **2013**, *113*, 2110-2142.

(52)   (a) Neese, F. Software Update: The ORCA Program System, Version 4.0. *Wiley Interdiscip. Rev.: Comput. Mol. Sci.* **2018,** *8*, No. e1327. (b) Neese, F. The ORCA Program System. *Wiley Interdiscip. Rev.: Comput. Mol. Sci.* **2012**, *2*, 73−78.

(53)   Adamo, C.; Barone, V. Toward Reliable Density Functional Methods without Adjustable Parameters: The PBE0 Model. *J. Chem. Phys.* **1999**, *110*, 6158−6170.

(54)   (a) Caldeweyher, E.; Ehlert, S.; Hansen, A.; Neugebauer, H.; Spicher, S.; Bannwarth, C.; Grimme, S. A Generally Applicable Atomic-Charge Dependent London Dispersion Correction. *J. Chem. Phys.* **2019**, *150*, 154122. (b)

Caldeweyher, E.; Bannwarth, C.; Grimme, S. Extension of the D3 Dispersion Coefficient Model. *J. Chem. Phys.* **2017**, *147*, 034112.

(55)   Cusumano, A. Q.; Goddard, W. A. I.; Stoltz, B. M. The Transition Metal Catalyzed [σ2s + σ2s + π2s + π2s] Pericyclic Reaction: Woodward–Hoffmann Rules, Aromaticity, and Electron Flow. *J. Am. Chem. Soc.* **2020**, *142*, 19033–19039.

(56)   Weigend, F.; Ahlrichs, R. Balanced Basis Sets of Split Valence, Triple Zeta Valence and Quadruple Zeta Valence Quality for H to Rn: Design and Assessment of Accuracy. *Phys. Chem. Chem. Phys.* **2005**, *7*, 3297–3305.

(57)   Peterson, K. A.; Figgen, D.; Goll, E.; Stoll, H.; Dolg, M. Systematically Convergent Basis Sets with Relativistic Pseudopotentials. II. Small-Core Pseudopotentials and Correlation Consistent Basis Sets for the Post- *d* Group 16–18 Elements. *J. Chem. Phys.* **2003**, *119*, 11113–11123.

(58)   Garcia-Ratés, M.; Neese, F. Effect of the Solute Cavity on the Solvation Energy and Its Derivatives within the Framework of the Gaussian Charge Scheme. *J. Comput. Chem.* **2020**, *41*, 922–939.

(59)   Ishida, K.; Morokuma, K.; Komornicki, A. The Intrinsic Reaction Coordinate. An Ab Initio Calculation for HNC→HCN and H−+CH4→CH4+H−. *J. Chem. Phys.* **1977**, *66*, 2153−2156.

(60)   Zhao, Y.; Truhlar, D. G. The M06 Suite of Density Functionals for Main Group Thermochemistry, Thermochemical Kinetics, Noncovalent Interactions, Excited States, and Transition Elements: Two New Functionals and Systematic Testing of

Four M06-Class Functionals and 12 Other Functionals. *Theor. Chem. Account.* **2008**, *120*, 215–241.

(61)   Grimme, S. Supramolecular Binding Thermodynamics by Dispersion-Corrected Density Functional Theory. *Chem. Eur. J.* **2012**, *18*, 9955–9964.

(62)   Izato, Y.; Matsugi, A.; Koshi, M.; Miyake, A. A Simple Heuristic Approach to Estimate the Thermochemistry of Condensed-Phase Molecules Based on the Polarizable Continuum Model. *Phys. Chem. Chem. Phys.* **2019**, *21*, 18920–18929.

(63)   Finkelstein, A. V.; Janin, J. The Price of Lost Freedom: Entropy of Bimolecular Complex Formation. *Protein Eng. Des. Sel.* **1989**, *3*, 1–3.

(64)   Neese, F.; Wennmohs, F.; Hansen, A.; Becker, U. Efficient, Approximate and Parallel Hartree-Fock and Hybrid DFT Calculations. A 'Chain-of-Spheres' Algorithm for the Hartree-Fock Exchange. *Chem. Phys.* **2009**, *356*, 98–109.

(65)   Weigend, F. Accurate Coulomb-Fitting Basis Sets for H to Rn. *Phys. Chem. Chem. Phys.* **2006**, *8*, 1057–1065.

(66)   Stoychev, G. L.; Auer, A. A.; Neese, F. Automatic Generation of Auxiliary Basis Sets. *J. Chem. Theory Comput.* **2017**, *13*, 554–562.

(67)   (a) Pracht, P.; Grimme, S. Calculation of Absolute Molecular Entropies and Heat Capacities Made Simple. *Chem. Sci.* **2021**, *12*, 6551–6568. (b) Gorges, J.; Grimme, S.; Hansen, A.; Pracht, P. Towards Understanding Solvation Effects on the Conformational Entropy of Non-Rigid Molecules. *Phys. Chem. Chem. Phys.* **2022**, *24*, 12249–12259.

(68) (a) DeTar, D. F. Theoretical Ab Initio Calculation of Entropy, Heat Capacity, and Heat Content. *J. Phys. Chem. A* **1998**, *102*, 5128–5141. See also: (b) Guthrie, J. P. Use of DFT Methods for the Calculation of the Entropy of Gas Phase Organic Molecules: An Examination of the Quality of Results from a Simple Approach. *J. Phys. Chem. A* **2001**, *105*, 8495–8499.

APPENDIX 2

Spectra Relevant to Chapter 3: Catalytic Asymmetric [4+2]

Cycloaddition of Pd Enolates
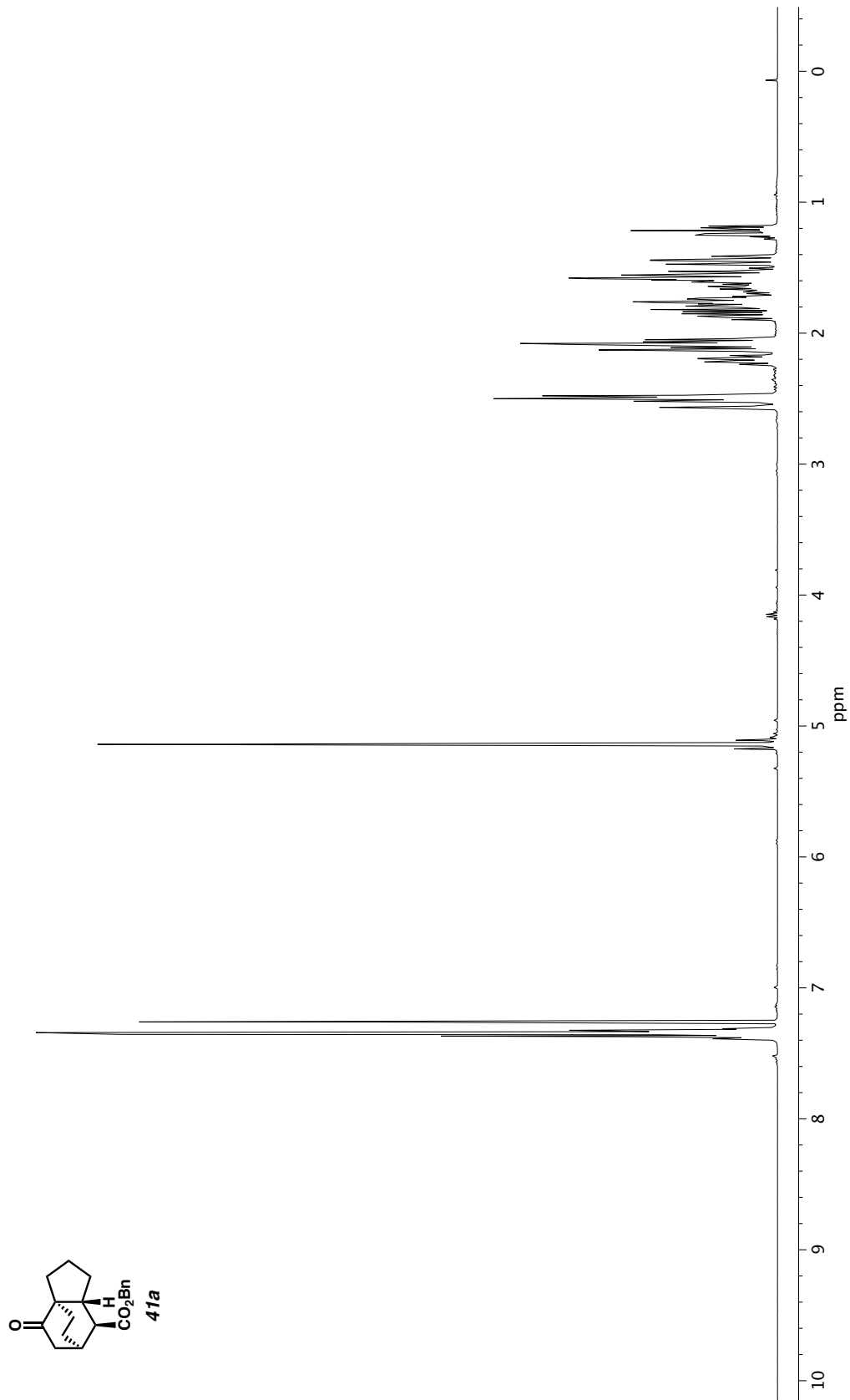
Figure A2.1. ^1H NMR (400 MHz, CDCl$_3$) of compound **41a**.
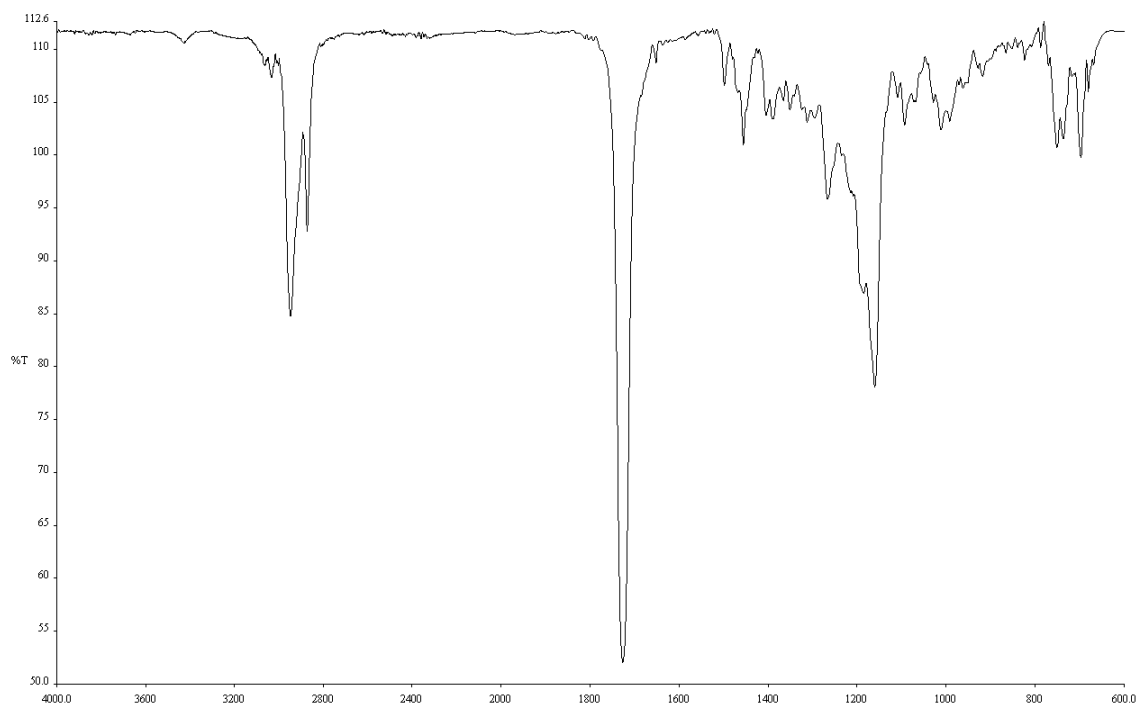
Figure A2.2. *Infrared spectrum (Thin Film, NaCl) of compound* **41a**.
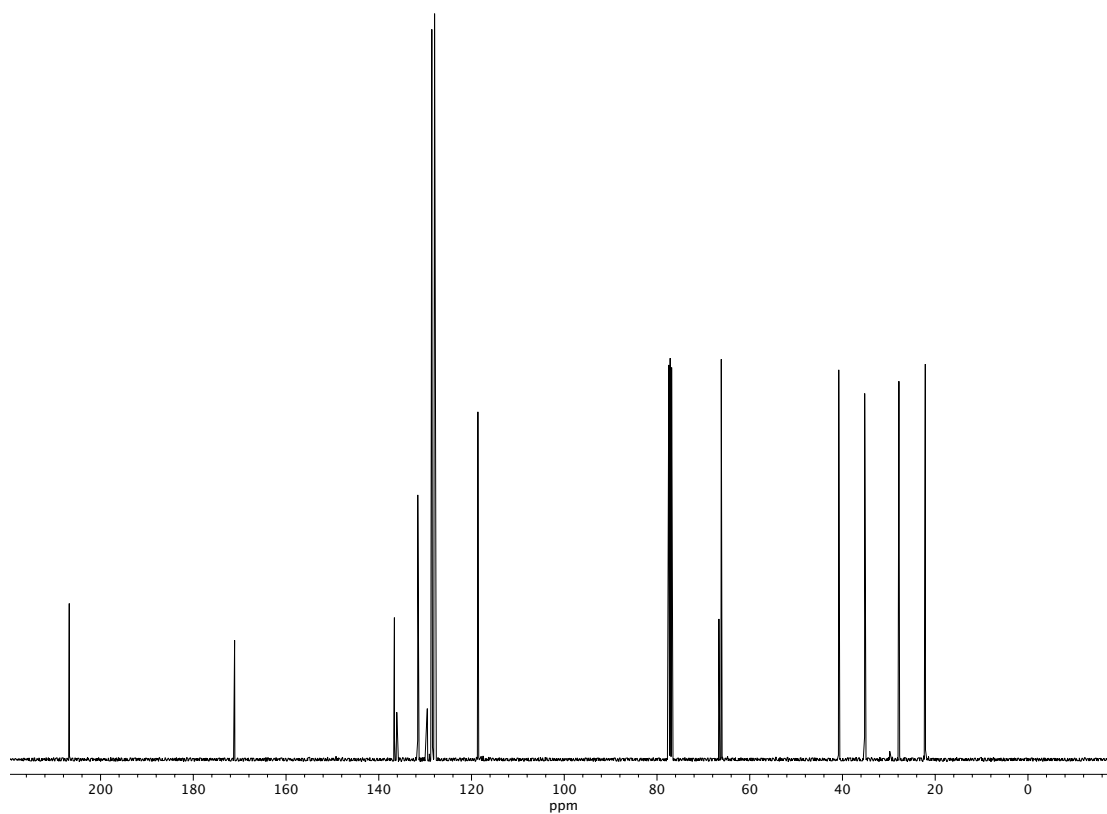
Figure A2.3. ^{13}C *NMR (100 MHz, CDCl$_3$) of compound* **41a**.
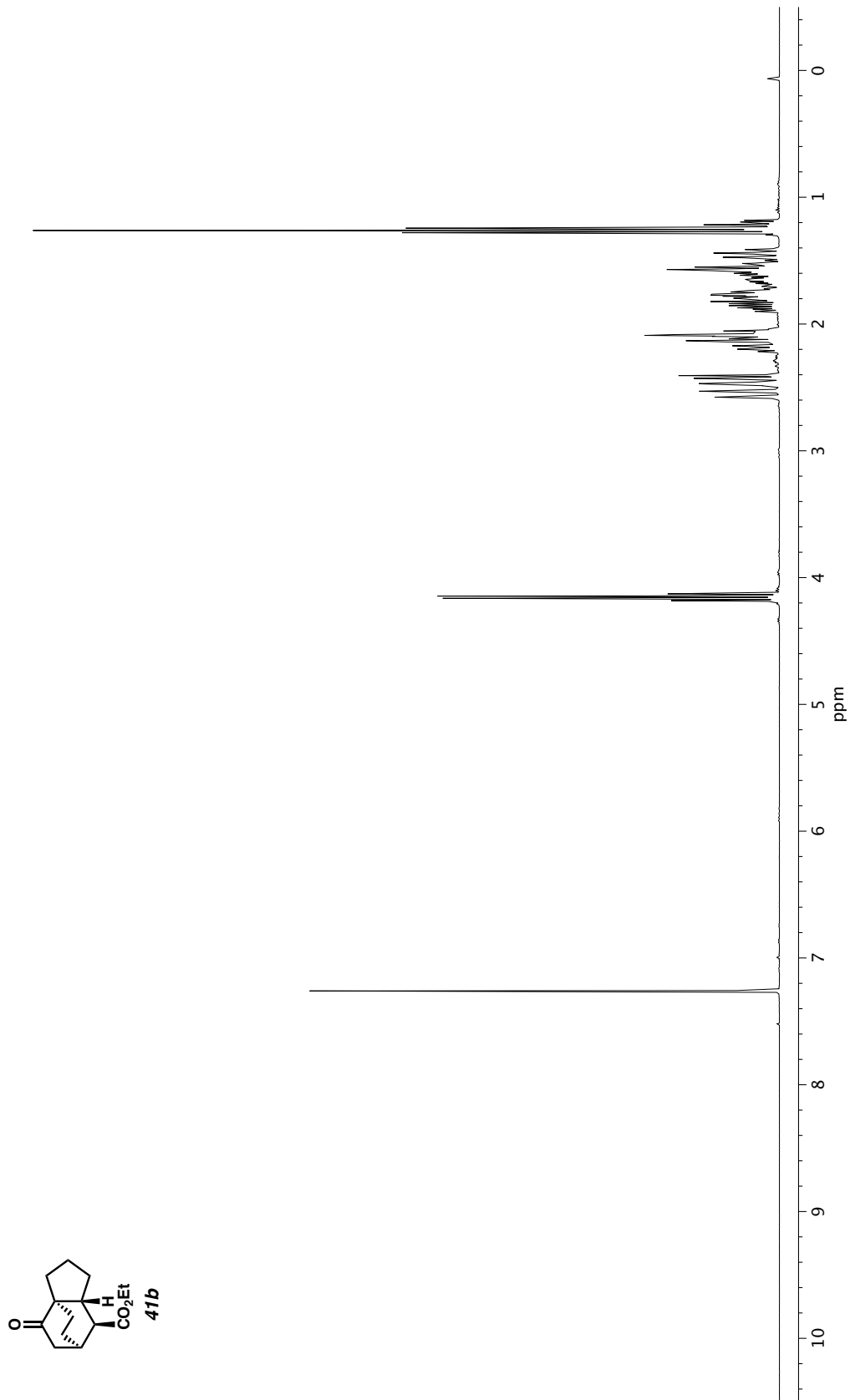
Figure A2.4. ^1H NMR (400 MHz, CDCl$_3$) of compound **41b**.
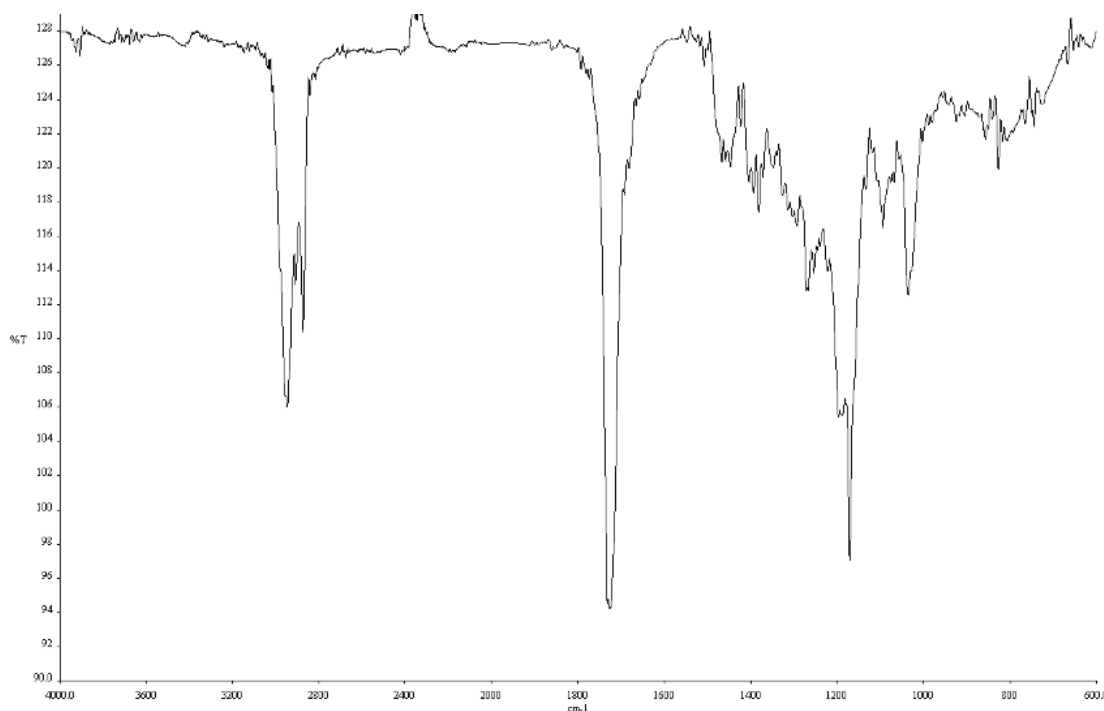
Figure A2.5. *Infrared spectrum (Thin Film, NaCl) of compound **41b**.*
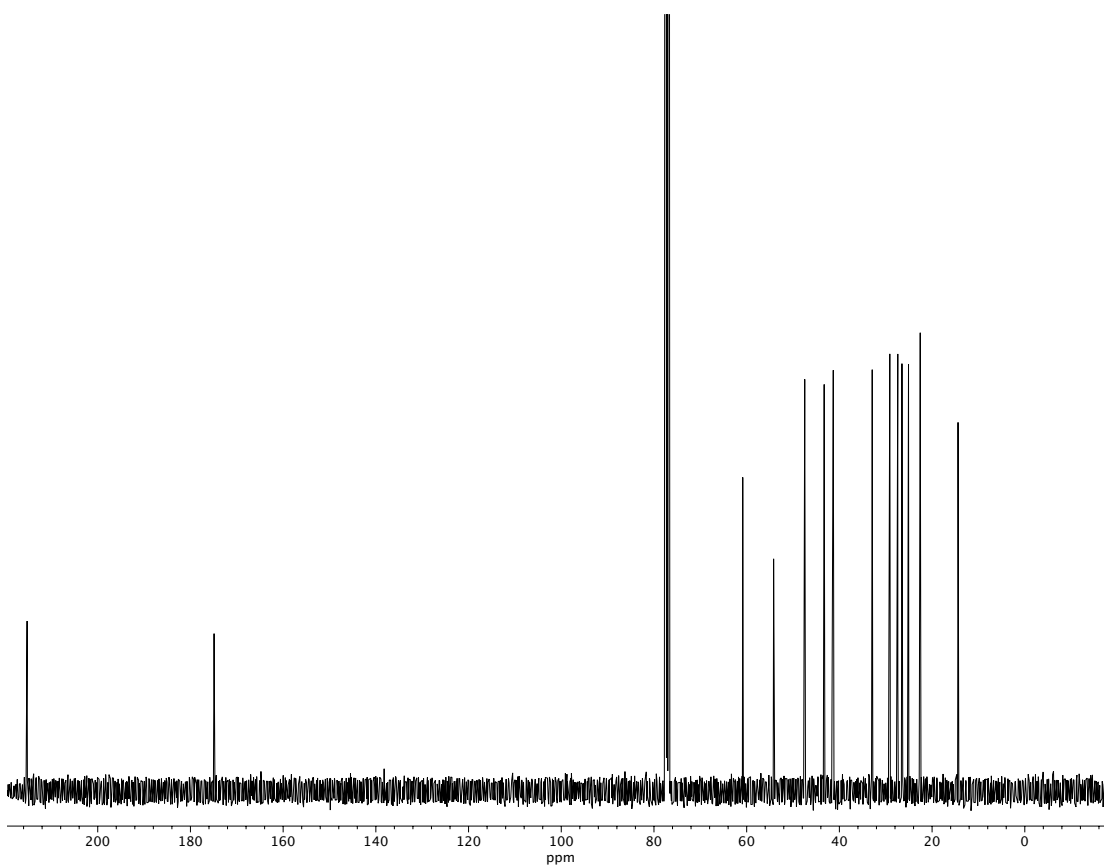
Figure A2.6. ^{13}C NMR (100 MHz, CDCl$_3$) of compound **41b**.
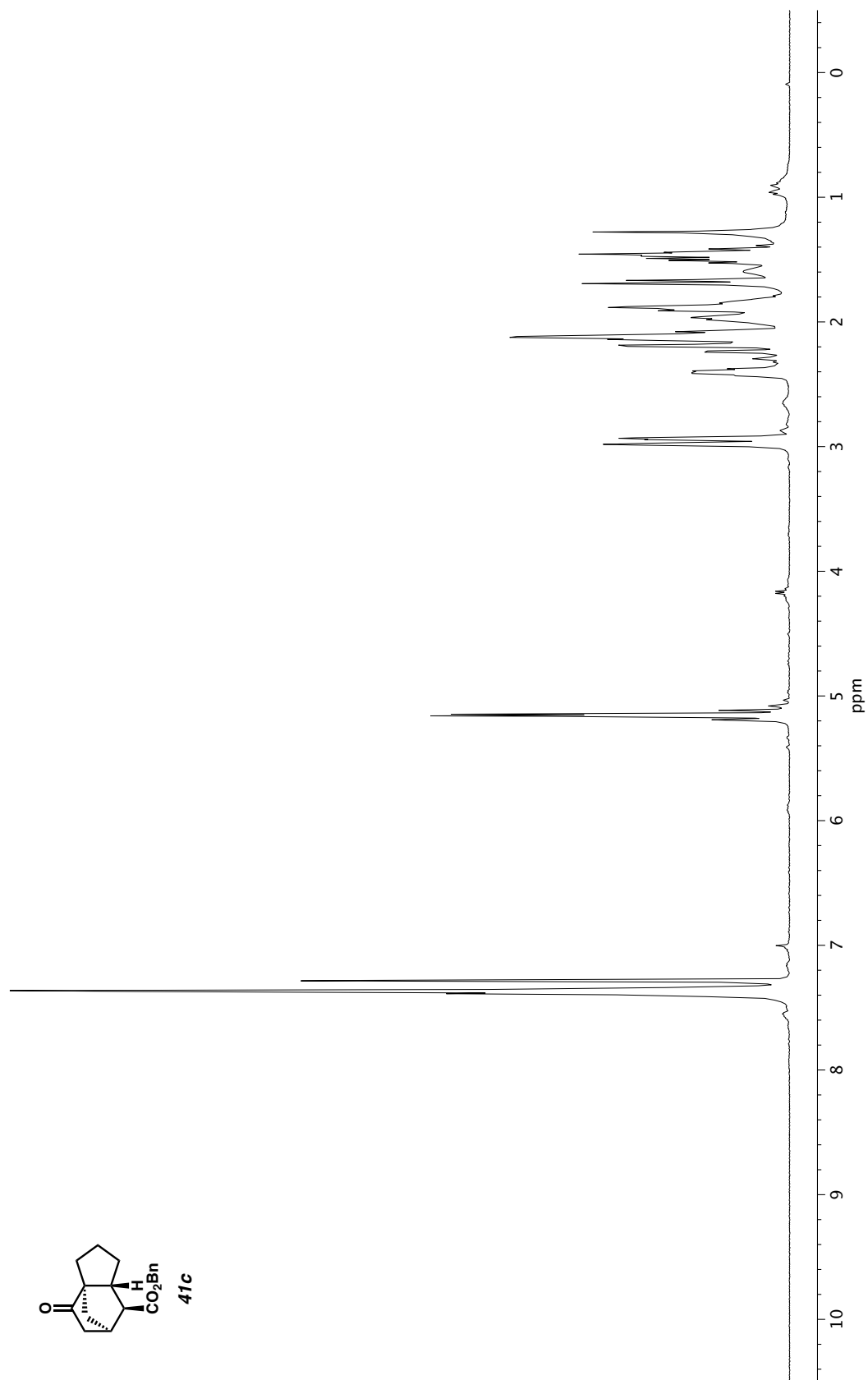
Figure A2.7. ^1H NMR (400 MHz, CDCl$_3$) of compound **41c**.
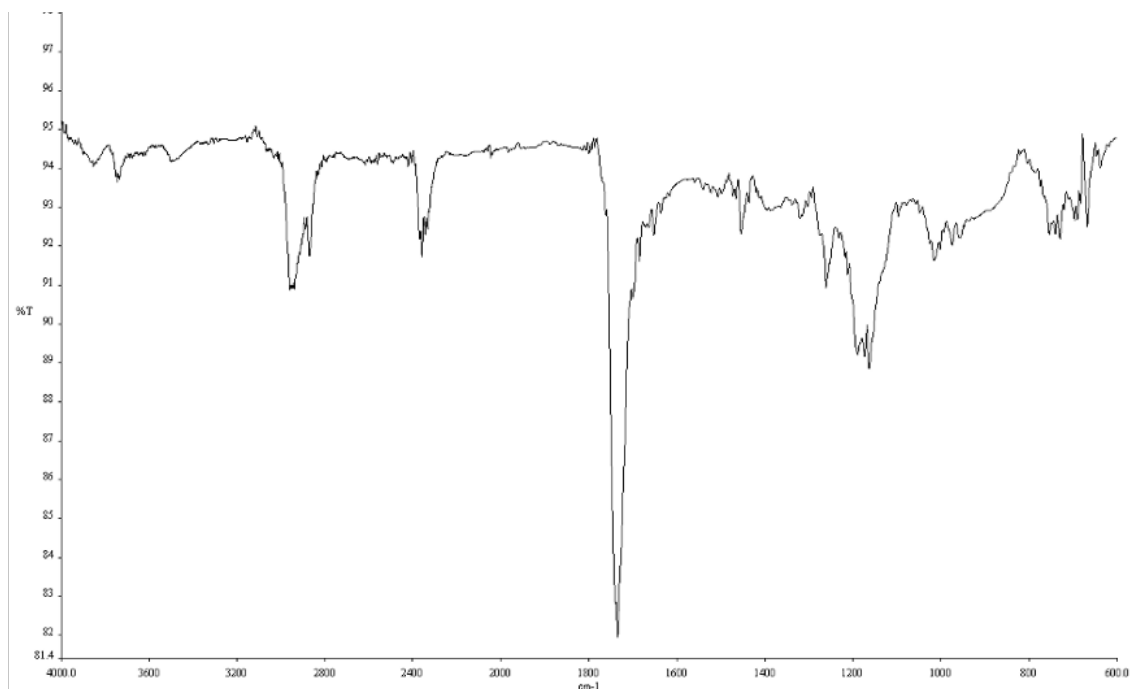
Figure A2.8. *Infrared spectrum (Thin Film, NaCl) of compound* **41c***.*
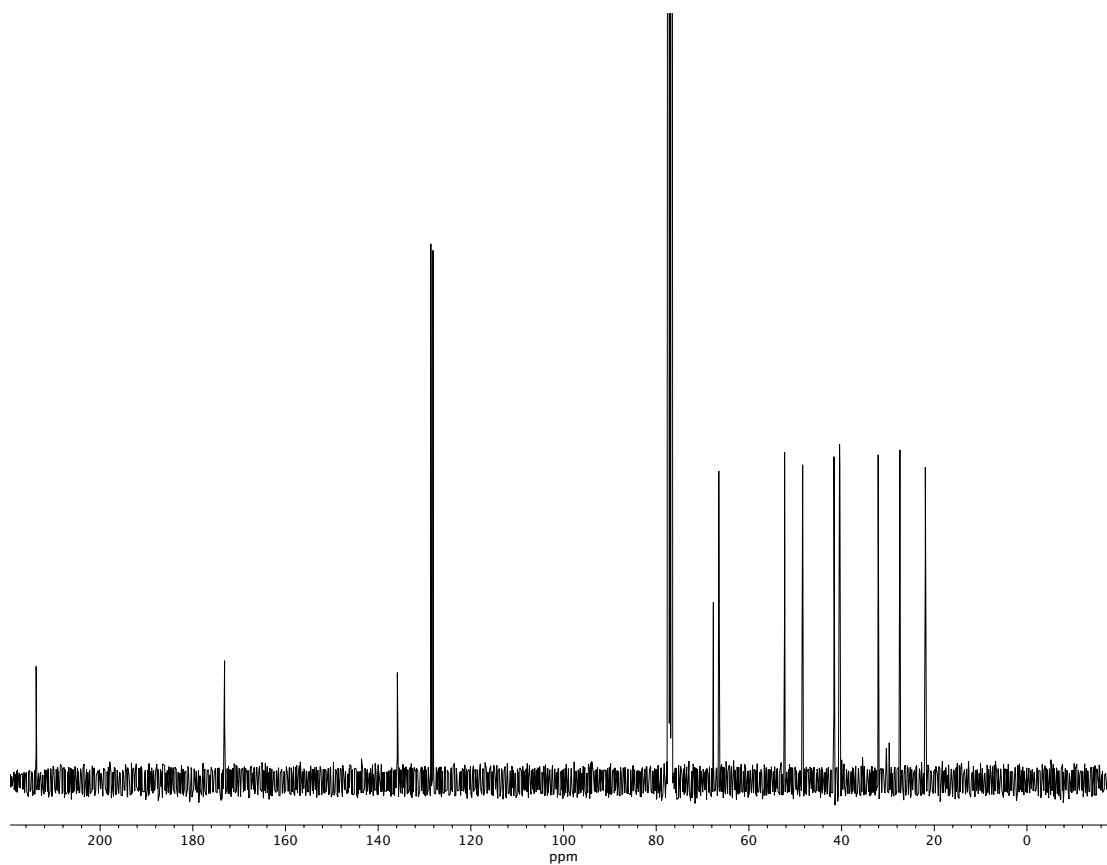
Figure A2.9. ^{13}C *NMR (100 MHz, CDCl$_3$) of compound* **41c***.*
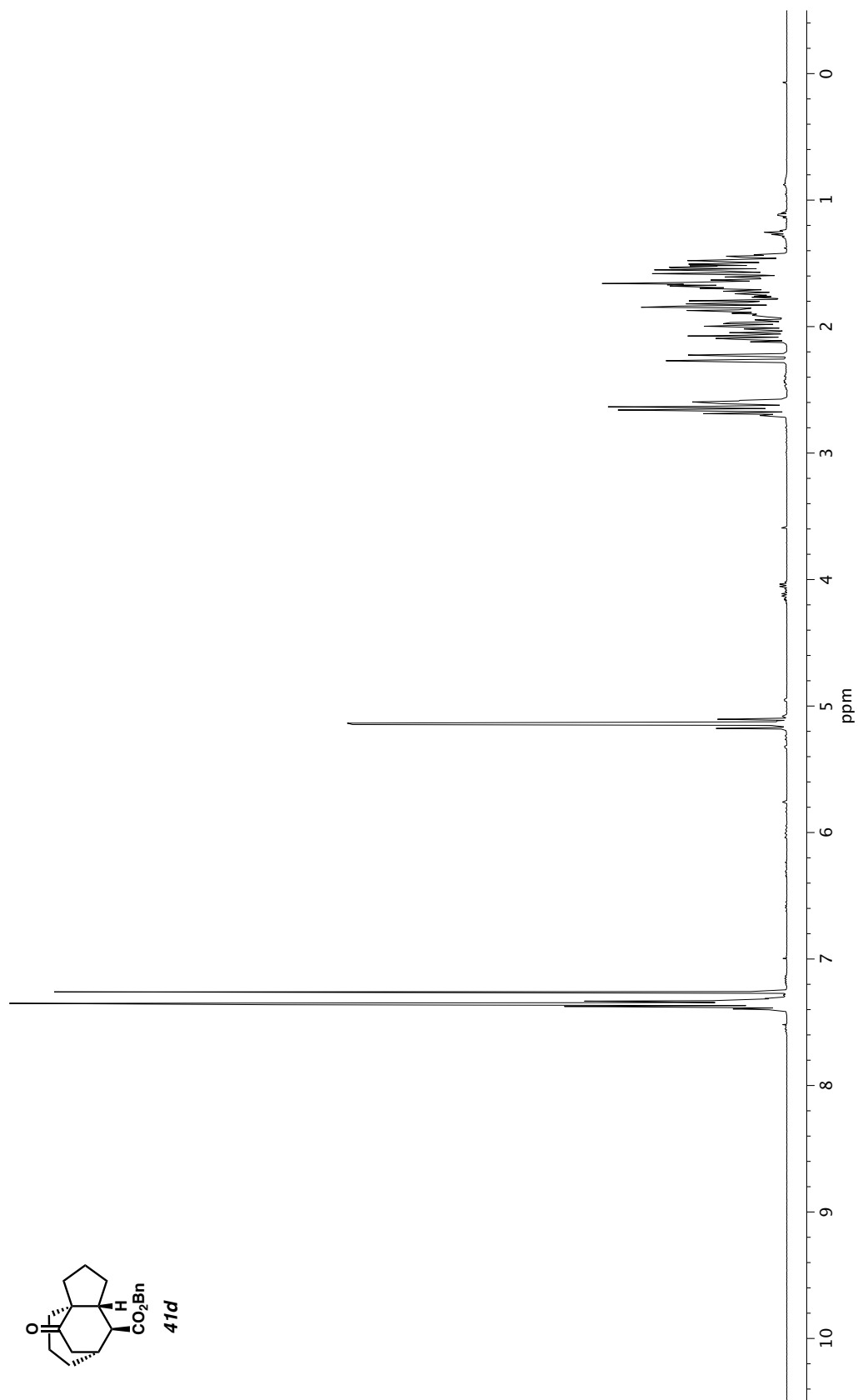
Figure A2.10. ^{1}H NMR (400 MHz, CDCl$_3$) of compound **41d**.
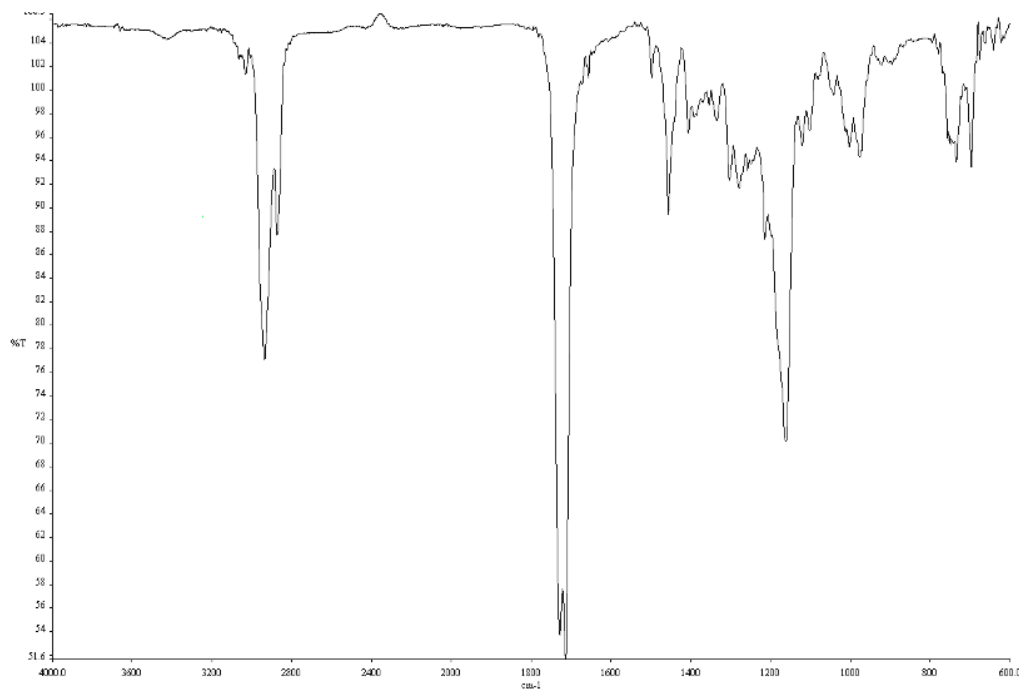
Figure A2.11. Infrared spectrum (Thin Film, NaCl) of compound **41d**.
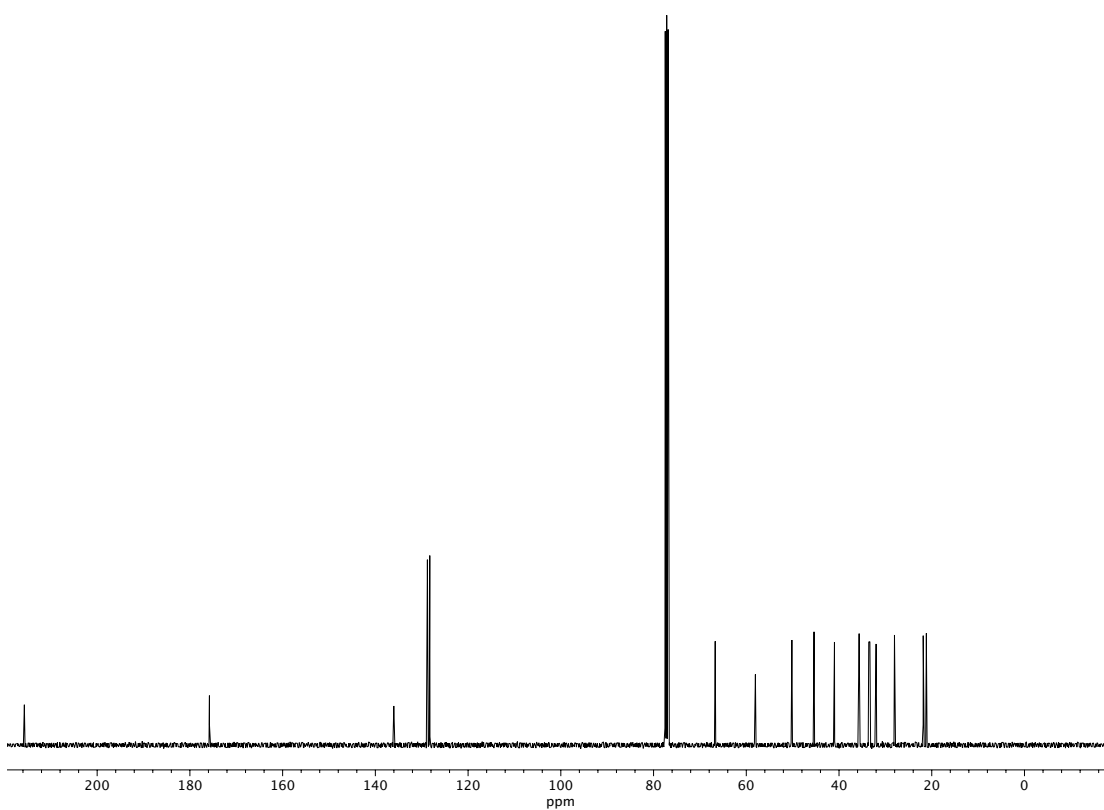
Figure A2.12. ^{13}C NMR (100 MHz, CDCl$_3$) of compound **41d**.
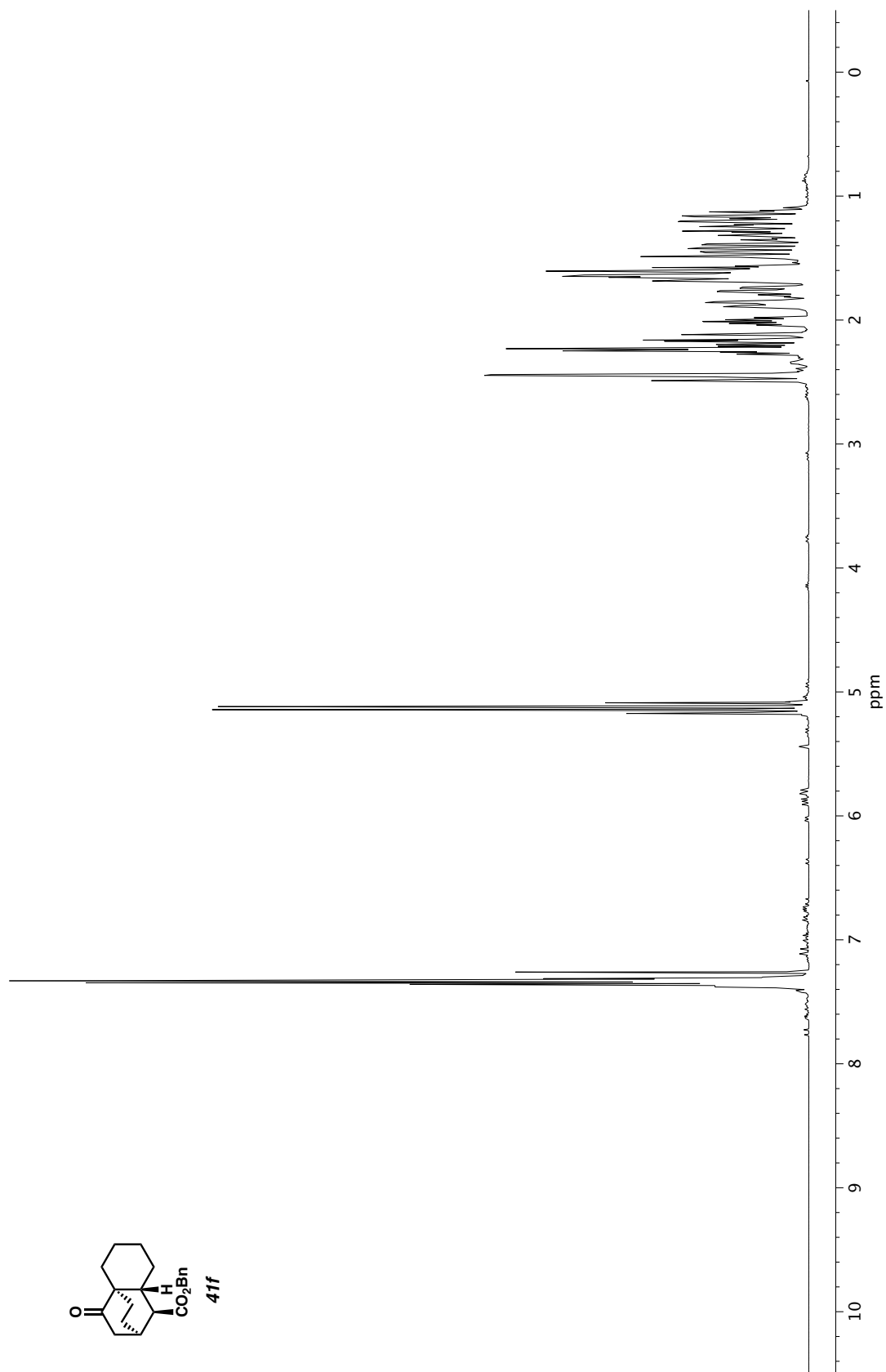
Figure A2.13. ^1H NMR (400 MHz, CDCl$_3$) of compound **41f**.
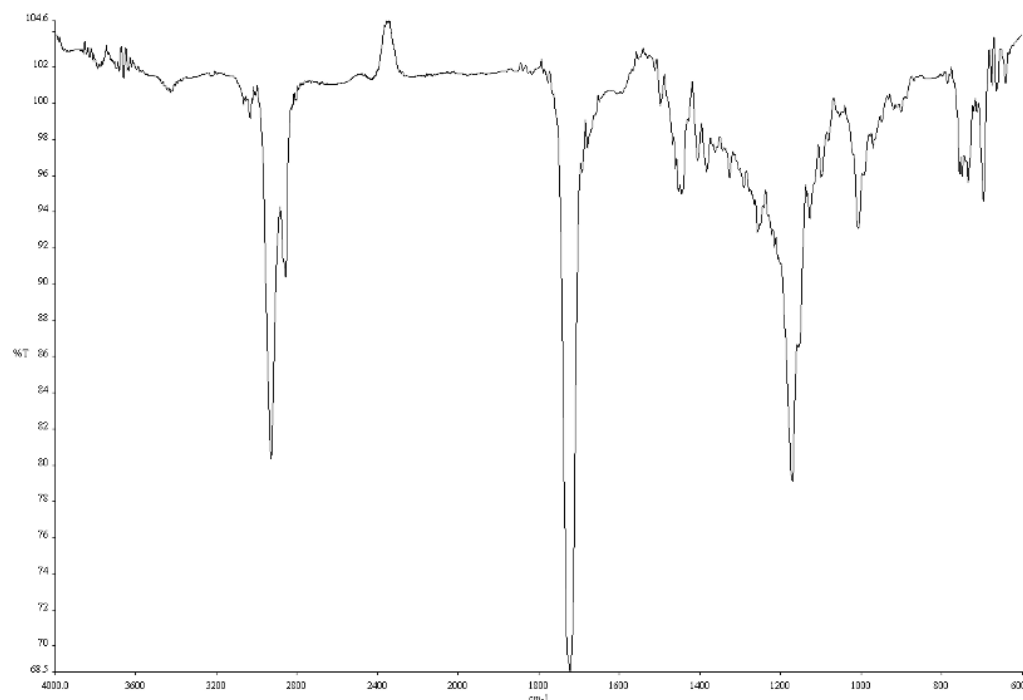
Figure A2.14. *Infrared spectrum (Thin Film, NaCl) of compound* **41f***.*
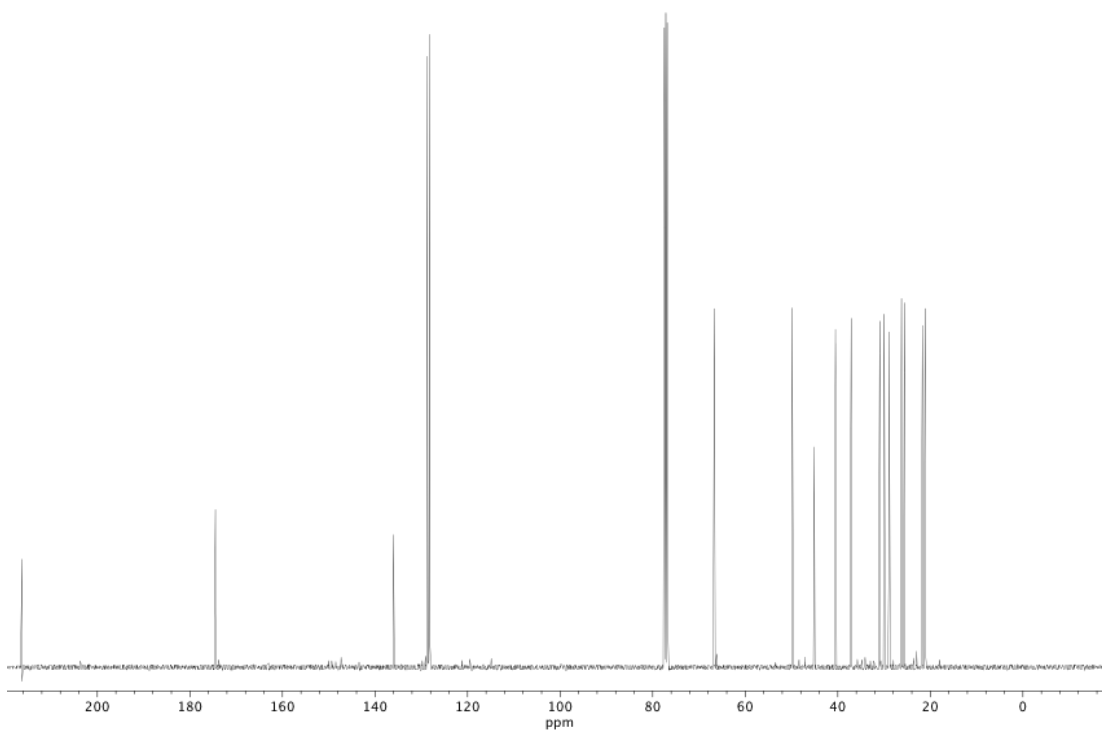
Figure A2.15. *^{13}C NMR (100 MHz, CDCl$_3$) of compound* **41f***.*
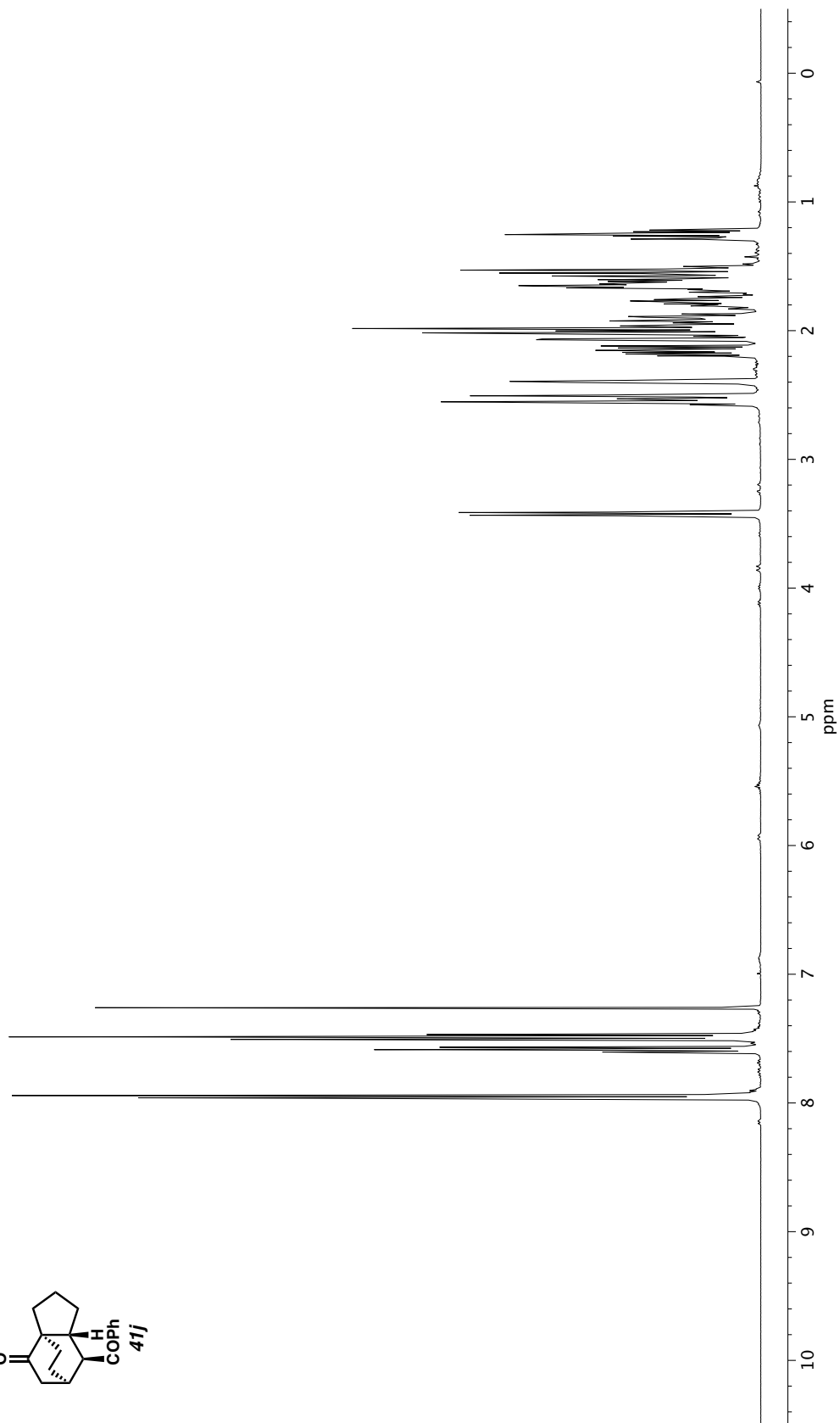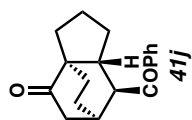
Figure A2.16. ^1H NMR (400 MHz, CDCl$_3$) of compound **41j**.
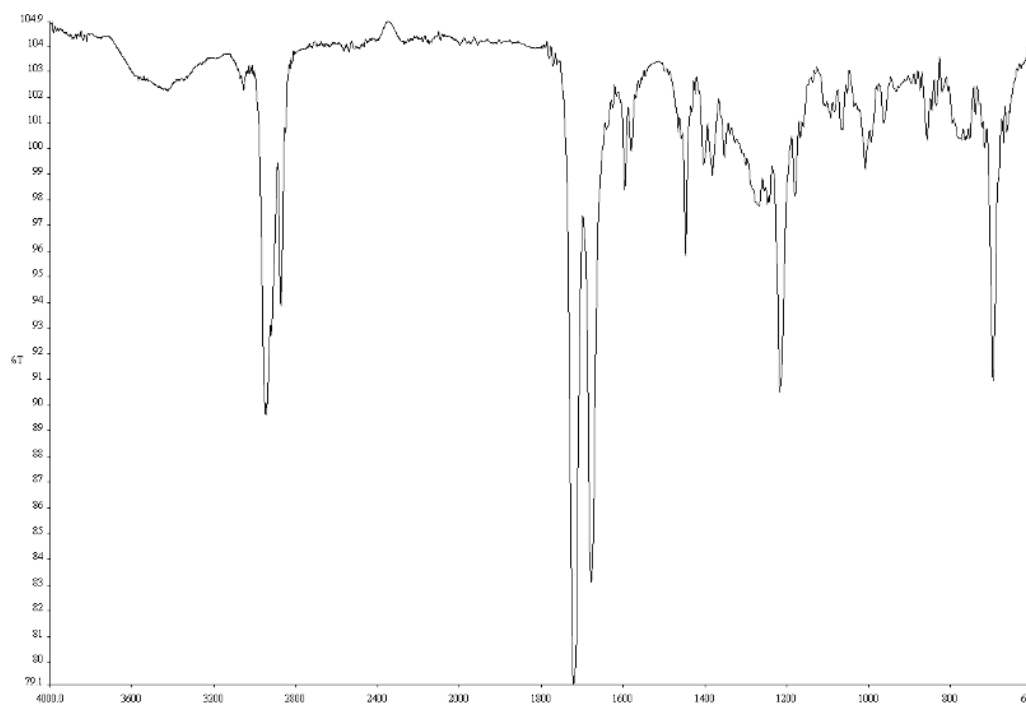
Figure A2.17. Infrared spectrum (Thin Film, NaCl) of compound **41j**.
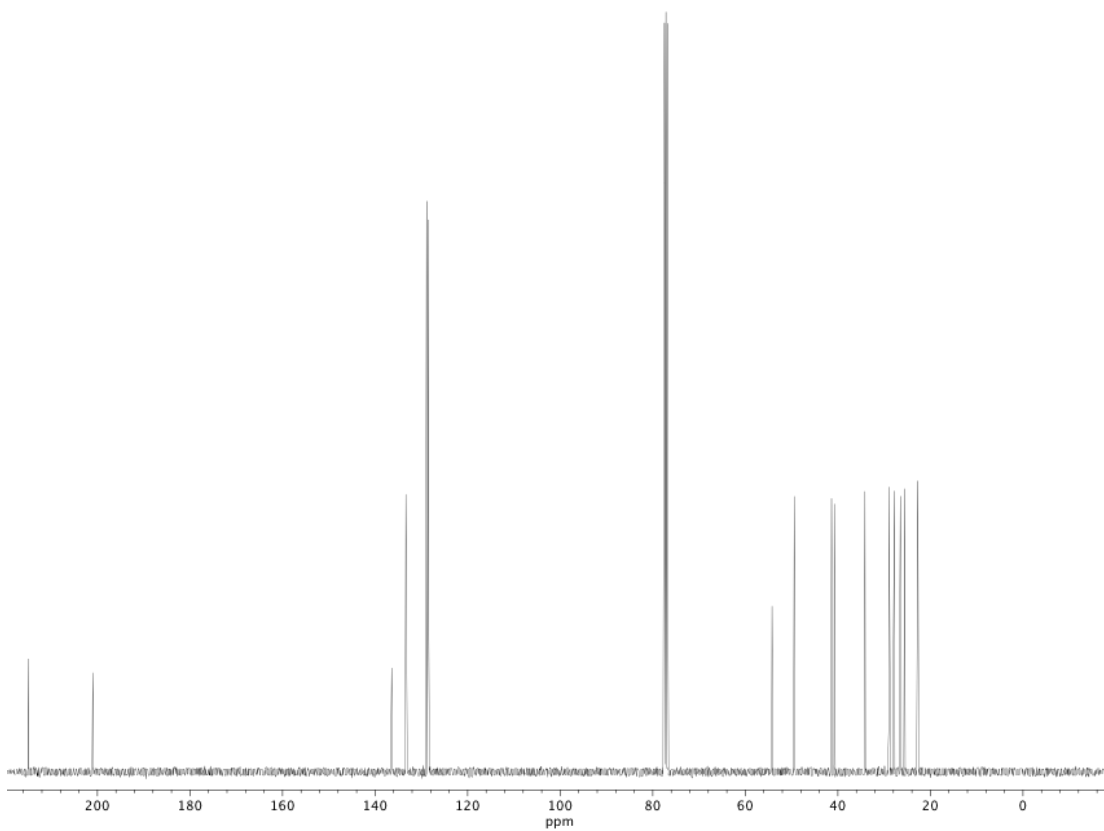
Figure A2.18. ^{13}C NMR (100 MHz, CDCl$_3$) of compound **41j**.
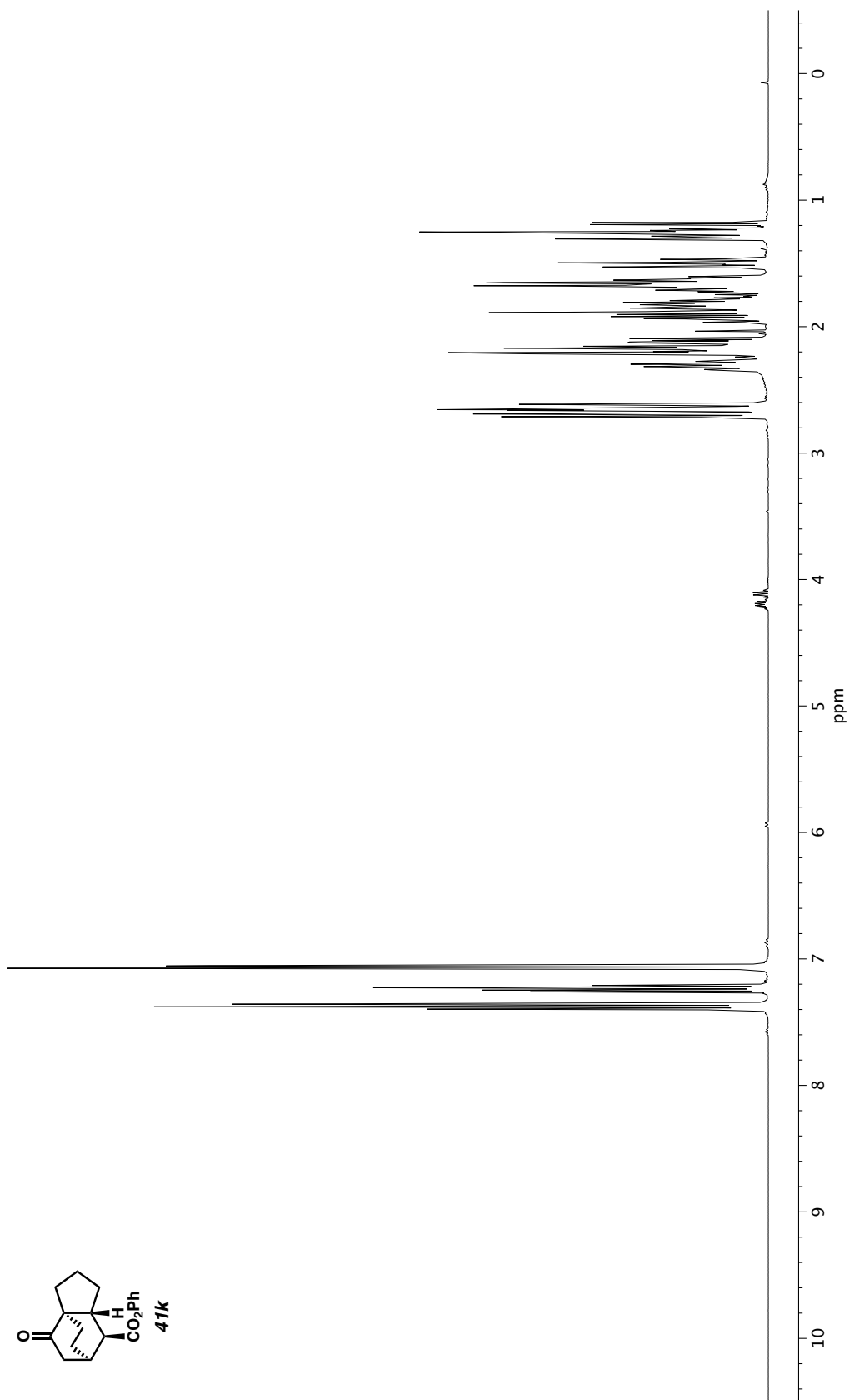
Figure A2.19. ^1H NMR (400 MHz, CDCl$_3$) of compound **41k**.
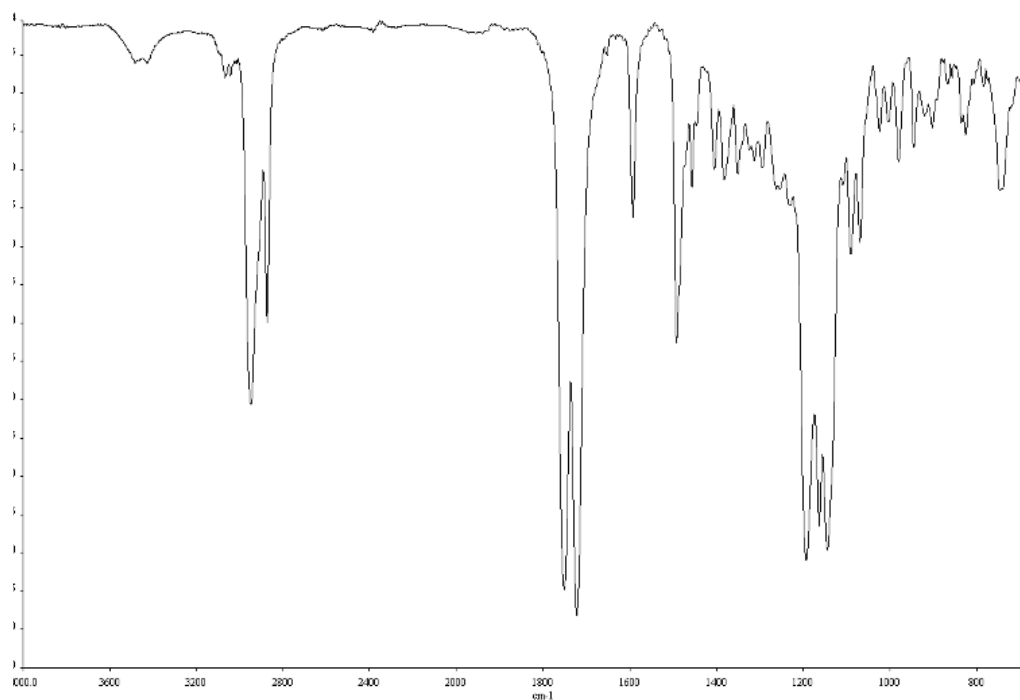
Figure A2.20. Infrared spectrum (Thin Film, NaCl) of compound **41k**.
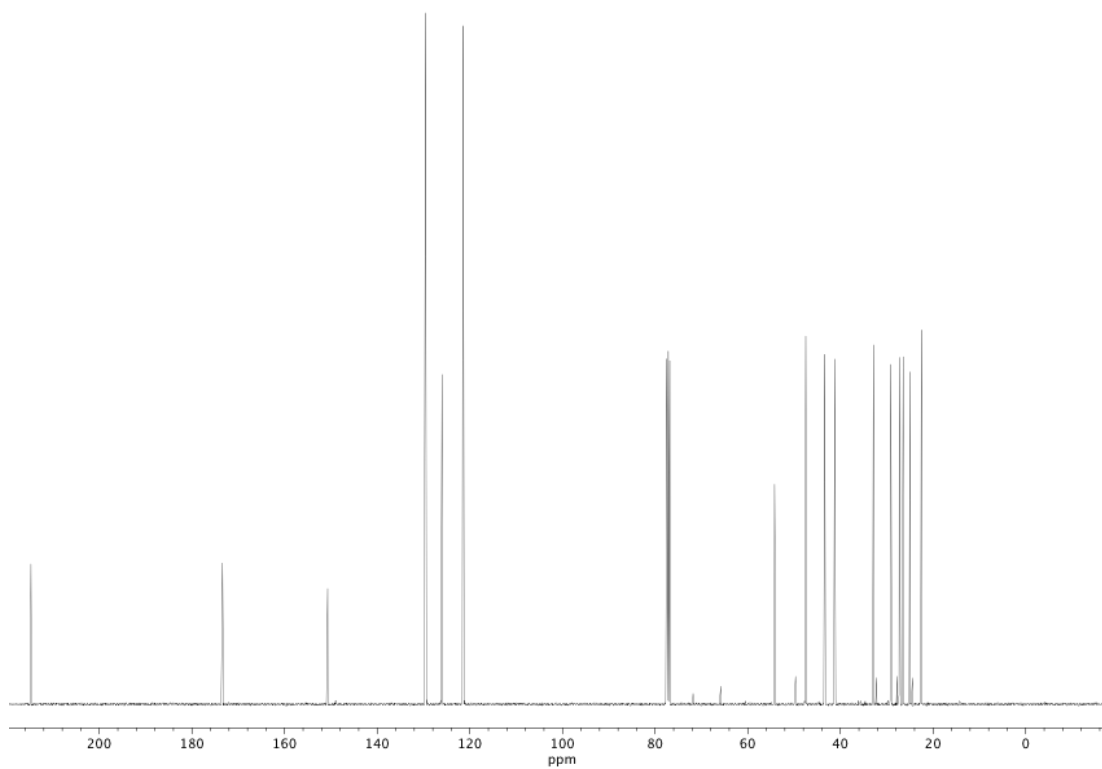
Figure A2.21. ^{13}C NMR (100 MHz, CDCl$_3$) of compound **41k**.
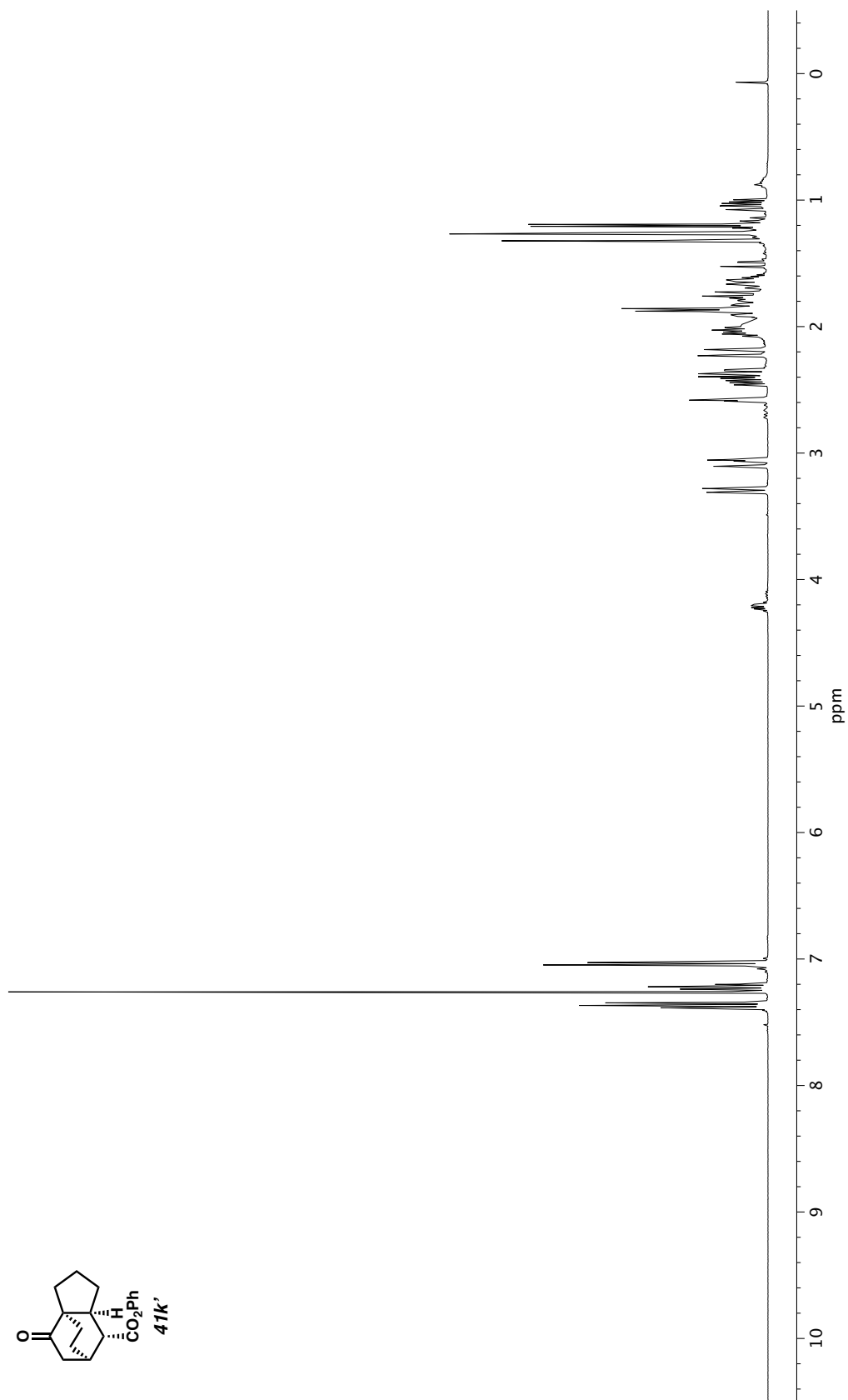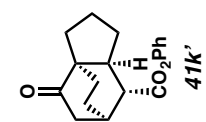
Figure A2.22. ^1H NMR (400 MHz, CDCl$_3$) of compound **41k'** .
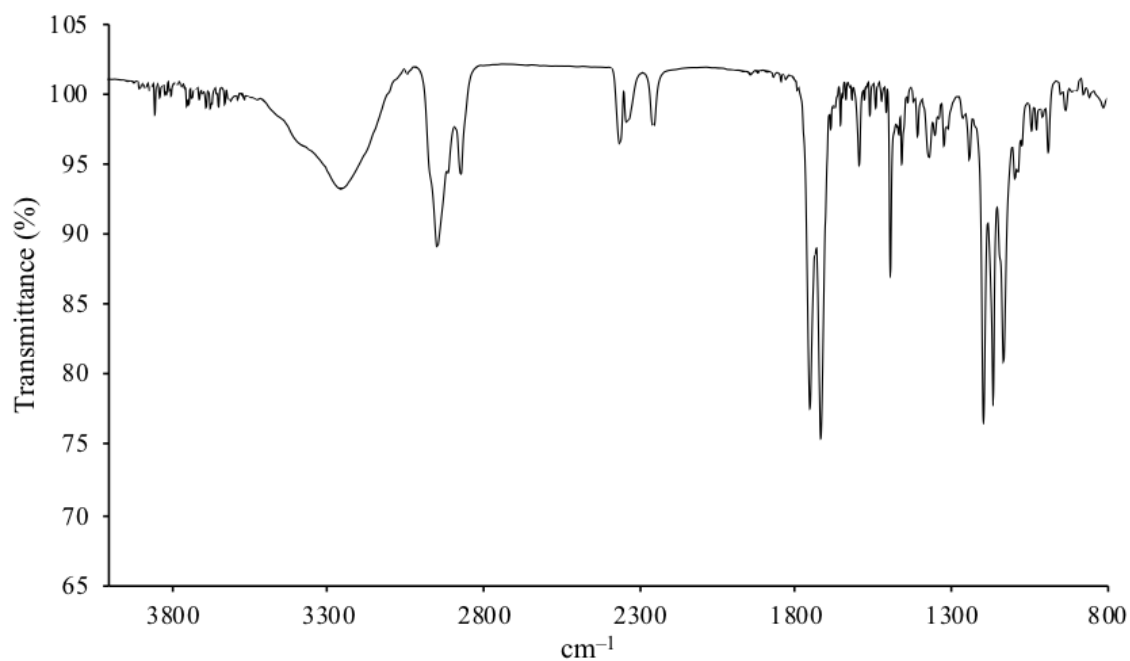
Figure A2.23. *Infrared spectrum (CDCl₃ solution) of compound **41k′**.*
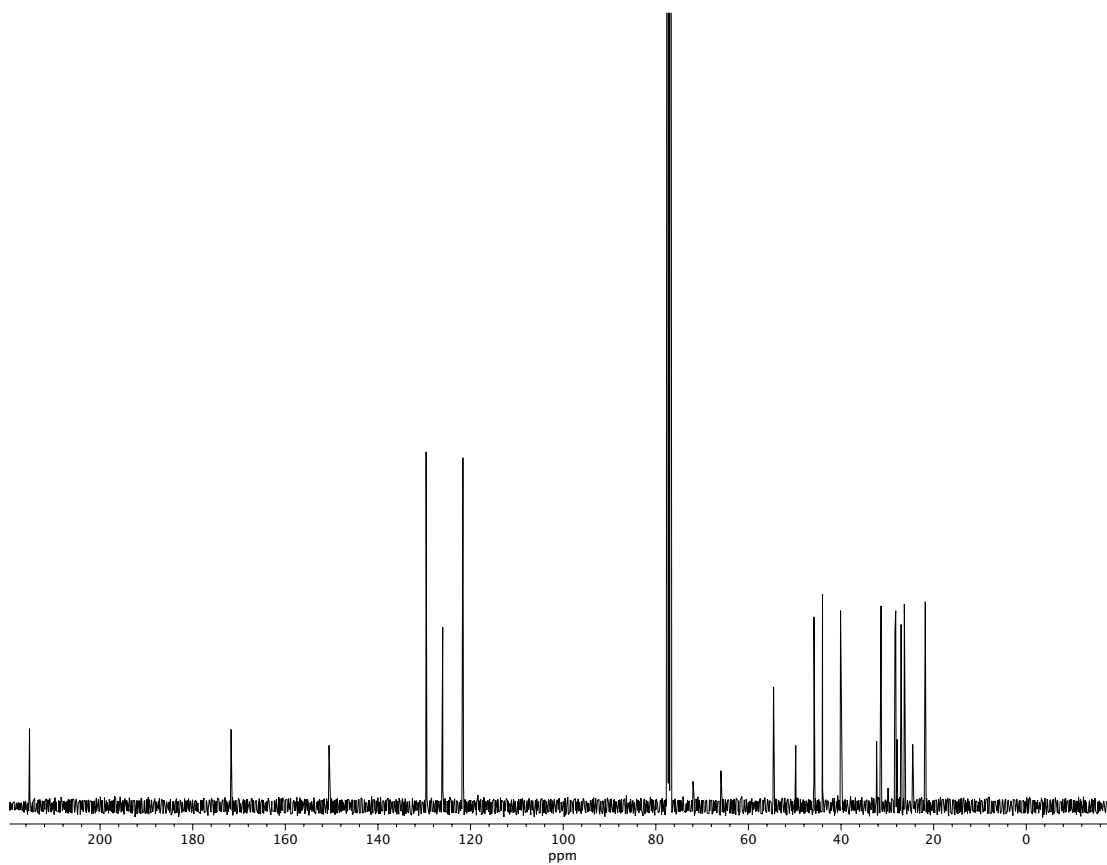
Figure A2.24. *¹³C NMR (100 MHz, CDCl₃) of compound **41k′**.*
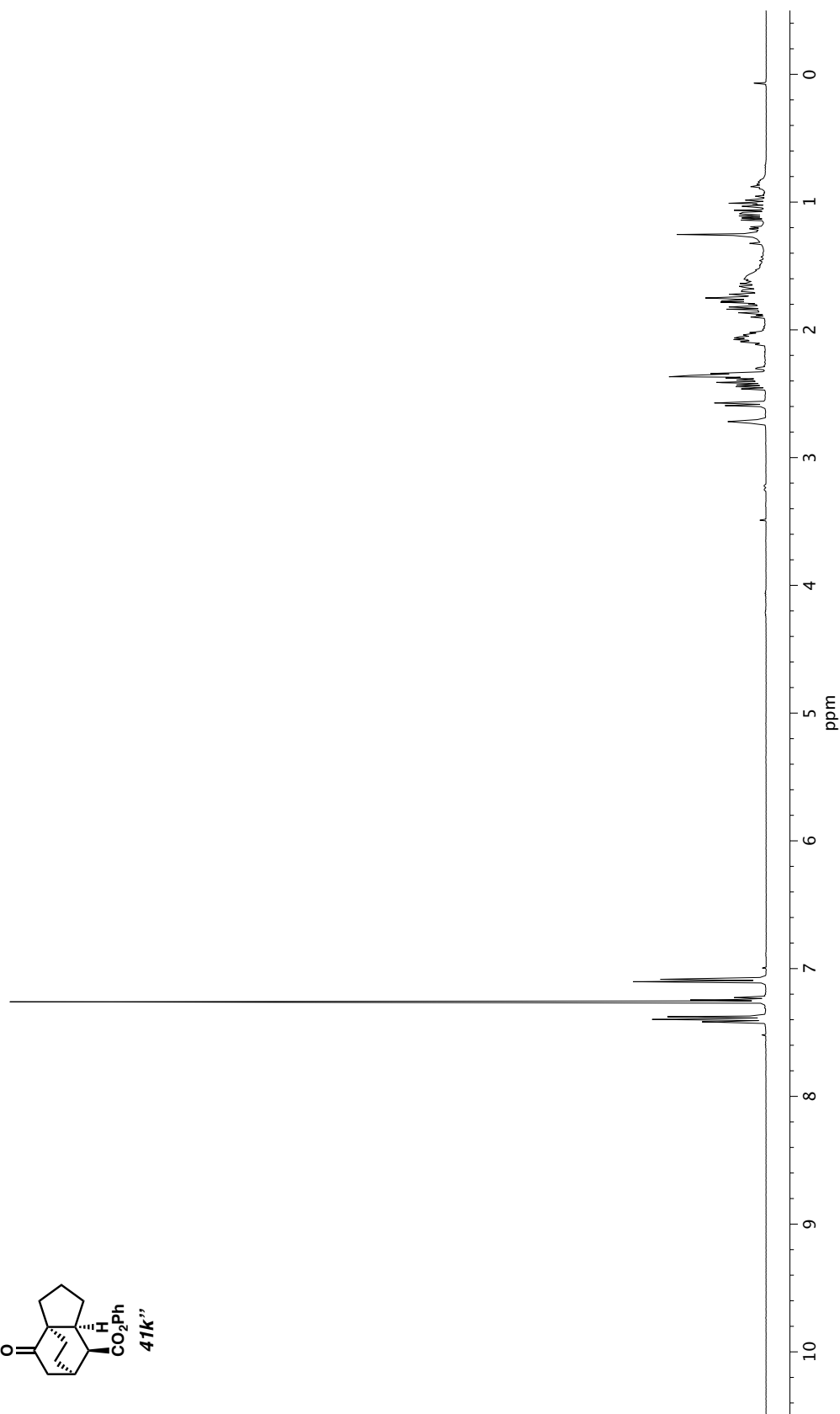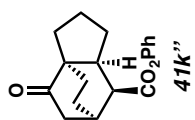
Figure A2.25. ^1H NMR (400 MHz, CDCl$_3$) of compound **41k''** .
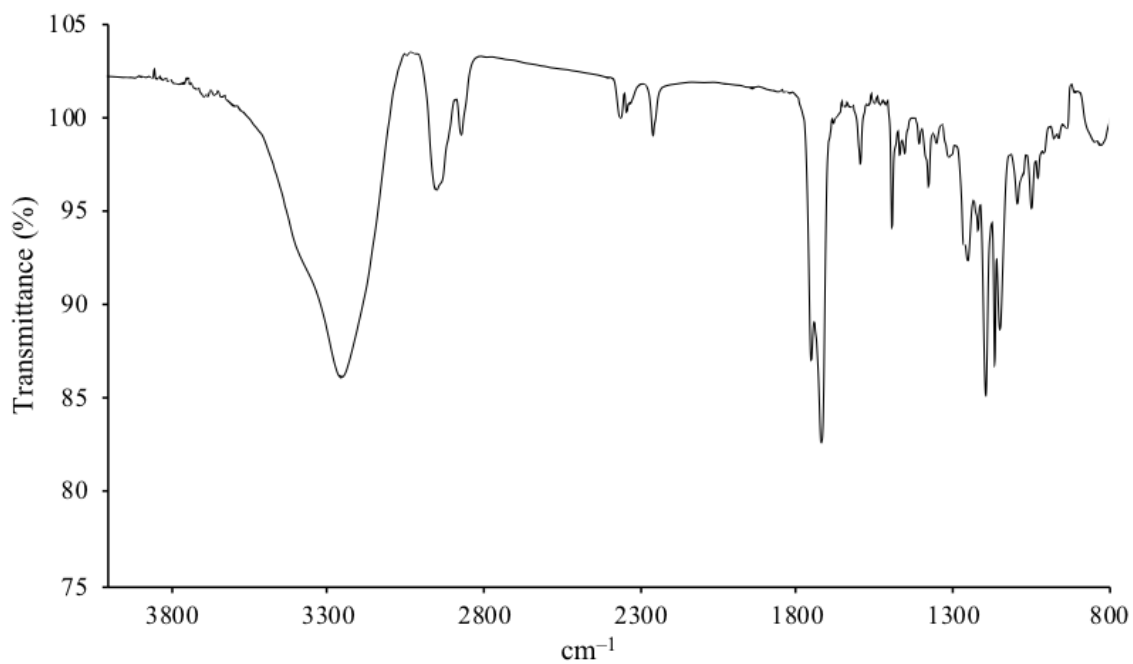
Figure A2.26. Infrared spectrum (CDCl₃ solution) of compound **41k″**.
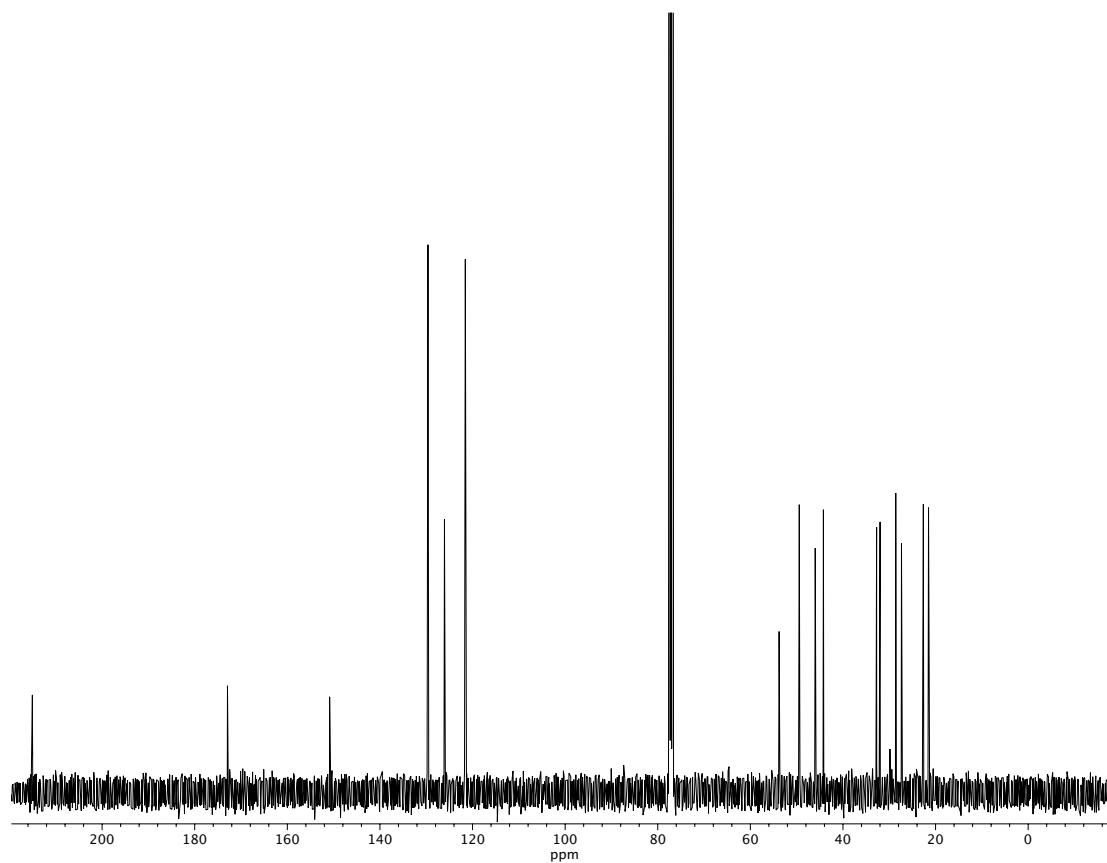
Figure A2.27. ¹³C NMR (100 MHz, CDCl₃) of compound **41k″**.
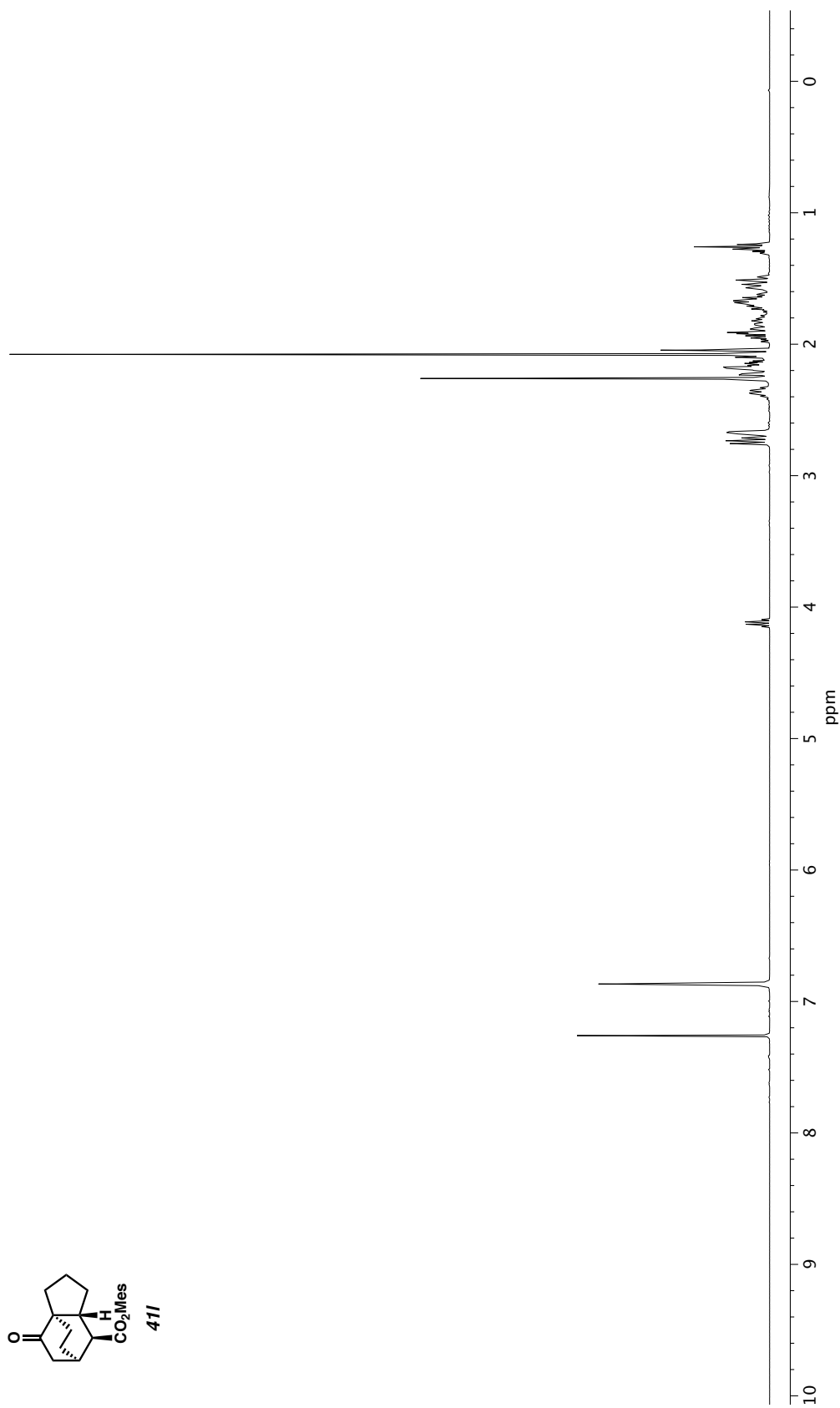
Figure A2.28. *^1H NMR (400 MHz, CDCl$_3$) of compound **41l***.
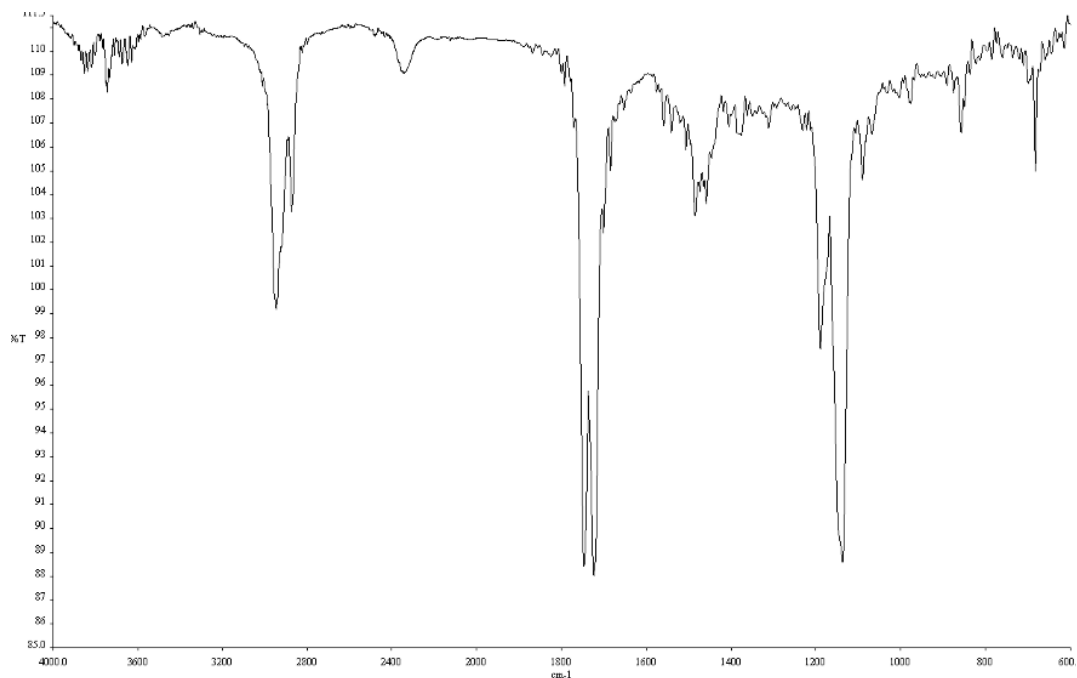
Figure A2.29. *Infrared spectrum (Thin Film, NaCl) of compound **41l**.*
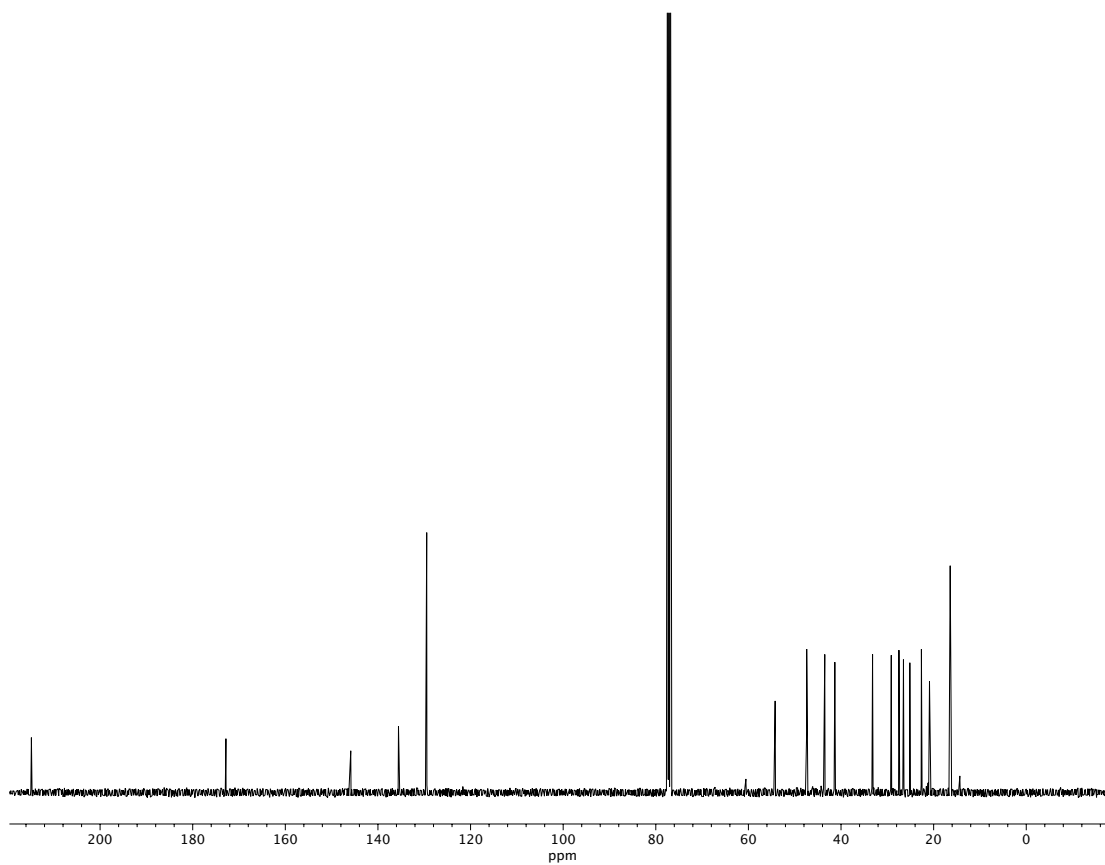
Figure A2.30. *^{13}C NMR (100 MHz, CDCl$_3$) of compound **41l**.*
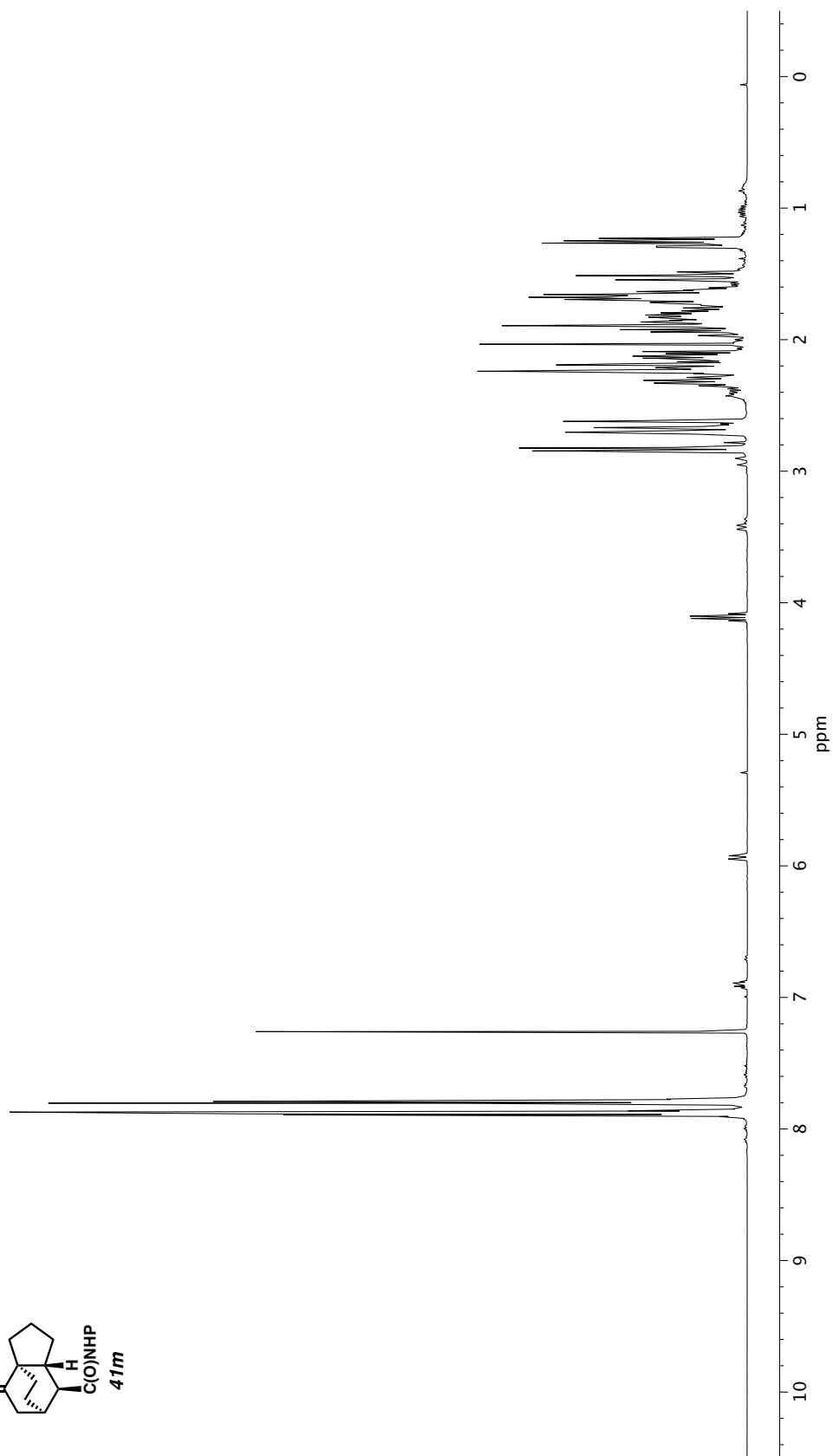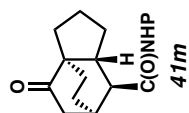
Figure A2.31. ^1H NMR (400 MHz, CDCl$_3$) of compound **41m**.
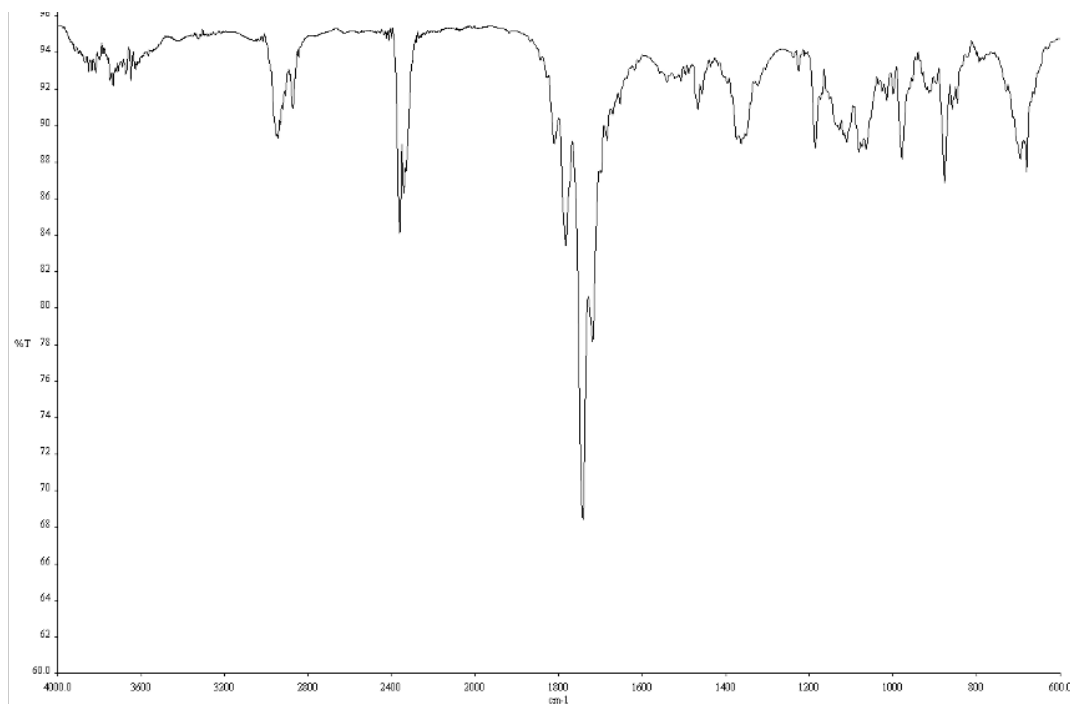
Figure A2.32. Infrared spectrum (Thin Film, NaCl) of compound **41m**.
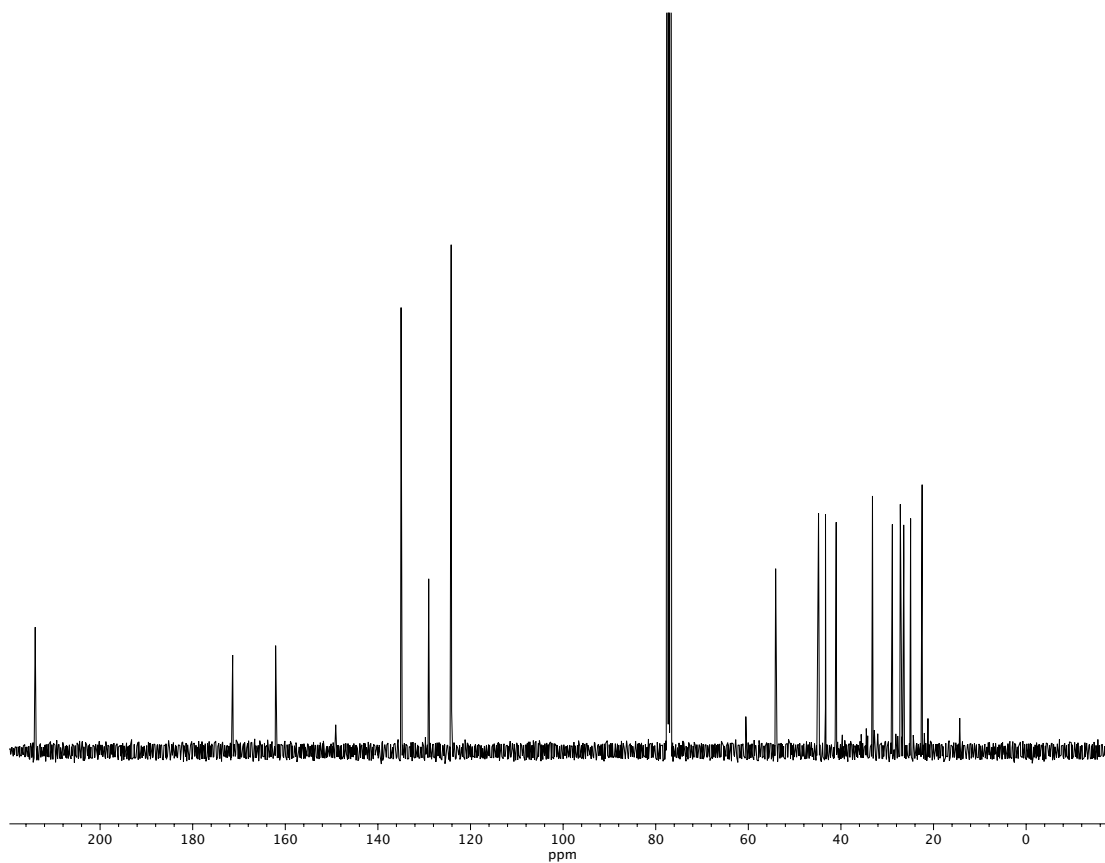
Figure A2.33. ^{13}C NMR (100 MHz, CDCl$_3$) of compound **41m**.

Figure A2.34. ^1H NMR (400 MHz, CDCl$_3$) of compound **41m'** .
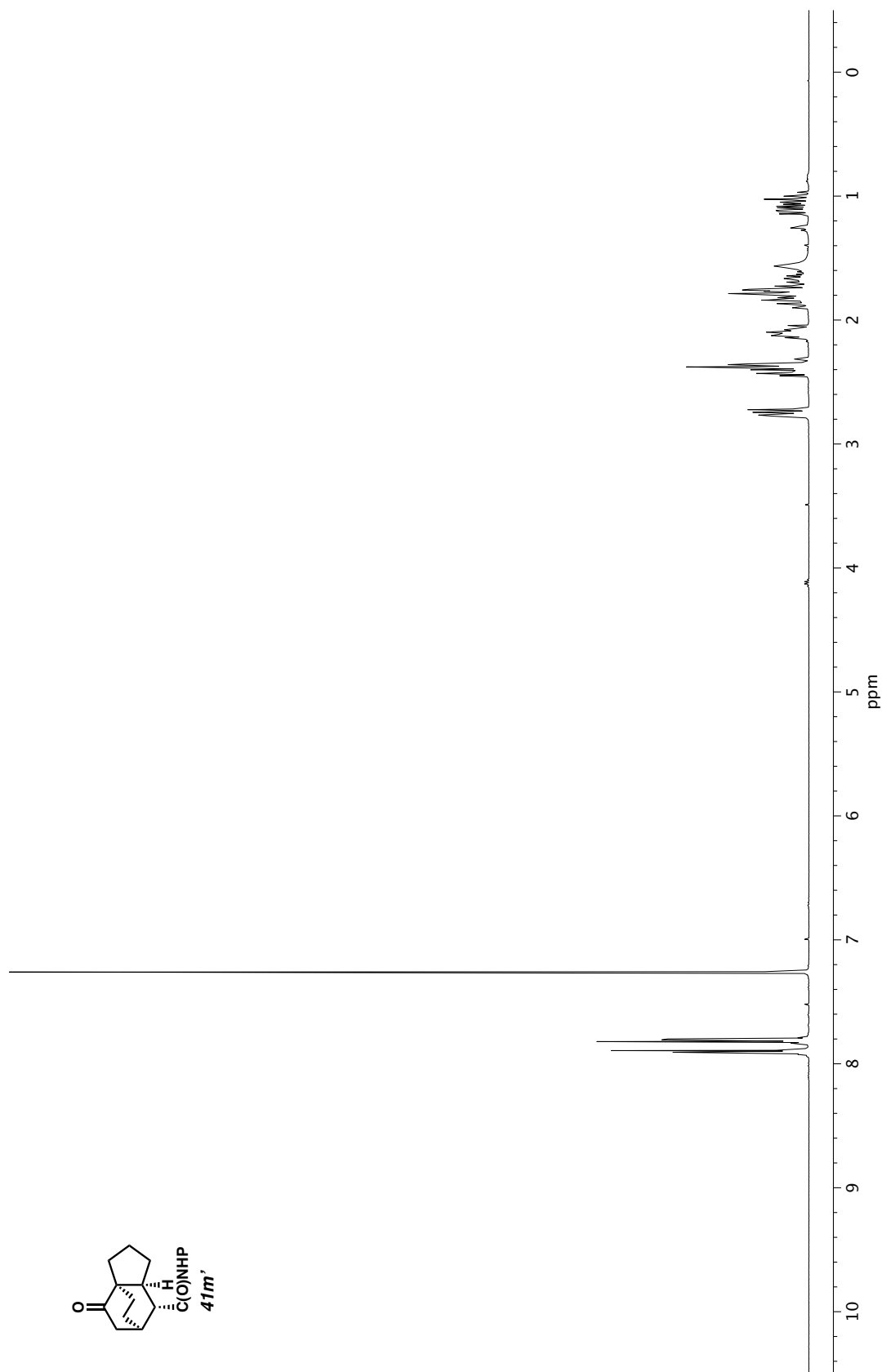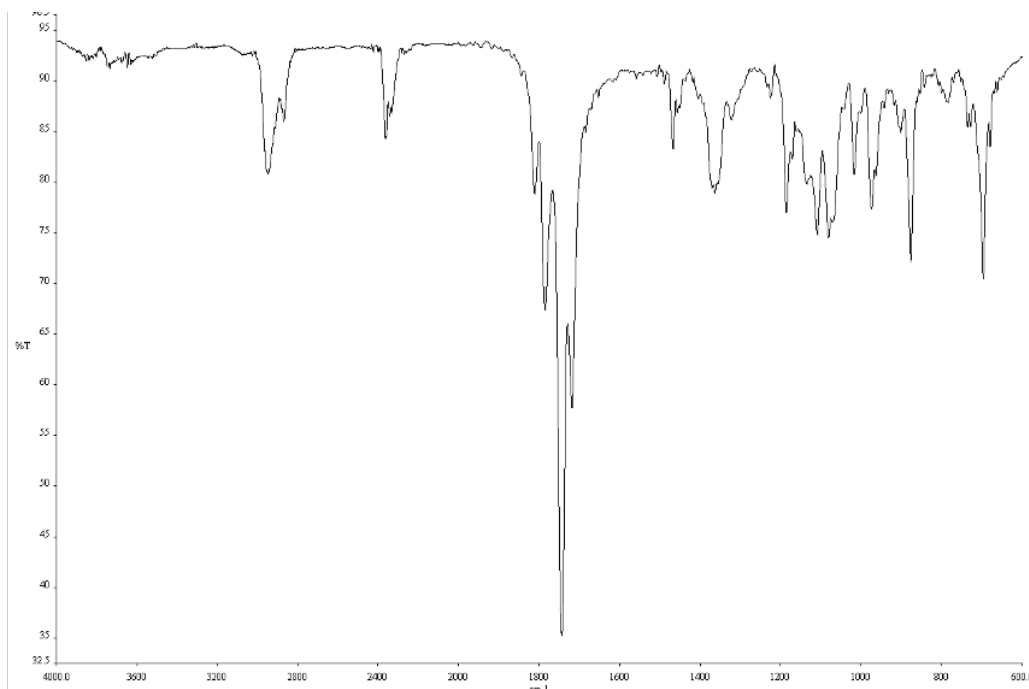
Figure A2.35. *Infrared spectrum (Thin Film, NaCl) of compound **41m'**.*
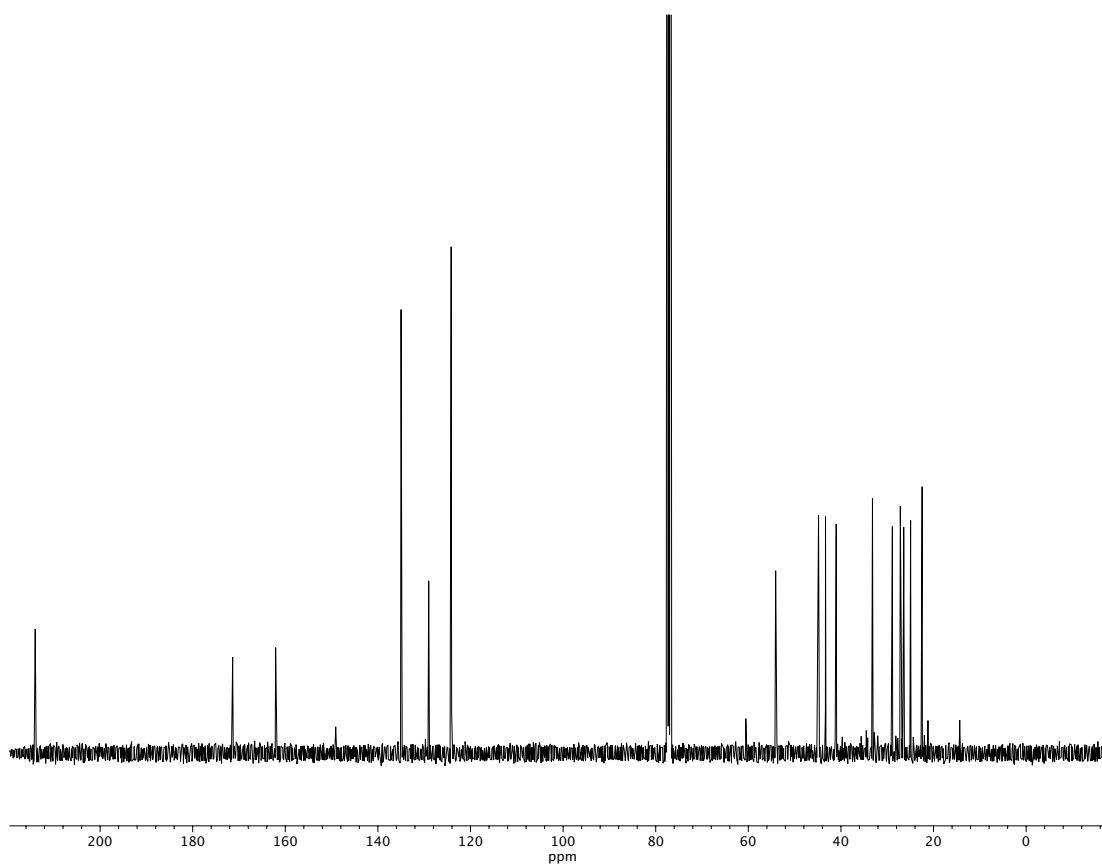
Figure A2.36. *^{13}C NMR (100 MHz, CDCl$_3$) of compound **41m'**.*
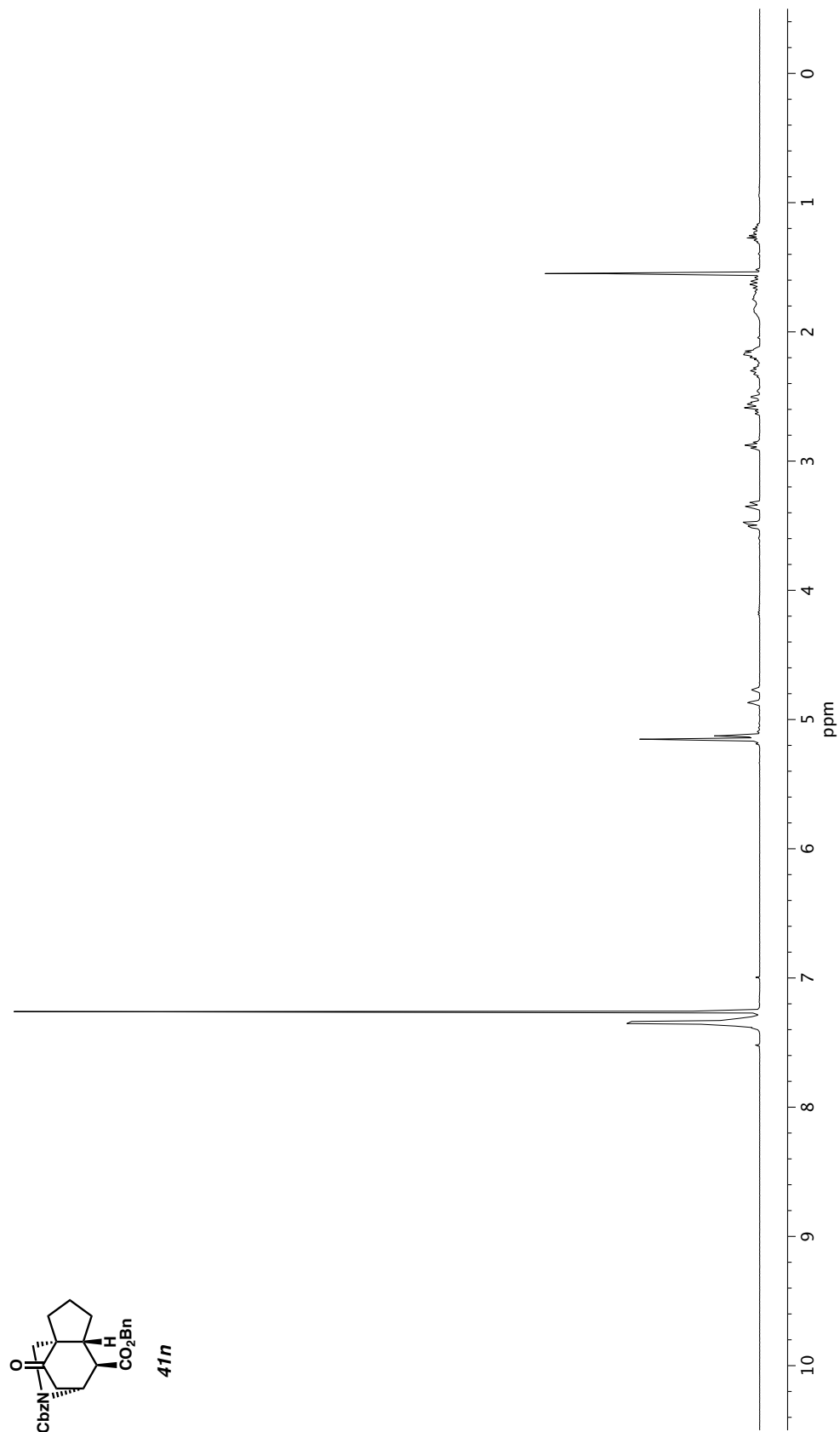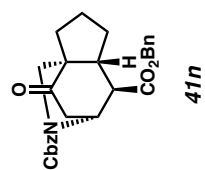
Figure A2.37. ^1H NMR (400 MHz, CDCl$_3$) of compound **41n**.
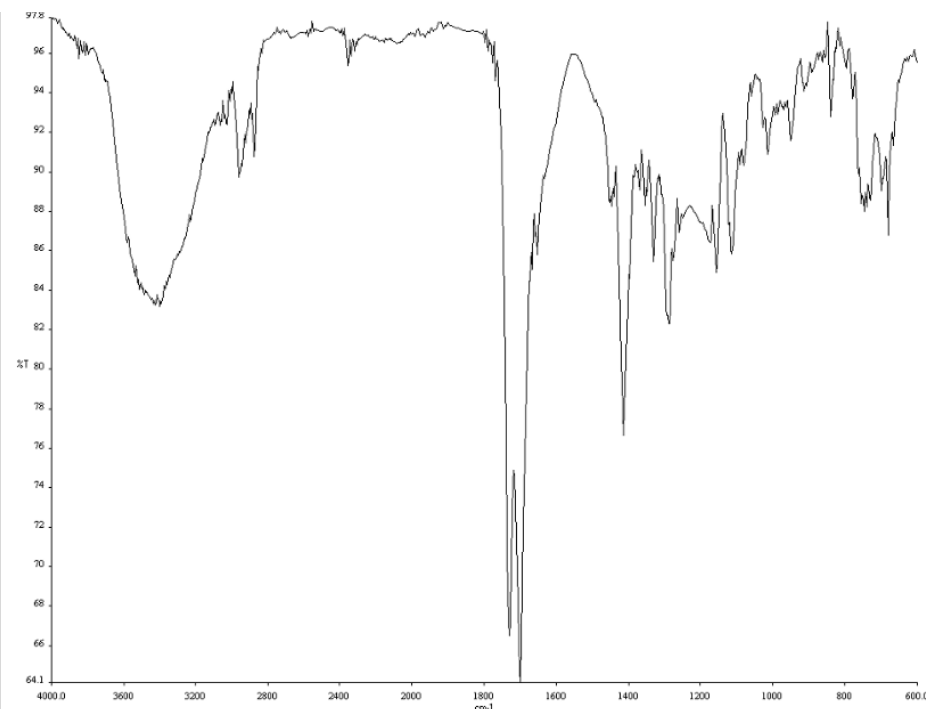
Figure A2.38. Infrared spectrum (Thin Film, NaCl) of compound **41n**.
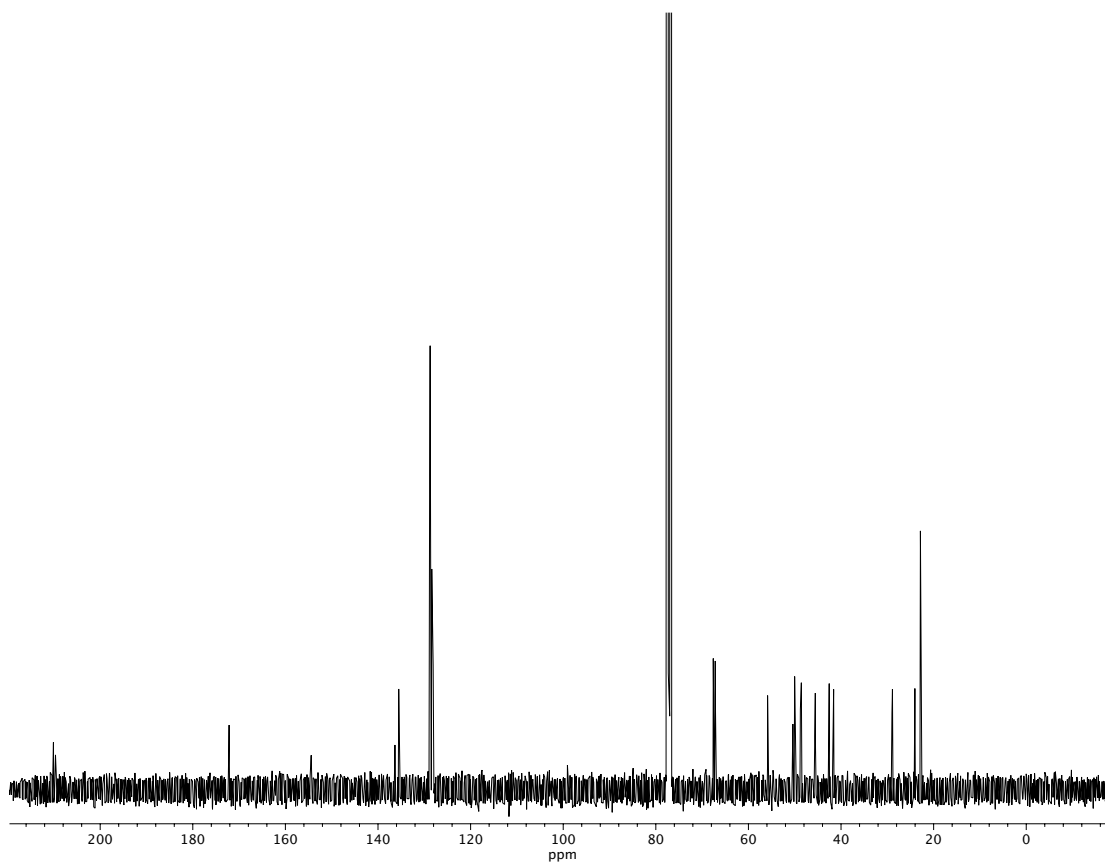
Figure A2.39. ^{13}C NMR (100 MHz, CDCl$_3$) of compound **41n**.
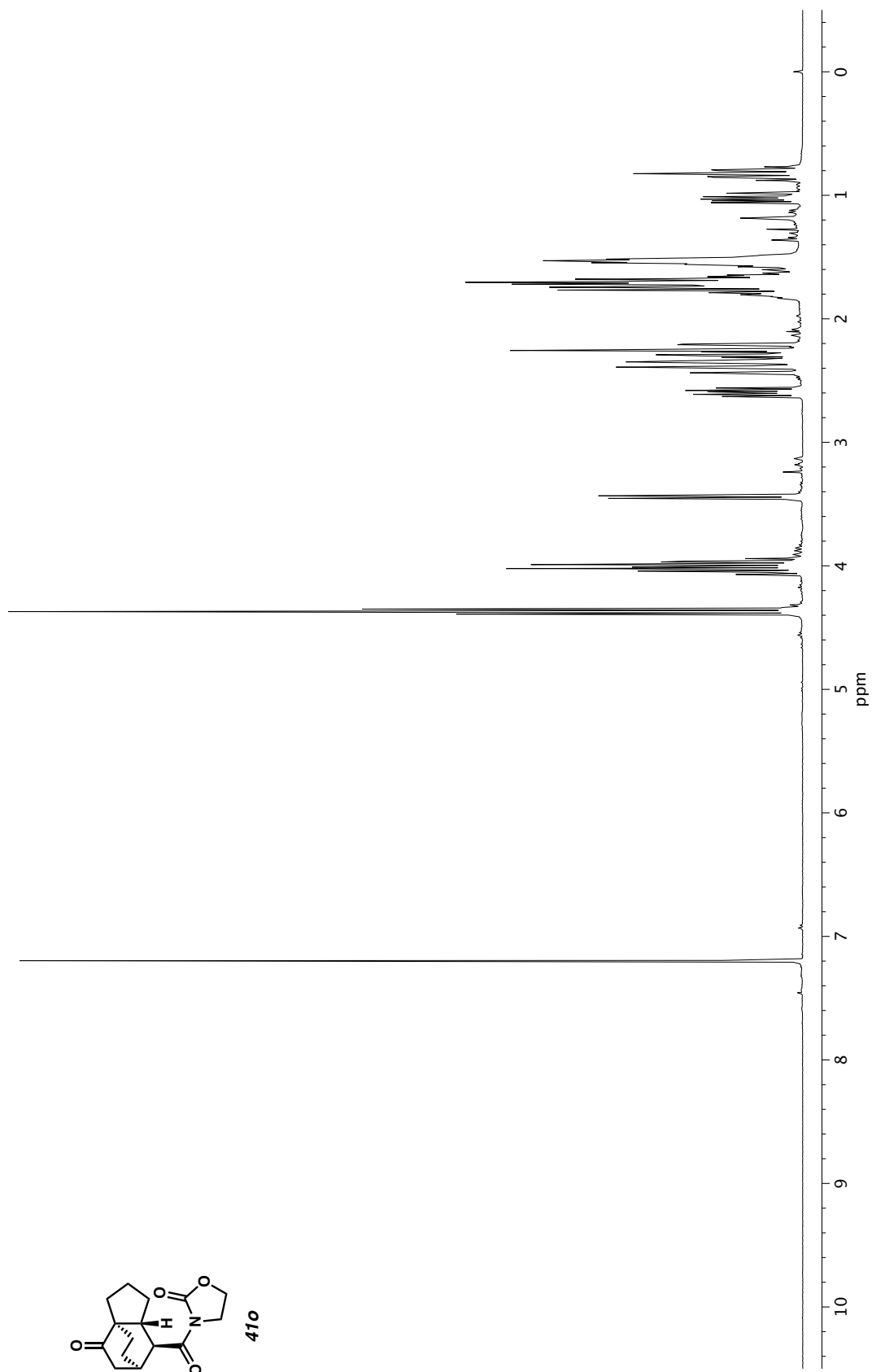
Figure A2.40. *^{1}H NMR (400 MHz, CDCl$_3$) of compound **41o**.*

41o
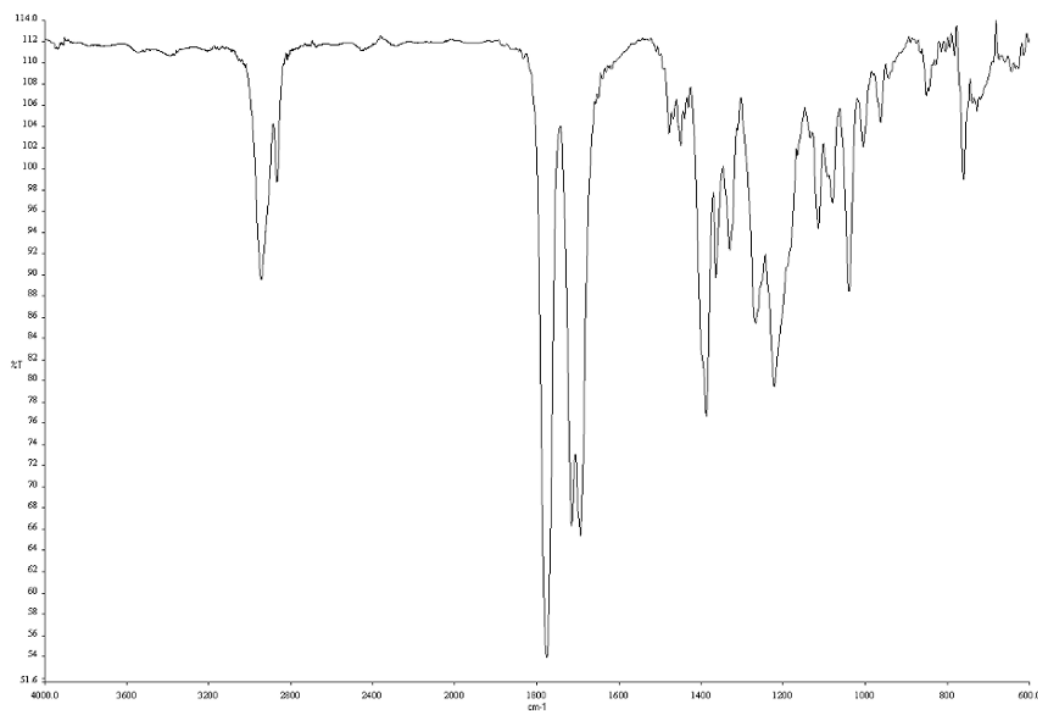
Figure A2.41. Infrared spectrum (Thin Film, NaCl) of compound **41o**.
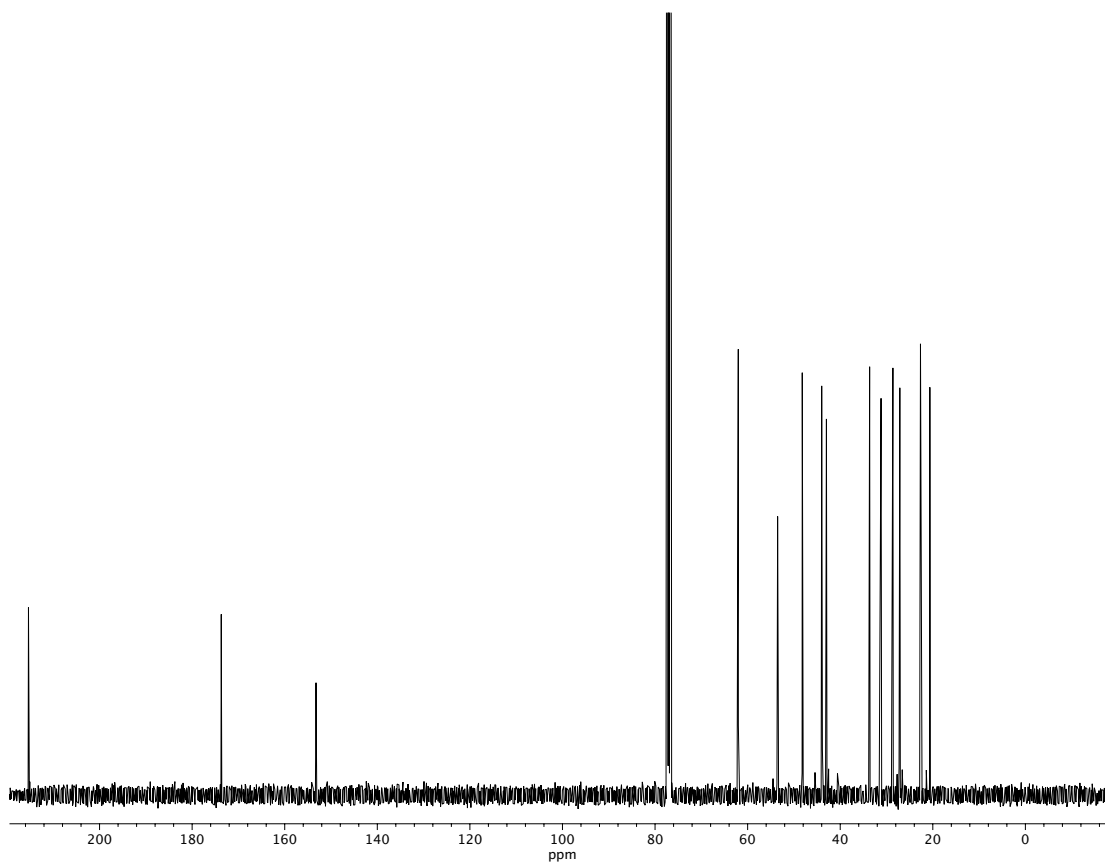
Figure A2.42. ^{13}C NMR (100 MHz, CDCl$_3$) of compound **41o**.
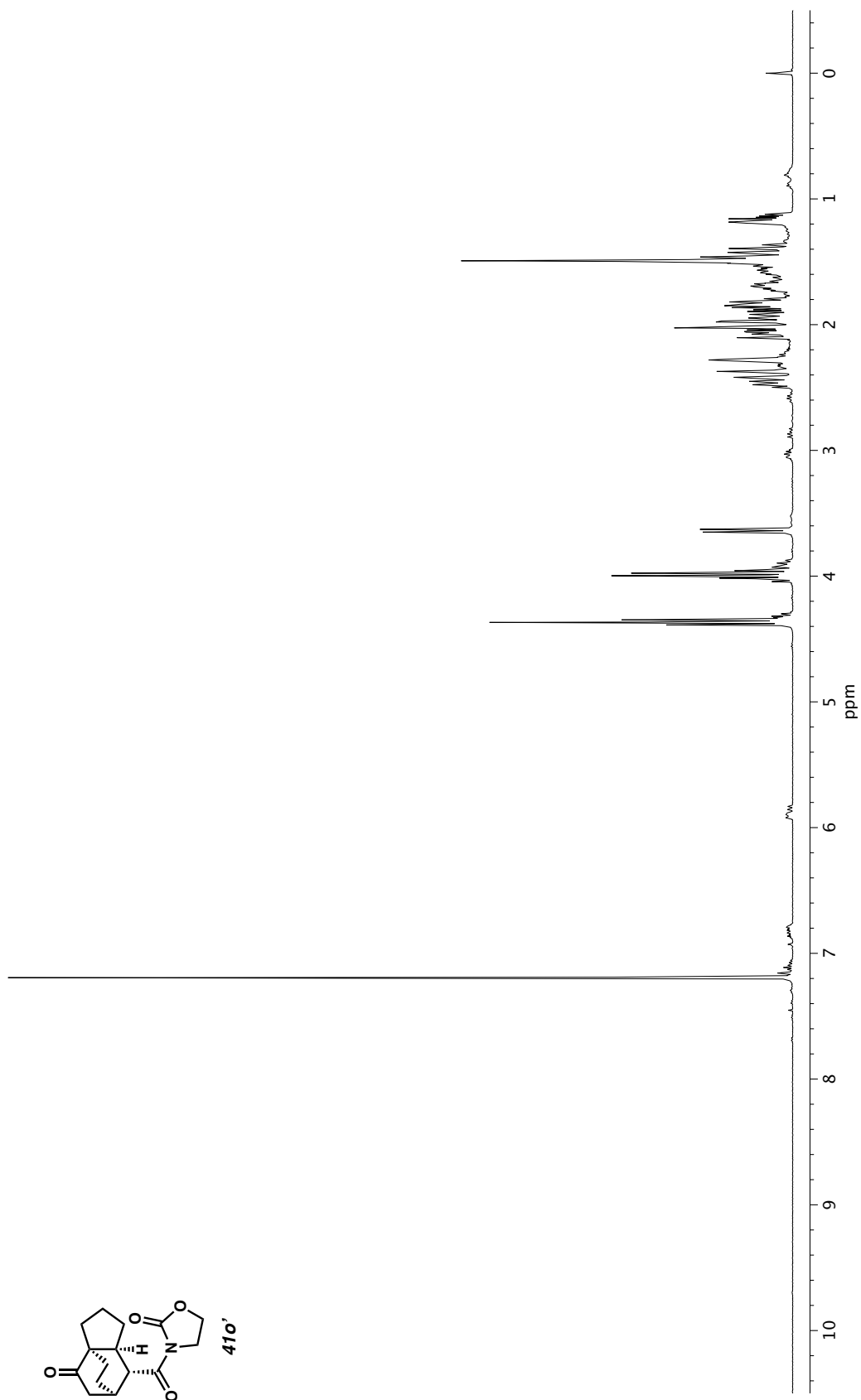
Figure A2.43. ^{1}H NMR (400 MHz, CDCl$_3$) of compound **41o'** .
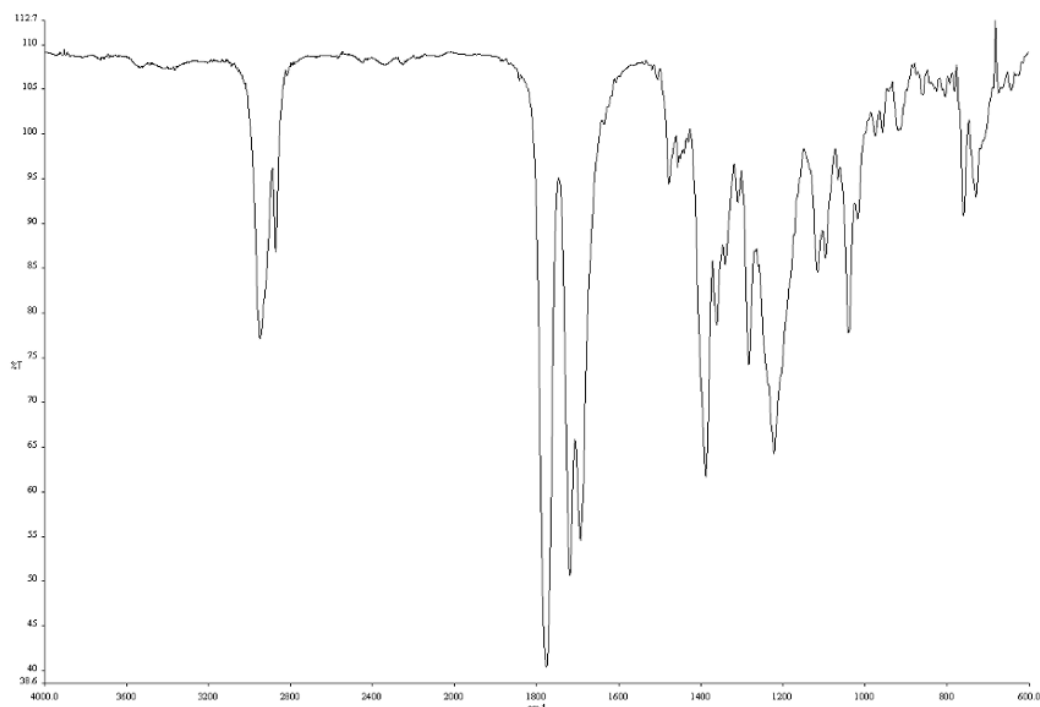
Figure A2.44. Infrared spectrum (Thin Film, NaCl) of compound **41o'**.
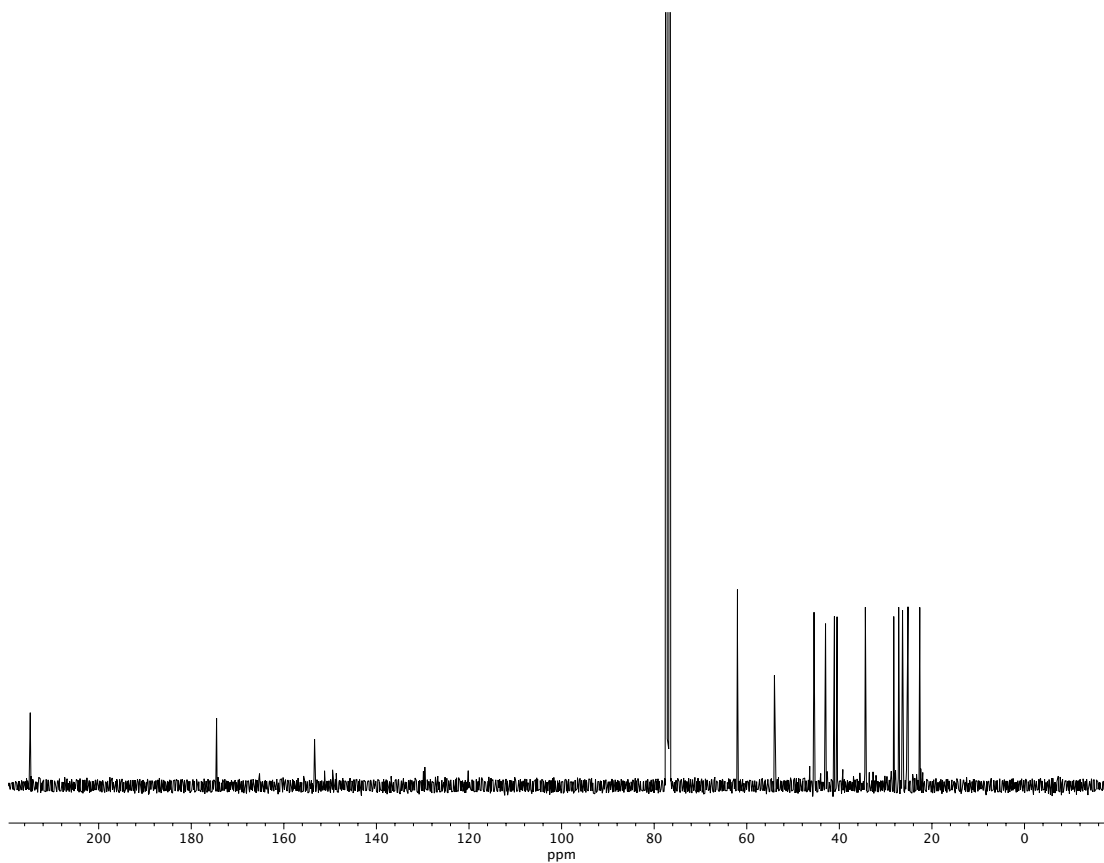
Figure A2.45. ^{13}C NMR (100 MHz, CDCl$_3$) of compound **41o'**.
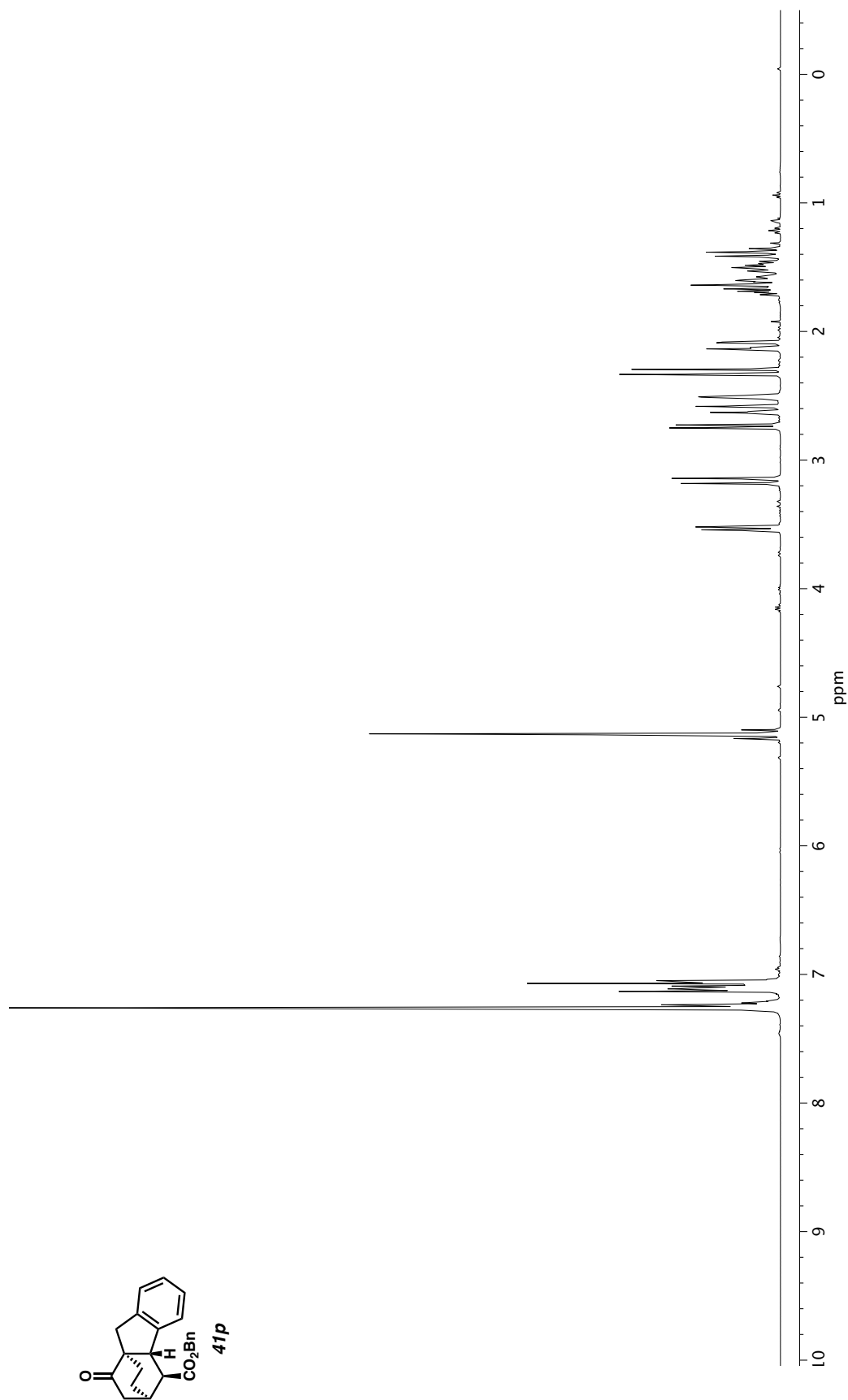
Figure A2.46. *^{1}H NMR (400 MHz, CDCl$_3$) of compound **41p**.*
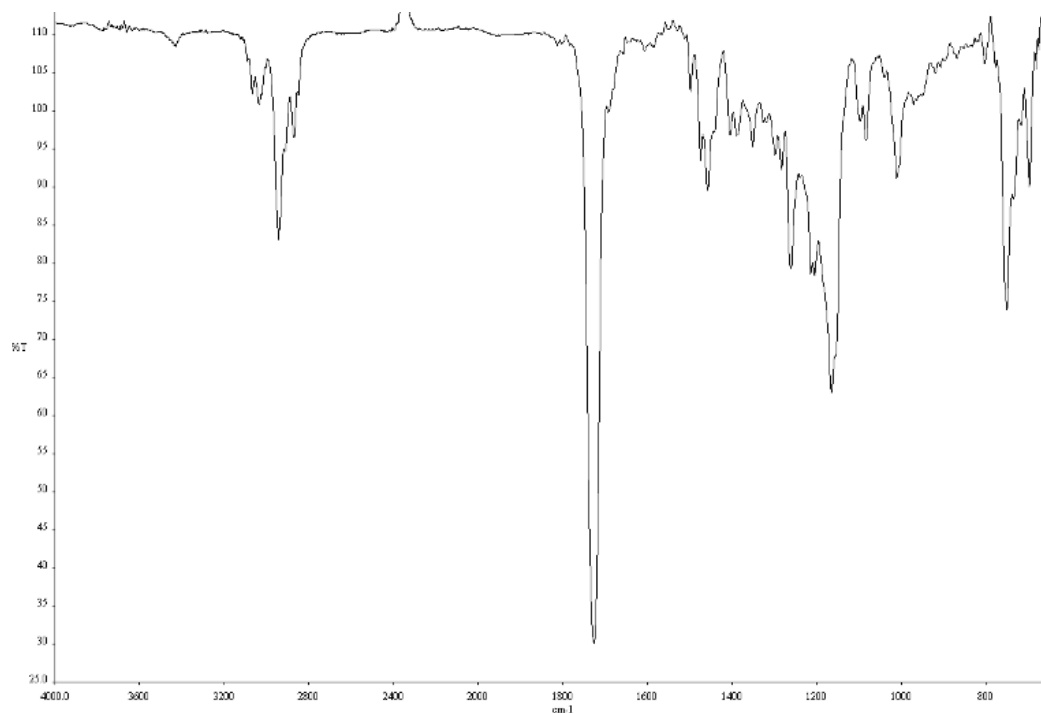
Figure A2.47. Infrared spectrum (Thin Film, NaCl) of compound **41p**.
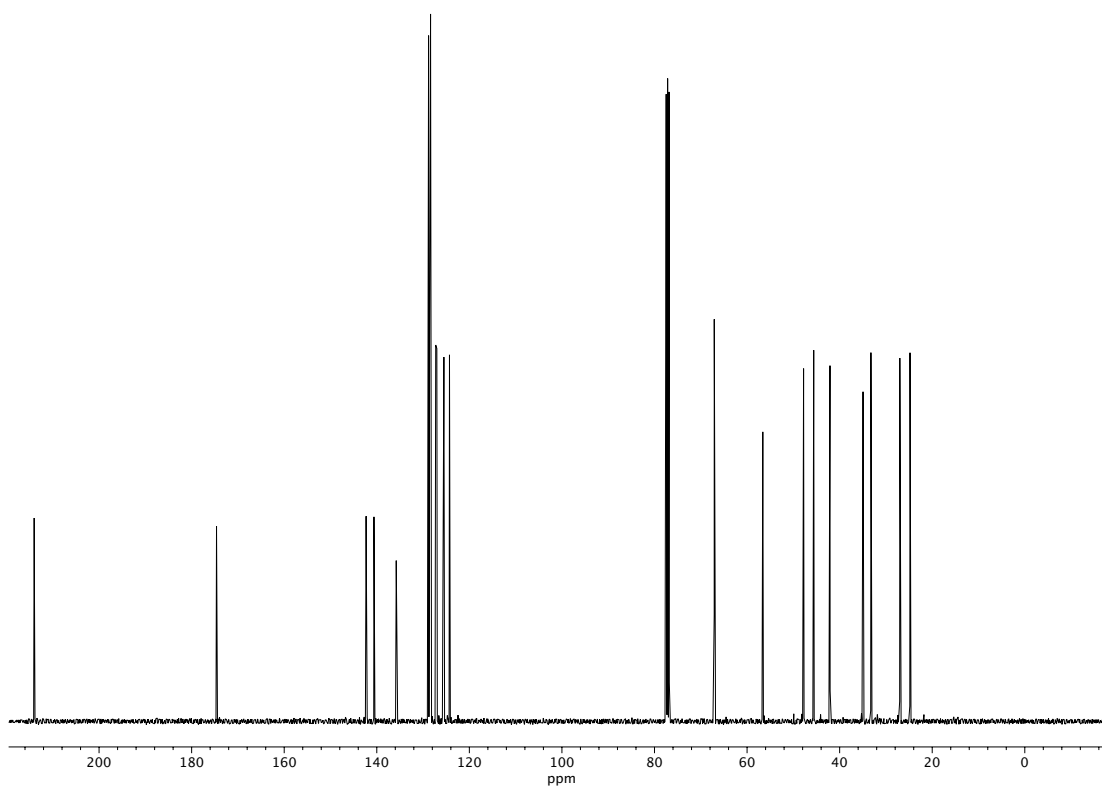
Figure A2.48. ^{13}C NMR (100 MHz, CDCl$_3$) of compound **41p**.

Figure A2.49. ^1H NMR (400 MHz, CDCl$_3$) of compound **41p'** .
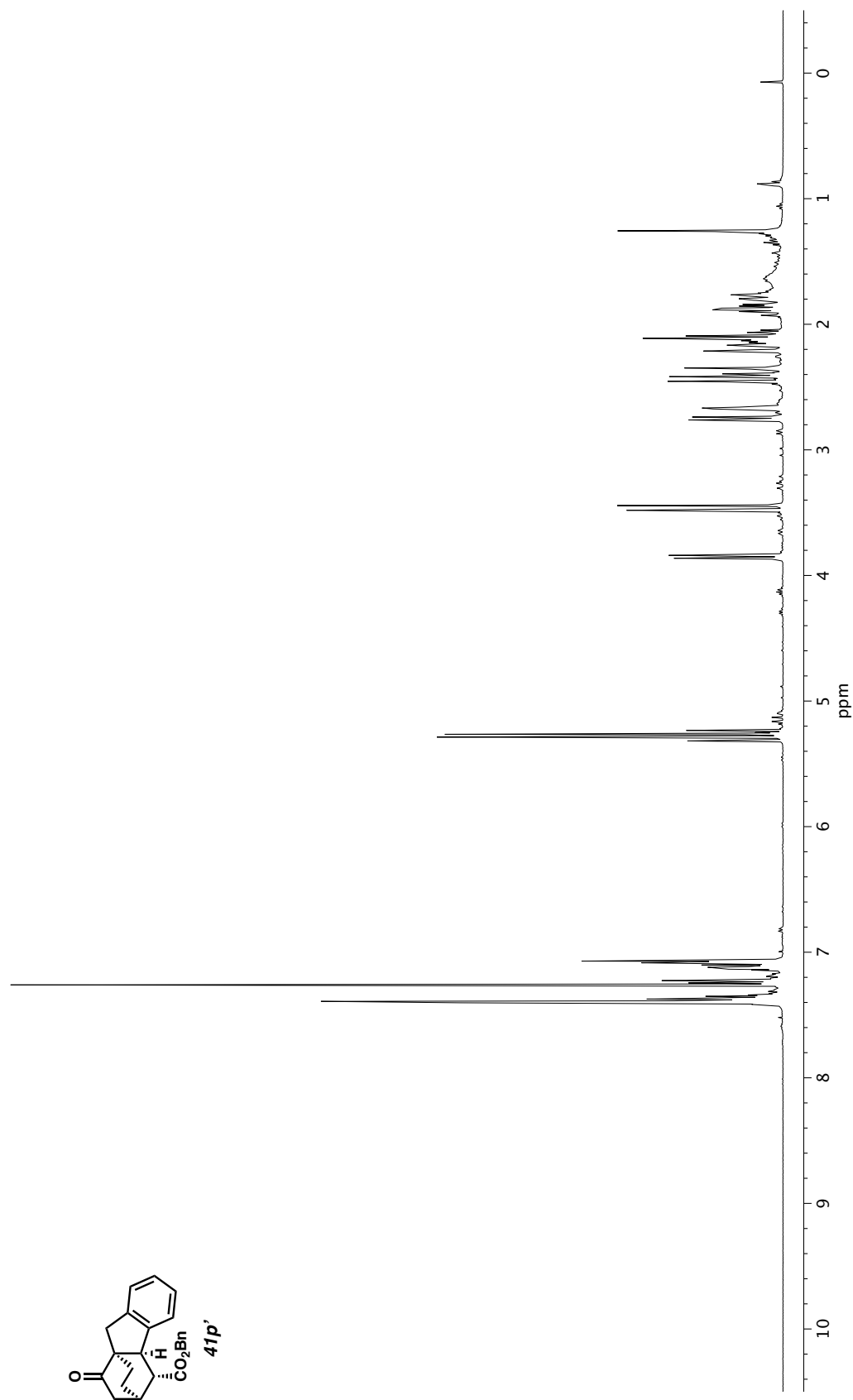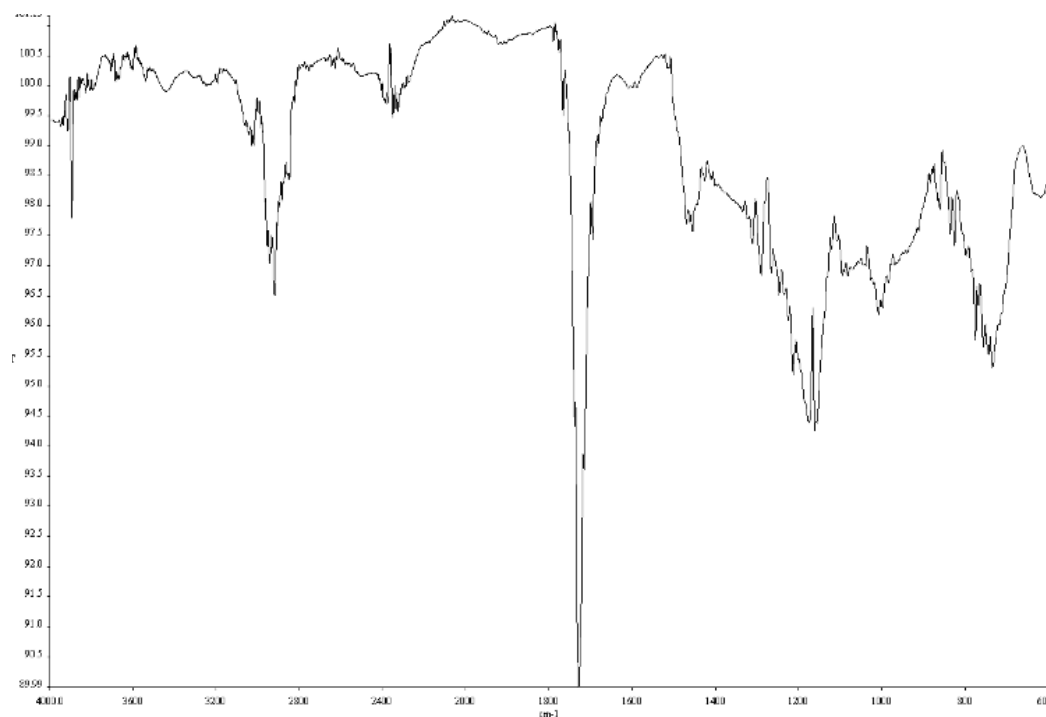
Figure A2.50. *Infrared spectrum (Thin Film, NaCl) of compound **41p′**.*
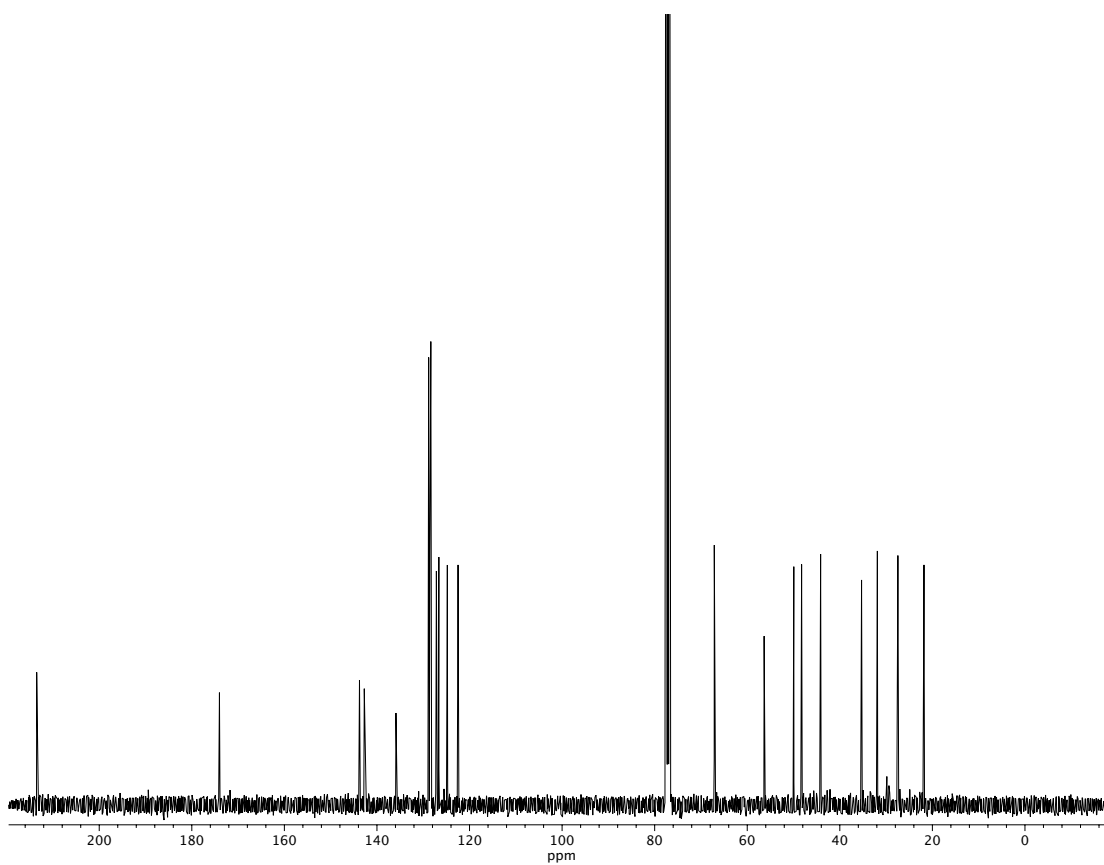
Figure A2.51. *^{13}C NMR (100 MHz, CDCl$_3$) of compound **41p′**.*
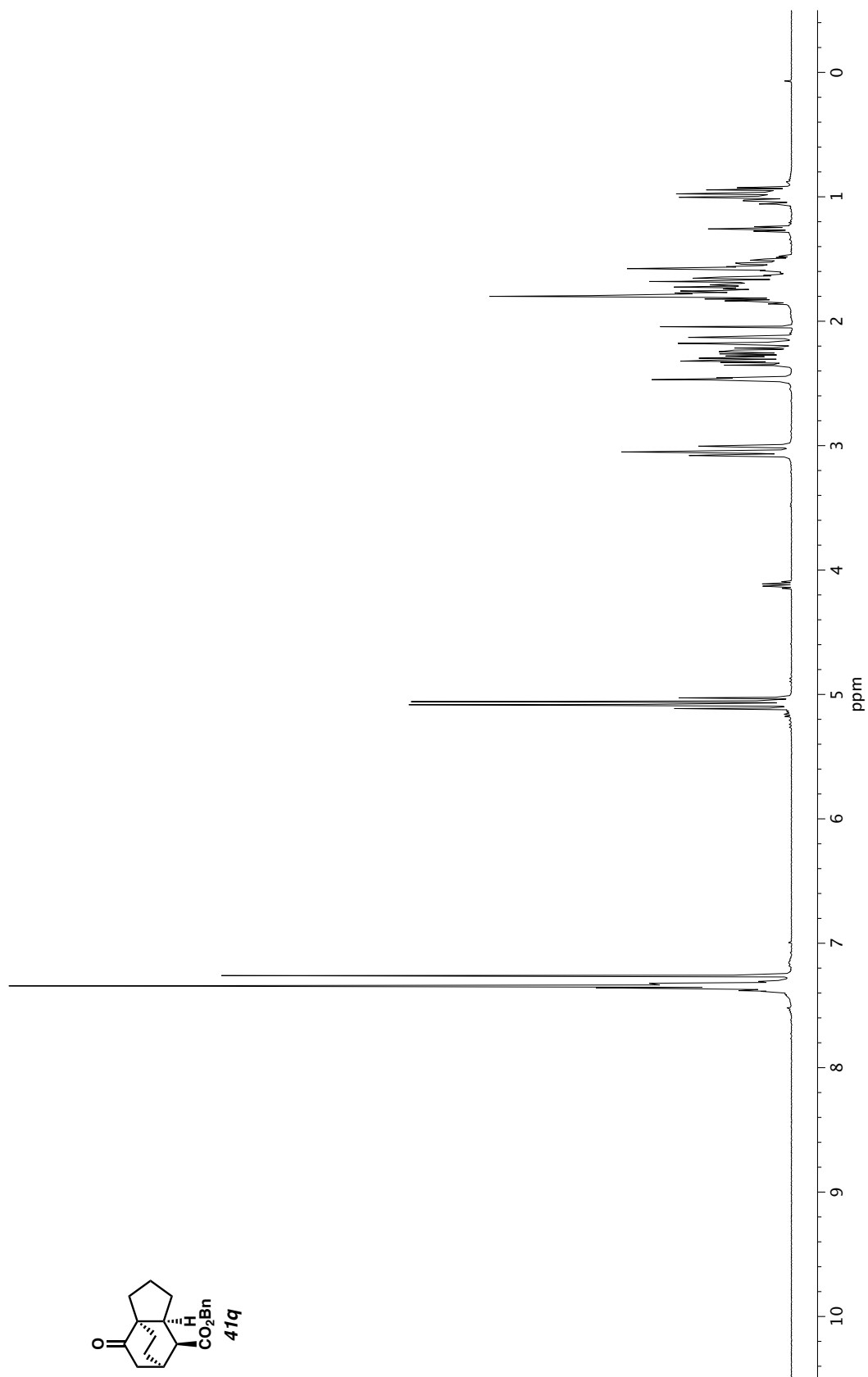
Figure A2.52. *^{1}H NMR (400 MHz, CDCl$_3$) of compound **41q**.*
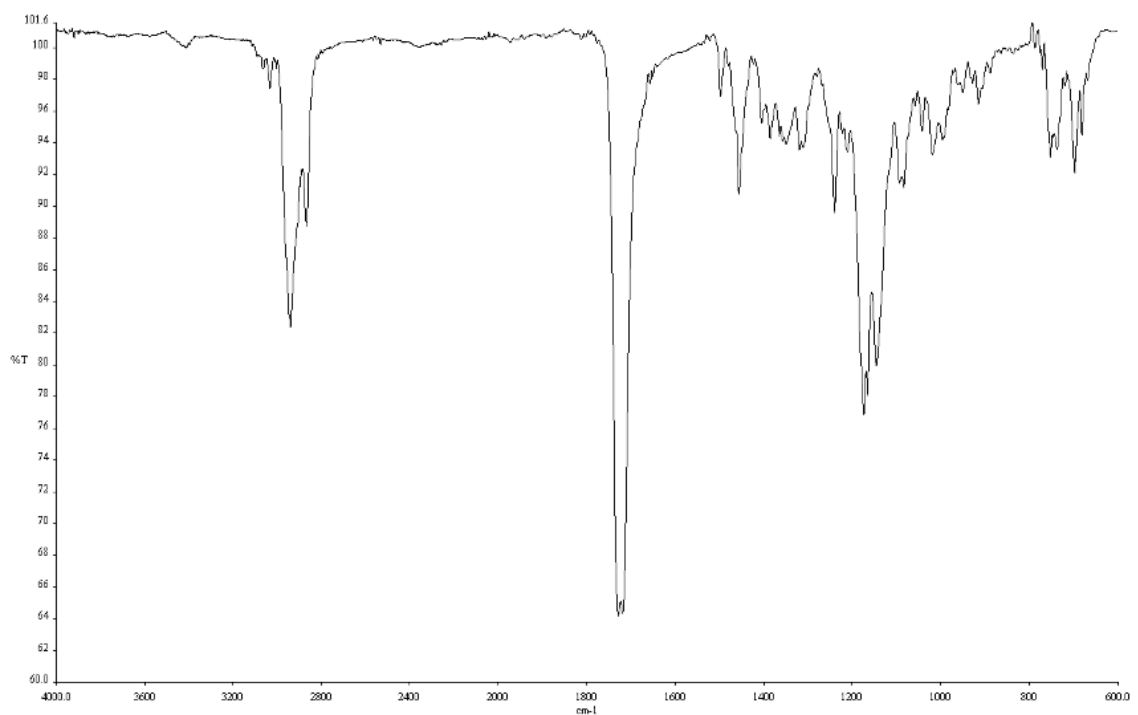
Figure A2.53. Infrared spectrum (Thin Film, NaCl) of compound **41q**.
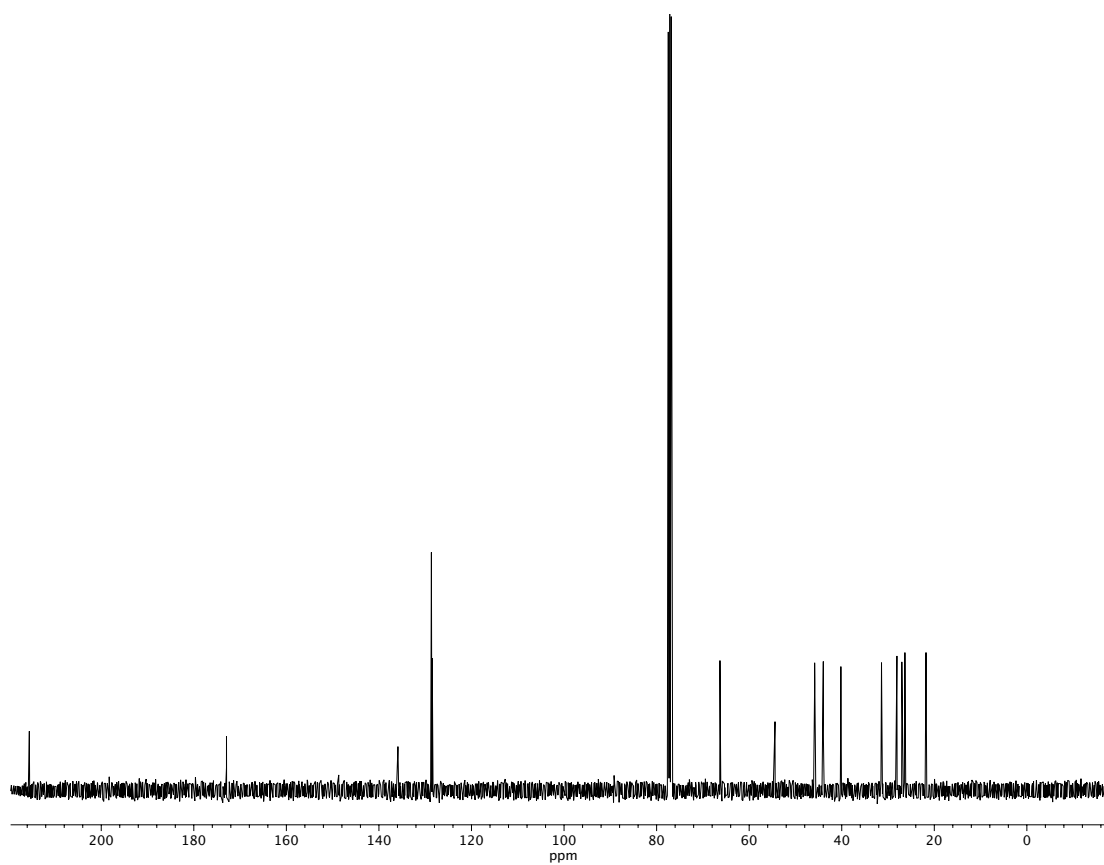
Figure A2.54. ^{13}C NMR (100 MHz, CDCl$_3$) of compound **41q**.
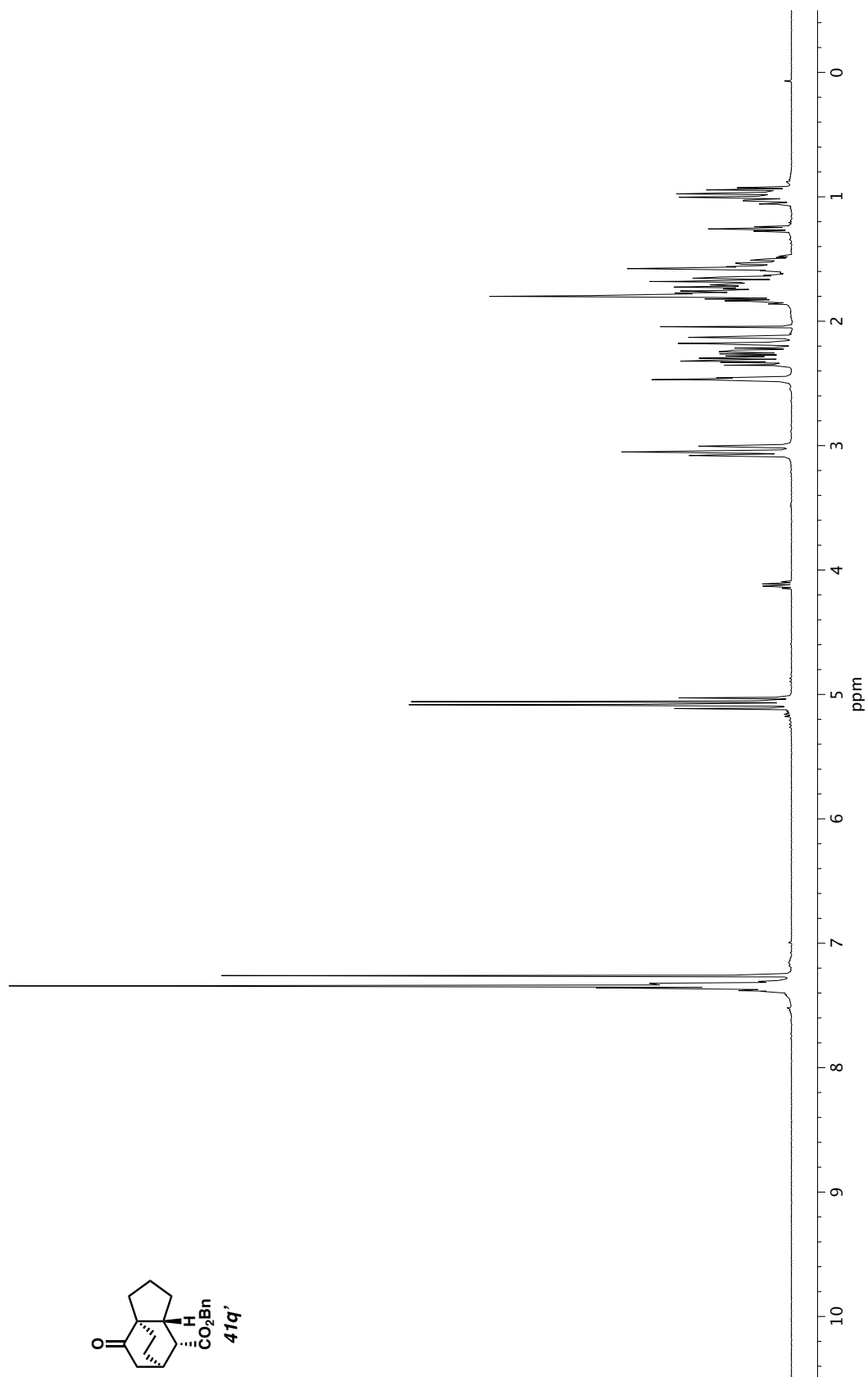
Figure A2.55. ^1H NMR (400 MHz, CDCl$_3$) of compound **41q'** .
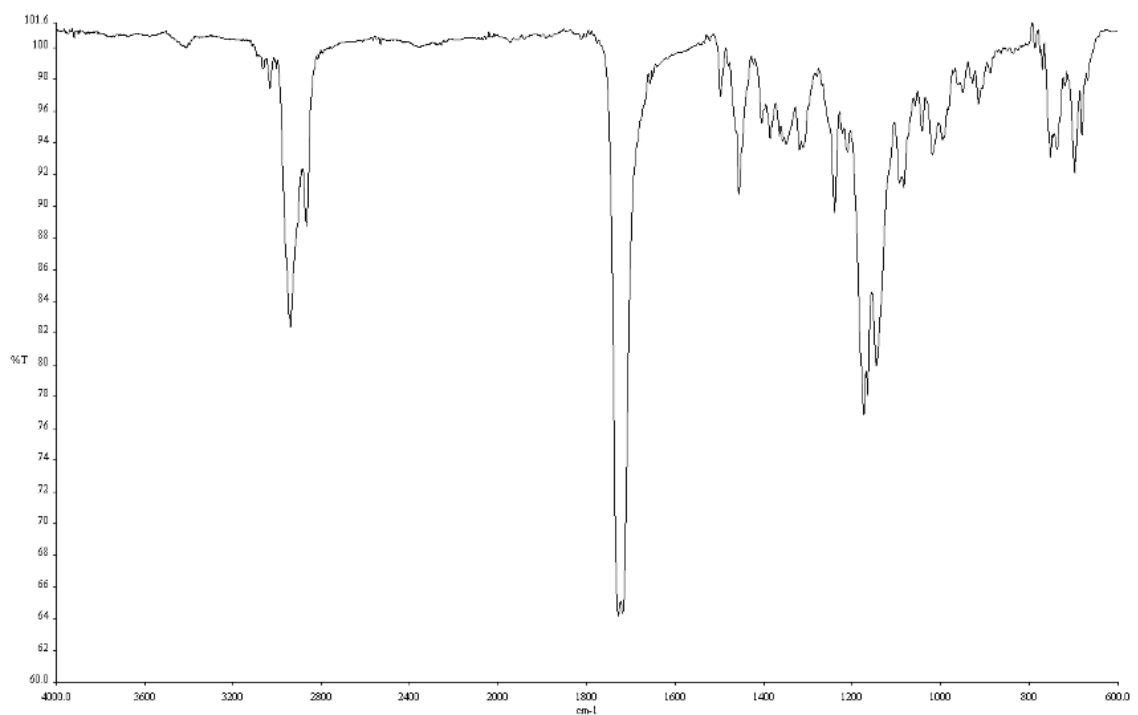
Figure A2.56. *Infrared spectrum (Thin Film, NaCl) of compound* **41q′**.
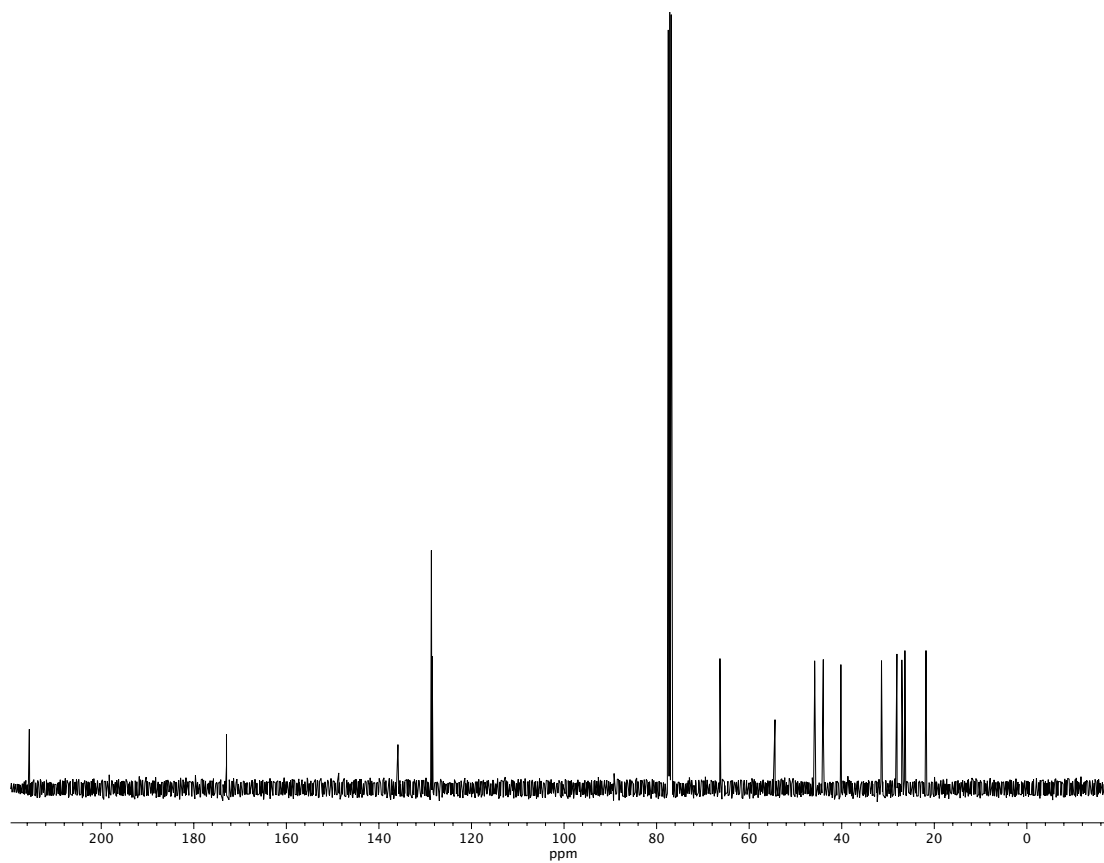
Figure A2.57. ^{13}C *NMR (100 MHz, CDCl$_3$) of compound* **41q′**.
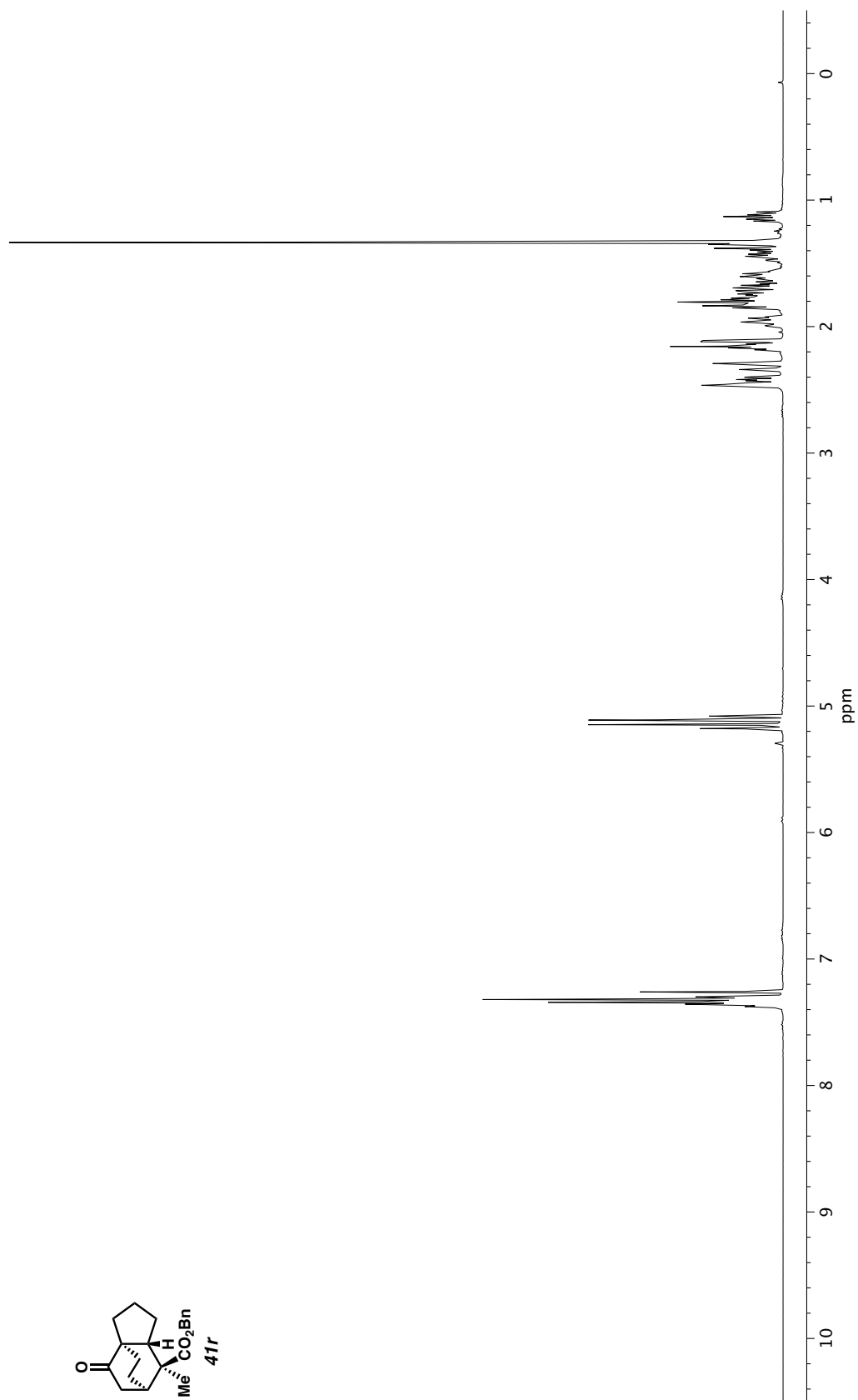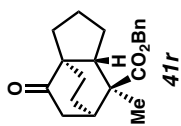
Figure A2.58. ^1H NMR (400 MHz, CDCl$_3$) of compound **41r**.
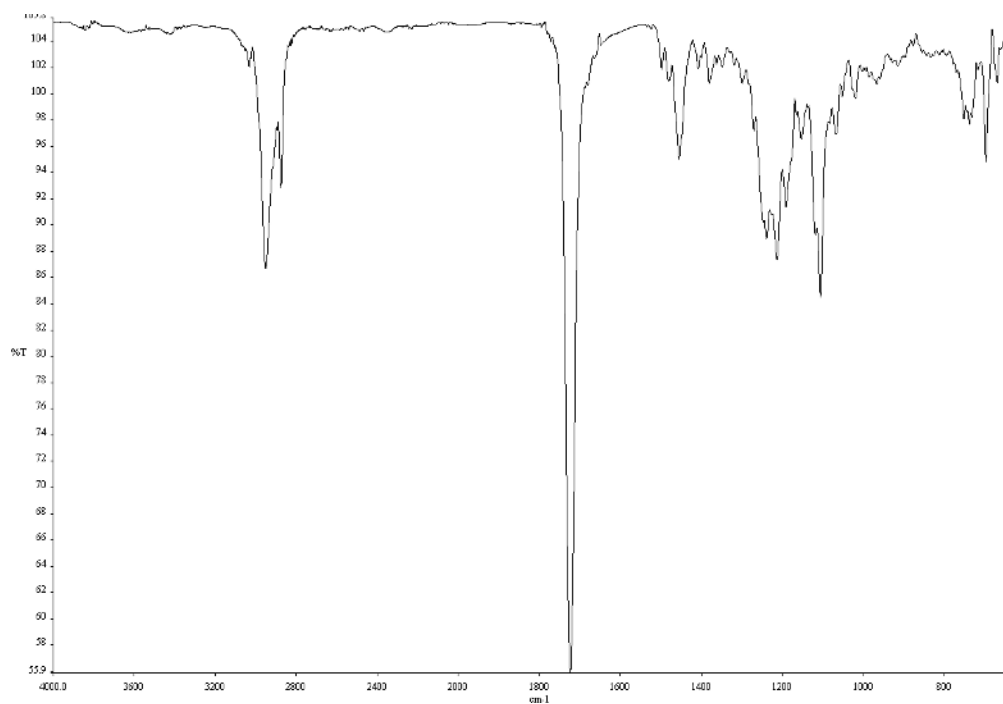
Figure A2.59. Infrared spectrum (Thin Film, NaCl) of compound **41r**.
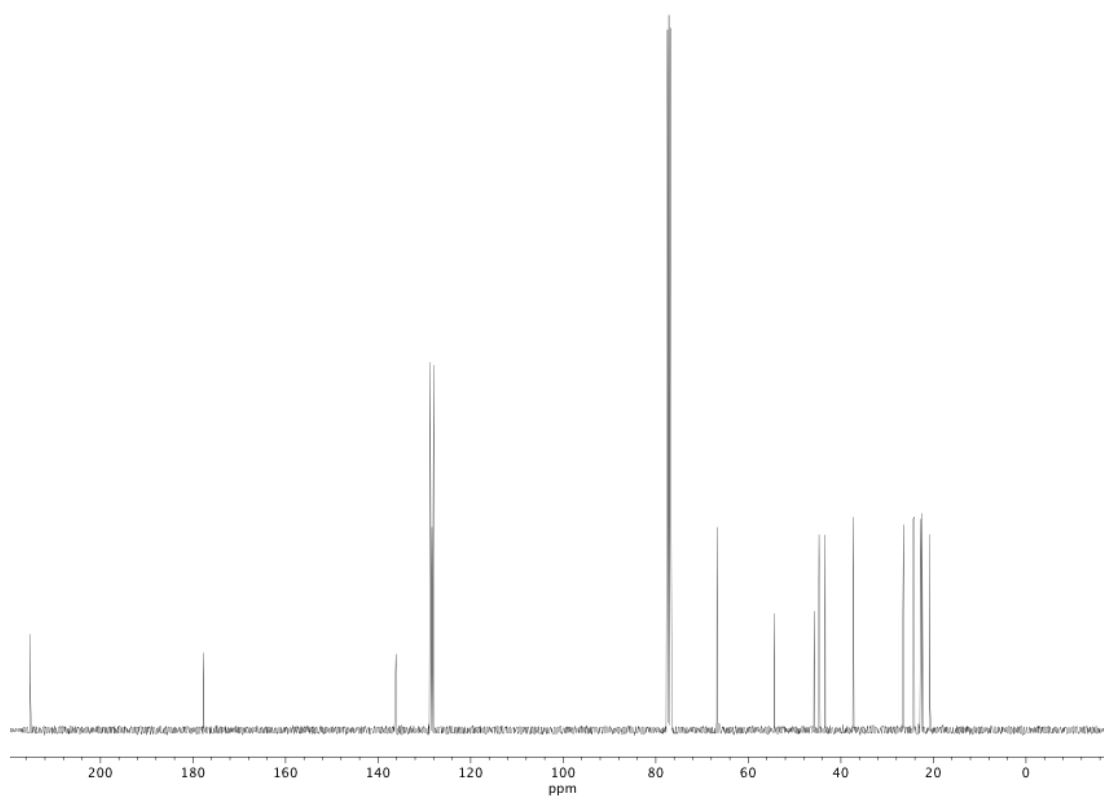
Figure A2.60. ^{13}C NMR (100 MHz, CDCl$_3$) of compound **41r**.
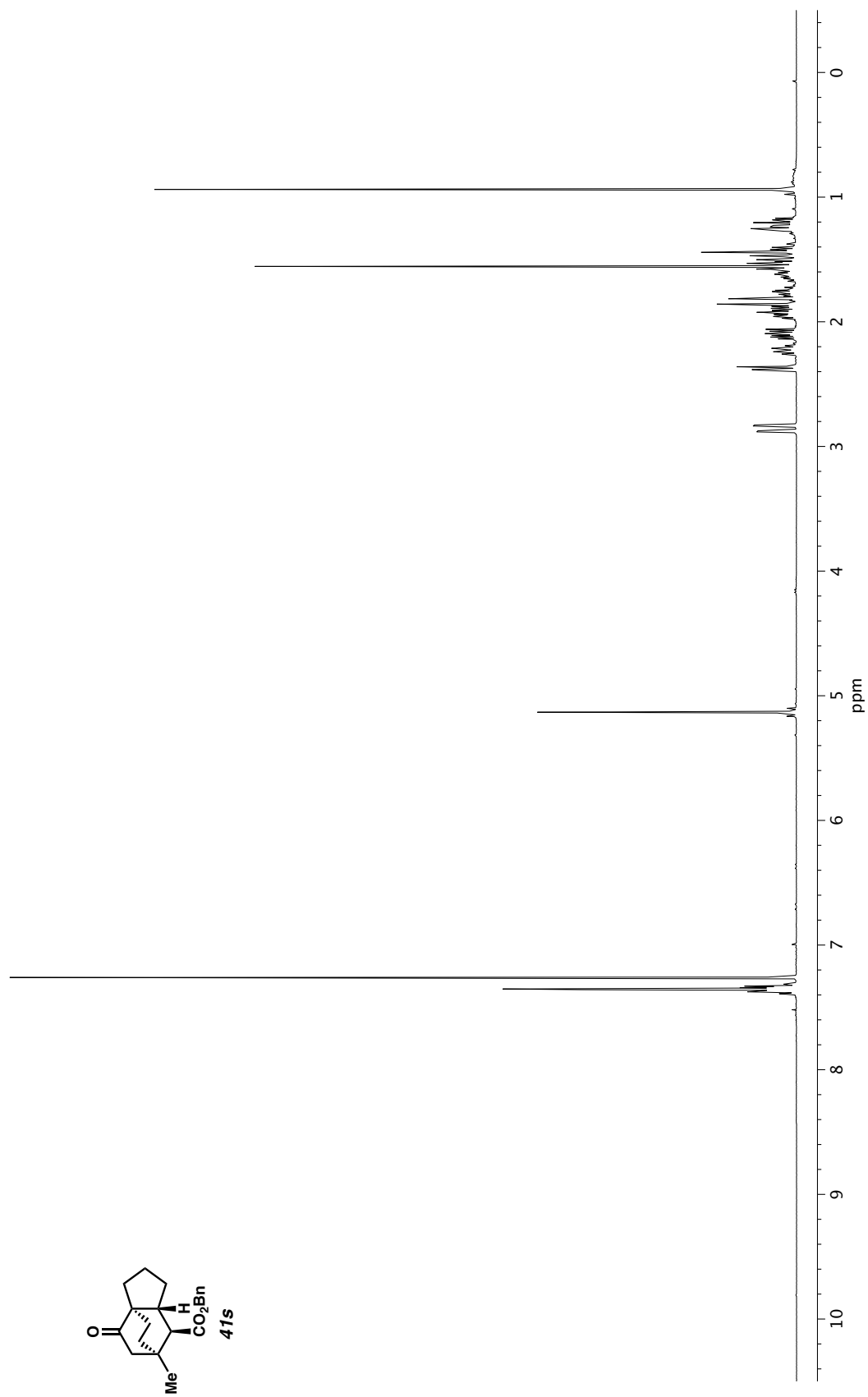
Figure A2.61. ^1H NMR (400 MHz, CDCl$_3$) of compound **41s**.
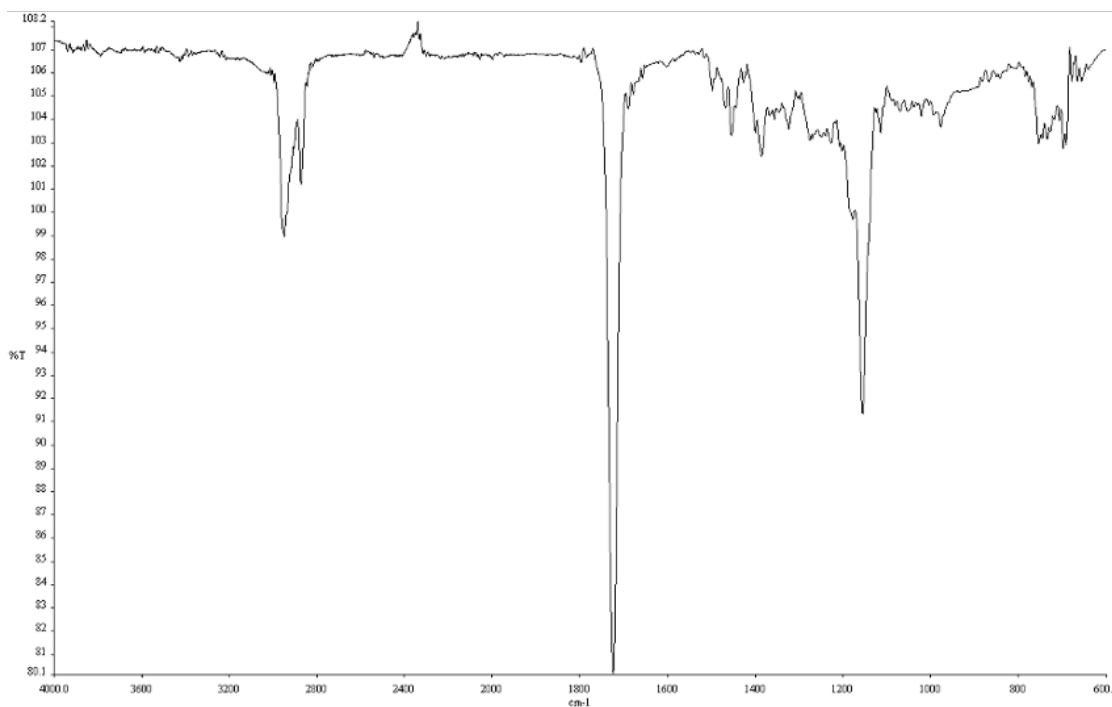
Figure A2.62. Infrared spectrum (Thin Film, NaCl) of compound **41s**.
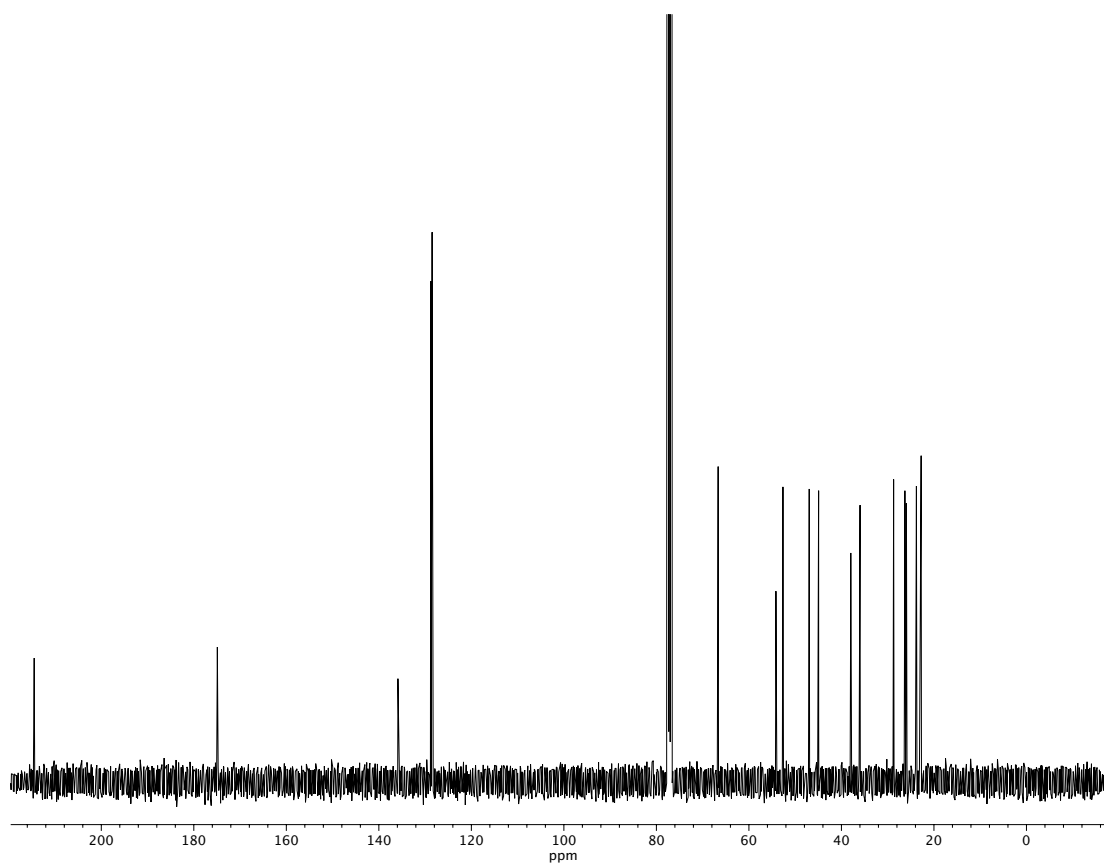
Figure A2.63. ^{13}C NMR (100 MHz, CDCl$_3$) of compound **41s**.
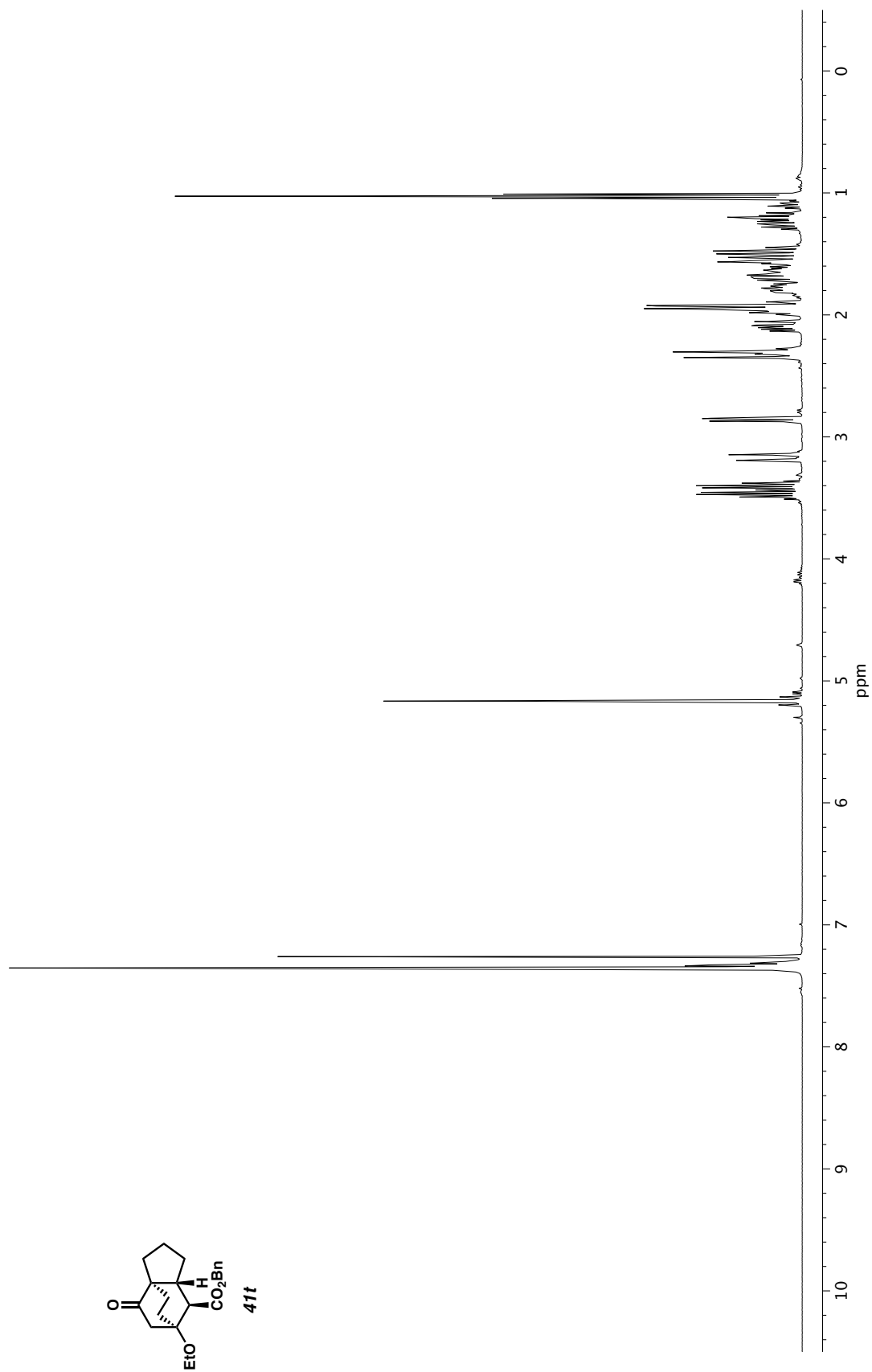
Figure A2.64. ^1H NMR (400 MHz, CDCl$_3$) of compound **41t**.
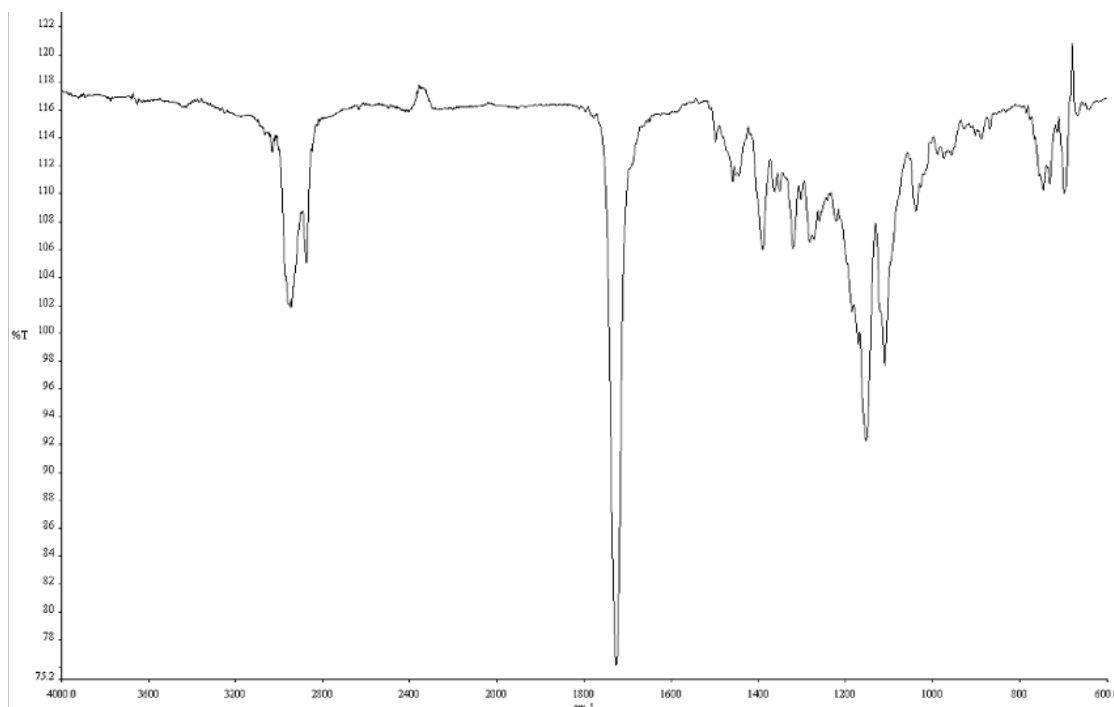
Figure A2.65. Infrared spectrum (Thin Film, NaCl) of compound **41t**.
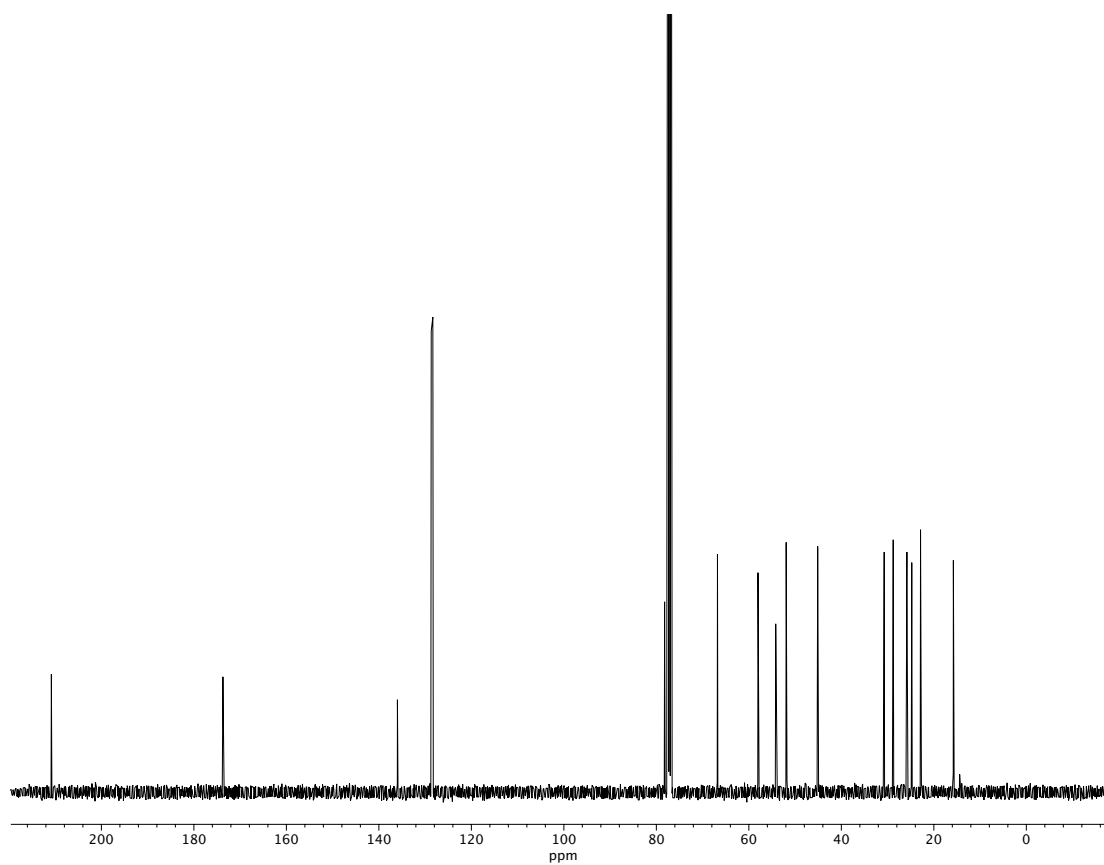
Figure A2.66. ^{13}C NMR (100 MHz, CDCl$_3$) of compound **41t**.
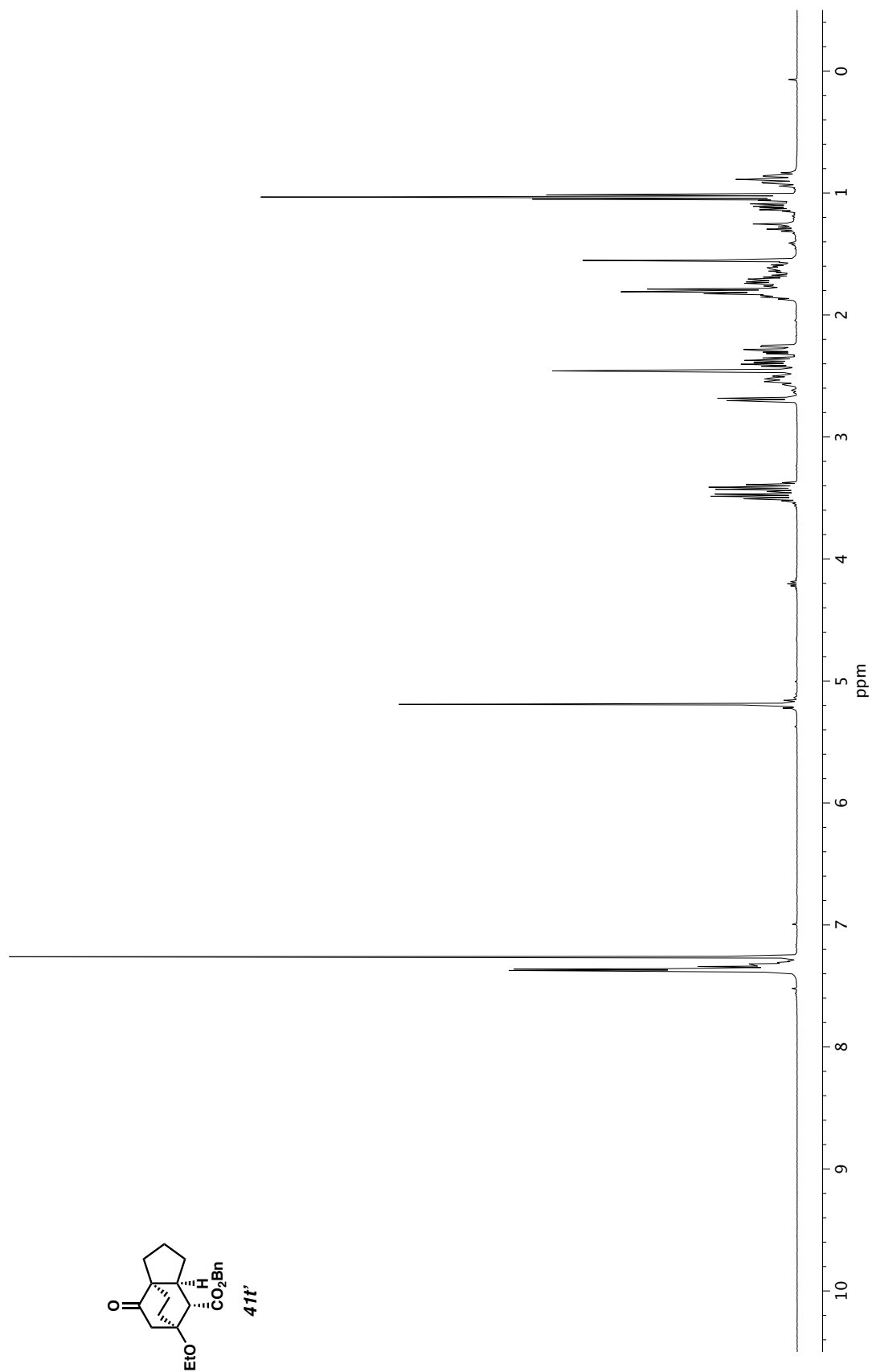
Figure A2.67. ^1H NMR (400 MHz, CDCl$_3$) of compound **41t'** .
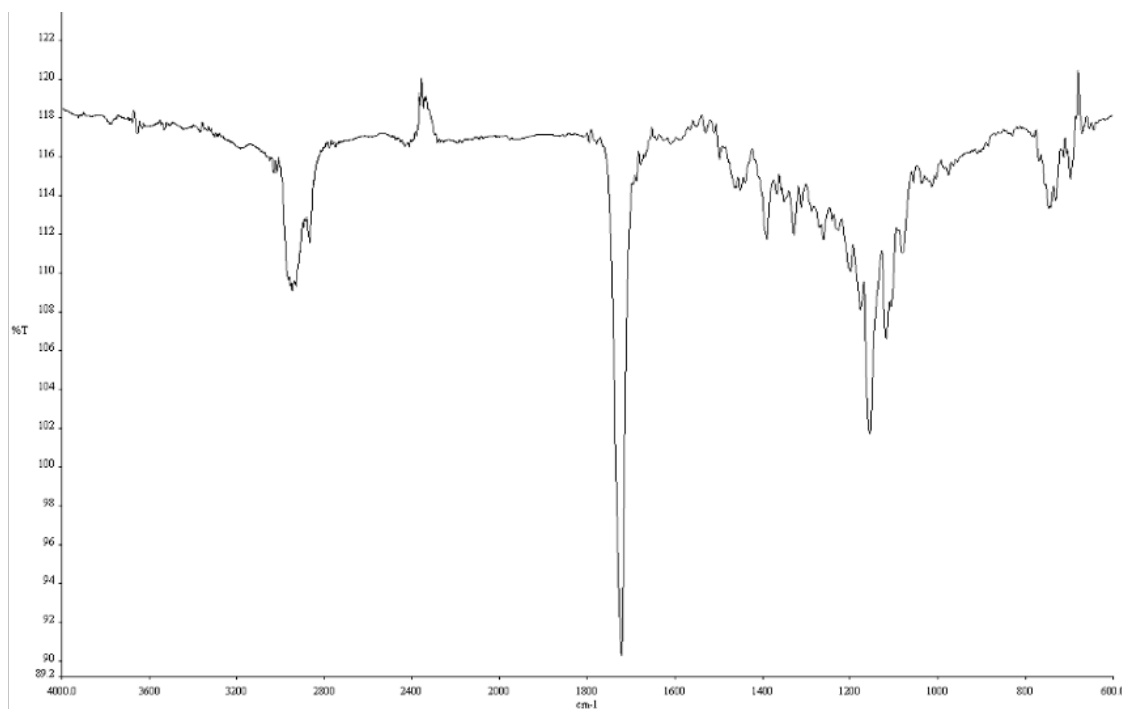
Figure A2.68. Infrared spectrum (Thin Film, NaCl) of compound **41t'**.
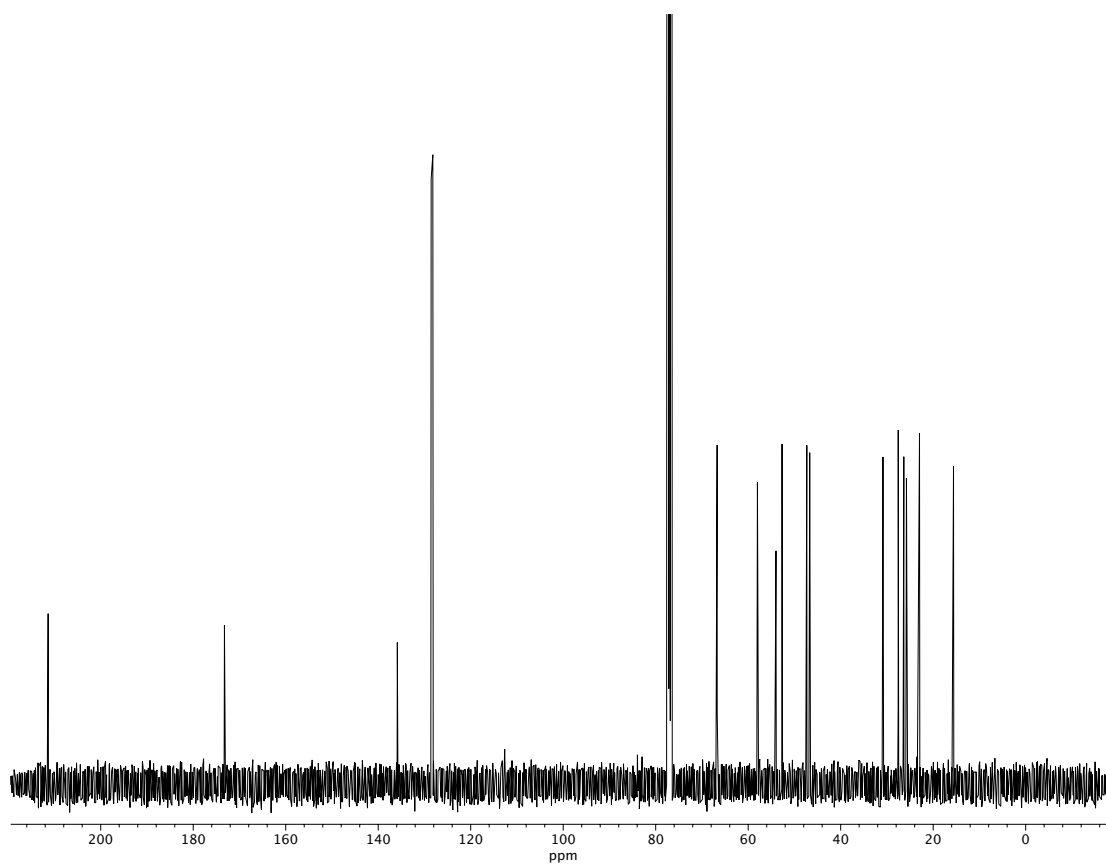
Figure A2.69. ^{13}C NMR (100 MHz, CDCl$_3$) of compound **41t'**.
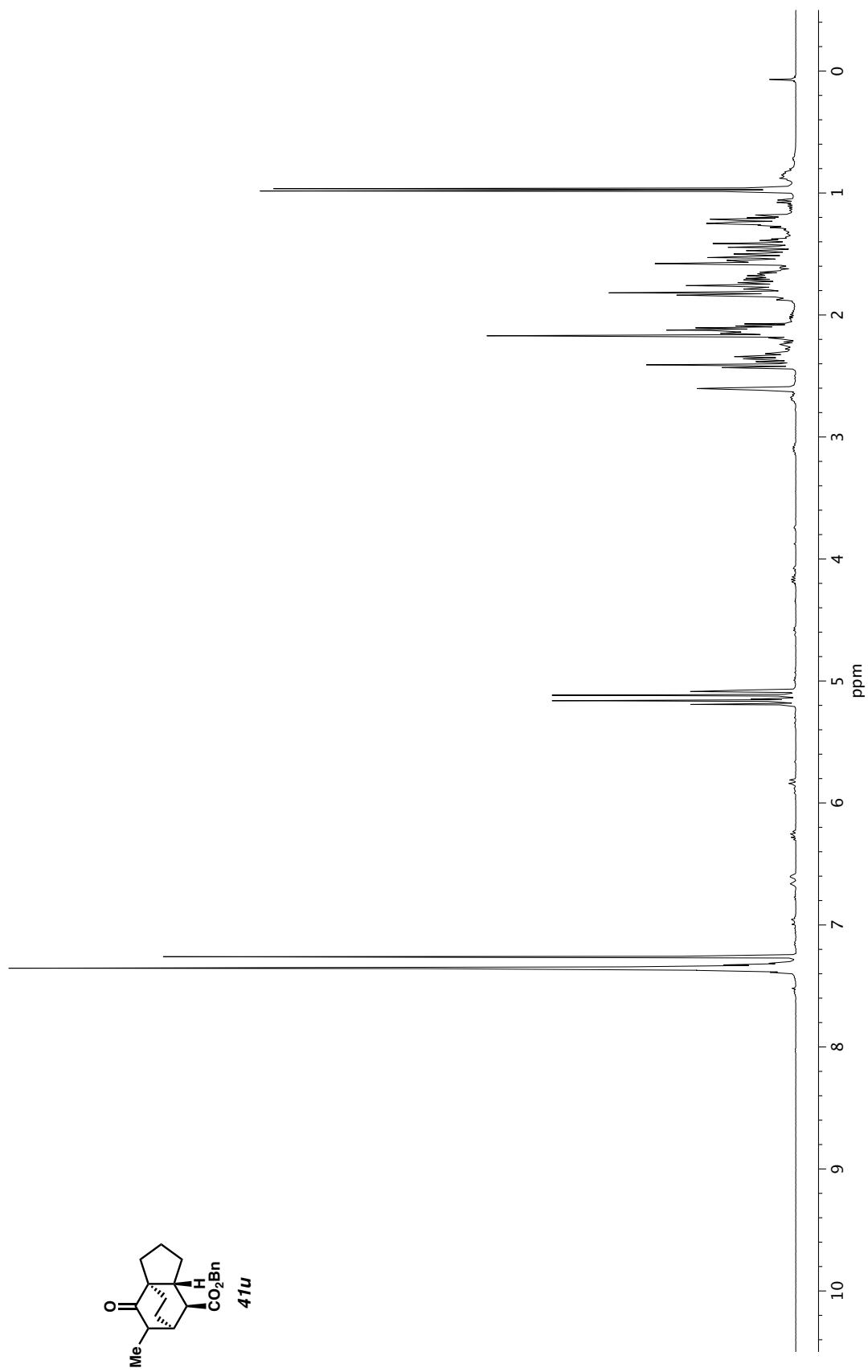
Figure A2.70. ^1H NMR (400 MHz, CDCl$_3$) of compound **41u**.
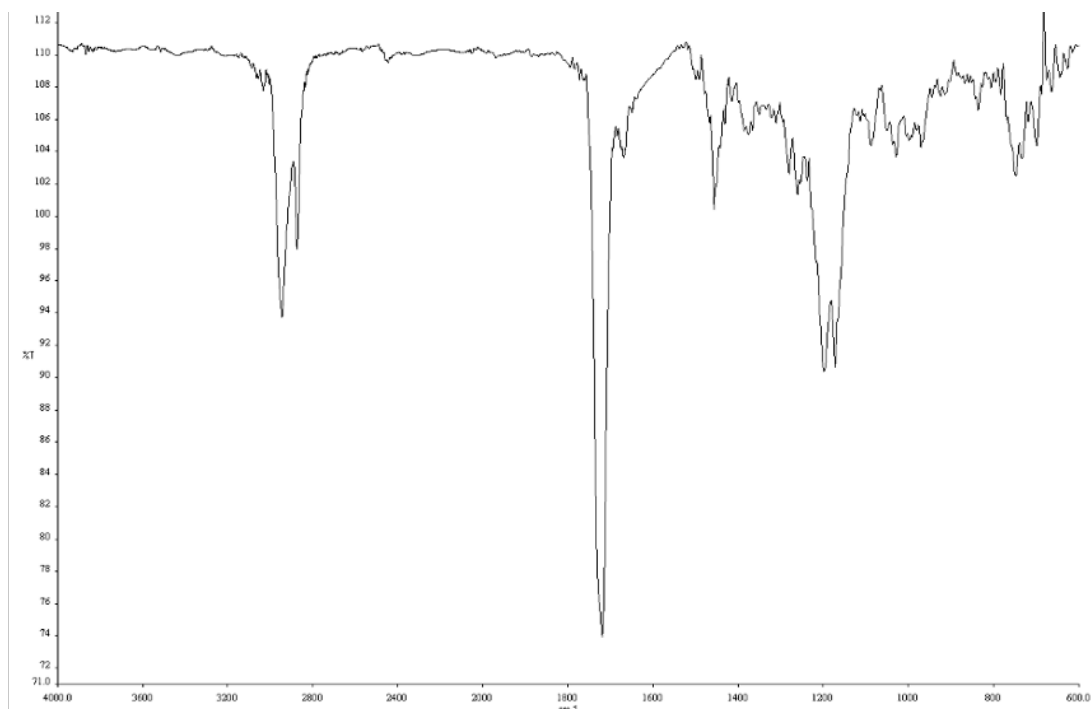
Figure A2.71. Infrared spectrum (Thin Film, NaCl) of compound **41u**.
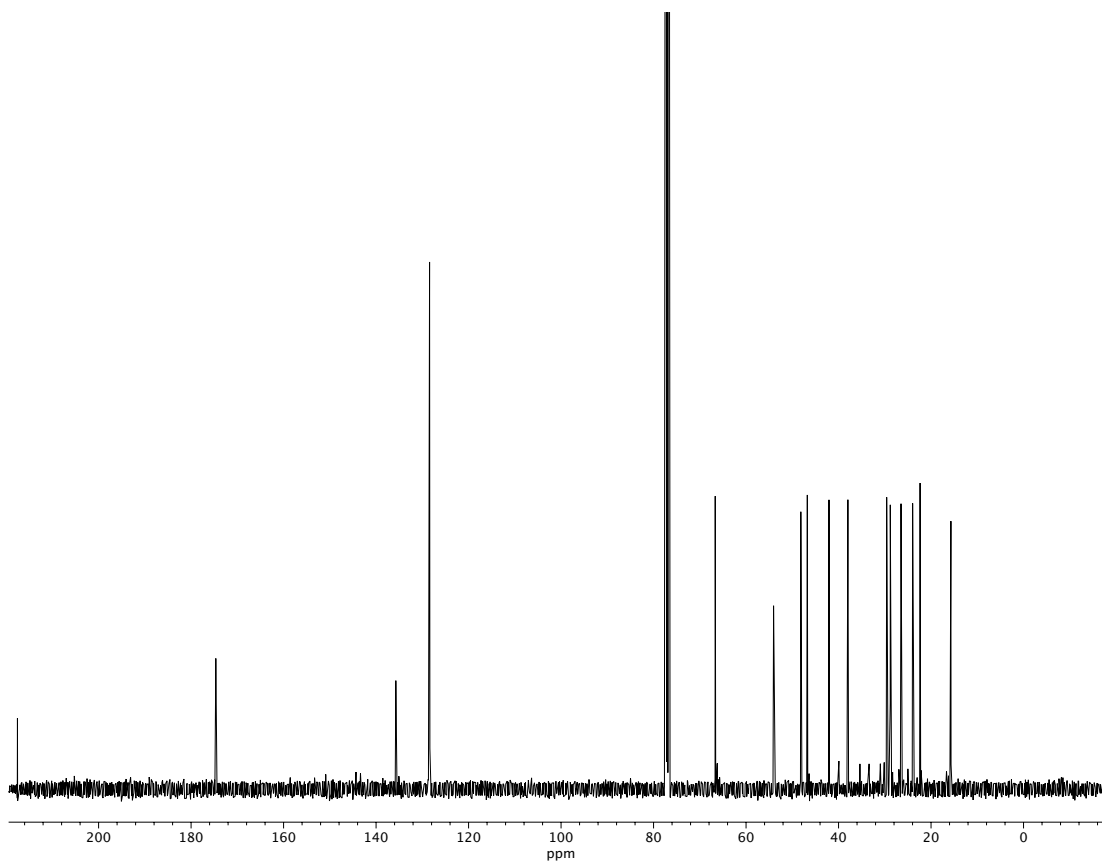
Figure A2.72. ^{13}C NMR (100 MHz, CDCl$_3$) of compound **41u**.
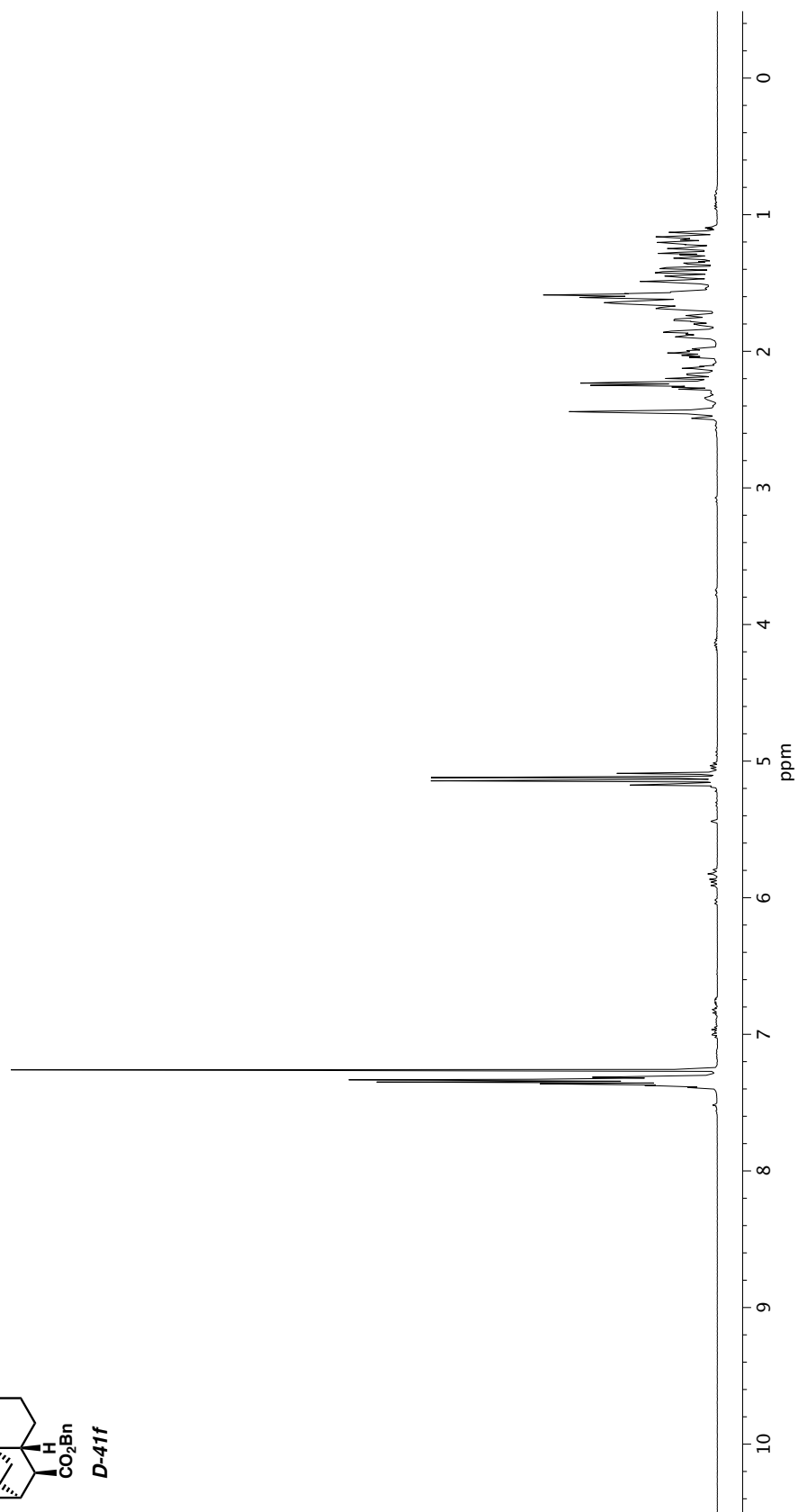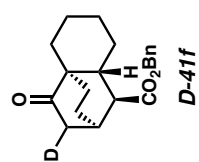
Figure A2.73. ^1H NMR (400 MHz, CDCl$_3$) of compound **D-41f**.
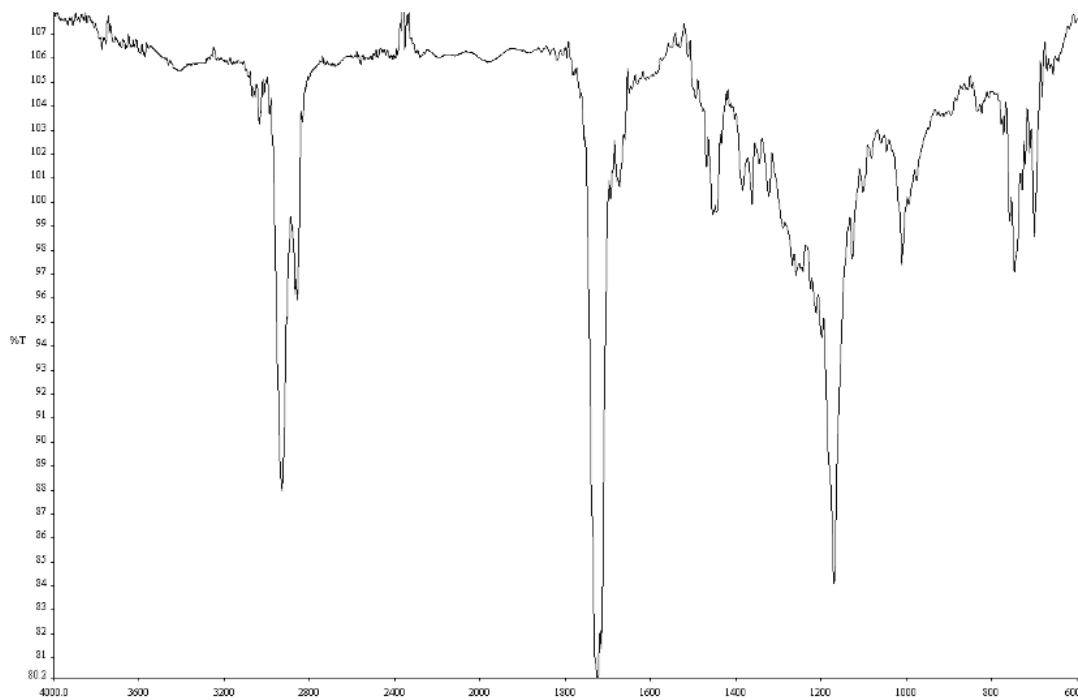
Figure A2.74. *Infrared spectrum (Thin Film, NaCl) of compound* **D-41f**.
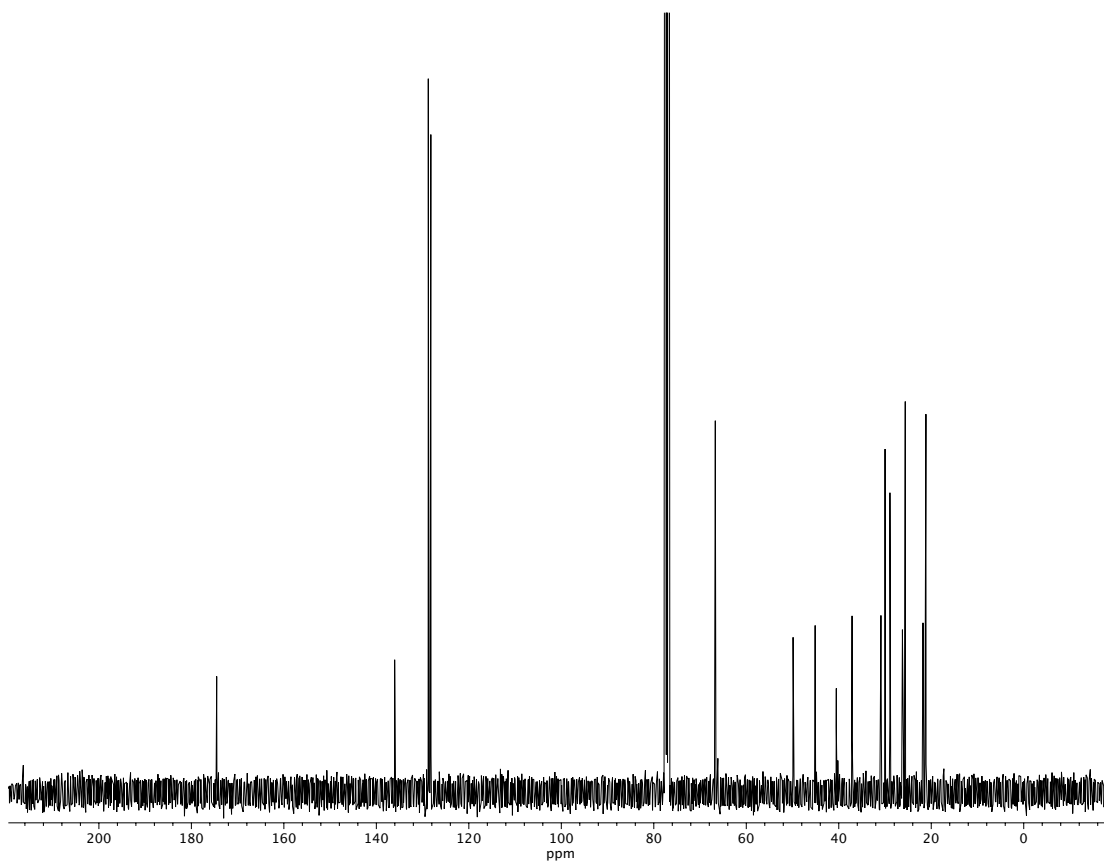
Figure A2.75. ^{13}C *NMR (100 MHz, CDCl$_3$) of compound* **D-41f**.
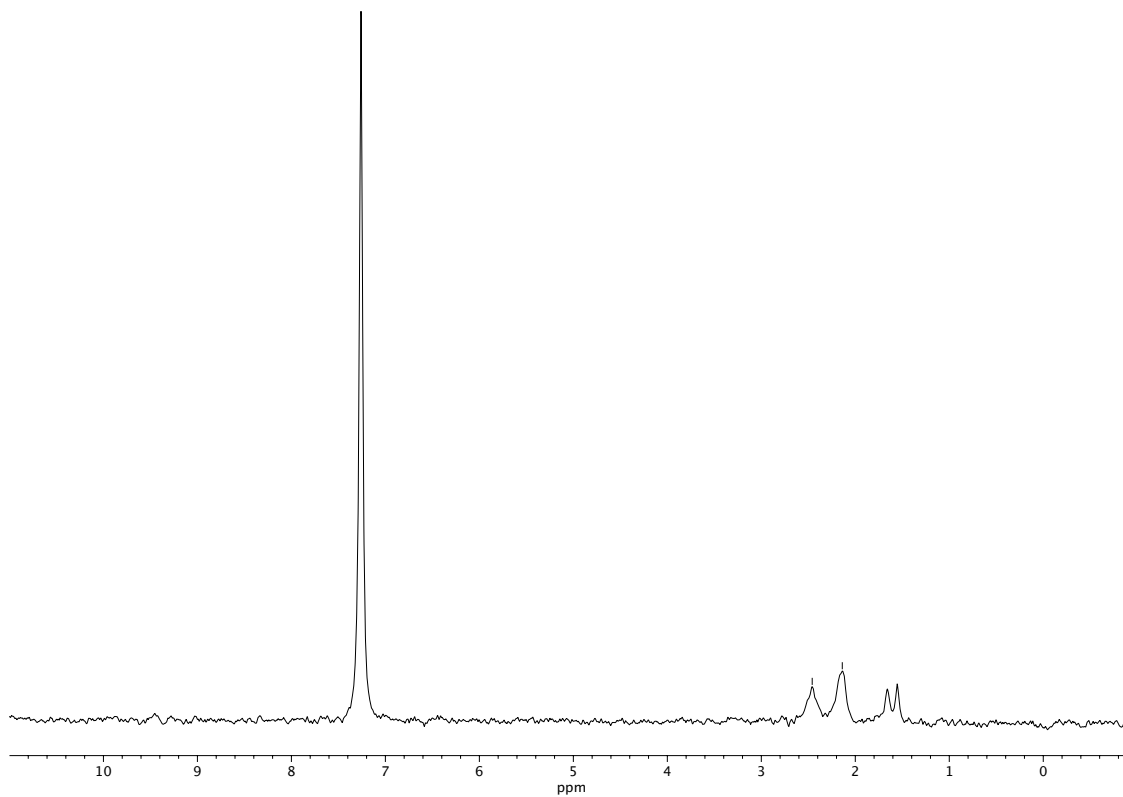
Figure A2.76. *²H NMR (61 MHz, CDCl₃) of compound **D-41f***.
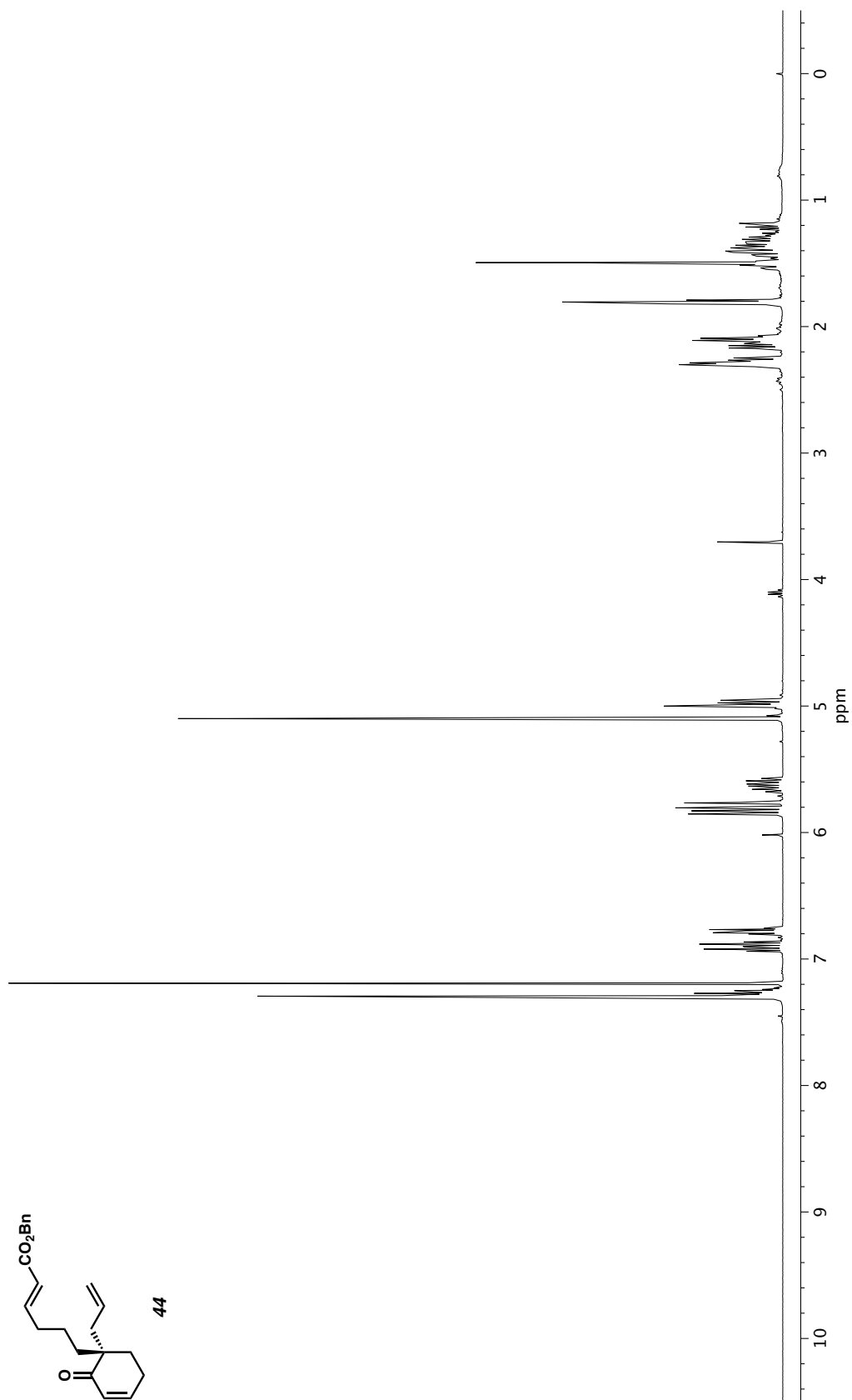
Figure A2.77. ^1H NMR (400 MHz, CDCl$_3$) of compound **44**.
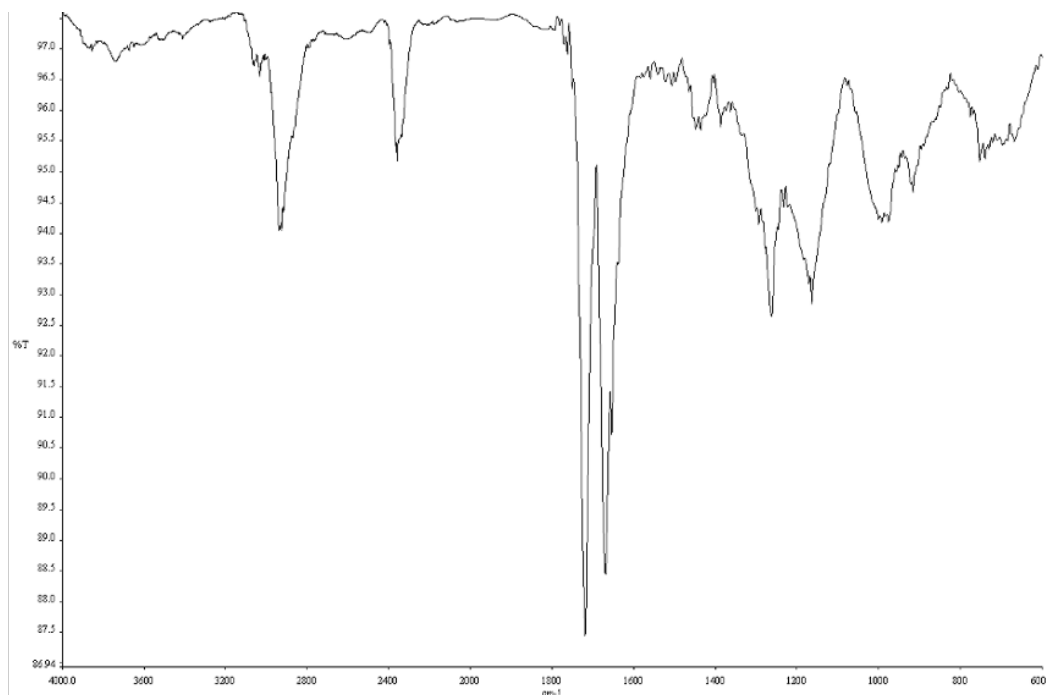
Figure A2.78. *Infrared spectrum (Thin Film, NaCl) of compound **44**.*
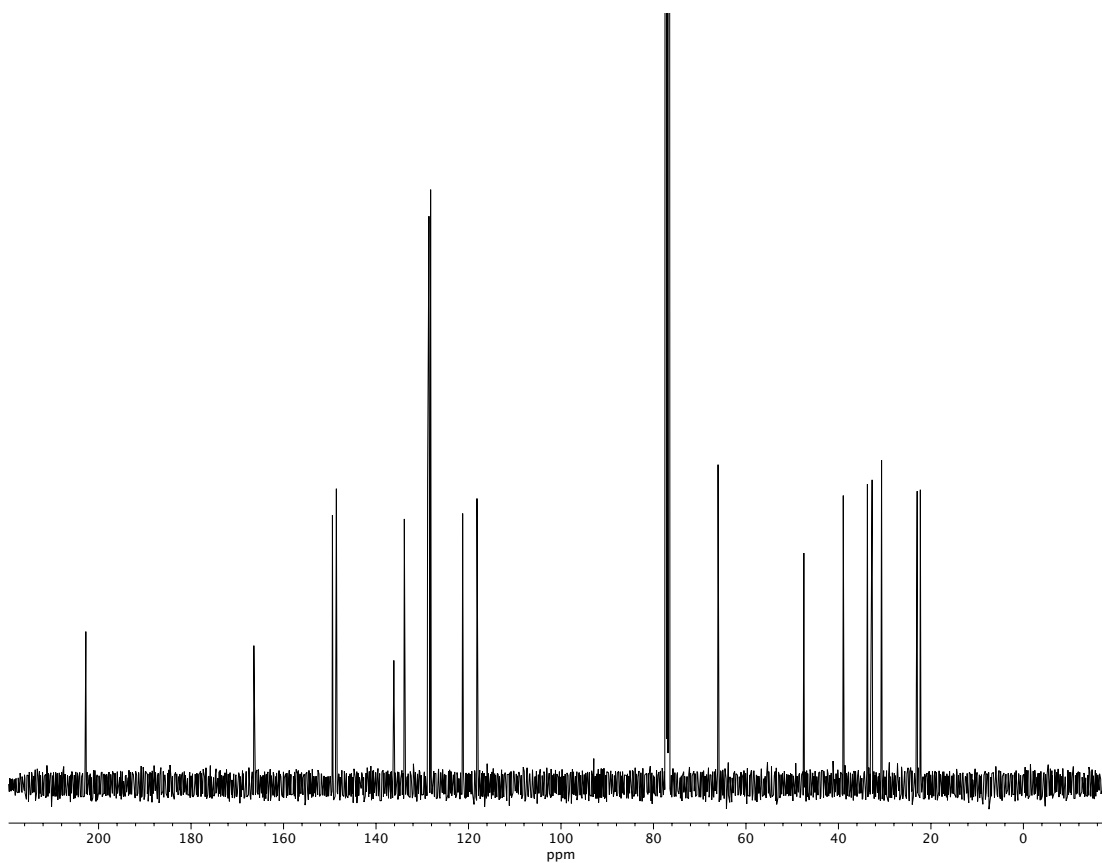
Figure A2.79. *^{13}C NMR (100 MHz, CDCl$_3$) of compound **44**.*
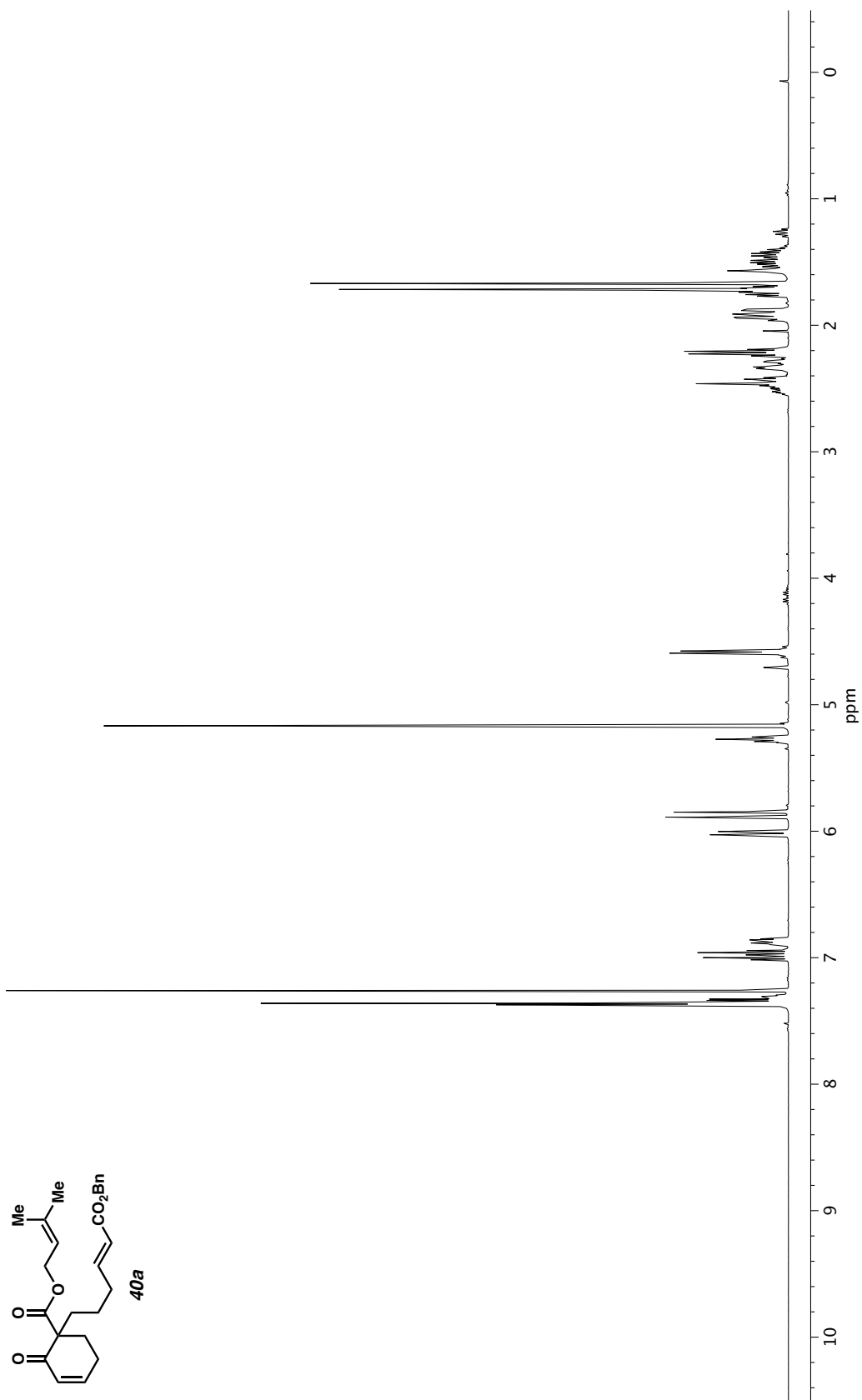
Figure A2.80. ^1H NMR (400 MHz, CDCl$_3$) of compound **40a**.
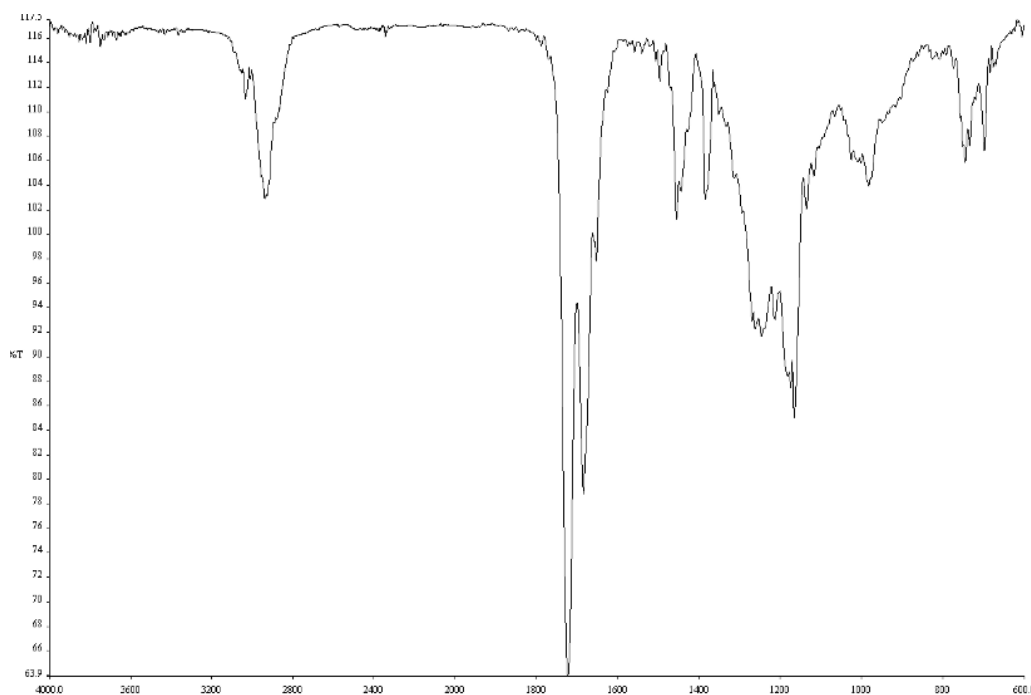
Figure A2.81. Infrared spectrum (Thin Film, NaCl) of compound **40a**.
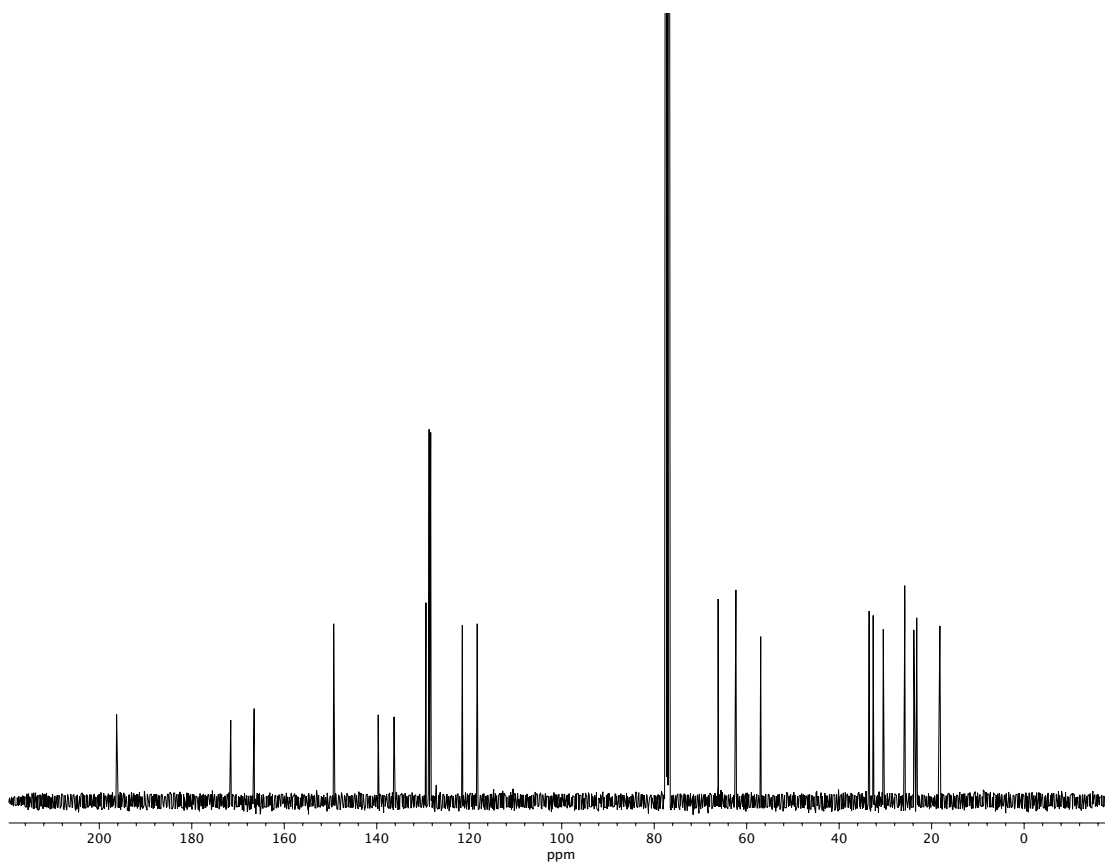
Figure A2.82. ^{13}C NMR (100 MHz, CDCl$_3$) of compound **40a**.
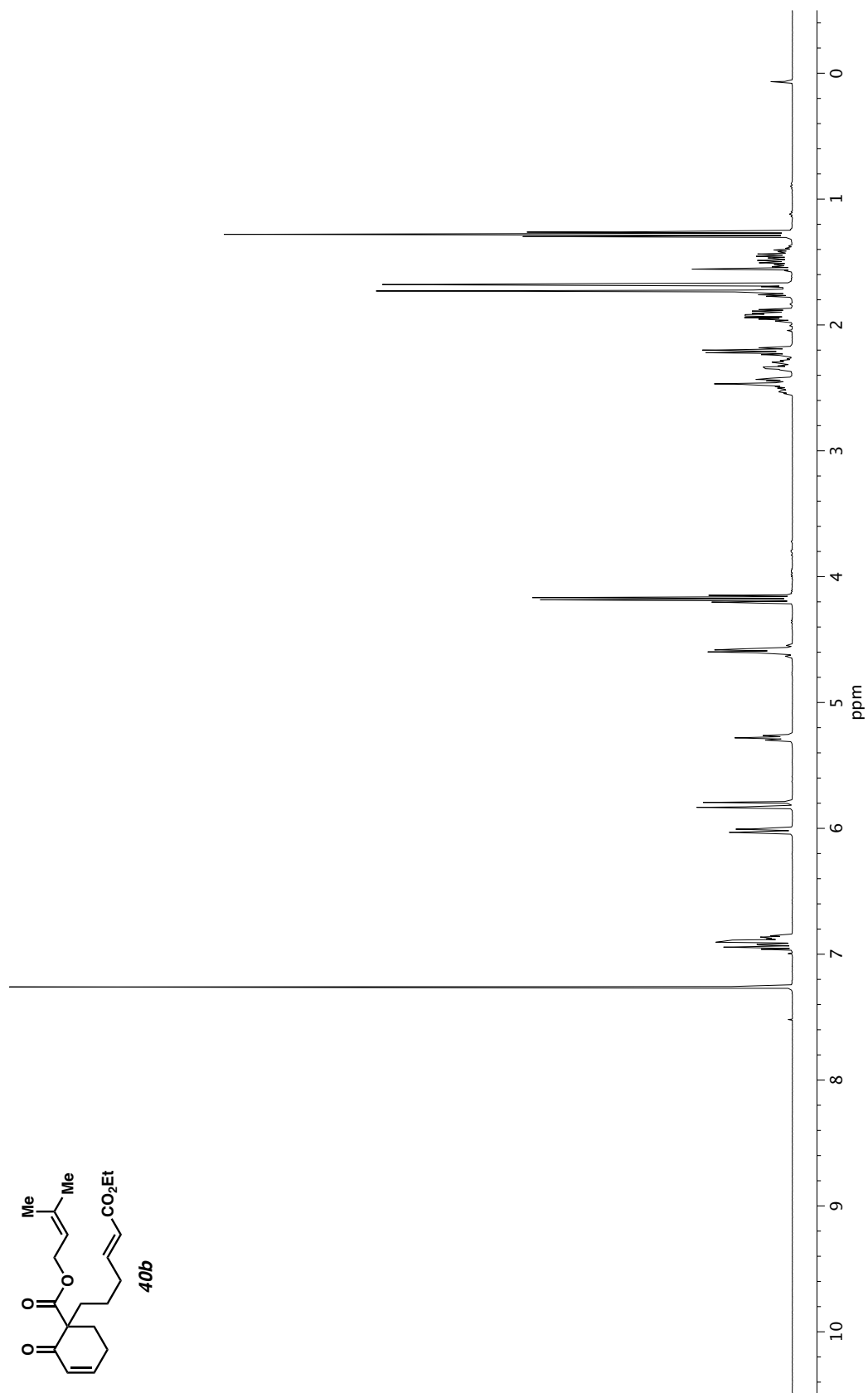
Figure A2.83. ^1H NMR (400 MHz, CDCl$_3$) of compound **40b**.
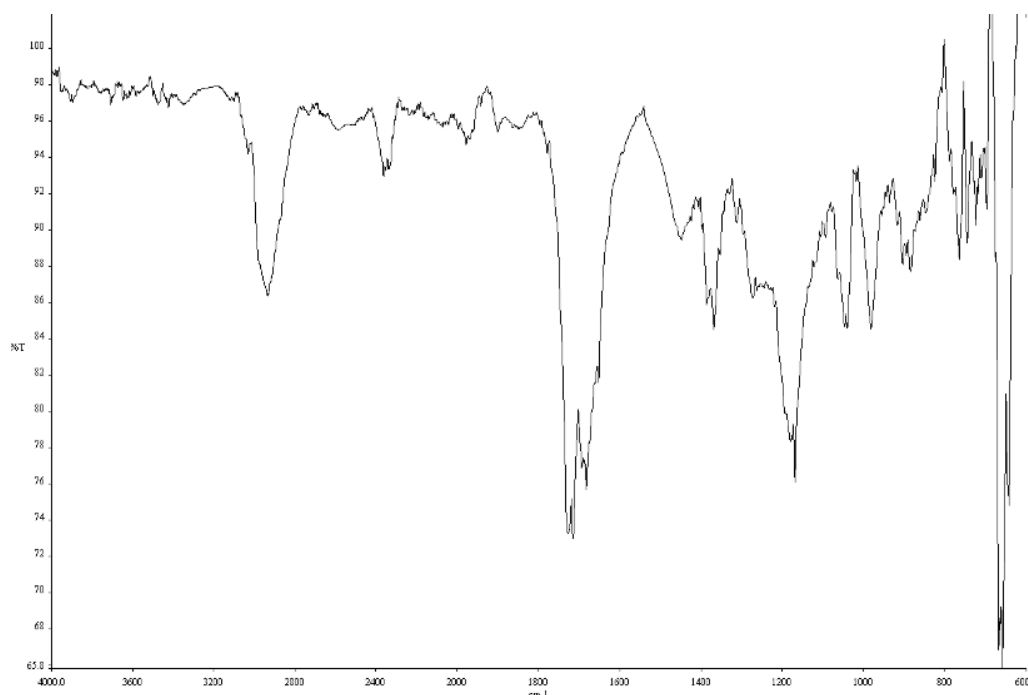
Figure A2.84. Infrared spectrum (Thin Film, NaCl) of compound **40b**.
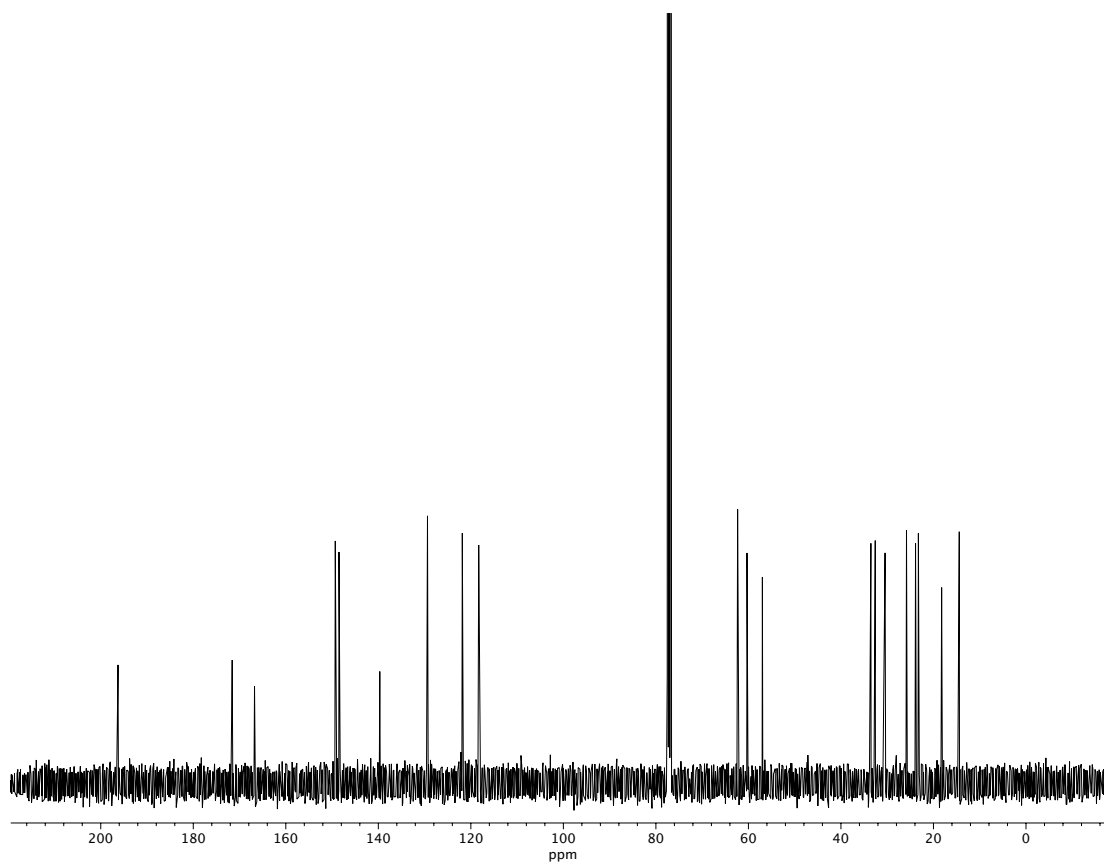
Figure A2.85. ^{13}C NMR (100 MHz, CDCl$_3$) of compound **40b**.
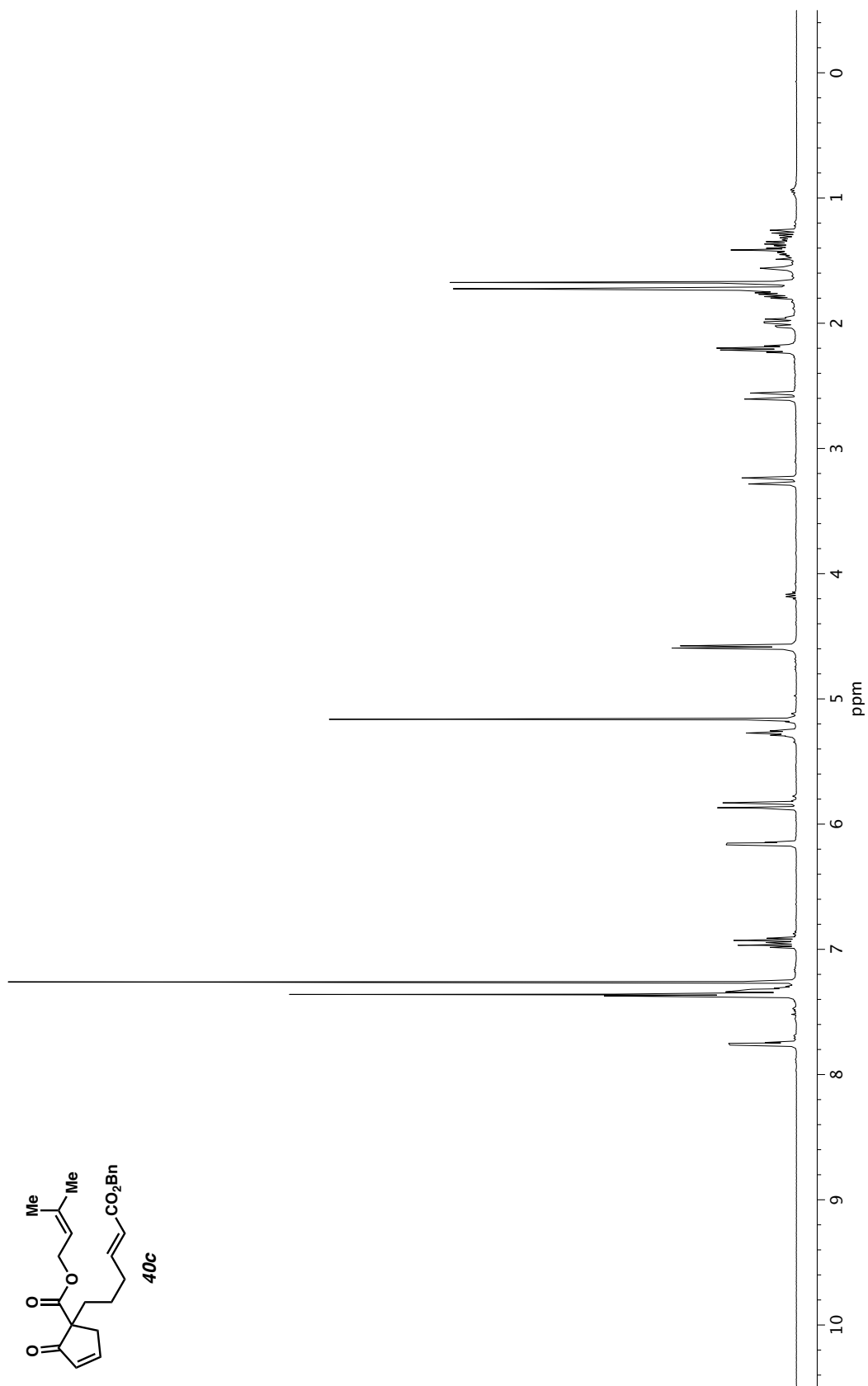
Figure A2.86. ^1H NMR (400 MHz, CDCl$_3$) of compound **40c**.
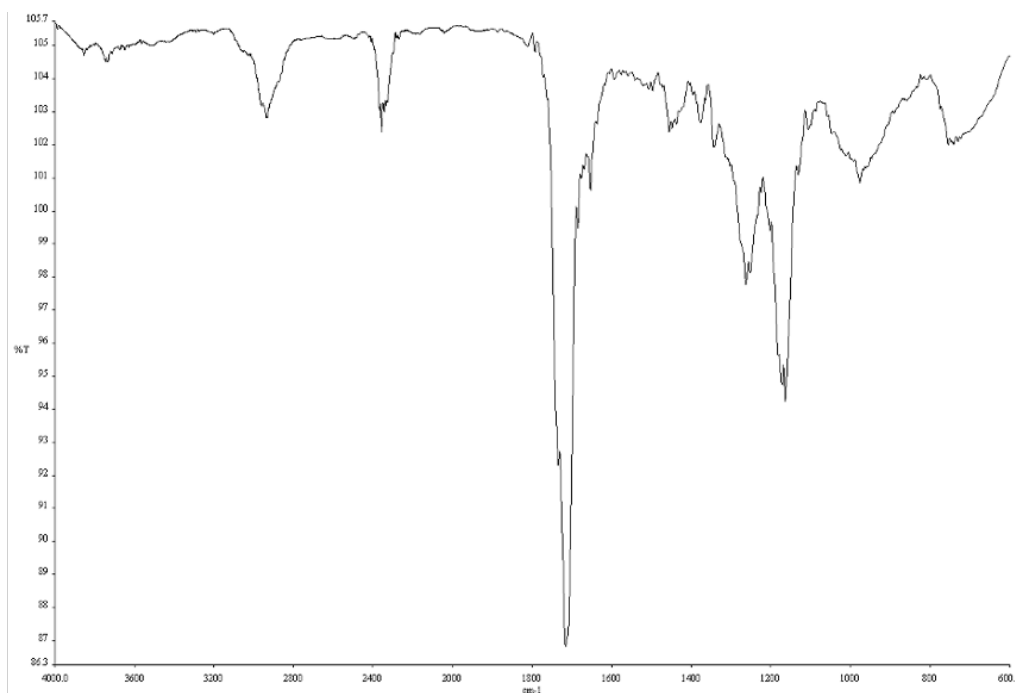
Figure A2.87. *Infrared spectrum (Thin Film, NaCl) of compound **40c**.*
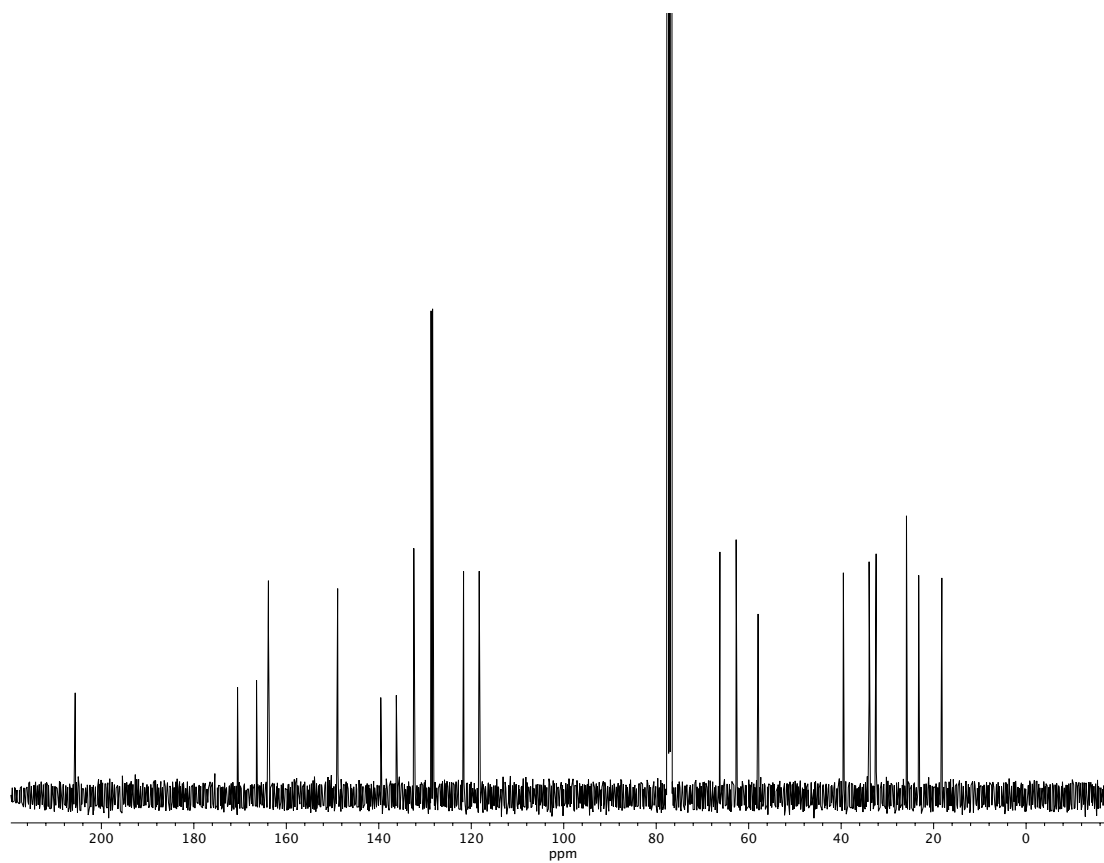
Figure A2.88. ^{13}C *NMR (100 MHz, CDCl$_3$) of compound **40c**.*
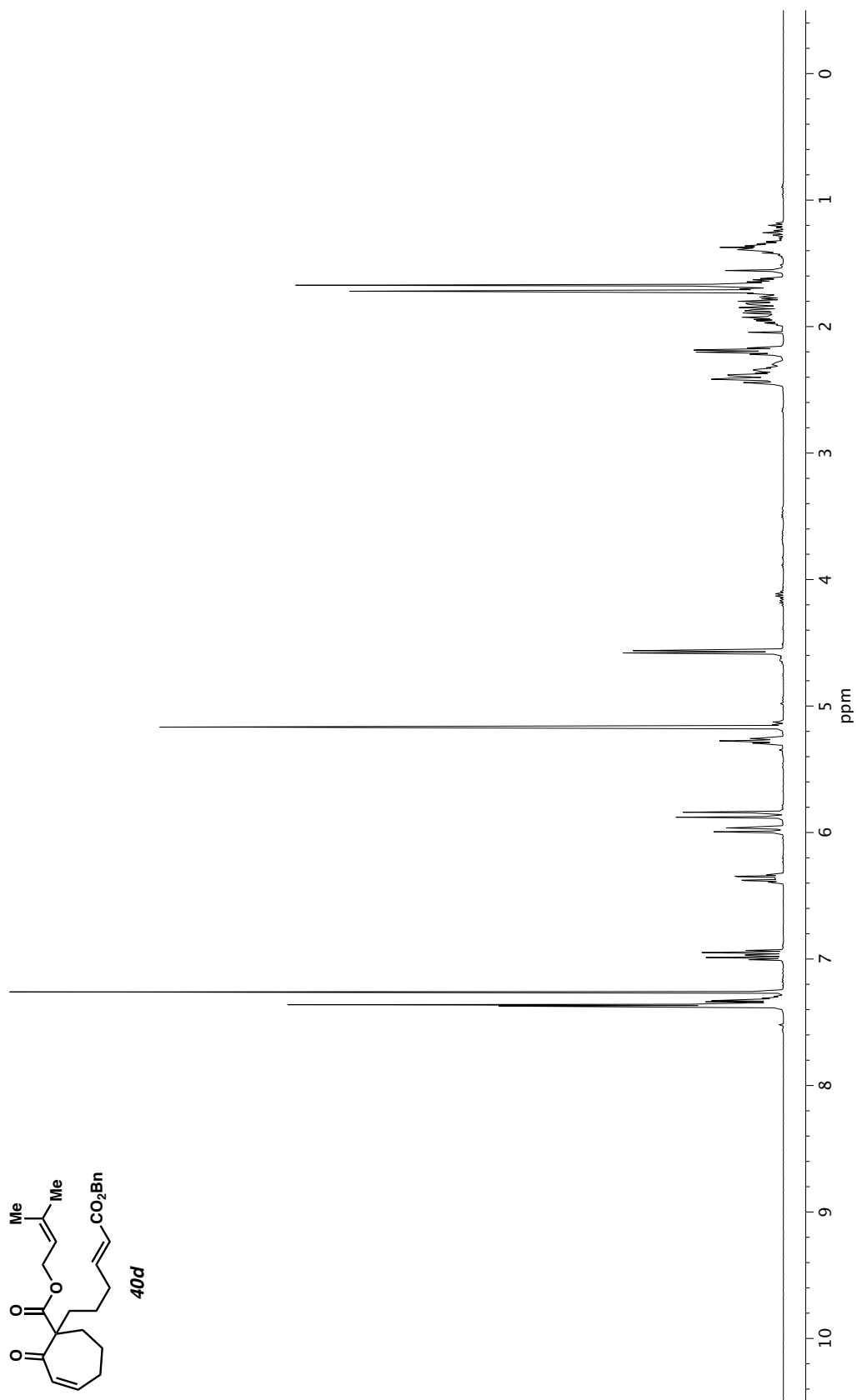
Figure A2.89. ^1H NMR (400 MHz, CDCl$_3$) of compound **40d**.
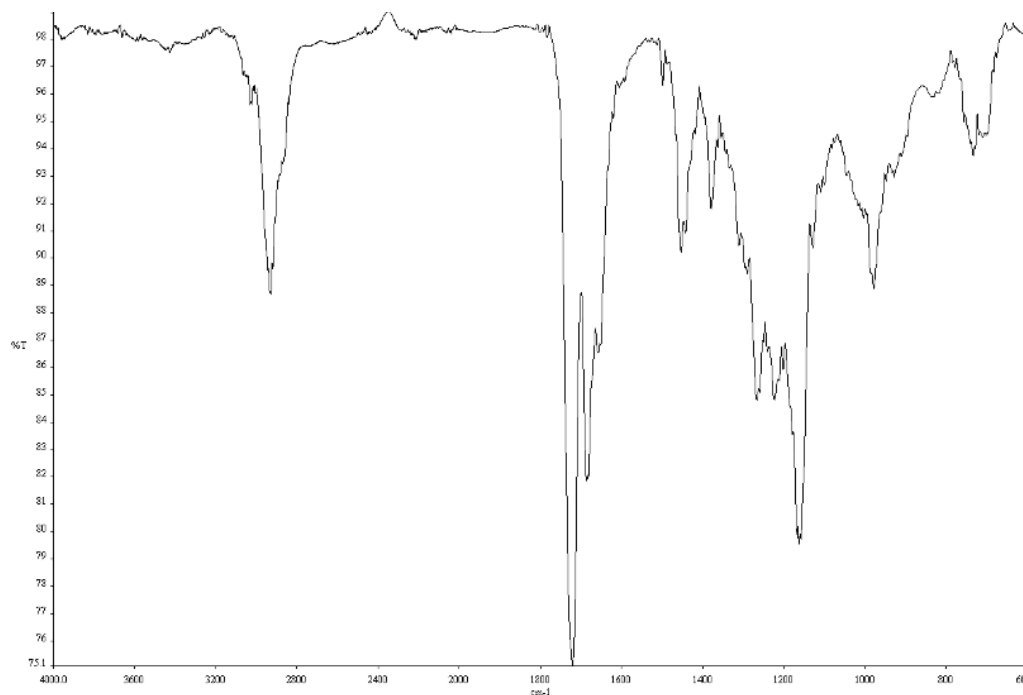
Figure A2.90. *Infrared spectrum (Thin Film, NaCl) of compound **40d**.*
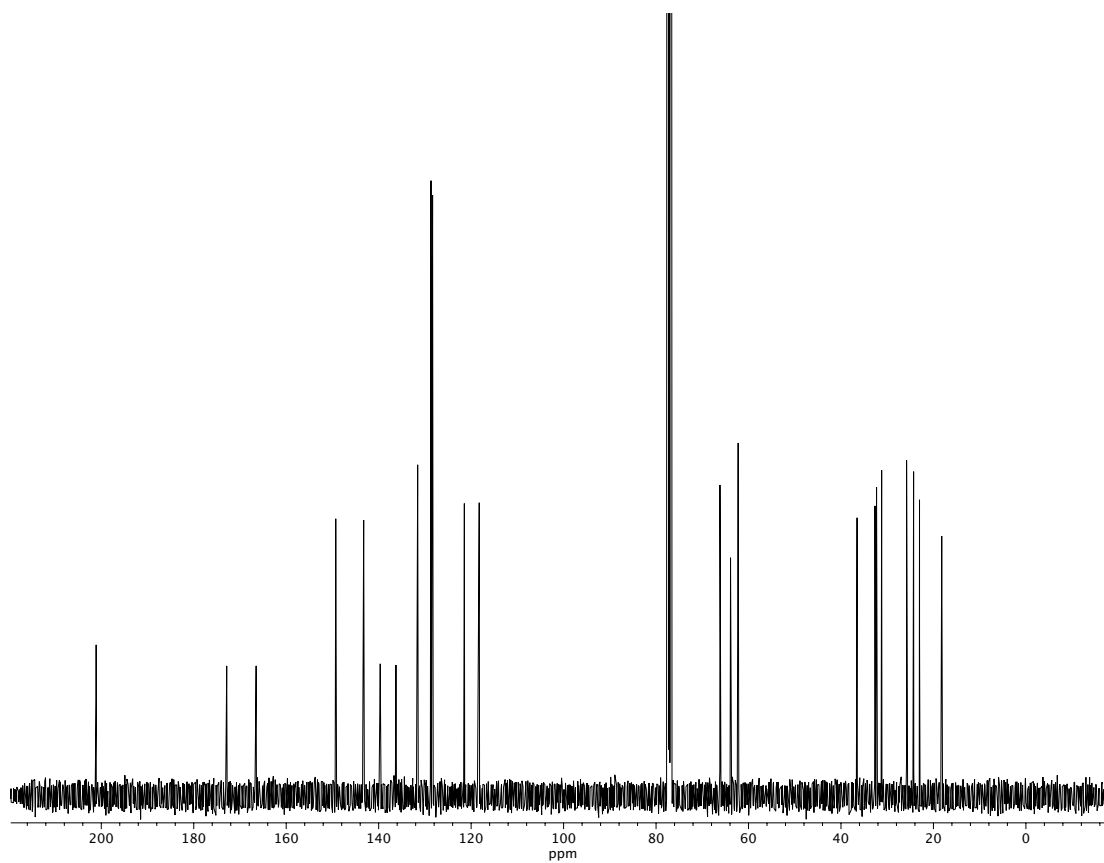
Figure A2.91. *^{13}C NMR (100 MHz, CDCl$_3$) of compound **40d**.*
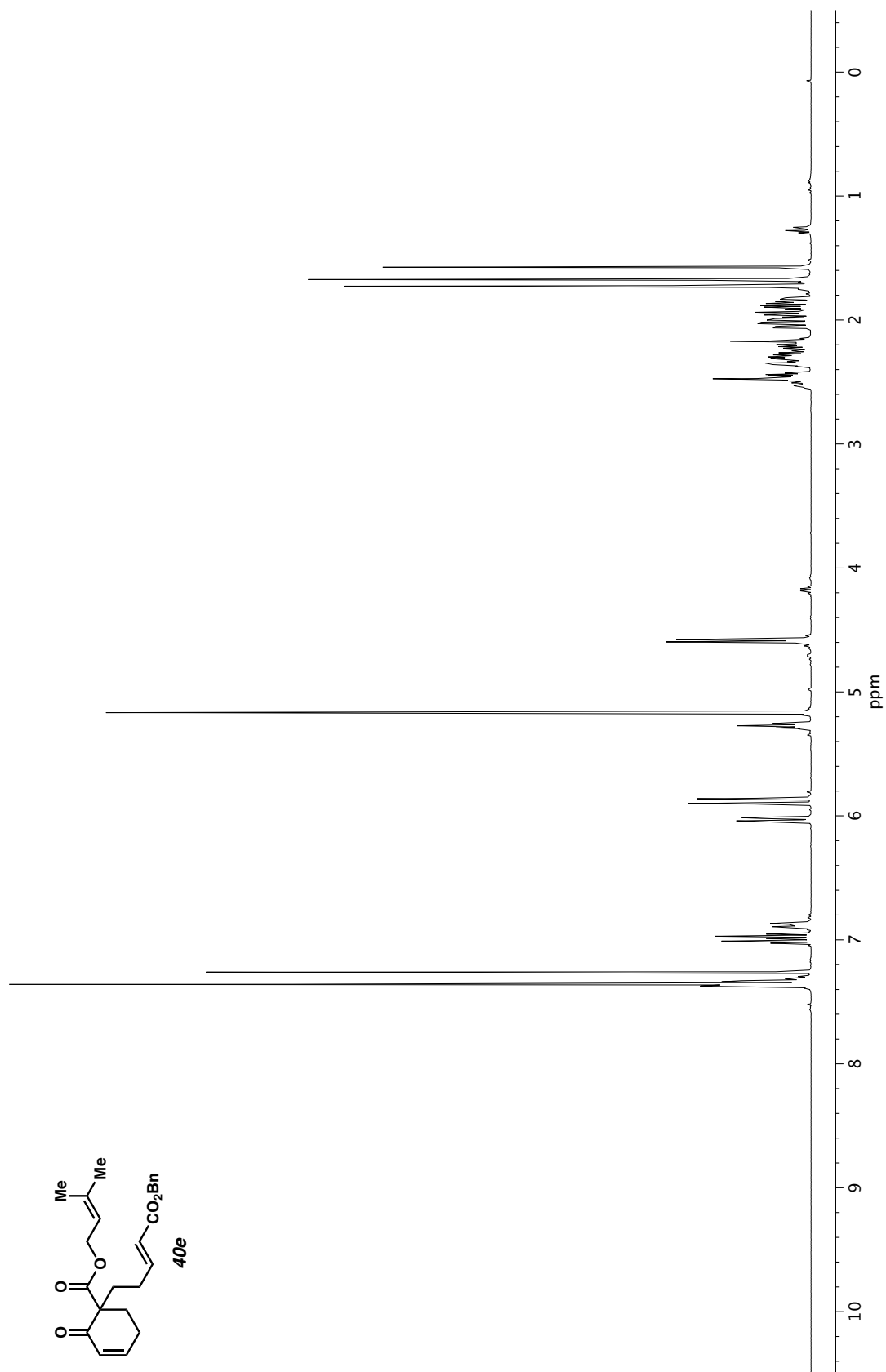
Figure A2.92. ^1H NMR (400 MHz, CDCl$_3$) of compound **40e**.
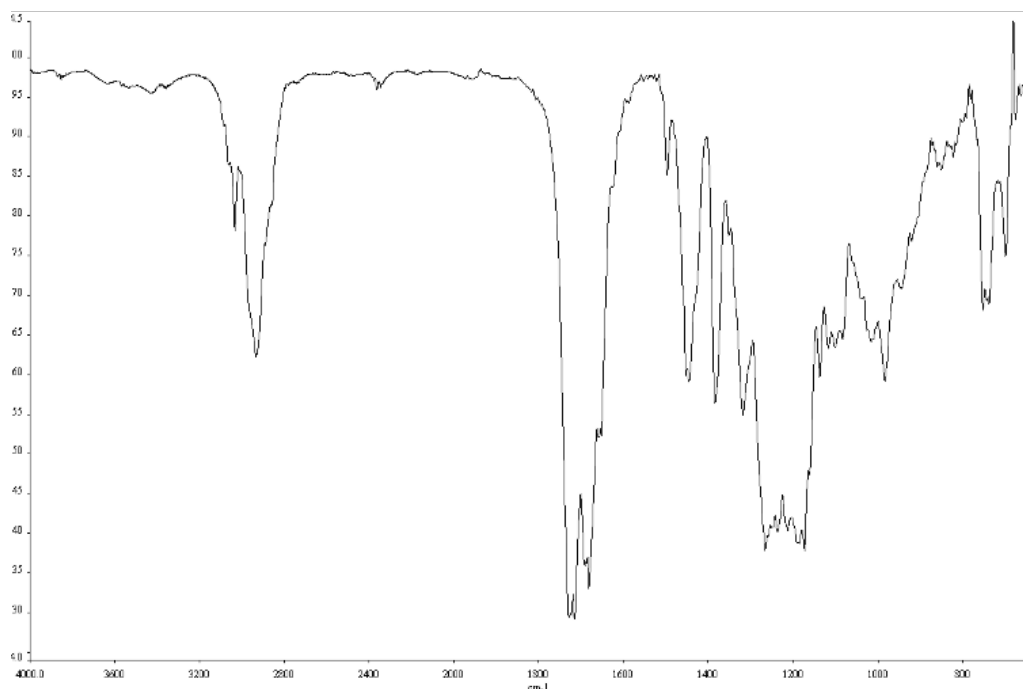
Figure A2.93. Infrared spectrum (Thin Film, NaCl) of compound **40e**.
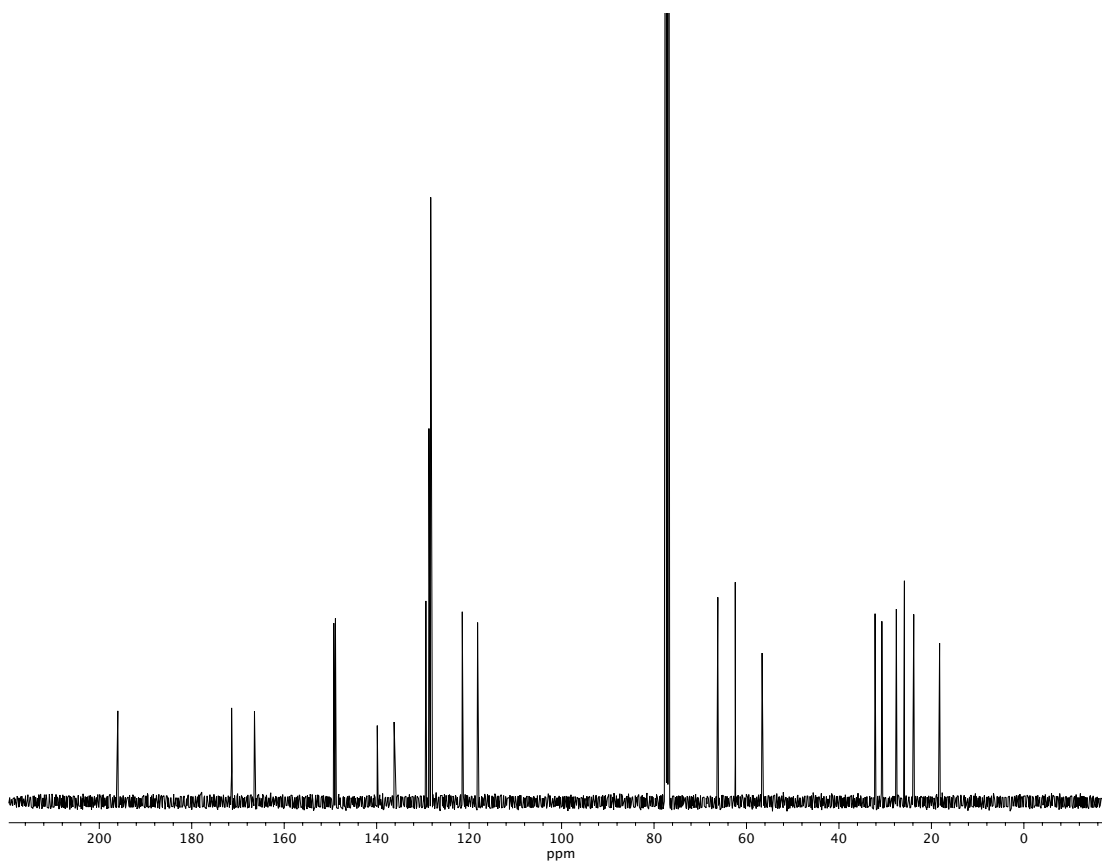
Figure A2.94. ^{13}C NMR (100 MHz, CDCl$_3$) of compound **40e**.
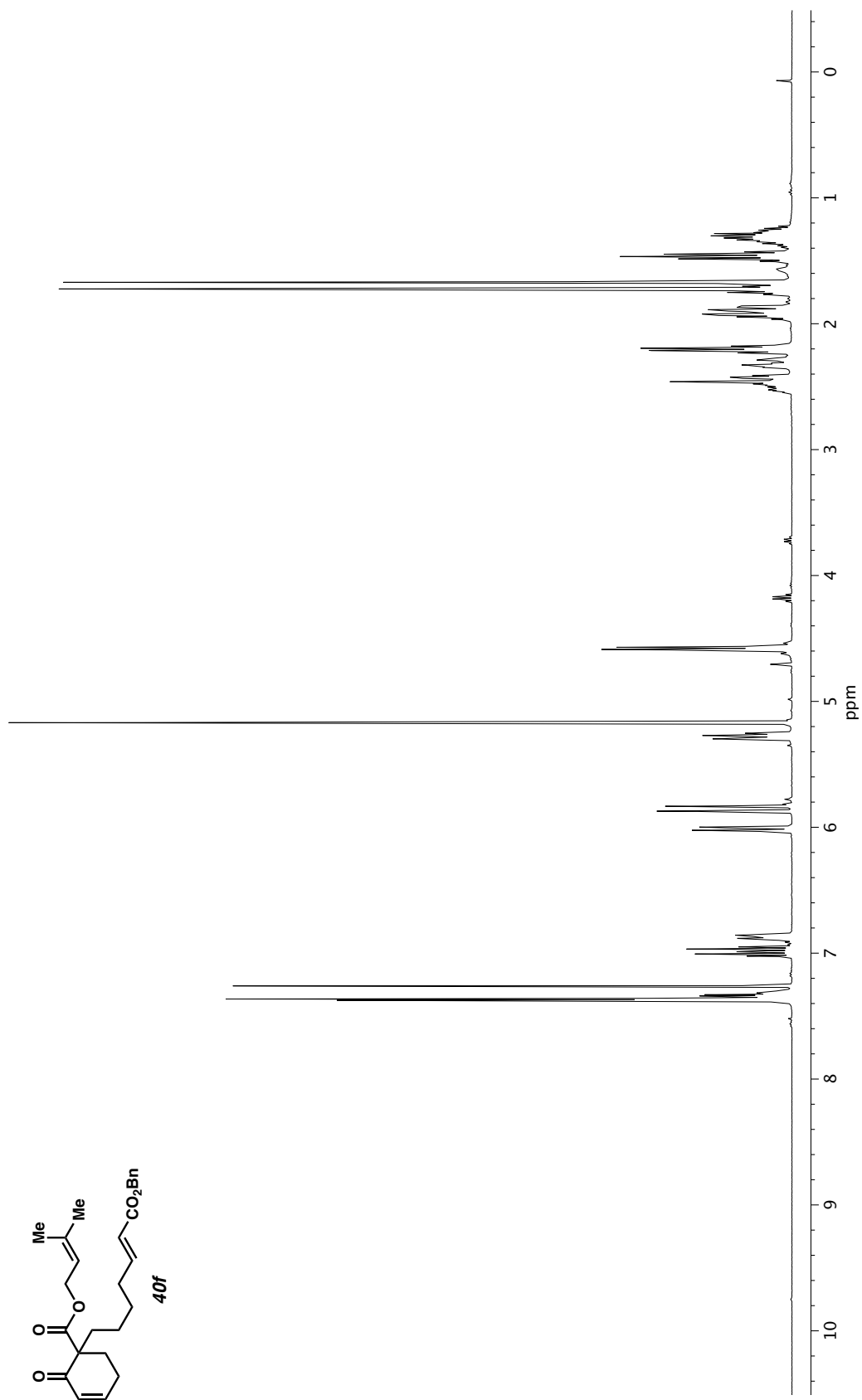
Figure A2.95. ^1H NMR (400 MHz, CDCl$_3$) of compound **40f**.
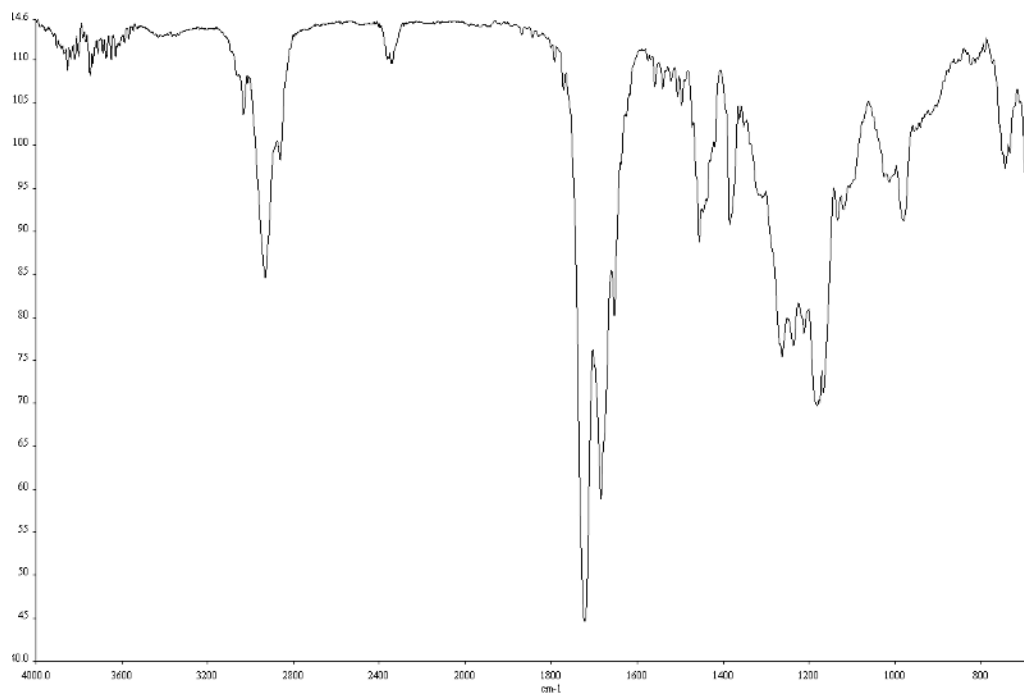
Figure A2.96. *Infrared spectrum (Thin Film, NaCl) of compound **40f**.*
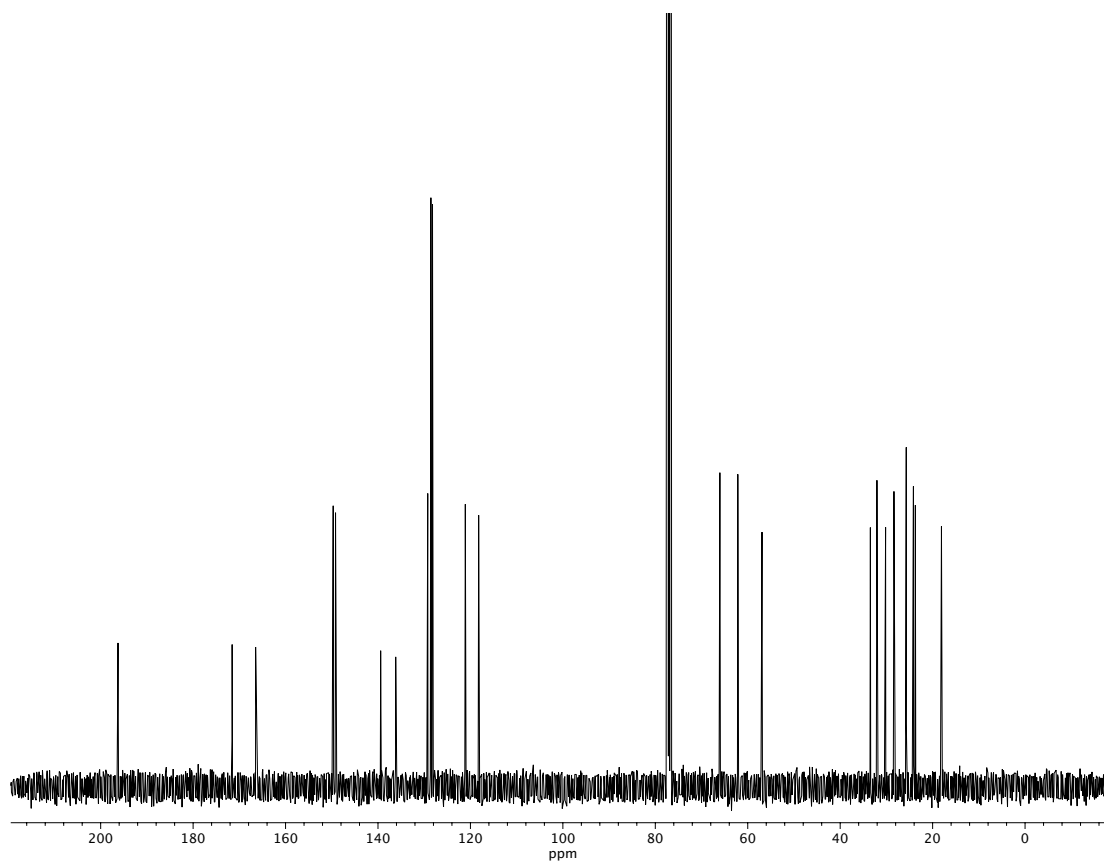
Figure A2.97. *^{13}C NMR (100 MHz, CDCl$_3$) of compound **40f**.*

Figure A2.98. *^{1}H NMR (400 MHz, CDCl$_3$) of compound **D-40f**.*
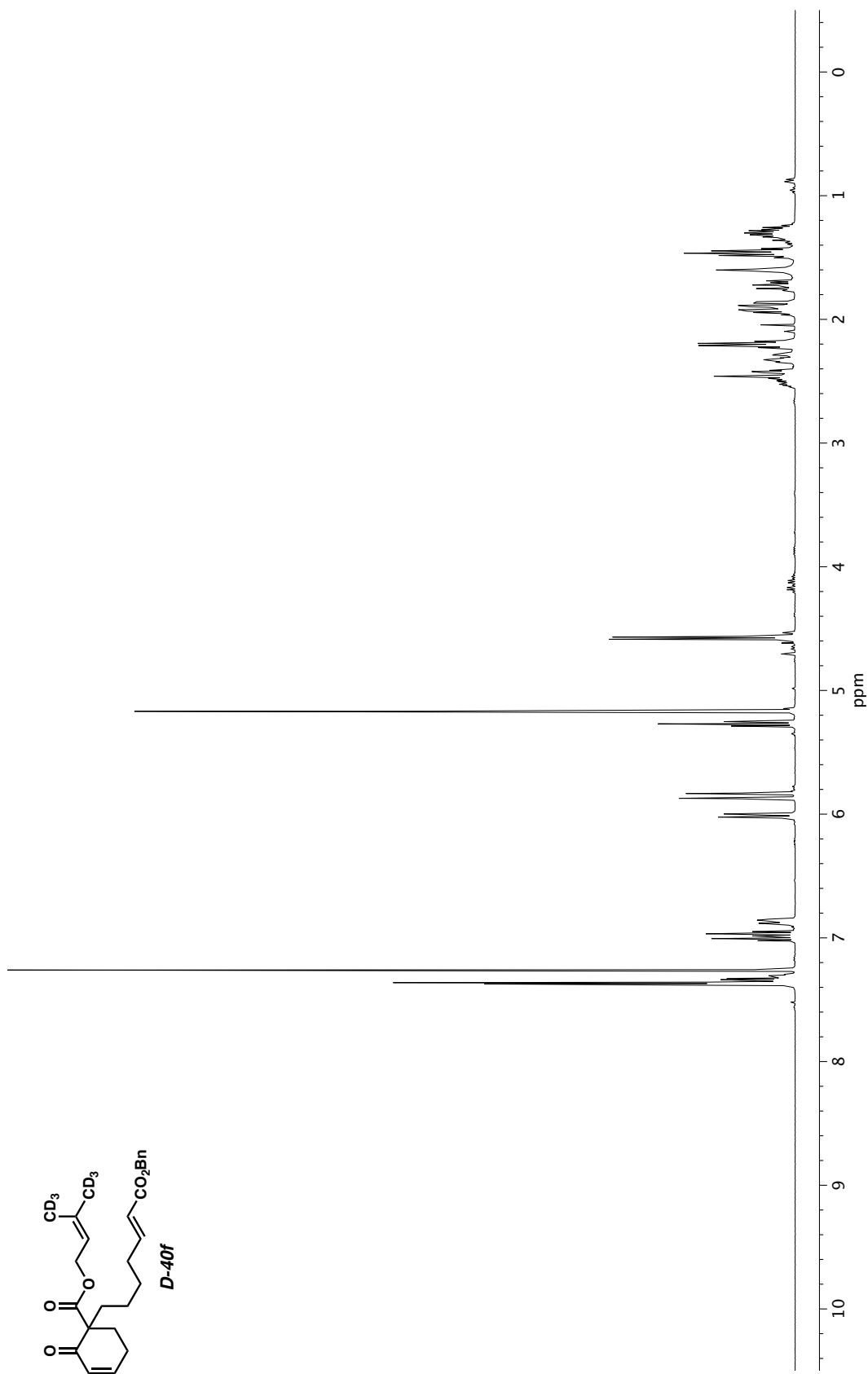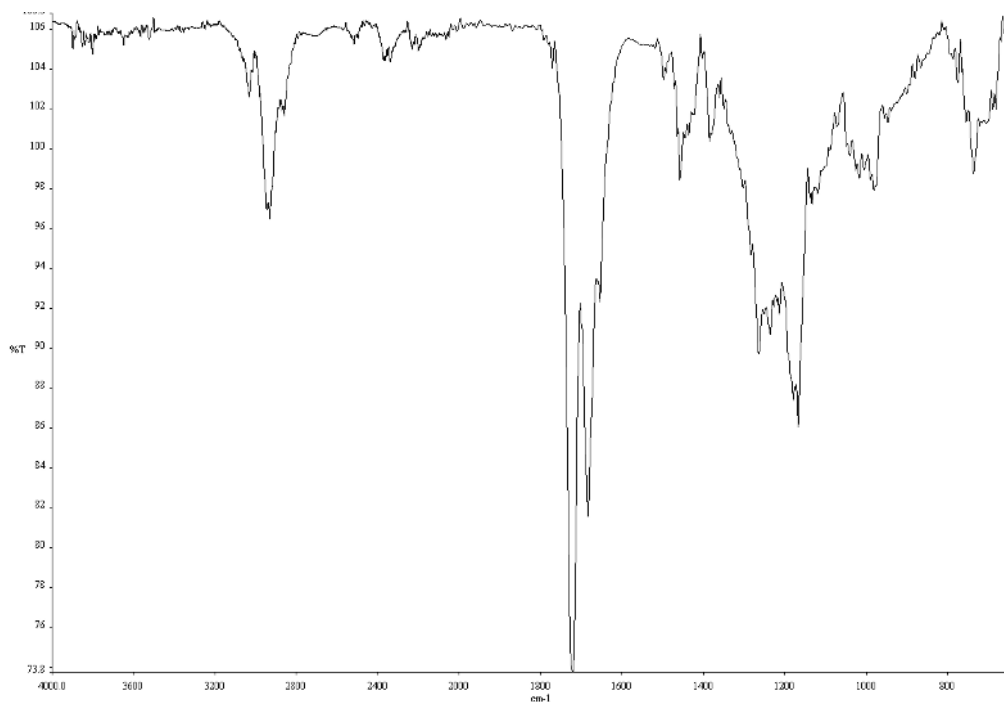
Figure A2.99. *Infrared spectrum (Thin Film, NaCl) of compound* **D-40f**.
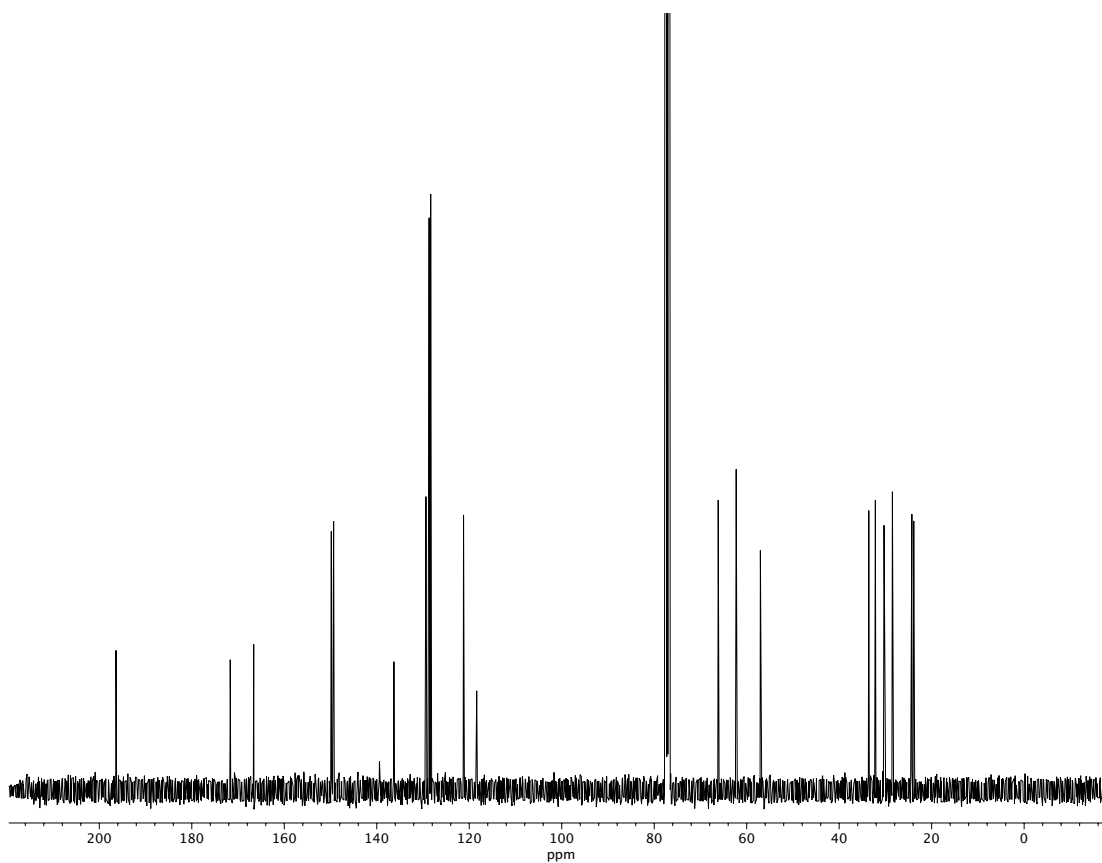
Figure A2.100. *^{13}C NMR (100 MHz, CDCl$_3$) of compound* **D-40f**.
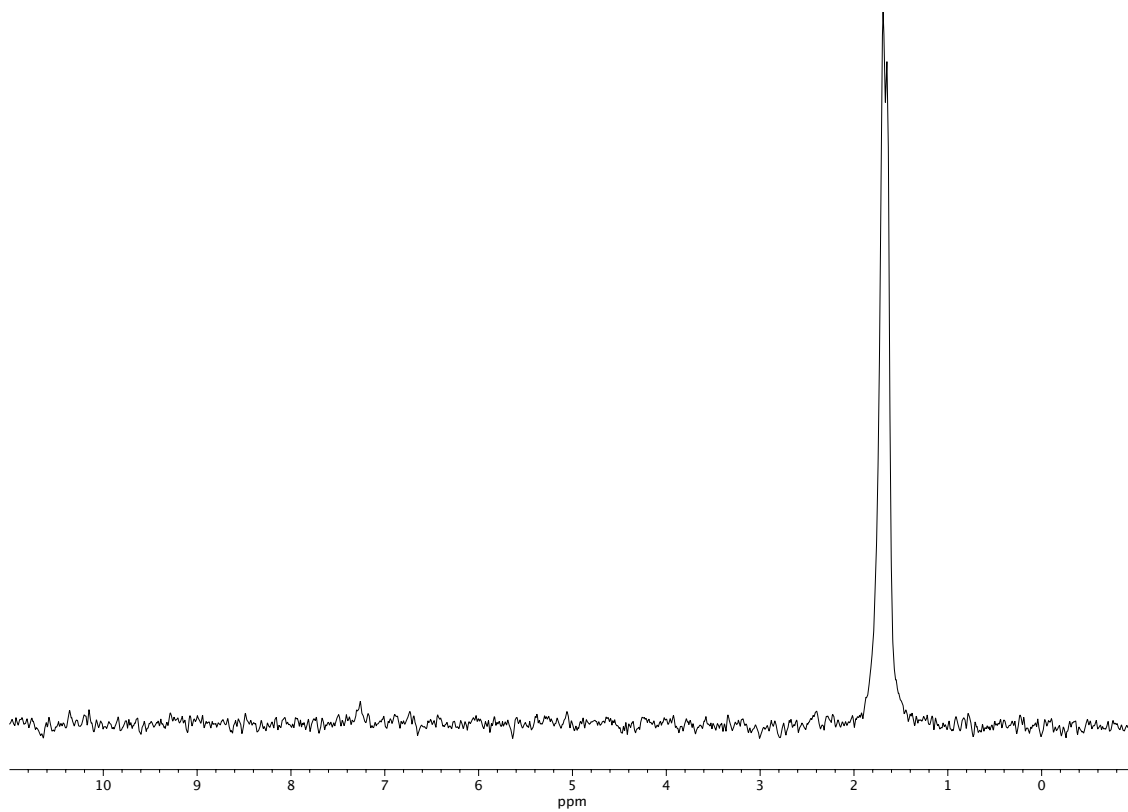
Figure A2.101. ^{2}*H NMR (61 MHz, CDCl$_3$) of compound* **D-40f**.

Figure A2.102. ^1H NMR (400 MHz, CDCl$_3$) of compound **40g**.
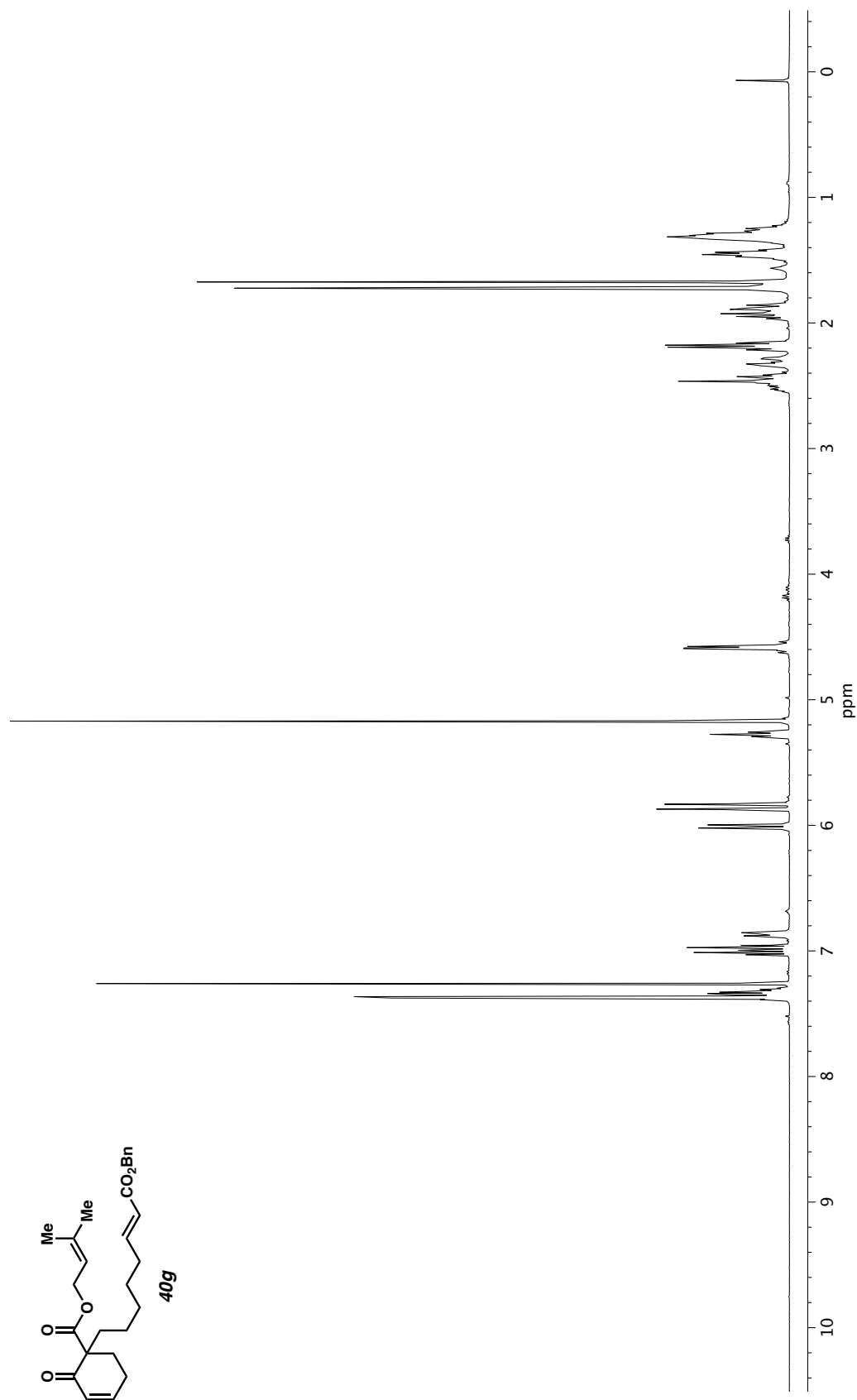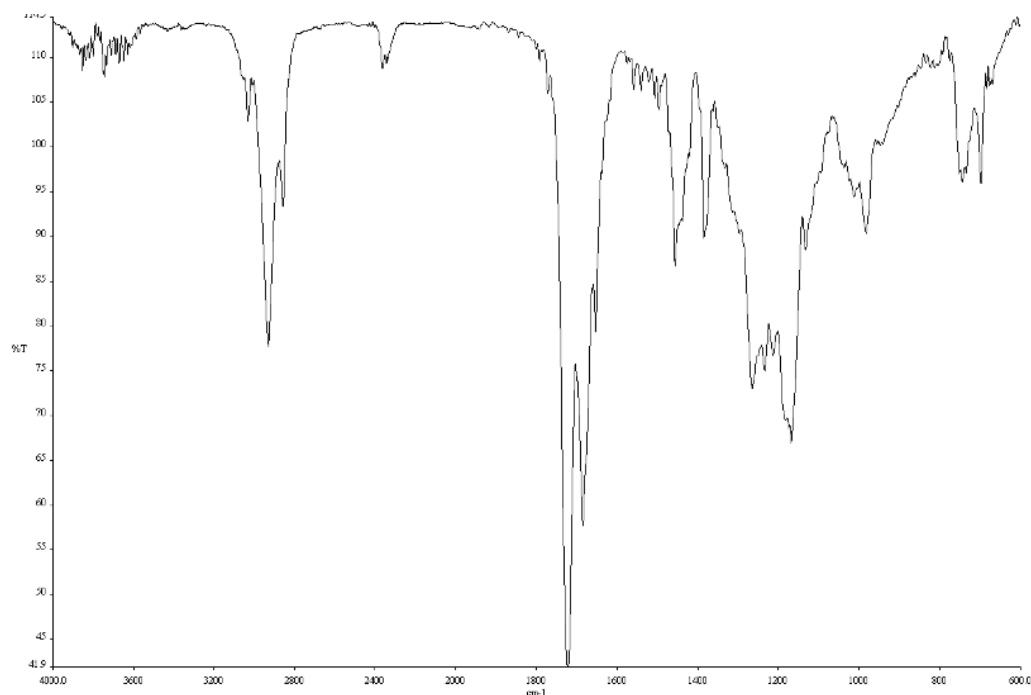
Figure A2.103. *Infrared spectrum (Thin Film, NaCl) of compound* **40g**.
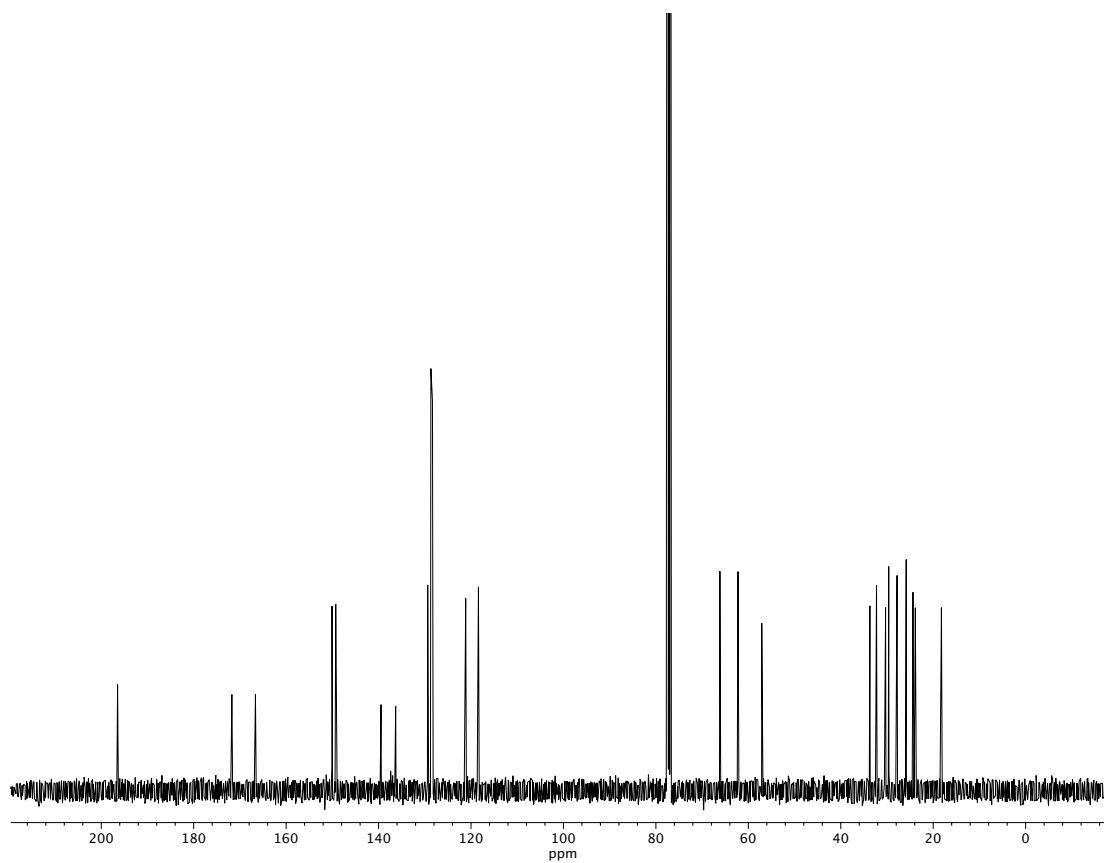
Figure A2.104. ^{13}C *NMR (100 MHz, CDCl$_3$) of compound* **40g**.
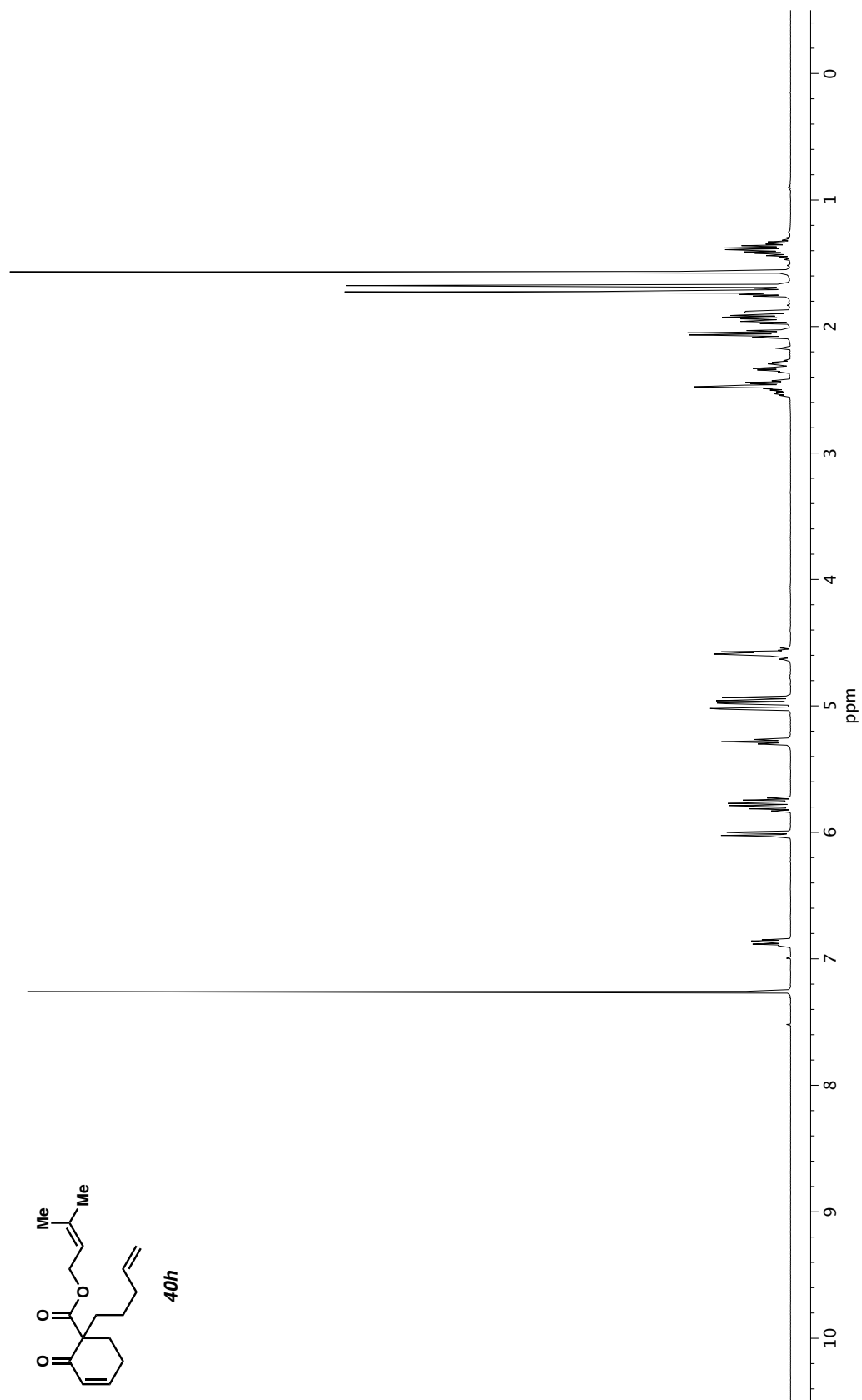
Figure A2.105. ^1H NMR (400 MHz, CDCl$_3$) of compound **40h**.
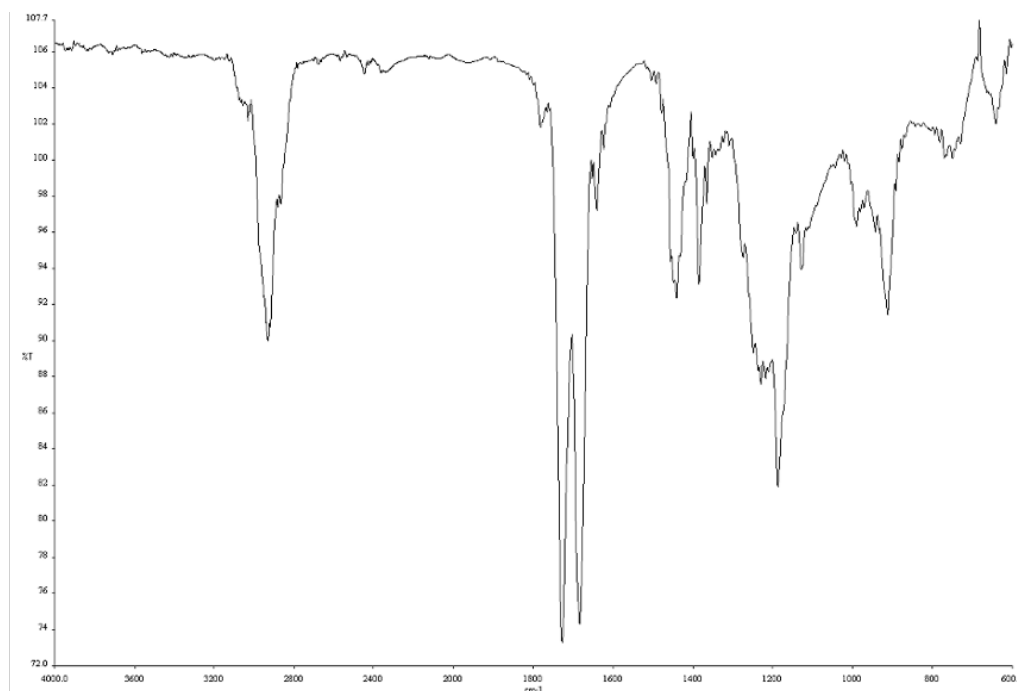
Figure A2.106. *Infrared spectrum (Thin Film, NaCl) of compound* **40h**.
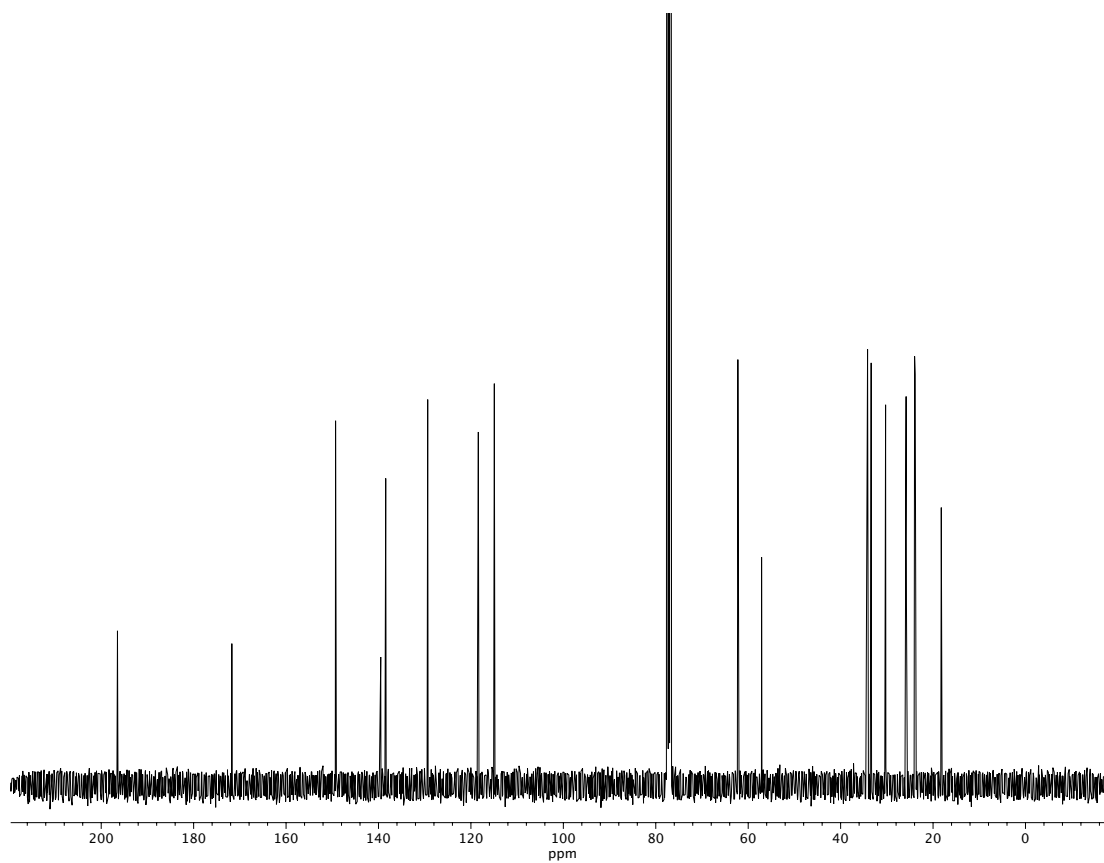
Figure A2.107. *^{13}C NMR (100 MHz, CDCl$_3$) of compound* **40h**.

Figure A2.108. ^1H NMR (400 MHz, CDCl$_3$) of compound **40i**.
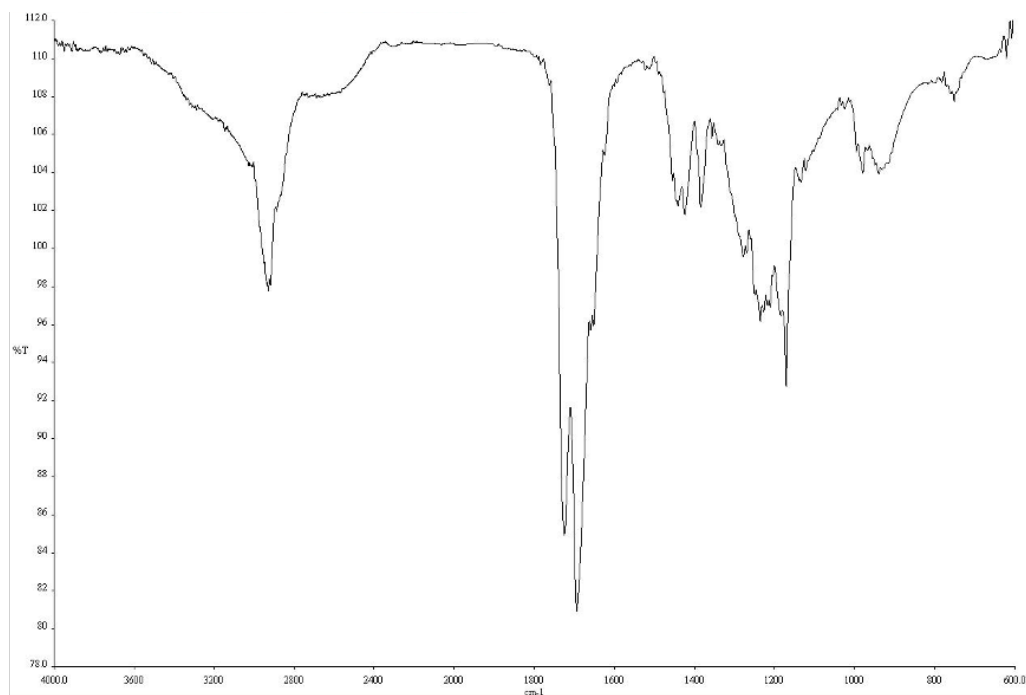
Figure A2.109. *Infrared spectrum (Thin Film, NaCl) of compound* **40i**.
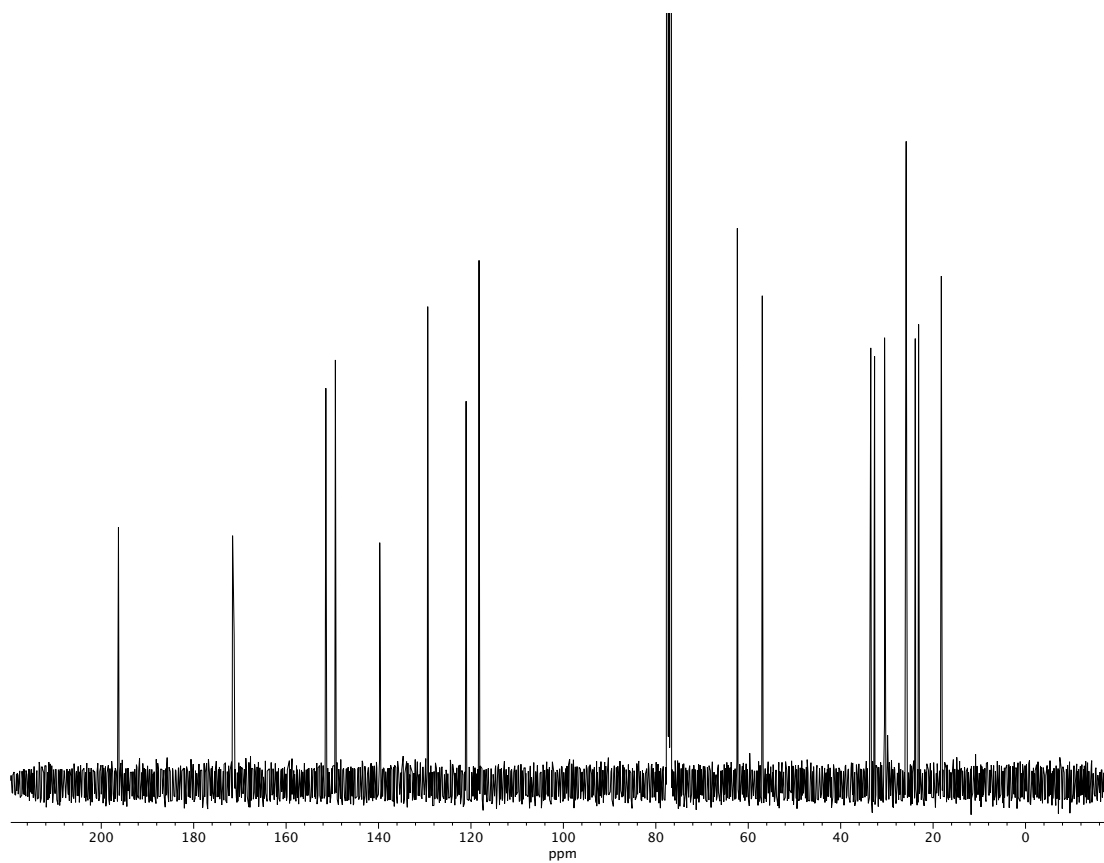
Figure A2.110. ^{13}C *NMR (100 MHz, CDCl$_3$) of compound* **40i**.
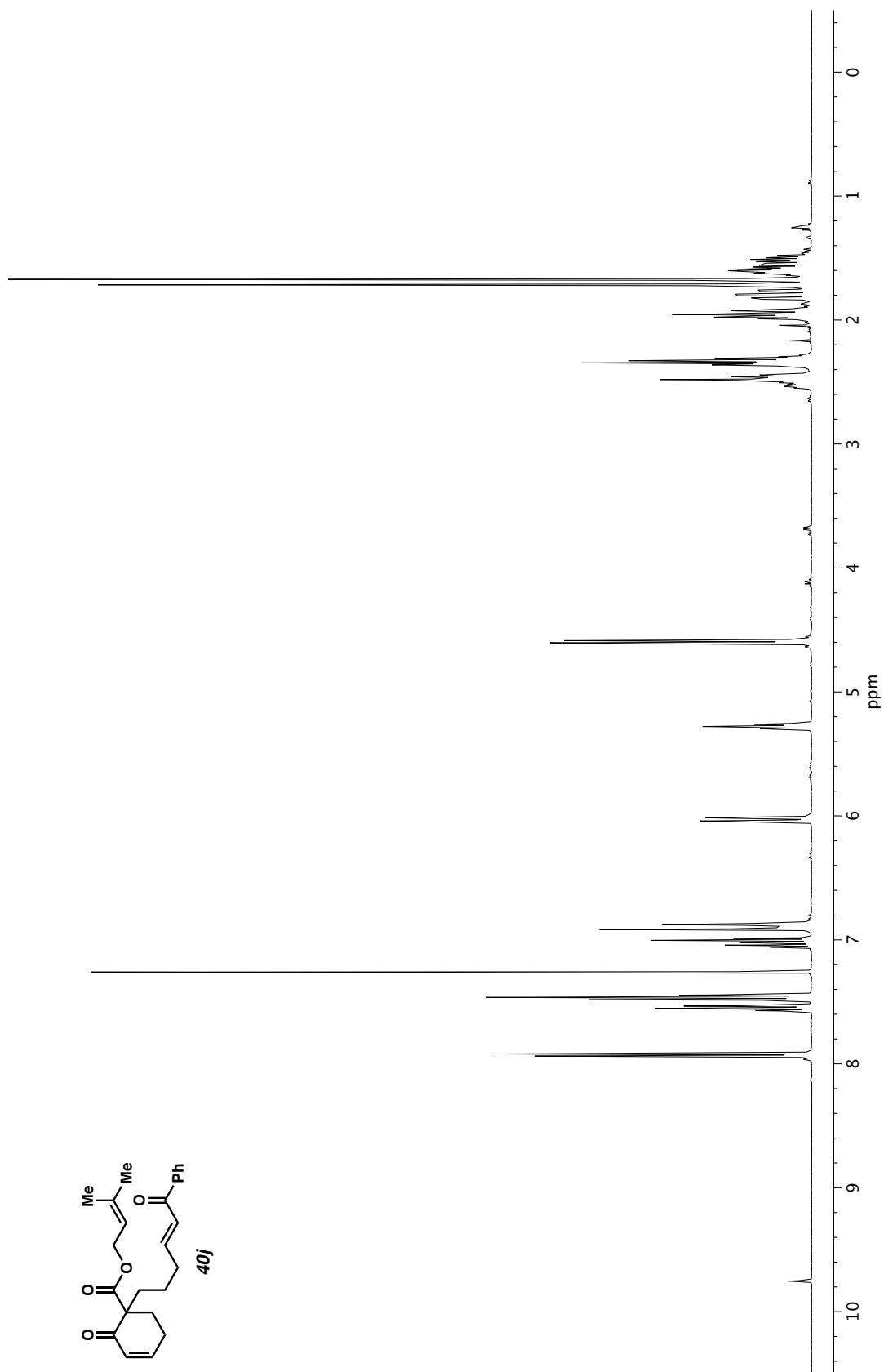
Figure A2.111. *¹H NMR (400 MHz, CDCl₃) of compound **40j***.
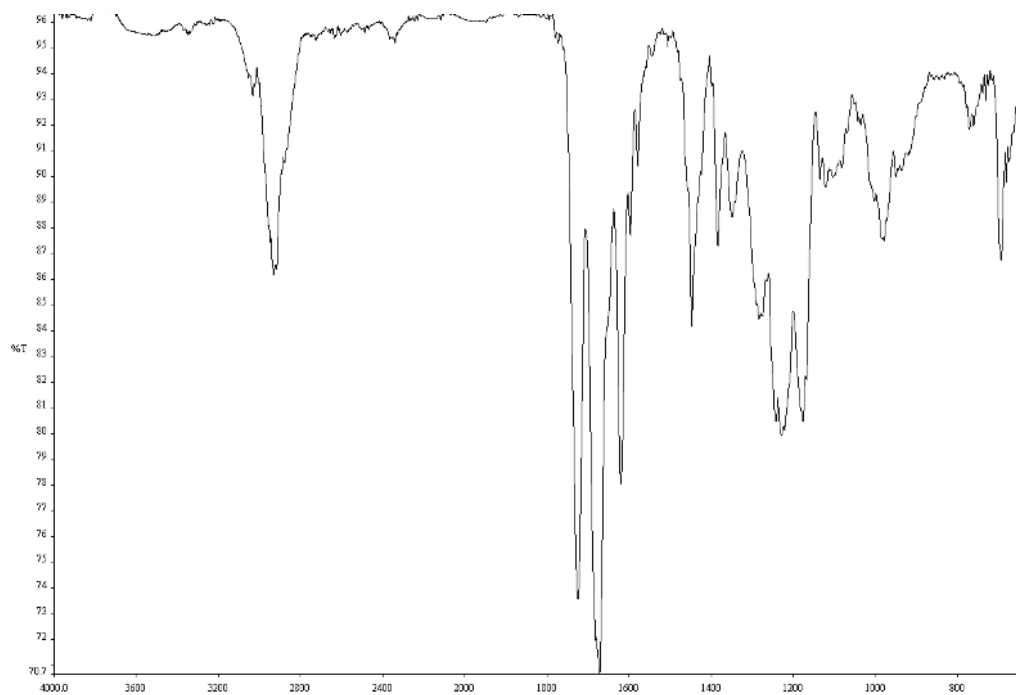
Figure A2.112. *Infrared spectrum (Thin Film, NaCl) of compound **40j***.
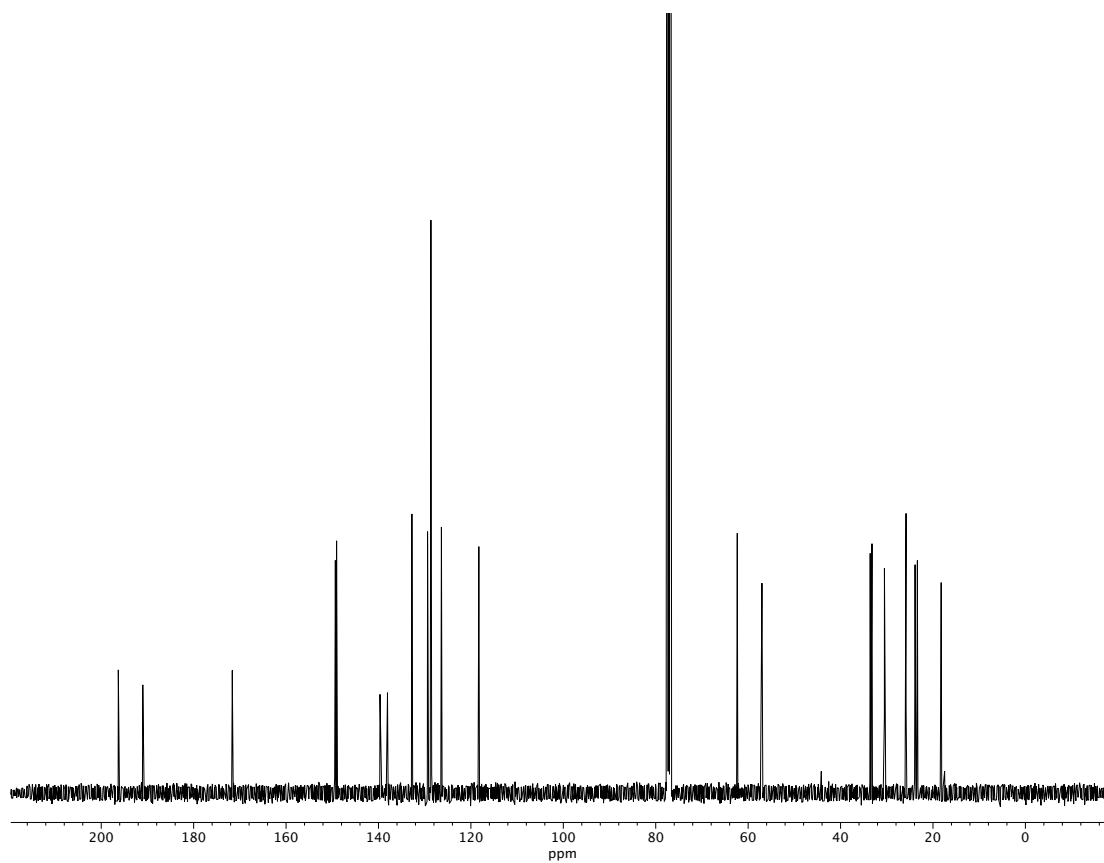
Figure A2.113. ^{13}C *NMR (100 MHz, CDCl$_3$) of compound **40j***.
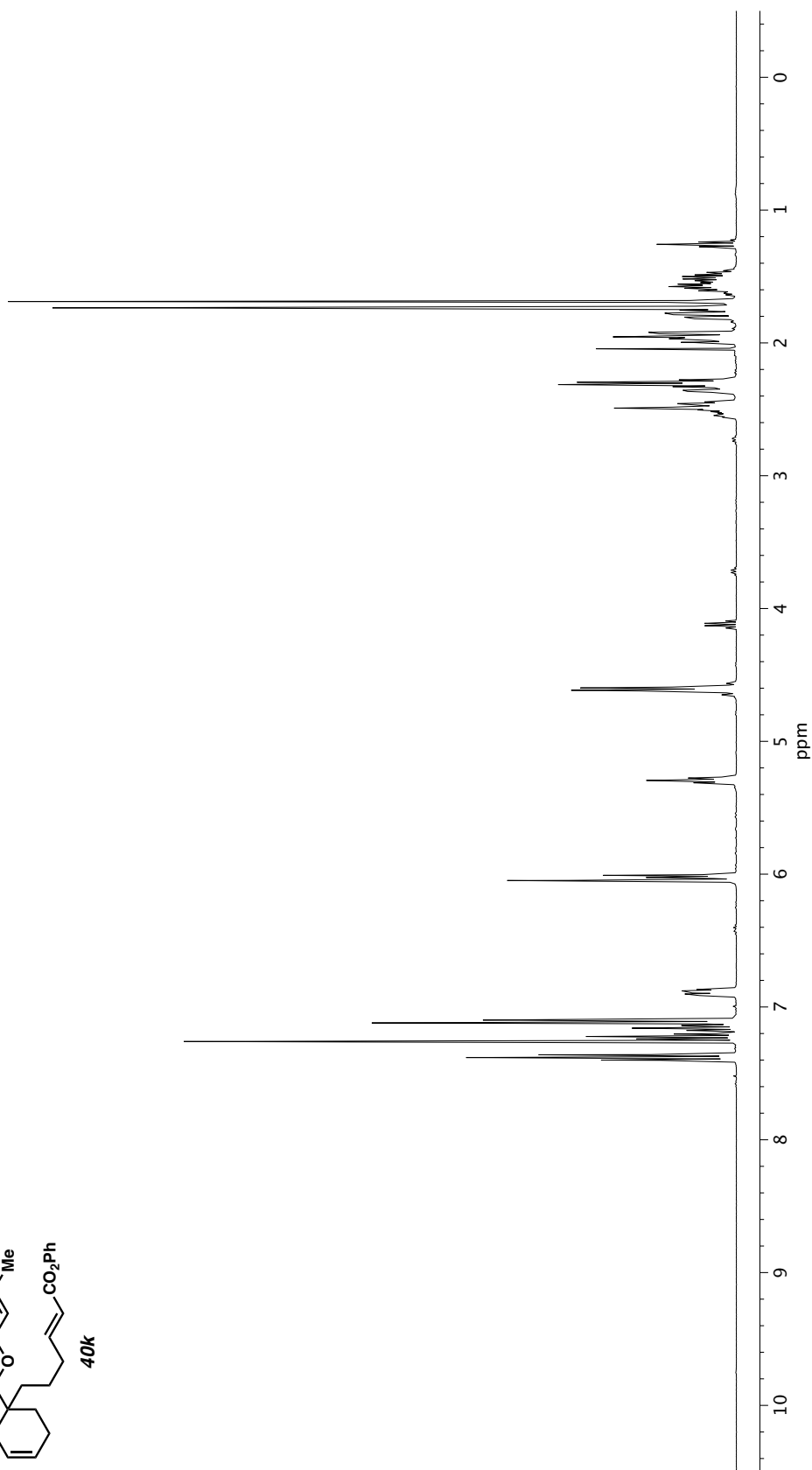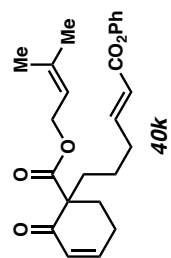
Figure A2.114. ^1H NMR (400 MHz, CDCl$_3$) of compound **40k**.
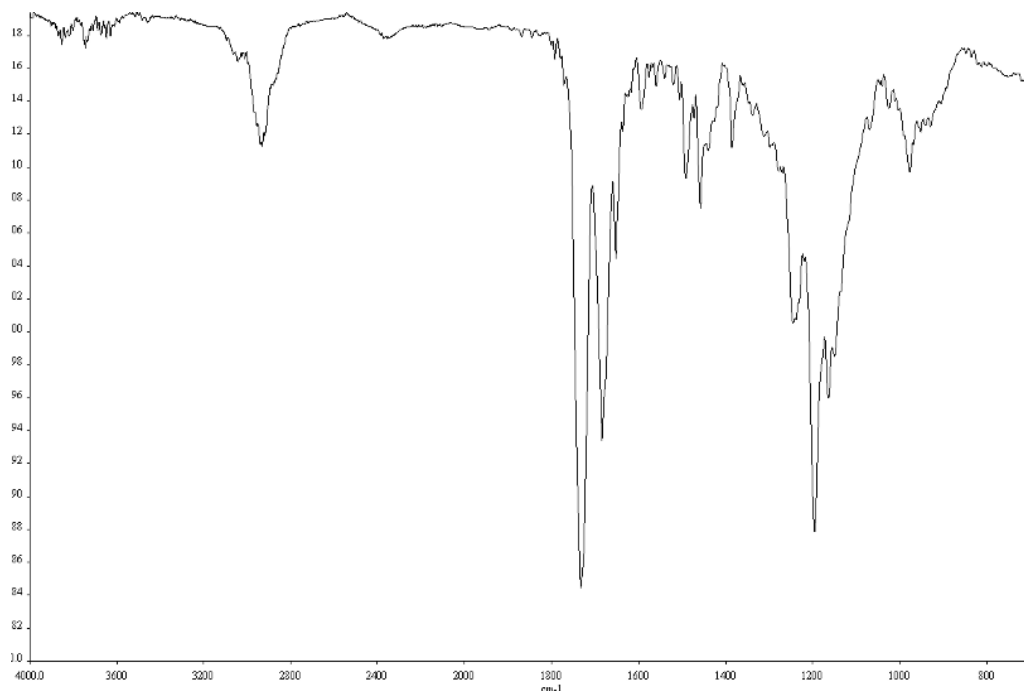
Figure A2.115. Infrared spectrum (Thin Film, NaCl) of compound **40k**.
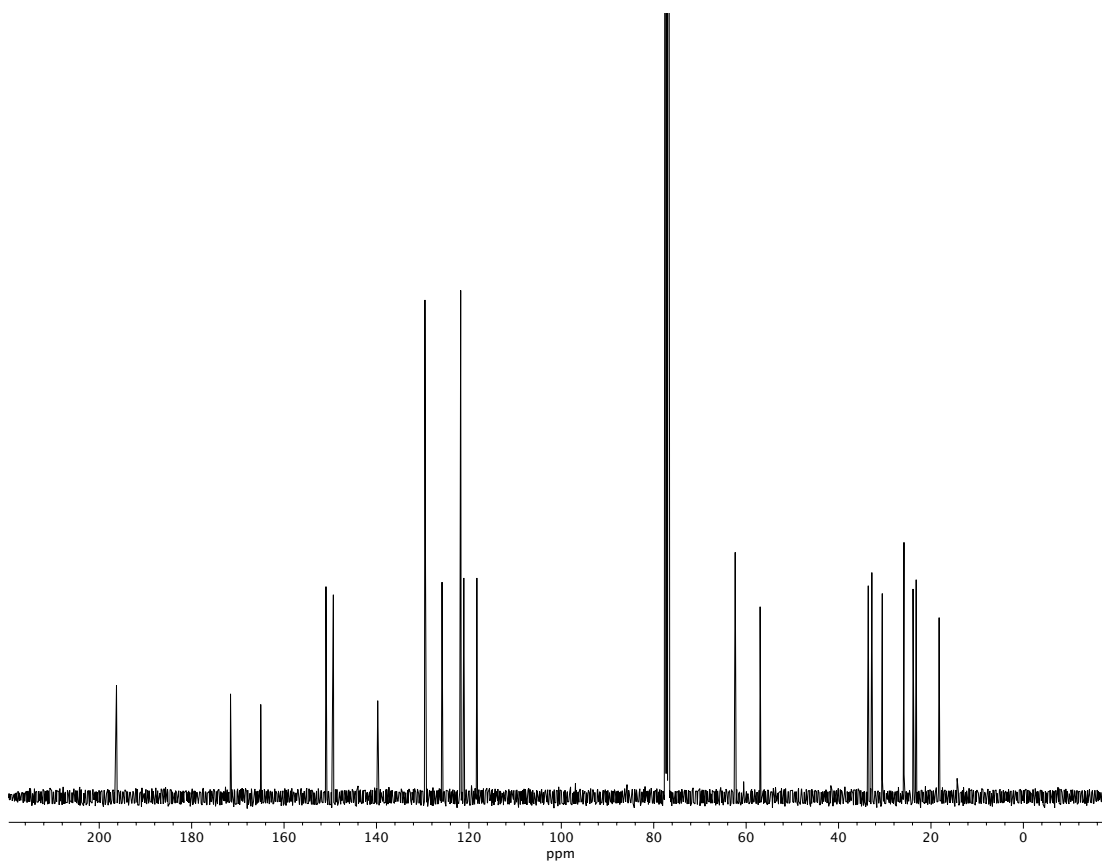
Figure A2.116. ^{13}C NMR (100 MHz, CDCl$_3$) of compound **40k**.
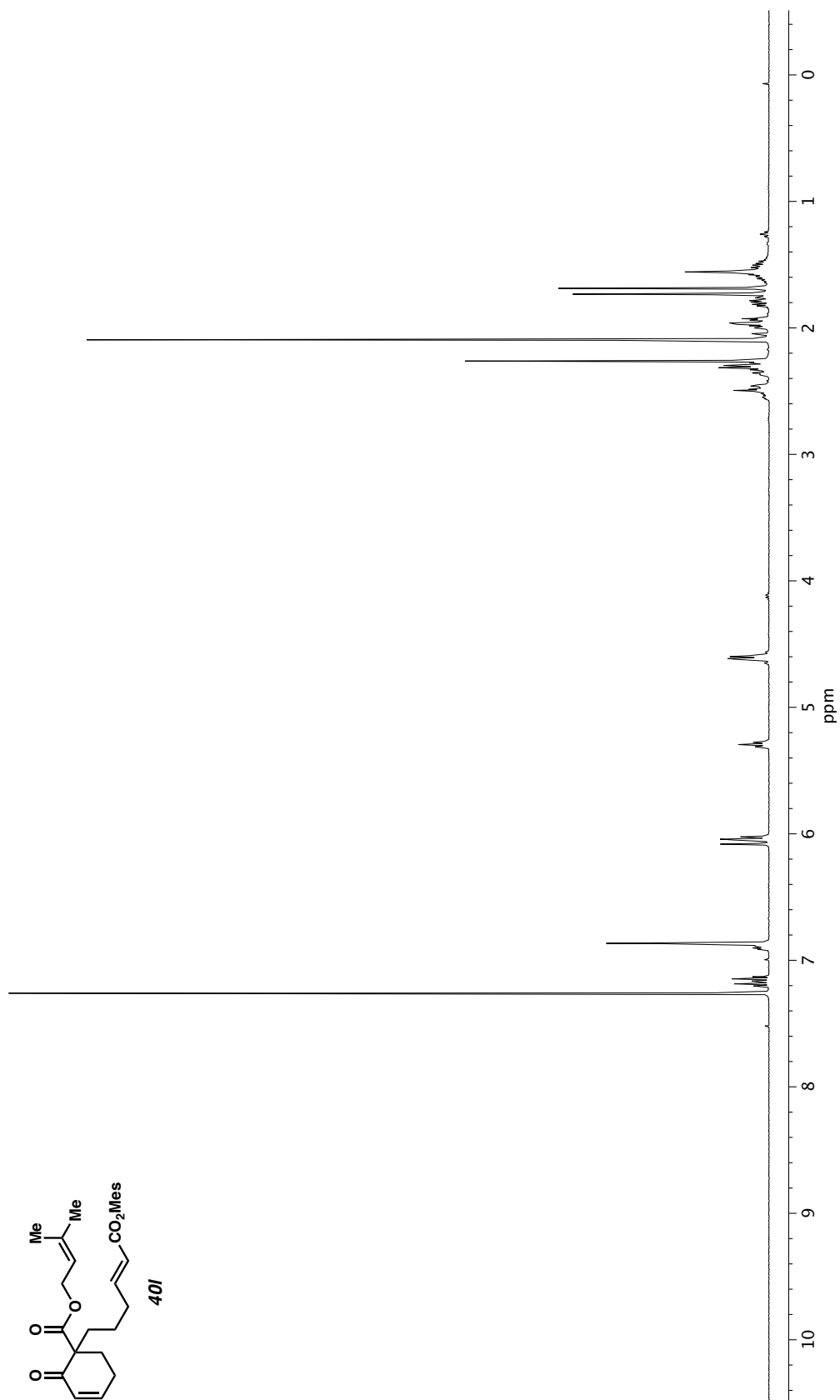
Figure A2.117. *¹H NMR (400 MHz, CDCl₃) of compound **40l**.*
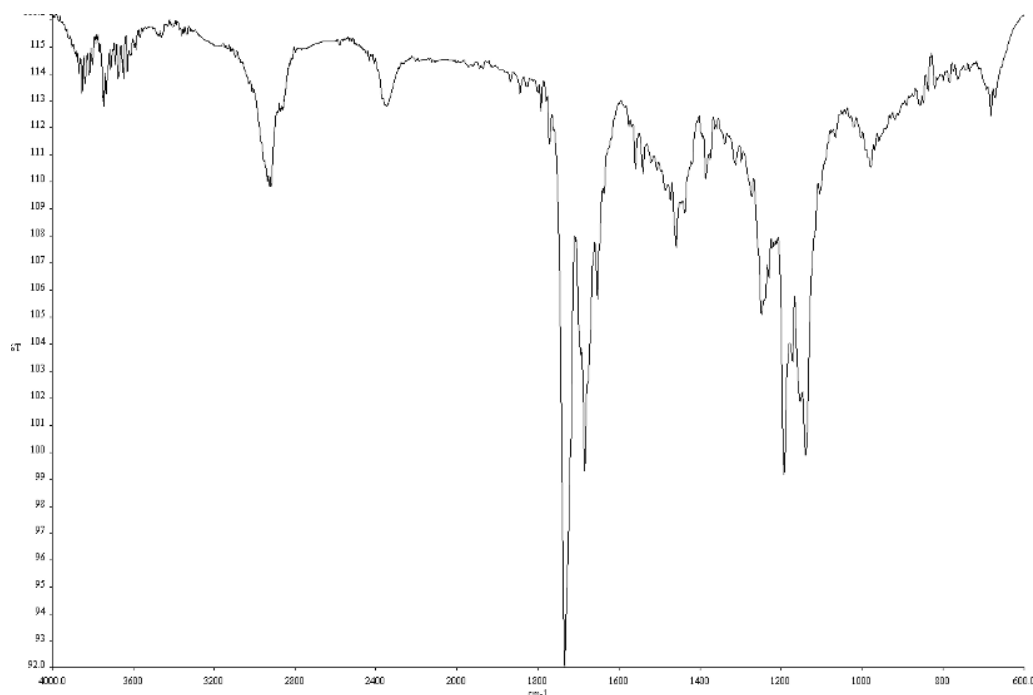
Figure A2.118. *Infrared spectrum (Thin Film, NaCl) of compound **40l**.*
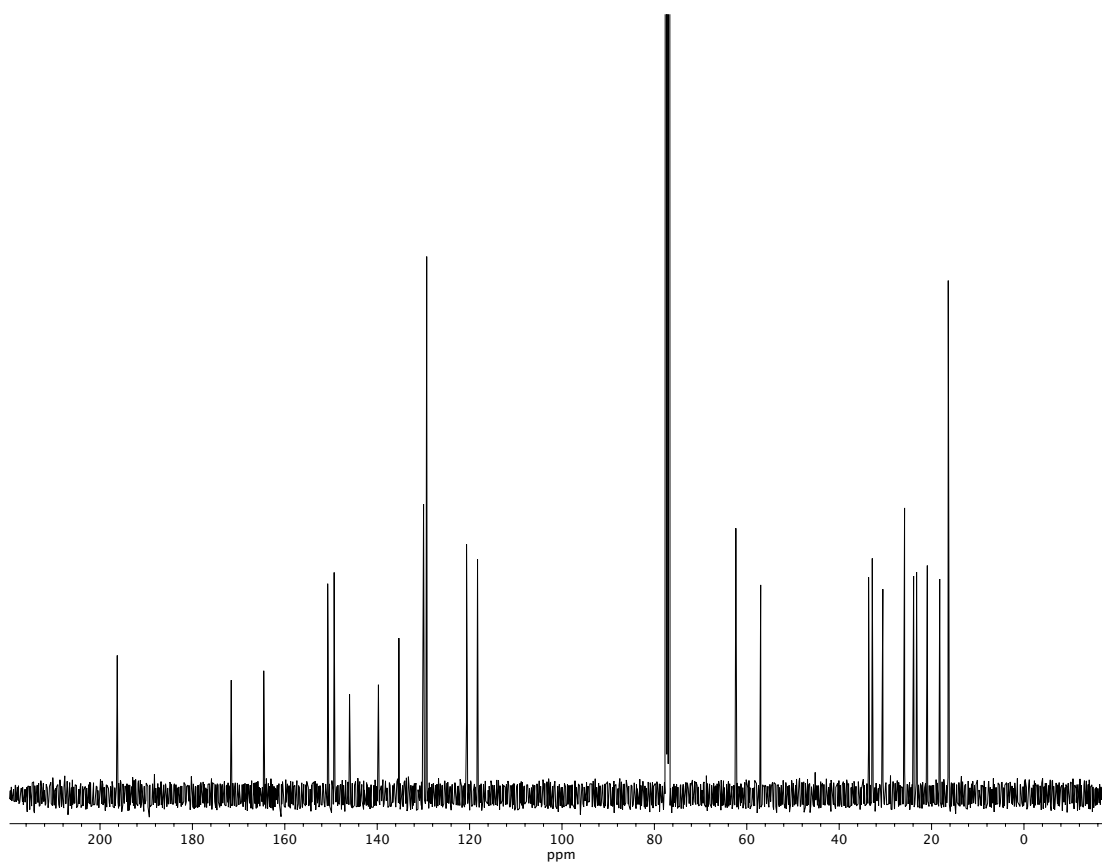
Figure A2.119. *^{13}C NMR (100 MHz, CDCl$_3$) of compound **40l**.*
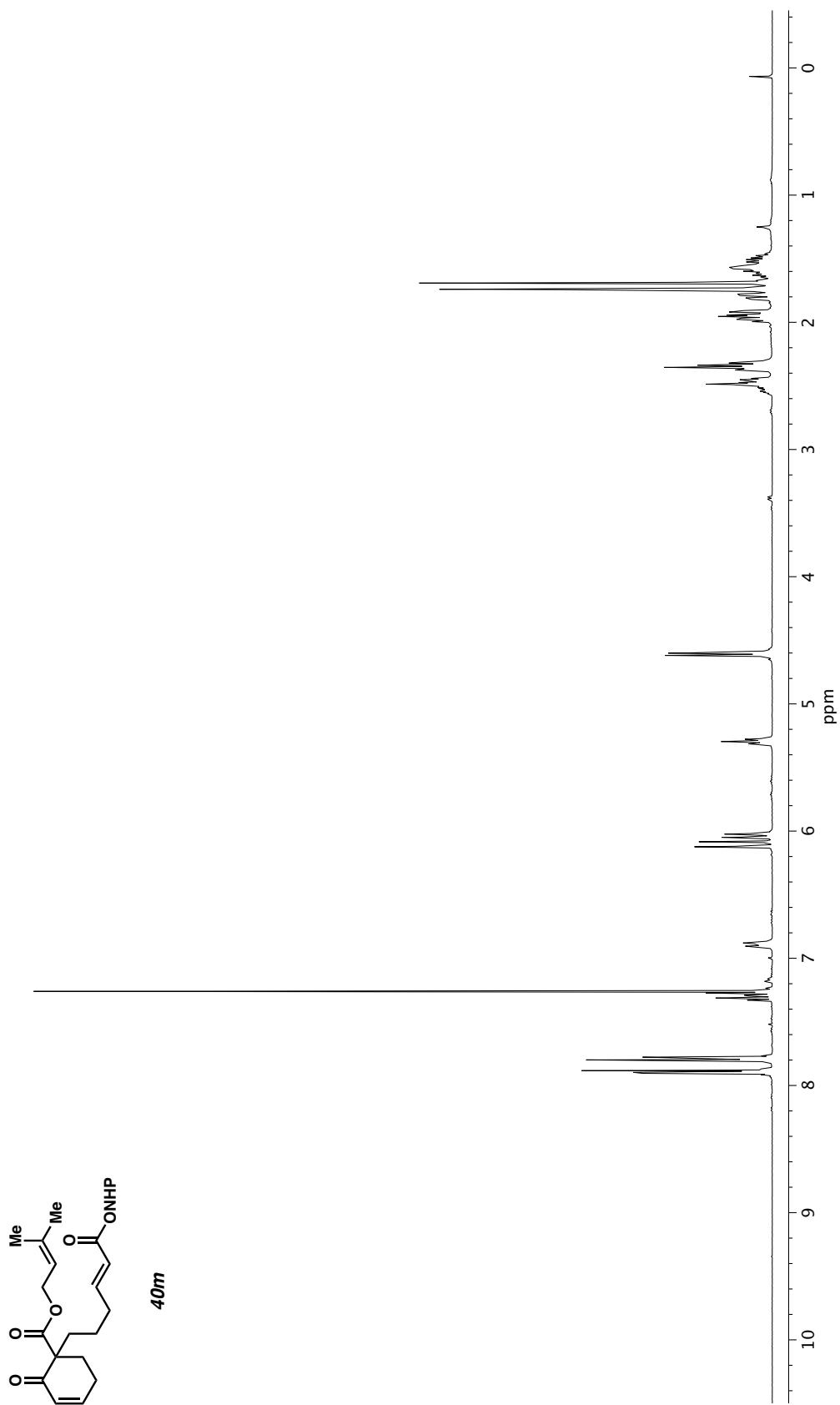
Figure A2.120. ^1H NMR (400 MHz, CDCl$_3$) of compound **40m**.
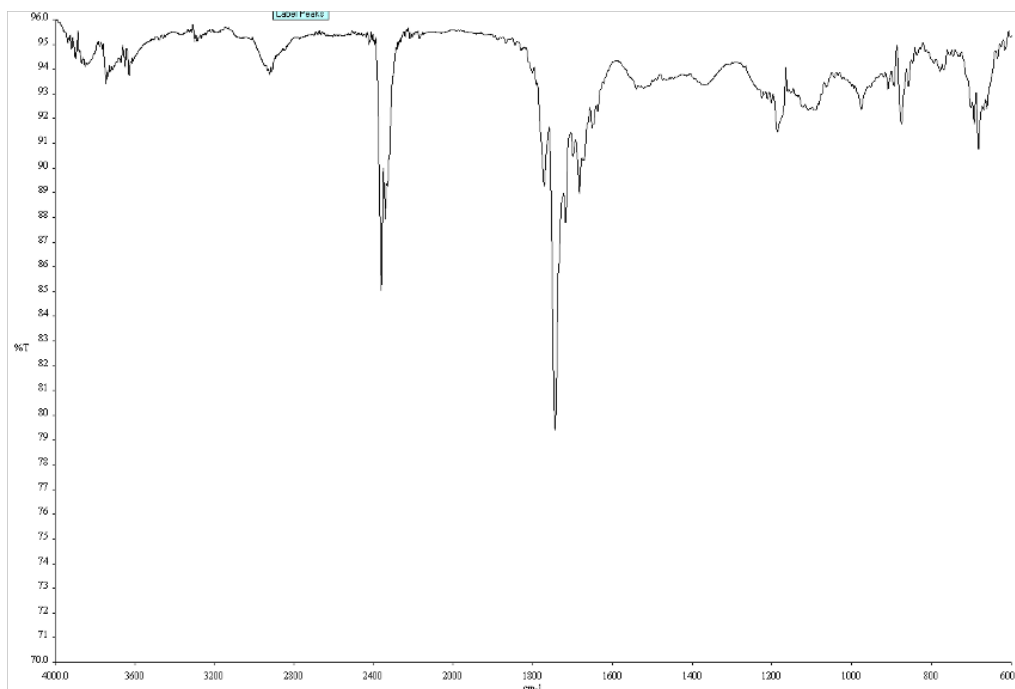
Figure A2.121. Infrared spectrum (Thin Film, NaCl) of compound **40m**.
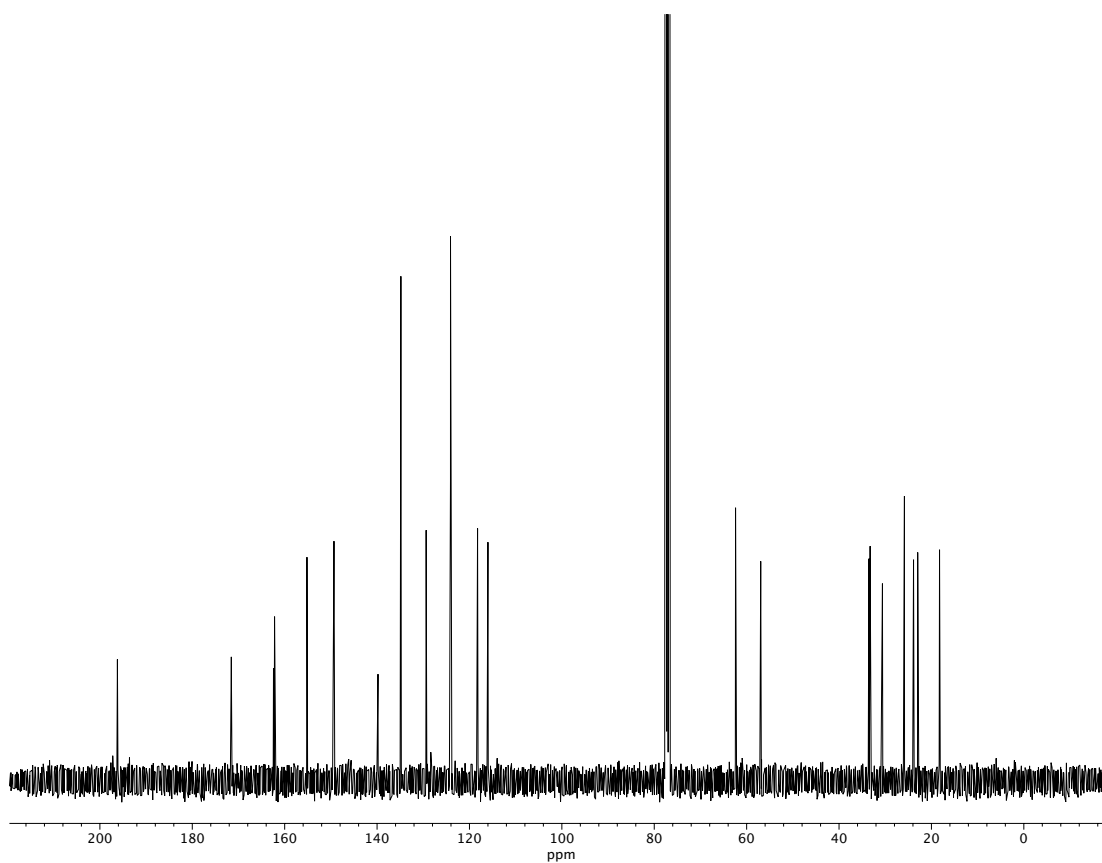
Figure A2.122. ^{13}C NMR (100 MHz, CDCl$_3$) of compound **40m**.
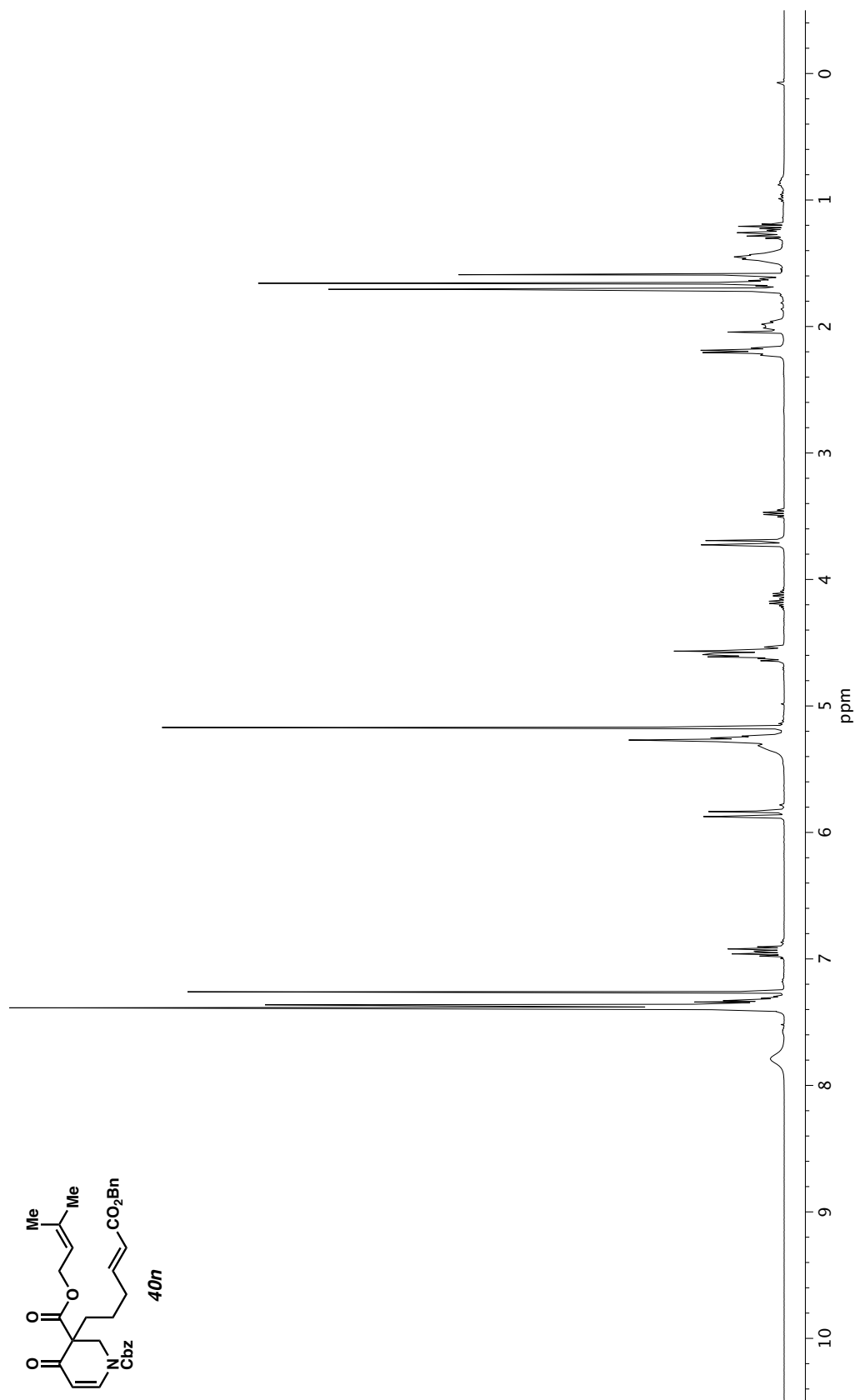
Figure A2.123. ^1H NMR (400 MHz, CDCl$_3$) of compound **40n**.
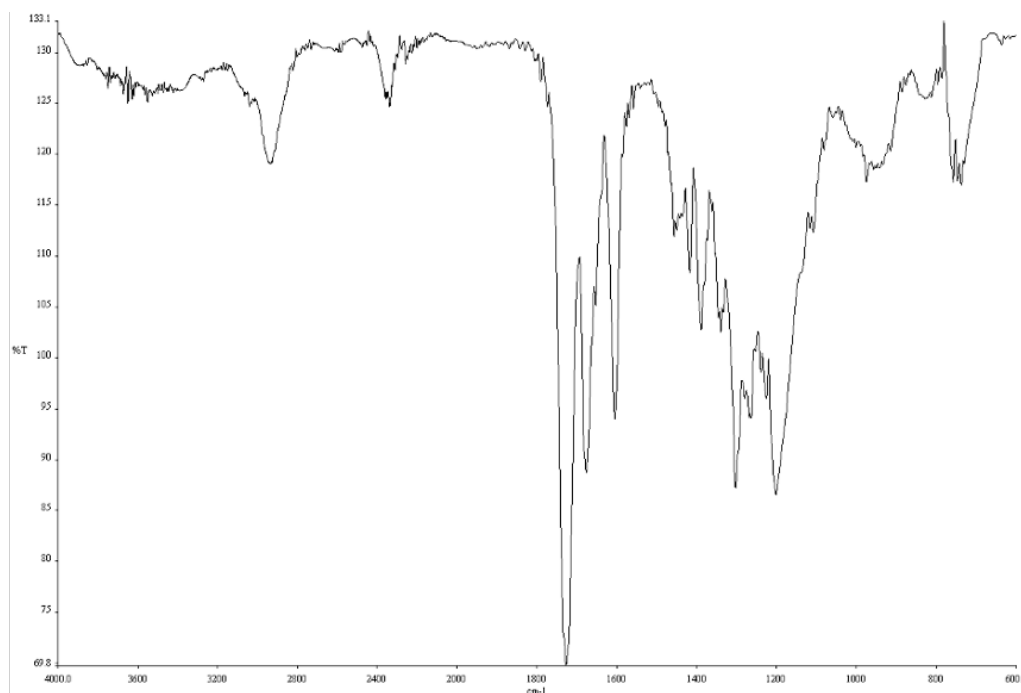
Figure A2.124. Infrared spectrum (Thin Film, NaCl) of compound **40n**.
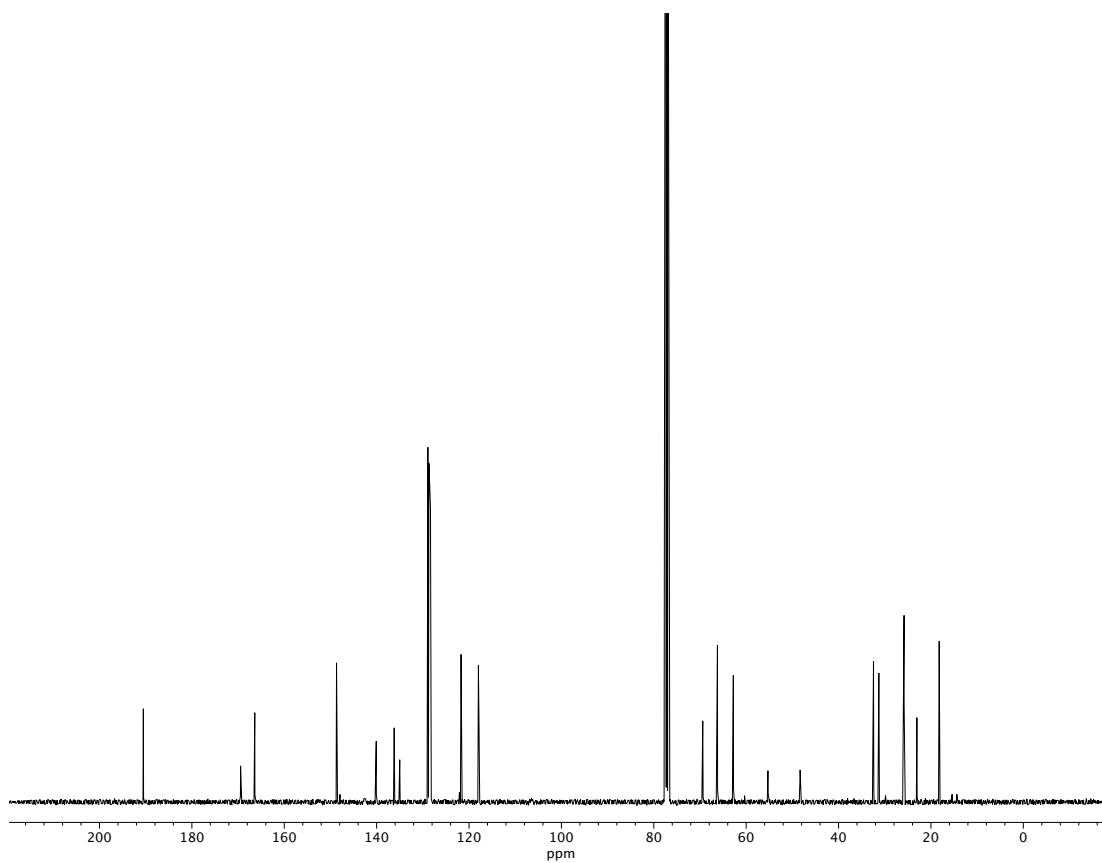
Figure A2.125. ^{13}C NMR (100 MHz, CDCl$_3$) of compound **40n**.

Figure A2.126. ^1H NMR (400 MHz, CDCl$_3$) of compound **40o**.
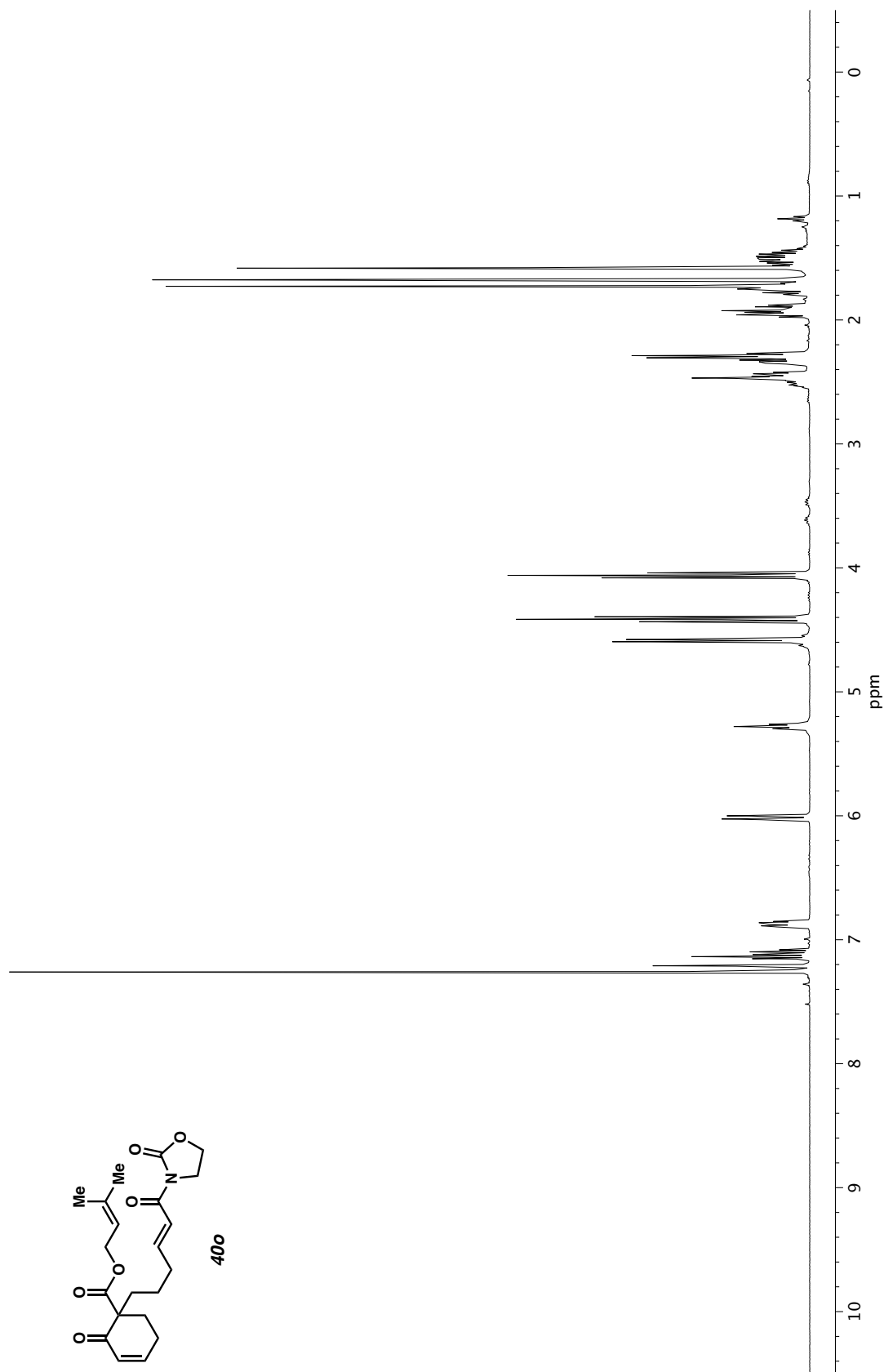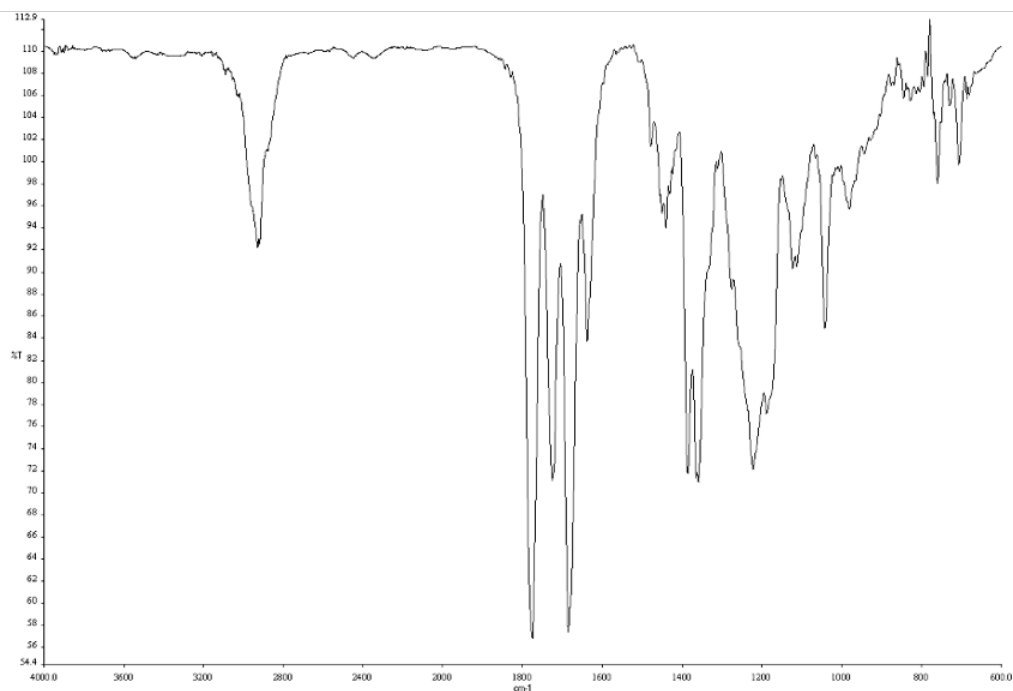
Figure A2.127. *Infrared spectrum (Thin Film, NaCl) of compound **40o**.*
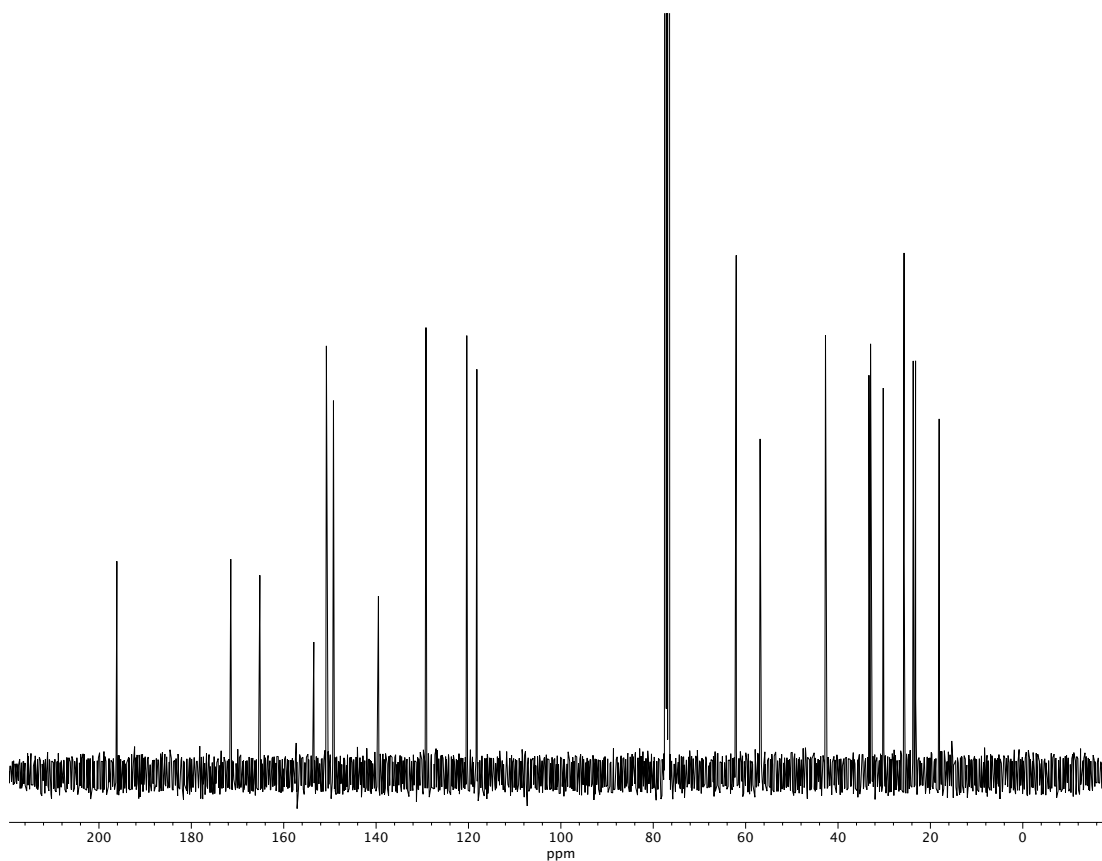
Figure A2.128. *^{13}C NMR (100 MHz, CDCl$_3$) of compound **40o**.*
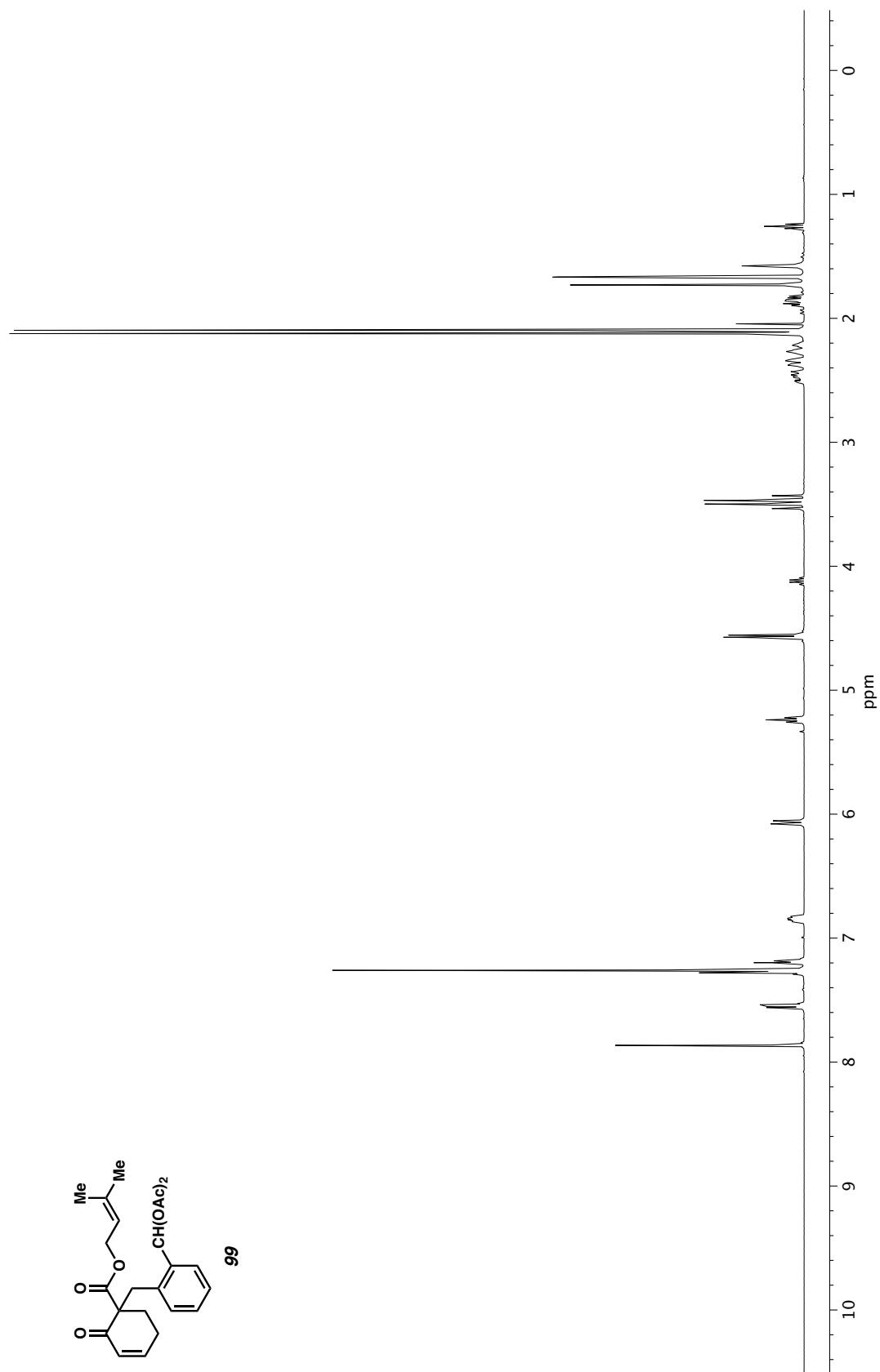
Figure A2.129. *^{1}H NMR (400 MHz, CDCl$_3$) of compound **99**.*
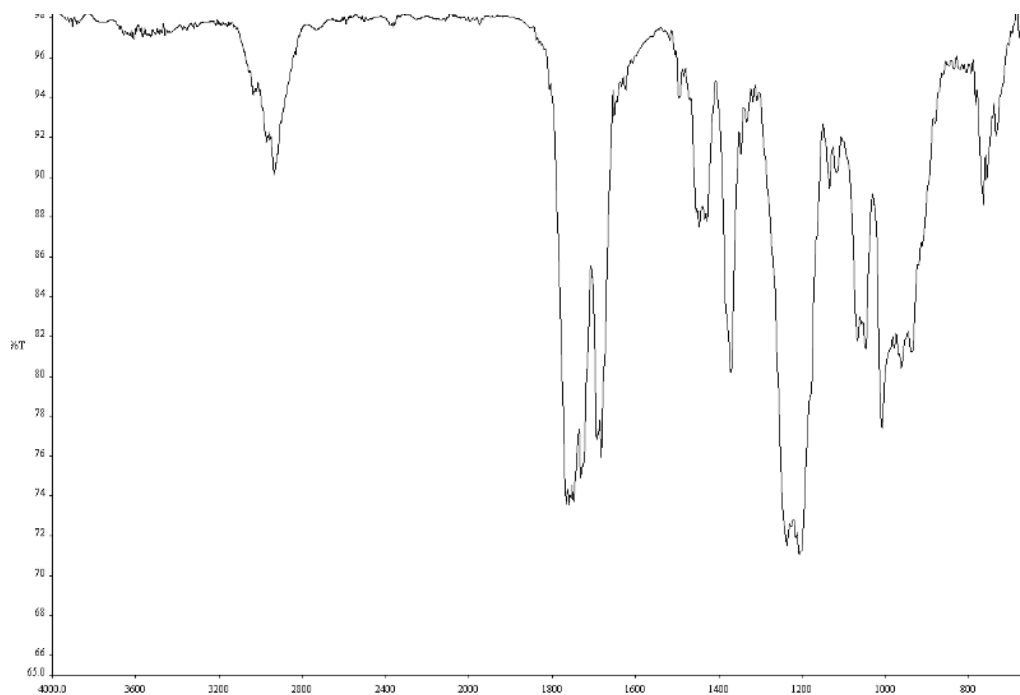
Figure A2.130. *Infrared spectrum (Thin Film, NaCl) of compound* **99**.
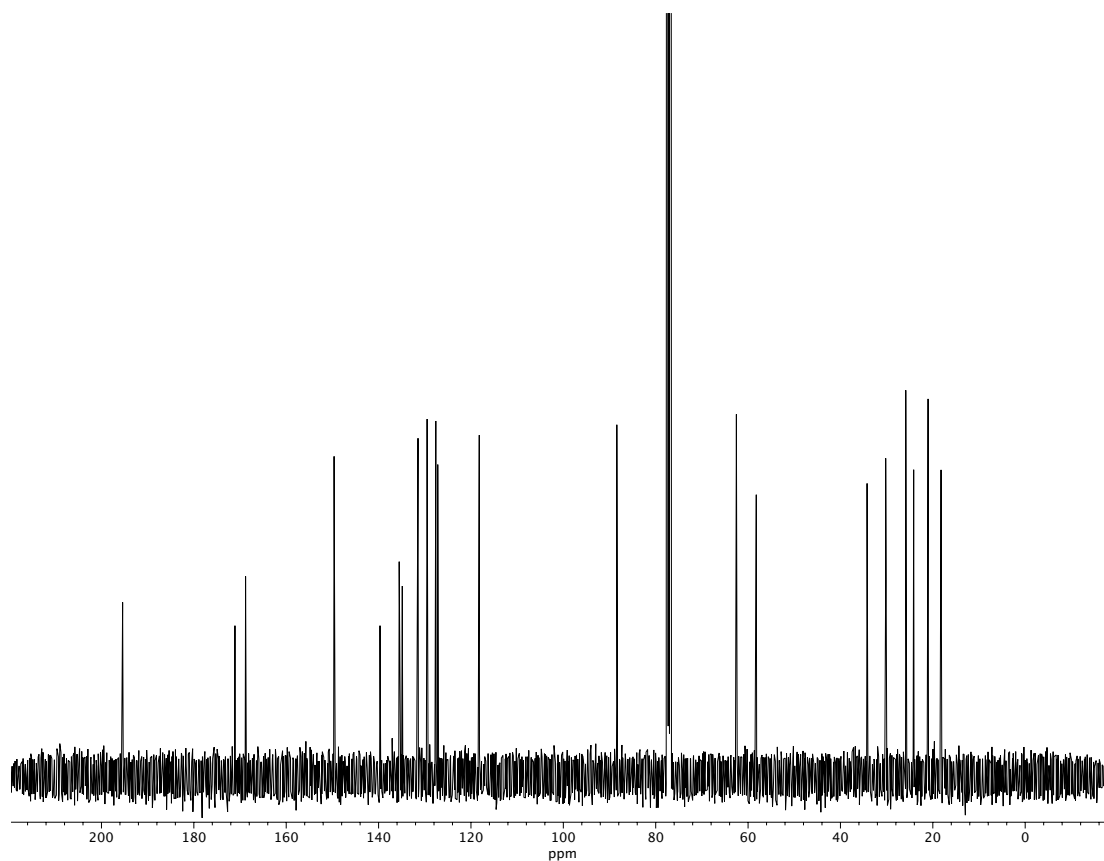
Figure A2.131. ^{13}C *NMR (100 MHz, CDCl$_3$) of compound* **99**.
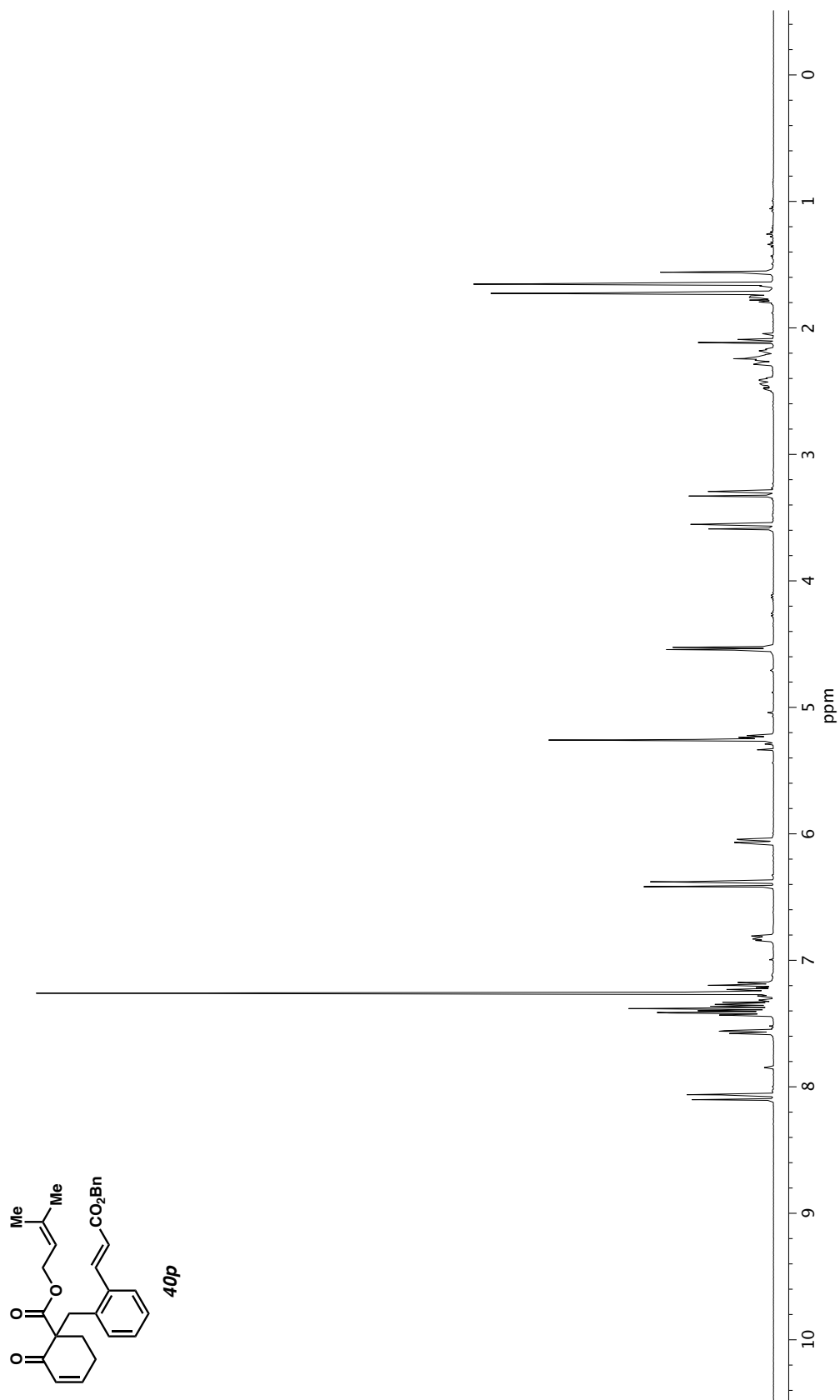
Figure A2.132. ^1H NMR (400 MHz, CDCl$_3$) of compound **40p**.
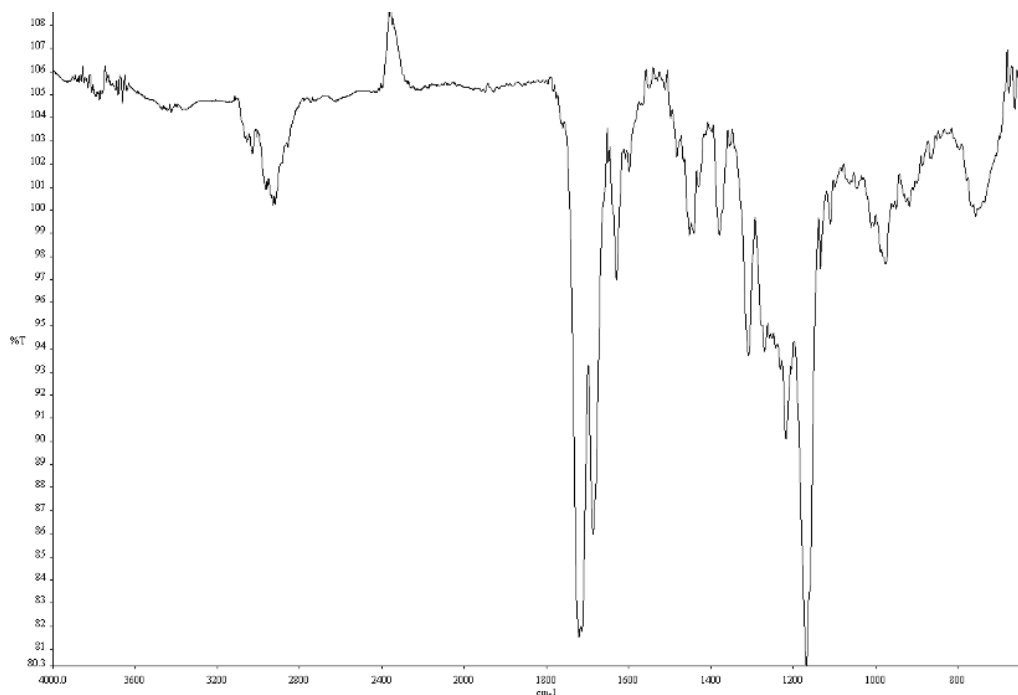
Figure A2.133. *Infrared spectrum (Thin Film, NaCl) of compound* **40p**.
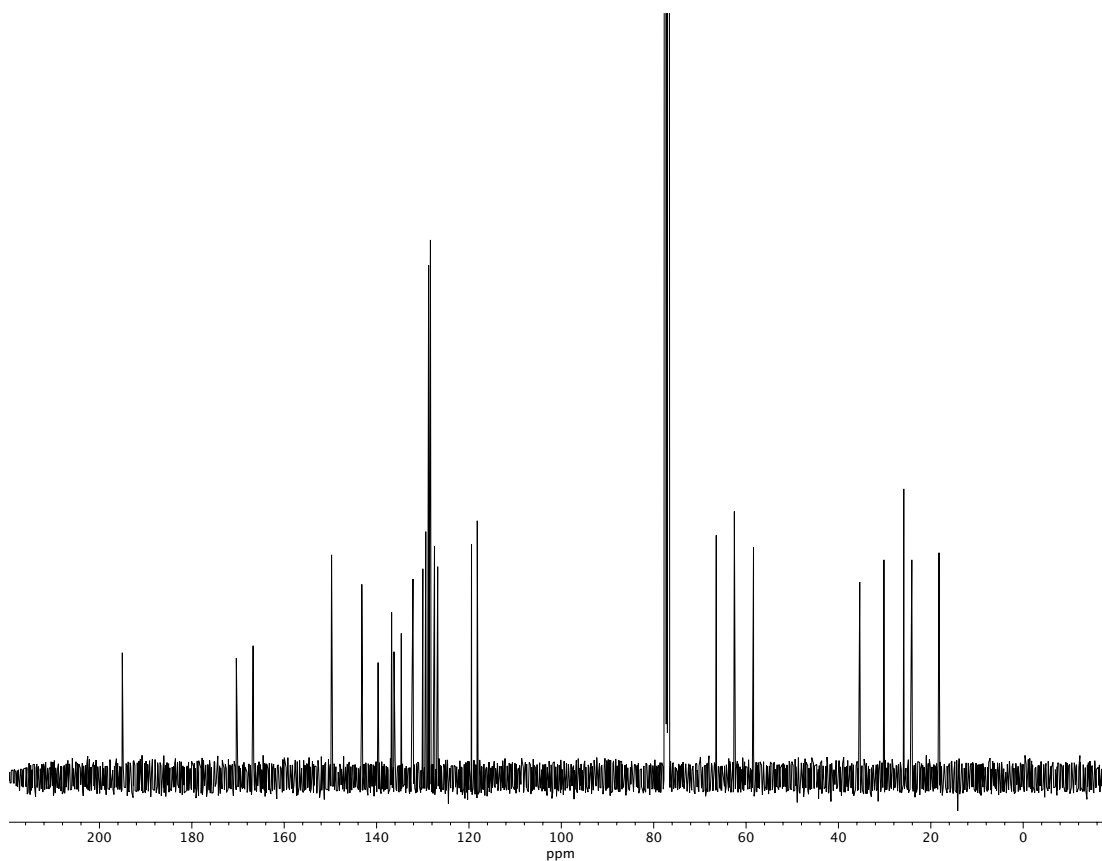
Figure A2.134. ^{13}C *NMR (100 MHz, CDCl$_3$) of compound* **40p**.
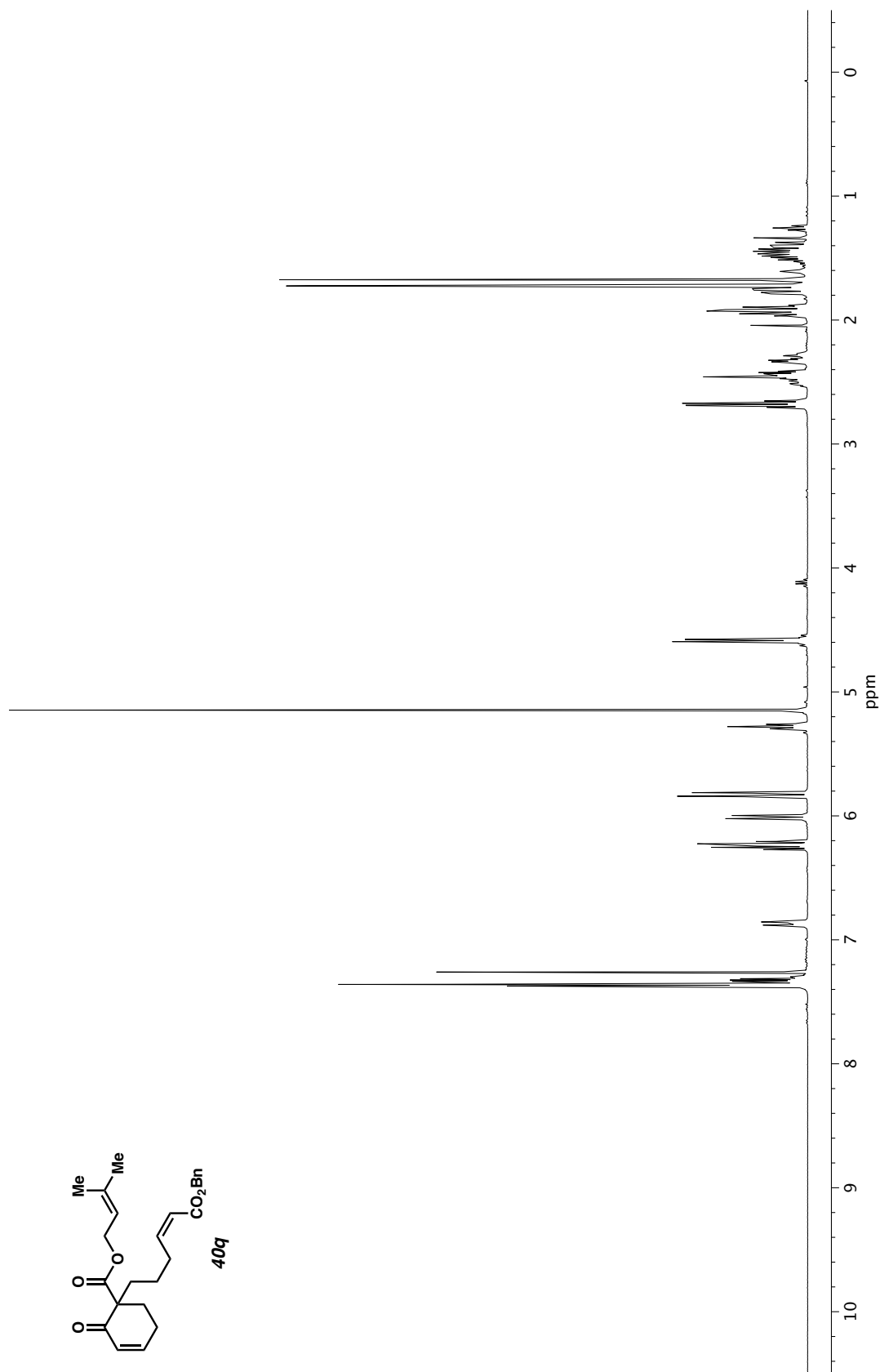
Figure A2.135. ^1H NMR (400 MHz, CDCl$_3$) of compound **40q**.
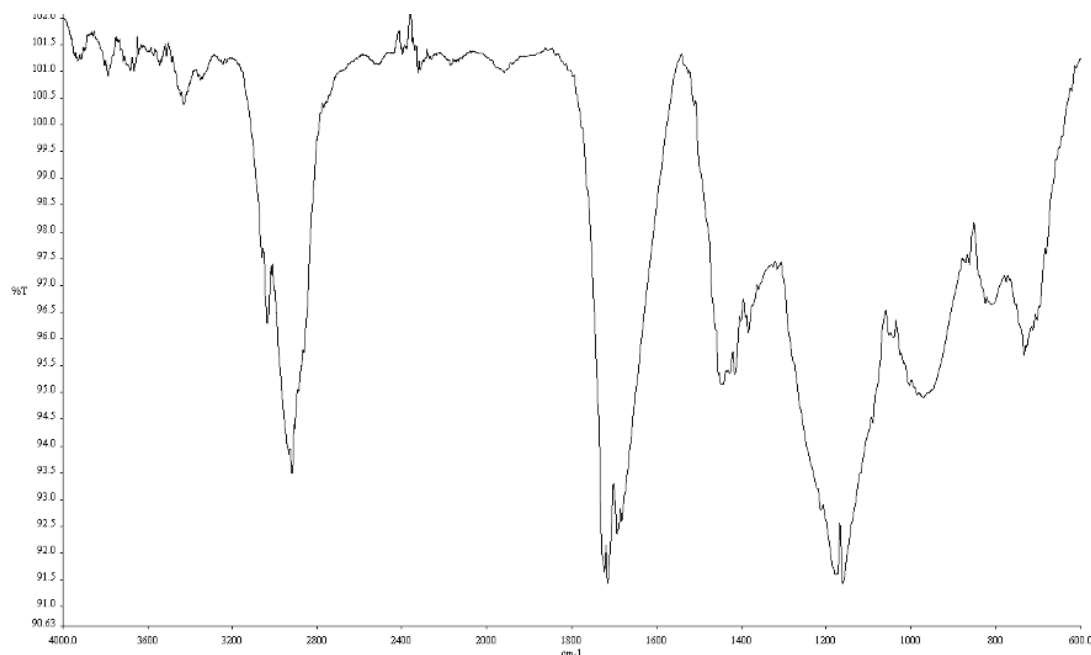
Figure A2.136. Infrared spectrum (Thin Film, NaCl) of compound **40q**.
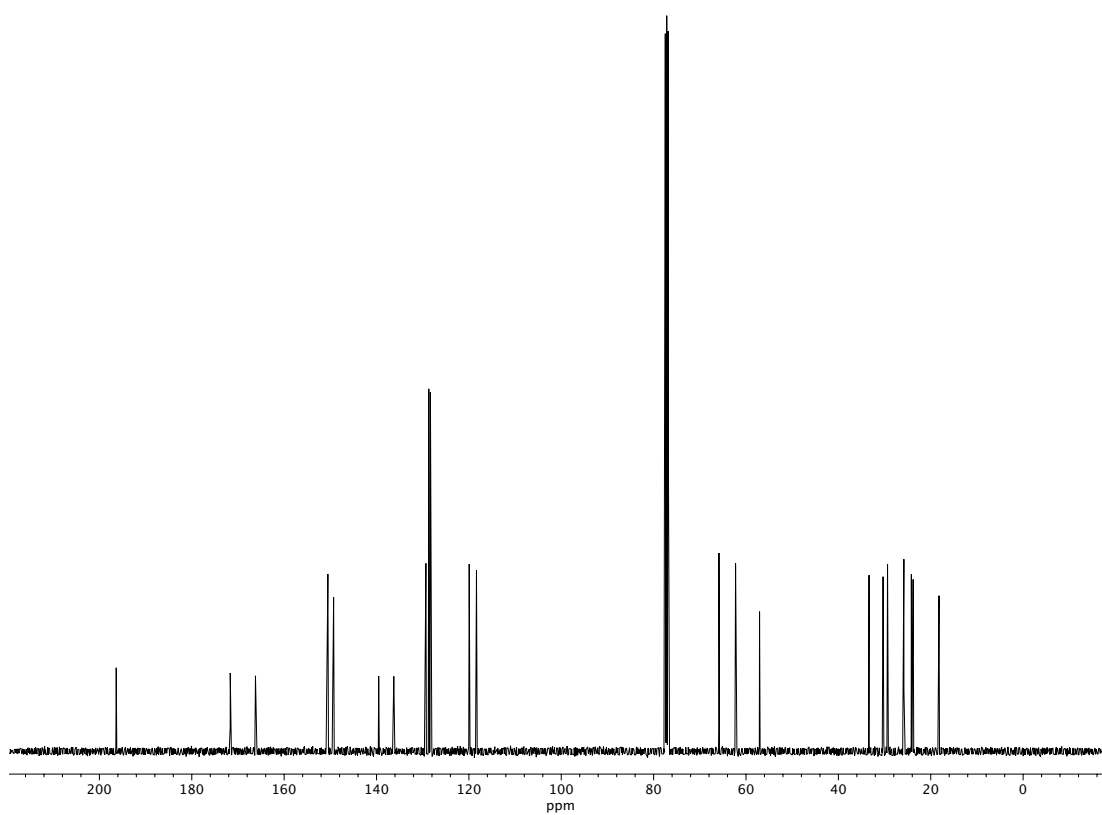
Figure A2.137. ^{13}C NMR (100 MHz, CDCl$_3$) of compound **40q**.

Figure A2.138. ^1H NMR (400 MHz, CDCl$_3$) of compound **40r**.
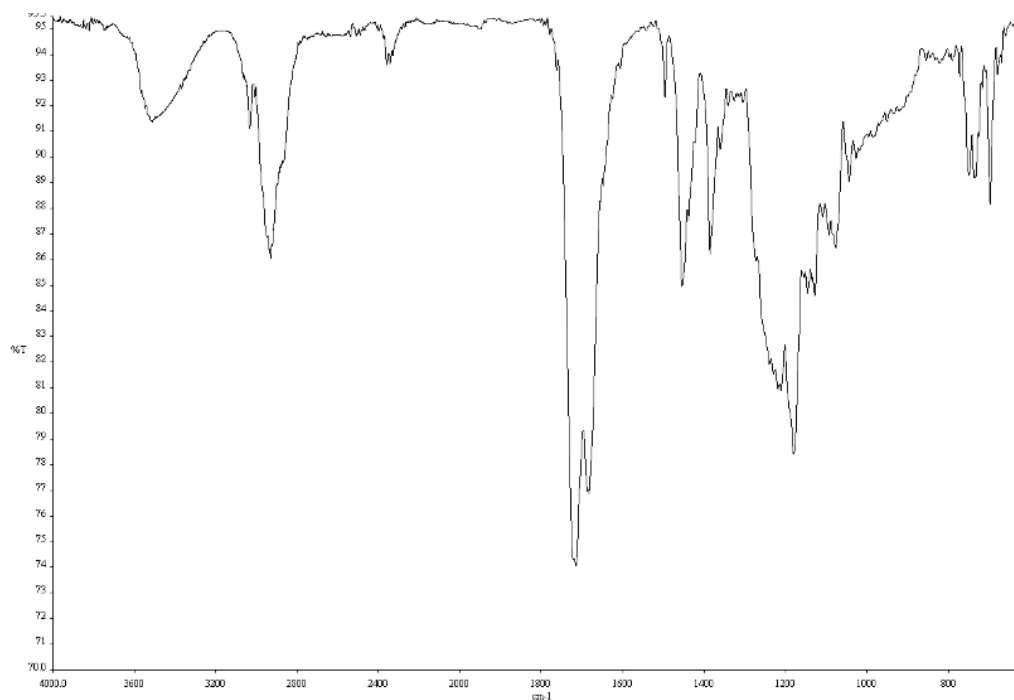
Figure A2.139. Infrared spectrum (Thin Film, NaCl) of compound **40r**.
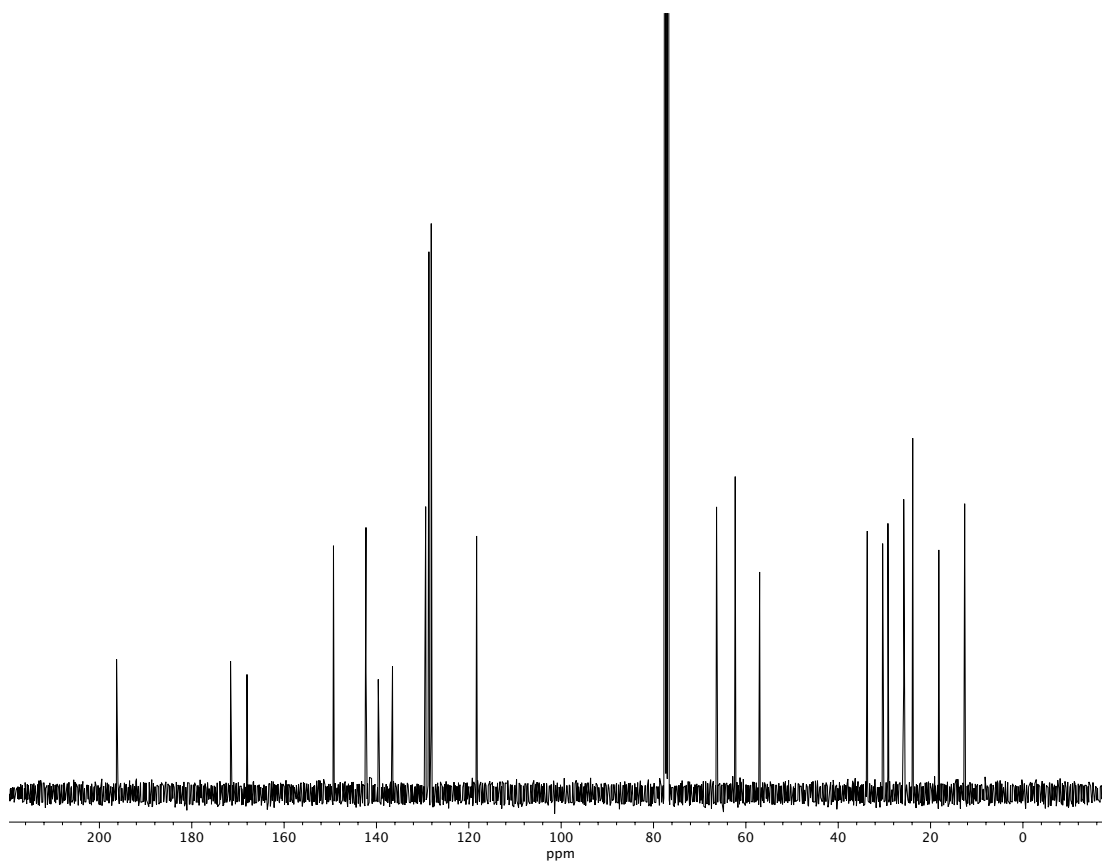
Figure A2.140. ^{13}C NMR (100 MHz, CDCl$_3$) of compound **40r**.
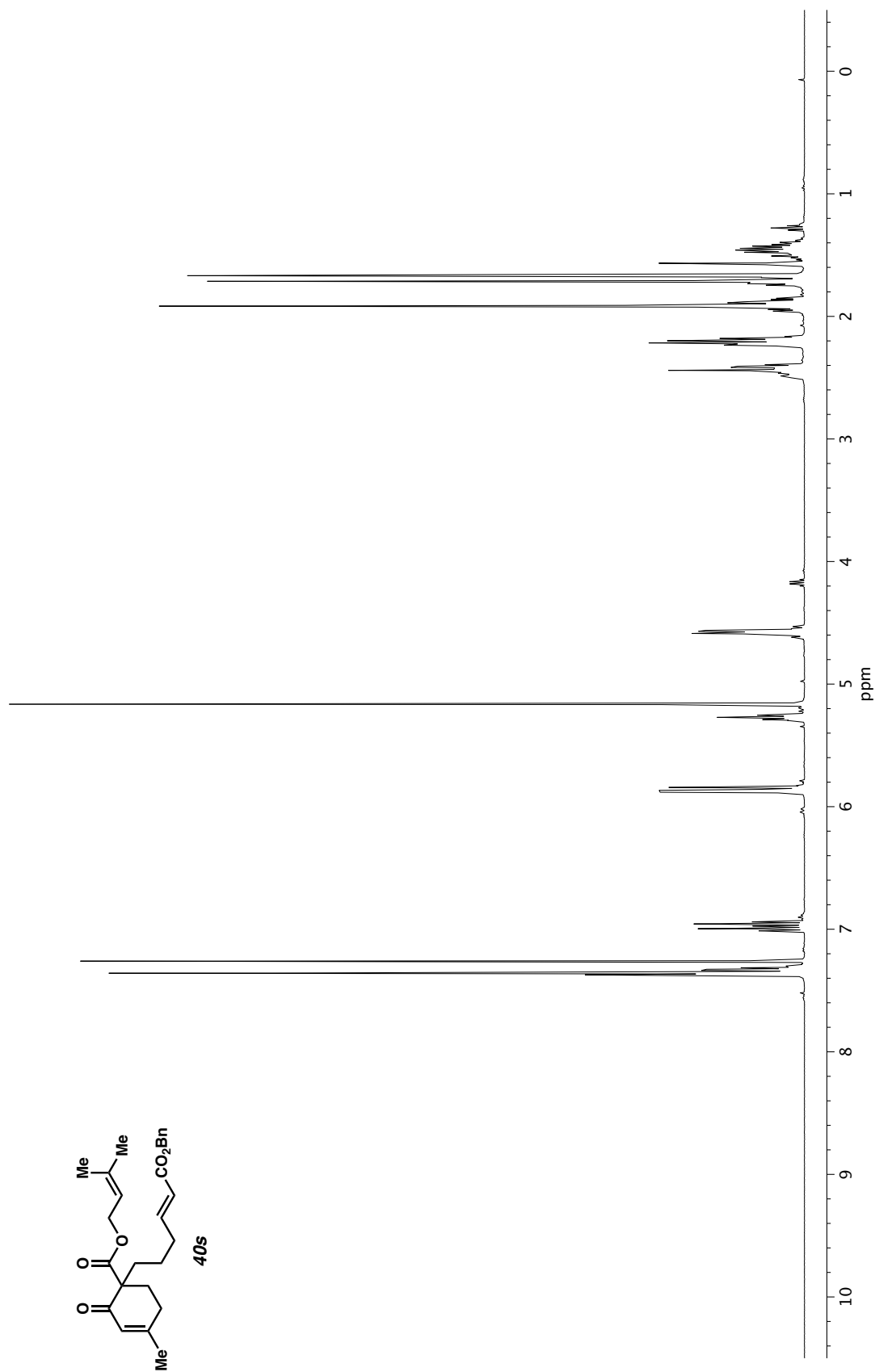
Figure A2.141. ^{1}H NMR (400 MHz, CDCl$_3$) of compound *40s.*
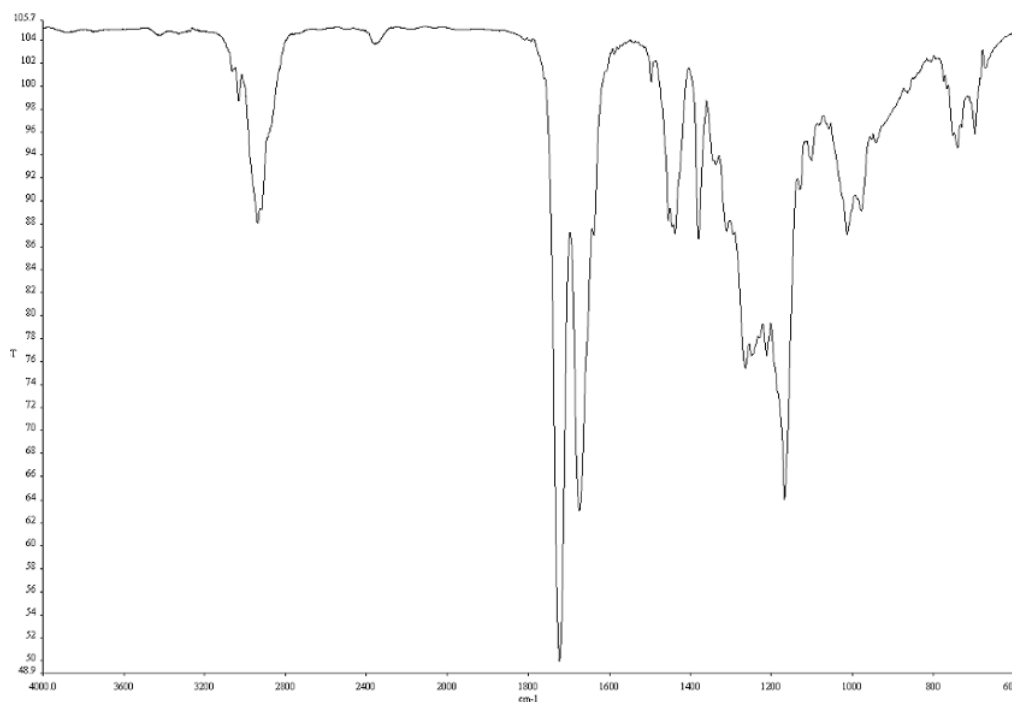
Figure A2.142. Infrared spectrum (Thin Film, NaCl) of compound **40s**.
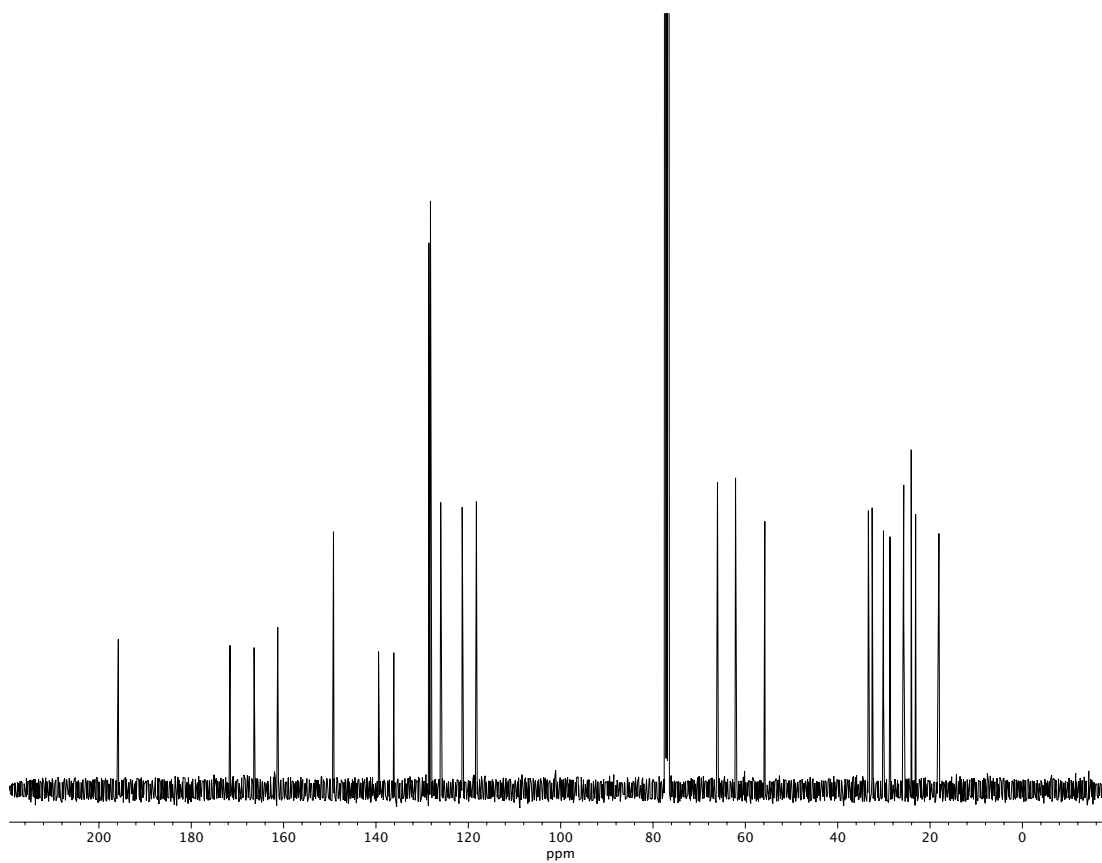
Figure A2.143. ^{13}C NMR (100 MHz, CDCl$_3$) of compound **40s**.
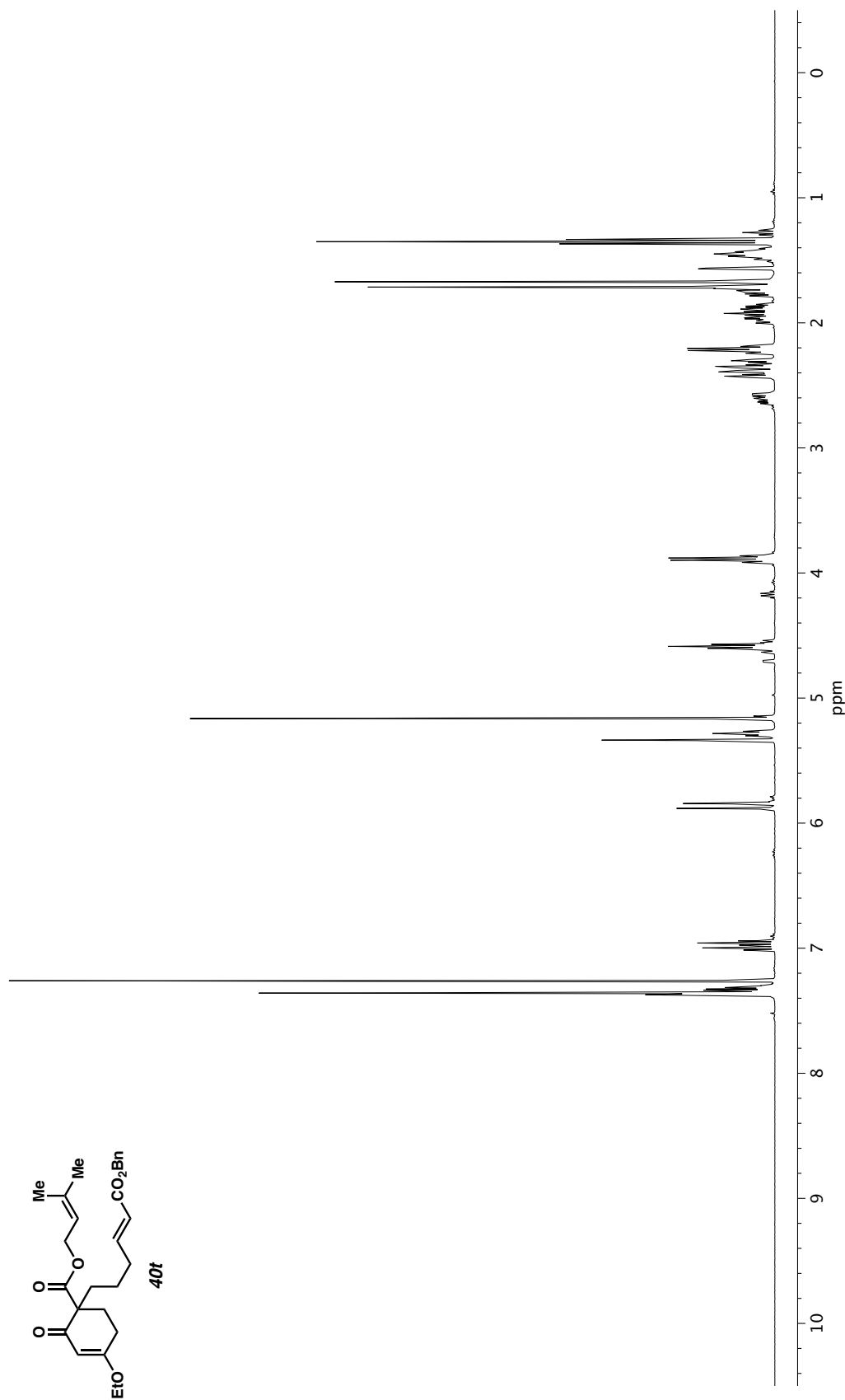
Figure A2.144. ^1H NMR (400 MHz, CDCl$_3$) of compound **40t**.
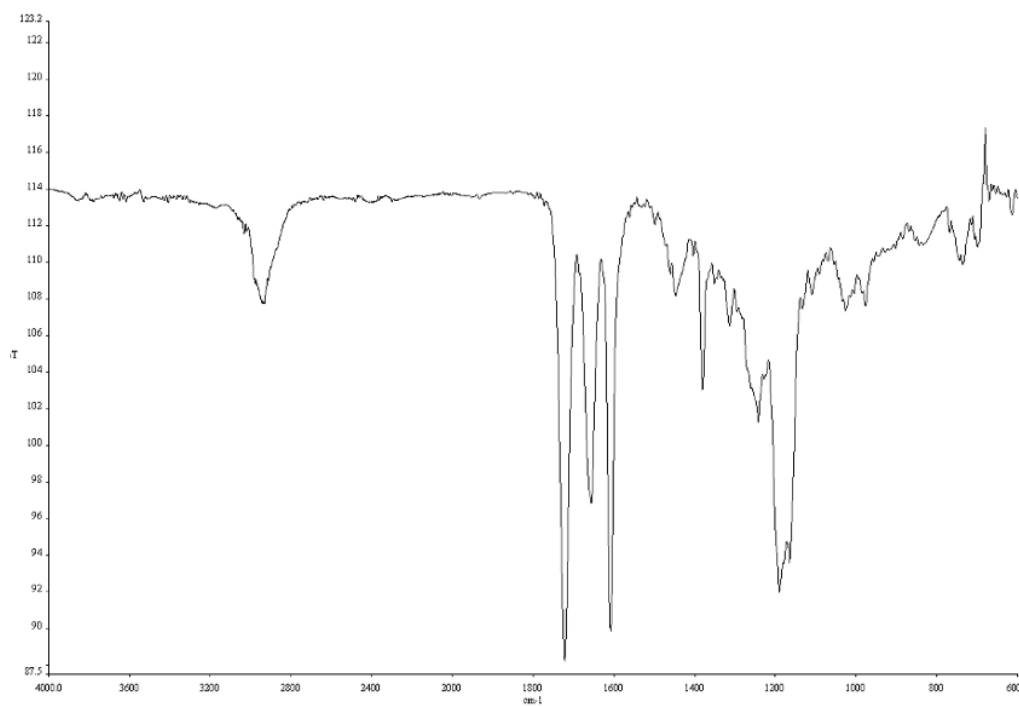
Figure A2.145. *Infrared spectrum (Thin Film, NaCl) of compound **40t**.*
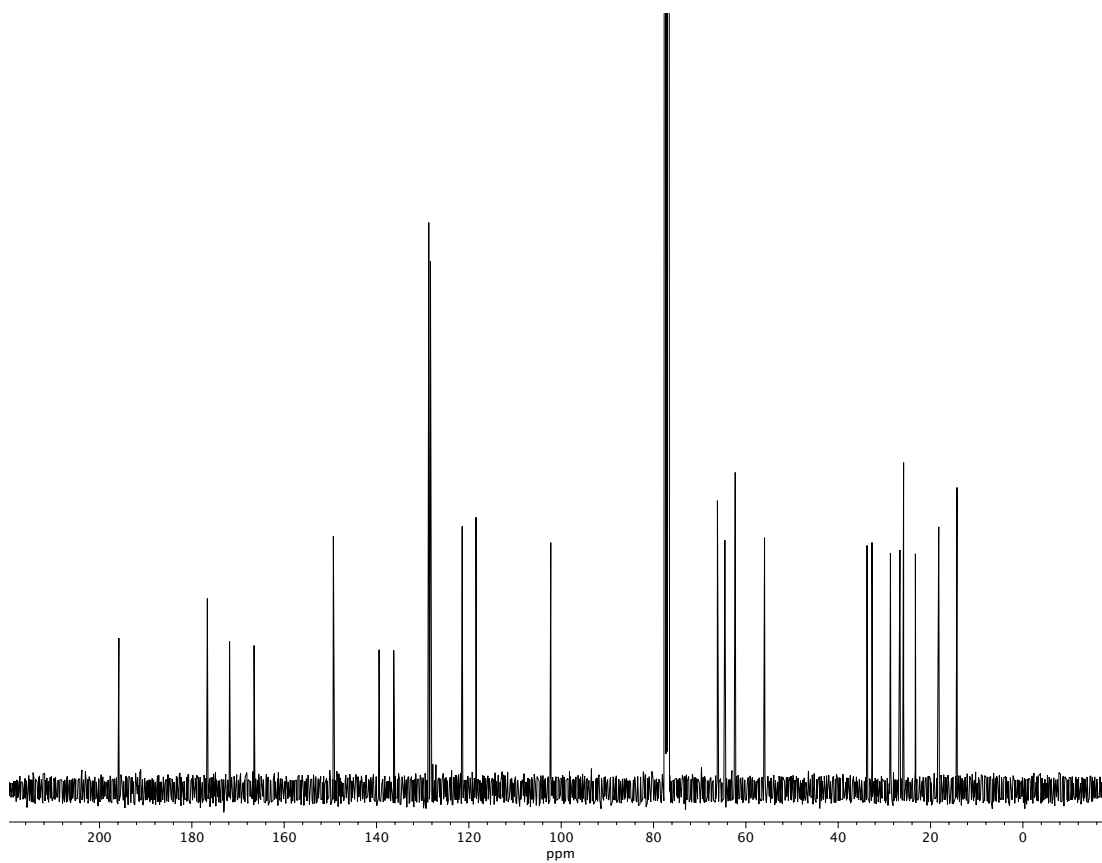
Figure A2.146. *^{13}C NMR (100 MHz, CDCl$_3$) of compound **40t**.*
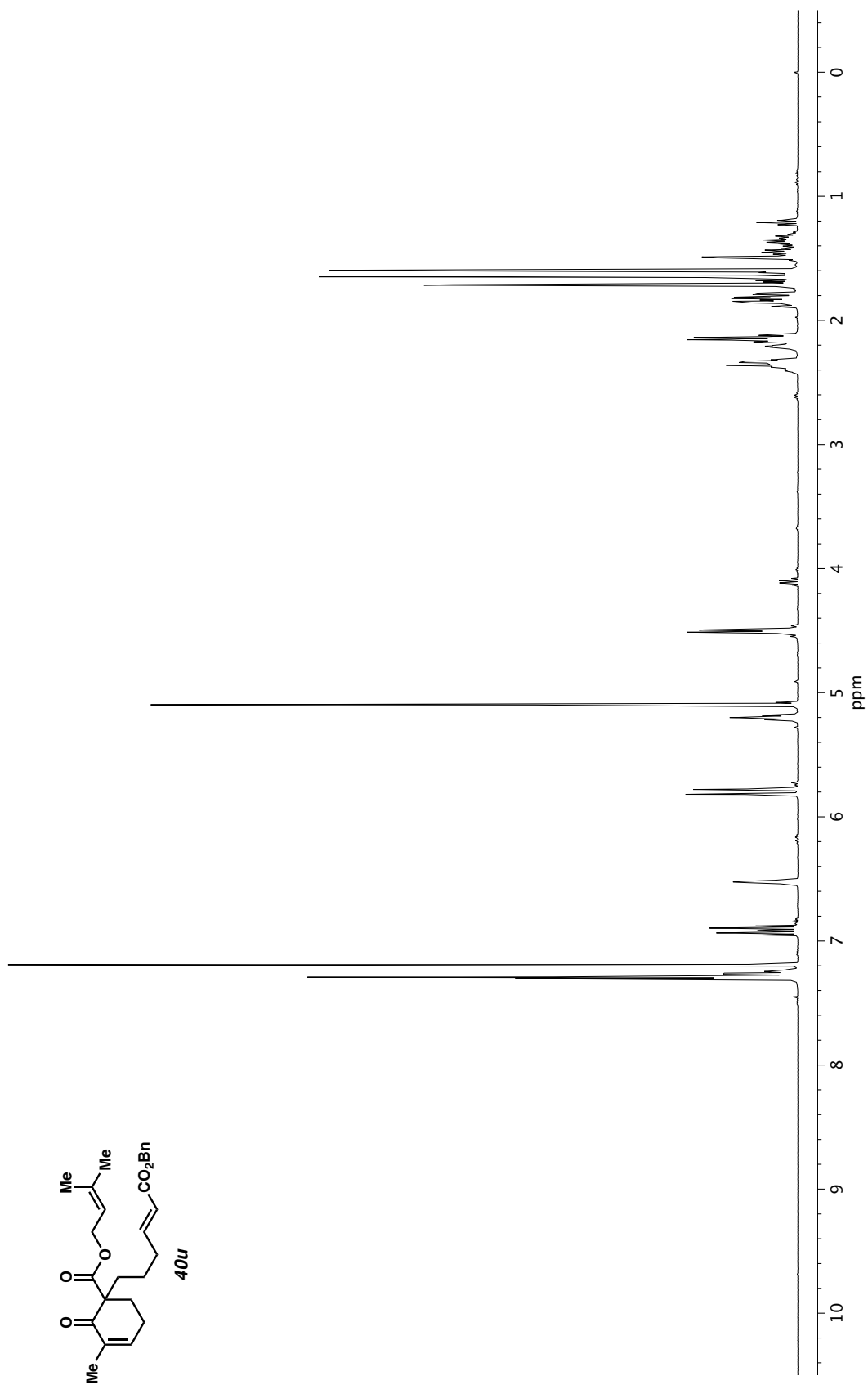
Figure A2.147. ^1H NMR (400 MHz, CDCl$_3$) of compound **40u**.
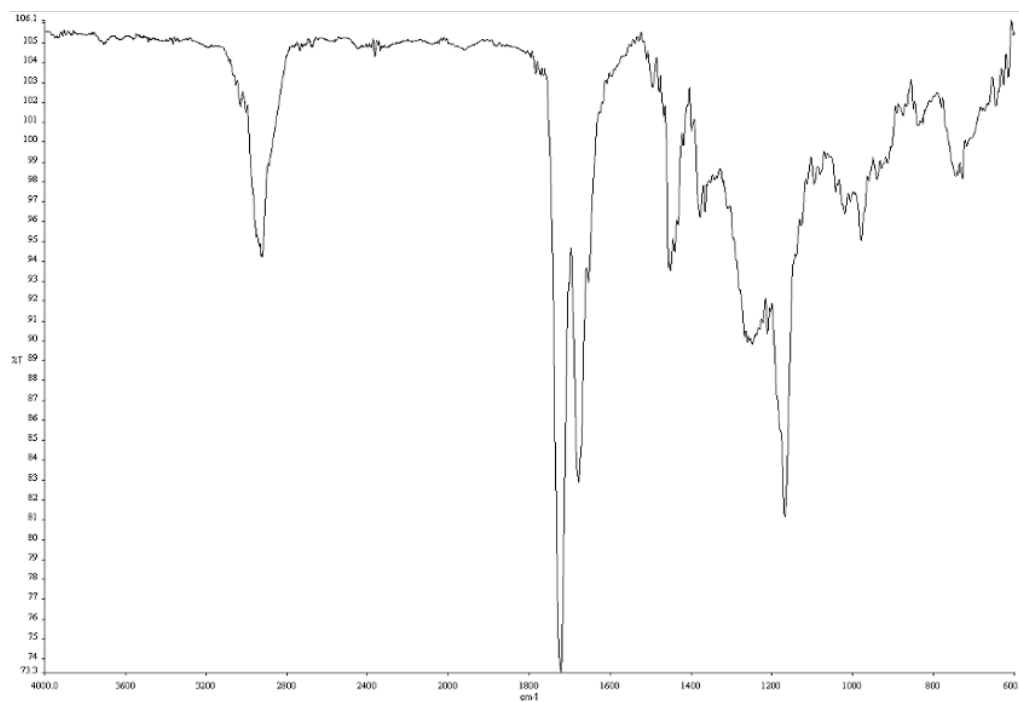
Figure A2.148. Infrared spectrum (Thin Film, NaCl) of compound **40u**.
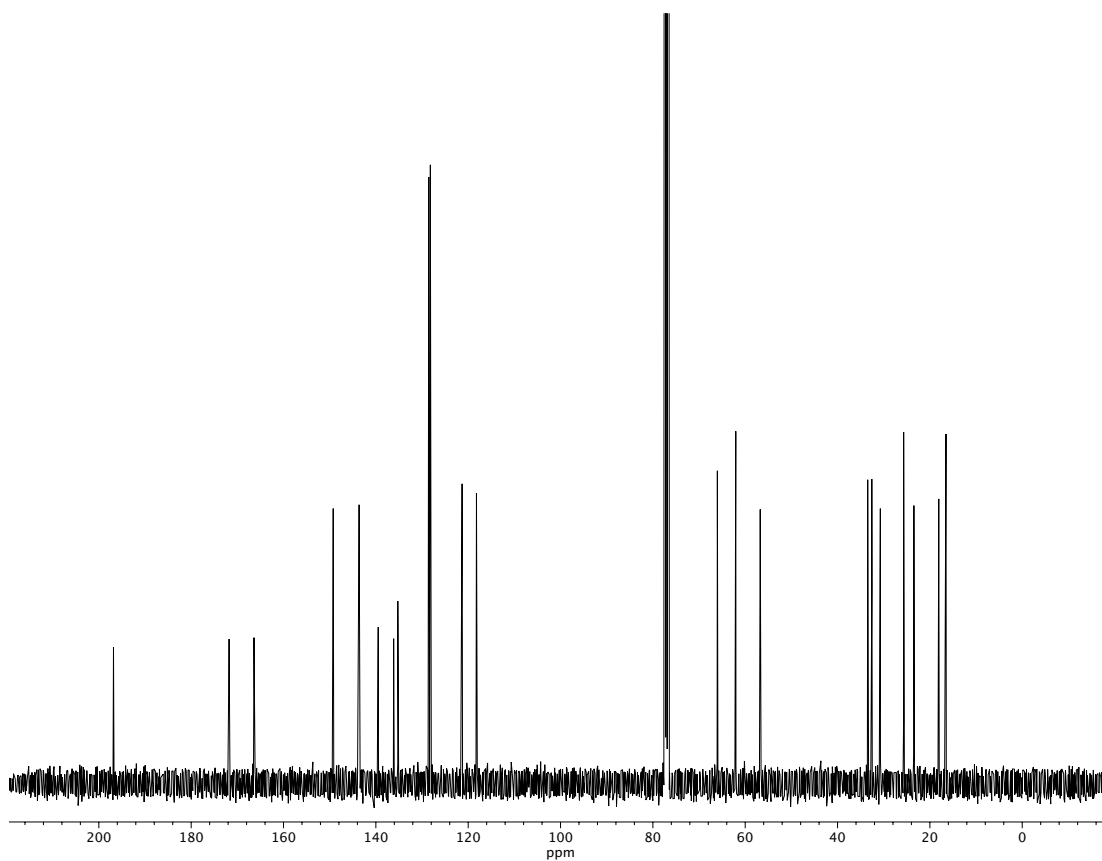
Figure A2.149. ^{13}C NMR (100 MHz, CDCl$_3$) of compound **40u**.
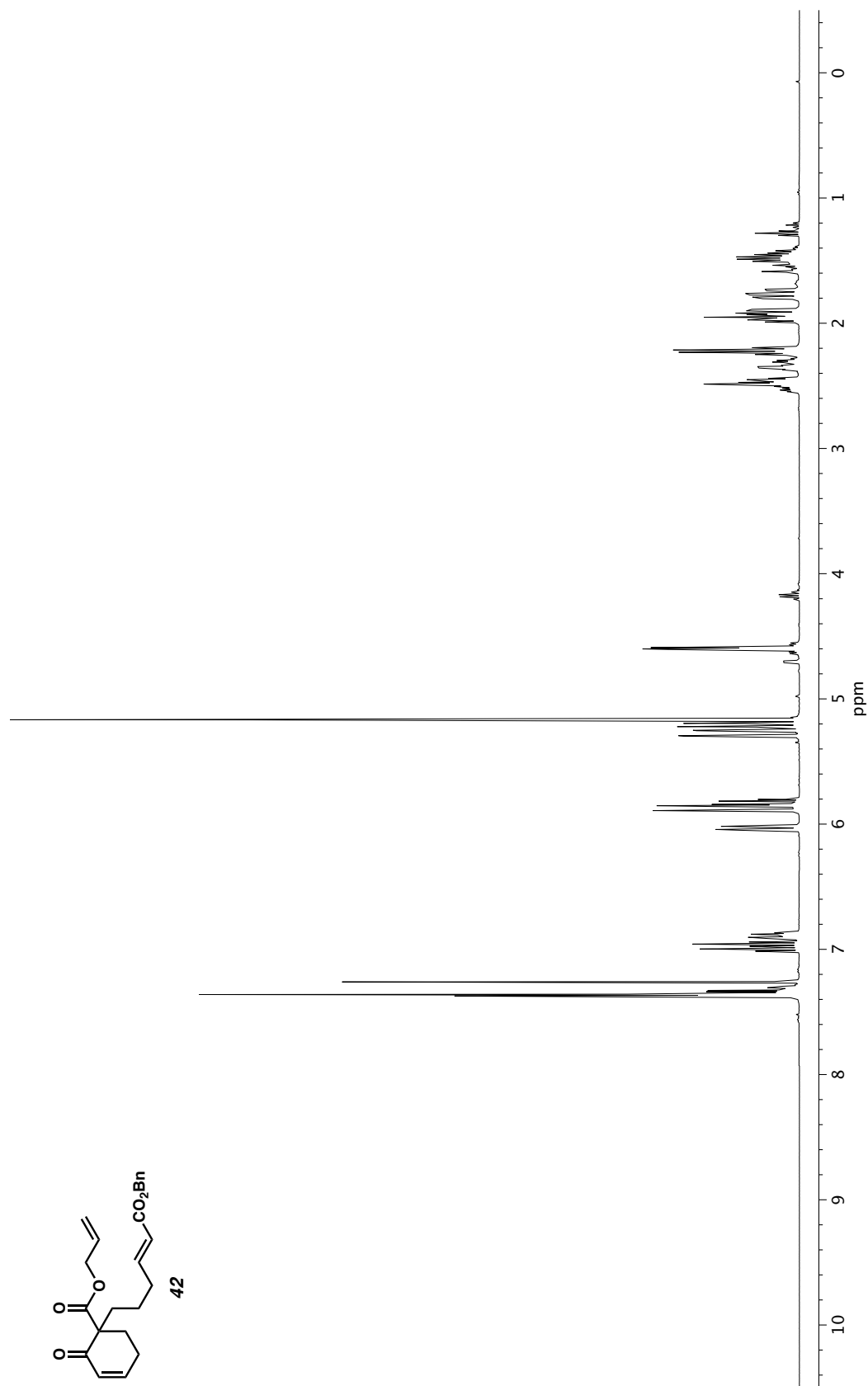
Figure A2.150. ^1H NMR (400 MHz, CDCl$_3$) of compound **42**.
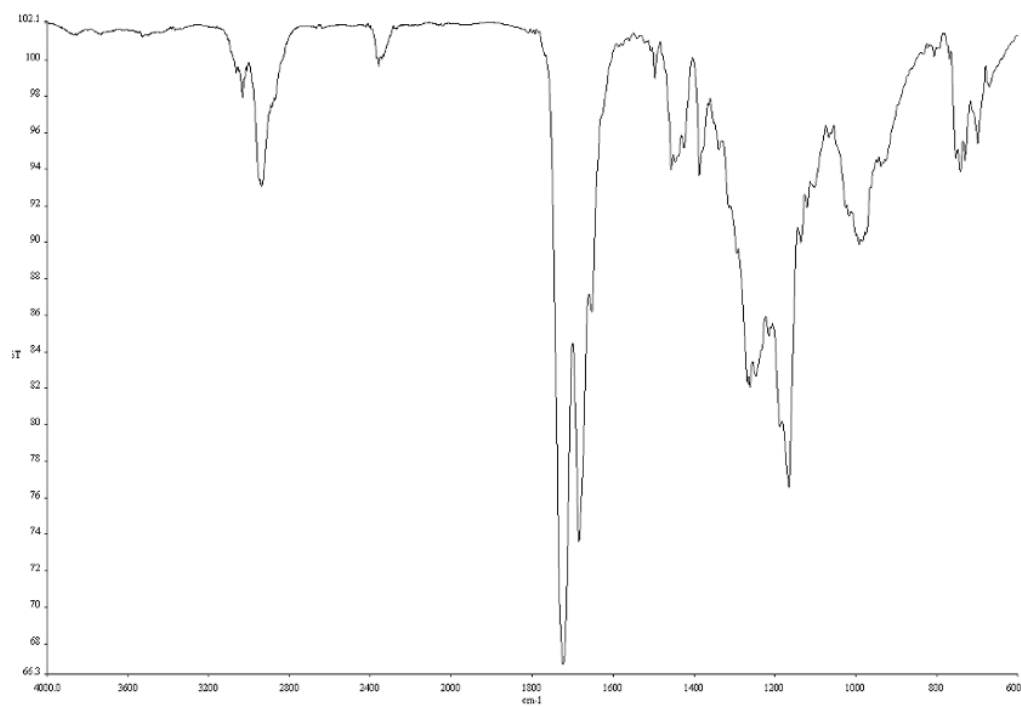
Figure A2.151. *Infrared spectrum (Thin Film, NaCl) of compound **42**.*
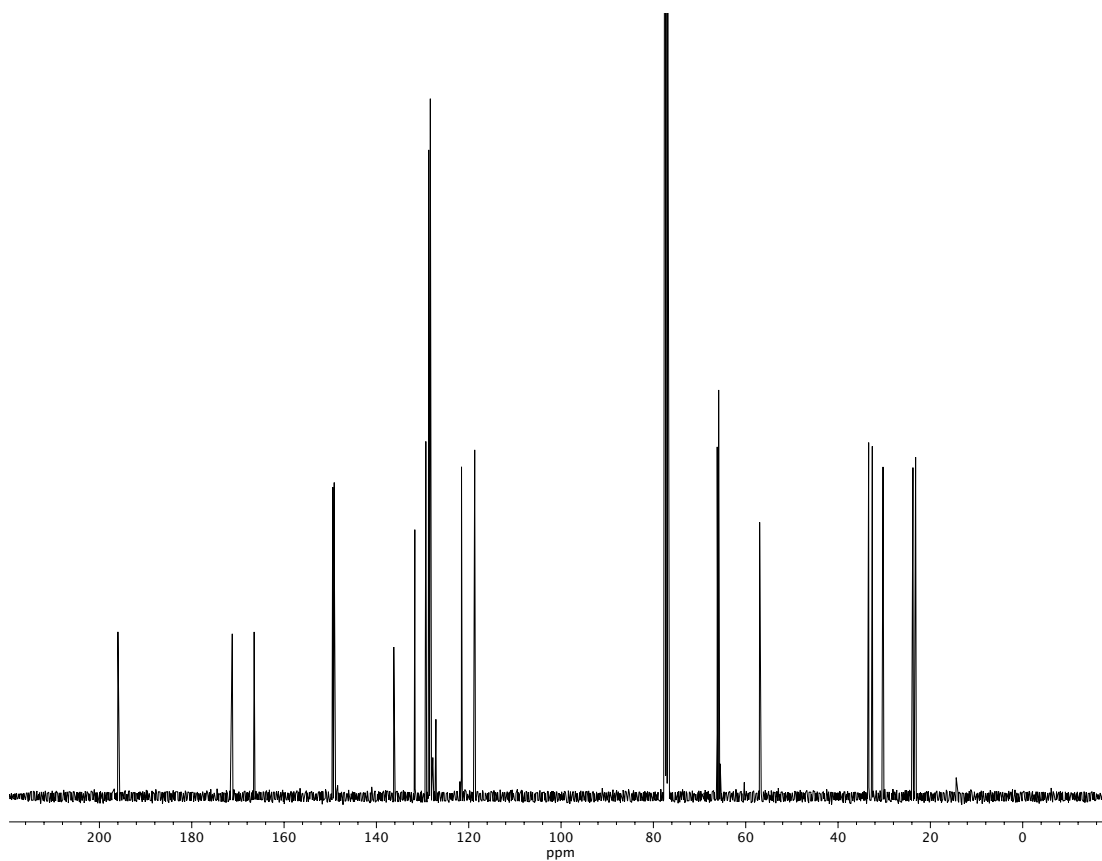
Figure A2.152. *^{13}C NMR (100 MHz, CDCl$_3$) of compound **42**.*
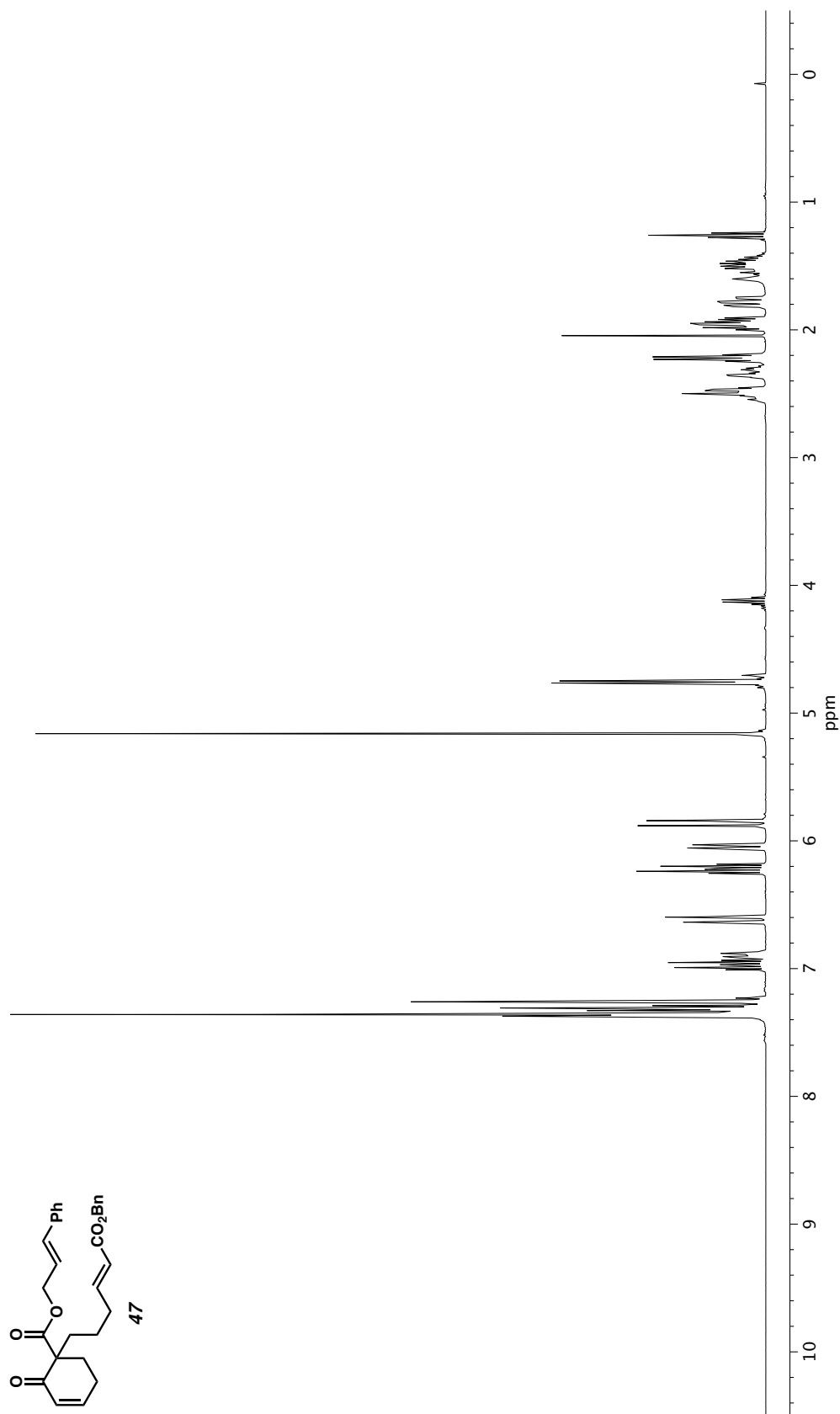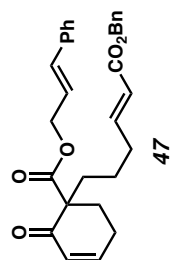
Figure A2.153. ^1H NMR (400 MHz, CDCl$_3$) of compound **47**.
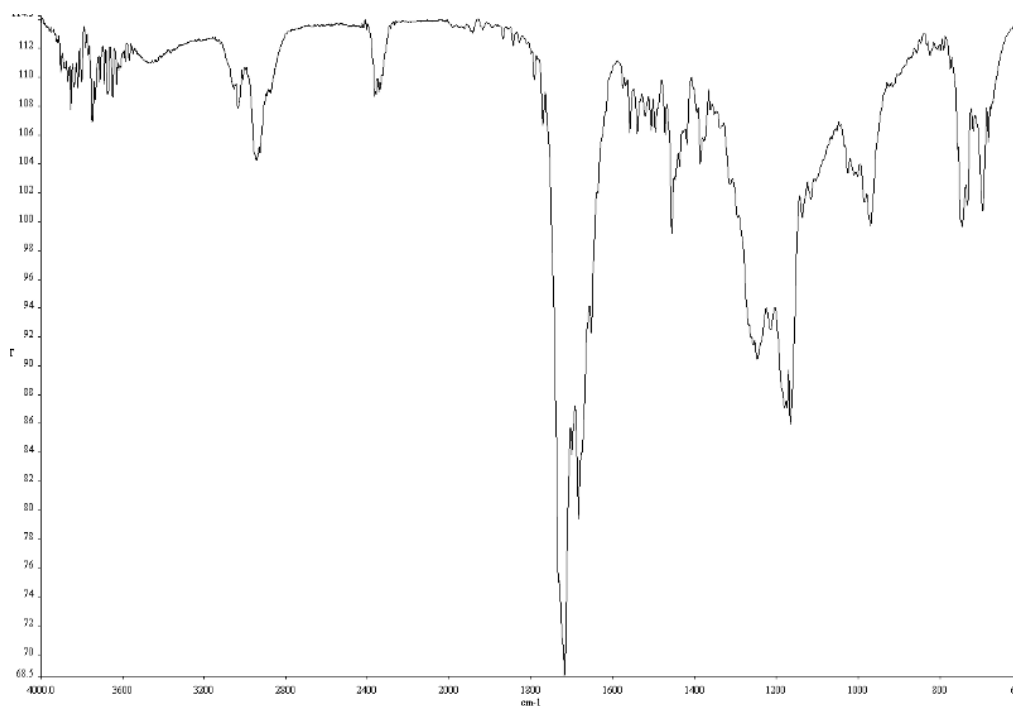
Figure A2.154. *Infrared spectrum (Thin Film, NaCl) of compound* **47**.
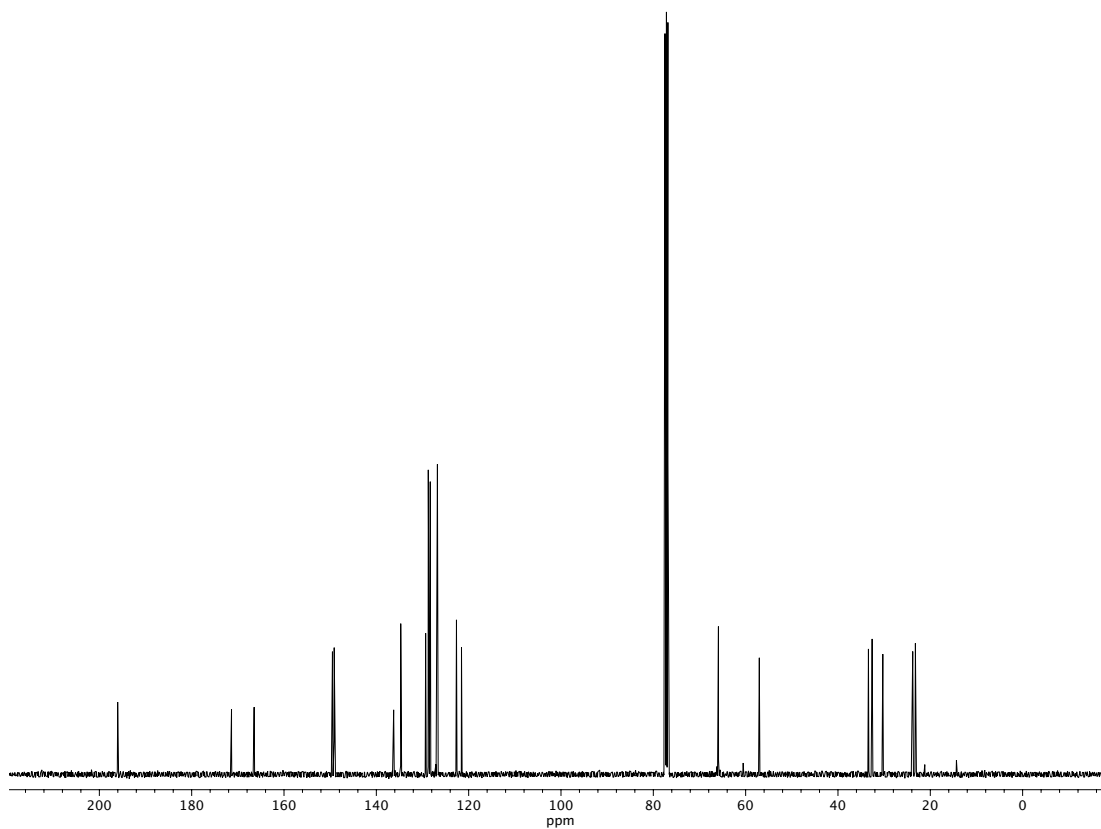
Figure A2.155. ^{13}C *NMR (100 MHz, CDCl$_3$) of compound* **47**.
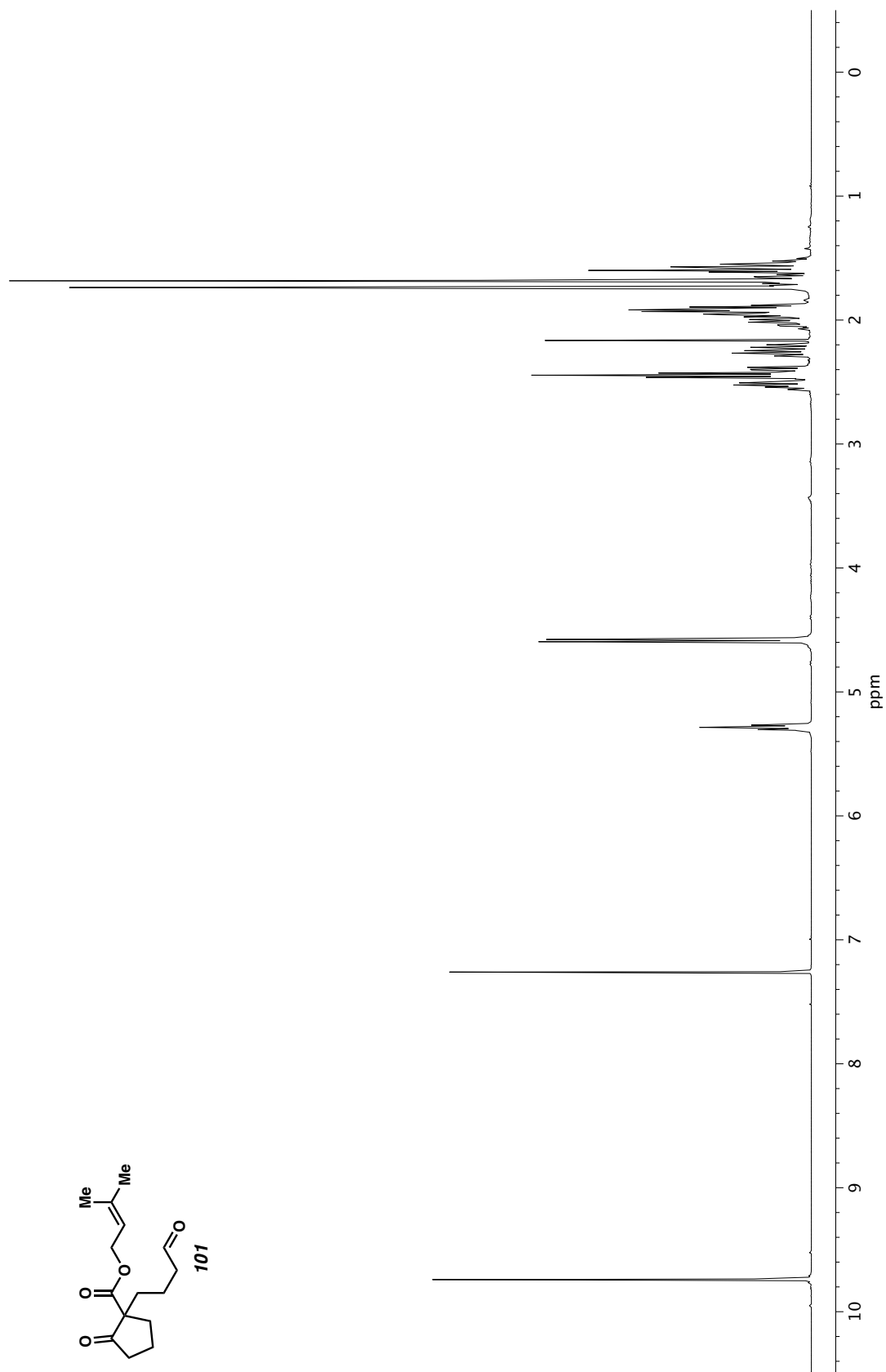
Figure A2.156. ^1H NMR (400 MHz, CDCl$_3$) of compound **101**.
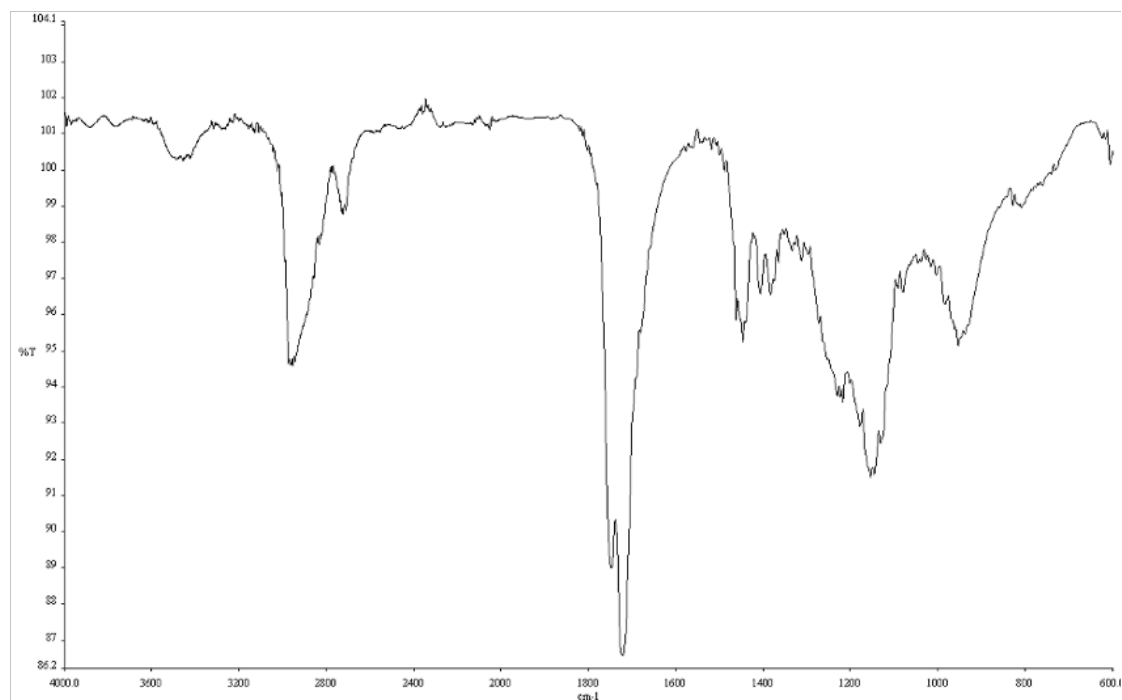
Figure A2.157. Infrared spectrum (Thin Film, NaCl) of compound **101**.
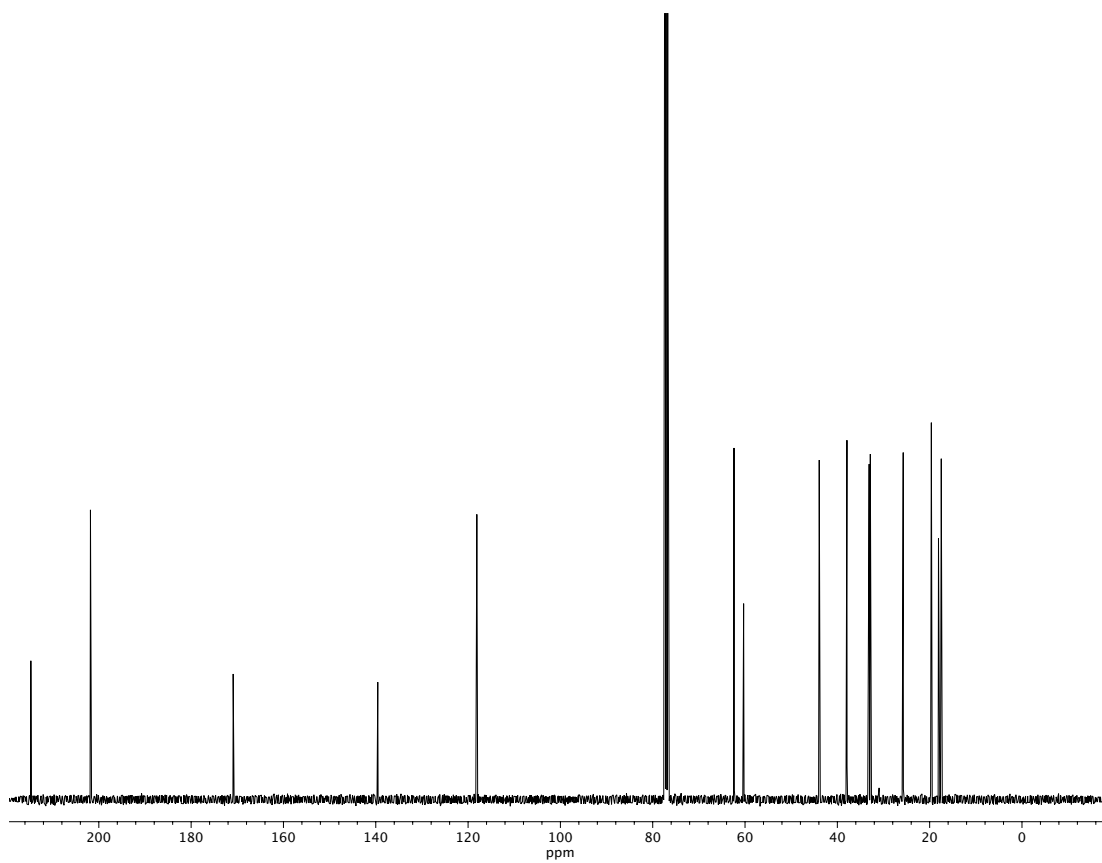
Figure A2.158. ^{13}C NMR (100 MHz, CDCl$_3$) of compound **101**.
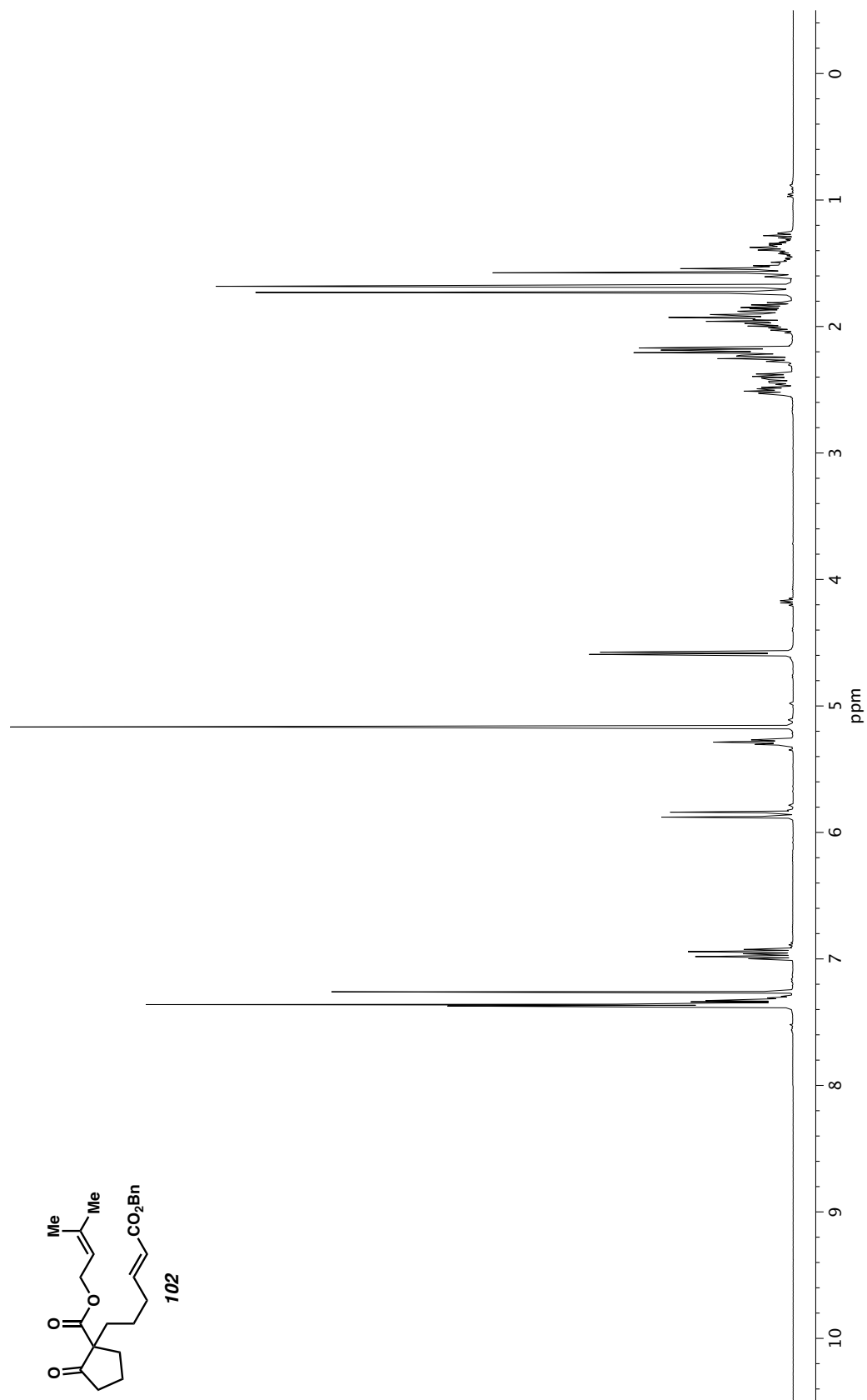
Figure A2.159. ^1H NMR (400 MHz, CDCl$_3$) of compound **102**.
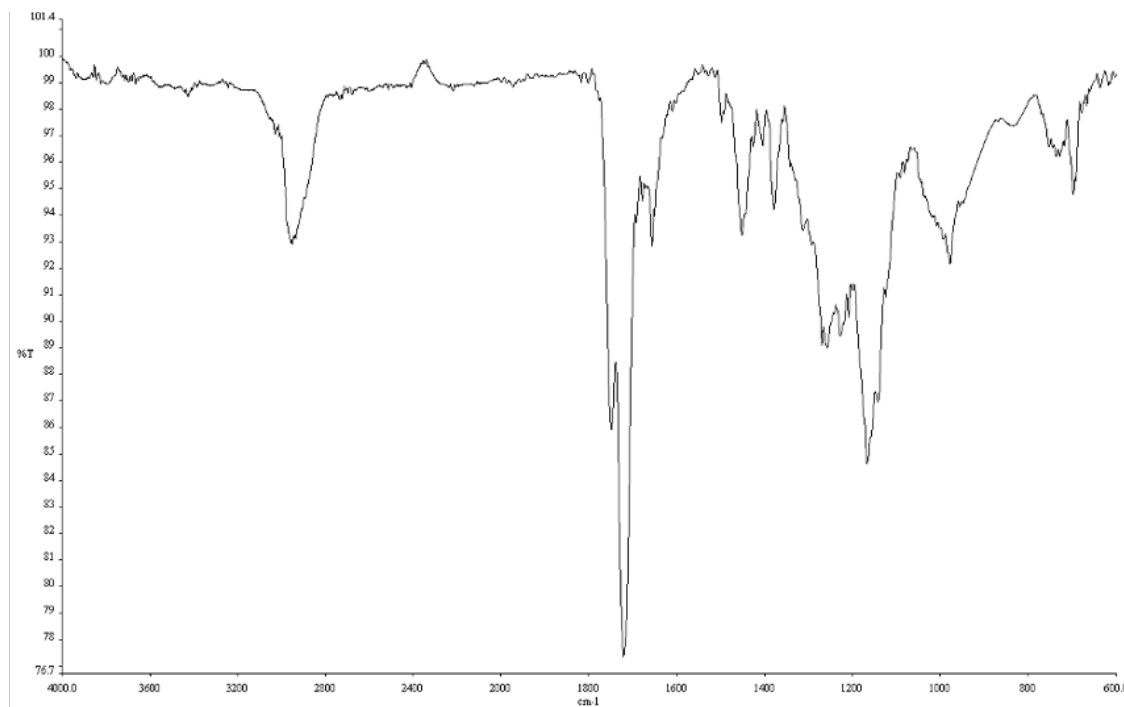
Figure A2.160. Infrared spectrum (Thin Film, NaCl) of compound **102**.
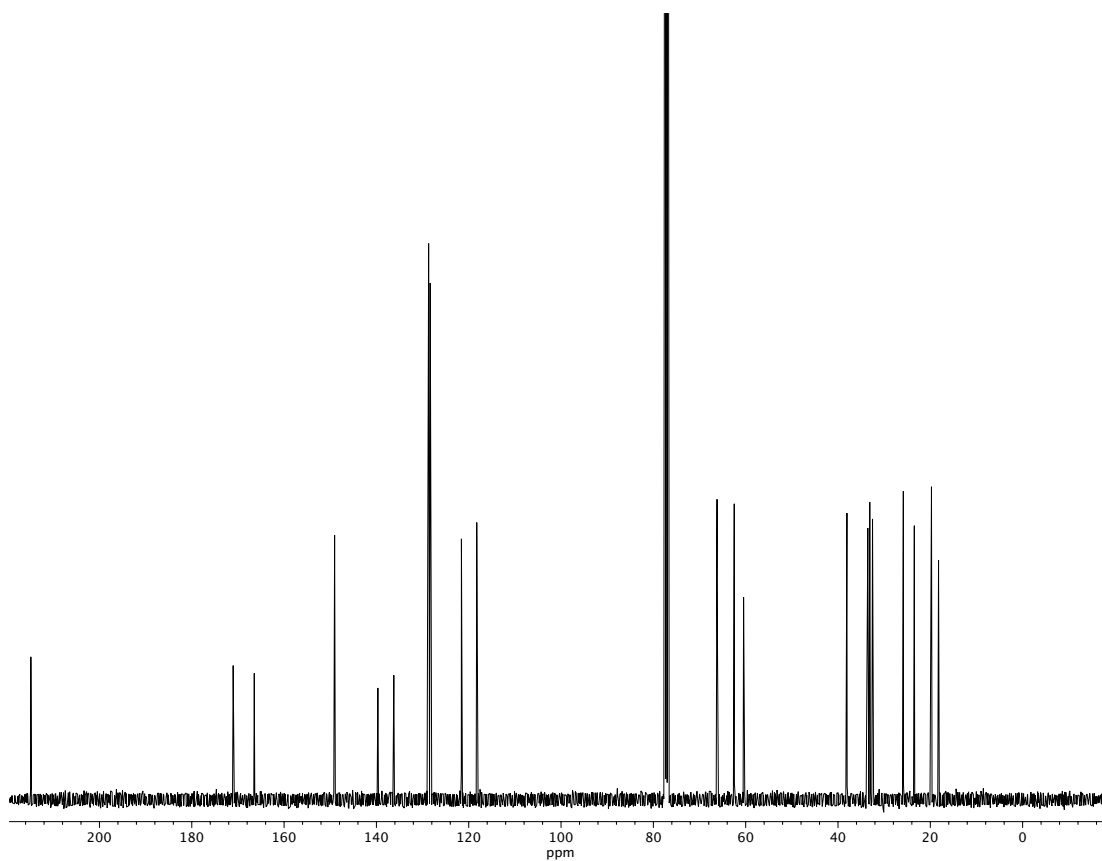
Figure A2.161. ^{13}C NMR (100 MHz, CDCl$_3$) of compound **102**.

Figure A2.162. ^1H NMR (400 MHz, CDCl$_3$) of compound **85**.
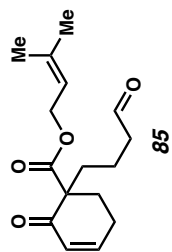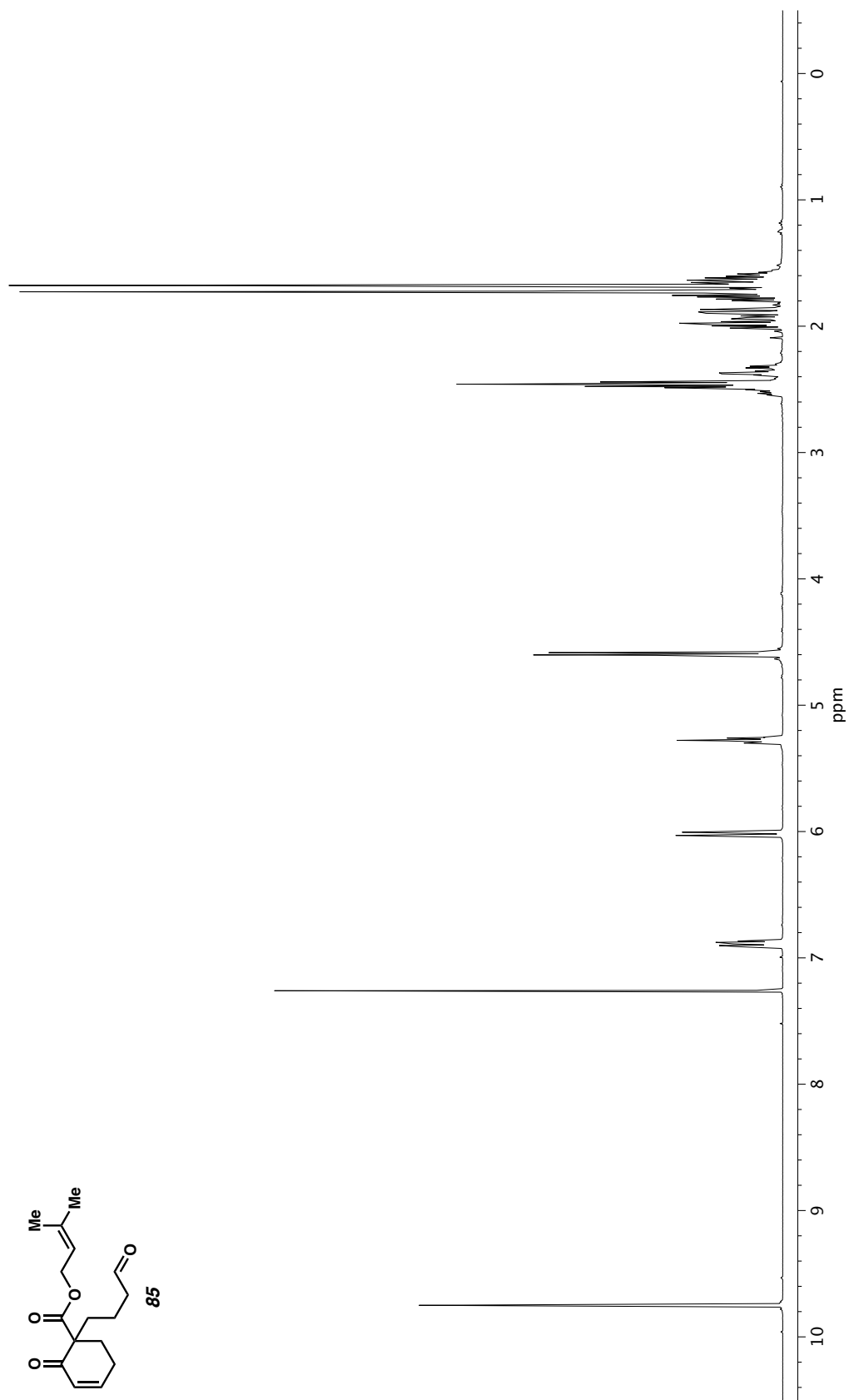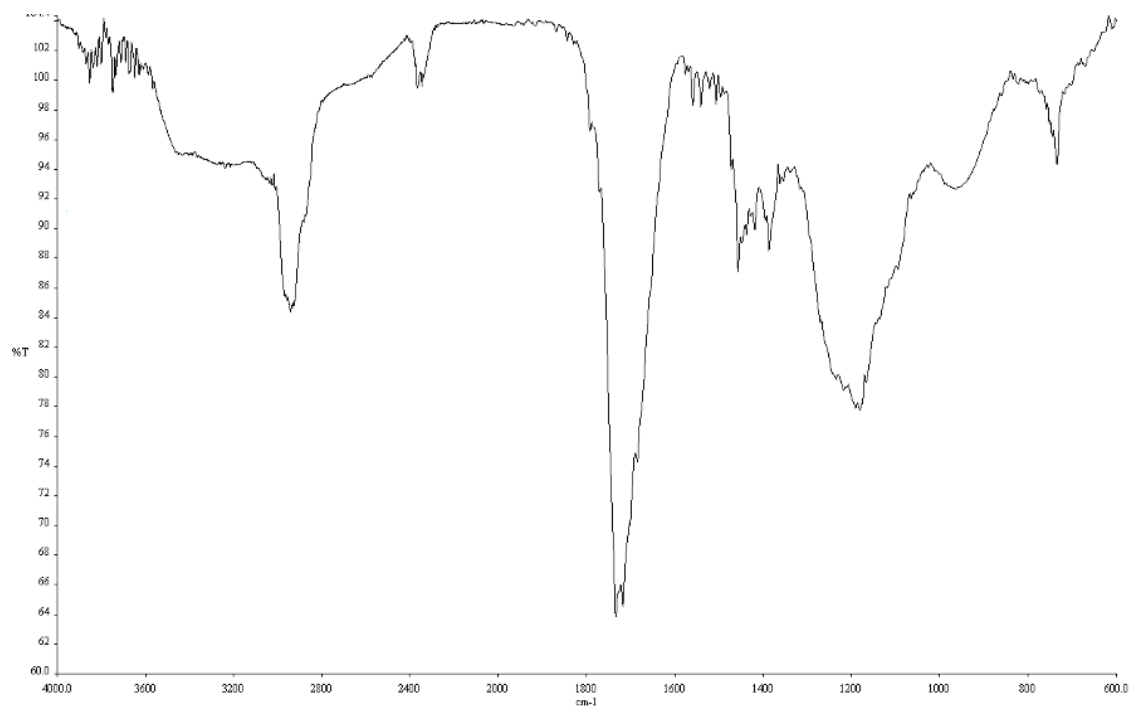
Figure A2.163. *Infrared spectrum (Thin Film, NaCl) of compound* **85**.
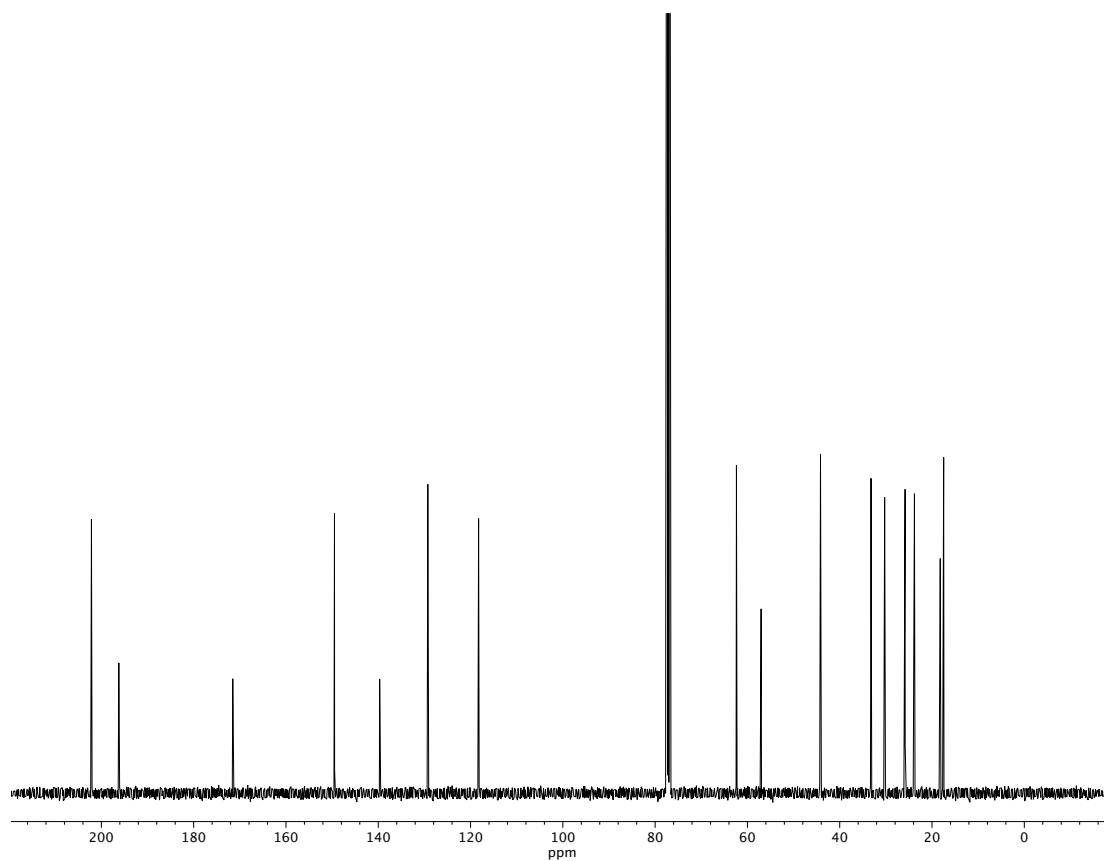
Figure A2.164. ^{13}C *NMR (100 MHz, CDCl$_3$) of compound* **85**.
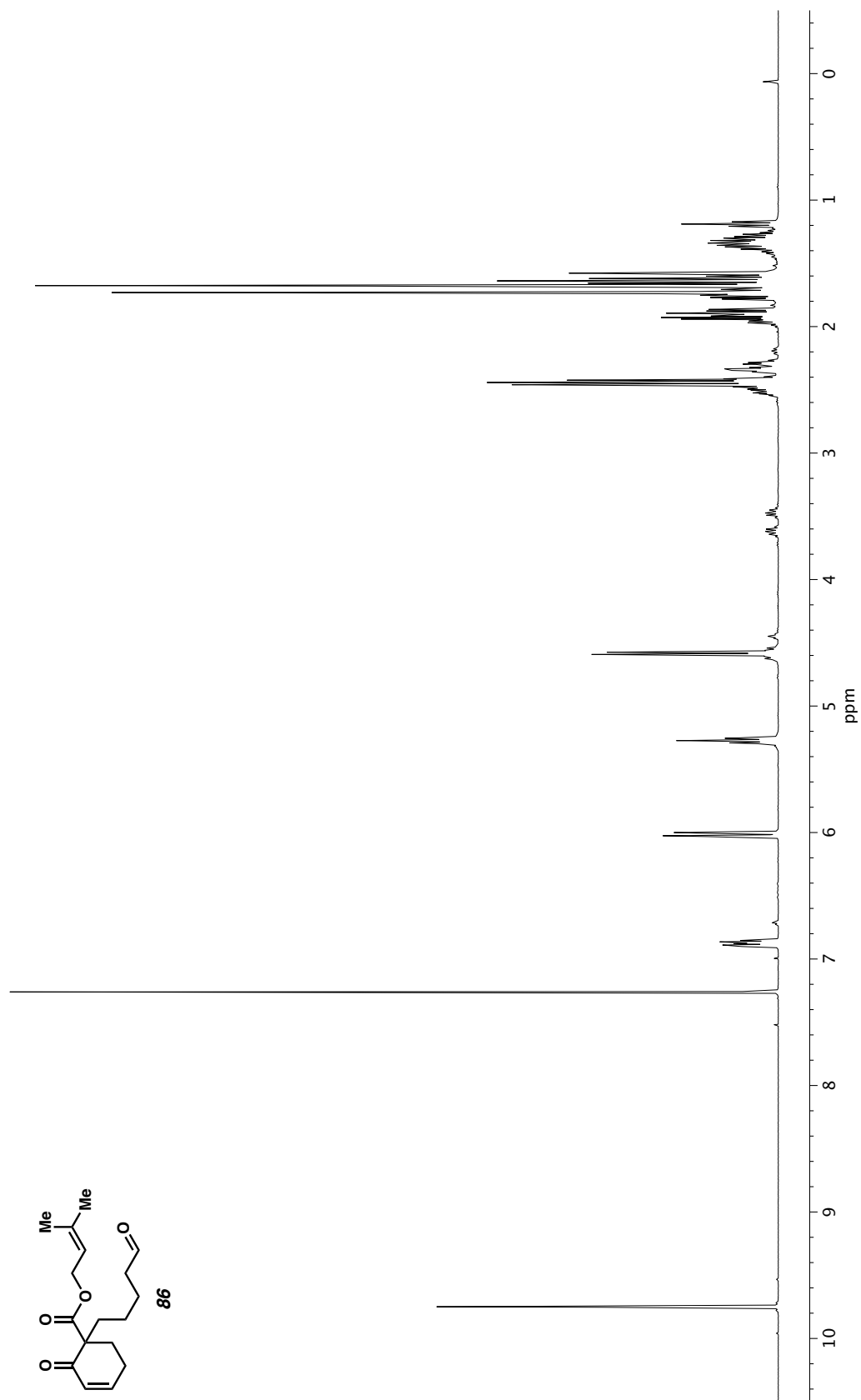
Figure A2.165. ^1H NMR (400 MHz, CDCl$_3$) of compound **86**.
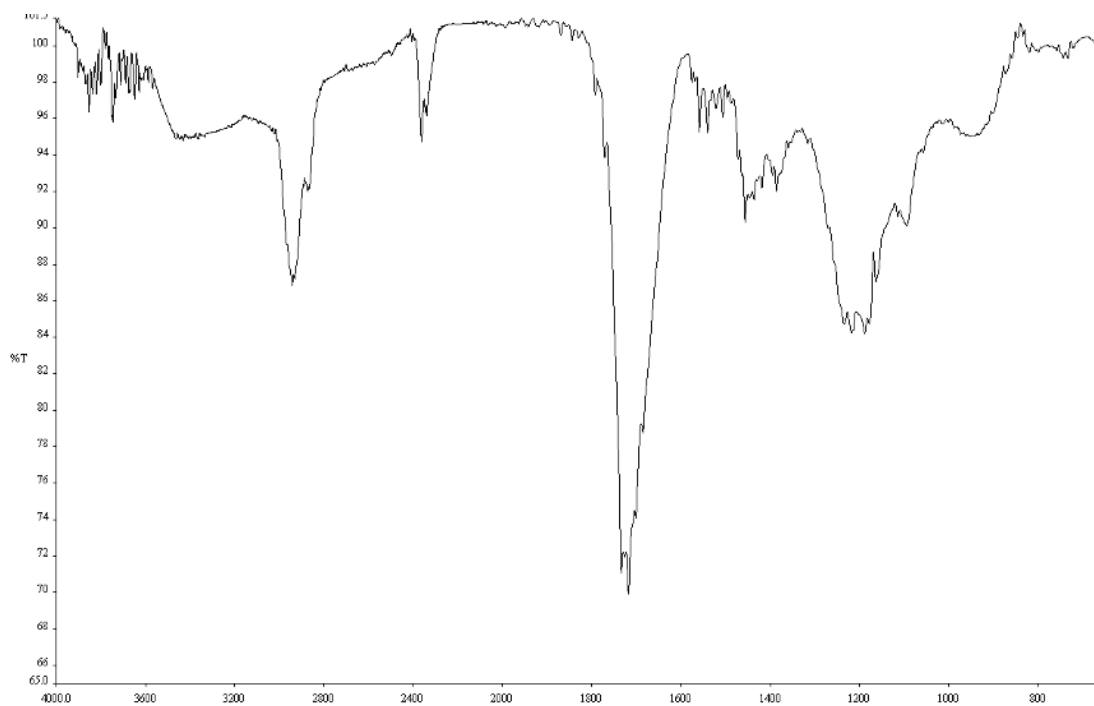
Figure A2.166. *Infrared spectrum (Thin Film, NaCl) of compound* **86**.
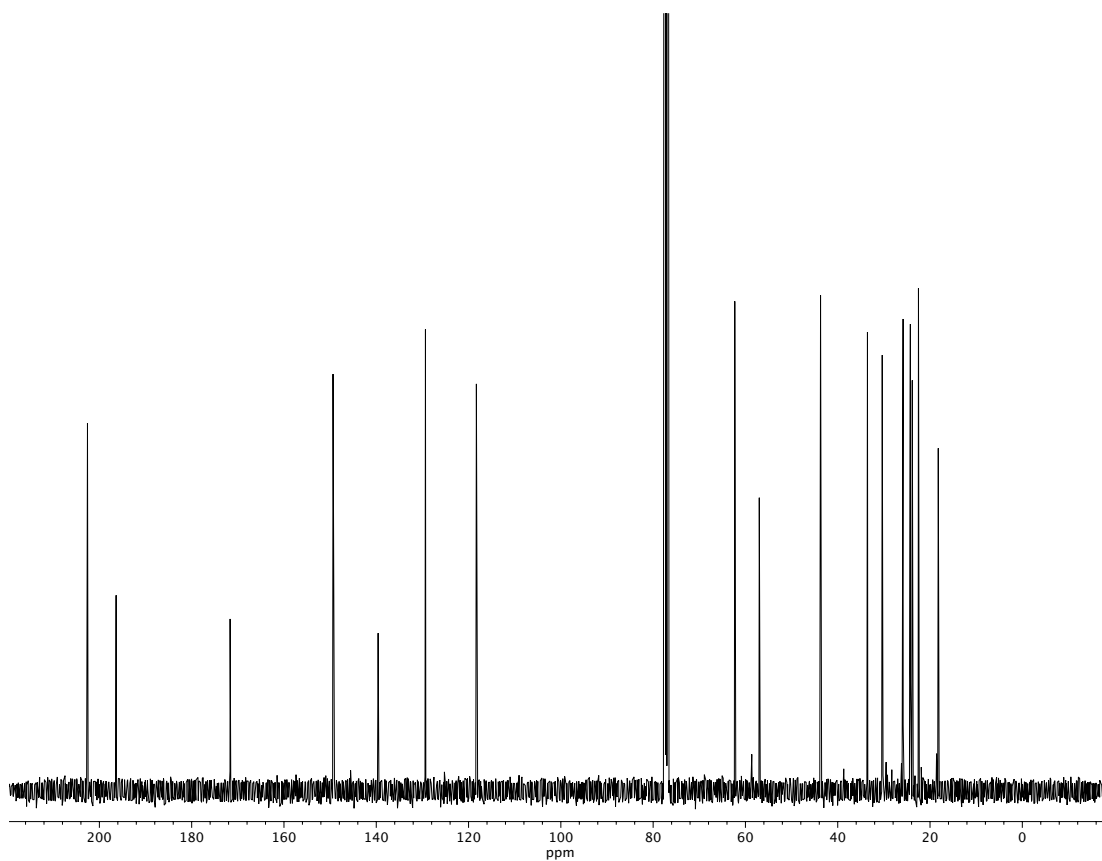
Figure A2.167. *^{13}C NMR (100 MHz, CDCl$_3$) of compound* **86**.
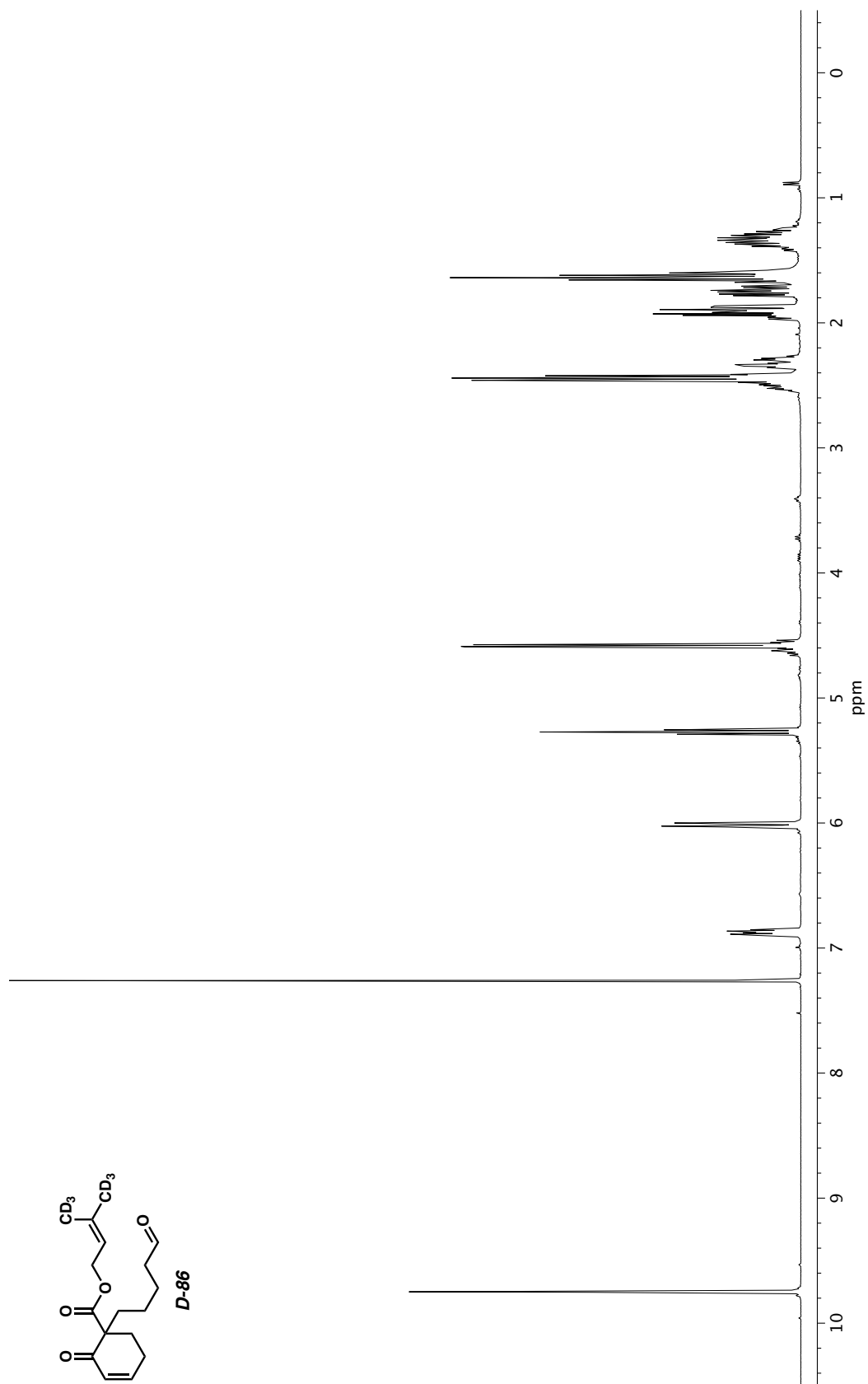
Figure A2.168. ^1H NMR (400 MHz, CDCl$_3$) of compound **D-86**.
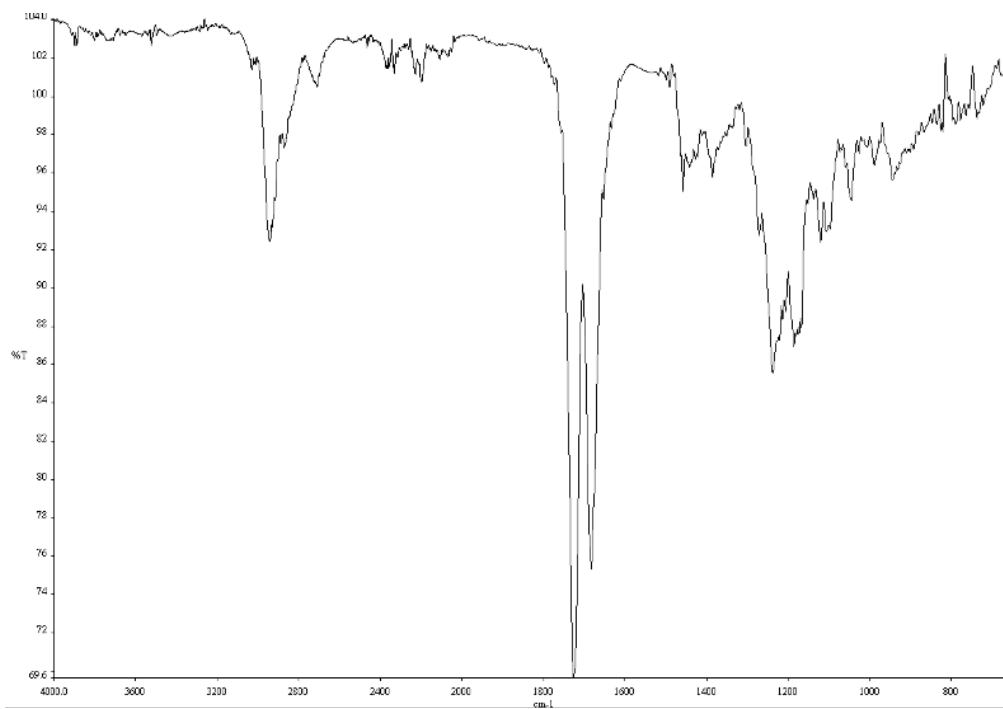
Figure A2.169. Infrared spectrum (Thin Film, NaCl) of compound **D-86**.
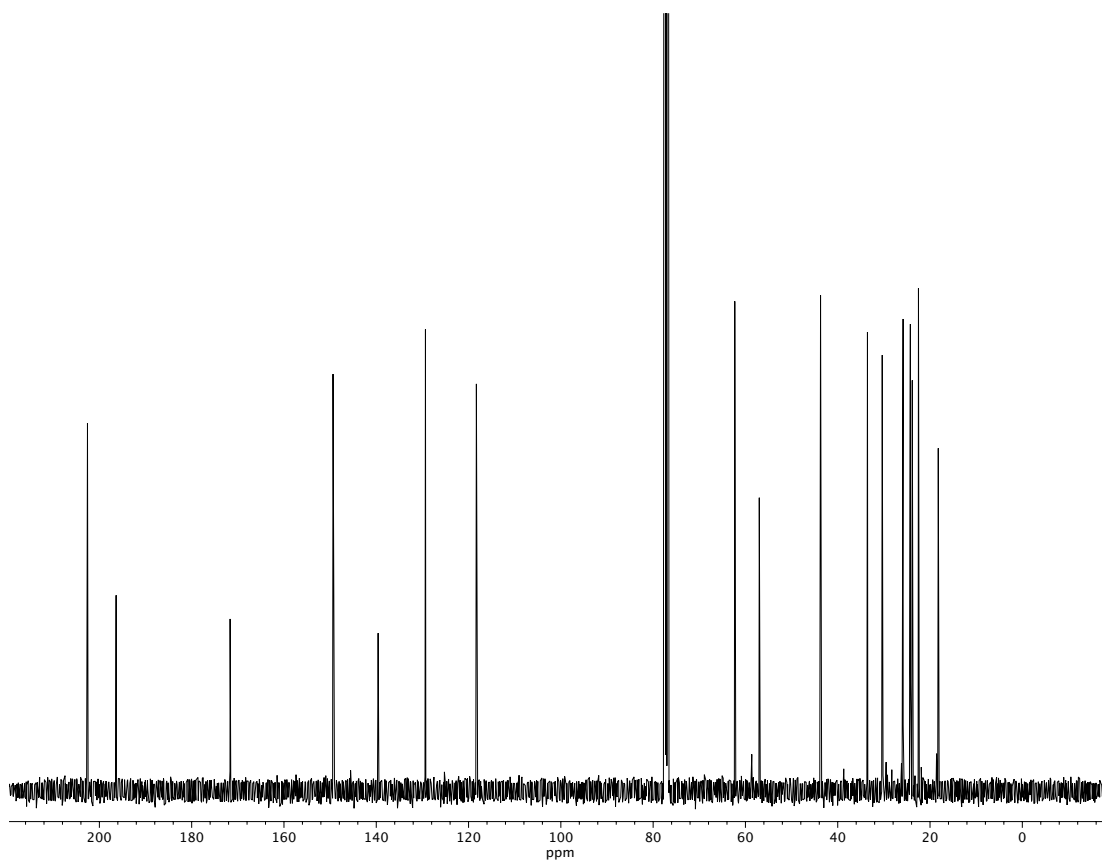
Figure A2.170. ^{13}C NMR (100 MHz, CDCl$_3$) of compound **D-86**.
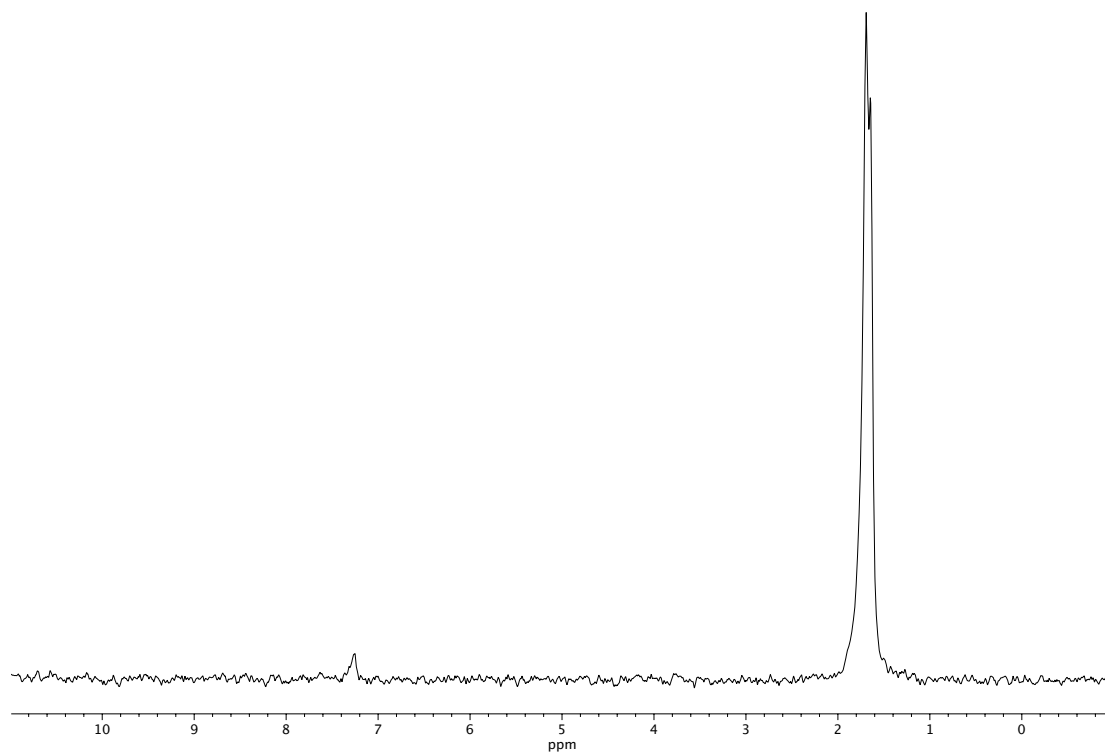
Figure A2.171. ^{2}H NMR (61 MHz, CHCl$_3$) of compound **D-86**.
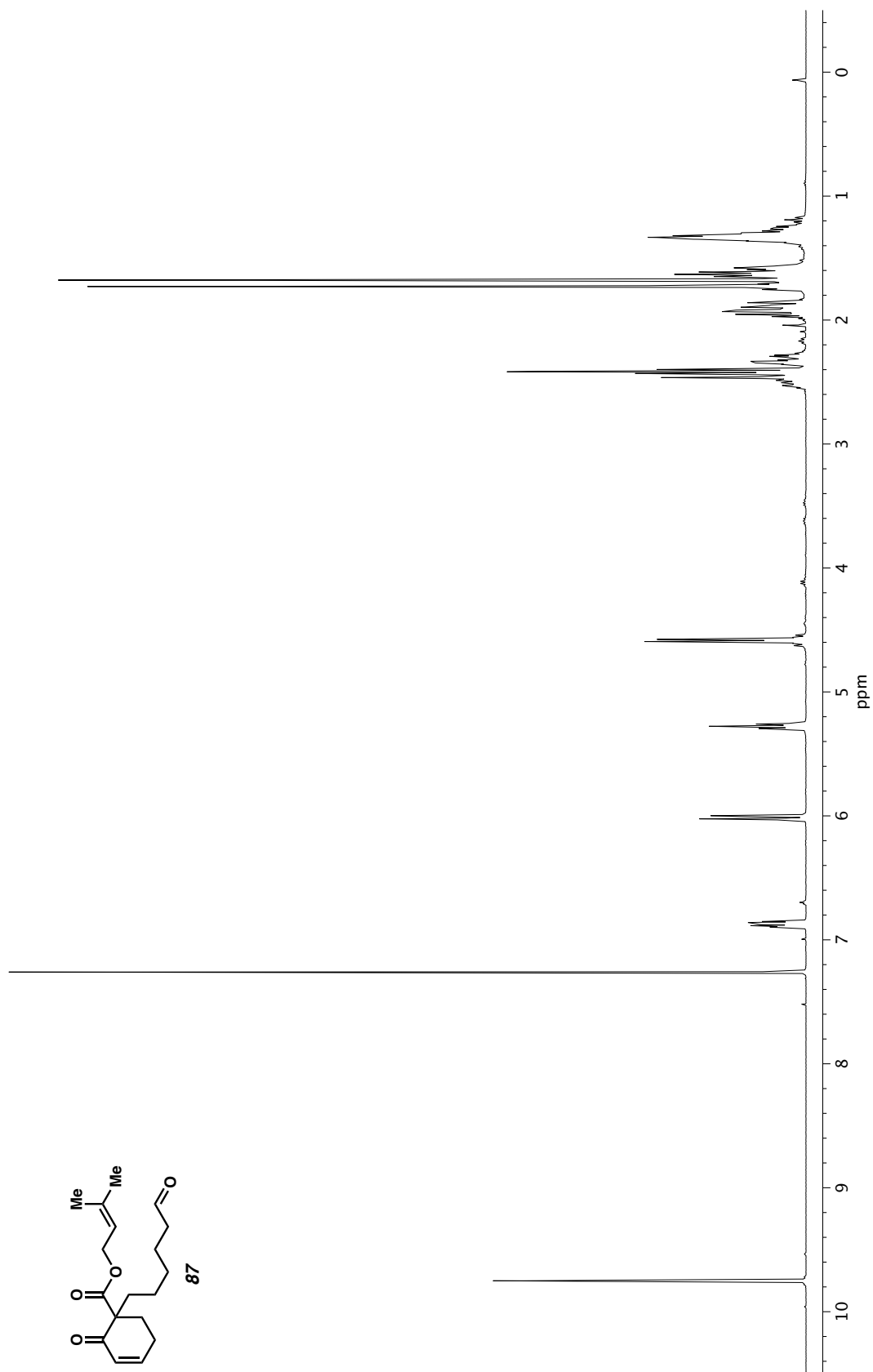
Figure A2.172. *^{1}H NMR (400 MHz, CDCl$_3$) of compound **87**.*
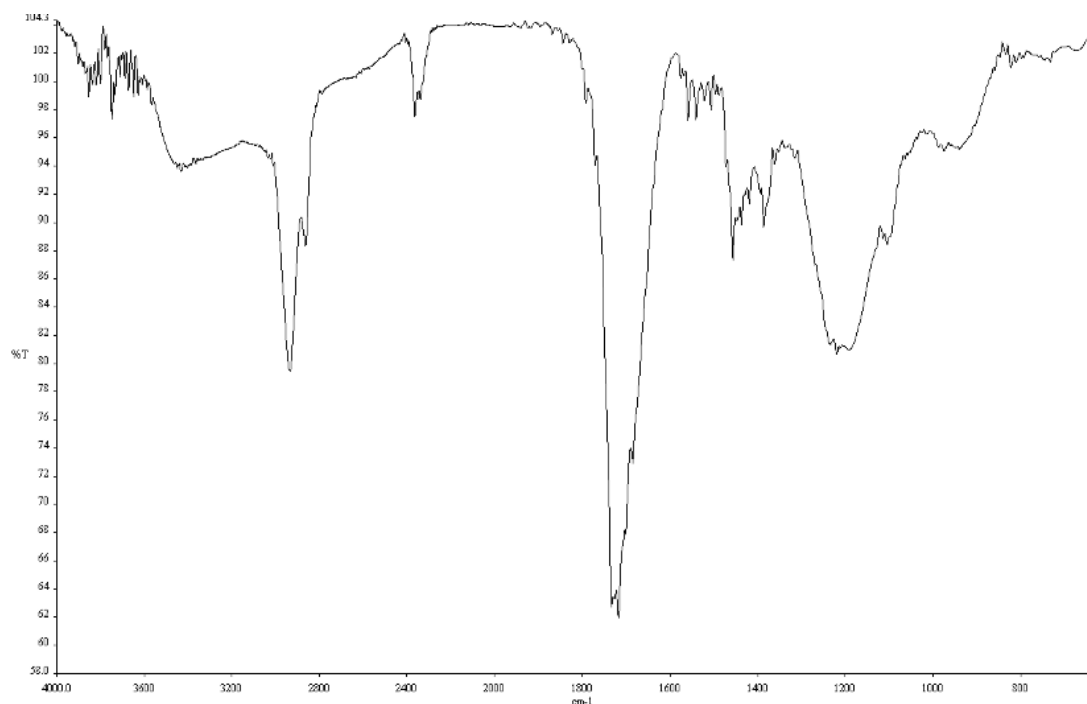
Figure A2.173. *Infrared spectrum (Thin Film, NaCl) of compound* **87**.
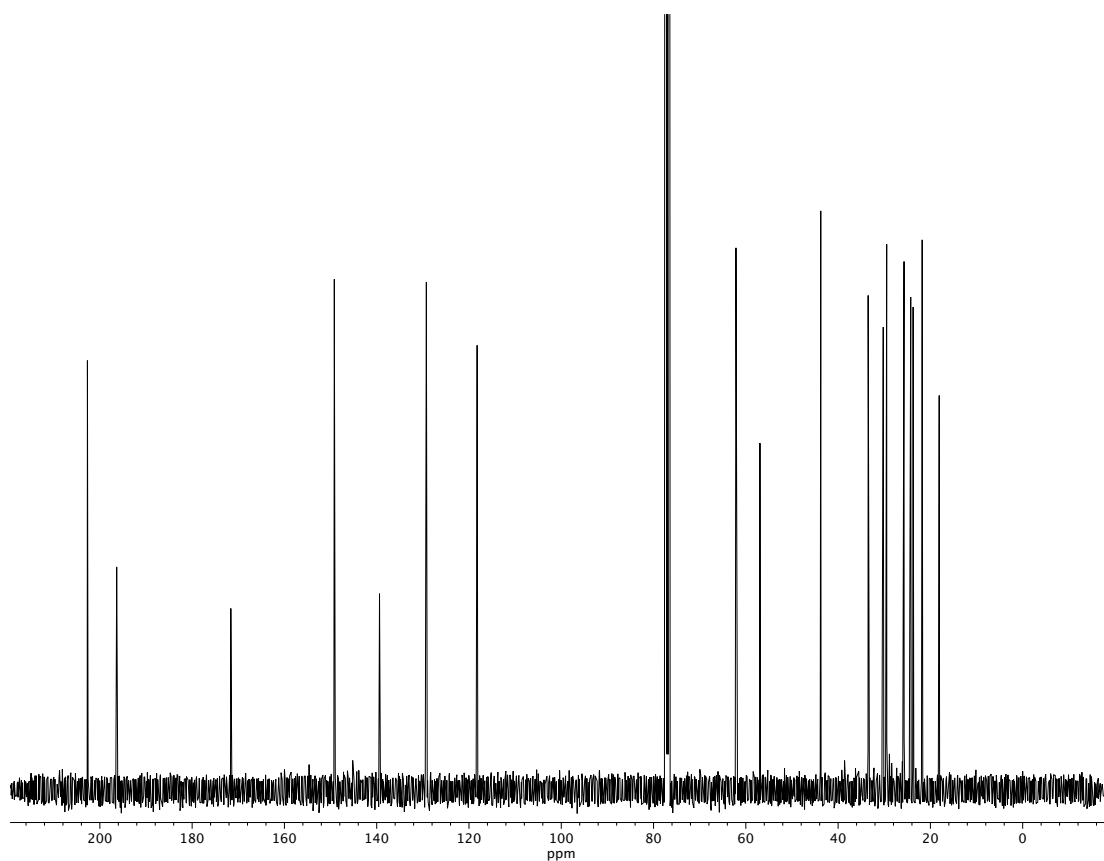
Figure A2.174. ^{13}C *NMR (100 MHz, CDCl$_3$) of compound* **87**.
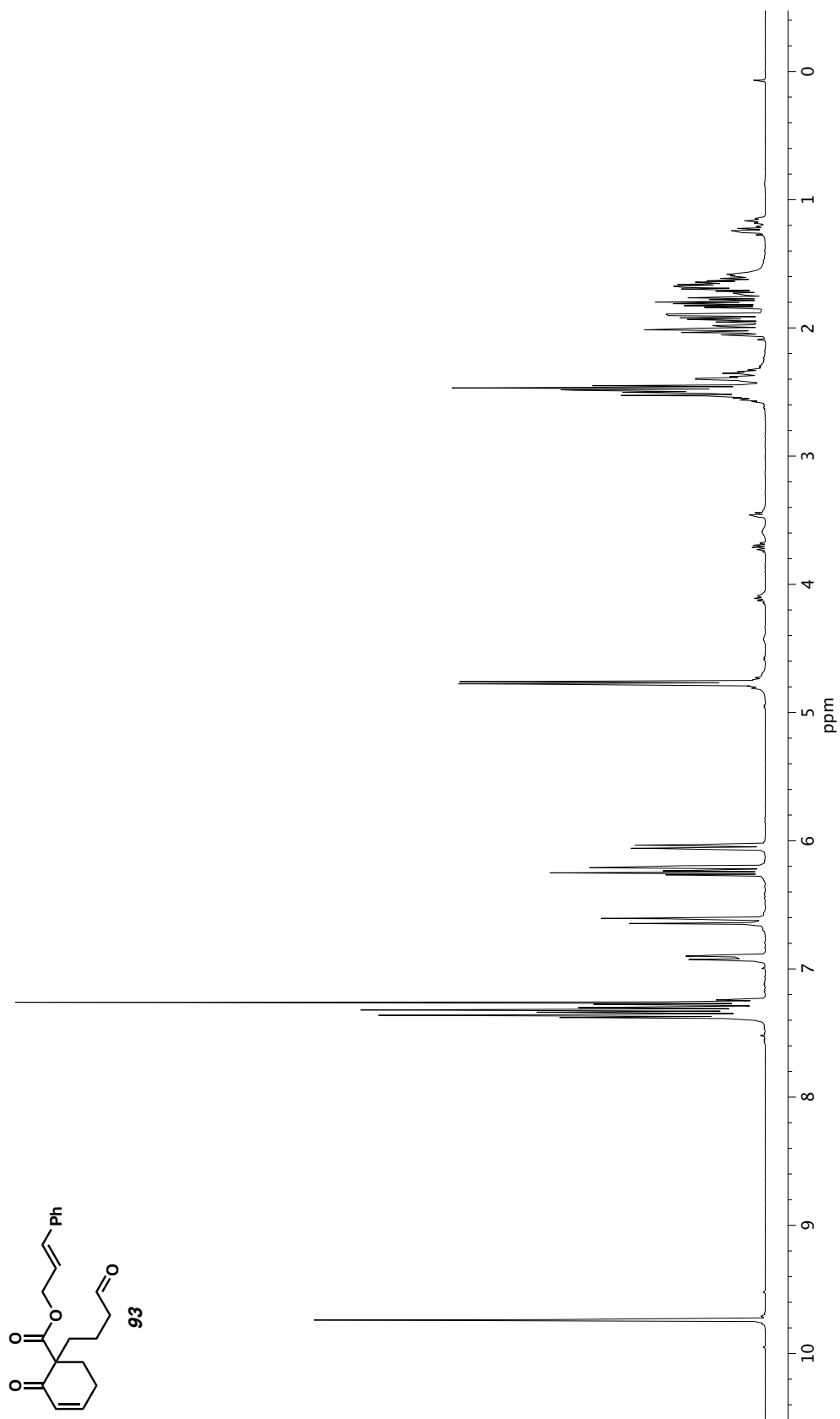
Figure A2.175. ^1H NMR (400 MHz, CDCl$_3$) of compound **93**.
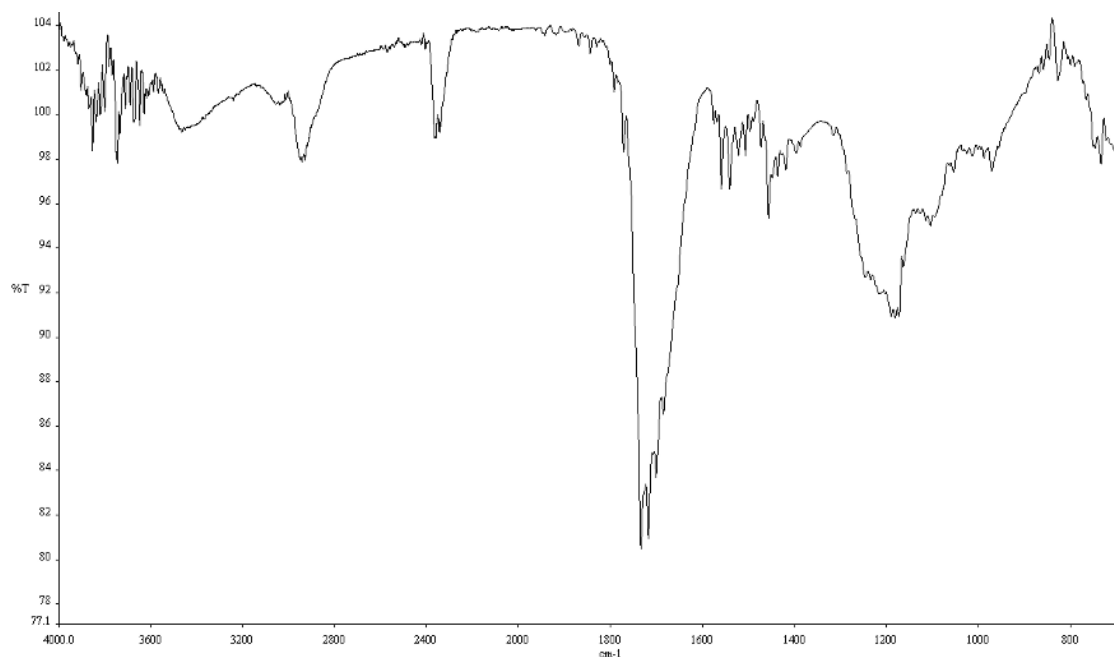
Figure A2.176. Infrared spectrum (Thin Film, NaCl) of compound **93**.
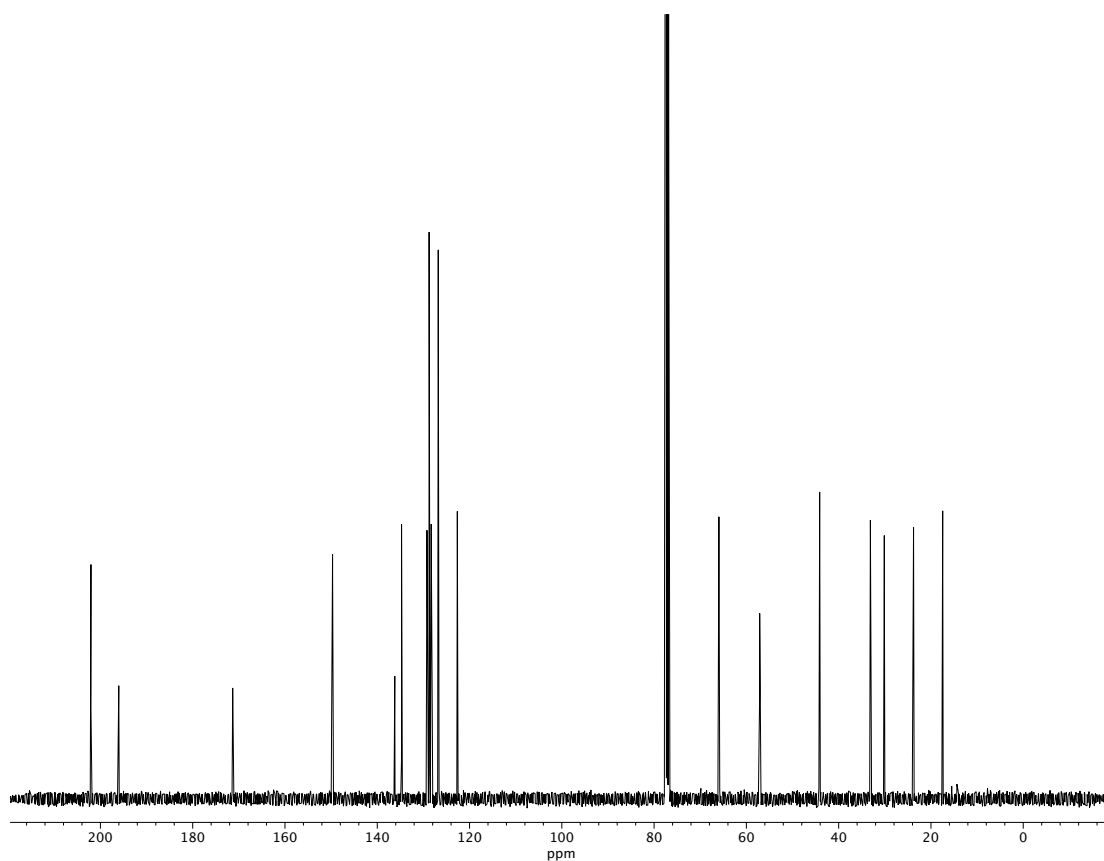
Figure A2.177. ^{13}C NMR (100 MHz, CDCl$_3$) of compound **93**.
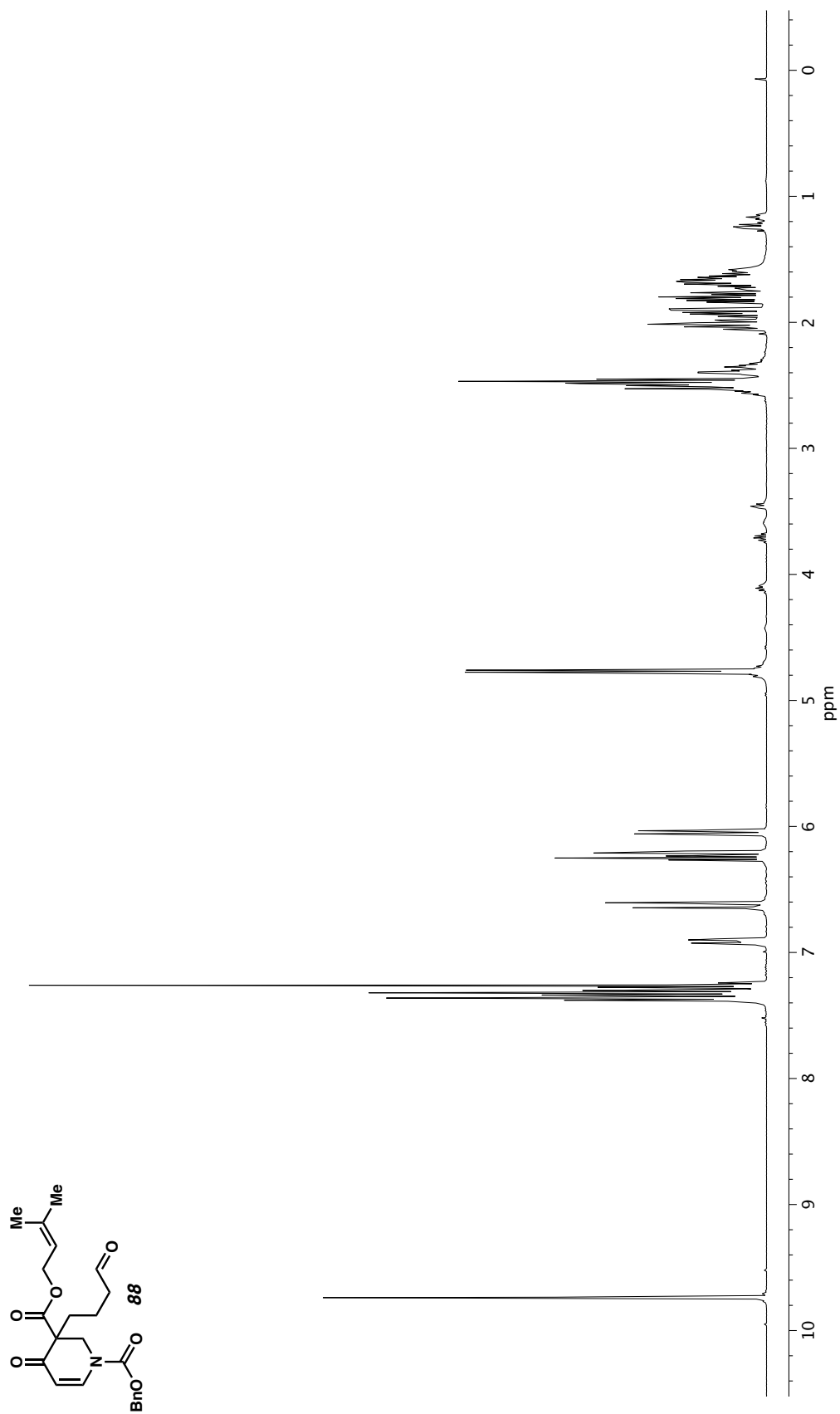
Figure A2.178. ^1H NMR (400 MHz, CDCl$_3$) of compound **88**.
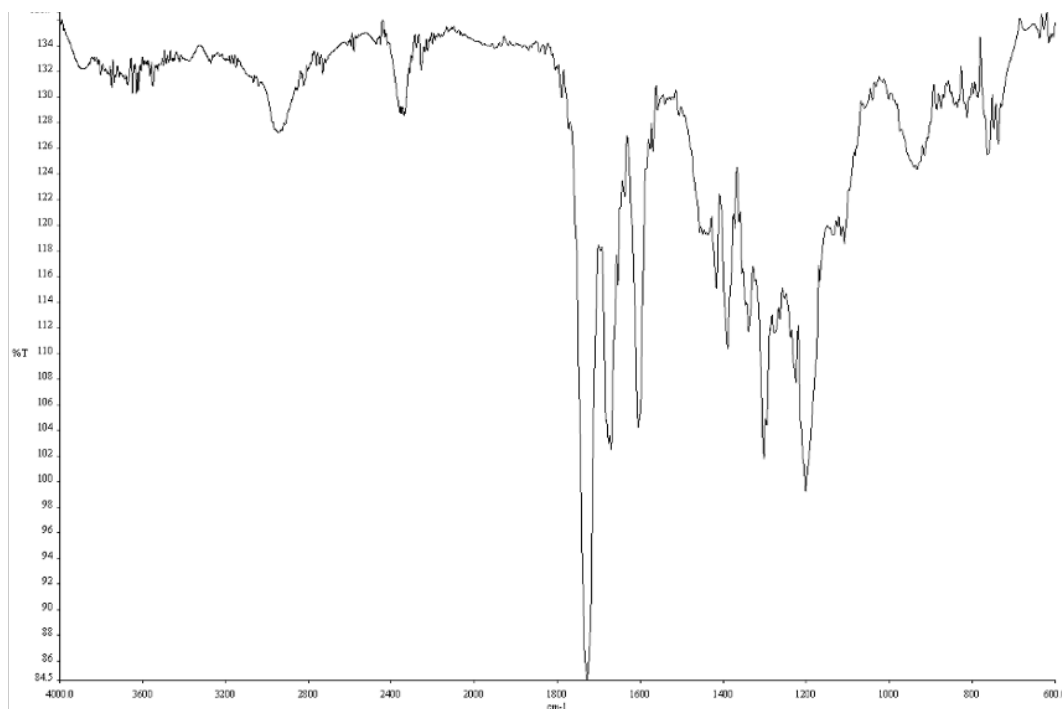
Figure A2.179. *Infrared spectrum (Thin Film, NaCl) of compound **88**.*
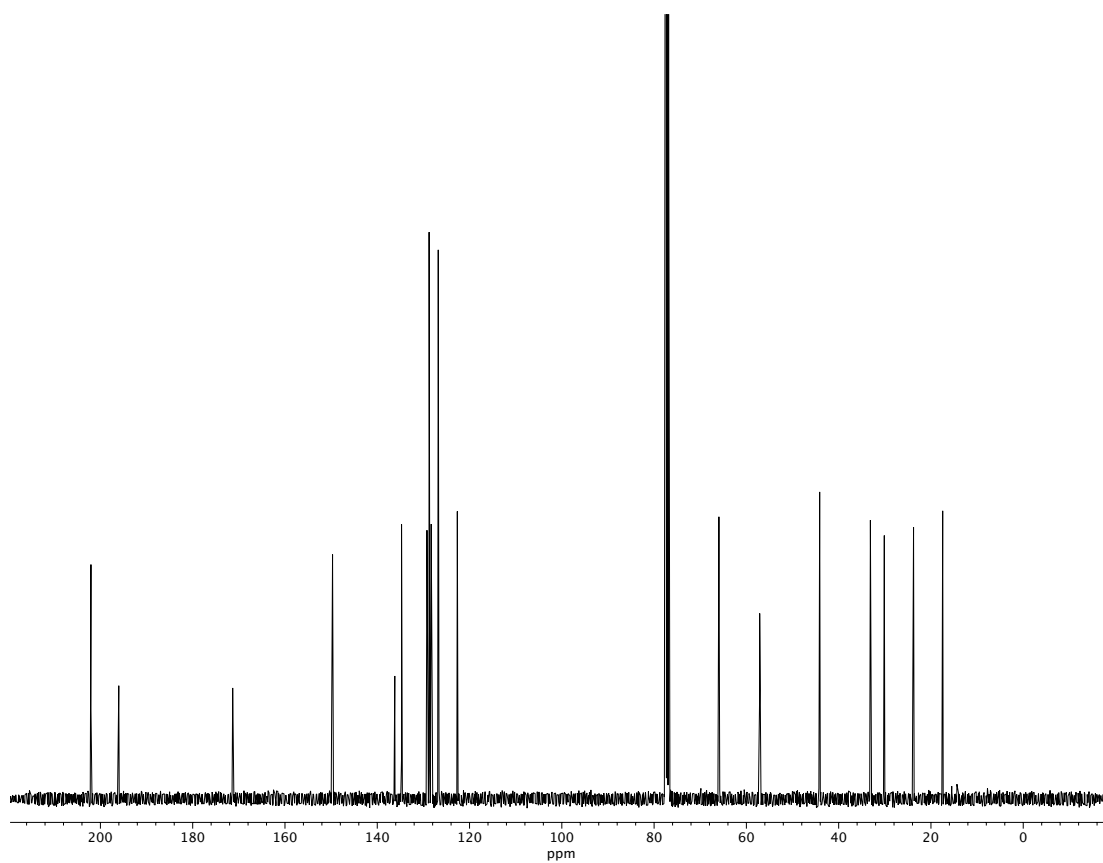
Figure A2.180. *^{13}C NMR (100 MHz, CDCl$_3$) of compound **88**.*
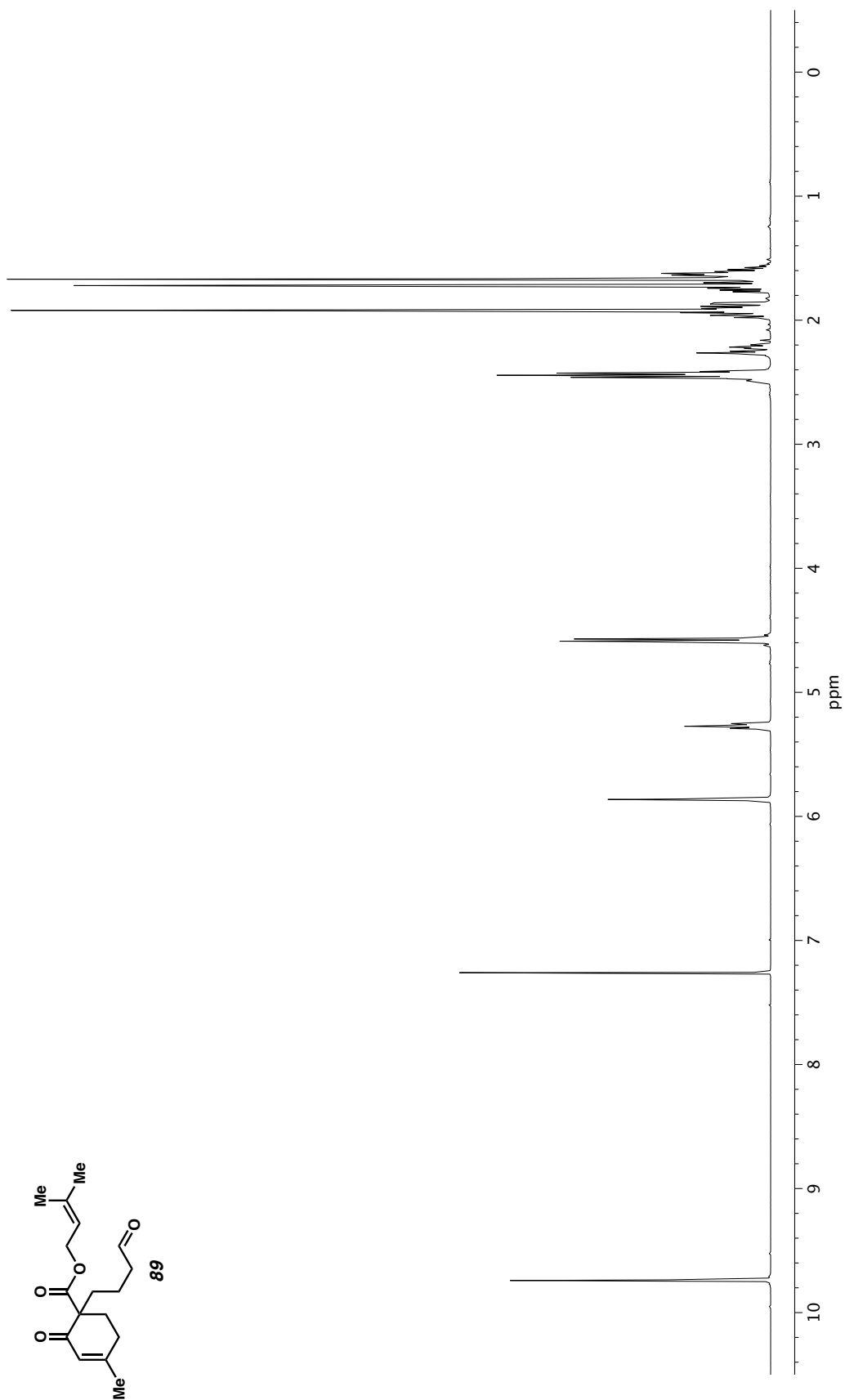
Figure A2.181. ^1H NMR (400 MHz, CDCl$_3$) of compound **89**.
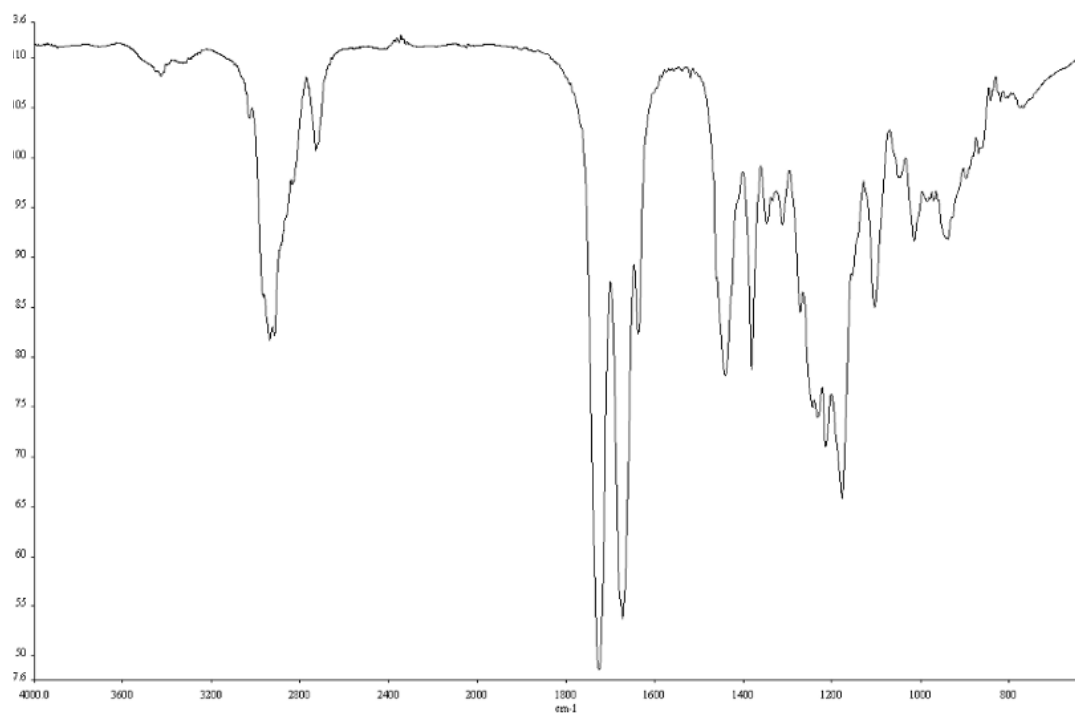
Figure A2.182. *Infrared spectrum (Thin Film, NaCl) of compound* **89**.
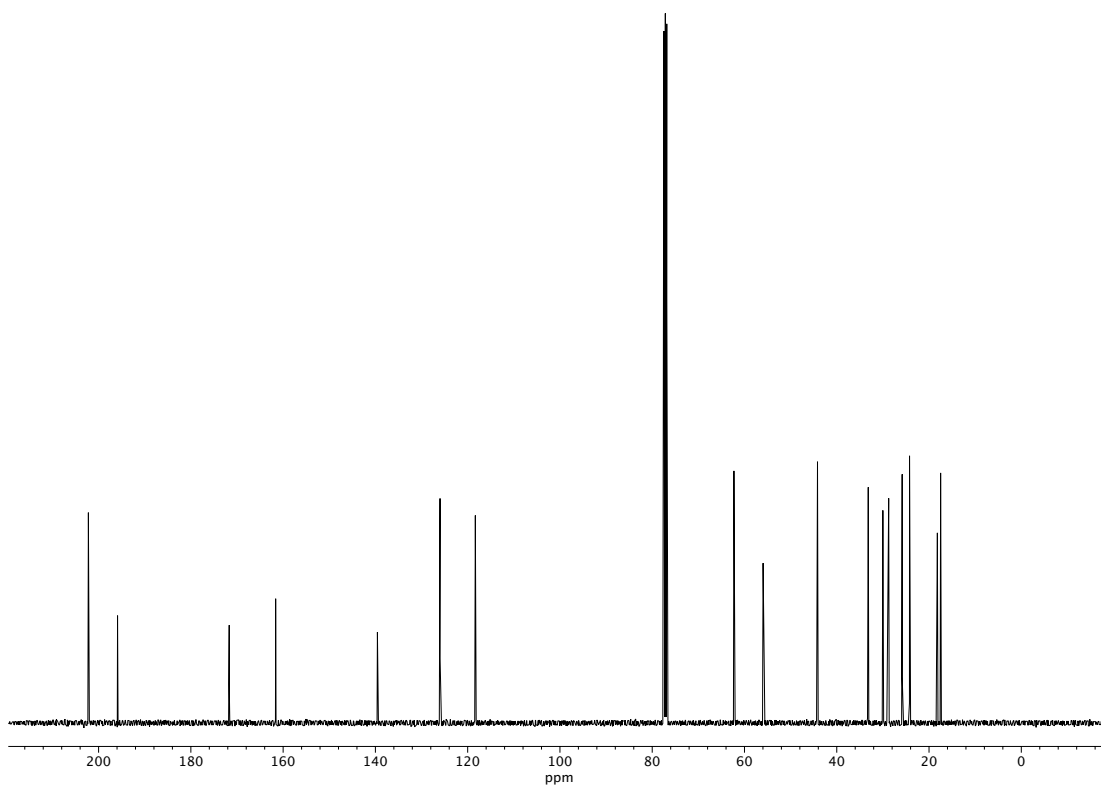
Figure A2.183. ^{13}C *NMR (100 MHz, CDCl$_3$) of compound* **89**.
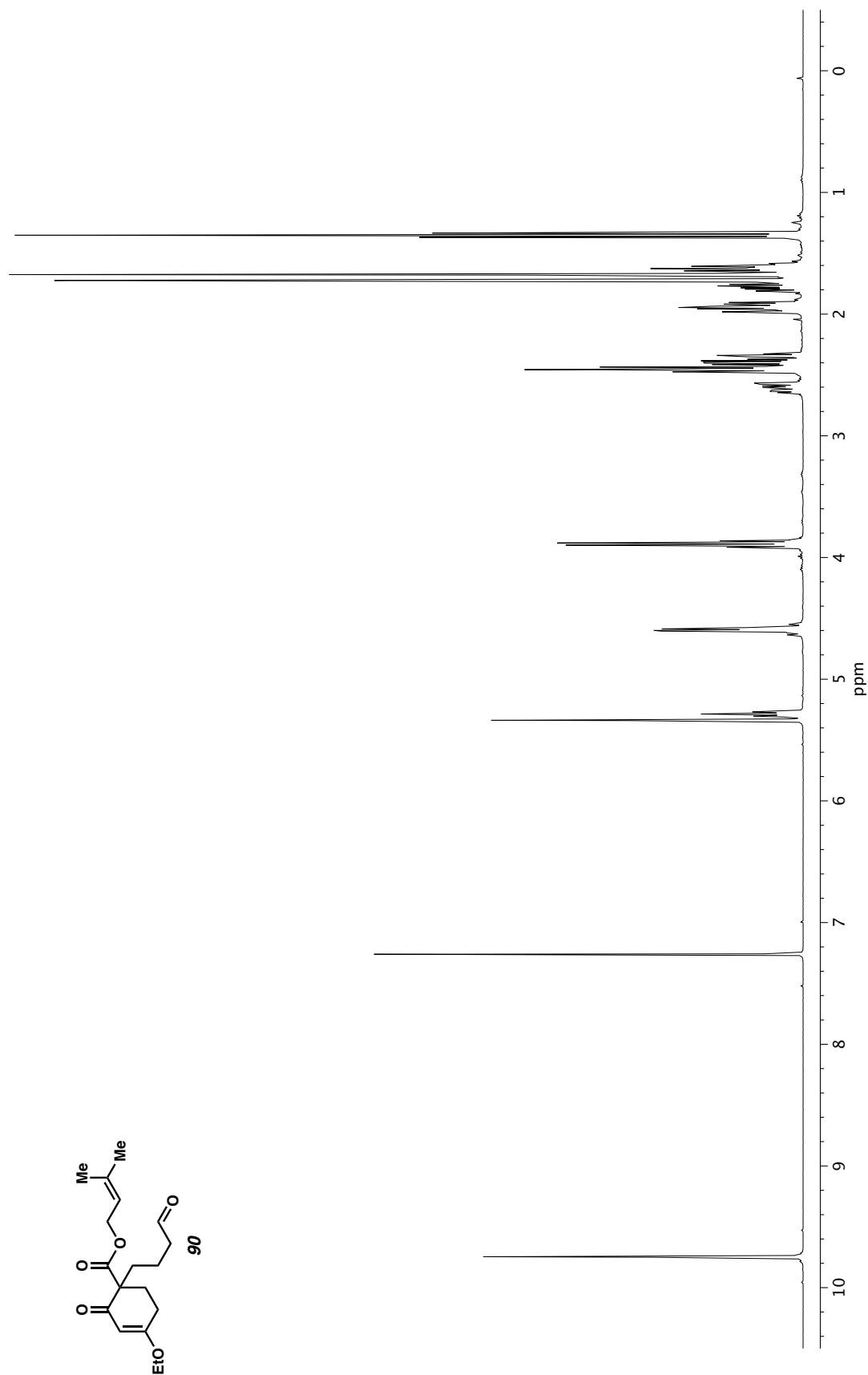
Figure A2.184. *^{1}H NMR (400 MHz, CDCl$_3$) of compound **90**.*
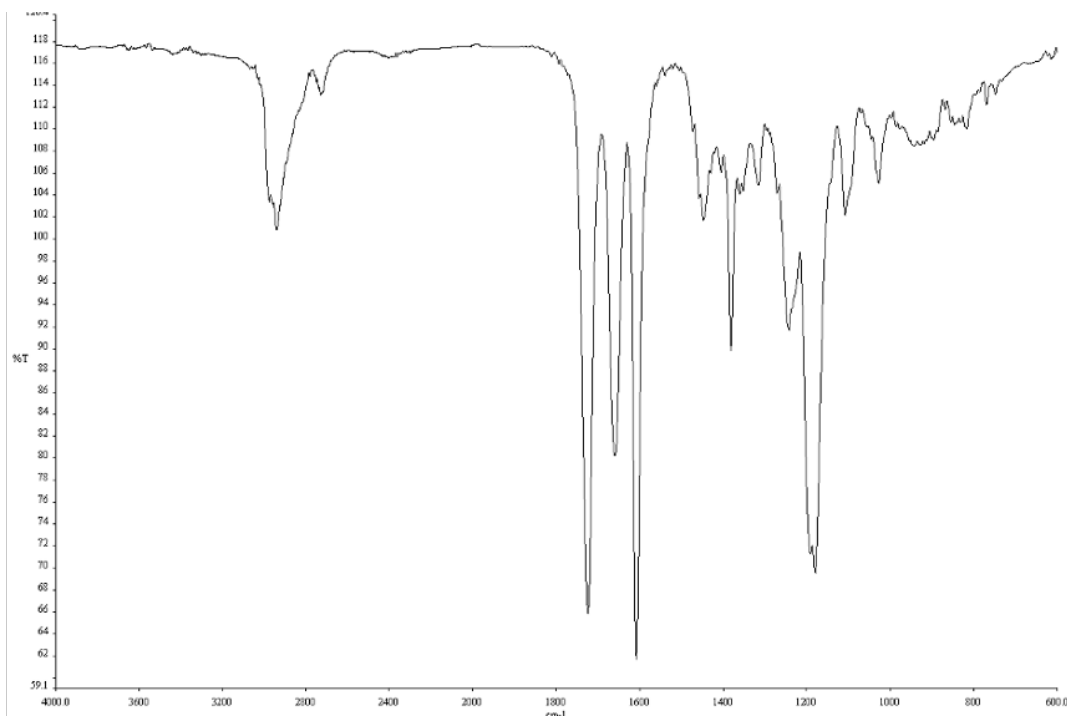
Figure A2.185. *Infrared spectrum (Thin Film, NaCl) of compound* **90**.
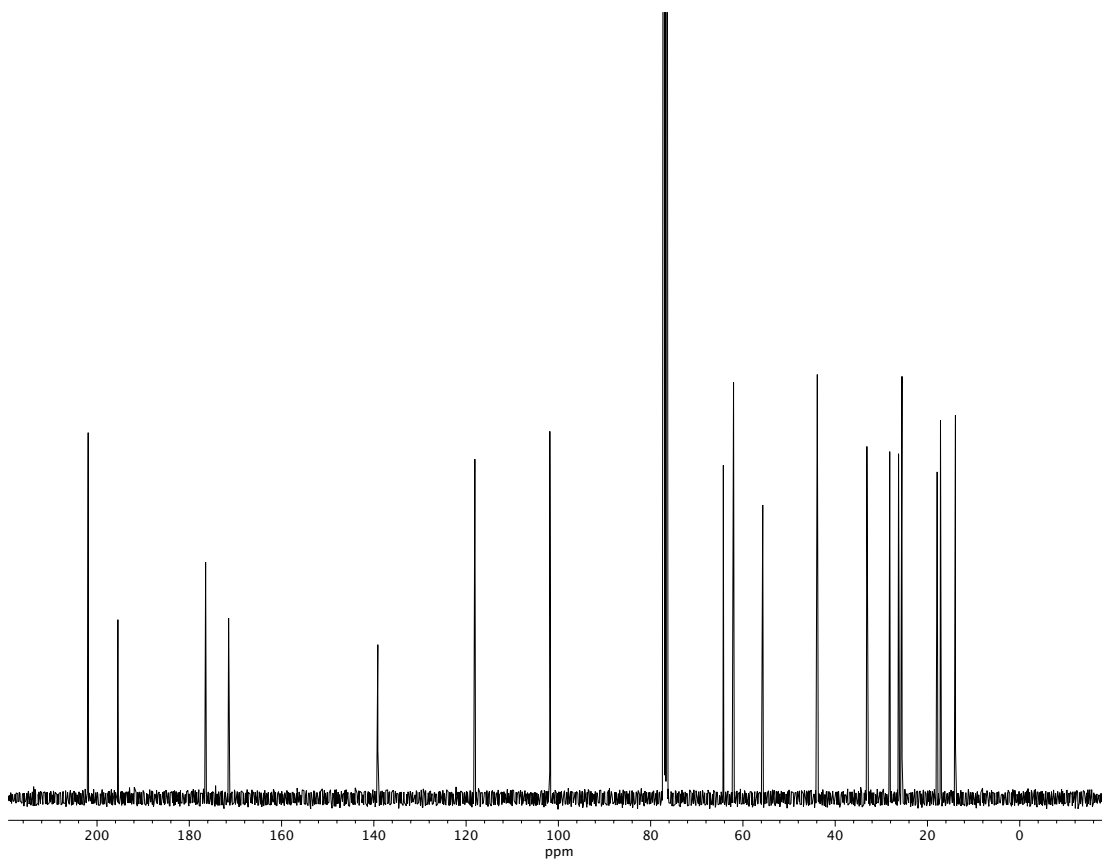
Figure A2.186. ^{13}C *NMR (100 MHz, CDCl$_3$) of compound* **90**.
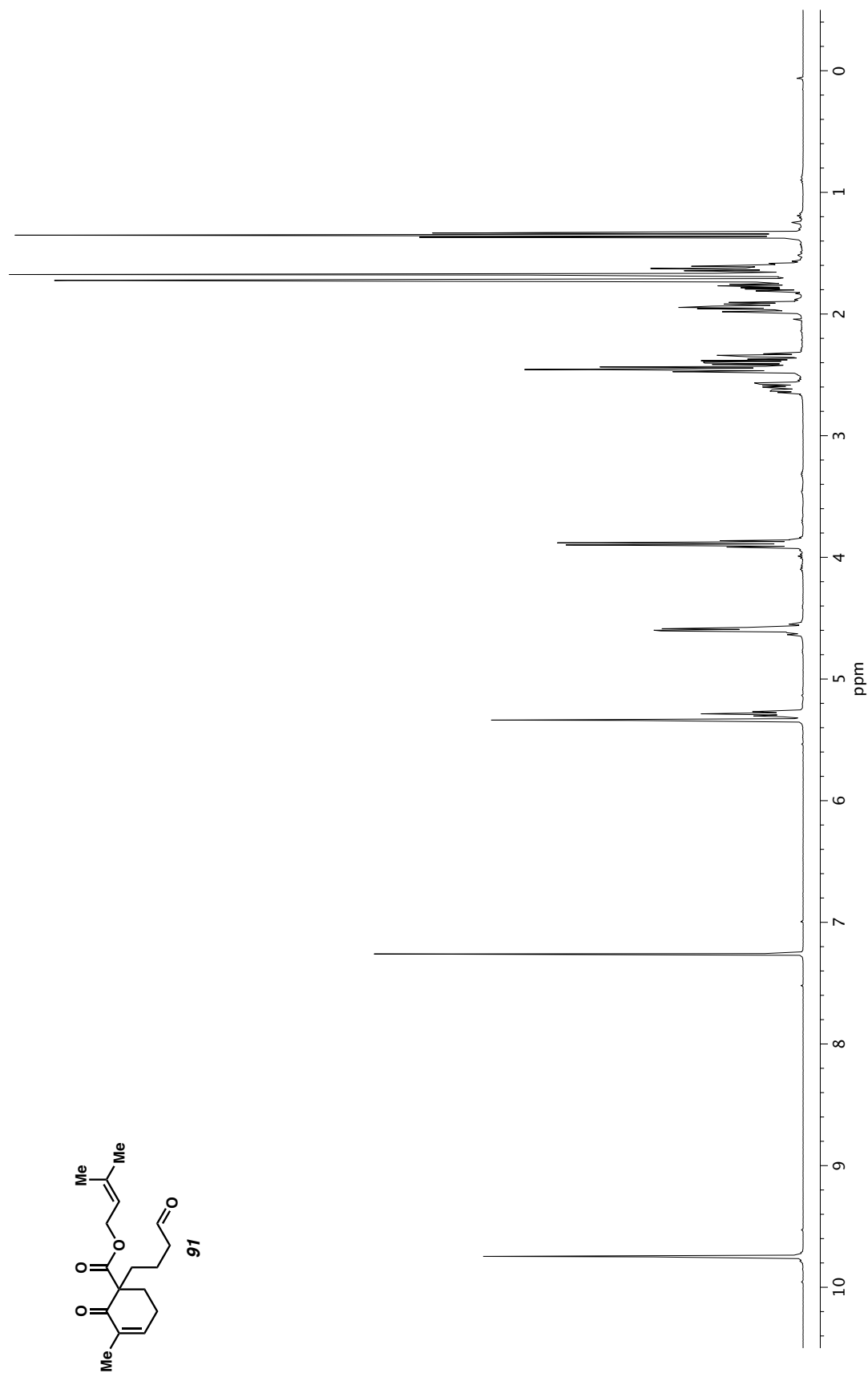
Figure A2.187. ^1H NMR (400 MHz, CDCl$_3$) of compound **91**.
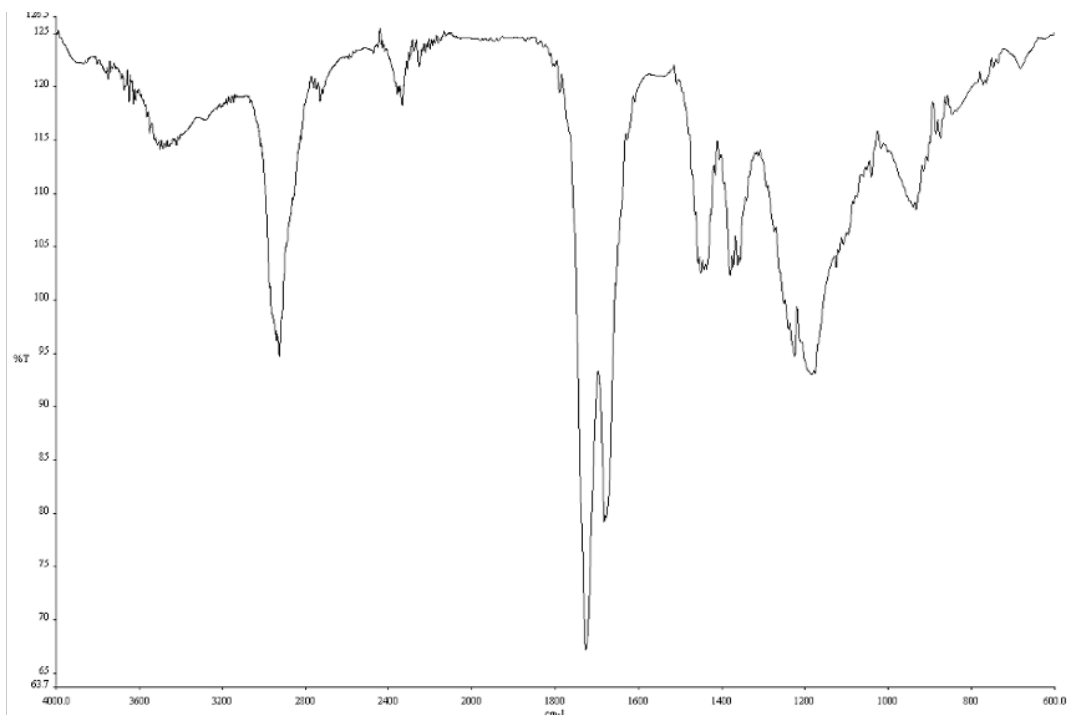
Figure A2.188. *Infrared spectrum (Thin Film, NaCl) of compound* **91**.
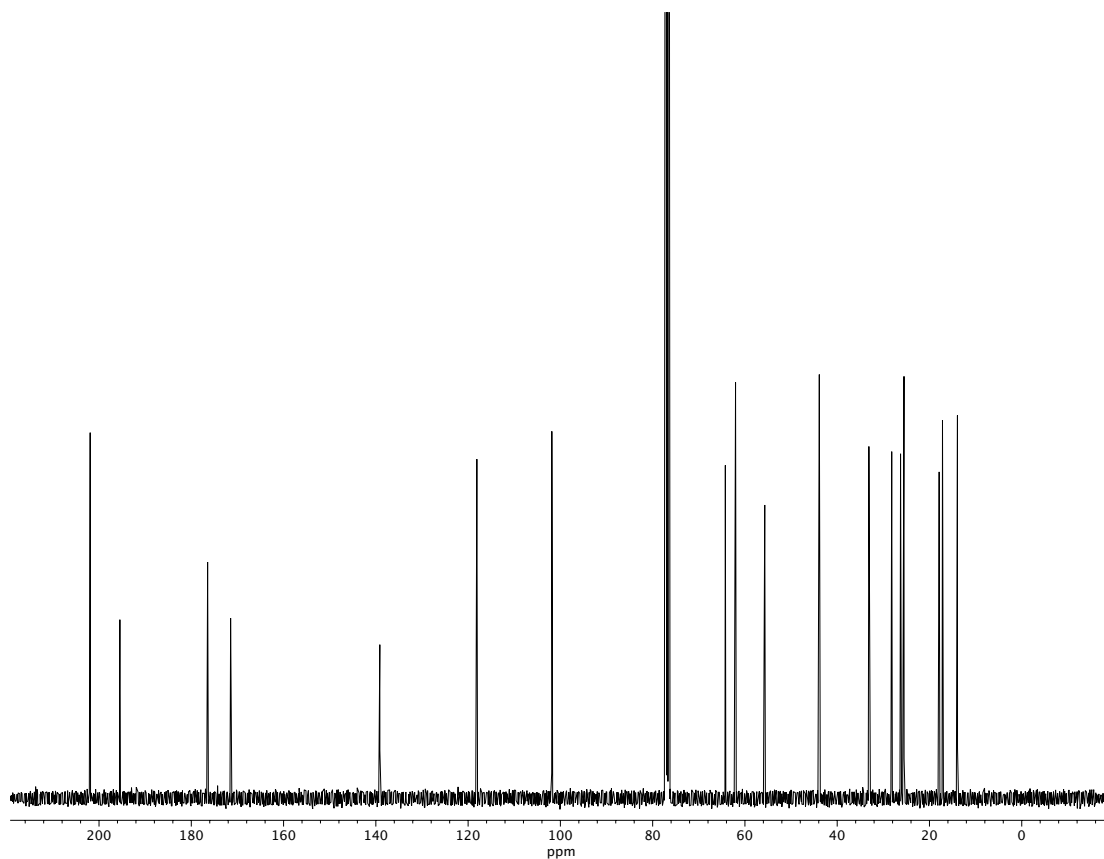
Figure A2.189. ^{13}C *NMR (100 MHz, CDCl$_3$) of compound* **91**.
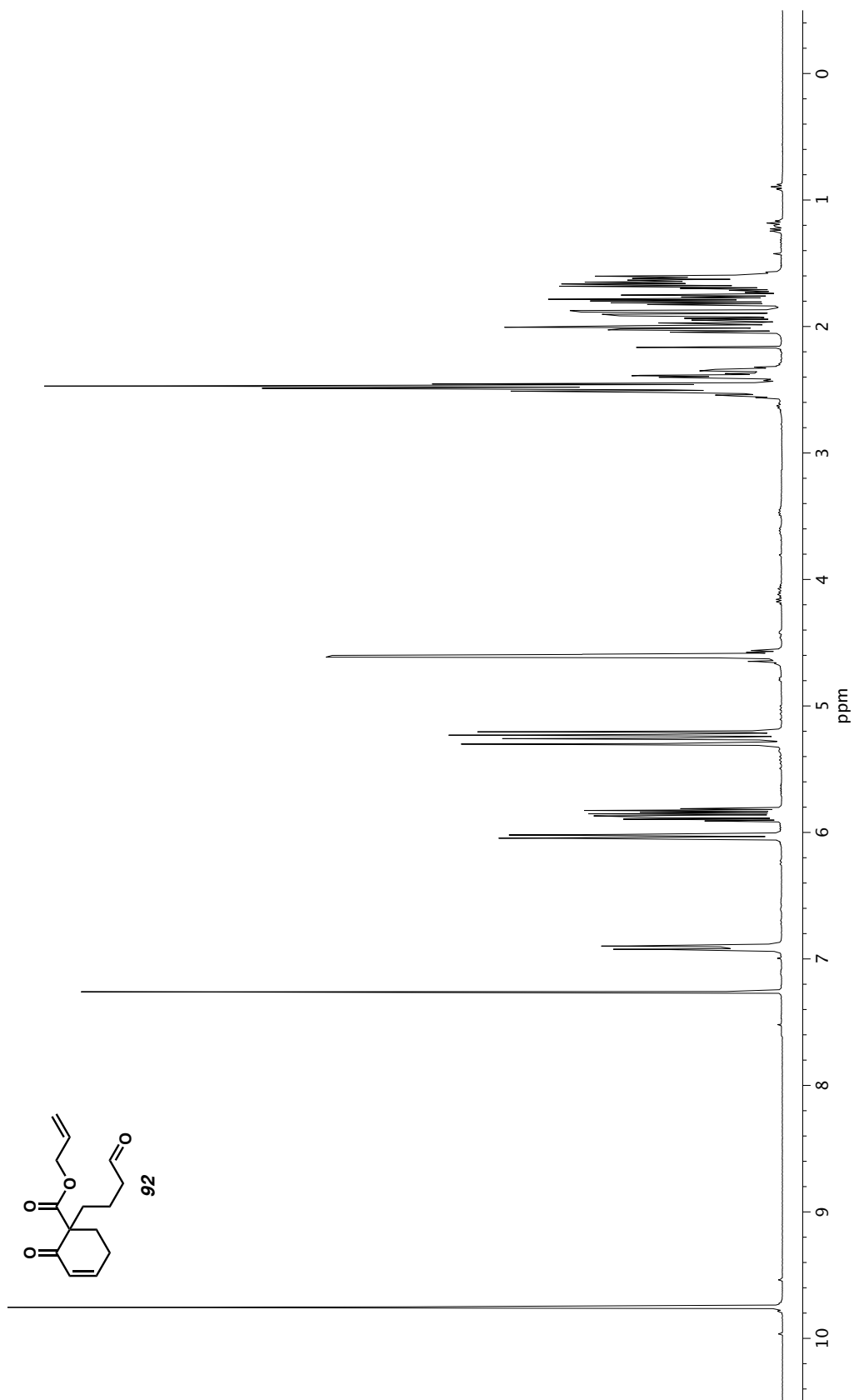
Figure A2.190. ^{1}H NMR (400 MHz, CDCl$_3$) of compound **92.**
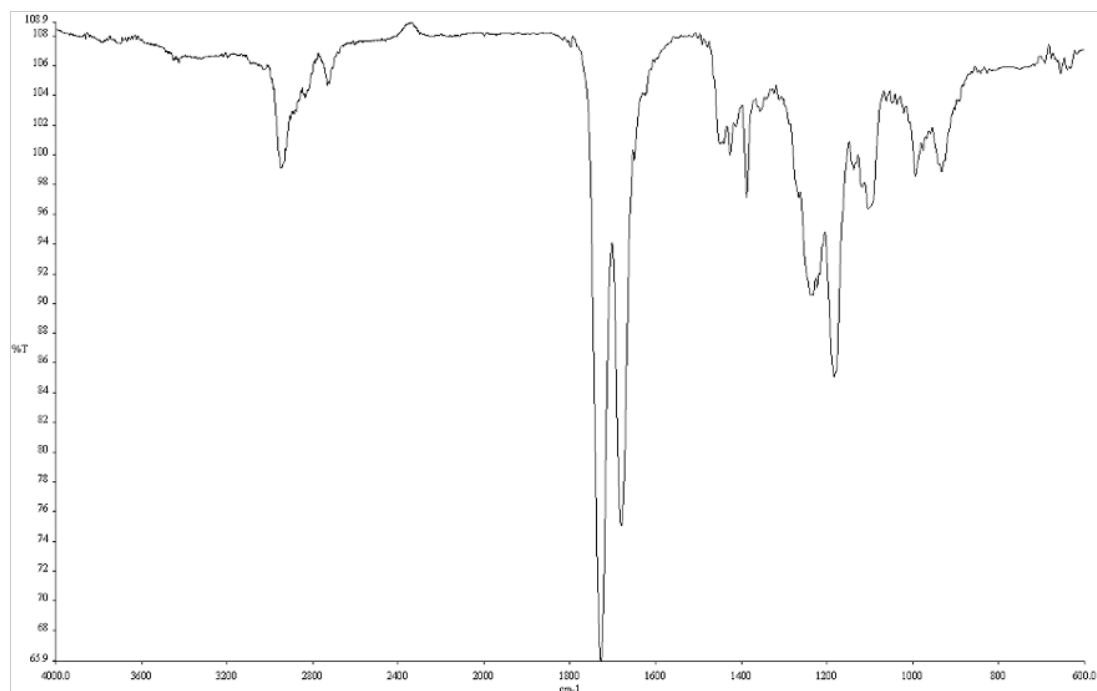
Figure A2.191. *Infrared spectrum (Thin Film, NaCl) of compound* **92**.
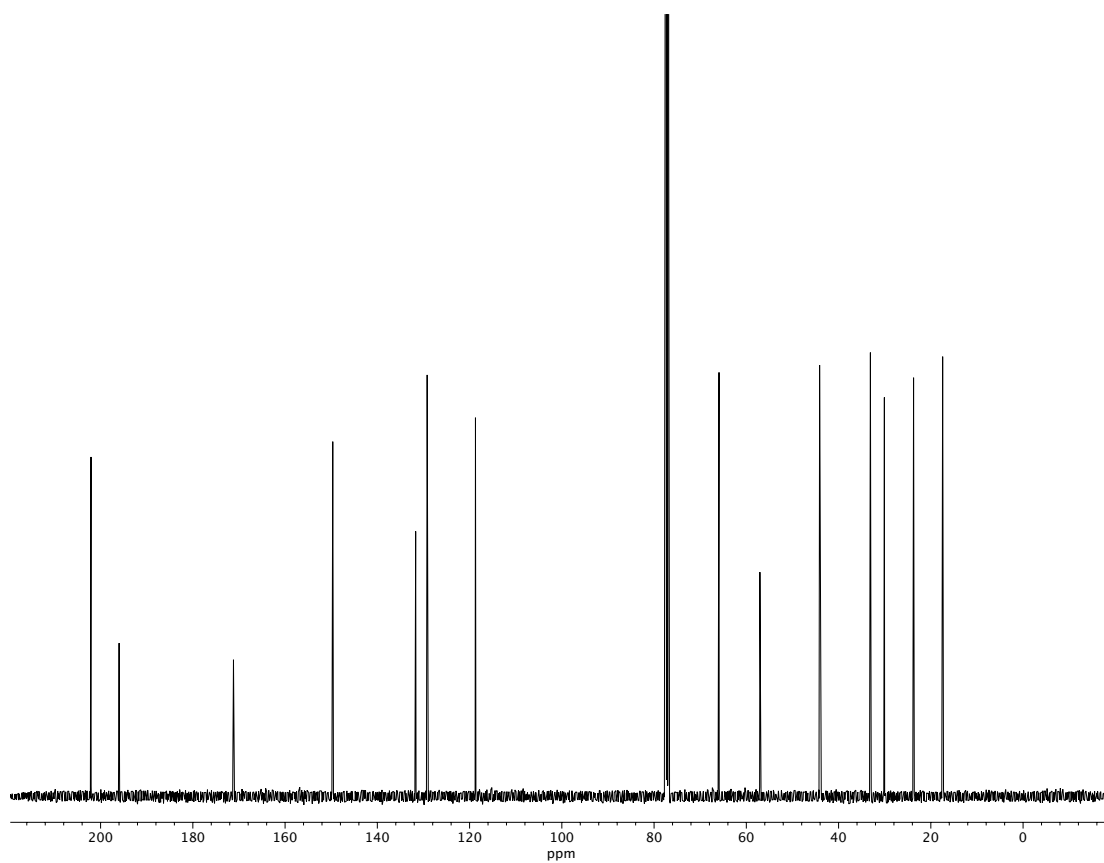
Figure A2.192. ^{13}C *NMR (100 MHz, CDCl₃) of compound* **92**.
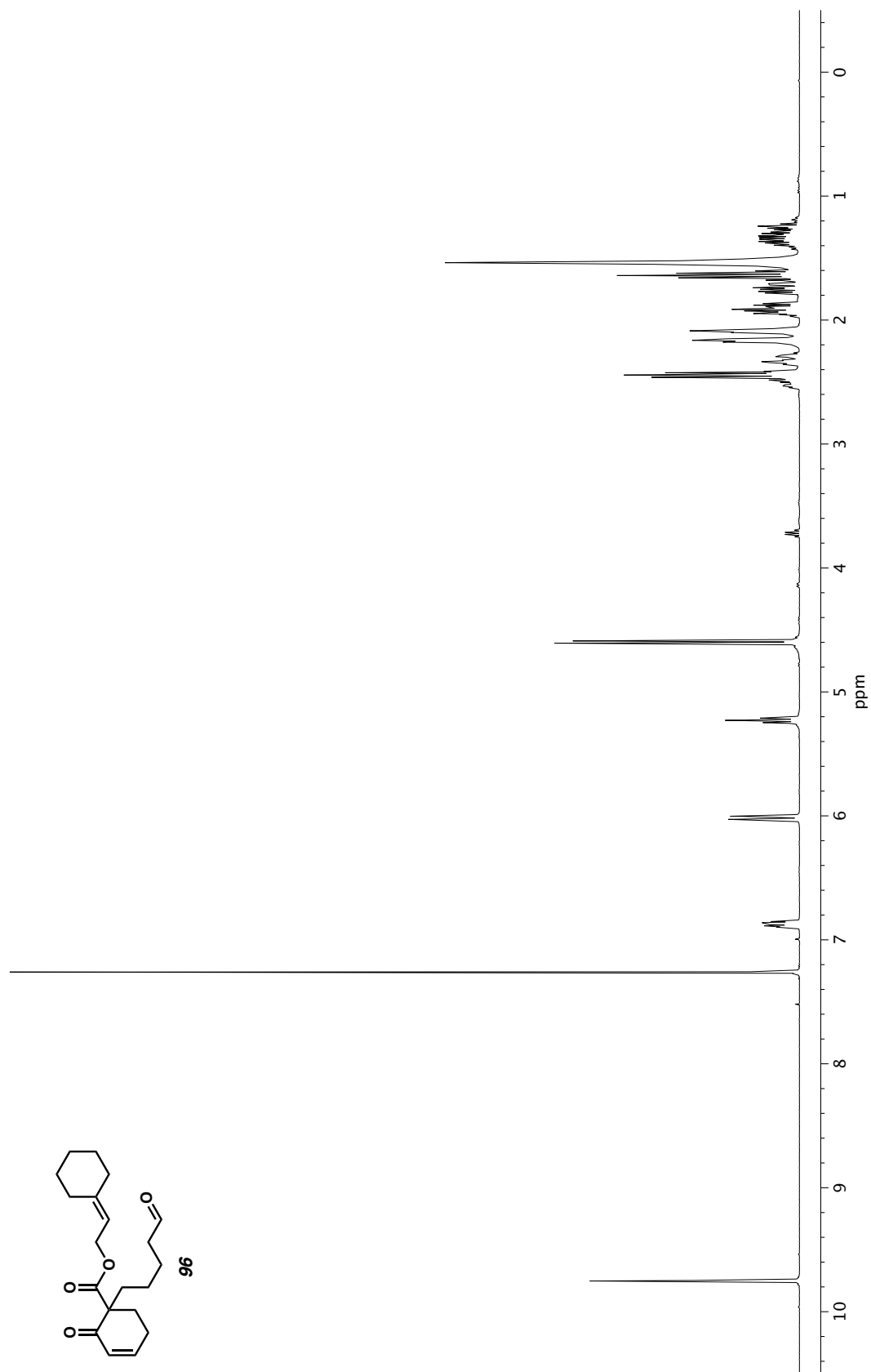
Figure A2.193. *^{1}H NMR (400 MHz, CDCl$_3$) of compound **96**.*
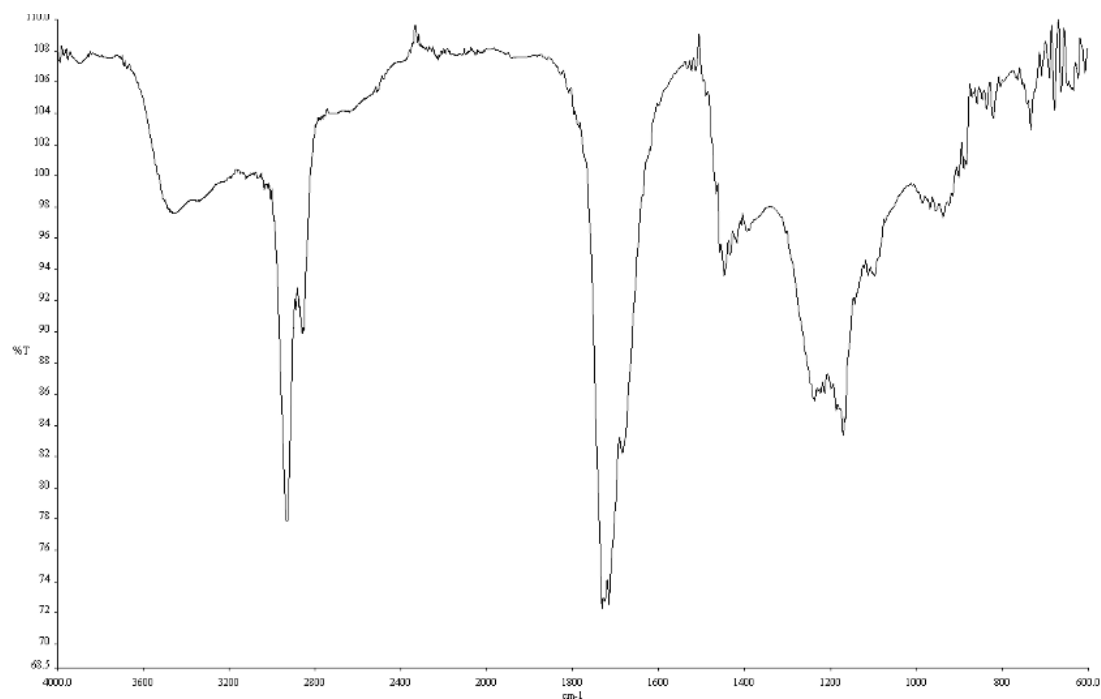
Figure A2.194. *Infrared spectrum (Thin Film, NaCl) of compound* **96**.
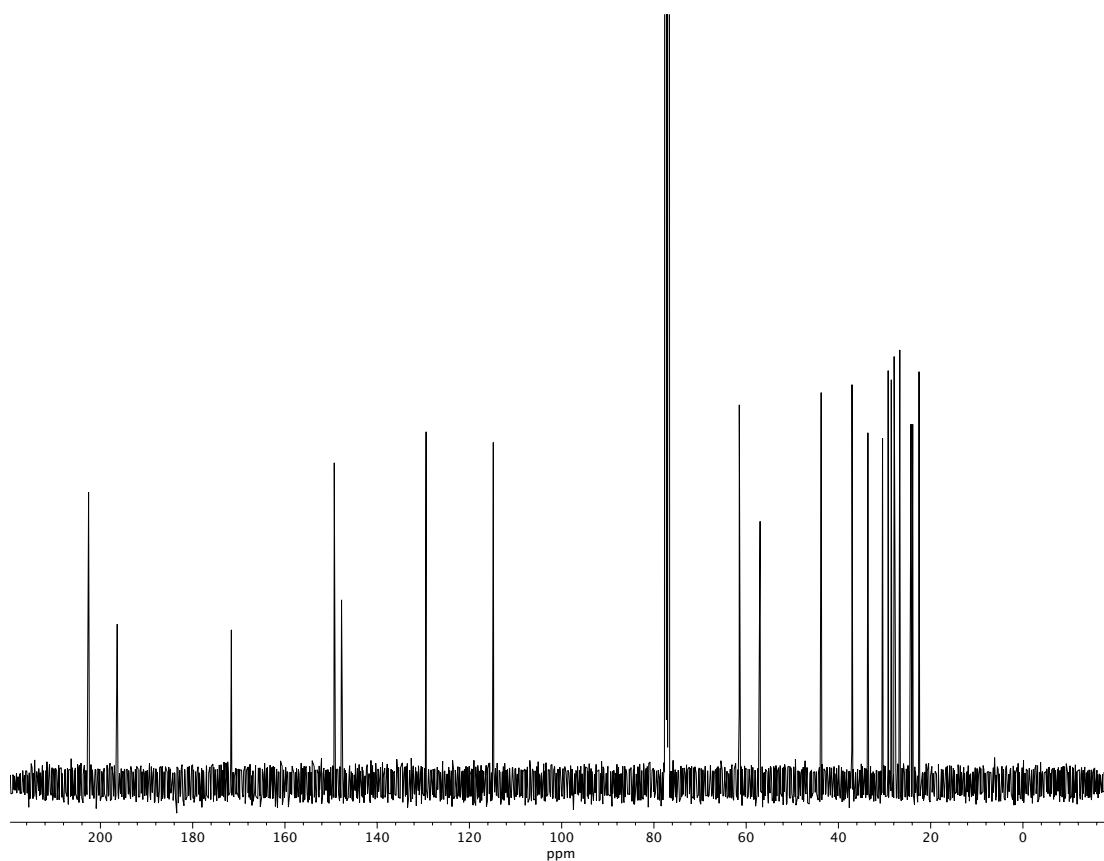
Figure A2.195. ^{13}C *NMR (100 MHz, CDCl$_3$) of compound* **96**.
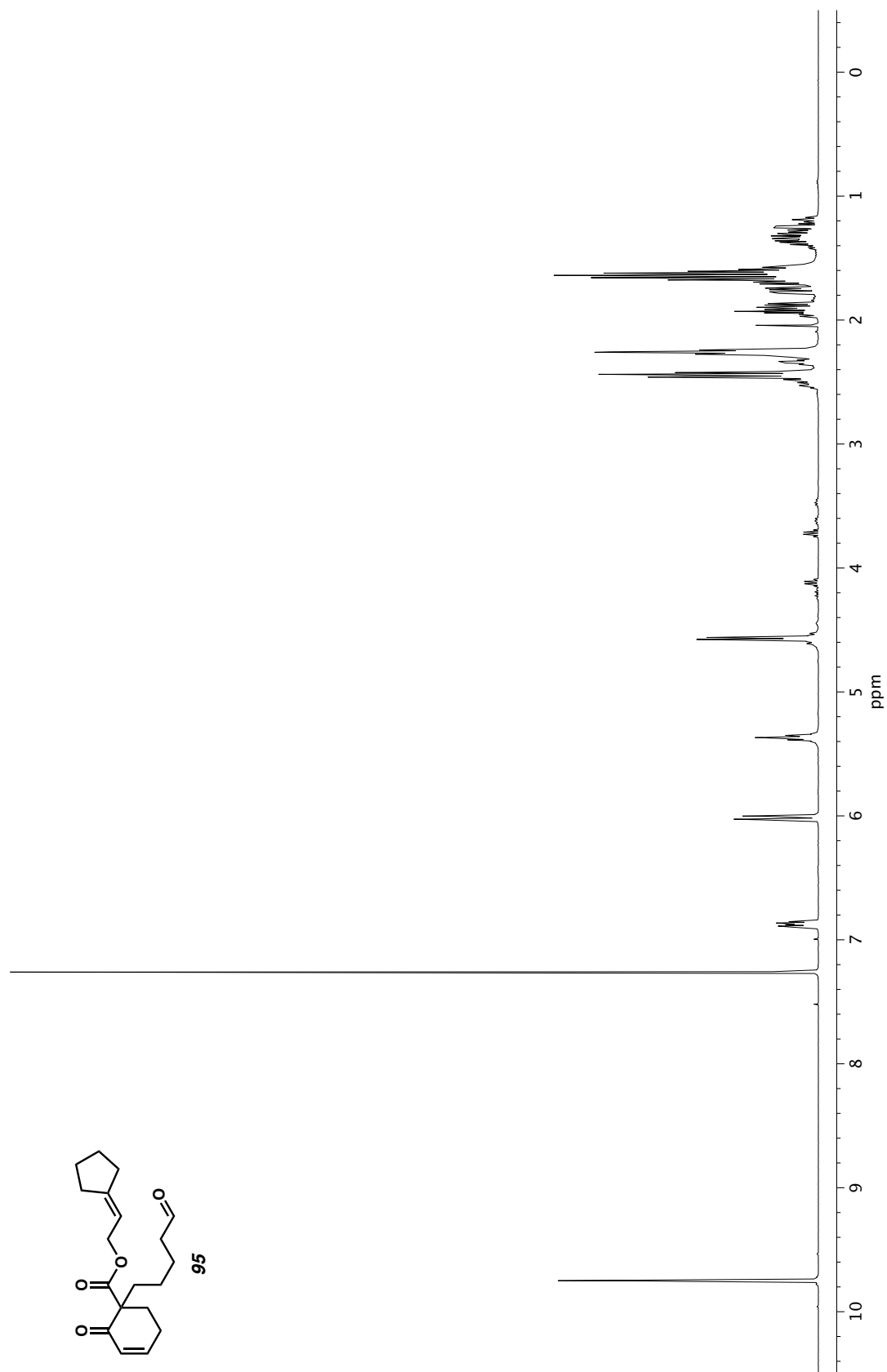
Figure A2.196. *^{1}H NMR (400 MHz, CDCl$_3$) of compound **95**.*
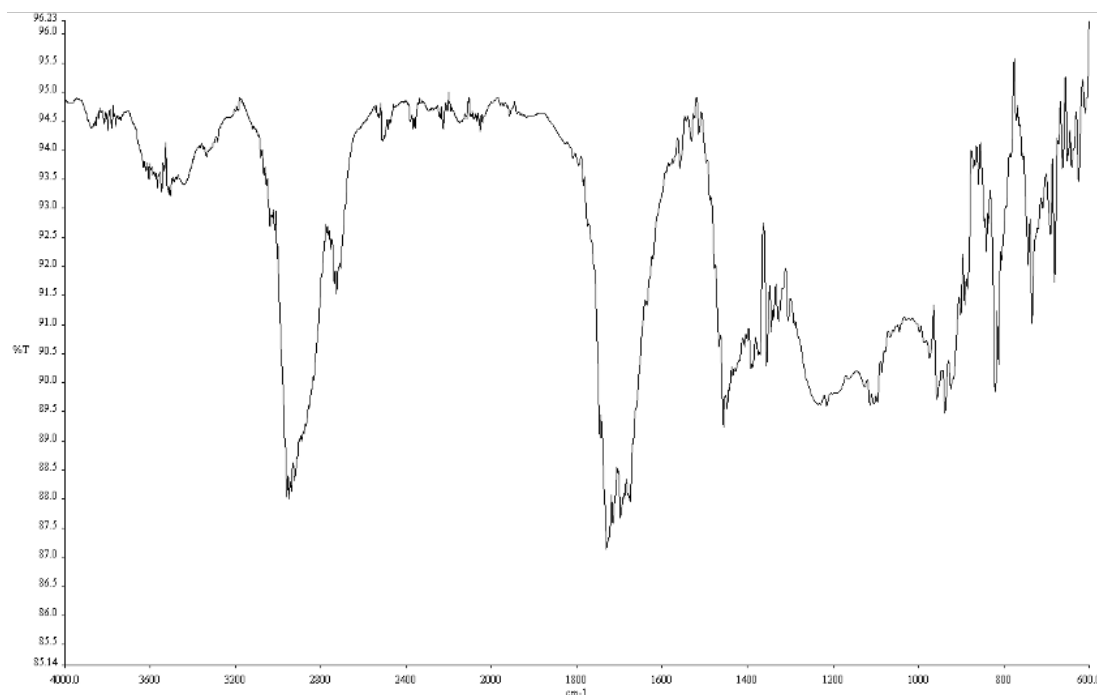
Figure A2.197. Infrared spectrum (Thin Film, NaCl) of compound **95**.
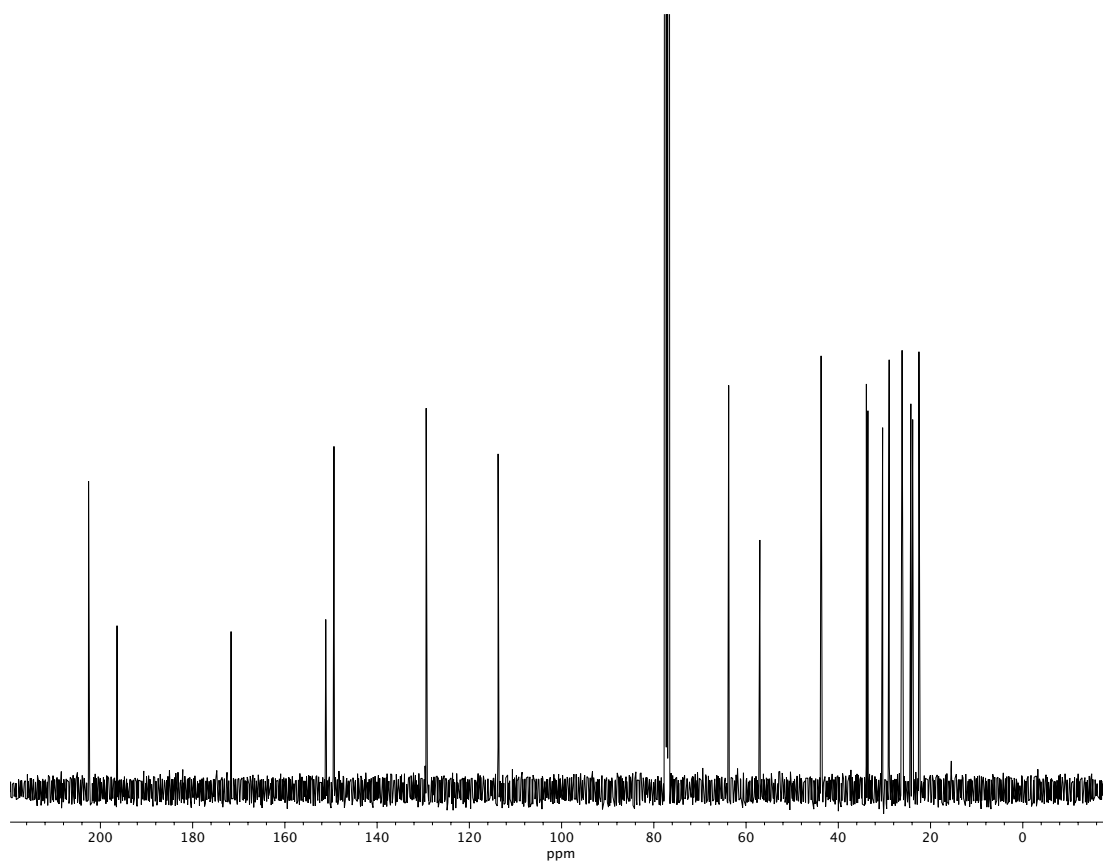
Figure A2.198. ^{13}C NMR (100 MHz, CDCl$_3$) of compound **95**.
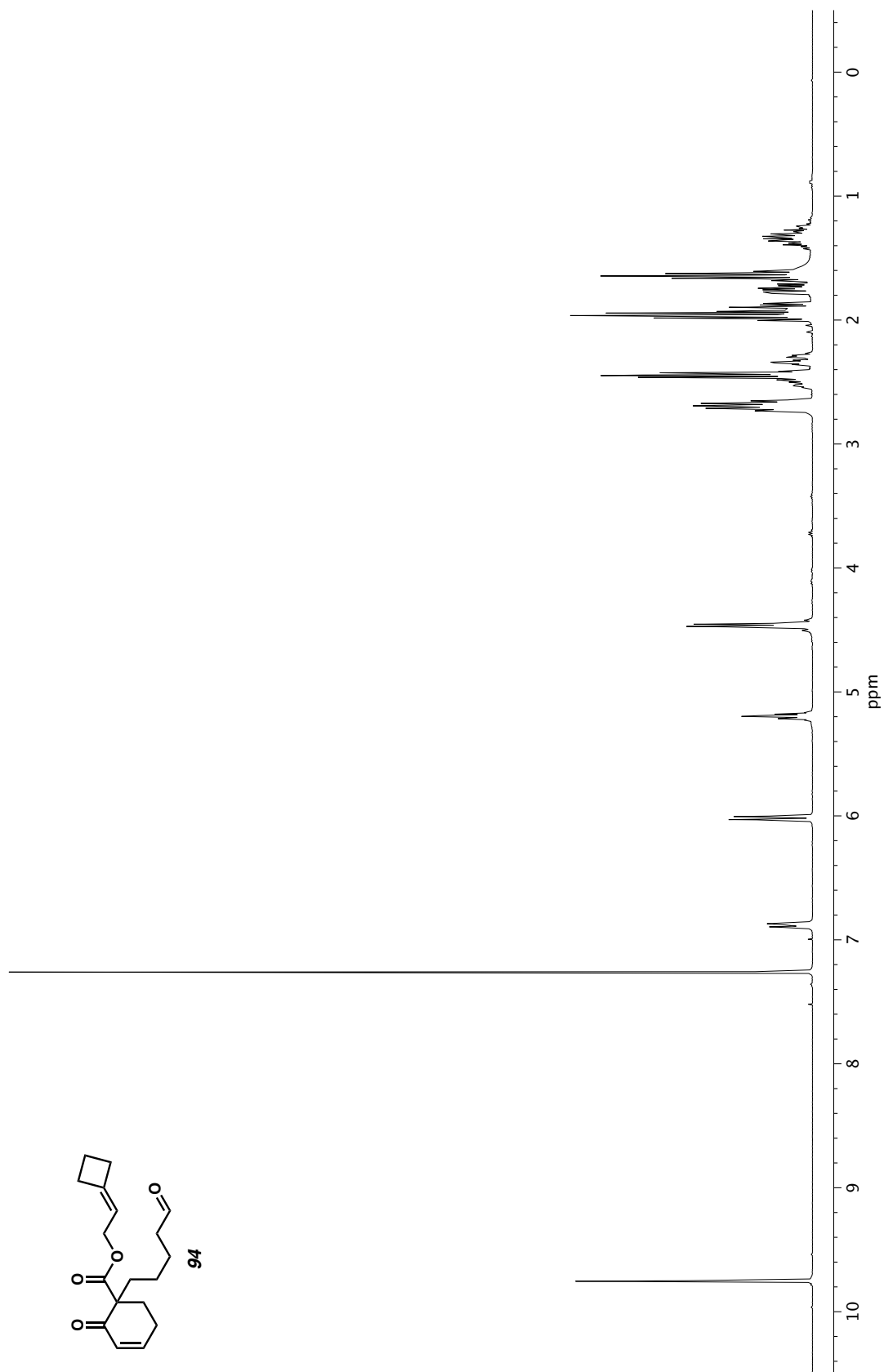
Figure A2.199. *^{1}H NMR (400 MHz, CDCl$_3$) of compound **94**.*
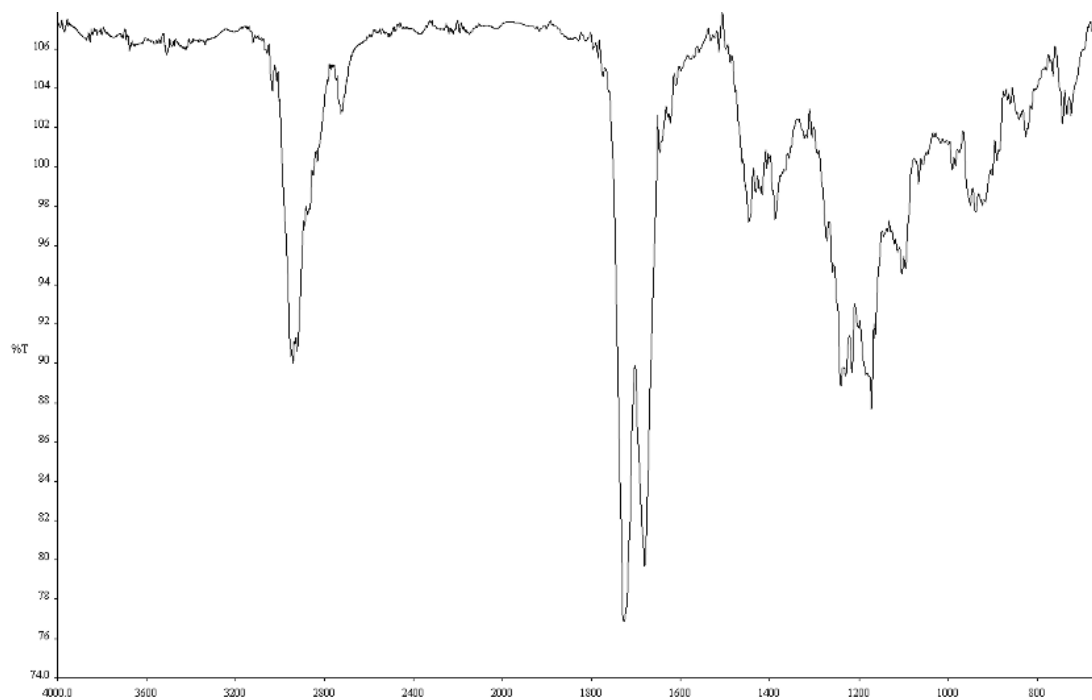
Figure A2.200. Infrared spectrum (Thin Film, NaCl) of compound **94**.
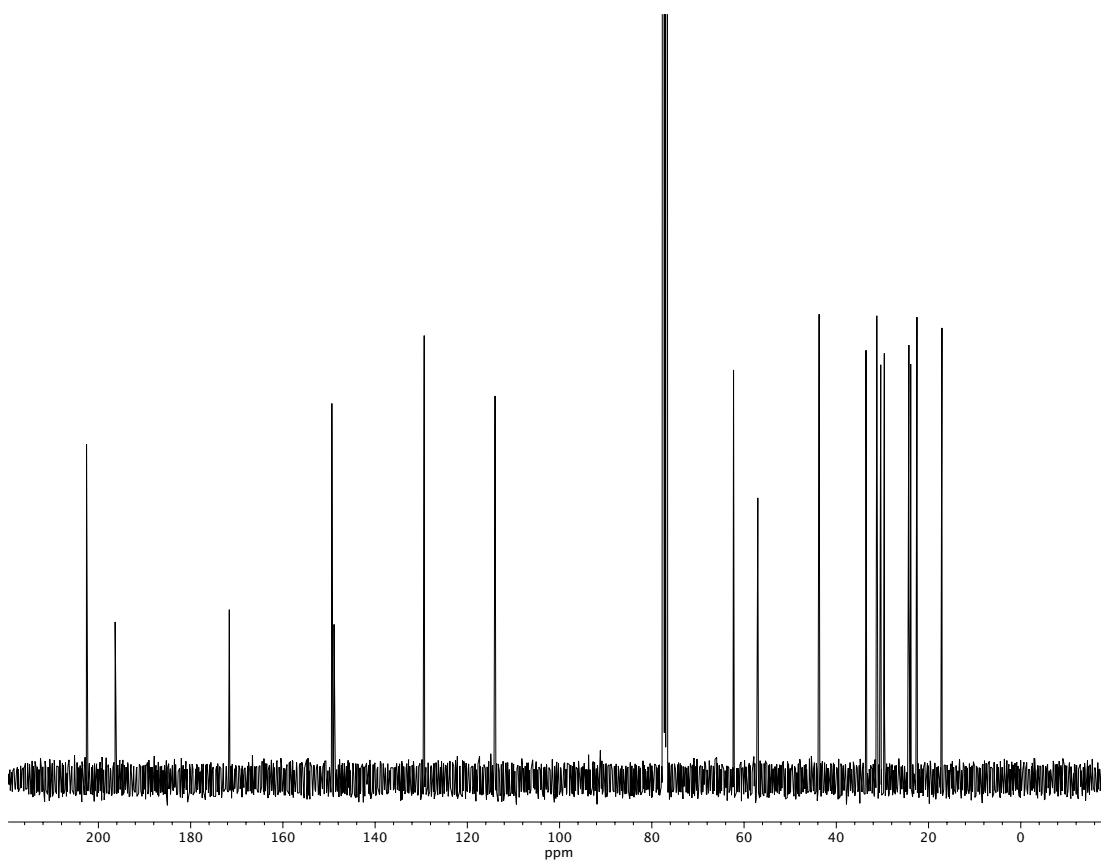
Figure A2.201. ^{13}C NMR (100 MHz, CDCl$_3$) of compound **94**.
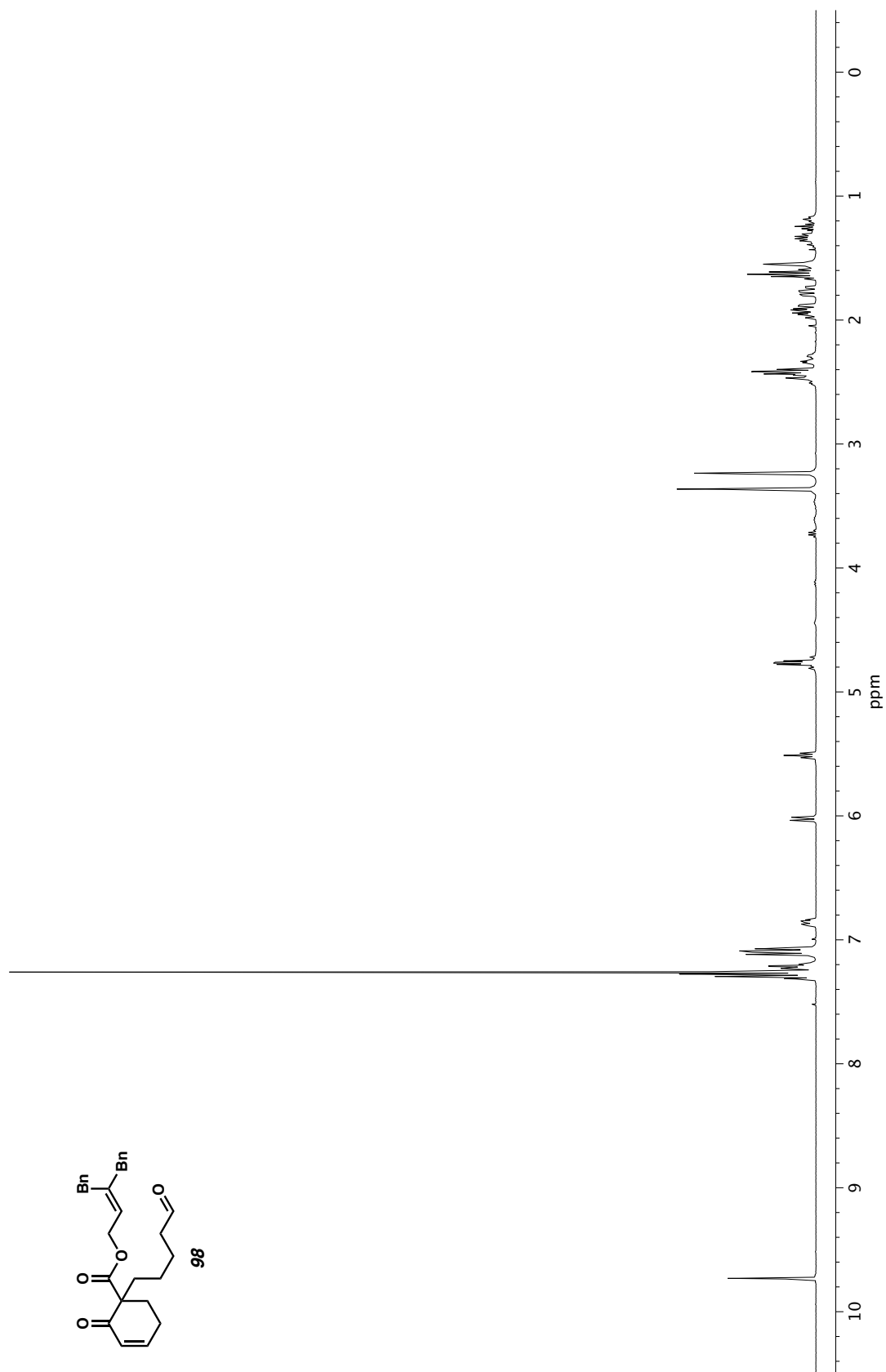
Figure A2.202. *¹H NMR (400 MHz, CDCl₃) of compound **98**.*
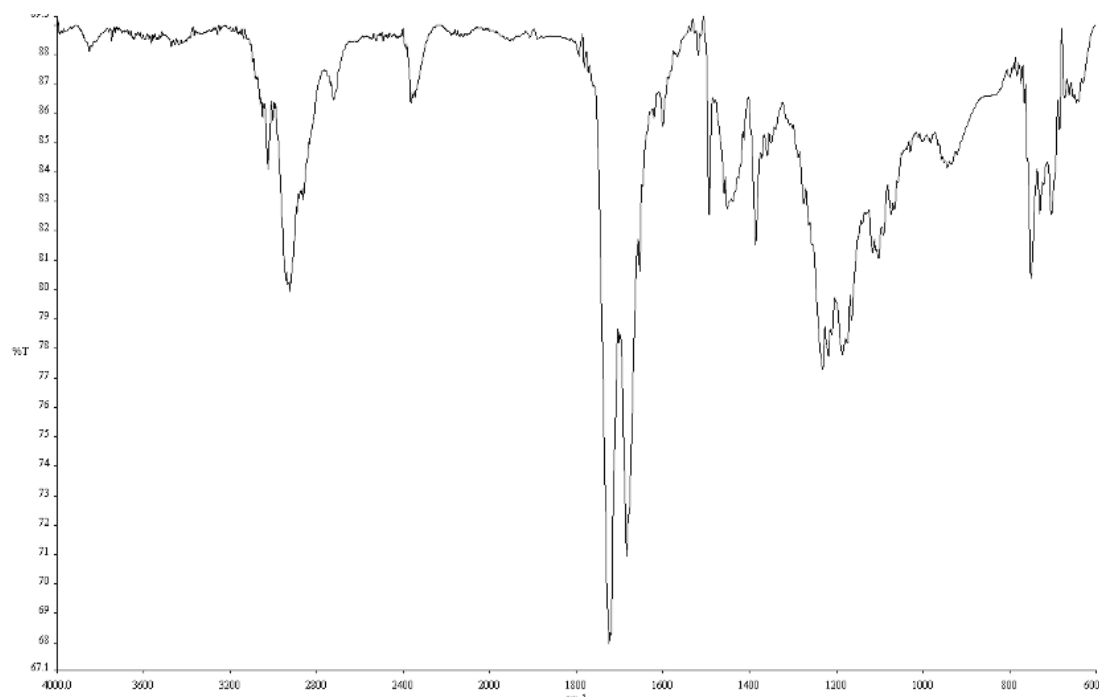
Figure A2.203. *Infrared spectrum (Thin Film, NaCl) of compound **98**.*
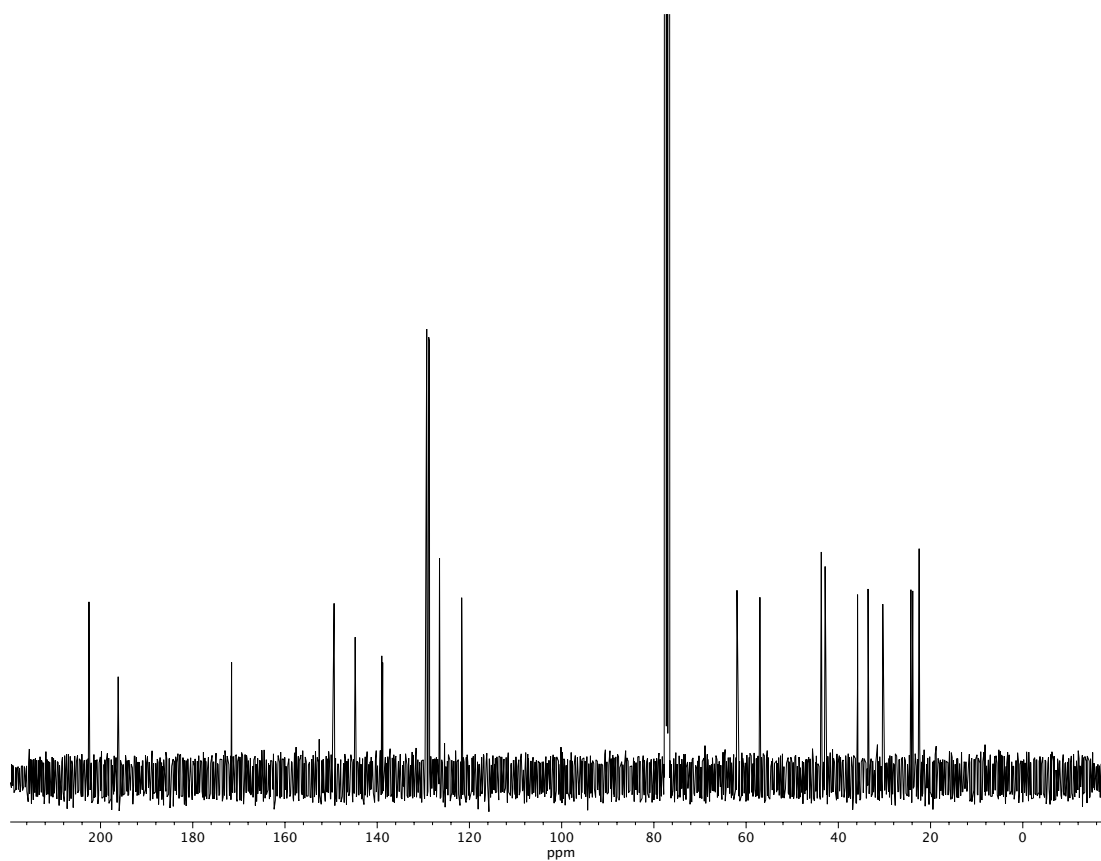
Figure A2.204. *^{13}C NMR (100 MHz, CDCl$_3$) of compound **98**.*

Figure A2.205. ^1H NMR (400 MHz, CDCl$_3$) of compound **97**.
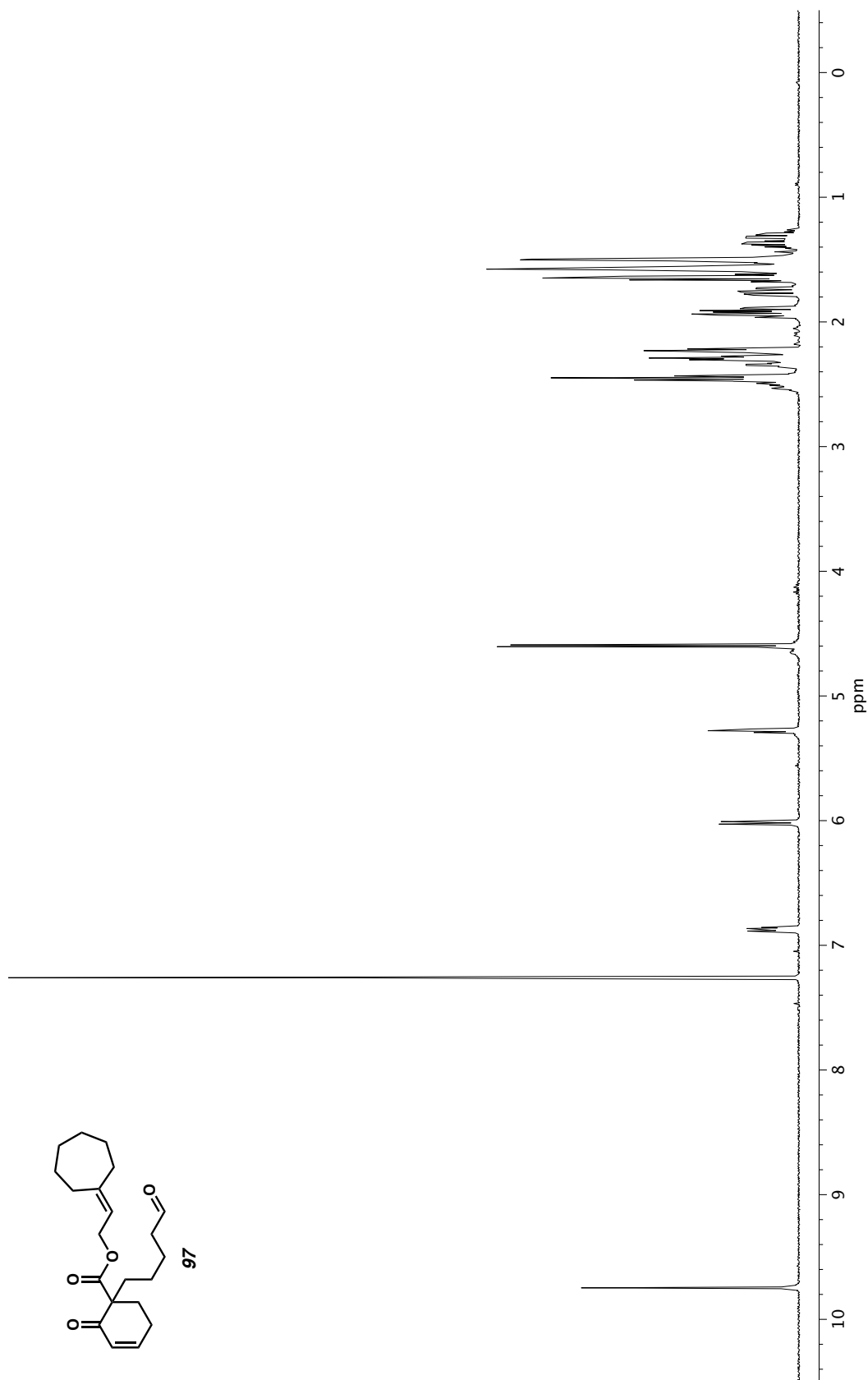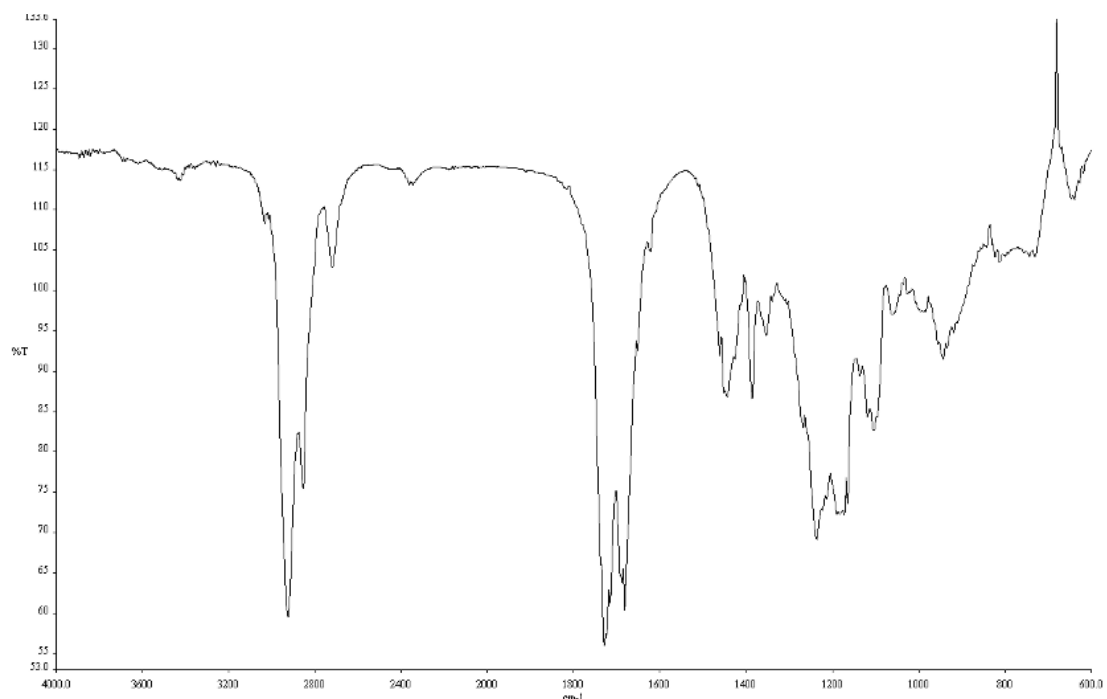
Figure A2.206. *Infrared spectrum (Thin Film, NaCl) of compound* **97**.
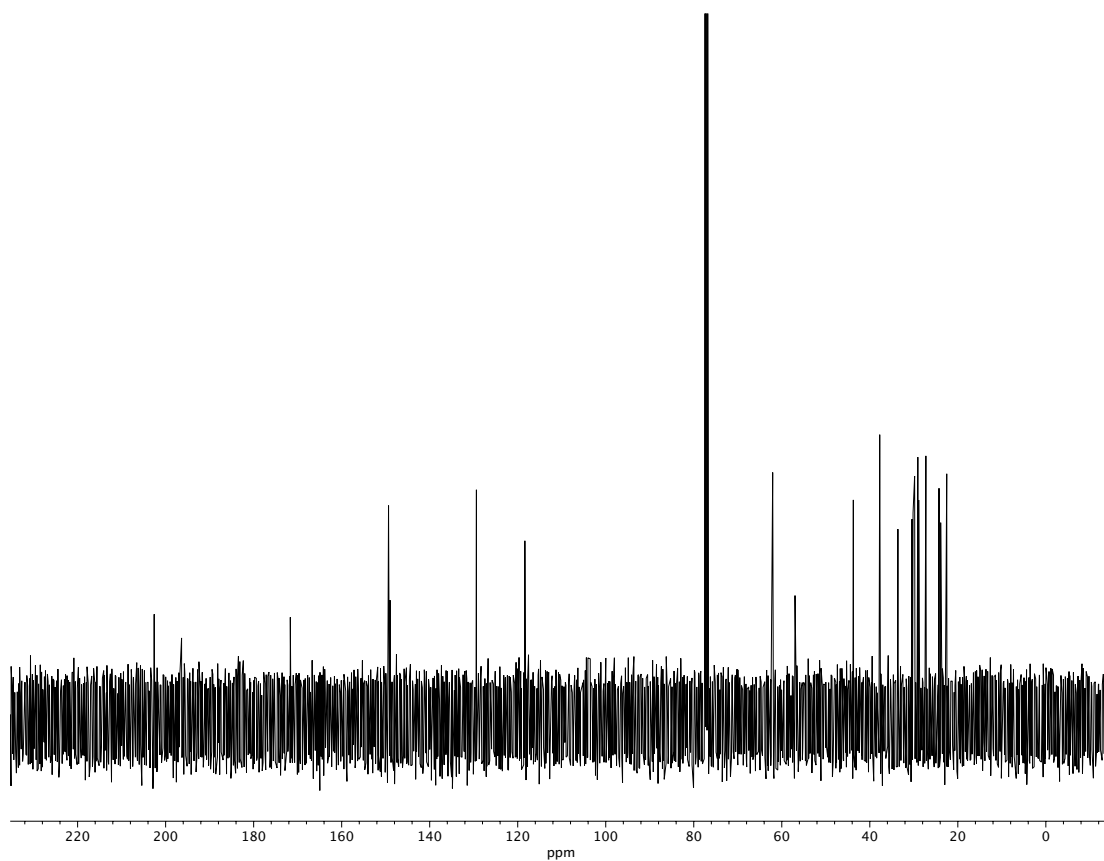
Figure A2.207. *^{13}C NMR (100 MHz, CDCl$_3$) of compound* **97**.
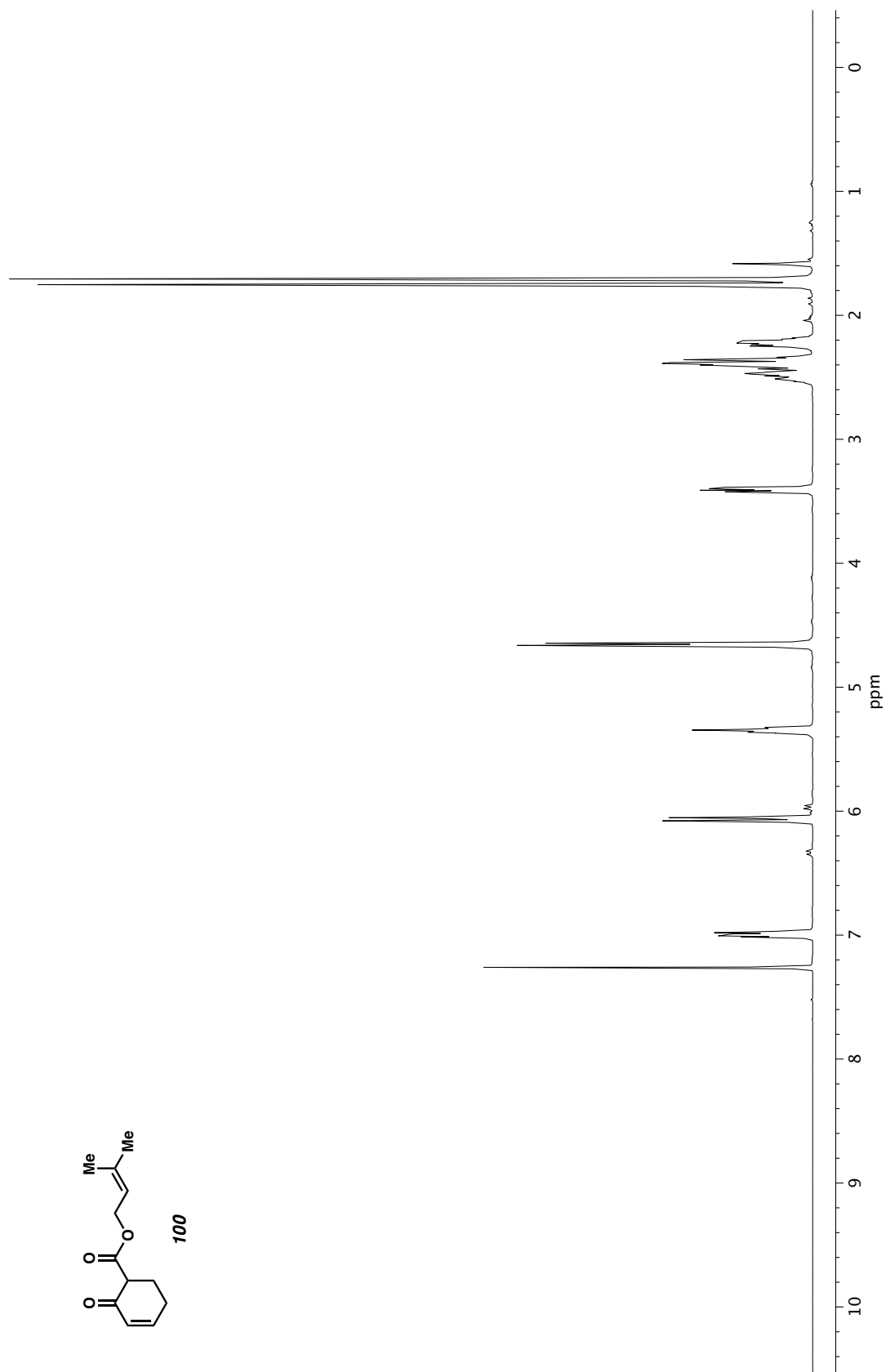
Figure A2.208. ^1H NMR (400 MHz, CDCl$_3$) of compound **100**.
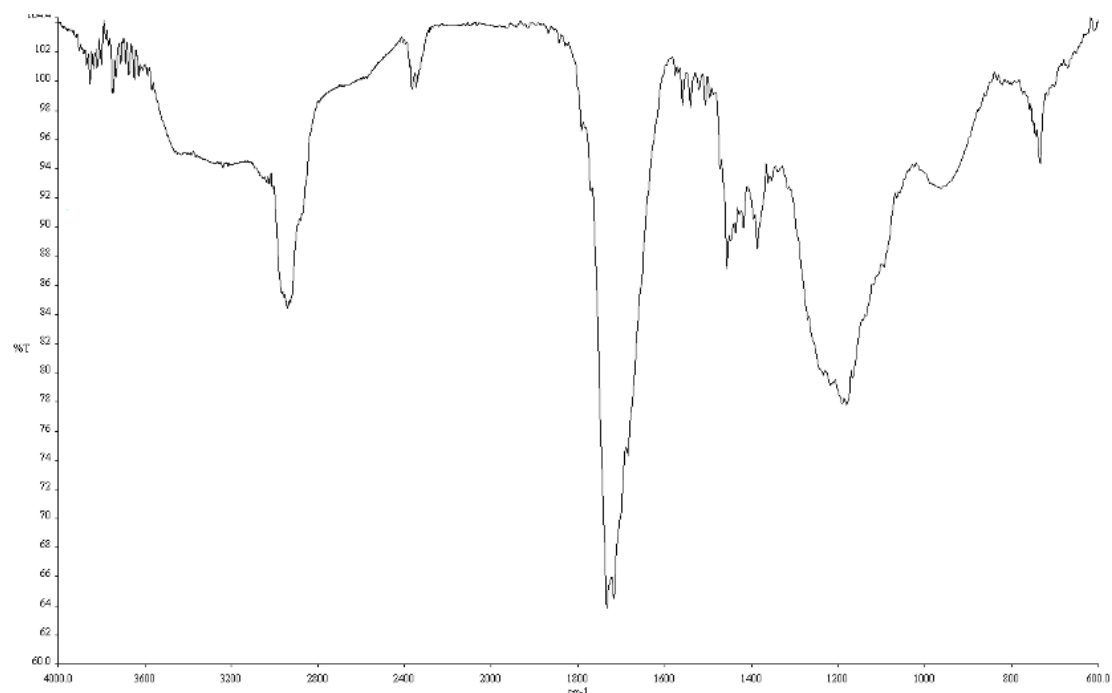
Figure A2.209. *Infrared spectrum (Thin Film, NaCl) of compound* **100**.
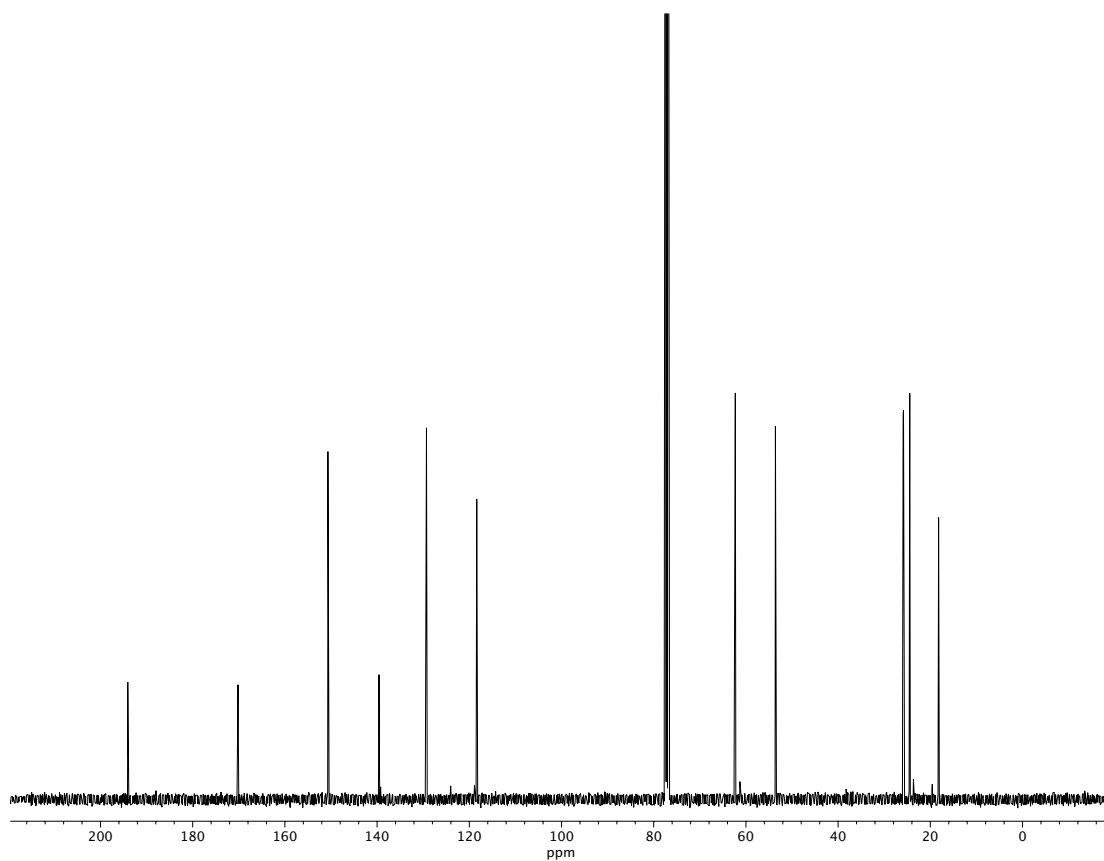
Figure A2.210. ^{13}C *NMR (100 MHz, CDCl$_3$) of compound* **100**.
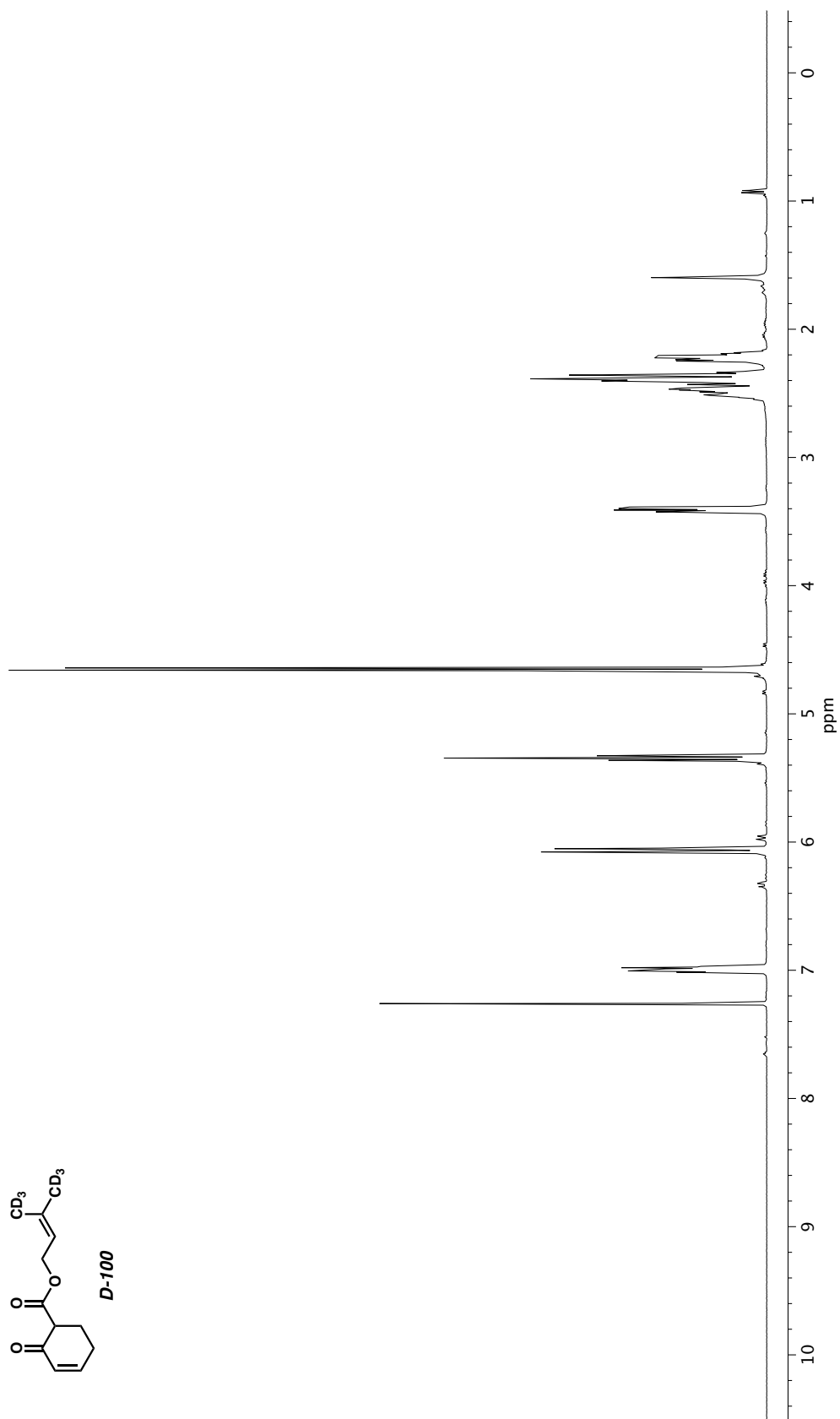
Figure A2.211. ^1H NMR (400 MHz, CDCl$_3$) of compound **D-100**.
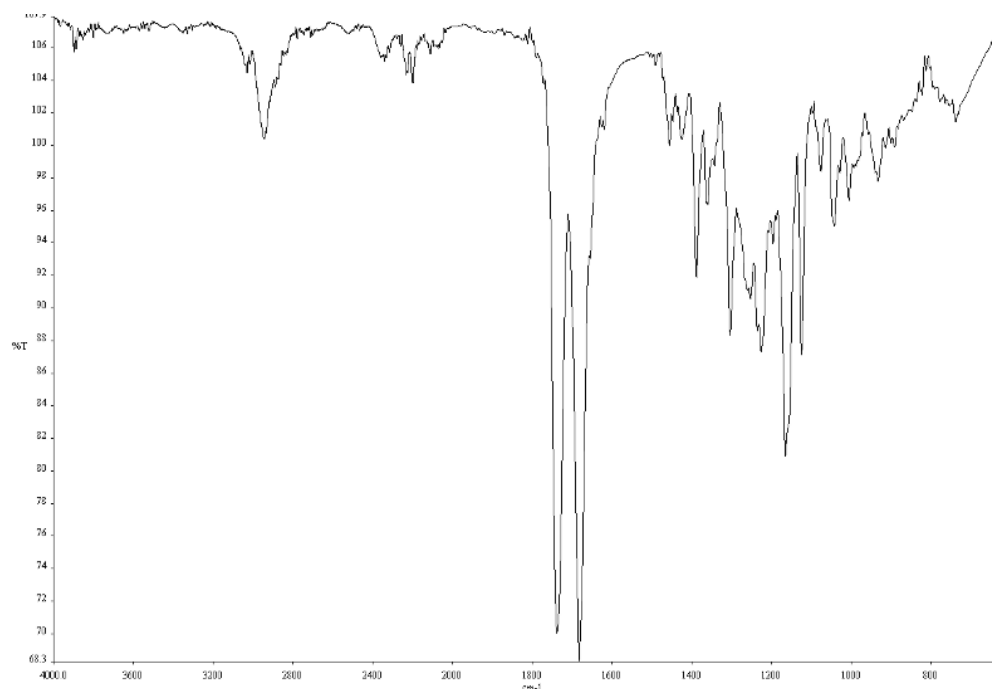
Figure A2.212. *Infrared spectrum (Thin Film, NaCl) of compound **D-100***.
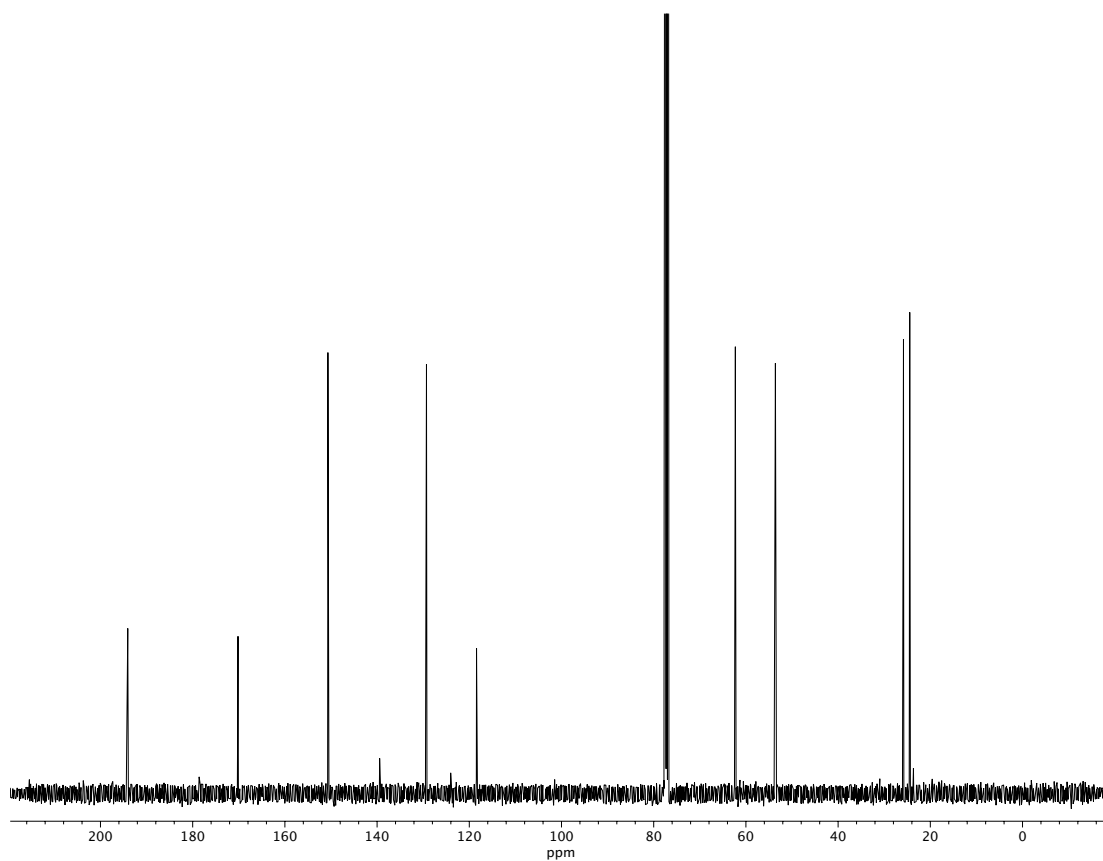
Figure A2.213. ^{13}C *NMR (100 MHz, CDCl$_3$) of compound **D-100***.
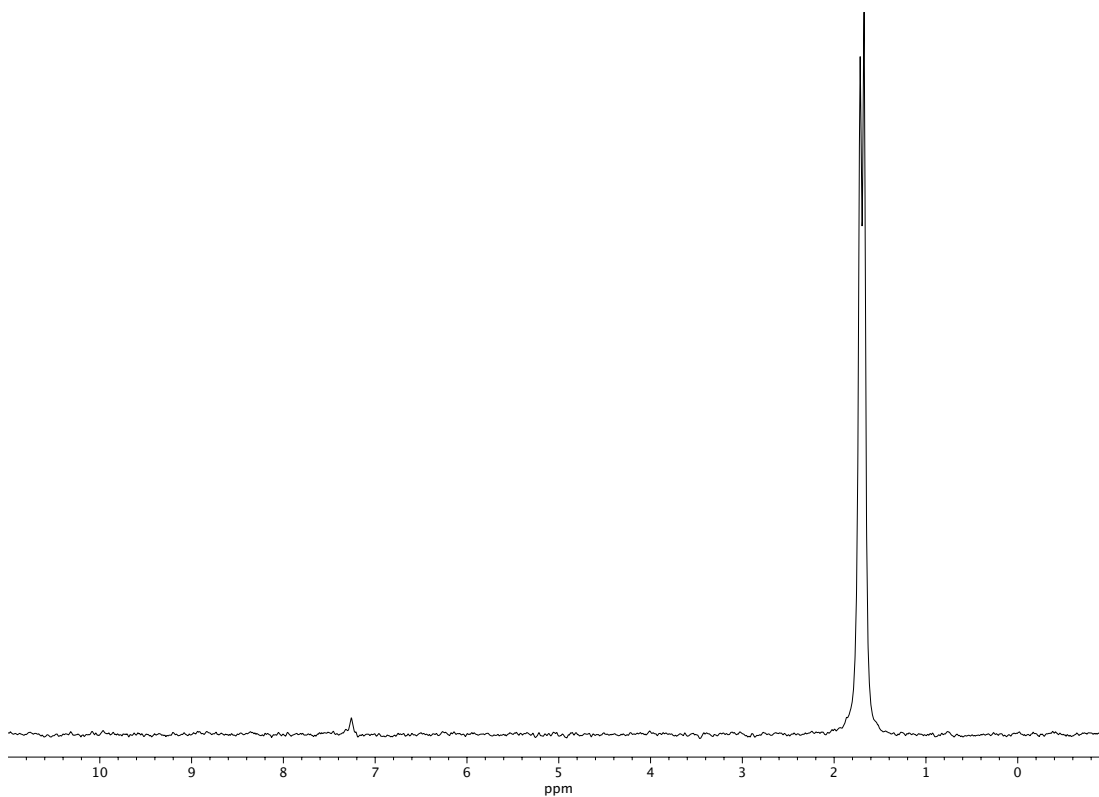
Figure A2.214. ^{2}H NMR (61 MHz, CHCl$_3$) of compound **D-100**.
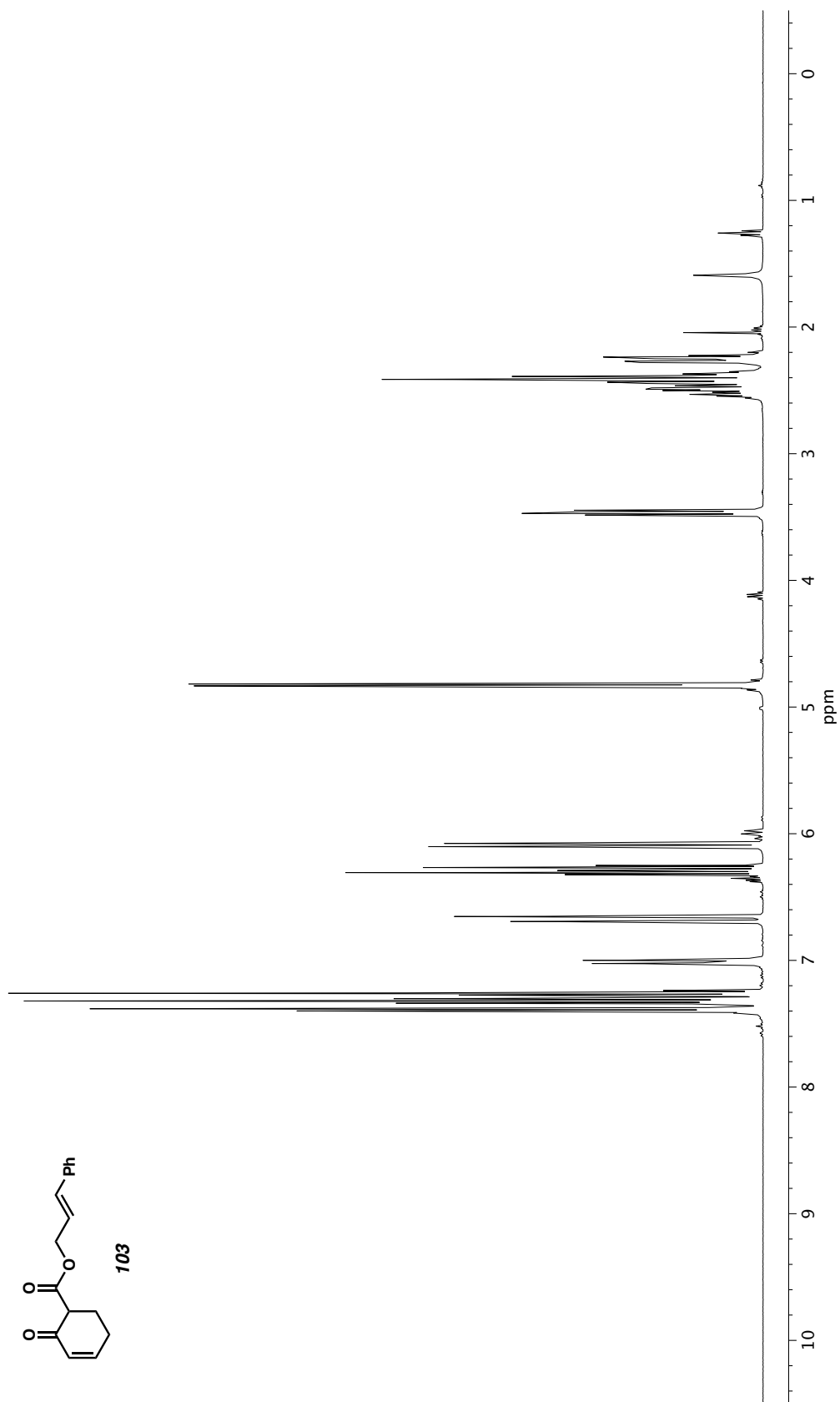
Figure A2.215. ^1H NMR (400 MHz, CDCl$_3$) of compound **103**.
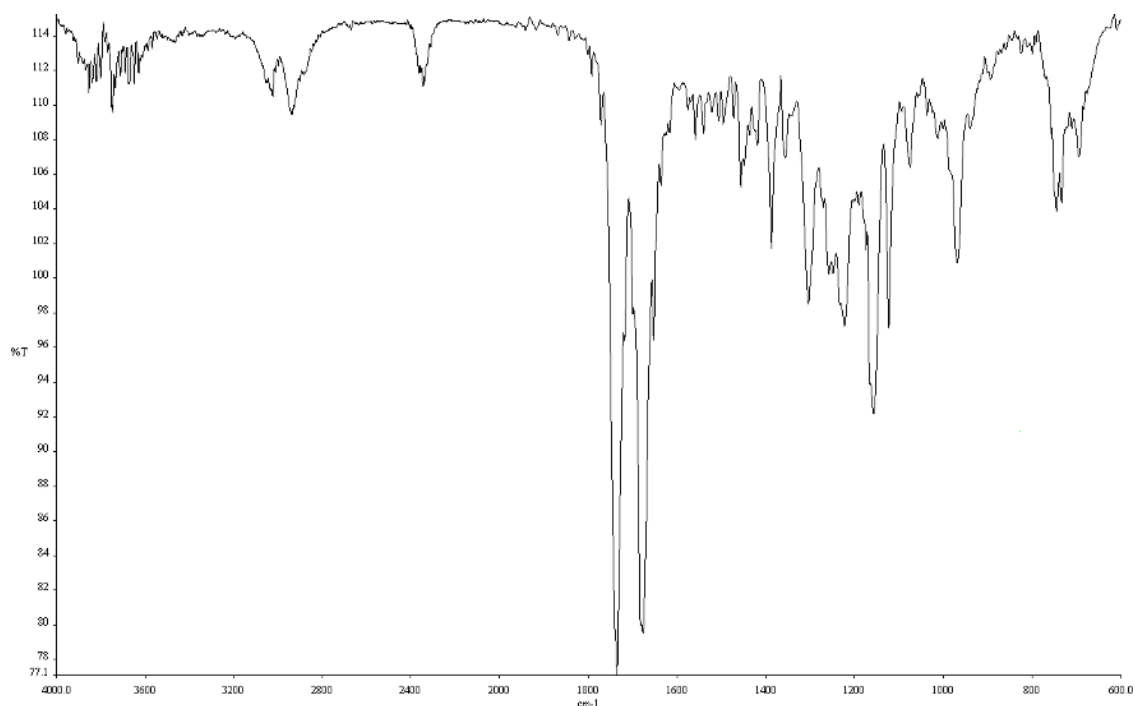
Figure A2.216. *Infrared spectrum (Thin Film, NaCl) of compound* **103**.
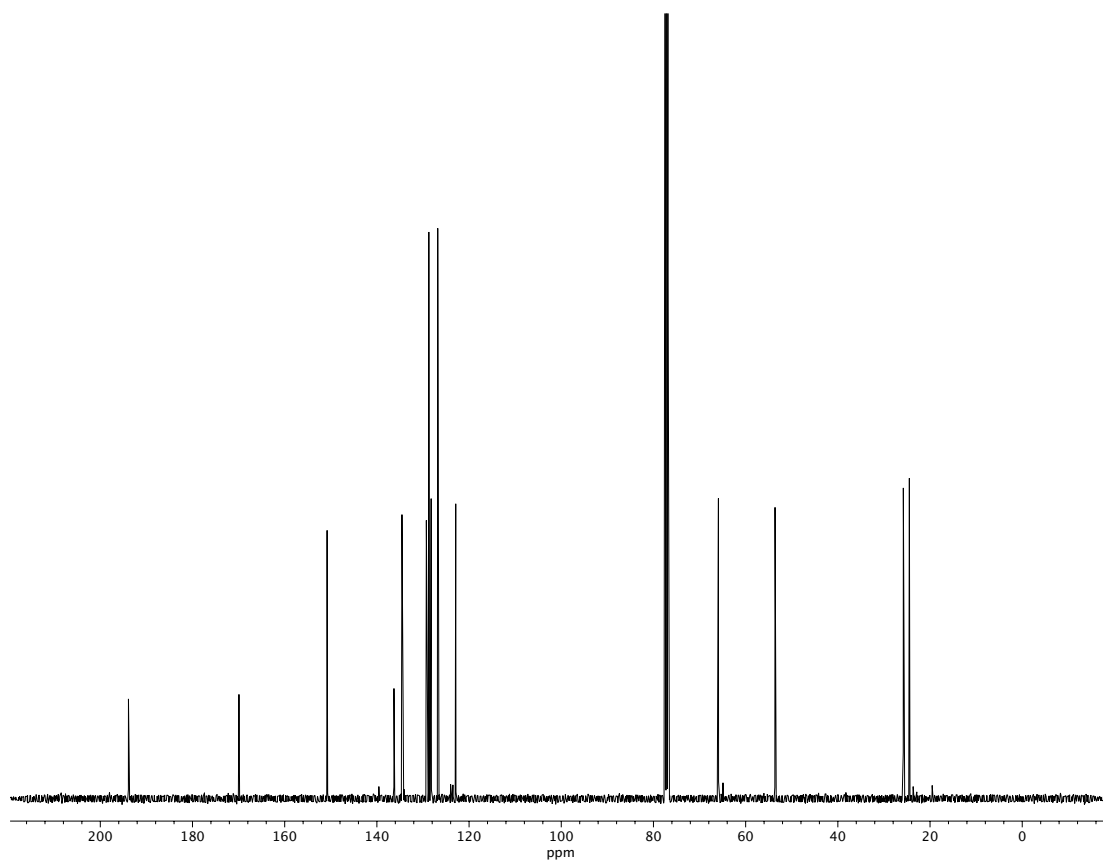
Figure A2.217. ^{13}C *NMR (100 MHz, CDCl$_3$) of compound* **103**.
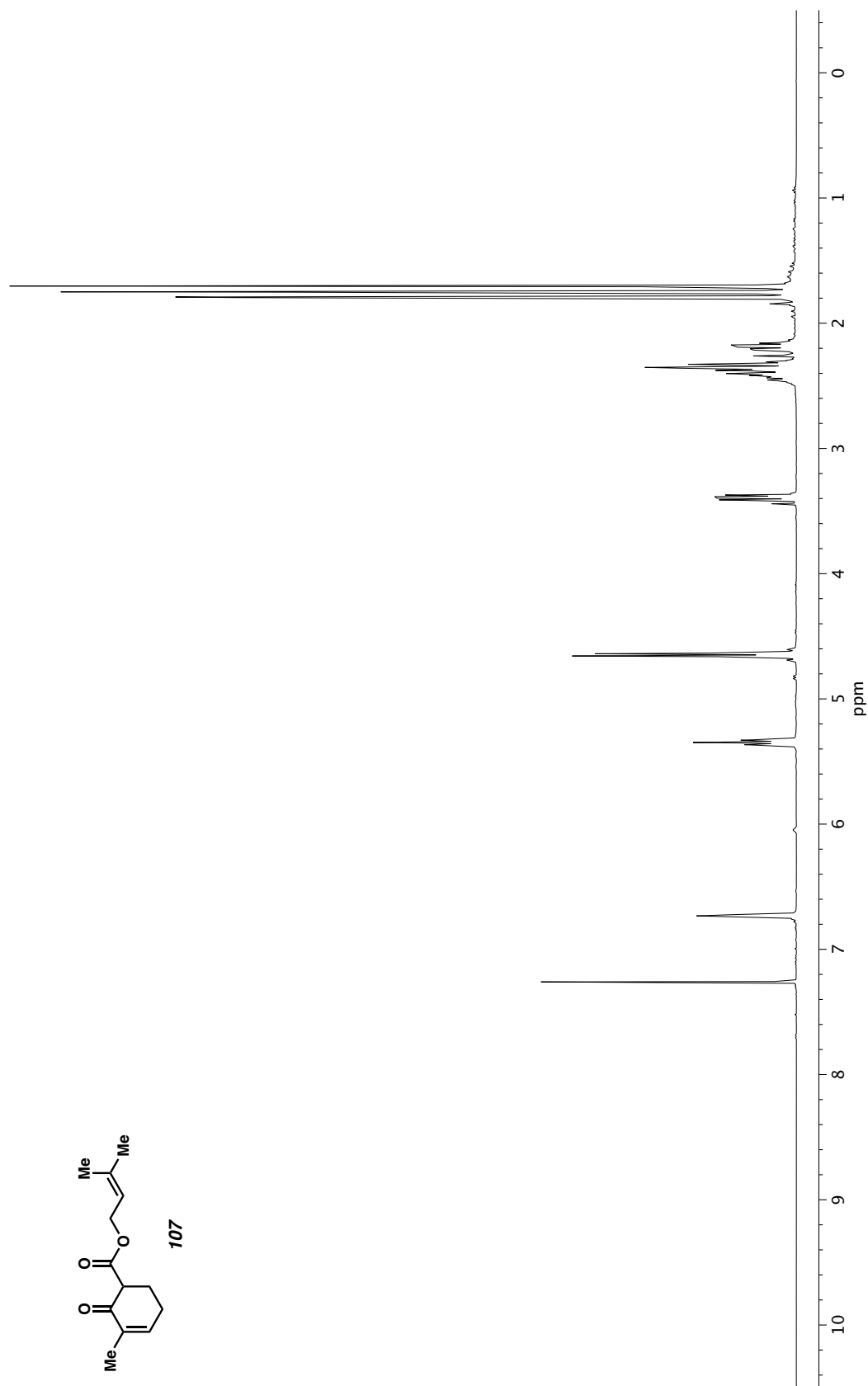
Figure A2.218. ^1H NMR (400 MHz, CDCl$_3$) of compound **107**.
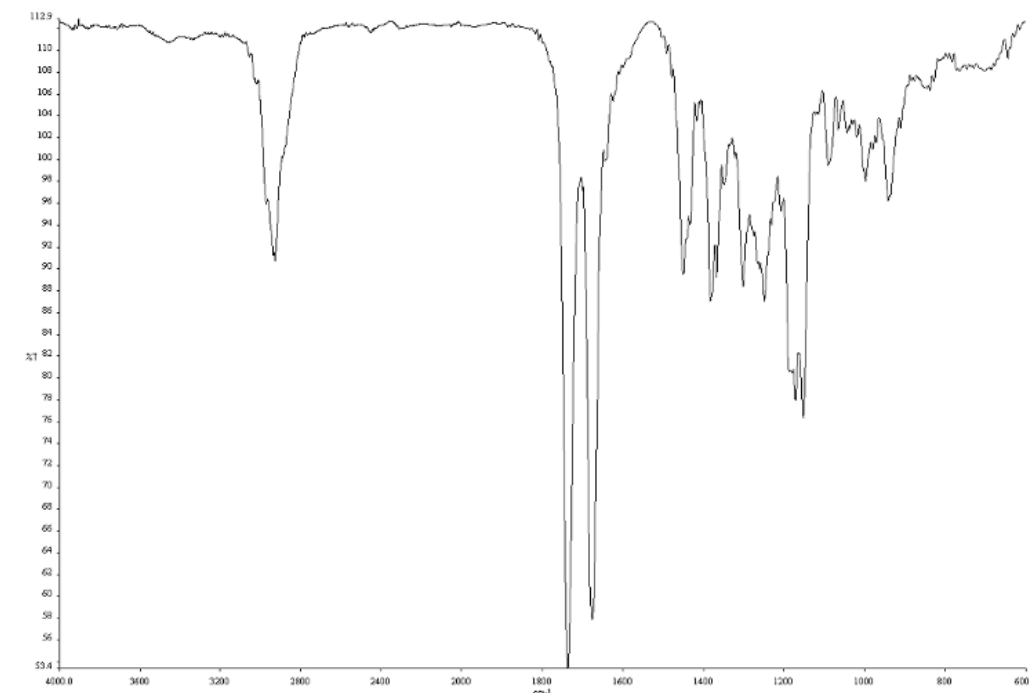
Figure A2.219. *Infrared spectrum (Thin Film, NaCl) of compound* **107**.
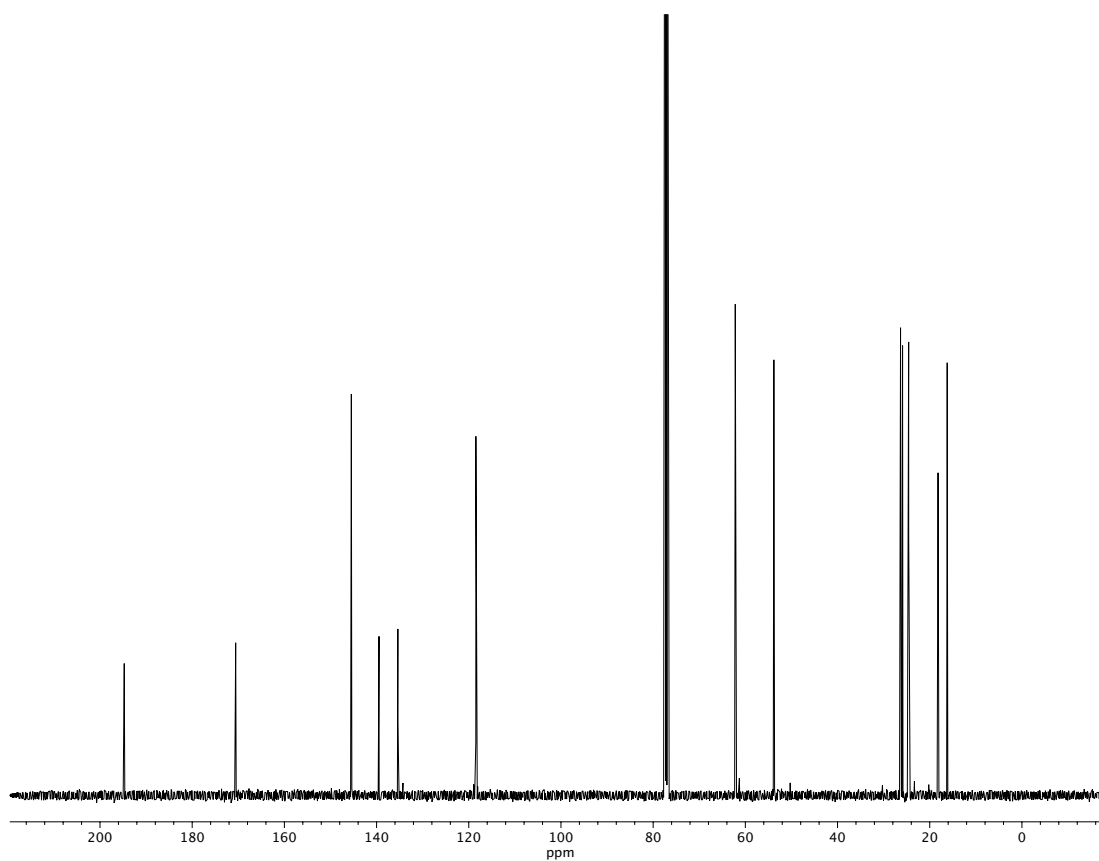
Figure A2.220. *^{13}C NMR (100 MHz, CDCl$_3$) of compound* **107**.
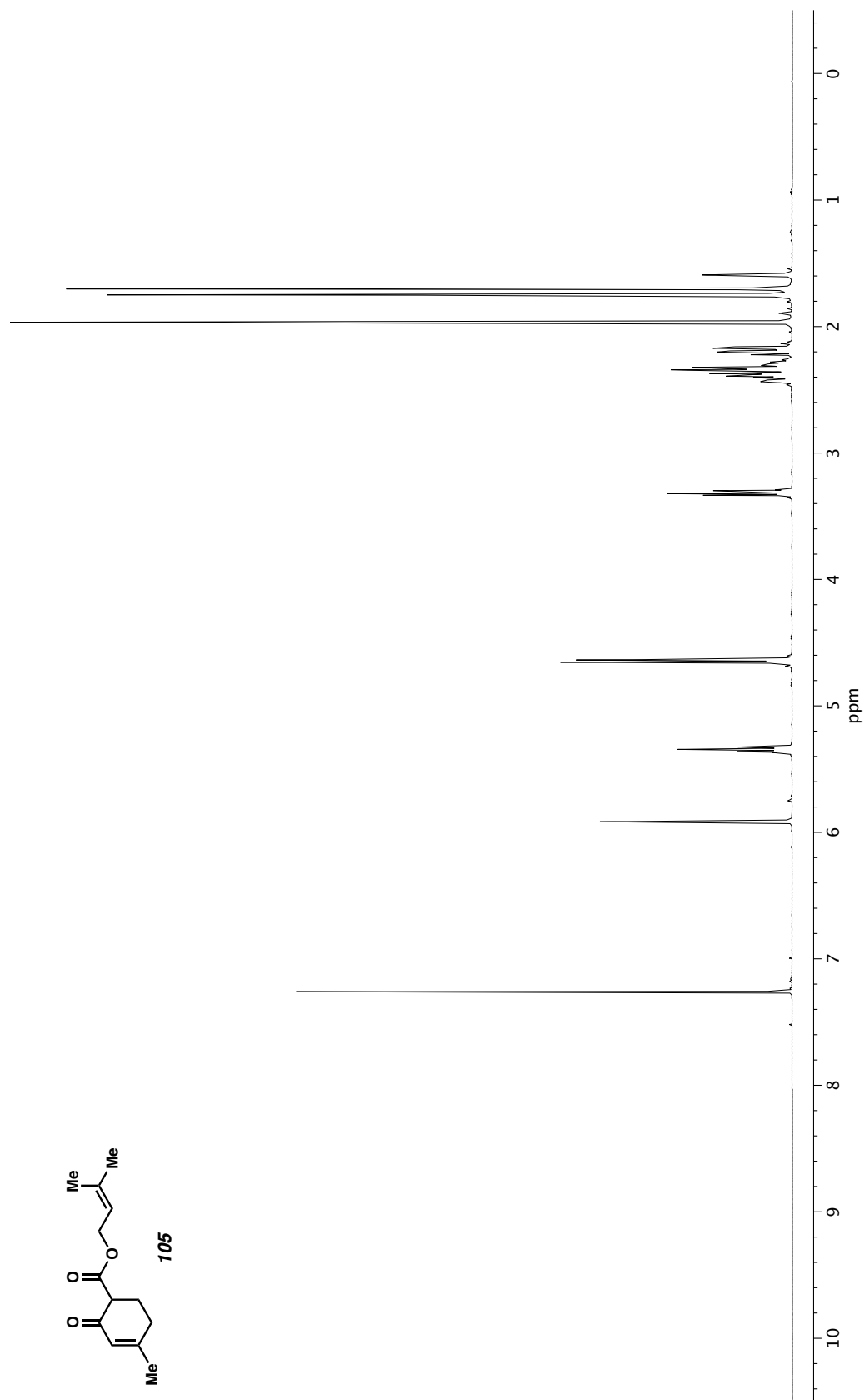
Figure A2.221. *^{1}H NMR (400 MHz, CDCl$_3$) of compound **105**.*
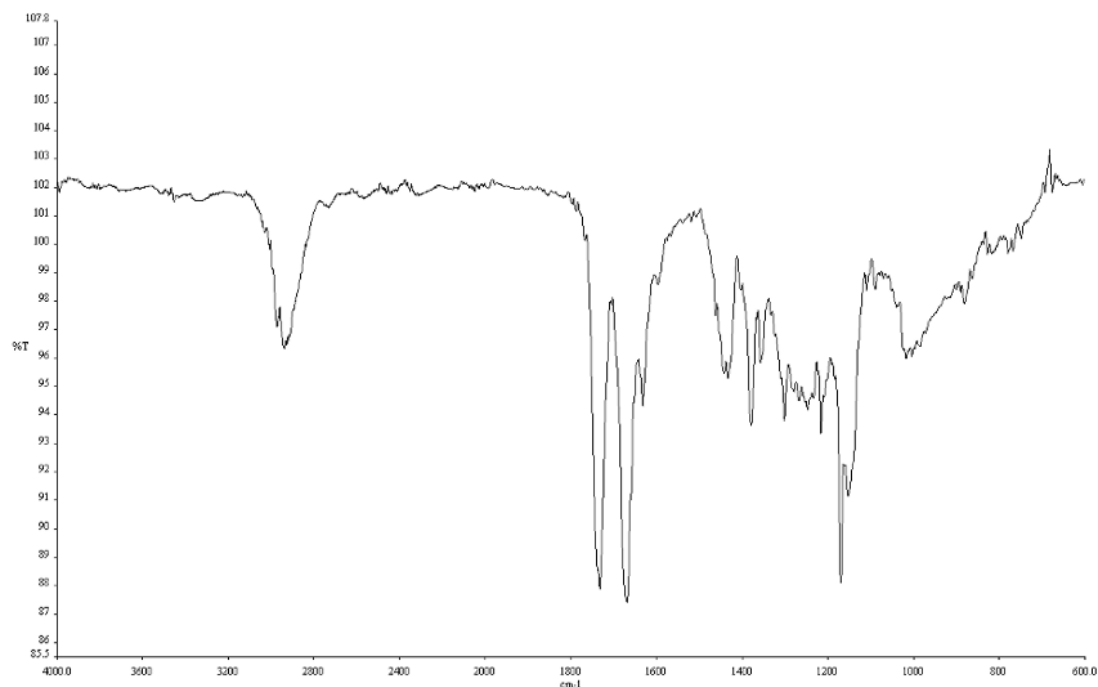
Figure A2.222. *Infrared spectrum (Thin Film, NaCl) of compound* **105**.
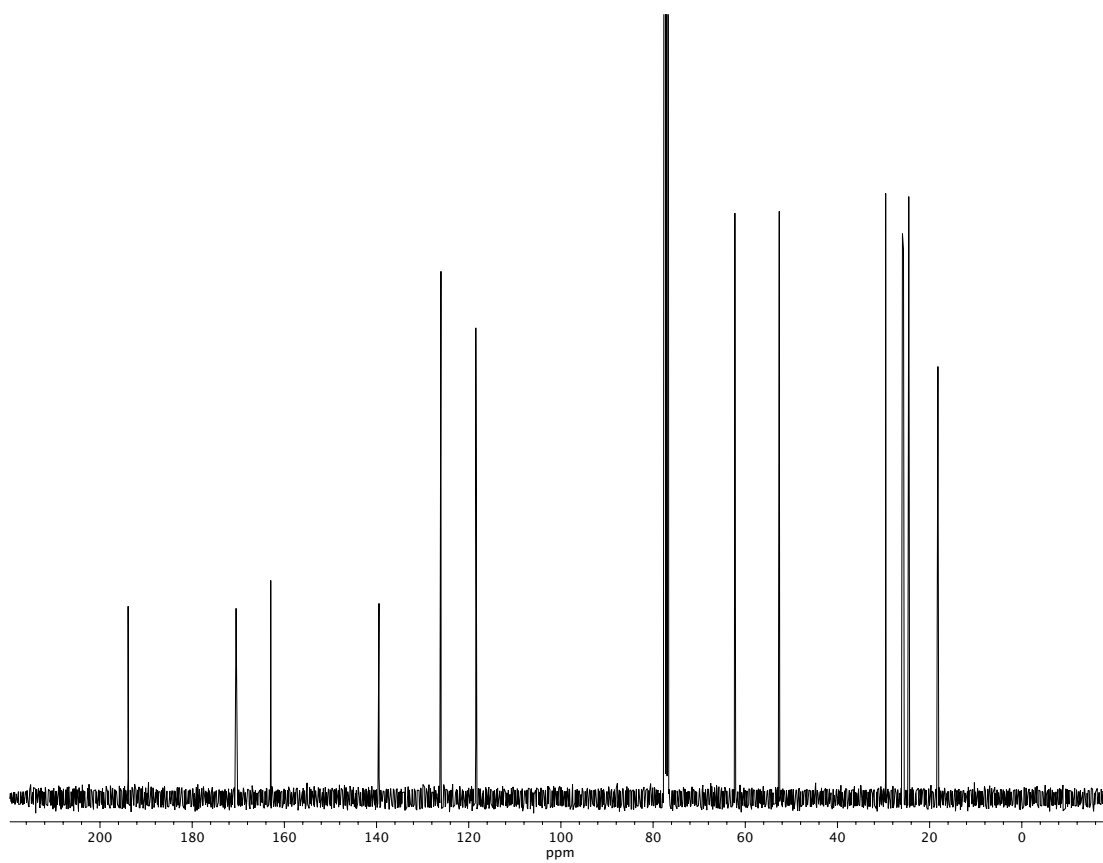
Figure A2.223. ^{13}C *NMR (100 MHz, CDCl$_3$) of compound* **105**.
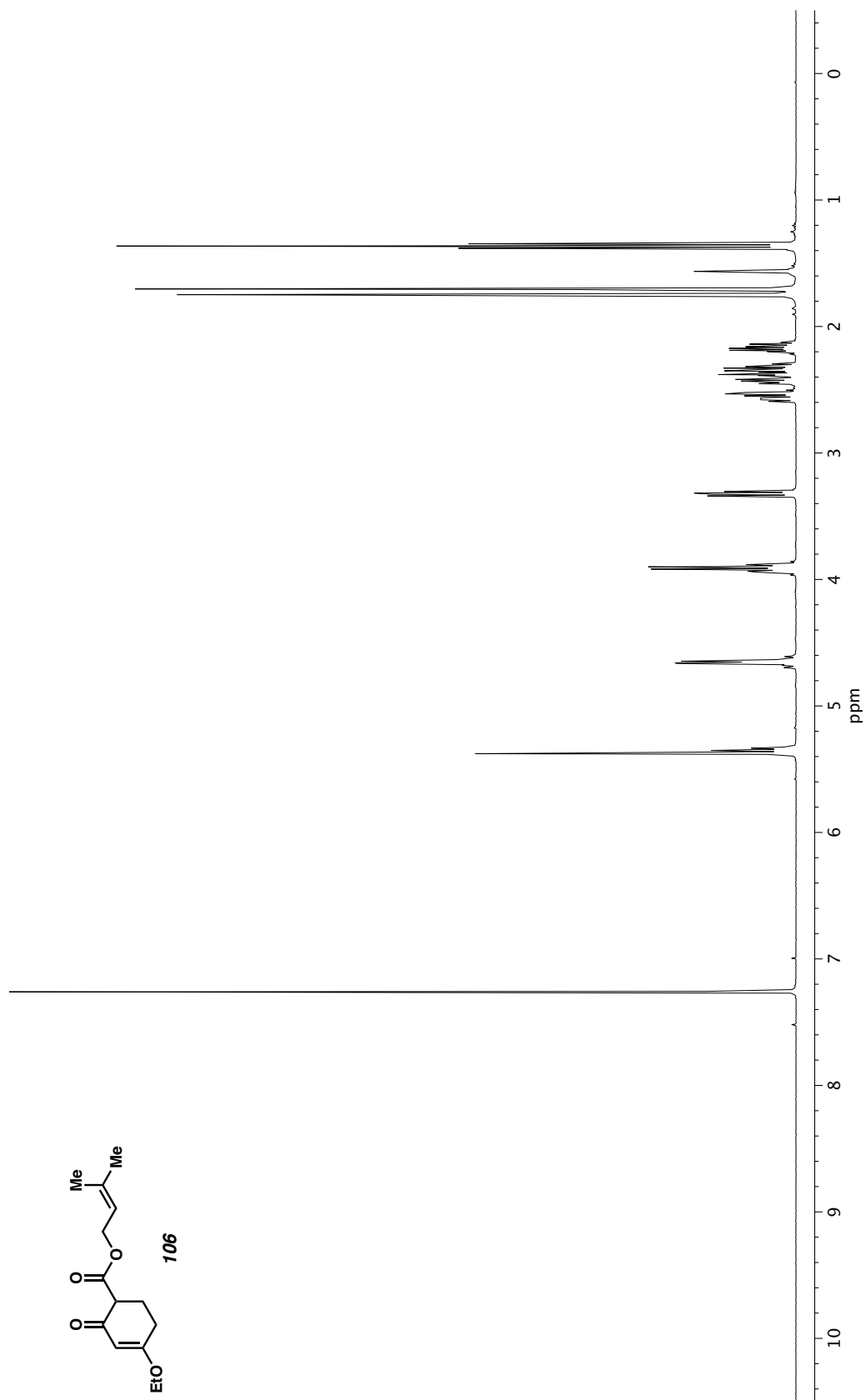
Figure A2.224. ^1H NMR (400 MHz, CDCl$_3$) of compound **106**.
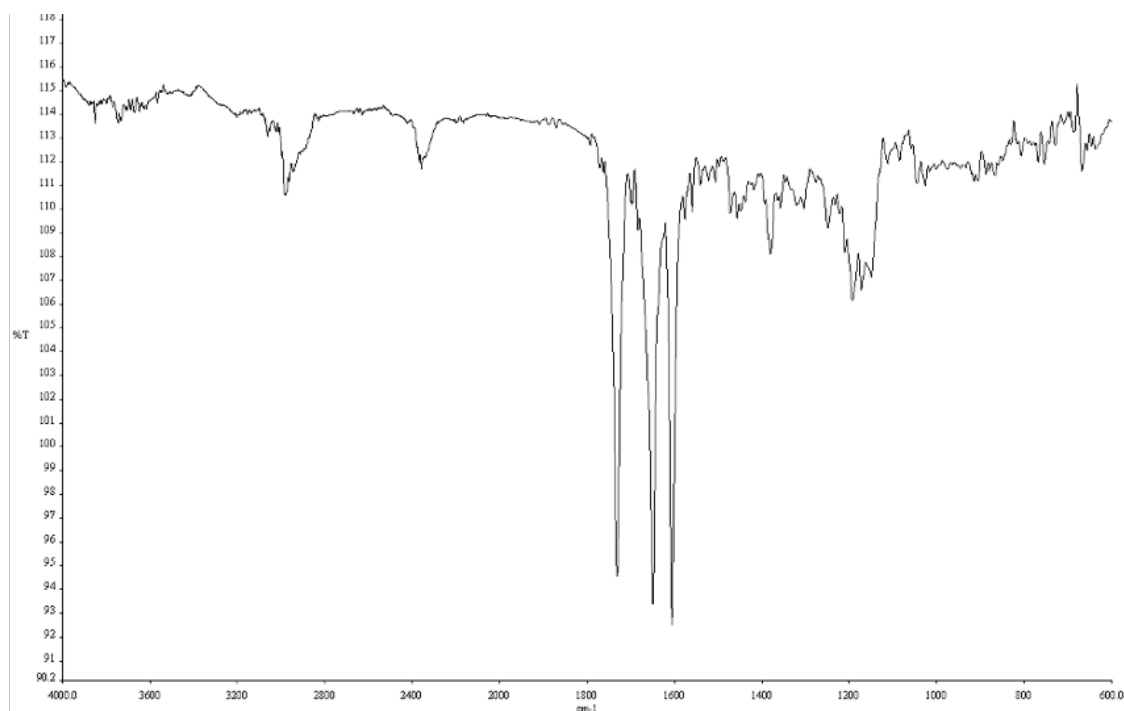
Figure A2.225. Infrared spectrum (Thin Film, NaCl) of compound **106**.
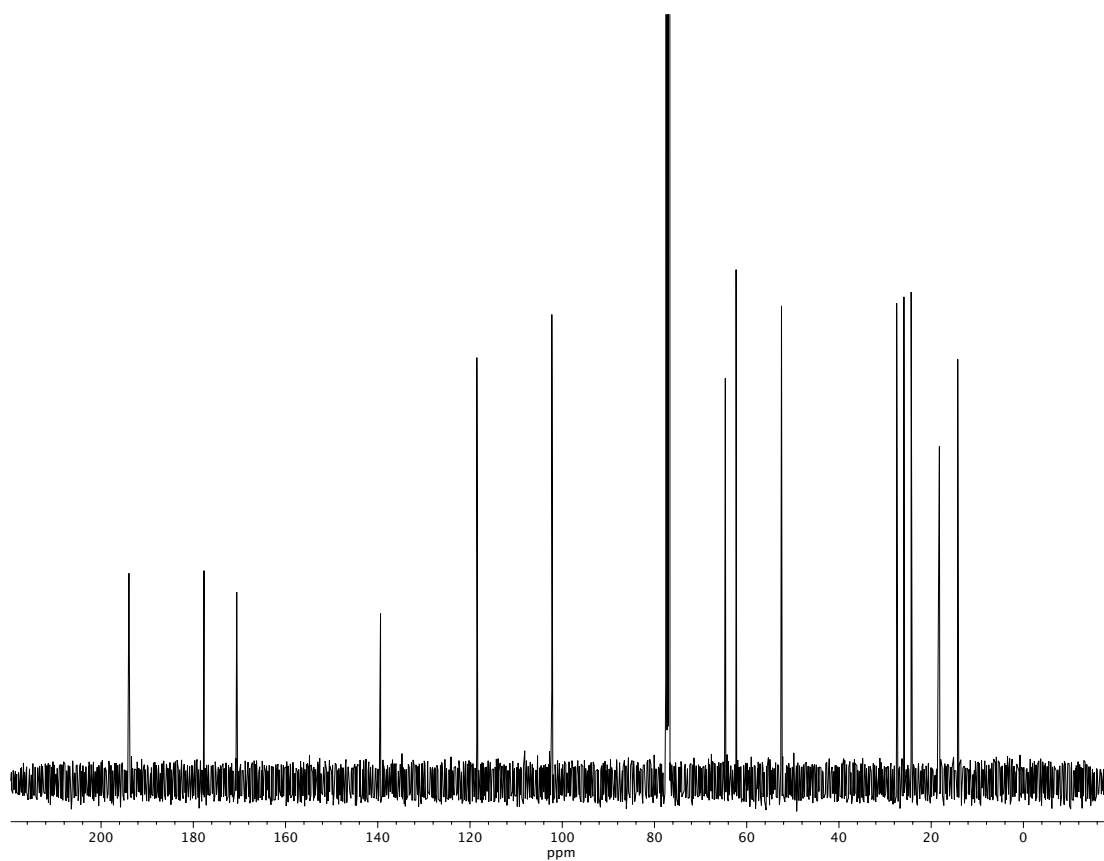
Figure A2.226. ^{13}C NMR (100 MHz, CDCl$_3$) of compound **106**.
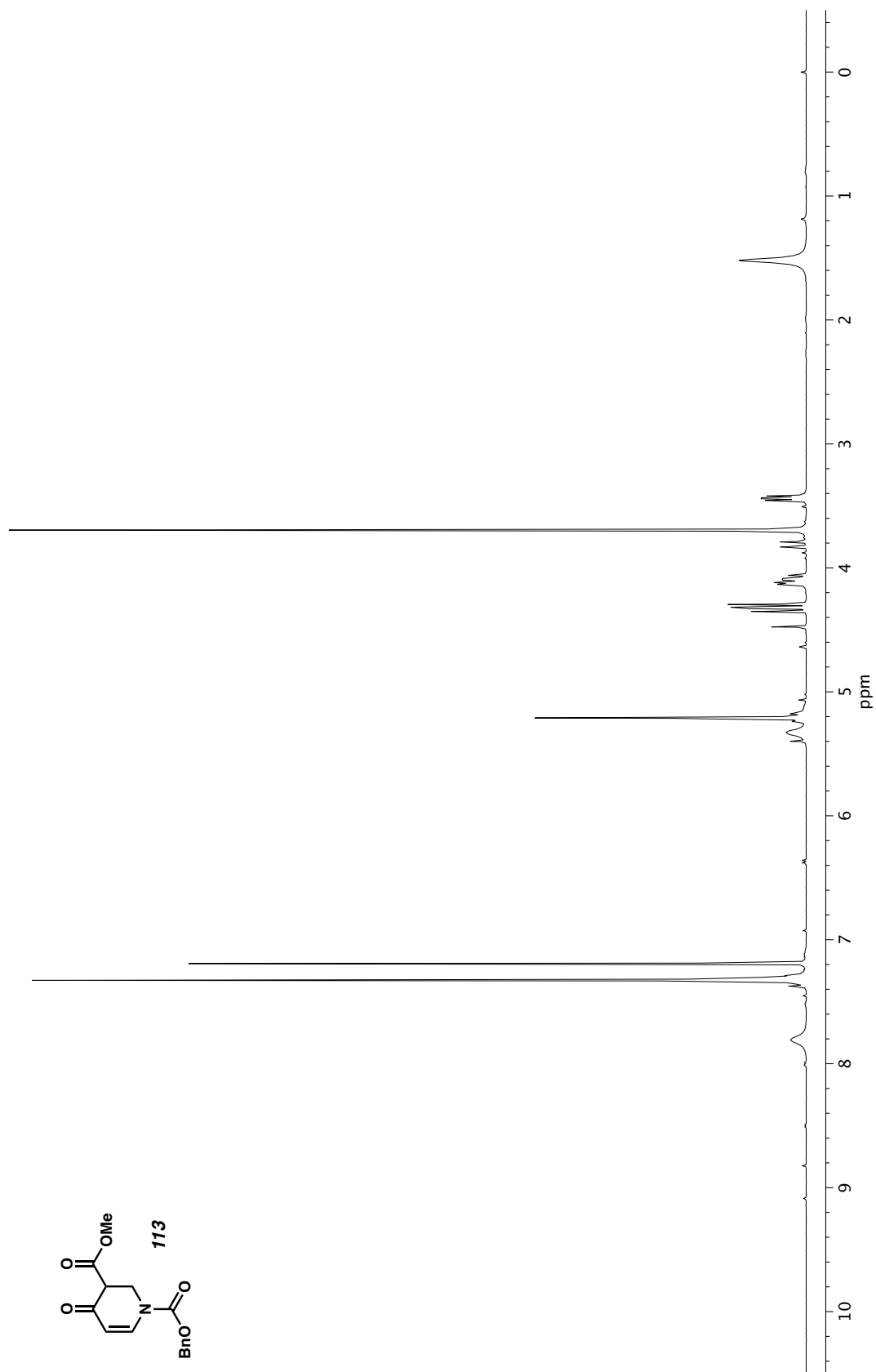
Figure A2.227. *¹H NMR (400 MHz, CDCl₃) of compound **113**.*
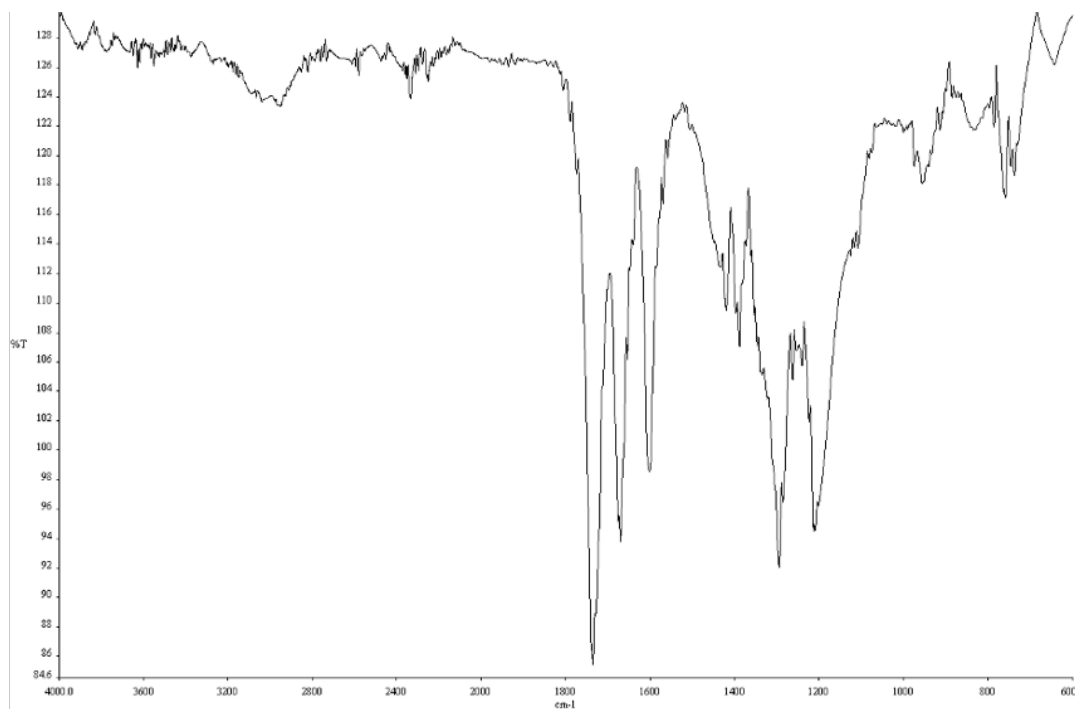
Figure A2.228. *Infrared spectrum (Thin Film, NaCl) of compound **113**.*
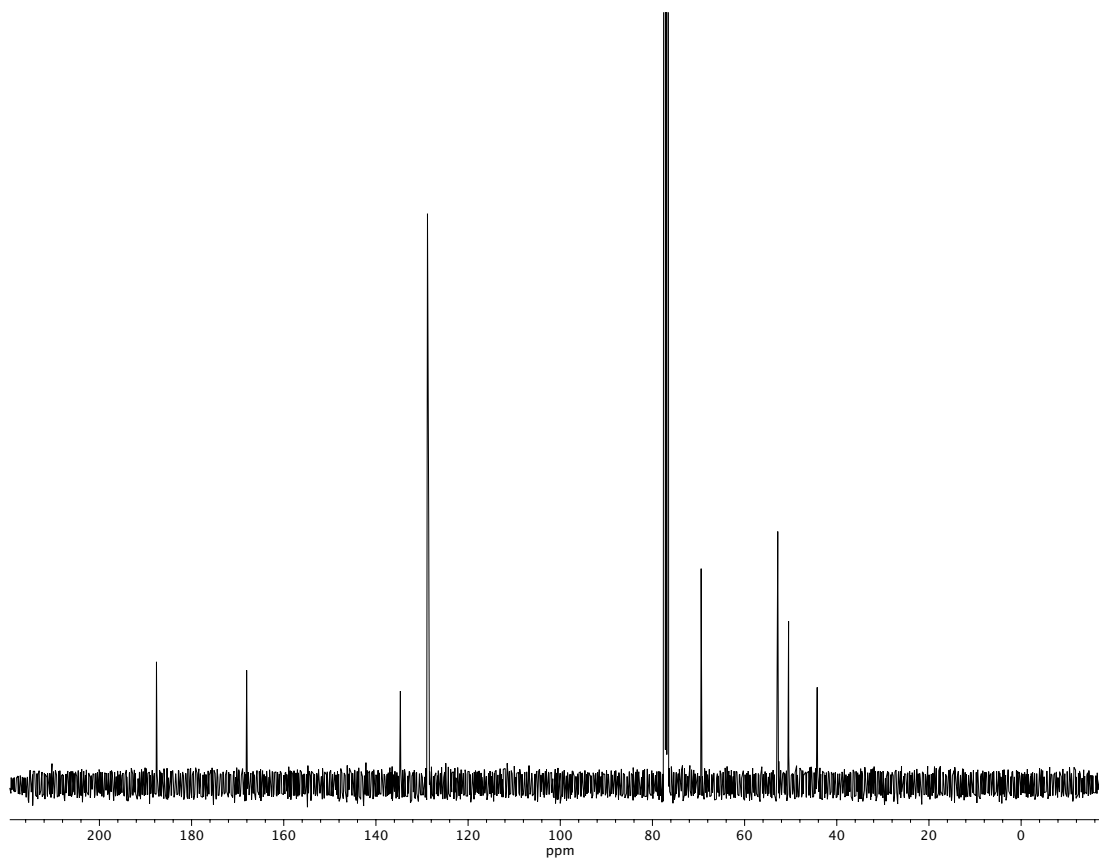
Figure A2.229. *^{13}C NMR (100 MHz, CDCl$_3$) of compound **113**.*
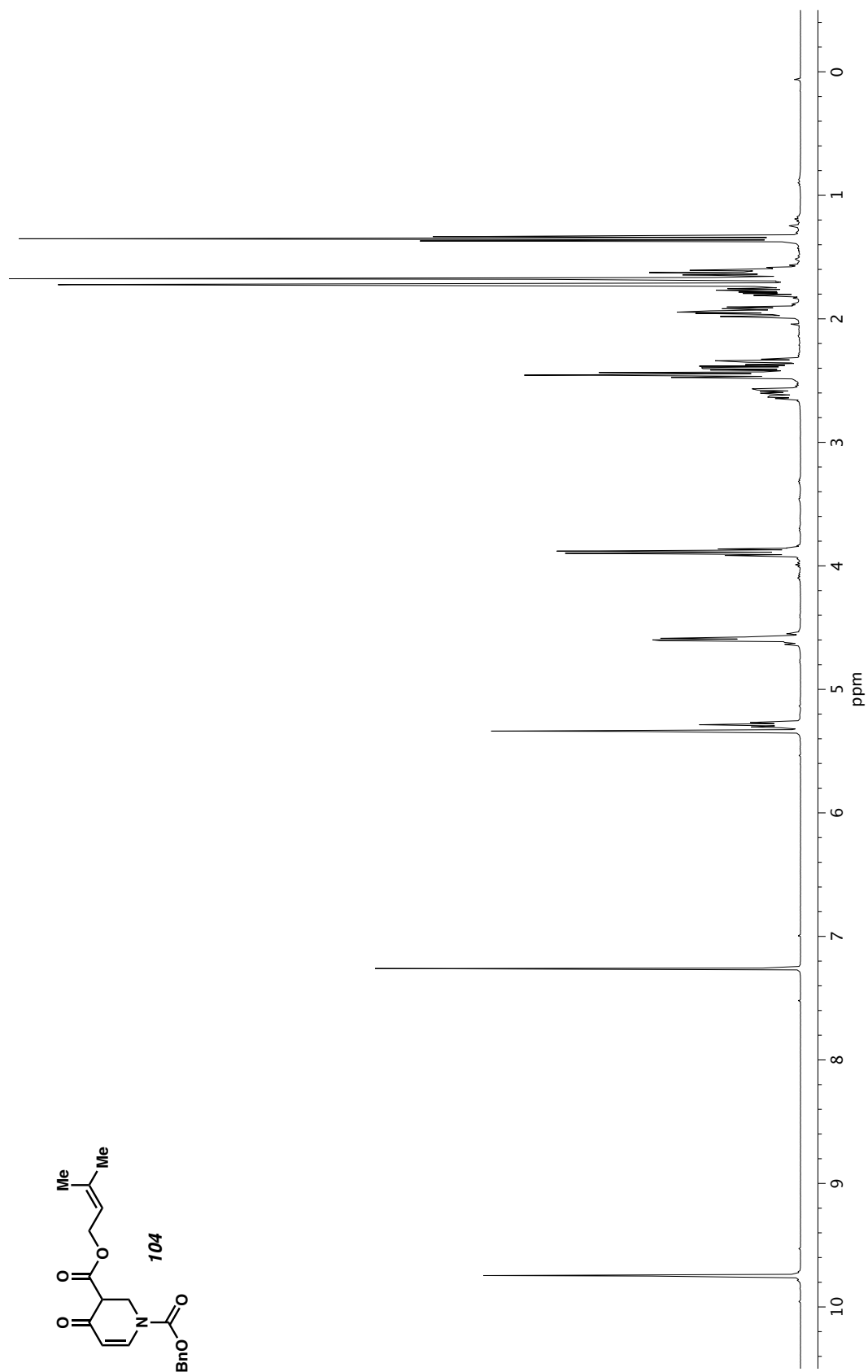
Figure A2.230. ^1H NMR (400 MHz, CDCl$_3$) of compound **104**.
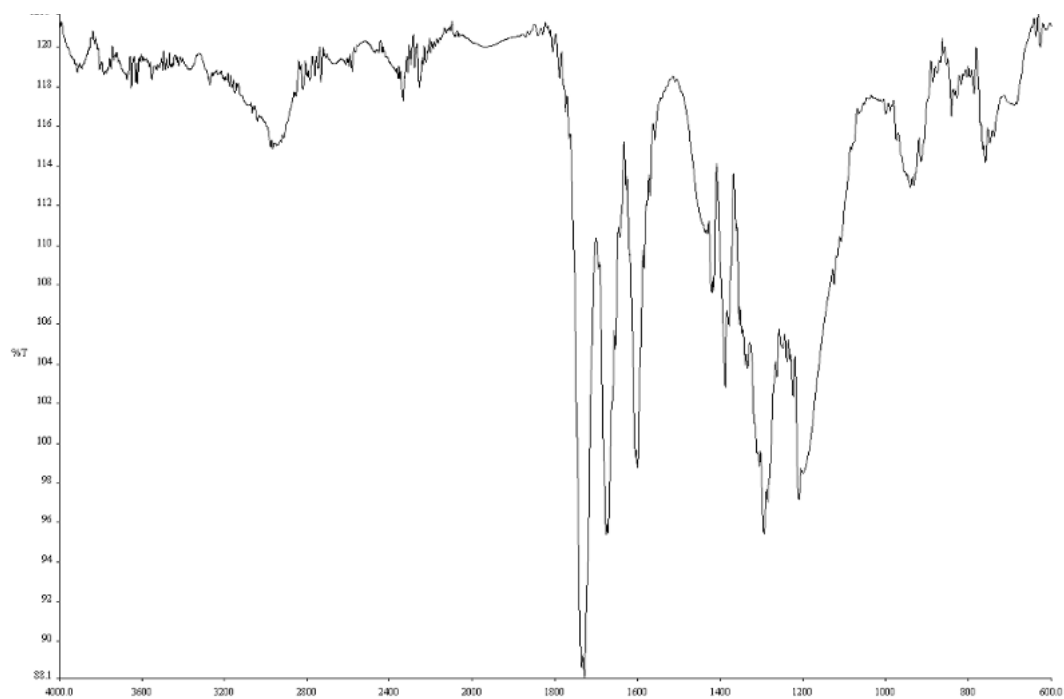
Figure A2.231. *Infrared spectrum (Thin Film, NaCl) of compound **104**.*
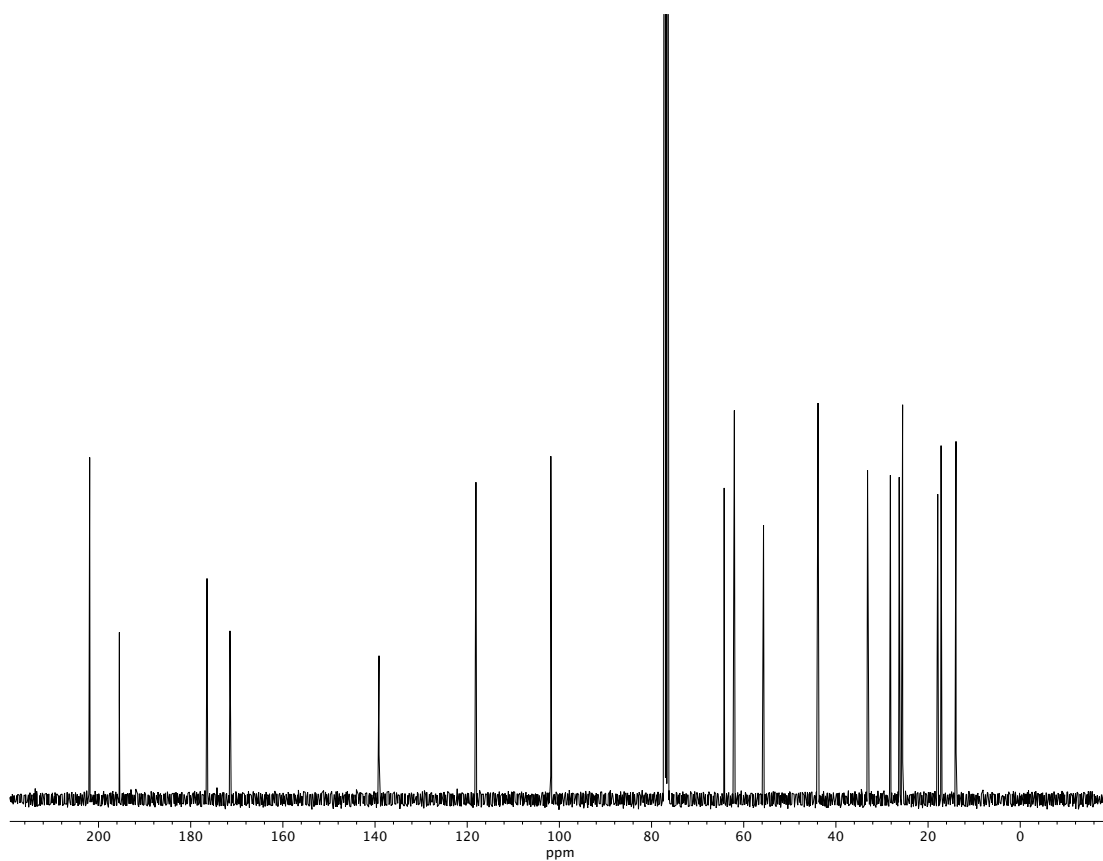
Figure A2.232. *^{13}C NMR (100 MHz, CDCl$_3$) of compound **104**.*
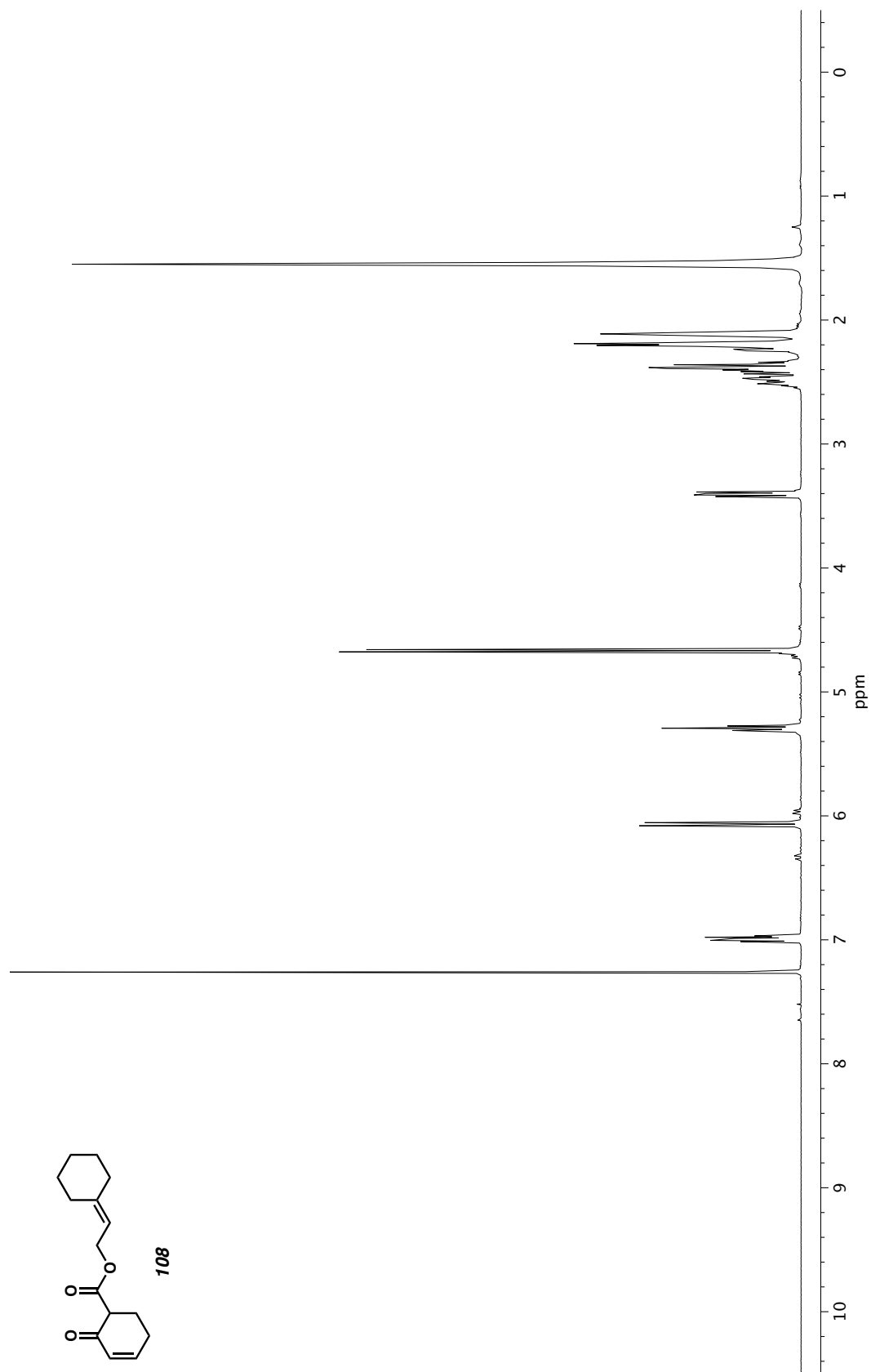
Figure A2.233. ^1H NMR (400 MHz, CDCl$_3$) of compound **108**.
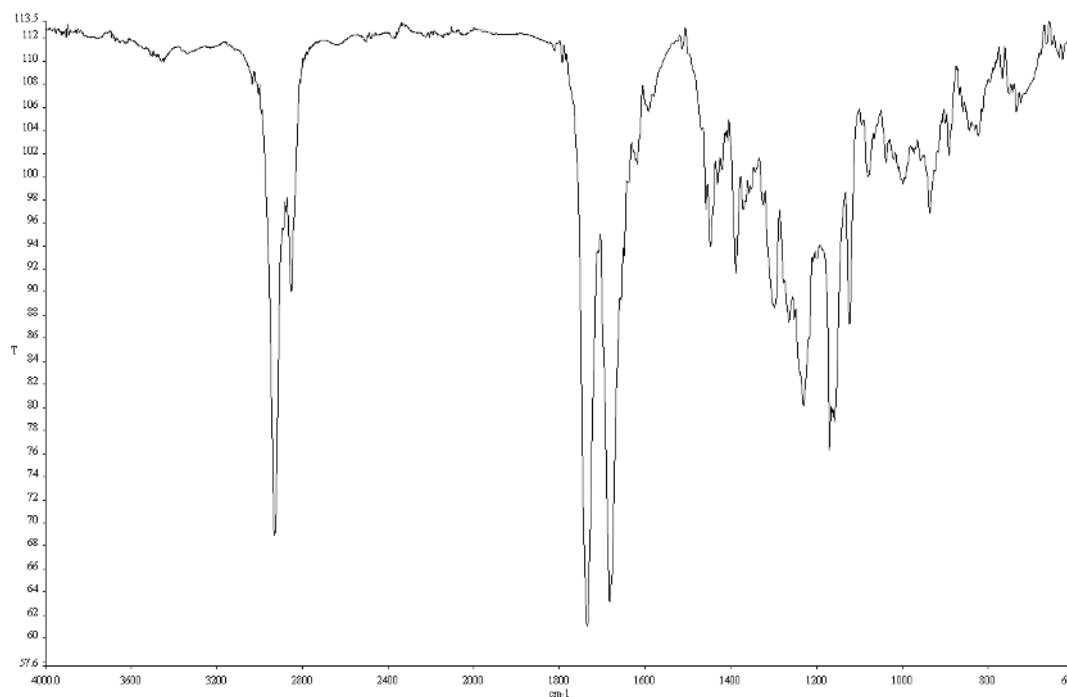
Figure A2.234. Infrared spectrum (Thin Film, NaCl) of compound **108**.
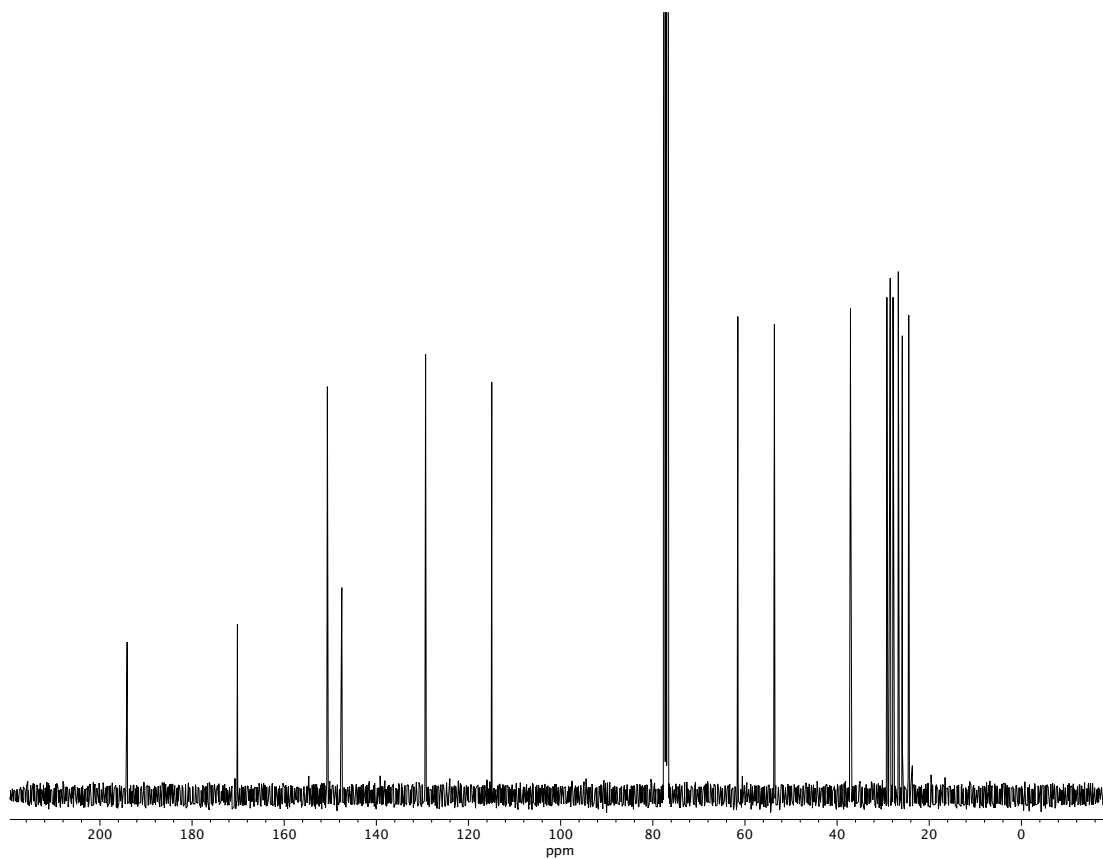
Figure A2.235. ^{13}C NMR (100 MHz, CDCl$_3$) of compound **108**.
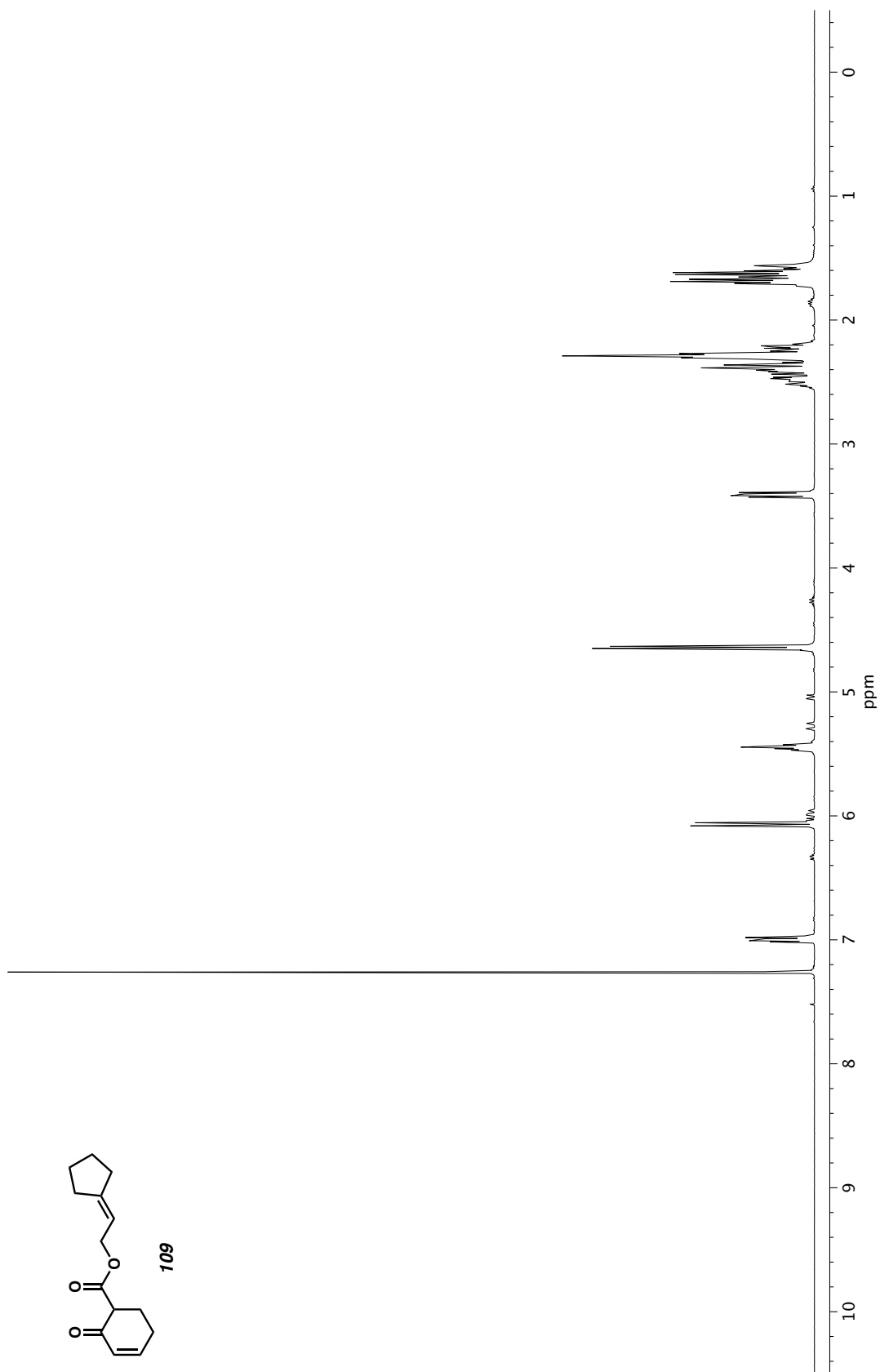
Figure A2.236. ^1H NMR (400 MHz, CDCl$_3$) of compound **109**.
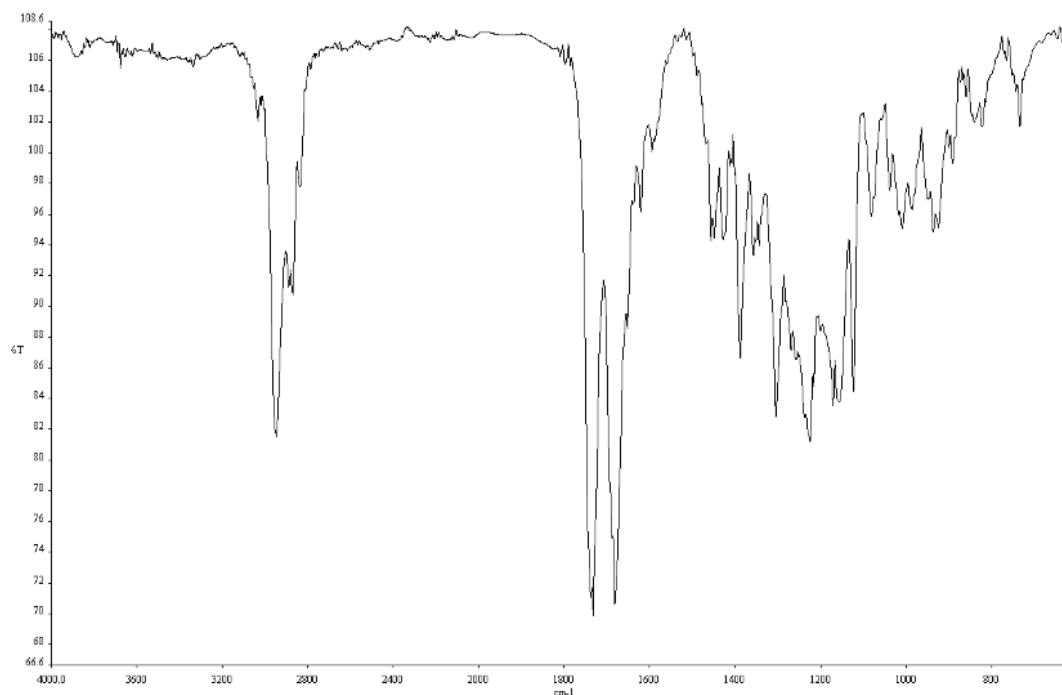
Figure A2.237. *Infrared spectrum (Thin Film, NaCl) of compound **109**.*
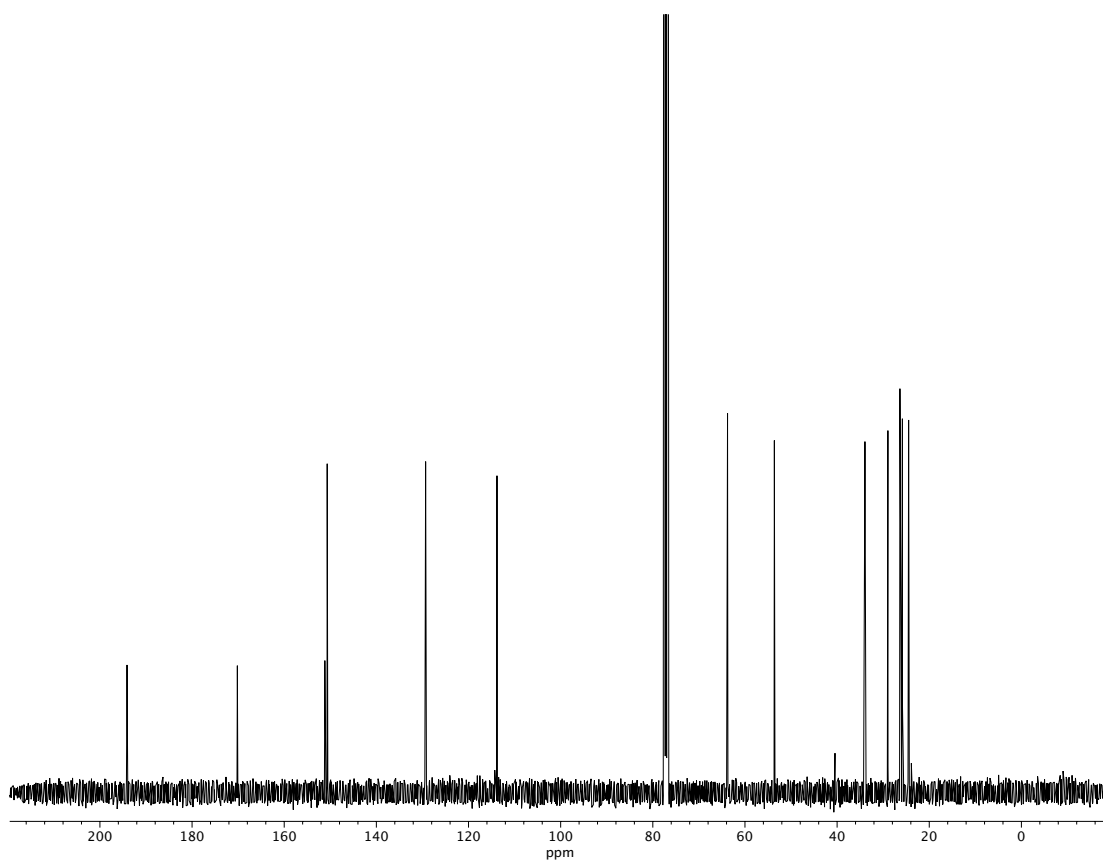
Figure A2.238. *^{13}C NMR (100 MHz, CDCl$_3$) of compound **109**.*
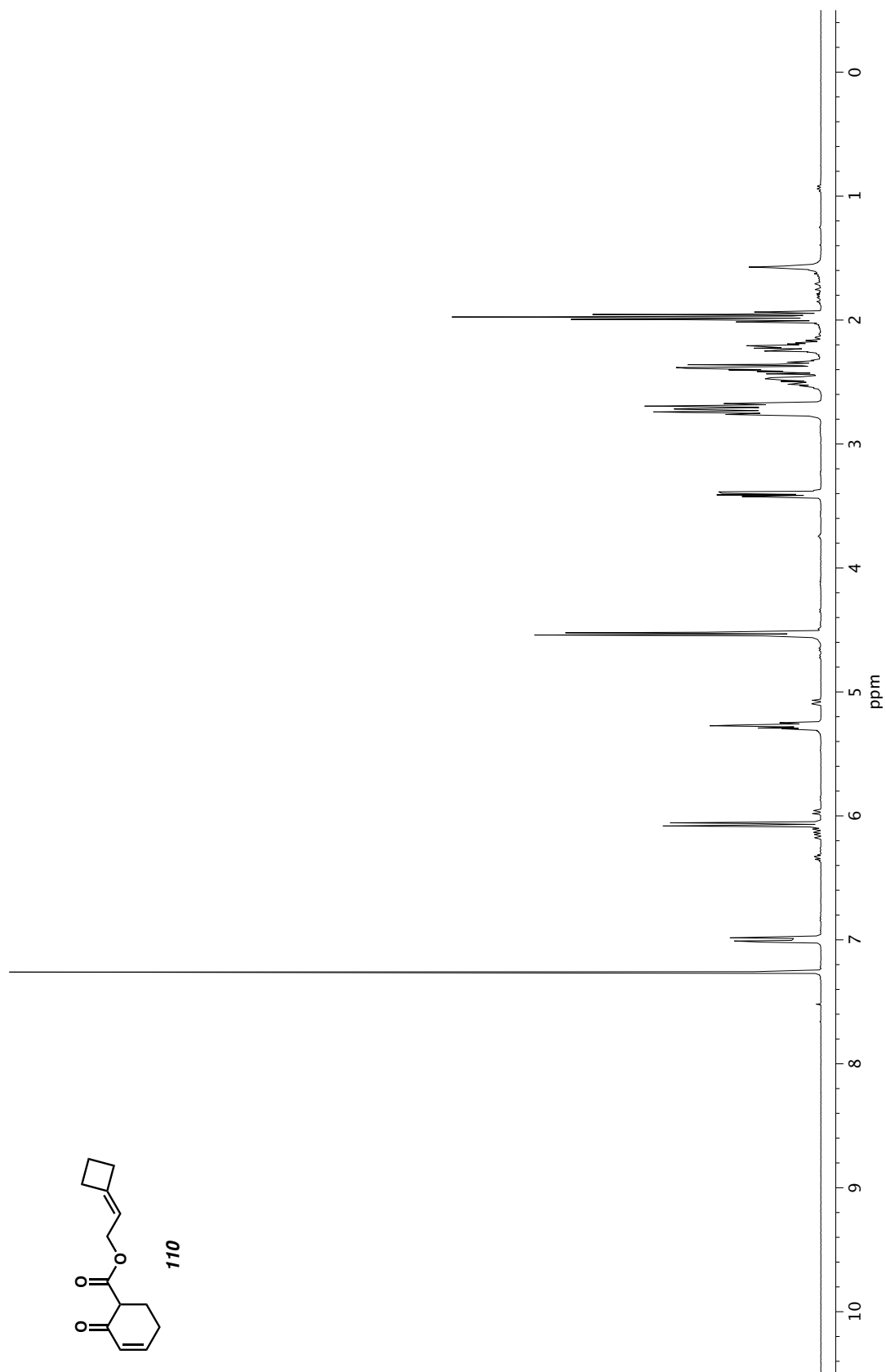
Figure A2.239. ^1H NMR (400 MHz, CDCl$_3$) of compound **110**.
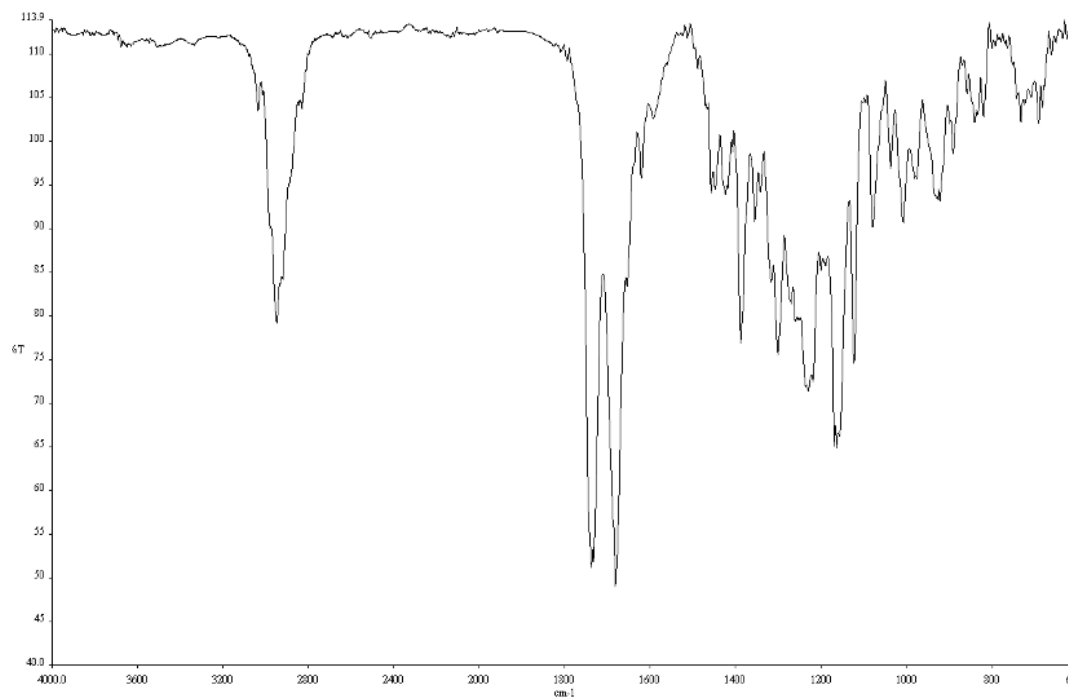
Figure A2.240. *Infrared spectrum (Thin Film, NaCl) of compound* **110**.
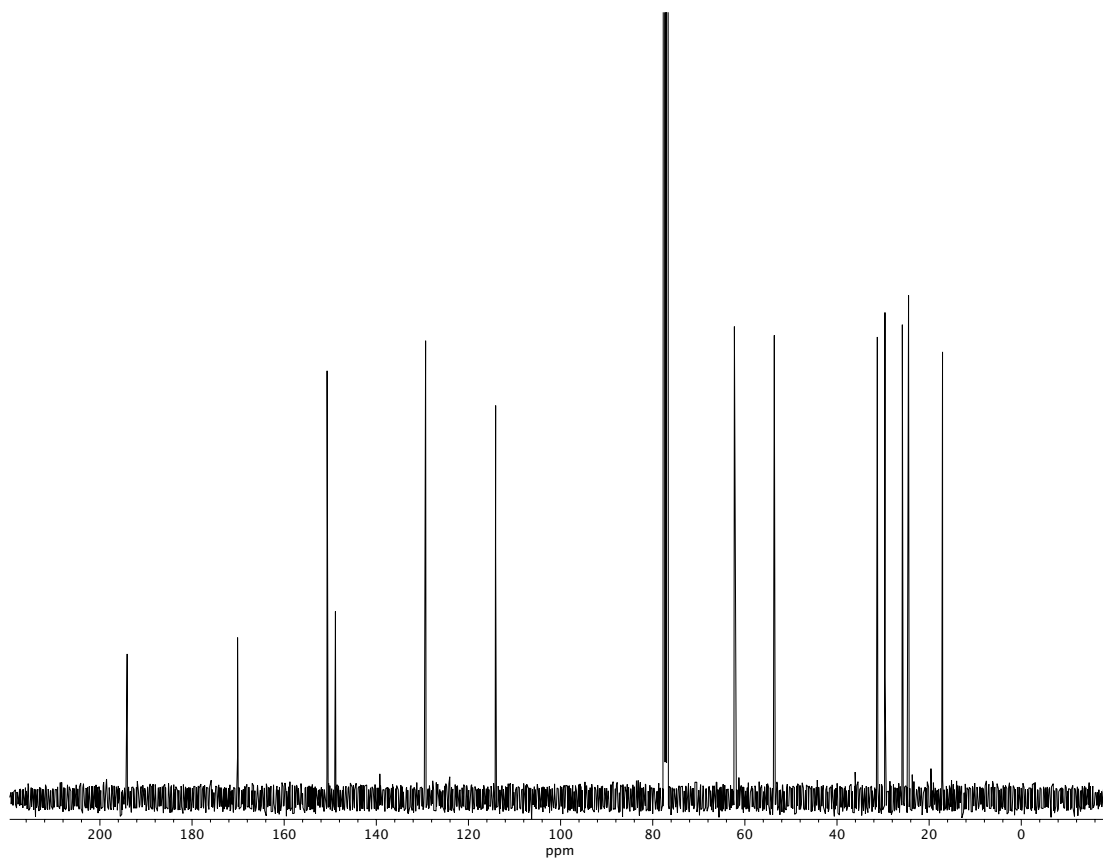
Figure A2.241. ^{13}C *NMR (100 MHz, CDCl$_3$) of compound* **110**.
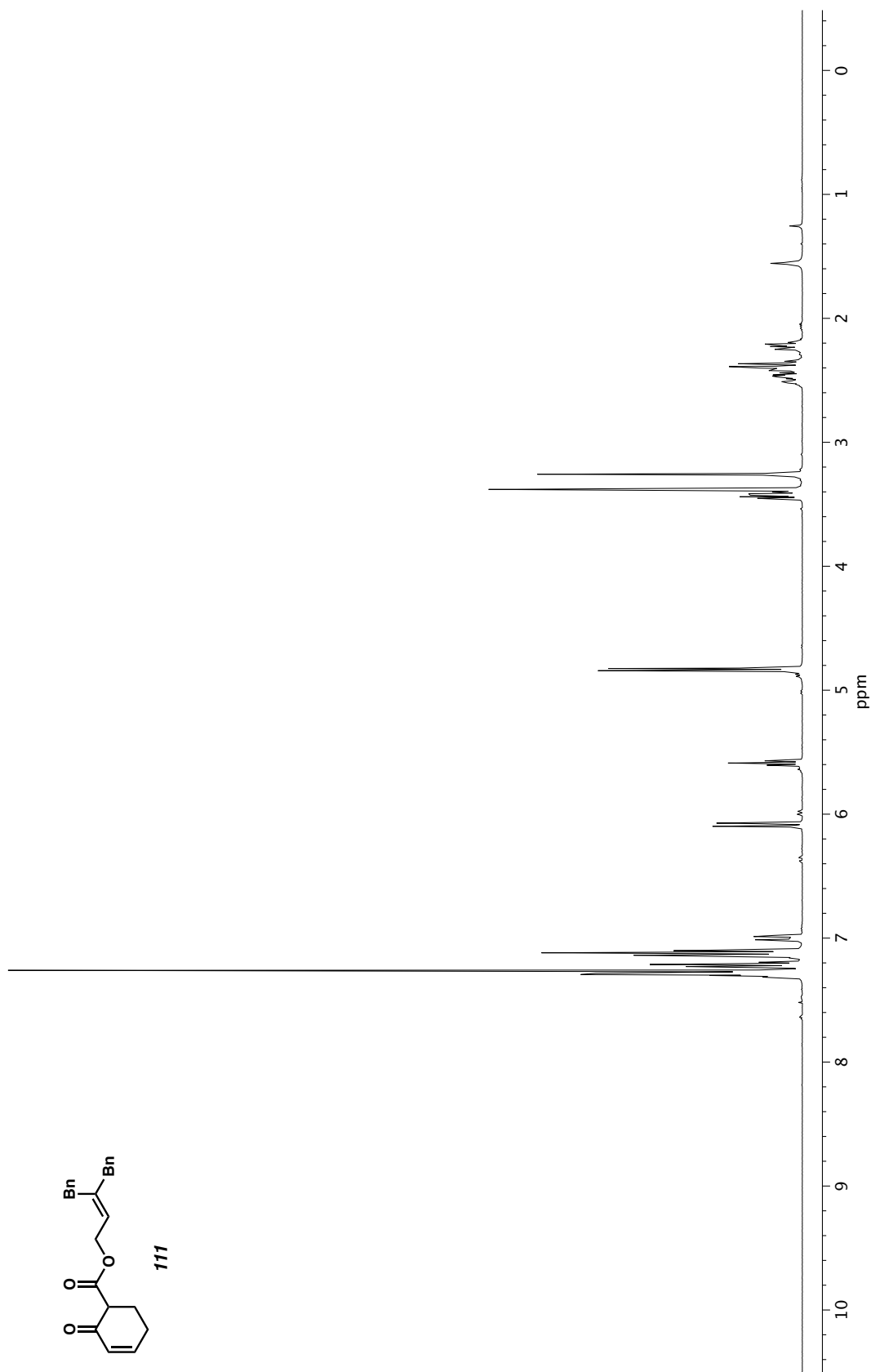
Figure A2.242. *^{1}H NMR (400 MHz, CDCl$_3$) of compound **111**.*
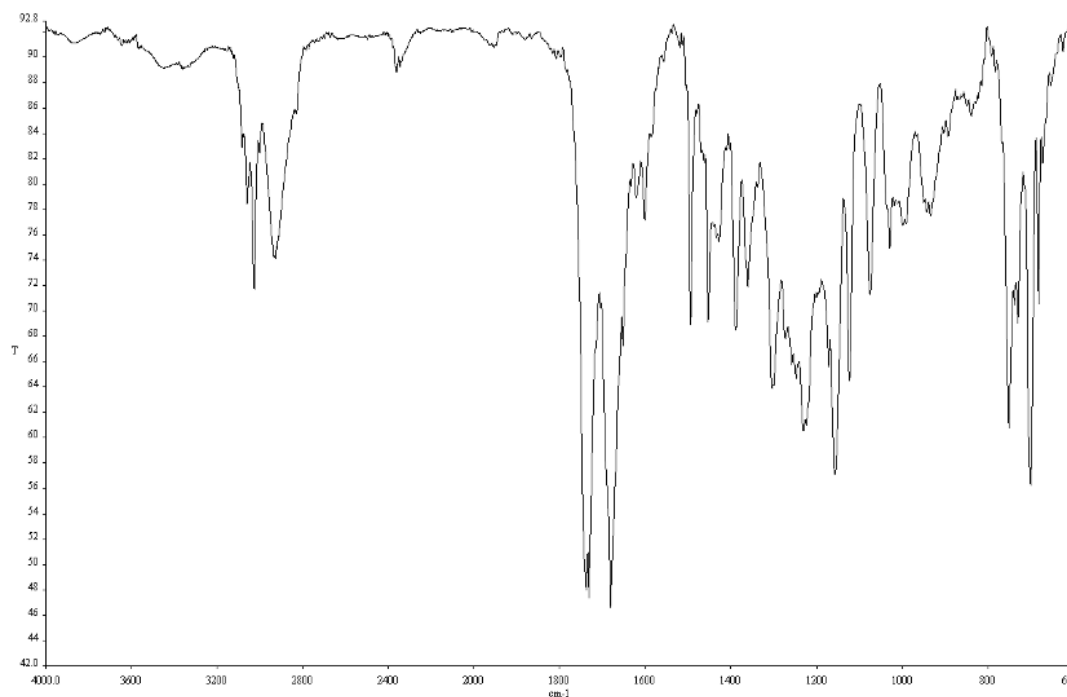
Figure A2.243. *Infrared spectrum (Thin Film, NaCl) of compound* **111**.
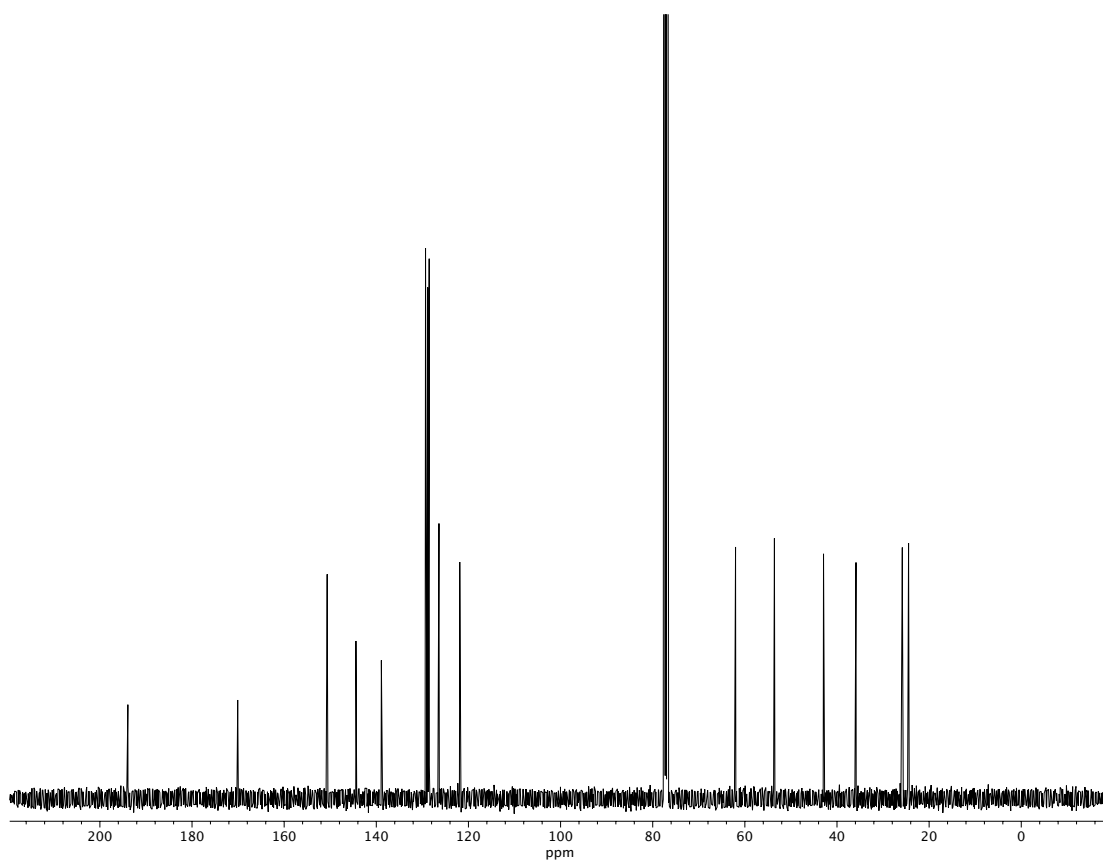
Figure A2.244. ^{13}C *NMR (100 MHz, CDCl$_3$) of compound* **111**.
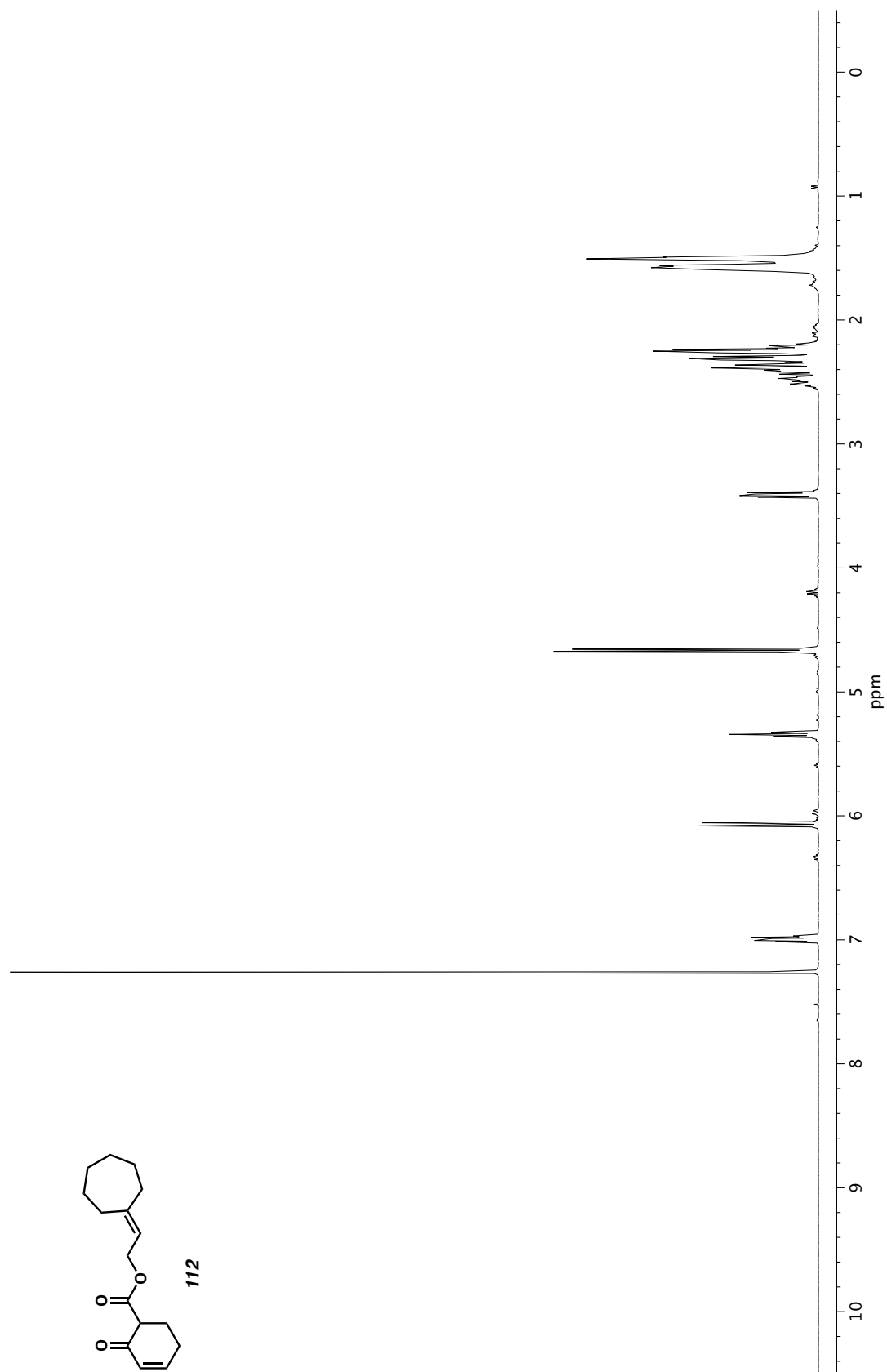
Figure A2.245. *¹H NMR (400 MHz, CDCl₃) of compound **112**.*
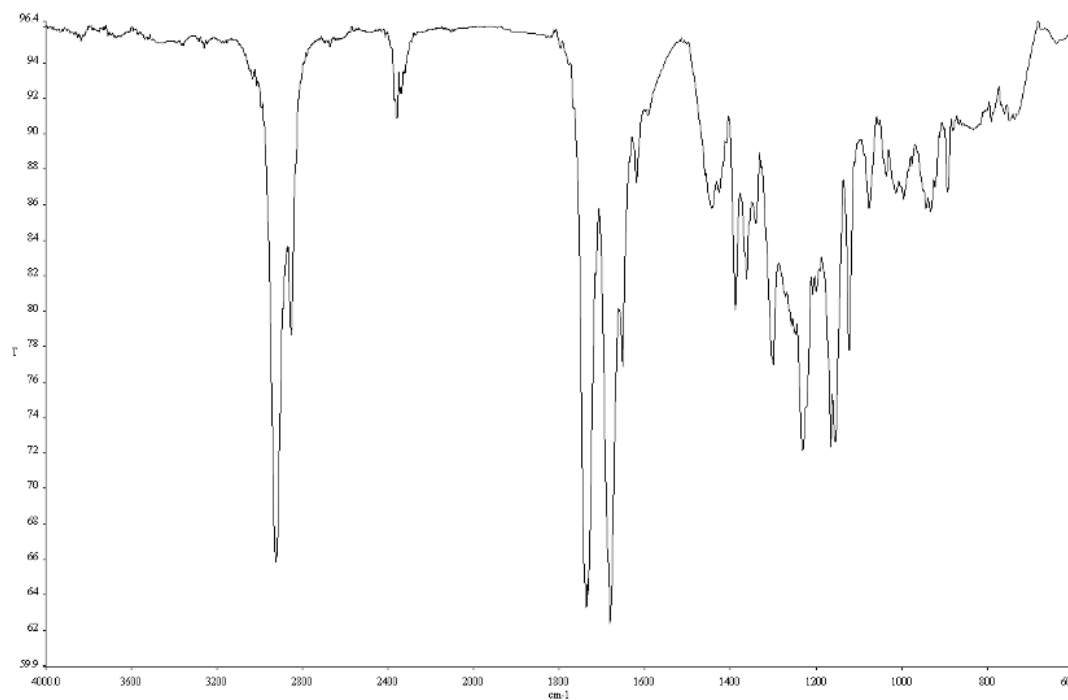
Figure A2.246. Infrared spectrum (Thin Film, NaCl) of compound **112**.
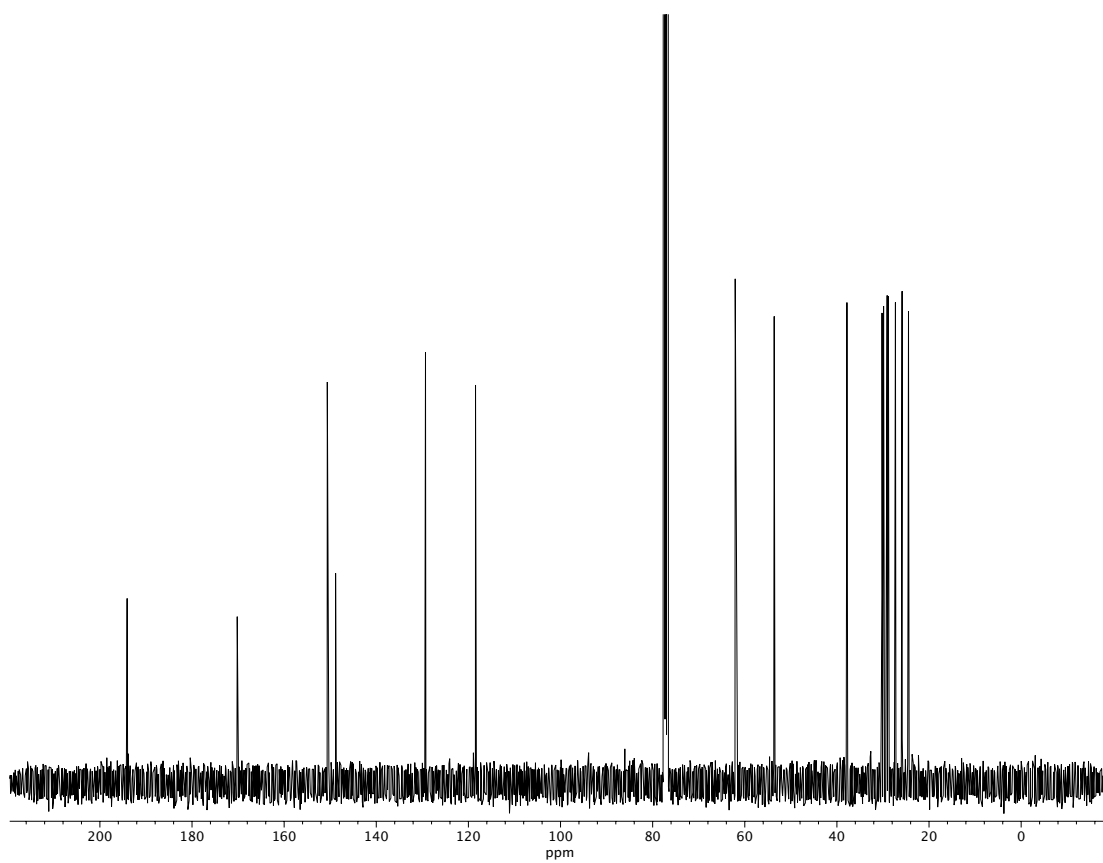
Figure A2.247. ^{13}C NMR (100 MHz, CDCl$_3$) of compound **112**.
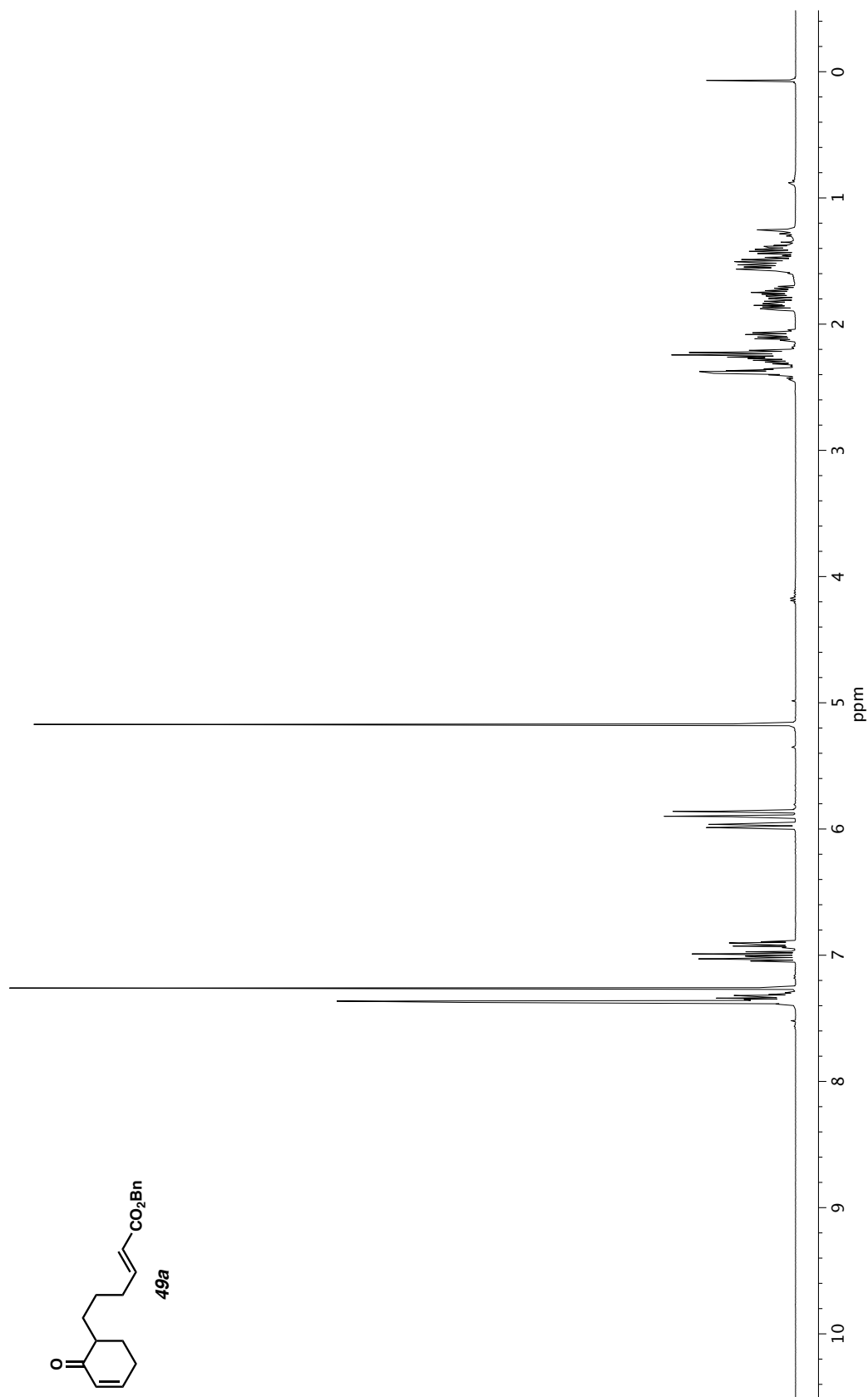
Figure A2.248. ^1H NMR (400 MHz, CDCl$_3$) of compound **49a**.
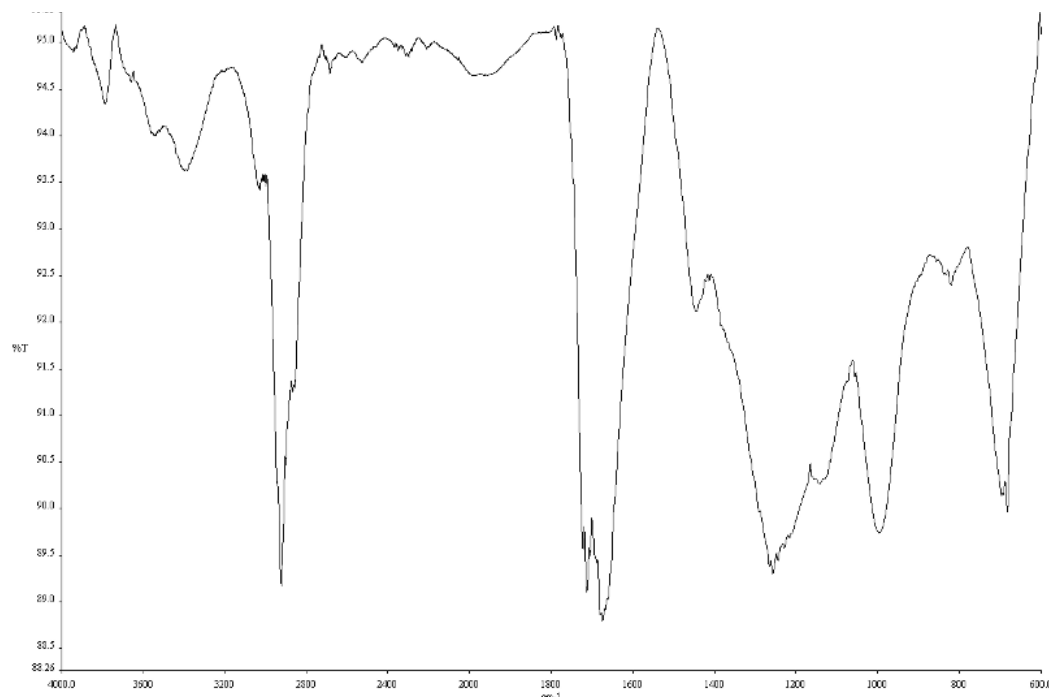
Figure A2.249. *Infrared spectrum (Thin Film, NaCl) of compound* **49a**.
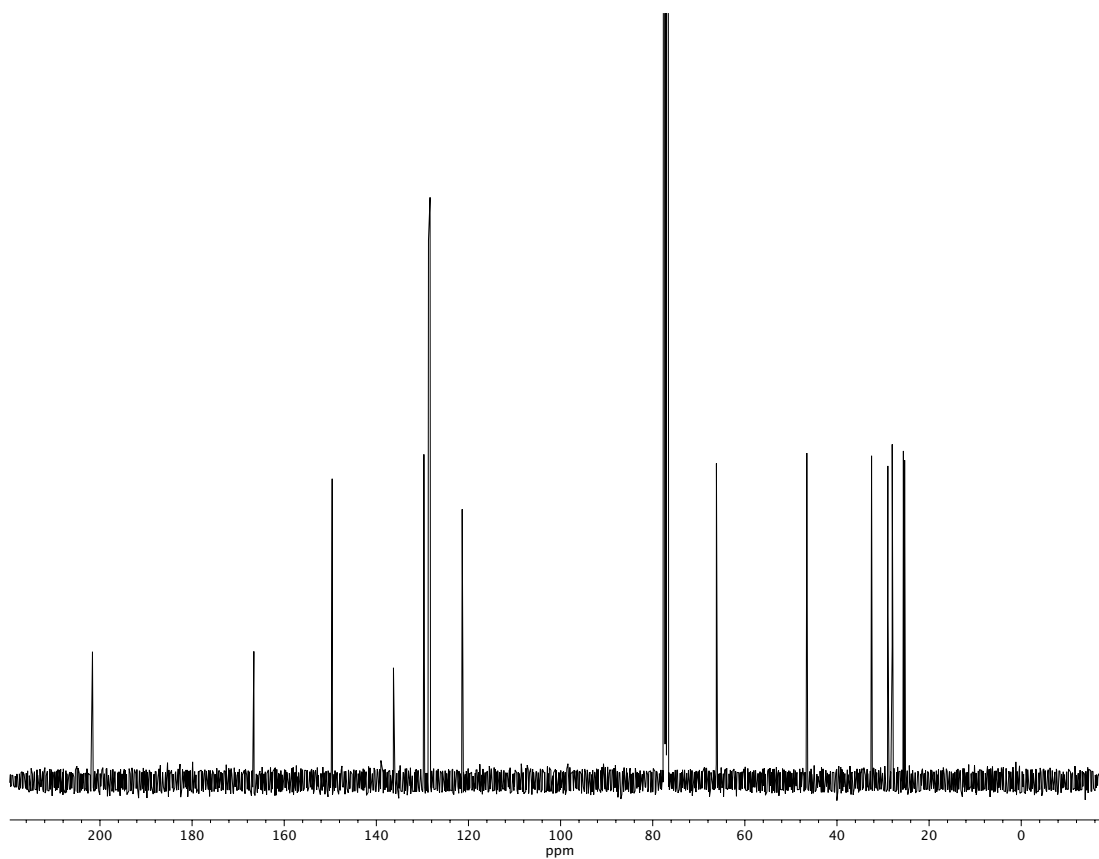
Figure A2.250. ^{13}C *NMR (100 MHz, CDCl$_3$) of compound* **49a**.
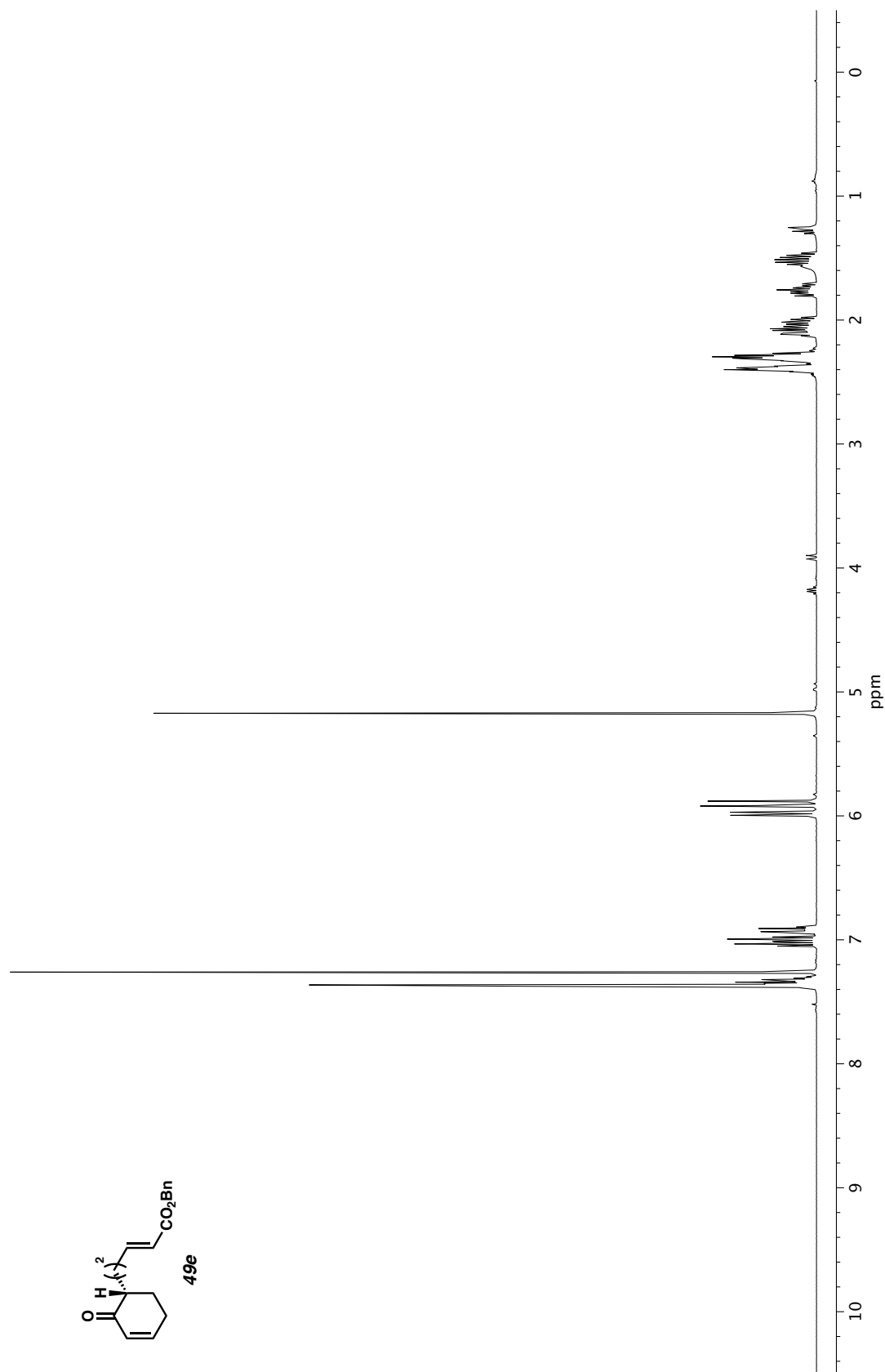
Figure A2.251. ^1H NMR (400 MHz, CDCl$_3$) of compound **49e**.
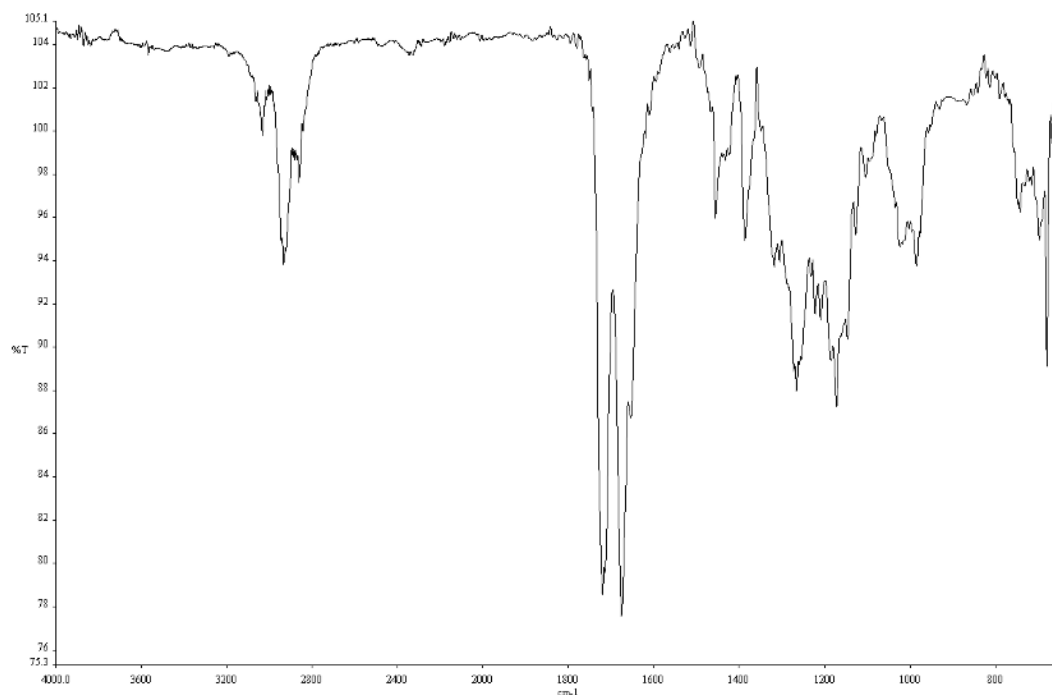
Figure A2.252. *Infrared spectrum (Thin Film, NaCl) of compound **49e**.*
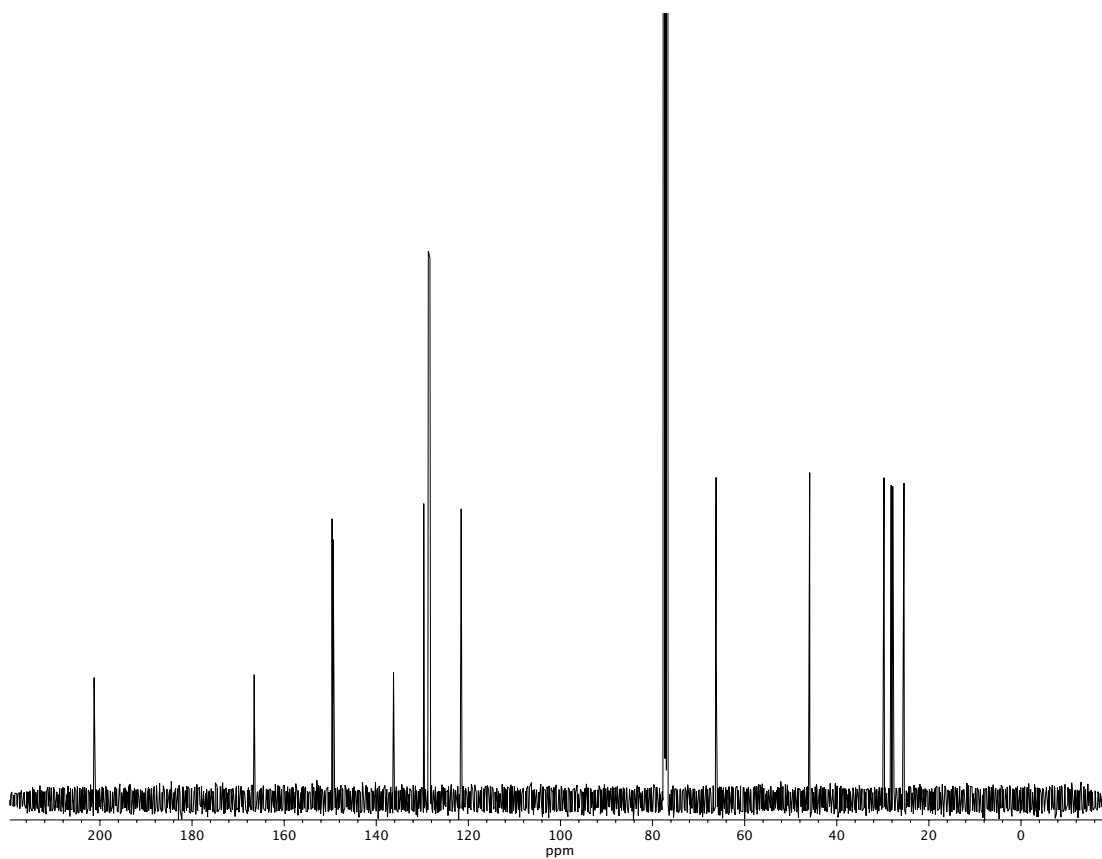
Figure A2.253. ^{13}C *NMR (100 MHz, CDCl$_3$) of compound **49e**.*
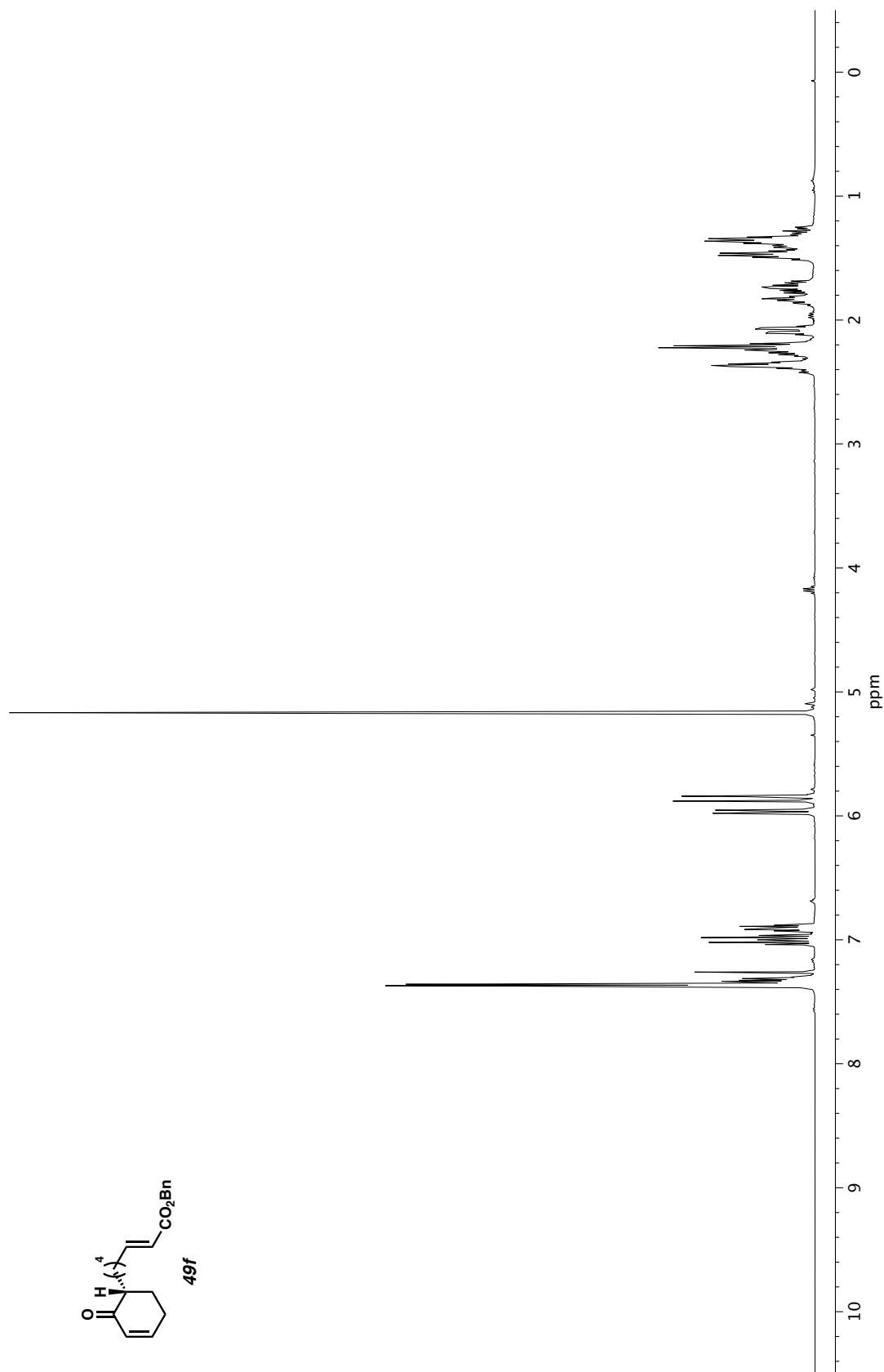
Figure A2.254. ^1H NMR (400 MHz, CDCl$_3$) of compound **49f**.
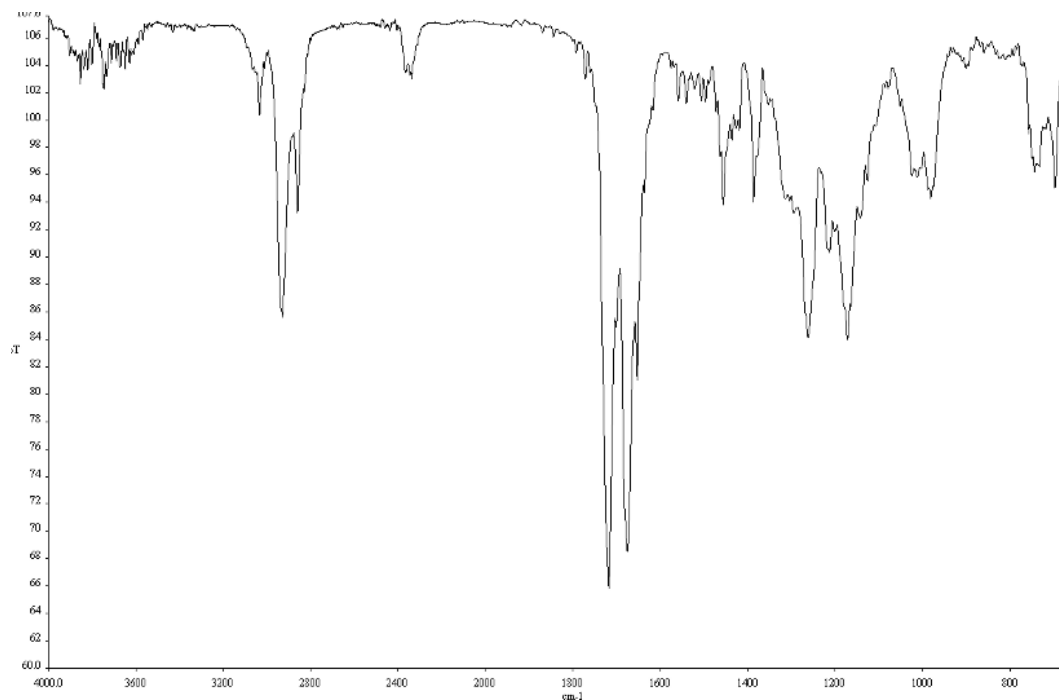
Figure A2.255. *Infrared spectrum (Thin Film, NaCl) of compound* **49f**.
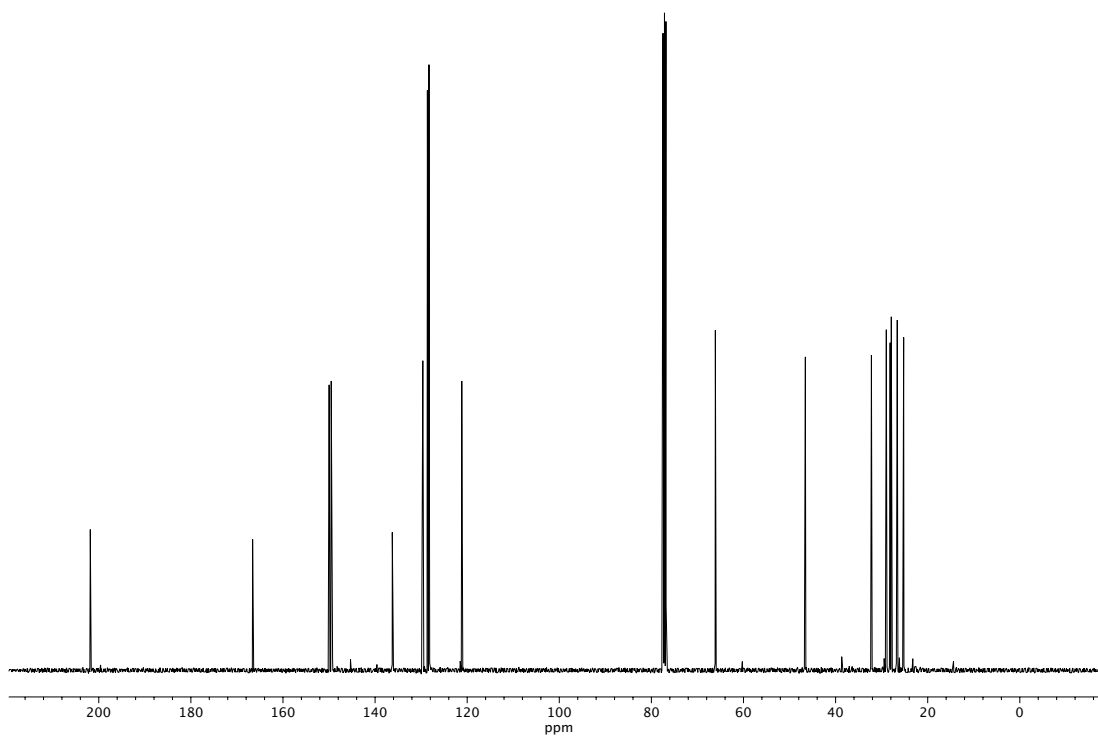
Figure A2.256. ^{13}C *NMR (100 MHz, CDCl$_3$) of compound* **49f**.
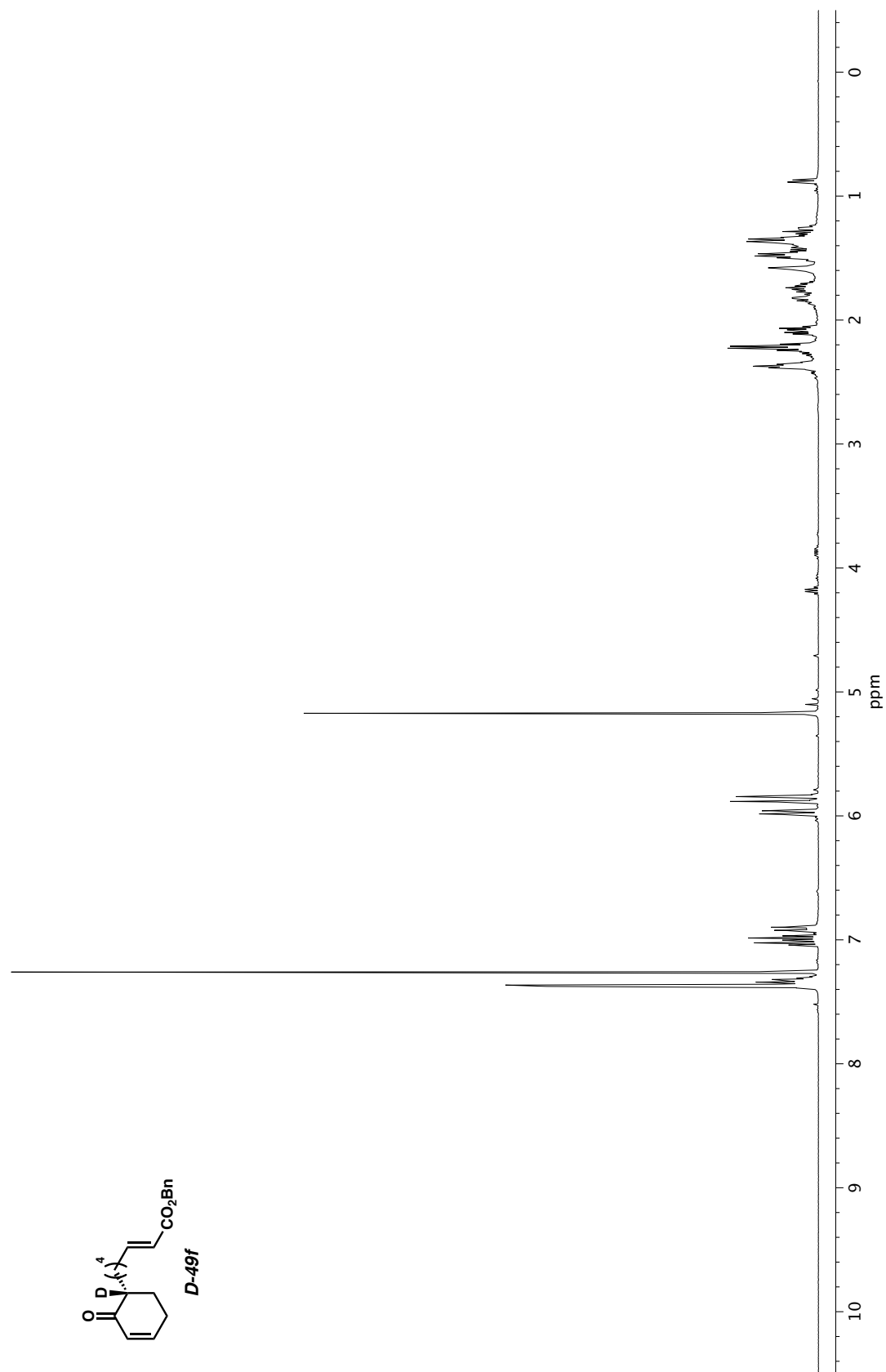
Figure A2.257. ^1H NMR (400 MHz, CDCl$_3$) of compound **D-49f**.
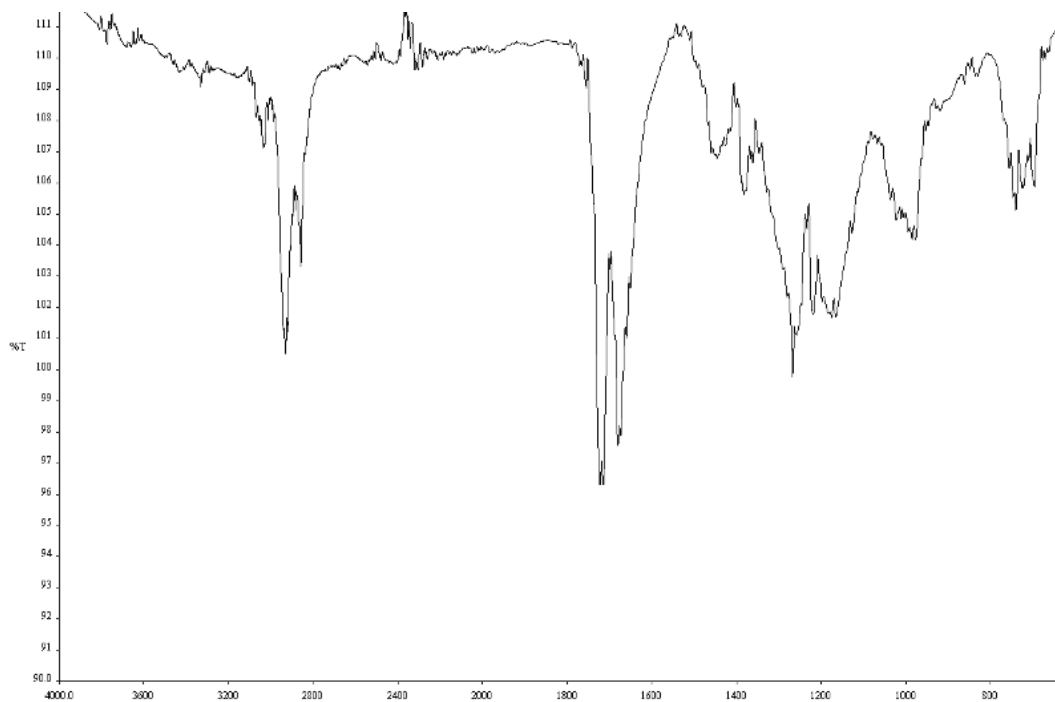
Figure A2.258. *Infrared spectrum (Thin Film, NaCl) of compound **D-49f**.*
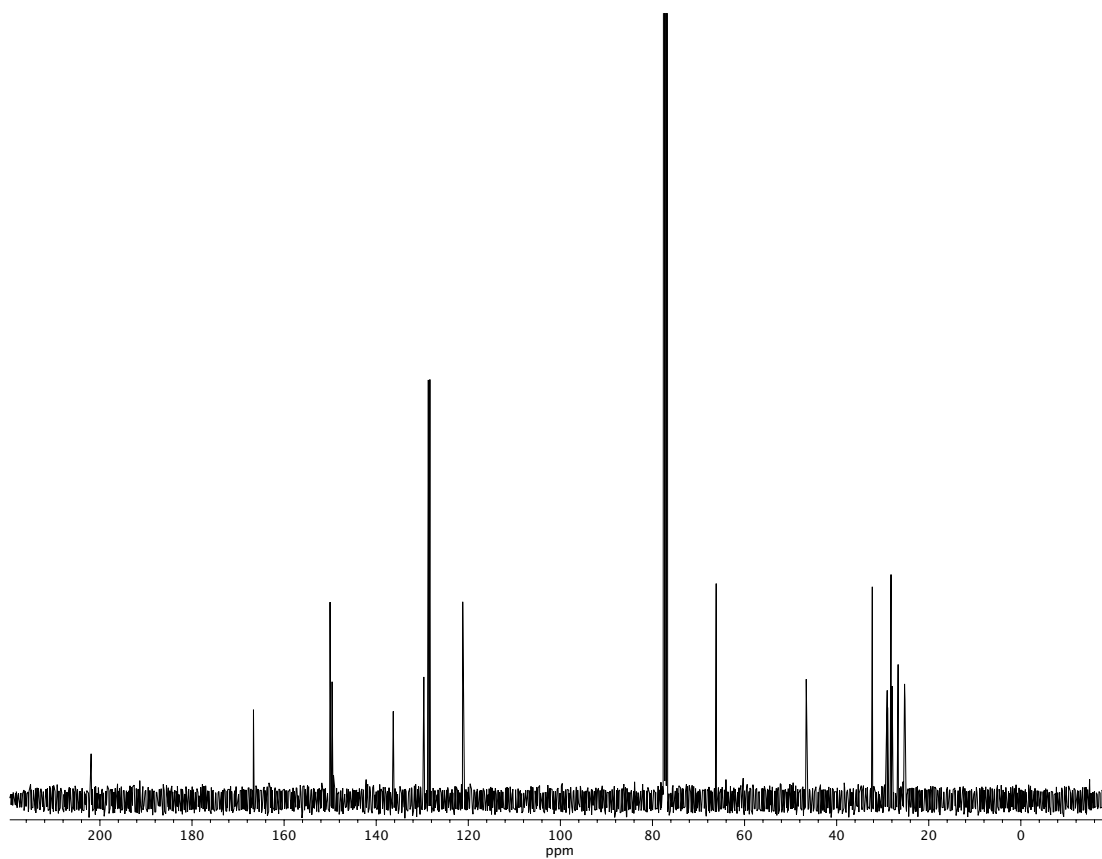
Figure A2.259. *^{13}C NMR (100 MHz, CDCl$_3$) of compound **D-49f**.*
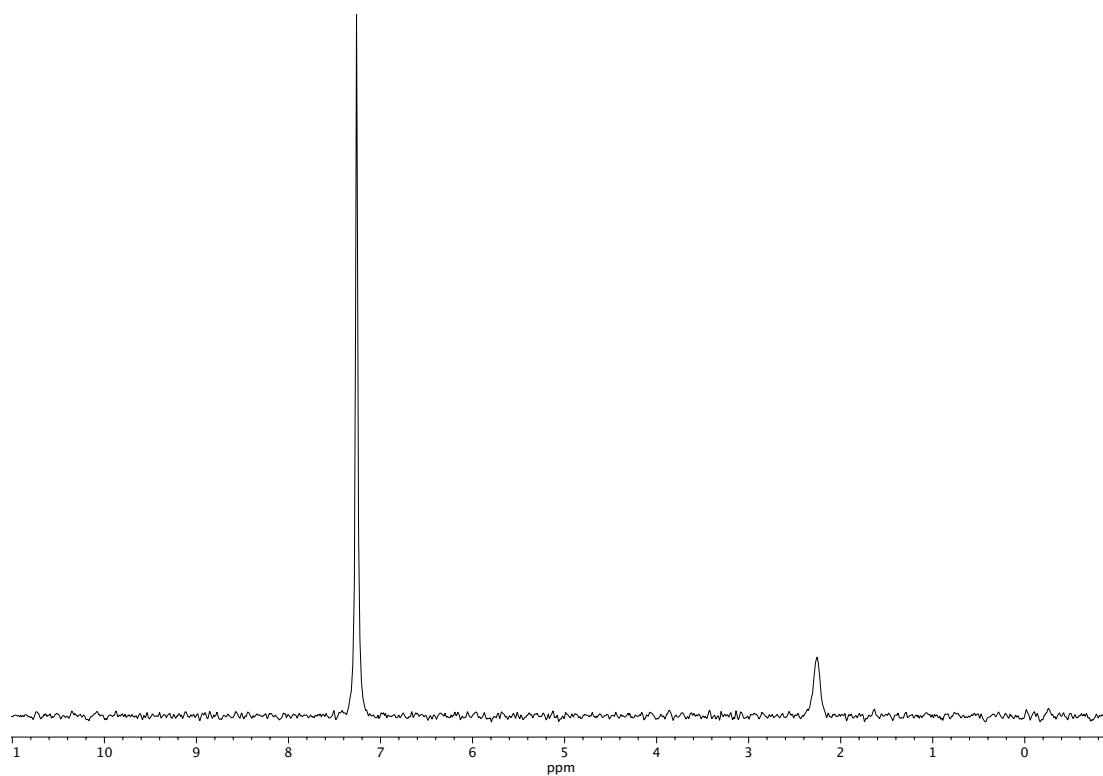
Figure A2.260. ^{2}H NMR (61 MHz, CHCl$_3$) of compound **D-49f**.
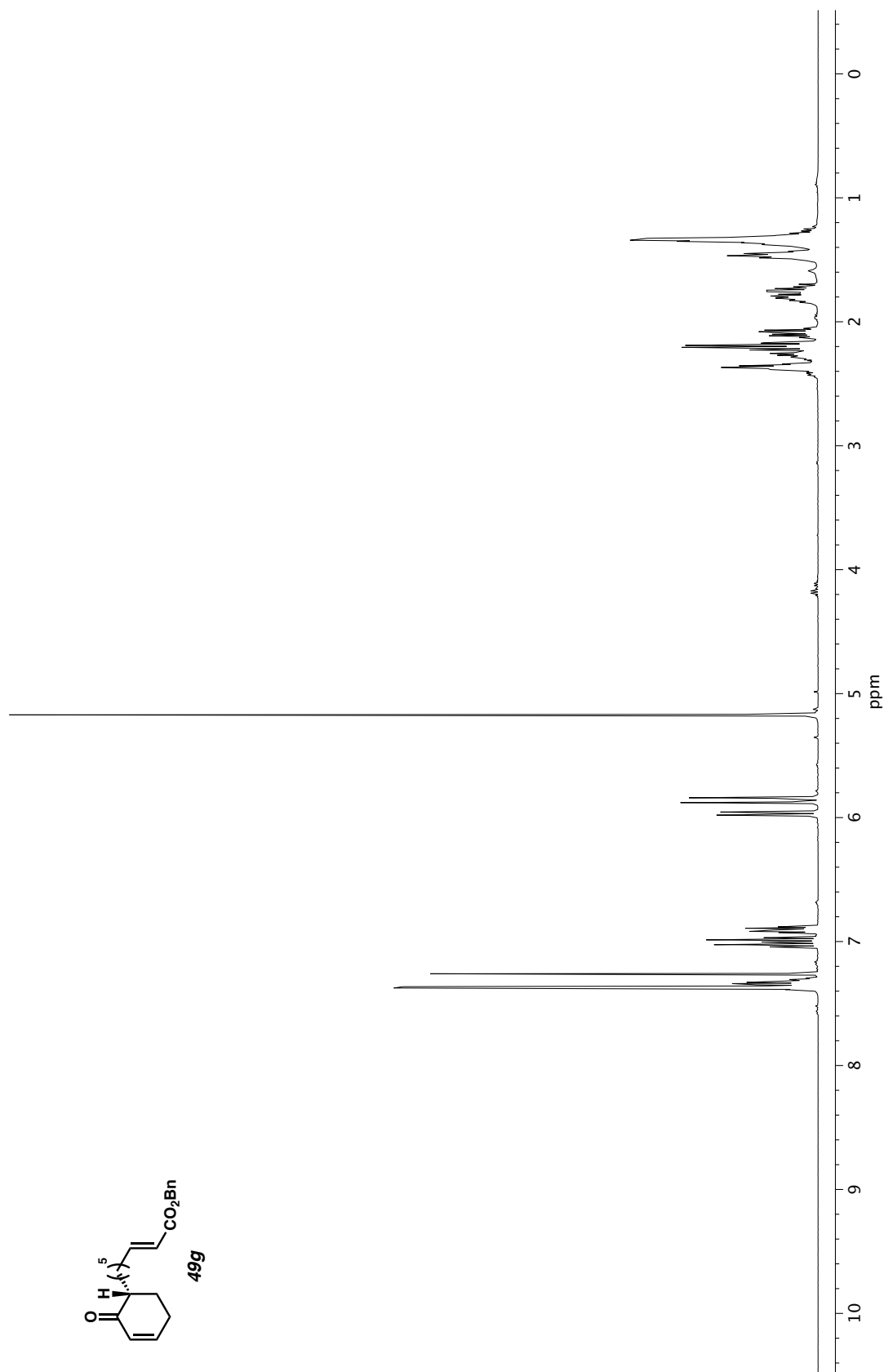
Figure A2.261. ^1H NMR (400 MHz, CDCl$_3$) of compound **49g**.
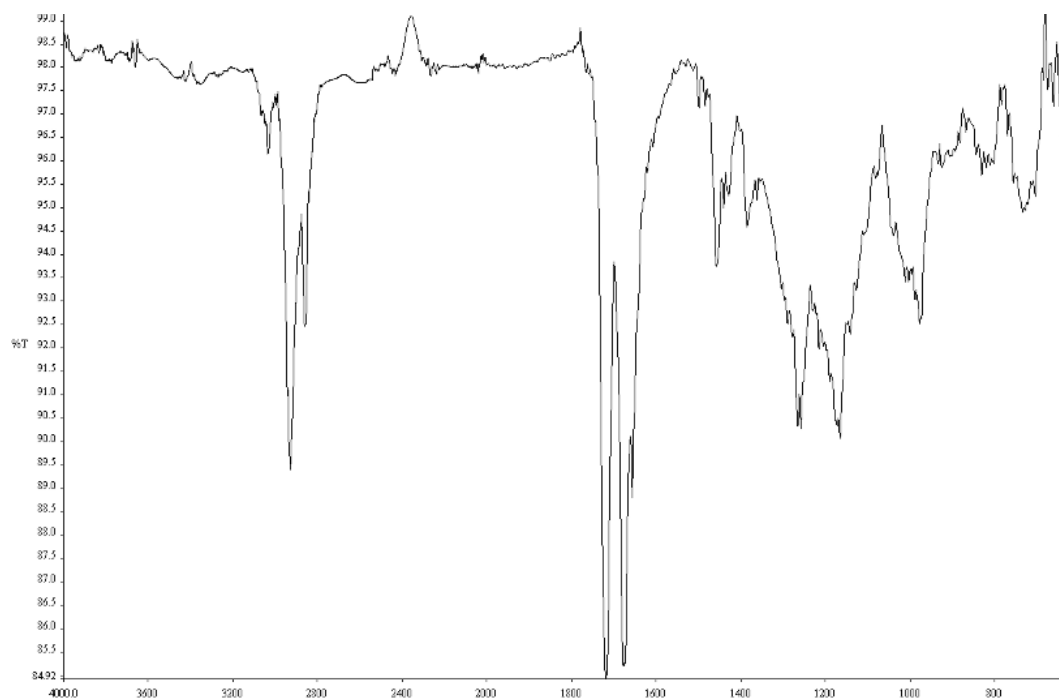
Figure A2.262. *Infrared spectrum (Thin Film, NaCl) of compound* **49g**.
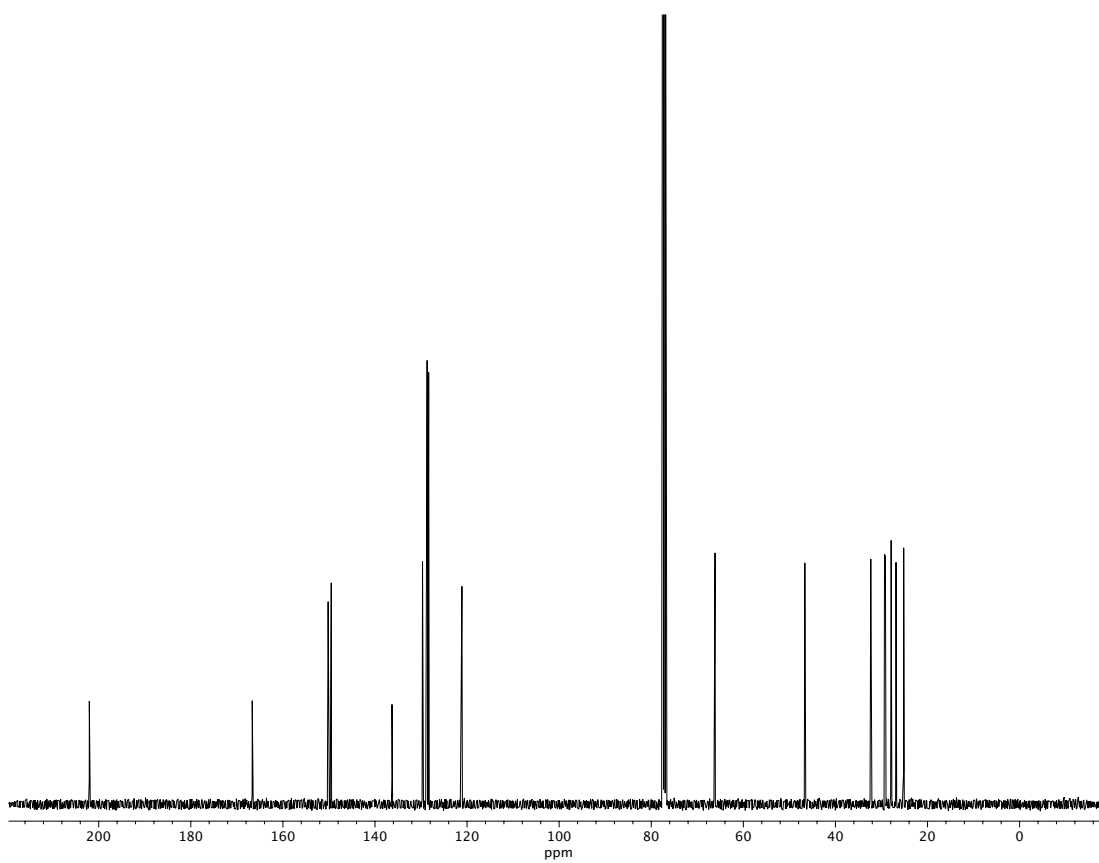
Figure A2.263. ^{13}C *NMR (100 MHz, CDCl$_3$) of compound* **49g**.
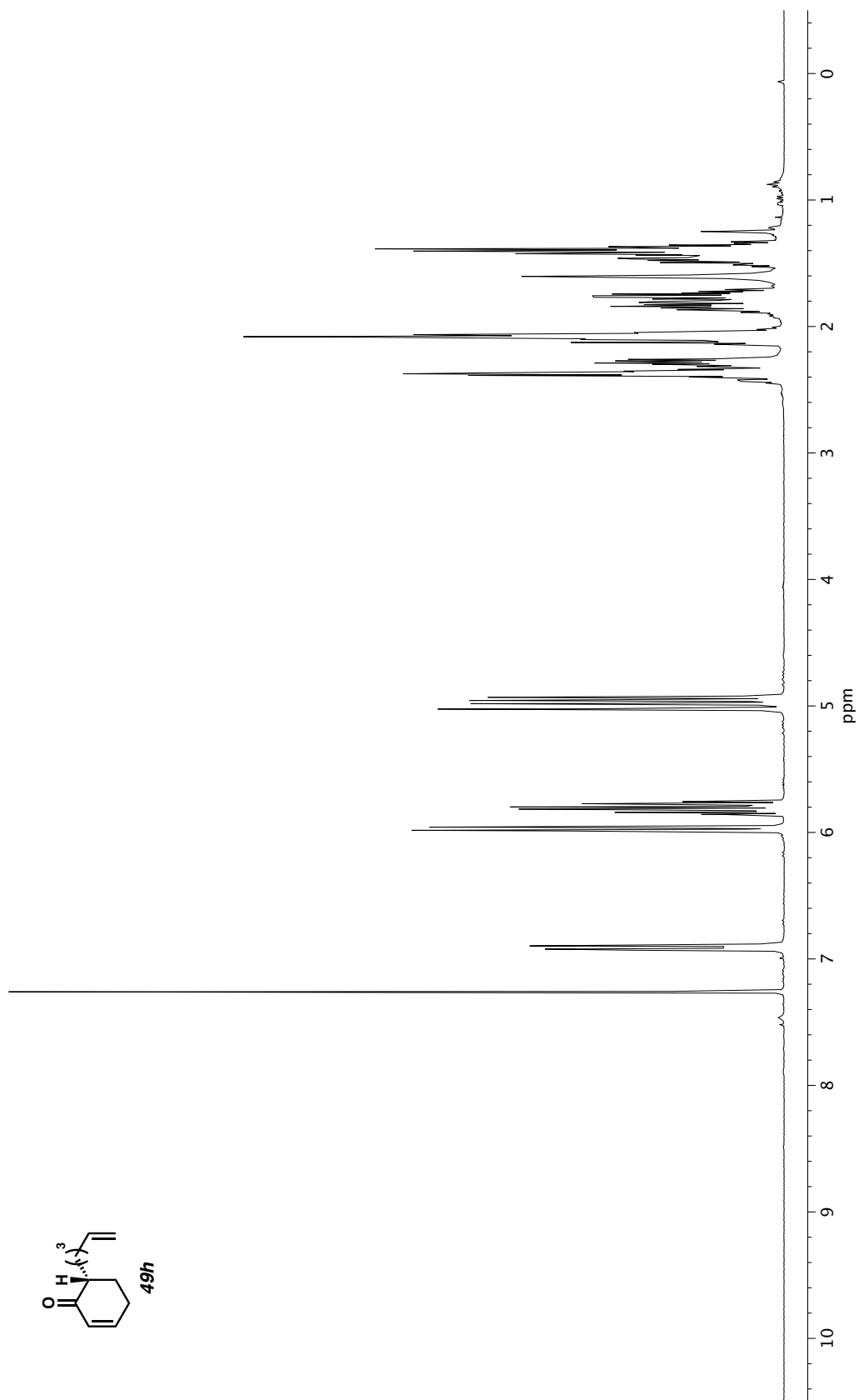
Figure A2.264. ^1H NMR (400 MHz, CDCl$_3$) of compound **49h**.
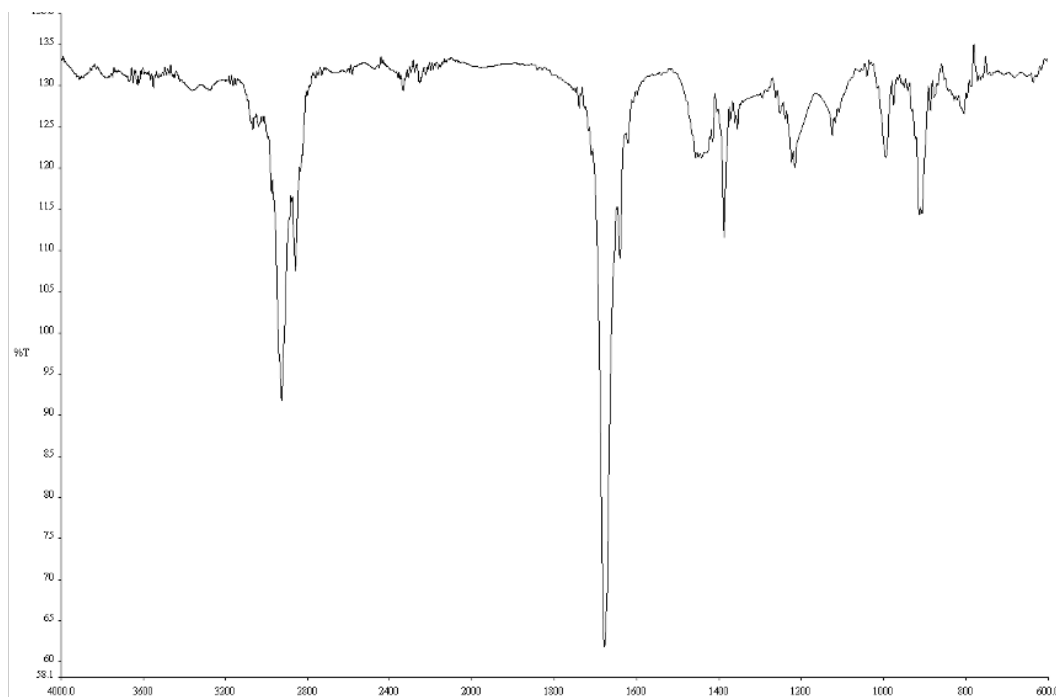
Figure A2.265. *Infrared spectrum (Thin Film, NaCl) of compound **49h**.*
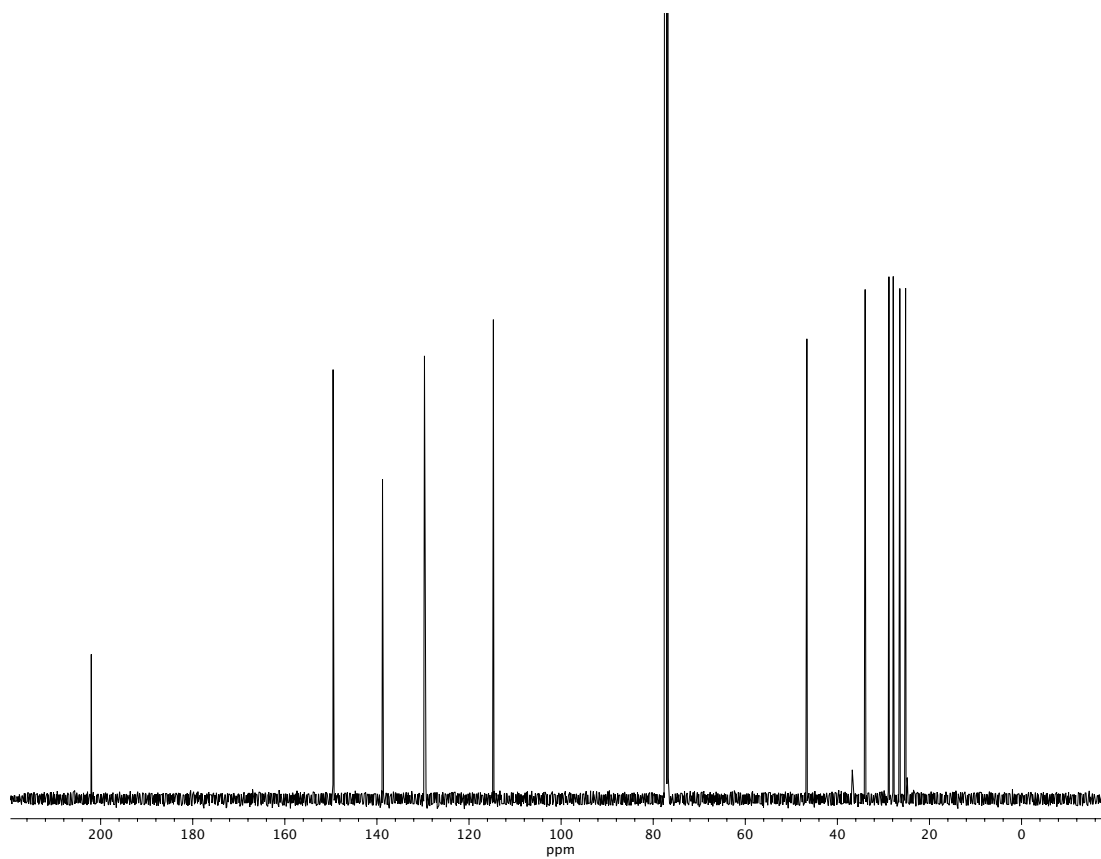
Figure A2.266. *^{13}C NMR (100 MHz, CDCl$_3$) of compound **49h**.*
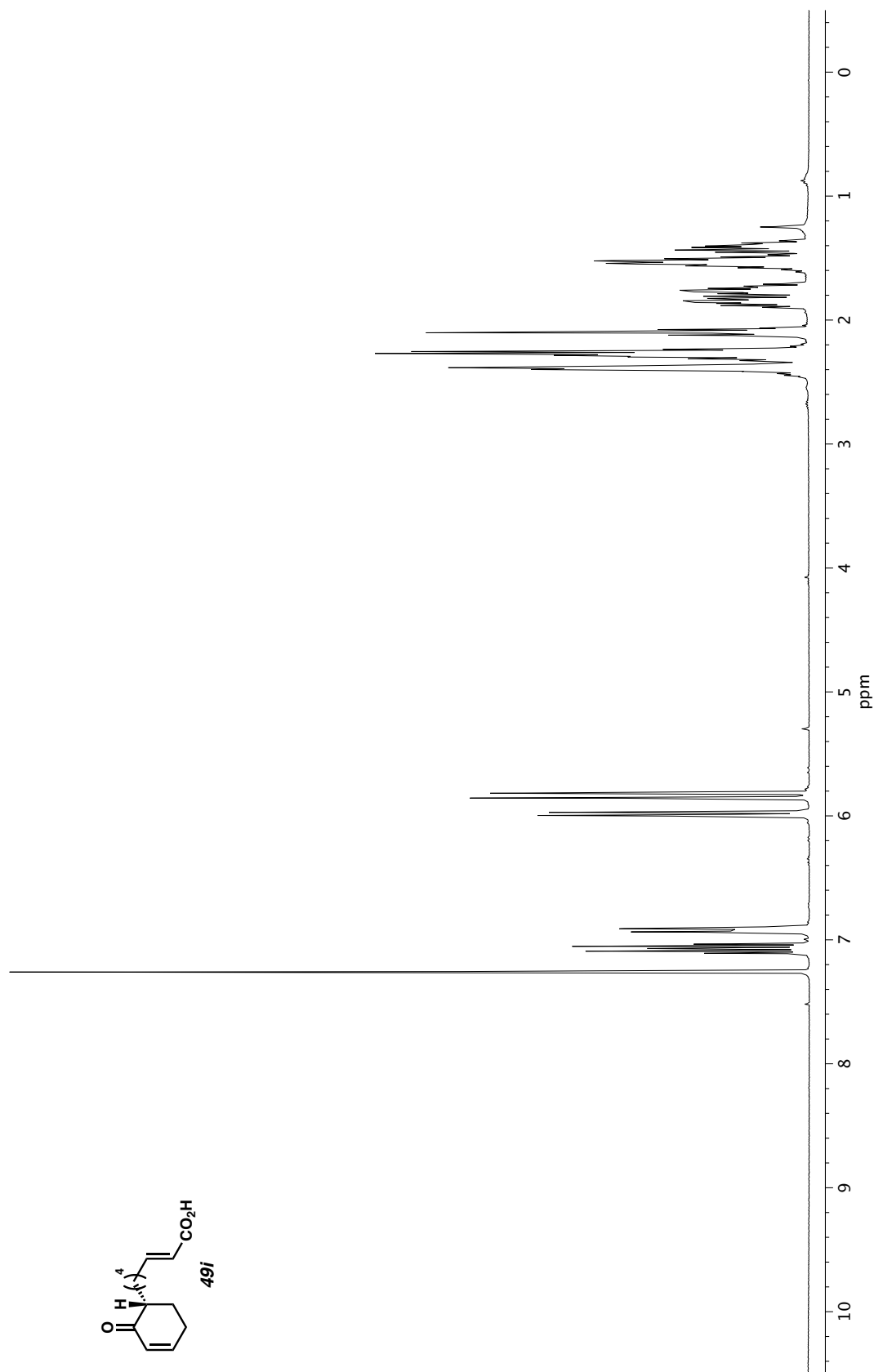
Figure A2.267. ^1H NMR (400 MHz, CDCl$_3$) of compound **49i**.
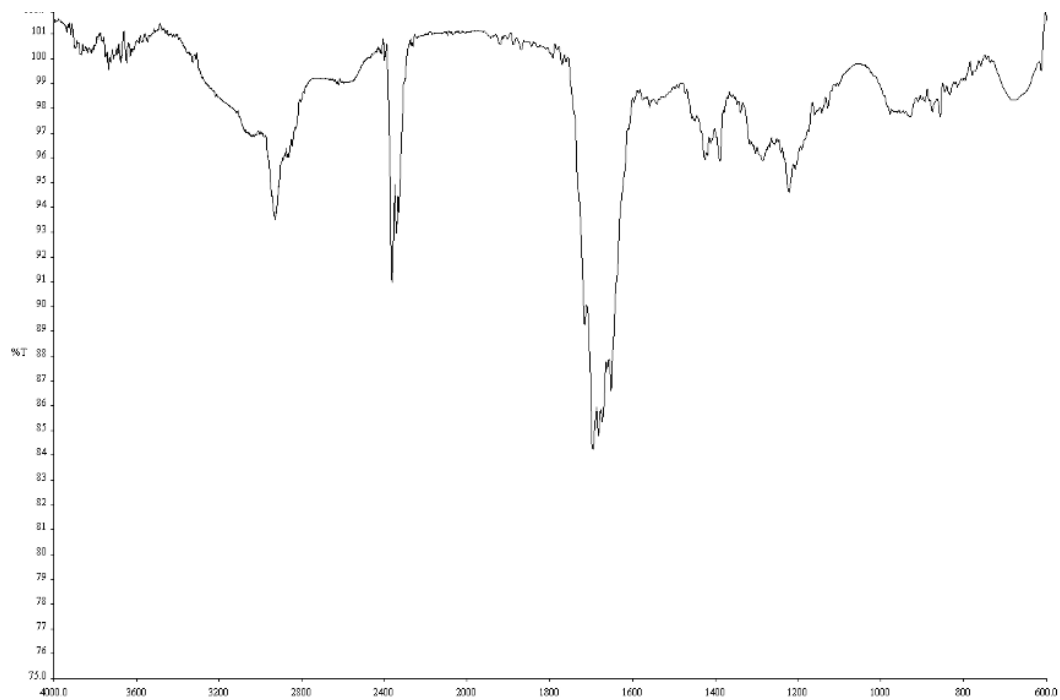
Figure A2.268. *Infrared spectrum (Thin Film, NaCl) of compound **49i**.*
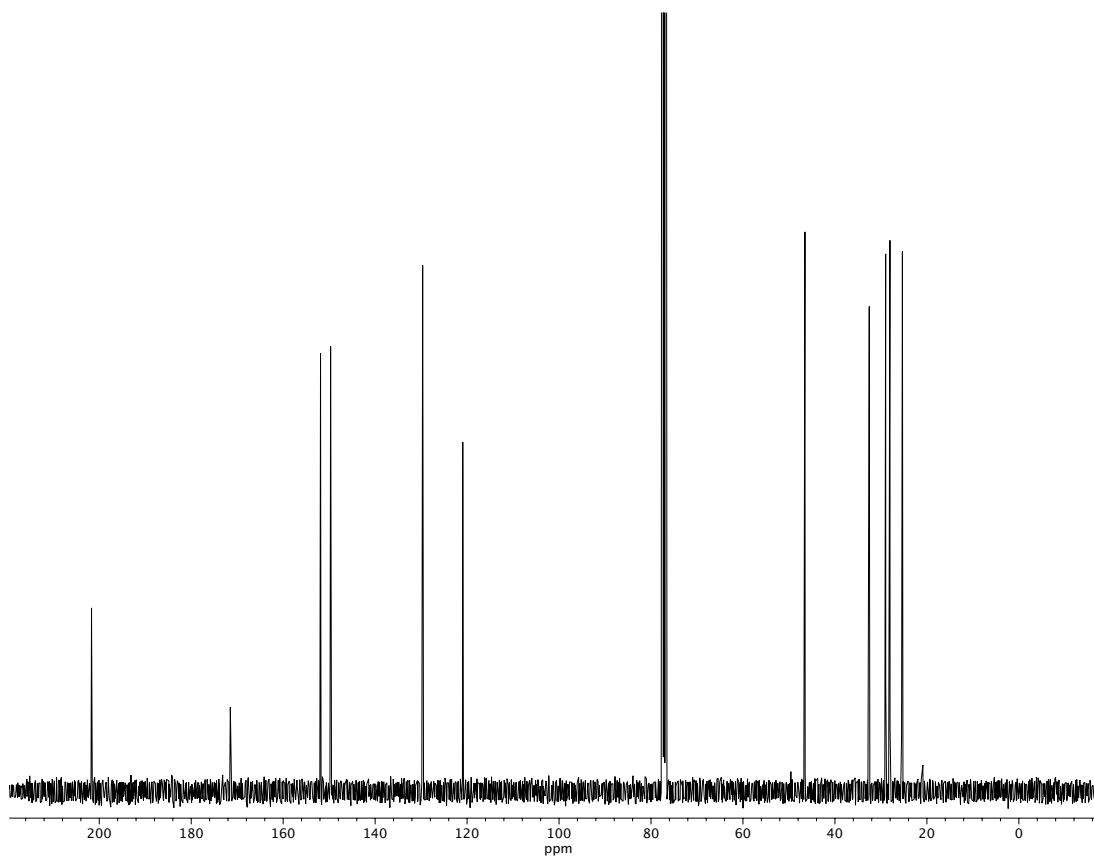
Figure A2.269. *^{13}C NMR (100 MHz, CDCl$_3$) of compound **49i**.*
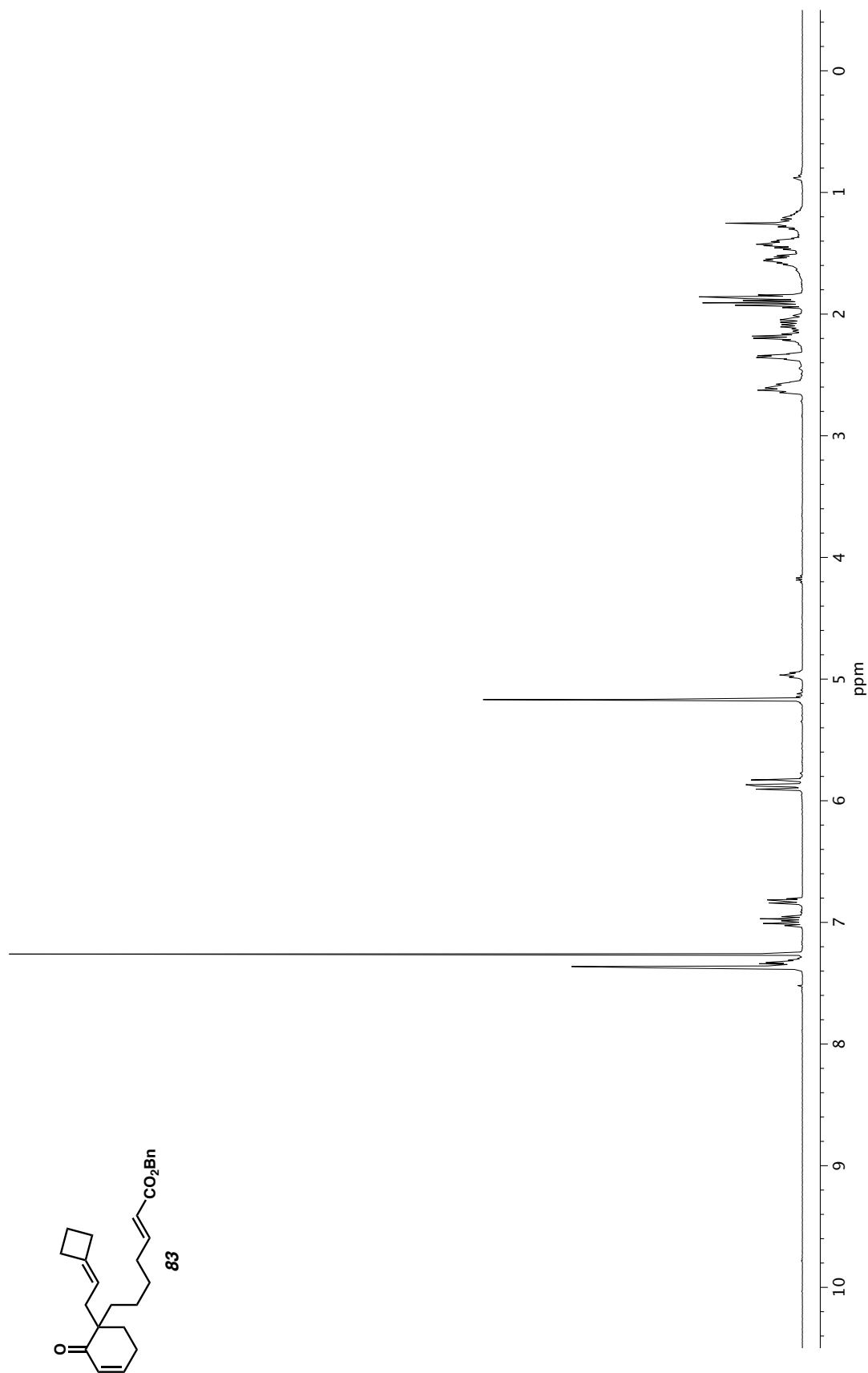
Figure A2.270. ^1H NMR (400 MHz, CDCl$_3$) of compound **83**.
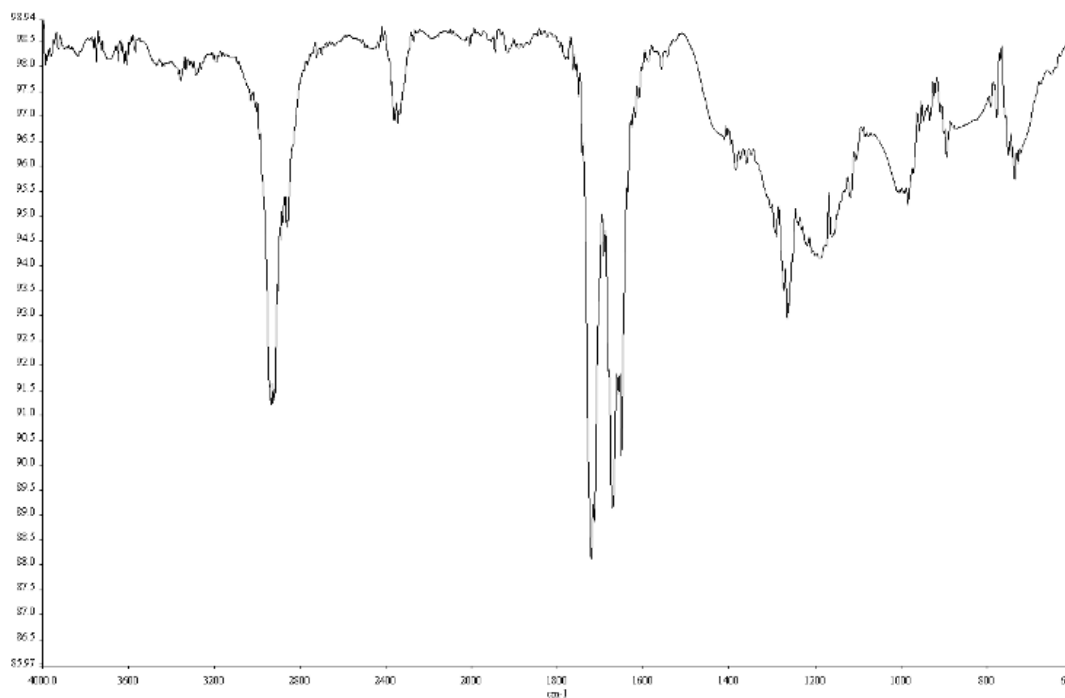
Figure A2.271. *Infrared spectrum (Thin Film, NaCl) of compound* **83**.
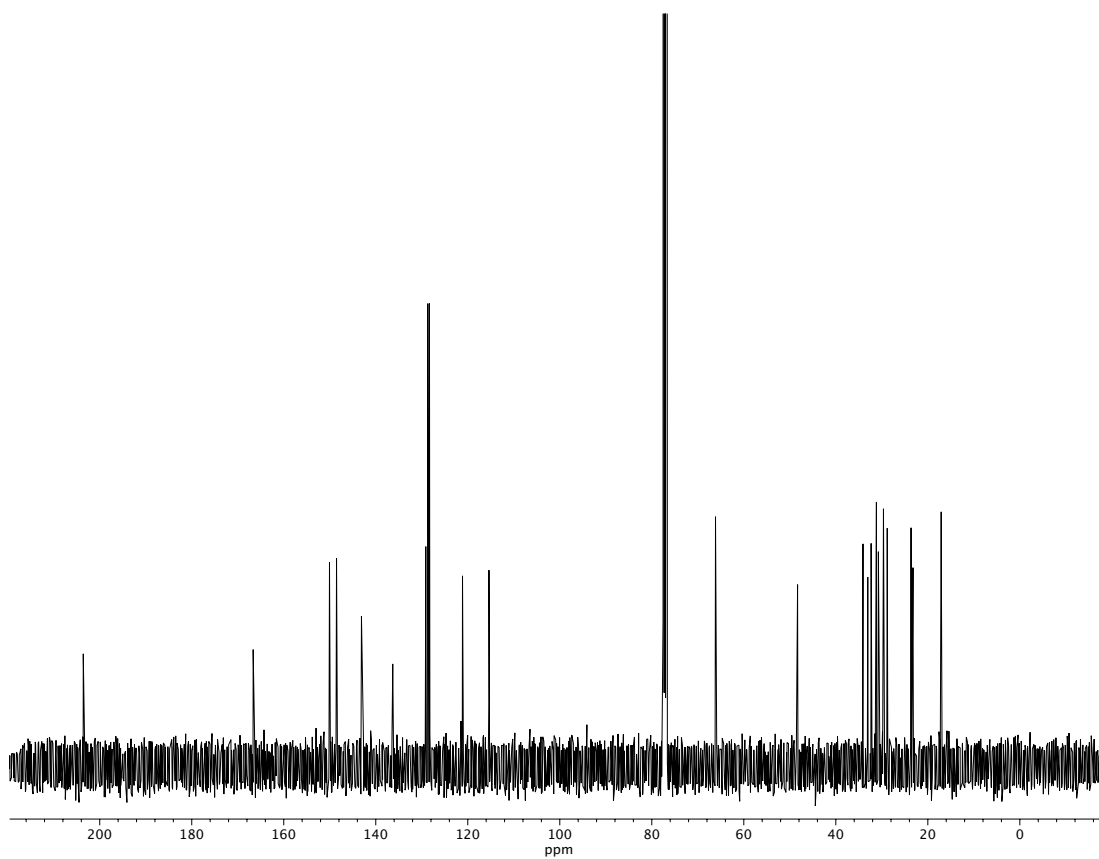
Figure A2.272. ^{13}C *NMR (100 MHz, CDCl$_3$) of compound* **83**.
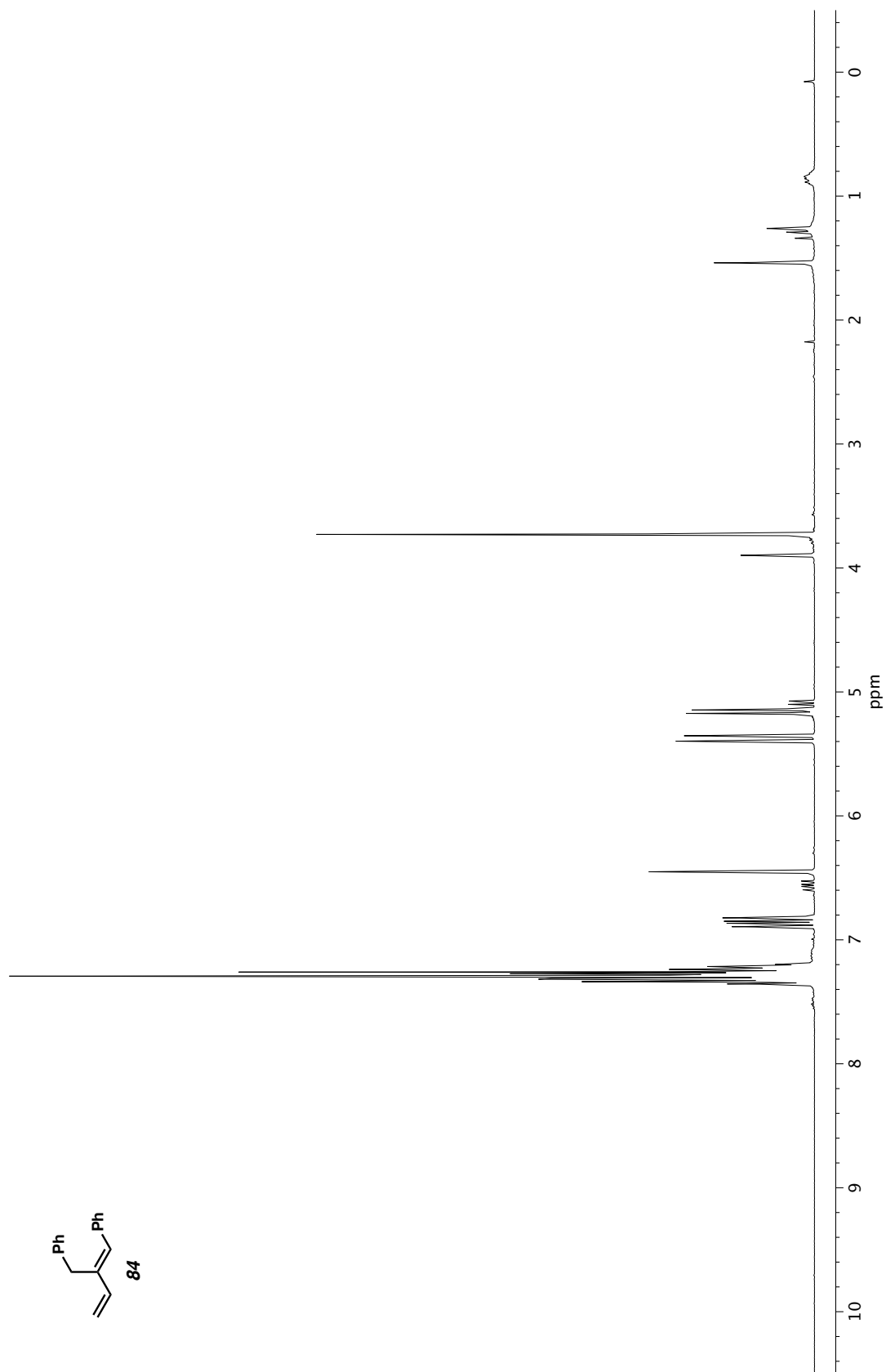
Figure A2.273. *^{1}H NMR (400 MHz, CDCl$_3$) of compound **84**.*
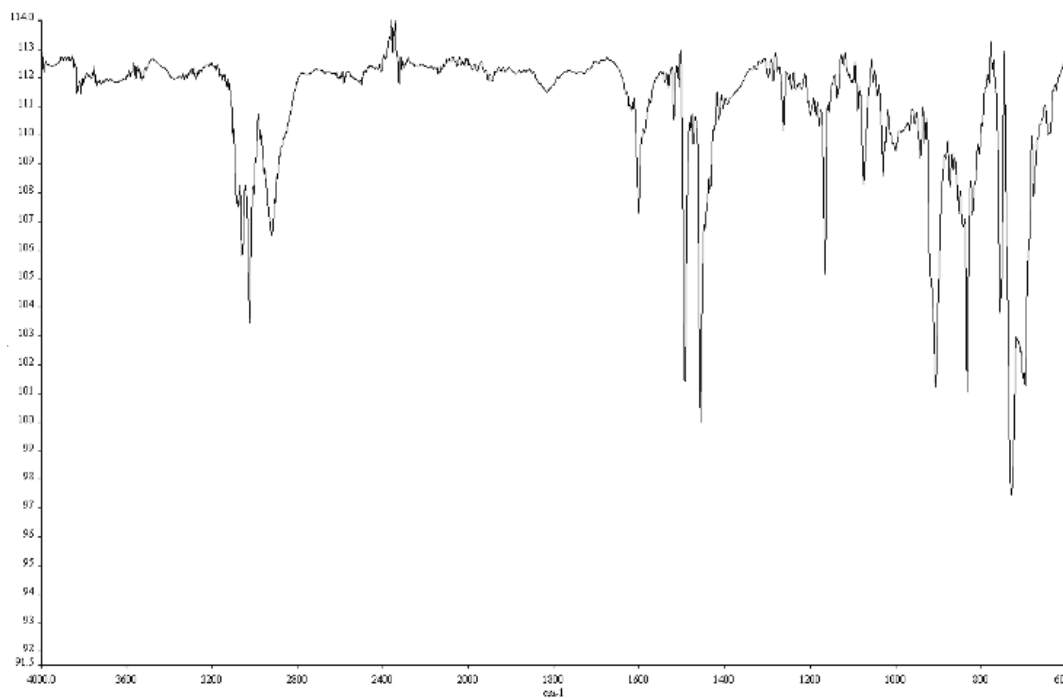
Figure A2.274. *Infrared spectrum (Thin Film, NaCl) of compound **84***.
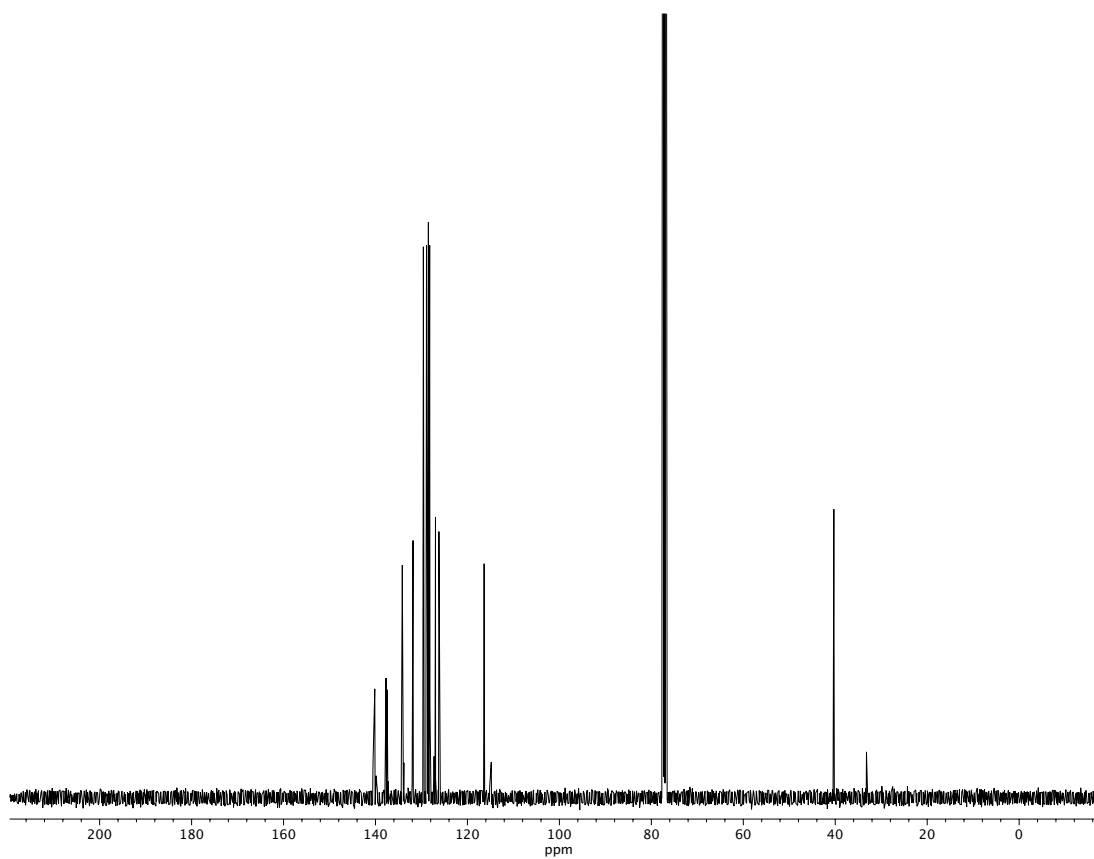
Figure A2.275. ^{13}C *NMR (100 MHz, CDCl$_3$) of compound **84***.
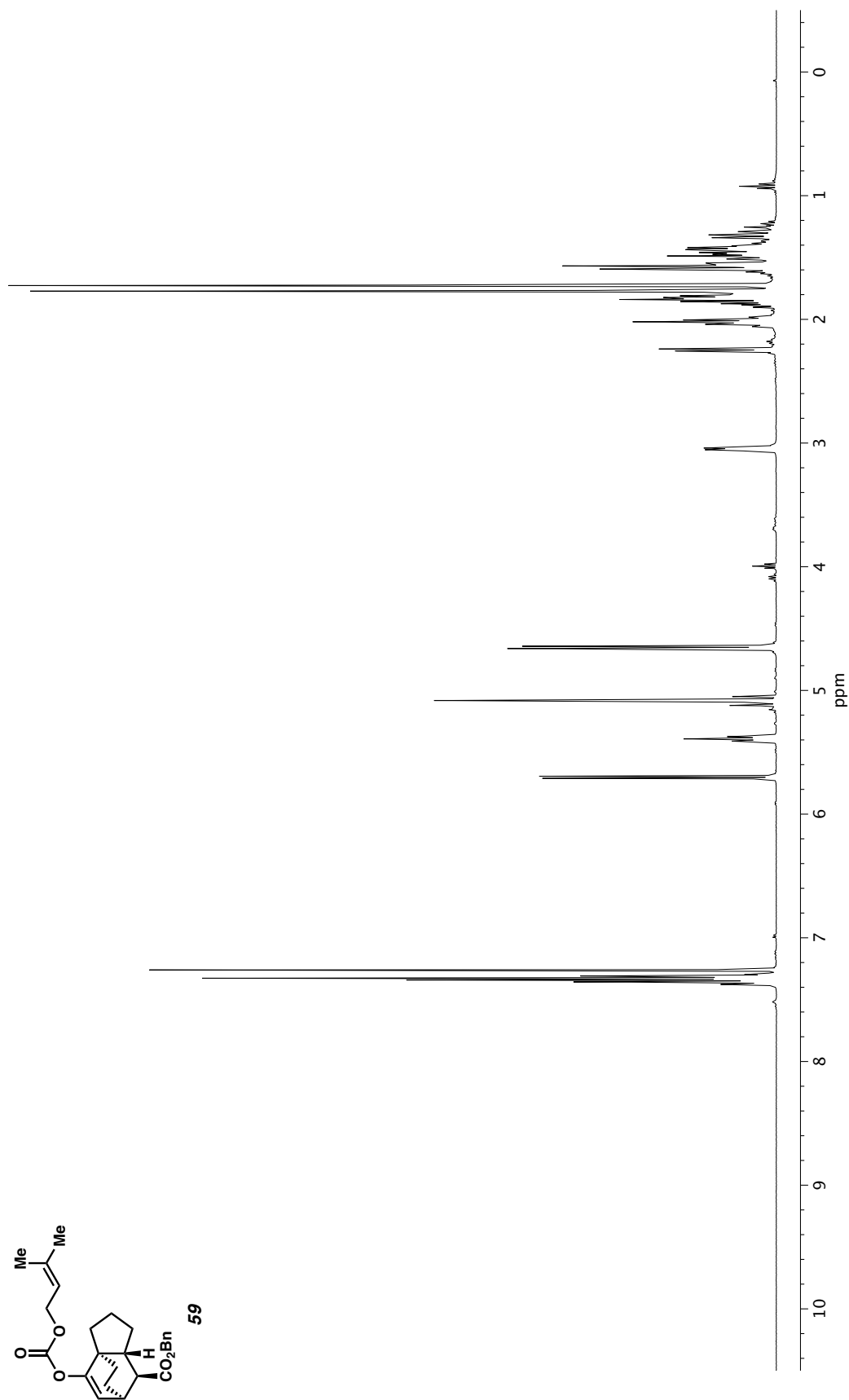
Figure A2.276. ^1H NMR (400 MHz, CDCl$_3$) of compound **59**.
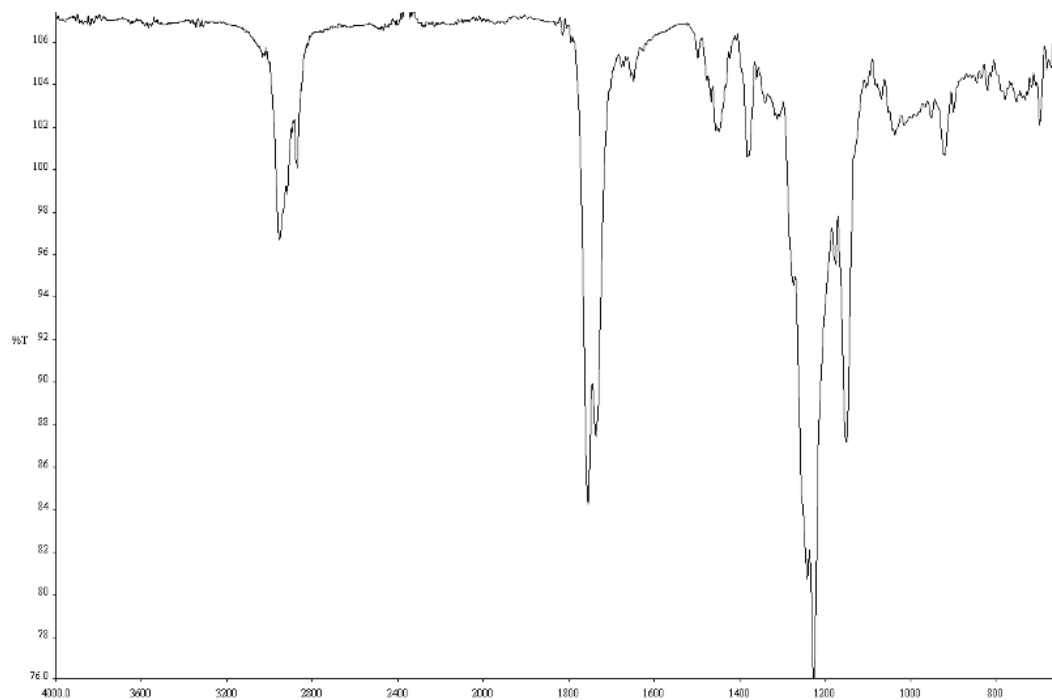
Figure A2.277. *Infrared spectrum (Thin Film, NaCl) of compound **59**.*
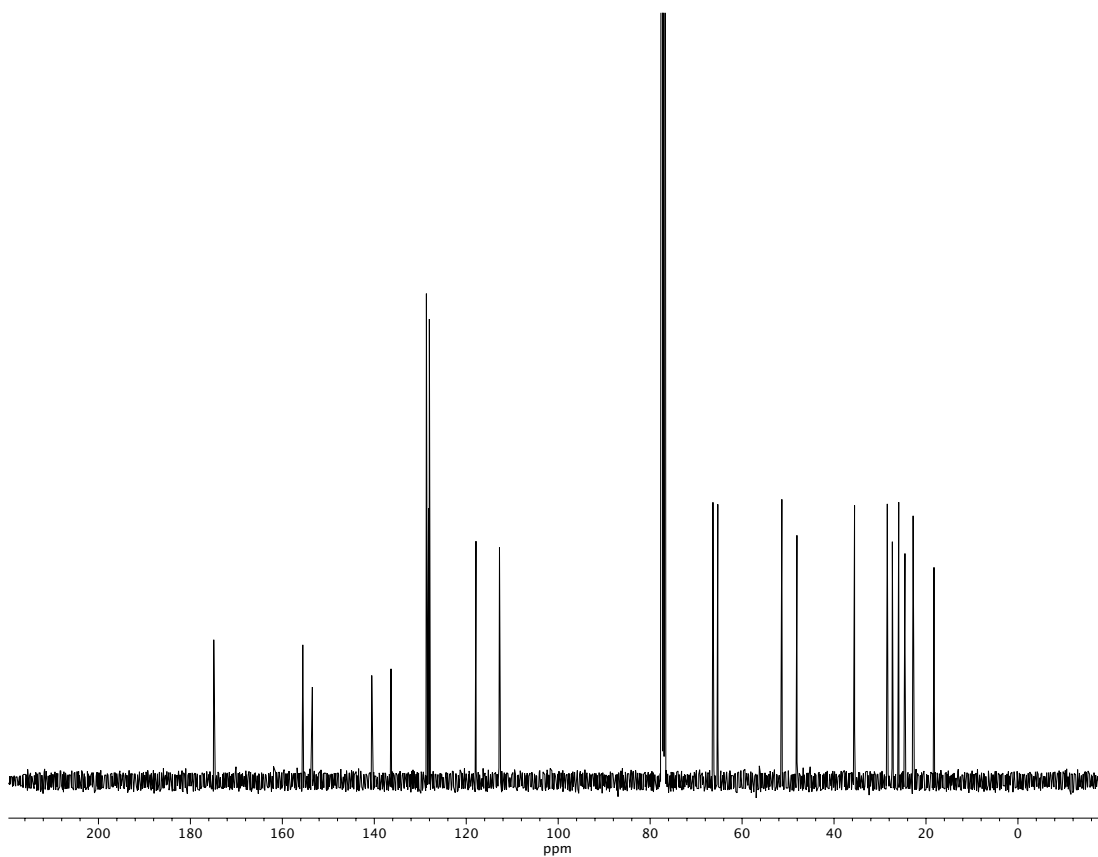
Figure A2.278. *^{13}C NMR (100 MHz, CDCl$_3$) of compound **59**.*
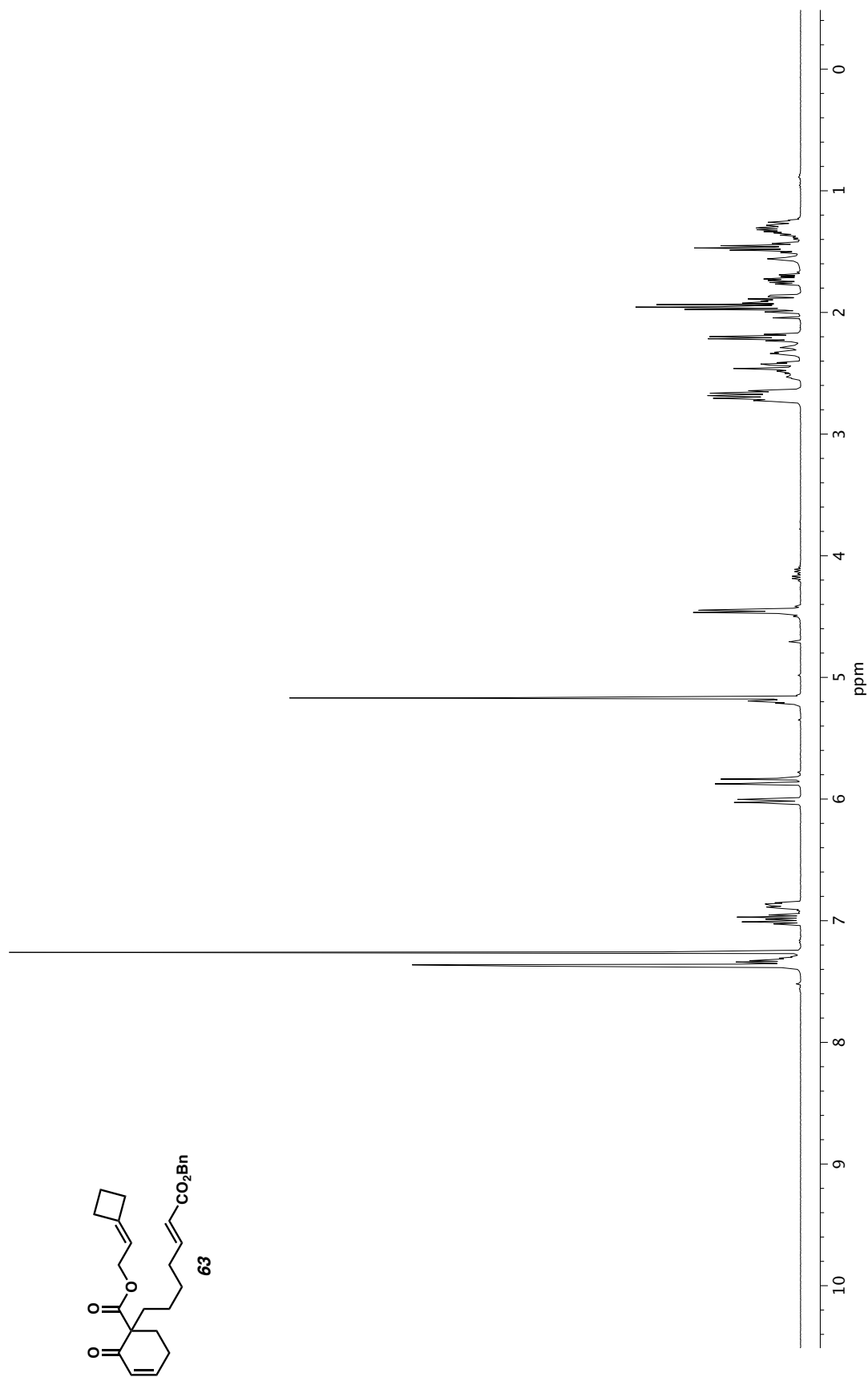
Figure A2.279. ^1H NMR (400 MHz, CDCl$_3$) of compound **63**.
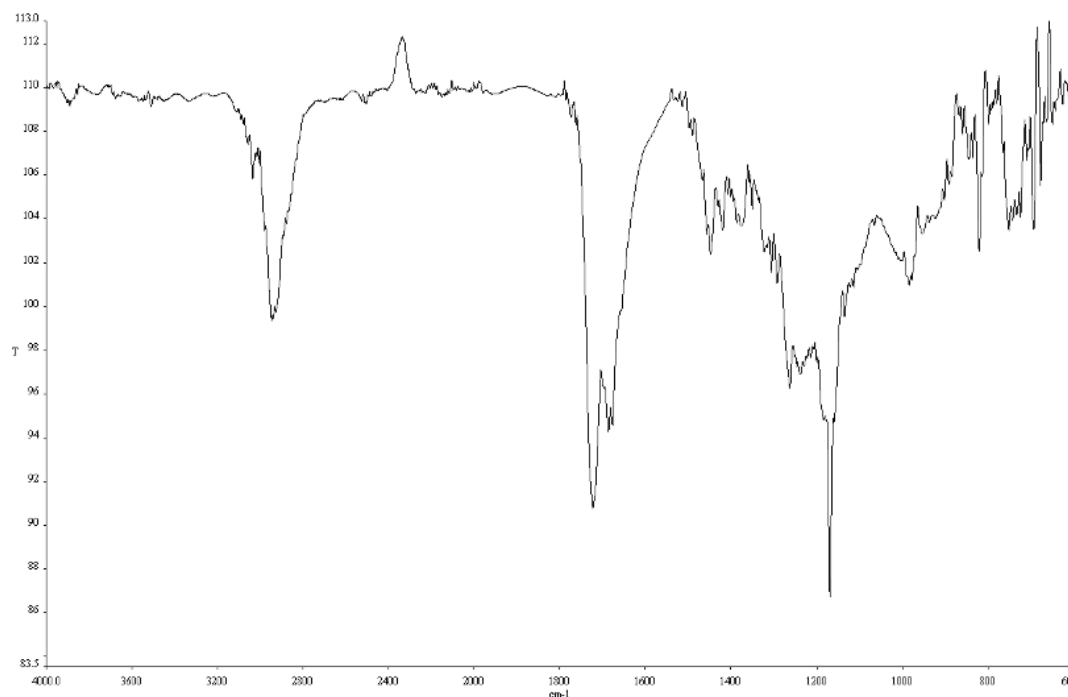
Figure A2.280. *Infrared spectrum (Thin Film, NaCl) of compound* **63**.
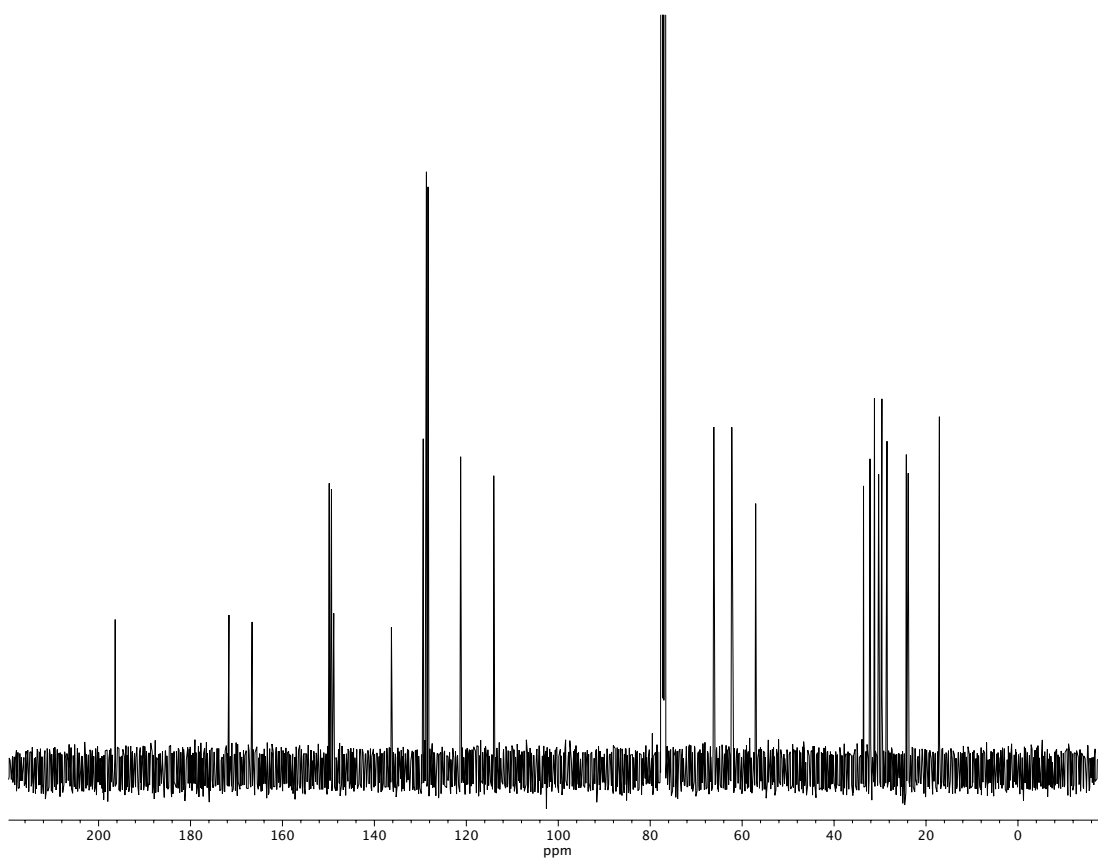
Figure A2.281. ^{13}C *NMR (100 MHz, CDCl$_3$) of compound* **63**.
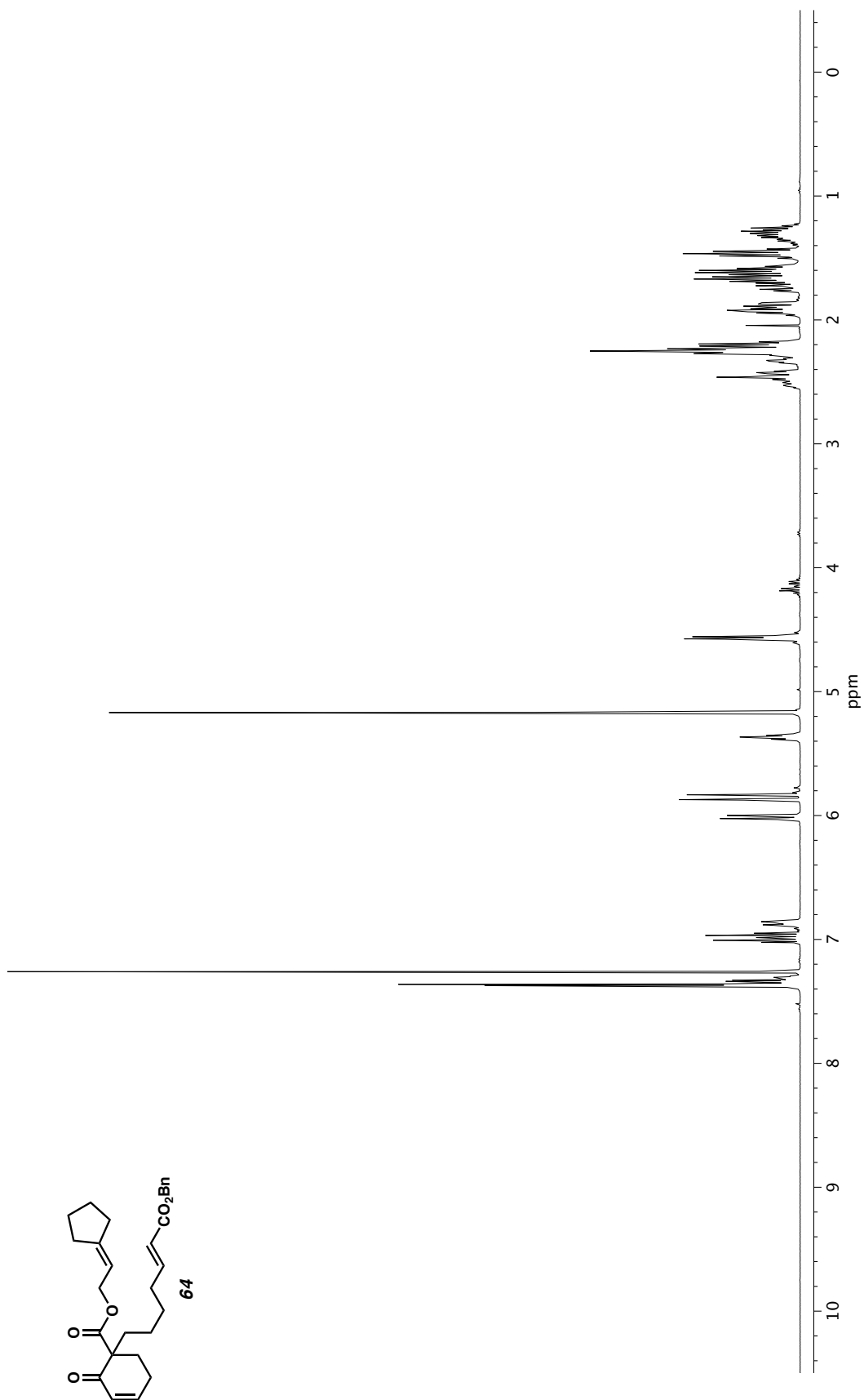
Figure A2.282. ^1H NMR (400 MHz, CDCl$_3$) of compound **64**.
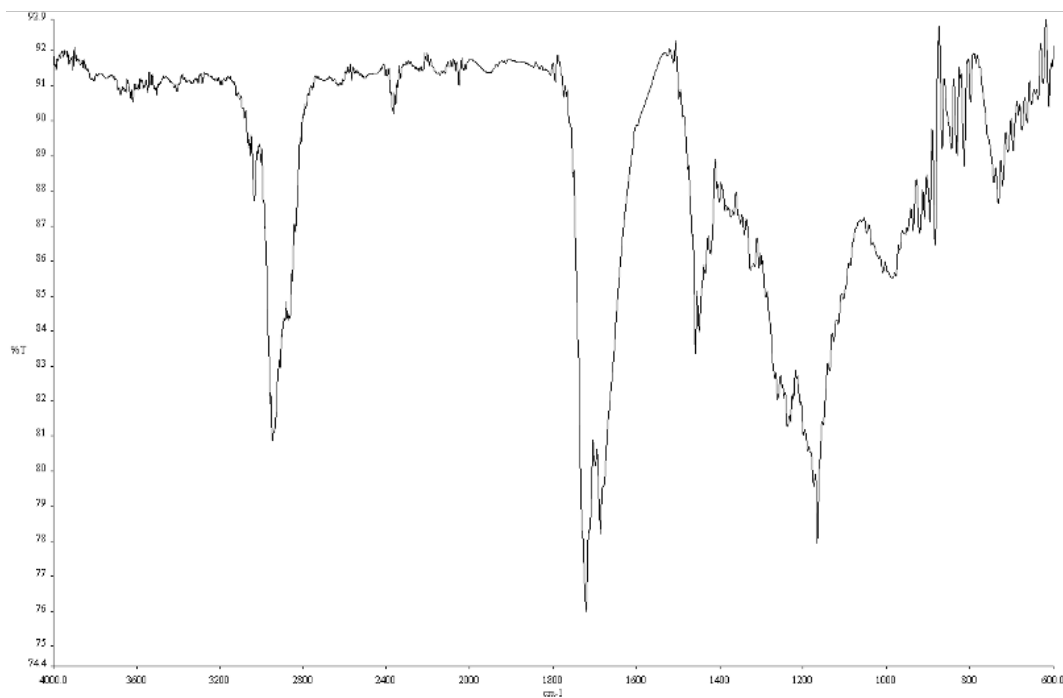
Figure A2.283. Infrared spectrum (Thin Film, NaCl) of compound **64**.
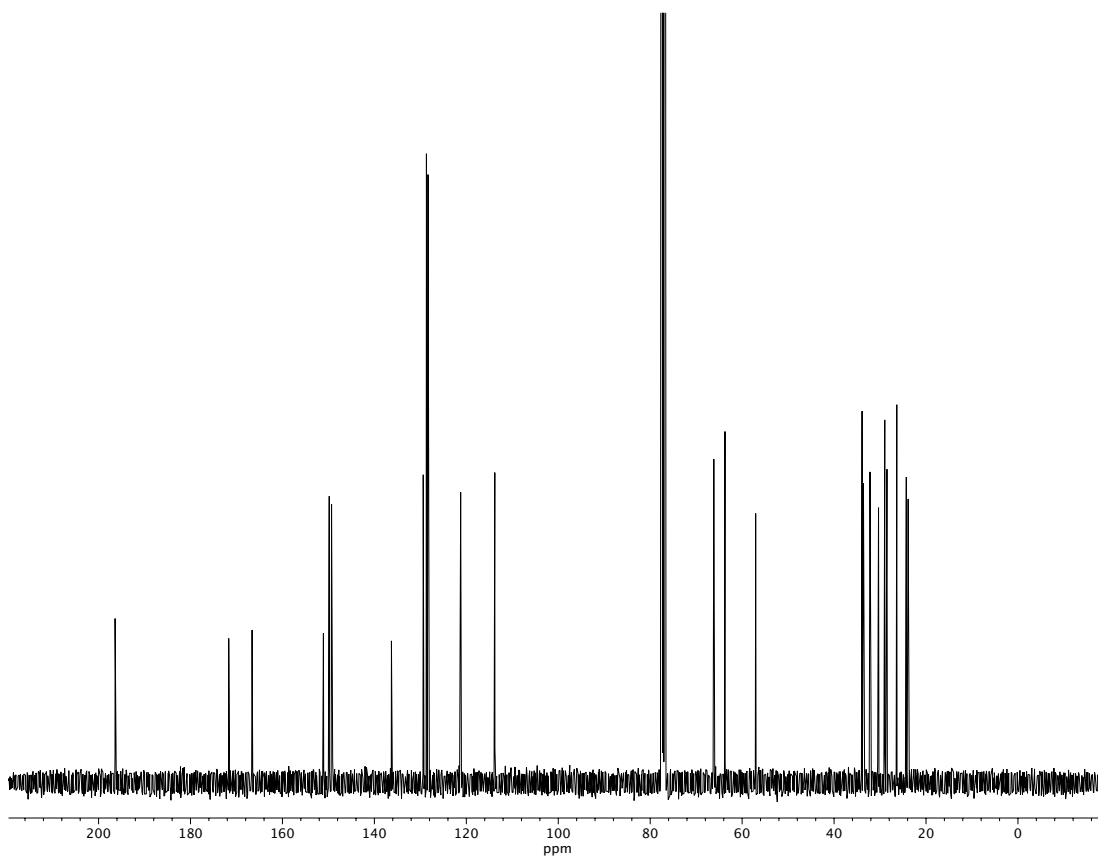
Figure A2.284. ^{13}C NMR (100 MHz, CDCl$_3$) of compound **64**.
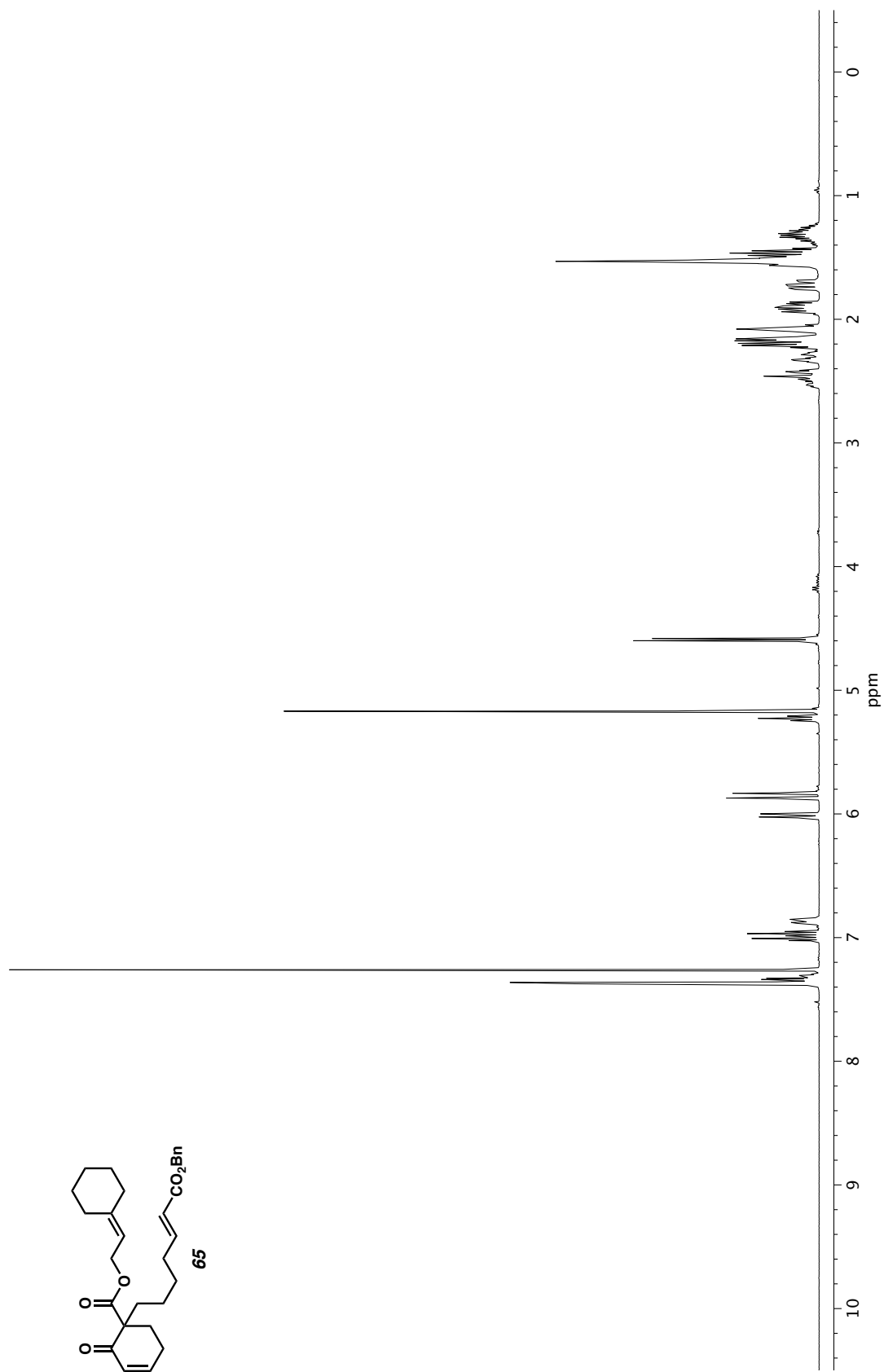
Figure A2.285. ^1H NMR (400 MHz, CDCl$_3$) of compound **65**.
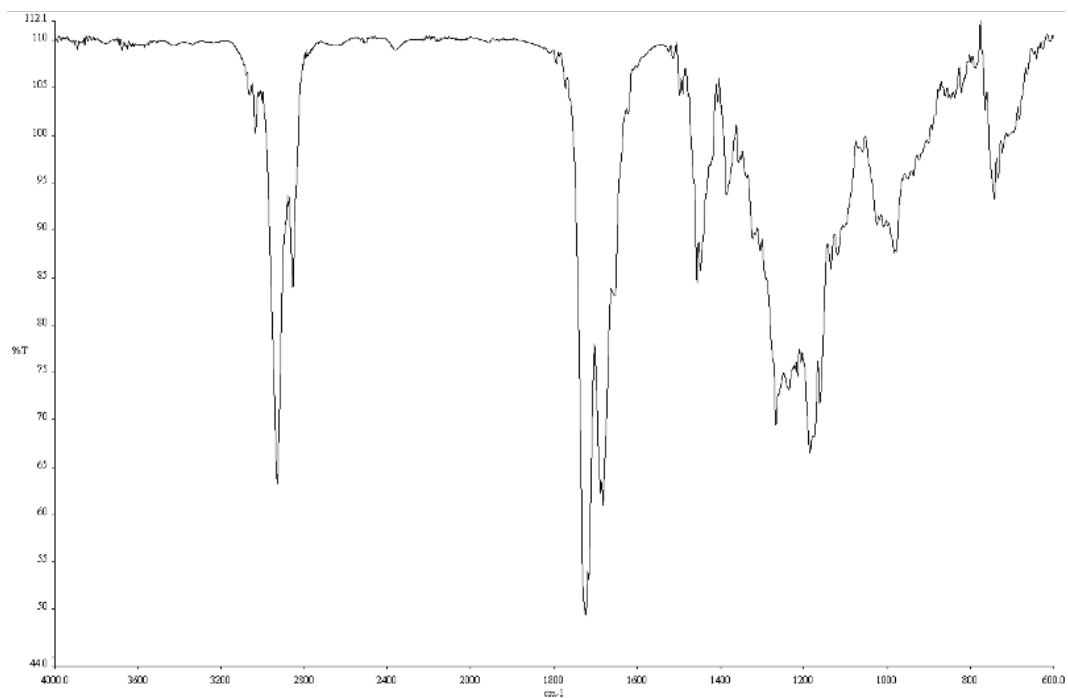
Figure A2.286. *Infrared spectrum (Thin Film, NaCl) of compound* **65**.
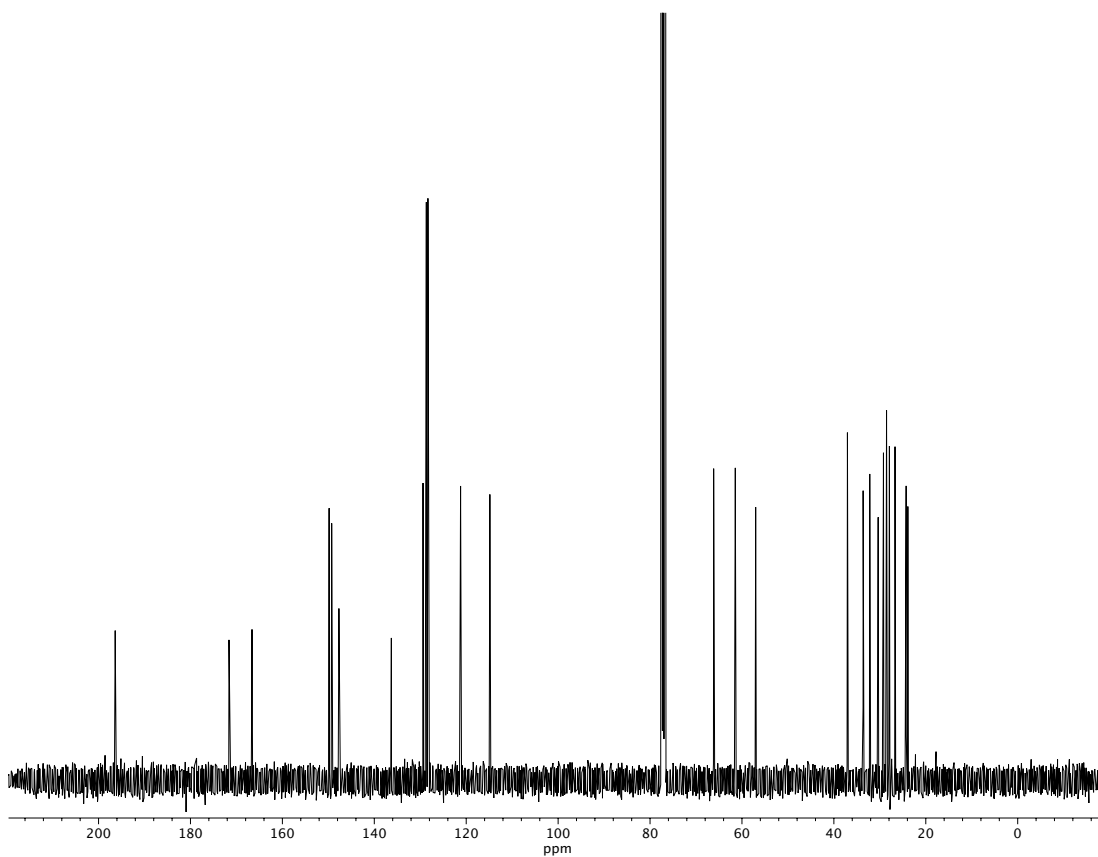
Figure A2.287. ^{13}C *NMR (100 MHz, CDCl₃) of compound* **65**.

Figure A2.288. ^1H NMR (400 MHz, CDCl$_3$) of compound **66**.
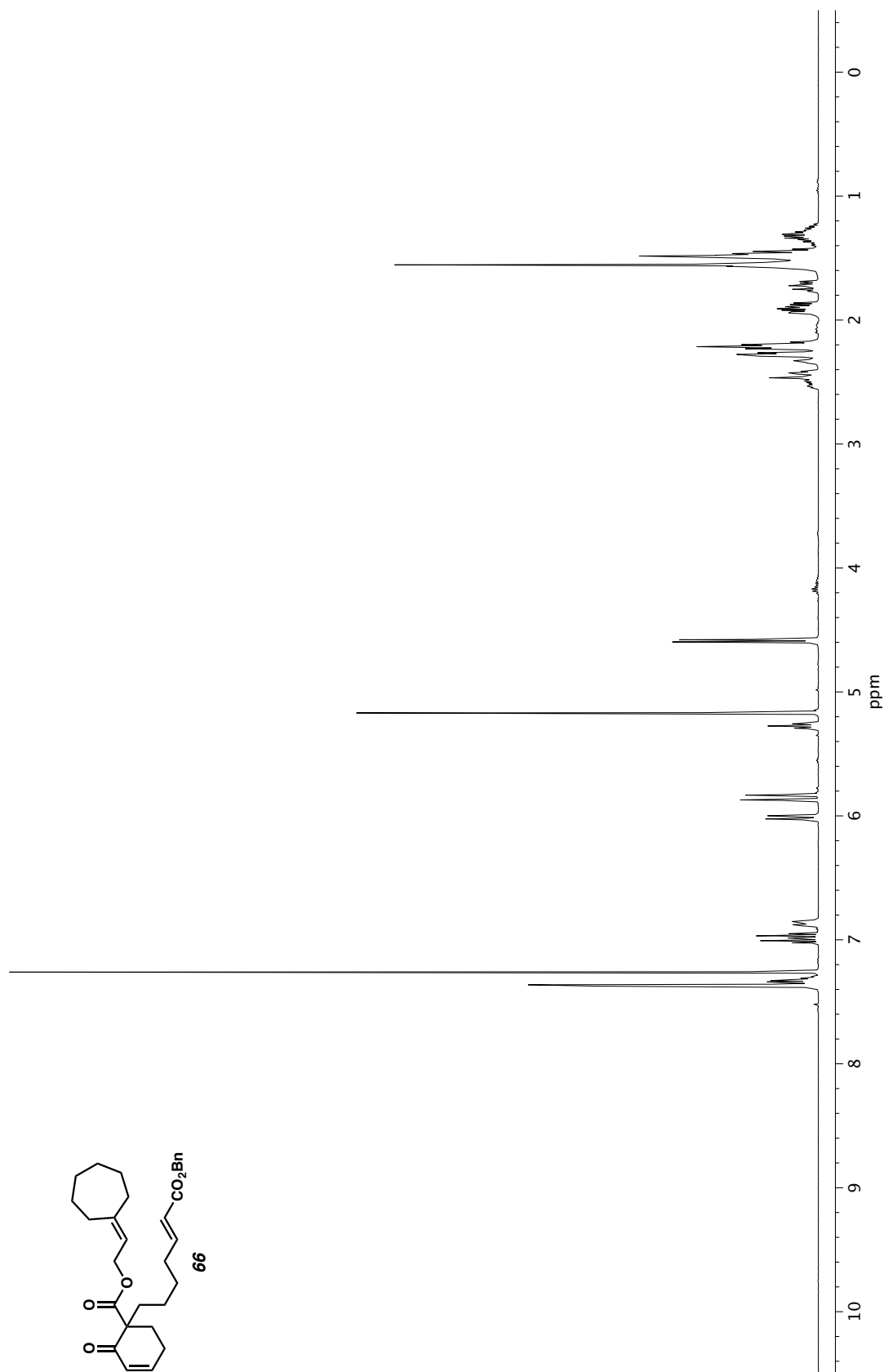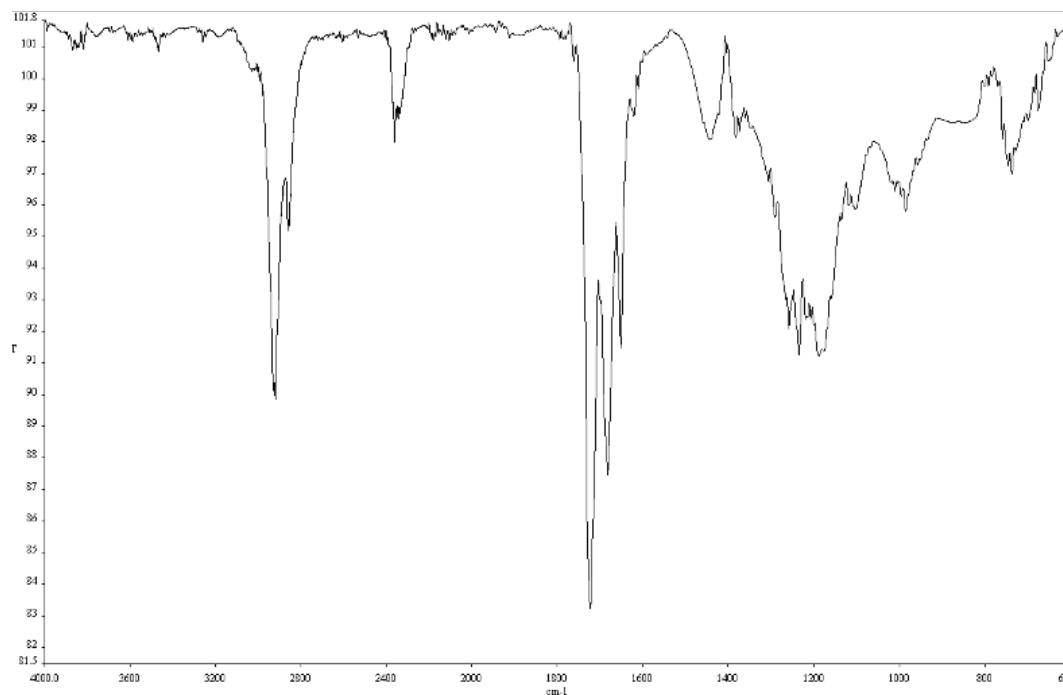
Figure A2.289. *Infrared spectrum (Thin Film, NaCl) of compound* **66**.
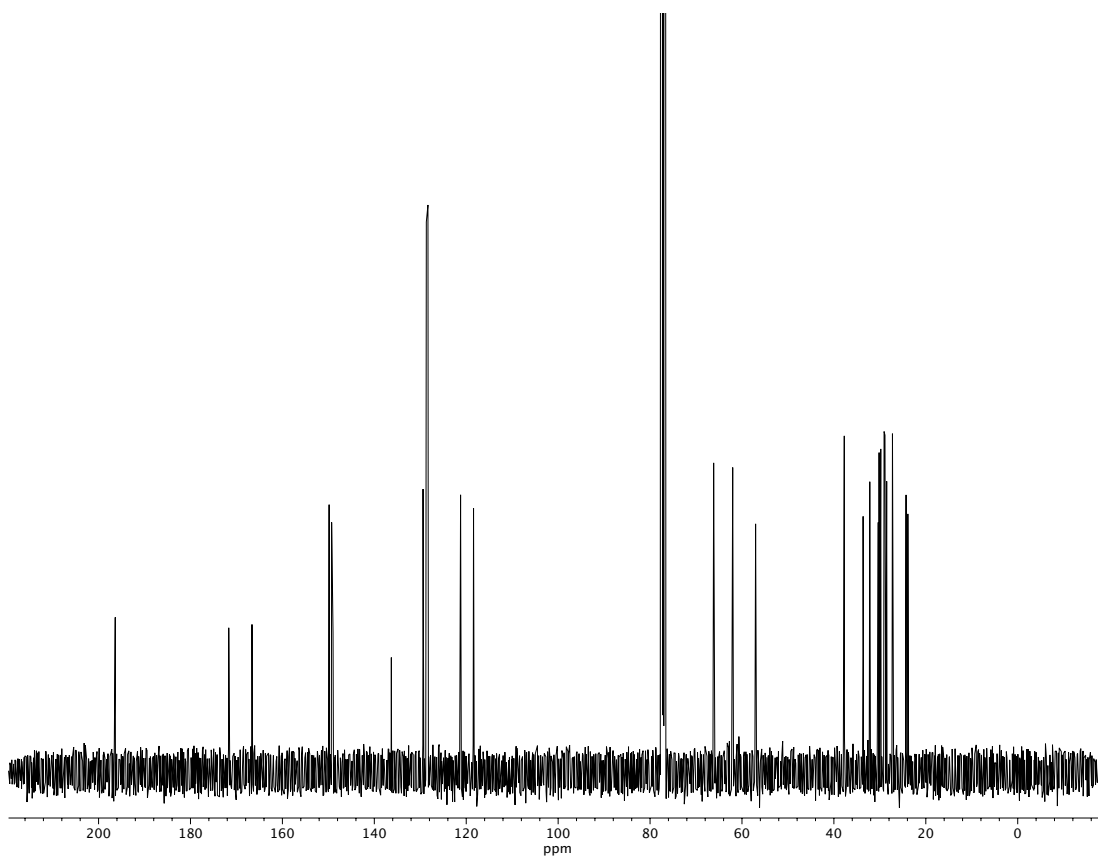
Figure A2.290. ^{13}C *NMR (100 MHz, CDCl$_3$) of compound* **66**.
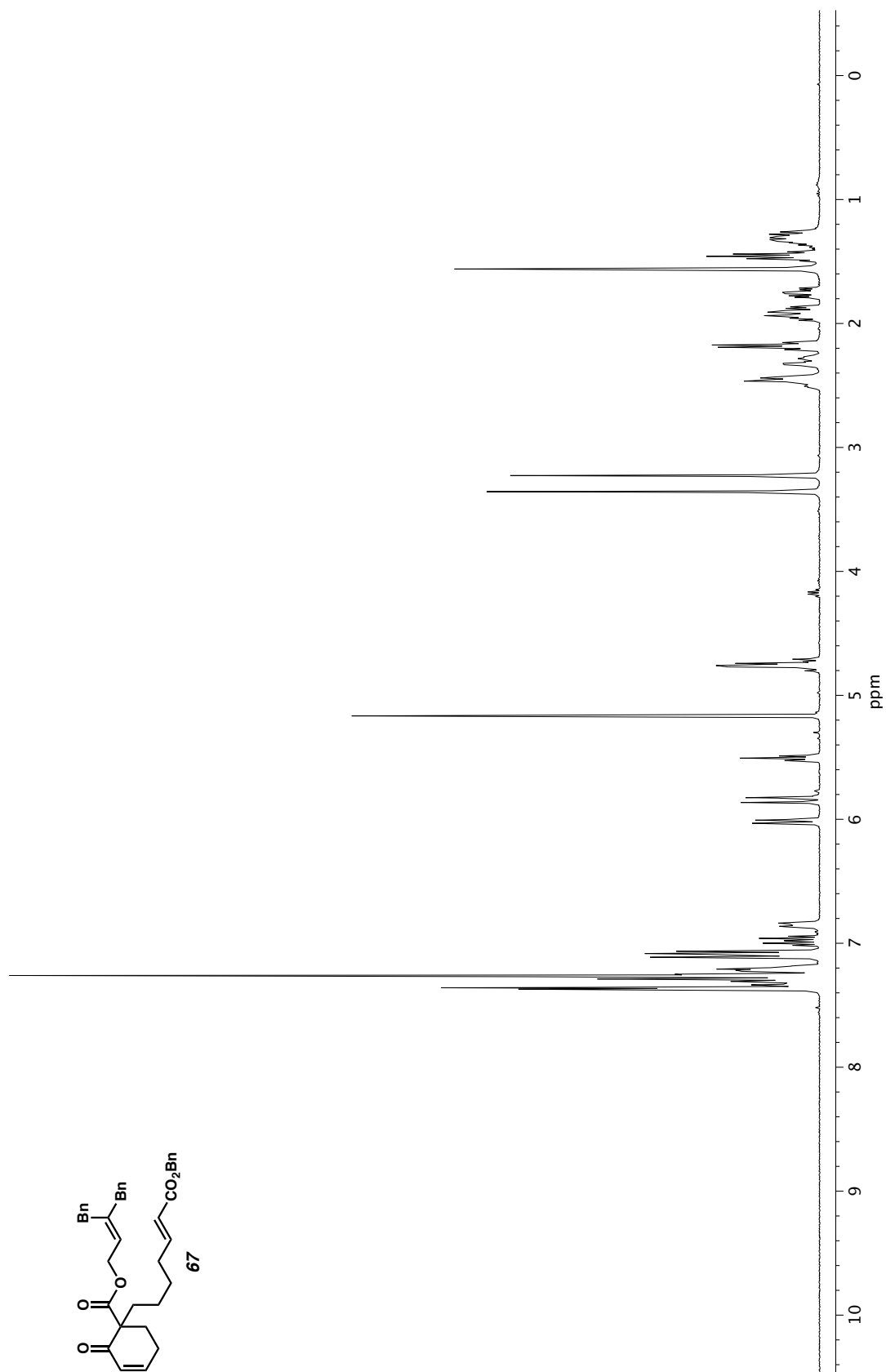
Figure A2.291. *^{1}H NMR (400 MHz, CDCl$_3$) of compound **67**.*
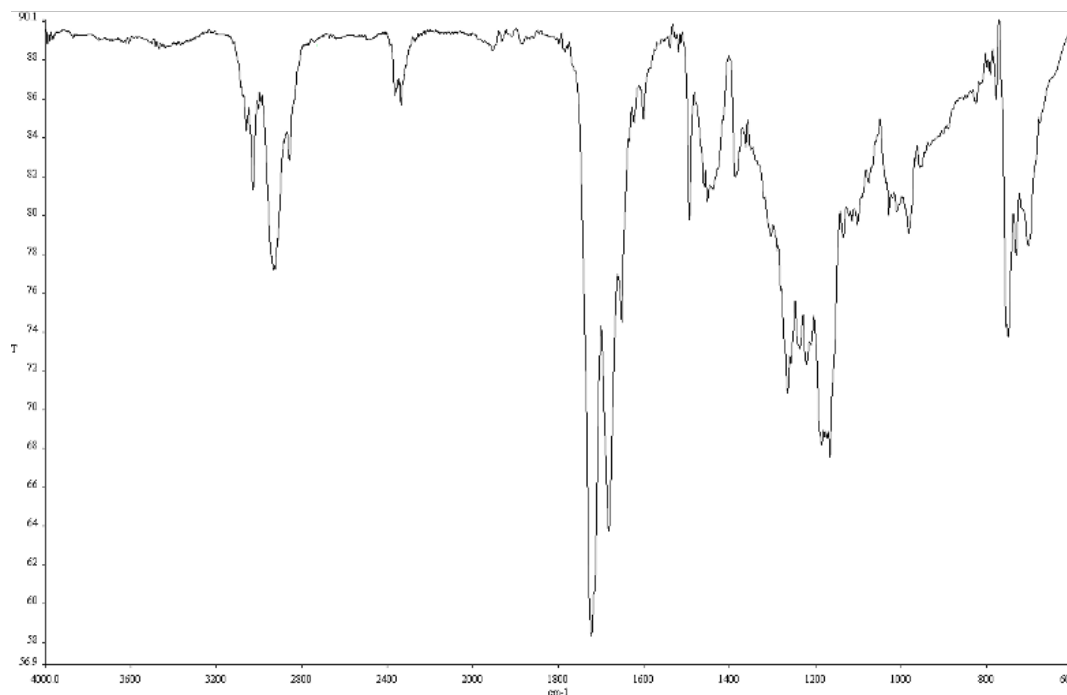
Figure A2.292. Infrared spectrum (Thin Film, NaCl) of compound **67**.
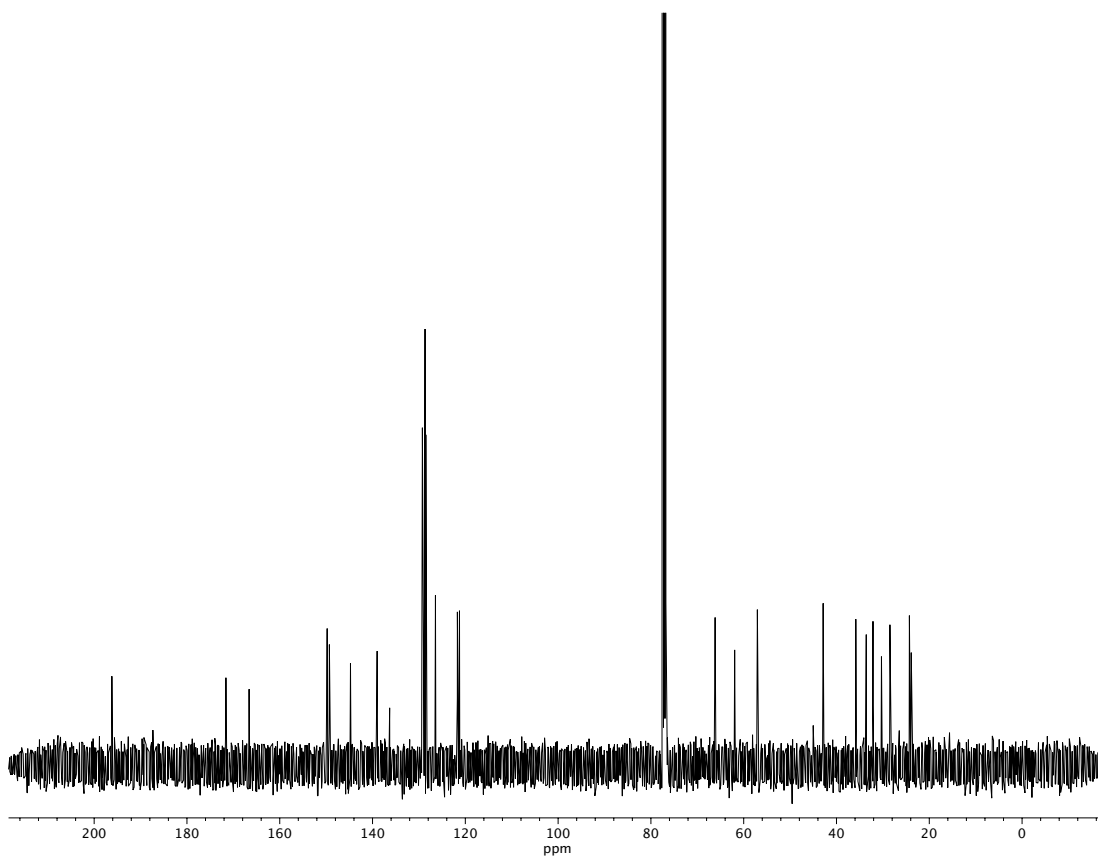
Figure A2.293. ^{13}C NMR (100 MHz, CDCl$_3$) of compound **67**.
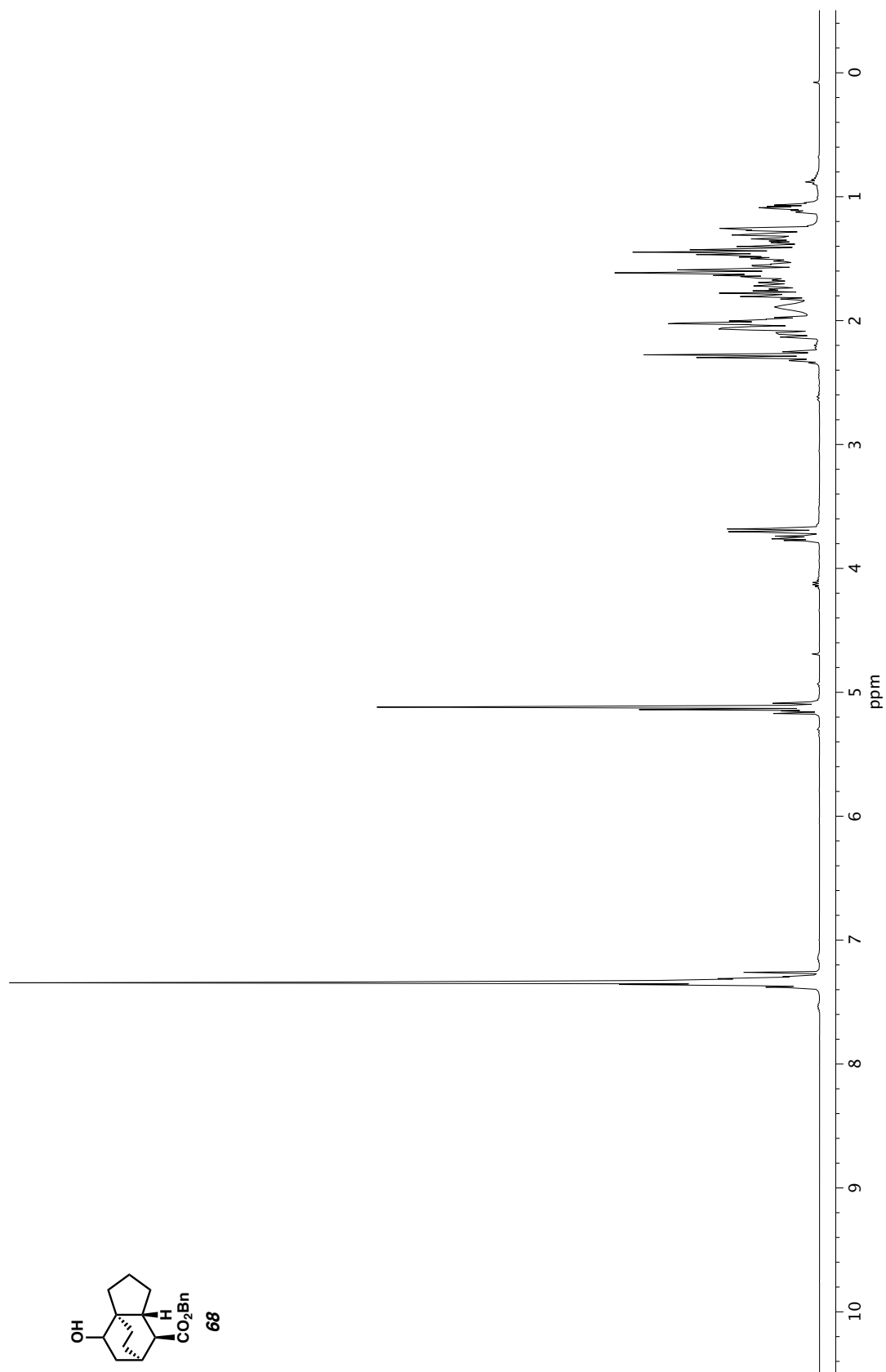
Figure A2.294. ^1H NMR (400 MHz, CDCl$_3$) of compound **68**.
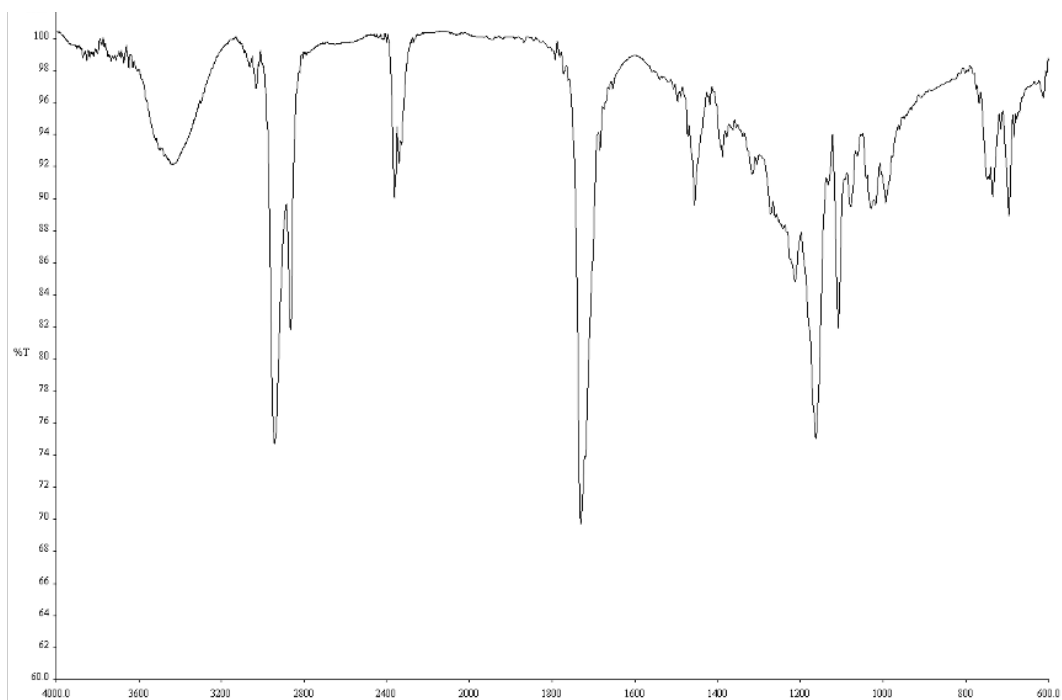
Figure A2.295. *Infrared spectrum (Thin Film, NaCl) of compound* **68**.
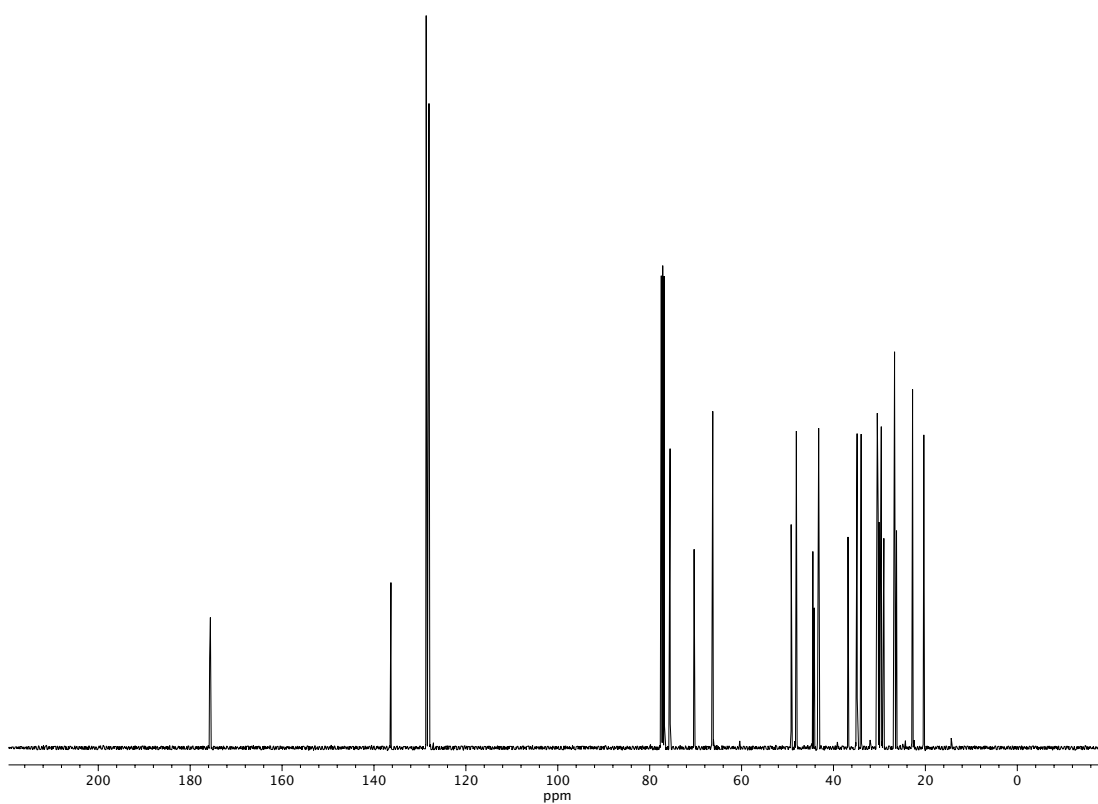
Figure A2.296. ^{13}C *NMR (100 MHz, CDCl$_3$) of compound* **68**.
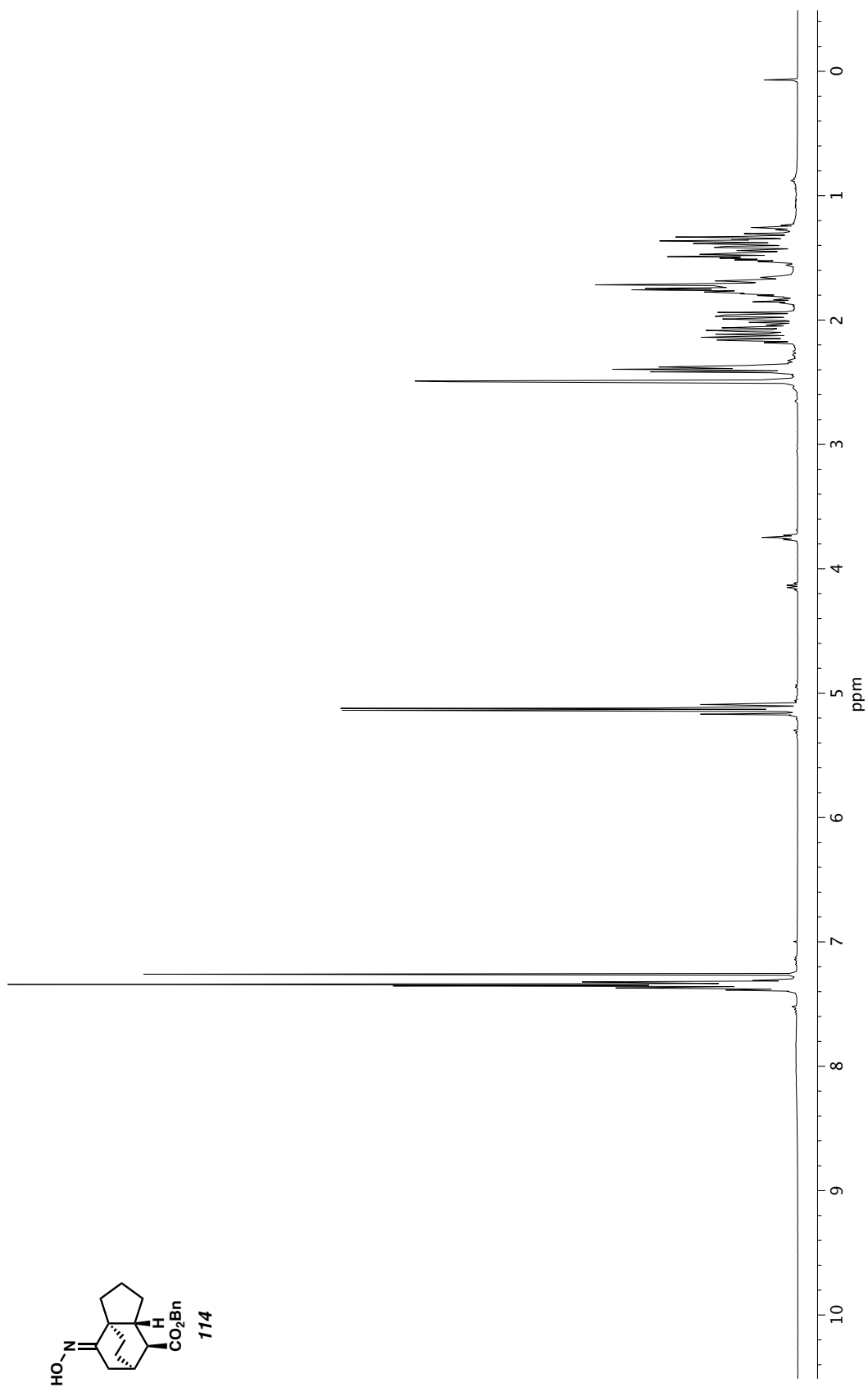
Figure A2.297. *^1H NMR (400 MHz, CDCl$_3$) of compound **114**.*
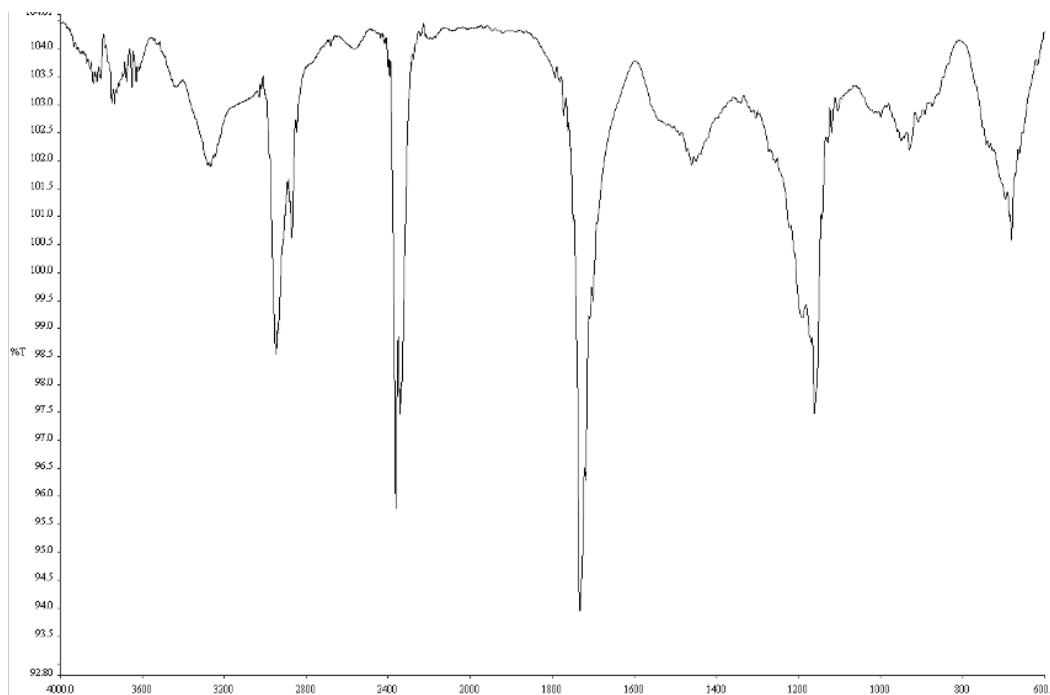
Figure A2.298. Infrared spectrum (Thin Film, NaCl) of compound **114**.
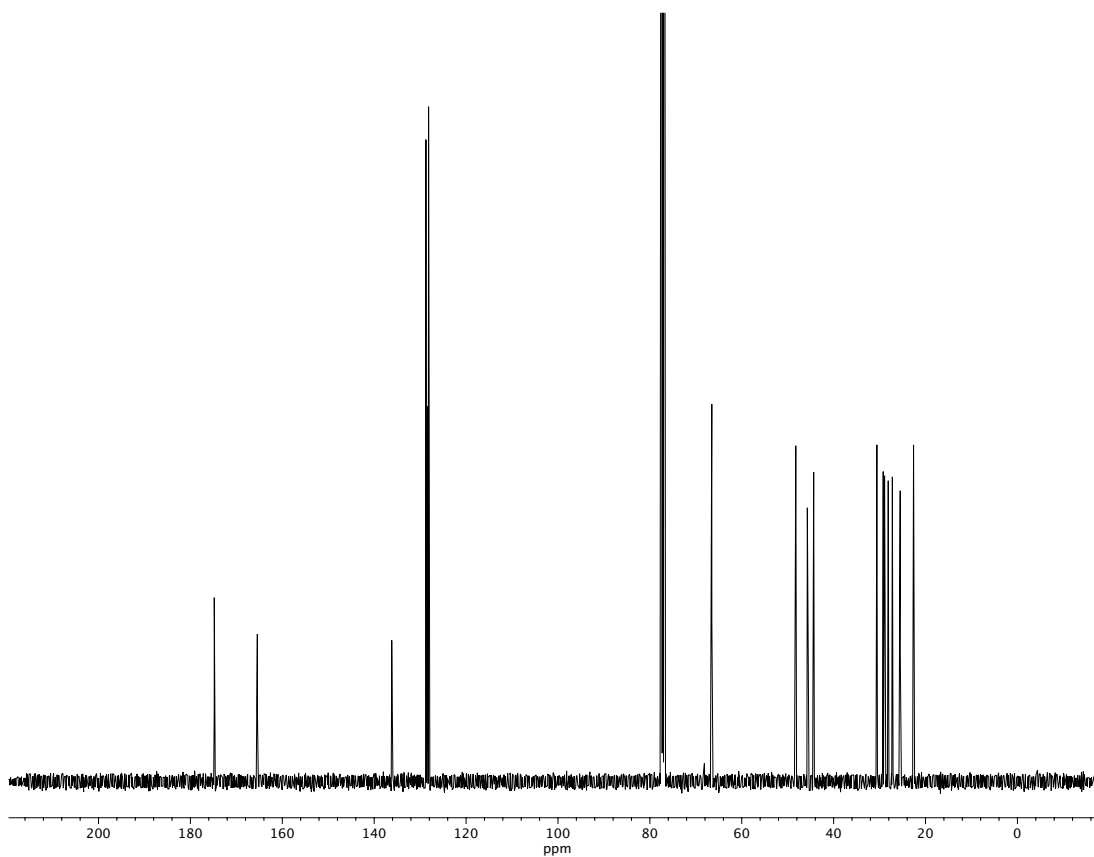
Figure A2.299. ^{13}C NMR (100 MHz, CDCl$_3$) of compound **114**.

Figure A2.300. ^1H NMR (400 MHz, CDCl$_3$) of compound **69**.
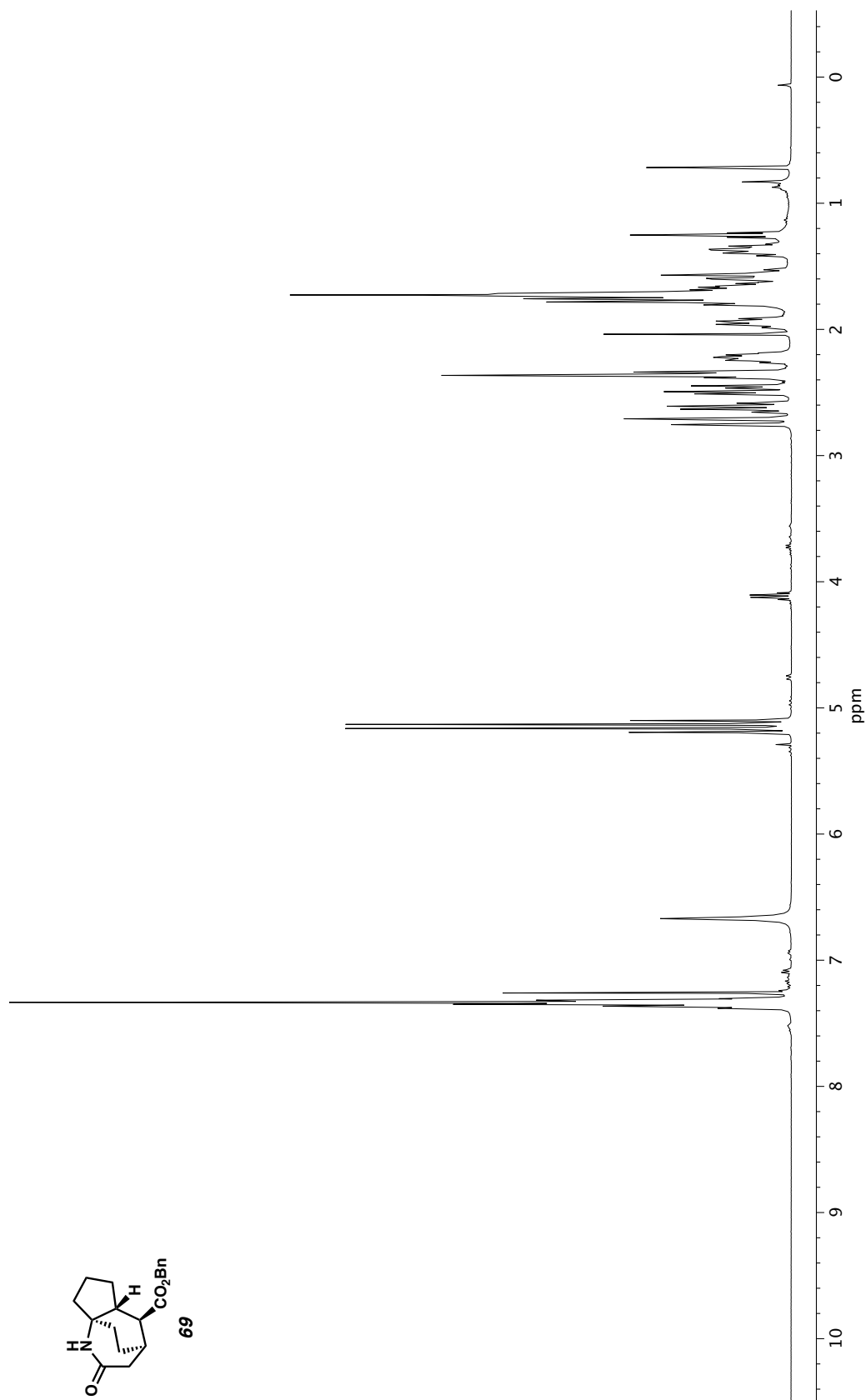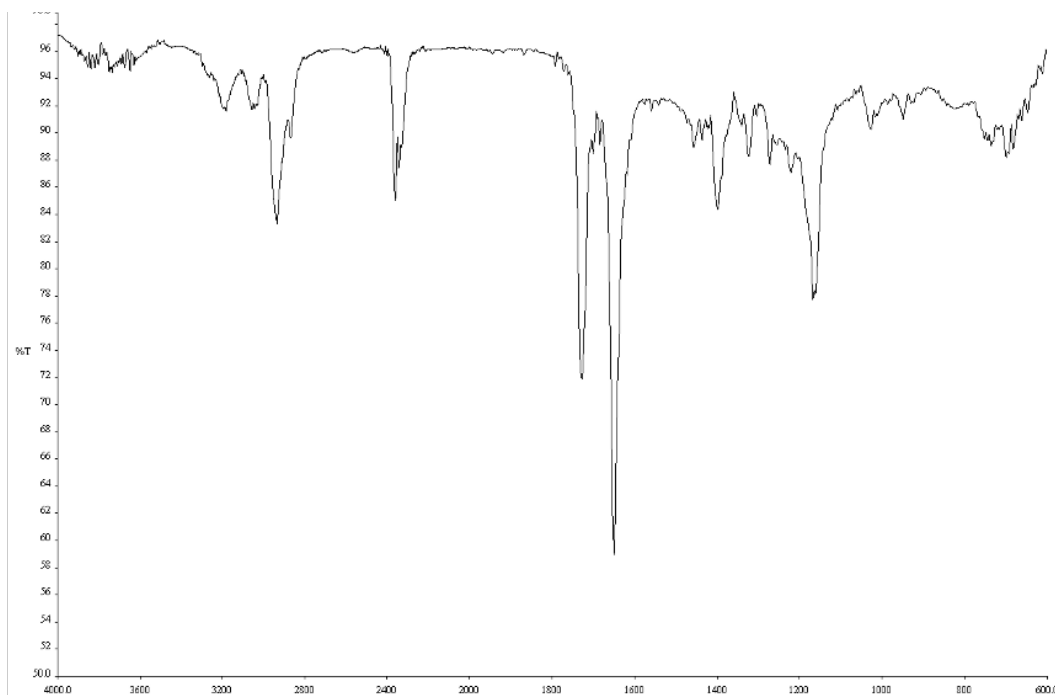
Figure A2.301. *Infrared spectrum (Thin Film, NaCl) of compound* **69**.
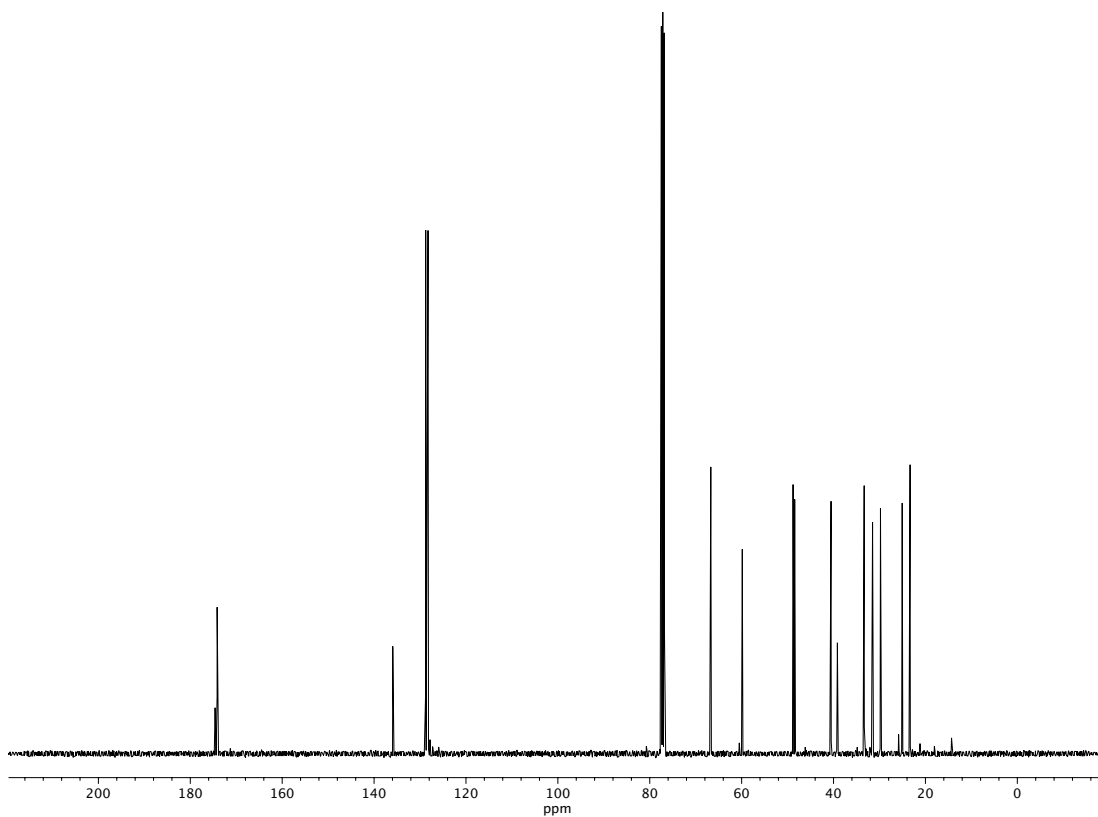
Figure A2.302. ^{13}C *NMR (100 MHz, CDCl$_3$) of compound* **69**.
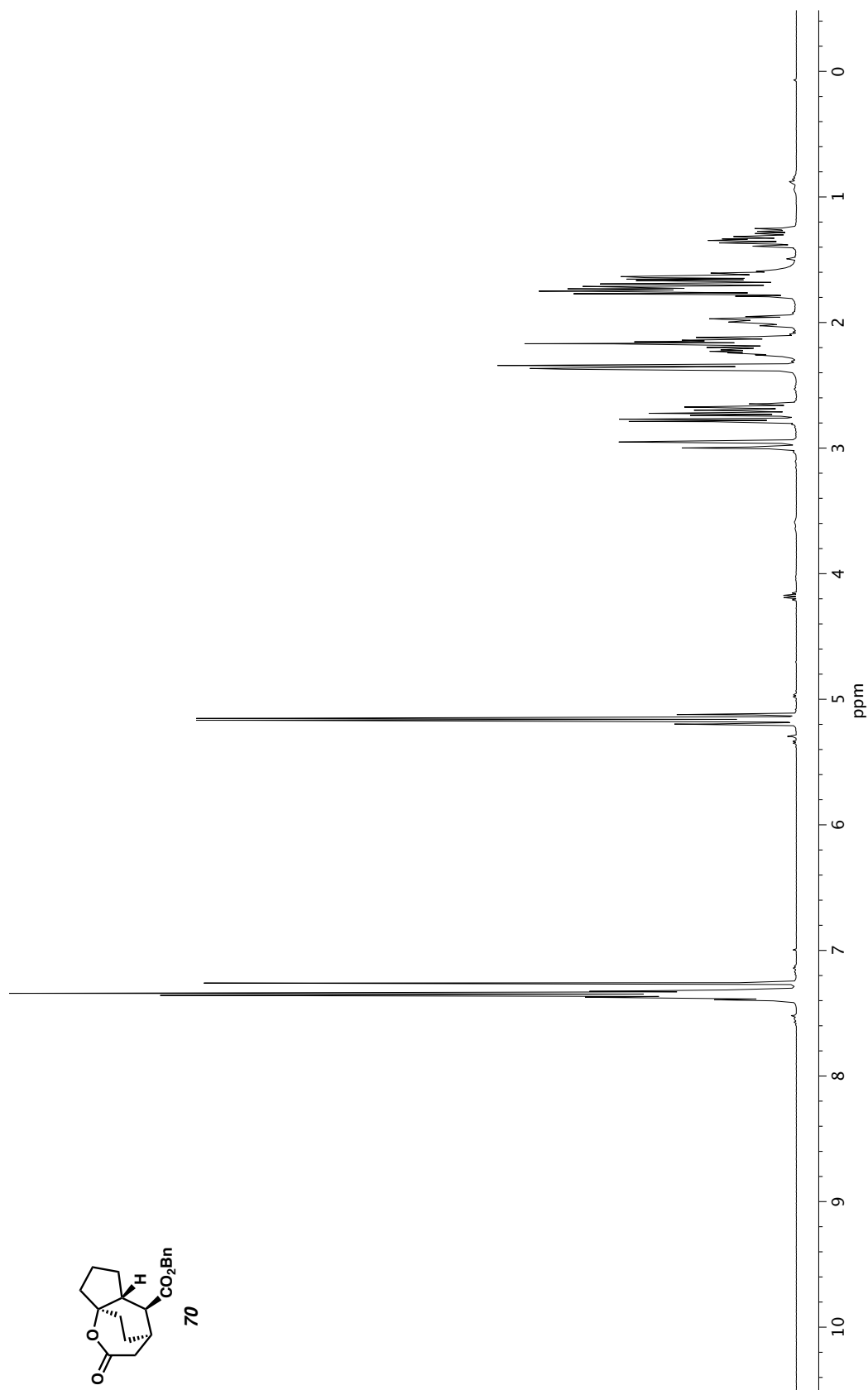
Figure A2.303. ^1H NMR (400 MHz, CDCl$_3$) of compound **70**.
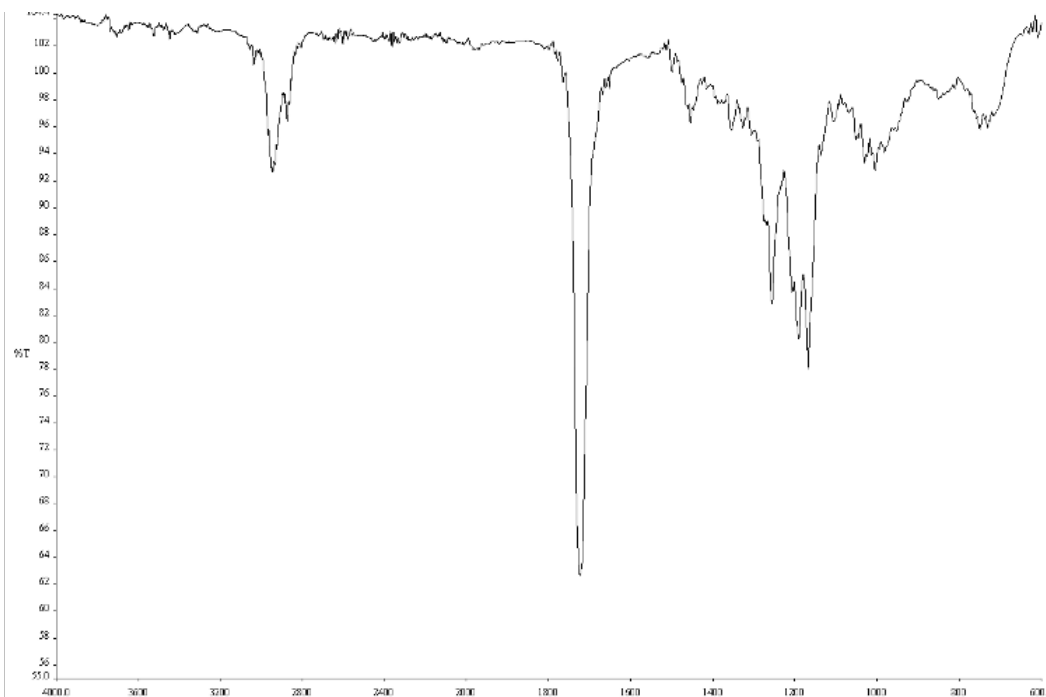
Figure A2.304. *Infrared spectrum (Thin Film, NaCl) of compound **70**.*
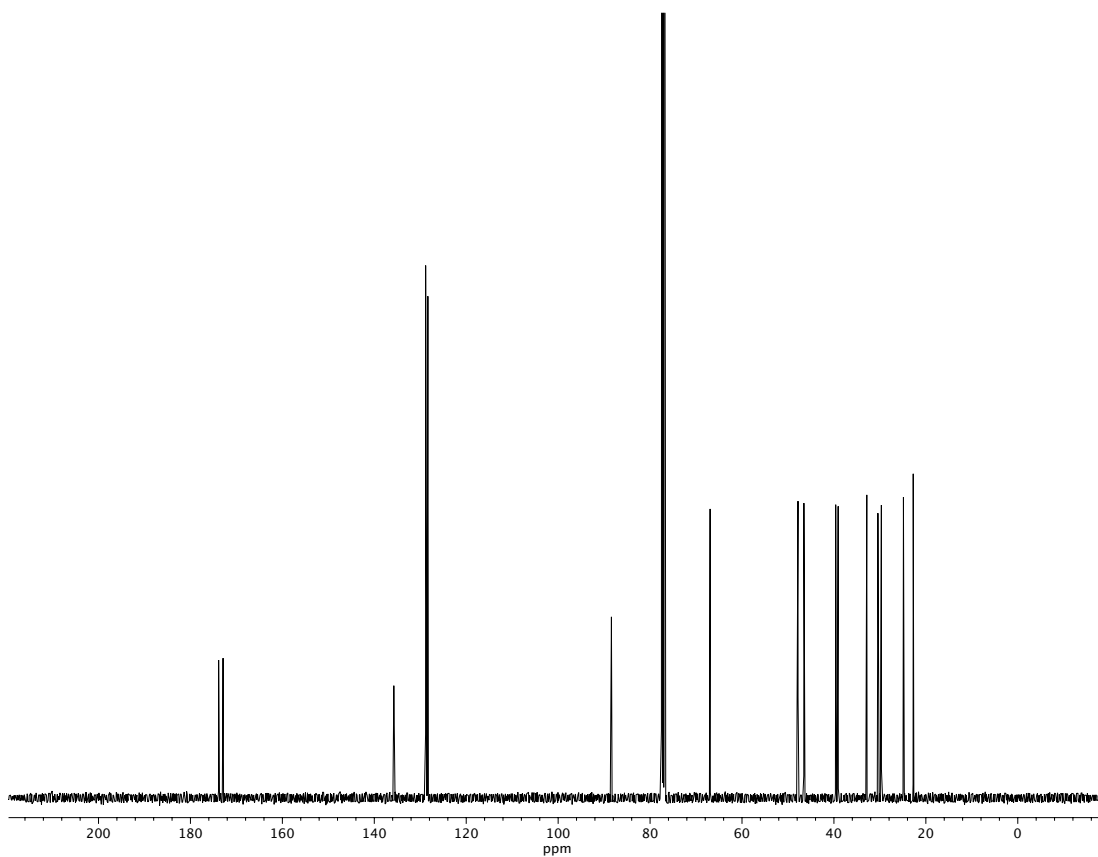
Figure A2.305. *^{13}C NMR (100 MHz, CDCl$_3$) of compound **70**.*

Figure A2.306. *¹H NMR (400 MHz, CDCl₃) of compound **75**.*
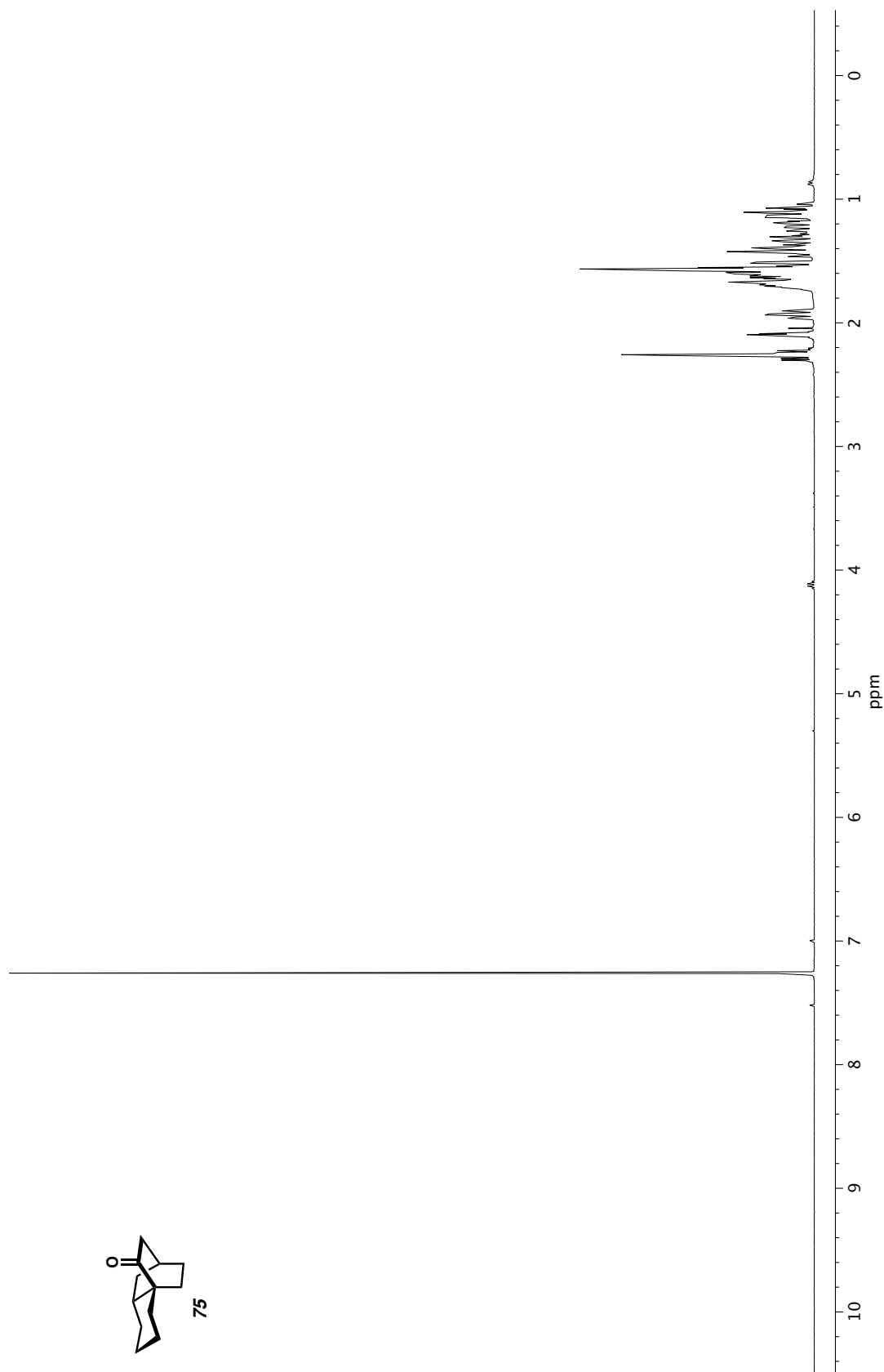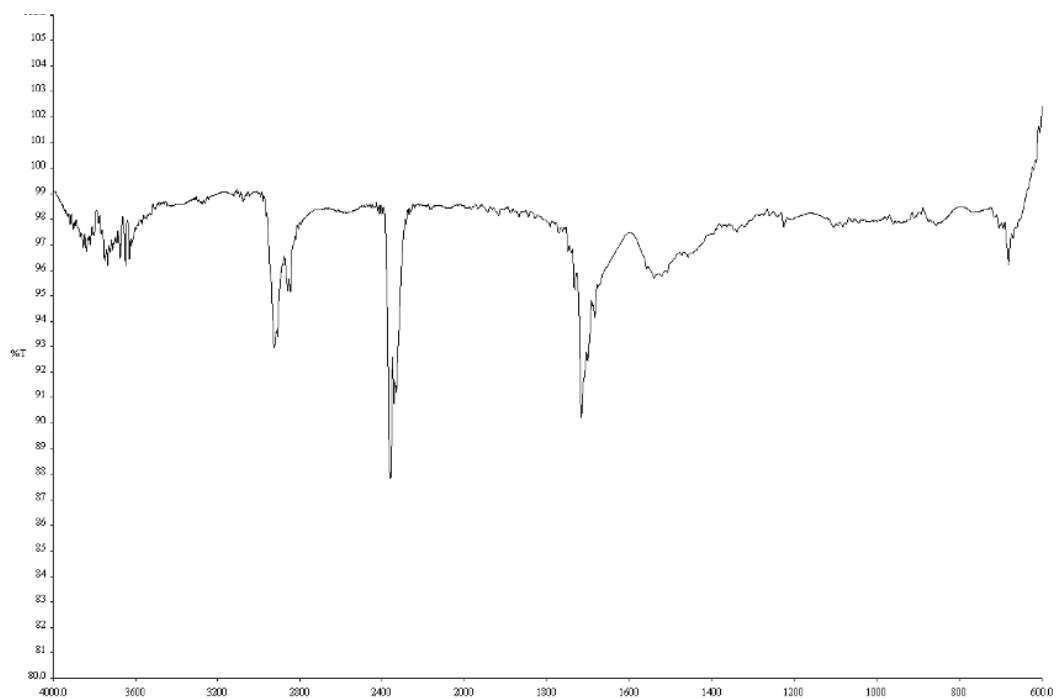
Figure A2.307. *Infrared spectrum (Thin Film, NaCl) of compound **75**.*
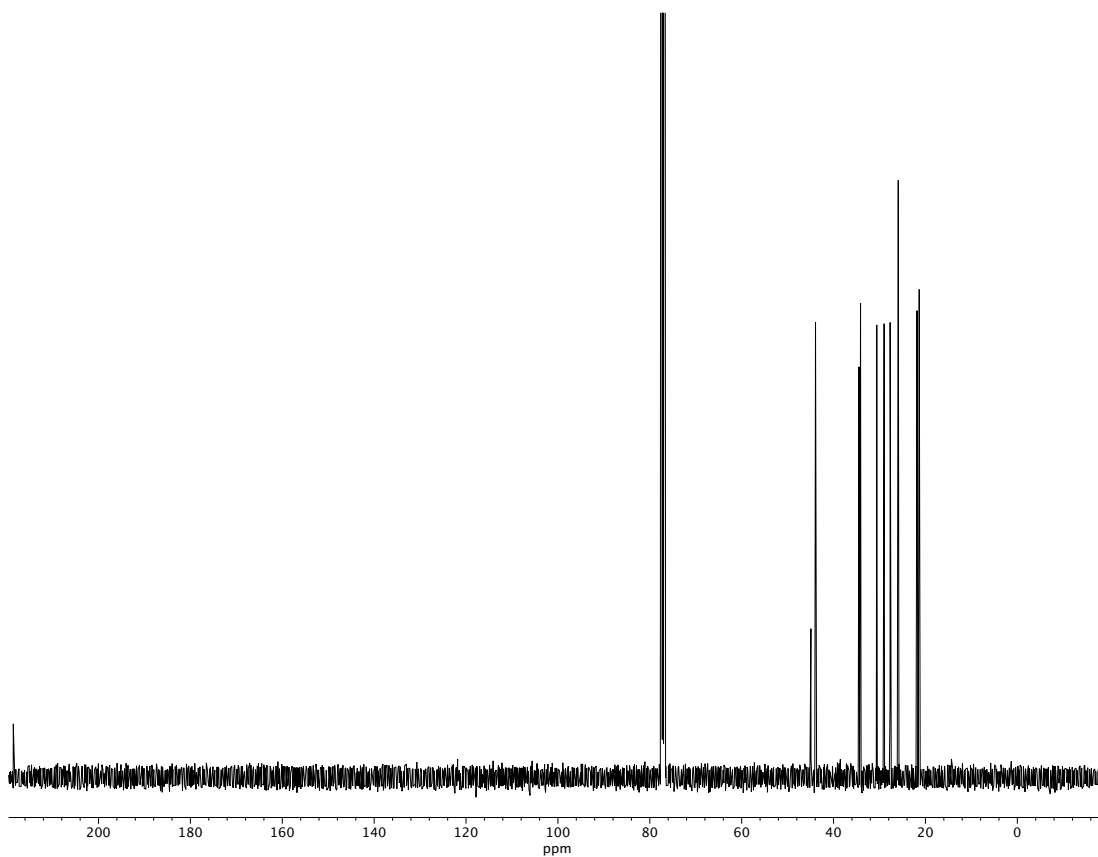
Figure A2.308. ^{13}C *NMR (100 MHz, CDCl$_3$) of compound **75**.*
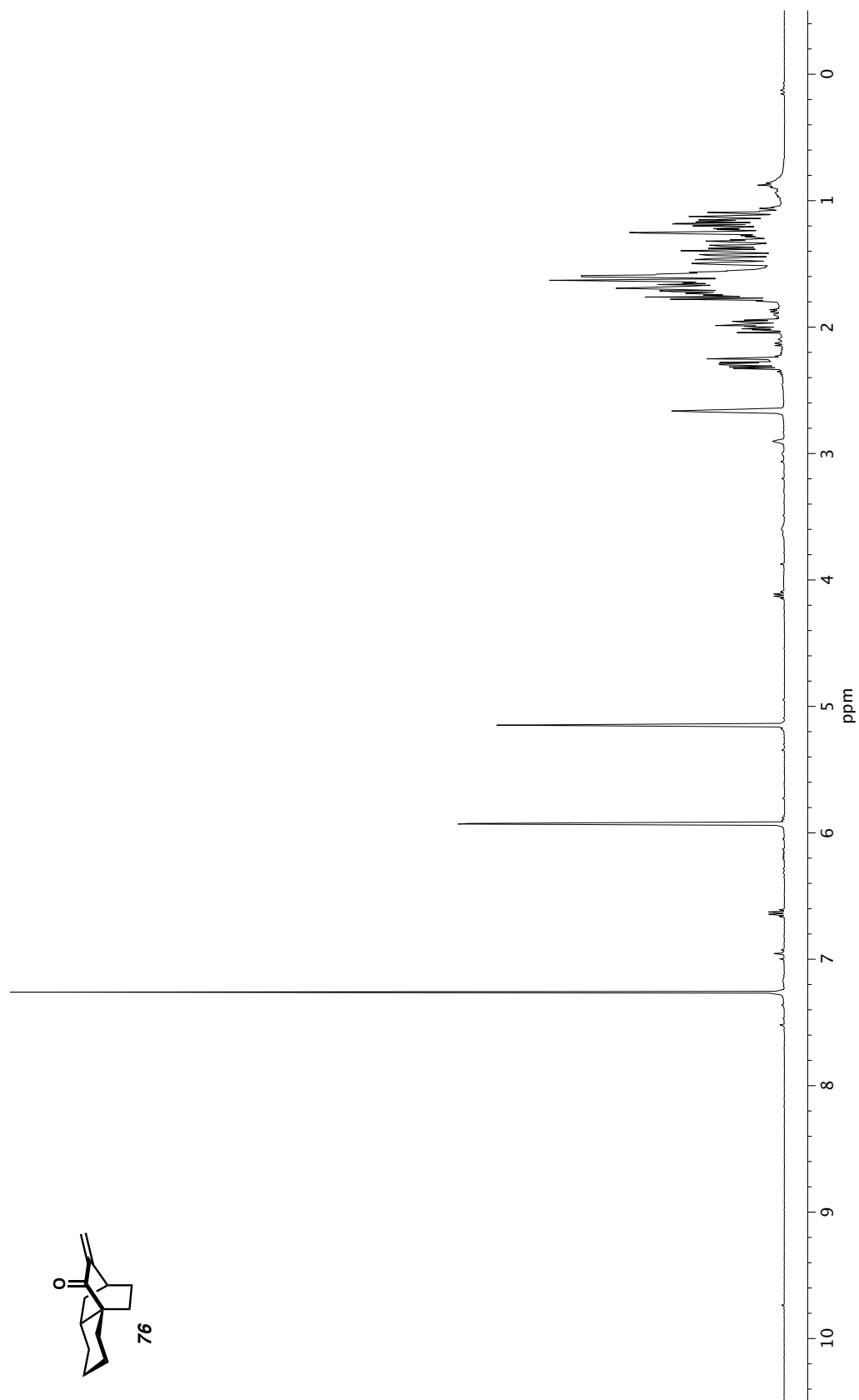
Figure A2.309. *¹H NMR (400 MHz, CDCl₃) of compound **76**.*
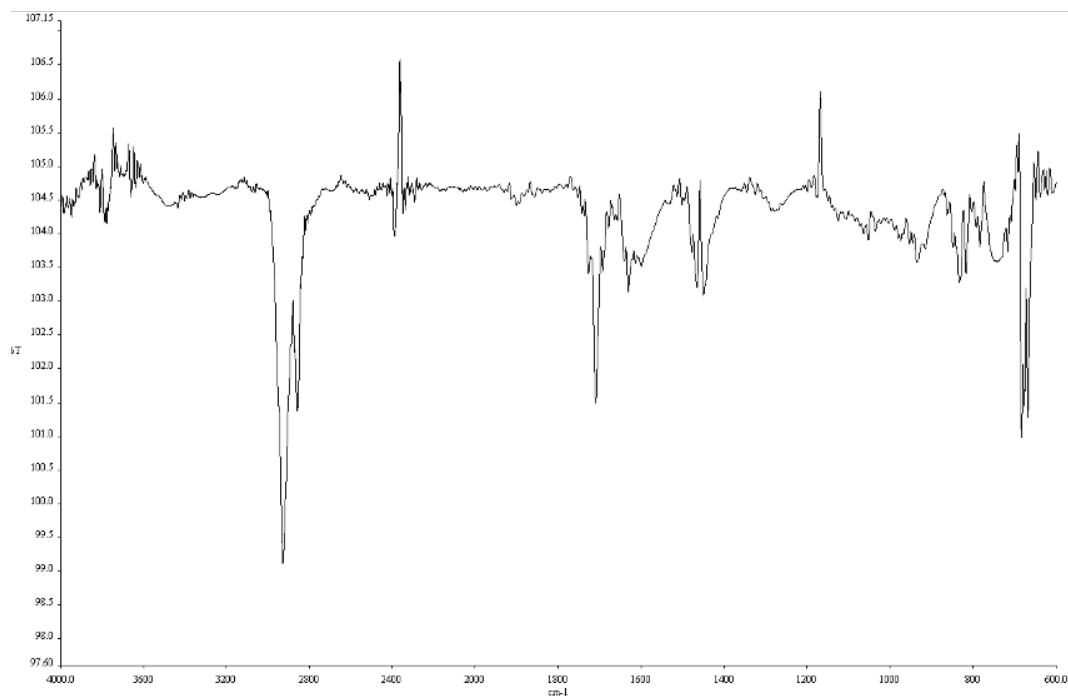
Figure A2.310. *Infrared spectrum (Thin Film, NaCl) of compound **76**.*
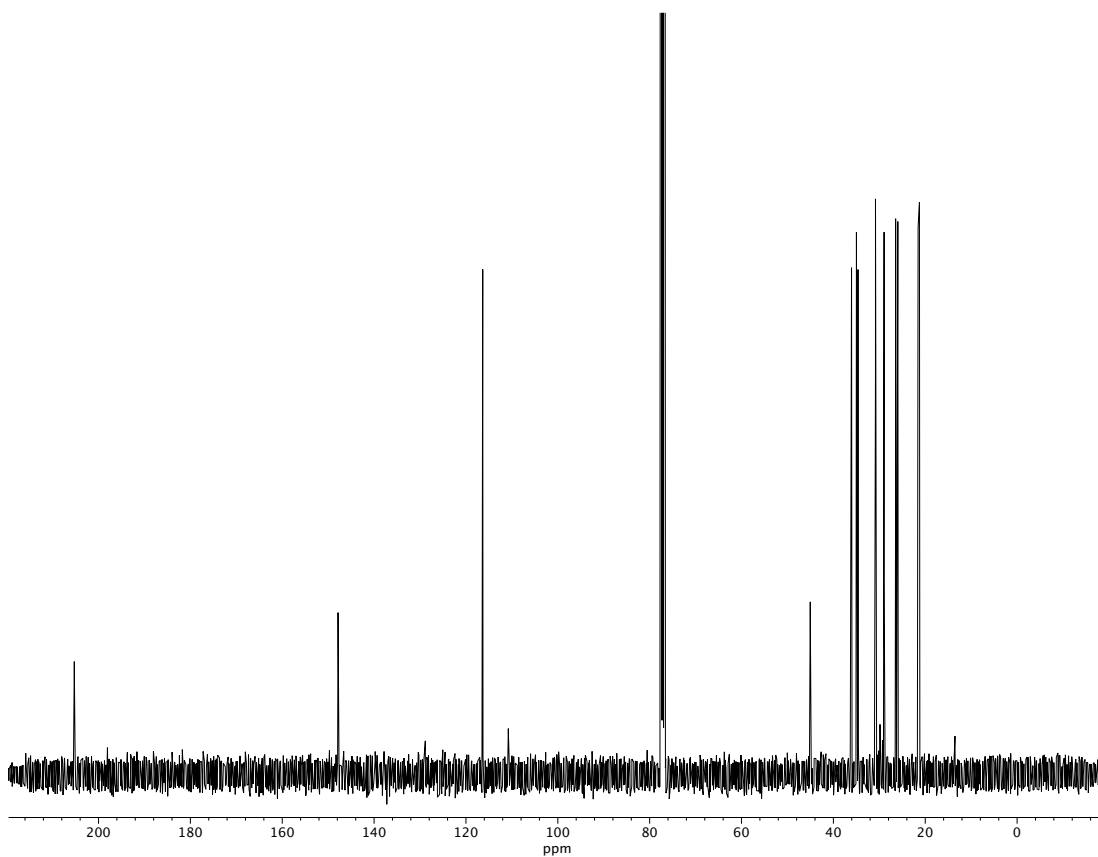
Figure A2.311. ^{13}C *NMR (100 MHz, CDCl$_3$) of compound **76**.*
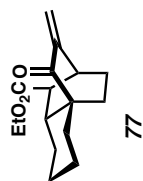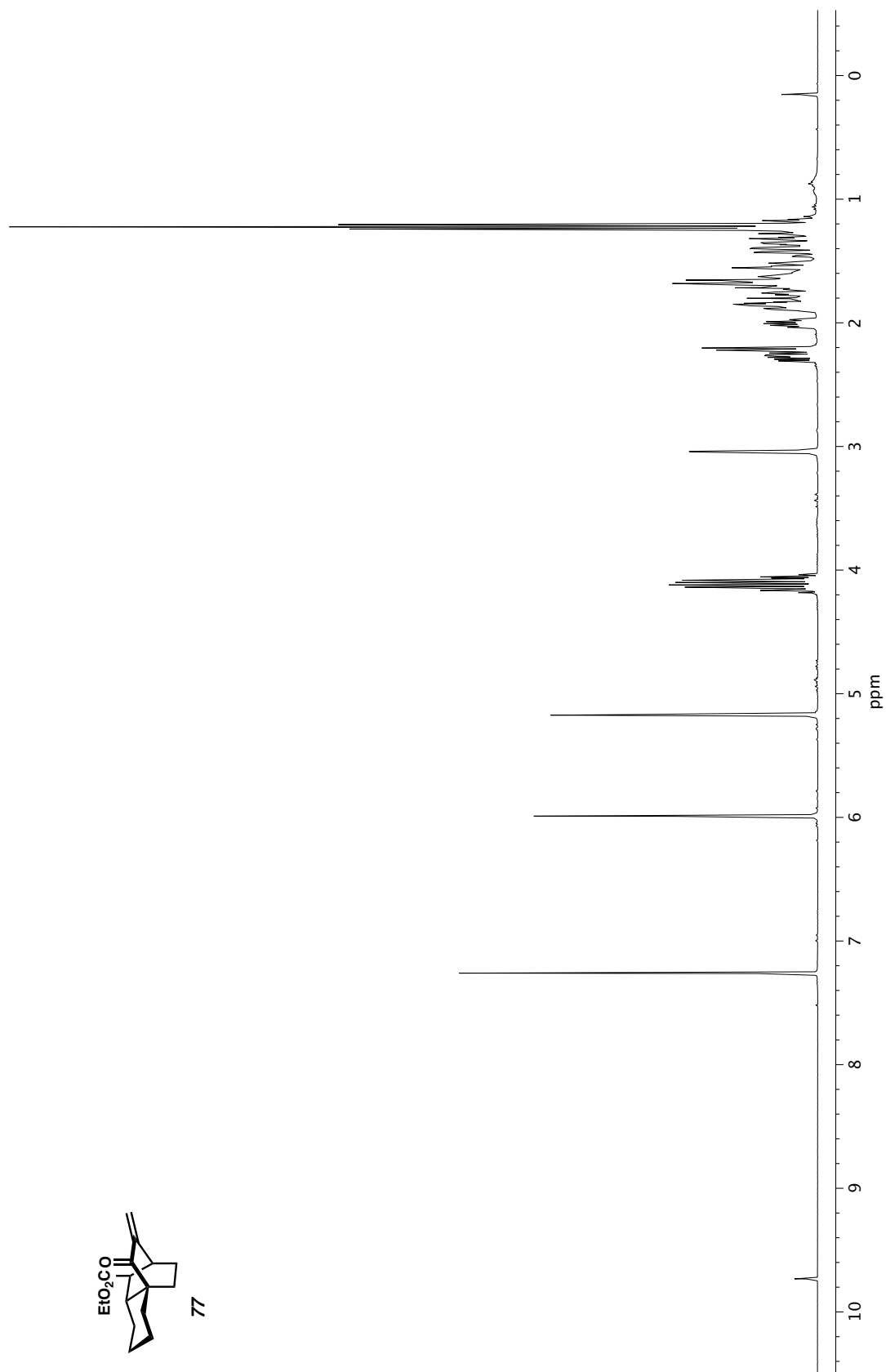
Figure A2.312. *¹H NMR (400 MHz, CDCl₃) of compound 77.*
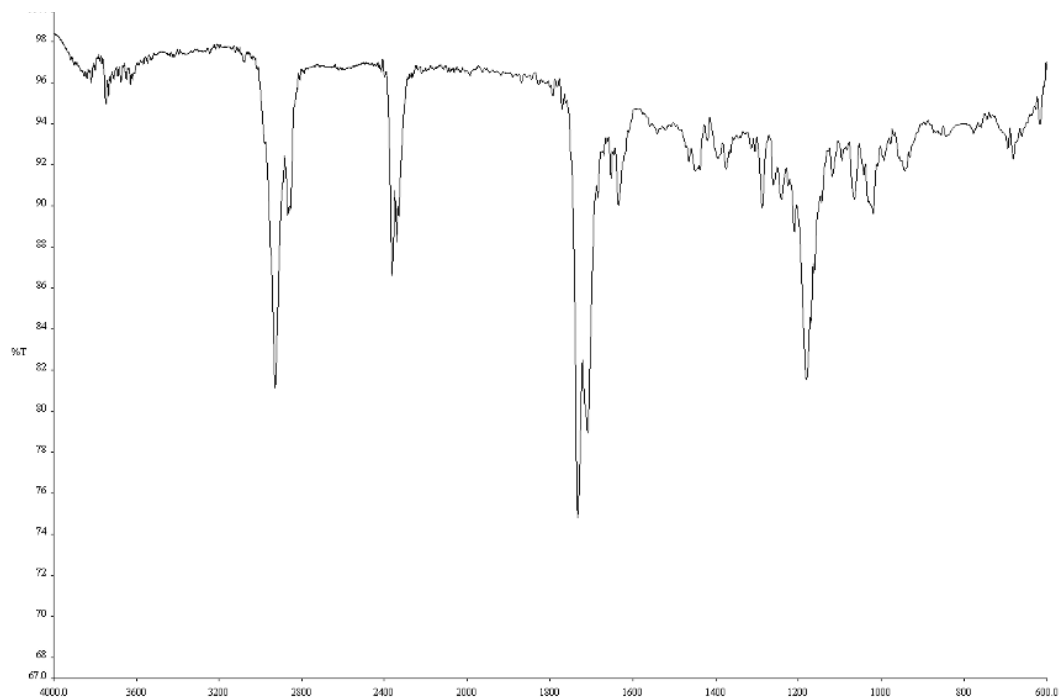
Figure A2.313. Infrared spectrum (Thin Film, NaCl) of compound **77**.
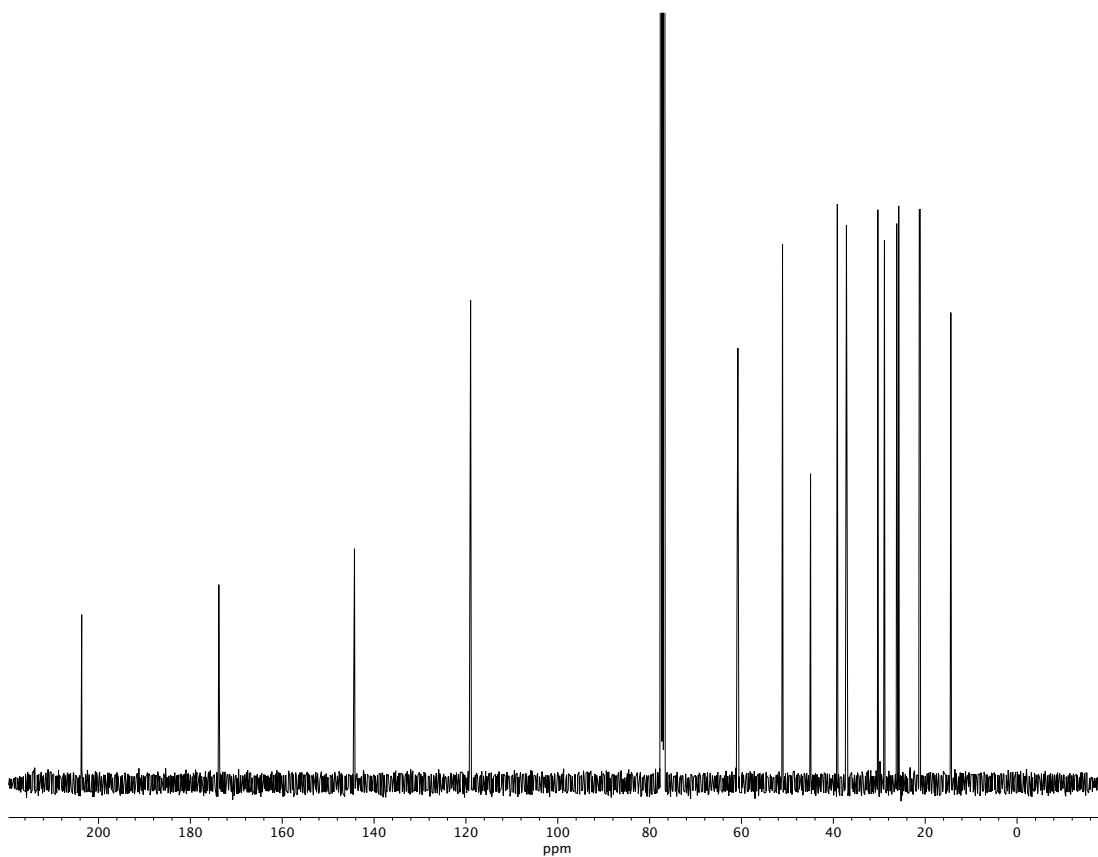
Figure A2.314. ^{13}C NMR (100 MHz, CDCl$_3$) of compound **77**.
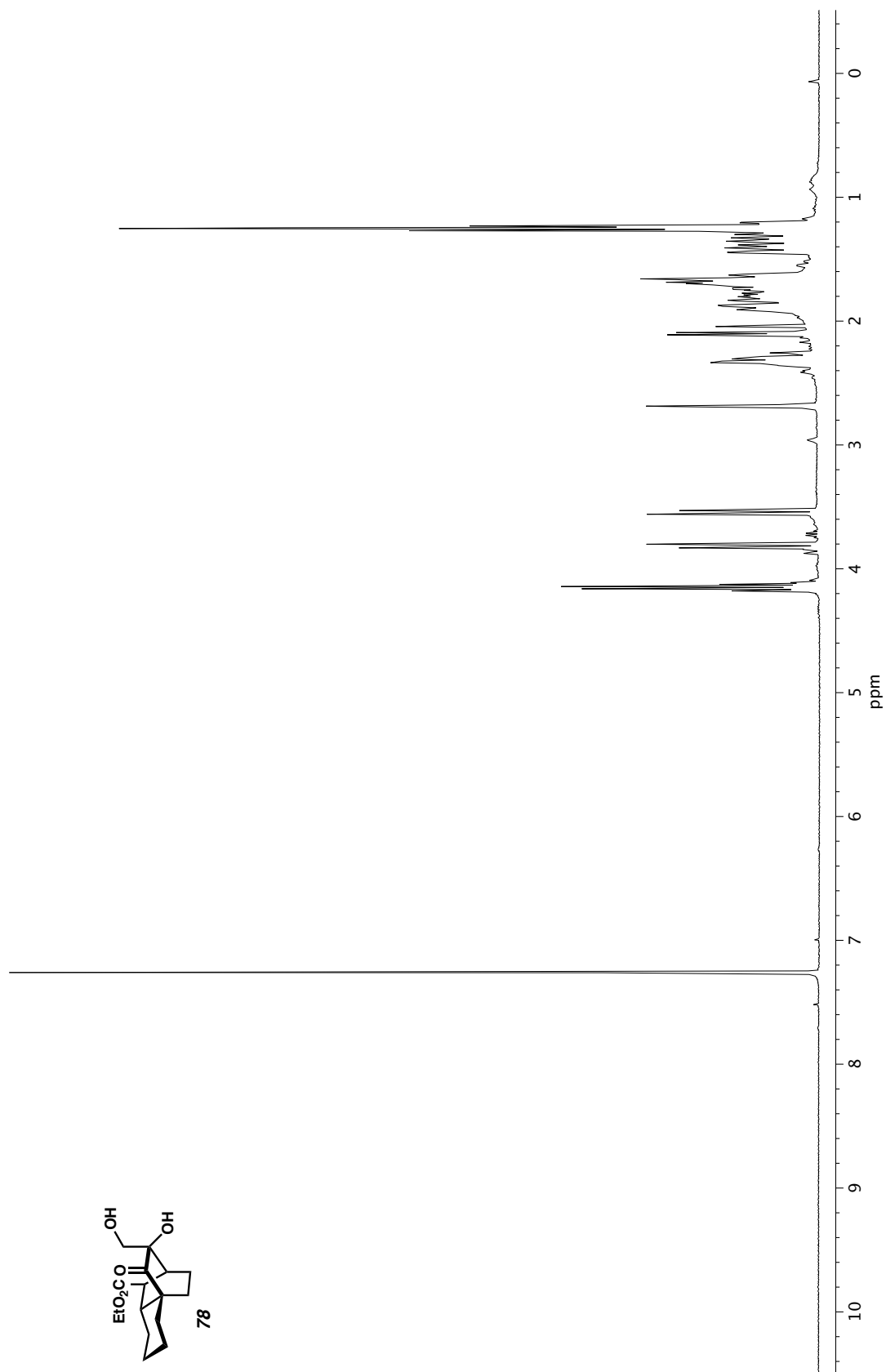
Figure A2.315. ^1H NMR (400 MHz, CDCl$_3$) of compound **78**.
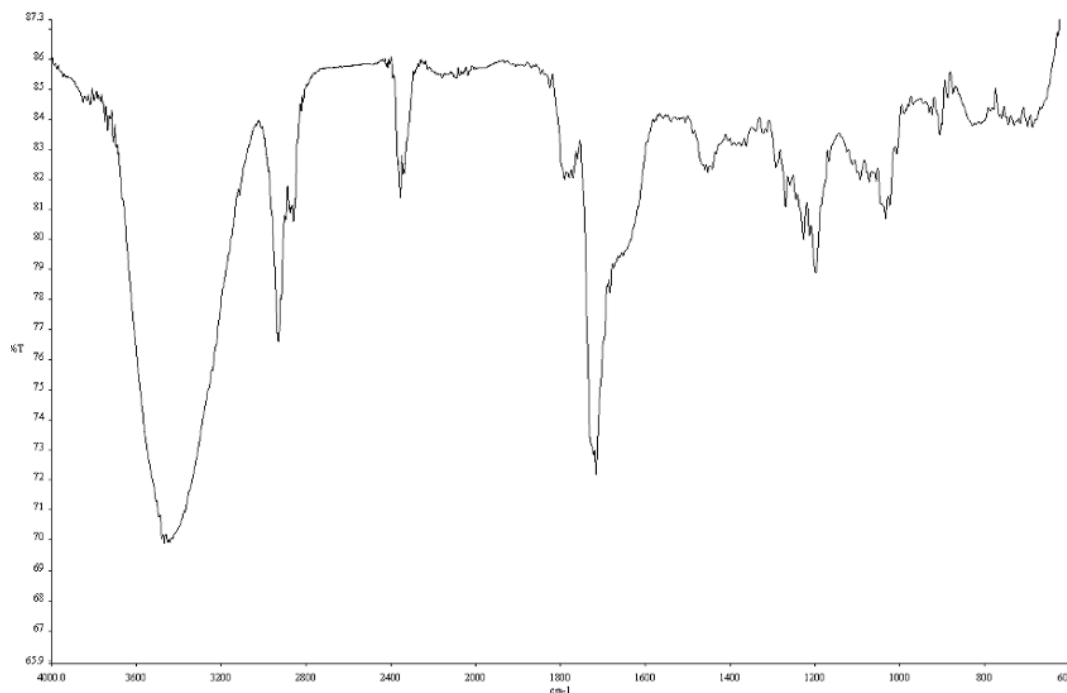
Figure A2.316. Infrared spectrum (Thin Film, NaCl) of compound **78**.
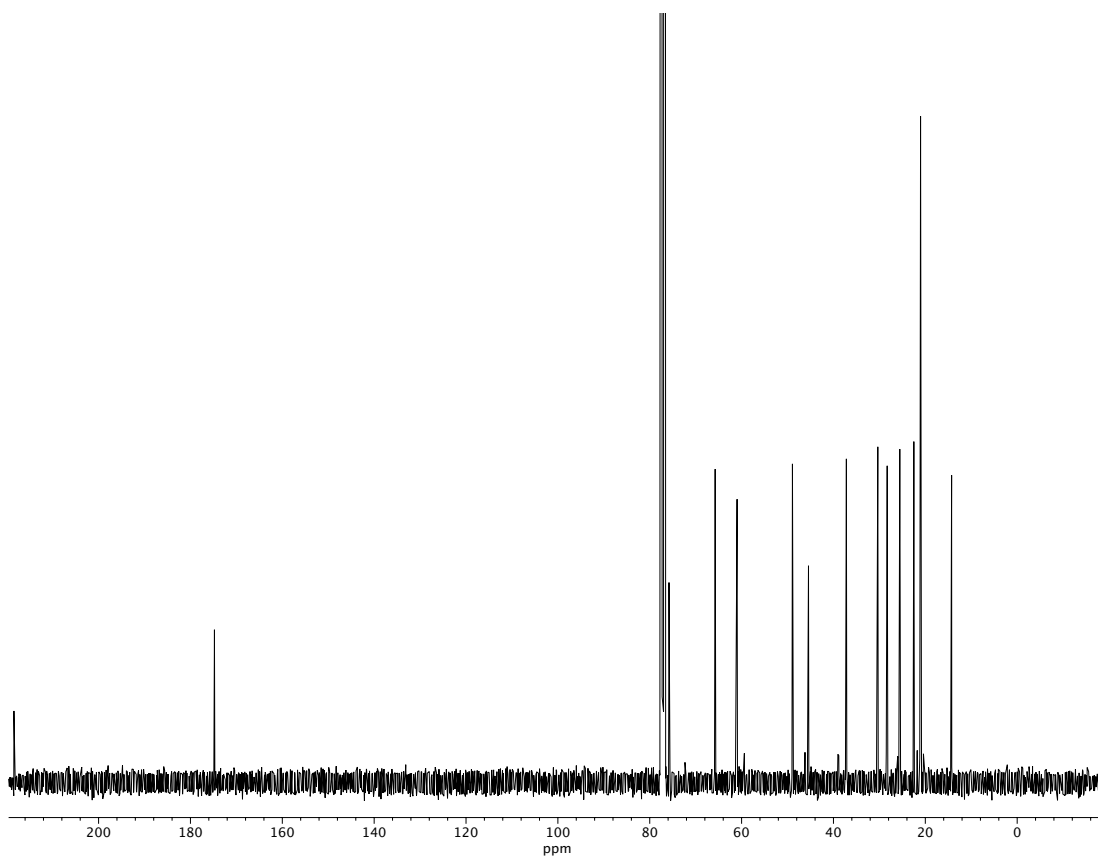
Figure A2.317. ^{13}C NMR (100 MHz, CDCl$_3$) of compound **78**.
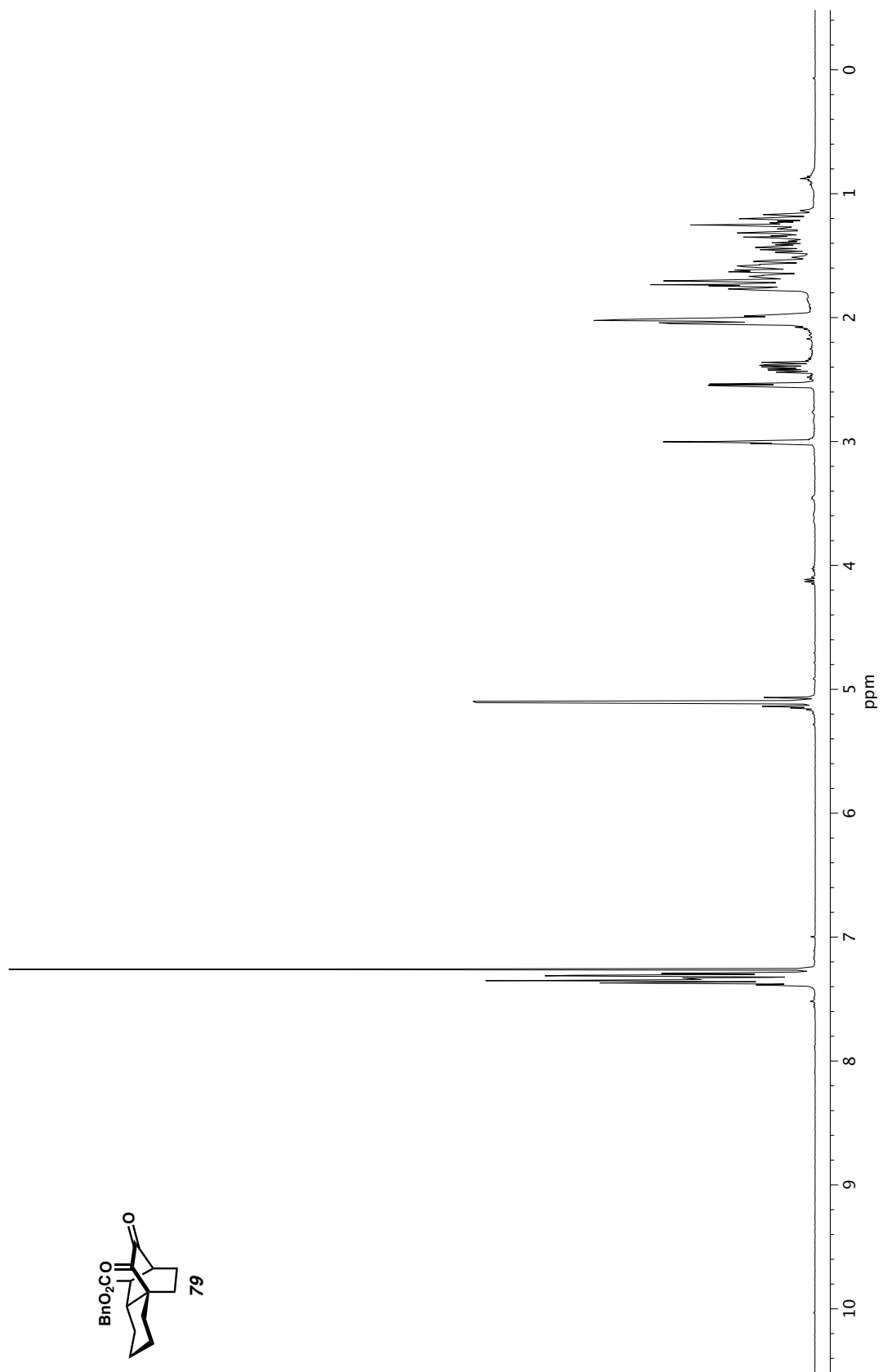
Figure A2.318. *^{1}H NMR (400 MHz, CDCl$_3$) of compound **79**.*
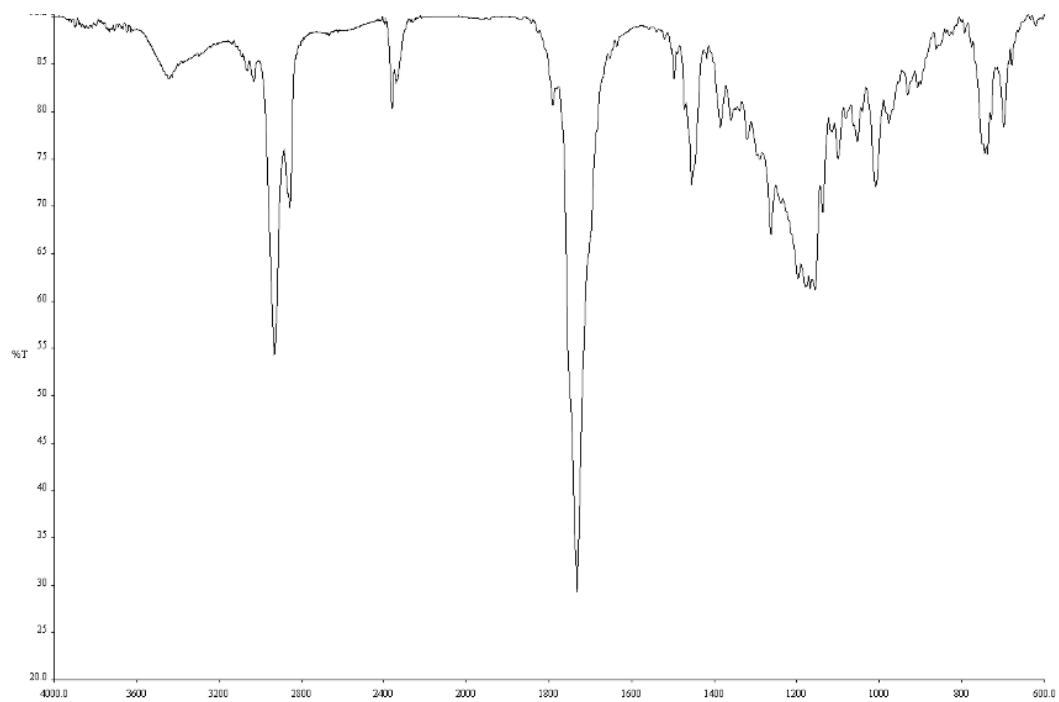
Figure A2.319. Infrared spectrum (Thin Film, NaCl) of compound **79**.
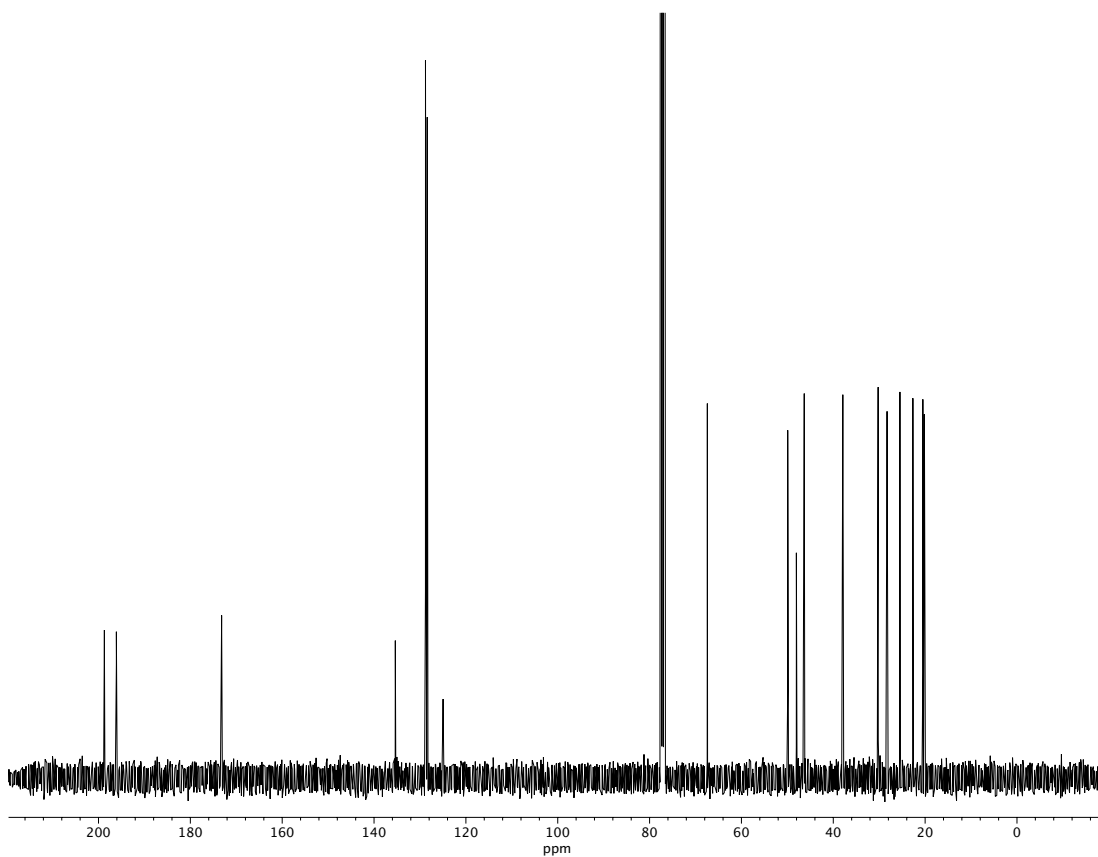
Figure A2.320. ^{13}C NMR (100 MHz, CDCl$_3$) of compound **79**.
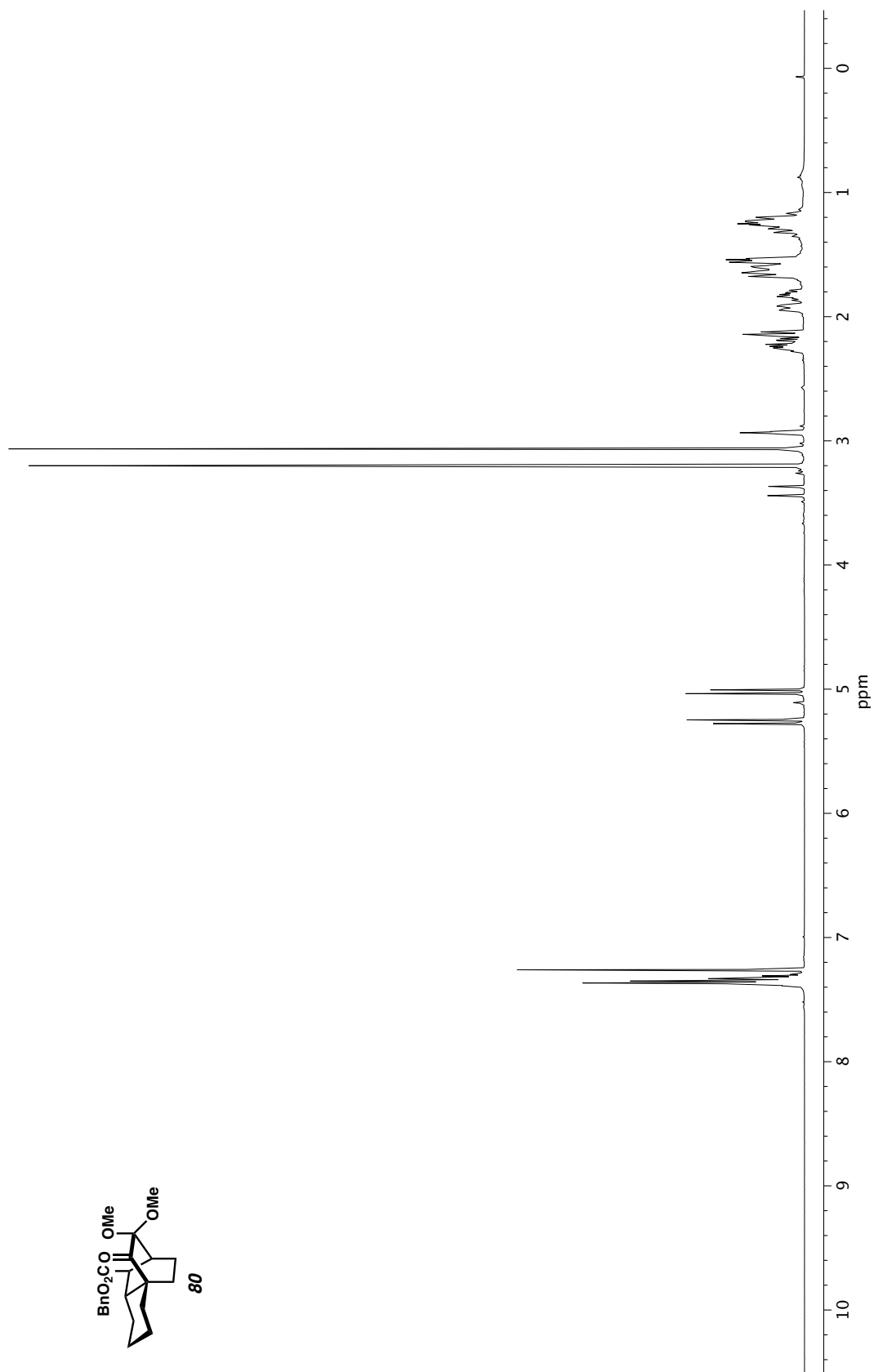
Figure A2.321. ^1H NMR (400 MHz, CDCl$_3$) of compound **80**.
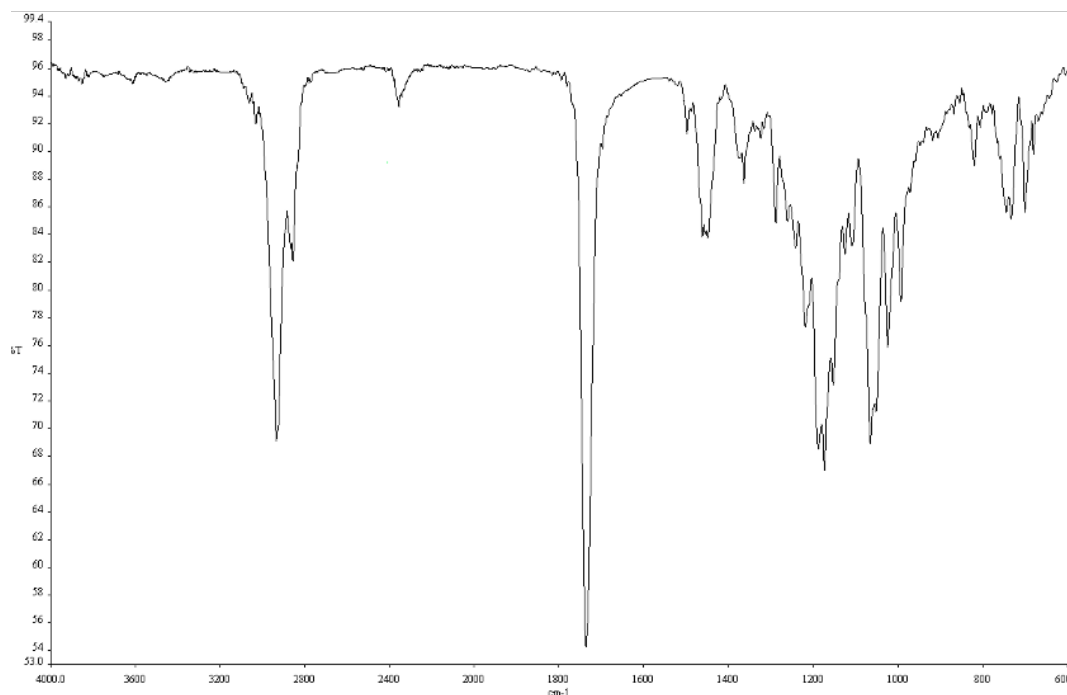
Figure A2.322. *Infrared spectrum (Thin Film, NaCl) of compound **80**.*
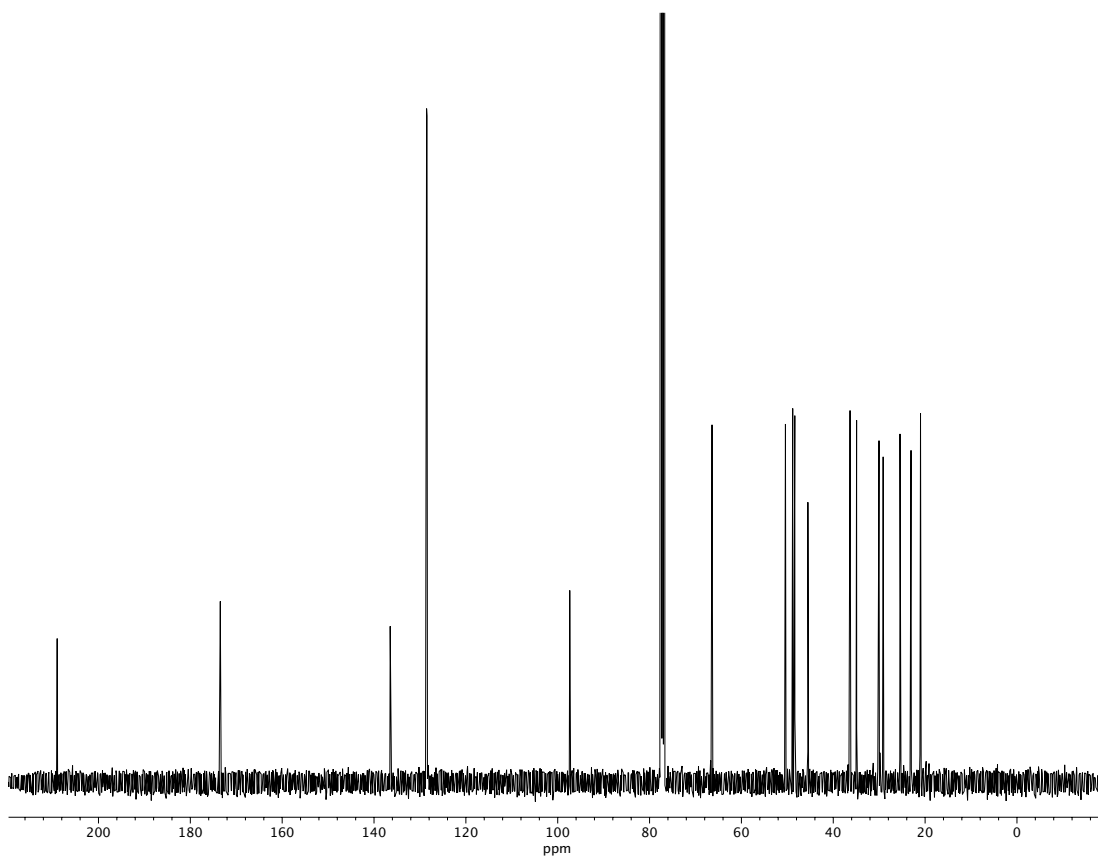
Figure A2.323. ^{13}C *NMR (100 MHz, CDCl₃) of compound **80**.*
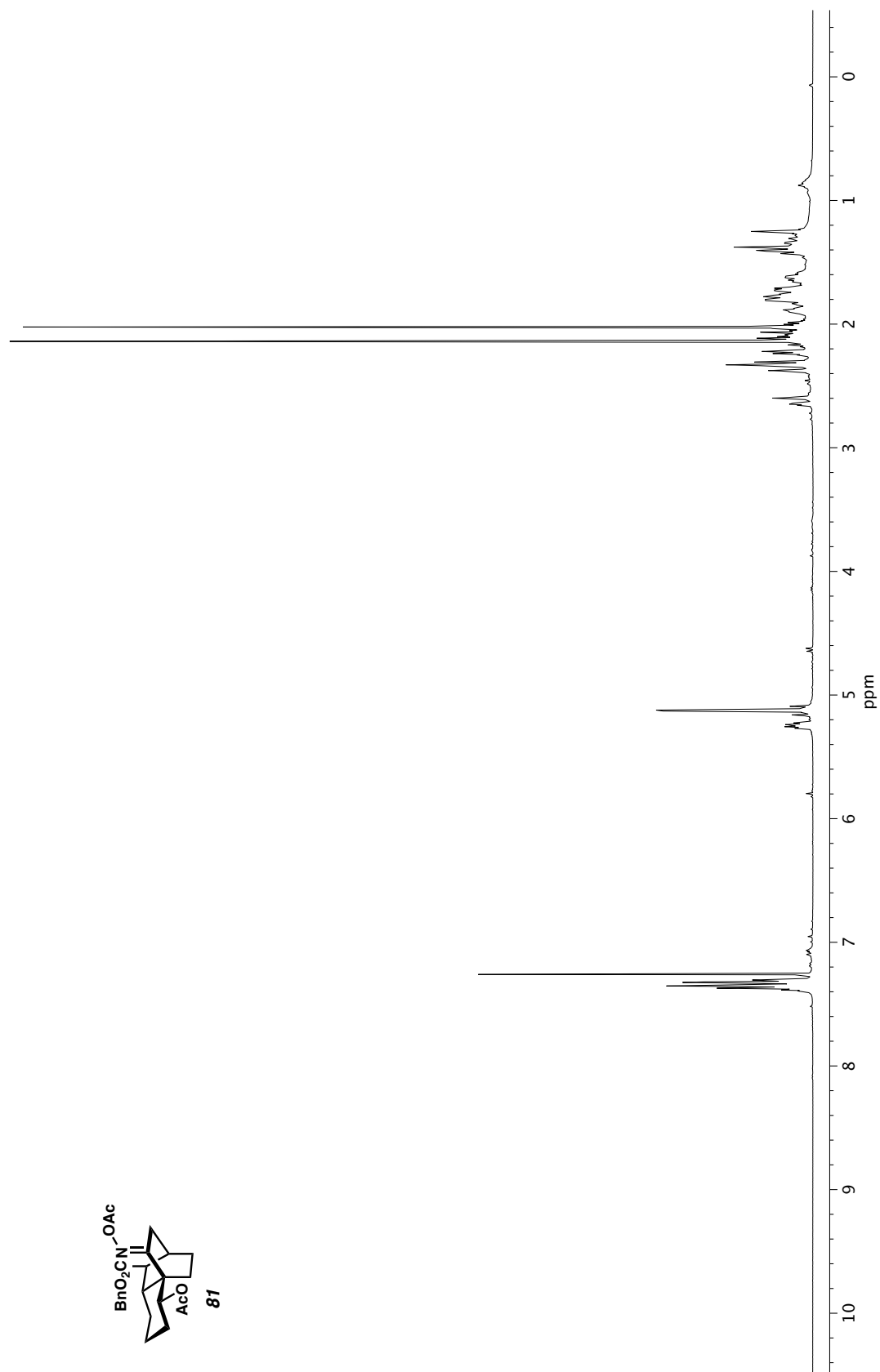
Figure A2.324. ^1H NMR (400 MHz, CDCl$_3$) of compound **81**.
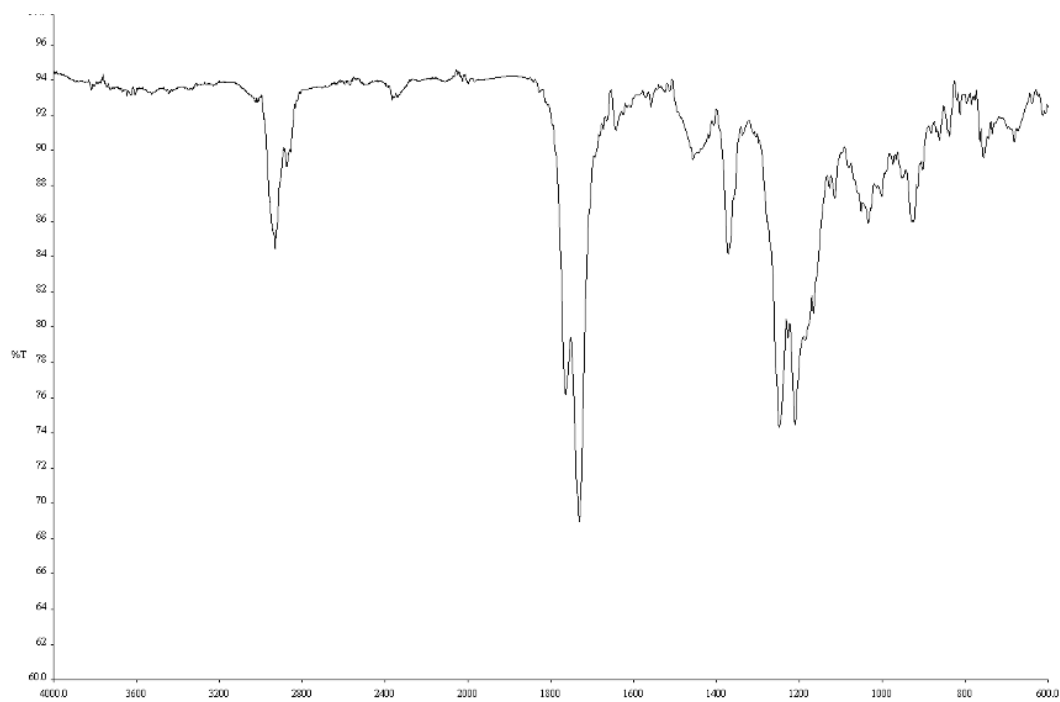
Figure A2.325. *Infrared spectrum (Thin Film, NaCl) of compound **81**.*
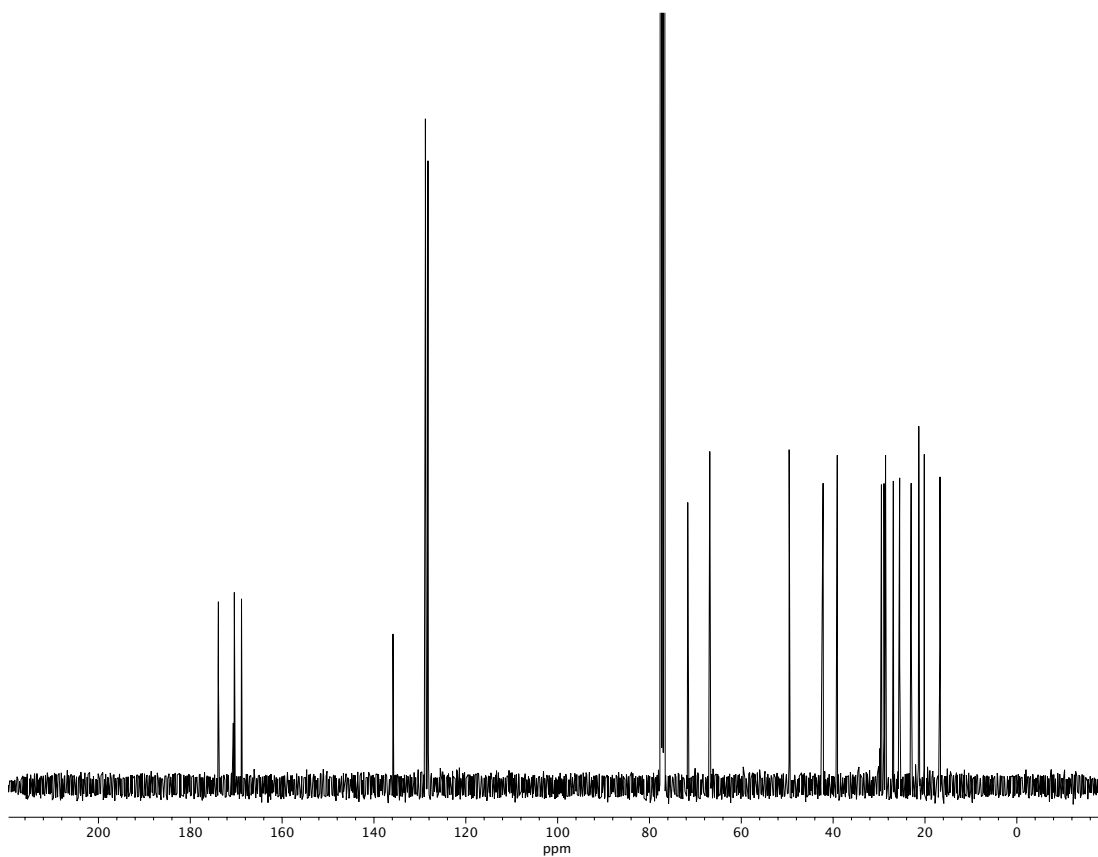
Figure A2.326. ^{13}C *NMR (100 MHz, CDCl$_3$) of compound **81**.*
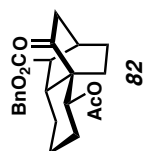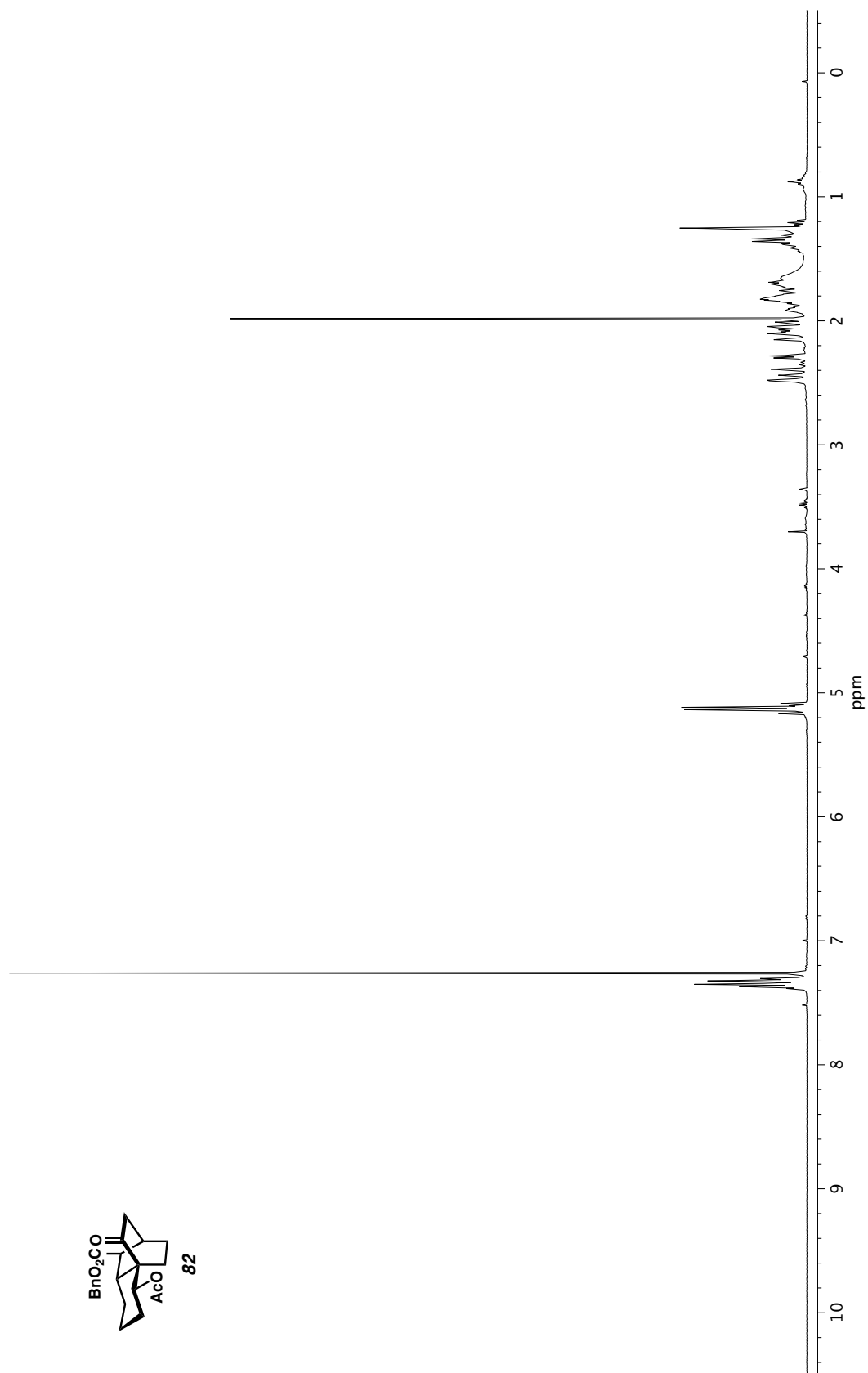
Figure A2.327. ^1H NMR (400 MHz, CDCl$_3$) of compound **82**.
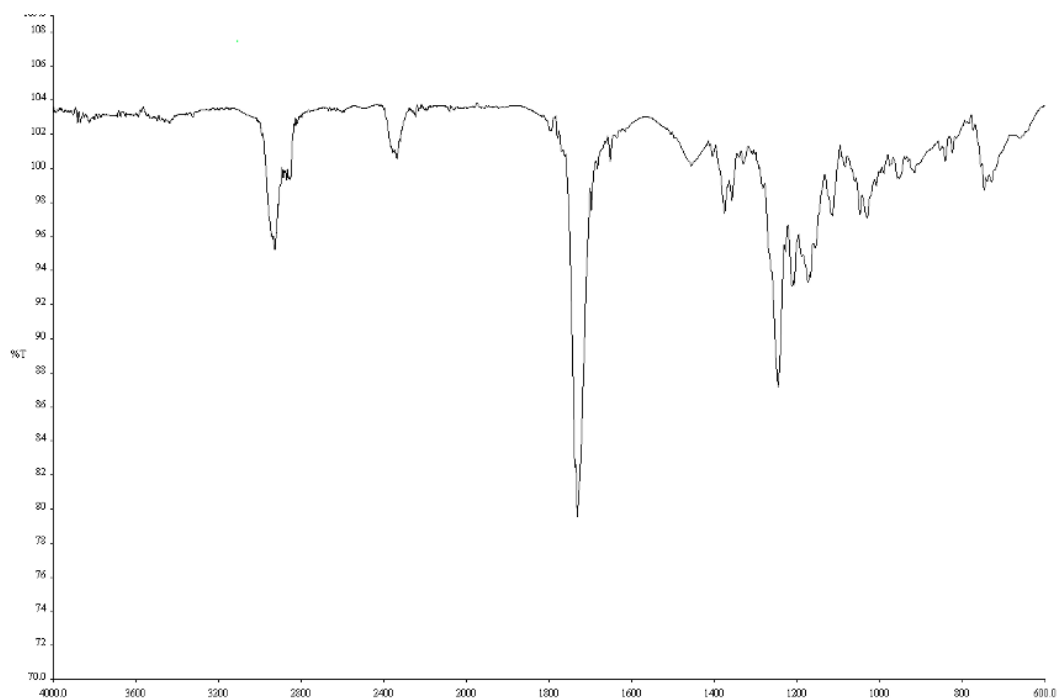
Figure A2.328. *Infrared spectrum (Thin Film, NaCl) of compound **82**.*
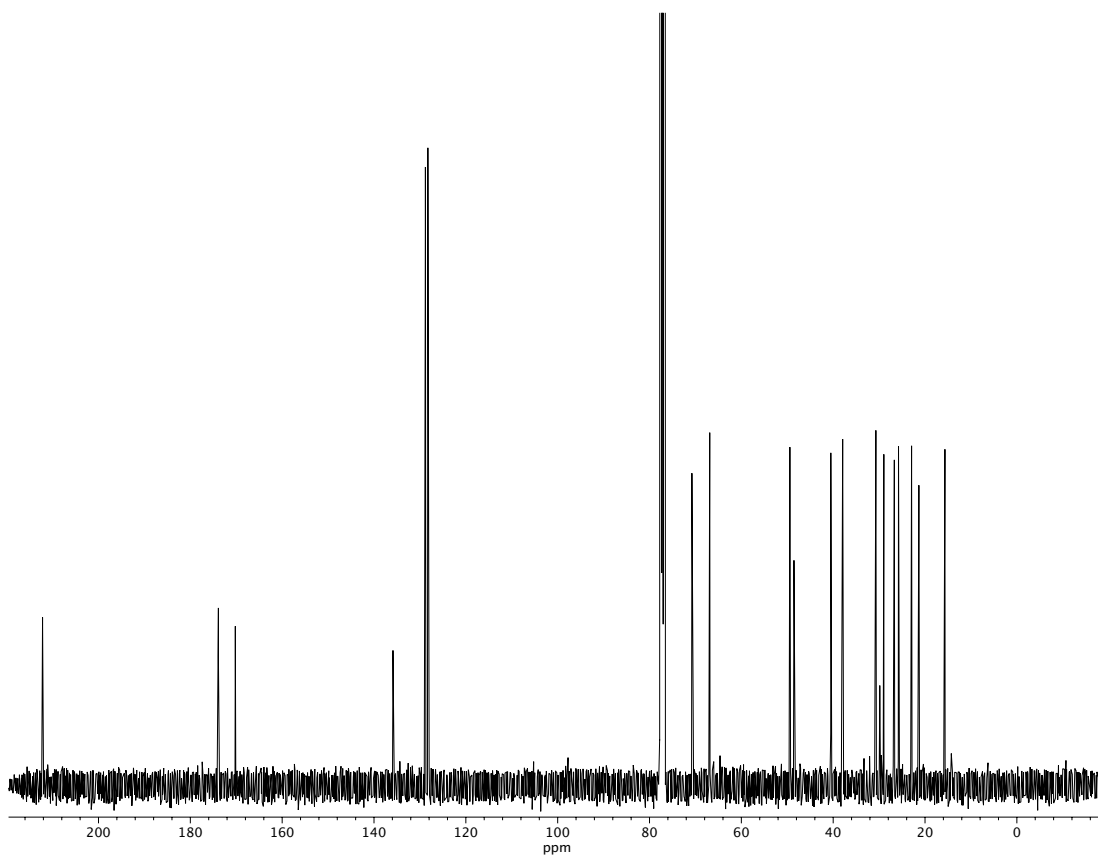
Figure A2.329. ^{13}C *NMR (100 MHz, CDCl$_3$) of compound **82**.*

CHAPTER 4

Quantum Mechanics Investigations of the [2+2] Photocycloaddition in the Synthesis of (−)-Scabrolide A [†]

4.1 INTRODUCTION

The [2+2] photocycloaddition serves as a powerful tool for the construction of carbon–carbon and carbon–heteroatom bonds.[1] The versatility of this transformation has led to numerous applications in the context of natural product synthesis,[2] particularly as the four-membered cycloadducts can be further employed in ring expansion processes through strain-release and C–C bond activation.[3]

In our recent total synthesis of (−)-scabrolide A (**119**), we sought to construct the 7-membered ring in the natural product through an oxidation/fragmentation sequence from cyclobutane **120**. Intermediate **120** would be accessed through an intramolecular photochemical [2+2] cycloaddition of an enone with a pendant vinyl silane (**121**) – derived from **122** and **123** – to forge the [4–5] ring system (**120**) (Scheme 4.1A).[4] Surprisingly, the desired [4–5] ring system (**120**) was not formed in this process; rather, a *cis*-fused [4–4] product **124** was produced as the exclusive product (Scheme 4.1B). The observed selectivity contrasts the "rule of five" generally attributed to enone-olefin cycloadditions, wherein the formation of five-membered rings is considered to be kinetically facile.[5] As a consequence of the undesirable reactivity, three additional steps to protect and

subsequently deprotect the isopropenyl olefin had to be incorporated into the synthesis.

Rectifying the chemoselectivity of the [2+2] photocycloaddition from **121** would improve

material throughput, support future synthetic efforts, and enable derivative-based

biological studies.[6] To explore this issue, we employ quantum mechanical calculations to

understand the mechanism by which the unexpected product **124** is formed and uncover

the origins of chemo- and diastereoselectivity.

Scheme 4.1. *Photochemical [2+2] approach to scabrolide A.*

A. Retrosynthetic approach to (–)-scabrolide A (119):
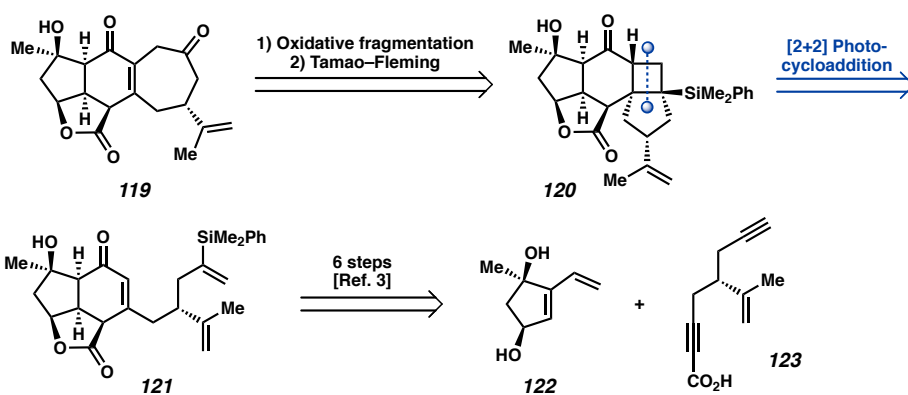
B. Unexpected reactivity:
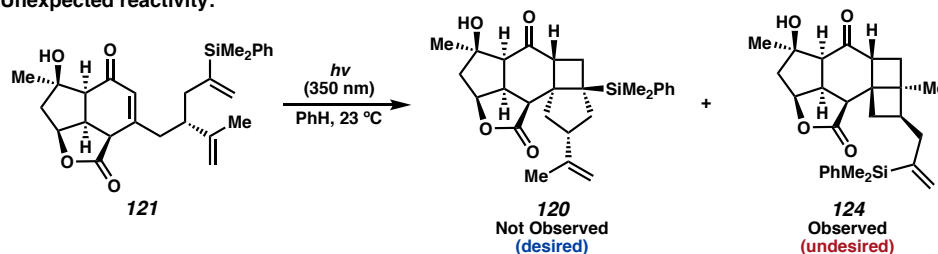
C. This research:
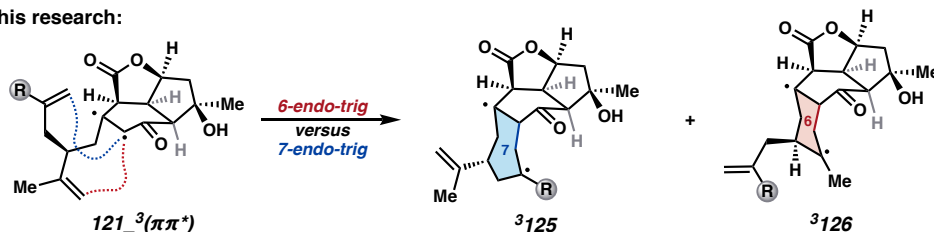
4.2   COMPUTATIONAL METHODS

All quantum mechanics calculations were carried out with the Orca program.[7] Geometries were optimized by density functional theory (DFT) using the B3LYP functional[8] paired with Grimme's D4 dispersion correction[9] and the def2-SV(P) basis set.[10] Vibrational frequency calculations were carried out at the same level of theory for all stationary points to verify their nature as minima or saddle points and to obtain thermal Gibbs free energy corrections at 298 K. Intrinsic reaction coordinate (IRC) analysis was performed to confirm that transition states lead to the appropriate minima.[11] Additional DFT single point calculations were carried out with the ωB97M-V functional[12] and the def2-TZVPP basis set with the SMD implicit solvation model for benzene. [13] Multiconfigurational single point calculations were carried out using complete active space self-consistent field (CASSCF) theory, with subsequent treatment of dynamical correlation by second order N-electron valence state perturbation theory (NEVPT2). [14] For state-averaged calculations, the Nakano quasi-degenerate (QD) formulation was employed.[15] These calculations employed the def2-TZVPP basis set with the SMD model for benzene. The (8,8) active space (eight electrons and eight orbitals) was chosen to contain the enone π system, the isopropenyl π/π^* and the vinyl silane π/π^*. The enone oxygen lone pair was included to obtain the (10,9) active space where nπ^* states are relevant. Unless otherwise specified, final Gibbs free energies are NEVPT2/def2-TZVPP/SMD(benzene) electronic energies with thermodynamical corrections obtained from the optimization level of theory. For full computational details, see section 4.5.

4.3   RESULTS AND DISCUSSION

The mechanism of the enone-olefin [2+2] photocycloaddition has been the subject of numerous theoretical and experimental investigations.[1b,16,17] The general mechanism begins with UVA irradiation to promote the n → π* excitation of α,β-unsaturated carbonyl **127** (Scheme 4.2, Step 1). The $^1(n\pi^*)$ excited state undergoes intersystem crossing (ISC) primarily to the $^3(\pi\pi^*)$ state (**128_$^3(\pi\pi^*)$**) (El Sayed's rule).[18] Occupation of the antibonding π* orbital would then result in elongation of the C=O and C=C bonds. For conformationally flexible enones, the adiabatically relaxed $^3(\pi\pi^*)$ state leads to a torsion about the α and β positions and typically becomes lower in energy than the $^3(n\pi^*)$ state. Prior studies unambiguously determined that the first C–C bond formation occurs from triplet excited states,[1b,17] preferentially from the $^3(\pi\pi^*)$ state.[16a] For intermolecular cases, the ensuing C–C bond formation between the enone and olefin typically occurs via β-attack of the enone (Scheme 4.2, Step 2), *i.e.*, an attack by the less stabilized spin center, to afford a triplet 1,4-diradical (**^{3}129**). Half-lives of the 1,4-triplet diradicals intermediates have been measured to range from 10 to 1,000 ns.[19] Subsequent ISC to the corresponding singlet diradical (**^{1}129**) then enables either productive ring closure to form **131** or unproductive C–C scission to return to enone **127** (Scheme 4.2, Steps 3 and 4). Weedon and coworkers find that the intermediacy of α-radicals (sp^2), such as **^{1}129**, tends to favor C–C bond scission, while ring closure is more likely with β-radicals (sp^3), such as **^{1}130**.[20]

Scheme 4.2. *General four-step mechanism for the olefin/α,β-unsaturated carbonyl*

[2+2] photocycloaddition.

| 1. Photoexcitation + ISC | 2. First bond formation | 3. ISC to singlet diradical | 4. Second bond formation |
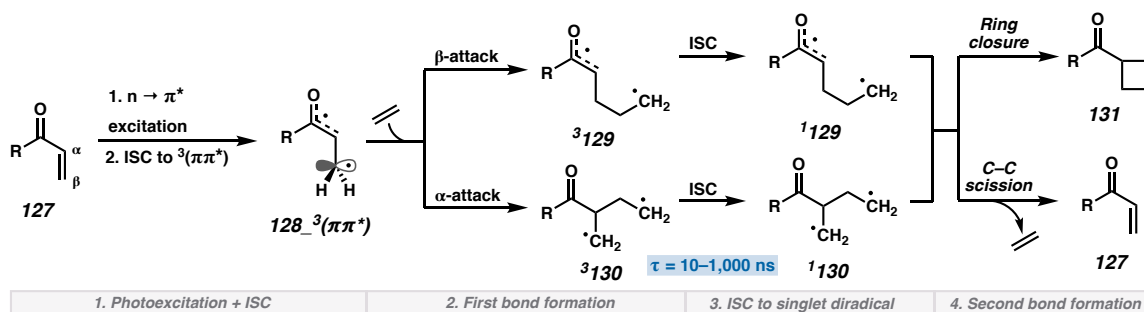
4.3.1   STEP 1: PHOTOEXCITATION

The [2+2] photocycloaddition of enone **121** (Scheme 4.1B) is achieved upon

irradiation with a standard UVA mercury vapor gas-discharge lamp ($\lambda_{max} \sim 350$ nm). The

initial singlet n $\rightarrow$ π* vertical excitation was calculated to be 3.96 eV (313 nm) (Scheme

4.3A) – in accord with known values for aliphatic cyclic enones.[19b] Energies of 3.73 and

4.01 eV were calculated for the vertical n $\rightarrow$ π* and π $\rightarrow$ π* excitations to the $^3(n\pi^*)$ and

$^3(\pi\pi^*)$ states, respectively, from the ground state minimum (**121_S$_0$**) (Scheme 4.3C).[21] The

second lowest singlet excitation is significantly higher in energy at 7.45 eV and is of $^1(\pi\pi^*)$

character.[22] In accord with prior studies, the singlet n $\rightarrow$ π* excitation is accessible under

UVA irradiation and is the excited state from which productive reactivity ensues.

Despite our best efforts, pervasive root-flipping made adiabatic optimization on the

$^1(n\pi^*)$ surface challenging. As such, we employed the optimized $^3(n\pi^*)$ geometry as a

surrogate for the $^1(n\pi^*)$ minimum.[23] The resulting adiabatic excitation energies of 3.34 and

3.37 eV (77.0 and 81.1 kcal/mol) are obtained for the $^3(n\pi^*)$ and $^1(n\pi^*)$ states, respectively.

Apart from elongation of the C(2)–O(1) and C(3)–C(4) bonds, the $^3(n\pi^*)$ geometry is

similar to that of the ground state enone (Scheme 4.3D). At the **121_^{1}(nπ*)** stationary point, the ^{3}(ππ*) surface lies 4.8 kcal/mol above the ^{1}(nπ*) surface. The ^{3}(nπ*) is the lowest energy triplet state at the **121_S$_0$** and **121_^{1}(nπ*)** stationary points (Scheme 4.3A); however, the adiabatic ^{3}(ππ*) excitation energies of simple enones are typically lower than that of the ^{3}(nπ*) state. Although it has been hypothesized that for highly rigid, cyclic systems the ^{3}(ππ*) state may remain higher in energy,[24] optimization of the ^{3}(ππ*) state of **121** yields a total adiabatic excitation energy of 3.26 eV (75.2 kcal/mol), 1.8 kcal/mol lower than the ^{3}(nπ*) minimum despite the rigidity of the tricyclic core. Given its comparative thermodynamic favorability, we hypothesized that the ^{3}(ππ*) surface can be readily accessed from the initially excited ^{1}(nπ*) state and account for the subsequent C–C bond formation. Hence, we sought to further interrogate the interaction of the excited state surfaces.

Beginning from the minimized **121_^{1}(nπ*)** geometry (still employing the ^{3}(nπ*) minimum as a surrogate), the nuclear coordinates were relaxed with energies and forces obtained from the ^{3}(ππ*) surface.[25] Single point calculations at the QD-NEVPT2 level of theory were carried out at points along the optimization trajectory to plot the corresponding energies of the ^{1}(nπ*), ^{3}(nπ*), and ^{3}(ππ*) surfaces. Moving along the reaction coordinate, the ^{3}(ππ*) state energy decreases, with elongation of the C(2)–O(1) and C(3)–C(4) bonds and subsequent twisting along the C(2)–C(3)–C(4)–C(5) dihedral (Scheme 4.3D). The nπ* states increase in energy as a result of these distortions, with the ^{1}(nπ*) crossing the ^{3}(ππ*) surface at C(2)–O(1) and C(3)–C(4) bond lengths of 1.33 and 1.45 Å, respectively.[26] Non-zero spin-orbit coupling (SOC) between the ^{1}(nπ*) and ^{3}(ππ*) states results in an avoided

crossing with a barrier (E_a) of 1.4 kcal/mol (Scheme 4.3B).[27] In contrast to the $^1(n\pi^*)$ to $^3(\pi\pi^*)$ crossing, ISC from the $^1(n\pi^*)$ state to the $^3(n\pi^*)$ state is symmetry-forbidden.[18] Additionally, non-productive phosphorescence from the $^3(n\pi^*)$ state to the closed-shell singlet ground state is symmetry-allowed and is anticipated to be rapid.[18] In summary, an n → π* transition at 3.96 eV (313 nm) followed by ISC to the $^3(\pi\pi^*)$ surface yields intermediate **121_$^3(\pi\pi^*)$** – which is 1.8 kcal/mol lower in energy than **121_$^3(n\pi^*)$** – poised to undergo the first C–C bond formation.

Scheme 4.3. *Photoexcitation of* **121_S_0** *and conversion to reactive triplet diradical* **121_$^3(n\pi^*)$**.
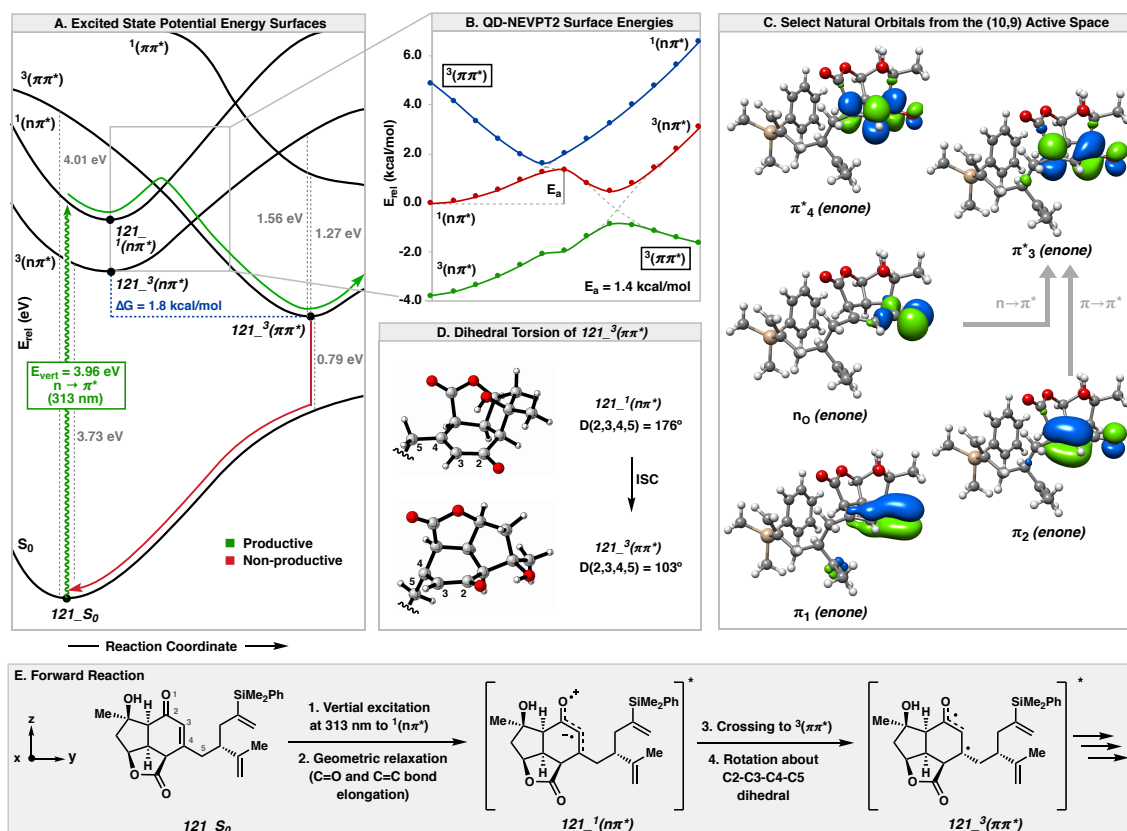
4.3.2   STEP 2: FIRST C–C BOND FORMATION

Triplet diradical **121_$^3(\pi\pi^*)$** may then undergo C–C bond formation with either of the

pendant olefins. A single reference approach such as DFT should provide a good

description of the triplet surface where the lowest triplet state is well isolated from other

excited states, as is the case for the **121_$^3(\pi\pi^*)$** (vide supra). Moreover, spin contamination

is generally minor.

As mentioned above, radical cyclizations during the first C–C bond formation may

occur from either the α or β positions (Scheme 4.2, Step 2). In the analogous reaction

between acrolein and ethylene, Houk and coworkers find a 3–4 kcal/mol preference for β-

attack due to the greater stability of the resulting delocalized α-acyl radical.[16a] In the system

at hand, β-attack may occur from the isopropenyl olefin in a 5-*exo*-trig fashion (**TS44**,

TS45) or the vinyl silane in a 4-*exo*-trig (**TS46**, **TS47**) fashion, respectively (Scheme

4.4A).[28] The corresponding 5-*endo*-trig and 6-*endo*-trig cyclizations that give rise to

spirocyclic 1,4-diradicals were also considered (see section 4.5). The cyclizations may

occur from either the *Re* or *Si* face of the enone in conjunction with either face of the olefin

(Schemes 4.7 and 4.8). In total, twelve diastereomeric transition states were considered for

the β-attack mechanism.

For reaction pathways involving α-attack, twelve diastereomeric transition states

were similarly derived from approach to either face of the enone with the isopropenyl olefin

in a 6-*endo*-trig (**TS48**, **TS49**) or 5-*exo*-trig cyclization (Scheme 4.7), or with the pendant

vinyl silane in a 7-*endo*-trig (**TS50, TS51**) or 6-*exo*-trig cyclization (Scheme 4.9).[29] All

diastereomeric transition states for α- and β-attack pathways were considered because the new stereocenters forged from the [2+2] photocycloaddition will be ablated during the ensuing synthetic transformations (oxidation and fragmentation, Scheme 4.1A). This causes diastereomeric diradicals – such as **³132** and **³133** (Scheme 4.4A) – to eventually give rise to the same [6–4–5] ring-containing synthetic intermediate. Therefore, only the chemoselectivity – not the diastereoselectivity – of the first C–C bond formation is relevant to the final synthetic outcome.

Given the vast number of energetically accessible conformers for each of the 24 relevant diastereomeric transition states, pre-screening with DFT ((U)ωB97M-V/def2-TZVPP/SMD(benzene)//(U)B3LYP-D4/def2-SV(P)) was carried out to efficiently eliminate high energy pathways. The eight most relevant pathways are discussed below (Scheme 4.4A) with additional discussion on alternative pathways in section 4.5.

During the course of our synthetic planning, we envisioned that the system would preferentially undergo β-attack in a 5-*exo*-trig cyclization with the vinyl silane (**TS44**), forging the 5-membered ring of a desirable cycloaddition adduct (**³132**). Approach of the enone *Si* face to give 1,4-diradical intermediate **³132** is met with a barrier of 8.0 kcal/mol. The analogous 5-*exo*-trig transition state corresponding to approach of the *Re* face (**TS45**) was not found. Rather, diradical **³133** converts to **121_³(ππ*)** via a stepwise mechanism from cycloheptyl diradical **³125** (Scheme 4.4B).[30]

Scheme 4.4. *Eight lowest energy reaction pathways from* **$121\_^3(\pi\pi^*)$**.[a]

A. Eight lowest energy reaction pathways from triplet diradical $121\_^3(\pi\pi^*)$.
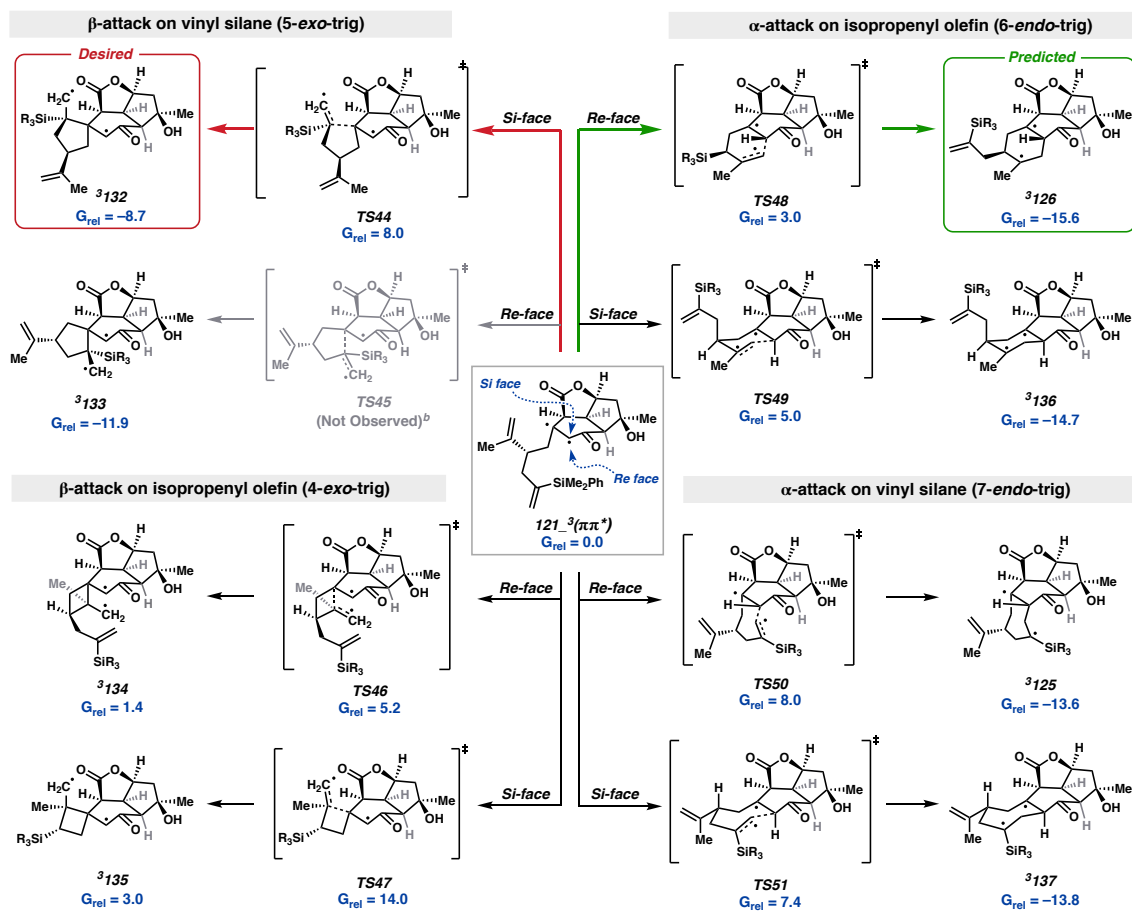
B. 5-*exo*-trig Transition States
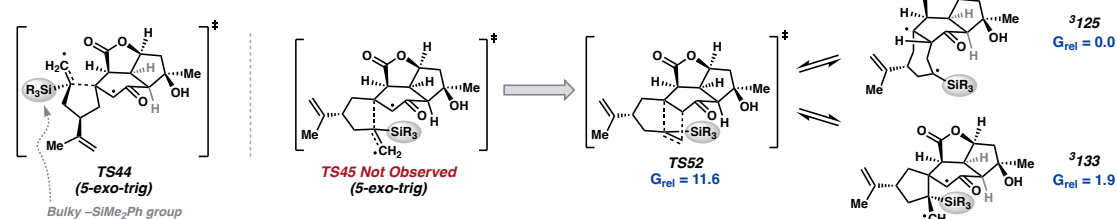
[a] Gibbs free energies (in kcal/mol) are calculated at the NEVPT2/def2-TZVPP/SMD(benzene)//(U)B3LYP-D4/def2-SV(P) level of theory. –SiR$_3$ = SiMe$_2$Ph. [b] All attempts to find a saddle point corresponding to **TS45** ultimately lead to **TS52** connecting ^{3}**125** to ^{3}**133**.

Prior studies suggest that bond formation occurs from the $^3(\pi\pi^*)$ state rather than along the higher energy $^3(n\pi^*)$ surface. Indeed, the $^3(n\pi^*)$ state is found to lie 1.69 eV (39.0 kcal/mol) above the $^3(\pi\pi^*)$ ground state triplet PES at the **TS44** saddle point.[31] At **TS44**, $^3(n\pi^*)$ character in the ground state triplet is negligible, contributing < 0.5% to the configuration interaction (CI) wavefunction.

Surprisingly, a barrier of 5.2 kcal/mol was found for *Re* face β-attack in a 4-*exo*-trig cyclization with the isopropenyl olefin (**TS46**), lower than that of the minimum energy 5-*exo*-trig pathway (**TS44**). Approaching from the *Re* face of the enone is favored (**TS46**), with a $\Delta G^{\ddagger}$ to *Si* face approach of 14.0 kcal/mol (**TS47**) (Scheme 4.4A). Unlike the generation of cyclopentanes **³132** and **³133**, the formation of both cyclobutane 1,4-diradicals (**³134** and **³135**) is thermodynamically unfavorable, with a change in reaction free energy (ΔG) of 1.4 and 3.0 kcal/mol, respectively.

We then turned our attention to reaction pathways featuring α-attack of the triplet enone diradical. Productive C–C bond formation may occur through either a 6-*endo*-trig or 7-*endo*-trig radical cyclization from either the *Re* or *Si* face of the enone (Scheme 4.4).[32] Barriers of 3.0 and 5.0 kcal/mol were found for 6-*endo*-trig cyclization from the *Re* (**TS48**) or *Si* face (**TS49**), respectively. Higher barriers were obtained for the 7-*endo*-trig cyclization at 8.0 and 7.4 kcal/mol for approach from the *Re* (**TS50**) or *Si* face (**TS51**), respectively. Triplet 1,4-diradical intermediates resulting from 6-*endo*-trig (**³126**) or 7-*endo*-trig (**³137**) radical cyclization are lower in free energy than **121_³(ππ*)** by at least 13 kcal/mol.

In summary, the global minimum energy pathway for the first C–C bond formation from **121_$^3(\pi\pi^*)$** is via 6-*endo*-trig cyclization with the isopropenyl olefin to forge triplet diradical ^{3}**126**. This process is accompanied by a $\Delta G^\ddagger$ of 3.0 kcal/mol and a ΔG of –15.6 kcal/mol, relative to **121_$^3(\pi\pi^*)$**. The transition state describing this minimum energy pathway (**TS48**) resides on the $^3(\pi\pi^*)$ surface, with a vertical excitation energy of 1.96 eV (45.2 kcal/mol) to the $^3(n\pi^*)$ state. At **TS48**, $^3(n\pi^*)$ character in the ground state triplet is negligible, contributing < 0.5% to the CI wavefunction.[33]

Prior studies suggest that in photochemical [2+2] cycloadditions, the first C–C bond formation on the triplet surface occurs irreversibly (*i.e.*, before ISC).[1b,16] We found forward and reverse barriers to C–C bond formation along the minimum energy pathway to be 3.0 and 18.6 kcal/mol, with rate constants at 298.15 K of 3.9 x10^{10} s^{-1} and 1.4 x10^{-1} s^{-1}, respectively. For simple enones, lifetimes of triplet 1,4-diradical intermediates derived from [2+2] photocycloadditions are on the scale of 10 to 1,000 ns, *i.e.*, unimolecular decay rate constants are on the order of magnitude of 10^6 – 10^8 s^{-1}.[19] Thus, C–C bond formation through **TS48** is irreversible, with the reverse process (k ~ 10^{-1} s^{-1}) being outcompeted by ISC (k ~ 10^8 – 10^6 s^{-1}). Meanwhile, productive bond formation (k ~ 10^{10} s^{-1}) is anticipated to be more rapid than ISC, and thus, proceeds on the triplet surface. Still, we consider the effect of a competitive ISC. Starting from the **121_$^3(\pi\pi^*)$** geometry, optimization along the ground state singlet surface smoothly affords the closed-shell singlet starting material **121_S$_0$**. Hence, premature spin flip would lower the efficiency of the overall process but likely does not lead to undesired reactivity.[16d]

4.3.3   STEP 3: SECOND C–C BOND FORMATION

The first ring closure generates a triplet 1,4-diradical, which was shown to be almost energetically degenerate with its singlet counterpart. The singlet-triplet gap for diradical **126** is calculated to be less than 1 kcal/mol, favoring anti-ferromagnetically coupled spins (Scheme 4.5).[34] After ISC to the singlet 1,4-diradical surface, the system undergoes relaxation to a stable diradical intermediate or a C–C bond cleavage to re-form **121** (Scheme 4.5). We hypothesized that the partitioning between the two outcomes depends on the conformation of the 1,4-diradical at the point at which ISC occurs (Scheme 4.10).[35] Starting from the triplet diradical geometries of low-energy conformers, relaxation of the nuclear coordinates on the broken-symmetry ($M_S = 0$) DFT (BS-DFT)[36,37] surface yields either singlet diradicals or enone **121**. For diradical **126** (Scheme 4.5), five of the 14 lowest-energy conformers relaxed to enone **121** (including the globally lowest-energy conformer), which accounts for 70% of the Boltzmann-weighted population of conformers. As such, only 30% of the triplet diradical population will relax to stable singlet diradicals.[38]

Unlike multi-configurational methods (such as NEVPT2/CASSCF), single-determinantal methods (such as BS-DFT) are unable to properly describe open-shell singlet states.[36,39] Hence, we sought to compare the final energies calculated on the BS-DFT potential energy surface (PES) to those from the NEVPT2 surface. We found significant discrepancies in the BS-DFT and NEVPT2 PESs along the reaction coordinate of the second C–C bond formation (see section 4.5), with BS-DFT calculations favoring a later transition state than NEVPT2. Consequently, a more accurate barrier was derived from a

PES obtained by calculating NEVPT2 electronic energies along the BS-DFT intrinsic

reaction coordinate (IRC) trajectory for the transition state in question.

Scheme 4.5. *Predicted reactivity from diradical* **126**.
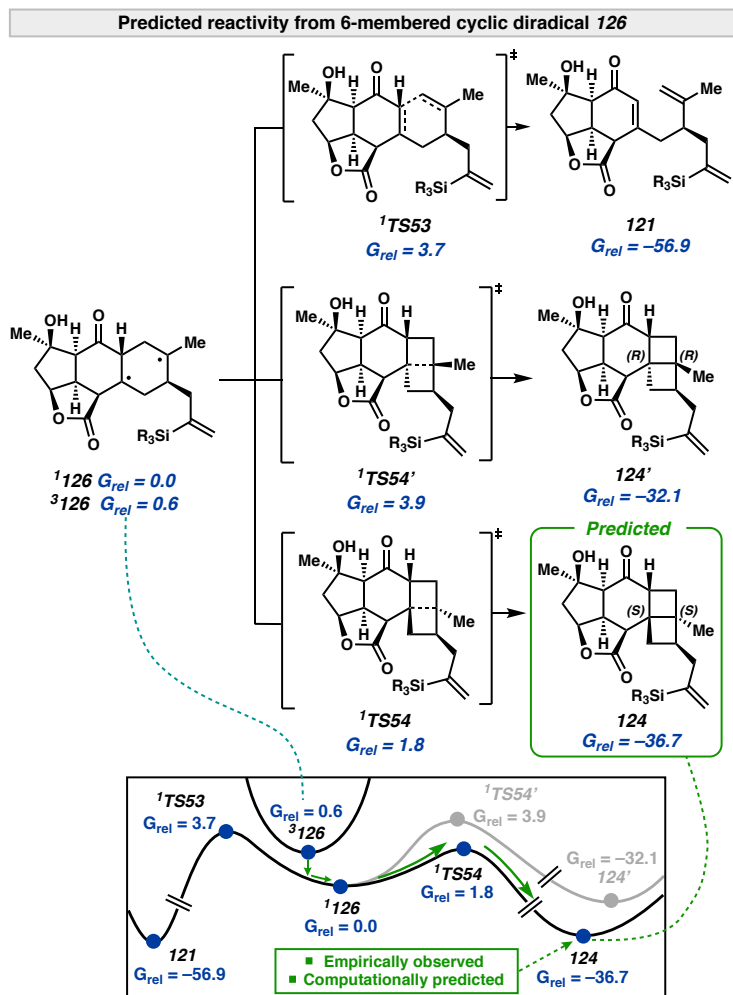
[a]   Gibbs   free   energies   (in   kcal/mol)   are   calculated   at   the   NEVPT2/def2-

TZVPP/SMD(benzene)//(U)B3LYP-D4/def2-SV(P) level of theory. –SiR$_3$ = SiMe$_2$Ph.

Scheme 4.6. *Predicted reactivity from diradical **125**.*
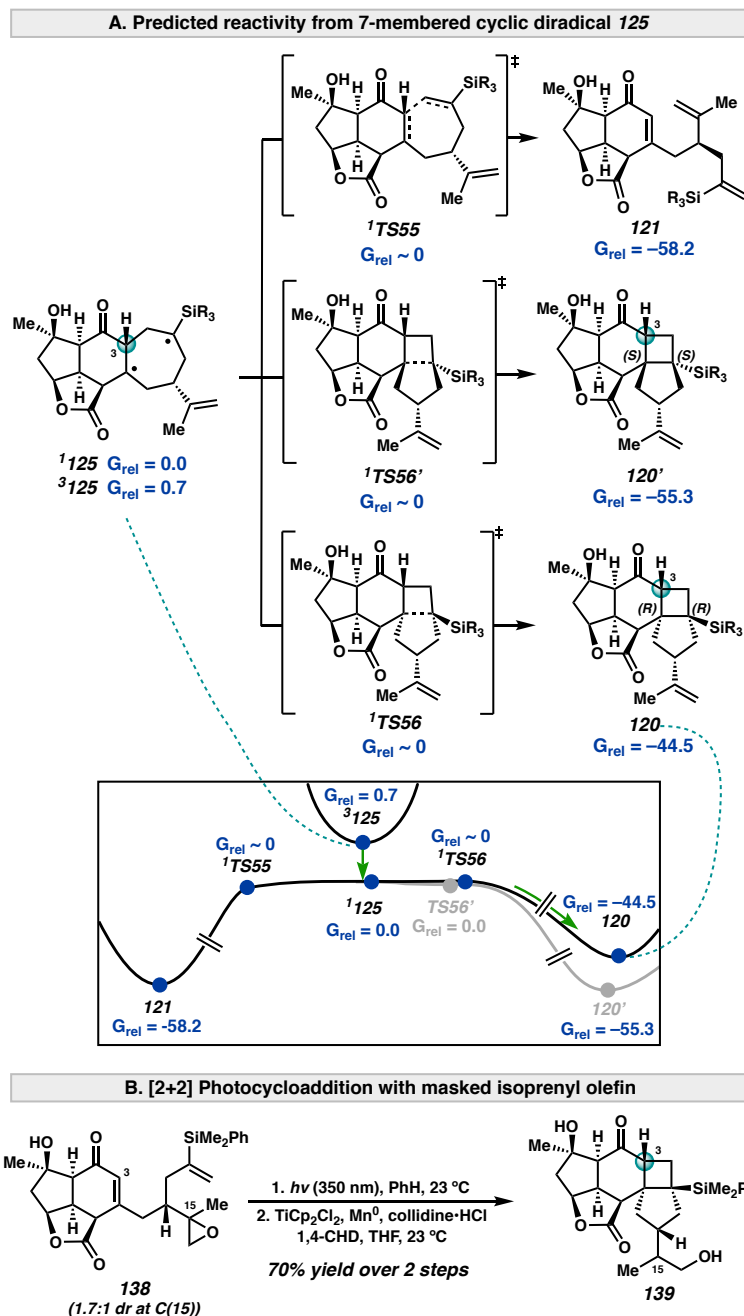
A. Predicted reactivity from 7-membered cyclic diradical 125

¹TS55
$G_{rel} \sim 0$

121
$G_{rel} = -58.2$

¹125 $G_{rel} = 0.0$
³125 $G_{rel} = 0.7$

¹TS56'
$G_{rel} \sim 0$

120'
$G_{rel} = -55.3$

¹TS56
$G_{rel} \sim 0$

120
$G_{rel} = -44.5$

$G_{rel} = 0.7$
³125

$G_{rel} \sim 0$
¹TS55

$G_{rel} \sim 0$
¹TS56

$G_{rel} = -44.5$
120

¹125
$G_{rel} = 0.0$

TS56'
$G_{rel} = 0.0$

121
$G_{rel} = -58.2$

120'
$G_{rel} = -55.3$

B. [2+2] Photocycloaddition with masked isoprenyl olefin

138
(1.7:1 dr at C(15))

1. *hv* (350 nm), PhH, 23 °C
2. TiCp₂Cl₂, Mn⁰, collidine·HCl
   1,4-CHD, THF, 23 °C

70% yield over 2 steps

139

[a] Gibbs free energies (in kcal/mol) are calculated at the NEVPT2/def2-TZVPP/SMD(benzene)//(U)B3LYP-D4/def2-SV(P) level of theory. –SiR₃ = SiMe₂Ph.

From the relaxed singlet diradical geometry, the second C–C bond formation could then occur. For diradical **126**, the formation of which is most facile during the first C–C bond formation (Scheme 4.4), the open-shell singlet PES for its lowest-energy conformer (Scheme 4.5) suggests that formation of the experimentally observed product **124** involves a barrier of 1.8 kcal/mol via **^{1}TS54**. This is significantly lower than the 3.9 kcal/mol barrier (**^{1}TS54'**) for the formation of the corresponding diastereomer **124'** or the 3.7 kcal/mol barrier (**^{1}TS53**) for the reversion back to enone **121**. This is consistent with exclusive formation of product **6**, as was observed experimentally.[4]

It was observed in the original synthesis of scabrolide A that protecting the isopropenyl olefin as an epoxide (**138**) afforded the desired [6–4–5] ring system as the *R* epimer at C(3) (**139**) (Scheme 4.6A). Analogously, we analyzed the open-shell singlet surface for diradical **125**, which would lead to the desired but experimentally non-observed product **120** containing the [6–4–5] ring system with the same stereochemistry at C(3). Its precursor triplet diradical **^{3}125** is generated via 7-*endo*-trig cyclization (**TS50**) of **121_^{3}(ππ*)** (Scheme 4.4A) and all of its low-energy conformers remained as stable singlet diradicals after ISC (with a singlet-triplet gap of less than 1.0 kcal/mol). NEVPT2 calculations suggest a highly flat open-shell singlet PES around the diradical geometry, with an approximately barrierless formation of target product **120** via **^{1}TS56**, or its diastereomer **120'** via **^{1}TS56'**, or re-formation of enone **121** via **^{1}TS55** (Scheme 4.6B).

The relative flat nature of the open-shell singlet PES introduces the possibility that dynamical effects might dictate the partitioning of reaction pathways from diradicals **^{1}126** and **^{1}125**. Ergo, ab initio molecular dynamics (AIMD) simulations were performed,

beginning from optimized triplet-diradical geometries (see section 4.5). AIMD were carried out with the PBE functional, as our controlled studies found that omission of Hartree–Fock exchange leads to a more qualitatively correct open-shell singlet PES with respect to NEVPT2 as a reference (Schemes 4.12 and 4.13). For [1]**126**, AIMD reveals an equal partitioning of low-energy conformers between substrate regeneration and product formation, which is qualitatively consistent with the distribution of outcomes from relaxation of nuclear coordinates of low-energy conformers along the broken-symmetry PES (Table 4.3). Similarly, AIMD trajectories suggest that the majority of the population of diradical [1]**125** terminate as the desired product **120**, while <1% affords substrate **121** or diastereomer **120'** (Table 4.4). These results suggest that dynamic effects on the singlet surface are not significant and the aforementioned results from relaxation of nuclear coordinates after the ISC are reliable.

In summary, our results demonstrate that if ISC from the triplet to the open-shell singlet surface affords a stable singlet diradical, then the second C–C bond formation (ring closure) will occur, albeit with variable efficiencies depending on the conformation of the singlet diradical. Equipped with this understanding, we hypothesized that the desired product **120** (or **120'**) can be accessed, as long as formation of triplet diradical [3]**125** is favored during the first C–C bond formation.

4.3.4   COMPLETE MECHANISM

As a result of these findings, we propose a mechanism that accounts for the chemo- and diastereoselectivity in the unexpected formation of **124** from enone **121** (Figure 4.1). The initial $n \rightarrow \pi^*$ excitation followed by intersystem crossing (ISC) to the $^3(\pi\pi^*)$ state

and geometric relaxation, characterized by twisting of the enone, affords triplet diradical

121_^{3}($\pi\pi^*$) (Scheme 4.3). From **121_^{3}($\pi\pi^*$)**, cyclizations can occur from α- or β-attack of

the enone triplet diradical with either the pendant isopropenyl olefin or vinyl silane.

Considering all modes of cyclization and *Re/Si* facial selectivity, a total of eight possible

ring-closed products are relevant (Scheme 4.4A). From **121_^{3}($\pi\pi^*$)** the most kinetically

favorable of these pathways is a 6-*endo*-trig cyclization involving α-attack of the enone

onto the isopropenyl olefin to give **^{3}126**, with ΔG‡ of 3.0 kcal/mol (**TS48**, Scheme 4.4A)

and ΔΔG‡ of 4.4 kcal/mol (relative to the second lowest activation barrier). This initial C–

C bond formation is thermodynamically favored by 15.6 kcal/mol. Experimentally derived

excited state lifetimes for related ^{3}($\pi\pi^*$) 1,4-diradical intermediates range from 10 to 1,000

ns. As a result, the initial C–C bond formation is irreversible. ISC from **^{3}126** affords the

corresponding singlet 1,4-diradical **^{1}126**. Along the singlet surface, C–C bond cleavage to

regenerate **121** or radical recombination to forge a second C–C bond may occur to form

ring-closed species **124** or **124'**. Given the flat nature of the singlet PES, the ultimate

outcome of ISC was found to be influenced by the conformation of the triplet diradical

prior to spin-flip. Relaxation to the ground state enone **121** was observed in a subset of

conformers accounting for approximately 70% of the Boltzmann population of the

conformer ensemble of **^{3}126**. For the conformers that persisted as singlet diradicals, radical

recombination to forge experimentally observed product **124** is favored over formation of

124' or **121** (Scheme 4.5).

Figure 4.1. *Complete mechanism describing formation of unexpected product **124***

*from the intramolecular [2+2] photocycloaddition of enone **121**.*

[a] Relative free energies (in kcal/mol) calculated at the (QD-)NEVPT2/def2-TZVPP/SMD(benzene)//(U)B3LYP-D4/def2-SV(P) level of theory. Relative energies in eV given in parentheses. Vertical excitation energies at selected stationary points are calculated with a state-averaged wavefunction. $^3(\pi\pi^*)/S_0$ intersection is not depicted.

4.4   CONCLUSIONS

We report a detailed quantum mechanics investigation of the mechanism of the intramolecular enone-olefin [2+2] photocycloaddition employed in our recent synthesis of (–)-scabrolide A (**119**). In our prior report, enone **121** was subjected to UV irradiation with the intent to forge a [6–4–5] ring system, which upon oxidative ring opening, would afford the fused [6–7] carbocyclic framework of (–)-scabrolide A (**119**). To our surprise, instead of forming the desired [6–4–5] ring scaffold (*i.e.*, **120**), **121** undergoes an unexpected cyclization to afford an undesired [6–4–4] ring system (*i.e.*, **124**). As a consequence of the undesirable reactivity, three additional synthetic steps to mask and subsequently reveal the isopropenyl olefin were incorporated into the synthesis.

Our QM calculations reveal that the preferential formation of the [6–4–4] ring system is a result of a facile 6-*endo*-trig radical cyclization on the $^3(\pi\pi^*)$ surface, outcompeting the alternative 7-*endo*-trig, 6-*exo*-trig, 5-*exo/endo*-trig, and 4-*exo*-trig pathways. Analysis of the open-shell singlet surfaces describing the hypothetical 1,4-diradical intermediates post-ISC reveals that C–C bond formation by radical recombination is favorable in each case. Moreover, our study has showcased the practicality and accuracy of combining ab initio wavefunction methods (CASSCF/NEVPT2) with DFT in modeling multiconfigurational and multideterminental open-shell systems. This approach thus serves as a model for future computational endeavors aiming at real-world systems involving complex spin configurations.

4.5   SUPPORTING INFORMATION

4.5.1   GENERAL COMPUTATIONAL DETAILS

All quantum mechanical calculations were performed with ORCA version 4.2.[7] The resolution of identity (RI) and chain-of-spheres[40] approximations were utilized for Coulomb and exchange integrals, respectively, with the def2/J auxiliary basis set.[41] Ultra-fine integration grids were employed throughout (keywords: "Grid7 NoFinalGrid GridX9"). The CYLview and Chimera[42] programs were used to generate graphical images in the main text.

DFT Calculations: Unless otherwise noted, geometry optimizations were carried out with the B3LYP global hybrid generalized gradient approximation (GGA) functional[8] with Grimme's D4 dispersion corrections[9] (henceforth referred to as B3LYP-D4) with the def2-SV(P) basis set[10] on all atoms. For open-shell species, unrestricted Kohn–Sham orbitals were employed. Spin contamination is generally minor. Thermal corrections at 298.15 K were calculated from the unscaled vibrational frequencies at this level of theory. The Quasi-RRHO method was applied to correct for the breakdown of the harmonic oscillator approximation for low frequency vibrations.[43] All stationary points are characterized by the appropriate number of imaginary vibrational modes (zero for optimized geometries and one for transition states). Intrinsic reaction coordinate (IRC) analyses were carried out to ensure all transition states connect the appropriate starting materials and products.[11] DFT electronic energies were further refined with the ωB97M-V functional,[12] def2-TZVPP basis set on all atoms, and the SMD implicit solvation model[13] for benzene. Outlying charge corrections were included in the final solvated energies. Final

(DFT) Gibbs free energies were derived by applying thermodynamic corrections obtained at the optimization level of theory to these refined electronic energies. While these DFT energies are found to be reliable for high-spin (S = 1) intermediates where the $n\pi^*$ and $\pi\pi^*$ surfaces are well separated, multiconfigurational calculations (here, CASSCF/NEVPT2) are employed for a more rigorous description of the electronic structure. However, DFT remains a cost-effective tool for rapid evaluation/screening of conformers. Hence, calculations at the (U)ωB97M-V/def2-TZVPP/SMD(benzene)//(U)-B3LYP-D4/def2-SV(P) level of theory were employed for exploring reactivity along the triplet $\pi\pi^*$ surface (see Schemes 4.7–4.9).

CASSCF/NEVPT2 Calculations: CASSCF calculations were performed in order to properly describe the multiconfigurational nature of the system in regions of state crossings, as well as open-shell singlet intermediates. The active space is chosen to incorporate the necessary bonding/anti-bonding orbitals. For enone **121_S$_0$**, this affords a 10 electron in 9 orbital active space [enone π/π^* orbitals, isopropyl π/π^*, vinyl silane π/π^*, carbonyl oxygen lone pair], henceforth abbreviated as (10,9). For intermediates where C–C bonds are formed from reactivity of these π systems, the corresponding C–C s/s* are included to maintain a consistent active space. The carbonyl oxygen lone pair of **121** and its subsequent intermediates is included only when necessary (*i.e.*, describing $n\pi^*$ states), as the lone pair is otherwise weakly correlated (occupation number > 1.999) leading to convergence issues. Additional dynamical correlation is recovered by subsequent N-Electron Valence State Perturbation Theory[14] (NEVPT2) calculations using the CASSCF wavefunction as a reference. For cases where state-averaged CASSCF wavefunctions are

employed, the quasi-degenerate formalism of Nakano[15] (QD-NEVPT2) was employed, allowing for re-mixing of CI coefficients under the effect of dynamical correlation. Unless otherwise notes, all energies in the main text are relative Gibbs free energies in kcal/mol derived from electronic energies at the NEVPT2/def2-TZVPP/SMD(benzene) level of theory with thermodynamic corrections from the (U)B3LYP/def2-SV(P) optimization level.

Excited State Surfaces in Scheme 4.3.

The initial singlet $n \rightarrow \pi^*$ vertical excitation energy of 3.96 eV (313 nm) was obtained from QD-NEVPT2-corrected CASSCF wavefunction with the (10,9) active space with averaging over two triplets ($n\pi^*$ and $\pi\pi^*$) and three singlet states (closed-shell singlet (ground state), $n\pi^*$, and $\pi\pi^*$). Nearly identical results are obtained regardless of state averaging scheme employed (see Table 4.1). From the ground state closed-shell singlet (S_0), the singlet $n \rightarrow \pi^*$ (S_1) and $\pi \rightarrow \pi^*$ (S_1) excitations are 3.96 and 7.45 eV, respectively (Table S1).

Table 4.1. *Comparison of vertical excitation energies calculated at the* **121_S₀** *with various state-averaging schemes.[a]*

State	2 triplets	2 singlets	3 singlets	2 triplets 3 singlets
S_0	–	0.00 [0.0]	0.00 [0.0]	0.00 [0.0]
S_1	–	4.01 [92.6]	3.99 [92.0]	3.96 [91.4]
S_2	–	–	7.42 [171.2]	7.45 [171.7]
T_1	0.00 [0.0]	–	–	3.73 [85.9]
T_2	0.28 [6.6]	–	–	4.01 [92.4]

[a] Calculations at the QD-NEVPT2/def2-TZVPP/SMD(benzene)//(U)B3LYP-D4/def2-SV(P) level of theory with the (10,9) active space at **121_S₀**.

In order to calculate the energy difference between the $^3(n\pi^*)$ and $^3(\pi\pi^*)$ minima (*i.e.*, **121_³(nπ*)** and **121_³(ππ*)**), single point calculations at the QD-NEVPT2/CASSCF level of theory with state averaging ($^3(n\pi^*)$ and $^3(\pi\pi^*)$)) were carried out at the **121_³(nπ*)** and **121_³(ππ*)** stationary points. State averaging was employed as at **121_³(ππ*)** the carbonyl oxygen lone pair is not significantly correlated in the ground-state triplet at **121_³(ππ*)** (occupation number > 1.999). This results in convergence issues in orbital optimization when included in the active space. Accordingly, the lowest triplet state at **121_³(ππ*)** does not contain significant $^3(n\pi^*)$ character and is well described by a single configuration of $\pi\pi^*$ character. Single point calculations with DFT ((U)ωB97M-V/def2-TZVPP/SMD(benzene)) also predict the **121_³(ππ*)** minimum to be 1.8 kcal/mol lower in energy than **121_³(nπ*)**.

An analogous strategy was employed when calculating the vertical excitation energies at the other relevant stationary points in Scheme 4.3 (**121_³(ππ*)**), scheme 4.4

(**TS48**), and when computing the vertical energy difference between $^3(n\pi^*)$ and $^3(\pi\pi^*)$ at C–C bond forming transition states. For computing the energy difference between stationary points with the same ground state (for example, $\Delta G^{\ddagger}$ between **121_$^3(\pi\pi^*)$** and **TS48**, both with $^3(\pi\pi^*)$ ground state), state-averaging is *not* employed.

Additional Stereochemical Considerations

In addition to the two 5-*exo*-trig β-attack pathways highlighted in the main discussion (**TS44** and **TS45** in Scheme 4.4), two additional diastereomeric pathways (**TS57** and **TS58**) are possible (Scheme 4.7). These pathways present higher barriers and are not accessible given the estimated kinetics of ISC. Moreover, the ensuing ring closure (after ISC) of the diradical intermediates would forge highly strained *trans* [4–5] fused ring systems. Hence, even if triplet diradical intermediates **140** and **141** were formed, C–C bond scission after ISC is anticipated, reforming starting material **121_S$_0$**.

In analogy to the discussion above, two additional diastereomeric 4-*exo*-trig β-attack transition states are possible (**TS59** and **TS60**, Scheme 4.8). These pathways are high in energy relative to the minimum energy pathways (Scheme 4.4) and are not responsible for the observed reactivity. Moreover, the formation of the resulting cyclobutane-containing products is accompanied by a positive change in free energy. Hence, equilibration prior to ISC will preferentially reform **121_$^3(\pi\pi^*)$**.

Scheme 4.7. *All four diastereomeric 5-exo-trig β-attack transition states and*
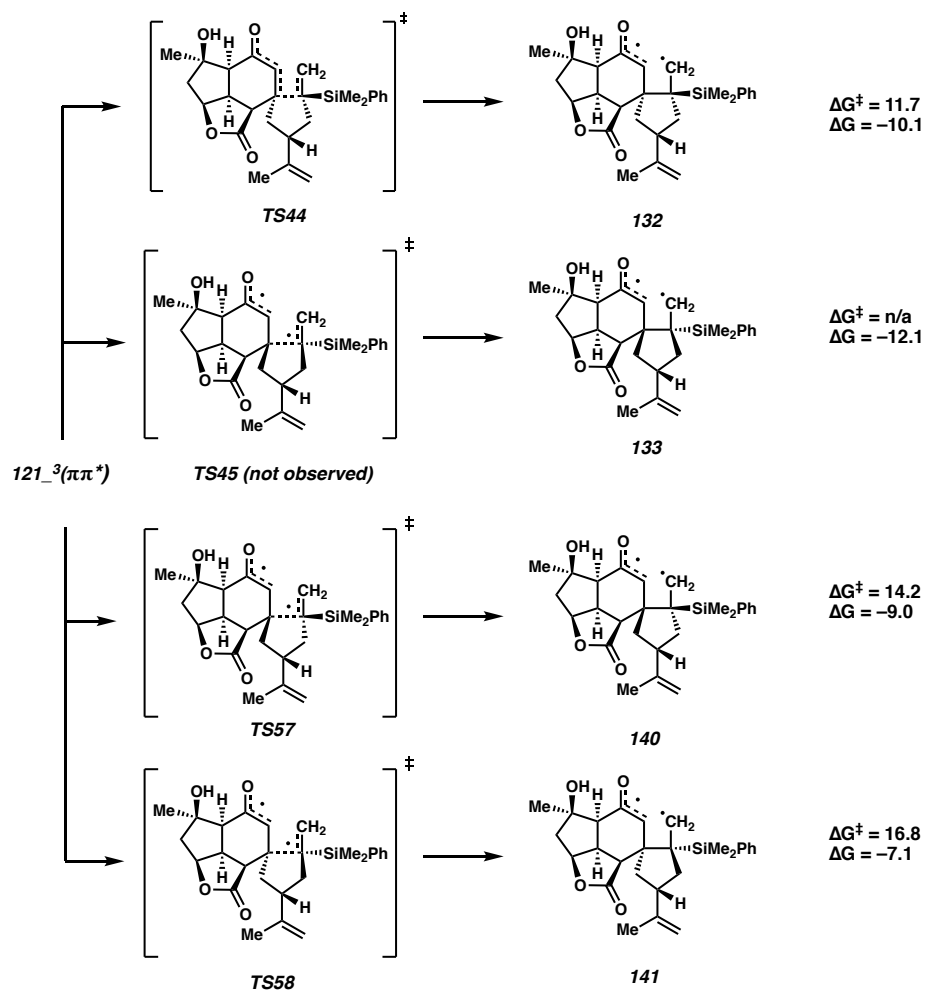
products.[a]

ΔG‡ = 11.7
ΔG = −10.1

ΔG‡ = n/a
ΔG = −12.1

ΔG‡ = 14.2
ΔG = −9.0

ΔG‡ = 16.8
ΔG = −7.1

[a] All diradicals are in the triplet spin state. Gibbs free energies in kcal/mol from the (U)ωB97M-

V/def2-TZVPP/SMD(benzene)//(U)B3LYP-D4/def2-SV(P) level of theory.

Scheme 4.8. *All four diastereomeric 4-exo-trig β-attack transition states and products.*
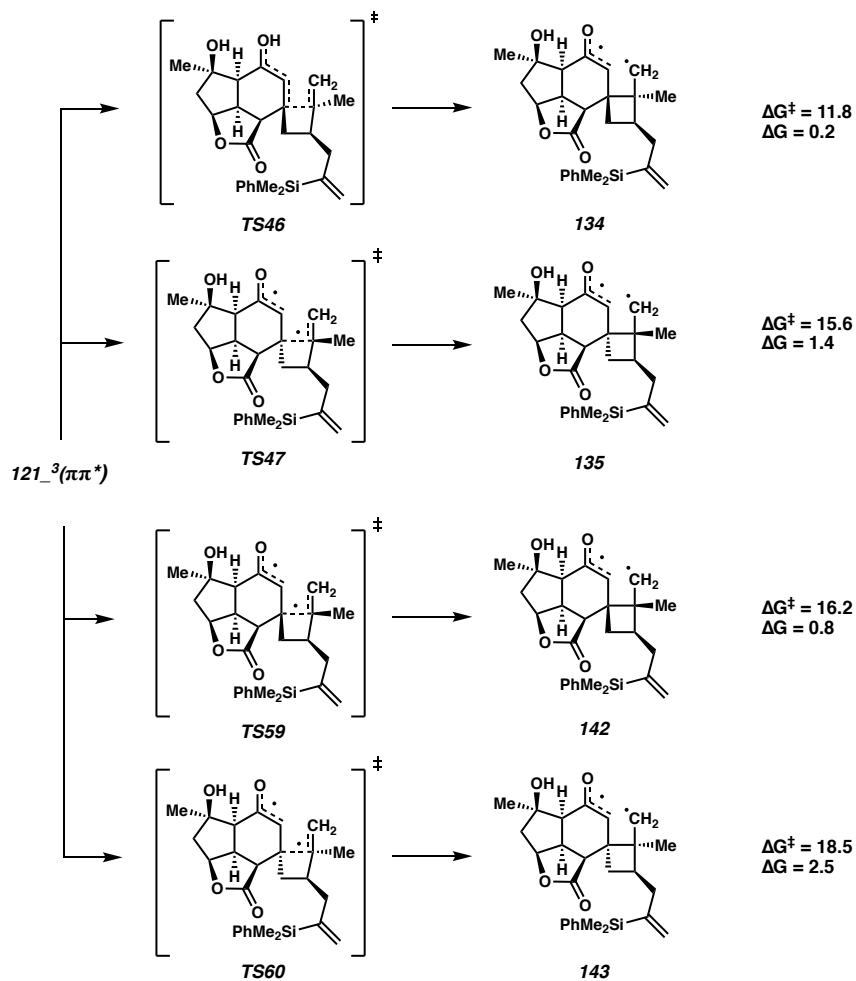
[a] All diradicals are in the triplet spin state. Gibbs free energies in kcal/mol from the (U)ωB97M-

V/def2-TZVPP/SMD(benzene)//(U)B3LYP-D4/def2-SV(P) level of theory.

Scheme 4.9. *All diastereomeric products for 6-exo-trig α-attack (**144–147**), 6-endo-trig β-attack (**148–149**), 5-endo-trig β-attack (**150–151**), and 5-exo-trig α-attack (**152–155**).*[a]
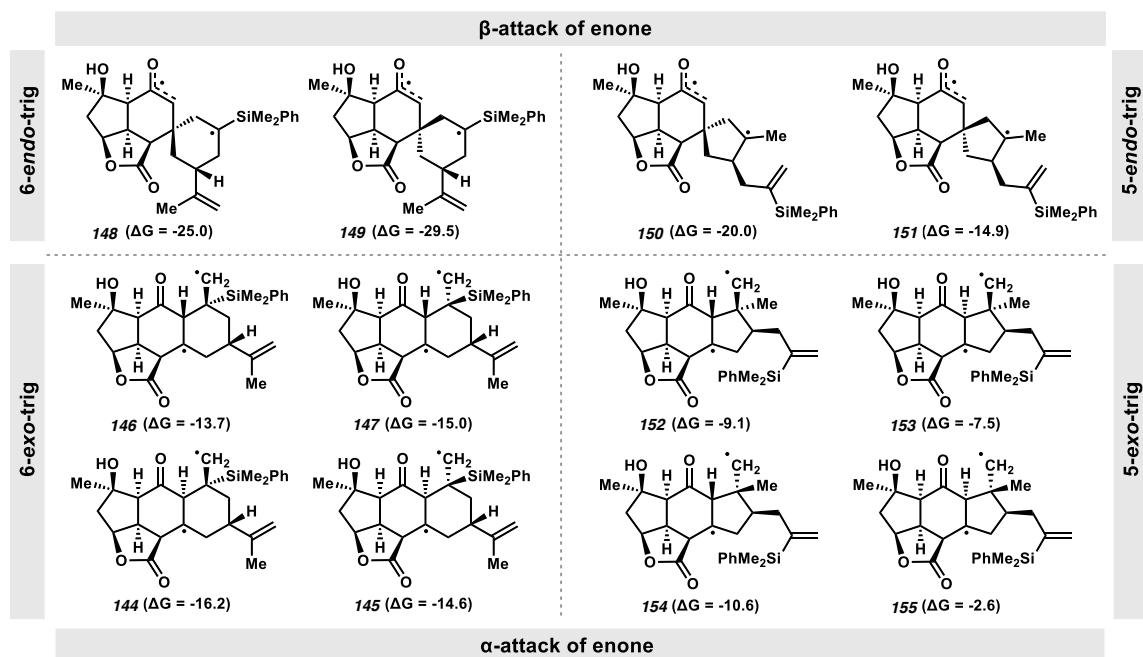
[a] All diracicals are in the triplet spin state. Gibbs free energies in kcal/mol from the (U)ωB97M-V/def2-TZVPP/SMD(benzene)//(U)B3LYP-D4/def2-SV(P) level of theory.

While the formation of cross adducts is not experimentally observed, the free energy of triplet diradicals derived from 6-*exo*-trig α-attack (**24–27**), 6-*endo*-trig β-attack (**28–29**), 5-*endo*-trig β-attack (**30–31**), and 5-*exo*-trig α-attack (**32–35**) were evaluated for reference (Scheme 4.9). Wolf and Agosta have also previously found that substitution on the internal carbon of pendant olefins leads to "straight" adducts rather than crossed products.[44]

Open-shell Singlet Potential Energy Surfaces

As the triplet diradical (such as [3]**126**) undergoes a spin flip (ISC), whether it geometrically relaxes to the stable open-shell singlet diradical (such as [1]**126**) or undergoes C–C bond cleavage back to the substrate **121** may be influenced by conformation (Scheme 4.10).

Scheme 4.10. *Conformational influence on outcome post-ISC.[a]*
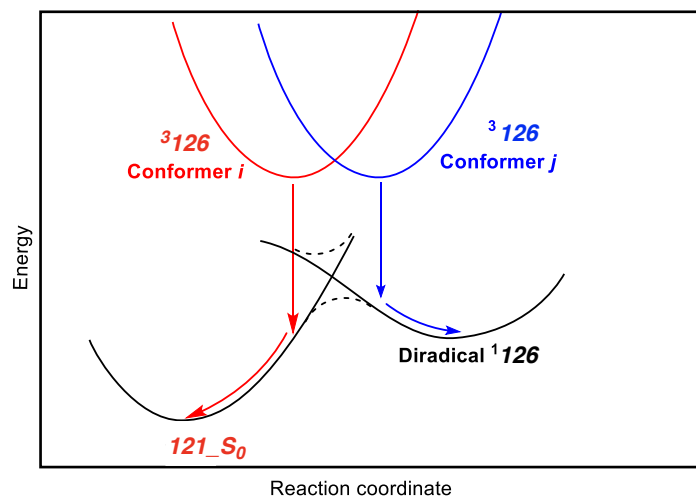
[a] Outcome of ISC would depend on the exact conformation of each conformer of triplet-spin diradical ([3]**126**). This led to a partitioning between geometry relaxation to a stable diradical ([1]**126**), or C–C bond cleavage to re-form substrate **121**, as illustrated by the example of diradical **126**.

Unfortunately, a single Slater determinant, as is used in DFT, does not afford a proper spin eigenfunction for an open-shell singlet state. However, the broken-symmetry formalism may be employed to obtain an $M_s = 0$ wavefunction with a qualitatively correct character. While the resulting wavefunction is spin contaminated, the energy of the "pure" singlet state can be estimated by a variety of spin projection methods. Here, we employ that of Yamaguchi:[45]

$$E_T - E_S = \frac{2}{\langle S^2 \rangle_T - \langle S^2 \rangle_{BS}} (E_T - E_{BS})$$

When applying this approach to calculate barriers for C–C bond formation/cleavage from the singlet diradical intermediates (**[1]126**, **[1]125**, etc.), some spin-projected values resulted in barriers of < 0 kcal/mol (Table 4.2). This indicates that the broken-symmetry (BS) DFT PES may be qualitatively incorrect, *i.e.*, stationary points on the BS-PES may not be stationary points on the true singlet surface. To test this, single point calculations with CASSCF/NEVPT2 were carried out along the IRC trajectories from the suspected saddle points (as obtained by BS-DFT) (Scheme 4.11). While BS-DFT predicts **TS11** to be a stationary point between [1]**8** and **6**, the NEVPT2 PES reveals no well-defined saddle point, and hence, $\Delta E(el)^{\ddagger} \sim 0.0$ kcal/mol.

While the relative energies along the BS-DFT PES are not necessarily accurate, the molecular geometries obtained along the IRC describing the simple C–C bond stretching/compressing should otherwise remain reliable. As such, a refined PES is derived from single point calculations with CASSCF/NEVPT2 carried out along the IRC trajectories from the saddle points as obtained by BS-DFT. $\Delta E(el)$ is then calculated from this new PES and thermodynamical corrections are applied accordingly to obtain free energy barriers ($\Delta G^{\ddagger}$).

Table 4.2. *Free energy barriers to C–C bond formation/cleavage from* [1]**126**.[a]

Species formed	ΔG‡ (kcal/mol)		
	BS-DFT	SP-BS-DFT	QD-NEVPT2
124	5.0	-1.5	1.8
124'	6.6	1.8	3.9
121	6.5	2.5	3.7
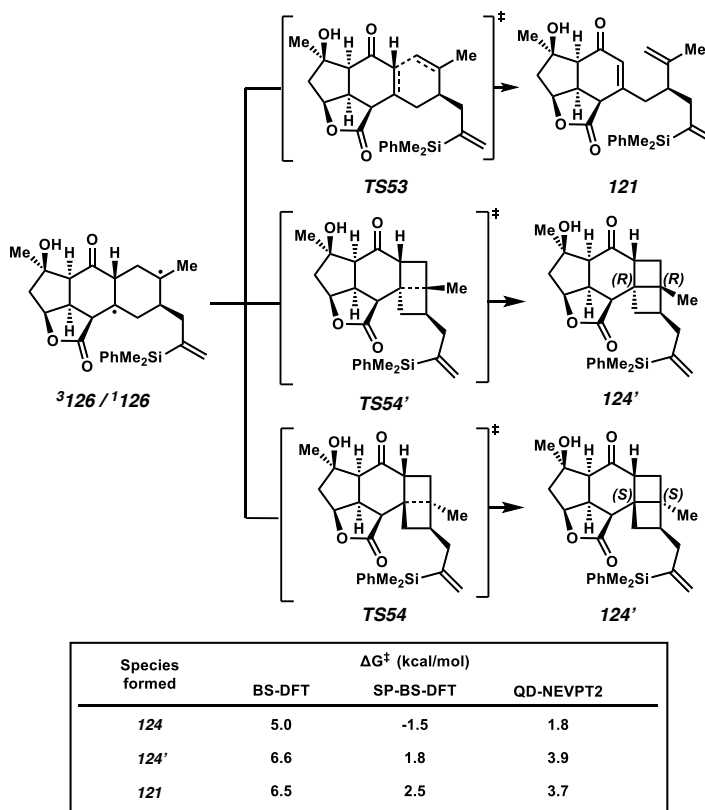
[a] Significant discrepancies between broken-symmetry DFT (BS-DFT), spin-projected BS-DFT, and QD-NEVPT2 calculations in the activation barrier for second C–C bond formation (**TS54** and **TS54'**) and reversion to substrate (**TS53**), as illustrated by the example of diradical **126**. Single-point energies were obtained using (U)B3LYP-D4/def2-SV(P) geometries at either the QD-NEVPT2/CASSCF/def2-TZVPP/SMD(benzene) or (U)B3LYP-D4/def2-TZVPP/SMD(benzene) level of theory. For SP-BS-DFT, Yamaguchi's formula for spin projection was applied.

Scheme 4.11. *PESs generated from single point calculations along the BS-DFT IRC*

trajectories of **¹126** *to* **TS54** *to* **124**.[a]
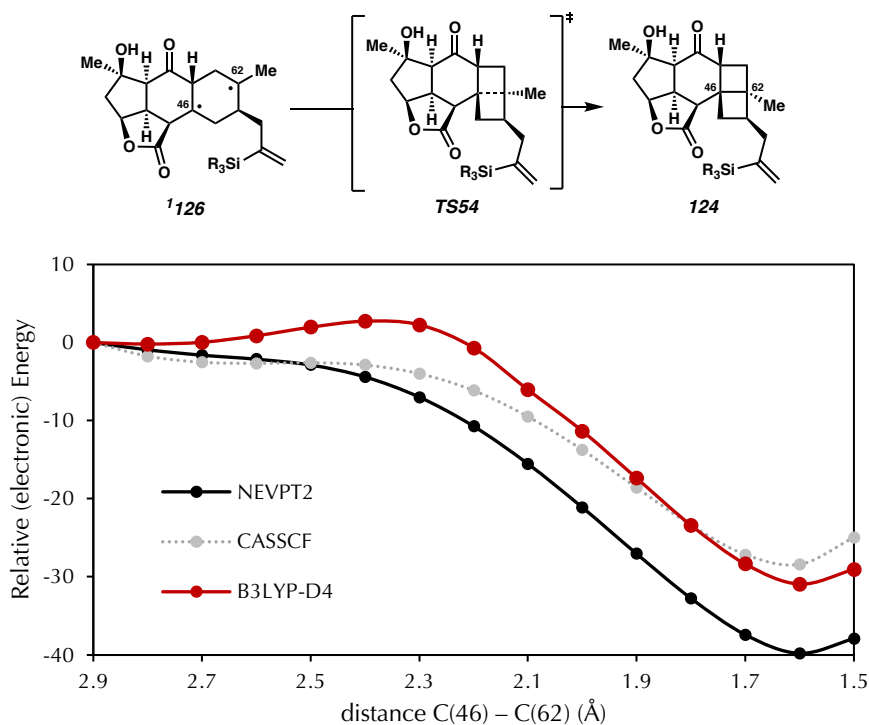
[a] The CASSCF PES is included for comparison, but the NEVPT2 PES should be taken as reference.

Considering the relatively flat nature of many of the open-shell singlet potential

energy surfaces, we sought to explore by means of ab initio molecular dynamics (AIMD)

simulations whether dynamic effects play a role in the final product distributions. For the

system at hand, AIMD would not be practical at the CASSCF/NEVPT2 level. Constrained

to DFT, we returned to the approach described above, now comparing the performance of

a variety of functionals to NEVPT2 references. This was carried out for the ring closure

step of diradicals **¹126** (Scheme 4.12) and **¹125** (Scheme 4.13). These results show that the

PBE-D4 functional bears the best resemblance to the NEVPT2 potential energy surface.

Employing the PBE-D4 functional, AIMD simulations were initiated from the lowest energy conformers (within a 1.0 kcal/mol window) of [3]**125** (Table 4.4) and [3]**126** (Table 4.3). AIMD simulations were propagated with a 1.0 fs timestep for up to 10 ps or until a bond formation/cleavage occurred. A Berendsen thermostat was employed with a time constant of 50 fs. Randomized initial velocities were set at 20 K, followed by a temperature ramp to 298 K.

Scheme 4.12. *Comparison of performance in relaxed surface scan of ring closure of*

diradical ¹**126** *to form observed but undesired product* **124** *of various DFT*

functionals with respect to NEVPT2.[a]
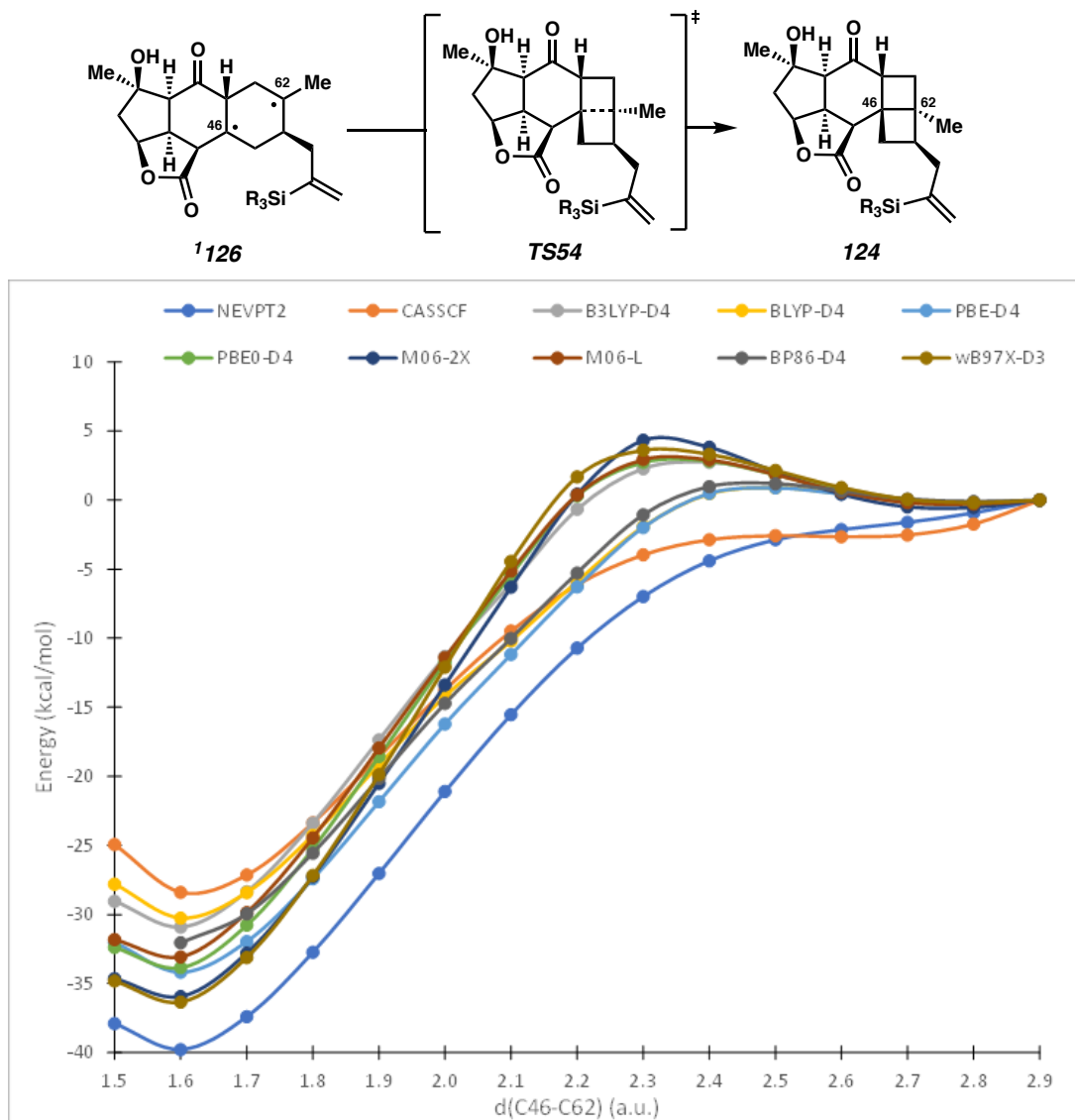
[a] Scans were performed from the lowest-energy conformer of ¹**126**. All single point energies were

calculated from each respective functional with the def2-TZVPP basis set and with the SMD(benzene)

implicit solvation.

Scheme 4.13. *Comparison of performance in relaxed surface scan of ring closure of diradical ¹**125** to form observed but undesired product **120** of various DFT functionals with respect to NEVPT2.[a]*
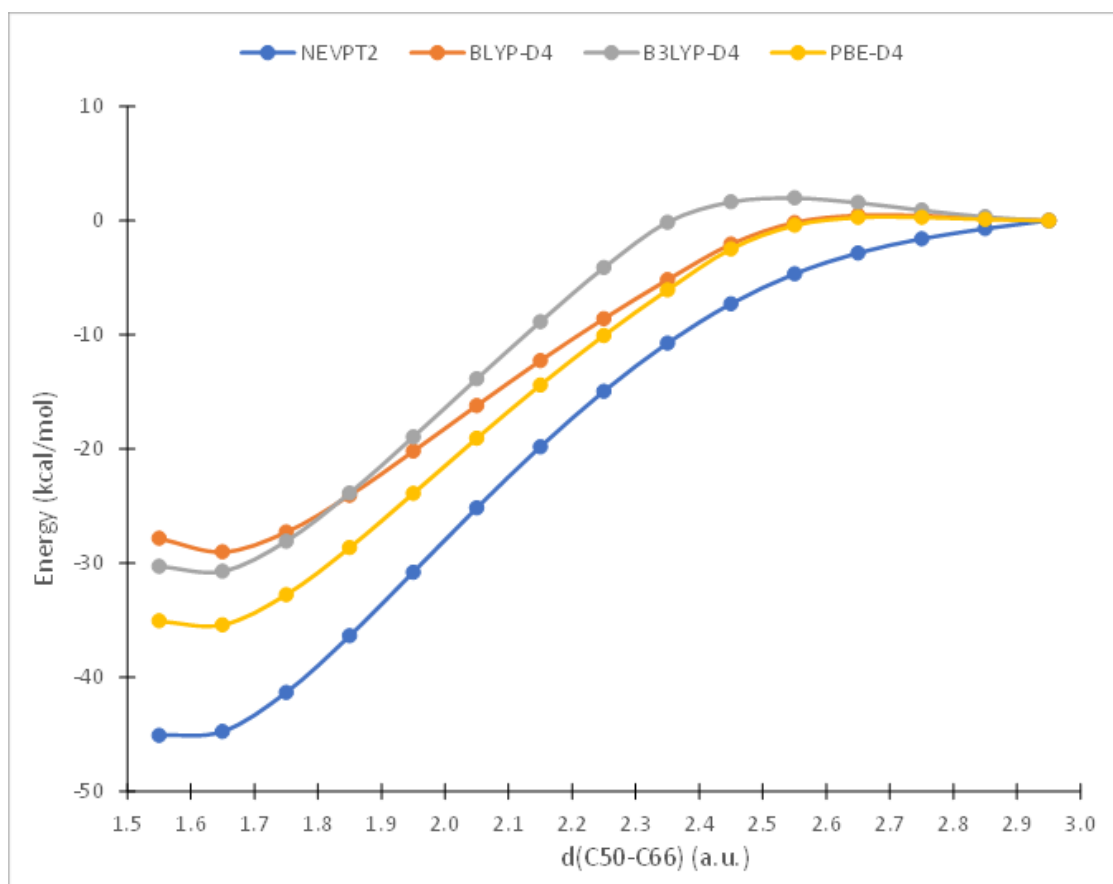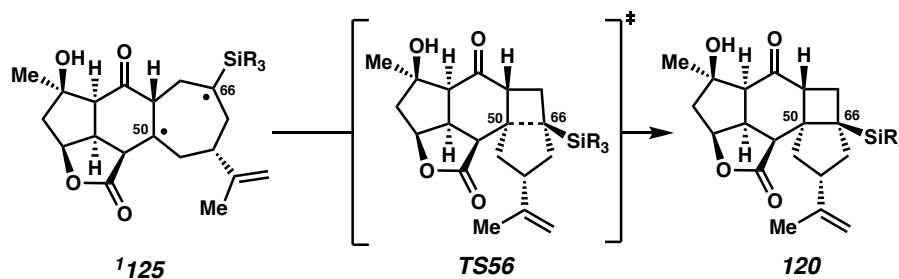
[a] Scans were performed from the lowest-energy conformer of ¹**125**. All single point energies were calculated from each respective functional with the def2-TZVPP basis set and with the SMD(benzene) implicit solvation.

Table 4.3. *Partitioning of five lowest-energy conformers of singlet diradical* **¹126**

between four outcomes based on picosecond-scale AIMD calculations.[a]
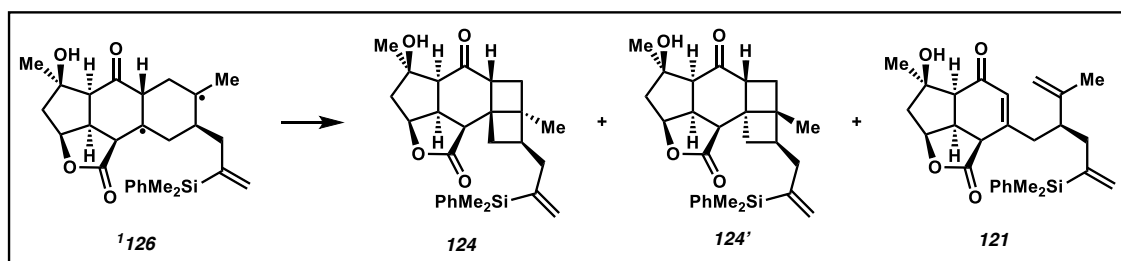
Conformer #	G_{rel} (kcal/mol)	% Boltzmann population	% ¹126	% 124	% 124'	% 121
4	0.9	8.6	0	0	0	100
7	1.0	6.6	0	100	0	0
10	0.5	16.8	0	100	0	0
11	0.0	38.8	0	0	0	100
13	1.0	7.1	0	100	0	0
14	0.4	20.1	0	0	0	100

[a] Percent remaining as diradical **¹126**, product **124** formation, diastereomer **124'** formation, and

substrate **121** formation. AIMD calculations were performed at (U)PBE-D4/def2-SV(P) level of theory.

Table 4.4. *Partitioning of five lowest-energy conformers of singlet diradical* **^{1}125**

between four outcomes based on picosecond-scale AIMD calculations.[a]
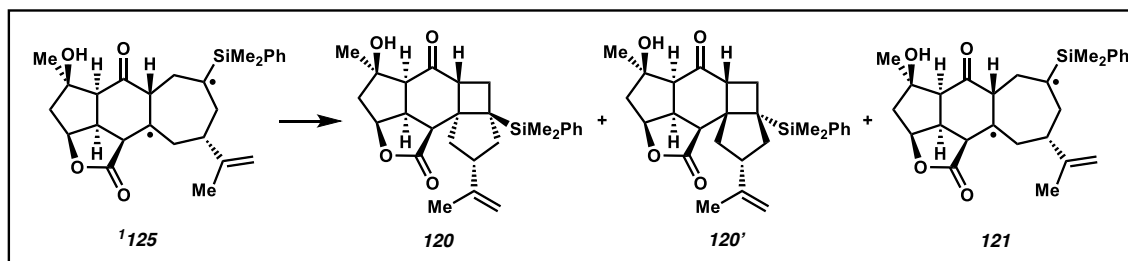
Conformer #	G_{rel} (kcal/mol)	% Boltzmann population	% ^{1}125	% 120	% 120'	% 121
4	0.00	28.8	32	68	0	0
7	0.84	6.9	10	80	0	5
8	0.37	15.4	25	75	0	0
11	0.50	12.3	35	65	0	0
13	0.01	28.4	23	77	0	0

[a] Percent remaining as diradical **^{1}125**, product **120** formation, diastereomer **120'** formation, and

substrate **121** formation. AIMD calculations were performed at (U)PBE-D4/def2-SV(P) level of theory.

4.6   REFERENCES AND NOTES

(1)   Initial reports: (a) Corey, E. J.; Bass, J. Dolf.; LeMahieu, Ronald.; Mitra, R. B. A

Study of the Photochemical Reactions of 2-Cyclohexenones with Substituted

Olefins. *J. Am. Chem. Soc.* **1964**, *86*, 5570–5583. (b) Eaton, P. E.; Hurt, W. S.

Photodimerization of Cyclopentenone. Singlet or Triplet? *J. Am. Chem. Soc.* **1966**,

88, 5038–5039. (c) Eaton, P. E. The Tricyclo[5.3.0.02,6]Decane System. The

Photodimers of Cyclopentenone. *J. Am. Chem. Soc.* **1962**, *84*, 2344–2348. For

broad reviews, see: (d) Crimmins, M. T. Synthetic Applications of Intramolecular

Enone-Olefin Photocycloadditions. *Chem. Rev.* **1988**, *88*, 1453–1473. (e) Poplata,

S.; Tröster, A.; Zou, Y.-Q.; Bach, T. Recent Advances in the Synthesis of

Cyclobutanes by Olefin [2 + 2] Photocycloaddition Reactions. *Chem. Rev.* **2016**,

116, 9748–9815. (f) Crimmins, M. T.; Reinhold, T. L. Enone Olefin [2 + 2]

Photochemical Cycloadditions. In *Organic Reactions*; John Wiley & Sons, Ltd,

2004; pp 297–588. For recent examples, see: (g) Ischay, M. A.; Ament, M. S.; Yoon,

T. P. Crossed Intermolecular [2 + 2] Cycloaddition of Styrenes by Visible Light

Photocatalysis. *Chem. Sci.* **2012**, *3*, 2807–2811. (h) Brimioulle, R.; and Bach, T.

Enantioselective Lewis Acid Catalysis of Intramolecular Enone [2+2]

Photocycloaddition Reactions. *Science* **2013**, *342*, 840–843. (i) Gravatt, C. S.;

Melecio-Zambrano, L.; Yoon, T. P. Olefin-Supported Cationic Copper Catalysts

for Photochemical Synthesis of Structurally Complex Cyclobutanes. *Angew. Chem.

Int. Ed.* **2021**, *60*, 3989–3993. (j) Scholz, S. O.; Kidd, J. B.; Capaldo, L.; Flikweert,

N. E.; Littlefield, R. M.; Yoon, T. P. Construction of Complex Cyclobutane Building Blocks by Photosensitized [2 + 2] Cycloaddition of Vinyl Boronate Esters. *Org. Lett.* **2021**, *23*, 3496–3501. (k) Sherbrook, E. M.; Genzink, M. J.; Park, B.; Guzei, I. A.; Baik, M.-H.; Yoon, T. P. Chiral Brønsted Acid-Controlled Intermolecular Asymmetric [2 + 2] Photocycloadditions. *Nat. Commun.* **2021**, *12*, 5735.

(2)   Early example of use in synthesis: (a) Corey, E. J.; Mitra, R. B.; Uda, H. Total Synthesis of d,l-Caryophyllene and d,l-Isocaryophyllene. *J. Am. Chem. Soc.* **1964**, *86*, 485–492. For review see: (b) Iriondo-Alberdi, J.; Greaney, M. F. Photocycloaddition in Natural Product Synthesis. *Eur. J. Org. Chem.* **2007**, 4801– 4815. (c) Bach, T.; Hehn, J. P. Photochemical Reactions as Key Steps in Natural Product Synthesis. *Angew. Chem. Int. Ed.* **2011**, *50*, 1000–1045. (d) Sarkar, D.; Bera, N.; Ghosh, S. [2+2] Photochemical Cycloaddition in Organic Synthesis. *Eur. J. Org. Chem.* **2020**, 1310–1326. (e) Winkler, J. D.; Bowen, C. M.; Liotta, F. [2 + 2] Photocycloaddition/Fragmentation Strategies for the Synthesis of Natural and Unnatural Products. *Chem. Rev.* **1995**, *95*, 2003–2020.

(3)   Reviews of fragmentation strategies and tactics: (a) Namyslo, J.C.; Kaufman, D.E. The Application of Cyclobutane Derivatives in Organic Synthesis. *Chem. Rev.* **2003**, *103*, 1485–1538. (b) Murakami, M.; Ishida, N. Cleavage of Carbon–Carbon s-Bonds for Four-Membered Rings. *Chem. Rev.* **2021**, *121*, 264–299. (c) Wang, B.; Parea, M.A.; Sarpong, R. Transition Metal-Mediated C–C Single Bond Cleavage:

Making the Cut in Total Synthesis. *Angew. Chem. Int. Ed.* **2020**, *59*, 18898–18919.

(d) Lee-Ruff, E.; Mladenova, G. Enantiomerically Pure Cyclobutane Derivatives

and Their Use in Organic Synthesis. *Chem. Rev.* **2003**, *103*, 1449–1484.

(4)   Hafeman, N. J.; Loskot, S. A.; Reimann, C. E.; Pritchett, B. P.; Virgil, S. C.; Stoltz,

B. M. The Total Synthesis of (−)-Scabrolide A. *J. Am. Chem. Soc.* **2020**, *142*, 8585–

8590.

(5)   (a) Srinivasan, Ramaswamy.; Carlough, K. H. Mercury(3P1) Photosensitized

Internal Cycloaddition Reactions in 1,4-, 1,5-, and 1,6-Dienes. *J. Am. Chem. Soc.*

1967, *89*, 4932–4936. (b) Liu, R. S. H.; Hammond, G. S. Photosensitized

Cyclization of Myrcene: The Problem of Addition of Dienes to Alkenes. *J. Am.*

Chem. Soc. **1964**, *86*, 1892–1893. For further discussion regarding the "Rule of

Five" in the context of [2+2] photocycloadditions, see Bradley, S. A.; Bresnan, B.

J.; Draper, S. M.; Geraghty, N. W. A.; Jeffares, M.; McCabe, T.; McMurry, T. B.

H.; O'Brien, J. E. Photochemical [2 + 2] Cycloaddition Reactions of 6-Alkenyl-3-

Phenylcyclohex-2-En-1-Ones: Using Biradical Conformation Control to Account

for Exceptions to the "Rule of Five." *Org. Biomol. Chem.* **2011**, *9*, 2959.

(6)   (a) Sheu, J.-H.; Ahmed, A. F.; Shiue, R.-T.; Dai, C.-F.; Kuo, Y.-H. Scabrolides

A−D, Four New Norditerpenoids Isolated from the Soft Coral Sinularia Scabra. *J.*

Nat. Prod. **2002**, *65*, 1904–1908. (b) Thao, N. P.; Nam, N. H.; Cuong, N. X.; Quang,

T. H.; Tung, P. T.; Dat, L. D.; Chae, D.; Kim, S.; Koh, Y.-S.; Kiem, P. V.; Minh,

C. V.; Kim, Y. H. Anti-Inflammatory Norditerpenoids from the Soft Coral Sinularia Maxima. *Bioorg. Med. Chem. Lett.* **2013**, *23*, 228–231.

(7)   (a) Neese, F. Software Update: The ORCA Program System, Version 4.0. *Wiley Interdisciplinary Reviews: Computational Molecular Science* **2018**, *8*, e1327. (b) Neese, F. The ORCA Program System. *Wiley Interdisciplinary Reviews: Computational Molecular Science* **2012**, *2*, 73–78.

(8)   Stephens, P. J.; Devlin, F. J.; Chabalowski, C. F.; Frisch, M. J. Ab Initio Calculation of Vibrational Absorption and Circular Dichroism Spectra Using Density Functional Force Fields. *J. Phys. Chem.* **1994**, *98*, 11623–11627.

(9)   Caldeweyher, E.; Ehlert, S.; Hansen, A.; Neugebauer, H.; Spicher, S.; Bannwarth, C.; Grimme, S. A Generally Applicable Atomic-Charge Dependent London Dispersion Correction. *J. Chem. Phys.* **2019**, *150*, 154122.

(10)   Weigend, F.; Ahlrichs, R. Balanced Basis Sets of Split Valence, Triple Zeta Valence and Quadruple Zeta Valence Quality for H to Rn: Design and Assessment of Accuracy. *Phys. Chem. Chem. Phys.* **2005**, *7*, 3297–3305.

(11)   Ishida, K.; Morokuma, K.; Komornicki, A. The Intrinsic Reaction Coordinate. An Ab Initio Calculation for HNC→HCN and $H^-+CH_4\rightarrow CH_4+H^-$. *J. Chem. Phys.* **1977**, *66*, 2153–2156.

(12)   Mardirossian, N.; Head-Gordon, M. ωB97M-V: A Combinatorially Optimized, Range-Separated Hybrid, Meta-GGA Density Functional with VV10 Nonlocal Correlation. *J. Chem. Phys.* **2016**, *144*, 214110.

(13)   Marenich, A. V.; Cramer, C. J.; Truhlar, D. G. Universal Solvation Model Based

on Solute Electron Density and on a Continuum Model of the Solvent Defined by

the Bulk Dielectric Constant and Atomic Surface Tensions. *J. Phys. Chem. B* **2009**,

113, 6378–6396.

(14)   (a) Angeli, C.; Cimiraglia, R.; Malrieu, J.-P. N-Electron Valence State Perturbation

Theory: A Fast Implementation of the Strongly Contracted Variant. *Chem. Phys.

Lett.* **2001**, *350*, 297–305. (b) Angeli, C.; Cimiraglia, R.; Malrieu, J.-P. N-Electron

Valence State Perturbation Theory: A Spinless Formulation and an Efficient

Implementation of the Strongly Contracted and of the Partially Contracted Variants.

J. Chem. Phys. **2002**, *117*, 9138–9153.

(15)   When a state-averaged CASSCF wavefunction employed as a zeroth order

reference, the Nakano quasi-degenerate formulation was used. (a) Nakano, H.

Quasidegenerate Perturbation Theory with Multiconfigurational Self-consistent-

field Reference Functions. *J. Chem. Phys.* **1993**, *99*, 7983–7992. (b) Angeli, C.;

Borini, S.; Cestari, M.; Cimiraglia, R. A Quasidegenerate Formulation of the

Second Order N-Electron Valence State Perturbation Theory Approach. *J. Chem.

Phys.* **2004**, *121*, 4043–4049.

(16)   (a) Wilsey, S.; González, L.; Robb, M. A.; Houk, K. N. Ground- and Excited-State

Surfaces for the [2+2]-Photocycloaddition of α,β-Enones to Alkenes. *J. Am. Chem.

Soc.* **2000**, *122*, 5866–5876. (b) Bertrand, C.; Bouquant, J.; Pete, J. P.; Humbel, S.

Theoretical Description of [2+2] Photocycloadditions: Enone and Ethylene as a

Model of the Reactivity of Cycloenones. *J. Mo. Struct.* **2001**, *538*, 165–177. (c) Cucarull-González, J. R.; Hernando, J.; Alibés, R.; Figueredo, M.; Font, J.; Rodríguez-Santiago, L.; Sodupe, M. [2 + 2] Photocycloaddition of 2(5*H*)-Furanone to Unsaturated Compounds. Insights from First Principles Calculations and Transient-Absorption Measurements. *J. Org. Chem.* **2010**, *75*, 4392–4401. (d) Reguero, M.; Olivucci, M.; Bernardi, F.; Robb, M. A. Excited-State Potential Surface Crossings in Acrolein: A Model for Understanding the Photochemistry and Photophysics of α,β-Enones. *J. Am. Chem. Soc.* **1994**, *116*, 2103–2114.

(17)   (a) Lam, E. Y. Y.; Valentine, Donald.; Hammond, G. S. Mechanisms of Photochemical Reactions in Solution. XLIV. Photodimerization of Cyclohexenone. *J. Am. Chem. Soc.* **1967**, *89*, 3482–3487. (b) Ruhlen, J. L.; Leermakers, P. A. Photochemistry of Cyclopentenone in Various Media. *J. Am. Chem. Soc.* **1967**, *89*, 4944–4948. (c) Chapman, O. L.; Koch, T. H.; Klein, F.; Nelson, P. J.; Brown, E. L. Photochemical Transformations. XXV. Two Triplet Mechanisms in Photochemical Addition of 2-Cyclohexenones to 1,1-Dimethoxyethylene. *J. Am. Chem. Soc.* **1968**, *90*, 1657–1658. (d) Bauslaugh, P. G. Photochemical Cycloaddition Reactions of Enones to Alkenes; Synthetic Applications. *Synthesis* **1970**, 287–300. For a review, see: (e) Schuster, D. I.; Lem, George.; Kaprinidis, N. A. New Insights into an Old Mechanism: [2 + 2] Photocycloaddition of Enones to Alkenes. *Chem. Rev.* **1993**, *93*, 3–22.

(18)   (a) El-Sayed, M. A. Spin—Orbit Coupling and the Radiationless Processes in Nitrogen Heterocyclics. *J. Chem. Phys.* **1963**, *38*, 2834–2838. (b) Baba, M. Intersystem Crossing in the ^{1}nπ* and ^{1}ππ* States. *J. Phys. Chem. A* **2011**, *115*, 9514–9519.

(19)   (a) Kaprinidis, N. A.; Lem, G.; Courtney, S. H.; Schuster, D. I. Determination of the Energies and Lifetimes of Triplet 1,4-Biradicals Involved in [2+2] Photocycloaddition Reactions of Enones with Alkenes Using Photoacoustic Calorimetry *J. Am. Chem. Soc.* **1993**, *115*, 3324–3325. (b) Schuster, D. I.; Dunn, D. A.; Heibel, G. E.; Brown, P. B.; Rao, J. M.; Woning, J.; Bonneau, R. Enone Photochemistry. Dynamic Properties of Triplet Excited States of Cyclic Conjugated Enones as Revealed by Transient Absorption Spectroscopy. *J. Am. Chem. Soc.* **1991**, *113*, 6245–6255. Here we assume a 1 M standard state of substrate.

(20)   Weedon, A. C., Enone photochemical cycloaddition in organic synthesis, in *Synthetic Organic Chemistry,* Horspool, W. M., Ed., Plenum Press, New York, 1984, chap. 2.

(21)   Similar results are obtained regardless of the state averaging scheme employed.

(22) $\Delta E_{ST}(\pi\pi^*)$ is larger in magnitude than $\Delta E_{ST}(n\pi^*)$ as the overlap of the π/π* orbitals is greater than that of the n/π* orbitals.

(23)   The ^{3}(nπ*) and ^{3}(nπ*) minima are expected to be qualitatively similar in geometry. The similarity of their PES is highlighted in Scheme 4.3B.

(24)   Schuster, D. I.; Woning, J.; Kaprinidis, N. A.; Pan, Y.; Cai, B.; Barra, M.; Rhodes, C. A. Photochemical and Photophysical Studies of Bicyclo[4.3.0]non-1(6)-en-2-one. *J. Am. Chem. Soc.* **1992**, *114*, 7029–7034.

(25)   Root-flipping between $^3(\pi\pi^*)$ and $^3(n\pi^*)$ states complicates this matter. In order to approximate the diabatic surface obtained by relaxation of the nuclear coordinates of the $^3(\pi\pi^*)$ state, the carbonyl oxygen lone pair is removed from the active space, rendering the $^3(\pi\pi^*)$ state the lowest energy triplet state for the portion of the PES of interest. Starting from the **120_^{3}(nπ*)** minimum geometry, triplet state geometries were then relaxed at the CASSCF(8,8)/def2-SV(P) level of theory. Points along the optimization trajectory were then taken for analysis.

(26)   The crossing point is not rigorously the *minimum* energy crossing point, rather the approximate surface rather serves as an upper bound.

(27)   At the $^3(\pi\pi^*)/^1(n\pi^*)$ minimum energy crossing point, SOC creates an energy gap of *ca.* 1 kcal/mol between the adiabatic surfaces.

(28)   For β-attack, 2 diastereomeric transition states arise from each of 4-*exo*-, 5-*endo*-, 5-*exo*-, and 6-*endo*-trig cyclizations, as the pendant olefin of interest approaches the β-radical from either the *Si* or *Re* face of the enone. There are 2 more diastereomeric transition states for each of the 4-*exo*- and 5-*exo*-trig cyclizations, as the β-radical can approach the more substituted and prochiral carbon in the isopropenyl olefin and the vinyl silane from either of the diastereotopic faces of the olefin.

(29)   For α-attack, 2 diastereomeric transition states arise from each of 5-*exo*-, 6-*endo*-, 6-*exo*-, and 7-*endo*-trig cyclizations, as the pendant olefin of interest approaches the β-radical from either the *Si* or *Re* face of the enone. There are 2 more diastereomeric transition states for each of the 5-*exo*- and 6-*exo*-trig cyclizations, as the α-radical can approach the more substituted and prochiral carbon in the isopropenyl olefin and the vinyl silane from either of the diastereotopic faces of the olefin.

(30)   No first-order saddle point exists describing **TS45**, not that the formation of **³133** is barrierless, but rather that the saddle structure that would have corresponded to **TS45** maintains non-zero energy gradient until ultimately reaching **TS52**. In other words, bringing the vinyl silane olefin to the $^3(\pi\pi^*)$ enone would more readily give rise to **TS50**. This is likely due to the steric congestion of forming vicinal tetrasubstituted centers in **TS45**. We note that there may be non-statistical dynamical affects that are not accounted for here – **TS52** may be near an inflection point on a bifurcated PES which could lead to **³133** or **³125** from **³121**.

(31)   The $^3(n\pi^*)$ transition structure is different than that along the $^3(\pi\pi^*)$ surface. However, the vertical excitation of *ca*. 40 kcal/mol at the $^3(\pi\pi^*)$ saddle point highlights the significant divergence of the two surfaces at this region of the PES.

(32)   Similar reactivity has been proposed in intermolecular enone/olefine photocycloadditions. Bowman, R. M.; Calvo, C.; McCullough, J. J.; Rasmussen, P.

W.; Snyder, F. F. Photoadditions of 2-Cyclohexenone Derivatives to Cyclopentene. Stereochemistry. *J. Org. Chem.* **1972**, *37*, 2084–2091.

(33)   Note that its <0.5% of QD-NEVPT2 wavefunction.

(34)   The vertical singlet-triplet gap was calculated at the same geometry optimized by (U)B3LYP-D4/def2-SV(P) on the open-shell singlet surface. Energy of the lowest singlet and triplet state was calculated with state-averaging using the QD-NEVPT2 method with an (8,8) active space.

(35)   Note the relative rates of ISC also depend on the geometry of the 1,4-diradical, with increasingly perpendicular valence orbitals giving rise to stronger SOC. Increased ionic character in the singlet state and decreasing distance between the two radical centers also serve to maximize SOC. See also: Carlacci, L.; Doubleday, C.; Furlani, T. R.; King, H. F.; McIver, J. W. Spin-Orbit Coupling in Biradicals. Ab Initio MCSCF Calculations on Trimethylene and the Methyl-Methyl Radical Pair. *J. Am. Chem. Soc.* **1987**, *109*, 5323–5329.

(36)   (a) Noodleman, L. Valence Bond Description of Antiferromagnetic Coupling in Transition Metal Dimers. *J. Chem. Phys.* **1981**, *74*, 5737–5743. (b) Noodleman, L.; Davidson, E. R. Ligand Spin Polarization and Antiferromagnetic Coupling in Transition Metal Dimers. *Chem. Phys.* **1986**, *109*, 131–143.

(37)   Broken symmetry energies were spin decontaminated following the approach of Yamaguchi and coworkers to approximate the energy of the pure singlet states.

(38)   Wagner, P. J.; Bucheck, D. J. Inefficiency and Reversibility in the Photodimerization of 2-Cyclopentenone. *Can. J. Chem.* **1969**, *47*, 713–714.

(39)   The single broken-symmetry determinant is not a proper spin eigenfunction of the $\hat{S}^2$ operator. For addition discussion, see: Neese, F. Definition of Corresponding Orbitals and the Diradical Character in Broken Symmetry DFT Calculations on Spin Coupled Systems. *J. Phys. Chem. Solids* **2004**, *65*, 781–785.

(40)   Neese, F.; Wennmohs, F.; Hansen, A.; Becker, U. Efficient, Approximate and Parallel Hartree-Fock and Hybrid DFT Calculations. A 'Chain-of-Spheres' Algorithm for the Hartree-Fock Exchange. *Chem. Phys.* **2009**, *356*, 98–109.

(41)   Weigend, F. Accurate Coulomb-Fitting Basis Sets for H to Rn. *Phys. Chem. Chem. Phys.* **2006**, *8*, 1057–1065.

(42)   Pettersen, E. F.; Goddard, T. D.; Huang, C. C.; Couch, G. S.; Greenblatt, D. M.; Meng, E. C.; Ferrin, T. E. UCSF Chimera—A Visualization System for Exploratory Research and Analysis. *J. Comput. Chem.* **2004**, *25*, 1605–1612.

(43)   Grimme, S. Supramolecular Binding Thermodynamics by Dispersion-Corrected Density Functional Theory. *Chem. Eur. J.* **2012**, *18*, 9955–9964.

(44)   Wolff, S.; Agosta, W. C. Preparation of Derivatives of Tricyclo[4.2.0.01,4]Octane, Broken Window Compounds. *J. Chem. Soc., Chem. Commun.* **1981**, *3*, 118–120.

(45)   (a) Yamaguchi, K.; Takahara, Y.; Fueno, T. Ab-Initio Molecular Orbital Studies of Structure and Reactivity of Transition Metal-OXO Compounds. In *Applied Quantum Chemistry*; Smith, V. H., Schaefer, H. F., Morokuma, K., Eds.; Springer

Netherlands: Dordrecht, 1986; pp 155–184. (b) Soda, T.; Kitagawa, Y.; Onishi, T.; Takano, Y.; Shigeta, Y.; Nagao, H.; Yoshioka, Y.; Yamaguchi, K. Ab Initio Computations of Effective Exchange Integrals for H–H, H–He–H and Mn_2O_2 Complex: Comparison of Broken-Symmetry Approaches. *Chemical Physics Letters* **2000**, *319*, 223–230. (c) Ferré, N.; Guihéry, N.; Malrieu, J.-P. Spin Decontamination of Broken-Symmetry Density Functional Theory Calculations: Deeper Insight and New Formulations. *Phys. Chem. Chem. Phys.* **2015**, *17*, 14375–14382.

CHAPTER 5

Development of a Branched-selective Asymmetric Allylic Alkylation of

Hard Pd-Enolate Nucleophiles.†

5.1   INTRODUCTION

The construction of chiral all-carbon quaternary centers featuring vicinal tertiary stereocenters exemplifies a prevalent challenge in synthetic chemistry. We envisioned the transition metal-catalyzed branched-selective allylic alkylation of prochiral hard enolate nucleophiles as a promising strategy for accessing such motifs. However, a multitude of challenges must be overcome, including regioselectivity in enolate formation, and regio-, enantio-, and diastereoselectivity in the alkylation event.[1] Ir catalyst systems have proven to be privileged for the branched-selective allylic alkylation of *soft* carbon nucleophiles.[2] Extending this reactivity paradigm to *hard*, prochiral enolate nucleophiles has remained a challenge.[3] To address this, Hartwig employed the in situ generation of Ba enolates to enable the branched-selective allylic alkylation of α-tetralone nucleophiles (**156**) (Figure 5.1A).[4] However, this approach is limited to select ketones due to the challenge of regioselective deprotonation. Related transformations are subject to similar constraints.[5] The Pd-catalyzed decarboxylative allylic alkylation of β-ketoesters represents a general, regiospecific-at-nucleohile strategy for the asymmetric allylic alkylation of *hard* enolates (Figure 5.1B).[6] However, canonical Pd-catalyzed decarboxylative allylic alkylation

---

† Unpublished research conducted with Dr. Stephen Sardini and Dr. Veronica Hubble

employing tetrasubstituted nucleophiles and substituted allyl esters (**158a**) gives rise to undesired regioselectivity, yielding linear alkylation products (**159a**) (Figure 5.1C).[3,7]

Figure 5.1. *Asymmetric allylic alkylation of tetrasubstituted enolate nucleophiles.*

A. Ir-catalyzed branched-selective allylic alkylation of Ba enolates.

B. Decarboxylative asymmetric allylic alkylation.

C. Standard Pd-catalyzed decarboxylative allylic alkylation of substituted allyl esters.[a]

D. This research: Branched-selective decarboxylative asymmetric allylic alkylation.
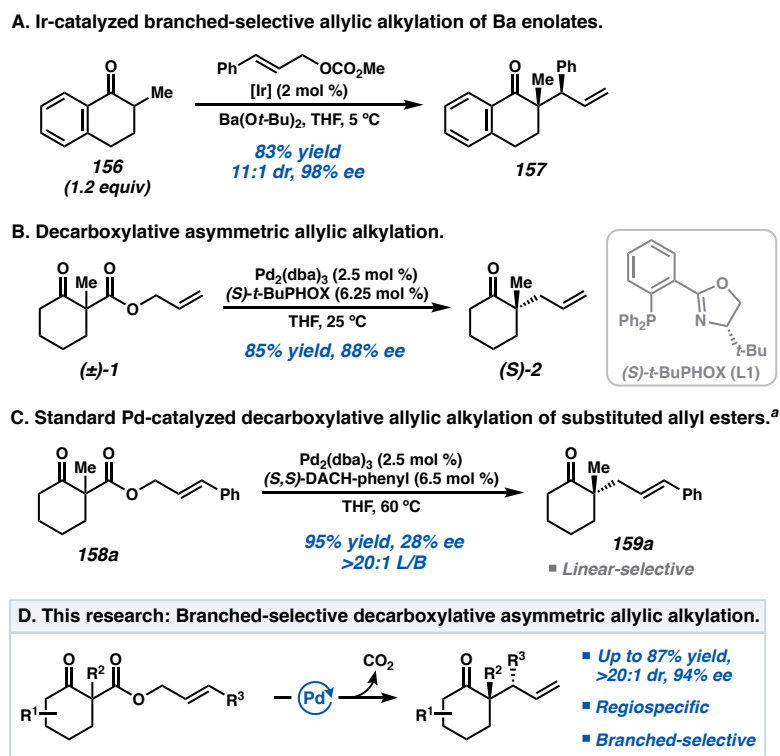
[a] Reaction conditions: **158a** (0.05 mmol), Pd₂(dba)₃ (2.5 mol %), *(S,S)*-DACH-Ph (6.5 mol %), and THF (2 mL) at 60 °C for 14 h. NMR yield determined with 1,3,5-trimethoxybenzene as an internal standard. Enantioselectivity measured by chiral SFC analysis.

Aided by our prior mechanistic studies, we sought to favor the formation of branched products through the design of ligands that bias key interactions in the inner-sphere seven-membered reductive elimination transition state.[8] Ultimately, we achieve a general approach to chiral all-carbon vicinal quaternary/tertiary stereocenters (Figure 5.1D). High diastereo- (>20:1) and enantioselectivity (>80% ee) are obtained, with the

majority of products featuring >20:1 branched/linear selectivity. Subsequent derivatization of these compounds highlights their utility as synthetic building blocks.

5.2   MECHANISM AND DEVELOPMENT

We began our investigation by considering the inner-sphere transition states that lead to the formation of the desired branched (**160a**) and undesired linear (**159a**) products from β-ketoester **158a** (Figure 5.2A). The two lowest energy transition states leading to linear (**159a**) and branched (**160a**) products are **TS61** and **TS62**, respectively. Unfortunately, with the prototypical *(S)-t*-BuPHOX ligand (**L1**), linear **TS61** is favored by 2.6 kcal/mol over its branched counterpart. Noting the proximity of the allyl substituent to the phenyl group of the PHOX backbone (red arrows in **TS61** at top of Figure 5.2A), we explored di-*ortho* substitution of the ligand aryl groups as a means to disfavor **TS61** by sterics.[9] Accordingly, with *(S)*-Mes-*t*-BuPHOX (**L2**), **TS62** now becomes favored over **TS61** by 3.5 kcal/mol. Enantioselectivity of the branched product (**160a**) from inner-sphere reactivity is computed to remain high, with $\Delta\Delta G^{\ddagger}$ between diastereomeric transition states of 2.4 and 3.9 kcal/mol with **L1** and **L2**, respectively. Moreover, 2.5 and 1.2 kcal/mol preferences for the chair-like over the boat-like transition states ensures good diastereoselectivity. In summary, our preliminary in silico studies highlight that (1) *ortho* substitution of the ligand arenes will introduce a bias for the desired branched product (**160a**), and (2) a purely inner-sphere reaction will maintain both high diastereo- and enantioselectivity.

Figure 5.2. *Computational studies and initial reaction development.*

A. Mechanistic hypothesis.[a]

TS61
Linear Transition State (to 159a)

TS62
Branch Transition State (to 160a)

▪ Exploit non-covalent interactions to favor TS62

TS61: (S)-t-BuPHOX (L1)

Ar =

$\Delta G^{\ddagger}_{rel}$ (L) = 0.0
$\Delta G^{\ddagger}_{rel}$ (B) = 2.6
Linear preferred

Favorable Linear TS

Potential edge–face interaction

TS61: (S)-Mes-t-BuPHOX (L2)

Ar =

$\Delta G^{\ddagger}_{rel}$ (L) = 3.5
$\Delta G^{\ddagger}_{rel}$ (B) = 0.0
Branched preferred

Disfavored Linear TS

Sterics to disrupt aryl positioning

B. Reaction optimization.[b]

158a

Pd₂(dba)₃ (2.5 mol %)
ligand (6.5 mol %)
solvent, 60 °C

160a
(branched)

159a
(linear)

Entry	Ligand	Solvent	Yield	B:L	dr	% ee
1	(S)-t-BuPHOX (L1)	THF	54	1:2.1	2.1:1	−12
2	(S)-t-BuPHOX (L1)	PhMe	97	1:1.9	7.0:1	65
3	(S)-(CF₃)₃-t-BuPHOX (L3)	PhMe	86	1:1.1	14:1	80
4	(S)-Mes-t-BuPHOX (L2)	PhMe	38	1.1:1	1.9:1	6
5	L4	PhMe	25	3.1:1	12:1	68
6	L5	PhMe	85	11:1	14:1	70
7	L6	PhMe	78	1.7:1	16:1	82
8	L7	PhMe	62	5.9:1	>20:1	76
9[c]	L7	PhMe	62	9.1:1	>20:1	82

Ligand electronics

R = H **L1**
CF₃ **L3**

ortho-Substitution

L4 L5 L6 L7

[a] Gibbs free energies in kcal/mol.[10] [b] Reaction conditions: **158a** (0.05 mmol), Pd₂(dba)₃ (2.5 mol %), *ligand* (6.5 mol %), and *solvent* (2 mL) at 60 °C for 14 h. NMR yield determined with 1,3,5-trimethoxybenzene as an internal standard. B:L and dr determined by crude ¹H NMR analysis. Enantioselectivity measured by chiral SFC analysis. [c] Isolated yield from 0.1 mmol of **158a** at 50 °C.

Encouraged by the prospect of rational ligand design as a means to affect branched-selective alkylation, we began our experimental investigations. As anticipated, subjecting β-ketoester **158a** to standard reaction conditions with *(S)-t*-BuPHOX (**L1**) in THF afforded the undesired linear isomer (**159a**) as the major reaction product with a branched-to-linear ratio (B/L) of 1:2.1 (Figure 5.2B, entry 1). Surprisingly, the branched ketone (**160a**) was furnished in poor enantio- and diastereoselectivity. Our computational studies found that branched product formation from inner-sphere reductive elimination to proceed with both high enantio- and diastereoselectivity. Hence, we suspected a deleterious outer-sphere

mechanism to be competitive with said inner-sphere processes. To disfavor charge-separated outer-sphere intermediates, a less polar solvent, such as toluene, and the electron-poor *(S)*-(CF$_3$)$_3$-*t*-BuPHOX (**L3**) ligand were explored. Under these conditions, the desired branched product is obtained in 86% yield, 80% ee, and an improved 14:1 dr (entries 2–3). As anticipated, regioselectivity remains poor, with a B/L ratio of 1:1.1. To improve branched-selectivity, *(S)*-Mes-*t*-BuPHOX (**L2**) from our in silico studies was explored; however, the electron rich nature of the ligand likely supports outer-sphere processes, affording **160a** in 6% ee and 1.9:1 dr (entry 4). Hence, a series of ligands that keep *ortho* aryl substitution yet feature electron-withdrawing groups were evaluated (**L4**–**L7**, entries 5–8). Ultimately, *o*-trifluoromethylether-containing PHOX ligand **L7** was found to be optimal for the branched-selective allylic alkylation of **158a**, affording the desired product (**160a**) in 62% isolated yield, 82% ee, >20:1 dr, and in a 9.1:1 B/L ratio at 50 ºC in toluene (entry 9).

5.3   SUBSTRATE SCOPE

With respect to the scope of the transformation, substrates that incorporate α,β-unsaturation led to a marked increase in the branched selectivity to 20:1 or greater (**160b** and **160c**) (Figure 5.3). We were delighted to find the increasingly electron-rich enolate nucleophiles derived from synthetically useful vinylogous esters are well tolerated, affording the corresponding products (**160d**–**160h**) in generally good yield, >20:1 B/L, >20:1 dr, and 82–87% ee. Both ligands **L6** and **L7** perform well for the vinylogous ester substrate class. A vinylogous thioester was also explored, albeit reduced branched selectivity was observed (**160i**). α-Enaminone-containing product **160j** was obtained in

lower yield but excellent diastereo- and enantioselectivity (>20:1 dr, 94% ee). We were excited to observe that aliphatic substituted allyl electrophiles are competent coupling partners. Crotyl alcohol-derived β-ketoester **158k** affords enone **160k** in 59% yield, 8.3:1 dr, and 73% ee, albeit with a diminished 2.5:1 B/L ratio. The reduction in branched selectivity likely arises from the smaller steric profile of the methyl substituent, making distinction between **TS61** and **TS62** more challenging. Employing a larger alkyl substituent restores branched-selectivity (**160l**). Additionally, α-fluoro enolate nucleophiles are highly competent substrates in this transformation. A variety of fluorinated tetrasubstituted/tertiary vicinal stereocenter-containing products (**160m**–**160q**) were furnished in generally good yield as predominantly a single isomer with high enantioselectivity (82–87% ee). Hence, the branched-selective decarboxylative allylic alkylation described herein represents a powerful strategy to access diverse, stereochemically rich building blocks.

Figure 5.3. *Substrate scope of branched-selective allylic alkylation.*[a]

Substrate scope for branched-selective allylic alkylation forging quaternary centers

160a
62% yield, 9.1:1 B/L
>20:1 dr, 82% ee

160b
51% yield, 20:1 B/L
>20:1 dr, 78% ee

160c
70% yield, >20:1 B/L
>20:1 dr, 80% ee

160d
70% yield, >20:1 B/L
>20:1 dr, 84% ee

160e
70% yield[c], >20:1 B/L
>20:1 dr, 87% ee

160f
42% yield[c], >20:1 B/L
>20:1 dr, 84% ee

160g
77% yield[c], >20:1 B/L
>20:1 dr, 84% ee

160h
70% yield[c], >20:1 B/L
>20:1 dr, 82% ee

160i
87% yield[c], 7.5:1 B/L
>20:1 dr, 78% ee

160j
30% yield[d], 9.1:1 B/L
>20:1 dr, 94% ee

160k
59% yield[c], 2.5:1 B/L
8.3:1 dr, 73% ee

160l
35% yield, >20:1 B/L
>20:1 dr, 82% ee

Vicinal stereocenters containing C–F bonds

160m
71% yield, >20:1 B/L
>20:1 dr, 85% ee

160n
75% yield, >20:1 B/L
>20:1 dr, 82% ee

160o
80% yield[c,e], >20:1 B/L
>20:1 dr, 87% ee

160p
48% yield, >20:1 B/L
14:1 dr, 84% ee

160q
78% yield[d], 3.6:1 B/L
4.5:1 dr, 87% ee

[a] Reaction conditions: **158** (0.1 mmol), Pd$_2$(dba)$_3$ (2.5 mol %), **L7** (6.5 mol %), and toluene (4 mL) at 50 °C for 14 h. [b] Pd$_2$(pmdba)$_3$ can be employed as a Pd source when dba is difficult to separate from desired product. [c] **L6** employed (comparable performance between **L7** and **L6**). [d] **L3** employed. [e] Reaction carried out at 60 °C.

5.4   PRODUCT TRANSFORMATIONS

Derivatization of allylic alkylation products showcases the synthetic utility of these building blocks. Stork–Danheiser ketone transposition of vinylogous ester **160d** afforded γ-substituted α,β-unsaturated ketone **161**. Selective olefin hydrogenation of **160d** smoothly furnishes vicinal stereocenter-containing product **162** in nearly quantitative yield. Wacker oxidation of the terminal olefin of **160c** yielded ketone **163**, now bearing a 1,4-dioxygenation pattern.

Figure 5.4. *Branched allylic alkylation product derivatizations.*
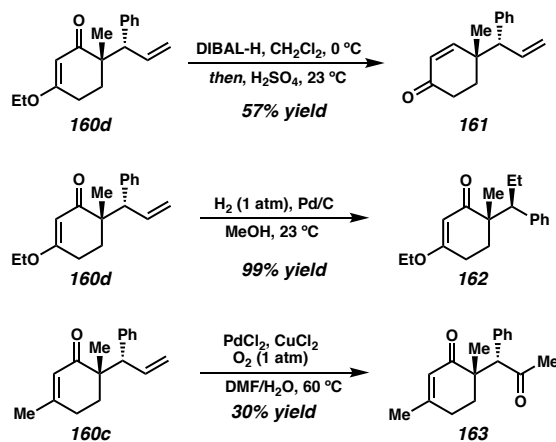
5.5   CONCLUSIONS

We report the development of a branched-selective Pd-catalyzed decarboxylative asymmetric allylic alkylation of *hard* enolate nucleophiles. Building on our prior studies on the inner-sphere seven-centered reductive elimination, we derive a set of design principles for rational ligand design that ultimately overturns the innate selectivity in prior systems. The transformation employs readily accessible β-ketoester precursors to furnish products containing vicinal all-carbon quaternary/tertiary stereocenters. Branched products

are obtained in up to 80% yield, >20:1 dr, and 87% ee. Studies further expanding the utility and scope of this transformation are underway and will be reported in due course.

5.6   SUPPORTING INFORMATION

5.6.1   MATERIALS AND METHODS

Unless otherwise stated, reactions were performed in flame-dried glassware under an argon or nitrogen atmosphere using dry, deoxygenated solvents. Solvents were dried by passage through an activated alumina column under argon.[11] Reaction progress was monitored by thin-layer chromatography (TLC) or Agilent 1290 UHPLC-MS. TLC was performed using E. Merck silica gel 60 F254 precoated glass plates (0.25 mm) and visualized by UV fluorescence quenching or $KMnO_4$ staining. Silicycle Silia*Flash*® P60 Academic Silica gel (particle size 40–63 nm) was used for flash chromatography. ^{1}H NMR spectra were recorded on a Bruker 400 MHz spectrometer and are reported relative to residual $CHCl_3$ (δ 7.26 ppm). ^{13}C NMR spectra were recorded on a Bruker 400 MHz spectrometer (100 MHz) and are reported relative to $CHCl_3$ (δ 77.16 ppm). ^{2}H NMR spectra were recorded on a Bruker 400 MHz (61 MHz) spectrometer and are reported relative to residual $CDCl_3$ (δ 7.26 ppm). Data for ^{1}H NMR are reported as follows: chemical shift (δ ppm) (multiplicity, coupling constant (Hz), integration). Multiplicities are reported as the peaks appear as follows: s = singlet, d = doublet, t = triplet, q = quartet, p = pentet, sept = septuplet, m = multiplet, br s = broad singlet, br d = broad doublet. Data for ^{13}C NMR are reported in terms of chemical shifts (δ ppm). Some reported spectra include minor solvent impurities of water (δ 1.56ppm), ethyl acetate (δ 4.12, 2.05, 1.26 ppm), methylene chloride (δ 5.30 ppm), acetone (δ 2.17 ppm), grease (δ 1.26, 0.86 ppm), and/or

silicon grease (δ 0.07 ppm), which do not impact product assignments. ^{13}C NMR spectra

of deuterated compounds are complicated by the low intensity of peaks of deuterium-

substituted carbon atoms. IR spectra were obtained by use of a Perkin Elmer Spectrum

BXII spectrometer or Nicolet 6700 FTIR spectrometer using thin films deposited on NaCl

plates and reported in frequency of absorption (cm^{-1}). Optical rotations were measured

with a Jasco P-2000 polarimeter operating on the sodium D-line (589 nm), using a 100 mm

path-length cell. Analytical SFC was performed with a Mettler SFC supercritical CO_2

analytical chromatography system utilizing Chiralpak (AD-H or IC) or Chiralcel (OD-H,

OJ-H, or OB-H) columns (4.6 mm x 25 cm) obtained from Daicel Chemical Industries, Ltd.

High resolution mass spectra (HRMS) were obtained from the Caltech Mass Spectral

Facility using a JEOL JMS-600H High Resolution Mass Spectrometer in Field Desorption

(FD+) mode. Absolute stereochemical assignments were made by vibrational circular

dichroism analysis for select compounds with related compounds assigned by analogy.

Reagents were purchased from commercial sources and used as received unless

otherwise stated. Ligands were prepared according to literature procedures.[12]

List of Abbreviations: ee – enantiomeric excess, SFC – supercritical fluid

chromatography, TLC – thin-layer chromatography, IPA – isopropanol, VCD – vibrational

circular dichroism, pmdba – bis(4-methoxybenzylidene)acetone.

5.6.2   EXPERIMENTAL PROCEDURES AND SPECTROSCOPIC DATA

Pd-Catalyzed Decarboxylative Asymmetric Allylic Alkylation

General Procedure A: Asymmetric Pd-Catalyzed Decarboxylative Allylic Alkylation.
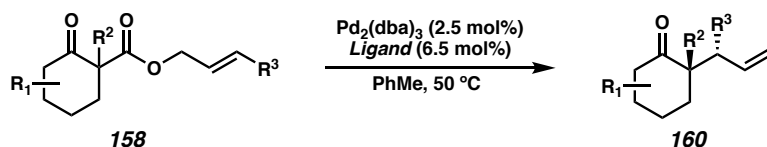
In a nitrogen filled glovebox, an oven-dried 1 dram vial was charged with a stir bar,

Pd₂(dba)₃ or Pd₂(pmdba)₃ (2.5 µmol, 2.5 mol %), ligand (0.0065 mmol, 6.5 mol %), and

toluene (1.0 mL). The catalyst solution was stirred at 23 ºC for 20 min, then added to a

solution of substrate **158** in toluene (3 mL) in a 2 dram vial. The reaction vial was then

sealed with electrical tape, removed from the glovebox, and heated to 50 ºC for 14 h. The

reaction mixture was let cool to ambient temperature, passed through a plug of silica gel,

and concentrated under reduced pressure. The crude reaction mixture was loaded directly

onto a flash column and the product (**160**) was isolated by silica gel flash column
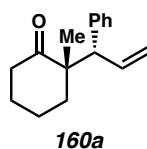
chromatography.

(S)-2-methyl-2-((S)-1-phenylallyl)cyclohexan-1-one (160a)

Prepared from **158a** (27.2 mg, 100 µmol) following General Procedure A using

Pd₂(pmdba)₃ and **L7**. Purification by flash column chromatography (0–15%

EtOAc/hexanes) afforded the title compund as a colorless oil (14.2 mg, 62.2 µmol, 62%

yield, 9.1:1 B/L, >20:1 dr (B), 82% ee(B)).

*Crude ^{1}H NMR analysis reveals a B/L of 5.6:1 prior to chromatography.

^{1}H NMR (400 MHz, CDCl$_3$): δ 7.35 – 7.28 (m, 2H), 7.25 – 7.19 (m, 3H), 6.21 – 6.07 (m, 1H), 5.09 – 5.03 (m, 2H), 3.93 (d, J = 9.4 Hz, 1H), 2.56 – 2.32 (m, 2H), 2.10 – 1.98 (m, 2H), 1.87 – 1.62 (m, 3H), 1.35 – 1.24 (m, 1H), 0.98 (s, 3H).

^{13}C NMR (100 MHz, CDCl$_3$): δ 215.0, 140.0, 136.6, 129.8, 128.2, 126.9, 117.2, 53.0, 52.5, 39.7, 37.4, 27.8, 21.1, 19.6.

IR (Neat Film, NaCl): 3062, 3027, 2933, 2863, 1704, 1453, 1124 cm^{-1}.

HRMS (MM: EI+): *m/z* calc'd for C$_{16}$H$_{20}$O [M]$^+$: 228.1514, found 228.1515.

Optical Rotation: $[\alpha]_D^{21}$ –25.1 (c 1.00, CHCl$_3$).

SFC conditions: 10% IPA, 2.5 mL/min, Chiralpak OJ-H column, λ = 210 nm, t$_R$ (min): minor = 3.59, major = 2.81.
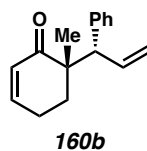
160b

(*S*)-6-methyl-6-((*S*)-1-phenylallyl)cyclohex-2-en-1-one (160b)

Prepared from **158b** (27.2 mg, 1.00 mmol) following General Procedure A using Pd$_2$(pmdba)$_3$ and **L7**. Purification by flash column chromatography (0–100% CH$_2$Cl$_2$/hexanes) afforded the title compound as a colorless oil (11.5 mg, 0.05 mmol, 51% yield, 20:1 B/L, >20:1 dr (B), 78% ee(B)).

^{1}H NMR (400 MHz, CDCl$_3$): δ 7.32 – 7.17 (m, 5H), 6.84 (dt, J = 10.0, 3.9 Hz, 1H), 6.20 (dt, J = 16.8, 9.9 Hz, 1H), 5.91 (dt, J = 10.0, 2.1 Hz, 1H), 5.12 – 4.98 (m, 2H), 3.86 (d, J =

9.7 Hz, 1H), 2.56 – 2.46 (m, 1H), 2.40 – 2.29 (m, 1H), 1.85 (dt, J = 13.8, 5.7 Hz, 1H), 1.73 (ddd, J = 13.9, 7.3, 5.5 Hz, 1H), 1.10 (s, 3H).

^{13}C NMR (101 MHz, CDCl$_3$): δ 203.0, 148.2, 140.8, 137.0, 129.8, 129.1, 128.1, 126.6, 117.4, 52.9, 48.8, 31.1, 23.4, 20.5.

IR (Neat Film, NaCl): 3028, 2935, 2343, 2357, 1699, 1670, 1636, 1387, 1222, 695 cm^{-1}.

HRMS [M+H]$^{+}$: *m/z* calc'd for C$_{16}$H$_{19}$O: 227.14359, found 227.14317.

Optical Rotation: [α]$_D^{22}$ +39.0° (*c* 0.48, CHCl$_3$).

SFC conditions: 20% IPA, 2.5 mL/min, Chiralpak OJ-H column, λ = 210 nm, t$_R$ (min): minor = 4.45, major = 4.08.
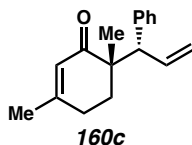
(*S*)-3,6-dimethyl-6-((*S*)-1-phenylallyl)cyclohex-2-en-1-one (160c)

Prepared from **158c** (28.4 mg, 100 μmol) following General Procedure A using Pd$_2$(pmdba)$_3$ and **L7**. Purification by flash column chromatography (0–20% EtOAc/hexanes) afforded the title compound as a colorless oil (16.8 mg, 69.9 μmol, 70% yield, >20:1 B/L, >20:1 dr, 80% ee).

^{1}H NMR (400 MHz, CDCl$_3$): δ 7.37 – 7.24 (m, 5H), 6.28 (dt, J = 16.8, 9.9 Hz, 1H), 5.83 (q, J = 1.4 Hz, 1H), 5.17 (dd, J = 10.0, 1.8 Hz, 1H), 5.11 (ddd, J = 16.8, 1.8, 0.9 Hz, 1H), 3.94 (d, J = 9.7 Hz, 1H), 2.51 – 2.42 (m, 1H), 2.37 – 2.28 (m, 1H), 1.98 (s, 3H), 1.92 (ddd, J = 13.8, 6.9, 5.4 Hz, 1H), 1.78 (ddd, J = 13.8, 7.0, 5.4 Hz, 1H), 1.16 (s, 3H).

¹³C NMR (100 MHz, CDCl₃): δ 202.8, 159.9, 141.0, 137.1, 129.8, 128.1, 126.5, 126.0,

117.4, 53.1, 47.5, 30.9, 28.3, 24.1, 20.8.

IR (Neat Film, NaCl): 3062, 3028, 2969, 2932, 1663, 1637, 1452, 1377, 1213 cm⁻¹.

HRMS (MM: FD+): *m/z* calc'd for $C_{17}H_{20}O$ [M]⁺: 240.1514, found 240.1522.

Optical Rotation: $[\alpha]_D^{21}$ +38.1 (c 1.00, CHCl₃)

SFC conditions: 10% IPA, 2.5 mL/min, Chiralpak AD-H column, λ = 210 nm, t_R (min):

minor = 2.95, major = 3.31.
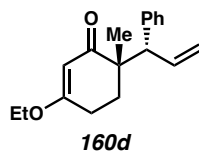
160d

(*S*)-3-ethoxy-6-methyl-6-((*S*)-1-phenylallyl)cyclohex-2-en-1-one (160d)

Prepared from **158d** (31.4 mg, 100 μmol) following General Procedure A using Pd₂(dba)₃

and **L7**. Purification by flash column chromatography (0–40% EtOAc/hexanes) afforded

the title compound as a colorless oil (18.8 mg, 70 μmol, 70% yield, >20:1 dr, 84% ee).

Ligand **L6** afforded identical results.

¹H NMR (400 MHz, CDCl₃): δ 7.28 – 7.16 (m, 5H), 6.23 (dt, *J* = 16.8, 9.9 Hz, 1H), 5.23

(s, 1H), 5.12 (dd, *J* = 10.1, 1.8 Hz, 1H), 5.06 (ddd, *J* = 16.8, 1.9, 0.9 Hz, 1H), 3.90 (d, *J* =

9.7 Hz, 1H), 3.87 (dd, *J* = 7.0, 2.8 Hz, 1H), 3.83 (dd, *J* = 7.0, 2.7 Hz, 1H), 2.48 (ddd, *J* =

18.1, 7.0, 5.6 Hz, 1H), 2.44 – 2.34 (m, 1H), 1.87 (ddd, *J* = 13.4, 7.6, 5.6 Hz, 1H), 1.73 –

1.66 (m, 2H), 1.33 (t, *J* = 7.0 Hz, 3H), 1.11 (s, 3H).

¹³C NMR (100 MHz, CDCl₃): δ 202.8, 175.5, 141.2, 137.1, 129.8, 128.1, 126.5, 117.4,

102.0, 64.3, 53.5, 47.5, 29.5, 26.1, 21.3, 14.3.

IR (Neat Film, NaCl): 2942, 1647, 1611, 1377, 1190 cm^{-1}.

HRMS (MM: FD+): *m/z* calc'd for $C_{18}H_{22}O_2$ [M]$^+$: 270.1620, found 270.1628.

Optical Rotation: $[\alpha]_D^{21}$ –1.3 (c 1.00, CHCl$_3$).

SFC conditions: 10% IPA, 2.5 mL/min, Chiralpak OJ-H column, λ = 254 nm, t_R (min):

minor = 2.70, major = 3.25.
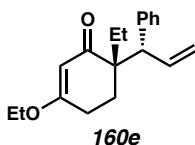
(*S*)-3-ethoxy-6-ethyl-6-((*S*)-1-phenylallyl)cyclohex-2-en-1-one (160e)

Prepared from **158e** (34.4 mg, 104 µmol) following General Procedure A using Pd$_2$(dba)$_3$

and **L6**. Purification by flash column chromatography (5–20% EtOAc/hexanes) afforded

the title compound as a colorless oil (21.0 mg, 74 µmol, 70% yield, >20:1 dr, 87% ee).

^{1}H NMR (400 MHz, CDCl$_3$): δ 7.26 – 7.21 (m, 4H), 7.19 – 7.13 (m, 1H), 6.26 (dt, *J* =

16.8, 10.1 Hz, 1H), 5.22 (s, 1H), 5.14 – 5.07 (m, 2H), 4.02 (d, *J* = 10.0 Hz, 1H), 3.86 –

3.78 (m, 2H), 2.47 – 2.33 (m, 2H), 1.96 – 1.74 (m, 3H), 1.50 (dq, *J* = 14.5, 7.4 Hz, 1H),

1.31 (t, *J* = 7.0 Hz, 3H), 0.83 (t, *J* = 7.4 Hz, 3H).

^{13}C NMR (100 MHz, CDCl$_3$): δ 201.0, 175.2, 141.6, 137.0, 130.1, 128.0, 126.3, 117.3,

103.0, 64.2, 51.7, 50.7, 26.7, 26.3, 26.0, 14.3, 8.3.

IR (Neat Film, NaCl): 2978, 2937, 1650, 1612, 1380, 1189 cm^{-1}.

HRMS (MM: ESI+): *m/z* calc'd for $C_{19}H_{25}O_2$ [M+H]$^+$: 285.1849, found 285.1859.

Optical Rotation: $[\alpha]_D^{21}$ +16.0 (c 1.00, CHCl$_3$).

SFC conditions: 10% IPA, 2.5 mL/min, Chiralpak OJ-H column, λ = 254 nm, t_R (min):

minor = 2.93, major = 3.50.
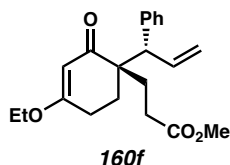
160f

methyl   3-((R)-4-ethoxy-2-oxo-1-((S)-1-phenylallyl)cyclohex-3-en-1-yl)propanoate

(160f)

Prepared from **158f** (38.2 mg, 98.9 μmol) following General Procedure A using Pd$_2$(dba)$_3$

and **L6**. Purification by flash column chromatography (5–20% EtOAc/hexanes) afforded

the title compound as a colorless oil (14.3 mg, 41.8 μmol, 42% yield, >20:1 dr, 84% ee).

^{1}H NMR (400 MHz, CDCl$_3$): δ 7.26 – 7.20 (m, 4H), 7.18 – 7.13 (m, 1H), 6.25 (dt, J =

16.8, 10.1 Hz, 1H), 5.20 (s, 1H), 5.19 – 5.10 (m, 2H), 4.07 (d, J = 10.1 Hz, 1H), 3.86 –

3.77 (m, 2H), 3.63 (s, 3H), 2.52 – 2.33 (m, 3H), 2.25 (ddd, J = 16.3, 11.4, 4.8 Hz, 1H), 2.00

(ddd, J = 14.0, 11.5, 5.2 Hz, 1H), 1.95 – 1.79 (m, 3H), 1.31 (t, J = 7.0 Hz, 3H).

^{13}C NMR (100 MHz, CDCl$_3$): δ 200.2, 175.3, 174.3, 141.0, 136.2, 130.0, 128.0, 126.4,

117.9, 102.6, 64.2, 51.6, 51.0, 49.6, 28.3, 28.1, 27.0, 25.7, 14.1.

IR (Neat Film, NaCl): 2980, 2946, 1737, 1643, 1610, 1381, 1191 cm^{-1}.

HRMS (MM: ESI+): *m/z* calc'd for C$_{21}$H$_{27}$O$_4$ [M+H]$^+$: 343.1904, found 343.1909.

Optical Rotation: $[\alpha]_D^{21}$ +24.6 (c 1.00, CHCl$_3$).

SFC conditions: 10% IPA, 2.5 mL/min, Chiralpak OJ-H column, λ = 254 nm, t_R (min):

minor = 2.54, major = 3.00.
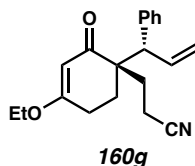
160g

3-((*S*)-4-ethoxy-2-oxo-1-((*S*)-1-phenylallyl)cyclohex-3-en-1-yl)propanenitrile (160g)

Prepared from **158g** (35.3 mg, 100 μmol) following General Procedure A using Pd$_2$(dba)$_3$

and **L6**. Purification by flash column chromatography (5–40% EtOAc/hexanes) afforded

the title compound as a colorless oil (23.9 mg, 77.2 μmol, 77% yield, >20:1 B/L, >20:1 dr,

84% ee).

^{1}H NMR (400 MHz, CDCl$_3$): δ 7.29 – 7.23 (m, 2H), 7.19 (td, *J* = 7.8, 1.4 Hz, 3H), 6.23

(dt, *J* = 16.9, 10.1 Hz, 1H), 5.24 (s, 1H), 5.20 (d, *J* = 10.2 Hz, 1H), 5.13 (d, *J* = 16.9 Hz,

1H), 3.97 (d, *J* = 9.9 Hz, 1H), 3.89 – 3.80 (m, 2H), 2.51 – 2.39 (m, 3H), 2.28 – 2.12 (m,

2H), 1.93 – 1.76 (m, 3H), 1.33 (t, *J* = 7.0 Hz, 3H).

^{13}C NMR (100 MHz, CDCl$_3$): δ 199.5, 175.8, 140.2, 135.8, 129.8, 128.3, 126.9, 120.4,

118.5, 102.6, 64.6, 51.0, 49.8, 29.3, 26.7, 25.7, 14.2, 12.1.

IR (Neat Film, NaCl): 2980, 2937, 2246, 1643, 1606, 1381, 1190 cm^{-1}.

HRMS (MM: ESI+): *m/z* calc'd for C$_{20}$H$_{24}$O$_2$N [M+H]$^+$: 310.1802, found 310.1804.

Optical Rotation: [α]$_D^{21}$ +13.1 (c 1.00, CHCl$_3$).

SFC conditions: 20% IPA, 2.5 mL/min, Chiralpak OJ-H column, λ = 254 nm, t$_R$ (min):

minor = 2.06, major = 3.05.
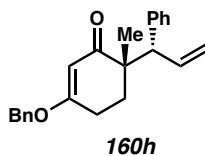
160h

(*S*)-3-(benzyloxy)-6-methyl-6-((*S*)-1-phenylallyl)cyclohex-2-en-1-one (160h)

Prepared from **158h** following General Procedure A using Pd$_2$(dba)$_3$ and **L6**. Purification

by flash column chromatography (0–40% EtOAc/hexanes) afforded the title compound as

a colorless oil (23.4 mg, 0.704 mmol, 70% yield, >20:1 dr, 82% ee).

^{1}H NMR (400 MHz, CDCl$_3$): δ 7.42 – 7.32 (m, 5H), 7.30 – 7.24 (m, 4H), 7.19 (ddd, J =

8.4, 5.3, 2.2 Hz, 1H), 6.24 (dt, J = 16.8, 9.9 Hz, 1H), 5.37 (s, 1H), 5.12 (dd, J = 10.1, 1.9

Hz, 1H), 5.06 (d, J = 16.8 Hz, 1H), 4.87 – 4.80 (m, 2H), 3.92 (d, J = 9.7 Hz, 1H), 2.55 (dt,

J = 18.1, 6.1 Hz, 1H), 2.45 (ddd, J = 18.1, 7.5, 5.6 Hz, 1H), 1.91 (ddd, J = 13.3, 7.6, 5.6

Hz, 1H), 1.73 (ddd, J = 13.7, 7.0, 5.6 Hz, 1H), 1.14 (s, 3H).

^{13}C NMR (100 MHz, CDCl$_3$): δ 202.6, 175.0, 141.1, 137.0, 135.2, 129.8, 128.8, 128.7,

128.1, 128.0, 126.5, 117.5, 102.6, 70.5, 53.5, 47.6, 29.4, 26.1, 21.3.

IR (Neat Film, NaCl): 2932, 1652, 1610, 1362, 1186 cm^{-1}.

HRMS (MM: FD+): *m/z* calc'd for C$_{23}$H$_{24}$O$_2$ [M]$^+$: 332.1776, found 332.1773.

Optical Rotation: [α]$_D^{21}$ –5.0 (c 1.00, CHCl$_3$).

SFC conditions: 25% IPA, 2.5 mL/min, Chiralpak OD-H column, λ = 254 nm, t$_R$ (min):

minor = 4.10, major = 3.72.
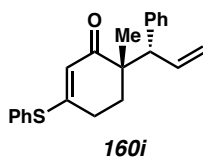
160i

(*S*)-6-methyl-6-((*S*)-1-phenylallyl)-3-(phenylthio)cyclohex-2-en-1-one (160i)

Prepared from **158i** following General Procedure A using Pd$_2$(dba)$_3$ and **L6**. Purification

by flash column chromatography (0–40% EtOAc/hexanes) afforded the title compound as

a colorless oil (29.2 mg, 0.873 mmol, 87% yield, 7.5:1 B/L, >20:1 dr, 78% ee).

¹H NMR (400 MHz, CDCl₃): δ 7.47 – 7.38 (m, 5H), 7.27 – 7.18 (m, 5H), 6.18 (dt, *J* =

16.8, 9.9 Hz, 1H), 5.37 (s, 1H), 5.11 (dd, *J* = 10.1, 1.9 Hz, 1H), 5.05 (d, *J* = 16.8 Hz, 1H),

3.91 (d, *J* = 9.7 Hz, 1H), 2.63 – 2.46 (m, 2H), 1.94 (ddd, *J* = 13.3, 7.7, 5.3 Hz, 1H), 1.78

(ddd, *J* = 13.7, 6.7, 5.2 Hz, 1H), 1.11 (s, 3H).

¹³C NMR (100 MHz, CDCl₃): δ 199.3, 164.0, 143.5, 140.9, 136.8, 135.6, 130.2, 129.9,

129.8, 128.1, 126.5, 120.3, 117.6, 53.3, 47.9, 31.0, 27.2, 21.3.

IR (Neat Film, NaCl): 2927, 1650, 1579, 1212 cm⁻¹.

HRMS (MM: FD+): *m/z* calc'd for C₂₂H₂₂O₂S [M]⁺: 334.1391, found 334.1392.

Optical Rotation: [α]$_D^{21}$ –64.9 (c 1.00, CHCl₃).

SFC conditions: 20% IPA, 2.5 mL/min, Chiralpak OJ-H column, λ = 210 nm, t$_R$ (min):

minor = 4.45, major = 4.08.
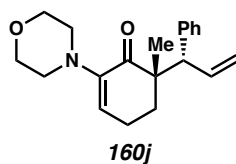
160j

***(S)*-6-methyl-2-morpholino-6-(*(S)*-1-phenylallyl)cyclohex-2-en-1-one (160j)**

Prepared from **158j** following General Procedure A using Pd₂(dba)₃ and **L3**. Purification

by preparatory TLC (10% acetone/toluene) afforded the title compound as a colorless oil

(9.2 mg, 0.030 mmol, 30% yield, 9.1:1 B/L, >20:1 dr, 94% ee).

¹H NMR (400 MHz, C₆D₆): δ 7.18 – 7.16 (m, 3H), 7.14 – 7.08 (m, 2H), 7.06 – 7.01 (m,

1H), 6.13 (dt, *J* = 16.8, 9.9 Hz, 1H), 5.24 (t, *J* = 4.4 Hz, 1H), 4.98 – 4.90 (m, 2H), 3.90 (d,

J = 9.6 Hz, 1H), 3.77 – 3.58 (m, 4H), 2.91 – 2.83 (m, 2H), 2.39 – 2.32 (m, 2H), 2.22 – 2.10

(m, 1H), 1.96 – 1.84 (m, 1H), 1.61 (dt, J = 13.8, 5.4 Hz, 1H), 1.33 (ddd, J = 13.8, 8.2, 5.6

Hz, 1H), 1.08 (s, 3H).

¹³C NMR (100 MHz, C₆D₆): δ 198.3, 146.3, 141.1, 137.6, 130.0, 128.2, 126.8, 121.6,

117.2, 67.0, 53.4, 50.5, 49.4, 31.5, 22.0, 20.5.

IR (Neat Film, NaCl): 3027, 2928, 2853, 1681, 1615, 1450, 1263, 1210, 1119 cm⁻¹.

HRMS (MM: ESI+): *m/z* calc'd for $C_{20}H_{27}O_2N$ [M+H]⁺: 312.1958, found 312.1961.

Optical Rotation: $[\alpha]_D^{21}$ +8.9 (c 0.90, CHCl₃).

SFC conditions: 30% IPA, 2.5 mL/min, Chiralpak OJ-H column, λ = 280 nm, t_R (min):

minor = 3.89, major = 2.05.
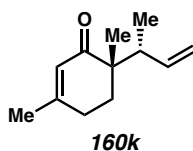
160k

***(S)*-6-methyl-2-morpholino-6-(*(S)*-1-phenylallyl)cyclohex-2-en-1-one (160k)**

Prepared from **158k** (0.094 mmol) following General Procedure A using Pd₂(pmdba)₃ and

L6. Purification by preparatory TLC (25% Et₂O/hexanes) afforded the title compound as a

colorless oil (10.0 mg, 0.056 mmol, 59% yield, 2.5:1 B/L, 9.0:1 dr, 73% ee).

¹H NMR (400 MHz, C₆D₆): δ 5.81 – 5.75 (m, 1.4H (linear + both branched)), 5.69 (ddd,

J = 16.5, 10.7, 8.4 Hz, 0.9H (branched)), 5.62 – 5.53 (m, 0.4H (linear)), 5.39 – 5.29 (m,

0.4H (linear)), 5.08 – 4.95 (m, 2H (branched major + branched minor)), 2.75 – 2.63 (m,

0.9H(branched major)), 2.64 – 2.56 (m, 0.1H (branched minor)), 2.31 – 2.21 (m, 3.6H),

2.01 (ddd, J = 13.7, 7.3, 6.3 Hz, 1H), 1.95 – 1.87 (m, 5H), 1.76 – 1.58 (m, 3.3H), 1.06 (s,

1.2H(linear)), 0.99 (s, 2.7H(branched major)), 0.98 (s, 0.4H(branched minor)), 0.94 (d, $J =$

6.8 Hz, 2.7H(branched major)), 0.88 (d, $J = 7.0$ Hz, 0.4H(branched minor)).

^{13}C NMR (100 MHz, CDCl$_3$): δ 204.0, 203.8, 160.5, 160.2, 140.4, 139.9, 126.8, 126.1,

125.8, 125.6, 125.5, 115.6, 115.4, 46.3, 46.0, 43.9, 41.6, 40.2, 33.8, 33.1, 31.9, 30.5, 29.8,

29.5, 28.4, 28.1, 28.0, 24.2, 24.1, 24.1, 21.9, 20.3, 18.1, 15.3, 14.4, 13.1.

IR (Neat Film, NaCl): 2965, 2930, 1666, 1638, 1433, 1378, 1213 cm^{-1}.

HRMS (MM: FI+): *m/z* calc'd for C$_{12}$H$_{18}$O [M]$^+$: 178.1358, found 178.1362.

Optical Rotation: [α]$_D^{21}$ +2.3 (c 1.00, CHCl$_3$).

SFC conditions: 4% IPA, 2.5 mL/min, Chiralpak IC column, λ = 210 nm, t$_R$ (min): minor

= 7.16, major = 8.11.
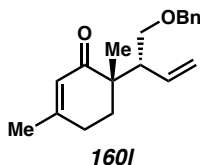
160l

(*S*)-6-methyl-2-morpholino-6-((*S*)-1-phenylallyl)cyclohex-2-en-1-one (160l)

Prepared from **158l** (0.105 mmol) following General Procedure A using Pd$_2$(pmdba)$_3$ and

L7. Purification by flash column chromatography (0–20% EtOAc/hexanes) afforded the

title compound as a colorless oil (10.6 mg, 0.037 mmol, 35% yield, >20:1 B/L, >20:1 dr,

82% ee).

^{1}H NMR (500 MHz, CDCl$_3$): δ 7.35 – 7.28 (m, 4H), 7.28 – 7.23 (m, 1H), 5.79 (s, 1H),

5.67 (dt, $J = 16.9, 9.9$ Hz, 1H), 5.19 – 5.10 (m, 2H), 4.47 (d, $J = 2.4$ Hz, 2H), 3.57 – 3.40

(m, 2H), 2.97 (ddd, $J = 9.4, 7.4, 5.6$ Hz, 1H), 2.37 – 2.17 (m, 2H), 2.08 – 1.97 (m, 1H),

1.91 (s, 3H), 1.70 – 1.61 (m, 2H), 1.02 (s, 3H).

^{13}C NMR (101 MHz, CDCl$_3$): δ 202.7, 159.9, 138.6, 136.0, 128.3, 127.5, 127.4, 125.9, 118.5, 72.8, 70.6, 48.1, 45.1, 29.7, 28.0, 24.1, 20.9.

IR (Neat Film, NaCl): 3026, 2918, 1665, 1453, 1214, 1096 cm^{-1}.

HRMS (MM: ESI+): *m/z* calc'd for C$_{19}$H$_{24}$O$_2$ [M]$^+$: 284.1766, found 284.1776.

Optical Rotation: [α]$_D^{21}$ +33.2 (c 1.05, CHCl$_3$).

SFC conditions: 10% IPA, 2.5 mL/min, Chiralpak OJ-H column, λ = 210 nm, t$_R$ (min): minor = 3.77, major = 2.81.
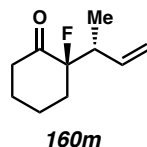
160m

(*S*)-2-fluoro-2-((*S*)-1-phenylallyl)cyclohexan-1-one (160m)

Prepared from **158m** (28.6 mg, 103 μmol) following General Procedure A using Pd$_2$(pmdba)$_3$ and **L7**. Purification by flash column chromatography (0–15% EtOAc/hexanes) afforded the title compound as a colorless crystalline solid (17.1 mg, 73.6 μmol, 71% yield, >20:1 B/L, >20:1 dr, 85% ee) as well as a fraction (1.5 mg, 6.5 μmol, 6% yield) containing mixed E/Z linear isomers with trace of the major diastereomer of the branched isomer. Overall yield: 18.6 mg, 80.1 μmol, 77% yield, 13:1 B/L, >20:1 dr (B), 85% ee (B)).

*Crude ^{1}H NMR analysis reveals a B/L of 12.5:1 prior to chromatography.

^{1}H NMR (400 MHz, CDCl$_3$): δ 7.39 – 7.24 (m, 5H), 6.18 (ddd, *J* = 17.1, 10.3, 8.8 Hz, 1H), 5.12 (d, *J* = 10.3 Hz, 1H), 5.08 (d, *J* = 17.1 Hz, 1H), 3.88 (dd, *J* = 32.4, 8.8 Hz, 1H), 2.71 – 2.63 (m, 1H), 2.54 – 2.45 (m, 1H), 2.06 – 1.98 (m, 1H), 1.86 – 1.68 (m, 5H).

*Trace isolated peaks of minor diastereomer (<5%) observed as 5.26 – 5.19 (m, 2H), 2.88 – 2.75 (m, 2H), 2.43 – 2.30 (m, 2H). Others overlap with major diastereomer.

¹³C NMR (100 MHz, CDCl₃): δ 207.5 (d, J_{C-F} = 18.2 Hz), 137.9, 135.3 (d, J_{C-F} = 5.4 Hz), 129.6 (d, J = 2.6 Hz), 128.8, 127.5, 117.9, 100.7 (d, J_{C-F} = 194.8 Hz), 53.1 (d, J_{C-F} = 20.0 Hz), 40.3, 36.7 (d, J_{C-F} = 21.7 Hz), 27.8, 22.2 (d, J_{C-F} = 9.1 Hz).

¹⁹F NMR (282 MHz, CDCl₃): δ –166.45 (d, J = 32.5 Hz).

IR (Neat Film, NaCl): 2948, 1724, 1454, 1047 cm⁻¹.

HRMS (MM: EI+): *m/z* calc'd for $C_{15}H_{17}OF$ [M]⁺: 232.1263, found 232.1259.

Optical Rotation: $[\alpha]_D^{21}$ –23.3 (c 1.00, CHCl₃).

SFC conditions: 10% IPA, 2.5 mL/min, Chiralpak OJ-H column, λ = 210 nm, t_R (min): minor = 3.23, major = 2.65.
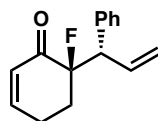
(*S*)-2-fluoro-2-((*S*)-1-phenylallyl)cyclohexan-1-one (160n)

Prepared from **158n** (27.0 mg, 98.4 μmol) following General Procedure A using Pd₂(pmdba)₃ and **L7**. Purification by flash column chromatography (0–20% EtOAc/hexanes) afforded the title compound as a colorless oil (17.1 mg, 74.3 μmol, 75% yield, >20:1 B/L, >20:1 dr, 82% ee).

¹H NMR (400 MHz, CDCl₃): δ 7.37 – 7.27 (m, 5H), 6.95 – 6.90 (m, 1H), 6.23 (ddd, J = 17.0, 10.1, 8.7 Hz, 1H), 6.06 (dddd, J = 10.0, 4.0, 2.8, 1.3 Hz, 1H), 5.11 (d, J = 10.1 Hz, 1H), 4.96 (d, J = 17.0 Hz, 1H), 3.67 (dd, J = 31.1, 8.7 Hz, 1H), 2.58 – 2.38 (m, 2H), 2.19 – 2.07 (m, 1H), 2.00 – 1.92 (m, 1H).

¹³C NMR (100 MHz, CDCl₃): δ 195.6 (d, $J_{C–F}$ = 17.2 Hz), 149.0, 138.5, 135.3 (d, $J_{C–F}$ =

5.5 Hz), 129.2 (d, $J_{C–F}$ = 2.8 Hz), 128.9, 128.2, 127.6, 118.0, 97.4 (d, $J_{C–F}$ = 194.5 Hz),

53.0 (d, $J_{C–F}$ = 20.2 Hz), 31.2 (d, $J_{C–F}$ = 22.1 Hz), 25.1 (d, $J_{C–F}$ = 11.3 Hz).

¹⁹F NMR (282 MHz, CDCl₃): –168.84 (d, J = 31.5 Hz).

IR (Neat Film, NaCl): 3031, 2922, 1695, 1489, 1452, 1425, 1383, 1219, 1060 cm⁻¹.

HRMS (MM: EI+): *m/z* calc'd for $C_{15}H_{15}OF$ [M]⁺: 230.1107, found 230.1113.

Optical Rotation: $[\alpha]_D^{21}$ +41.1 (c 1.00, CHCl₃).

SFC conditions: 10% IPA, 2.5 mL/min, Chiralpak OJ-H column, λ = 210 nm, t_R (min):

minor = 4.74, major = 3.92.
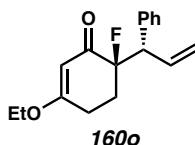
160o

(*R*)-3-ethoxy-6-fluoro-6-((*S*)-1-phenylallyl)cyclohex-2-en-1-one (160o)

Prepared from **158o** (31.8 mg, 100 μmol) following General Procedure A using $Pd_2(dba)_3$

and **L6**. Purification by flash column chromatography (5–20% EtOAc/hexanes) afforded

the title compound as a colorless oil (21.9 mg, 79.8 μmol, 80% yield, >20:1 dr, 87% ee).

¹H NMR (400 MHz, CDCl₃): δ 7.37 – 7.26 (m, 5H), 6.36 – 6.22 (m, 1H), 5.35 – 5.32 (m,

1H), 5.13 (d, J = 10.2 Hz, 1H), 4.97 (d, J = 17.0 Hz, 1H), 3.92 (q, J = 7.1 Hz, 2H), 3.71

(dd, J = 29.7, 8.5 Hz, 1H), 2.61 – 2.50 (m, 1H), 2.45 – 2.36 (m, 1H), 2.16 – 2.03 (m, 1H),

1.94 – 1.85 (m, 1H), 1.38 (t, J = 7.1 Hz, 3H).

¹³C NMR (100 MHz, CDCl₃): δ 194.4 (d, $J_{C–F}$ = 18.1 Hz), 194.3, 175.6 (d, $J_{C–F}$ = 1.6 Hz),

138.8, 135.4 (d, $J_{C–F}$ = 5.6 Hz), 129.3 (d, $J_{C–F}$ = 2.5 Hz), 128.8, 127.5, 117.8, 100.8, 96.4

(d, J_{C-F} = 191.3 Hz), 65.1, 53.3 (d, J_{C-F} = 20.8 Hz), 29.3 (d, J_{C-F} = 23.5 Hz), 27.2 (d, J_{C-F}

= 11.0 Hz), 14.2.

^{19}F NMR (282 MHz, CDCl$_3$): δ –168.60– –168.67 (m, 1F).

IR (Neat Film, NaCl): 2981, 2938, 1672, 1603, 1379, 1243, 1193 cm^{-1}.

HRMS (MM: ESI+): *m/z* calc'd for C$_{17}$H$_{20}$O$_2$F [M+H]$^+$: 275.1442, found 275.1440.

Optical Rotation: [α]$_D^{21}$ –11.2 (c 0.70, CHCl$_3$).

SFC conditions: 20% IPA, 2.5 mL/min, Chiralpak OJ-H column, λ = 254 nm, t$_R$ (min):

minor = 2.25, major = 2.58.

(*R*)-6-((*S*)-1-(benzyloxy)but-3-en-2-yl)-6-fluoro-3-methylcyclohex-2-en-1-one (160p)

Prepared from **158p** (36.0 mg, 108 µmol) following General Procedure A using Pd$_2$(dba)$_3$

and **L7**. Purification by flash column chromatography (0–30% EtOAc/hexanes) afforded

the branched product (**160p**) as a colorless oil (14.8 mg, 51.3 µmol, 48% yield, 14.3:1 dr,

84% ee) and the *(Z)*-linear product (**160p_linear**) also as a colorless oil (2.9 mg, 10.1 µmol,

9% yield, >20:1 Z/E, 53% ee)). Overall yield: 17.7 mg, 61.4 µmol, 57% yield, 5.1:1

B/L, >16.1 dr (B), 84% ee (B)).

*Crude ^{1}H NMR analysis reveals a B/L of 5.6:1 and a dr (B) of 12.9:1 prior to

*chromatography. In the tabulated NMR data for **160p**, the minor diastereomer is denoted.*

160p:

¹H NMR (400 MHz, CDCl₃): δ 7.36 – 7.27 (m, 5H), 5.88 – 5.74 (m, 2H), 5.34 – 5.24 (m,

0.15H(minor)), 5.17 (dd, *J* = 10.3, 1.7 Hz, 1H), 5.12 (d, *J* = 17.8 Hz, 1H), 4.50 (s, 2H),

4.45 (d, *J* = 11.8 Hz, 0.07H(minor)), 4.34 (d, *J* = 11.7 Hz, 0.07H(minor)), 3.76 (dd, *J* = 9.8,

6.7 Hz, 1H), 3.65 (dd, *J* = 9.6, 6.3 Hz, 0.07H(minor)), 3.52 (ddd, *J* = 9.8, 5.6, 0.9 Hz, 1H),

2.99 (ddt, *J* = 21.4, 9.2, 6.1 Hz, 1H), 2.91 – 2.82 (m, 0.07H(minor)), 2.53 – 2.33 (m, 3H),

2.26 – 2.14 (m, 1H), 1.96 (s, 3H), 1.93 (s, 0.19H(minor)).

¹³C NMR (100 MHz, CDCl₃): δ 194.0 (d, J_{C-F} = 17.9 Hz), 162.3, 138.2, 133.8 (d, J_{C-F} =

4.6 Hz), 128.5, 127.8, 127.7, 125.1, 119.1, 95.6 (d, J_{C-F} = 185.9 Hz), 73.3, 69.7 (d, J_{C-F} =

5.7 Hz), 47.1 (d, J_{C-F} = 21.4 Hz), 30.6 (d, J_{C-F} = 22.7 Hz), 29.6 (d, J_{C-F} = 9.5 Hz), 24.2.

¹⁹F NMR (282 MHz, CDCl₃): δ –167.64 – –167.85 (m).

IR (Neat Film, NaCl): 2923, 1681, 1633, 1104 cm⁻¹.

HRMS (MM: FD+): *m/z* calc'd for $C_{18}H_{21}O_2F$ [M]⁺: 289.1604, found 289.1590.

Optical Rotation: $[\alpha]_D^{21}$ –34.2 (c 1.00, CHCl₃).

SFC conditions: 10% IPA, 2.5 mL/min, Chiralpak OJ-H column, λ = 210 nm, t_R (min):

minor = 4.59, major = 3.43.

160p_linear:

¹H NMR (400 MHz, CDCl₃): δ 7.37 – 7.27 (m, 5H), 5.89 – 5.80 (m, 2H), 5.66 (dddt, *J* =

11.2, 8.4, 6.9, 1.5 Hz, 1H), 4.54 – 4.48 (m, 2H), 4.13 – 4.08 (m, 1H), 4.09 – 4.00 (m, 1H),

2.68 – 2.49 (m, 2H), 2.48 – 2.30 (m, 2H), 2.28 – 2.09 (m, 2H), 1.94 (s, 3H).

¹³C NMR (100 MHz, CDCl₃): δ 194.3 (d, J_{C-F} = 17.9 Hz), 162.8, 138.3, 130.6, 128.6,

128.0, 127.8, 125.5 (d, J_{C-F} = 4.5 Hz), 124.9, 93.9 (d, J_{C-F} = 183.0 Hz), 72.5, 65.8, 32.1 (d,

J_{C-F} = 23.8 Hz), 31.6 (d, J_{C-F} = 22.9 Hz), 29.2 (d, J_{C-F} = 9.0 Hz), 24.3.

¹⁹F NMR (282 MHz, CDCl₃): δ –161.29 – –161.59 (m).

IR (Neat Film, NaCl): 2917, 1682, 1631, 1072 cm⁻¹.

HRMS (MM: FD+): *m/z* calc'd for $C_{18}H_{21}O_2F$ [M]⁺: 289.1604, found 289.1597.

Optical Rotation: $[\alpha]_D^{21}$ –5.3 (c 0.30, CHCl₃).

SFC conditions: 10% IPA, 2.5 mL/min, Chiralpak OJ-H column, λ = 210 nm, t_R (min):

minor = 6.68, major = 5.86.
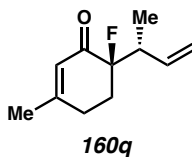
160q

(*R*)-3-ethoxy-6-fluoro-6-((*S*)-1-phenylallyl)cyclohex-2-en-1-one (160q)

Prepared from **158q** (23.3 mg, 103 μmol) following General Procedure A using

Pd₂(pmdba)₃ and **L3**. Purification by flash column chromatography (5–20% Et₂O/hexanes)

afforded the title compound as a colorless oil (14.7 mg, 80.8 μmol, 78% yield, >20:1 dr,

87% ee). For further characterization, the mixture of isomers was subsequently purified by

C18 reverse-phase preparatory HPLC (40–65% MeCN/H₂O) to afford the major

diastereomer of **160q** as a single isomer.

Compound **160q was found to be volatile, avoid excessive exposure to high vacuum.*

Yields are corrected for trace Et₂O in sample after purification.*

¹H NMR (400 MHz, CDCl₃): δ 5.93 – 5.83 (m, 2H), 5.10 – 5.01 (m, 2H), 2.91 – 2.74 (m,

1H), 2.47 (dt, *J* = 18.9, 5.6 Hz, 1H), 2.36 (dt, *J* = 19.0, 6.5 Hz, 1H), 2.29 – 2.18 (m, 2H),

1.97 (s, 3H), 1.09 (d, *J* = 7.0 Hz, 3H).

^{13}C NMR (100 MHz, CDCl$_3$): 194.3 (d, J_{C-F} = 18.0 Hz), 162.0, 137.5, 125.4, 116.5, 95.8

(d, J_{C-F} = 184.7 Hz), 40.29 (d, J_{C-F} = 21.9 Hz), 30.5, 29.8, 29.5, 29.3, 29.2, 29.1, 14.2 (d,

J_{C-F} = 5.7 Hz).

^{19}F NMR (282 MHz, CDCl$_3$): δ –168.13– –168.31 (m, 1F).

IR (Neat Film, NaCl): 2919, 2849, 1681, 1633, 1434, 1380, 1225 cm^{-1}.

HRMS (MM: FI+): *m/z* calc'd for C$_{11}$H$_{15}$OF [M]$^+$: 182.1107, found 182.1107.

Optical Rotation: [α]$_D^{21}$ –32.3 (c 0.40, CHCl$_3$).

SFC conditions: 10% IPA, 2.5 mL/min, Chiralpak IC column, λ = 254 nm, t$_R$ (min): minor

= 4.76, major = 5.45.

Synthesis of β-ketoester substrates (158a–158q)

General Procedure B: Alkylation of β-ketoesters.

165a–xx   *158a–q*
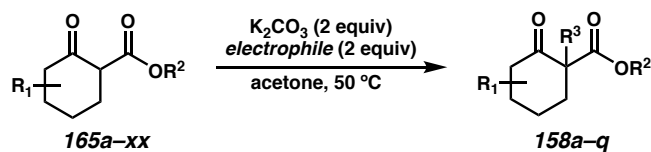
     To a solution of β-ketoester **165** (1 equiv) in acetone (0.5 M) is added anhydrous

K$_2$CO$_3$ (2 equiv), followed by the relevant electrophile (2 equiv). The reaction is heated to

50 ºC and stirring is continued until complete consumption of starting material is observed

(typically 24–36 h). The reaction mixture is then filtered, and volatiles are removed in

vacuo. Purification by flash silica gel column chromatography affords the desired alkylated

β-ketoester.
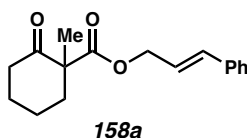
158a

cinnamyl 1-methyl-2-oxocyclohexane-1-carboxylate (158a)

Prepared from cinnamyl 2-oxocyclohexane-1-carboxylate and methyl iodide following

General Procedure B. Purification by flash column chromatography (5–40%

EtOAc/hexanes) afforded the title compound as a colorless oil (0.458 g, 1.39 mmol, 84%

yield).

^{1}H NMR (600 MHz, CDCl$_3$): δ 7.45 – 7.36 (m, 2H), 7.36 – 7.30 (m, 2H), 7.30 – 7.22 (m,

1H), 6.65 (d, J = 15.9 Hz, 1H), 6.26 (dt, J = 15.9, 6.5 Hz, 1H), 4.81 (ddd, J = 12.8, 6.4, 1.2

Hz, 1H), 4.77 (ddd, J = 12.8, 6.4, 1.2 Hz, 1H), 2.57 – 2.52 (m, 1H), 2.51 – 2.43 (m, 2H),

2.06 – 1.98 (m, 1H), 1.79 – 1.61 (m, 3H), 1.53 – 1.44 (m, 1H), 1.33 (s, 3H).

^{13}C NMR (101 MHz, CDCl$_3$): δ 208.3, 173.0, 136.2, 135.0, 128.8, 128.4, 126.8, 126.6,

65.9, 57.4, 40.8, 38.4, 27.6, 22.8, 21.4.

IR (Neat Film, NaCl): 2938, 1714, 1453 (m), 1142 (m), 961 (m) cm^{-1}.

HRMS (MM: FD+): *m/z* calc'd for C$_{17}$H$_{20}$O$_3$ [M]$^+$: 272.1412, found 272.1410.
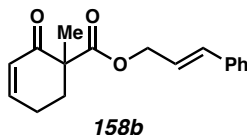
cinnamyl 1-methyl-2-oxocyclohex-3-ene-1-carboxylate (158b)

Prepared from cinnamyl 2-oxocyclohex-3-ene-1-carboxylate (prepared following General

Procedure D and used crude) and methyl iodide following General Procedure B.

Purification by flash column chromatography (5–40% EtOAc/hexanes) afforded the title

compound as a colorless oil (0.48 g, 1.78 mmol, 23% yield).

^{1}H NMR (400 MHz, CDCl$_3$): δ 7.40 – 7.27 (m, 5H), 6.92 (dddd, J = 10.1, 4.4, 3.3, 1.0 Hz,

1H), 6.62 (d, J = 15.9 Hz, 1H), 6.23 (dt, J = 15.9, 6.3 Hz, 1H), 6.07 (ddd, J = 10.1, 2.4, 1.7

Hz, 1H), 4.83 – 4.70 (m, 2H), 2.57 – 2.43 (m, 2H), 2.40 – 2.30 (m, 1H), 1.92 (ddd, J = 14.6,

8.9, 5.2 Hz, 1H), 1.42 (s, 3H).

¹³C NMR (100 MHz, CDCl₃): δ 197.0, 172.6, 149.6, 136.3, 134.5, 129.0, 128.8, 128.3,

126.8, 122.8, 65.9, 53.6, 33.5, 23.8, 20.8.

IR (Neat Film, NaCl): 3025, 1731, 1681, 1250, 1096 cm⁻¹.

HRMS (MM: FD+): *m/z* calc'd for $C_{17}H_{18}O_3$ [M]⁺: 270.1256, found 270.1259.
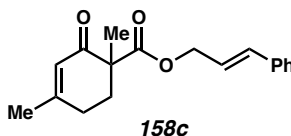
cinnamyl 1,4-dimethyl-2-oxocyclohex-3-ene-1-carboxylate (158c)

Prepared from **165a** and methyl iodide following General Procedure B. Purification by

flash column chromatography (15% EtOAc/hexanes) afforded the title compound as a

colorless oil (0.65 g, 2.1 mmol, 63% yield).

¹H NMR (600 MHz, CDCl₃): δ 7.37 (d, J = 7.5 Hz, 2H), 7.31 (d, J = 7.4 Hz, 2H), 7.28 –

7.23 (m, 1H), 6.61 (d, J = 15.8 Hz, 1H), 6.23 (dt, J = 15.8, 6.4 Hz, 1H), 5.92 (s, 1H), 4.81

– 4.70 (m, 2H), 2.51 (dt, J = 13.3, 4.8 Hz, 1H), 2.48 – 2.39 (m, 1H), 2.25 (dt, J = 19.0, 5.3

Hz, 1H), 1.94 (s, 3H), 1.92 – 1.86 (m, 1H), 1.41 (s, 3H).

¹³C NMR (101 MHz, CDCl₃): δ 196.7, 172.8, 161.7, 136.3, 134.3, 128.7, 128.2, 126.8,

125.7, 122.9, 65.8, 52.5, 33.3, 28.7, 24.3, 20.5.

IR (Neat Film, NaCl): 3026, 2935, 1731, 1668, 1448, 1253 cm⁻¹.

HRMS (MM: ESI+): *m/z* calc'd for $C_{18}H_{23}O_3Na$ [M+Na]⁺: 307.1305, found 307.1308.
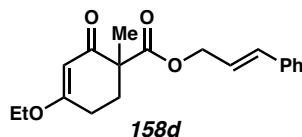
158d

cinnamyl 4-ethoxy-1-methyl-2-oxocyclohex-3-ene-1-carboxylate (158d)

Prepared from **165b** and methyl iodide following General Procedure B. Purification by flash column chromatography (10–50% EtOAc/hexanes) afforded the title compound as a colorless oil (0.65 g, 2.1 mmol, 63% yield).

^{1}H NMR (400 MHz, CDCl$_3$): δ 7.38 – 7.25 (m, 5H), 6.62 (d, J = 15.9 Hz, 1H), 6.24 (dt, J = 15.9, 6.3 Hz, 1H), 5.37 (s, 1H), 4.82 – 4.72 (m, 2H), 3.90 (q, J = 7.0 Hz, 2H), 2.61 – 2.47 (m, 2H), 2.38 (dt, J = 17.1, 5.3 Hz, 1H), 1.88 (ddd, J = 13.7, 8.5, 5.2 Hz, 1H), 1.43 (s, 3H), 1.34 (t, J = 7.0 Hz, 3H).

^{13}C NMR (100 MHz, CDCl$_3$): δ 196.9, 176.7, 172.9, 136.3, 134.3, 128.7, 128.2, 126.8, 123.0, 101.9, 65.8, 64.6, 52.6, 31.9, 26.6, 20.7, 14.2.

IR (Neat Film, NaCl): 2980, 2942, 1731, 1656, 1606, 1377, 1250, 1195 cm^{-1}.

HRMS (MM: FD+): *m/z* calc'd for C$_{19}$H$_{22}$O$_4$ [M]$^+$: 314.1518, found 314.1516.
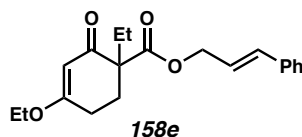
158e

cinnamyl 4-ethoxy-1-ethyl-2-oxocyclohex-3-ene-1-carboxylate (158e)

Prepared from **165b** and ethyl iodide following General Procedure B. Purification by flash column chromatography (5–40% EtOAc/hexanes) afforded the title compound as a colorless oil (0.458 g, 1.39 mmol, 84% yield).

¹H NMR (400 MHz, CDCl₃): δ 7.38 – 7.35 (m, 2H), 7.33 – 7.29 (m, 2H), 7.27 – 7.23 (m, 1H), 6.62 (d, *J* = 15.9 Hz, 1H), 6.24 (dt, *J* = 15.8, 6.3 Hz, 1H), 5.36 (s, 1H), 4.77 (dd, *J* = 6.3, 1.4 Hz, 2H), 3.93 – 3.84 (m, 2H), 2.64 (dddd, *J* = 17.9, 9.8, 5.0, 1.2 Hz, 1H), 2.45 (dt, *J* = 13.3, 5.0 Hz, 1H), 2.36 (dt, *J* = 17.9, 5.0 Hz, 1H), 2.13 – 2.01 (m, 1H), 1.93 (ddd, *J* = 13.3, 9.6, 5.2 Hz, 1H), 1.83 (dq, *J* = 13.9, 7.5 Hz, 1H), 1.33 (t, *J* = 7.0 Hz, 3H), 0.92 (t, *J* = 7.5 Hz, 3H).

¹³C NMR (100 MHz, CDCl₃): δ 196.0, 176.7, 171.8, 136.4, 134.3, 128.7, 128.2, 126.8, 123.1, 102.3, 65.7, 64.5, 56.5, 27.9, 27.1, 26.6, 14.2, 9.2.

IR (Neat Film, NaCl): 3025, 2979, 2938, 1728, 1659, 1603, 1446, 1378, 1235, 1186 cm⁻¹.

HRMS (MM: ESI+): *m/z* calc'd for C₂₀H₂₅O₄ [M+H]⁺: 329.1747, found 329.1747.
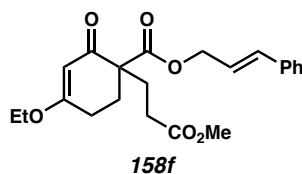
158f

cinnamyl 4-ethoxy-1-(3-methoxy-3-oxopropyl)-2-oxocyclohex-3-ene-1-carboxylate (158f)

Prepared from **165b** and methyl acrylate following General Procedure B. Purification by flash column chromatography (5–30% EtOAc/hexanes) afforded the title compound as a colorless oil (0.48 g, 1.24 mmol, 75% yield).

¹H NMR (400 MHz, CDCl₃): δ 7.39 – 7.35 (m, 2H), 7.34 – 7.29 (m, 2H), 7.28 – 7.23 (m, 1H), 6.62 (d, *J* = 15.9 Hz, 1H), 6.23 (dt, *J* = 15.9, 6.3 Hz, 1H), 5.36 (s, 1H), 4.82 – 4.72 (m, 2H), 3.88 (qd, *J* = 7.1, 2.0 Hz, 2H), 3.65 (s, 3H), 2.64 – 2.53 (m, 1H), 2.49 – 2.36 (m, 4H),

2.33 – 2.25 (m, 1H), 2.13 (ddd, J = 13.9, 10.0, 6.1 Hz, 1H), 1.95 – 1.87 (m, 1H), 1.34 (t, J

= 7.0 Hz, 3H).

¹³C NMR (100 MHz, CDCl₃): δ 195.4, 176.6, 173.7, 171.5, 136.3, 134.6, 128.7, 128.2,

126.8, 122.8, 102.2, 66.0, 64.7, 55.4, 51.8, 29.8, 29.0, 28.9, 26.4, 14.2.

IR (Neat Film, NaCl): 2946, 1737, 1731, 1659, 1651, 1606, 1246, 1192 cm⁻¹.

HRMS (MM: ESI+): *m/z* calc'd for $C_{22}H_{27}O_6$ [M+H]⁺: 387.1802, found 387.1806.
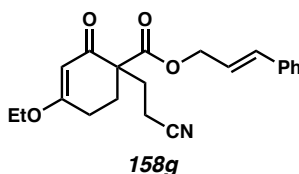
158g

cinnamyl 1-(2-cyanoethyl)-4-ethoxy-2-oxocyclohex-3-ene-1-carboxylate (158g)

Prepared from **165b** and acrylonitrile following General Procedure B. Purification by flash

column chromatography (5–30% EtOAc/hexanes) afforded the title compound as a

colorless oil (349 mg, 0.987 mmol, 59% yield).

¹H NMR (400 MHz, CDCl₃): δ 7.40 – 7.27 (m, 5H), 6.64 (d, J = 15.9 Hz, 1H), 6.23 (dt, J

= 15.9, 6.5 Hz, 1H), 5.38 (s, 1H), 4.85 – 4.74 (m, 2H), 3.96 – 3.86 (m, 2H), 2.65 – 2.39 (m,

5H), 2.31 – 2.13 (m, 2H), 2.01 – 1.94 (m, 1H), 1.35 (t, J = 7.0 Hz, 3H).

¹³C NMR (100 MHz, CDCl₃): δ 194.8, 176.9, 171.0, 136.1, 135.2, 128.8, 128.4, 126.8,

122.3, 119.8, 102.2, 66.4, 64.9, 55.1, 30.0, 29.4, 26.4, 14.2, 13.4.

IR (Neat Film, NaCl): 2981, 2939, 1730, 1651, 1605, 1381, 1186 cm⁻¹.

HRMS (MM: EI+): *m/z* calc'd for $C_{21}H_{23}O_4N$ [M]⁺: 353.1629, found 353.1627.
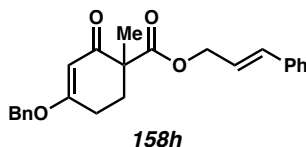
158h

cinnamyl 4-(benzyloxy)-1-methyl-2-oxocyclohex-3-ene-1-carboxylate (158h)

Prepared from **165c** and methyl iodide following General Procedure B. Purification by flash column chromatography (5–30% EtOAc/hexanes) afforded the title compound as a colorless oil (179 mg, 0.475 mmol, 57% yield).

^{1}H NMR (400 MHz, CDCl$_3$): δ 7.41 – 7.26 (m, 10H), 6.63 (d, J = 15.9 Hz, 1H), 6.25 (dt, J = 15.9, 6.3 Hz, 1H), 5.52 (s, 1H), 4.89 (s, 2H), 4.83 – 4.72 (m, 2H), 2.65 (dddd, J = 17.6, 9.8, 4.5, 1.1 Hz, 1H), 2.56 – 2.41 (m, 2H), 1.92 (ddd, J = 12.8, 8.8, 4.7 Hz, 1H), 1.44 (s, 3H).

^{13}C NMR (100 MHz, CDCl$_3$): δ 196.7, 176.4, 172.8, 136.3, 135.0, 134.4, 128.9, 128.8, 128.7, 128.2, 128.0, 126.8, 123.0, 102.5, 70.8, 65.9, 52.6, 31.9, 26.6, 20.7.

IR (Neat Film, NaCl): 3027, 2935, 1730, 1659, 1607, 1251, 1189, 1170 cm^{-1}.

HRMS (MM: ESI+): *m/z* calc'd for C$_{24}$H$_{24}$O$_4$ [M]$^+$: 376.1675, found 376.1665.
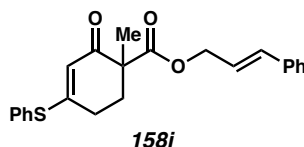
cinnamyl 1-methyl-2-oxo-4-(phenylthio)cyclohex-3-ene-1-carboxylate (158i)

Prepared from **165d** and methyl iodide following General Procedure B. Purification by flash column chromatography (5–30% EtOAc/hexanes) afforded the title compound as a colorless oil (232 mg, 0.853 mmol, 62% yield).

^{1}H NMR (400 MHz, CDCl$_3$): δ 7.46 – 7.27 (m, 10H), 6.62 (d, J = 15.9 Hz, 1H), 6.24 (dt, J = 15.9, 6.3 Hz, 1H), 5.52 (s, 1H), 4.81 (dd, J = 12.9, 6.3 Hz, 1H), 4.73 (dd, J = 13.0, 6.3 Hz, 1H), 2.73 – 2.64 (m, 1H), 2.59 – 2.46 (m, 2H), 2.01 – 1.93 (m, 1H), 1.41 (s, 3H).

^{13}C NMR (100 MHz, CDCl$_3$): δ 193.3, 172.5, 165.9, 136.2, 135.5, 134.3, 130.3, 129.9,

128.6, 128.1, 127.8, 126.7, 122.7, 119.9, 65.8, 52.8, 33.6, 27.6, 20.4.

IR (Neat Film, NaCl): 2934, 1729, 1655, 1577, 1303, 1250, 1167, 1108 cm^{-1}.

HRMS (MM: FD+): *m/z* calc'd for C$_{23}$H$_{22}$O$_3$S [M]$^+$: 378.1290, found 378.1293.

158j
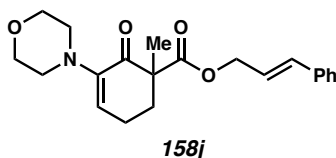
cinnamyl 1-methyl-3-morpholino-2-oxocyclohex-3-ene-1-carboxylate (158i)

Prepared from **165e** and methyl iodide following General Procedure B. Purification by

flash column chromatography (15–50% EtOAc/hexanes) afforded the title compound as a

colorless oil (0.43 g, 1.24 mmol, 81% yield).

^{1}H NMR (400 MHz, C$_6$D$_6$): δ 7.14 – 7.10 (m, 2H), 7.09 – 6.99 (m, 3H), 6.36 (d, *J* = 15.9

Hz, 1H), 6.00 (dt, *J* = 15.9, 6.4 Hz, 1H), 5.17 (ddd, *J* = 4.9, 3.5, 1.0 Hz, 1H), 4.56 (ddd, *J*

= 12.9, 6.5, 1.4 Hz, 1H), 4.50 (ddd, *J* = 12.8, 6.3, 1.4 Hz, 1H), 3.67 (ddd, *J* = 11.2, 6.4, 3.0

Hz, 1H), 3.58 (ddd, *J* = 11.2, 6.4, 2.9 Hz, 1H), 2.91 (ddd, *J* = 11.5, 6.3, 2.9 Hz, 1H), 2.47

– 2.30 (m, 4H), 1.92 – 1.81 (m, 1H), 1.53 – 1.46 (m, 1H), 1.45 (s, 3H).

^{13}C NMR (100 MHz, C$_6$D$_6$): δ 192.8, 172.4, 146.9, 136.5, 134.7, 128.9, 128.6, 126.9,

123.0, 121.8, 66.9, 65.6, 54.4, 50.2, 33.3, 22.7, 20.9.

IR (Neat Film, NaCl): 2936, 2856, 1736, 1730, 1692, 1613, 1448 cm^{-1}.

HRMS (MM: ESI+): *m/z* calc'd for C$_{21}$H$_{26}$O$_4$N [M+H]$^+$: 356.1856, found 356.1867.
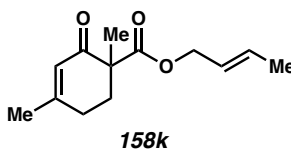
158k

(*E*)-but-2-en-1-yl 1,4-dimethyl-2-oxocyclohex-3-ene-1-carboxylate (158k)

Prepared from **165g** and methyl iodide following General Procedure B. Purification by flash column chromatography (5–25% EtOAc/hexanes) afforded the title compound as a colorless oil (0.29 g, 1.30 mmol, 55% yield).

^{1}H NMR (400 MHz, CDCl$_3$): δ 5.89 (s, 1H), 5.74 (dqt, *J* = 15.3, 6.5, 1.2 Hz, 1H), 5.57 – 5.47 (m, 1H), 4.56 – 4.47 (m, 2H), 2.51 – 2.37 (m, 2H), 2.28 – 2.19 (m, 1H), 1.94 (s, 3H), 1.90 – 1.82 (m, 1H), 1.70 (d, *J* = 6.5 Hz, 3H), 1.37 (s, 3H).

^{13}C NMR (100 MHz, CDCl$_3$): δ 196.9, 172.8, 161.6, 131.4, 125.8, 124.8, 65.9, 52.4, 33.3, 28.7, 24.3, 20.4, 17.9.

IR (Neat Film, NaCl): 3027, 2938, 2917, 1730, 1679, 1636, 1440, 1250 cm^{-1}.

HRMS (MM: ESI+): *m/z* calc'd for C$_{13}$H$_{18}$O$_3$Na [M+Na]$^+$: 245.1148, found 245.1159.
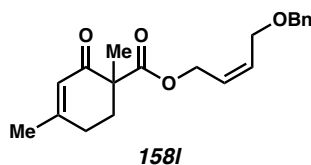
158l

(Z)-**4-(benzyloxy)but-2-en-1-yl 1,4-dimethyl-2-oxocyclohex-3-ene-1-carboxylate**

(158l)

Prepared from **165f** and methyl iodide following General Procedure B. Purification by flash column chromatography (20% EtOAc/hexanes) afforded the title compound as a colorless oil (361 mg, 1.1 mmol, 73% yield).

^{1}H NMR (500 MHz, CDCl$_3$): δ 7.39 – 7.31 (m, 1H), 7.31 – 7.26 (m, 1H), 5.88 (q, *J* = 1.5 Hz, 1H), 5.80 (dtt, *J* = 11.2, 6.2, 1.4 Hz, 1H), 5.70 – 5.59 (m, 1H), 4.72 – 4.59 (m, 2H), 4.11 (ddd, *J* = 6.3, 1.6, 0.8 Hz, 1H), 2.47 (dt, *J* = 13.2, 5.1 Hz, 1H), 2.43 – 2.35 (m, 1H),

2.24 (dt, J = 18.9, 5.2 Hz, 1H), 1.94 (d, J = 1.4 Hz, 1H), 1.87 (ddd, J = 13.2, 8.3, 5.1 Hz,

1H), 1.37 (s, 3H).

¹³C NMR (101 MHz, CDCl₃): δ 196.6, 172.7, 161.6, 138.1, 131.2, 128.6, 127.9, 127.8,

126.4, 125.6, 72.6, 65.8, 61.1, 52.4, 33.2, 28.7, 24.3, 20.3.

IR (Neat Film, NaCl): 3031 (m), 2933 (m), 1731 (s), 1681 (s), 1454 (m), 1214 (m) cm⁻¹.

HRMS (MM: ESI+): *m/z* calc'd for $C_{20}H_{24}O_4Na$ [M+Na]⁺: 351.1567, found 351.1565.
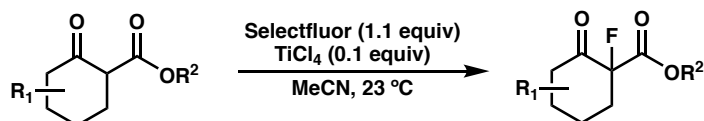
General Procedure C: Fluorination of β-ketoesters.

      To a solution of β-ketoester (1 equiv) in anhydrous acetonitrile (0.2 M) at 23 ºC is

added neat titanium(IV) chloride (0.1 equiv). After 5 minutes, Selectfluor® was added in

one portion. The reaction mixture is stirred at 23 ºC until complete consumption of starting

material as observed by TLC (typically 2 hours). Water is then added, and the reaction

mixture is extracted three times with Et₂O. The combined organic layers was washed with

saturated aqueous brine, dried over anhydrous sodium sulfate, and volatiles were removed

in vacuo. The crude reaction mixture was purified by silica gel flash column

chromatography to yield the desired α-fluoro-β-ketoester.
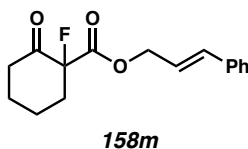
158m

cinnamyl 1-fluoro-2-oxocyclohexane-1-carboxylate (158m)

Prepared from cinnamyl 2-oxocyclohexane-1-carboxylate following General Procedure C. Purification by flash column chromatography (5–40% EtOAc/hexanes) afforded the title compound as a colorless oil (0.80 g, 2.9 mmol, 75% yield).

¹H NMR (400 MHz, CDCl₃): δ 7.40 (d, *J* = 7.3 Hz, 2H), 7.37 – 7.29 (m, 2H), 7.29 – 7.26 (m, 1H), 6.70 (d, *J* = 15.9 Hz, 1H), 6.29 (dt, *J* = 15.9, 6.6 Hz, 1H), 4.89 (d, *J* = 6.5 Hz, 2H), 2.81 – 2.69 (m, 1H), 2.67 – 2.56 (m, 1H), 2.57 – 2.40 (m, 1H), 2.25 – 2.11 (m, 1H), 1.99 – 1.82 (m, 4H).

¹³C NMR (100 MHz, CDCl₃): δ 201.9 (d, $J_{C–F}$ = 20.0 Hz), 166.9 (d, $J_{C–F}$ = 24.9 Hz), 136.0, 135.6, 128.8, 128.5, 126.9, 121.9, 96.6 (d, $J_{C–F}$ = 197.2 Hz), 66.9, 39.7, 36.2 (d, $J_{C–F}$ = 21.7 Hz), 26.7, 21.0 (d, $J_{C–F}$ = 5.7 Hz).

¹⁹F NMR (282 MHz, CDCl₃): δ –160.82 (ddd, *J* = 21.5, 13.5, 5.1 Hz, 1F).

IR (Neat Film, NaCl): 2943, 1731, 1457, 1281 cm⁻¹

HRMS (MM: FD+): *m/z* calc'd for C₁₆H₁₇O₃F [M]⁺: 276.1162, found 276.1165.
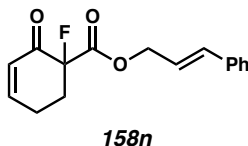
158n

cinnamyl 1-fluoro-2-oxocyclohex-3-ene-1-carboxylate (158n)

Prepared from cinnamyl 2-oxocyclohex-3-ene-1-carboxylate (prepared following General Procedure D and used crude) following General Procedure C. Purification by flash column chromatography (0–20% EtOAc/hexanes) afforded the title compound as a colorless oil (0.54 g, 2.0 mmol, 50% yield).

¹H NMR (400 MHz, CDCl₃): δ 7.41 – 7.37 (m, 2H), 7.35 – 7.30 (m, 2H), 7.30 – 7.26 (m, 1H), 7.10 (dt, *J* = 10.2, 4.0 Hz, 1H), 6.69 (d, *J* = 15.9 Hz, 1H), 6.27 (dt, *J* = 15.8, 6.5 Hz,

1H), 6.18 (dq, *J* = 10.2, 2.0 Hz, 1H), 4.94 – 4.84 (m, 2H), 2.72 – 2.58 (m, 3H), 2.48 – 2.39 (m, 1H).

¹³C NMR (100 MHz, CDCl₃): δ 188.9 (d, *J* = 18.7 Hz), 167.0 (d, *J* = 25.9 Hz), 151.9, 135.9, 135.4, 128.7, 128.4, 127.7, 126.8, 121.8, 92.9 (d, *J* = 194.8 Hz), 66.8, 31.3 (d, *J* = 22.5 Hz), 23.3 (d, *J* = 7.2 Hz).

¹⁹F NMR (282 MHz, CDCl₃): δ –164.30 (dd, *J* = 22.8, 12.5 Hz).

IR (Neat Film, NaCl): 3027, 2940, 1759, 1693, 1265 cm⁻¹.

HRMS (MM: FD+): *m/z* calc'd for $C_{16}H_{15}O_3F$ [M]⁺: 274.1005, found 274.1004.

1580
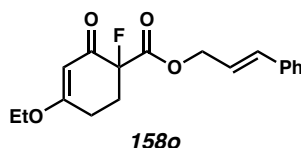
cinnamyl 4-ethoxy-1-fluoro-2-oxocyclohex-3-ene-1-carboxylate (158o)

Prepared from **165b** following General Procedure C. Purification by flash column chromatography (0–25% EtOAc/hexanes) afforded the title compound as a colorless oil (0.16 g, 0.50 mmol, 31% yield).

¹H NMR (400 MHz, CDCl₃): δ 7.42 – 7.35 (m, 2H), 7.36 – 7.27 (m, 2H), 7.31 – 7.22 (m, 2H), 6.68 (d, *J* = 15.9 Hz, 1H), 6.28 (dd, *J* = 16.0, 6.2 Hz, 1H), 5.46 (s, 1H), 4.94 – 4.85 (m, 2H), 3.97 (q, *J* = 7.1 Hz, 2H), 2.72 – 2.53 (m, 3H), 2.44 – 2.33 (m, 1H), 1.38 (t, *J* = 7.0 Hz, 3H).

¹³C NMR (100 MHz, CDCl₃): δ 188.6 (d, $J_{C–F}$ = 18.9 Hz), 178.2, 167.7 (d, $J_{C–F}$ = 26.0 Hz), 136.1, 135.3, 128.7, 128.4, 126.9, 122.0, 101.0, 92.3 (d, $J_{C–F}$ = 193.6 Hz), 66.8, 65.3, 29.7 (d, $J_{C–F}$ = 23.0 Hz), 25.7 (d, $J_{C–F}$ = 6.0 Hz), 14.2.

¹⁹F NMR (282 MHz, CDCl₃): δ –163.76 – –163.93 (m).

IR (Neat Film, NaCl): 2983, 2943, 1765, 1666, 1599, 1382, 1264 cm^{-1}

HRMS (MM: ESI+): *m/z* calc'd for $C_{18}H_{19}O_4FNa$ [M+Na]$^+$: 341.1148, found 341.1158.
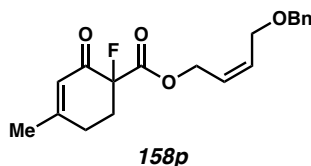
158p

(*Z*)-4-(benzyloxy)but-2-en-1-yl 1-fluoro-4-methyl-2-oxocyclohex-3-ene-1-carboxylate

(158p)

Prepared from **165f** following General Procedure C. Purification by flash column chromatography (10–60% EtOAc/hexanes) afforded the title compound as a colorless oil (0.39 g, 1.2 mmol, 75% yield).

^{1}H NMR (400 MHz, CDCl$_3$): δ 7.38 – 7.27 (m, 5H), 6.00 (s, 1H), 5.89 – 5.82 (m, 1H), 5.73 – 5.66 (m, 1H), 4.79 (d, *J* = 6.7 Hz, 2H), 4.51 (s, 2H), 4.13 (d, *J* = 6.2 Hz, 2H), 2.63 – 2.33 (m, 4H), 2.03 (s, 3H).

^{13}C NMR (100 MHz, CDCl$_3$): δ 188.5 (d, J_{C-F} = 18.6 Hz), 167.4 (d, J_{C-F} = 25.8 Hz), 164.6, 138.1, 132.1, 128.6, 128.0, 127.9, 125.6, 124.7, 92.2 (d, J_{C-F} = 194.0 Hz), 72.7, 65.8, 62.0, 31.1 (d, J_{C-F} = 22.5 Hz), 28.0 (d, J_{C-F} = 6.5 Hz), 24.7.

^{19}F NMR (282 MHz, CDCl$_3$): δ –165.21 (dd, *J* = 26.4, 12.0 Hz).

IR (Neat Film, NaCl): 2914, 1764, 1681, 1627, 1264, 1088 cm^{-1}

HRMS (MM: ESI+): *m/z* calc'd for $C_{19}H_{22}O_4F$ [M+H]$^+$: 333.1502, found 333.1491.
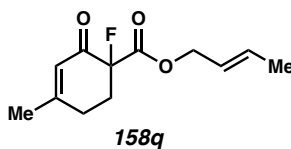
158q

(*E*)-but-2-en-1-yl 1-fluoro-4-methyl-2-oxocyclohex-3-ene-1-carboxylate (158q)

Prepared from **165g** following General Procedure C. Purification by flash column

chromatography (10–60% EtOAc/hexanes) afforded the title compound as a colorless oil

(326 mg, 1.44 mmol, 60% yield).

^{1}H NMR (400 MHz, CDCl$_3$): δ 6.00 (s, 1H), 5.87 – 5.77 (m, 1H), 5.58 (dtq, J = 15.0, 6.7,

1.7 Hz, 1H), 4.64 (ddt, J = 6.7, 2.5, 1.2 Hz, 2H), 2.65 – 2.49 (m, 3H), 2.43 – 2.33 (m, 1H),

2.03 (s, 3H), 1.72 (d, J = 6.5 Hz, 3H).

^{13}C NMR (100 MHz, CDCl$_3$): δ 188.7 (d, J_{C-F} = 18.6 Hz), 167.4 (d, J_{C-F} = 25.7 Hz), 164.5,

132.8, 124.7, 124.1, 92.3 (d, J_{C-F} = 194.1 Hz), 67.0, 31.2 (d, J_{C-F} = 22.5 Hz), 28.2 (d, J_{C-F}

= 6.8 Hz), 24.6, 18.0.

^{19}F NMR (282 MHz, CDCl$_3$): δ –165.04 (d, J = 22.2 Hz).

IR (Neat Film, NaCl): 3029, 2940, 1760, 1681, 1631, 1436, 1271, 1263, 1019 cm^{-1}.

HRMS (MM: ESI+): *m/z* calc'd for C$_{12}$H$_{15}$O$_3$FNa [M+Na]$^+$: 249.0897, found 249.0901.
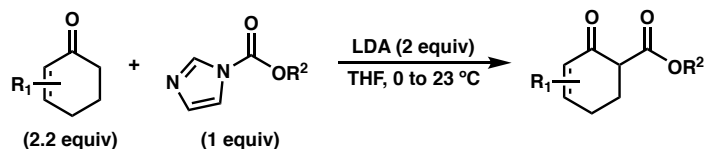
General Procedure D: β-ketoester synthesis through ketone acylation.

A flame dried round bottom flask was charged with iPr$_2$NH (2.2 equiv) and THF (1.75 M).

The solution was cooled to 0 ºC and *n*-BuLi (2.5 M in hexanes, 2.1 equiv) was added

dropwise. The resultant solution was stirred for 30 min at 0 ºC. The corresponding

cyclohexenone (2.0 equiv) in THF (1.25 M) was added dropwise and stirring was continued

at 0 ºC for 30 minutes. The solution was cooled to –78 ºC, and the appropriate N-acyl

imidazole (1.0 equiv) in THF (3.25 M) was added dropwise. After 2 h, the reaction was

gradually warmed to 23 ºC and diluted with 2 M aqueous HCl until reaching a pH < 7. The

reaction mixture was extracted three times with EtOAc. The combined organic layers were

washed with brine, dried over Na$_2$SO$_4$, filtered, and concentrated under reduced pressure.

The crude product was purified by flash silica gel column chromatography to afford the

corresponding acylated enone.
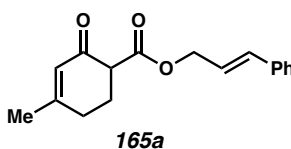
165a

cinnamyl 4-methyl-2-oxocyclohex-3-ene-1-carboxylate (165a)

Prepared from 3-methylcyclohex-2-en-1-one and cinnamyl 1*H*-imidazole-1-carboxylate

following General Procedure D. Purification by flash column chromatography (20%

EtOAc/hexanes) afforded the title compound as a colorless oil (5.5 g, 20.3 mmol, 51%

yield).

^{1}H NMR (600 MHz, CDCl$_3$): δ 7.42 – 7.36 (m, 2H), 7.32 (t, *J* = 7.6 Hz, 2H), 7.29 – 7.19

(m, 1H), 6.67 (d, *J* = 15.8 Hz, 1H), 6.28 (dt, *J* = 15.8, 6.4 Hz, 1H), 5.94 (d, *J* = 1.5 Hz, 1H),

4.82 (d, *J* = 6.4 Hz, 2H), 3.46 – 3.28 (m, 1H), 2.49 – 2.25 (m, 4H), 2.25 – 2.17 (m, 1H),

1.97 (d, *J* = 1.2 Hz, 3H).

^{13}C NMR (101 MHz, CDCl$_3$): δ 193.7, 170.2, 163.1, 136.3, 134.5, 128.7, 128.2, 126.8,

126.0, 123.0, 65.8, 52.7, 29.6, 25.6, 24.5.

IR (Neat Film, NaCl): 3026, 2935, 1737, 1666, 1445, 970 cm^{-1}.

HRMS (MM: ESI+): *m/z* calc'd for C$_{17}$H$_{18}$O$_3$Na [M+Na]$^+$: 293.1148, found 293.1152.
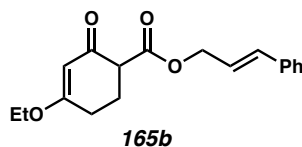
165b

cinnamyl 4-ethoxy-2-oxocyclohex-3-ene-1-carboxylate (165b)

Prepared from 3-ethoxycyclohex-2-en-1-one following General Procedure D. Purification by flash column chromatography (10–60% EtOAc/hexanes) afforded the title compound as a colorless oil (2.13 g, 7.09 mmol, 35% yield).

^{1}H NMR (400 MHz, CDCl₃): δ 7.41 – 7.37 (m, 2H), 7.32 (tt, J = 6.5, 1.0 Hz, 2H), 7.28 – 7.23 (m, 1H), 6.67 (d, J = 15.9 Hz, 1H), 6.29 (dt, J = 15.9, 6.4 Hz, 1H), 5.40 (s, 1H), 4.82 (dd, J = 6.4, 1.4 Hz, 2H), 3.96 – 3.88 (m, 2H), 3.41 – 3.36 (m, 1H), 2.62 – 2.52 (m, 1H), 2.48 – 2.33 (m, 2H), 2.25 – 2.15 (m, 2H), 1.37 (t, J = 7.0 Hz, 3H).

^{13}C NMR (100 MHz, CDCl₃): δ 193.6, 177.6, 170.2, 136.2, 134.3, 128.6, 128.1, 126.7, 122.9, 102.1, 65.8, 64.6, 52.4, 27.4, 24.2, 14.1.

IR (Neat Film, NaCl): 2980, 2942, 1736, 1654, 1602, 1380, 1192 cm^{-1}.

HRMS (MM: FD+): *m/z* calc'd for $C_{18}H_{20}O_4$ [M]$^+$: 300.1362, found 300.1353.
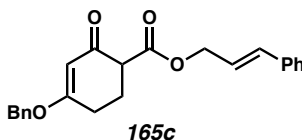
165c

cinnamyl 4-(benzyloxy)-2-oxocyclohex-3-ene-1-carboxylate (165c)

Prepared from 3-(benzyloxy)cyclohex-2-en-1-one following General Procedure D. Purification by flash column chromatography (10–60% EtOAc/hexanes) afforded the title compound as a colorless oil (0.79 g, 2.2 mmol, 22% yield).

^{1}H NMR (400 MHz, CDCl$_3$): δ 7.42 – 7.27 (m, 10H), 6.68 (d, *J* = 15.9 Hz, 1H), 6.29 (dt,

J = 15.9, 6.4 Hz, 1H), 5.54 (s, 1H), 4.91 (d, *J* = 2.5 Hz, 2H), 4.83 (dd, *J* = 6.4, 1.3 Hz, 2H),

3.41 (dd, *J* = 9.0, 5.0 Hz, 1H), 2.65 (ddd, *J* = 17.5, 6.4, 5.0 Hz, 1H), 2.56 – 2.46 (m, 1H),

2.41 (dtd, *J* = 13.7, 8.7, 5.0 Hz, 1H), 2.23 (ddt, *J* = 13.5, 6.6, 5.0 Hz, 1H).

^{13}C NMR (100 MHz, CDCl$_3$): δ 193.6, 177.3, 170.1, 136.2, 134.7, 134.4, 128.8, 128.7,

128.6, 128.1, 127.9, 126.7, 122.9, 102.8, 70.8, 65.8, 52.4, 27.4, 24.2.

IR (Neat Film, NaCl): 3030, 2942, 1736, 1657, 1603, 1362, 1186, 1150 cm^{-1}.

HRMS (MM: FD+): *m/z* calc'd for C$_{23}$H$_{22}$O$_4$ [M]$^+$: 362.1518, found 362.1510.
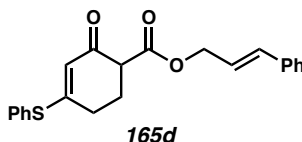
165d

cinnamyl 2-oxo-4-(phenylthio)cyclohex-3-ene-1-carboxylate (165d)

Prepared from 3-(phenylthio)cyclohex-2-en-1-one following General Procedure D.

Purification by flash column chromatography (10–60% EtOAc/hexanes) afforded the title

compound as a colorless oil (1.59 g, 4.36 mmol, 44% yield).

trace 3-(phenylthio)cyclohex-2-en-1-one coeluted with **165d. The material can be carried*

through alkylation and separated without issue*

^{1}H NMR (400 MHz, CDCl$_3$): δ 7.49 – 7.37 (m, 8H), 7.34 – 7.25 (m, 2H), 6.66 (d, *J* = 15.9

Hz, 1H), 6.27 (dt, *J* = 15.9, 6.3 Hz, 1H), 5.53 (s, 1H), 4.81 (dd, *J* = 6.4, 1.4 Hz, 2H), 3.41

(dd, *J* = 9.3, 4.9 Hz, 1H), 2.75 – 2.66 (m, 1H), 2.62 – 2.51 (m, 1H), 2.50 – 2.36 (m, 1H),

2.32 – 2.25 (m, 1H).

^{13}C NMR (100 MHz, CDCl$_3$): δ 190.2, 169.9, 167.5, 136.3, 135.6, 134.5, 130.5, 130.1,

128.7, 128.2, 127.7, 126.8, 122.9, 120.1, 65.9, 52.9, 28.6, 26.1.

IR (Neat Film, NaCl): 3054, 2939, 1736, 1656, 1576, 1300, 1167, 1146 cm^{-1}.

HRMS (MM: FD+): *m/z* calc'd for $C_{22}H_{20}O_3S$ [M]$^+$: 364.1133, found 364.1133.
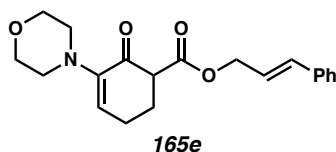
165e

cinnamyl 3-morpholino-2-oxocyclohex-3-ene-1-carboxylate (165e)

Prepared from 2-morpholinocyclohex-2-en-1-one [13] following General Procedure D. Purification by flash column chromatography (30–60% EtOAc/hexanes) afforded the title compound as a colorless oil (1.34 g, 3.92 mmol, 33% yield).

^{1}H NMR (400 MHz, C$_6$D$_6$): δ 7.16 – 7.13 (m, 2H), 7.10 – 6.98 (m, 3H), 6.43 (d, *J* = 15.9 Hz, 1H), 6.12 (dt, *J* = 15.9, 6.4 Hz, 1H), 5.22 (t, *J* = 4.5 Hz, 1H), 4.71 – 4.61 (m, 2H), 3.64 – 3.56 (m, 4H), 3.28 (dd, *J* = 9.6, 4.6 Hz, 1H), 2.67 – 2.55 (m, 4H), 2.20 – 2.12 (m, 1H), 2.02 (dq, *J* = 17.5, 4.9, 4.3 Hz, 1H), 1.81 – 1.65 (m, 2H).

^{13}C NMR (100 MHz, C$_6$D$_6$): δ 190.4, 169.7, 146.5, 136.7, 134.5, 128.8, 128.2, 127.0, 124.3, 123.4, 66.9, 65.6, 55.2, 50.3, 26.0, 23.6.

IR (Neat Film, NaCl): 3024, 2953, 2854, 1736, 1685, 1610, 1448, 1262, 1118 cm^{-1}.

HRMS (MM: ESI+): *m/z* calc'd for $C_{20}H_{24}O_4N$ [M+H]$^+$: 342.1700, found 342.1710.
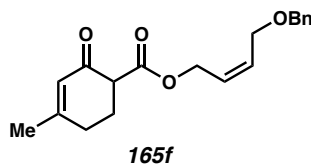
165f

(Z)-4-(benzyloxy)but-2-en-1-yl 4-methyl-2-oxocyclohex-3-ene-1-carboxylate (165f)

Prepared from 3-methylcyclohex-2-en-1-one and (Z)-4-(benzyloxy)but-2-en-1-yl 1*H*-imidazole-1-carboxylate following General Procedure D. Purification by flash column

chromatography (20% EtOAc/hexanes) afforded the title compound as a colorless oil (5.5 g, 20.3 mmol, 51% yield). *Due to difficult separation, the NMR contains signals associated with the starting material. However, this can be used in the next step without consequence.*

^{1}H NMR (600 MHz, CDCl$_3$): δ 7.41 – 7.32 (m, 4H), 7.32 – 7.27 (m, 1H), 5.91 (t, J = 1.5 Hz, 1H), 5.86 – 5.78 (m, 1H), 5.76 – 5.63 (m, 1H), 4.72 (dd, J = 6.6, 1.3 Hz, 2H), 4.51 (s, 2H), 4.13 (dd, J = 6.2, 1.5 Hz, 2H), 3.40 – 3.21 (m, 1H), 2.48 – 2.25 (m, 5H), 2.25 – 2.14 (m, 1H), 2.05 – 1.96 (m, 4H).

^{13}C NMR (101 MHz, CDCl$_3$): δ 193.6, 170.2, 163.1, 138.1, 131.2, 128.6, 127.9, 127.8, 126.5, 126.0, 72.6, 65.8, 61.1, 52.6, 29.5, 25.6, 24.5.

IR (Neat Film, NaCl): 3457, 3031, 2936, 1738, 1667, 1453 cm^{-1}.

HRMS (MM: ESI+): *m/z* calc'd for C$_{19}$H$_{22}$O$_4$Na [M+Na]$^+$: 337.1410, found 337.1415.
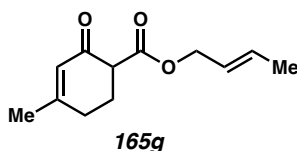
(*E*)-but-2-en-1-yl 4-methyl-2-oxocyclohex-3-ene-1-carboxylate (165g)

Prepared from 3-methylcyclohex-2-en-1-one following General Procedure D. Purification by flash column chromatography (20–40% EtOAc/hexanes) afforded the title compound as a colorless oil (1.98 g, 9.49 mmol, 63% yield).

^{1}H NMR (400 MHz, CDCl$_3$): δ 5.92 (q, J = 1.4 Hz, 1H), 5.84 – 5.74 (m, 1H), 5.63 – 5.54 (m, 1H), 4.58 (dt, J = 6.5, 1.1 Hz, 2H), 3.32 (dd, J = 9.6, 5.1 Hz, 1H), 2.45 – 2.27 (m, 3H), 2.21 – 2.16 (m, 1H), 1.97 (s, 3H), 1.71 (dq, J = 6.5, 1.2 Hz, 3H).

¹³C NMR (100 MHz, CDCl₃): δ 193.8, 170.2, 163.0, 131.7, 126.0, 124.9, 66.0, 52.6, 29.5,

25.6, 24.5, 17.9.

IR (Neat Film, NaCl): 3027, 2941, 1737, 1671, 1632, 1439, 1166, 1153 cm⁻¹.

HRMS (MM: ESI+): *m/z* calc'd for $C_{12}H_{16}O_3Na$ $[M+Na]^+$: 231.0992, found 231.1000.
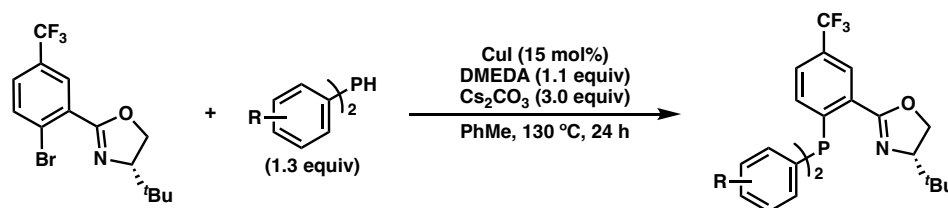
General Procedure E: Preparation of Novel (S)-t-BuPHOX Ligands.

A flame-dried 3-neck round-bottom flask attached to a reflux condenser under nitrogen

atmosphere was charged with CuI (0.15 equiv). Anhydrous toluene (0.03 M) was added

followed by DMEDA (1.1 equiv), and the reaction mixture was stirred at ambient

temperature for 20 minutes. To the pre-stirred catalyst solution was added the requisite aryl

bromide (1.0 equiv), Cs₂CO₃ (3.0 equiv), and the aryl phosphine (1.3 equiv). Minimal

additional toluene was added to rinse any solids off the sides of the flask. The reaction

mixture was heated to reflux (*ca.* 130 °C) and stirred for a minimum of 21 h. Upon

completion, the reaction mixture was cooled to ambient temperature, filtered through a

pad of celite, and washed with CH₂Cl₂. The filtrate was concentrated and purified by flash

silica gel column chromatography.
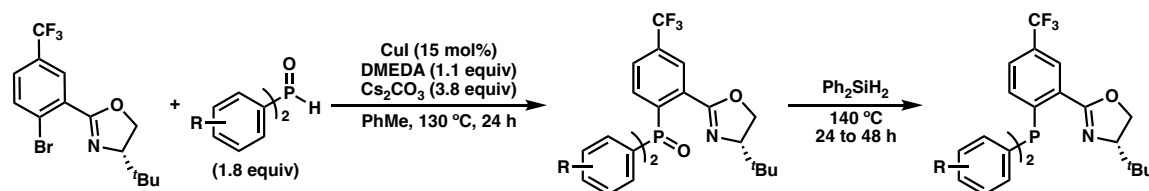
General Procedure F: Preparation of Novel (S)-t-BuPHOX Ligands.

A flame-dried 3-neck round-bottom flask attached to a reflux condenser under nitrogen atmosphere was charged with CuI (0.15 equiv). Anhydrous toluene (0.03 M) was added followed by DMEDA (1.1 equiv), and the reaction mixture was stirred at ambient temperature for 20 minutes. To the pre-stirred catalyst solution was added aryl bromide (1.0 equiv), Cs_2CO_3 (3.8 equiv), and aryl phosphine oxide (1.8 equiv). Minimal additional toluene was added to rinse any solids off the sides of the flask. The reaction mixture was heated to reflux (*ca.* 130 °C) and stirred for a minimum of 21 h. Upon completion, the reaction mixture was cooled to ambient temperature, filtered through a pad of celite, and washed with CH_2Cl_2. The filtrate was concentrated and purified by flash silica gel column chromatography.

The isolated phosphine oxide was placed in an oven-dried vial along with a magnetic stir bar and degassed using an Argon balloon for 10 min. Ph_2SiH_2 (1.2 mL, 6.5 mmol, 7.0 equiv) was added to the reaction vial, which fully dissolved the phosphine oxide residue. The reaction vial was then placed in a pre-heated oil bath at 140 °C and stirred until complete reduction of phosphine oxide (typically 24–120 h). Once complete as determined by ^{31}P NMR, the reaction was cooled to ambient temperature adsorbed onto silica gel then purified by flash silica gel column chromatography.

L4
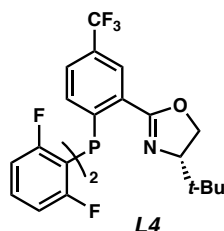
(*S*)-2-(2-(bis(2,6-difluorophenyl)phosphaneyl)-5-(trifluoromethyl)phenyl)-4-(*tert*-

butyl)-4,5-dihydrooxazole (L4)

Prepared from bis(2,6-difluorophenyl)phosphane (190 mg, 0.74 mmol, 1.2 equiv)
following General Procedure E. Purification by flash column chromatography (0–50%
CH$_2$Cl$_2$/hexanes) afforded the title compound as a white solid (67 mg, 0.13 mmol, 20%
yield).

Note: Ullmann coupling using the aryl phosphine oxide does not yield any product.

¹H NMR (300 MHz, CDCl₃): δ 8.23 (dd, *J* = 4.4, 2.0 Hz, 1H), 7.61 – 7.50 (m, 1H), 7.42
– 7.26 (m, 3H), 6.83 (qd, *J* = 7.8, 2.3 Hz, 4H), 4.30 (dd, *J* = 10.1, 8.5 Hz, 1H), 4.13 (t, *J* =
8.7 Hz, 1H), 3.94 (dd, *J* = 10.1, 8.9 Hz, 1H), 0.69 (s, 9H).

¹³C NMR (101 MHz, CDCl₃): δ 165.8 (td, *J* = 9.0, 3.7 Hz), 163.3 (td, *J* = 9.0, 4.1 Hz),
161.2 (d, *J* = 4.9 Hz), 140.9 (d, *J* = 28.6 Hz), 133.1, 132.1, 131.6 (dt, *J* = 28.6, 10.9 Hz),
130.5 (qd, *J* = 33.2, 1.6 Hz), 128.0, 126.4 (q, *J* = 3.7 Hz), 126.2 – 126.0 (m), 125.3, 122.6,
119.8, 114.7 – 113.3 (m), 111.9 – 111.2 (m), 68.9, 33.5, 25.8.

³¹P NMR (121 MHz, CDCl₃): δ –55.81 – –56.51 (m).

¹⁹F NMR (282 MHz, CDCl₃): δ –62.83 – –62.88 (m, 3F), –100.06 – –100.19 (m, 1F), –
100.24 – –100.34 (m, 1F), –100.43 – –100.54 (m, 1F), –100.58 – –100.70 (m, 1F).

IR (Neat Film, NaCl): 3080, 2958, 2907, 2870, 1657, 1607, 1574, 1454, 1326, 1228, 1176,

1131, 1083, 986, 784 cm^{-1}.

HRMS (MM: ESI+): *m/z* calc'd for $C_{26}H_{21}NOF_7P$ [M]$^+$: 527.12490, found 527.12391.

Optical Rotation: $[\alpha]_D^{21}$ +18.1° (*c* 0.10, CHCl$_3$)
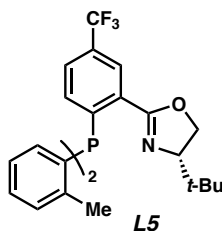
(*S*)-4-(*tert*-butyl)-2-(2-(di-*o*-tolylphosphaneyl)-5-(trifluoromethyl)phenyl)-4,5-

dihydrooxazole (L5)

Prepared from di-*o*-tolylphosphane (240 mg, 1.1 mmol, 1.3 equiv) following General

Procedure E. Purification by flash column chromatography (0–30% EtOAc/hexanes)

afforded the title compound as a tan solid (130 mg, 0.27 mmol, 31% yield).

^{1}H NMR (400 MHz, CDCl$_3$): δ 8.21 (t, *J* = 2.7 Hz, 1H), 7.51 (dd, *J* = 8.1, 2.0 Hz, 1H),

7.26 – 7.16 (m, 4H), 7.11 – 6.97 (m, 3H), 6.73 – 6.64 (m, 2H), 4.13 (dd, *J* = 10.1, 8.5 Hz,

1H), 4.04 (t, *J* = 8.3 Hz, 1H), 3.94 (dd, *J* = 10.1, 8.3 Hz, 1H), 2.38 (dd, *J* = 4.1, 1.7 Hz, 6H),

0.70 (s, 9H).

^{13}C NMR (101 MHz, CDCl$_3$): δ 161.61, 143.48 – 143.01 (m), 142.75 (d, *J* = 27.4 Hz),

142.31 (d, *J* = 28.0 Hz), 135.93 – 135.60 (m), 134.81, 133.49, 133.26, 133.05, 130.85,

130.53, 130.25 (d, *J* = 4.9 Hz), 128.90 (d, *J* = 15.1 Hz), 126.81 (dq, *J* = 11.3, 3.7 Hz),

126.38 (d, *J* = 16.2 Hz), 125.30, 122.59, 68.63, 33.76, 25.79, 21.48, 21.25.

^{31}P NMR (121 MHz, CDCl$_3$): δ –20.8 (s).

¹⁹F NMR (282 MHz, CDCl₃): δ –62.8 (s).

IR (Neat Film, NaCl): 3056, 2957, 2867, 2356, 1653, 1471, 1454, 1341, 1324, 1169, 1130, 1079, 970 cm⁻¹.

HRMS (MM: ESI+): *m/z* calc'd for C₂₈H₂₉NOF₃P [M+H]⁺: 483.19389, found 483.19472.

Optical Rotation: [α]$_D^{22}$ –55.4 ° (*c* 0.28, CHCl₃).
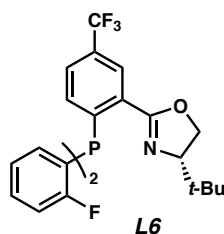
(*S*)-2-(2-(bis(2-fluorophenyl)phosphaneyl)-5-(trifluoromethyl)phenyl)-4-(*tert*-butyl)-4,5-dihydrooxazole (L6)

Prepared from bis(2-fluorophenyl)phosphine oxide (408 mg, 1.7 mmol, 1.8 equiv) following General Procedure F. Purification by flash column chromatography (0–50% EtOAc/hexanes) afforded the title compound as a white solid (408 mg, 0.81 mmol, 85% yield).

¹H NMR (500 MHz, CDCl₃): δ 8.28 (t, *J* = 2.8 Hz, 1H), 7.59 (dd, *J* = 8.2, 2.0 Hz, 1H), 7.41 – 7.32 (m, 2H), 7.20 (dd, *J* = 8.2, 3.0 Hz, 1H), 7.11 – 7.02 (m, 4H), 6.88 – 7.84 (m, 1H), 6.82 – 6.77 (m, 1H), 4.26 (dd, *J* = 10.1, 8.6 Hz, 1H), 4.12 (t, *J* = 8.6 Hz, 1H), 4.00 (dd, *J* = 10.1, 8.6 Hz, 1H), 0.74 (s, 9H).

¹³C NMR (101 MHz, CDCl₃): δ 165.7 (dd, *J* = 17.9, 16.1 Hz), 163.5 – 163.0 (m), 161.3, 141.6 (d, *J* = 29.5 Hz), 135.0 – 134.8 (m), 134.7 – 134.4 (m), 132.3 (d, *J* = 21.8 Hz), 131.4

(dd, $J = 25.3$, 8.3 Hz), 131.0 (d, $J = 33.2$ Hz), 127.0 (q, $J = 3.7$ Hz), 126.7 (t, $J = 3.5$ Hz),

125.2, 124.8 (dd, $J = 9.7$, 3.3 Hz), 124.4 – 123.7 (m), 122.5, 68.9, 33.7, 25.8.

^{31}P NMR (121 MHz, CDCl$_3$): δ –32.10 (t, $J = 63.2$ Hz).

^{19}F NMR (282 MHz, CDCl$_3$): δ –62.90 (s, 3F), –103.64 – –103.88 (m, 1), –103.88 – –

104.11 (m, 1F).

IR (Neat Film, NaCl): 3069, 2956, 2357, 1654, 1469, 1324, 1170, 1132, 1081, 756 cm^{-1}.

HRMS (MM: ESI+): *m/z* calc'd for C$_{26}$H$_{23}$NOF$_5$P [M+H]$^+$: 491.14374, found 491.14451.

Optical Rotation: [α]$_D^{22}$ –20.5° (*c* 0.73, CHCl$_3$).
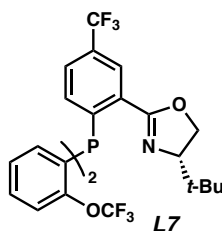
(*S*)-2-(2-(bis(2-(trifluoromethoxy)phenyl)phosphaneyl)-5-(trifluoromethyl)phenyl)-

4-(*tert*-butyl)-4,5-dihydrooxazole (L7)

Prepared from bis(2-(trifluoromethoxy)phenyl)phosphine oxide (700 mg, 1.9 mmol, 1.8

equiv) following General Procedure F. Purification by flash column chromatography (0–

50% EtOAc/hexanes) afforded the title compound as a tan solid (632 mg, 0.99 mmol, 94%

yield).

^{1}H NMR (300 MHz, CDCl$_3$): δ 8.25 – 8.23 (m, 1H), 7.62 – 7.50 (m, 1H), 7.45 – 7.37 (m,

2H), 7.31 – 7.27 (m, 2H), 7.20 – 7.14 (m, 2H), 7.03 (dd, $J = 8.2$, 2.7 Hz, 1H), 6.90 – 6.74

(m, 2H), 4.21 (dd, $J = 10.2$, 8.5 Hz, 1H), 4.12 (t, $J = 8.2$ Hz, 1H), 3.98 (dd, $J = 10.2$, 7.8

Hz, 1H), 0.71 (s, 9H).

¹³C NMR (101 MHz, CDCl₃): δ 161.24, 151.82 (dd, J = 27.3, 19.9 Hz), 141.42 (d, J =

30.8 Hz), 135.41 (d, J = 2.8 Hz), 135.00, 134.49, 133.09 (d, J = 23.3 Hz), 131.50, 131.18,

130.94, 130.85, 130.66, 130.45 (d, J = 17.5 Hz), 130.23, 129.78 (d, J = 21.2 Hz), 128.00,

127.86 (d, J = 1.3 Hz), 126.95 – 126.41 (m), 125.16, 124.33 (d, J = 3.0 Hz), 122.45, 121.76

(d, J = 3.0 Hz), 119.60, 119.27 – 119.01 (m), 116.60, 69.01, 33.82, 25.66.

³¹P NMR (121 MHz, CDCl₃): δ –27.4 (m).

¹⁹F NMR (282 MHz, CDCl₃): δ –56.5 (s, 6F), –62.9 (s, 3F).

IR (Neat Film, NaCl): 3062, 2964, 2870, 2363, 2342, 1653, 1472, 1326, 1251, 1216, 1200,

1168, 1160, 1128, 1081 cm⁻¹.

HRMS (MM: ESI+): *m/z* calc'd for $C_{28}H_{23}NO_3F_9P$ [M+H]⁺: 623.12718, found 623.12455.

Optical Rotation: $[\alpha]_D^{21}$ –20.3 ° (*c* 1.48, CHCl₃).

5.7   REFERENCES AND NOTES

(1)   Junk, L.; Kazmaier, U. The Allylic Alkylation of Ketone Enolates. *ChemistryOpen* **2020**, *9*, 929–952.

(2)   (a) Hethcox, J. C.; Shockley, S. E.; Stoltz, B. M. Iridium-Catalyzed Diastereo-, Enantio-, and Regioselective Allylic Alkylation with Prochiral Enolates. *ACS Catal.* **2016**, *6*, 6207–6213. (b) Qu, J.; Helmchen, G. Applications of Iridium-Catalyzed Asymmetric Allylic Substitution Reactions in Target-Oriented Synthesis. *Acc. Chem. Res.* **2017**, *50*, 2539–2555. (c) Shockley, S. E.; Hethcox, J. C.; Stoltz, B. M. Intermolecular Stereoselective Iridium-Catalyzed Allylic Alkylation: An Evolutionary Account. *Synlett* **2018**, *29*, 2481–2492. (d) Cheng, Q.; Tu, H.-F.; Zheng, C.; Qu, J.-P.; Helmchen, G.; You, S.-L. Iridium-Catalyzed Asymmetric Allylic Substitution Reactions. *Chem. Rev.* **2019**, *119*, 1855–1969. (e) Moghadam, F. A.; Hicks, E. F.; Sercel, Z. P.; Cusumano, A. Q.; Bartberger, M. D.; Stoltz, B. M. Ir-Catalyzed Asymmetric Allylic Alkylation of Dialkyl Malonates Enabling the Construction of Enantioenriched All-Carbon Quaternary Centers. *J. Am. Chem. Soc.* **2022**, *144*, 7983–7987.

(3)   Trost, B. M.; Schroeder, G. M. Palladium-Catalyzed Asymmetric Allylic Alkylation of Ketone Enolates. *Chem. Eur. J.* **2005**, *11*, 174–184.

(4)   Chen, W.; Chen, M.; Hartwig, J. F. Diastereo- and Enantioselective Iridium-Catalyzed Allylation of Cyclic Ketone Enolates: Synergetic Effect of Ligands and Barium Enolates. *J. Am. Chem. Soc.* **2014**, *136*, 15825–15828.

(5)   (a) Chen, J.-P.; Peng, Q.; Lei, B.-L.; Hou, X.-L.; Wu, Y.-D. Chemo- and Regioselectivity-Tunable Pd-Catalyzed Allylic Alkylation of Imines. *J. Am. Chem. Soc.* **2011**, *133*, 14180–14183. (b) Braun, M.; Laicher, F.; Meier, T. Diastereoselective and Enantioselective Palladium-Catalyzed Allylic Substitution with Nonstabilized Ketone Enolates. *Angew. Chem. Int. Ed.* **2000**, *39*, 3494–3497. (c) Yu, F.-L.; Bai, D.-C.; Liu, X.-Y.; Jiang, Y.-J.; Ding, C.-H.; Hou, X.-L. Pd-Catalyzed Allylic Alkylation of Gem-Alkyl,Aryl-Disubstituted Allyl Reagents with Ketones: Diastereoselective Construction of Vicinal Tertiary and Quaternary Carbon Centers. *ACS Catal.* **2018**, *8*, 3317–3321. (d) Zheng, W.-H.; Zheng, B.-H.; Zhang, Y.; Hou, X.-L. Highly Regio-, Diastereo-, and Enantioselective Pd-Catalyzed Allylic Alkylation of Acyclic Ketone Enolates with Monosubstituted Allyl Substrates. *J. Am. Chem. Soc.* **2007**, *129*, 7718–7719.

(6)   (a) Behenna, D. C.; Stoltz, B. M. The Enantioselective Tsuji Allylation. *J. Am. Chem. Soc.* **2004**, *126*, 15044–15045. (b) Mohr, J. T.; Behenna, D. C.; Harned, A. M.; Stoltz, B. M. Deracemization of Quaternary Stereocenters by Pd-Catalyzed Enantioconvergent Decarboxylative Allylation of Racemic β-Ketoesters. *Angew. Chem. Int. Ed.* **2005**, *44*, 6924–6927. (c) Ngamnithiporn, A.; Iwayama, T.; Bartberger, M. D.; Stoltz, B. M. Enantioselective Synthesis of Highly Oxygenated Acyclic Quaternary Center-Containing Building Blocks via Palladium-Catalyzed Decarboxylative Allylic Alkylation of Cyclic Siloxyketones. *Chem. Sci.* **2020**, *11*, 11068–11071. (d) Alexy, E. J.; Fulton, T. J.; Zhang, H.; Stoltz, B. M. Palladium-

Catalyzed Enantioselective Decarboxylative Allylic Alkylation of Fully Substituted N-Acyl Indole-Derived Enol Carbonates. *Chem. Sci.* **2019**, *10*, 5996–6000. (e) Lu, Y.; Goldstein, E. L.; Stoltz, B. M. Palladium-Catalyzed Enantioselective C(sp³)–C(sp³) Cross-Coupling for the Synthesis of (Poly)Fluorinated Chiral Building Blocks. *Org. Lett.* **2018**, *20*, 5657–5660. (f) Alexy, E. J.; Zhang, H.; Stoltz, B. M. Catalytic Enantioselective Synthesis of Acyclic Quaternary Centers: Palladium-Catalyzed Decarboxylative Allylic Alkylation of Fully Substituted Acyclic Enol Carbonates. *J. Am. Chem. Soc.* **2018**, *140*, 10109–10112. (g) Alexy, E. J.; Virgil, S. C.; Bartberger, M. D.; Stoltz, B. M. Enantioselective Pd-Catalyzed Decarboxylative Allylic Alkylation of Thiopyranones. Access to Acyclic, Stereogenic α-Quaternary Ketones. *Org. Lett.* **2017**, *19*, 5007–5009.

(7)   (a) Reaction conditions: **158a** (0.05 mmol), Pd₂(dba)₃ (2.5 mol %), *(S,S)*-DACH-Ph (6.5 mol %), and THF (2 mL) at 60 ºC for 14 h. (b) An analogous result was found by Wolfe and coworkers: Bornowski, E. C.; Hinds, E. M.; White, D. R.; Nakamura, Y.; Wolfe, J. P. Pd-Catalyzed Alkene Difunctionalization Reactions of Enolates for the Synthesis of Substituted Bicyclic Cyclopentanes. *Org. Process Res. Dev.* **2019**, *23*, 1610–1630.

(8)   (a) Keith, J. A.; Behenna, D. C.; Mohr, J. T.; Ma, S.; Marinescu, S. C.; Oxgaard, J.; Stoltz, B. M.; Goddard, W. A. The Inner-Sphere Process in the Enantioselective Tsuji Allylation Reaction with *(S)-t*-Bu-Phosphinooxazoline Ligands. *J. Am. Chem.*

Soc. **2007**, *129*, 11876–11877. (b) Keith, J. A.; Behenna, D. C.; Sherden, N.; Mohr, J. T.; Ma, S.; Marinescu, S. C.; Nielsen, R. J.; Oxgaard, J.; Stoltz, B. M.; Goddard, W. A. The Reaction Mechanism of the Enantioselective Tsuji Allylation: Inner-Sphere and Outer-Sphere Pathways, Internal Rearrangements, and Asymmetric C–C Bond Formation. *J. Am. Chem. Soc.* **2012**, *134*, 19050–19060. (c) Cusumano, A. Q.; Stoltz, B. M.; William A. Goddard, III. Reaction Mechanism, Origins of Enantioselectivity, and Reactivity Trends in Asymmetric Allylic Alkylation: A Comprehensive Quantum Mechanics Investigation of a $C(sp^3)$–$C(sp^3)$ Cross-Coupling. *J. Am. Chem. Soc.* **2020**, *142*, 13917–13933. (d) McPherson, K. E.; Croatt, M. P.; Morehead, A. T.; Sargent, A. L. DFT Mechanistic Investigation of an Enantioselective Tsuji–Trost Allylation Reaction. *Organometallics* **2018**, *37*, 3791–3802.

(9)   For an example of the use of ligand sterics to influence regioselectivity in Pd-catalyzed allylic alkylation, see: (b) Yang, M.-H.; Orsi, D. L.; Altman, R. A. Ligand-Controlled Regiodivergent Palladium-Catalyzed Decarboxylative Allylation Reaction to Access α,α-Difluoroketones. *Angew. Chem. Int. Ed.* **2015**, *54*, 2361–2365.

(10)   Free energies at the PBE0-D4/def2-TZVPP/SMD(PhMe)//PBE-D4/def2-TZVP[Pd], ma-def2-SVP[O], def2-SV(P) level of theory at 333.15 K.

(11)   Pangborn, A. M.; Giardello, M. A.; Grubbs, R. H.; Rosen, R. K.; Timmers, F. J. Safe and Convenient Procedure for Solvent Purification. *Organometallics* **1996**, *15*, 1518–1520.

(12)   McDougal, N. T.; Streuff, J.; Mukherjee, H.; Virgil, S. C.; Stoltz, B. M. Rapid synthesis of an electron-deficient *t*-BuPHOX ligand: cross-coupling of aryl bromides with secondary phosphine oxides. *Tetrahedron Lett*. **2010**, *51*, 5550–5554.

(13)   Tobias, M. A.; Strong, J. G.; Napier, R. P. Preparation of 2-substituted 2-cyclohexen-1-ones *J. Org. Chem.* **1970**, *35*, 1709–1711.

APPENDIX 3

Spectra Relevant to Chapter 5: Development of a Branched-selective

Asymmetric Allylic Alkylation of Hard Pd-Enolate Nucleophiles
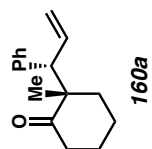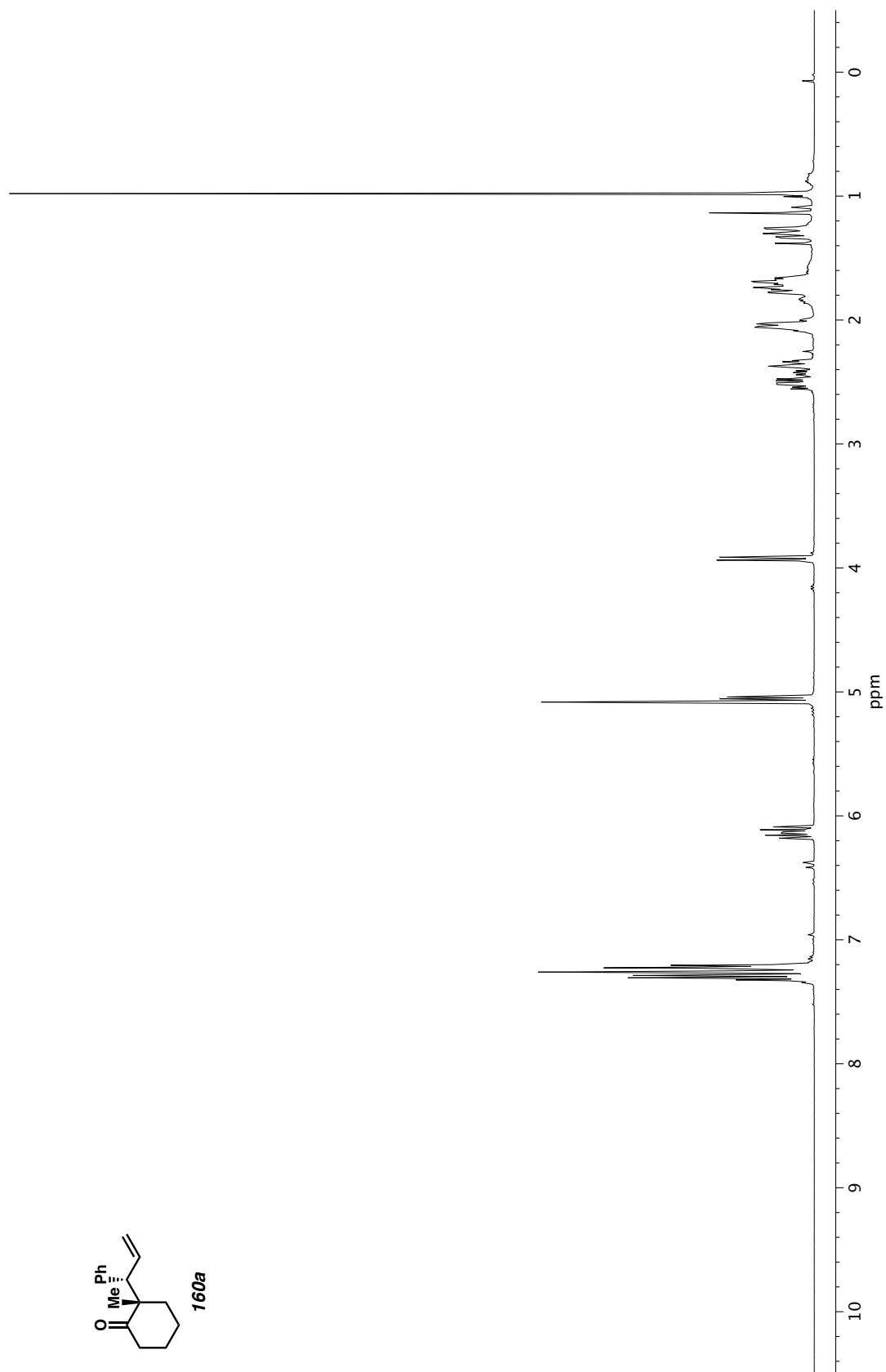
Figure A3.1. ^1H NMR (400 MHz, CDCl$_3$) of compound **160a**.
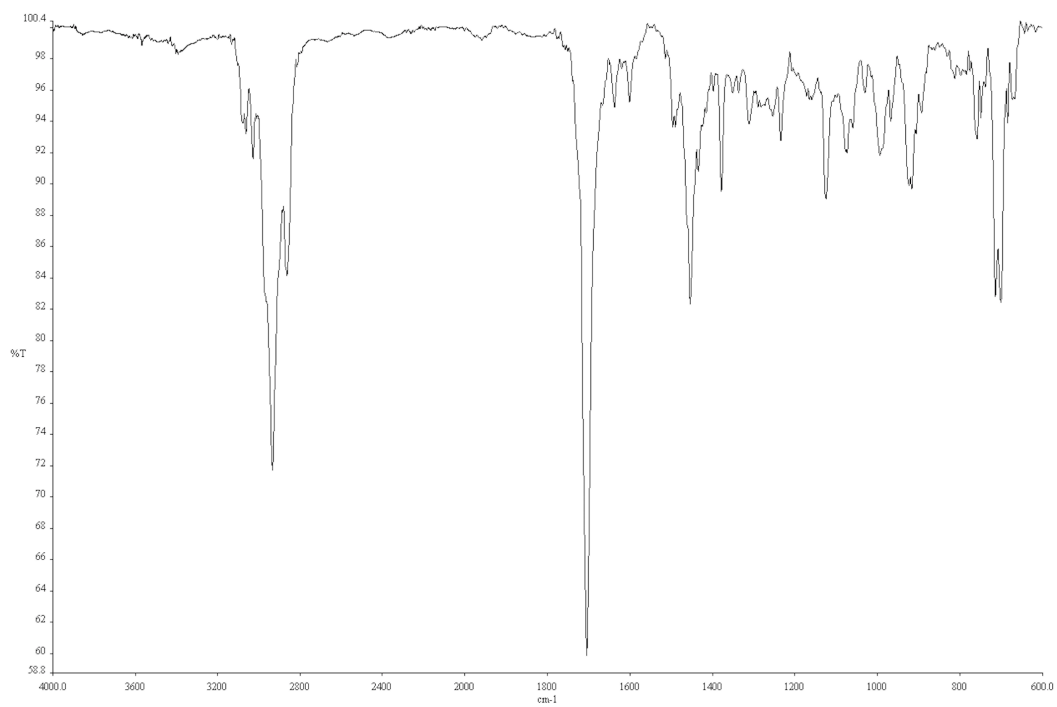
Figure A3.2. *Infrared spectrum (Thin Film, NaCl) of compound* **160a**.
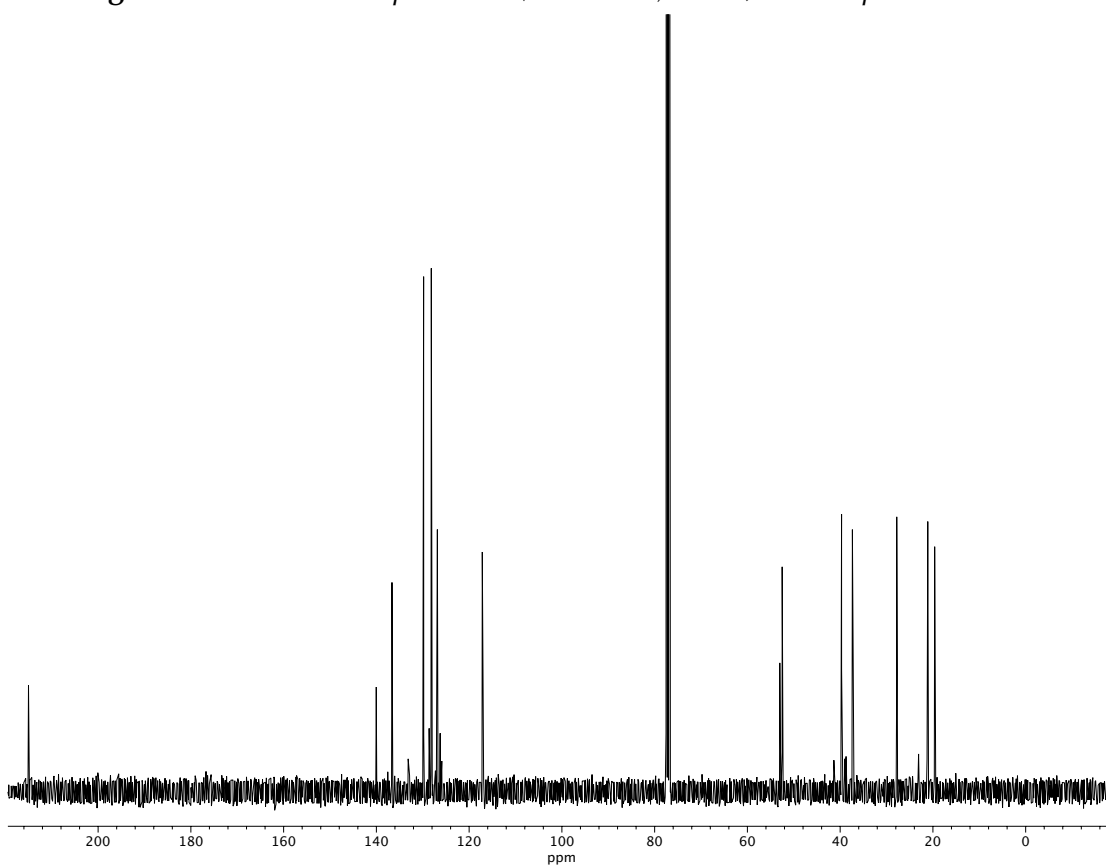
Figure A3.3. ^{13}C *NMR (100 MHz, CDCl$_3$) of compound* **160a**.
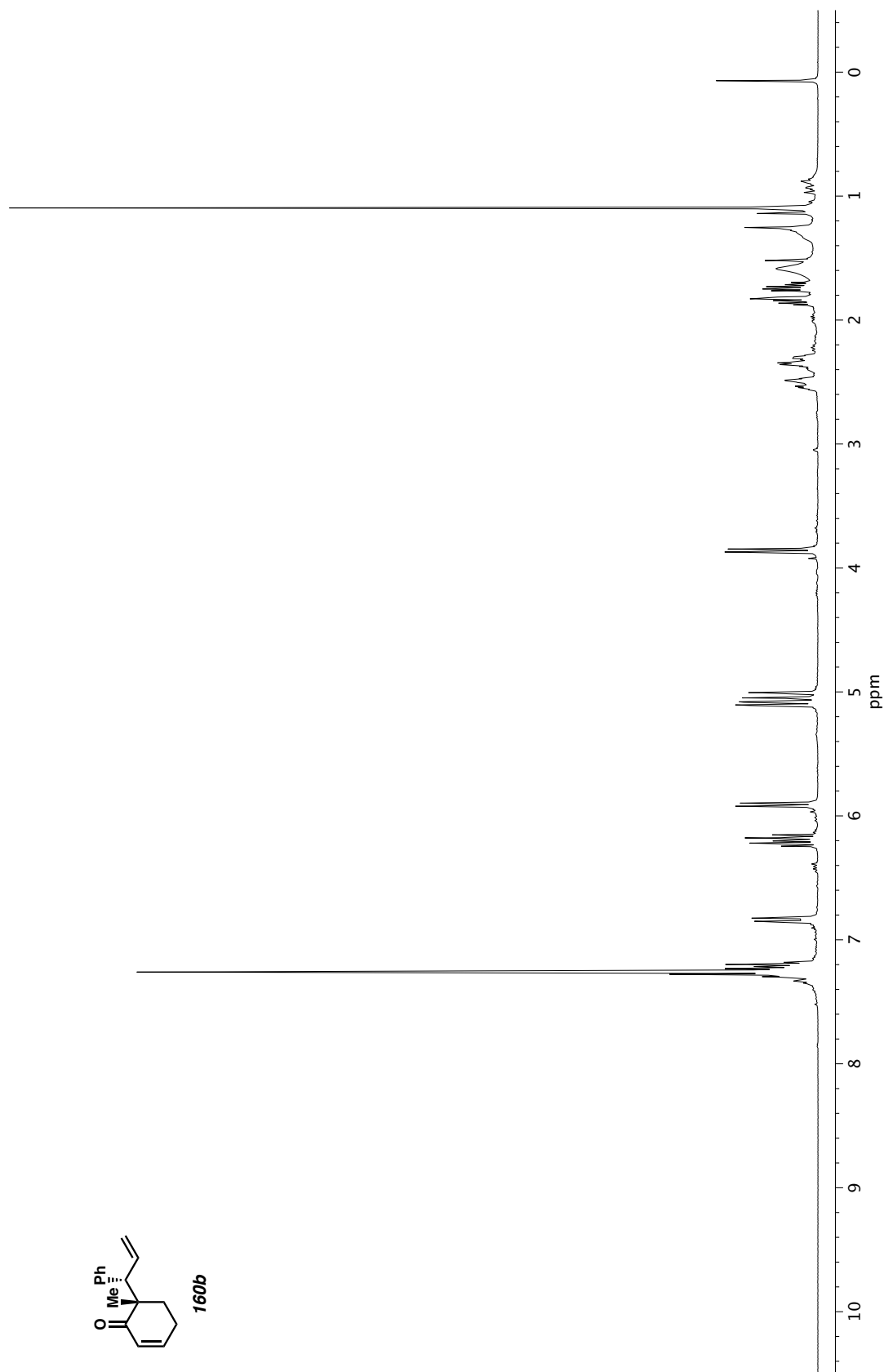
Figure A3.4. ^1H NMR (400 MHz, CDCl$_3$) of compound **160b**.
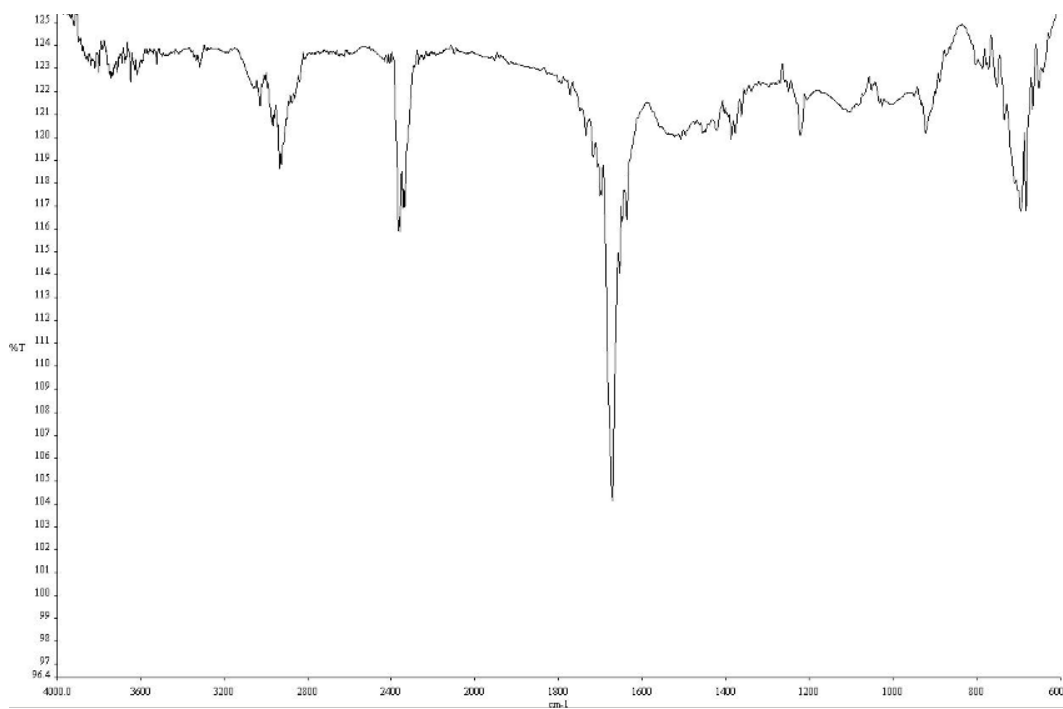
Figure A3.5. *Infrared spectrum (Thin Film, NaCl) of compound **160b***.
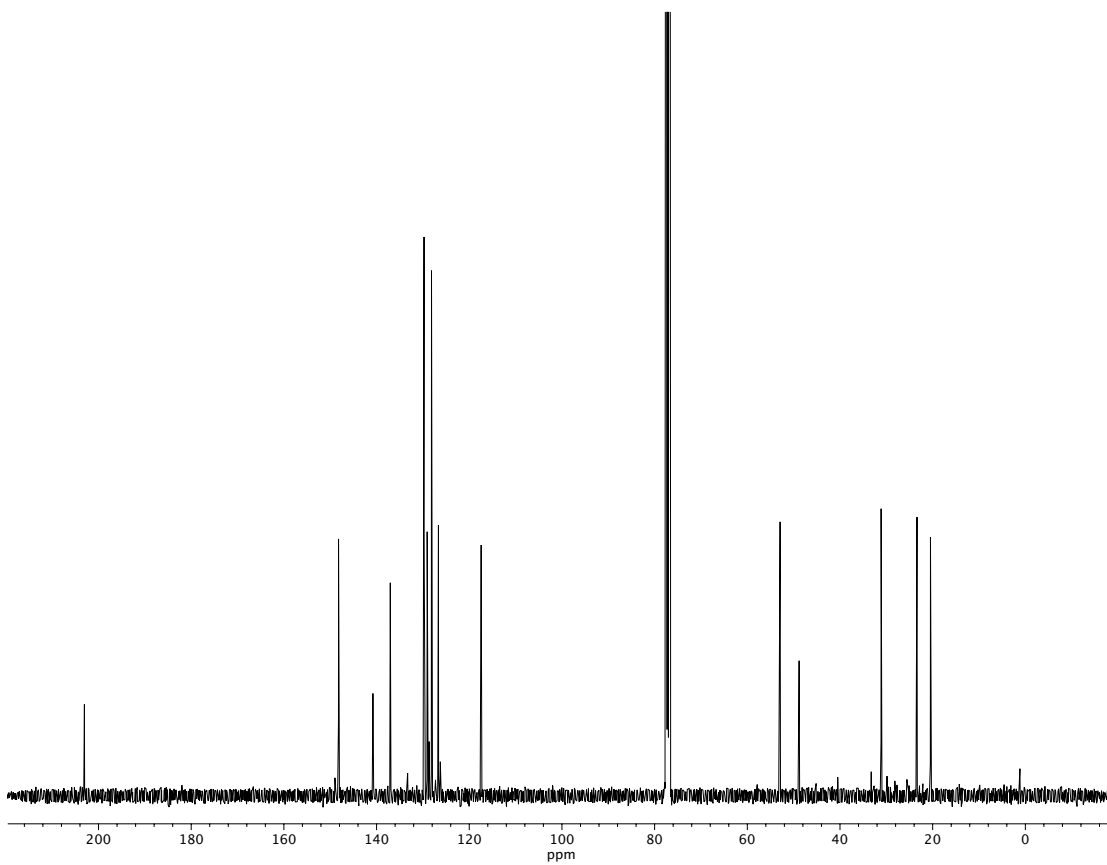
Figure A3.6. *^{13}C NMR (100 MHz, CDCl$_3$) of compound **160b***.
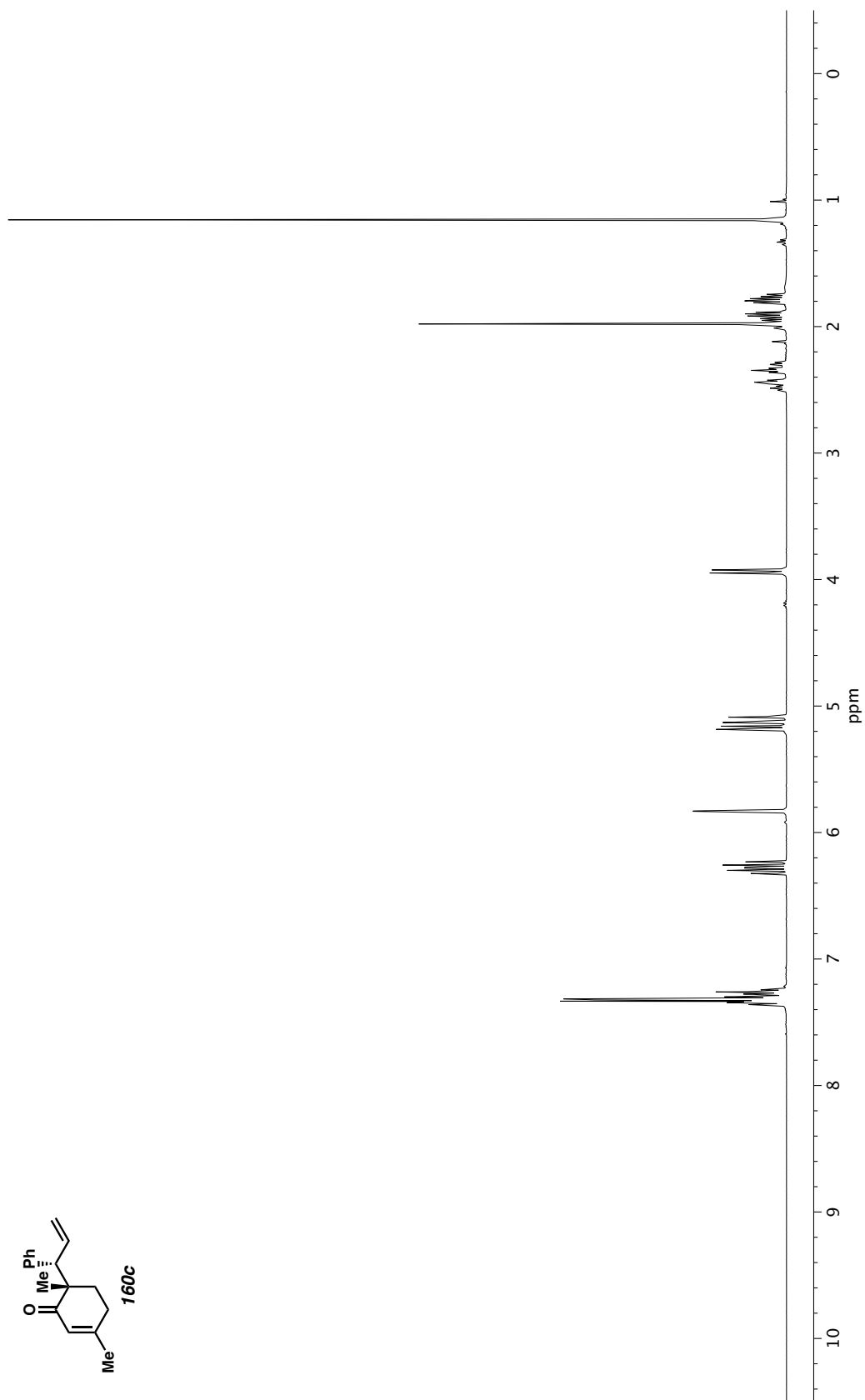
Figure A3.7. ^1H NMR (400 MHz, CDCl$_3$) of compound **160c**.
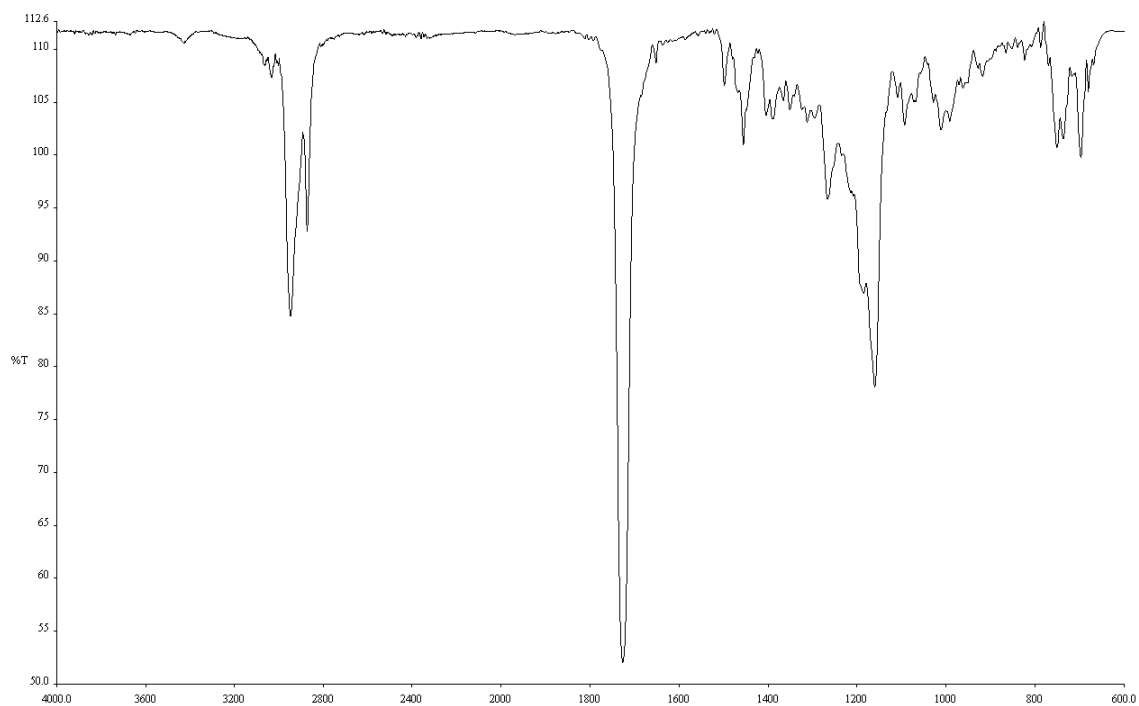
Figure A3.8. *Infrared spectrum (Thin Film, NaCl) of compound **160c**.*
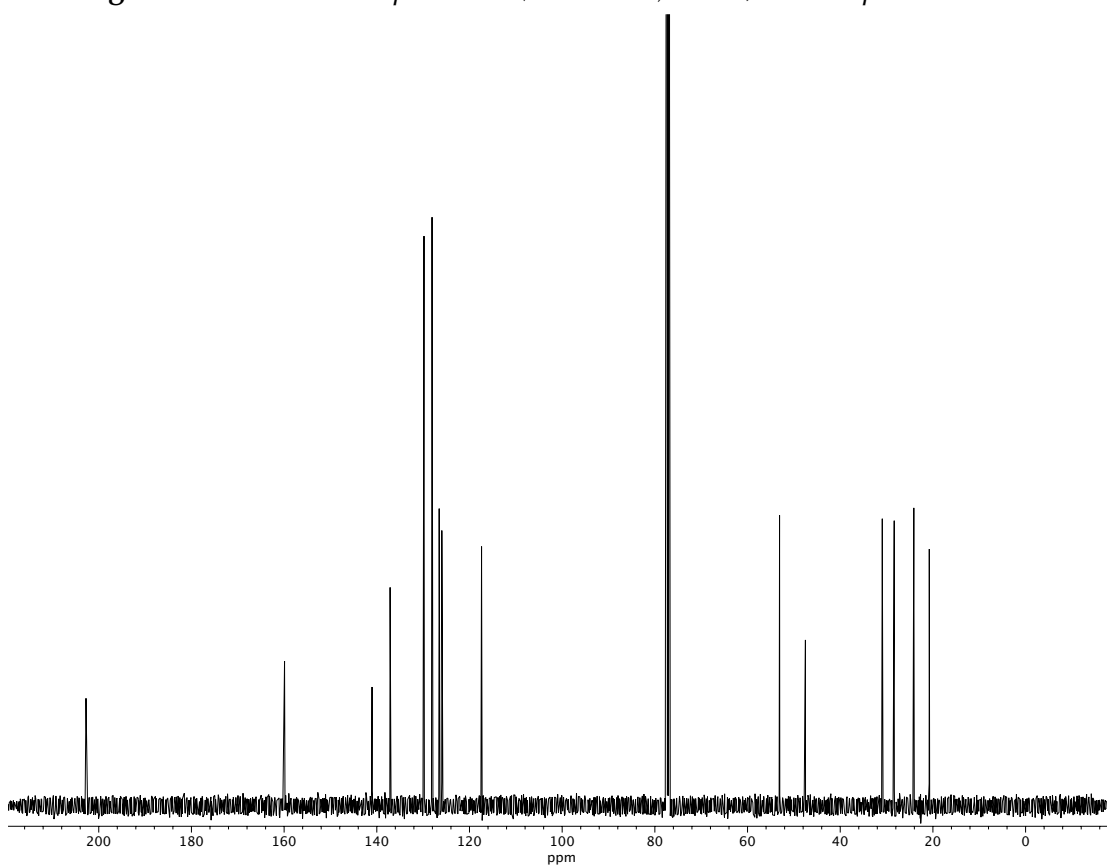
Figure A3.9. ^{13}C *NMR (100 MHz, CDCl$_3$) of compound **160c**.*
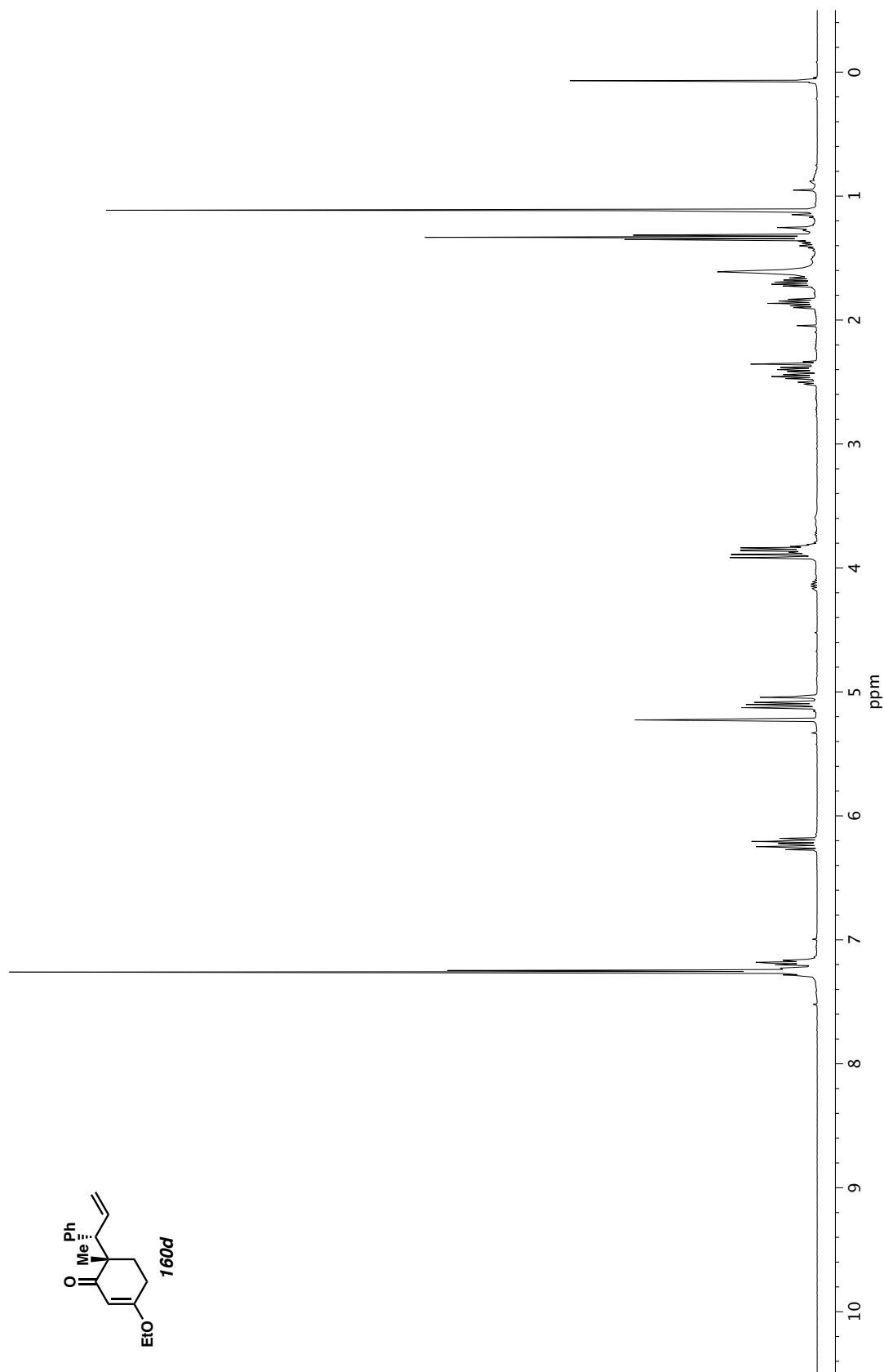
Figure A3.10. ^1H NMR (400 MHz, CDCl$_3$) of compound **160d**.
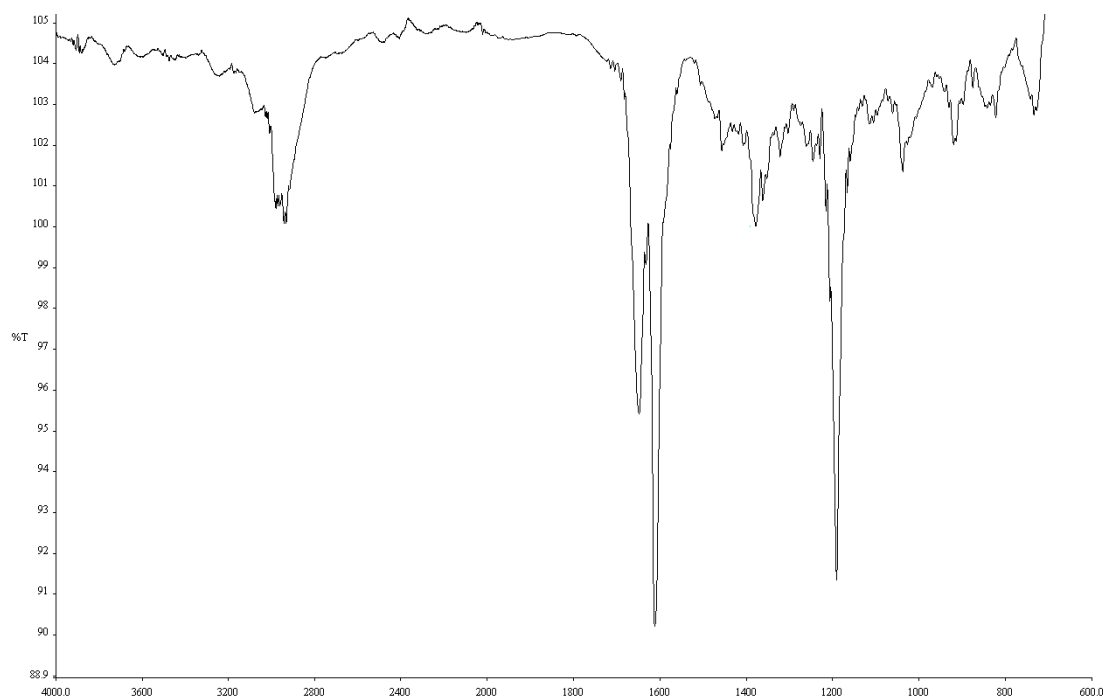
Figure A3.11. Infrared spectrum (Thin Film, NaCl) of compound **160d**.
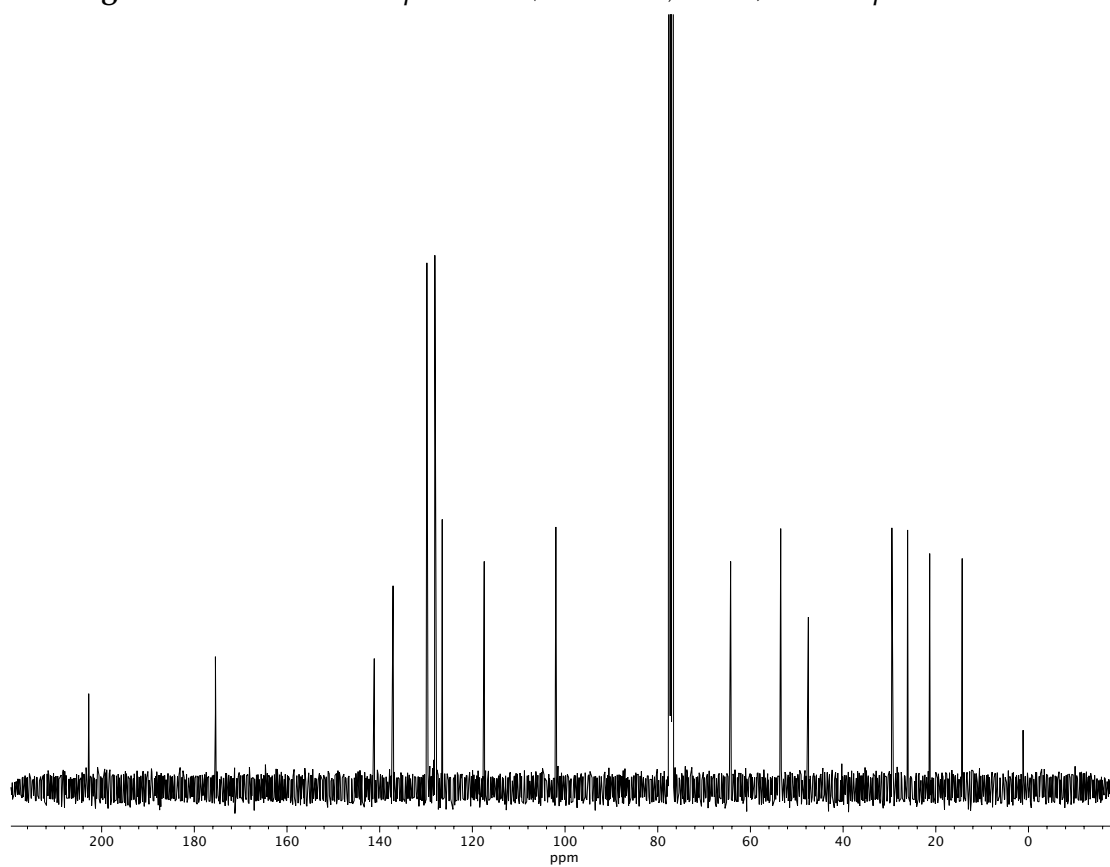
Figure A3.12. ^{13}C NMR (100 MHz, CDCl$_3$) of compound **160d**.
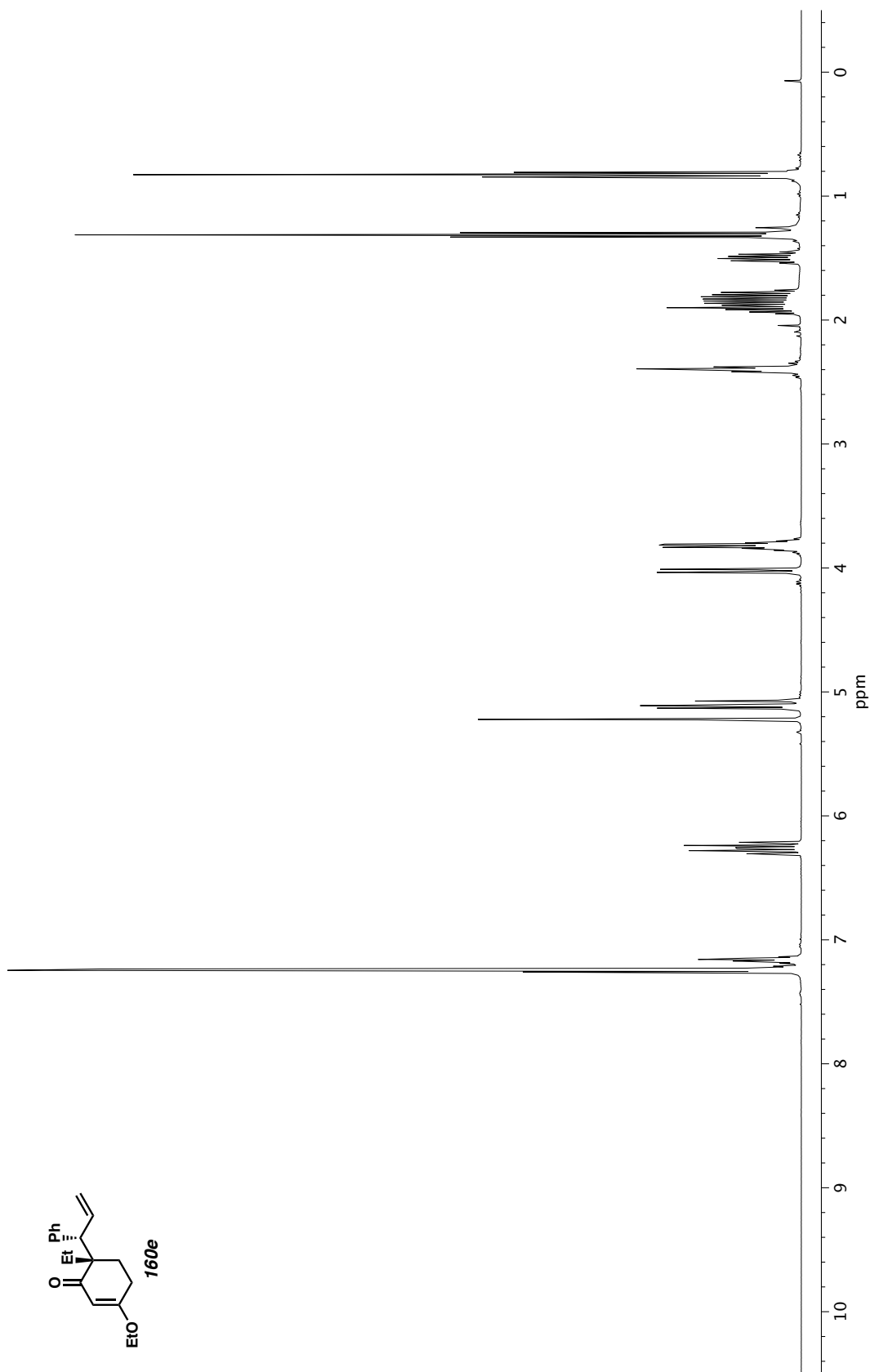
Figure A3.13. ^1H NMR (400 MHz, CDCl$_3$) of compound **160e**.
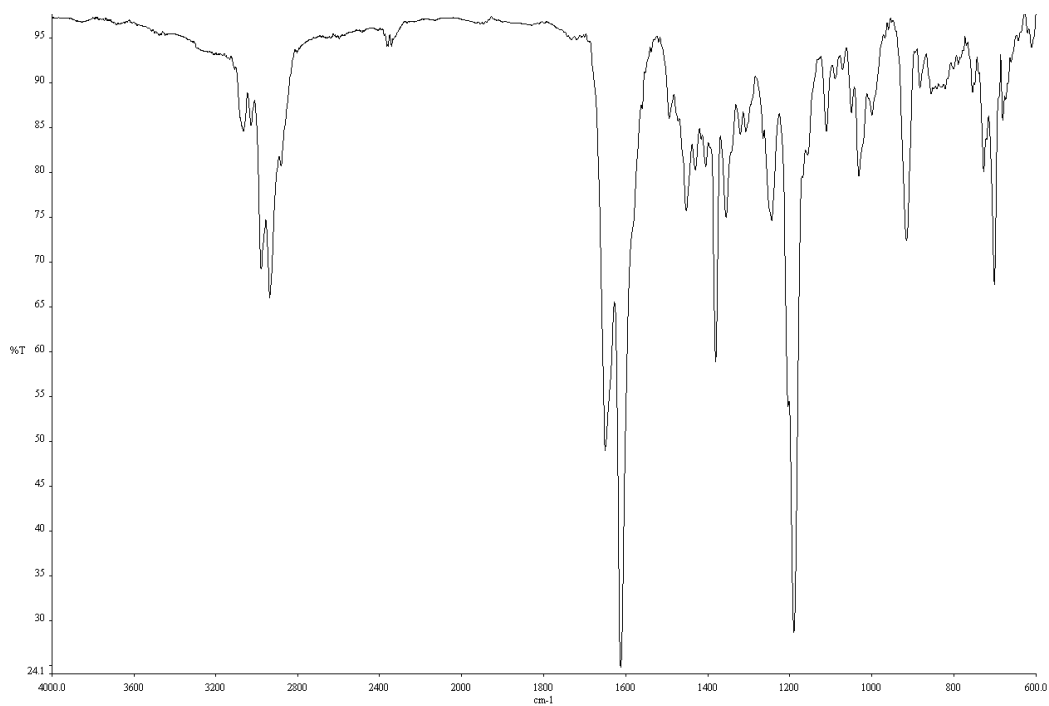
Figure A3.14. *Infrared spectrum (Thin Film, NaCl) of compound* **160e**.
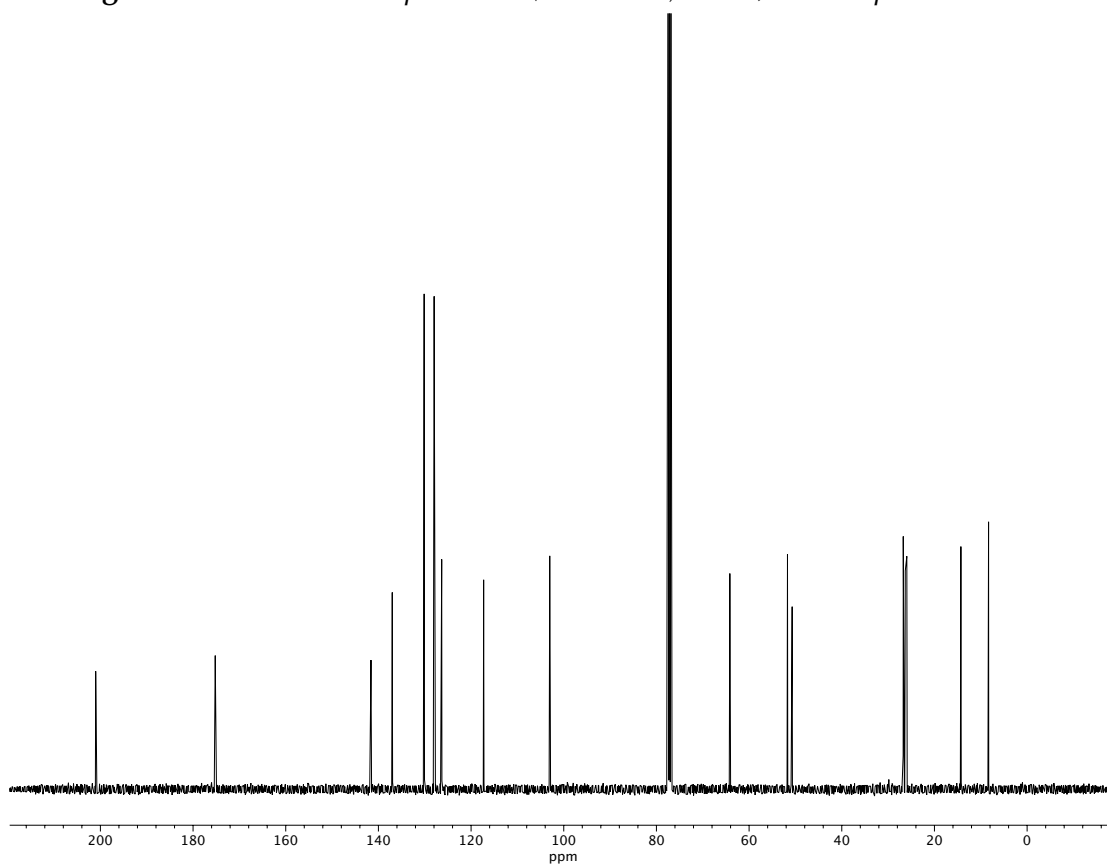
Figure A3.15. ^{13}*C NMR (100 MHz, CDCl$_3$) of compound* **160e**.
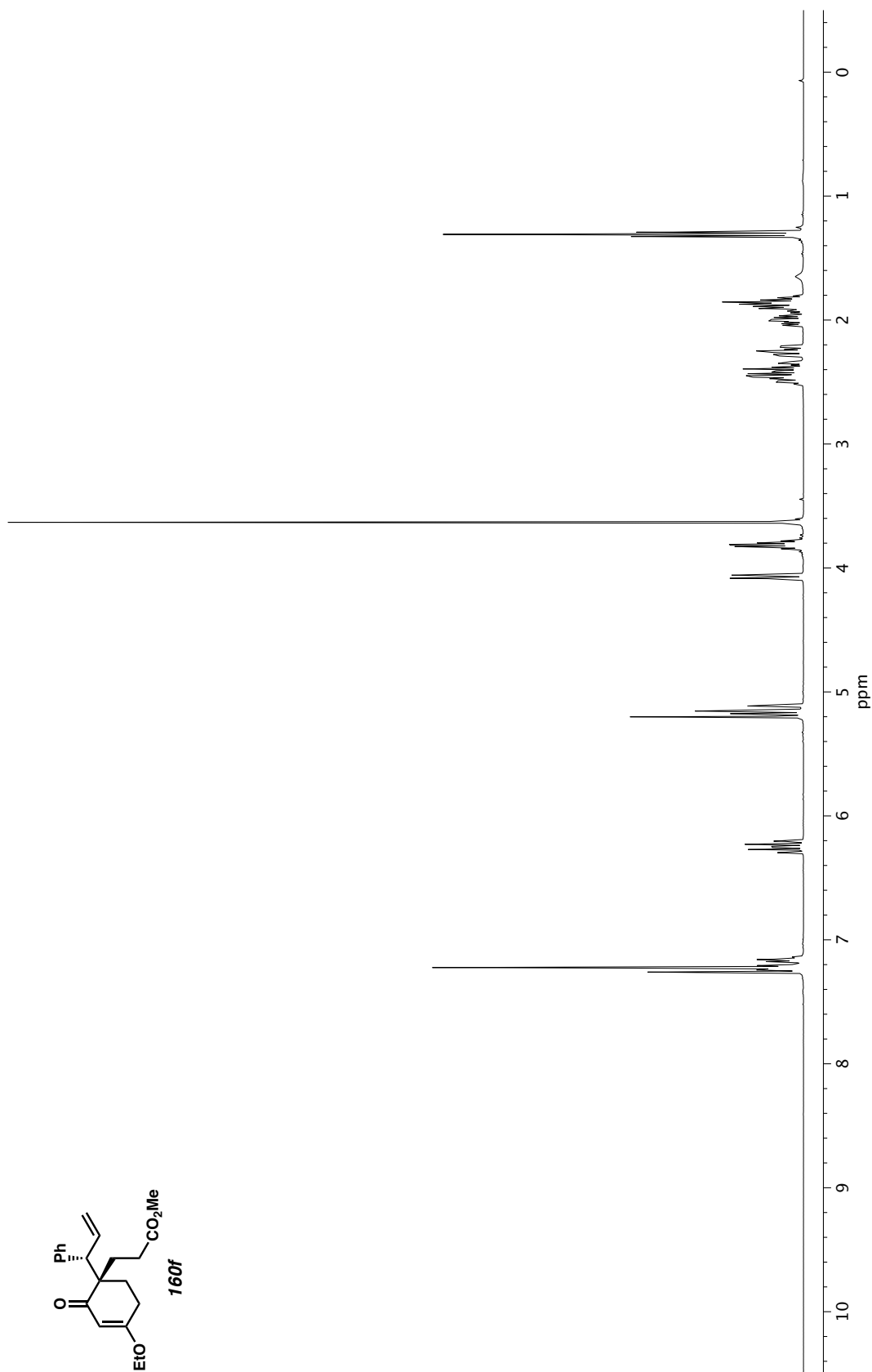
Figure A3.16. ^1H NMR (400 MHz, CDCl$_3$) of compound **160f**.
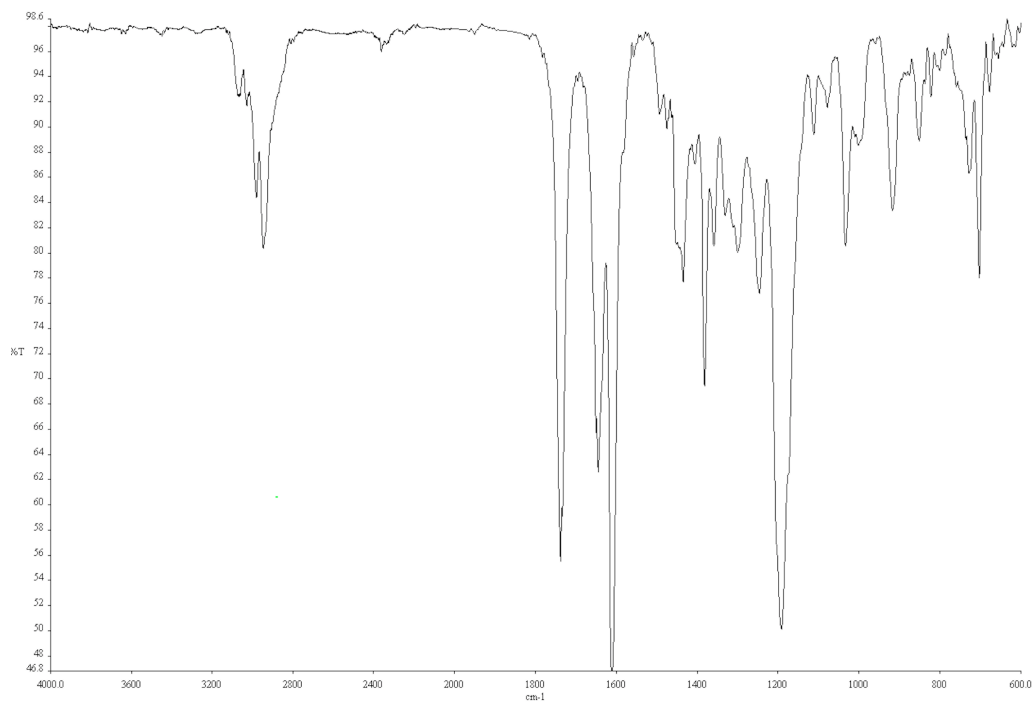
Figure A3.17. *Infrared spectrum (Thin Film, NaCl) of compound **160f**.*
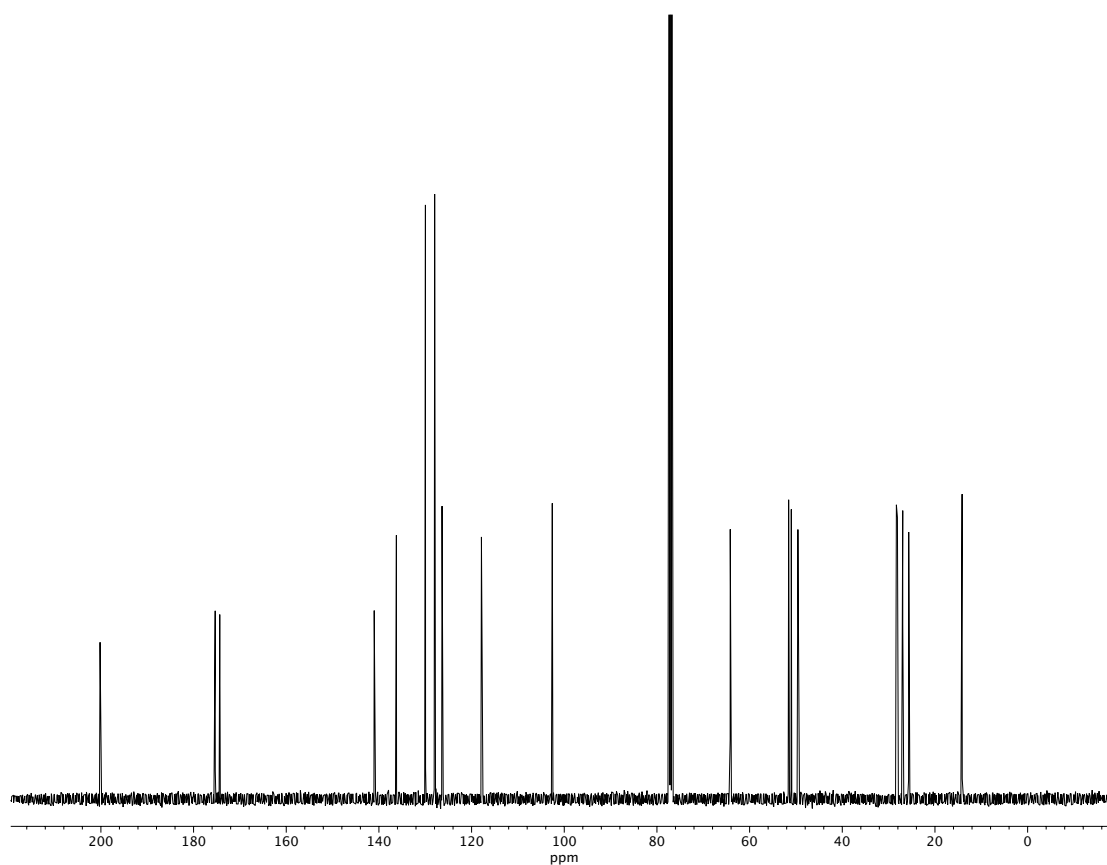
Figure A3.18. *^{13}C NMR (100 MHz, CDCl$_3$) of compound **160f**.*

Figure A3.19. ^1H NMR (400 MHz, CDCl$_3$) of compound **160g**.
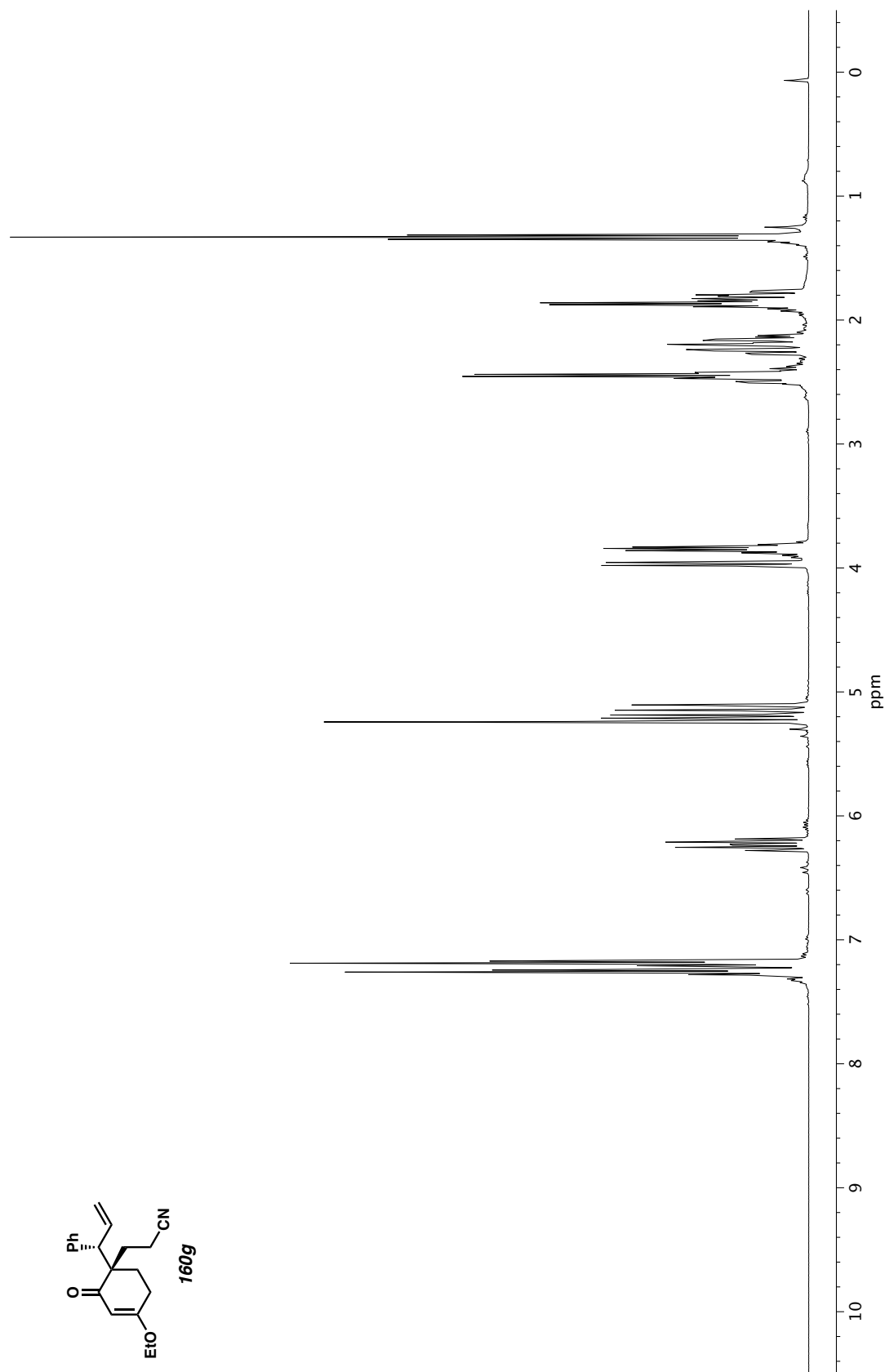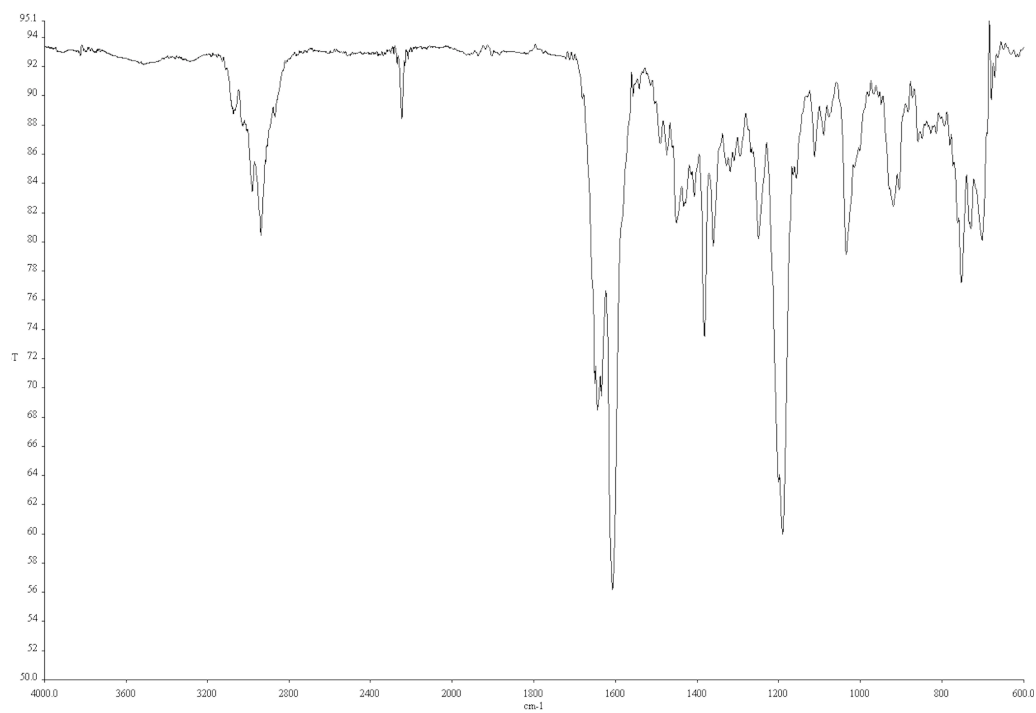
Figure A3.20. Infrared spectrum (Thin Film, NaCl) of compound **160g**.
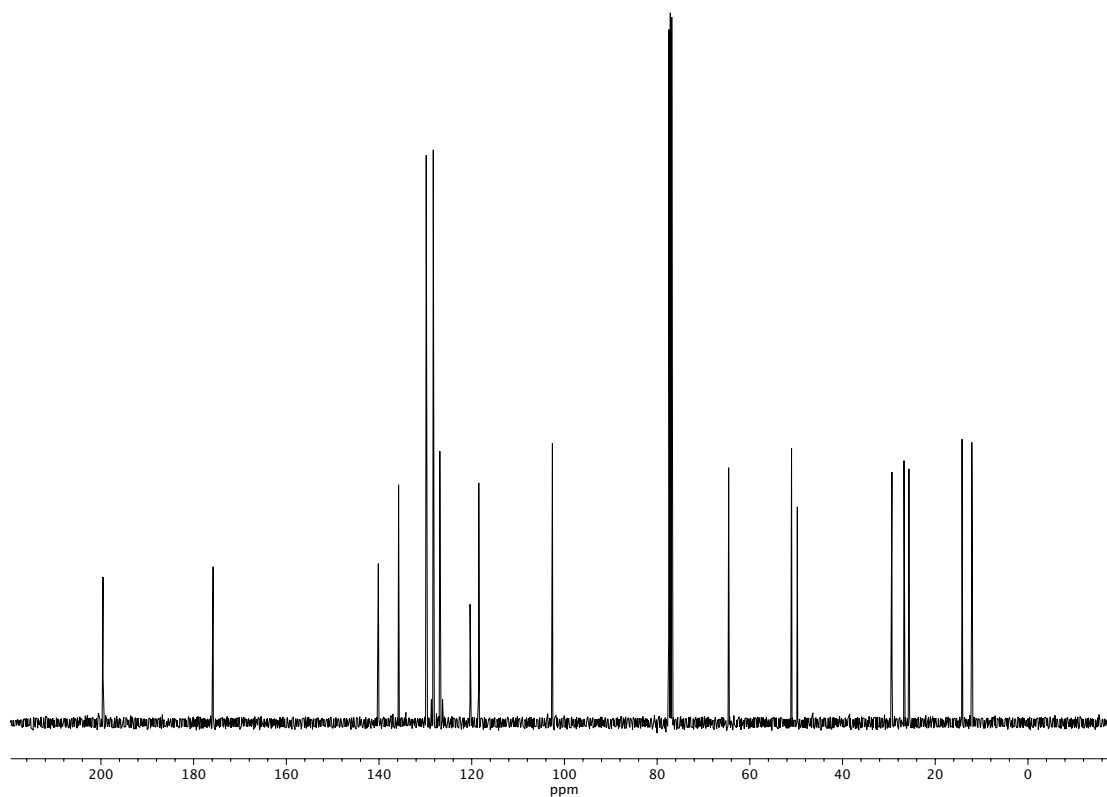
Figure A3.21. ^{13}C NMR (100 MHz, CDCl$_3$) of compound **160g**.
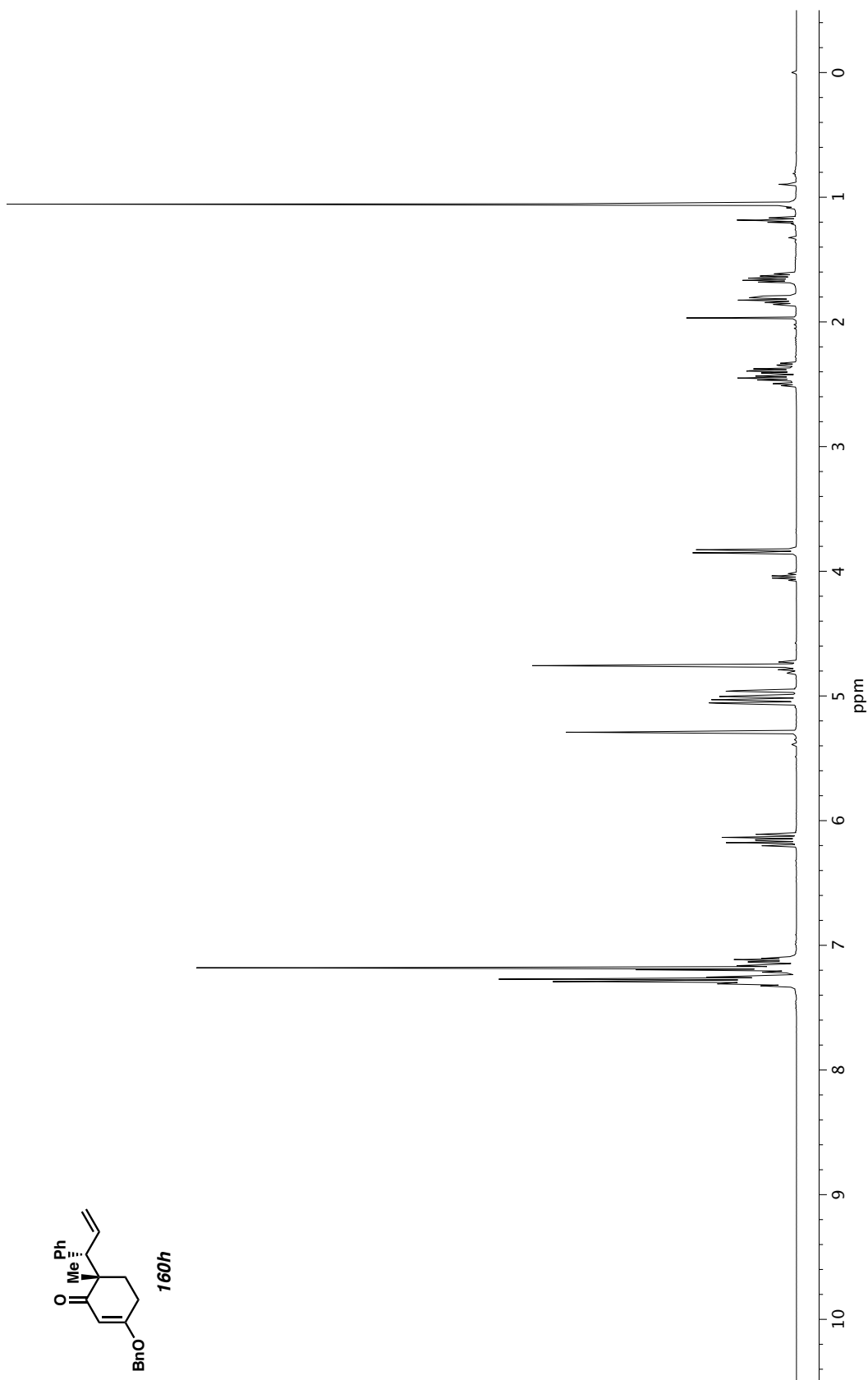
Figure A3.22. ^1H NMR (400 MHz, CDCl$_3$) of compound *160h*.
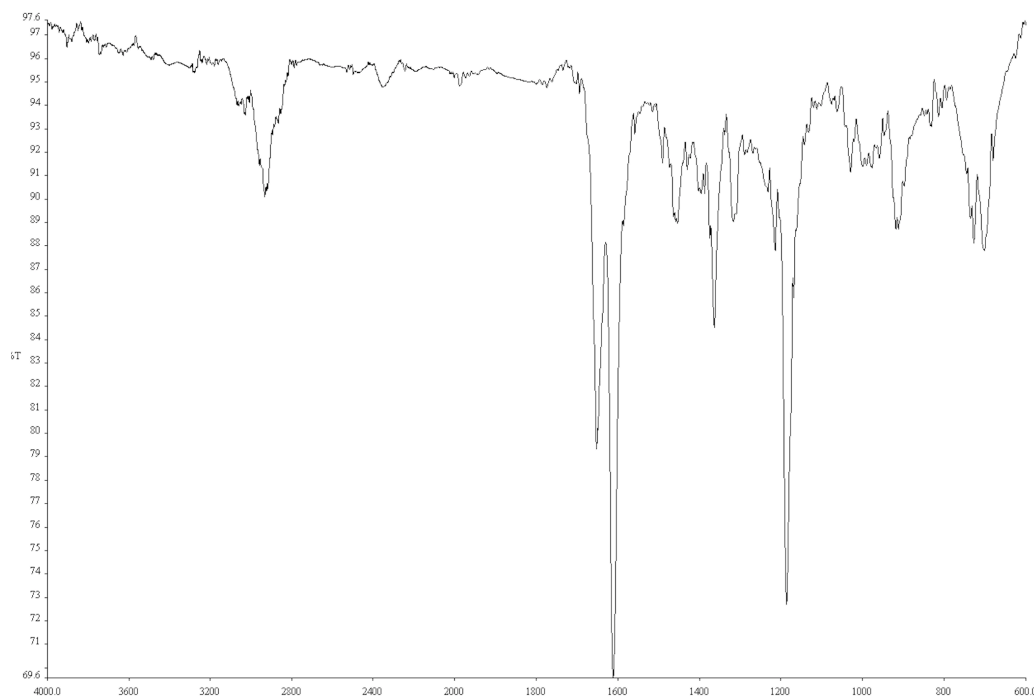
Figure A3.23. *Infrared spectrum (Thin Film, NaCl) of compound* **160h**.
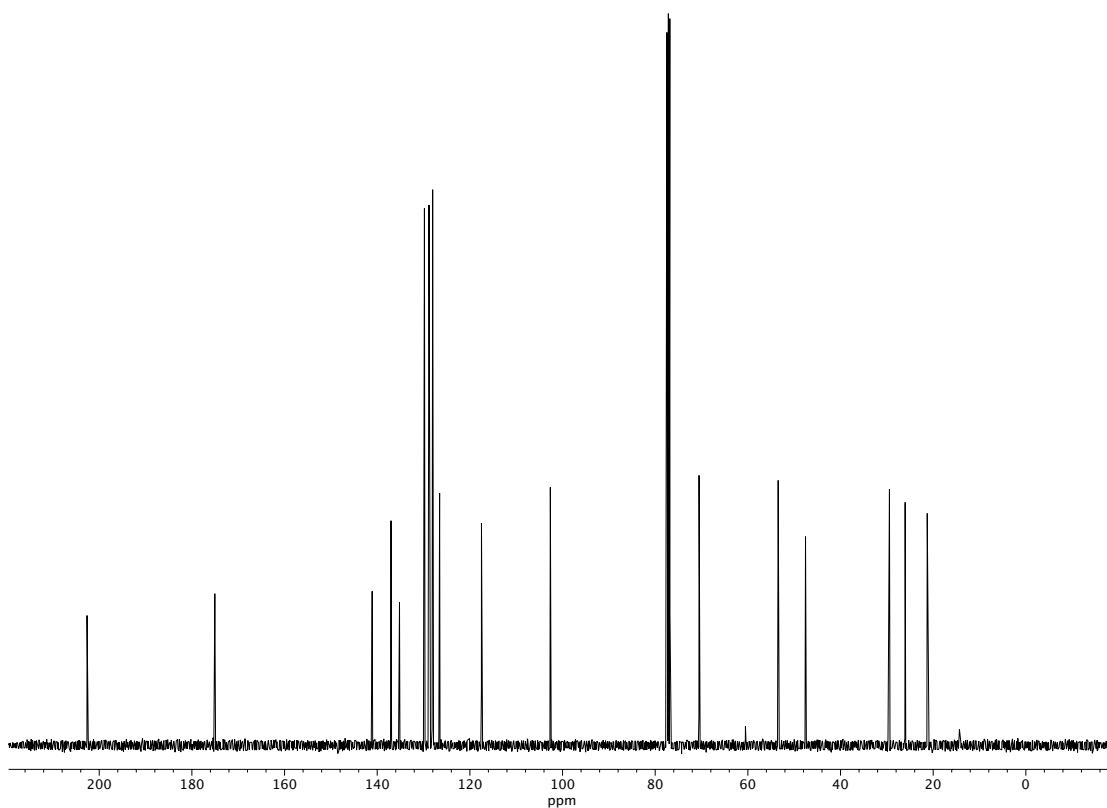
Figure A3.24. *¹³C NMR (100 MHz, CDCl₃) of compound* **160h**.

Figure A3.25. ^1H NMR (400 MHz, CDCl$_3$) of compound **160i**.
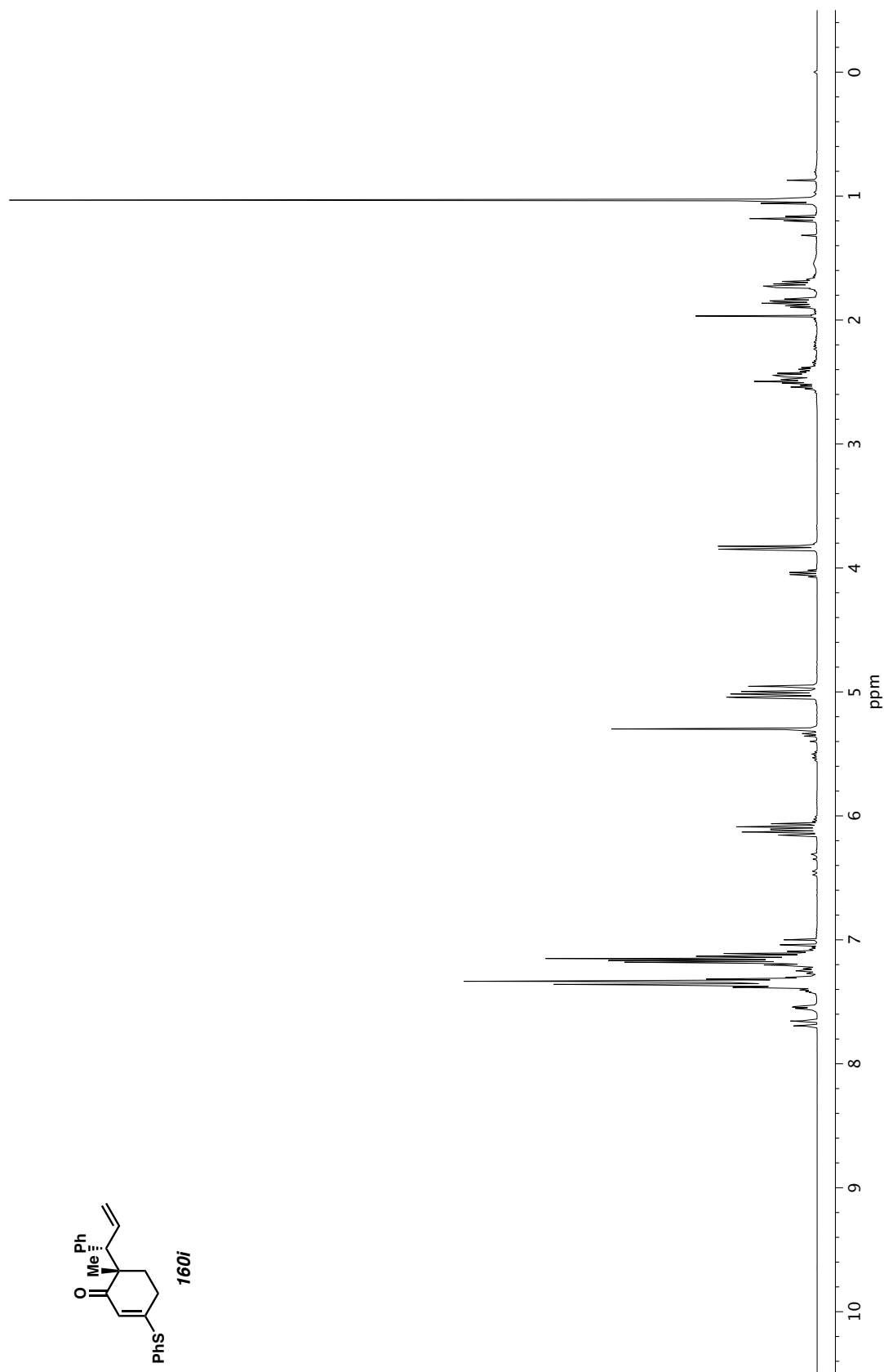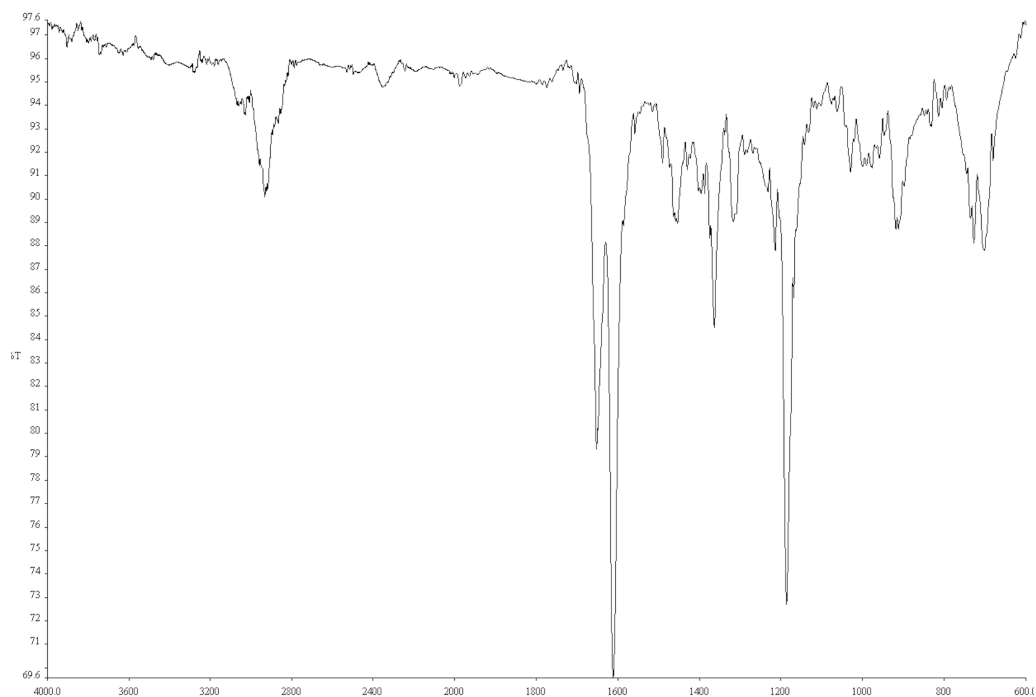
Figure A3.26. Infrared spectrum (Thin Film, NaCl) of compound **160i**.
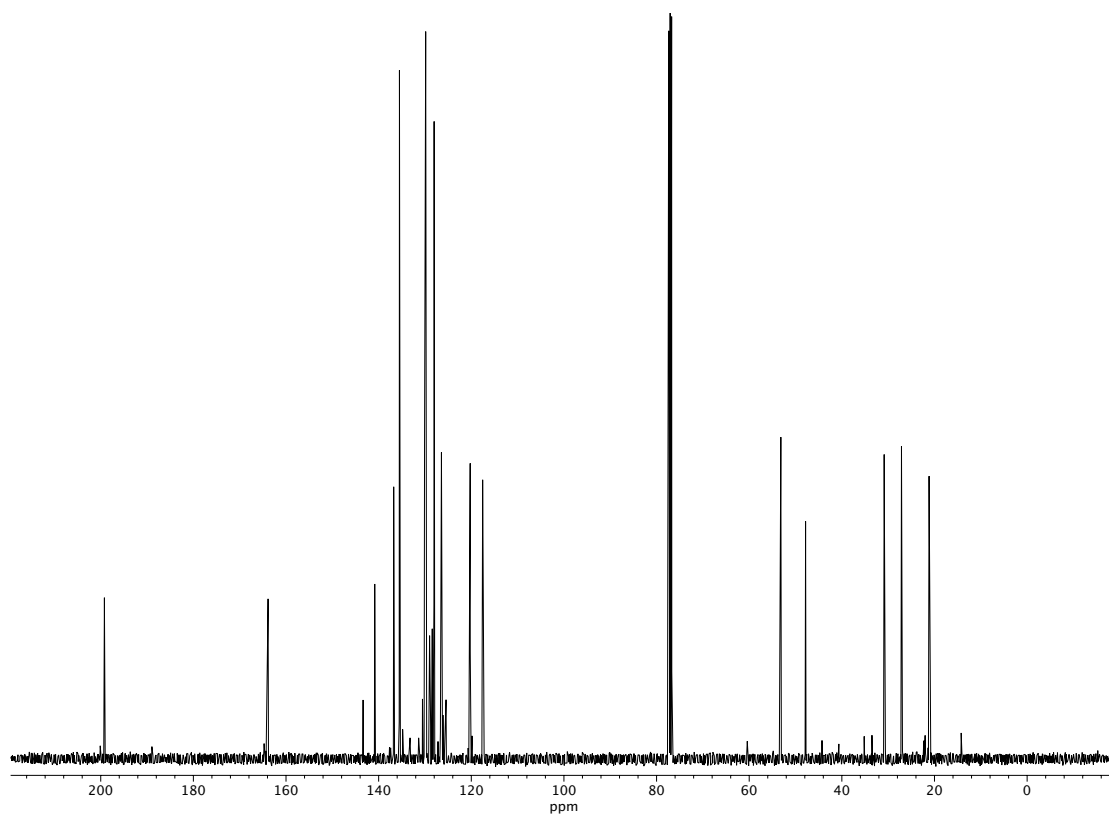
Figure A3.27. ^{13}C NMR (100 MHz, CDCl$_3$) of compound **160i**.
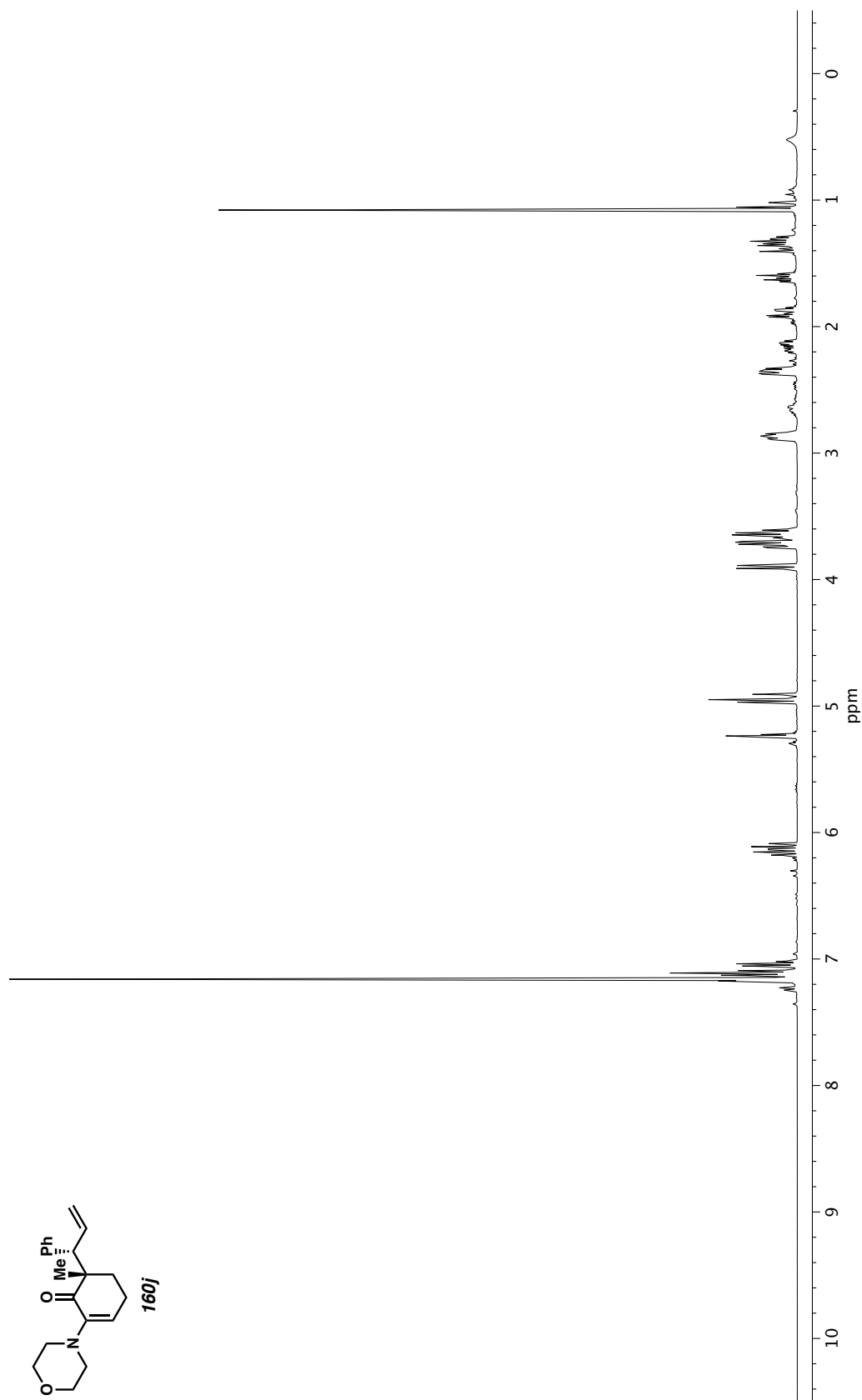
Figure A3.28. ^1H NMR (400 MHz, C_6D_6) of compound *160j*.
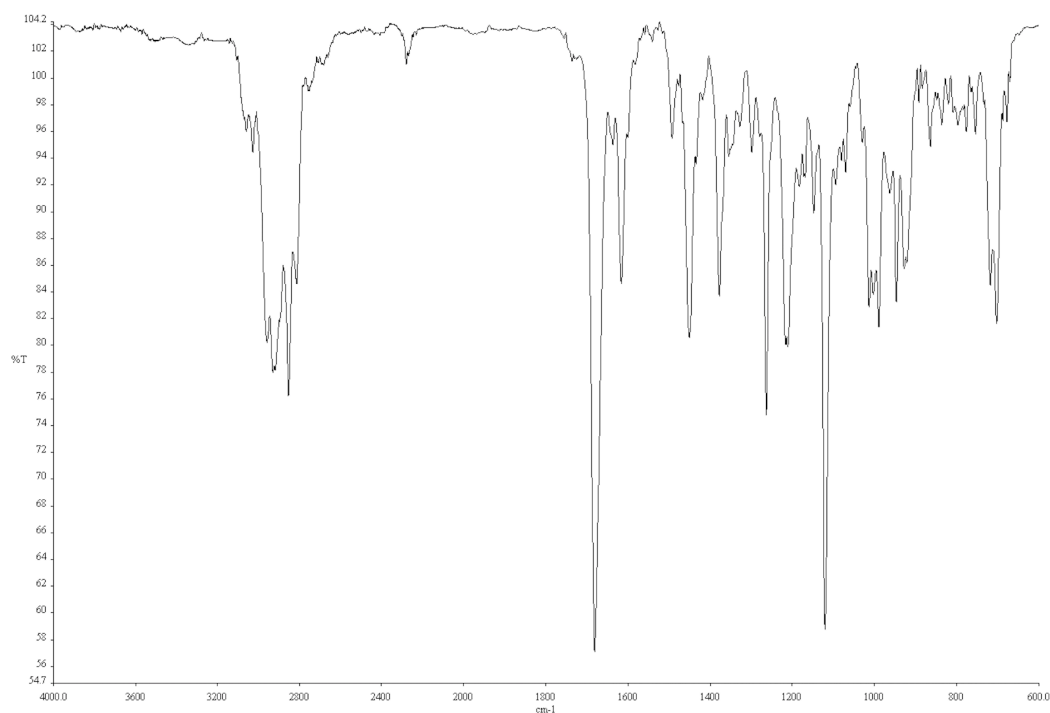
Figure A3.29. *Infrared spectrum (Thin Film, NaCl) of compound **160j**.*
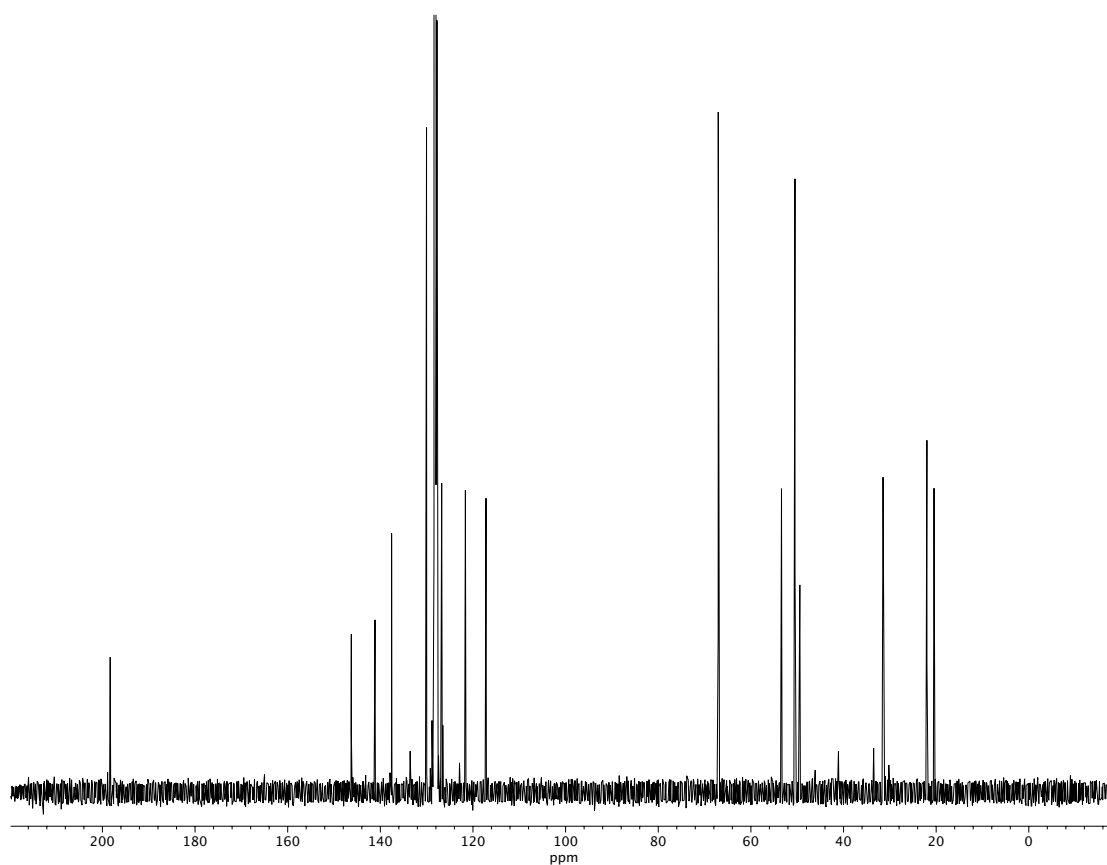
Figure A3.30. ^{13}C *NMR (100 MHz, C_6D_6) of compound **160j**.*

Figure A3.28. ^1H NMR (400 MHz, CDCl$_3$) of compound **160k**.
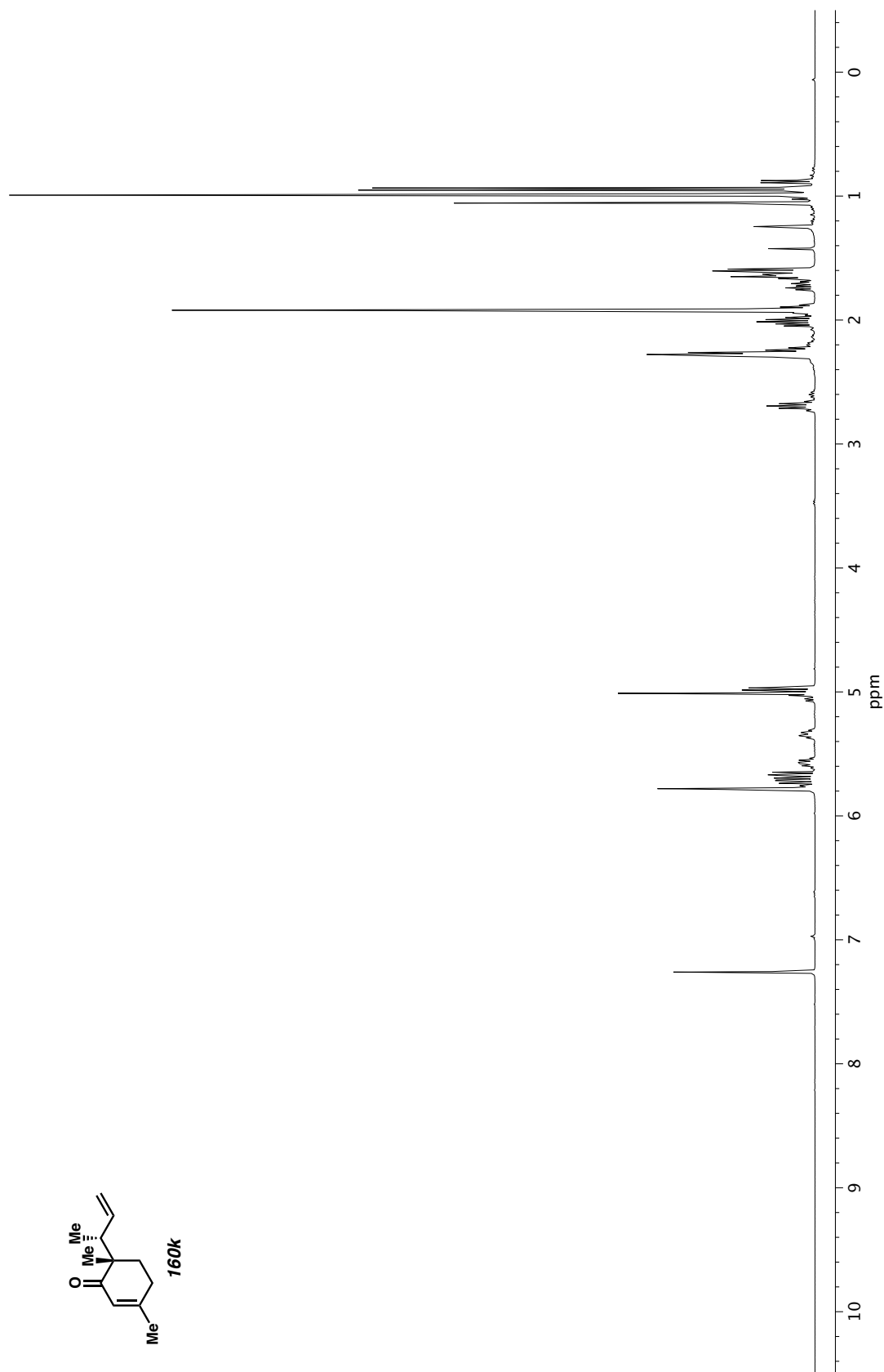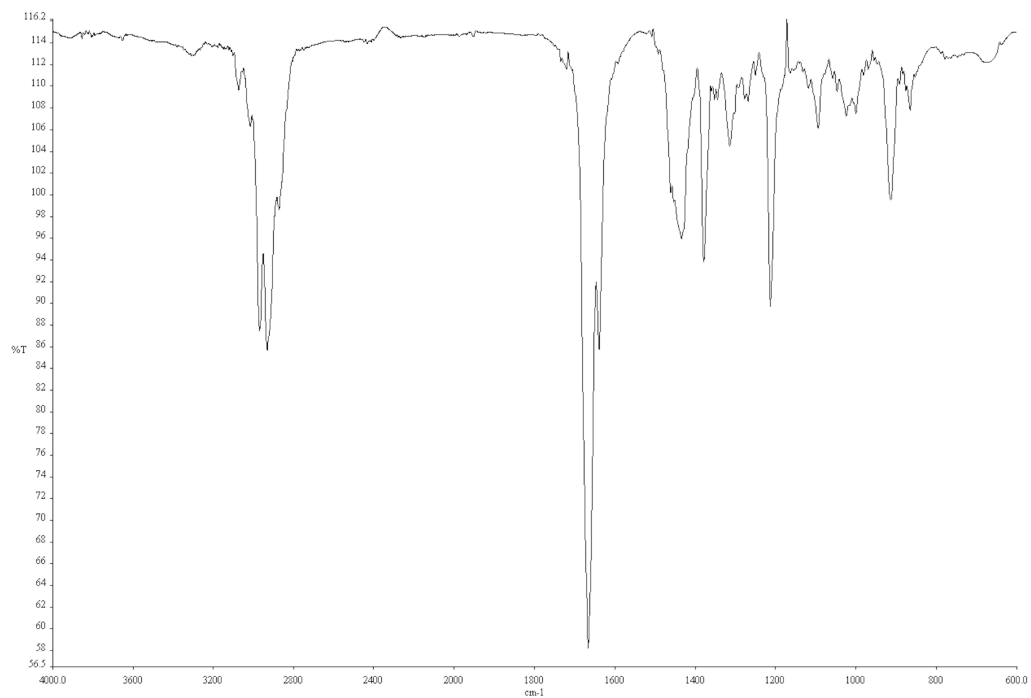
Figure A3.32. *Infrared spectrum (Thin Film, NaCl) of compound* **160k***.*
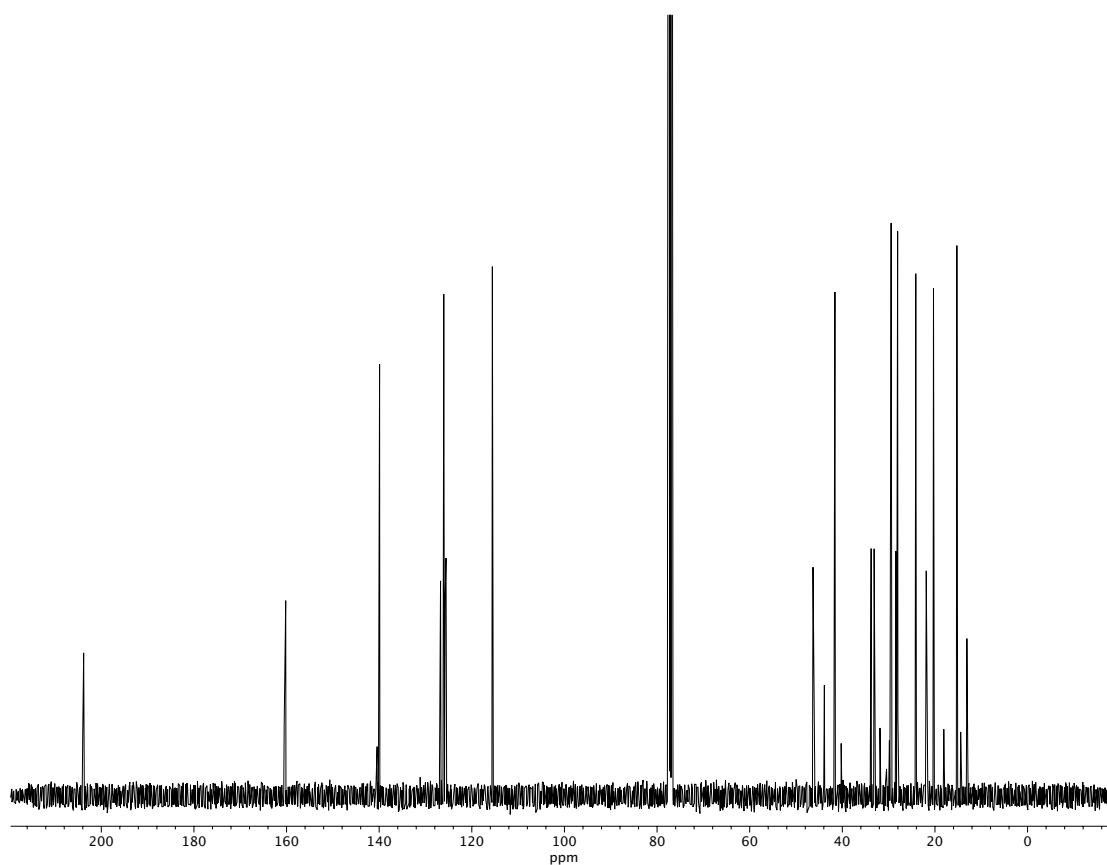
Figure A3.33. ^{13}C *NMR (100 MHz, CDCl$_3$) of compound* **160k***.*
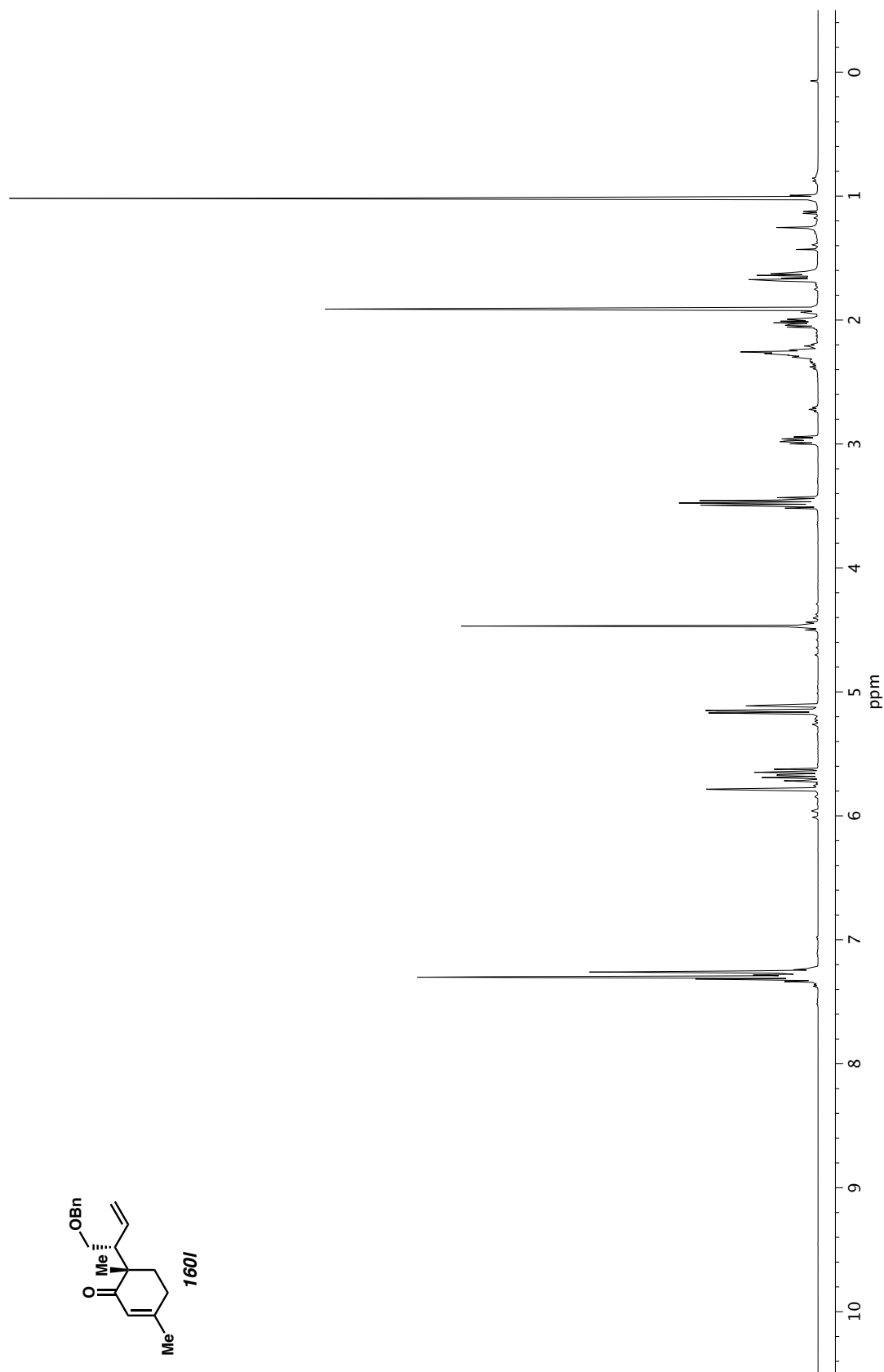
Figure A3.34. ^1H NMR (400 MHz, CDCl$_3$) of compound **160l**.
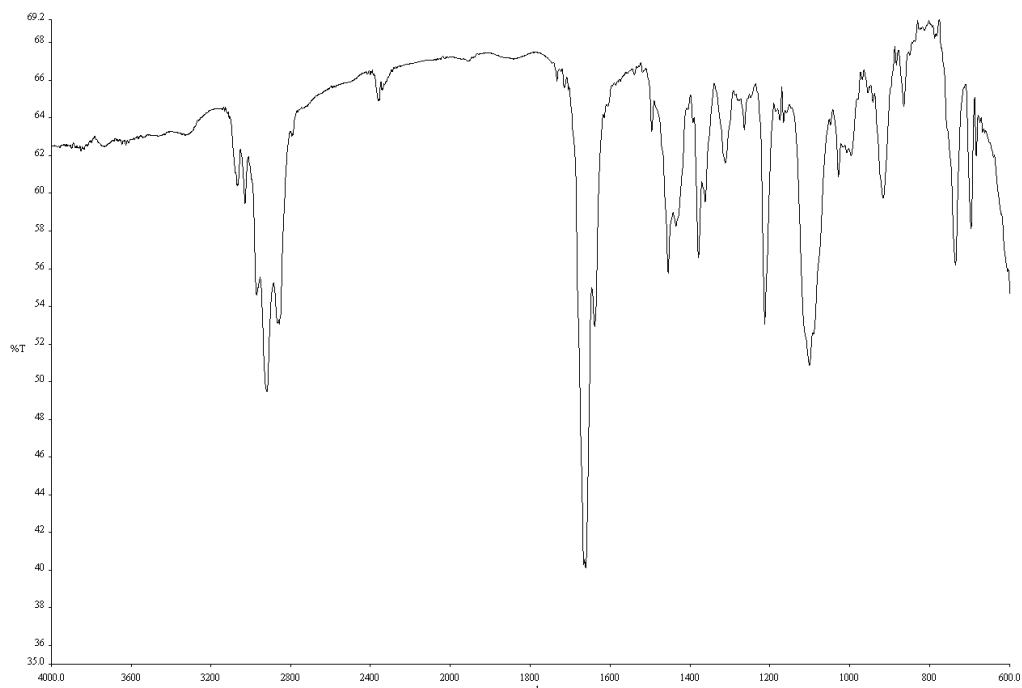
Figure A3.35. *Infrared spectrum (Thin Film, NaCl) of compound **160l**.*
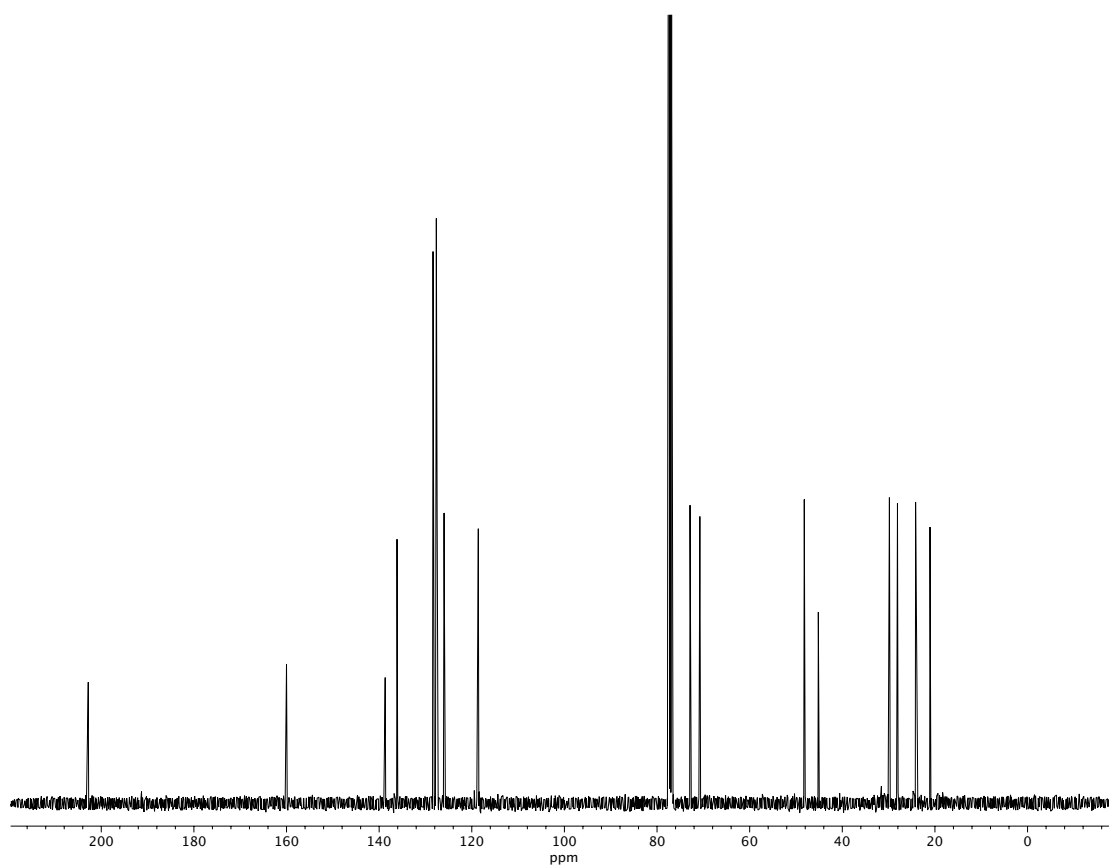
Figure A3.36. ^{13}C *NMR (100 MHz, CDCl$_3$) of compound **160l**.*
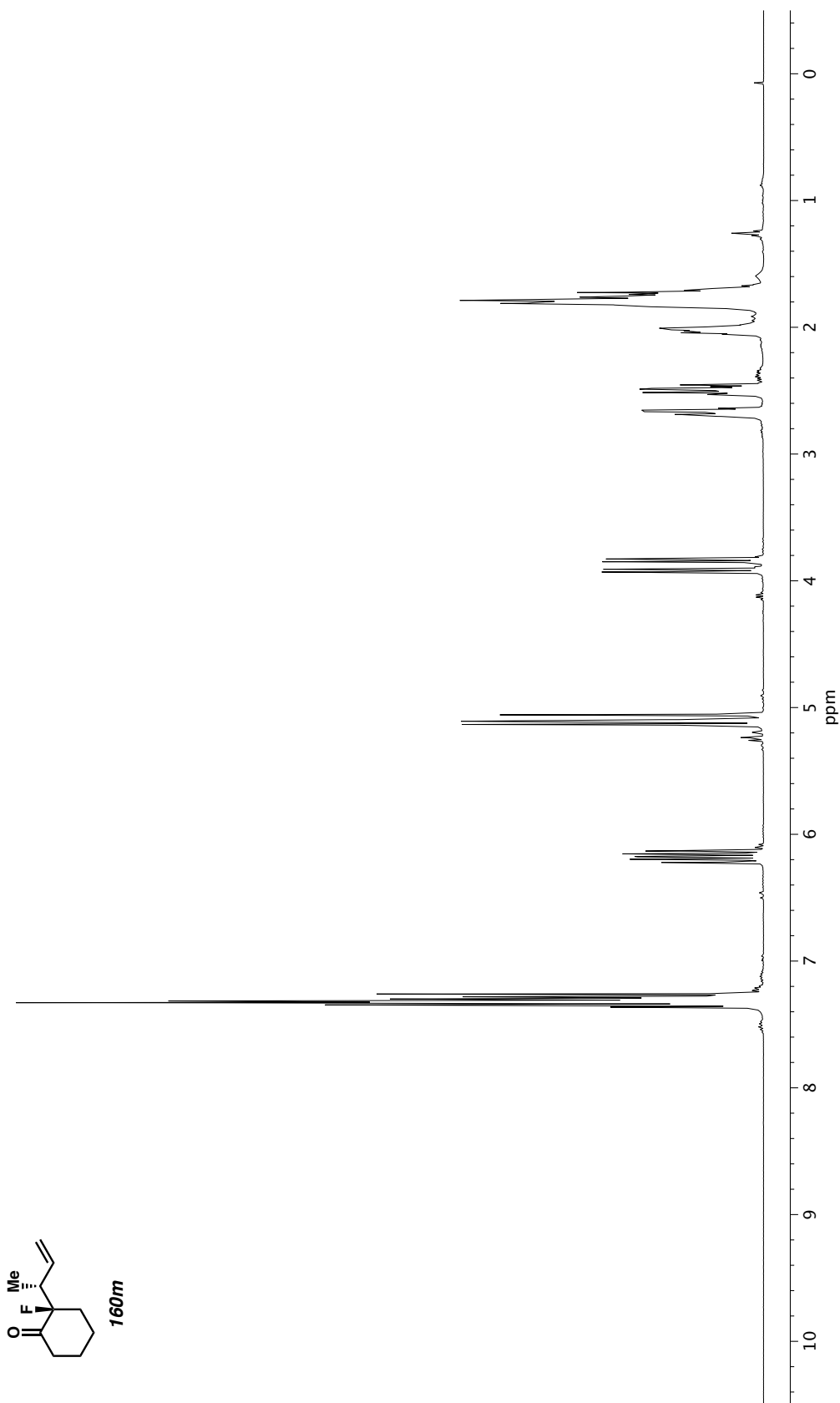
Figure A3.37. *^1H NMR (400 MHz, CDCl$_3$) of compound **160m**.*
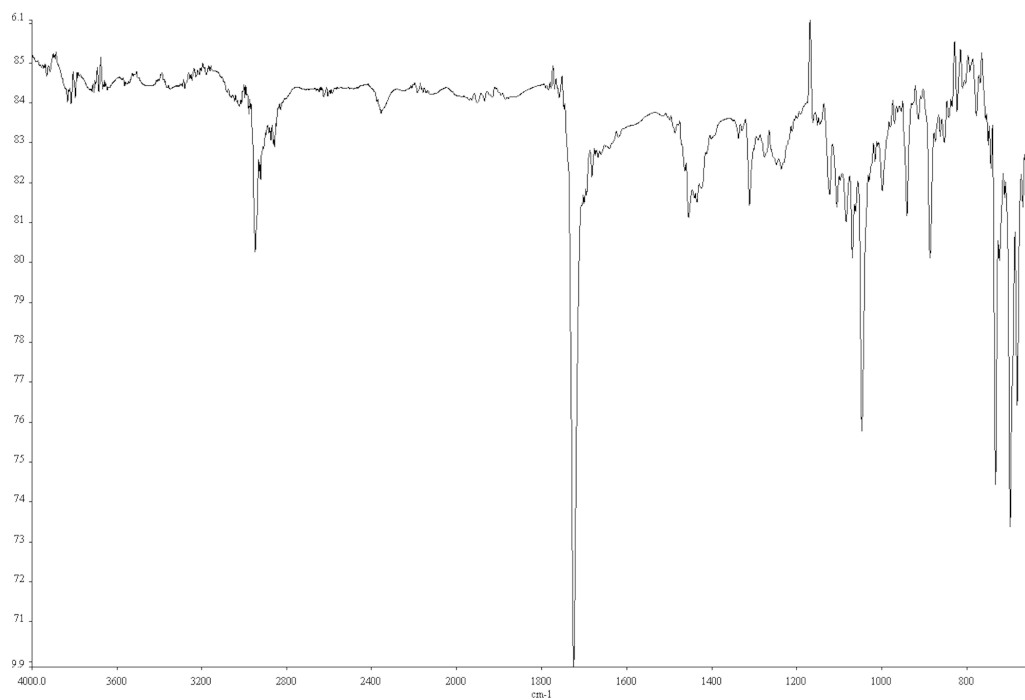
Figure A3.38. Infrared spectrum (Thin Film, NaCl) of compound **160m**.
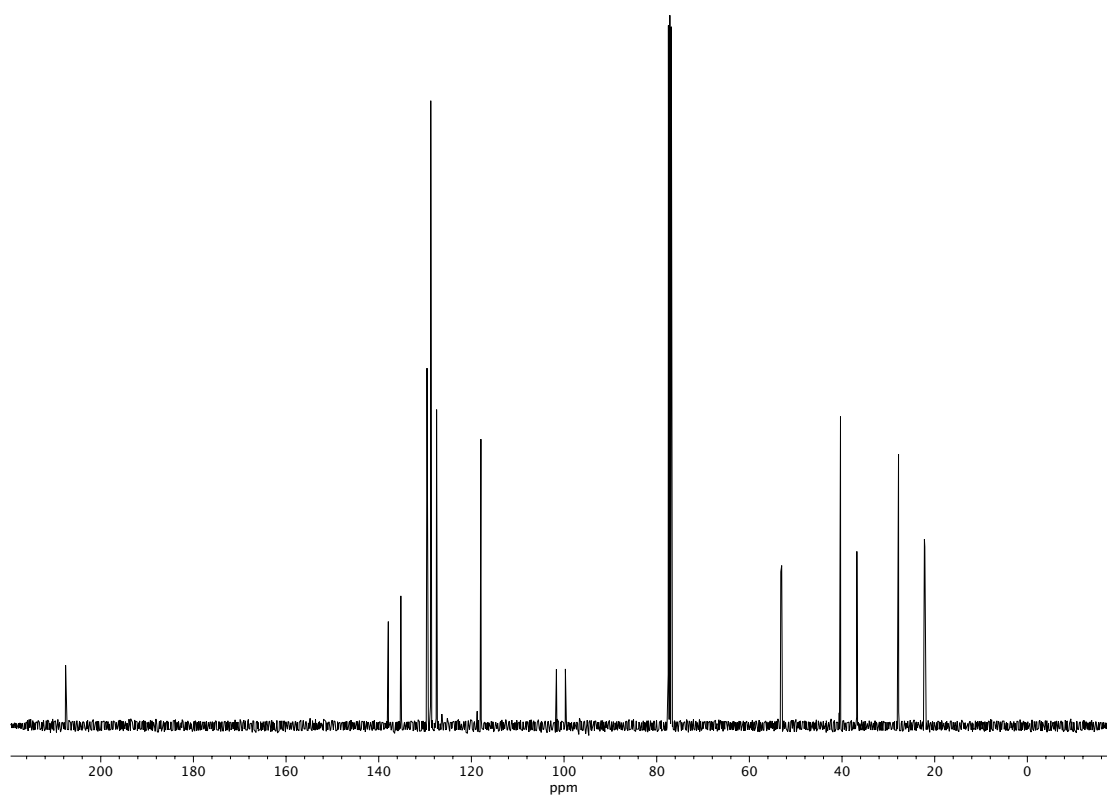
Figure A3.39. ^{13}C NMR (100 MHz, CDCl$_3$) of compound **160m**.
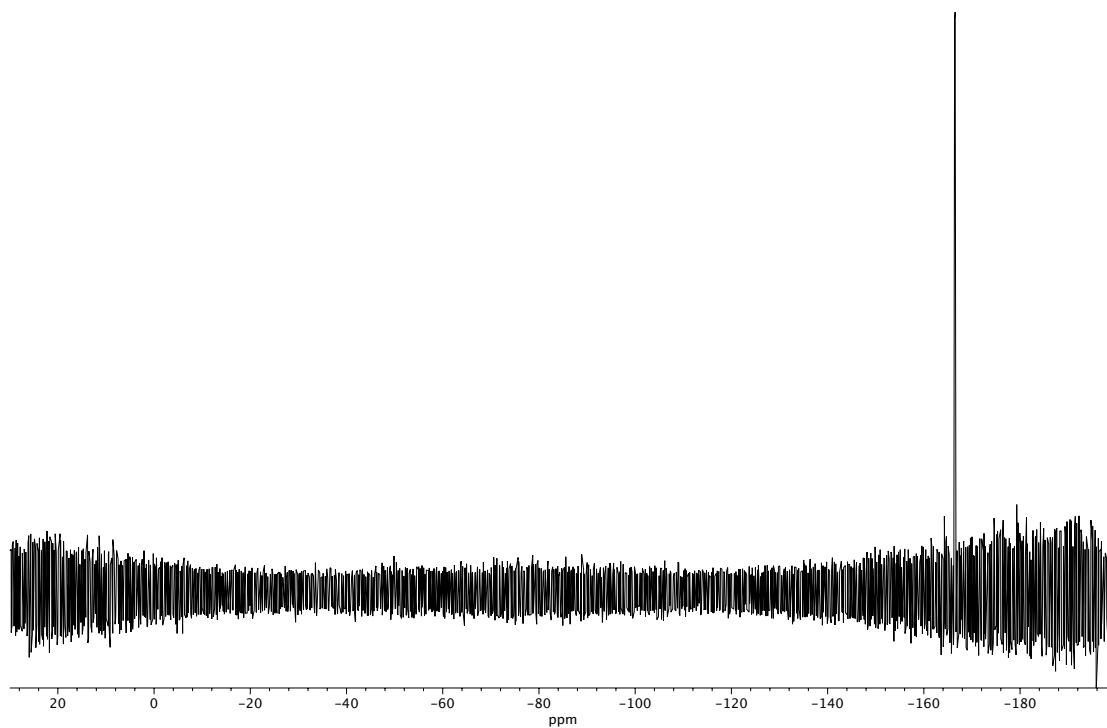
Figure A3.40. ^{19}F NMR (282 MHz, CDCl$_3$) of compound **160m**.
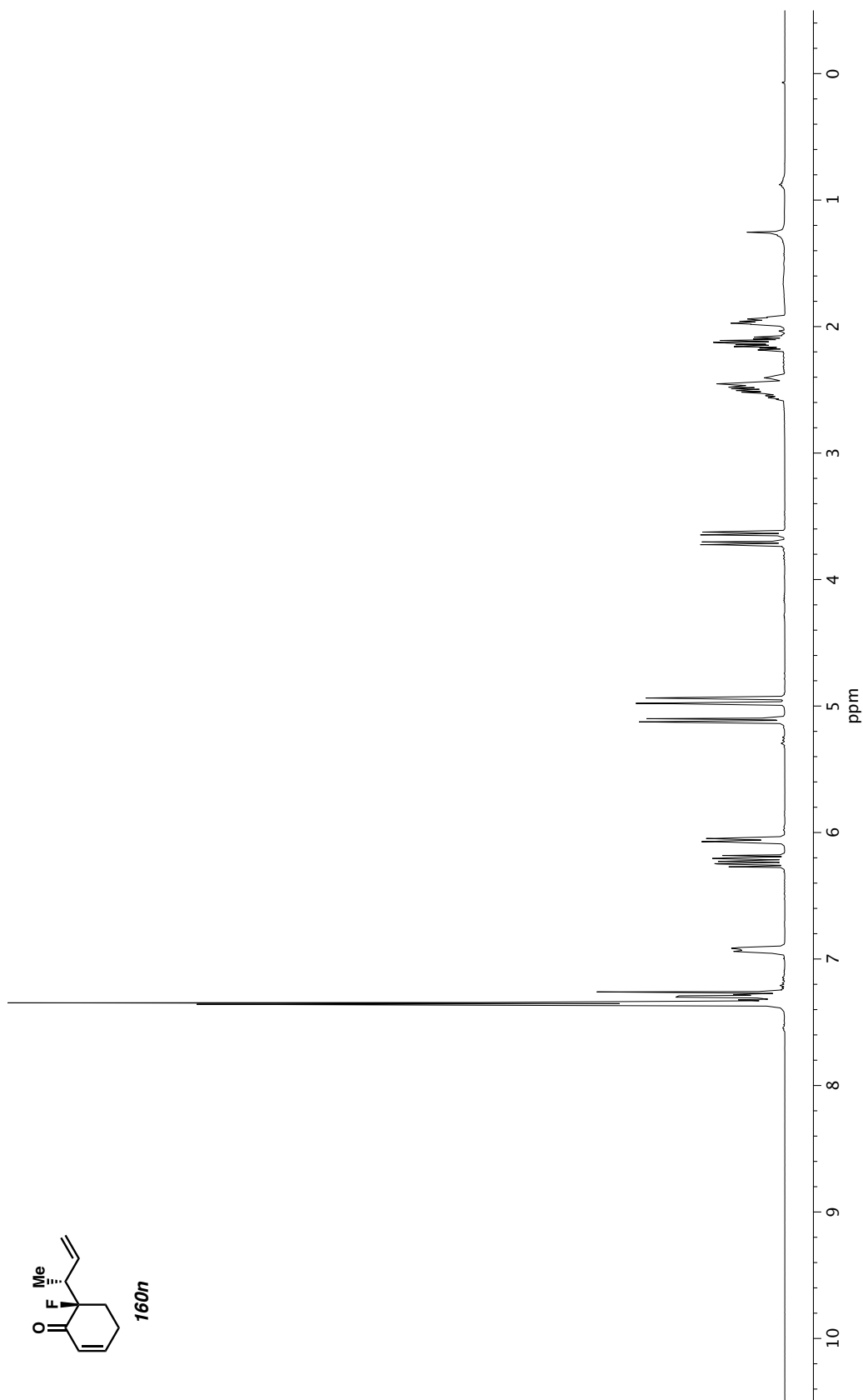
Figure A3.41. *^{1}H NMR (400 MHz, CDCl$_3$) of compound **160n**.*
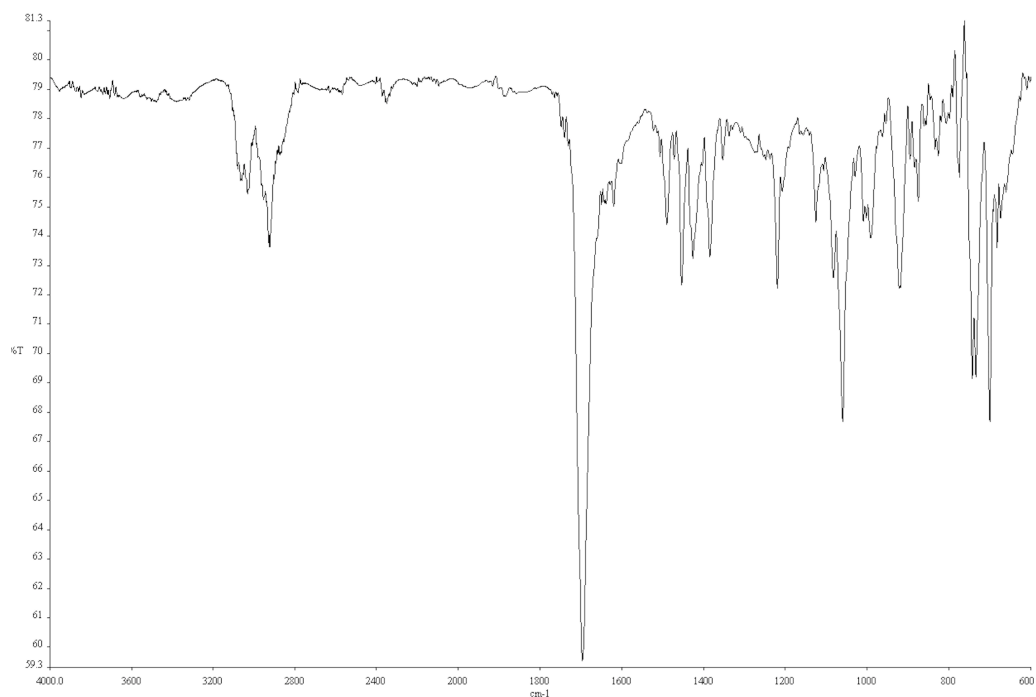
Figure A3.42. *Infrared spectrum (Thin Film, NaCl) of compound **160n**.*
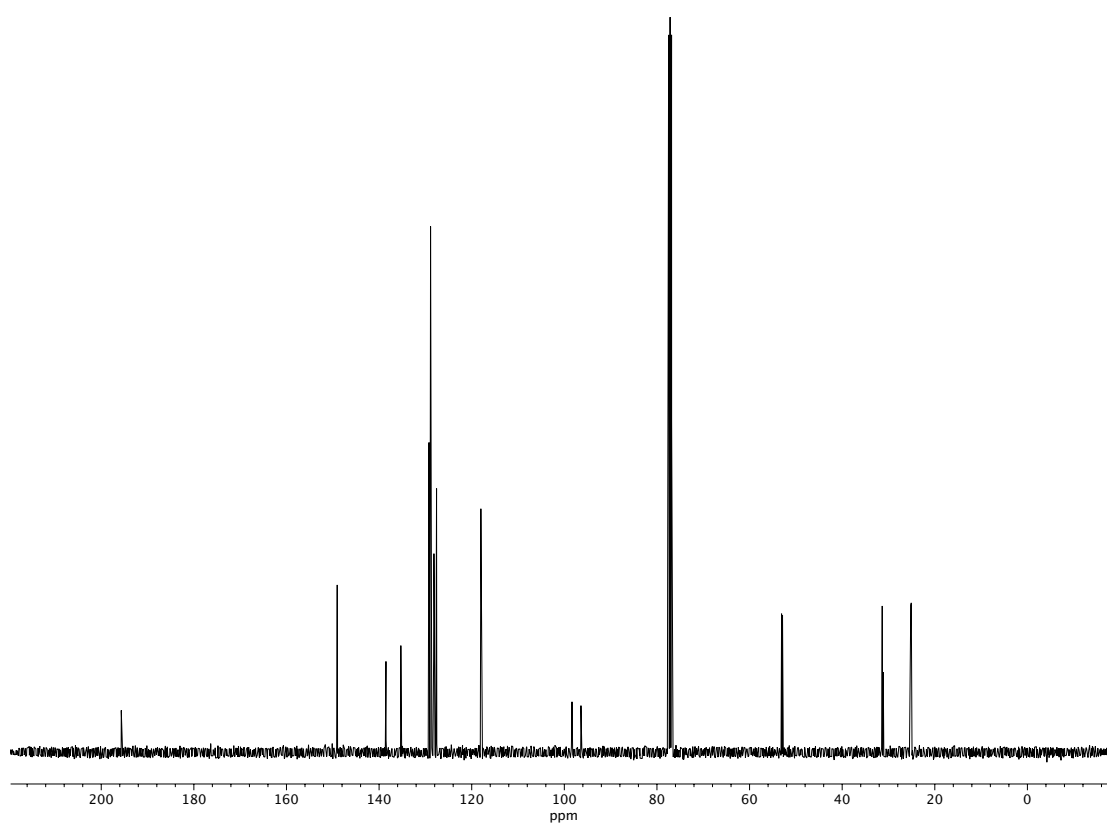
Figure A3.43. *^{13}C NMR (100 MHz, CDCl$_3$) of compound **160n**.*
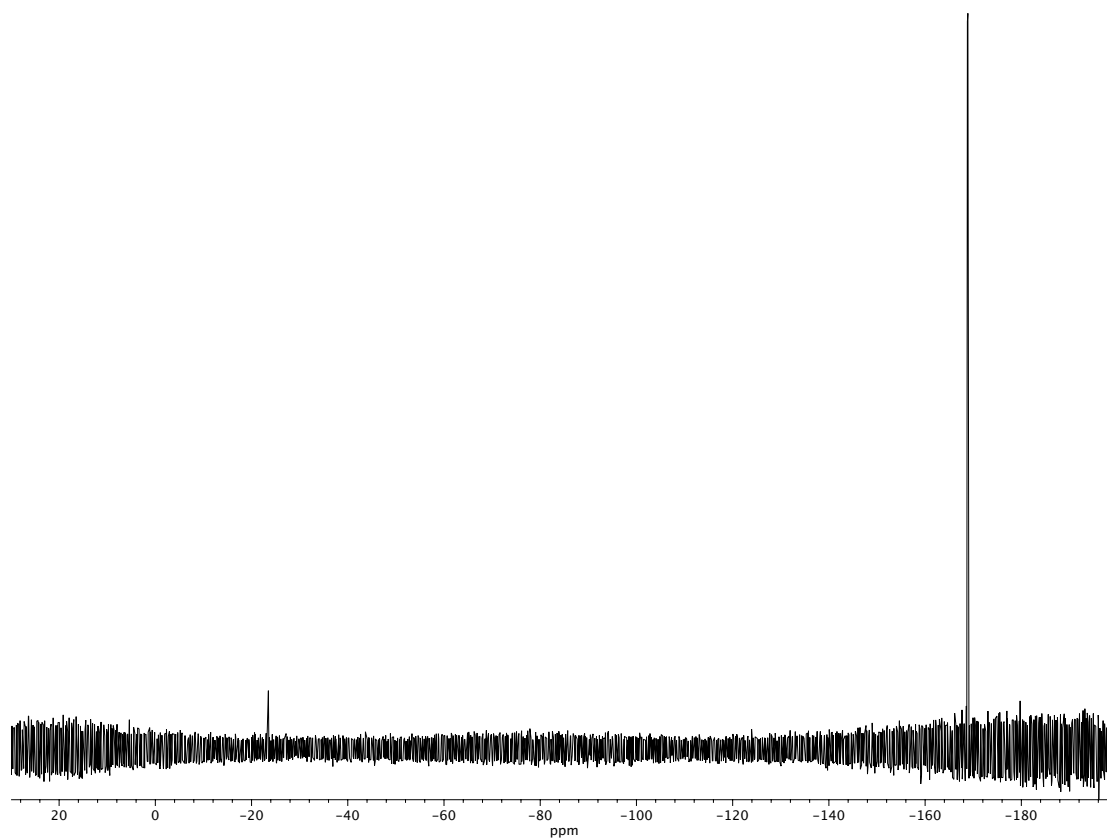
Figure A3.44. *^{19}F NMR (282 MHz, CDCl$_3$) of compound **160n**.*
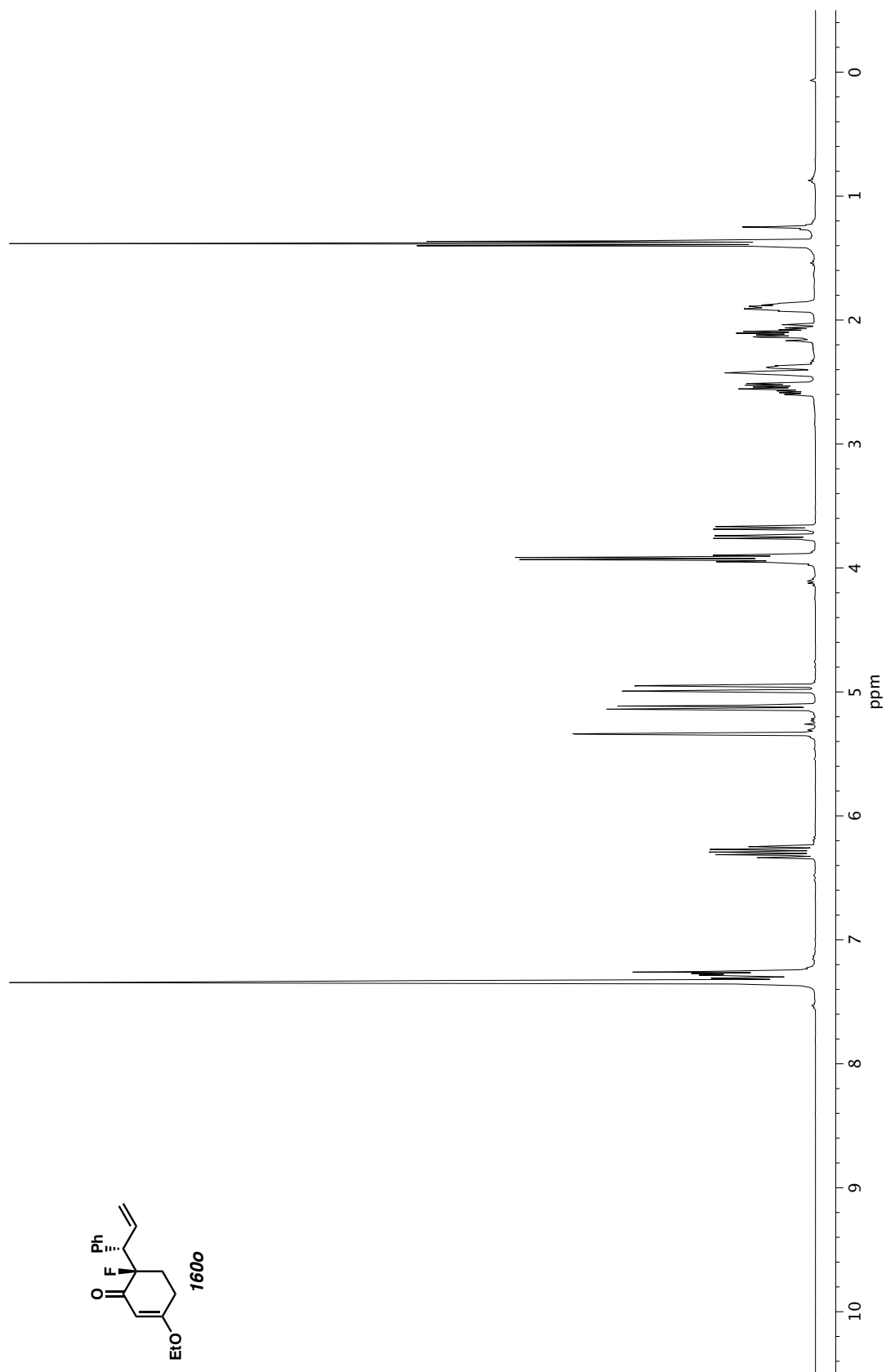
Figure A3.45. ^1H NMR (400 MHz, CDCl$_3$) of compound **160o**.
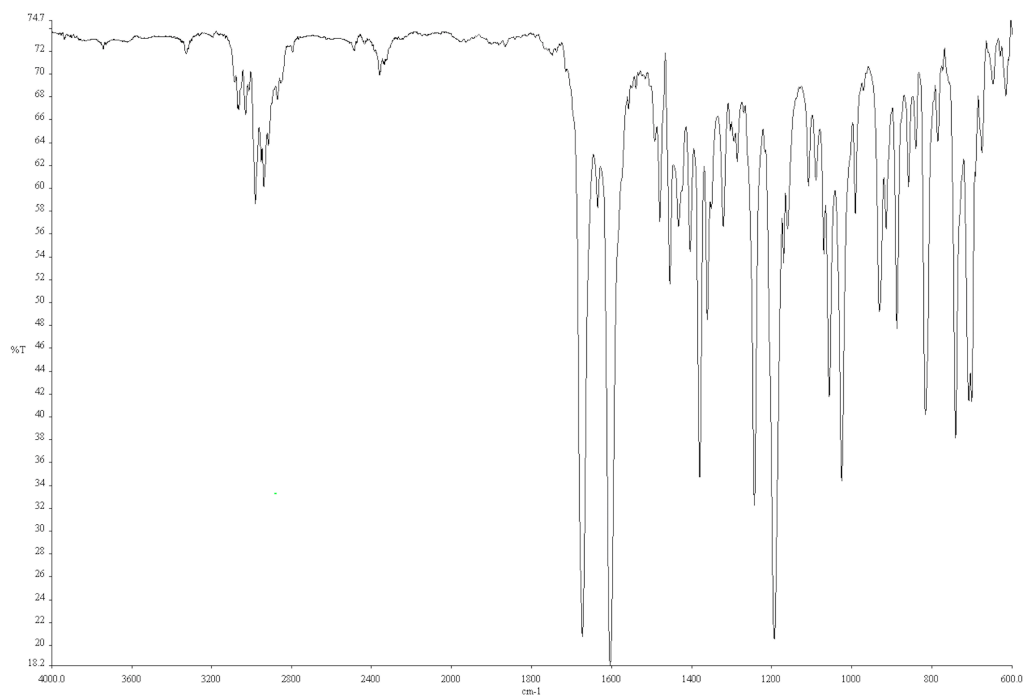
Figure A3.46. *Infrared spectrum (Thin Film, NaCl) of compound **160o**.*
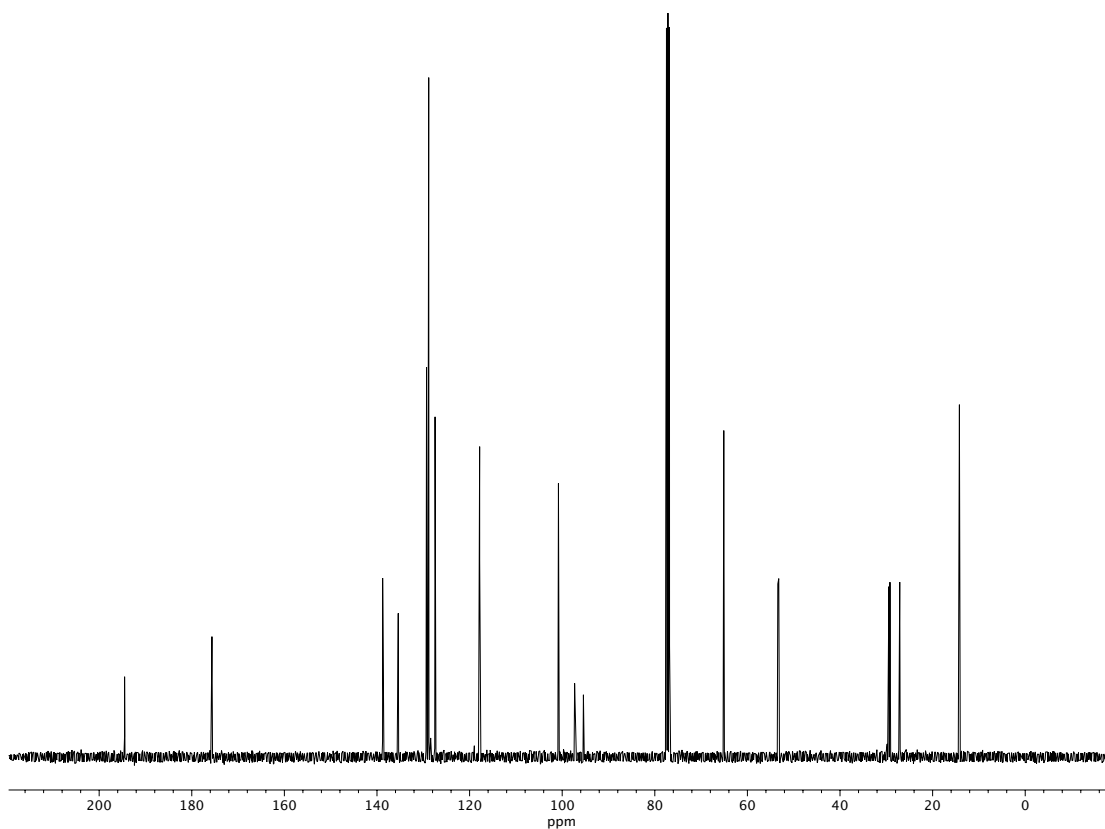
Figure A3.47. *^{13}C NMR (100 MHz, CDCl$_3$) of compound **160o**.*
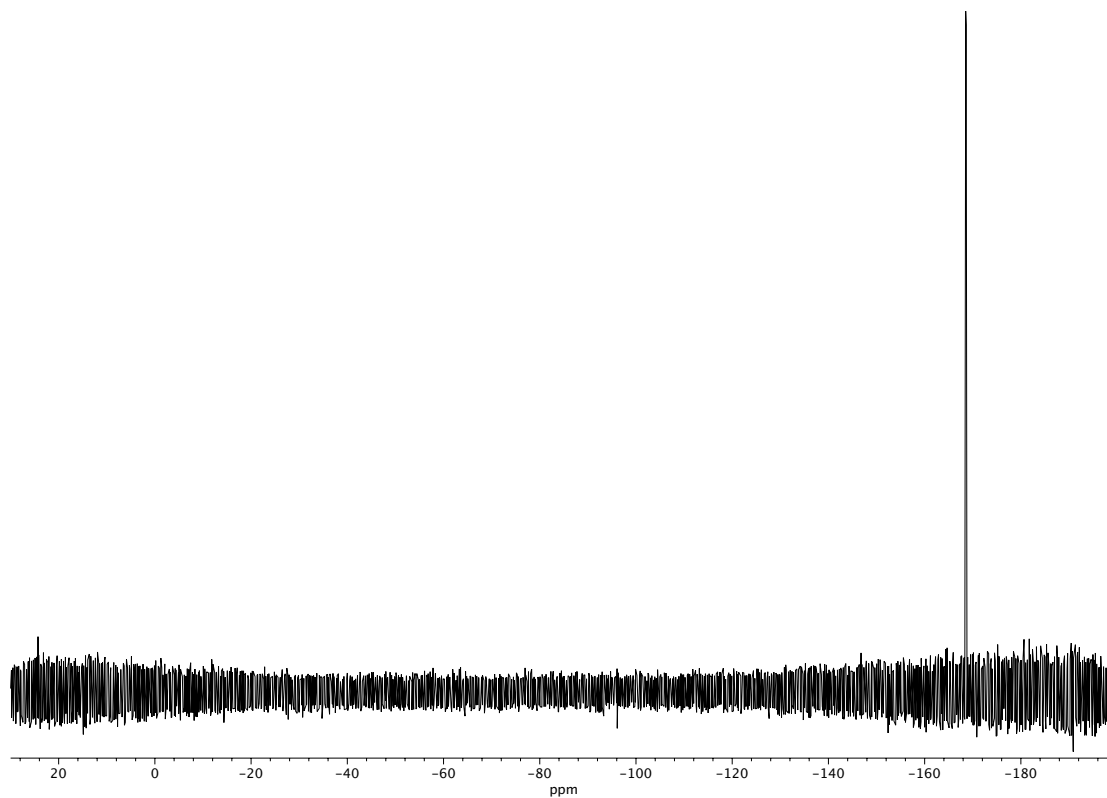
Figure A3.48. ^{19}F *NMR (282 MHz, CDCl$_3$) of compound* **160o**.
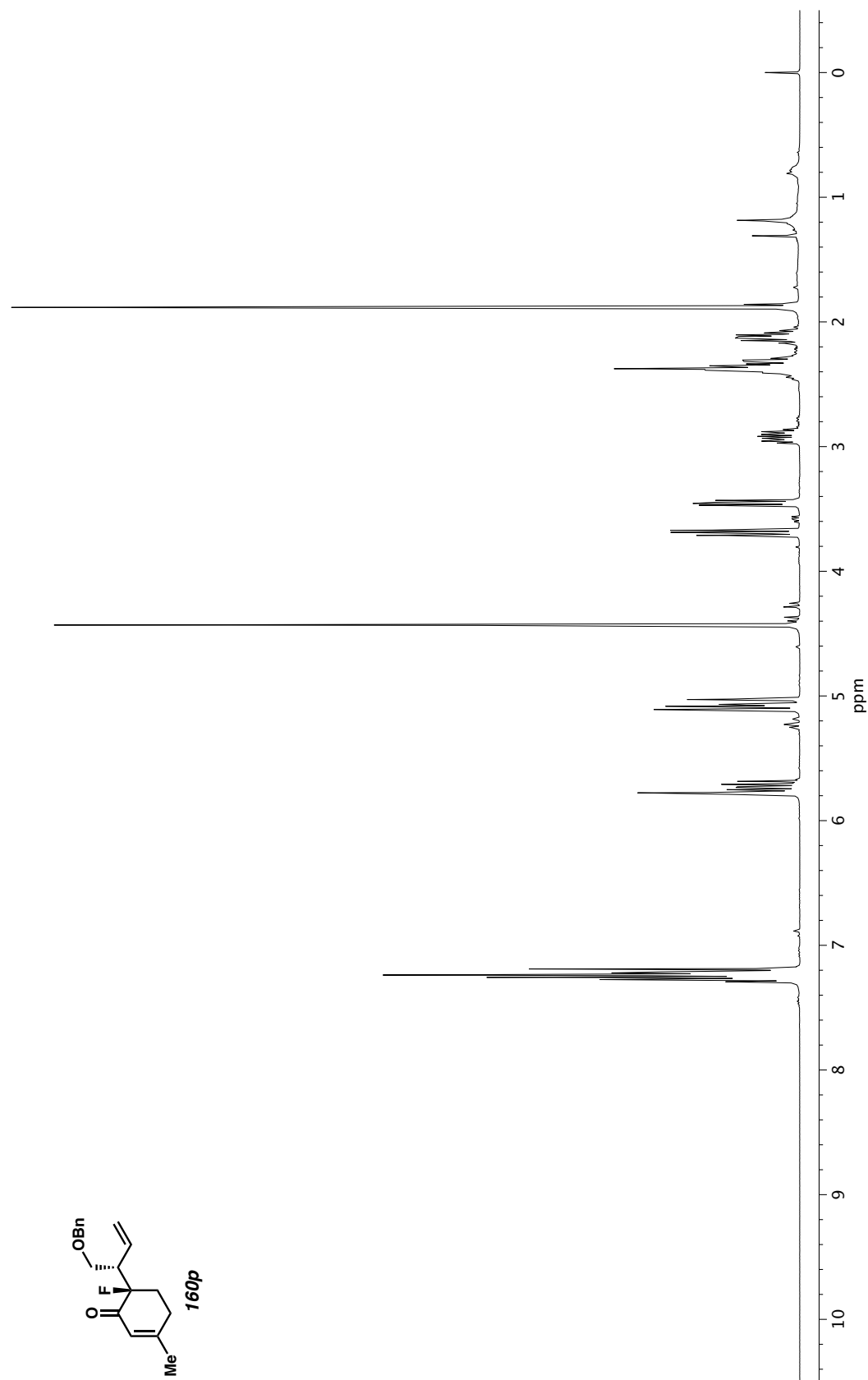
Figure A3.49. ^1H NMR (400 MHz, CDCl$_3$) of compound **160p**.
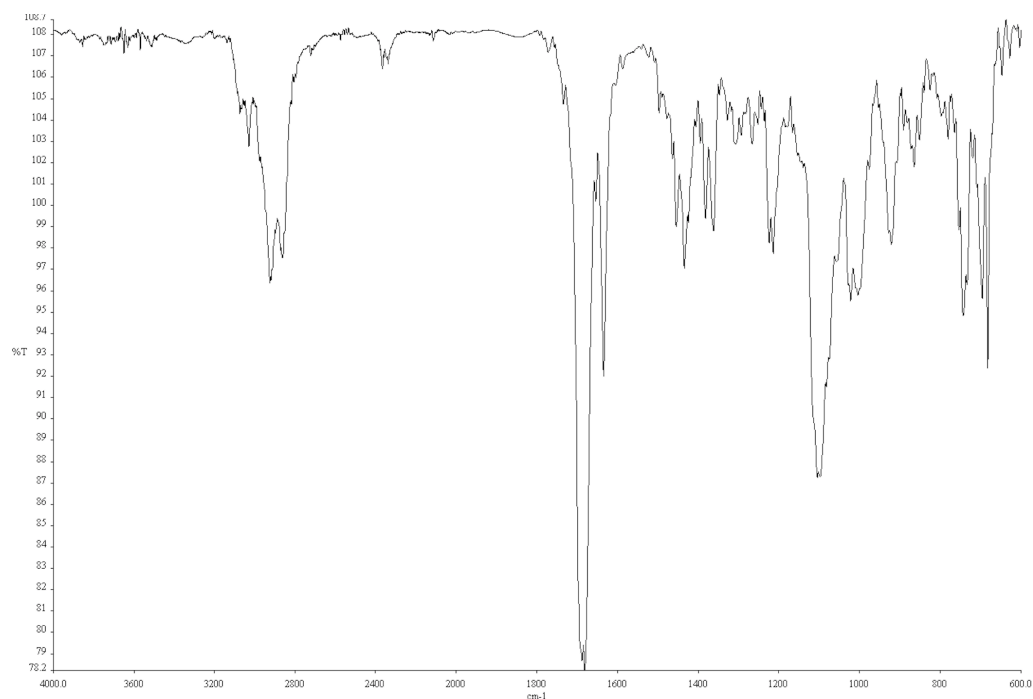
Figure A3.50. *Infrared spectrum (Thin Film, NaCl) of compound* **160p**.
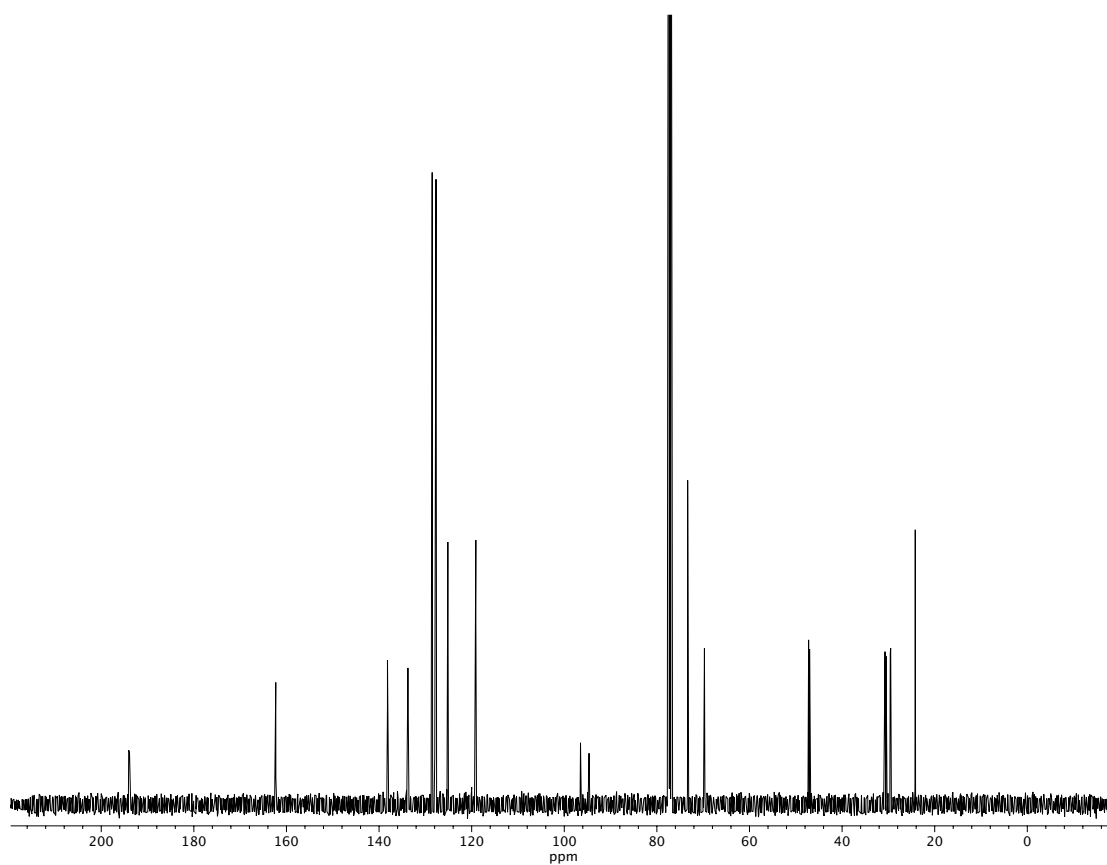
Figure A3.51. ^{13}C *NMR (100 MHz, CDCl$_3$) of compound* **160p**.
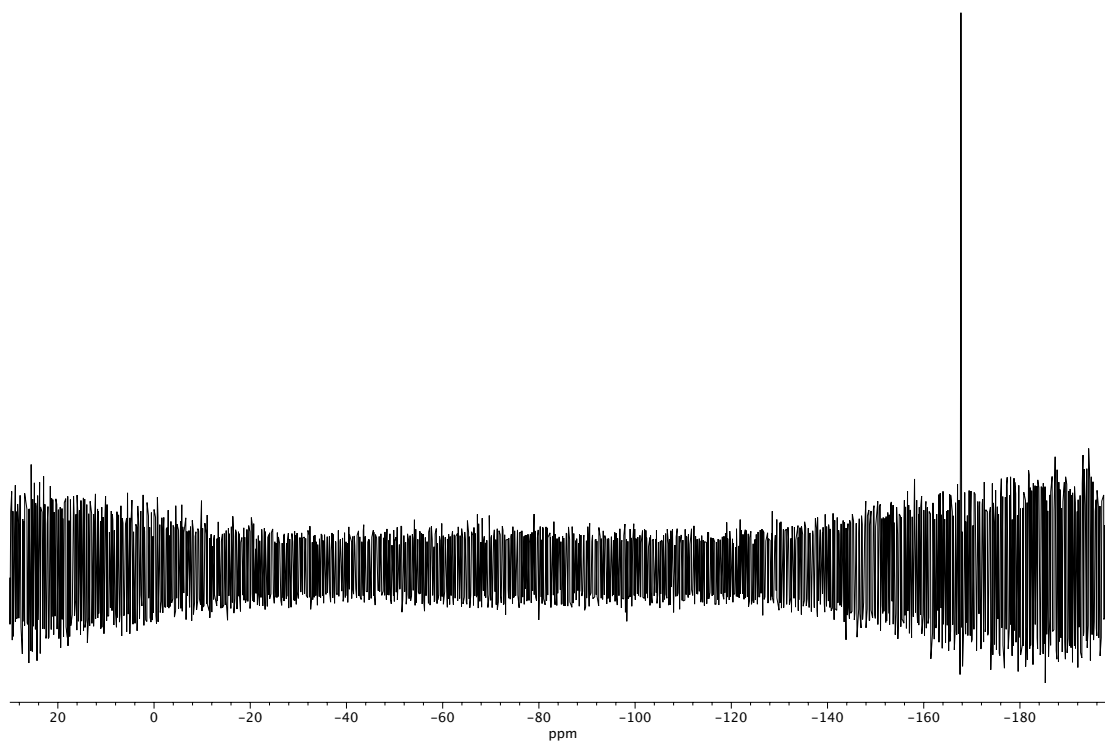
Figure A3.52. ^{19}F NMR (282 MHz, CDCl$_3$) of compound **160p**.

Figure A3.53. ^1H NMR (400 MHz, CDCl$_3$) of compound **160p_linear**.
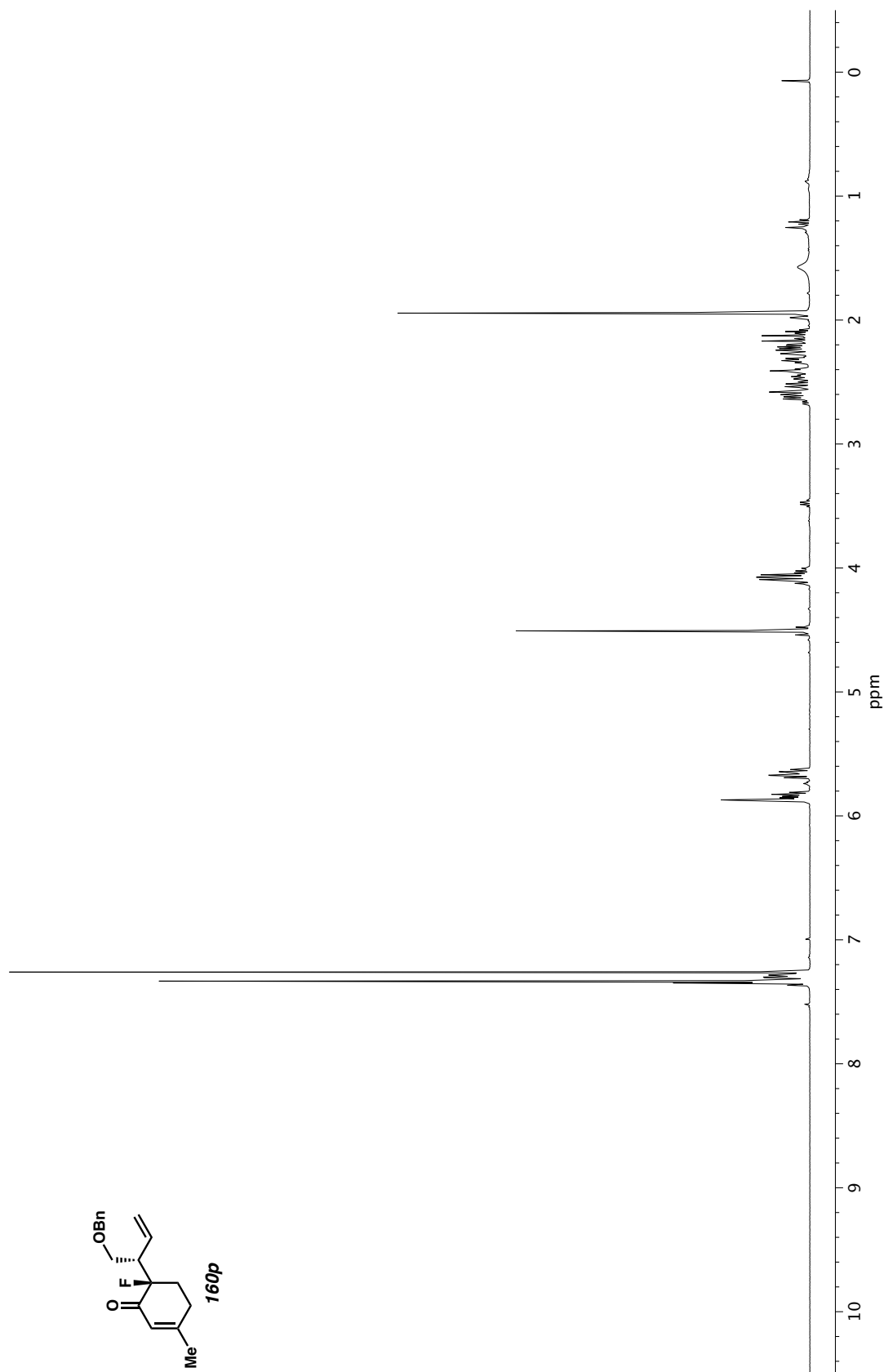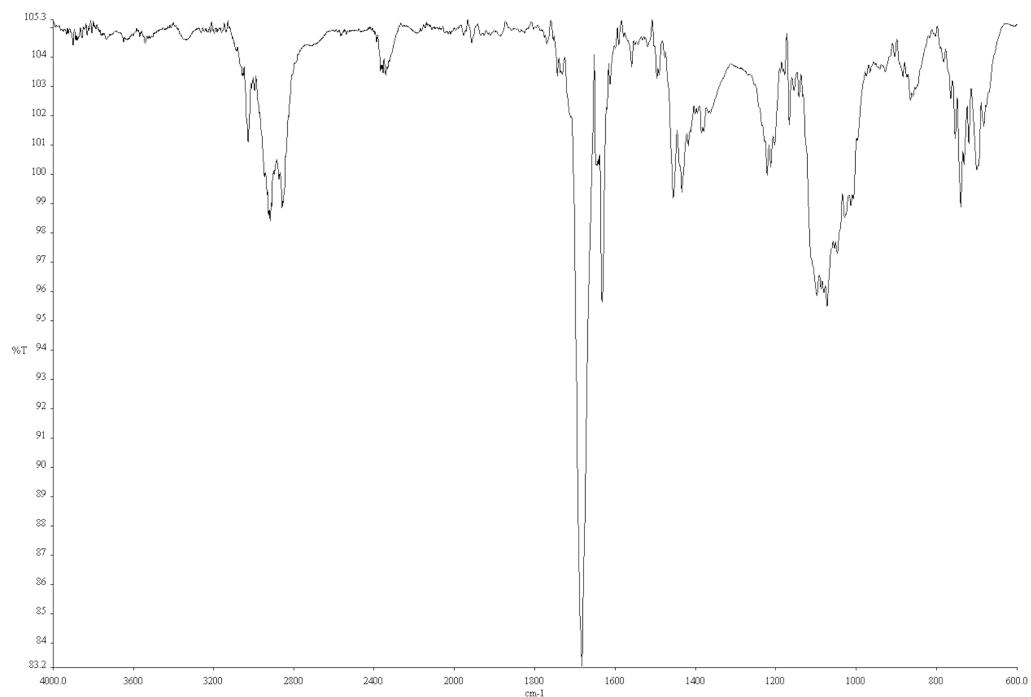
Figure A3.54. Infrared spectrum (Thin Film, NaCl) of compound **160p_linear**.
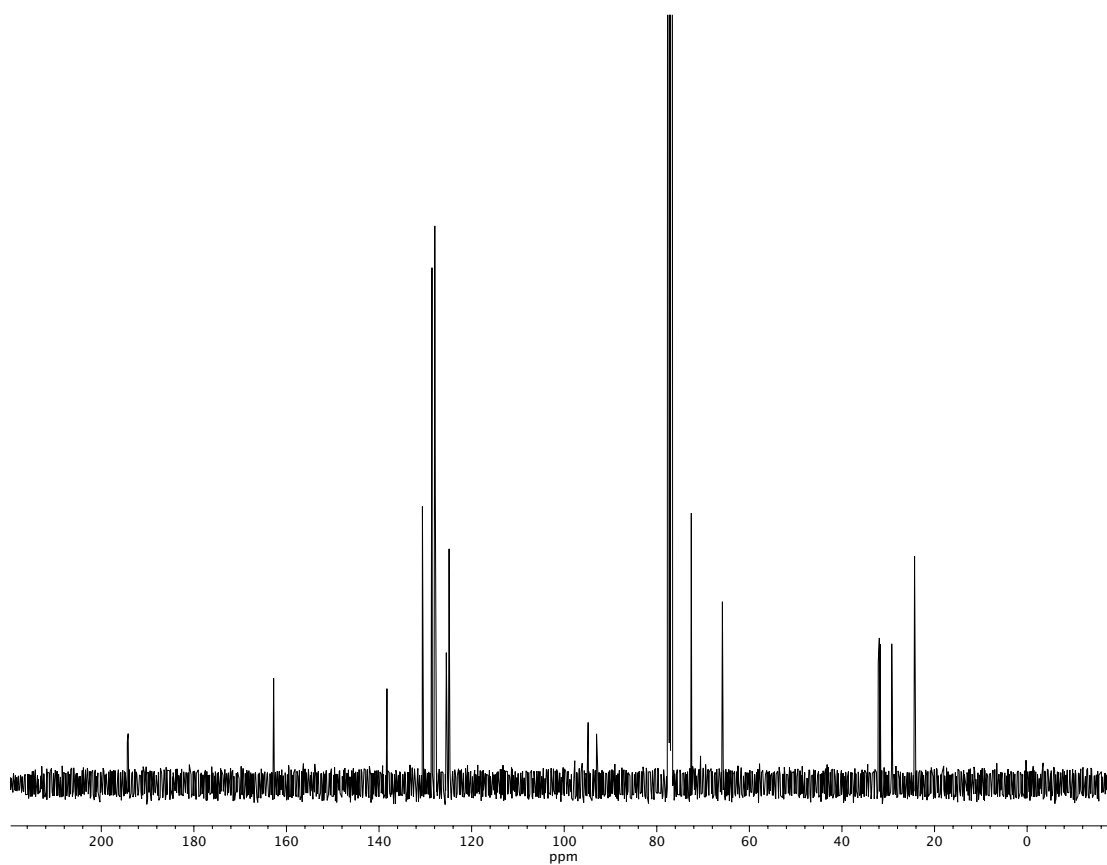
Figure A3.55. ^{13}C NMR (100 MHz, CDCl$_3$) of compound **160p_linear**.
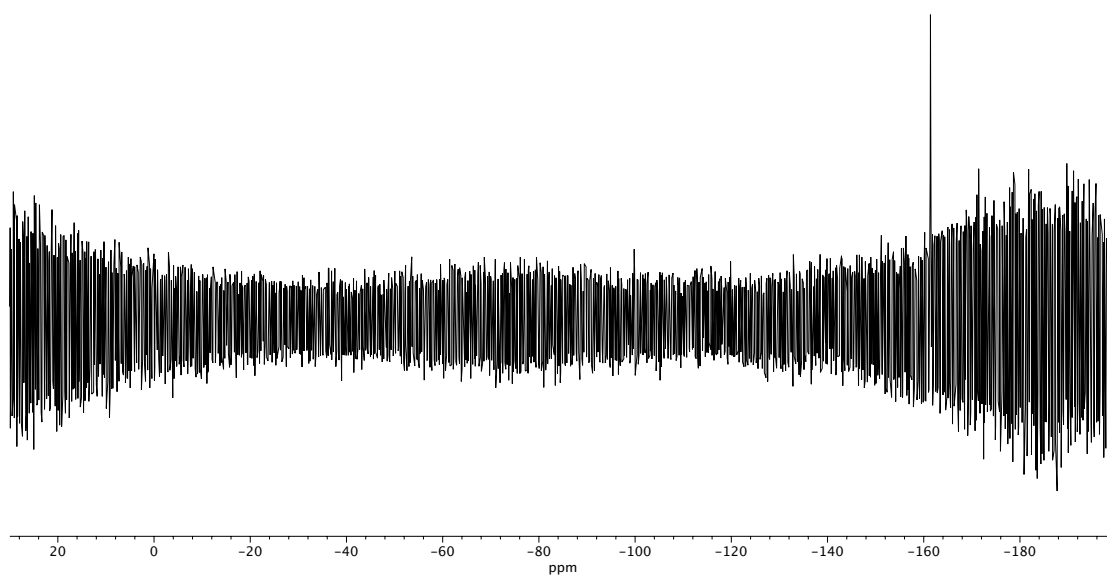
Figure A3.56. ^{19}F NMR (282 MHz, CDCl$_3$) of compound **160p_linear**.
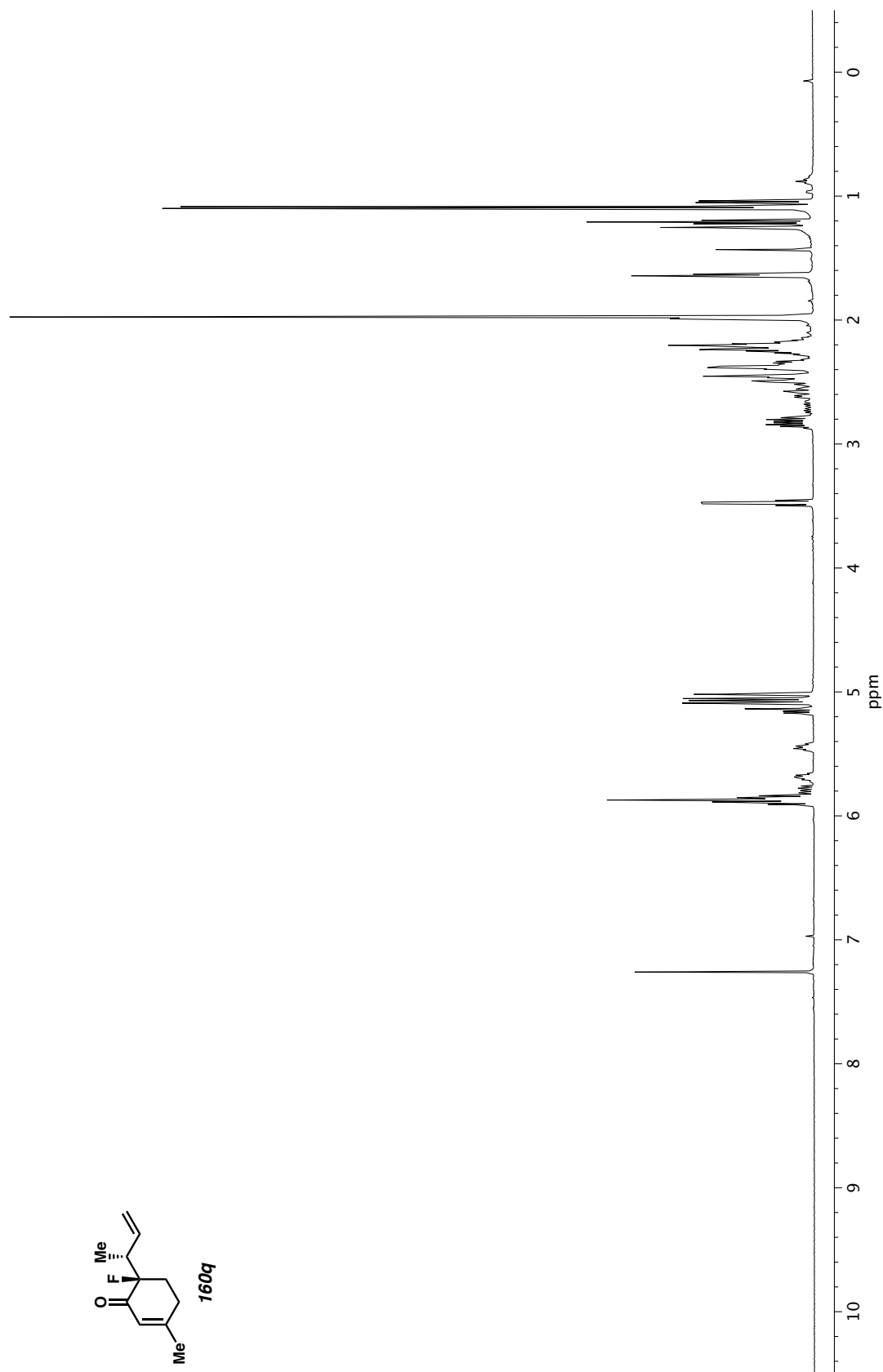
Figure A3.57. ^1H NMR (500 MHz, CDCl$_3$) of compound **160q** (mixture).
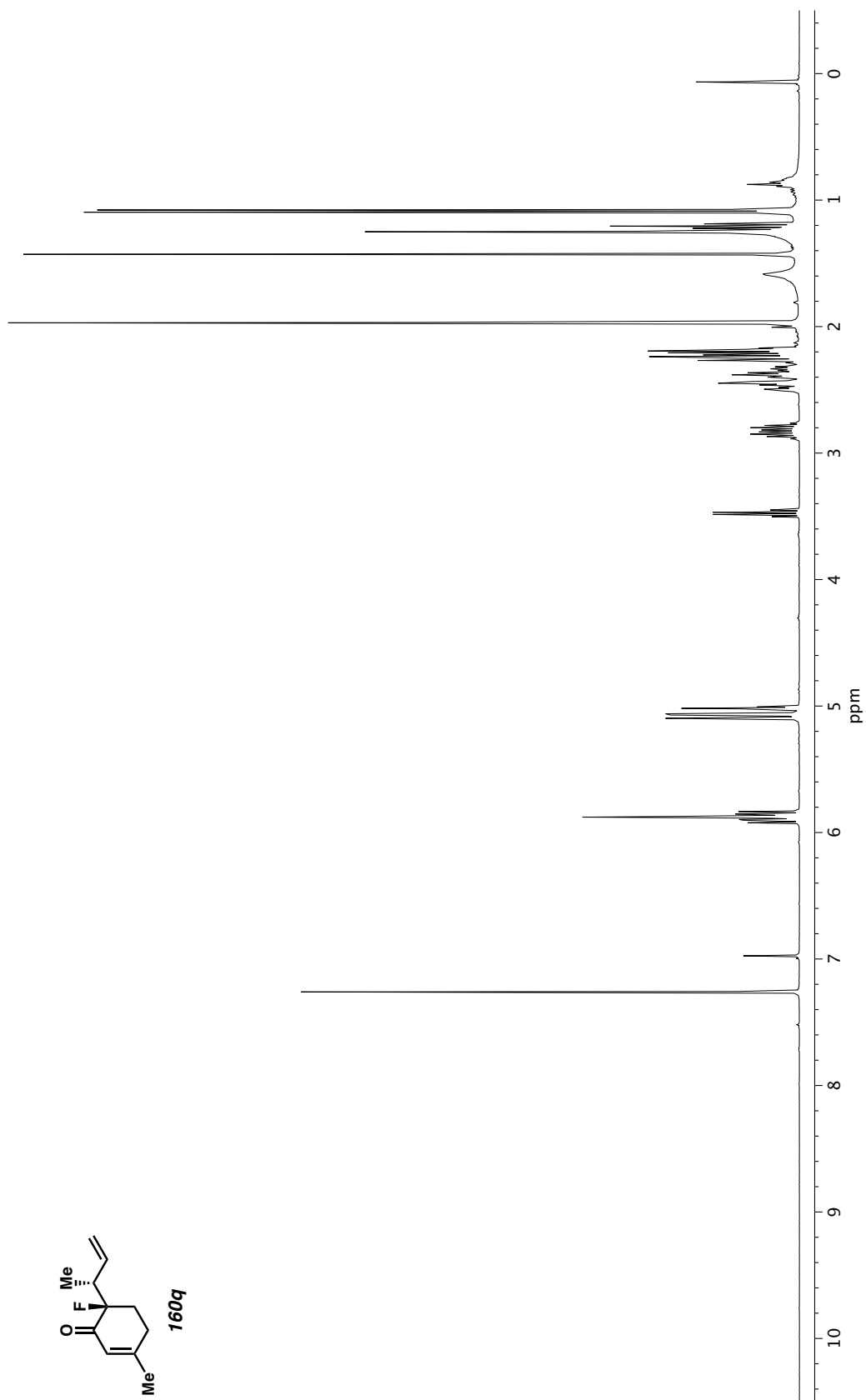
Figure A3.58. ^1H NMR (400 MHz, CDCl$_3$) of compound **160q**.
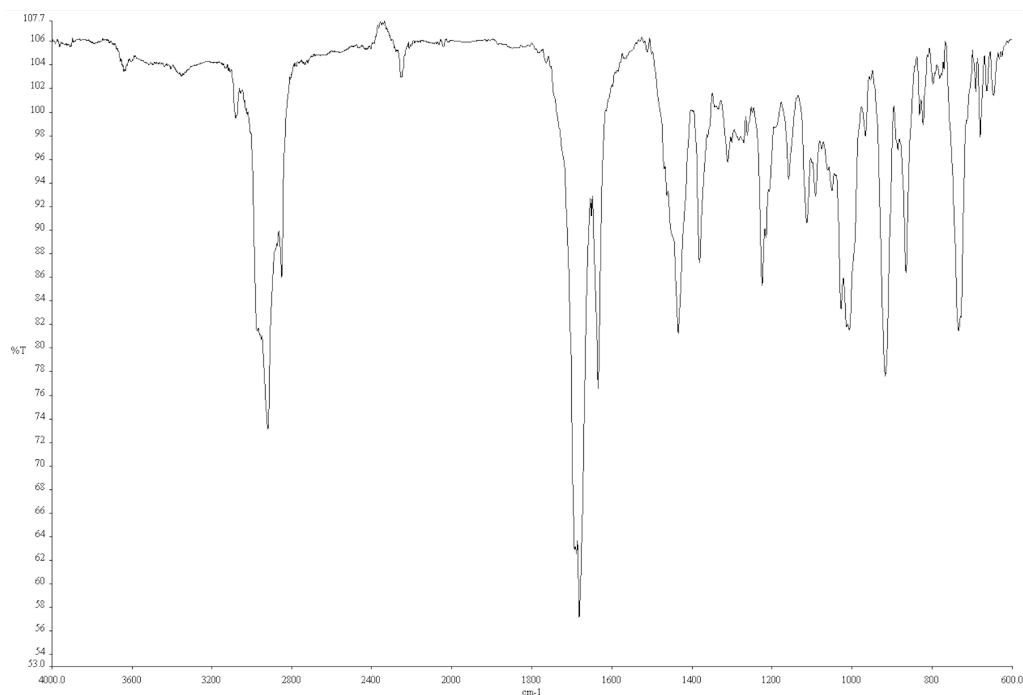
Figure A3.59. *Infrared spectrum (Thin Film, NaCl) of compound **160q**.*
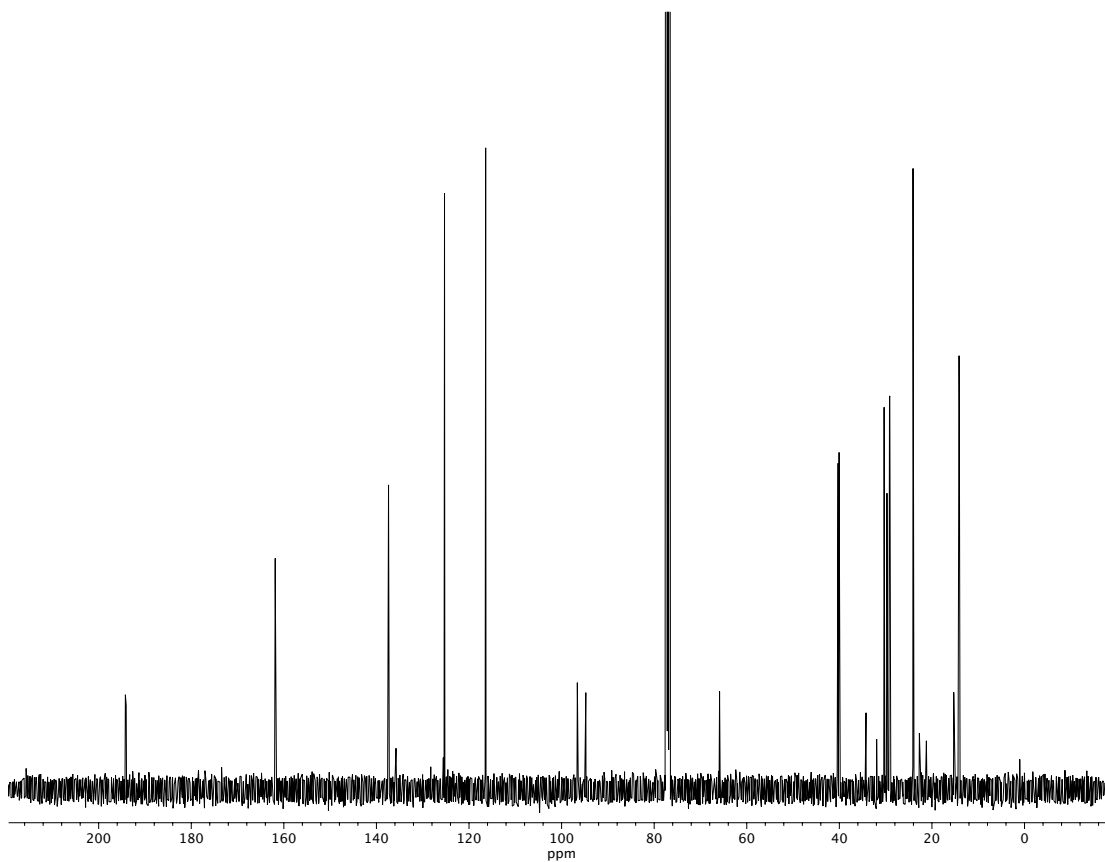
Figure A3.60. ^{13}C *NMR (100 MHz, CDCl₃) of compound **160q**.*
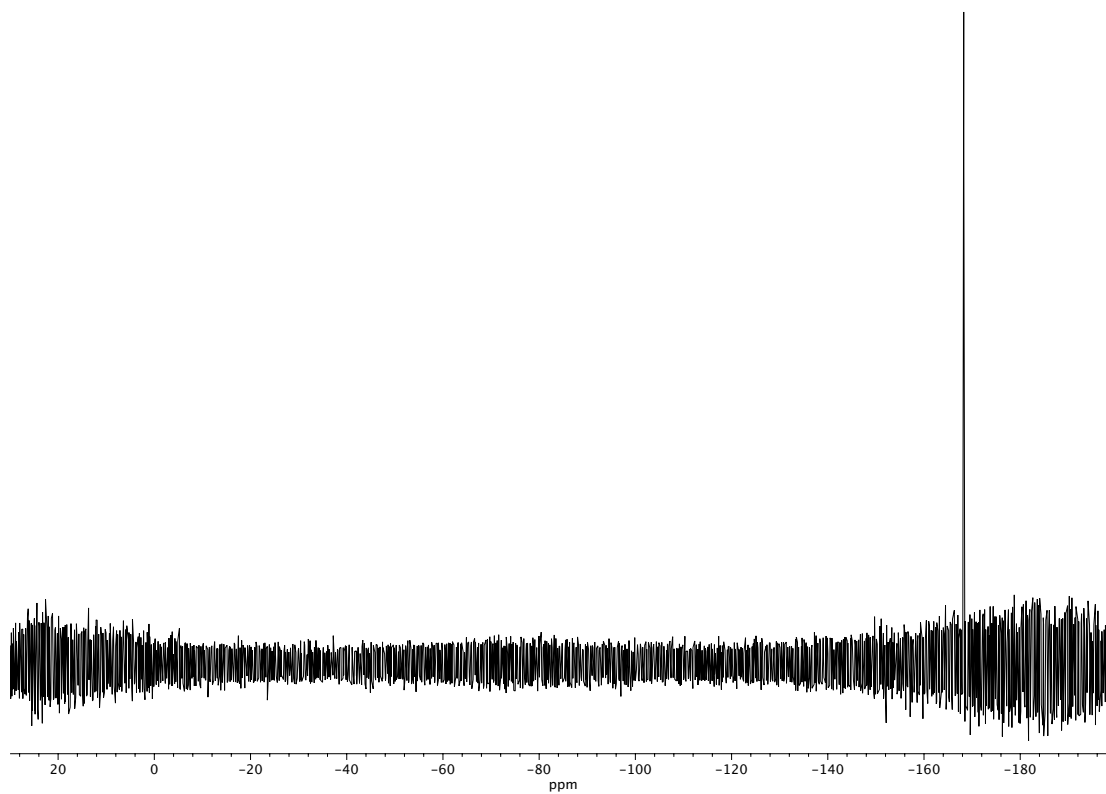
Figure A3.61. ^{19}F NMR (282 MHz, CDCl$_3$) of compound **160q**.
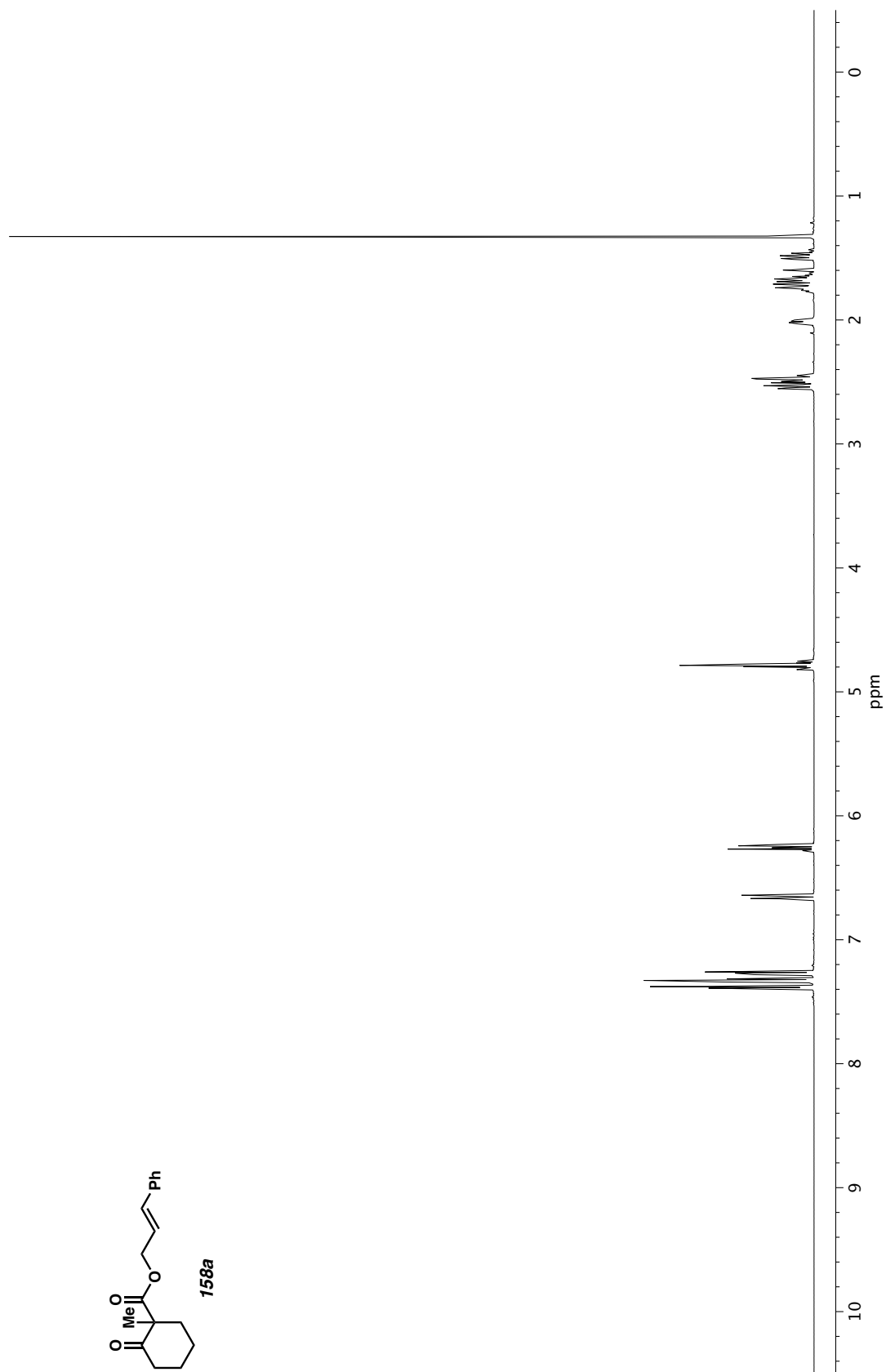
Figure A3.62. ^1H NMR (600 MHz, CDCl$_3$) of compound **158a**.
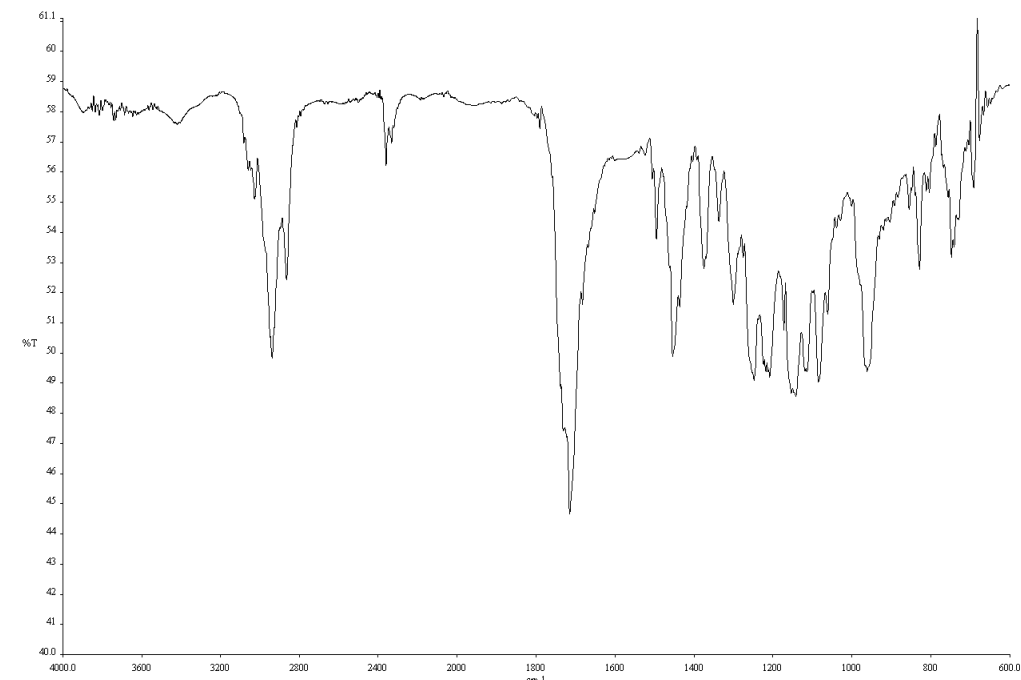
Figure A3.63. Infrared spectrum (Thin Film, NaCl) of compound **158a**.
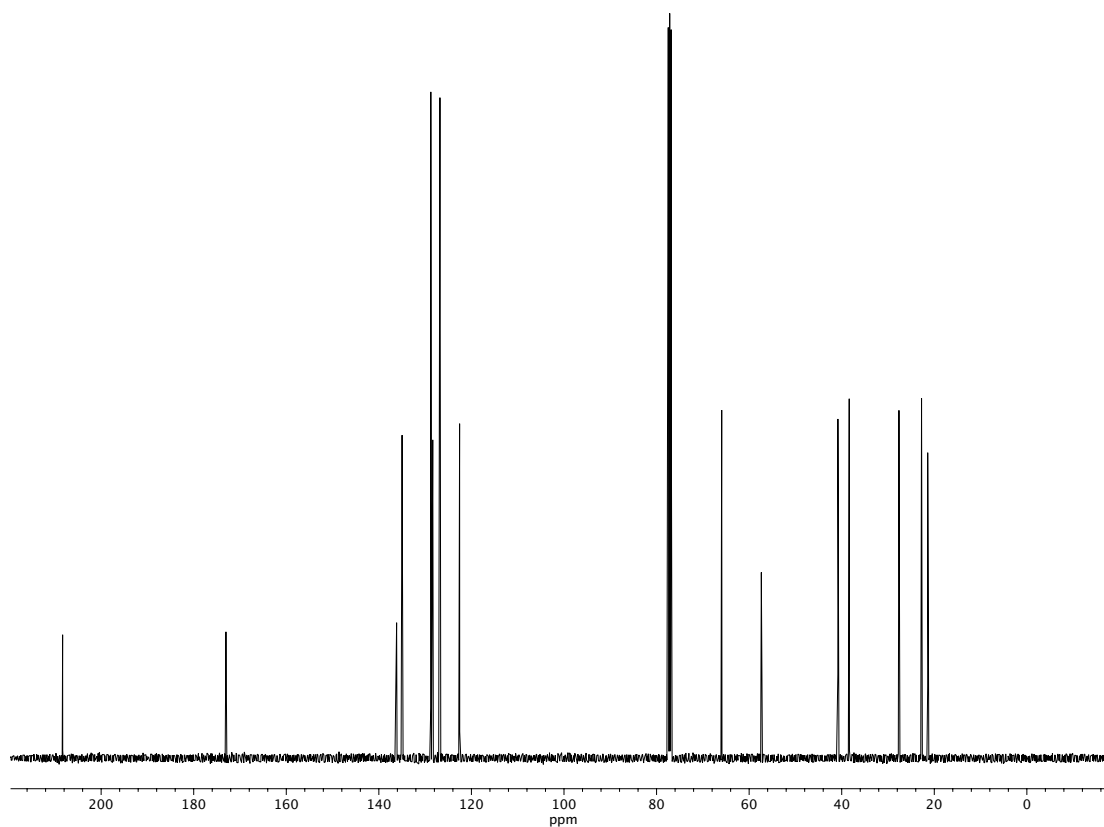
Figure A3.64. ^{13}C NMR (100 MHz, CDCl$_3$) of compound **158a**.
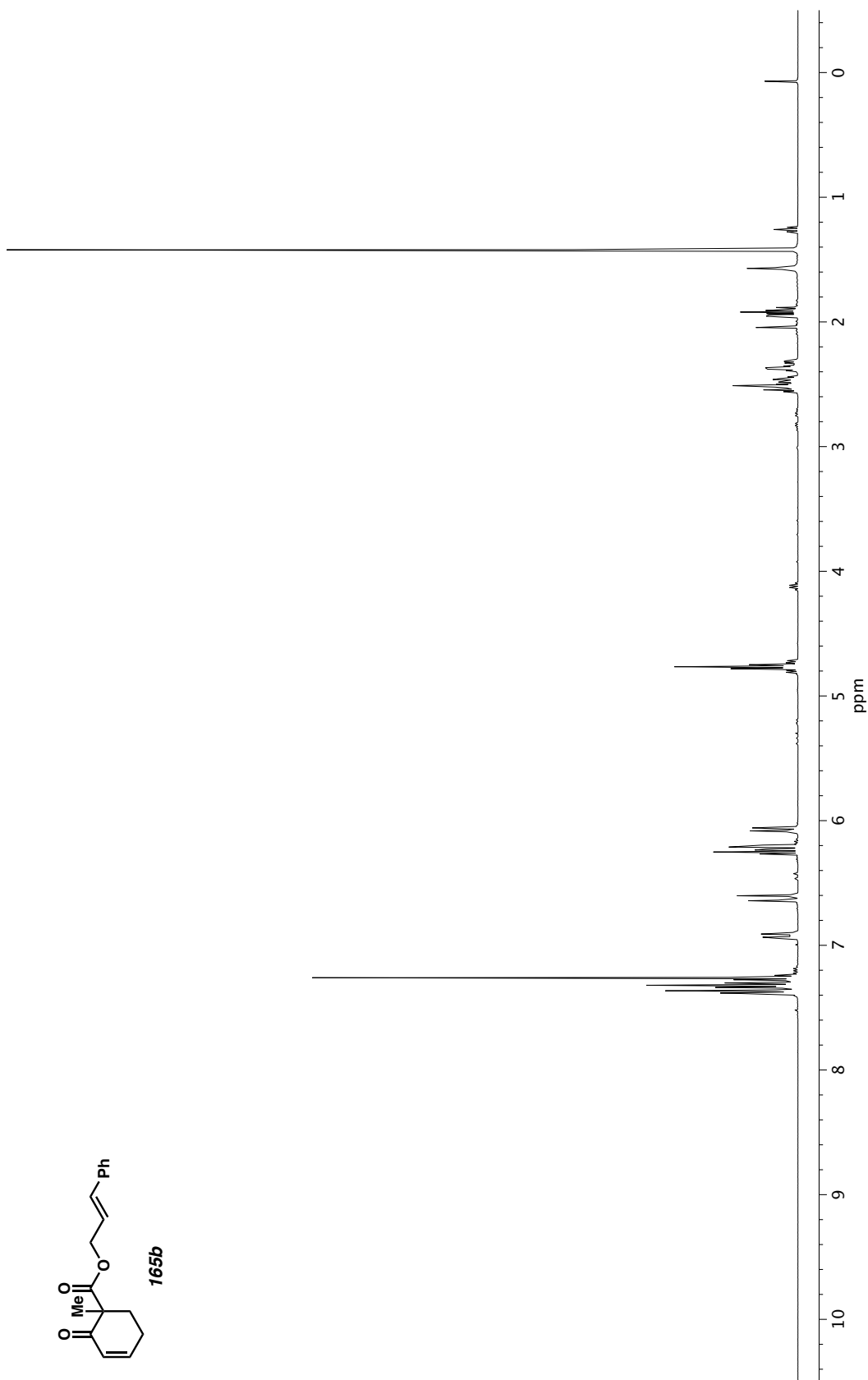
Figure A3.65. *^{1}H NMR (400 MHz, CDCl$_3$) of compound **158b**.*
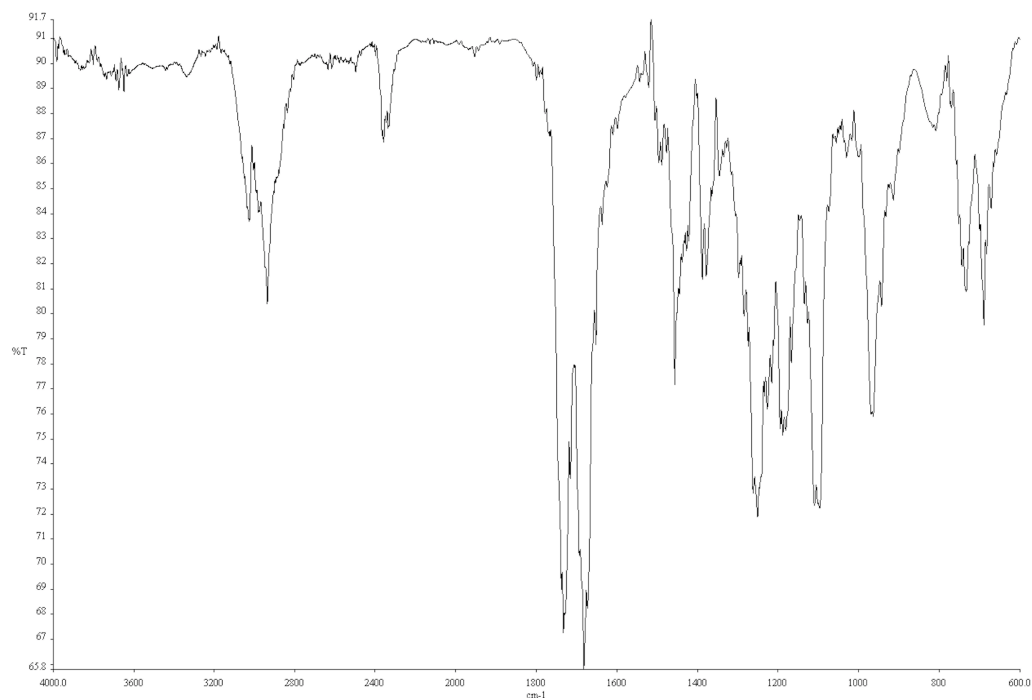
Figure A3.66. *Infrared spectrum (Thin Film, NaCl) of compound **158b***.
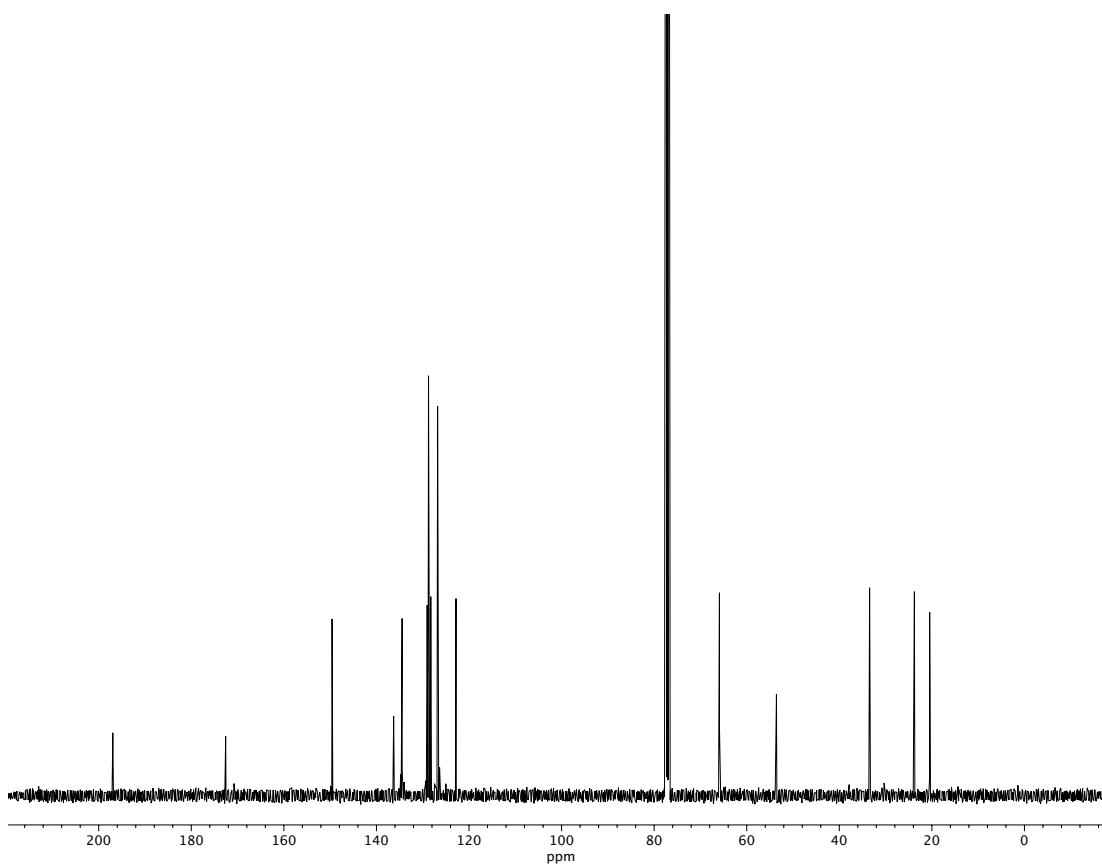
Figure A3.67. ^{13}C *NMR (100 MHz, CDCl$_3$) of compound **158b***.
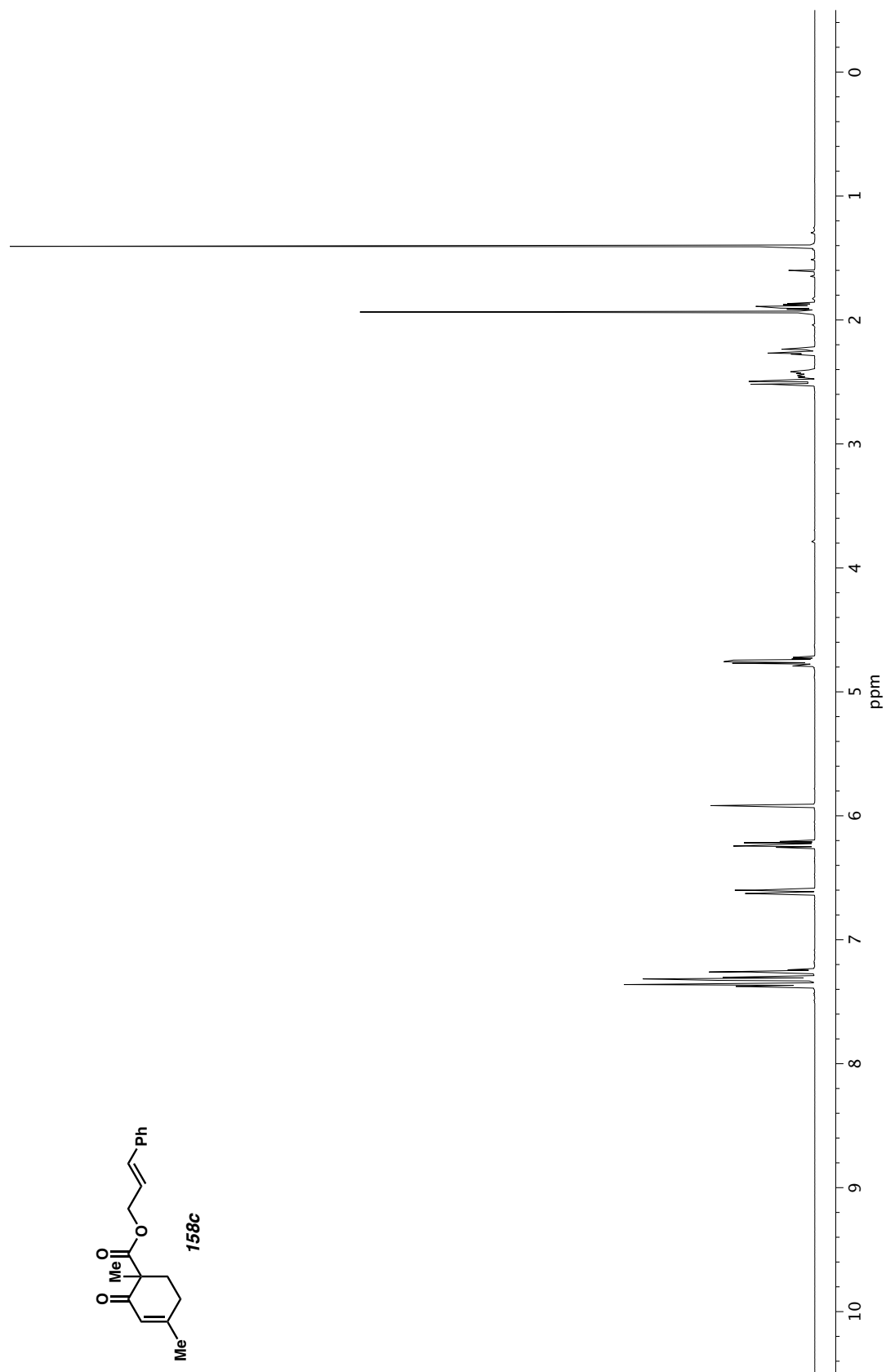
Figure A3.68. ^1H NMR (600 MHz, CDCl$_3$) of compound **158c**.
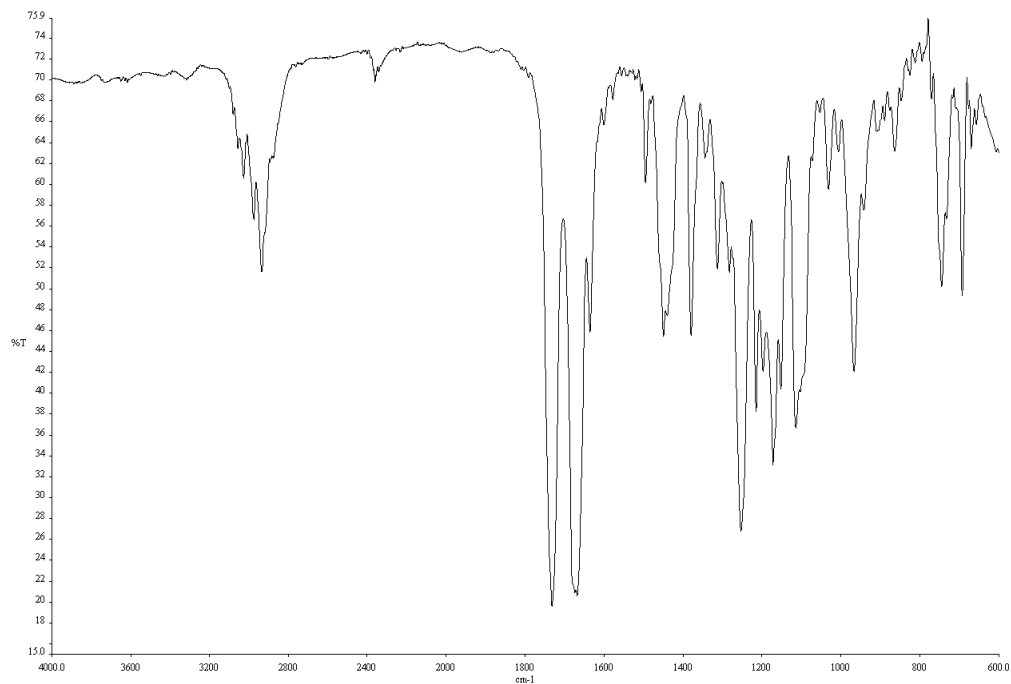
Figure A3.69. *Infrared spectrum (Thin Film, NaCl) of compound* **158c***.*
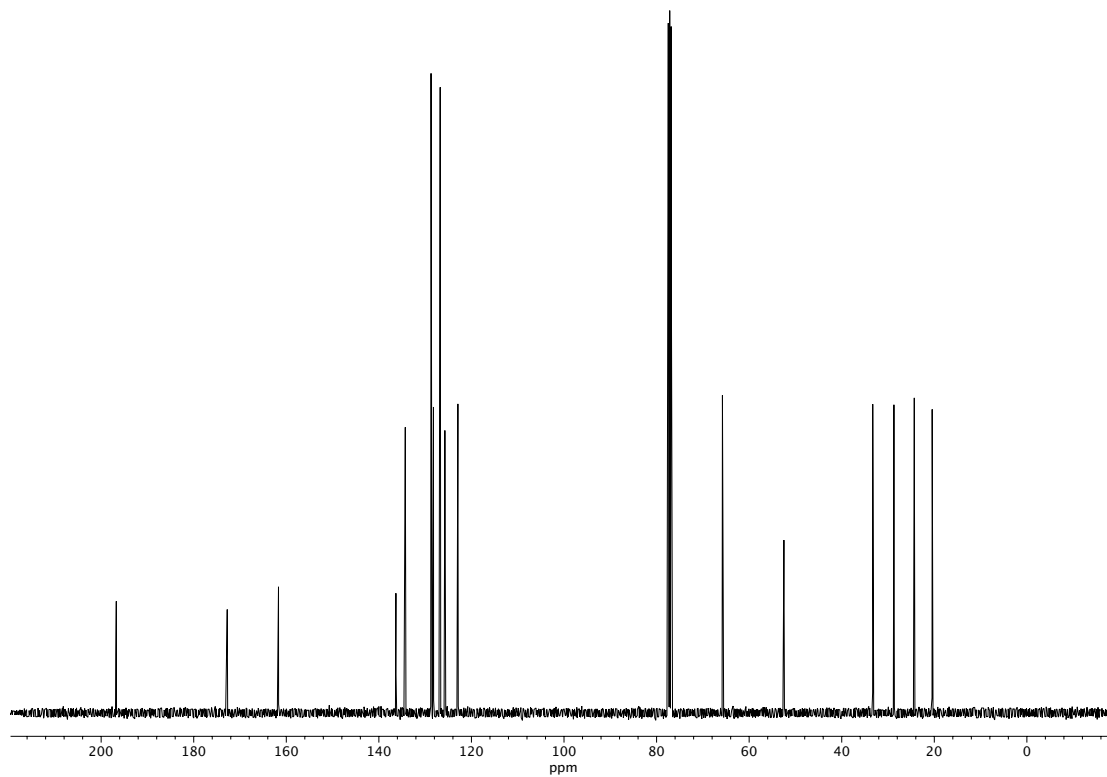
Figure A3.70. *^{13}C NMR (100 MHz, CDCl$_3$) of compound* **158c***.*
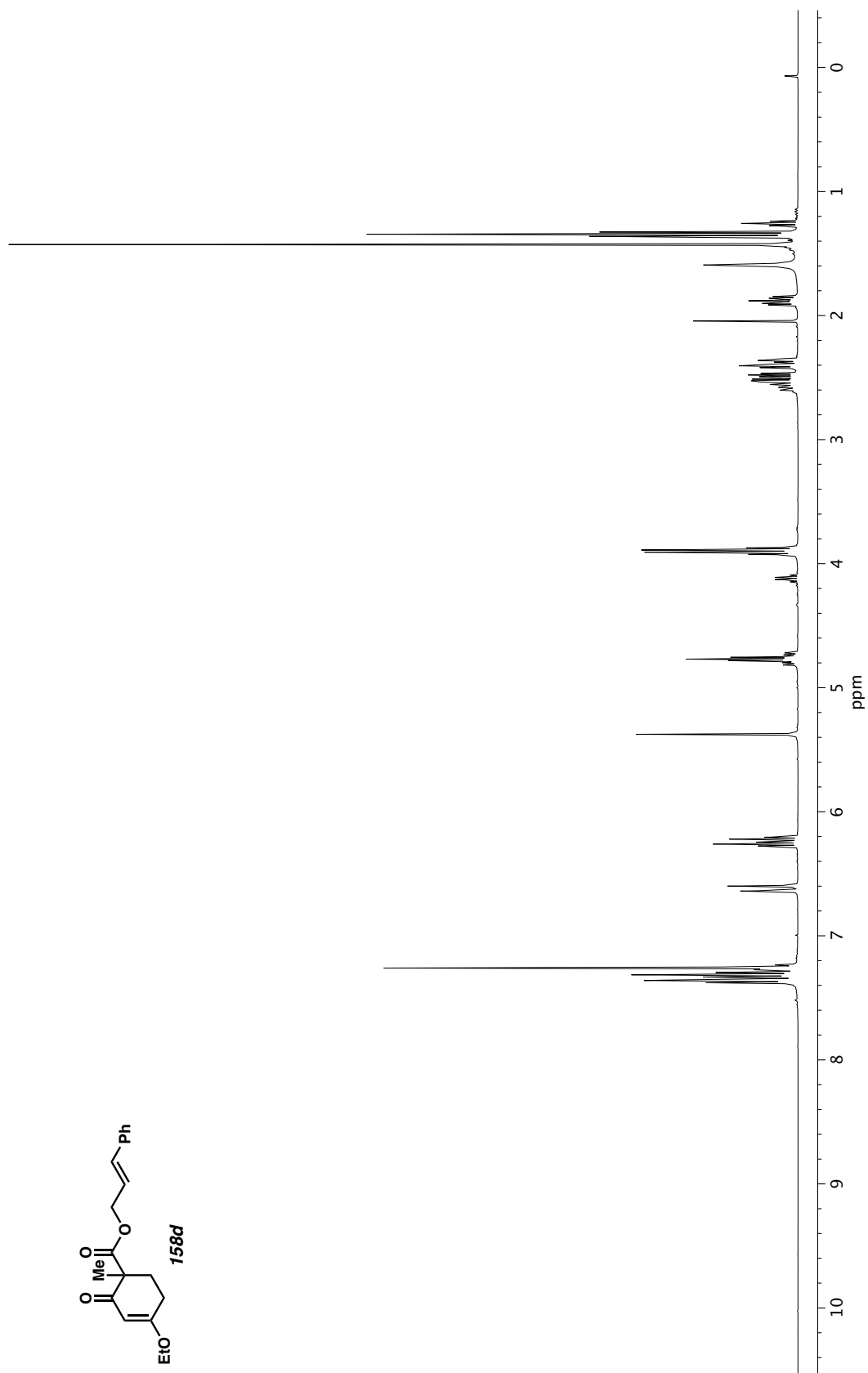
Figure A3.71. ^1H NMR (400 MHz, CDCl$_3$) of compound **158d**.
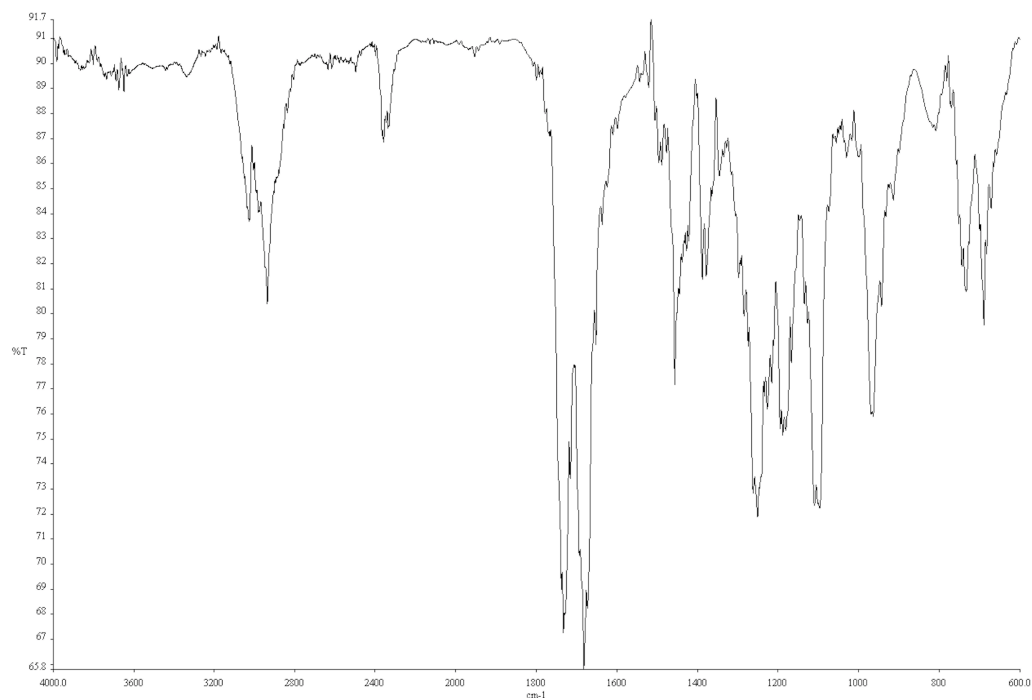
Figure A3.72. *Infrared spectrum (Thin Film, NaCl) of compound* **158d**.
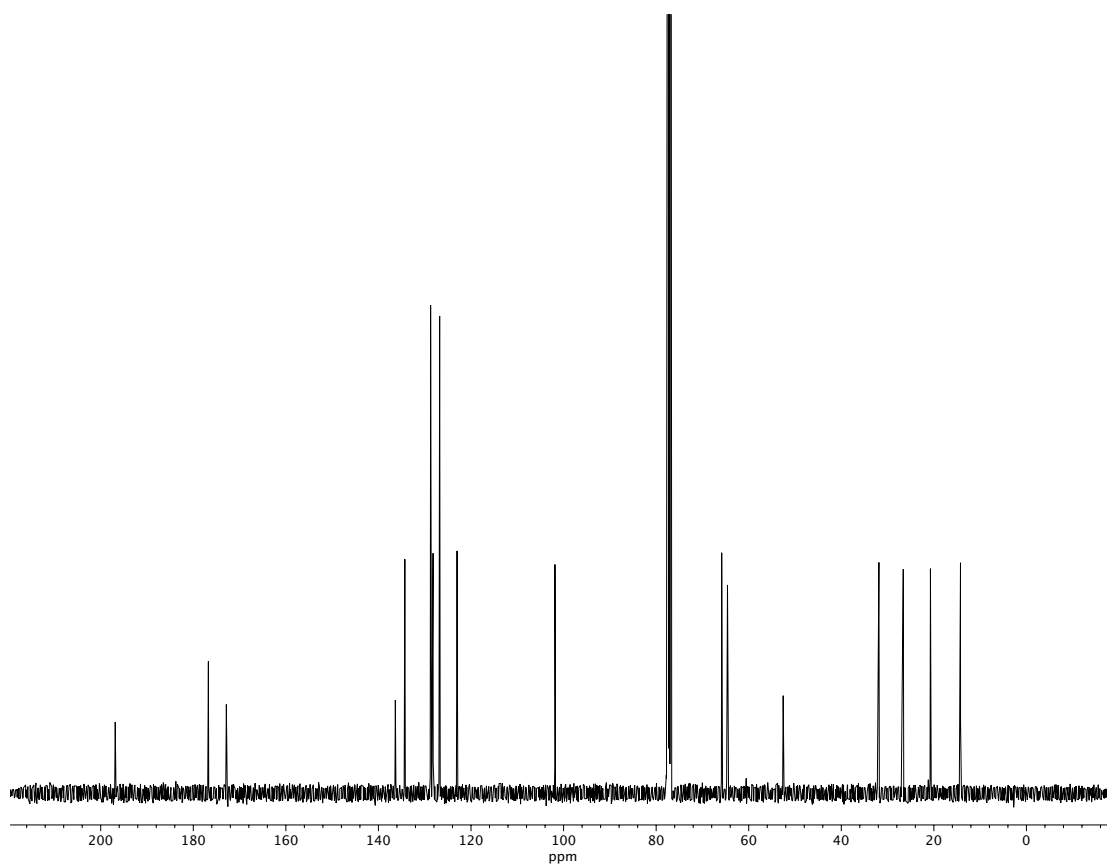
Figure A3.73. ^{13}C *NMR (100 MHz, CDCl$_3$) of compound* **158d**.
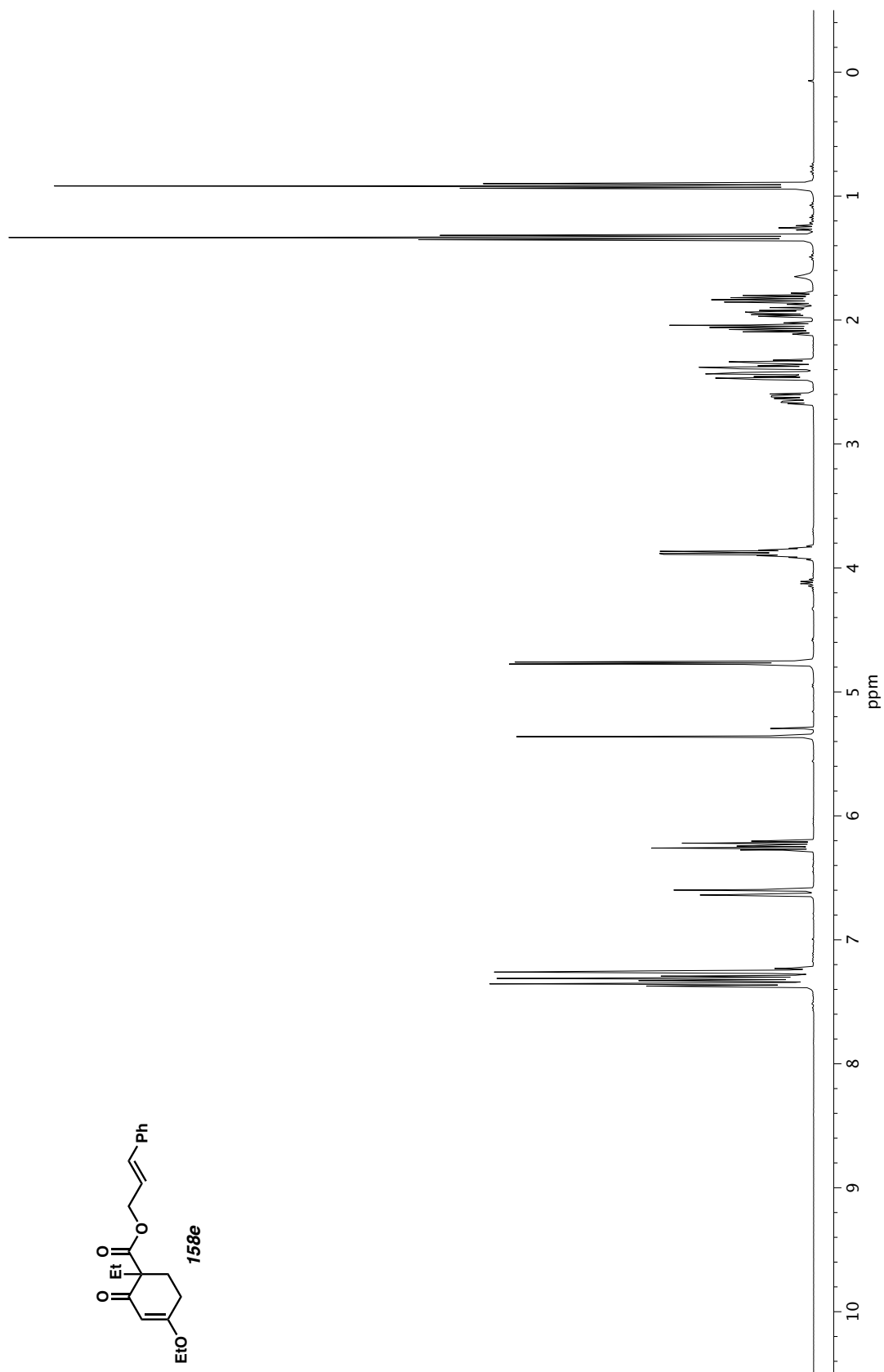
Figure A3.74. ^1H NMR (400 MHz, CDCl$_3$) of compound **158e**.
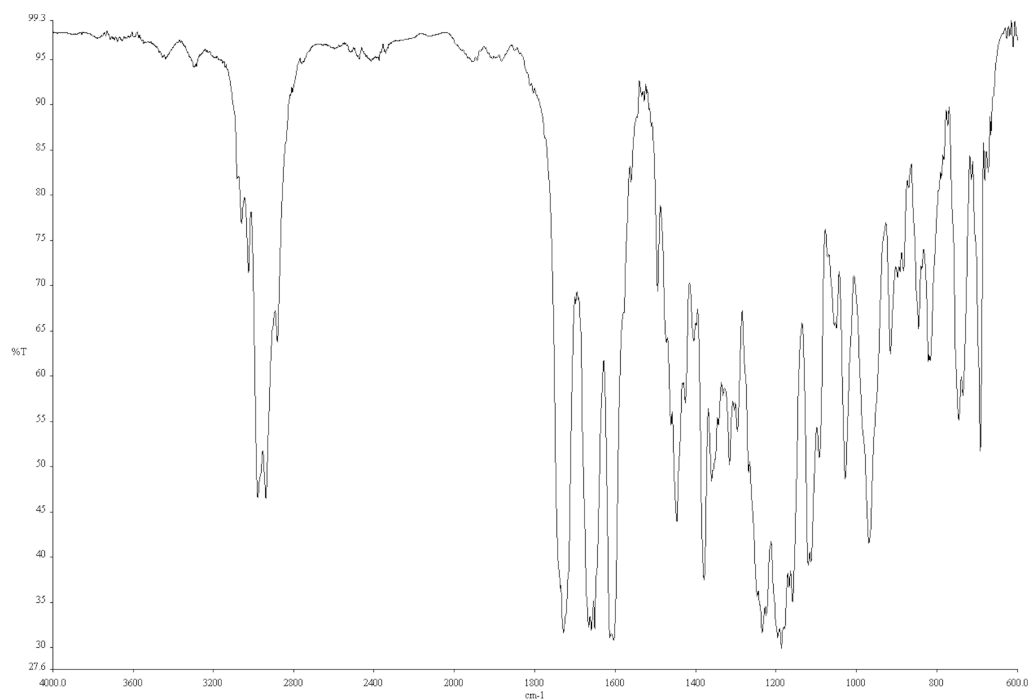
Figure A3.75. *Infrared spectrum (Thin Film, NaCl) of compound **158e**.*
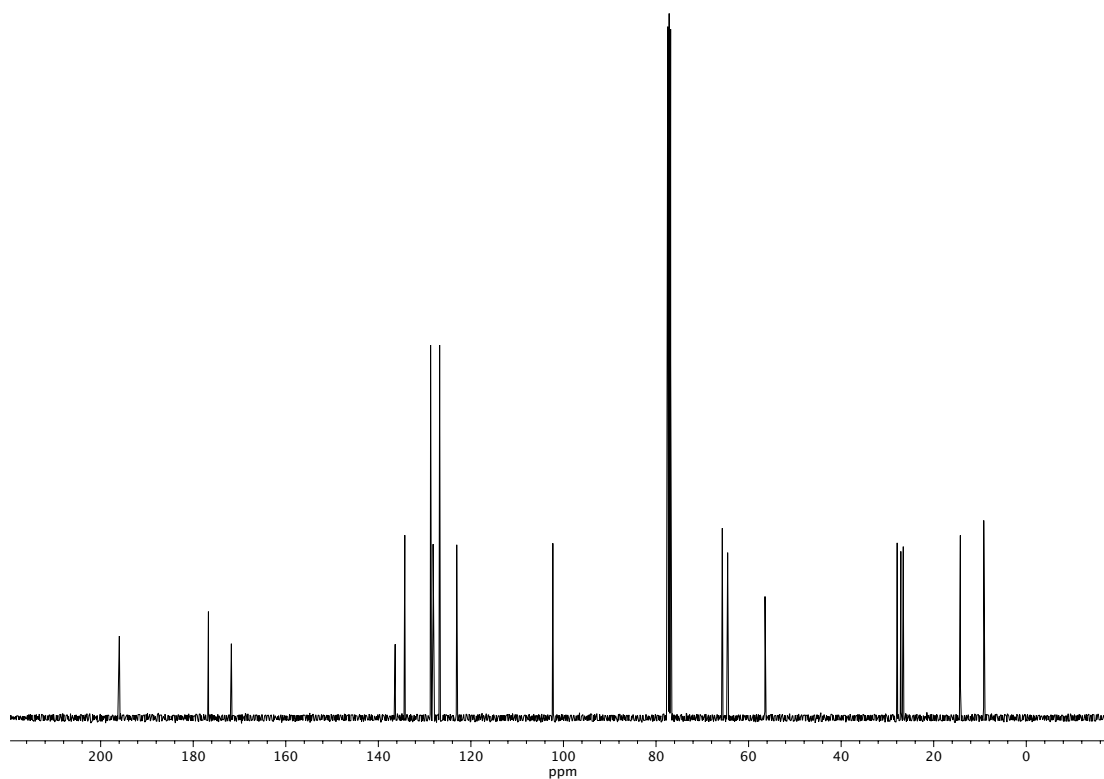
Figure A3.76. ^{13}C *NMR (100 MHz, CDCl$_3$) of compound **158e**.*
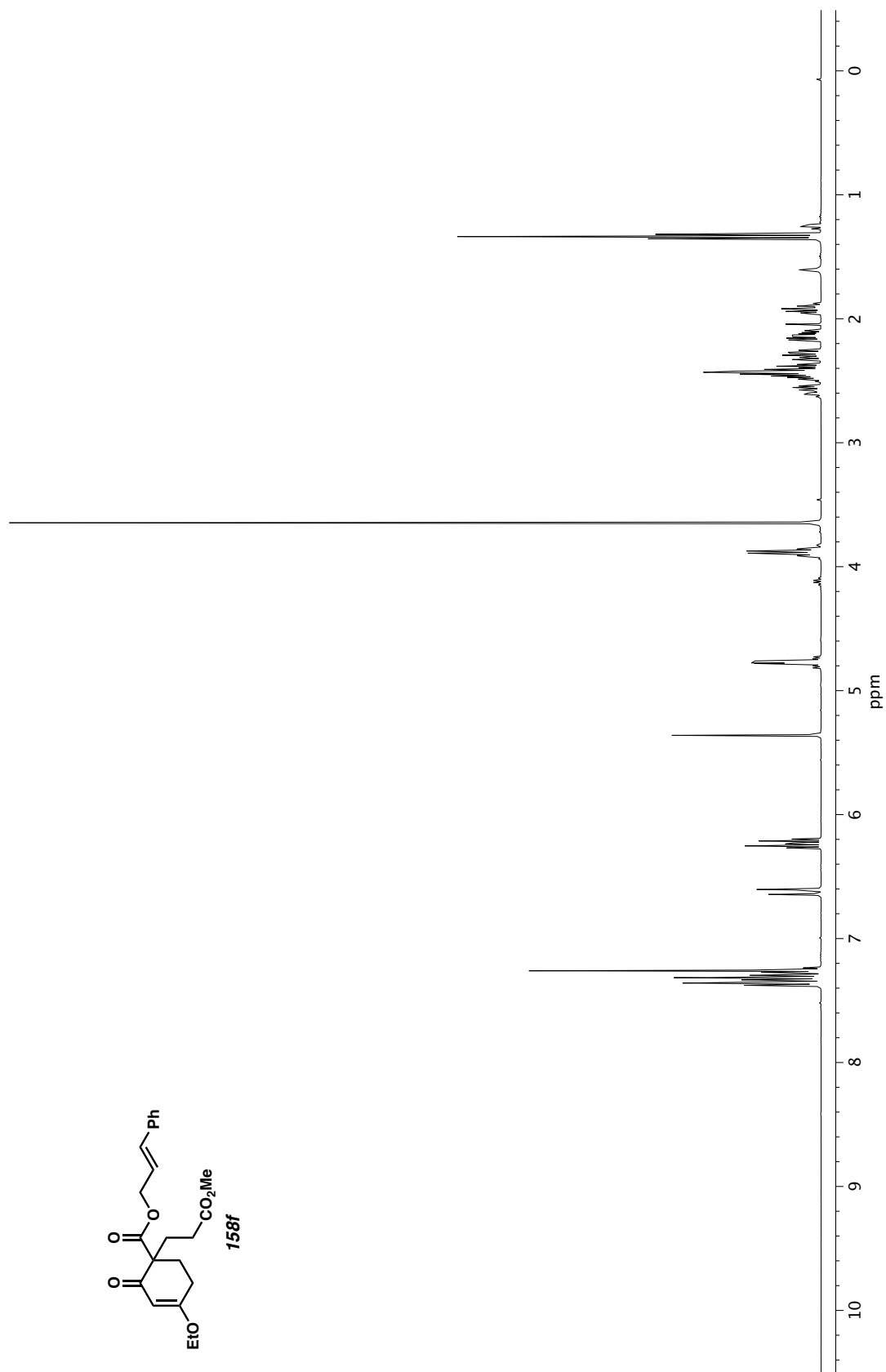
Figure A3.77. ^1H NMR (400 MHz, CDCl$_3$) of compound **158f**.
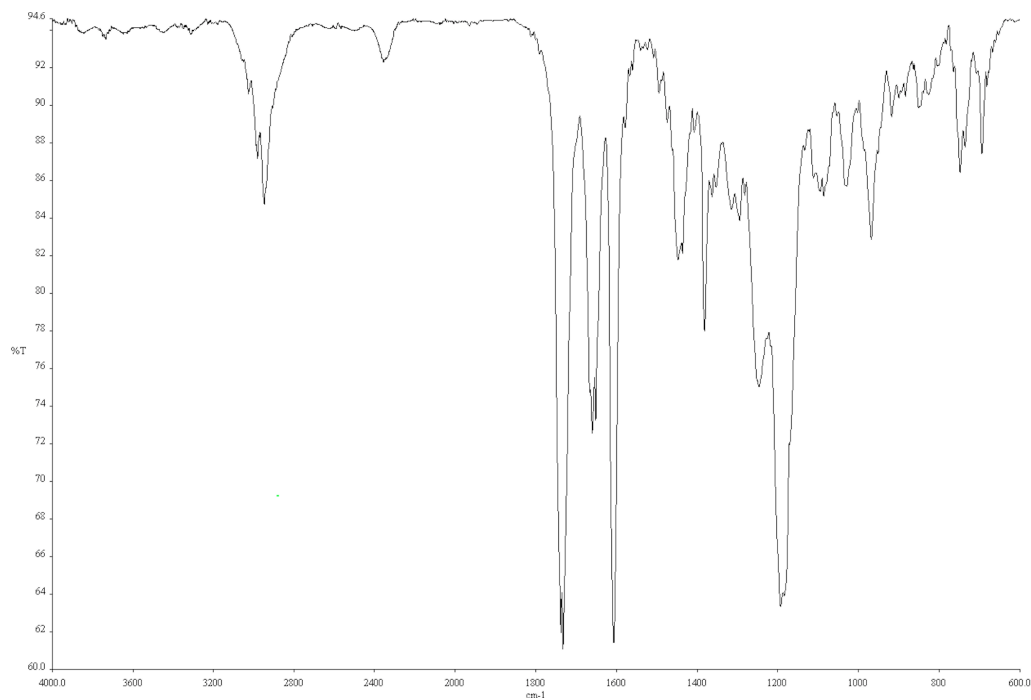
Figure A3.78. Infrared spectrum (Thin Film, NaCl) of compound **158f**.
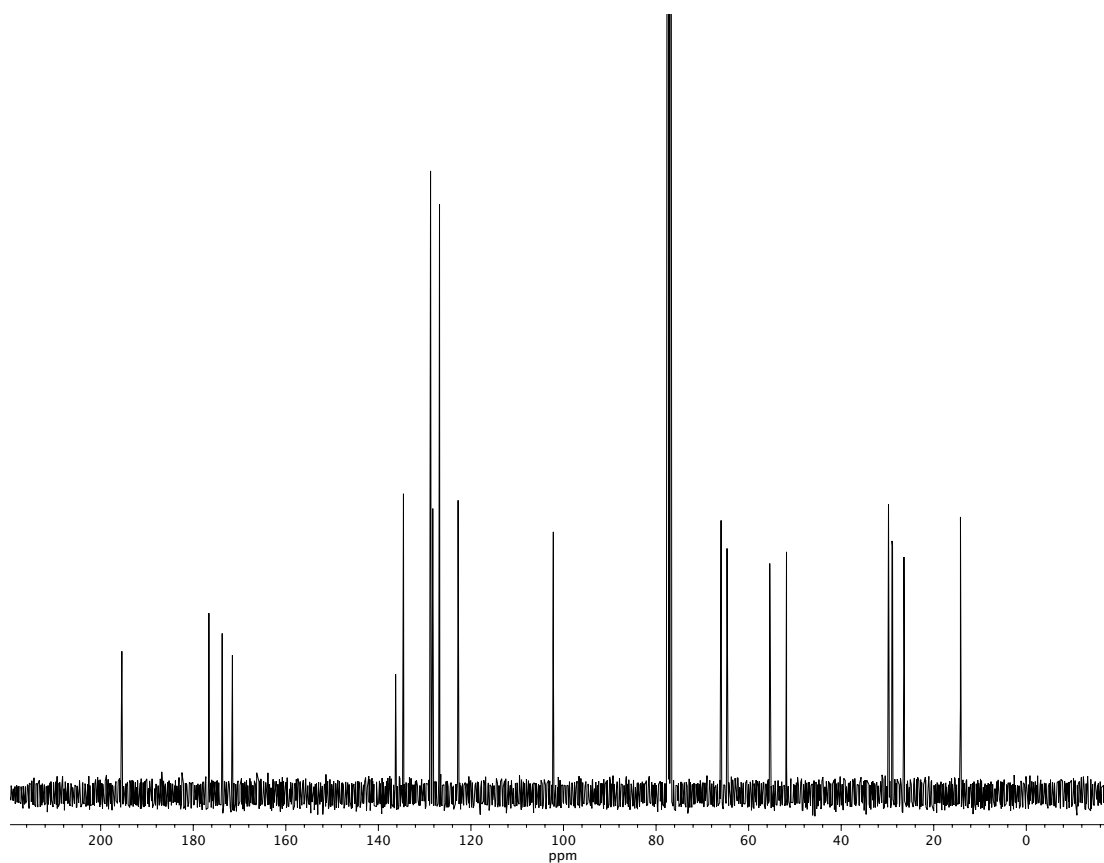
Figure A3.79. ^{13}C NMR (100 MHz, CDCl$_3$) of compound **158f**.
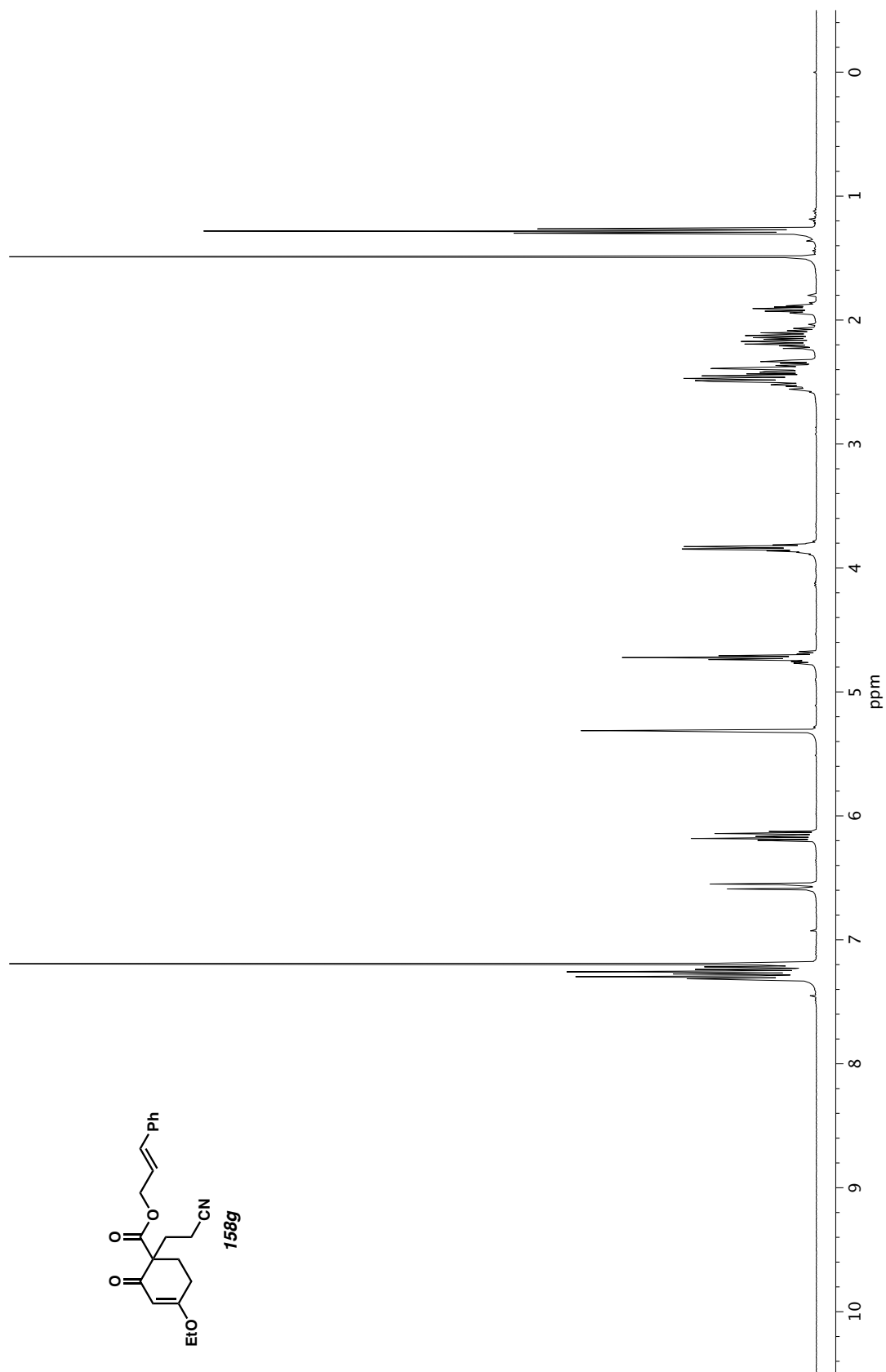
Figure A3.80. *¹H NMR (400 MHz, CDCl₃) of compound **158g**.*
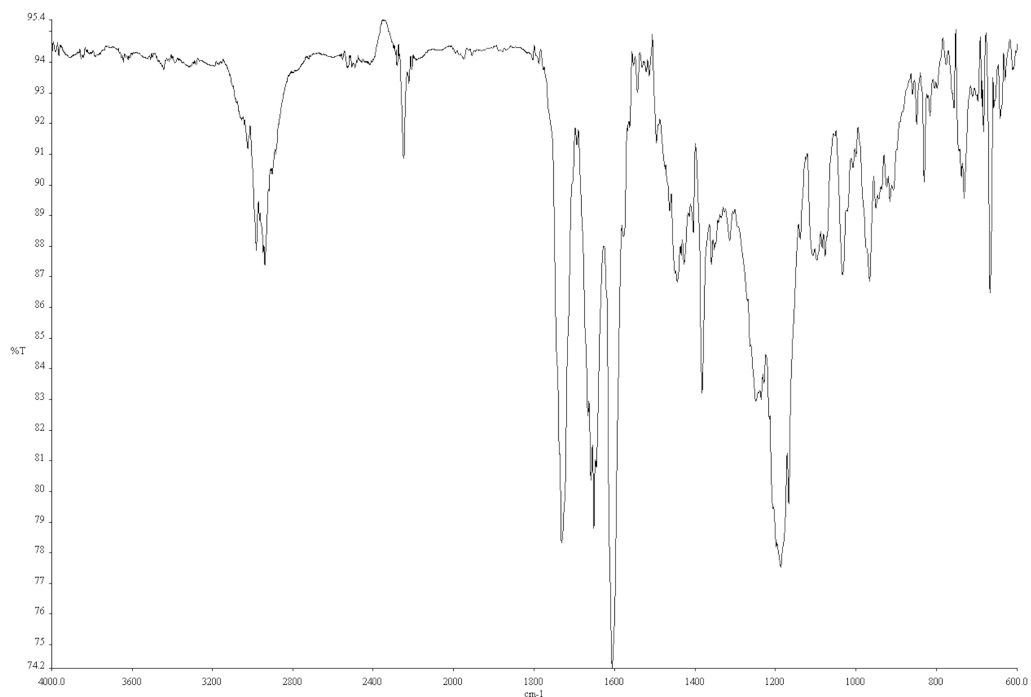
Figure A3.81. *Infrared spectrum (Thin Film, NaCl) of compound* **158g**.
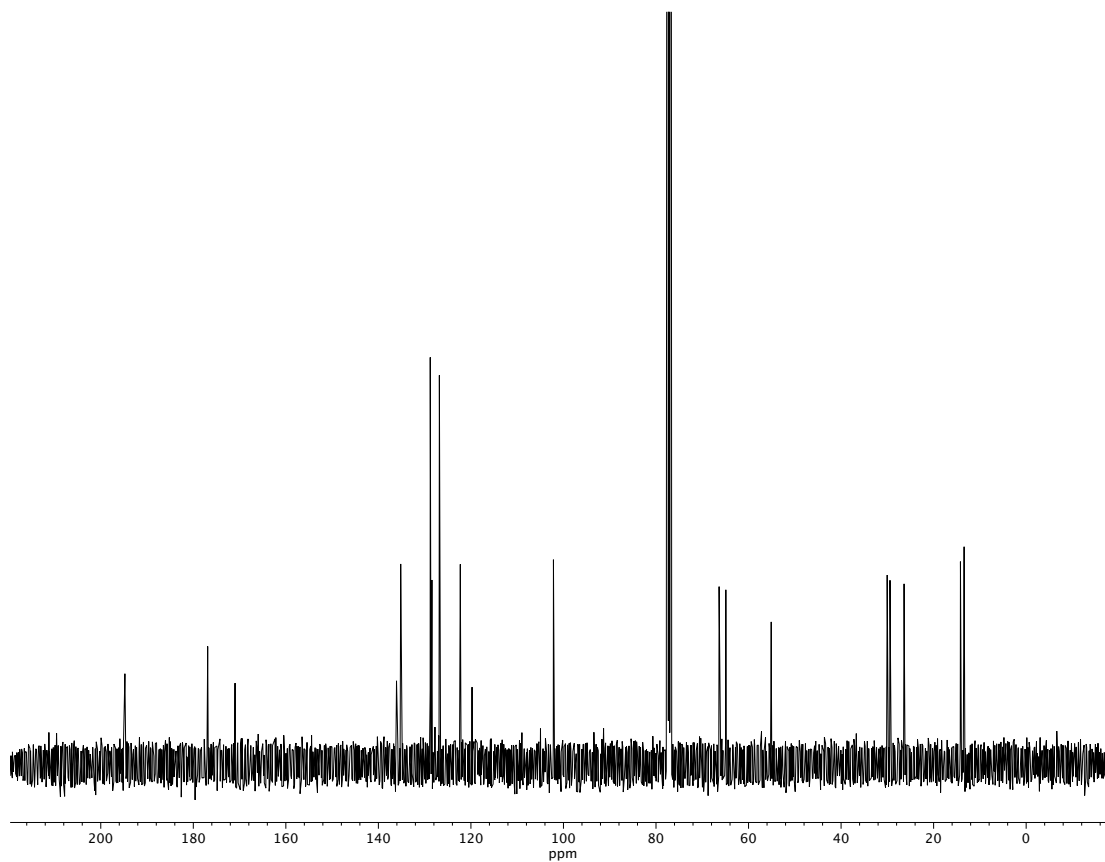
Figure A3.82. ^{13}C *NMR (100 MHz, CDCl$_3$) of compound* **158g**.
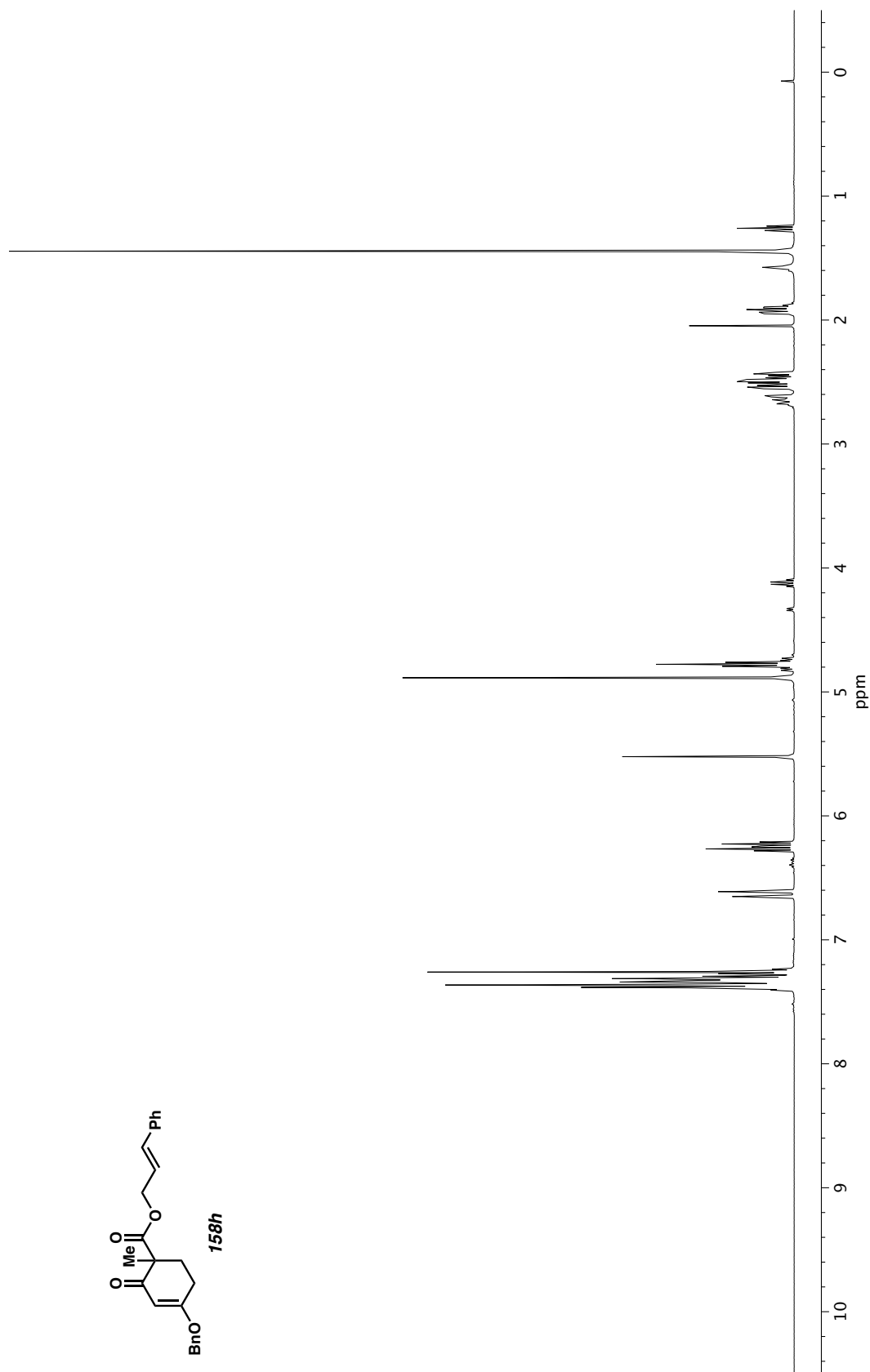
Figure A3.83. ¹H NMR (400 MHz, CDCl₃) of compound **158h**.
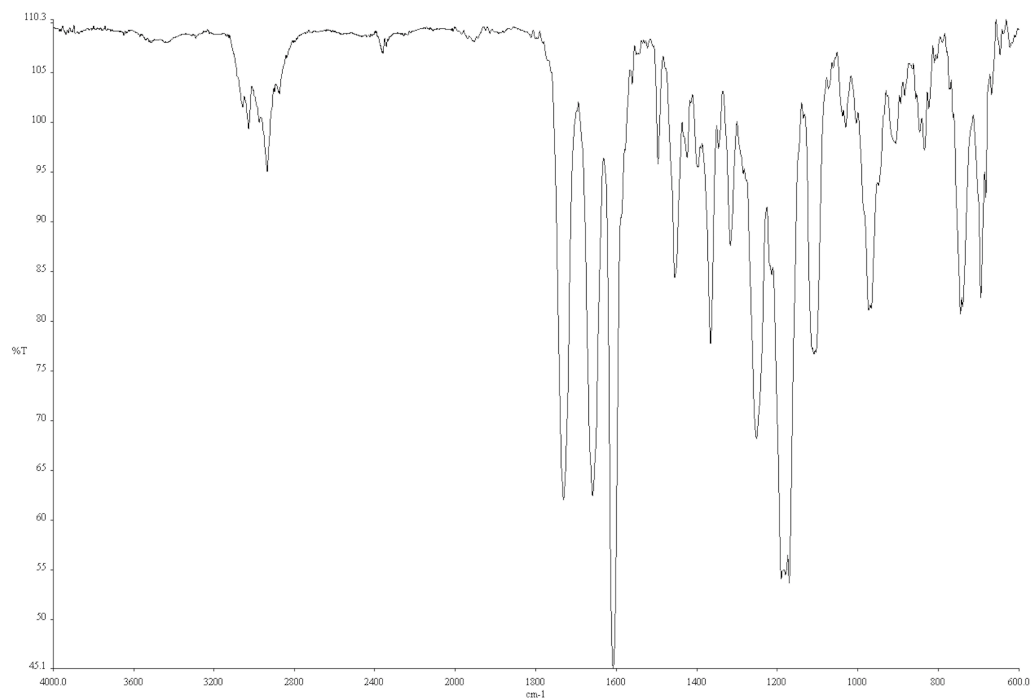
Figure A3.84. Infrared spectrum (Thin Film, NaCl) of compound **158h**.
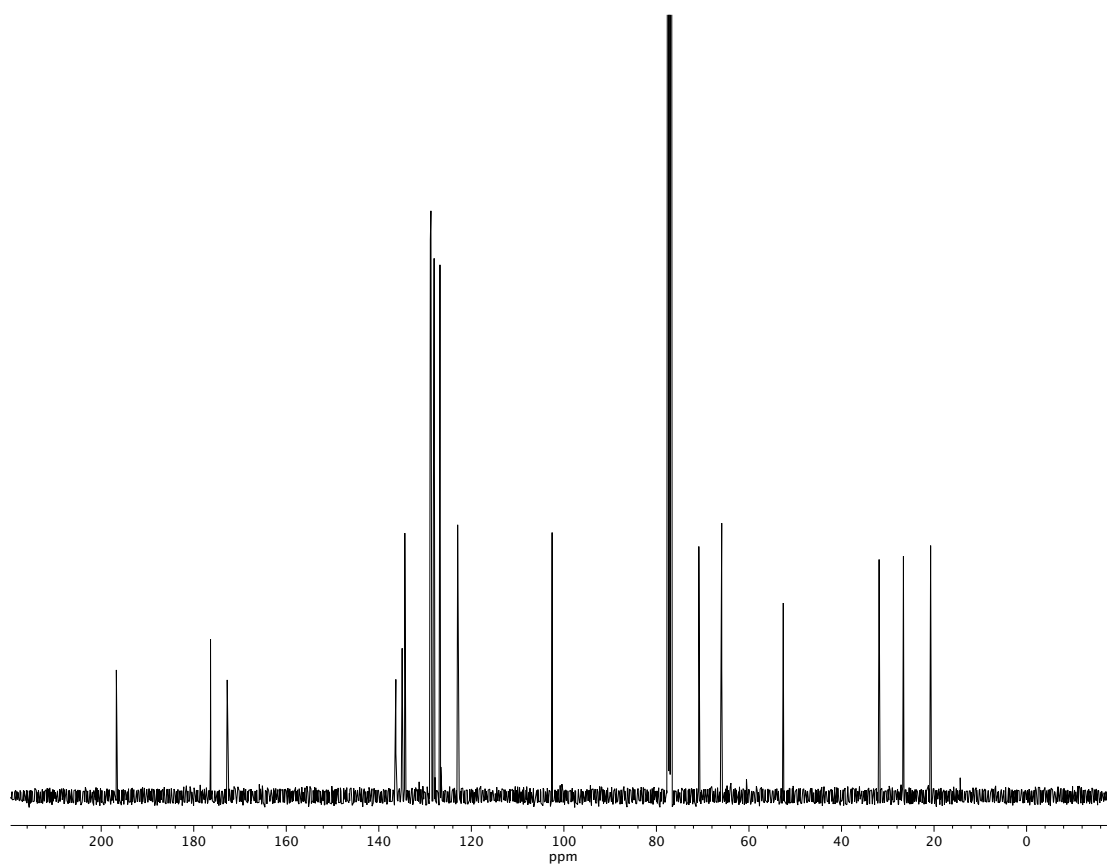
Figure A3.85. ^{13}C NMR (100 MHz, CDCl$_3$) of compound **158h**.
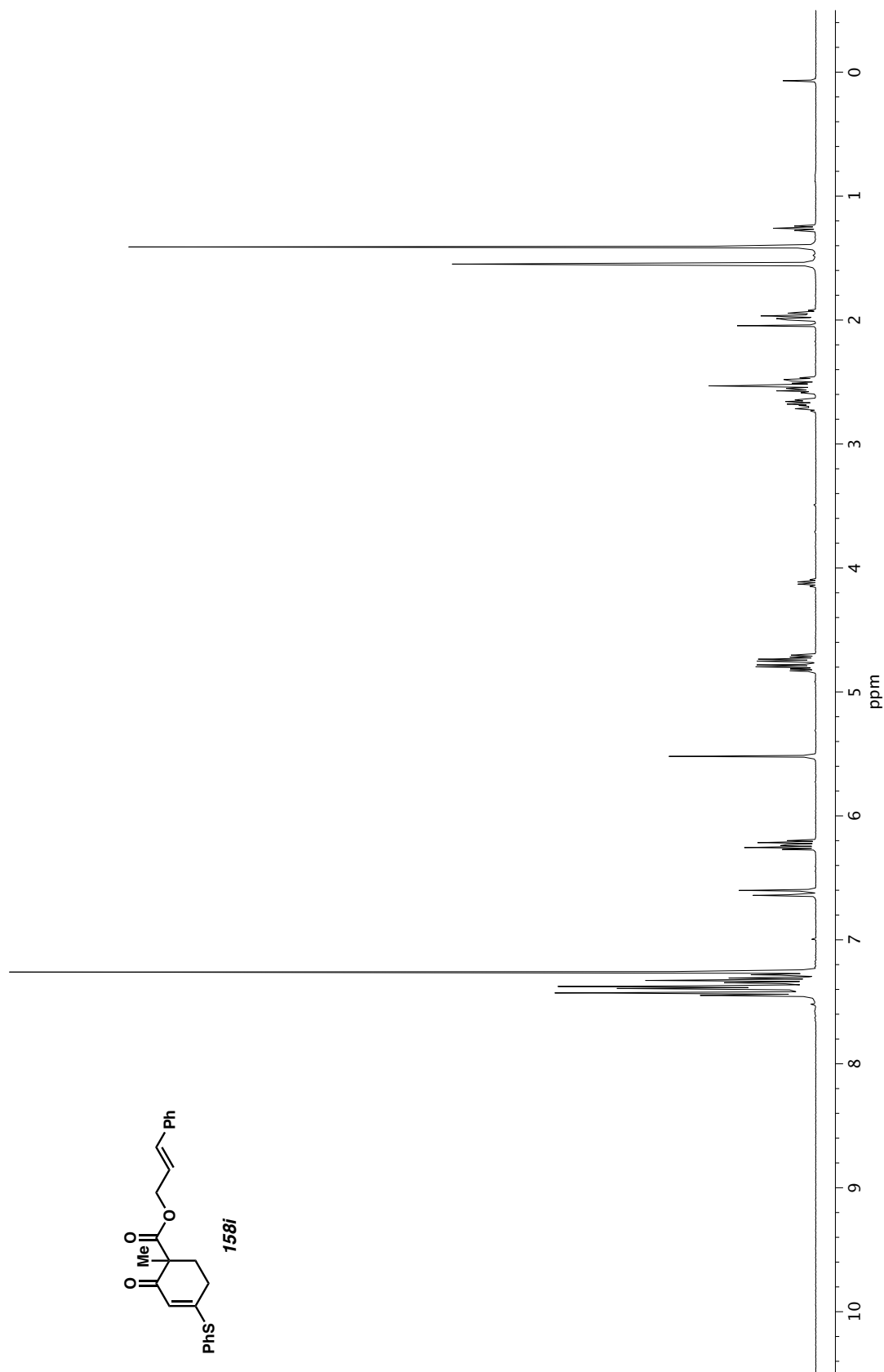
Figure A3.86. ^1H NMR (400 MHz, CDCl$_3$) of compound **158i**.
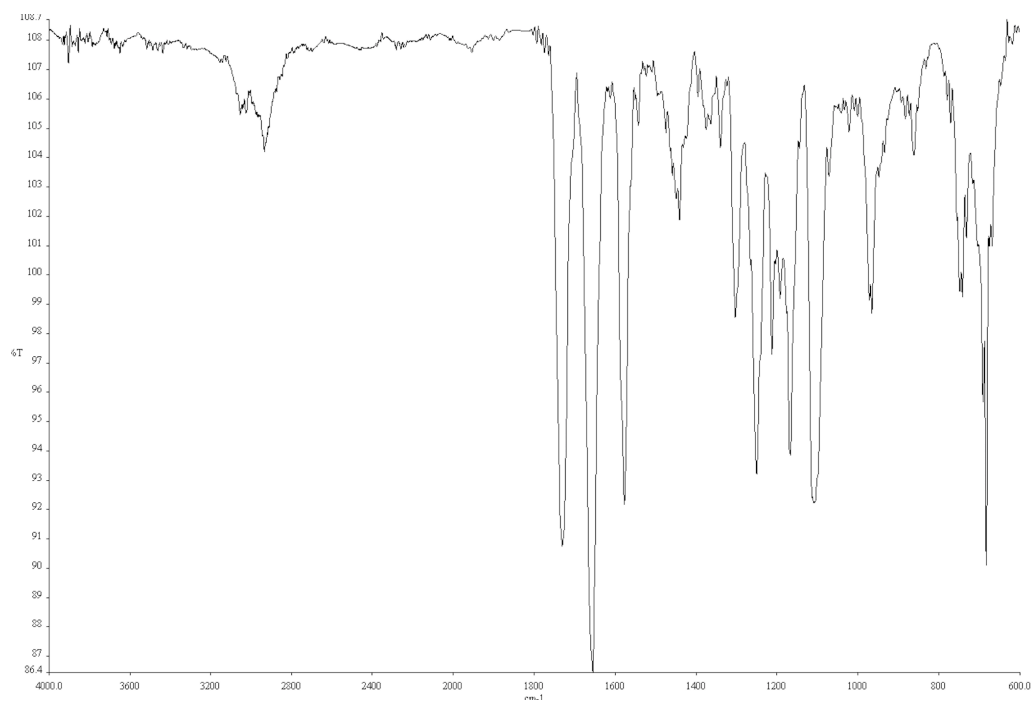
Figure A3.87. *Infrared spectrum (Thin Film, NaCl) of compound* **158i**.
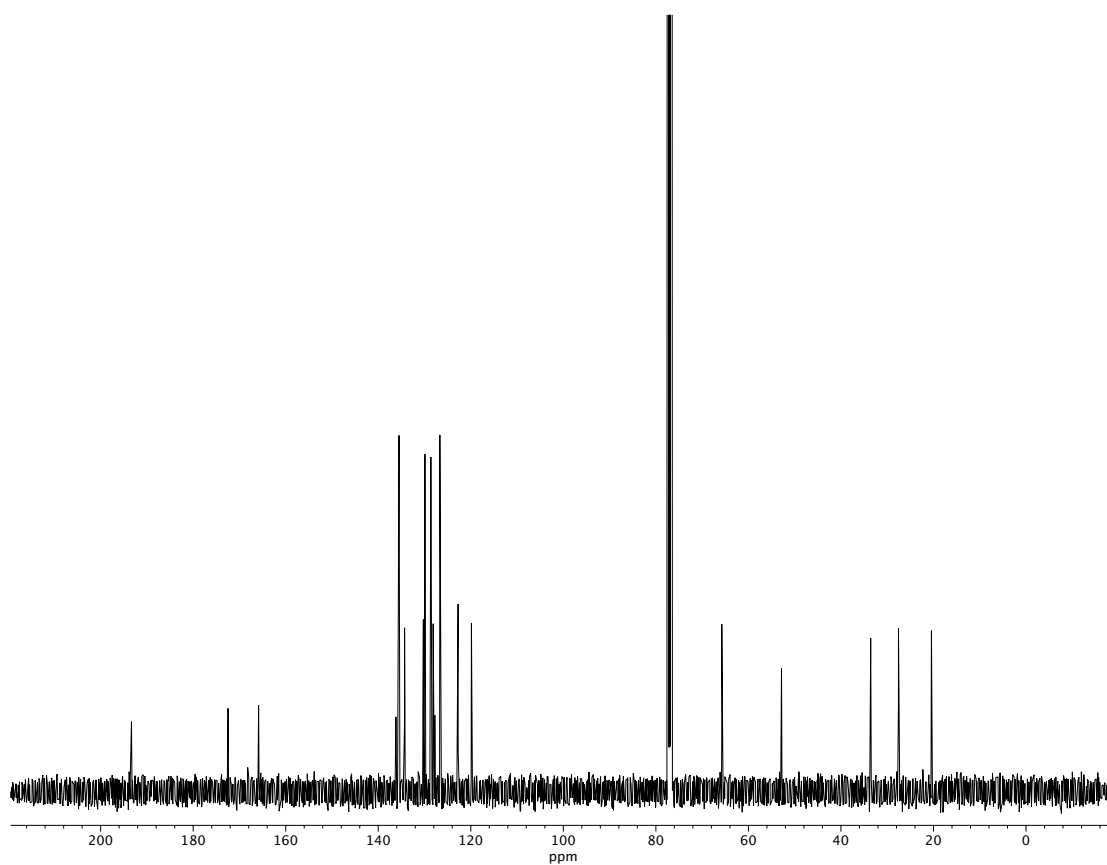
Figure A3.88. ^{13}C *NMR (100 MHz, CDCl$_3$) of compound* **158i**.
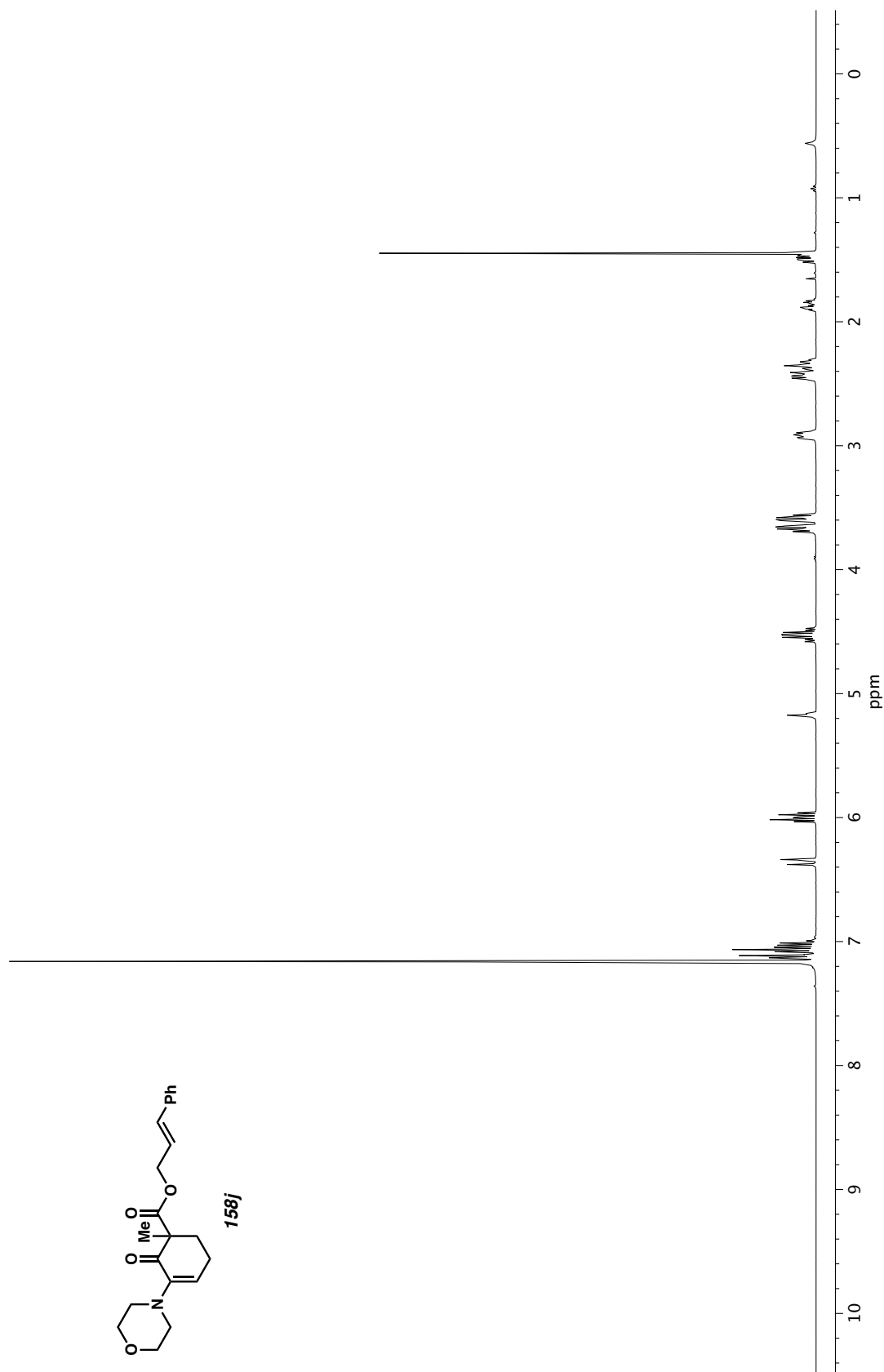
Figure A3.89. ^1H NMR (400 MHz, C_6D_6) of compound **158j**.
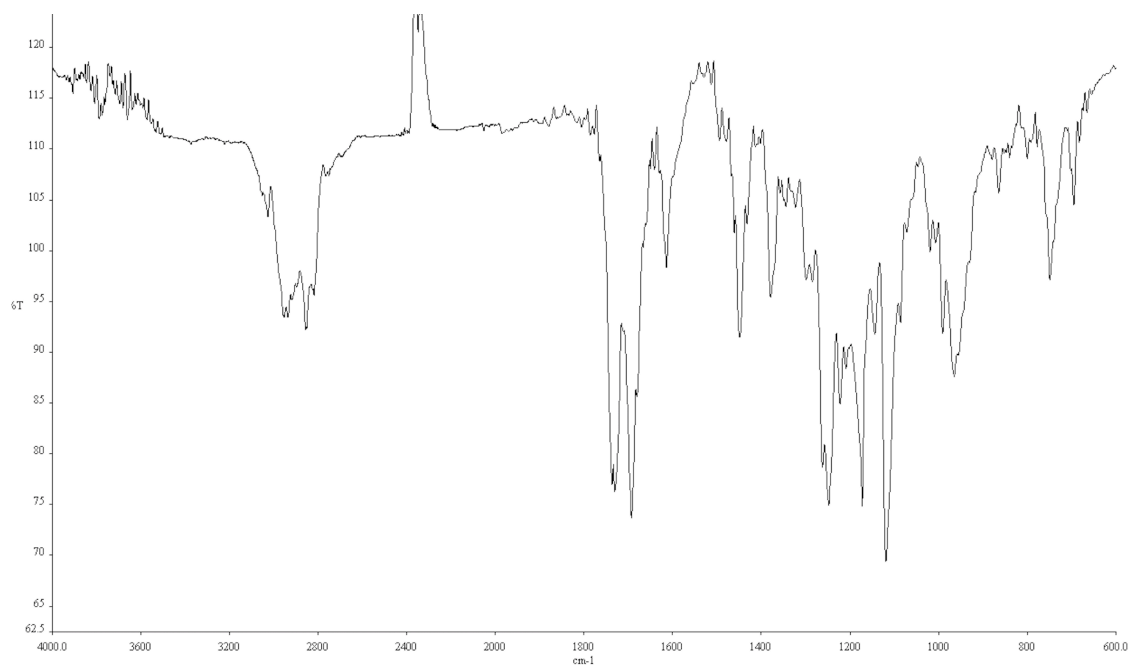
Figure A3.90. *Infrared spectrum (Thin Film, NaCl) of compound* **158j**.
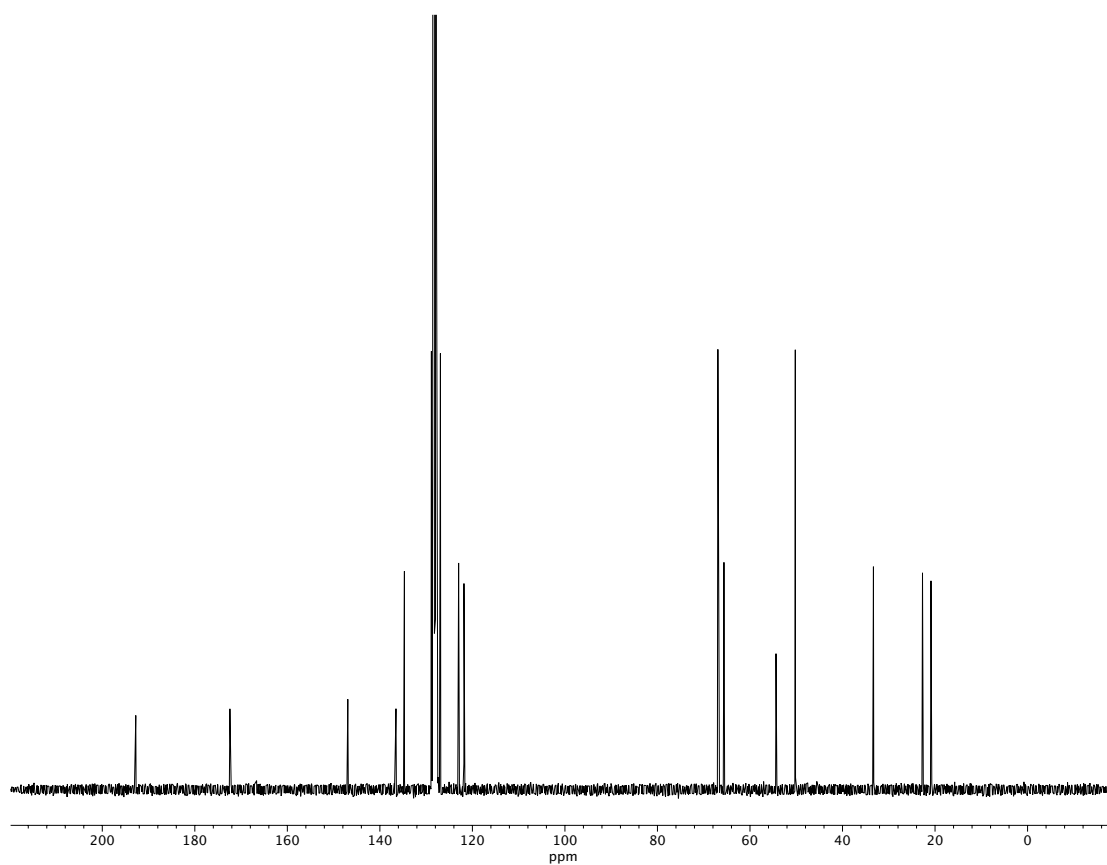
Figure A3.91. *^{13}C NMR (100 MHz, C_6D_6) of compound* **158j**.
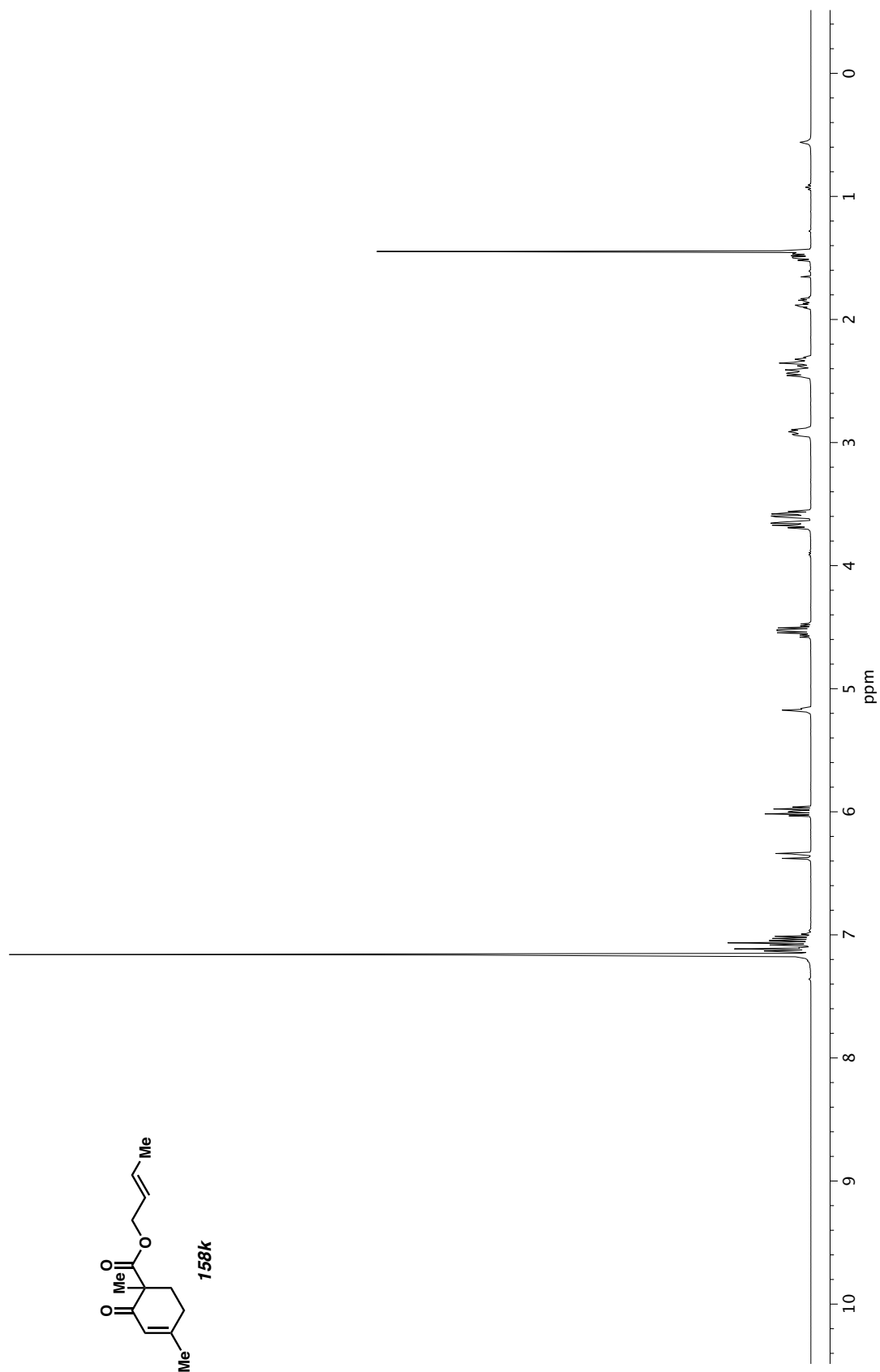
Figure A3.92. *¹H NMR (400 MHz, CDCl₃) of compound **158k**.*
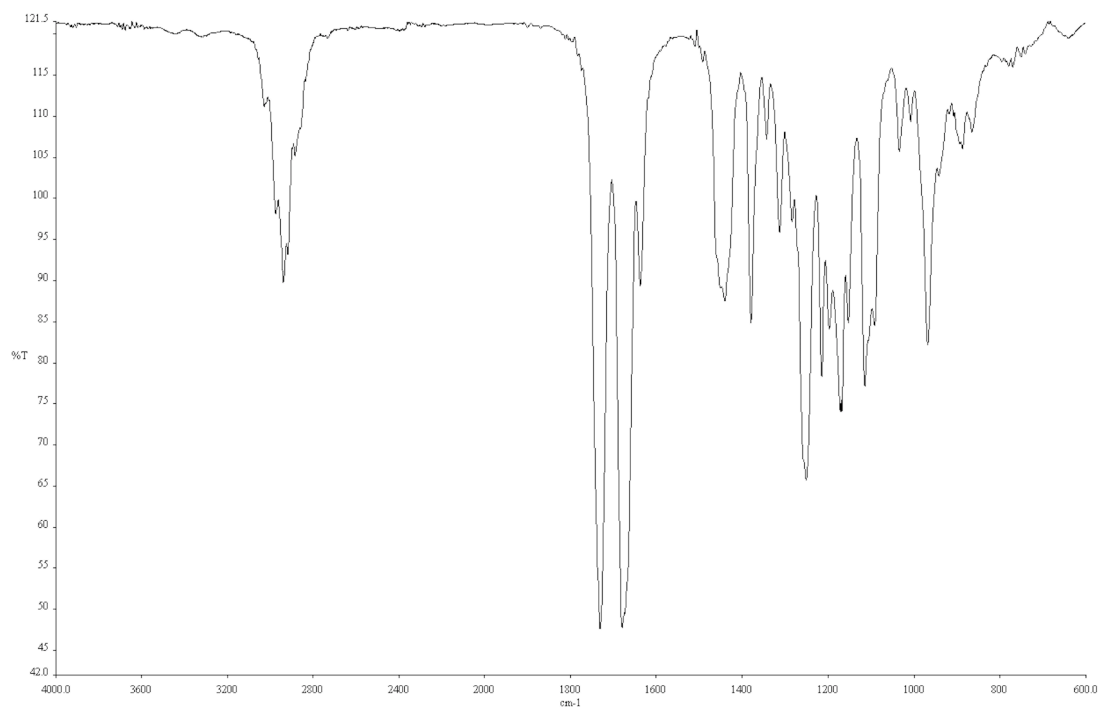
Figure A3.93. *Infrared spectrum (Thin Film, NaCl) of compound* **158k**.
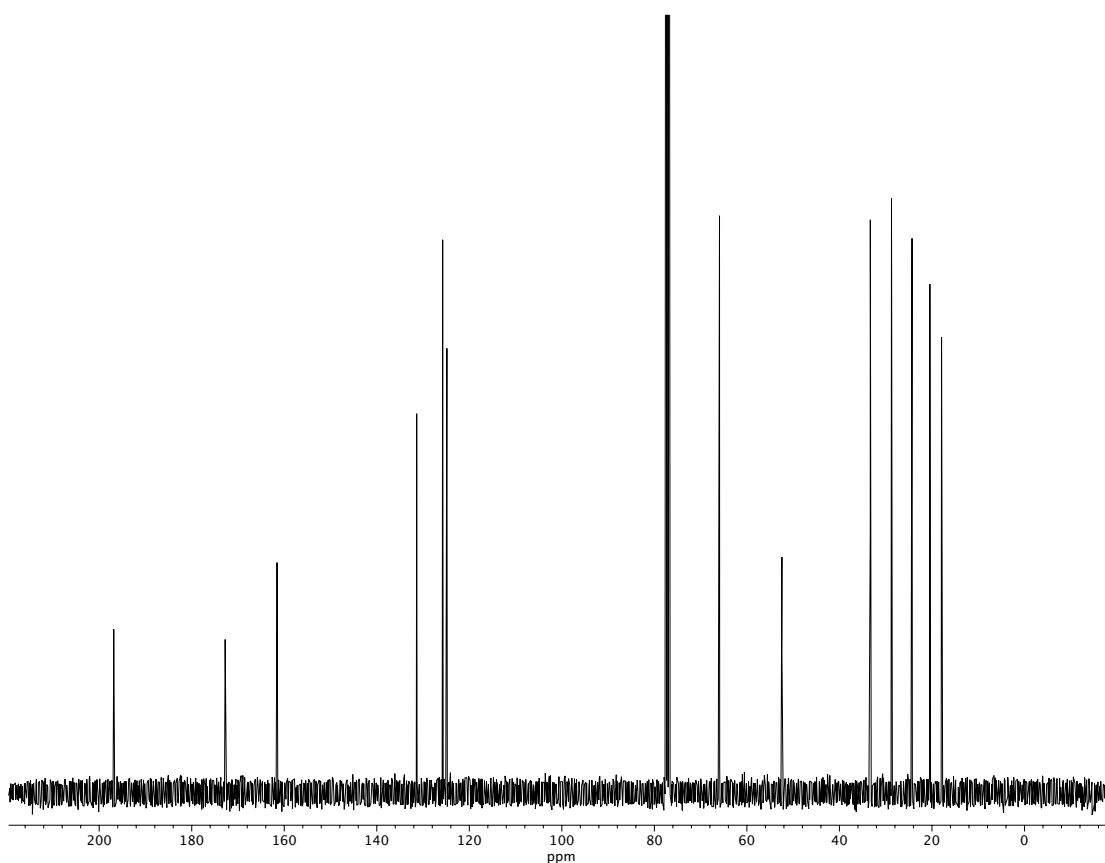
Figure A3.94. ^{13}C *NMR (100 MHz, CDCl$_3$) of compound* **158k**.
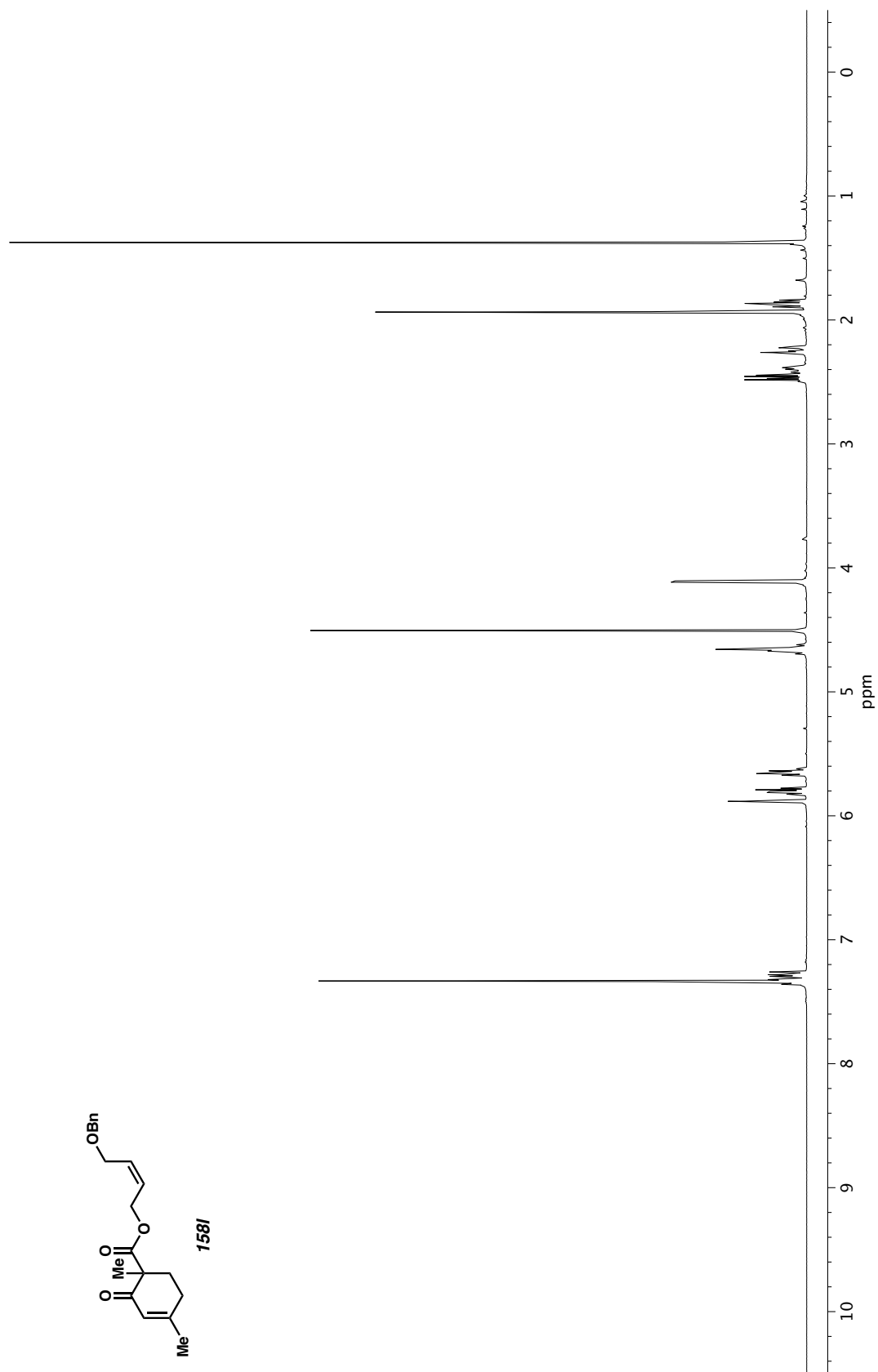
Figure A3.95. ^1H NMR (400 MHz, CDCl$_3$) of compound *158l*.
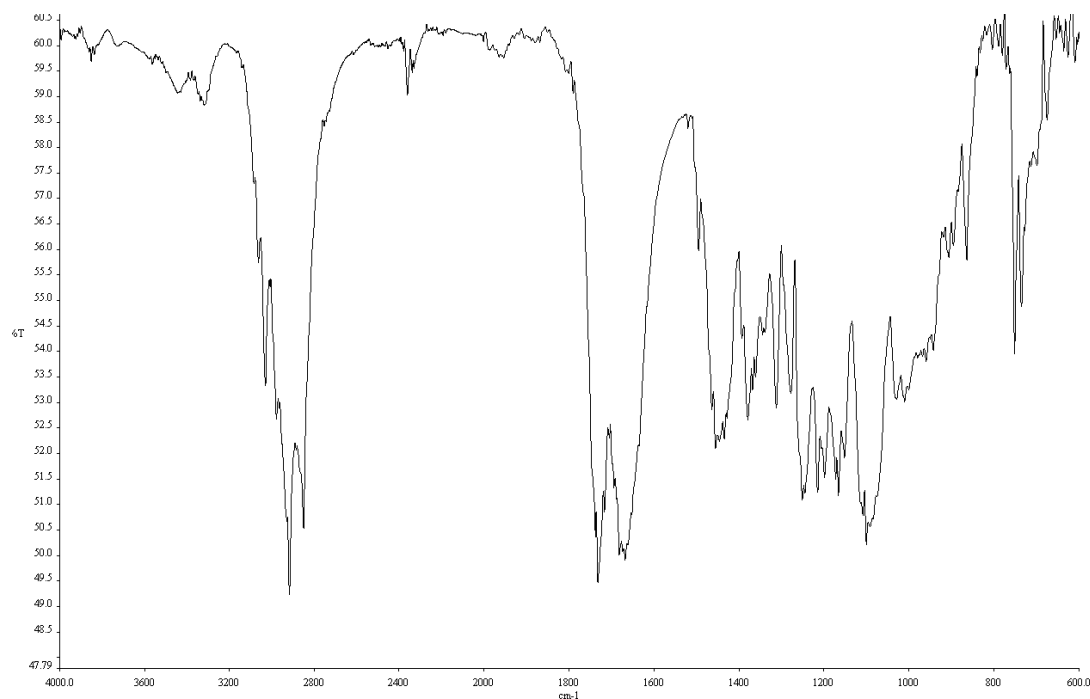
Figure A3.96. Infrared spectrum (Thin Film, NaCl) of compound **158l**.
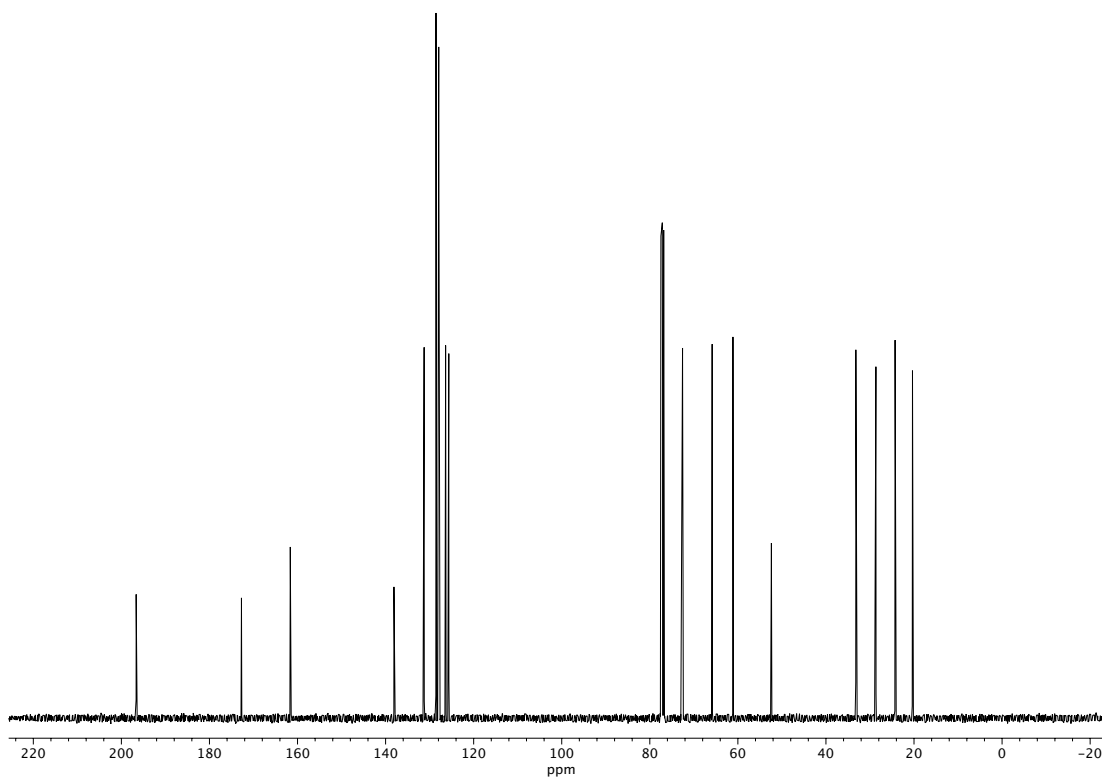
Figure A3.97. ^{13}C NMR (100 MHz, CDCl$_3$) of compound **158l**.
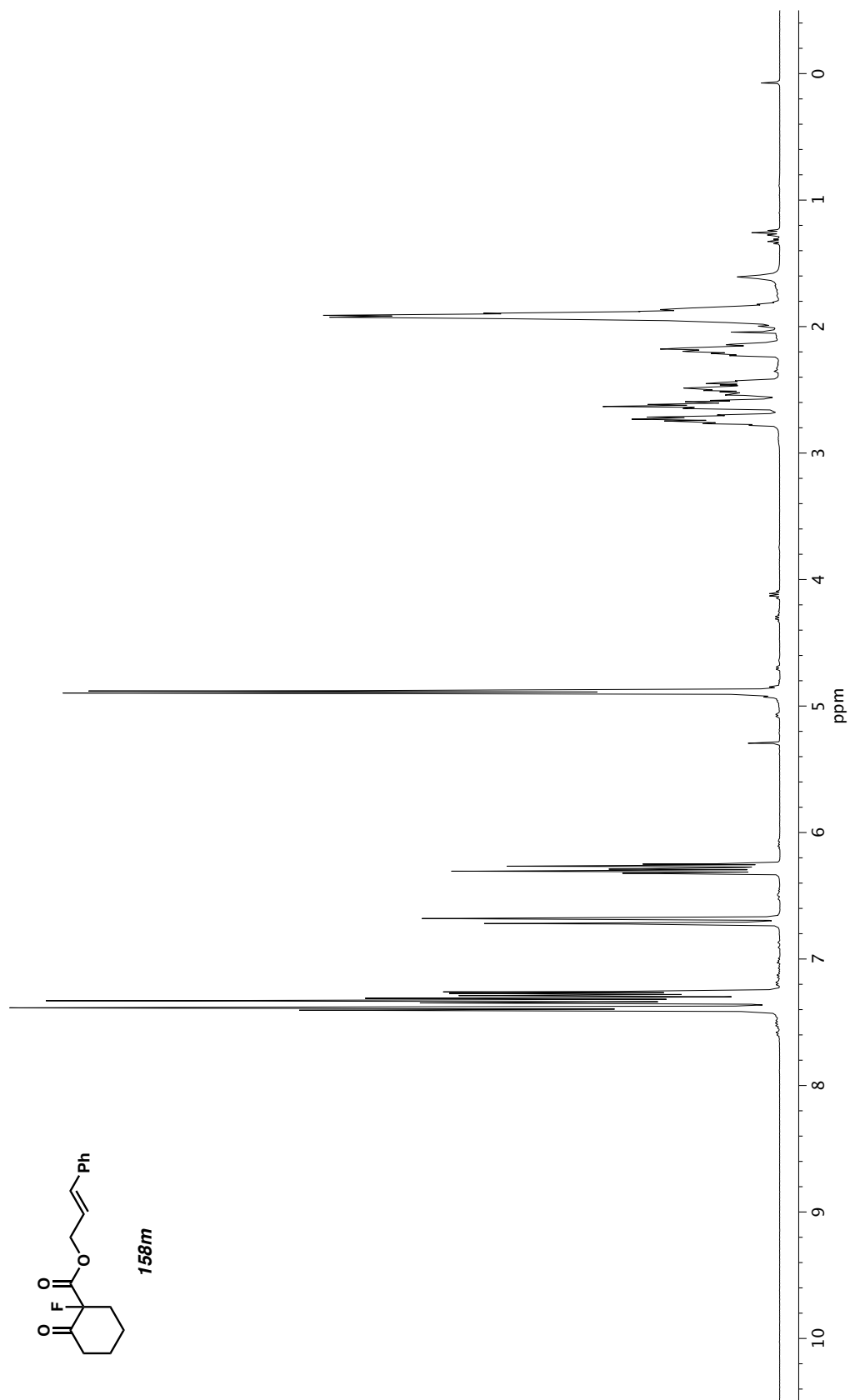
Figure A3.98. ^1H NMR (400 MHz, CDCl$_3$) of compound **158m**.
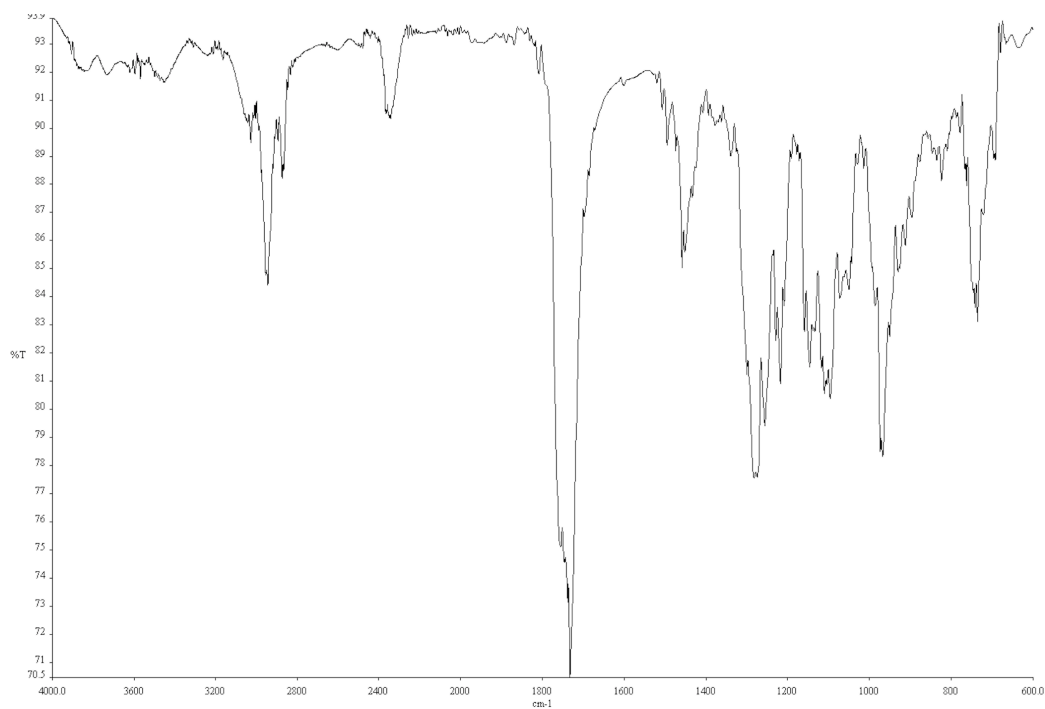
Figure A3.99. *Infrared spectrum (Thin Film, NaCl) of compound **158m**.*
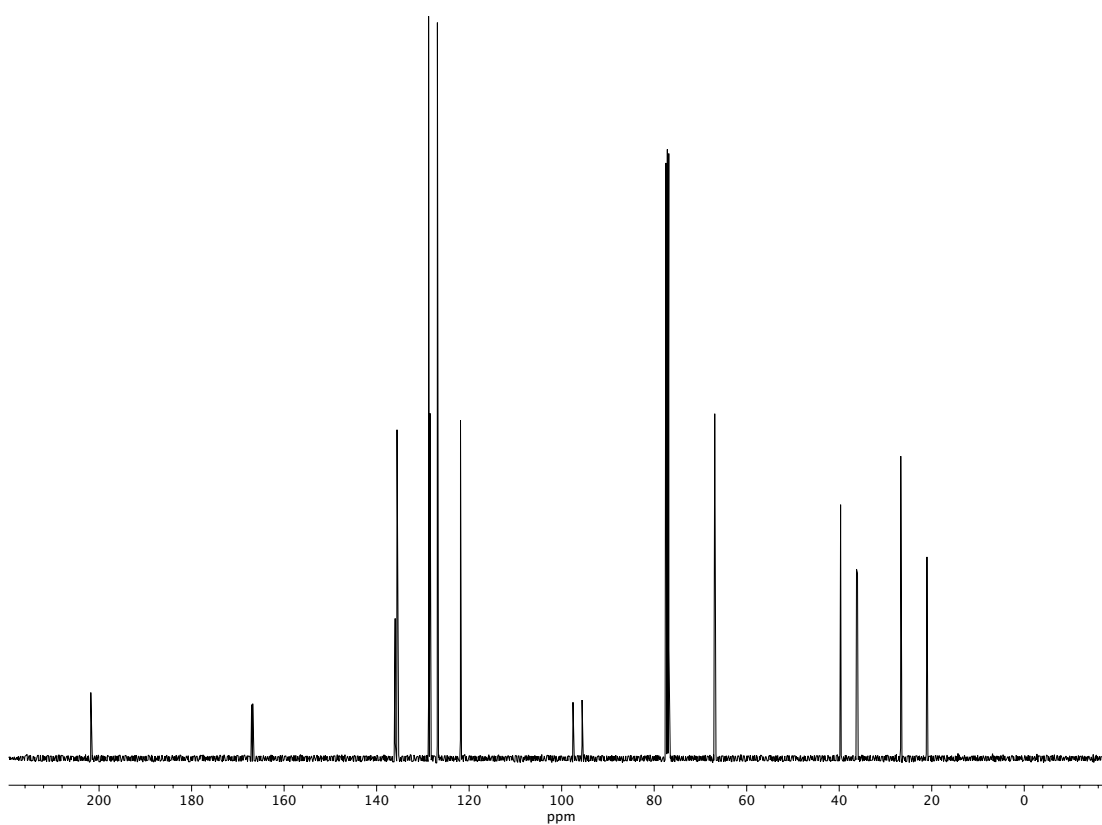
Figure A3.100. *^{13}C NMR (100 MHz, CDCl$_3$) of compound **158m**.*
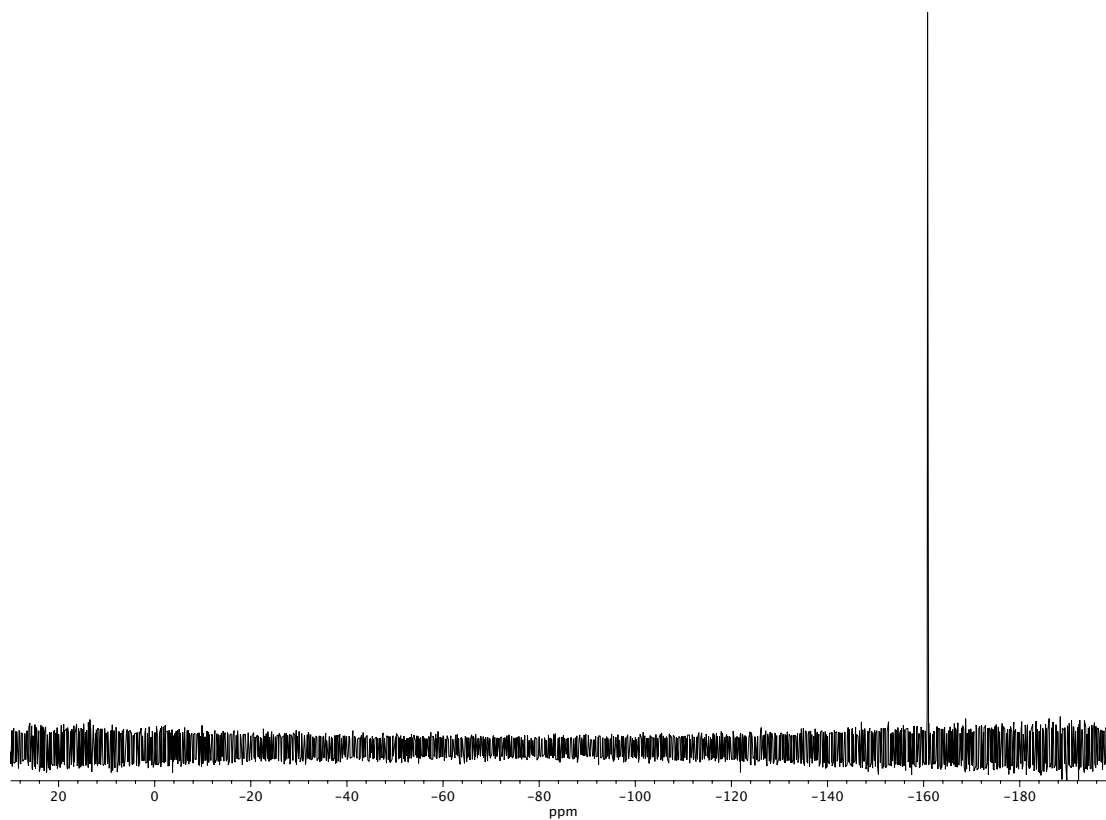
Figure A3.101. ^{19}F NMR (282 MHz, CDCl$_3$) of compound **158m**.
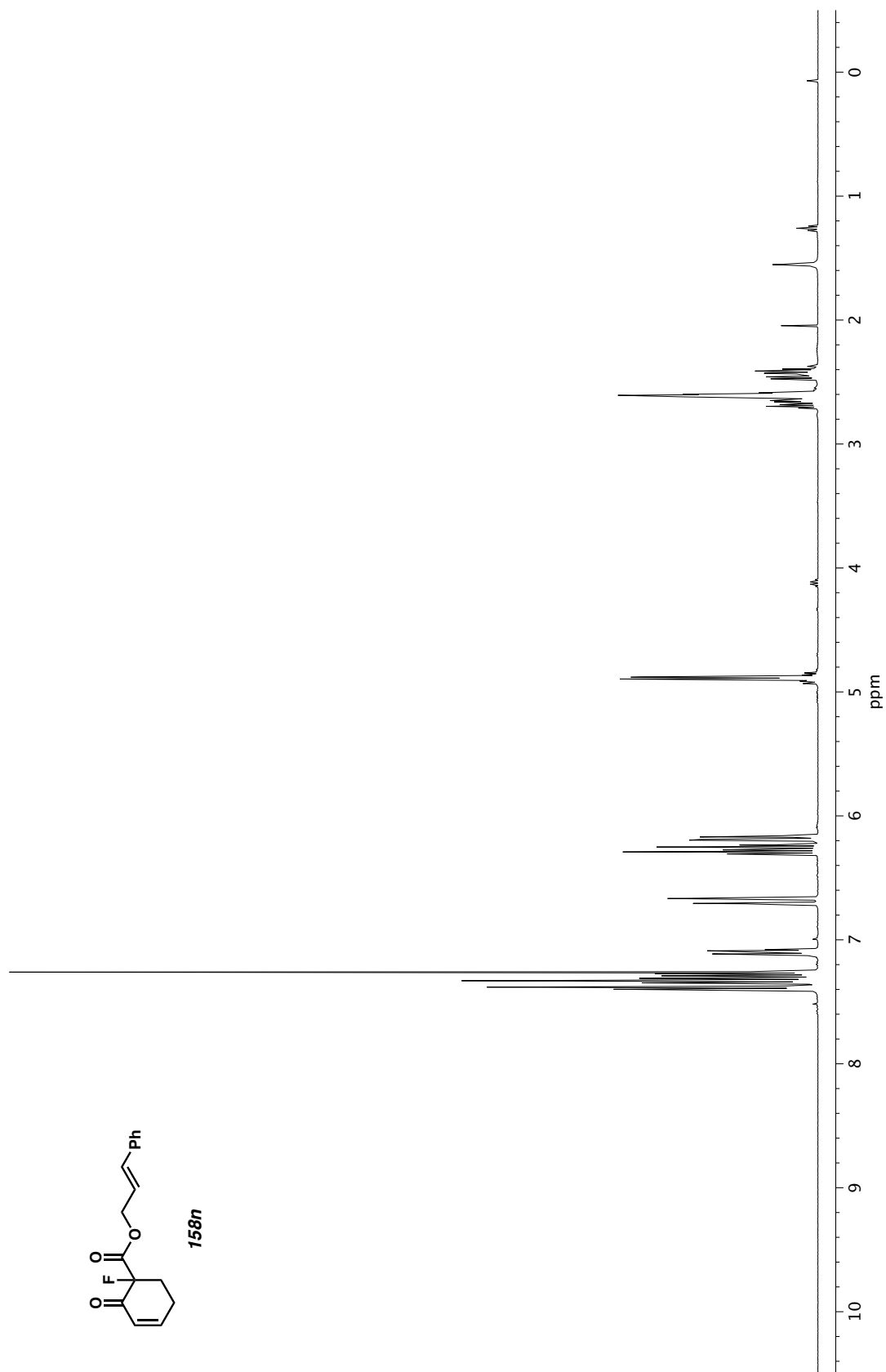
Figure A3.102. ^1H NMR (400 MHz, CDCl$_3$) of compound **158n**.
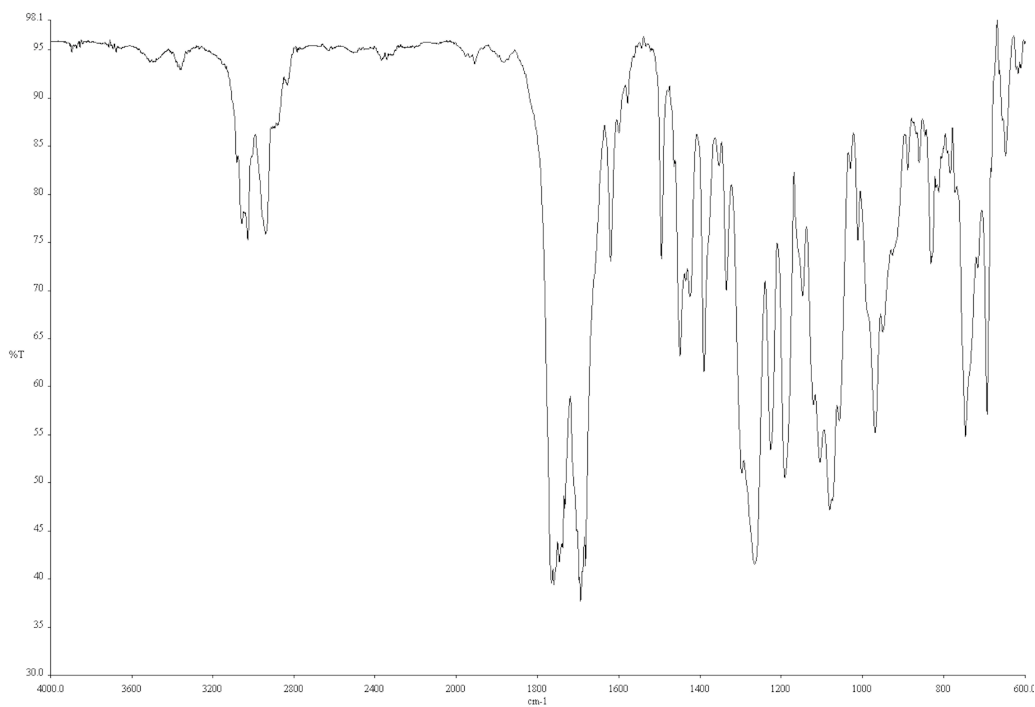
Figure A3.103. *Infrared spectrum (Thin Film, NaCl) of compound* **158n**.
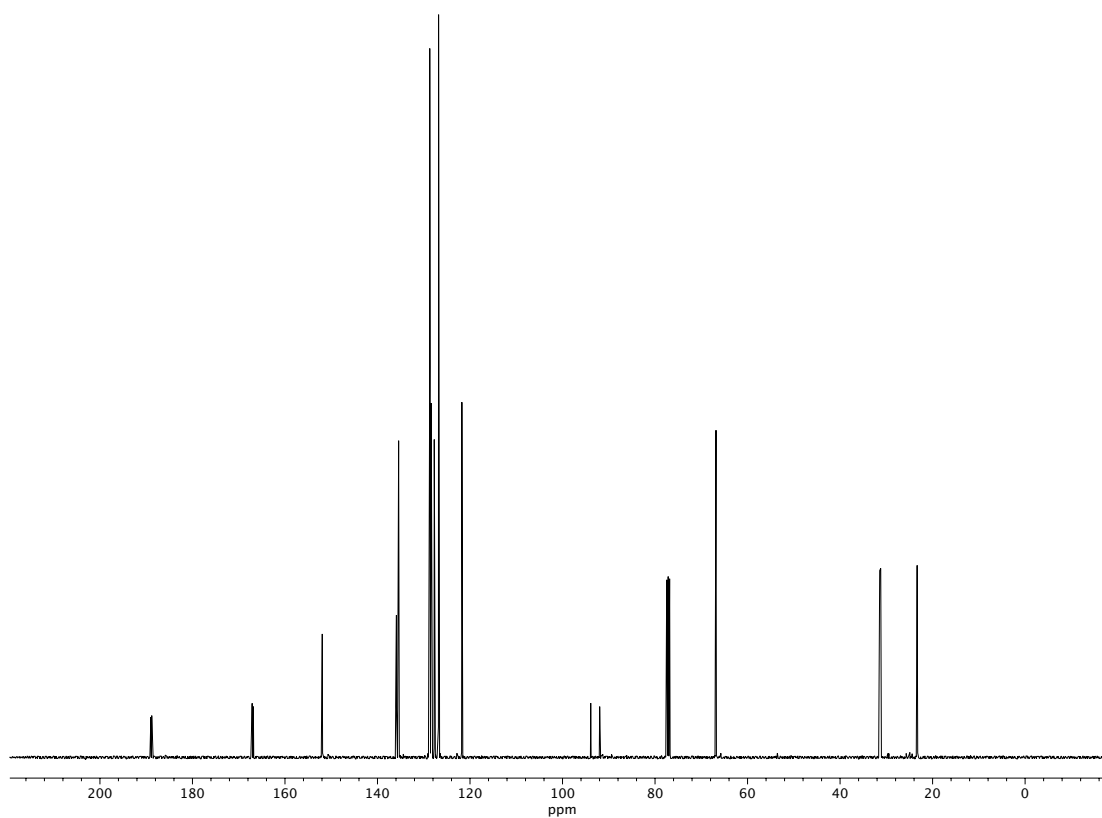
Figure A3.104. ^{13}C *NMR (100 MHz, CDCl$_3$) of compound* **158n**.
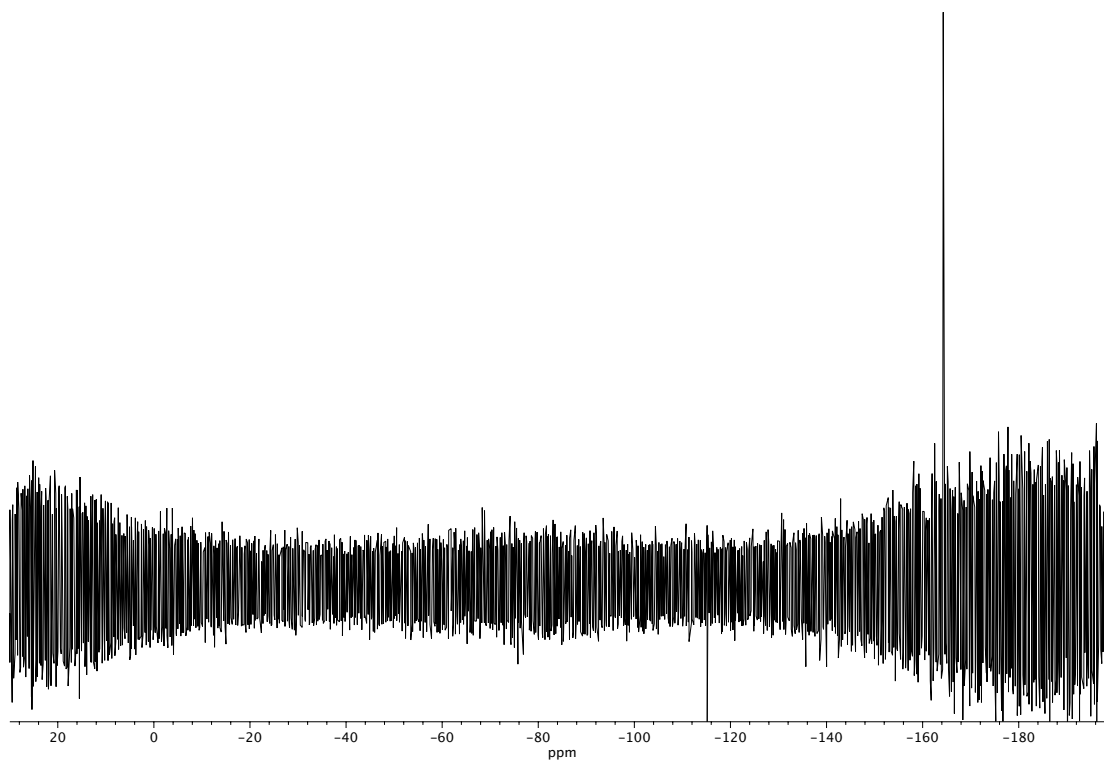
Figure A3.105. ^{19}F NMR (282 MHz, CDCl$_3$) of compound **158n**.

Figure A3.106. *^1H NMR (400 MHz, CDCl$_3$) of compound 158o.*
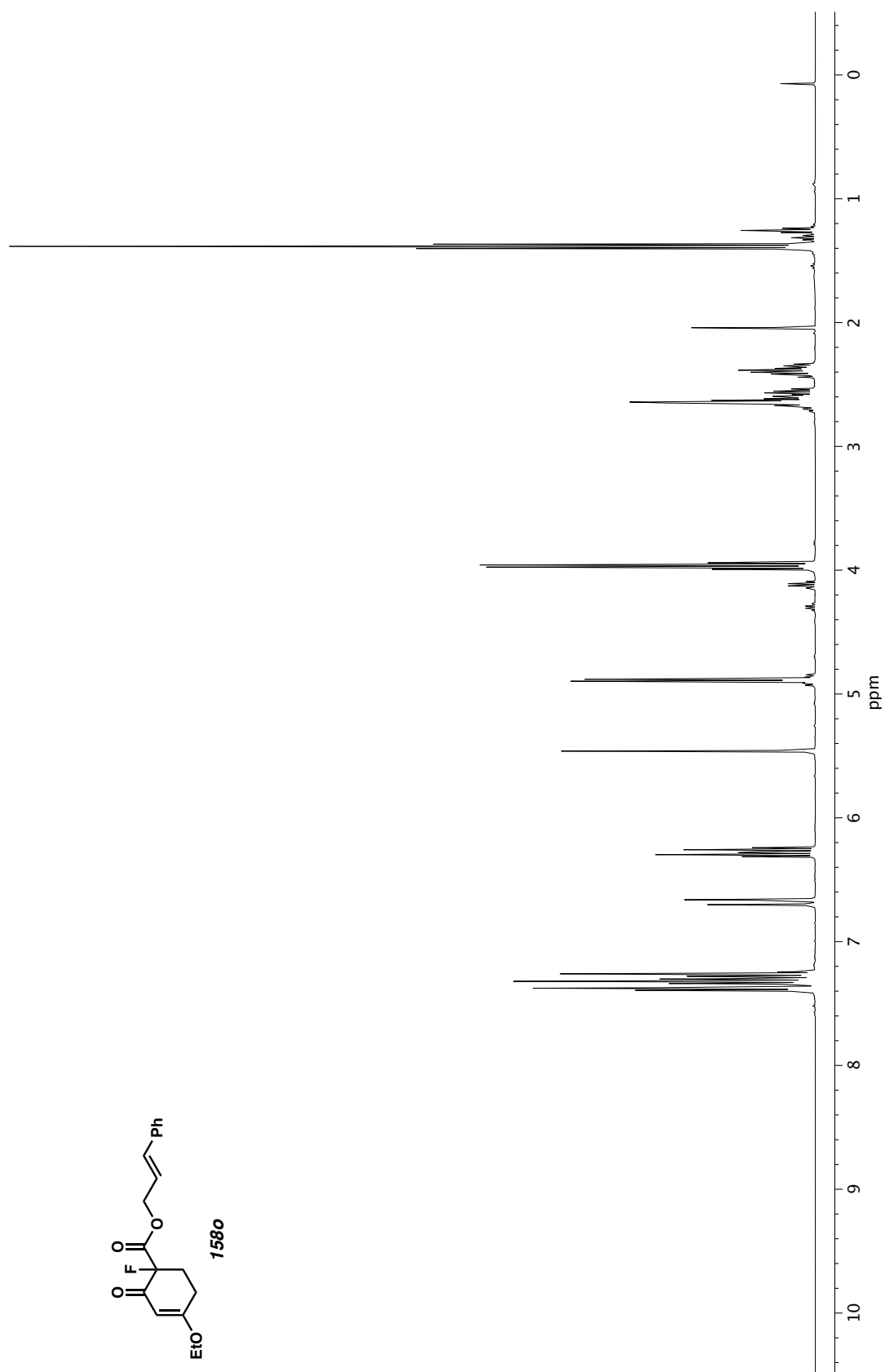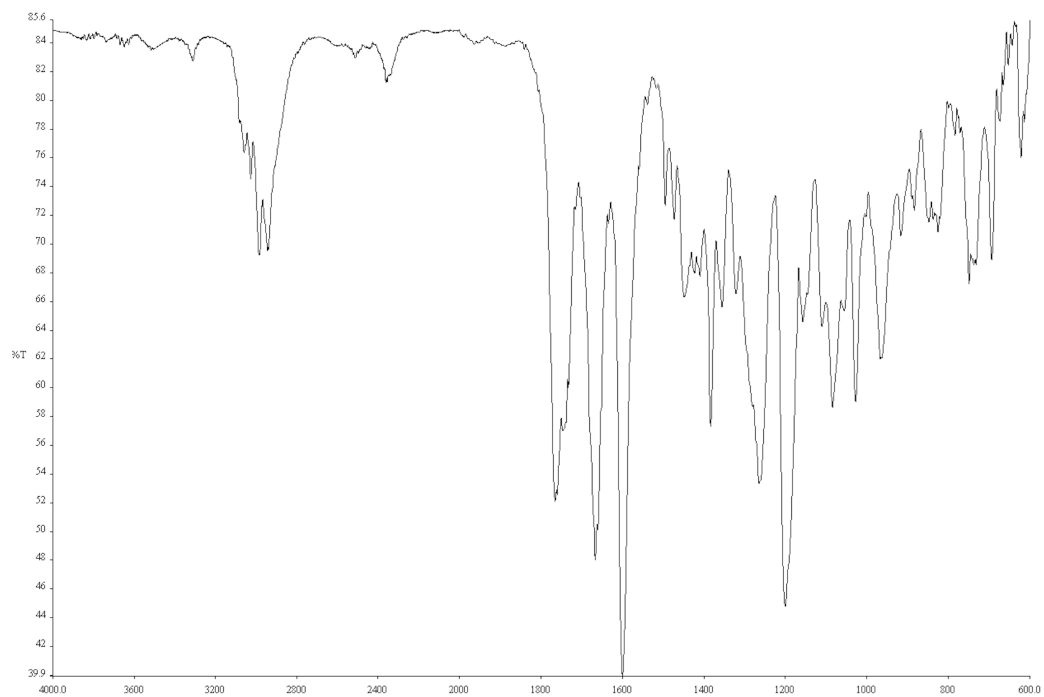
Figure A3.107. Infrared spectrum (Thin Film, NaCl) of compound **158o**.
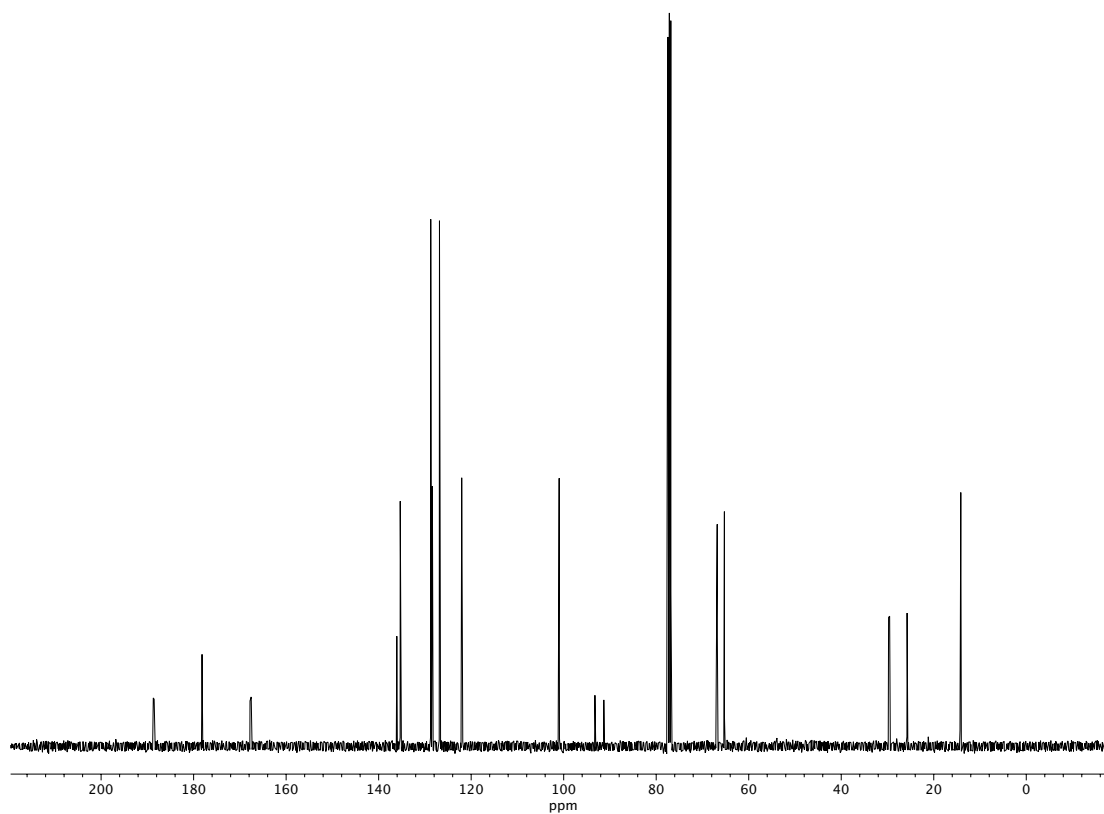
Figure A3.108. ^{13}C NMR (100 MHz, CDCl$_3$) of compound **158o**.
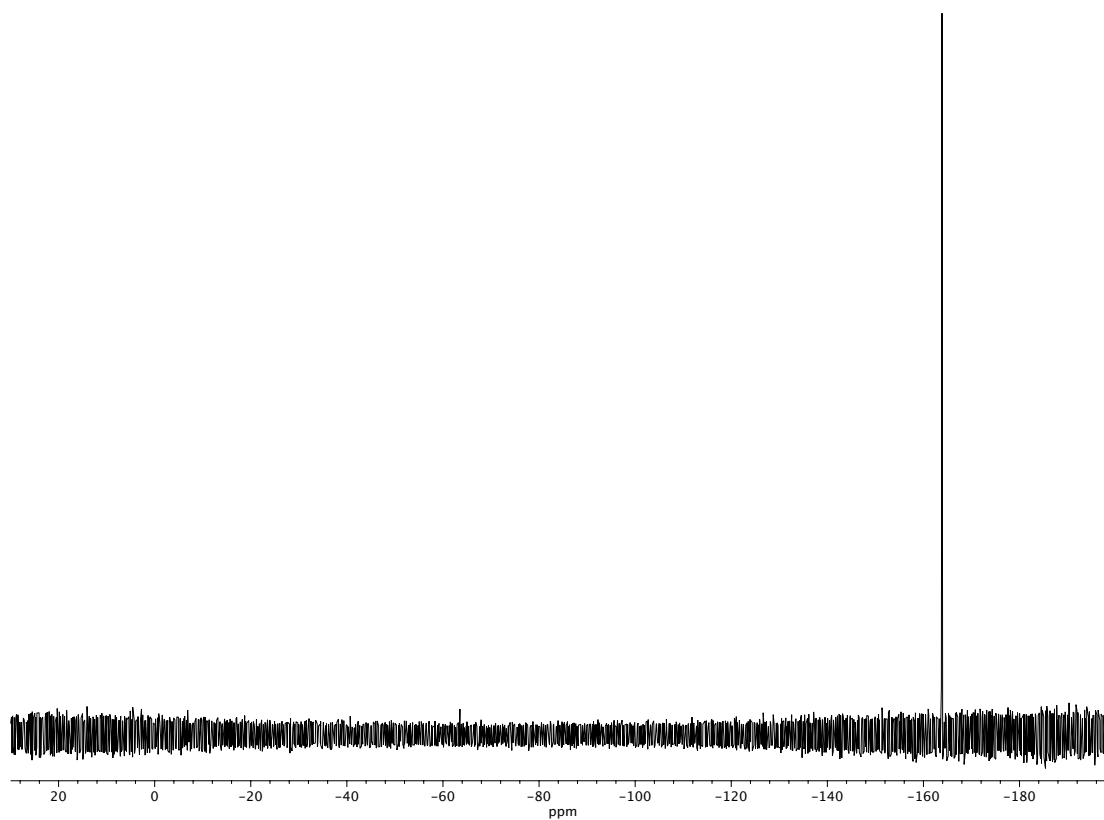
Figure A3.109. ^{19}F NMR (282 MHz, CDCl$_3$) of compound **158o**.
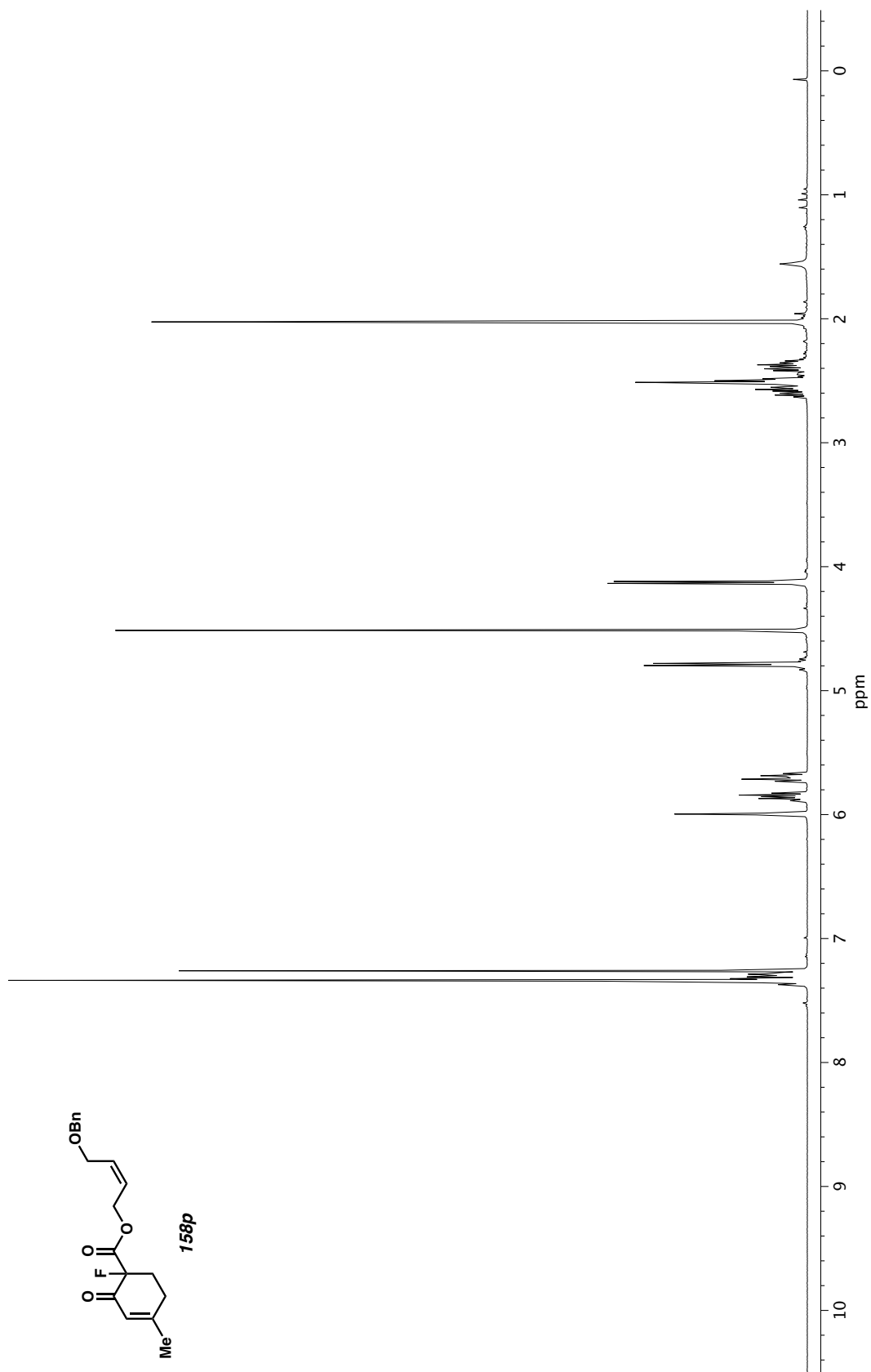
Figure A3.110. ^{1}H NMR (400 MHz, CDCl$_3$) of compound **158p**.
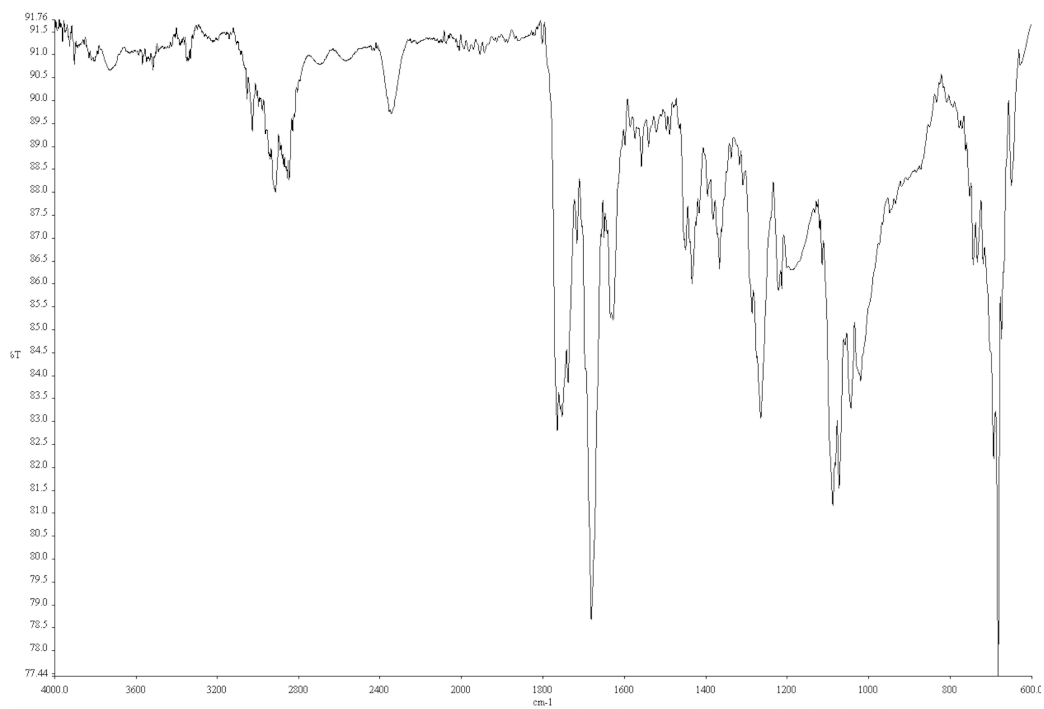
Figure A3.111. Infrared spectrum (Thin Film, NaCl) of compound **158p**.
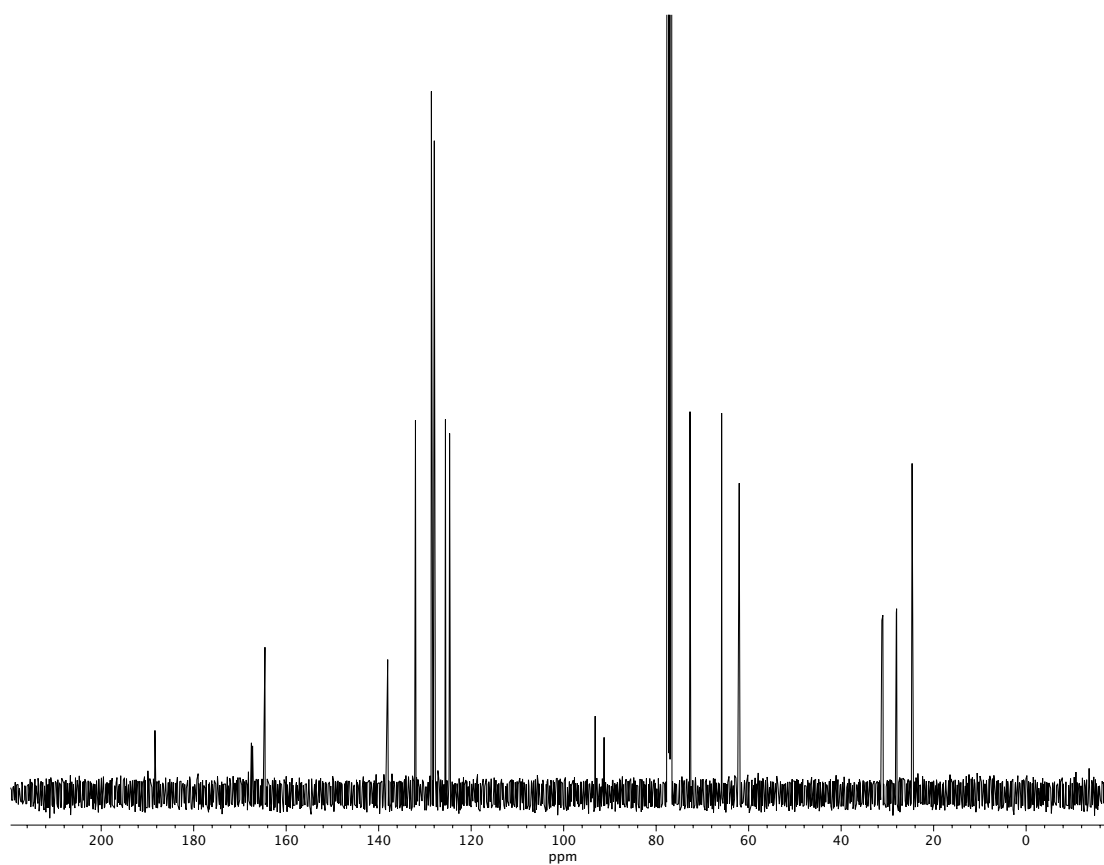
Figure A3.112. ^{13}C NMR (100 MHz, CDCl$_3$) of compound **158p**.
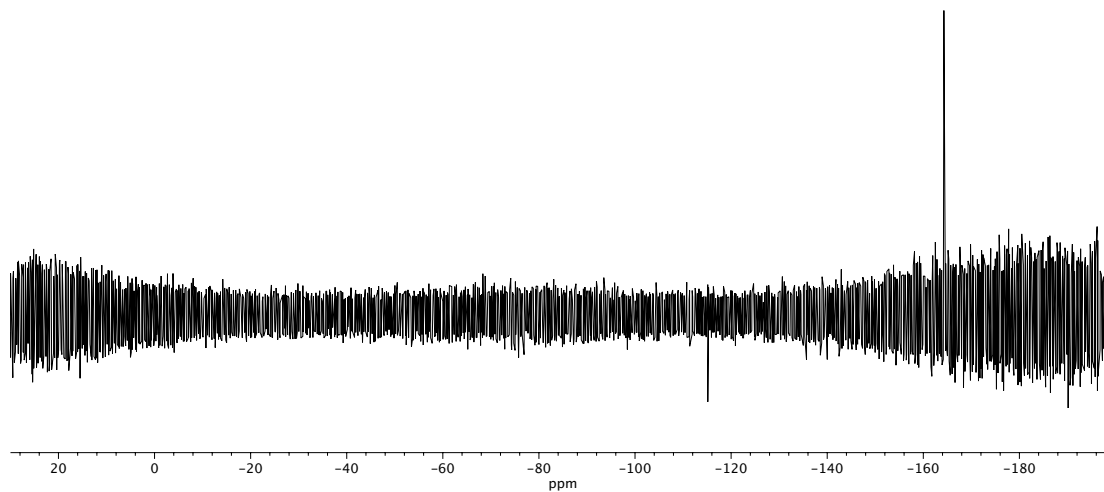
Figure A3.113. ^{19}F NMR (282 MHz, CDCl$_3$) of compound **158p**.
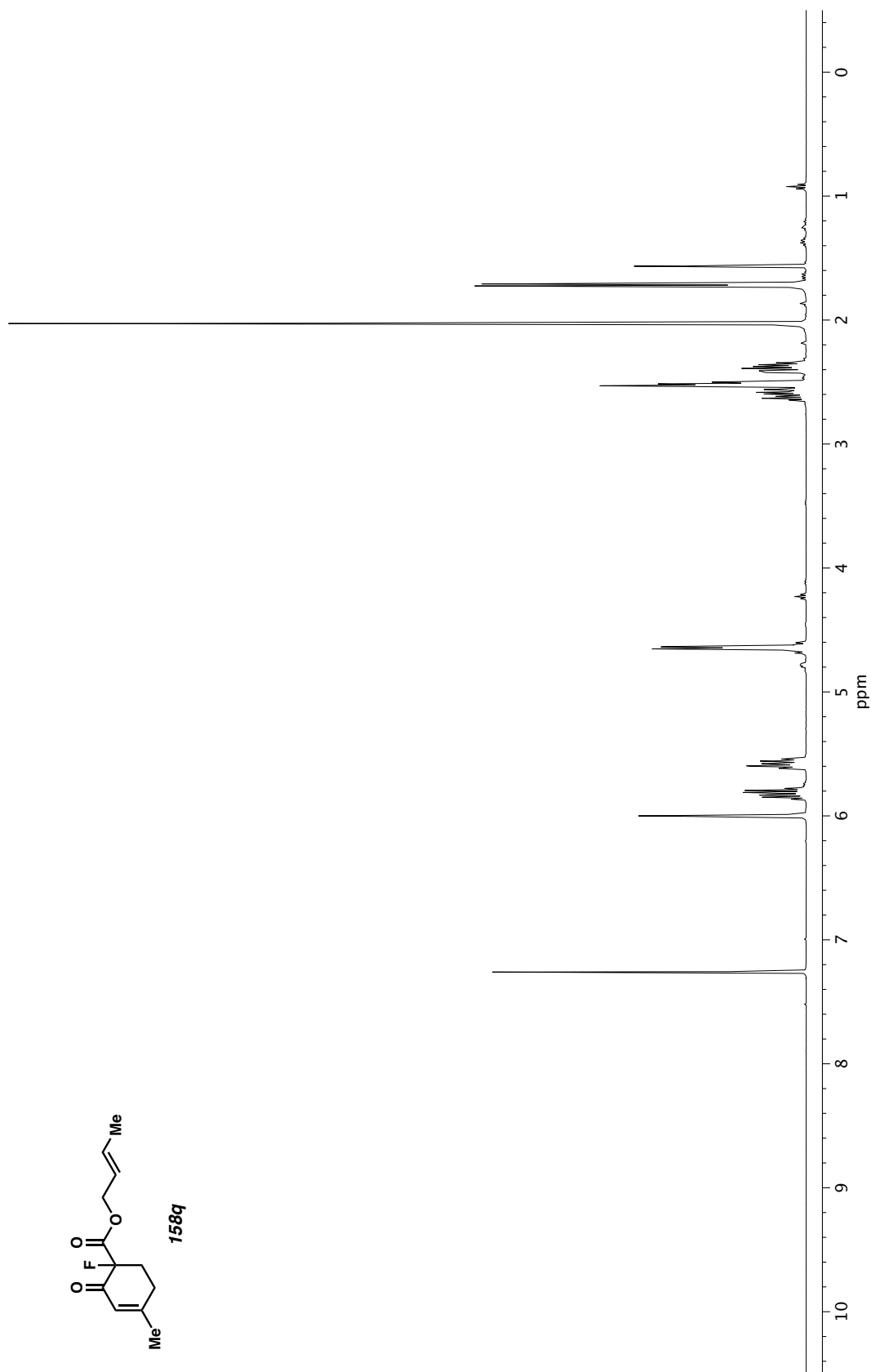
Figure A3.114. ^1H NMR (400 MHz, CDCl$_3$) of compound **158q**.
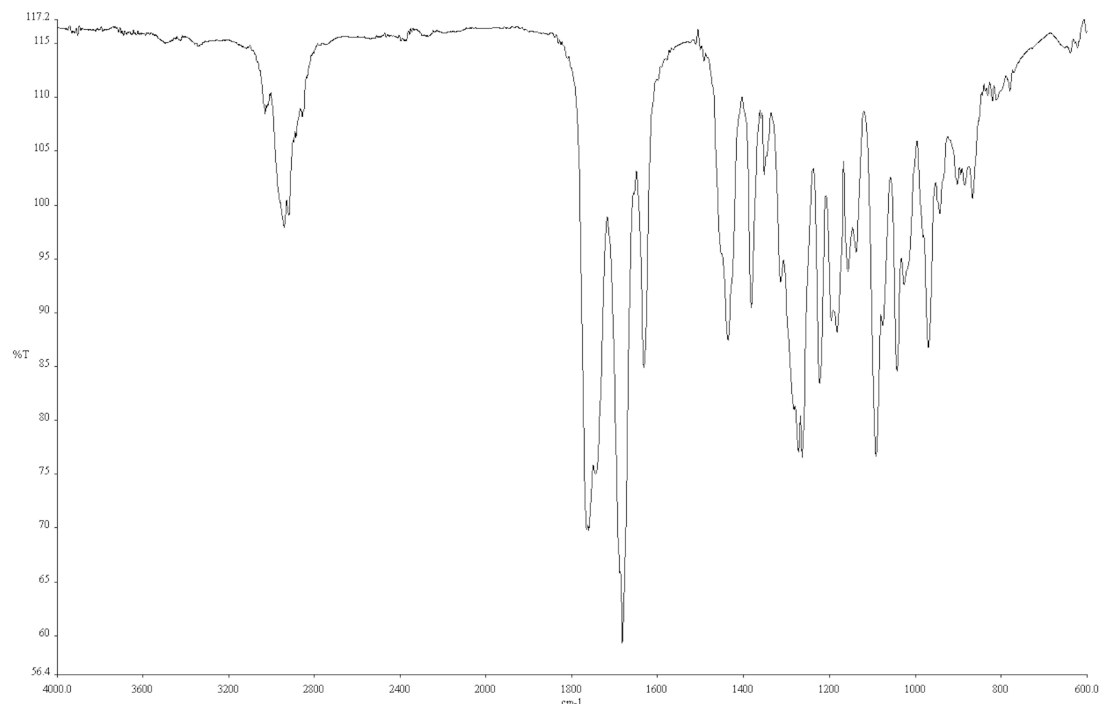
Figure A3.115. *Infrared spectrum (Thin Film, NaCl) of compound **158q**.*
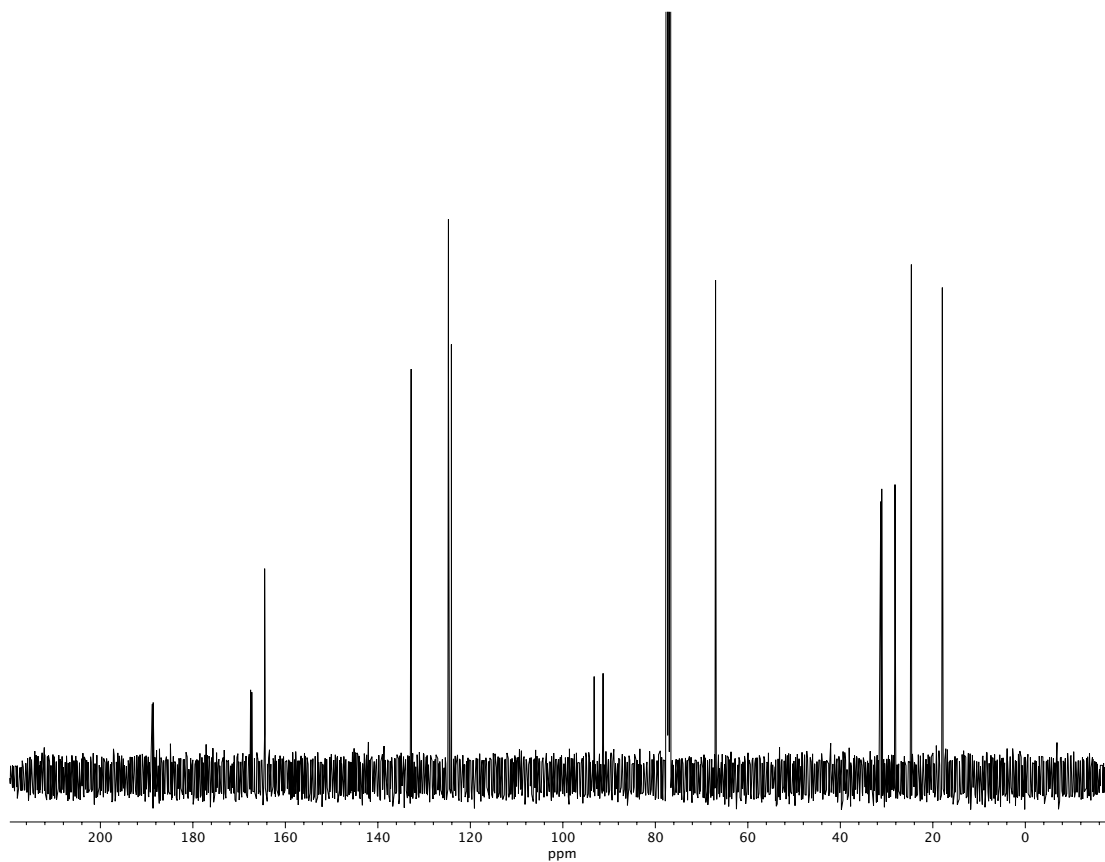
Figure A3.116. ^{13}C *NMR (100 MHz, CDCl$_3$) of compound **158q**.*
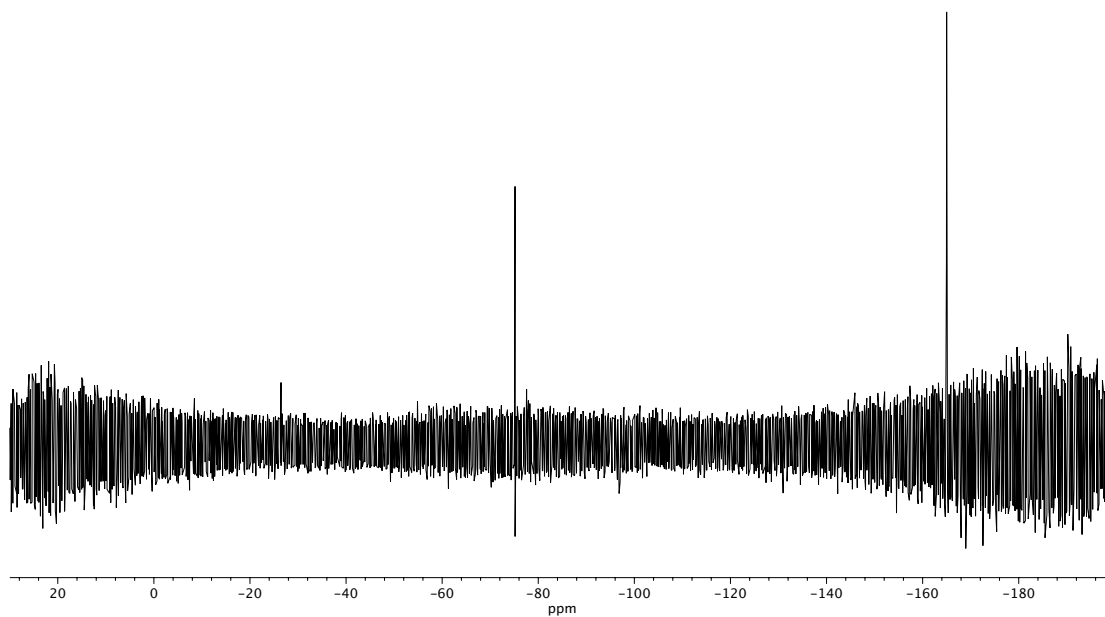
Figure A3.117. ^{19}F NMR (282 MHz, CDCl$_3$) of compound **158q**.
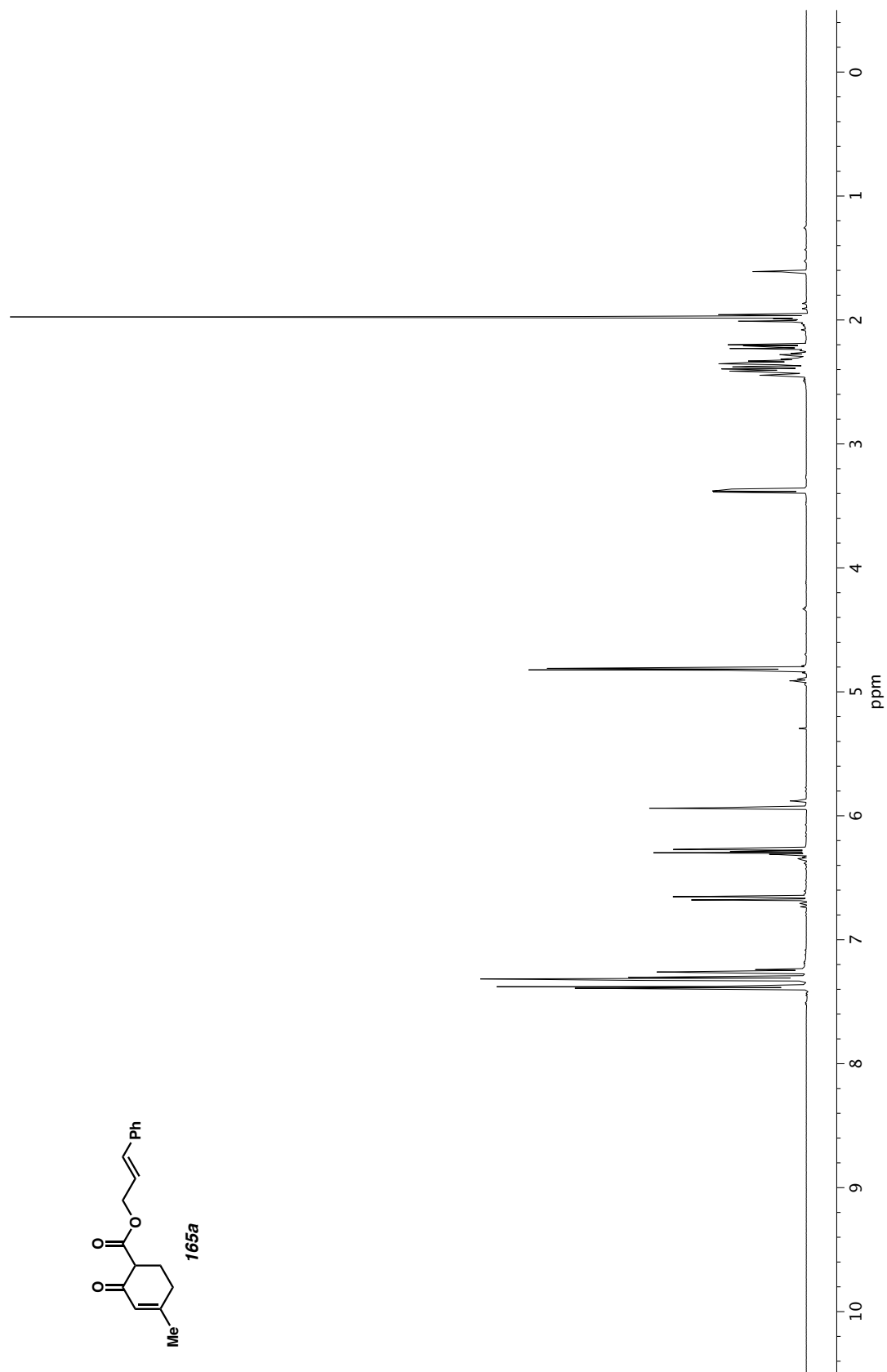
Figure A3.118. *^{1}H NMR (400 MHz, CDCl$_3$) of compound **165a**.*
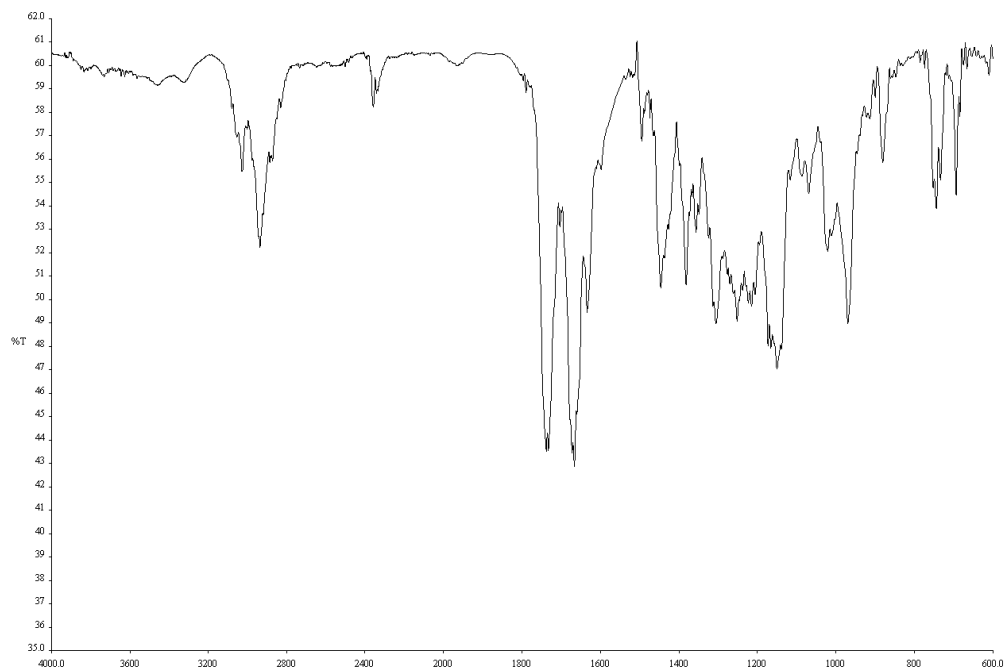
Figure A3.119. *Infrared spectrum (Thin Film, NaCl) of compound* **165a**.
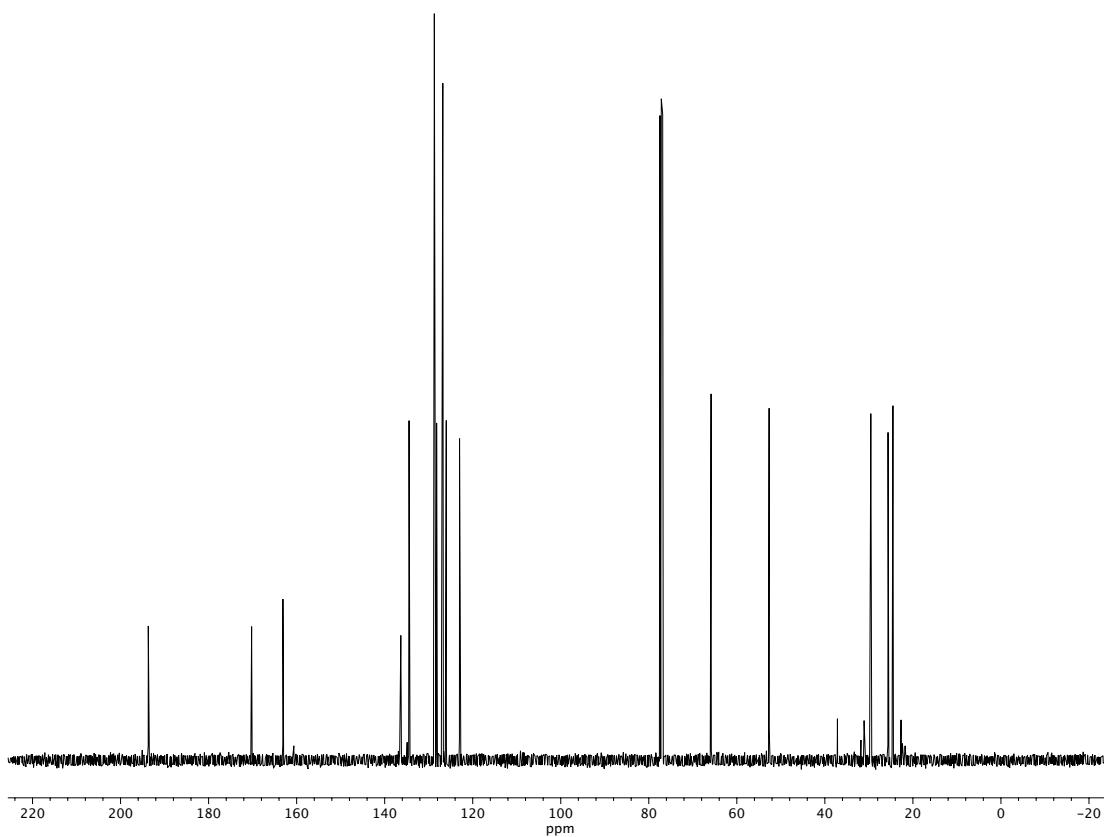
Figure A3.120. *^{13}C NMR (100 MHz, CDCl$_3$) of compound* **165a**.
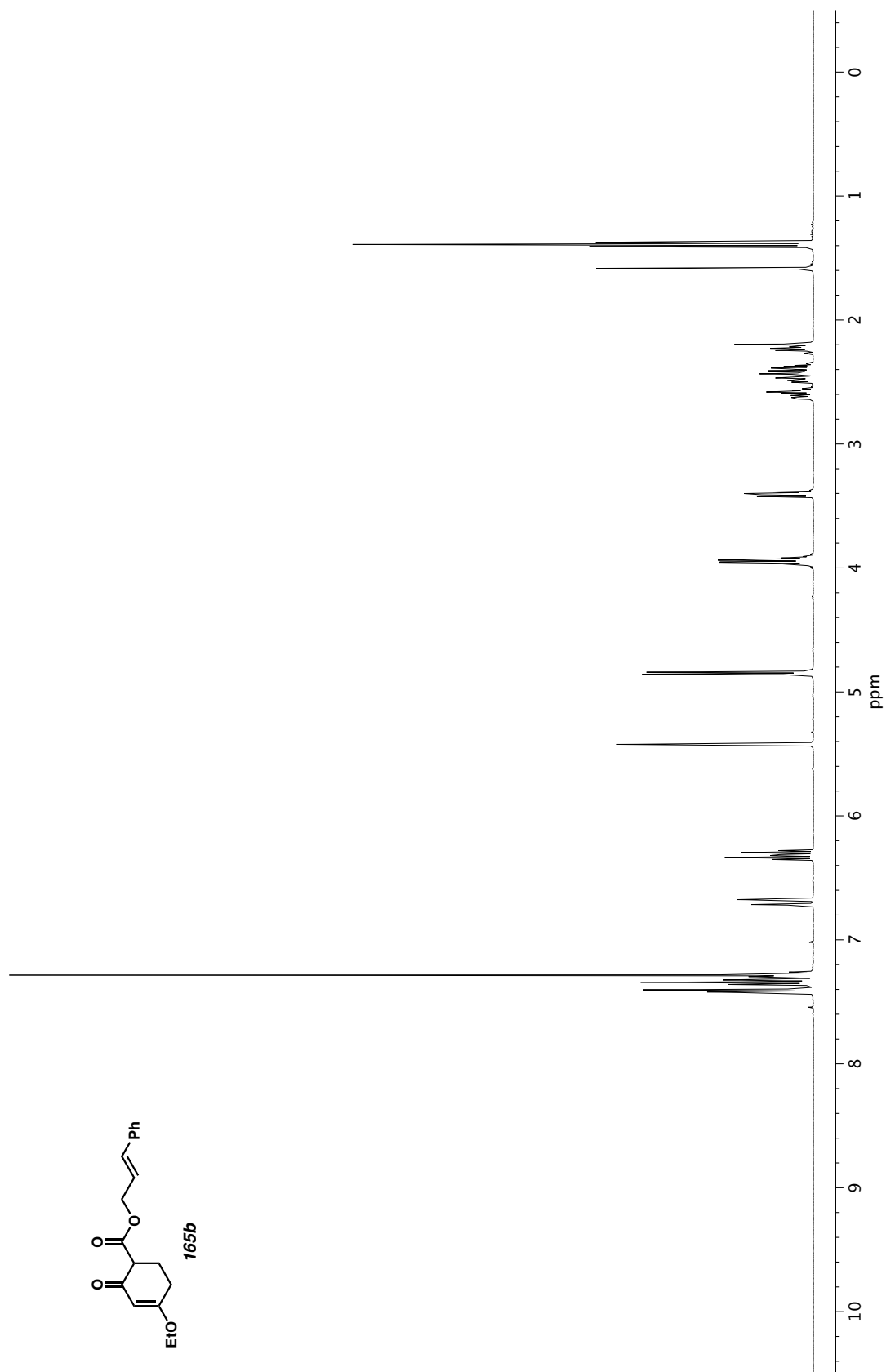
Figure A3.121. ^1H NMR (400 MHz, CDCl$_3$) of compound **165b**.
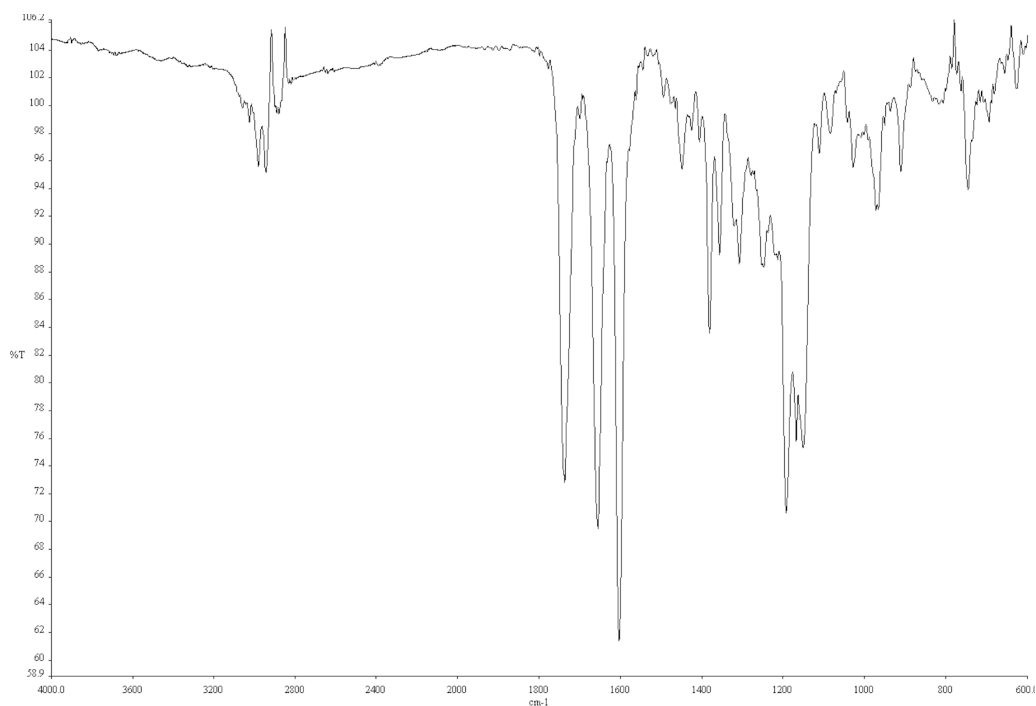
Figure A3.122. Infrared spectrum (Thin Film, NaCl) of compound **165b**.
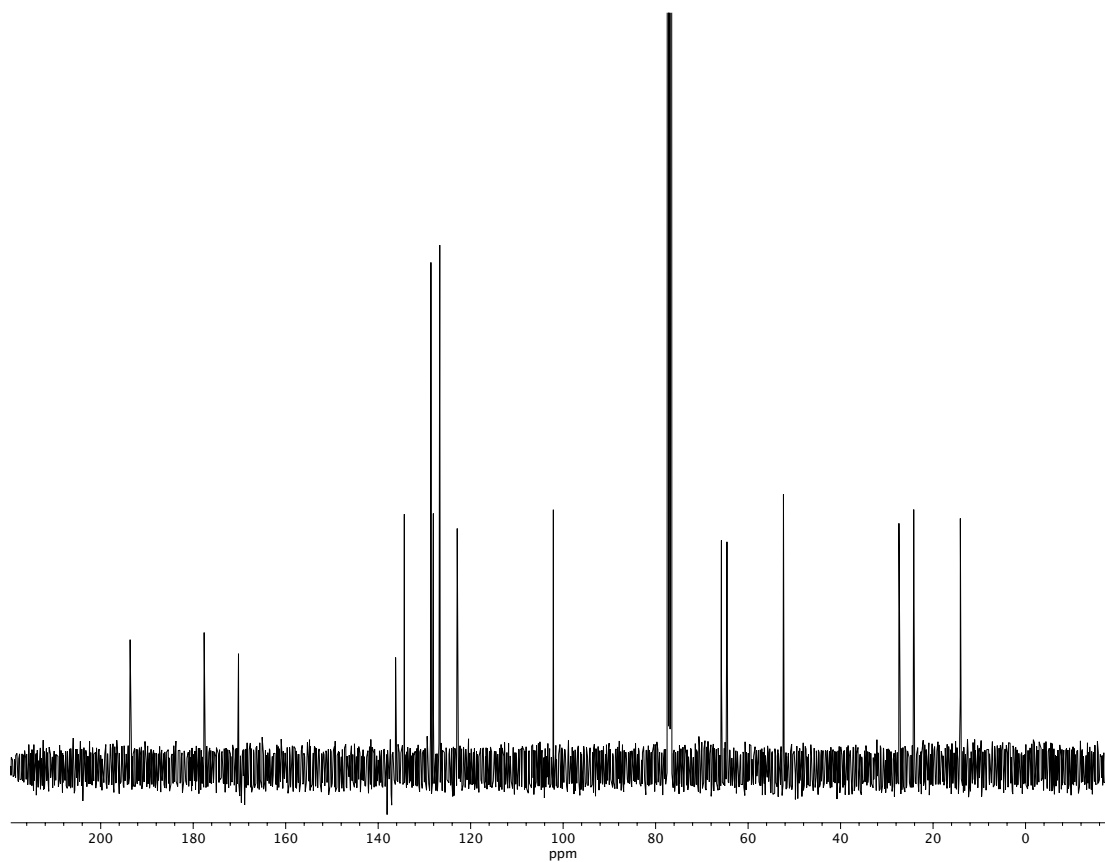
Figure A3.123. ^{13}C NMR (100 MHz, CDCl$_3$) of compound **165b**.
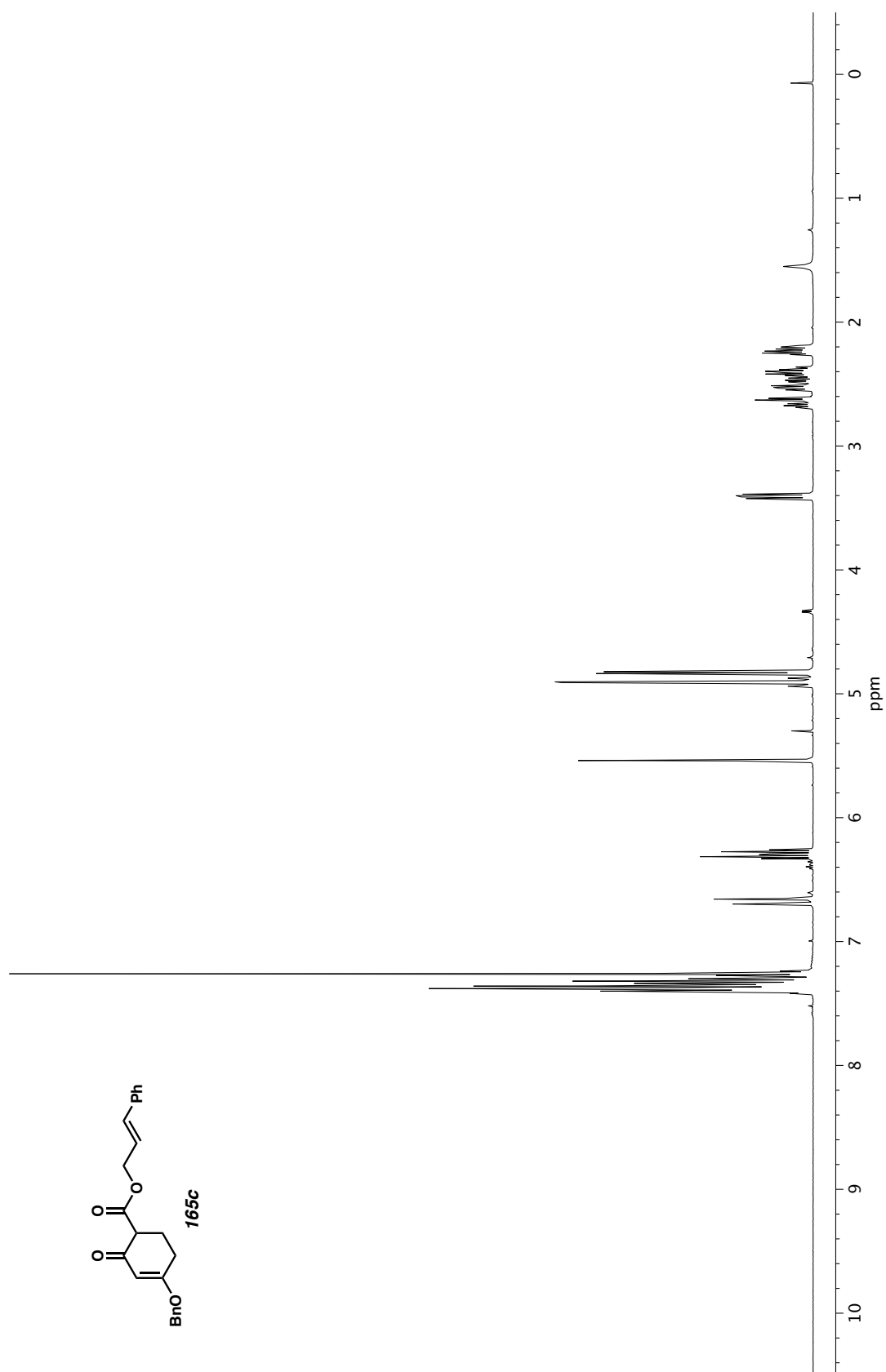
Figure A3.124. ^1H NMR (400 MHz, CDCl$_3$) of compound **165c**.
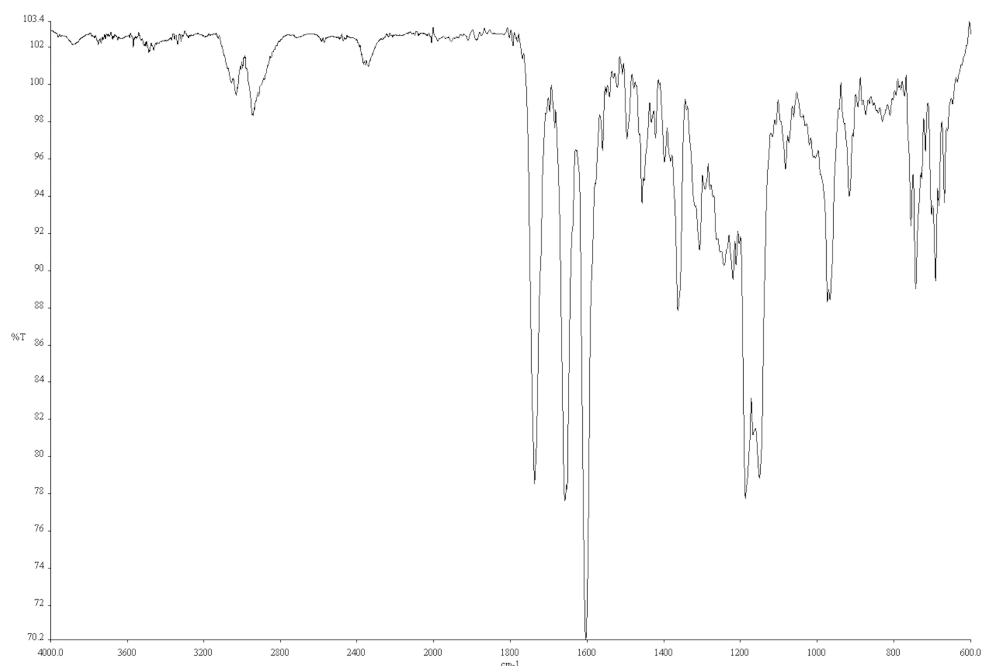
Figure A3.125. *Infrared spectrum (Thin Film, NaCl) of compound* **165c**.
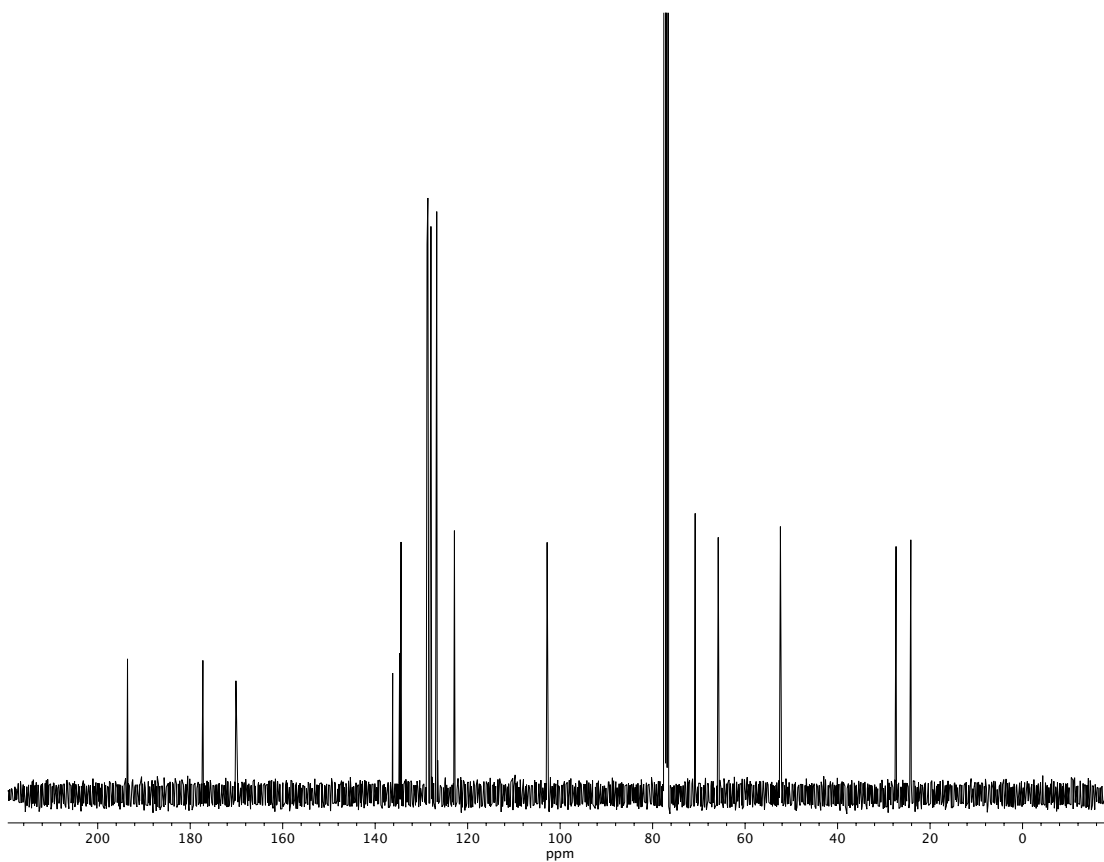
Figure A3.126. ^{13}C *NMR (100 MHz, CDCl$_3$) of compound* **165c**.
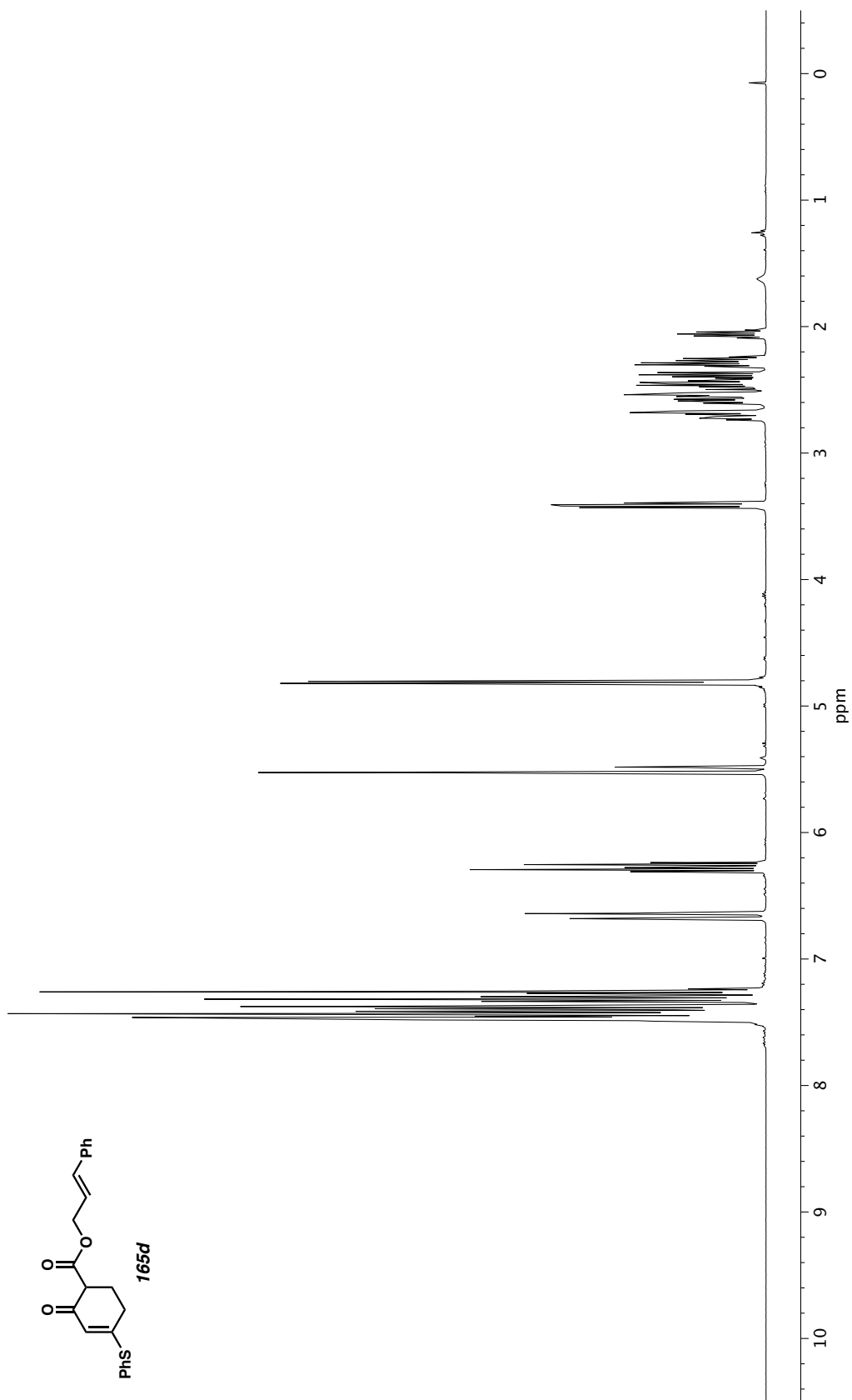
Figure A3.127. ^1H NMR (400 MHz, CDCl$_3$) of compound **165d**.
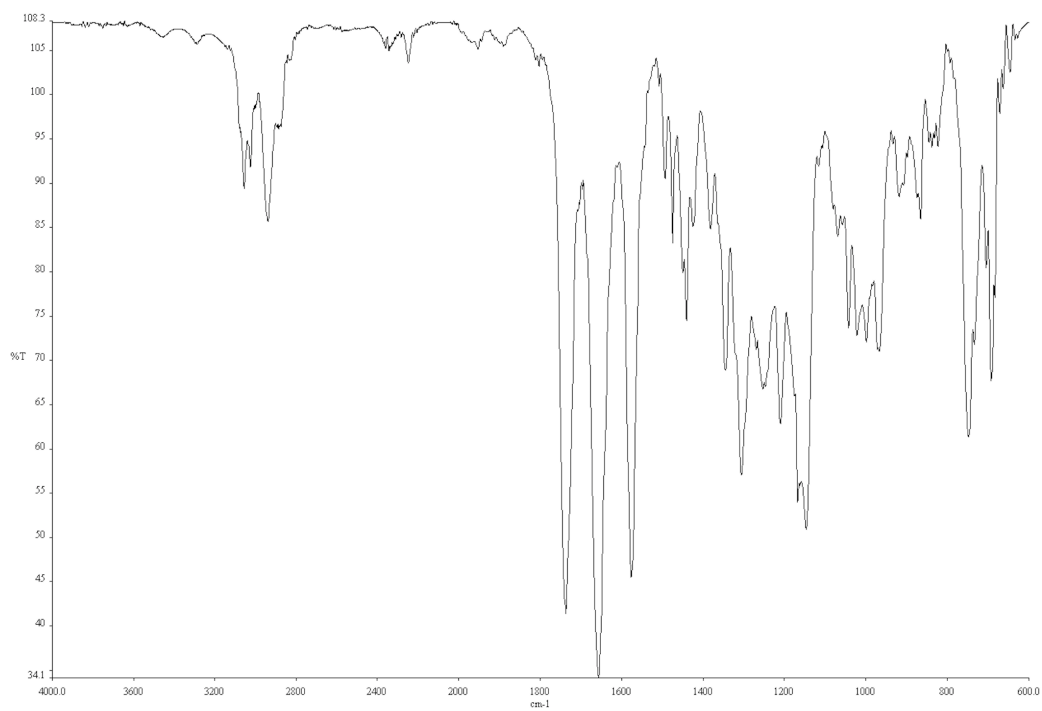
Figure A3.128. Infrared spectrum (Thin Film, NaCl) of compound **165d**.
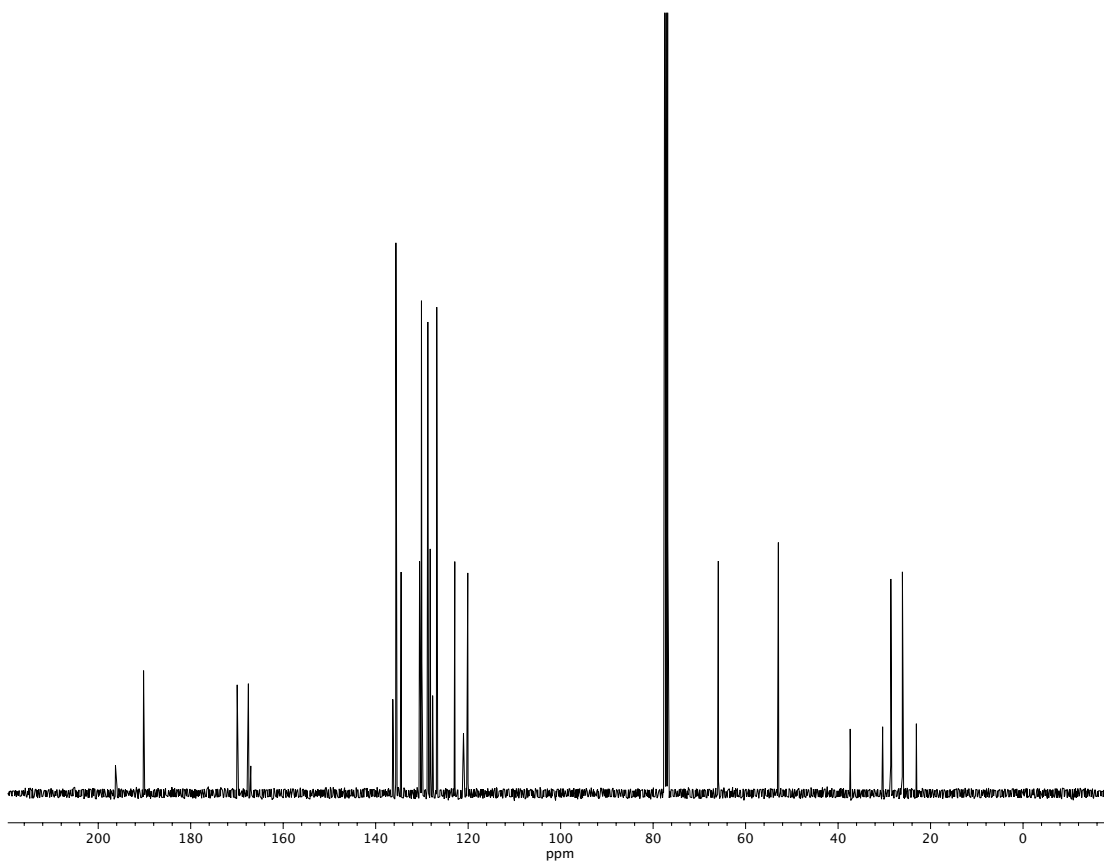
Figure A3.129. ^{13}C NMR (100 MHz, CDCl$_3$) of compound **165d**.
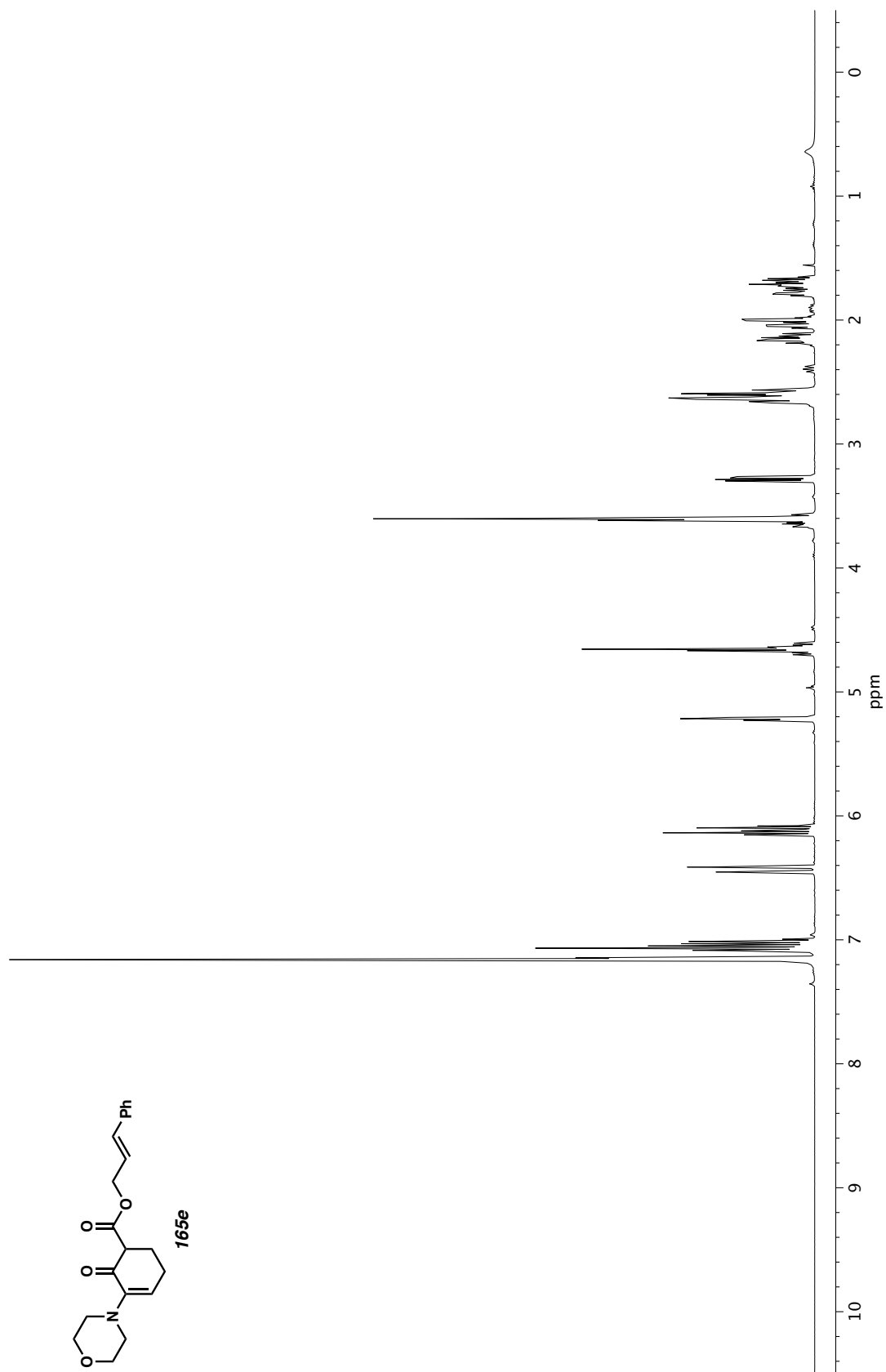
Figure A3.130. ^1H NMR (400 MHz, C_6D_6) of compound **165e**.
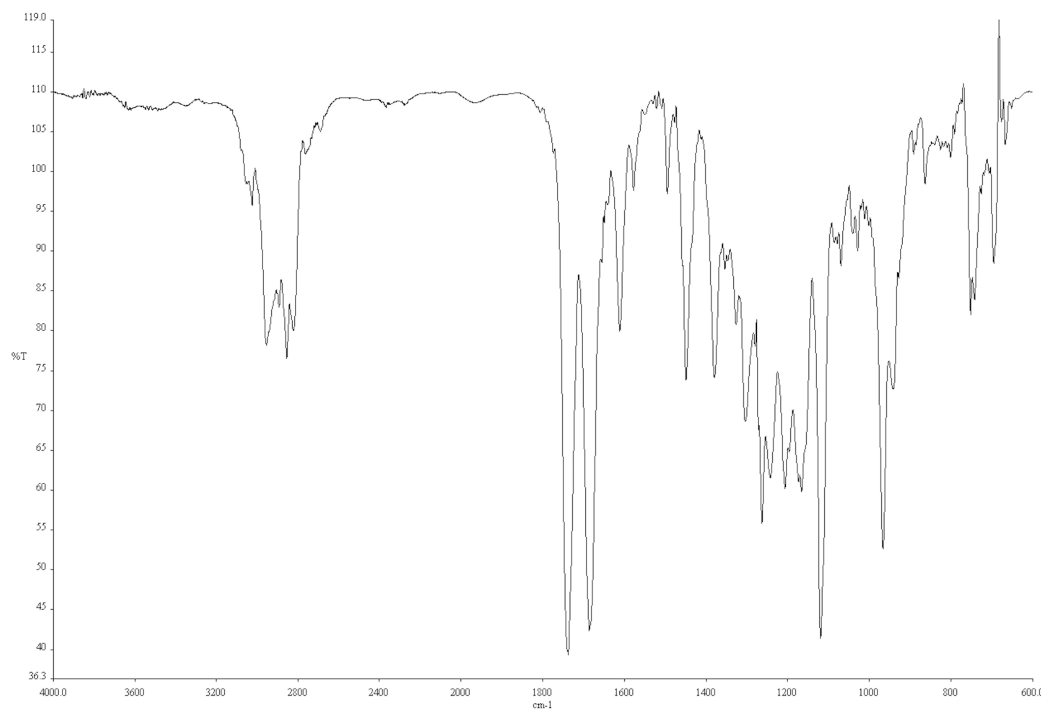
Figure A3.131. *Infrared spectrum (Thin Film, NaCl) of compound* **165e**.
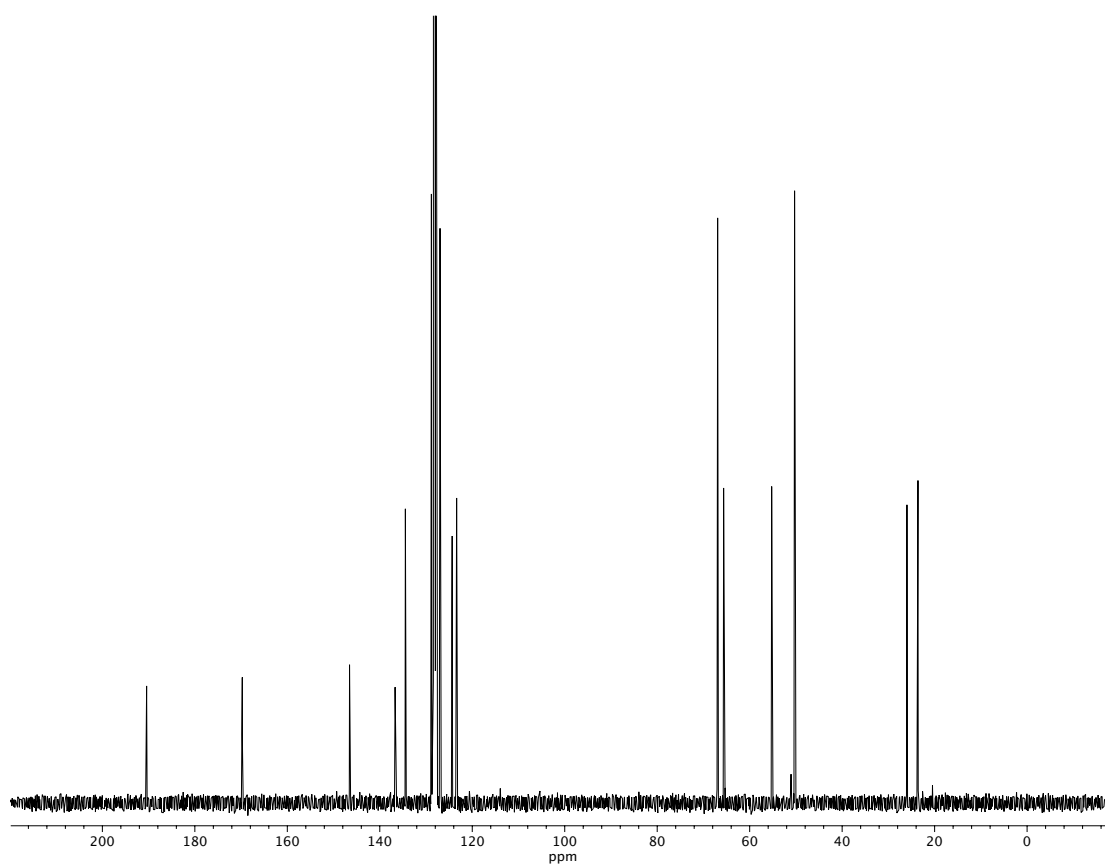
Figure A3.132. ^{13}C *NMR (100 MHz, C_6D_6) of compound* **165e**.
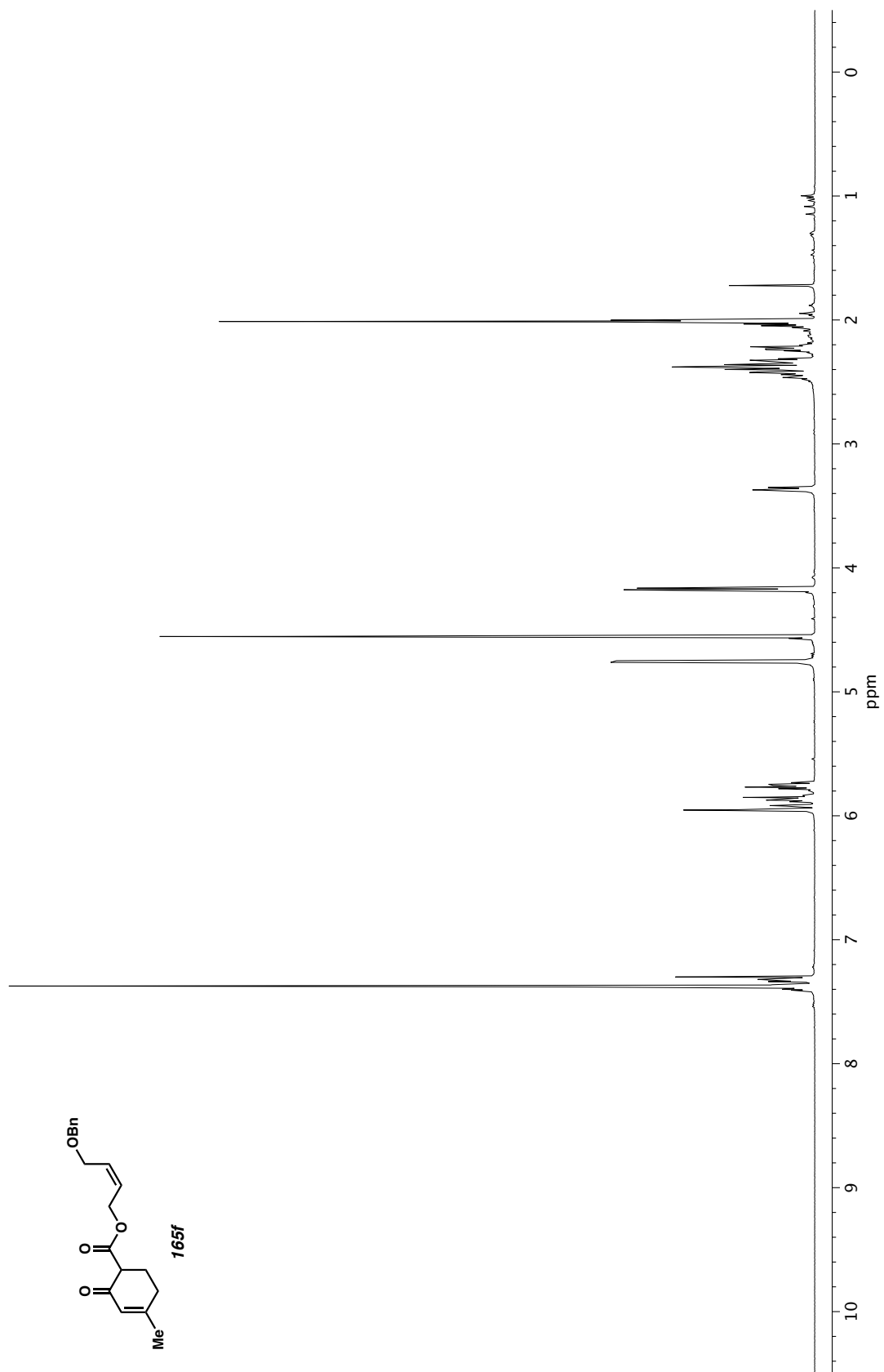
Figure A3.133. ^1H NMR (400 MHz, CDCl$_3$) of compound **165f**.
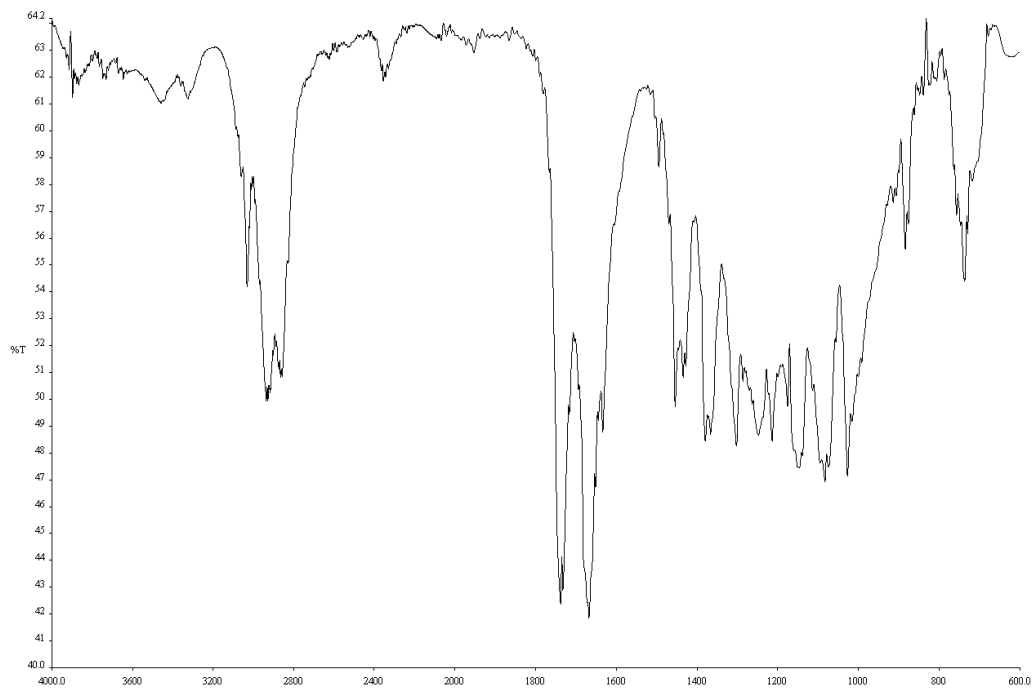
Figure A3.134. *Infrared spectrum (Thin Film, NaCl) of compound* **165f**.
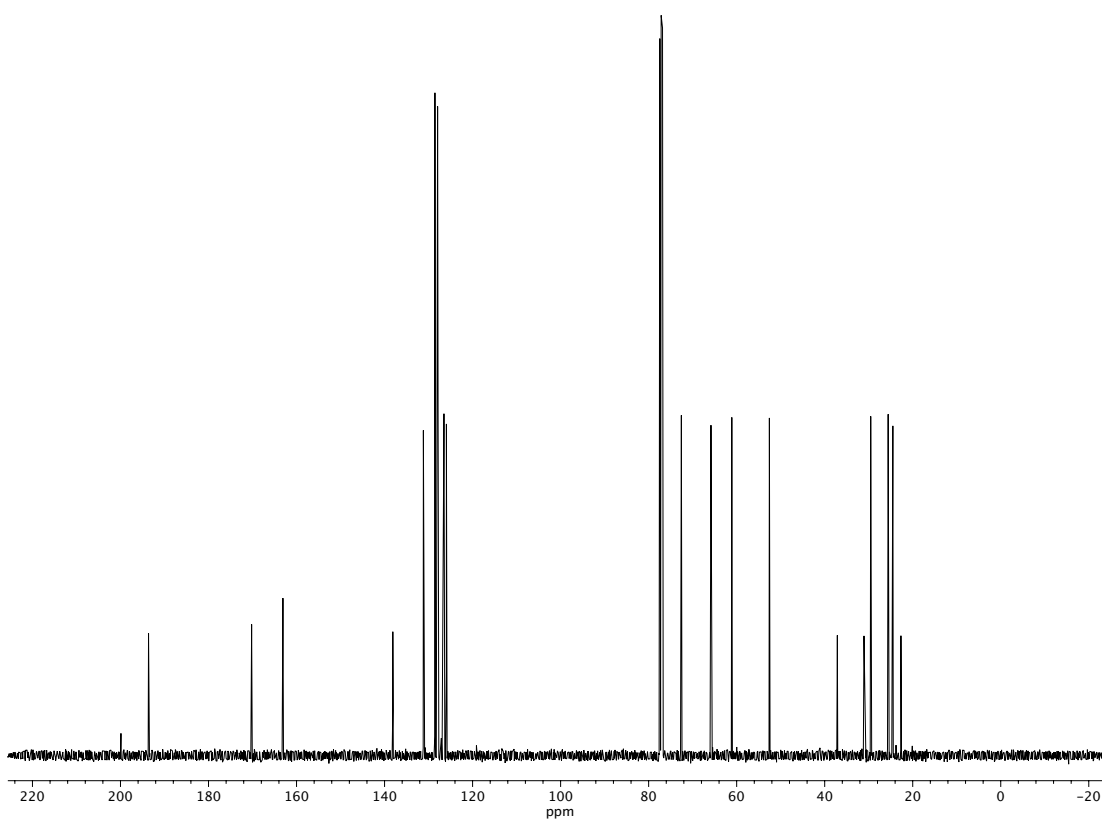
Figure A3.135. ^{13}C *NMR (100 MHz, CDCl$_3$) of compound* **165f**.
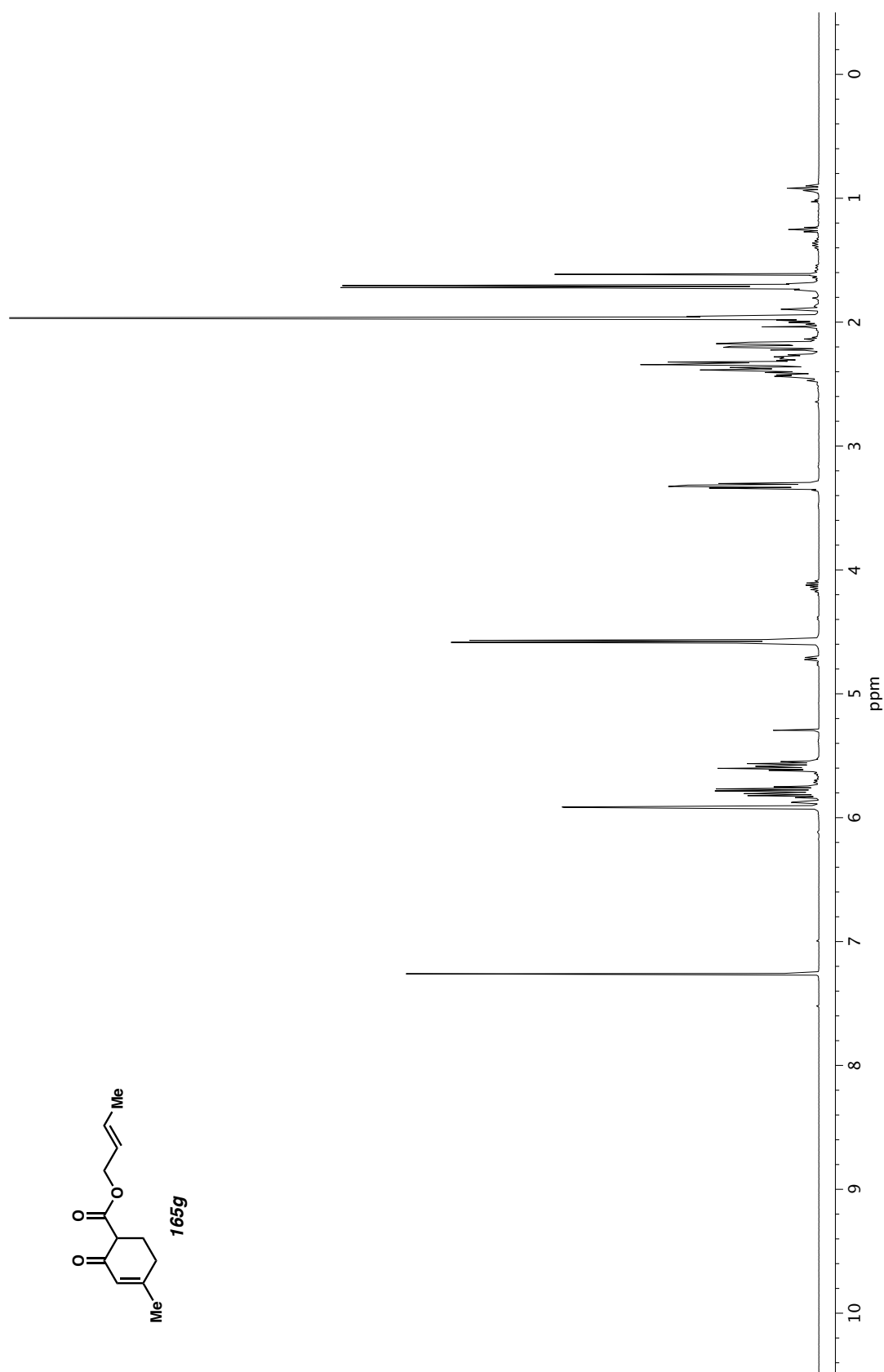
Figure A3.136. ^1H NMR (400 MHz, CDCl$_3$) of compound **165g**.
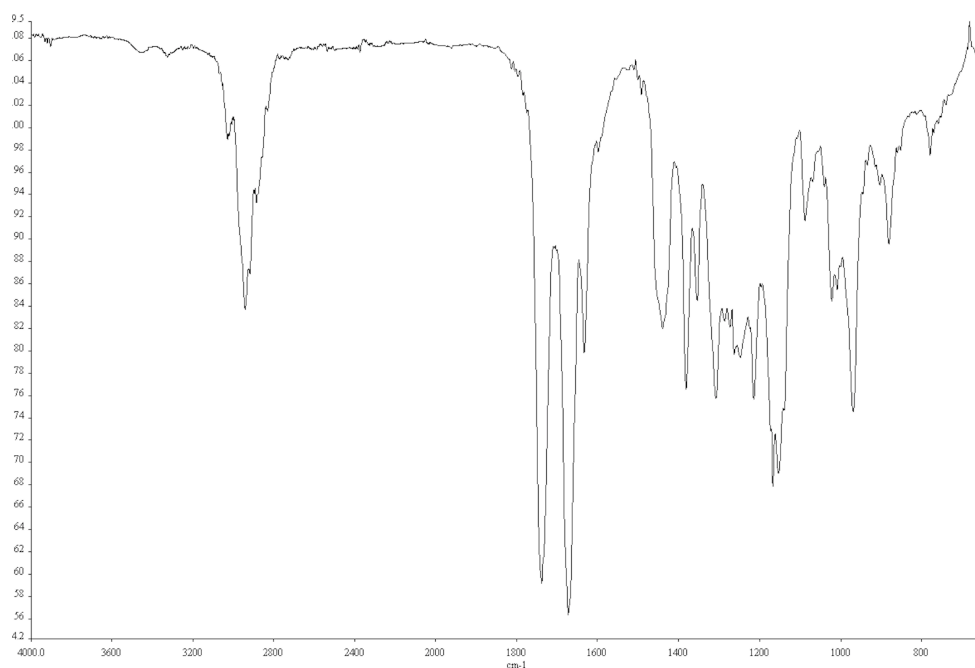
Figure A3.137. Infrared spectrum (Thin Film, NaCl) of compound **165g**.
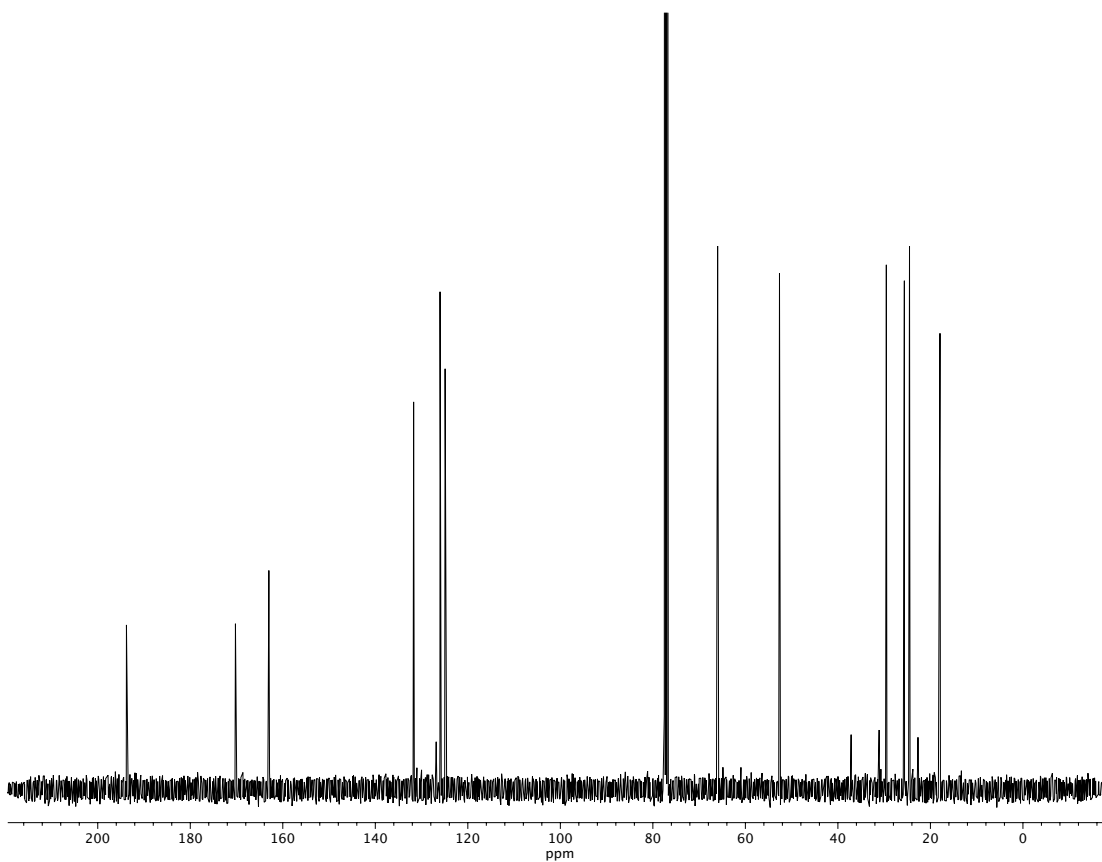
Figure A3.138. ^{13}C NMR (100 MHz, CDCl$_3$) of compound **165g**.

Figure A3.139. ^1H NMR (400 MHz, CDCl$_3$) of compound **L4**.
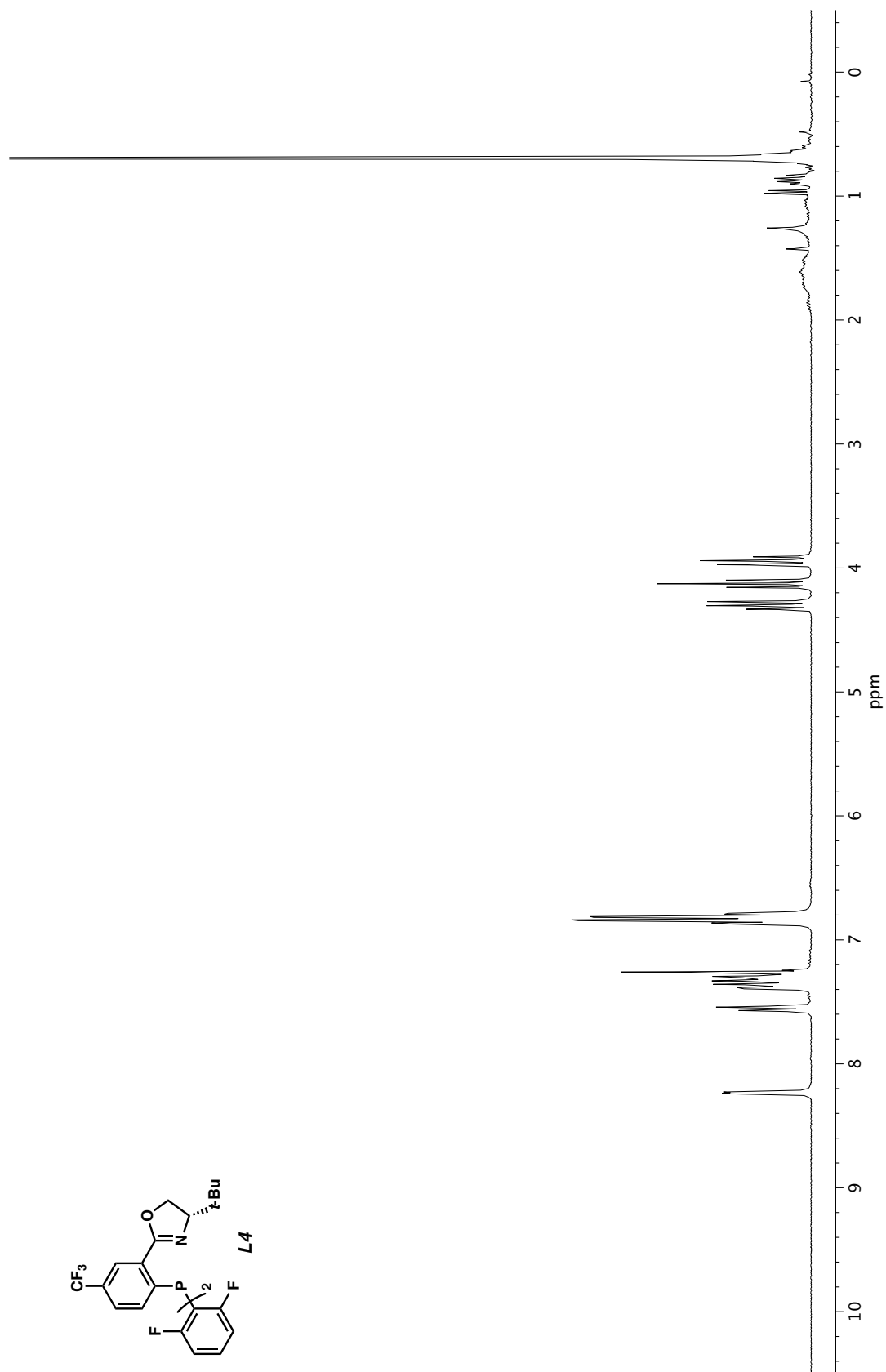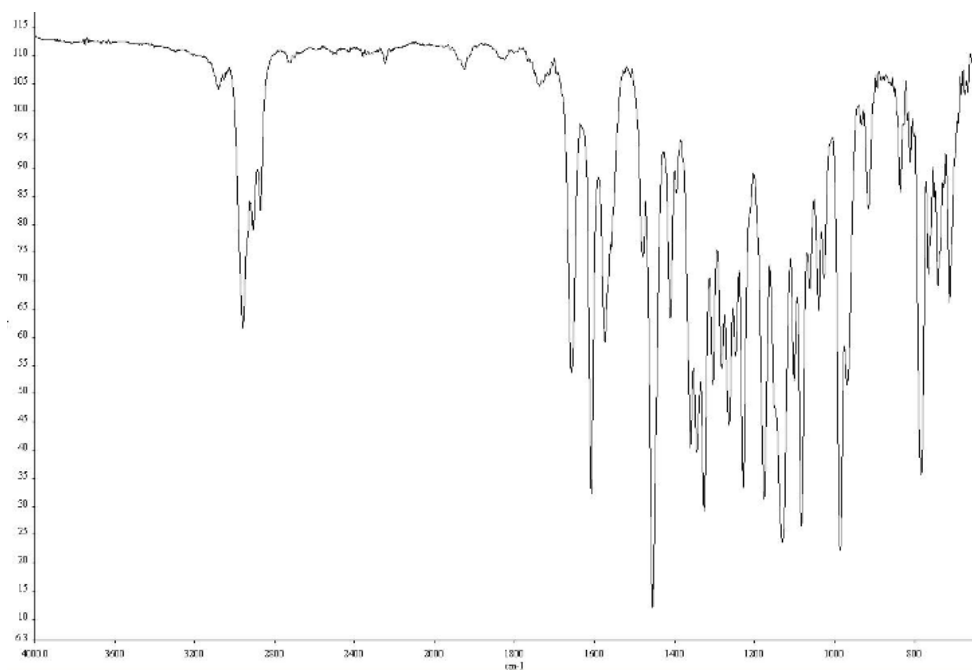
Figure A3.140. *Infrared spectrum (Thin Film, NaCl) of compound **L4**.*
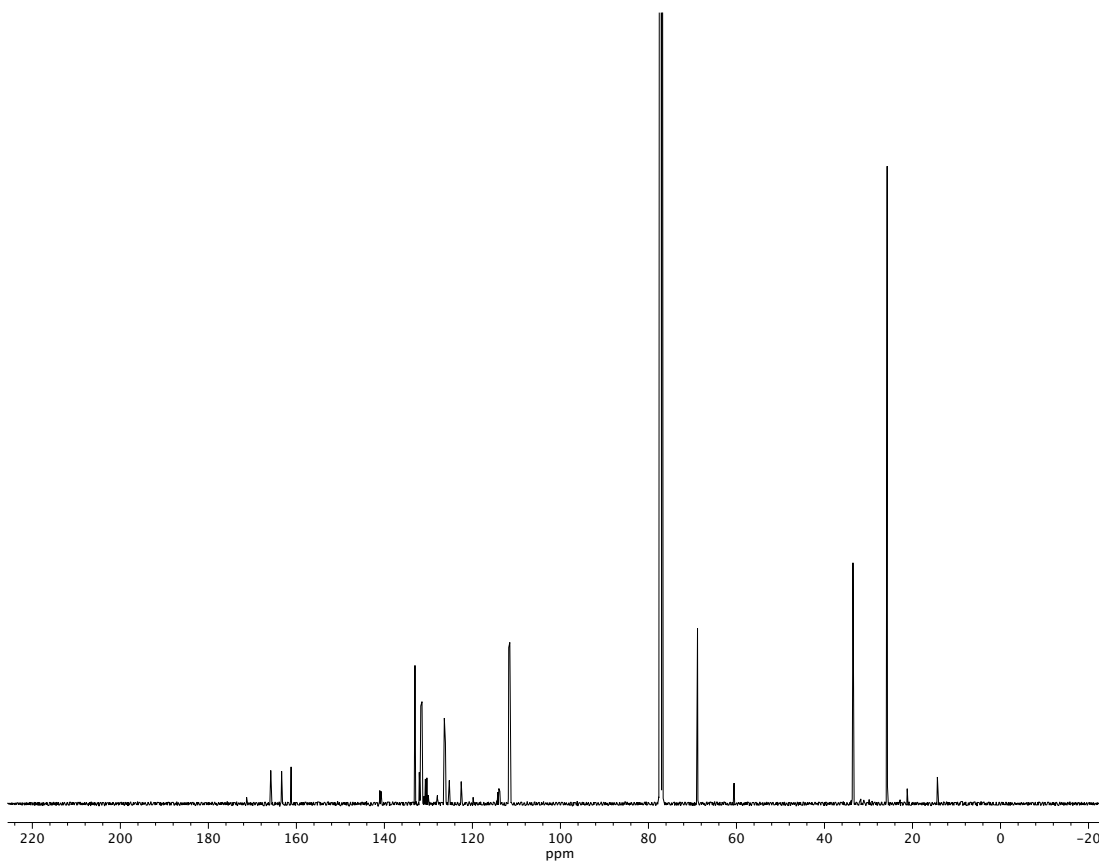
Figure A3.141. *^{13}C NMR (100 MHz, CDCl$_3$) of compound **L4**.*
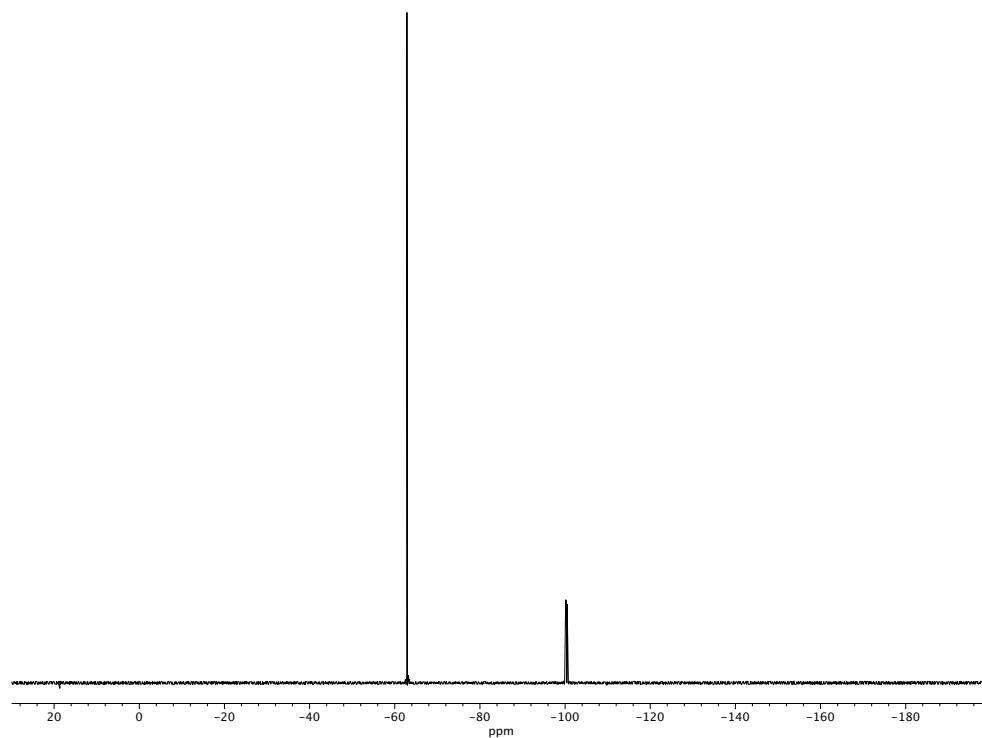
Figure A3.142. ^{19}F *NMR (282 MHz, CDCl$_3$) of compound* **L4**.
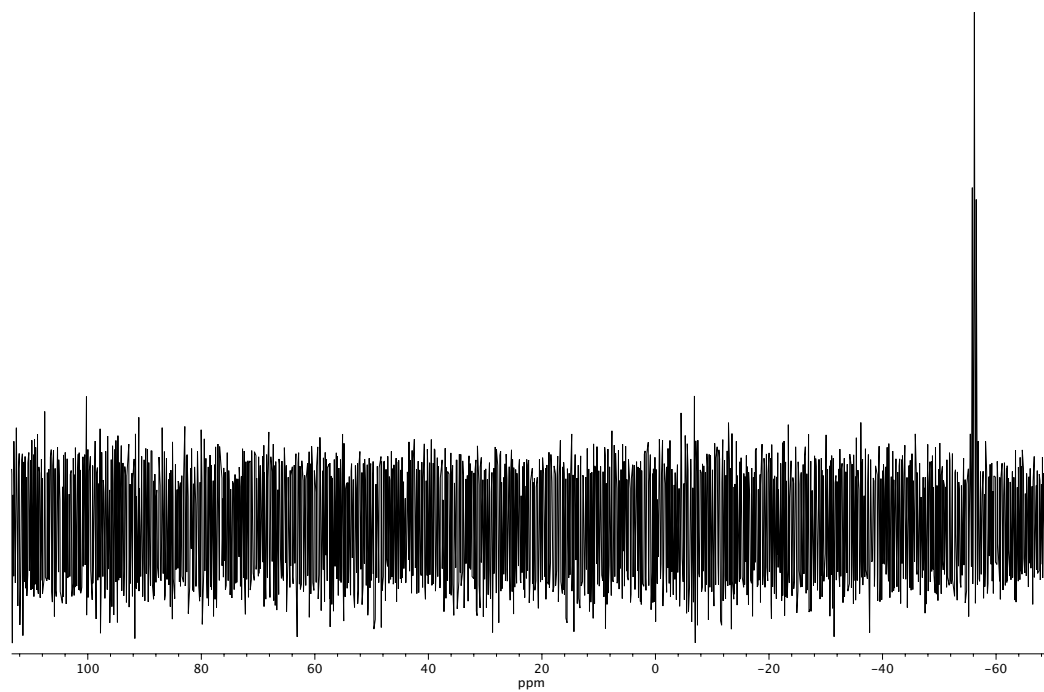
Figure A3.143. ^{31}P *NMR (121 MHz, CDCl$_3$) of compound* **L4**.

Figure A3.144. ^1H NMR (400 MHz, CDCl$_3$) of compound **L5**.
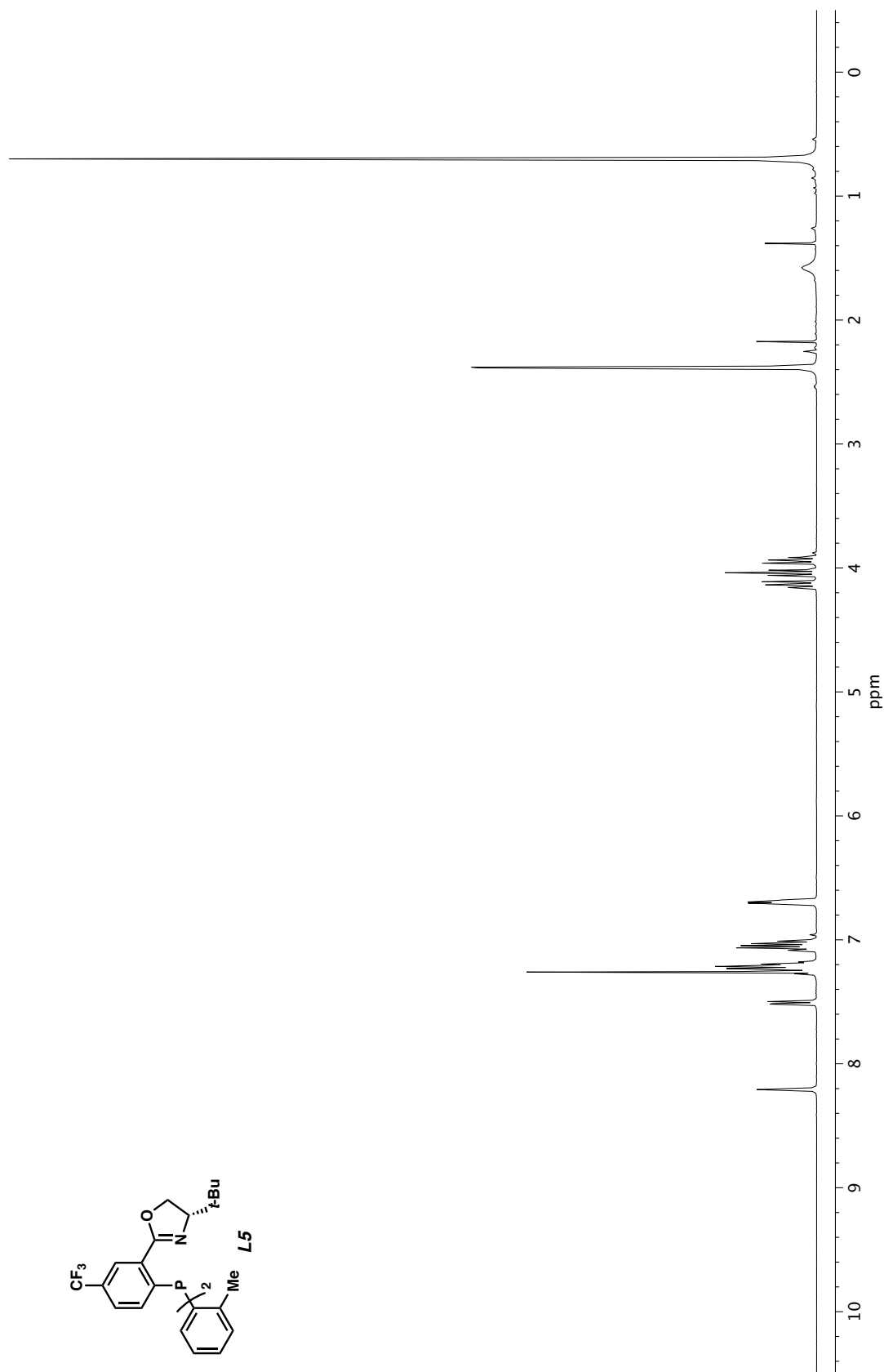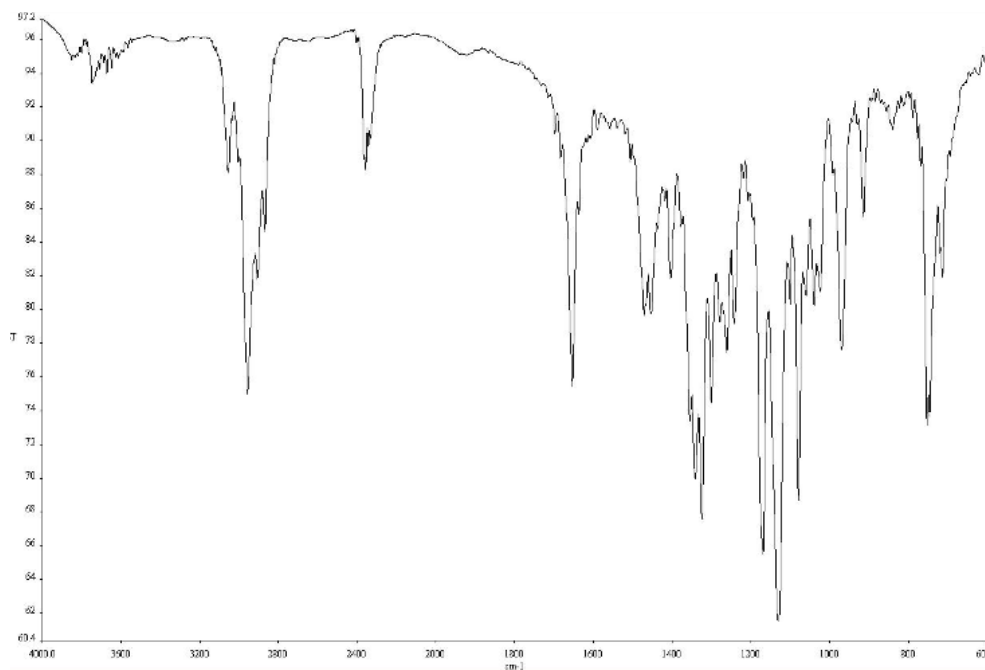
Figure A3.145. Infrared spectrum (Thin Film, NaCl) of compound **L5**.
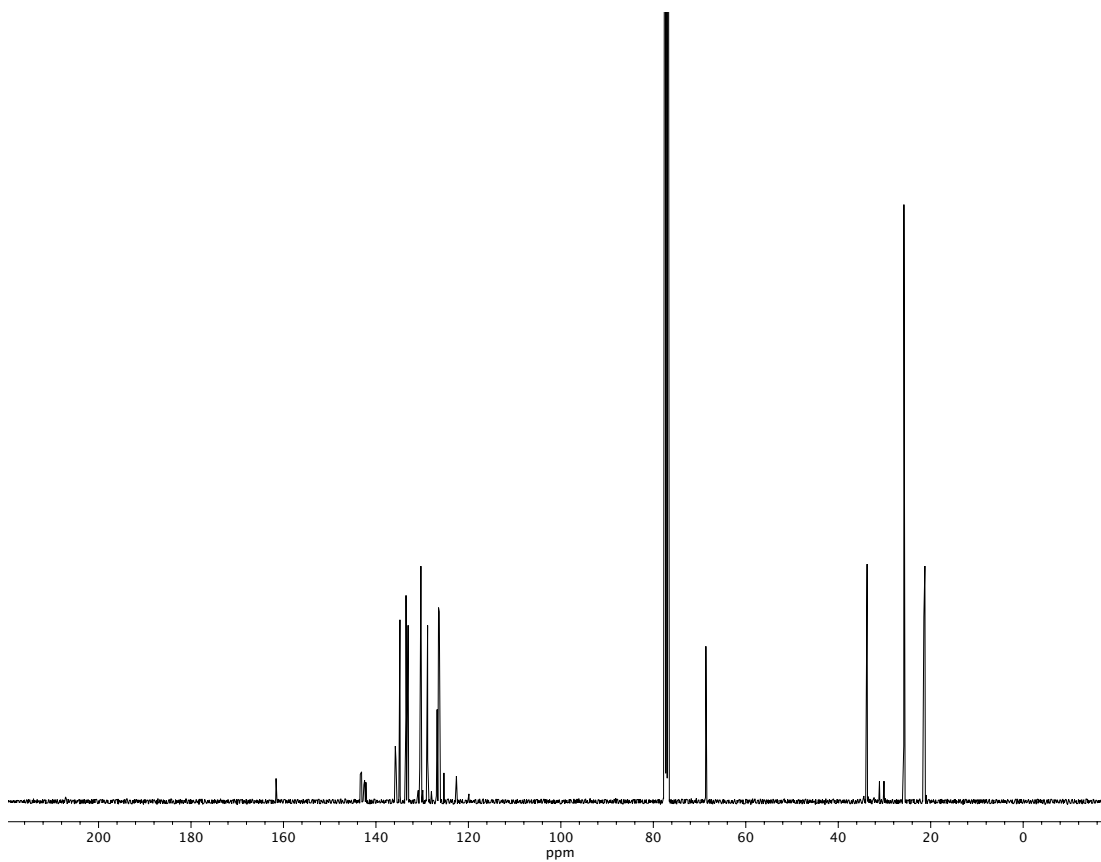
Figure A3.146. ^{13}C NMR (100 MHz, CDCl$_3$) of compound **L5**.
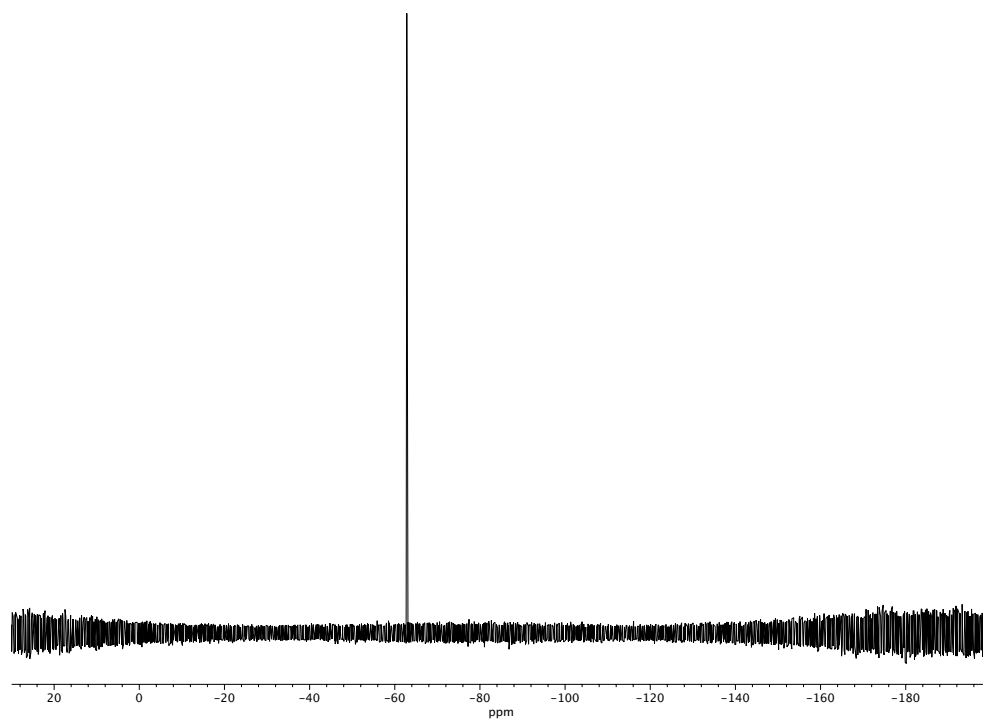
Figure A3.147. ^{19}F NMR (282 MHz, CDCl$_3$) of compound **L5**.
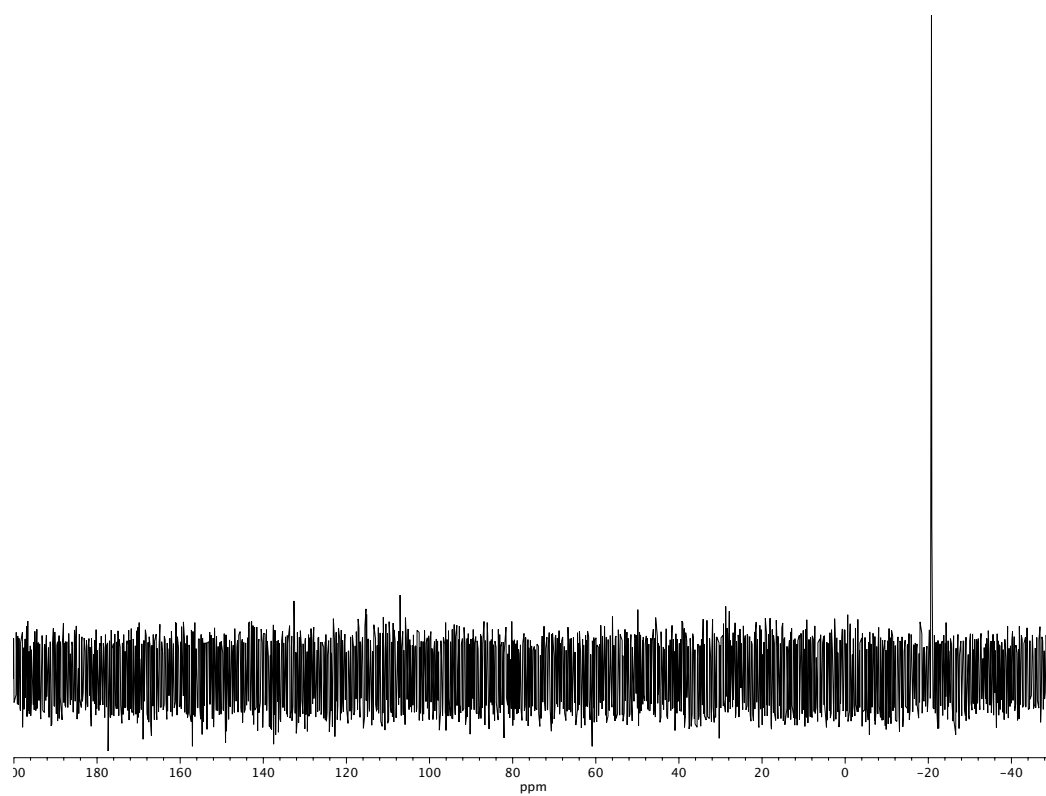
Figure A3.148. ^{31}P NMR (121 MHz, CDCl$_3$) of compound **L5**.
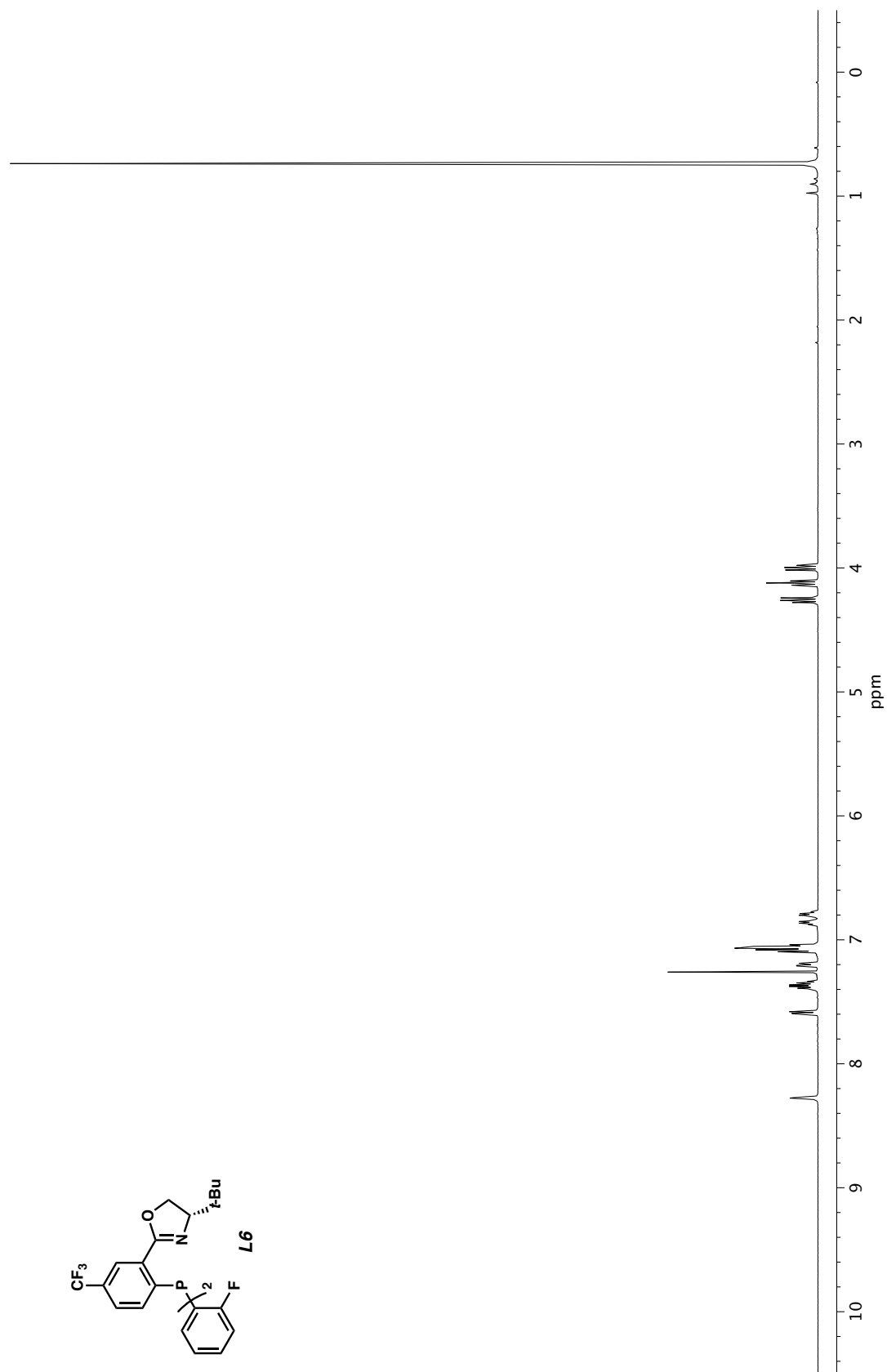
Figure A3.149. ^1H NMR (400 MHz, CDCl$_3$) of compound **L6**.
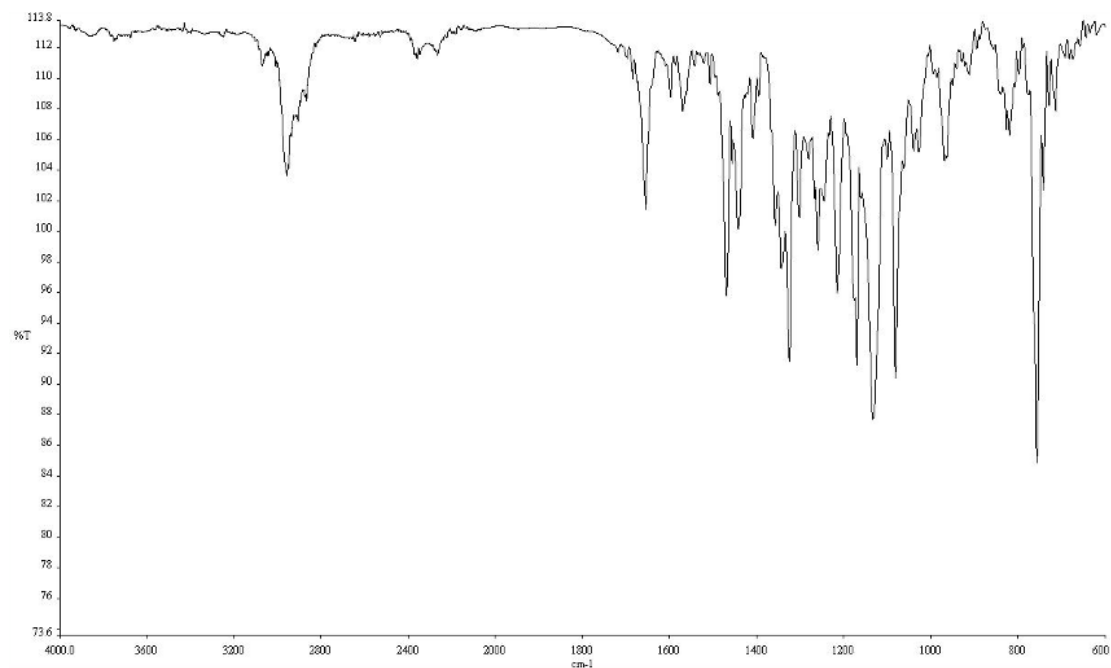
Figure A3.150. *Infrared spectrum (Thin Film, NaCl) of compound **L6**.*
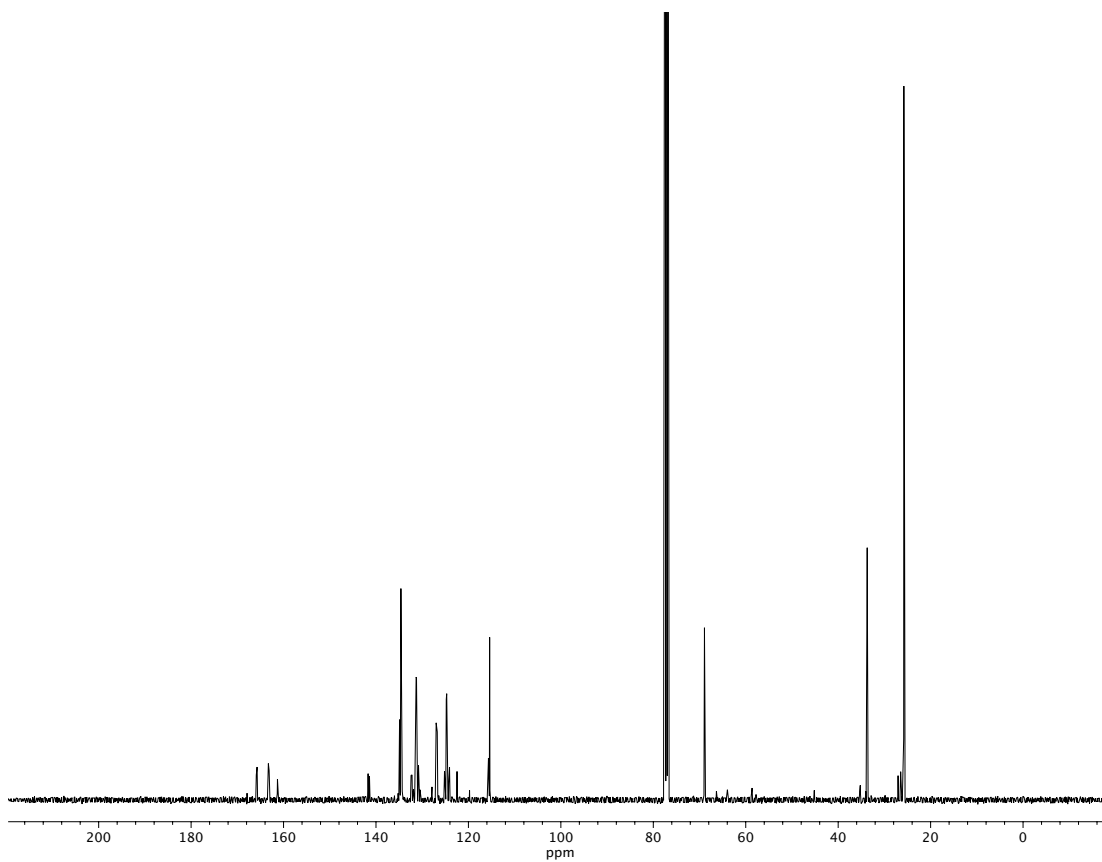
Figure A3.151. *^{13}C NMR (100 MHz, CDCl$_3$) of compound **L6**.*
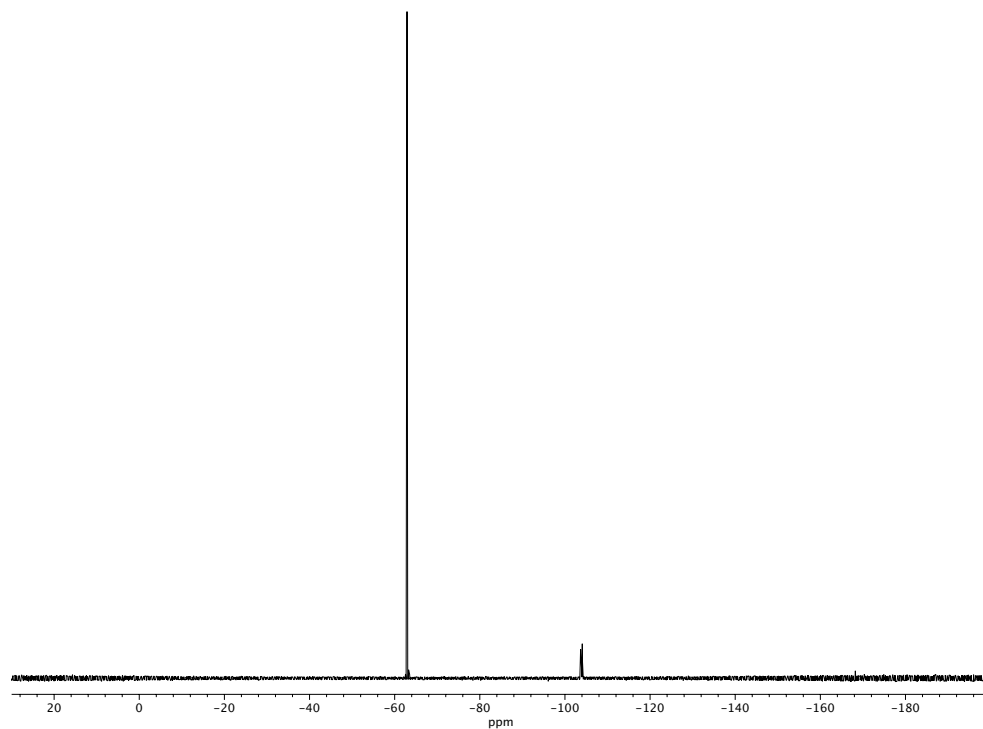
Figure A3.152. ^{19}F NMR (282 MHz, CDCl$_3$) of compound **L6**.
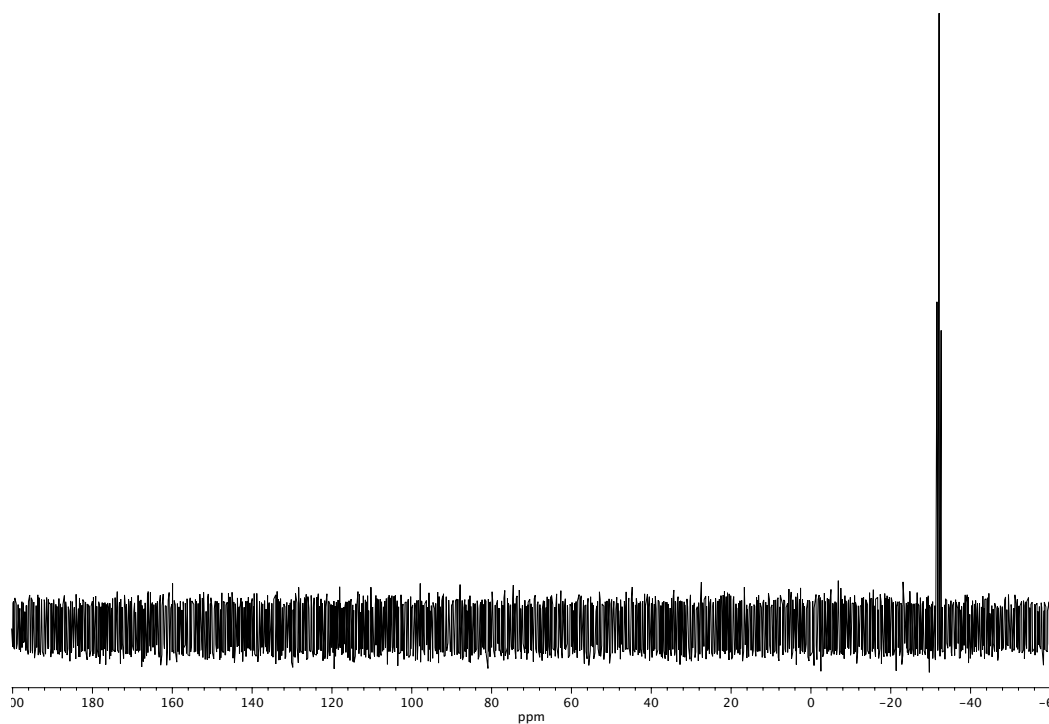
Figure A3.153. ^{31}P NMR (121 MHz, CDCl$_3$) of compound **L6**.
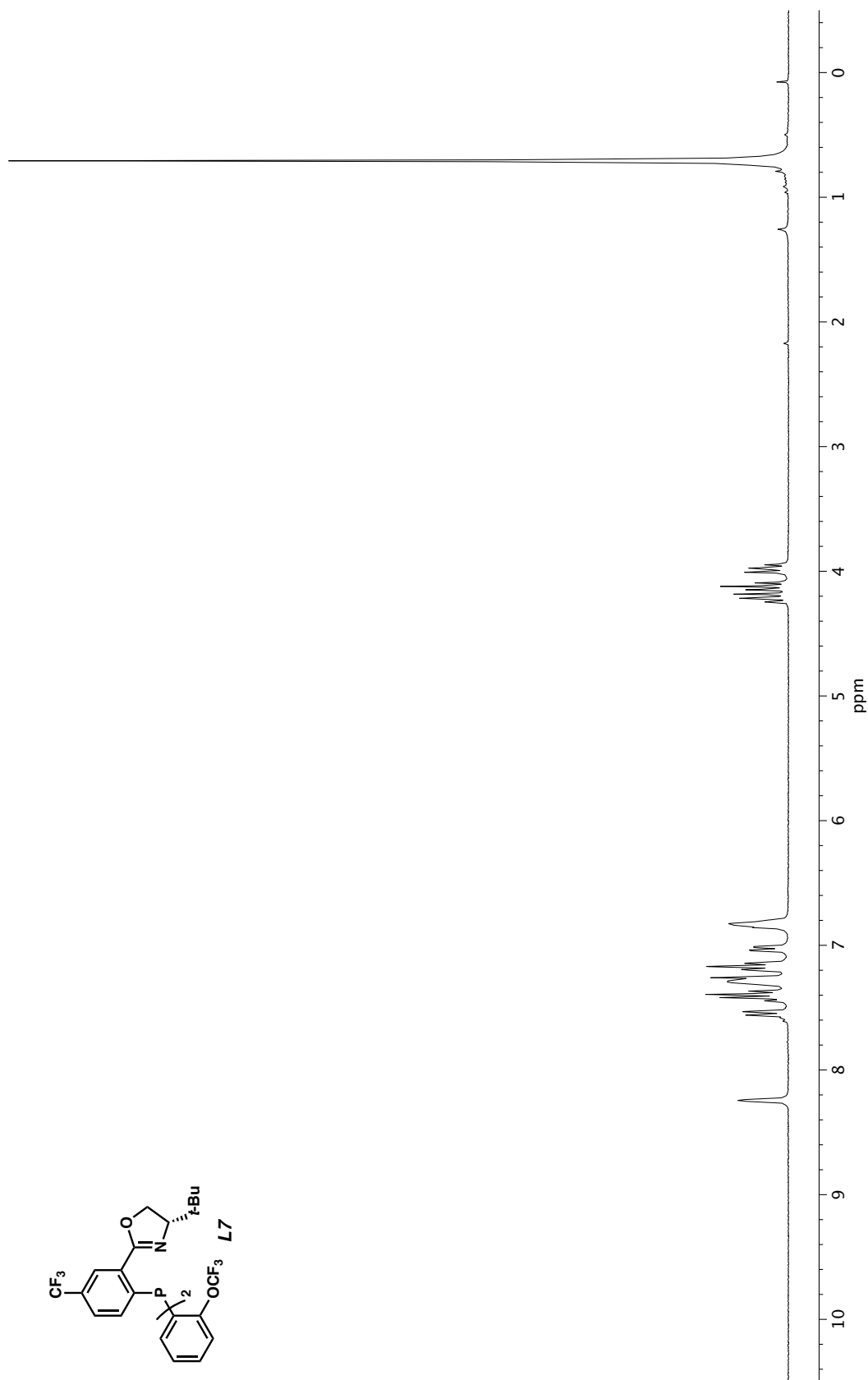
Figure A3.154. ^1H NMR (400 MHz, CDCl$_3$) of compound **L7**.
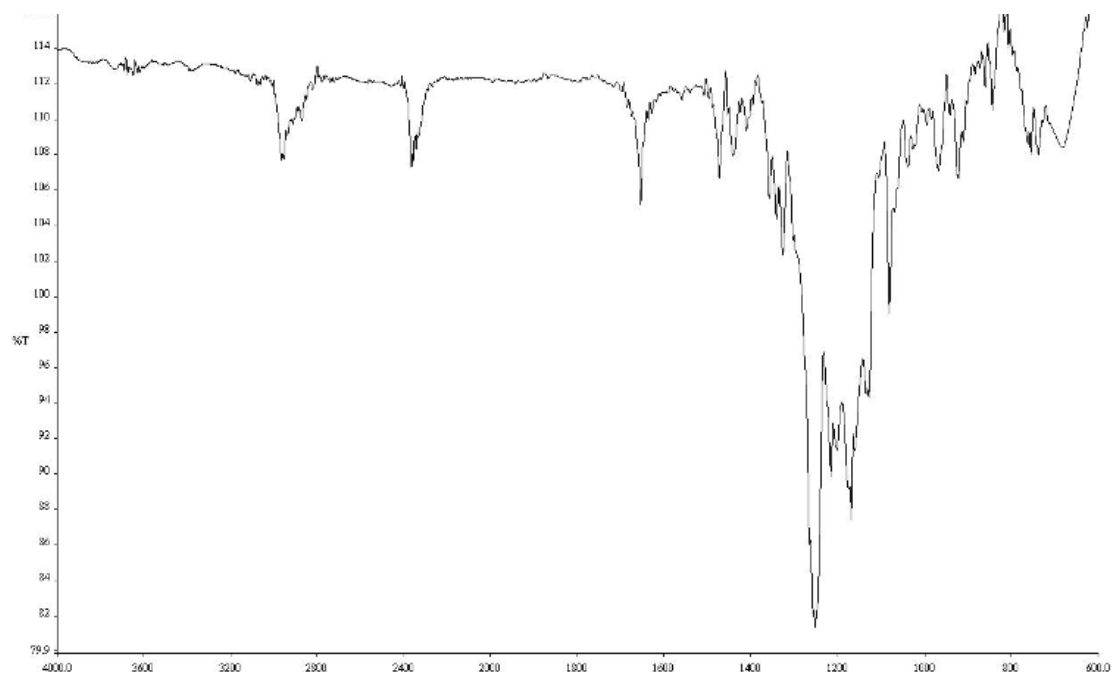
Figure A3.155. *Infrared spectrum (Thin Film, NaCl) of compound **L7**.*
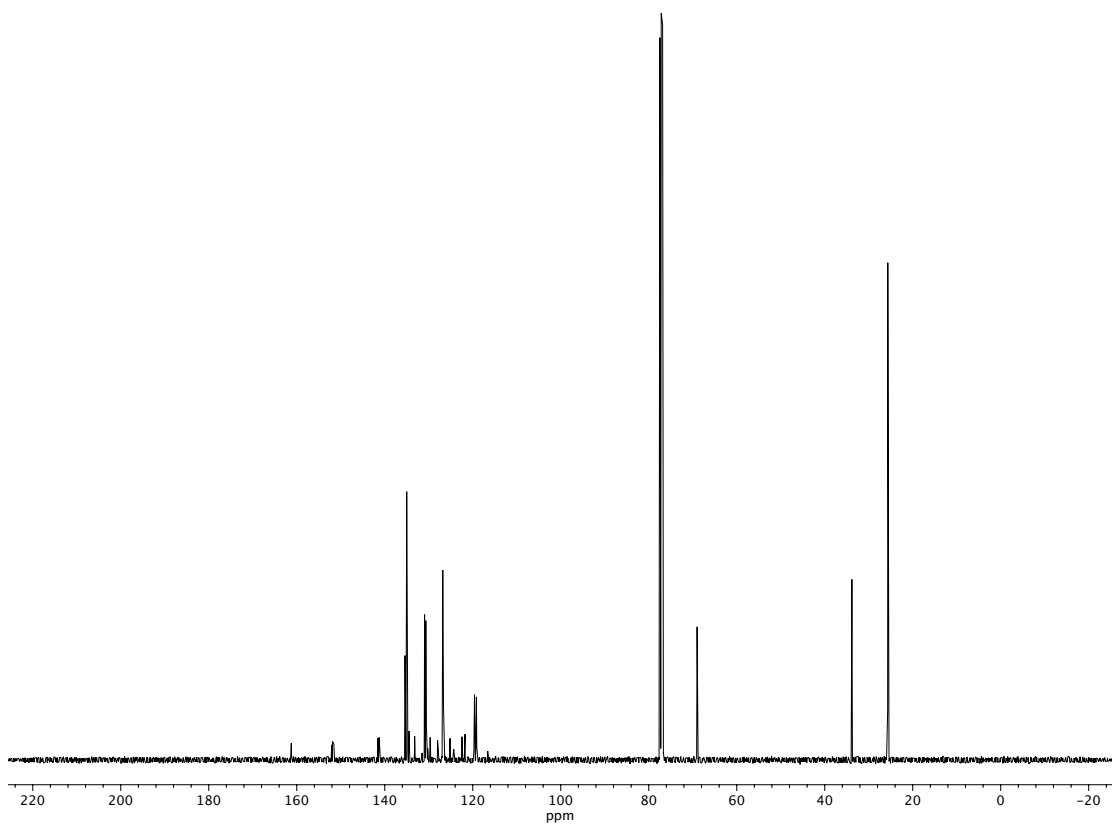
Figure A3.156. ^{13}C *NMR (100 MHz, CDCl$_3$) of compound **L7**.*
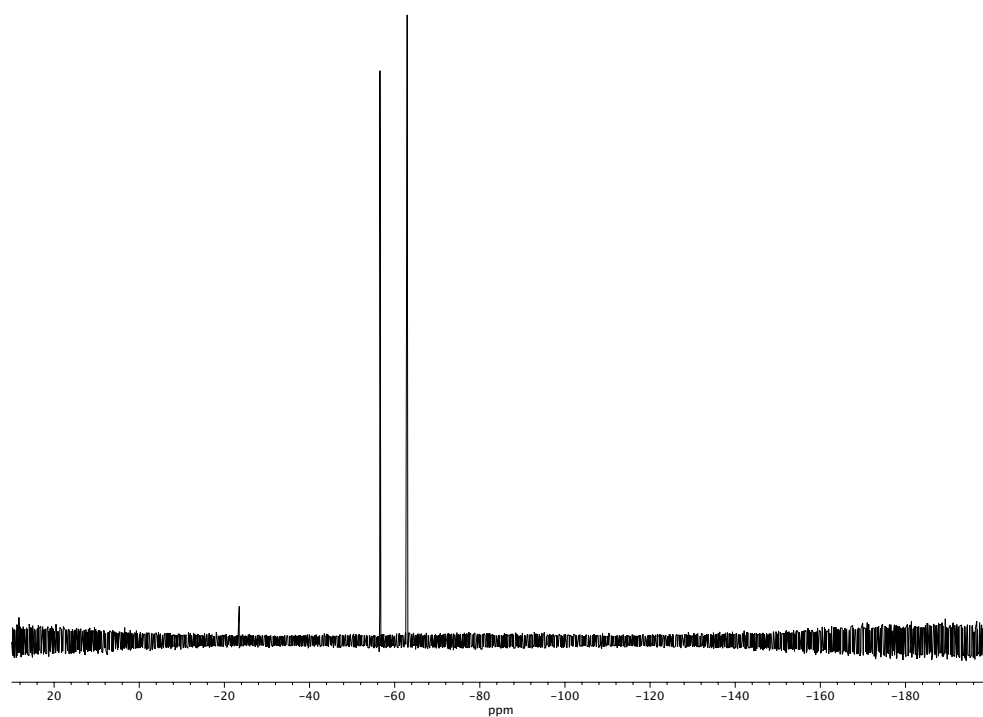
Figure A3.157. *^{19}F NMR (282 MHz, CDCl$_3$) of compound **L7**.*
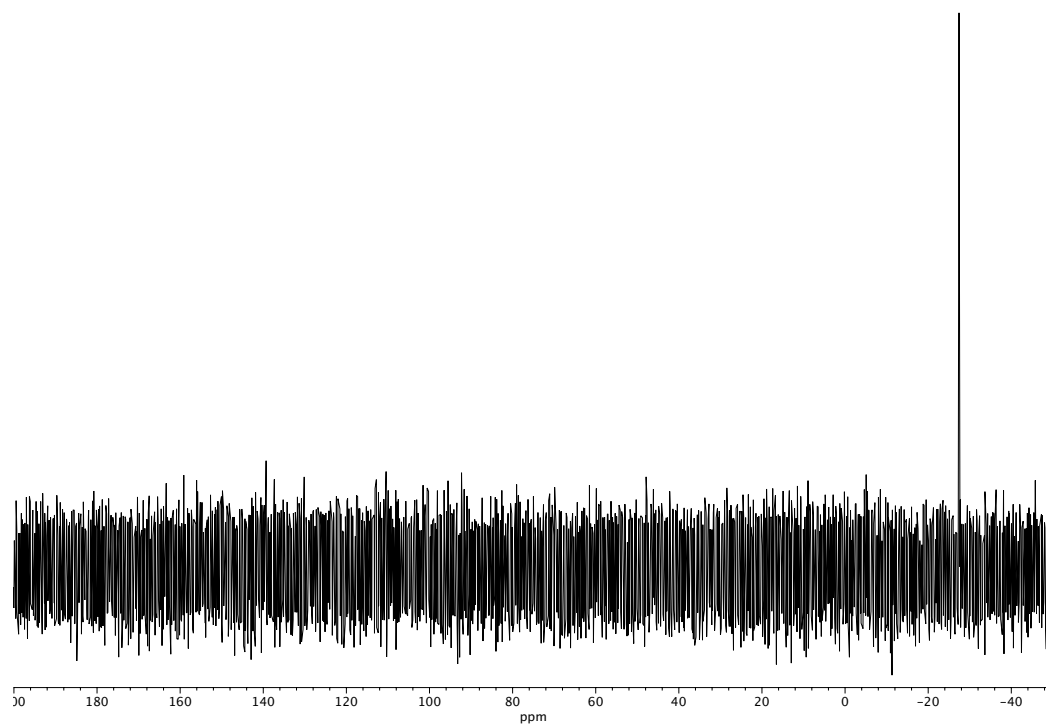
Figure A3.158. *^{31}P NMR (121 MHz, CDCl$_3$) of compound **L7**.*

APPENDIX 4

Notebook Cross-Reference for New Compounds.

Table A4.1 *Notebook cross-reference for Chapter 3.*

Compound	Notebook Ref.	Compound	Notebook Ref.
40a	AQC3-189	41n	KNF-3-043-B
40b	AQC5-245	41o	KNF-2-221A
40c	KNF-2-145	41o'	KNF-2-221B
40d	AQC4-33	41p	AQC4-61
40e	CS-I-153	41p'	AQC4-181_p2
40f	AQC4-274	41q	AQC3-275_p2
40g	AQC3-213	41r	AQC4-69_p1
40h	KNF-2-219	41s	KNF-1-295
40i	RC-I-99	41t	KNF-2-161_A
40j	AQC4-109	41t'	KNF-2-161_B
40k	AQC3-263	41u	KNF-2-229_C
40l	AQC3-277	42	KNF-1-289
40m	RC-I-75	44	KNF-1-293
40n	KNF-3-033	47	AQC3-137
40o	KNF-2-207	49a	AQC3-229
40p	AQC4-55	49e	CS-I-163
40q	AQC3-281	49f	AQC4-19_p2
40r	AQC4-67	49g	AQC4-21
40s	KNF-1-287	49h	KNF-3-031
40t	KNF-2-157	49i	RC-I-119A
40u	ED-2-043	63	CS-I-225
41a	AQC3-291	64	CS-I-223
41b	AQC5-251	65	CS-I-183
41c	KNF-2-151	66	CS-I-271
41d	AQC4-35_p1	67	CS-I-257
41f	AQC4-19_p1	68	RC-I-111
41j	AQC4-117	69	RC-I-129
41k	AQC3-265B_p4	70	CS-I-51
41k'	AQC3-265B_p3	75	RC-II-35
41k"	AQC3-265B_p1	76	RC-II-39
41l	AQC3-287	77	RC-II-41
41m	RC-I-181A	78	KNF-3-177
41m'	RC-I-181A	79	RC-I-301

80	RC-II-67		**D-40f**	AQC4-143
81	RC-II-65		**D-41f**	AQC4-153_p1
82	RC-II-77		**D-49f**	AQC4-153_p2
83	CS-I-229		**D-86**	AQC4-139
84	CS-I-279		**D-100**	AQC4-133
85	AQC3-187			
86	AQC3-201			
87	AQC3-203			
89	KNF-1-283			
90	KNF-2-155			
92	KNF-1-275-B			
93	AQC3-129			
94	CS-I-217			
95	CS-I-215			
96	CS-I-179			
97	CS-I-267			
98	CS-I-249			
99	AQC4-159			
100	AQC3-183			
101	KNF-2-121			
102	KNF-2-123			
103	AQC3-117			
104	KNF-2-155			
105	KNF-1-279			
106	KNF-2-147			
107	ED-2-035			
108	CS-I-175			
109	CS-I-203			
110	CS-I-207			
111	CS-I-237			
112	CS-I-253			
113	KNF-2-283			
114	RC-I-113			

Table A4.2 *Notebook cross-reference for Chapter 5.*

Compound	Notebook Ref.
158a	SRS-II-294
158b	AQC5-65
158c	SRS-III-128
158d	AQC5-47
158e	AQC5-193
158f	AQC5-173
158g	AQC5-235
158h	AQC5-117
158i	AQC5-115
158j	AQC6-87
158k	AQC6-123
158l	SRS-III-31
158m	AQC5-41
158n	AQC5-67
158o	AQC5-153
158p	AQC5-103
158q	AQC5-125
160a	AQC5-265
160b	VH-II-197
160c	AQC5-271
160d	AQC5-143
160e	AQC5-201
160f	AQC5-181
160h	AQC5-145
160i	AQC5-147
160j	AQC6-147
160k	AQC6-151
160l	AQC6-151
160m	AQC5-267
160n	AQC5-269
160o	AQC5-171
160p	AQC5-257_p1
160p_linear	AQC5-107B_p2
160q	AQC6-145_p1

Compound	Notebook Ref.
165a	SRS-III-16
165b	AQC5-37
165c	AQC5-111
165d	AQC5-109
165e	AQC6-83
165f	SRS-III-30
165g	AQC6-113
L4	VH-II-264
L5	VH-II-195
L6	VH-II-281
L7	VH-II-291

ABOUT THE AUTHOR

Alexander Quinn Cusumano was born in St. Petersburg, Florida on June 7th, 1997 to Dave and Dale Cusumano. After 10 years in Florida, Alex, his parents, and his younger sister Nicki moved to Charlotte, North Carolina. His interest in organic chemistry began in high school after carrying out research in the lab of Professor Markus Etzkorn at the University of North Carolina at Charlotte.

In the fall of 2014, Alex started attending North Carolina State University in Raleigh, North Carolina as a chemistry major. While an undergraduate at NCSU, he conducted research under the advisory of Professor Joshua Pierce regarding the development of methods for the synthesis of functionalized heterocycles in the context of natural product synthesis. With the continued support and guidance from Dr. Pierce, his passion for academic research was solidified, leading him to continue his studies in graduate school.

Upon completion of his studies at NCSU, Alex moved to Pasadena, California to pursue graduate studies at the California Institute of Technology under the advisory of Professor Brian Stoltz, with additional guidance from Professor William A. Goddard III. His research focused on the development of novel asymmetric transformations, with an emphasis on transition-metal catalysis and computational chemistry. Upon completion of his Ph.D. at Caltech in June 2023, Alex will continue to broaden his research horizons with a postdoctoral appointment under the guidance of Professor Abigail Doyle at the University of California at Los Angeles.